

The nuclear Cooper pair

Structure and Reactions

G. Potel and R. A. Broglia

April 21, 2020

Preface

The elementary modes of nuclear excitation are vibrations and rotations, single-particle motion, and pairing vibrations and rotations. The specific reactions probing these modes are inelastic scattering and Coulomb excitation, single- and two-particle transfer processes respectively.

The interweaving of the elementary modes of excitation lead to renormalization of the energy, wavefunction and particle content of the single-particles, as well as of the energy, width and collectivity of vibrations and rotations. This implies renormalization of the formfactors and transition densities, Q -value and effective deformation parameters both in 3D- and in gauge-space, and state and mass number dependence of the optical potential. As a consequence, the emergence of long range correlations. Also of resonant phenomena as a function of the bombarding energy of the projectile inducing the anelastic and/or transfer processes, implying the need to go beyond lowest order distorted wave Born approximation (DWBA).

Within this context one can posit that nuclear structure (bound) and reactions (continuum) are but two aspects of the same physics. Even more so concerning the study of light exotic halo nuclei, in which case the distinction between bound and continuum states is almost completely blurred. This is also the reason why these two aspects of nuclear physics are treated in the present monograph on equal footing, within the framework of a unified nuclear field theory of structure and reactions (NFT)_(s+r).

This theory provides the (graphical) rules to diagonalize in a compact and economic way the nuclear Hamiltonian for both bound and continuum states. It does so in terms of Feynman diagrams which describe the coupling of elementary modes of excitation, correcting for the overcompleteness of the basis (structure) and for the non-orthogonality of the scattering states (reaction), as well as for Pauli principle violation. The outcome connects directly with observables: absolute reaction cross sections and decay probabilities.

In other words (NFT)_(s+r) focuses on the scattering amplitudes which determine the absolute cross sections for the variety of physical processes, involving also those in which bosons and fermions are created or annihilated, connecting such processes to formfactors and transition densities. Processes where one set of particles with given energies, momenta angular momenta, etc. go in and another group (or the same), comes out. That is, as it happens in the laboratory, let alone in nature.

Pairing vibrations and rotations, closely connected with nuclear superfluidity are paradigms of quantal nuclear phenomena. They thus play an important role within the field of nuclear structure. It is only natural that two-nucleon transfer plays a similar role concerning the probing of the nucleus.

At the basis of fermionic pairing phenomena one finds Cooper pairs, weakly bound, largely extended, strongly overlapping (quasi-) bosonic entities, made out of pairs of nucleons dressed by collective vibrations and interacting through the exchange of these vibrations as well as through the bare NN -interaction, eventually corrected by $3N$ contributions. Cooper pairs not only change the statistics of the nuclear stuff around the Fermi surface and, condensing, the properties of nuclei close to their ground state. They also display a rather remarkable mechanism of tunneling between target and projectile in direct two-nucleon transfer reaction.

Cooper pair partners being weakly bound ($\ll \epsilon_F$, Fermi energy), are correlated over distances (correlation length) much larger than nuclear dimensions ($\gg R$, nuclear radius). On the other hand, Cooper pairs are forced to be confined within regions in which normal, single-particle density is present and thus, within nuclear dimensions. Within this context the mean field acts as a strong external field, distorting its spatial structure. The correlation length paradigm comes into evidence, for example, when two nuclei are set into weak contact in a direct reaction. In such a case, the partner nucleons of a Cooper pair have a finite probability to be confined each within the mean field of a different nucleus, equally well pairing correlated that when both nucleons are in the same nucleus. It is then natural that a Cooper pair can tunnel between target and projectile, also equally well correlated, through simultaneous than through successive transfer processes. But because of the weak binding of the Cooper pair, let alone the fact that tunneling probability falls off with increasing mass successive is the dominant transfer process.

Although one does not expects supercurrents in nuclei, one can study long-range pairing correlations in terms of individual quantal states and of the tunneling of single Cooper pairs. Such weak coupling Cooper pair transfer reminds the tunneling mechanism of electronic Cooper pairs across a barrier (e.g. a dioxide layer of dimensions much smaller than the correlation length) separating two superconductors, known as a Josephson junction¹. The main difference is that, as a rule, in the nuclear time dependent junction eimereley established in direct two-nucleon transfer process, only one or even none of the two weakly interacting nuclei are superfluid. On the other hand in nuclei, paradigmatic example of fermionic quantum finite many-body system, zero point fluctuations (ZPF) in general, and those associated with pair addition and pair subtraction modes known as pairing vibrations in particular, are much stronger than in condensed matter. Thus, pairing correlations based on even a single Cooper pair can lead to distinct pairing correlation effects in two-nucleon transfer processes.

Nucleonic Cooper pair tunneling has played and is playing a central role in the probing of these subtle quantal phenomena, both in the case of light exotic nuclei

¹Josephson (1962); Anderson (1964b).

as well as of medium and heavy nuclei lying along the stability valley. They have been instrumental in shedding light on the subject of pairing in nuclei at large, and on nuclear superfluidity in particular. Consequently, and as already said, the subject of two-nucleon transfer occupies a central place in the present monograph. Both concerning the conceptual and the computational aspects of the description of nuclear pairing, as well as regarding the quantitative confrontation of the theoretical results with the experimental findings, in terms of absolute differential cross sections.

Concerning exotic nuclei, recent experiments carried out at TRIUMF (Canada) have provided, through the magnifying glass of $(NFT)_{(s+r)}$, a microscopic view of what can be considered a unique embodiment of Cooper's pair model²: a pair of fermions (neutrons) moving in time reversal states on top of a Fermi surface and interacting through the exchange of a long wavelength vibration (phonon)³, leading to a barely bound system. The two neutrons give rise to an isotropic halo. Because the vibration (phonon) results from the sloshing back and forth of the neutron halo against the nucleons of the core moving in phase, one is in presence of a realization of Nambu's tumbling⁴ or, more precisely, symbiotic mechanism of spontaneously broken symmetry in gauge space.

Regarding the case of medium heavy nuclei lying along the stability valley, recent studies of heavy ion reactions between superfluid nuclei carried out at energies below the Coulomb barrier at the National Laboratory of Legnaro (Italy) have provided a measure of the neutron Cooper pair correlation length. Within this context, in the present monograph interdisciplinarity is used as a tool to attack concrete nuclear problems. But also, making use of the unique laboratory provided by the finite quantum many-body system of which the atomic nucleus is a paradigmatic example⁵, to shed light on condensed matter results, in terms of analogies involving individual, quantal single-particle states, let alone tunneling of single Cooper pairs.

Because of the central role the interweaving of the variety of elementary modes of nuclear excitation, namely single-particle motion and collective vibrations and rotations play in nuclear superfluidity, the study of Cooper pair tunneling in nuclei requires a consistent description of nuclear structure in terms of dressed quasiparticles and, making use of the resulting renormalized wavefunctions (formfactors), of one-nucleon transfer processes⁶. This is similar to the situation encountered in superconductors, in connection with strongly coupled systems, and experimentally studied through one-electron tunneling experiments⁷

²Cooper (1956).

³Fröhlich (1952); Bardeen and Pines (1955); Bardeen et al. (1957a,b).

⁴Nambu (1991).

⁵Broglia (2019a) (Overview).

⁶Within this context one recognizes the difficulties of extracting spectroscopic factors from experiment, in terms of single-particle transfer cross sections calculated making use of mean field wavefunctions.

⁷Giaver (1973).

Thus, in the present monograph the general physical arguments and technical computational details concerning the calculation of absolute one-and two nucleon transfer differential cross sections, making use of state of the art NFT structure input, are discussed in detail.

As a result of this approach, theoretical and experimental nuclear practitioners can use the present monograph at profit. To help this use, the basic nuclear structure formalism, in particular that associated with pairing and with collectives modes in nuclei, is economically introduced through general physical arguments. This is also in keeping with the availability in the current literature, of detailed discussions of the corresponding material. Within this context, the monographs *Nuclear Superfluidity* by Brink and Broglia and *Oscillations in Finite Quantum Systems* by Bertsch and Broglia, published also by Cambridge University Press, can be considered companion volumes to the present one. Volume which shares with those a similar aim: to provide a broad physical view of central issues in the study of finite quantal many-body nuclear systems accessible to motivated students and practitioners. However, neither the present one, nor the other two are introductory texts. In particular the present one in which an attempt at unifying structure and reactions as it happens in nature, is made. On the other hand, unifying discrete (mainly structure) and continuum (reactions) configuration spaces, implies that one will be dealing with those structure results which can be tested by means of experiment. A fact which makes the subject of the present monograph a chapter of quantum mechanics, and thus opened to a wide range of practitioners⁸.

Concerning the notation, we have divided each chapter into sections. Each section may, in turn, be broken down into subsections. Equations and Figures are identified by the number of the chapter and that of the section. Thus (5.1.33) labels the thirtythird equation of section 1 of chapter 5. Similarly, Fig. 5.1.2 labels the second figure of section 1 of chapter 5. Concerning the Appendices, they are labelled by the chapter number and by a Latin letter in alphabetical order, e.g. App. 2.A, App. 2.B, etc. Concerning equations and Figures, a sequential number is added. Thus (2.B.2) labels the second equation of Appendix B of chapter 2,

⁸Within this context let us mention the intimately correlated subjects of Random Phase Approximation (RPA) and Particle Vibration Coupling (PVC) not found in a fourth year curriculum. They are explained and refer to in a number of places throughout the present monograph, starting from a pedestrian level and for both surface (particle-hole) and pairing (particle-particle and hole-hole) vibrations (Sects. 1.2 and 1.3), and then extended to include further details and facets (see Sects. 1.6, 2.3 Fig. (2.3.1), Sect. 2.3.2 (Fig. 2.3.10), App. 2.C (Fig. 2.C.1), Sect. 3.1 (Fig. 3.1.5). Furthermore, in the case of RPA of pairing vibrations around the closed shell system ^{208}Pb , one provides in Sect. 3.5, detailed documentation of the numerical calculation of the associated wavefunctions (X - and Y -amplitudes) at the level of an exercise in a fourth year course. A similar situation is encountered in connection with the subject of the Distorted Wave Born Approximation (DWBA), again a subject not found in fourth year curricula. It is treated at the pedestrian level in Apps. 2.A, 5.F and 6.B in connection with inelastic, one-particle and two-particle transfer reactions respectively. And once more in full detail, without eschewing complexities, but again in the style of an example-exercise (“Sometimes one has to say difficult things, but one ought to say them as simply as one know-how” (G. H. Hardy, *A mathematician’s apology*, Cambridge University Press, Cambridge (1969))) in Sects. 5.1, 6.2.1, 6.2.2 and 6.2.3 for one- and two-particle transfer reactions respectively.

while Fig. 2.B.1 labels the first figure of Appendix B of Chapter 2. References are called in terms of the author's surname and publication year and are found in alphabetic order in the bibliography at the end of the monograph.

A methodological approach used in the present monograph concerns a certain degree of repetition. Similar, but not the same issues are dealt with more than once using different but equatable terminologies. This approach reflects the fact that useful concepts like reaction channels, or correlation length, let alone elementary modes of excitation, are easy to understand but difficult to define⁹. This is because their validity is not exhausted in a single perspective. But even more important, because their power in helping at connecting¹⁰ seemingly unrelated results and phenomena is difficult to be fully appreciated the first time around, spontaneous symmetry breaking and associated emergent properties providing an example of this fact.

⁹“Gentagelsen den er virkeligheden, og Tilverelsens Alvor” (Repetition is reality, and life’s seriousness: S. Kierkegaard Gjentagelsen (1843)) повторение маты обучение : repetition is learning’s mother.

¹⁰“The concepts and propositions get “meaning” viz. “content”, only through their connection with sense-experience... The degree of certainty with which this connection, viz., intuitive combination, can be undertaken, and nothing else, differentiates empty fantasy from scientific “truth”... A correct proposition borrows its “truth” from the truth-content of the system to which it belongs” (A. Einstein, Autobiographical notes, in Albert Einstein, Ed. P. A. Schilpp, Harper, New York (1951)) p.1, Vol I.

Throughout, a number of footnotes are found. This is in keeping with the fact that footnotes can play a special role within the framework of an elaborated presentation. In particular, they are useful to emphasize relevant issues in an economic way. Being outside the main text, they give the possibility of stating eventual important results, without the need of elaborating on the proof, but referring to the corresponding sources. Within this context, and keeping the natural distances, one can mention that in the paper in which Born¹¹ introduces the probabilistic interpretation of Schrödinger's wavefunction, the fact that this probability is connected with its modulus squared and not with the wavefunction itself, is only referred to in a footnote.

Most of the material contained in this monograph have been the subject of lectures of the four year course "Nuclear Structure Theory" which RAB delivered throughout the years at the Department of Physics of the University of Milan, as well as at the Niels Bohr Institute and at Stony Brook (State University of New York). It was also presented by the authors in the course Nuclear Reactions held at the PhD School of Physics of the University of Milan.

GP wants to thank the tutoring of Ben Bayman concerning specific aspects of two-particle transfer reactions. Discussions with Ian Thompson and Filomena Nunes on a variety of reaction subjects are gratefully acknowledged. RAB acknowledges the essential role the collaboration with Francisco Barranco and Enrico Vigezzi has played concerning nuclear structure aspects of the present monograph. Its debt with the late Aage Winther regarding the reaction aspects of it is difficult to express in words. The overall contributions of Daniel Bès, Ben Bayman and Pier Francesco Bortignon¹² are only too explicitly evident throughout the text and constitute a daily source of inspiration. G. P. and R. A. B. have received important suggestions and comments regarding concrete points and the overall presentation of the material discussed below from Ben Bayman, Pier Francesco Bortignon, David Brink, Willem Dickhoff and Vladimir Zelevinsky and are here gratefully acknowledged. We are specially beholden to Elena Litvinova and Horst Lenske for much constructive criticism and suggestions.

Gregory Potel Aguilar
East Lansing

Ricardo A. Broglia
Copenhagen

¹¹Born (1926a). Within this context, it is of notice that the extension of Born probabilistic interpretation to the case of many-particle systems is also found in a footnote (Pauli (1927), footnote on p. 83 of the paper). Source of information Pais (1986).

¹²Deceased August 27, 2018.

Contents

1	Introduction	15
1.1	Views of the nucleus	15
1.1.1	The liquid drop and the shell model	15
1.1.2	Nuclear excitations	18
1.2	The particle-vibration coupling	22
1.3	Pairing vibrations	31
1.4	Spontaneously broken symmetry	34
1.4.1	Quadrupole deformations in 3D-space	34
1.4.2	Deformation in gauge space	41
1.5	Giant dipole resonance	48
1.6	Giant pairing vibrations	50
1.7	Sum rules	51
1.8	Ground state correlations	52
1.9	Interactions	59
1.10	Hindsight	62
2	Structure and reactions	63
2.1	Elementary modes of excitation and specific probes	63
2.2	Sum rules revisited	72
2.2.1	Empirical two-nucleon transfer sum rules	76
2.3	Particle-vibration coupling	79
2.3.1	Fluctuation and damping	81
2.3.2	Induced interaction	87
2.4	Well funneled nuclear structure landscape	90
2.5	Non-orthogonality	94
2.6	Coupling between intrinsic and relative motion	101
2.7	Nuclear Field Theory for pedestrians	103
2.7.1	The concept of elementary modes of excitation	108
2.7.2	NFT rules and applications	111
2.7.3	Spurious states	119
2.7.4	Applications	127
2.8	Elementary modes of excitation and specific probes	133
2.9	Competition between ZPF	134

2.10	Coupling between structure and reaction channels	138
2.10.1	Bare particles and Hartree-Fock field	138
2.10.2	Physical particles and optical potential	139
2.10.3	$^3_3\text{Li}_8$ structure in a nutshell	140
2.10.4	$^{11}\text{Li}(p, p)^{11}\text{Li}$ and transfer reaction channels	144
2.11	Characterization of an open-shell nucleus: ^{120}Sn	151
2.12	Summary	154
2.A	Inelastic Scattering	155
2.A.1	(α, α') -scattering	155
2.B	Technical details NFT	159
2.B.1	Graphical solution	160
2.B.2	Overlap	161
2.B.3	NFT($r+s$): linear theory	162
2.C	NFT and reactions	164
2.C.1	Potential scattering	166
2.C.2	Transfer	167
2.D	NFT vacuum polarization	173
3	Pairing with transfer	175
3.1	Nuclear Structure in a nutshell	175
3.2	Renormalization and spectroscopic amplitudes	187
3.3	Quantality Parameter	190
3.4	Cooper pairs	192
3.4.1	independent-particle motion	193
3.4.2	independent-pair motion	197
3.5	Pair vibration spectroscopic amplitudes	199
3.5.1	Pair removal mode	205
3.5.2	Pair addition mode	207
3.6	Halo pair addition mode and pygmy	212
3.6.1	Cooper pair binding: a novel embodiment of the Axel-Brink hypothesis	215
3.A	Nuclear van der Waals Cooper pair	223
3.B	Renormalized coupling constants ^{11}Li : resumé	225
3.C	Lindemann criterion and quantality parameter	226
3.C.1	Lindemann (“disorder”) parameter for a nucleus	228
3.D	The van der Waals interaction	228
3.D.1	van der Waals interaction between two hydrogen atoms	229
3.D.2	Critical dimension for van der Waals H-H interaction (protein folding domain)	233
3.D.3	van der Waals between two amino acids	234
3.D.4	Average interaction between two side chains	234
3.E	Phase transition and fluctuations	235
3.E.1	Pairing phase transition in small particles	237
3.E.2	Fine Sn particles	239

3.E.3	Time-reversal response function	239
4	Simultaneous versus successive transfer	243
4.1	Simultaneous versus successive Cooper pair transfer in nuclei	243
4.2	Transfer probabilities, enhancement factor	244
4.3	Phase correlation and enhancement factor	251
4.3.1	Interplay between mean field and correlation length	257
4.4	Correlations in Cooper pair tunneling	260
4.5	Pair transfer	263
4.5.1	Cooper pair dimensions	264
4.6	Comments on the optical potential	269
4.7	Weak link between superconductors	274
4.8	Rotation in gauge space	279
4.8.1	Phase coherence	280
4.9	Hindsight	286
4.A	Medium polarization effects and pairing	288
4.A.1	Nuclei	288
4.A.2	Metals	298
4.A.3	Elementary theory of phonon dispersion relation	299
4.A.4	Pairing condensation (correlation) energy beyond level density	304
4.A.5	Hindsight	306
4.B	Cooper pair: radial dependence	306
4.B.1	Number of overlapping pairs	312
4.B.2	Coherence length and quantality parameter for (<i>ph</i>) vibrations	314
4.B.3	tunneling probabilities	319
4.B.4	Nuclear correlation (condensation) energy	320
4.B.5	Summary	321
4.C	Absolute Cooper pair tunneling cross section	323
4.C.1	Saturation density, spill out and halo	324
4.D	Pairing spatial correlation: simple estimate	330
4.E	Coherent state	332
5	One-particle transfer	335
5.1	General derivation	336
5.1.1	Coordinates	343
5.1.2	Zero-range approximation	343
5.2	Examples and Applications	344
5.2.1	$^{120}\text{Sn}(p, d)^{119}\text{Sn}$ and $^{120}\text{Sn}(d, p)^{121}\text{Sn}$ reactions	344
5.2.2	Dressing of single-particle states: parity inversion in ^{11}Li	349
5.A	Minimal mean field theory	354
5.A.1	Density of levels	357
5.B	Single-particle strength function	359

5.C	Vacuum and medium polarization	361
5.D	The Lamb Shift	363
5.E	Self-energy and vertex corrections	364
5.F	Single-nucleon transfer for pedestrians	366
5.F.1	Plane-wave limit	370
5.G	One-particle knockout within DWBA	372
5.G.1	Spinless particles	372
5.G.2	Particles with spin	379
5.G.3	One-particle transfer	385
5.H	Dynamical shell model in a nutshell	388
6	Two-particle transfer	393
6.1	Summary of second order DWBA	394
6.2	Detailed derivation of second order DWBA	398
6.2.1	Simultaneous transfer: distorted waves	398
6.2.2	matrix element for the transition amplitude	399
6.2.3	Coordinates for the calculation of simultaneous transfer .	407
6.2.4	Matrix element for the transition amplitude (alternative derivation)	410
6.2.5	Coordinates used to derive Eq. (6.2.89)	413
6.2.6	Successive transfer	415
6.2.7	Coordinates for the successive transfer	420
6.2.8	Simplifying the vector coupling	421
6.2.9	non-orthogonality term	422
6.2.10	Arbitrary orbital momentum transfer	423
6.2.11	Successive transfer contribution	425
6.A	ZPF and Pauli principle	429
6.B	Coherence and effective formfactors	432
6.C	Succesive, simultaneous, non-orthogonality	437
6.C.1	Independent particle limit	444
6.C.2	Strong correlation (cluster) limit	445
6.D	Spherical harmonics and angular momenta	446
6.D.1	Addition theorem	447
6.D.2	Expansion of the delta function	447
6.D.3	Coupling and complex conjugation	447
6.D.4	Angular momenta coupling	448
6.D.5	Integrals	448
6.D.6	Symmetry properties	449
6.E	distorted waves	450
6.F	hole states and time reversal	451
6.G	Spectroscopic amplitudes in the BCS approximation	453
6.H	Bayman's two-nucleon transfer amplitudes	455

7 Probing Cooper pairs with pair transfer	457
7.1 Evidence for phonon mediated pairing	458
7.1.1 Structure	458
7.1.2 Reaction	462
7.2 NFT of ^{11}Be : one-particle transfer in halo nuclei	465
7.2.1 Outlook	466
7.2.2 Calculations	466
7.3 Summary	471
7.4 Pairing rotational bands	471
7.4.1 Structure–reaction: stability of the order parameter α_0 . .	473
7.4.2 A two-nucleon transfer physical sum rule	475
7.5 Virtual states forced to become real	476
7.5.1 Empirical renormalization: $(\text{NFT})_{\text{ren}}(\mathbf{r}+\mathbf{s})$ (Feynman + S –matrix)	478
7.5.2 On-shell energy	480
7.6 Perturbation and beyond	480
7.6.1 One-particle transfer and optical potential	481
7.6.2 $(\text{NFT})_{\text{ren}}(\mathbf{s}+\mathbf{r})$ diagrams, S –matrix	481
7.6.3 The structure of “observable” Cooper pairs	482
7.6.4 Closing the circle	487
7.7 Summary	488
7.A Bootstrap mechanism to break gauge invariance	490
7.A.1 Gedanken eksperiment	490
7.B Alternative processes to populate $ ^9\text{Li}(1/2^-)\rangle$	492
7.C Software	494
7.D Statistics.	499
7.E Correlation length and quantity parameter.	500
7.F Multipole pairing vibrations.	502
7.G Vacuum fluctuations: the Casimir effect	507
7.G.1 Measuring QED quantum fluctuations	508
7.G.2 The hydrophobic force	512

Chapter 1

Introduction

Toute théorie physique est fondée sur l'analogie qu'on établi entre des choses malconnues et des choses simples

Simone Weil (Leçons de philosophie, Plon, Paris (1959))

1.1 Views of the nucleus

In the atom, the nucleus provides the Coulomb field in which negatively charged electrons ($-e$) move independently of each other in single-particle orbitals. The filling of these orbitals explains Mendeleev's periodic table. Thus the valence of the chemical elements as well as the particular stability of the noble gases associated with the closing of shells (2(He), 10(Ne), 18(Ar), 36(Kr), 54(Xe), 86(Ra)). The dimension of the atom is measured in angstroms ($\text{\AA}=10^{-8}\text{cm}$), and typical energies in eV, the electron mass being $m_e \approx 0.5 \text{ MeV} (\text{MeV}=10^6 \text{eV})$.

The atomic nucleus is made out of positively charged protons ($+e$) and of (uncharged) neutrons, nucleons, of mass $\approx 10^3 \text{ MeV}$ ($m_p = 938.3 \text{ MeV}$, $m_n = 939.6 \text{ MeV}$). Nuclear dimensions are of the order of few fermis ($\text{fm}=10^{-13} \text{ cm}$). While the stability of the atom is provided by a source external to the electrons, namely the atomic nucleus, this system is self-bound as a result of the strong interaction of range $a_0 \approx 0.9 \text{ fm}$ and strength $v_0 \approx -100 \text{ MeV}$ acting among nucleons.

1.1.1 The liquid drop and the shell model

While most of the atom is empty space, the density of the atomic nucleus is conspicuous ($\rho = 0.17 \text{ nucleon/fm}^3$). The “closed packed” nature of this system implies a short mean free path as compared to nuclear dimensions. This can be estimated from classical kinetic theory $\lambda \approx (\rho\sigma)^{-1} \approx 1 \text{ fm}$, where $\sigma \approx 2\pi a_0^2$ is

the nucleon–nucleon cross section. It seems then natural to liken the atomic nucleus to a liquid drop (Bohr and Kalckar). This picture of the nucleus provided the framework to describe the basic features of the fission process¹.

The leptodermic properties of the atomic nucleus are closely connected with the semi-empirical mass formula².

$$m(N, Z) = (Nm_n + Zm_p) - \frac{1}{c^2}B(N, Z), \quad (1.1.1)$$

the binding energy being

$$B(N, Z) = \left(b_{vol}A - b_{surf}A^{2/3} - \frac{1}{2}b_{sym}\frac{(N-Z)^2}{A} - \frac{3}{5}\frac{Z^2e^2}{R_c} \right). \quad (1.1.2)$$

The first term is the volume energy representing the binding energy in the limit of large A , $N = Z$ and in the absence of the Coulomb interaction ($b_{vol} \approx 15.6$ MeV). The second term represents the surface energy, where

$$b_{surf} = 4\pi r_0^2 \gamma. \quad (1.1.3)$$

The nuclear radius is written as $R = r_0 A^{1/3}$, with $r_0 = 1.2$ fm, the surface tension energy being $\gamma \approx 0.95$ MeV/fm². The third term in (1.1.2) is the symmetry term which reflects the tendency towards stability for $N = Z$, with $b_{sym} = 50$ MeV. The symmetry energy can be divided into a kinetic and a potential energy part. A simple estimate of the kinetic energy part can be obtained by making use of the Fermi gas model which gives $(b_{sym})_{kin} \approx (2/3)\epsilon_F \approx 25$ MeV ($\epsilon_F \approx 36$ MeV). Consequently,

$$V_1 = (b_{sym})_{pot} = b_{sym} - (b_{sym})_{kin} \approx 25 \text{ MeV}. \quad (1.1.4)$$

The last term of (1.1.2) is the Coulomb energy corresponding to a uniformly charged sphere of radius $R_c = 1.24 A^{1/3}$ fm.

When, in a heavy-ion reaction, two nuclei come within the range of the nuclear forces, the Coulomb trajectory of relative motion will be changed by the attraction which will act between the nuclear surfaces. This surface interaction is a fundamental quantity in all heavy ion reactions. Assuming two spherical nuclei at a relative distance $r_{AA} = R_a + R_A$, where R_a and R_A are the corresponding half-density radii, the force acting between the two surfaces is

$$\left(\frac{\partial U_{AA}^N}{\partial r} \right)_{r_{AA}} = 4\pi\gamma \frac{R_a R_A}{R_a + R_A} \quad (1.1.5)$$

This result allows for the calculation of the ion-ion (proximity) potential which, supplemented with a position dependent absorption, can be used to accurately describe heavy ion reactions³.

¹Meitner and Frisch (1939); Bohr and Wheeler (1939).

²Weizsäcker (1935).

³Broglia and Winther (2004) and refs. therein.

In such reactions, not only elastic processes are observed, but also anelastic reactions in which one, or both surfaces of the interacting nuclei are set into vibration (Fig. 1.1.1). The restoring force parameter associated with oscillations of multipolarity λ is

$$C_\lambda = (\lambda - 1)(\lambda + 2)R_0^2\gamma - \frac{3}{2\pi} \frac{\lambda - 1}{2\lambda + 1} \frac{Z^2 e^2}{R_c}, \quad (1.1.6)$$

where the second term corresponds to the contribution of the Coulomb energy to C_λ . Assuming the flow associated with surface vibration to be irrotational, the associated inertia for small amplitude oscillations is,

$$D_\lambda = \frac{3}{4\pi} \frac{1}{\lambda} A M R^2, \quad (1.1.7)$$

the energy of the corresponding mode being

$$\hbar\omega_\lambda = \hbar \sqrt{\frac{C_\lambda}{D_\lambda}}. \quad (1.1.8)$$

The label λ stands for the angular momentum of the vibrational mode, μ being its third component (see Eq. (1.2.1)). Aside from λ, μ , surface vibrations can also be characterized by an integer $n (= 1, 2, \dots)$, an ordering number indicating increasing energy. For simplicity, a single common label α will also be used.

Experimental information associated with low-energy quadrupole vibrations, namely $\hbar\omega_2$ and the electromagnetic transition probabilities $B(E2)$, allows to determine C_2 and D_2 . The resulting C_2 values exhibit variations by more than a factor of 10 both above and below the liquid-drop estimate. The observed values of D_2 are large as compared with the mass parameter for irrotational flow, a fact connected with the role played by pairing in nuclei⁴.

A picture apparently antithetic to that of the liquid drop, the shell model, emerged from the study of experimental data, plotting them against either the number of protons (atomic number), or the number of neutrons in the nuclei, rather than against the mass number. One of the main nuclear features which led to the development of the shell model was the study of the stability and abundance of nuclear species and the discovery of what are usually called magic numbers⁵. What makes a number magic is that a configuration of a magic number of neutrons, or of protons, is unusually stable whatever the associated number of other nucleons is⁶.

The strong binding of a magic number of nucleons and weak binding for one more, reminds the results concerning the atomic stability of rare gases. In the nuclear case, at variance with the atomic case, the spin-orbit coupling play an important role, as can be seen from the level scheme shown in Fig. 1.1.2, obtained by assuming that nucleons move independently of each other in an average potential of spherical symmetry.

⁴See footnote 7; see also Bohr and Mottelson (1975) p. 75.

⁵Elsasser (1933); Mayer (1948); Haxel et al. (1949).

⁶Mayer (1949); Mayer and Teller (1949).

A closed shell, or a filled level, has angular momentum zero. Thus, nuclei with one nucleon outside (missing from) closed shell, should have the spin and parity of the orbital associated with the odd nucleon (-hole), a prediction confirmed by the data (available at that time) throughout the mass table. Such a picture implies that the nucleon mean free path is large compared to nuclear dimensions.

The systematic studies of the binding energies leading to the shell model found also that the relation (1.1.2), has to be supplemented to take into account the fact that nuclei with both odd number of protons and of neutrons are energetically unfavored compared with even-even ones by a quantity of the order of $\delta \approx 33 \text{ MeV}/A^{3/4}$ called the pairing energy⁷ and at the basis of the odd-even staggering effect.

1.1.2 Nuclear excitations

In addition to the quantum numbers λ and μ one can characterize nuclear excitations by additional quantum numbers such as parity π , isospin τ and spin σ . Furthermore one can assign a particle (baryon or transfer) quantum number β . For a nucleon moving above the Fermi surface one has $\beta = +1$, while for a hole in the Fermi sea $\beta = -1$. For (quasi-) bosonic excitations $\beta = 0$ for a mode associated with e.g. surface oscillation, which can also be viewed as a correlated particle-hole excitation (within this context see Fig. 1.2.3). In particular, the low-lying quadrupole vibrations of even-even nuclei have quantum numbers $\lambda^\pi = 2^+$, $\tau = 0$ (protons and neutrons oscillate in phase) and $\sigma = 0$ (no spin-flips in the excitation).

For modes which involve the addition or subtraction of two correlated nucleons to the nucleus, $\beta = +2$ (Fig. 1.3.1) and $\beta = -2$ respectively. The excitation which connects the ground state of an even nucleus, to the ground state of the next even nucleus, i.e. monopole pairing vibration (e.g. $\lambda^\pi = 0^+, \beta = +2$) is of this type. The structure of excitations with $|\beta| > 2$, expresses the various possible clustering effects of corresponding order.

The low-lying excited state of closed shell nuclei can be interpreted as a rule, as a harmonic quadrupole or octupole collective vibration (Fig. 1.1.3) described by the Hamiltonian⁸

$$H_{coll} = \sum_{\lambda\mu} \left(\frac{1}{2D_\lambda} |\Pi_{\lambda\mu}|^2 + \frac{C_\lambda}{2} |\alpha_{\lambda\mu}|^2 \right) \quad (1.1.9)$$

⁷ Mayer and Jensen (1955) p.9. Connecting with further developments associated with the BCS theory of superconductivity (Bardeen et al. (1957a,b)) and its extension to the atomic nucleus (Bohr et al. (1958)), the quantity δ is identified with the pairing gap Δ parametrized according to $\Delta = 12 \text{ MeV}/\sqrt{A}$ (Bohr and Mottelson (1969)). It is of notice that for typical superfluid nuclei like ¹²⁰Sn, the expression of δ leads to a numerical value which can be parametrized as $\delta \approx 33 \text{ MeV}/(A^{1/4} \times A^{1/2}) \approx 10 \text{ MeV}/\sqrt{A}$.

⁸Classically $\Pi_{\lambda\mu} = D_\lambda \dot{\alpha}_{\lambda\mu}$.

Following Dirac (1930) one can describe the oscillatory motion introducing boson creation (annihilation) operator $\Gamma_{\lambda\mu}^\dagger$ ($\Gamma_{\lambda\mu}$) obeying

$$[\Gamma_\alpha, \Gamma_{\alpha'}^\dagger] = \delta(\alpha, \alpha'), \quad (1.1.10)$$

leading to

$$\hat{a}_{\lambda\mu} = \sqrt{\frac{\hbar\omega_\lambda}{2C_\lambda}} (\Gamma_{\lambda\mu}^\dagger + (-1)^\mu \Gamma_{\lambda-\mu}), \quad (1.1.11)$$

and a similar expression for the conjugate momentum variable $\hat{\Pi}_{\lambda\mu}$, resulting in

$$\hat{H}_{coll} = \sum \hbar\omega_\lambda ((-1)^\mu \Gamma_{\lambda\mu}^\dagger \Gamma_{\lambda-\mu} + 1/2). \quad (1.1.12)$$

The frequency is $\omega_\lambda = (C_\lambda/D_\lambda)^{1/2}$, while $(\hbar\omega_\lambda/2C_\lambda)^{1/2}$ is the amplitude of the zero-point fluctuation of the vacuum state $|0\rangle_B, |n_{\lambda\mu} = 1\rangle = \Gamma_{\lambda\mu}^\dagger |0\rangle_B$ being the one-phonon state. To simplify the notation, in many cases one writes $|n_\alpha = 1\rangle$.

The ground and low-lying states of nuclei with one nucleon outside closed shell can be described by the Hamiltonian

$$H_{sp} = \sum_\nu \epsilon_\nu a_\nu^\dagger a_\nu, \quad (1.1.13)$$

where $a_\nu^\dagger (a_\nu)$ is the single-particle creation (annihilation) operator,

$$|\nu\rangle = a_\nu^\dagger |0\rangle_F, \quad (1.1.14)$$

being the single-particle state of quantum numbers $\nu (\equiv nljm)$ and energy ϵ_ν , while $|0\rangle_F$ is the Fermion vacuum. It is of notice that

$$[H_{coll}, \Gamma_{\lambda'\mu'}^\dagger] = \hbar\omega_{\lambda'} \Gamma_{\lambda'\mu'}^\dagger \quad (1.1.15)$$

and

$$[H_{sp}, a_{\nu'}^\dagger] = \epsilon_{\nu'} a_{\nu'}^\dagger. \quad (1.1.16)$$

This is an obvious outcome resulting from the bosonic

$$[\Gamma_\alpha, \Gamma_{\alpha'}^\dagger] = \delta(\alpha, \alpha') \quad (1.1.17)$$

and fermionic

$$\{a_\nu, a_{\nu'}^\dagger\} = \delta(\nu, \nu') \quad (1.1.18)$$

commutation (anti-commutation) relations.

Both the existence of drops of nuclear matter displaying collective surface vibrations, and of independent-particle motion in a self-confining mean field are

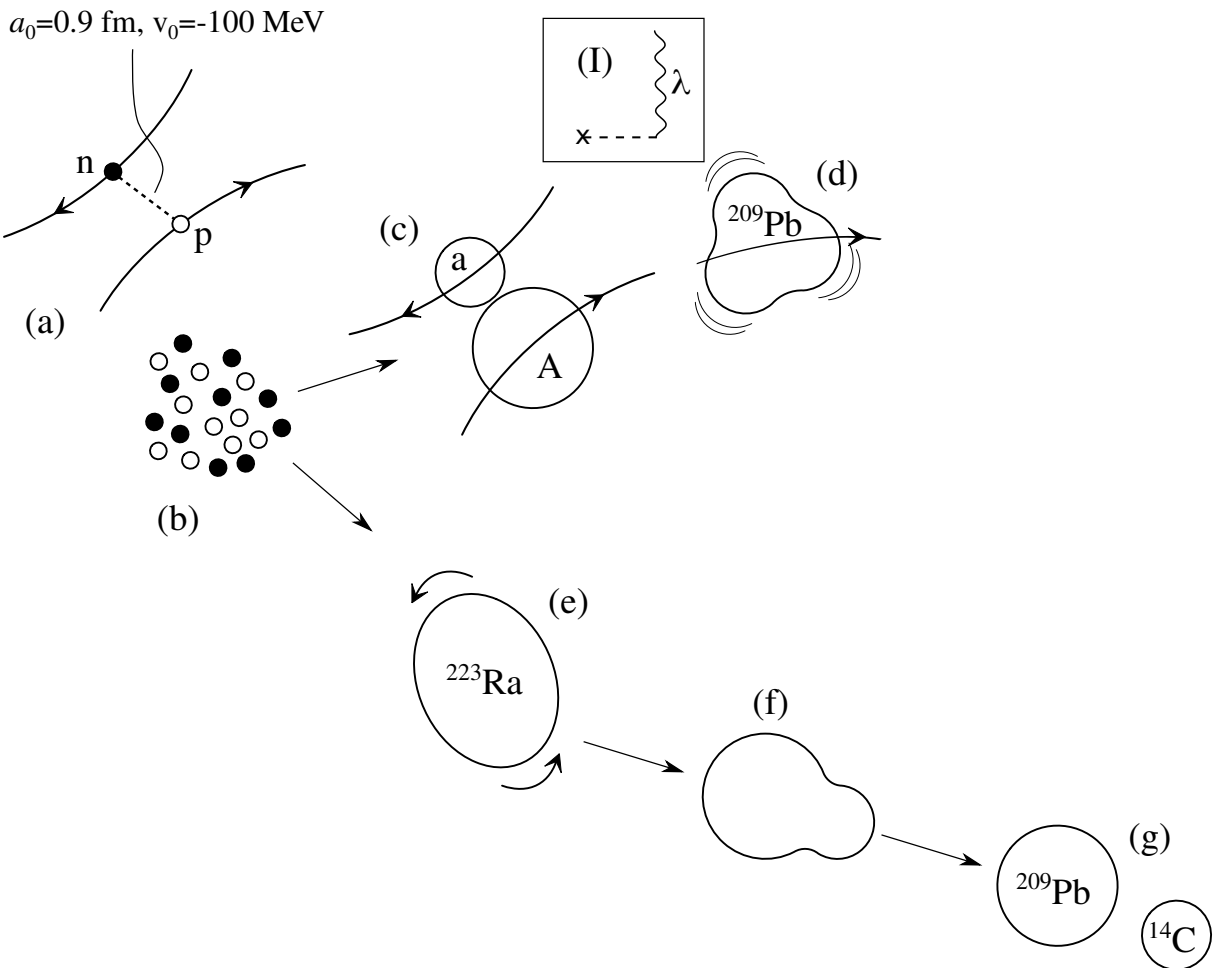


Figure 1.1.1: Emergent properties (collective nuclear modes) (a) Nucleon-Nucleon (NN) interaction in a scattering experiment; (b) assembly of a swarm of nucleons condensing into drops of nuclear matter, examples shown in (c) and (e); (c) anelastic heavy ion reaction $a + A \rightarrow a + A^*$ setting the nucleus A into an octupole surface oscillations (d); in inset (I) the time-dependent nuclear plus Coulomb fields associated with the reaction (c) is represented by a cross followed by a dashed line, while the wavy line labeled λ describes the propagation of the surface vibration shown in (d), time running upwards; (e) another possible outcome of nucleon condensation: the (weakly) quadrupole deformed nucleus ^{223}Ra which can rotate as a whole with moment of inertia smaller than the rigid moment of inertia, but much larger than the irrotational one; (f) the surface zero point fluctuations (quadrupole ($\lambda = 2$), octupole ($\lambda = 3$), etc.) can get, with a small but finite probability ($P \approx 10^{-10}$), spontaneously in phase and produce a neck-in (saddle conformation) leading eventually to the (exotic) decay mode $^{223}\text{Ra} \rightarrow ^{209}\text{Pb} + ^{14}\text{C}$, as experimentally observed (g) (Rose and Jones (1984), see Brink and Broglia (2005), Ch. 7 and refs. therein).

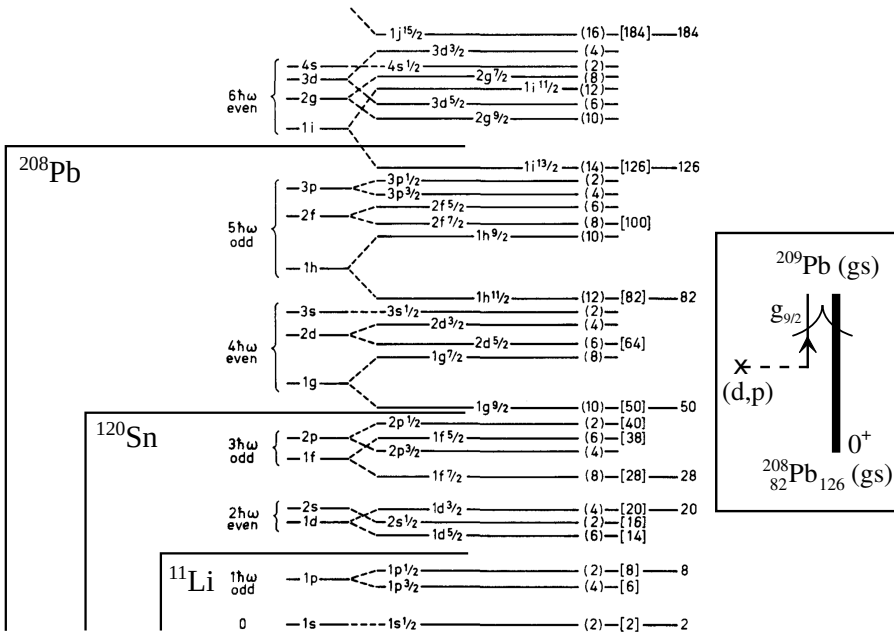


Figure 1.1.2: Sequence of levels of the harmonic oscillator potential labeled with the principal oscillator quantum number ($N = 0, 1(\hbar\omega), 2(\hbar\omega), \dots$ the parity being $\pi = (-1)^N$). The next column shows the splitting of major shell degeneracies obtained using a more realistic potential (Woods-Saxon), the quantum number being the number of radial nodes of the associated single-particle s, p, d , etc., states. The levels shown at the center result when a spin-orbit term is also considered, the quantum numbers n, l, j characterizing the states of degeneracy ($2j+1$) ($j = l \pm 1/2$). To the left we schematically (in particular in the case of Li which displays non Meyer and Jensen sequence) indicate the Fermi energy associated with a light (exotic), medium, and heavy nucleus, namely ^{11}Li , ^{120}Sn and ^{208}Pb . In the inset, a schematic graphical representation of the reaction $^{208}\text{Pb}(d, p)^{209}\text{Pb}(\text{gs})$ is shown. A cross followed by a horizontal dashed line represents, in the present case, the (d, p) field, while a single arrowed line describes the odd nucleon moving in the $g_{9/2}$ orbital above the $N = 126$ shell closure (and belonging to the $N = 6$ major shell) drawn as a bold line labeled 0^+ .

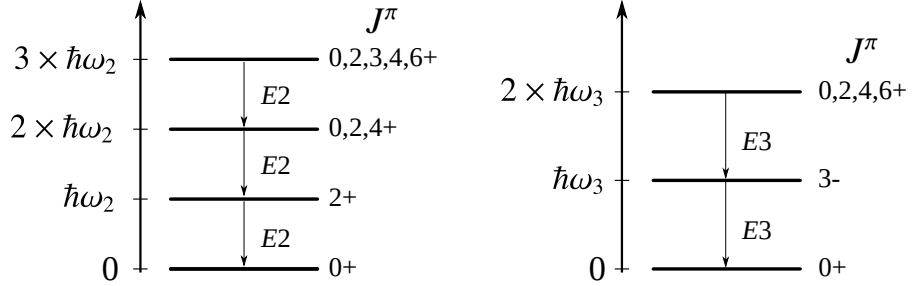


Figure 1.1.3: Schematic representation of harmonic quadrupole and octupole liquid drop collective surface vibrational modes.

emergent properties not contained in the particles forming the system, neither in the NN -force, but on the fact that these particles behave according to the rules of quantum mechanics, move in a confined volume and that there are many of them.

Expressed it differently, generalized rigidity closely connected to the inertial parameter D_λ implies that acting on a nucleus with an external $\beta = 0$, time-dependent (nuclear/Coulomb) field, the system reacts as a whole (collective vibrations; also rotations see Sect. 1.4), while acting with fields which change particle number by one ($\beta = \pm 1$; e.g. (d, p) and (p, d) reactions) the system reacts in terms of independent particle motion, feeling the pushings and pullings of the other nucleons only when trying to leave the nucleus. Such a behaviour can hardly be inferred from the study of the NN -forces in free space, being truly emergent properties of the finite, quantum many-body nuclear system.

Collective surface vibrations and independent particle motion are examples of what are called elementary modes of excitation in finite many-body physics, and collective variables in soft-matter physics.

1.2 The particle-vibration coupling

The oscillation of the nucleus under the influence of the surface tension implies that the potential $U(r, R)$ in which nucleons move independently of each other change with time. For low-energy collective vibrations this change is slow as compared with single-particle motion. Within this scenario the nuclear radius can be written as

$$R = R_0 \left(1 + \sum_{\lambda\mu} \alpha_{\lambda\mu} Y_{\lambda\mu}^*(\hat{r}) \right) \quad (1.2.1)$$

Assuming small amplitude motion,

$$U(r, R) = U(r, R_0) + \delta U(r), \quad (1.2.2)$$

where

$$\delta U = \kappa \hat{\alpha} \hat{F} = \Lambda_\alpha \left(\Gamma_{\lambda\mu}^\dagger + (-1)^\mu \Gamma_{\lambda-\mu} \right) \hat{F}, \quad (1.2.3)$$

with

$$\Lambda_\alpha = \kappa \sqrt{\frac{\hbar\omega_\lambda}{2C_\lambda}}, \quad (1.2.4)$$

is the particle-vibration coupling (PVC) (Fig. 1.2.1), product of the dynamic deformation

$$\beta_\lambda = \sqrt{2\lambda + 1} \sqrt{\frac{\hbar\omega_\lambda}{2C_\lambda}}, \quad (1.2.5)$$

and of the strength κ , while

$$\hat{F} = \sum_{\nu_1 \nu_2} \langle \nu_1 | F | \nu_2 \rangle a_{\nu_1}^\dagger a_{\nu_2}, \quad (1.2.6)$$

is a single-particle field with dimensionless form factor,

$$F = -\frac{R_0}{\kappa} \frac{\partial U}{\partial r} Y_{\lambda\mu}^*(\hat{r}). \quad (1.2.7)$$

An estimate of κ is provided below (Eq. 1.2.13). The coupling between surface oscillations and single-particle motion reflects, in the nuclear case, the fact that collective vibrations (quasi-bosons) are composites of the nucleons (fermions) degrees of freedom⁹

Diagonalizing δU making use of the graphical (Feynman) rules of nuclear field theory (NFT) to be discussed in following Chapter, one obtains structure results which can be used in the calculation of absolute transition probabilities and differential reaction cross sections, quantities which can be compared with experimental findings.

In fact, within the framework of NFT, single-particles are to be calculated as the Hartree–Fock solution of the NN –interaction $v(|\mathbf{r} - \mathbf{r}'|)$ (Fig. 1.2.2) – e.g. a regularized NN -bare interaction in terms of renormalization group methods or alternative techniques (v_{low-k}), taking eventually also $3N$ terms into account¹⁰ – leading, in particular to

$$U(r) = \int d\mathbf{r}' \rho(r') v(|\mathbf{r} - \mathbf{r}'|) \quad (1.2.8)$$

that is, the Hartree field¹¹ expressing the selfconsistency between density ρ and potential U (Fig. 1.2.2 (b) (1) and (3)), while vibrations are to be calculated in the

⁹The associated overcompleteness does not imply particular worries as the elimination of the spurious degrees of freedom can be carried out in a systematic fashion (see Sect. 2.7, in particular 2.7.2 and 2.7.3).

¹⁰?

¹¹To this potential one has to add the Fock potential resulting from the fact that nucleons are fermions. This exchange potential (Fig. 1.2.2 (b) (2 and 4)) is essential in the determination of single-particle energies and wavefunctions. Among other things, it takes care of eliminating the nucleon self interaction from the Hartree field.

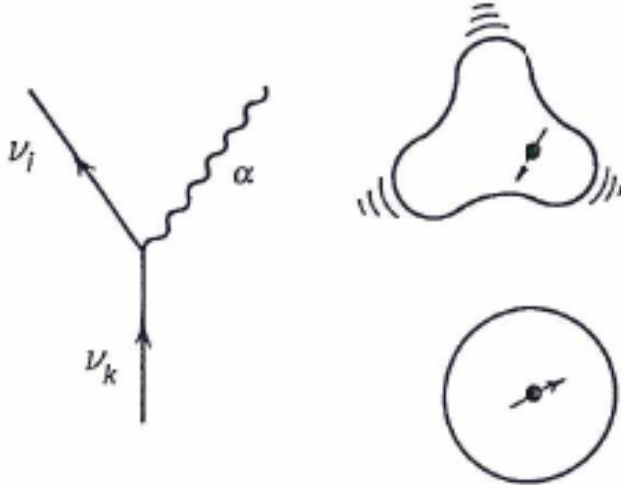


Figure 1.2.1: Graphical representation of process by which a fermion, bouncing inelastically off the surface, sets it into vibration. Particles are represented by an arrowed line pointing upwards which is also the direction of time, while the vibration is represented by a wavy line. In the cartoon to the right, the black dot represents a nucleon moving in a spherical mean field of which it excites, through the PVC vertex, an octupole vibration after bouncing inelastically off the surface.

Random Phase Approximation (RPA) making use of the same interaction¹² (Fig. 1.2.3), extending the selfconsistency to fluctuations $\delta\rho$ of the density and δU of the mean field, that is (see (1.2.2)),

$$\delta U(r) = \int d\mathbf{r}' \delta\rho(r') v(|\mathbf{r} - \mathbf{r}'|). \quad (1.2.9)$$

Making use of the solution to this relation one obtains the transition density $\delta\rho$. The matrix elements $\langle n_\lambda = 1, \nu_i | \delta\rho | \nu_k \rangle$ provide the particle-vibration coupling matrix elements to work out the variety of coupling processes between single-particle and collective motion (Fig. 1.2.1). That is, the matrix element of the PVC Hamiltonian H_c . However, the role of the NN -interaction v is not exhausted neither by H_{HF} nor by $H_{RPA} + H_c$. Diagonalizing

$$H = H_{HF} + H_{RPA} + H_c + v, \quad (1.2.10)$$

by applying, in the basis of single-particle and collective modes, that is solutions of H_{HF} and of H_{RPA} respectively, the graphical NFT rules (see next chapter) one obtains an exact solution of the total Hamiltonian, to order $1/\Omega$ of the Feynman

¹²Bohm and Pines (1951, 1953). The sum of the so called bubble (ring) diagrams (see Fig. 1.2.3) are taken into account to infinite order in RPA. This is the reason why bubble contributions in the diagonalization of Eq. (1.2.10) are not allowed in NFT, being already contained in the basis states (see next chapter, Sect. 2.7).

diagrams calculated. The quantity Ω is the effective degeneracy in which the nucleonic excitations are allowed to correlate through v to give rise to the collective modes, $1/\Omega$ being the small parameter of the NFT diagrams¹³ (see Sect. 2.7.2, see also 7.6.2). Concerning the rules of NFT (Sect. 2.7), they codify the way in which H_c (three-point vertices) and v (four-point vertices) are to be treated to all orders of perturbation theory. Also which processes (diagrams) are not allowed because they will imply overcounting of correlations already included in the basis states¹⁴.

Before proceeding let us make a simple estimate of the coupling strength κ , making use of a schematic separable interaction

$$v = \kappa \hat{F} \hat{F}^\dagger \quad (1.2.11)$$

and of an expansion of the nuclear density $\rho(r, R)$ similar to (1.2.2), that is,

$$\delta\rho(\mathbf{r}) = R_0 \frac{\partial\rho(r)}{\partial r} Y_{\lambda\mu}^*(\hat{r}). \quad (1.2.12)$$

With the help of the dynamical selfconsistent relation (1.2.9) on obtains¹⁵,

$$\kappa = \int r^2 dr R_0 \frac{\partial\rho(r)}{\partial r} R_0 \frac{\partial U(r)}{\partial r}. \quad (1.2.13)$$

For attractive fields, both U and κ are negative.

Because of quantal zero point fluctuations, a nucleon propagating in the nuclear medium moves through a cloud of bosonic virtual excitations to which it couples becoming dressed and acquiring effective mass, charge, etc. (Fig. 1.2.4; see also App. 5.A and 5.H). Vice versa, vibrational modes can become renormalized through the coupling to dressed nucleons which, in intermediate virtual states, can exchange the vibrations which produce their clothing, with the second fermion (hole state). Such a process leads to a renormalization of the PVC vertex¹⁶ (Fig.

¹³ According to renormalized NFT v is the NN -interaction which eventually combined with a k -mass, is used to calculate the bare single-particle states (HF-approximation), collective vibrations (RPA) and particle-vibration coupling vertices so that once the corresponding renormalization (dressing) diagrams (including also four-point vertices, i.e. v) to the order of $1/\Omega$ required (eventually infinite order if needed), reproduce the experimental findings. It is of notice that if one is interested in the collective vibrations, only to dress the single-particle degrees of freedom, one can take them from experiment (empirical renormalization). In other words, determine the Λ -values by making use of the experimental dynamical deformation parameter $\beta_\lambda = \sqrt{\frac{\hbar\omega_\lambda}{2C_\lambda}} \frac{1}{\sqrt{2t+1}}$ and energies $\hbar\omega_\lambda$ (Broglia et al. (2016)), in conjunction to the expression of the RPA amplitudes X and Y and dispersion relation collected in caption to Fig. 1.2.3.

¹⁴ A simple, although not directly related example is provided by Eq. (2A-31) of Bohr and Mottelson (1969) i.e. $G = \frac{1}{4} \sum_{v_1 v_2 v_3 v_4} \langle v_3 v_4 | G | v_1 v_2 \rangle_a a^\dagger(v_4) a^\dagger(v_3) a(v_1) a(v_2) = \frac{1}{2} \sum_{v_1 v_2 v_3 v_4} \langle v_3 v_4 | G | v_1 v_2 \rangle a^\dagger(v_4) a^\dagger(v_3) a(v_1) a(v_2)$ where $\langle \rangle_a$ is the antisymmetric matrix element.

¹⁵ Bohr and Mottelson (1975).

¹⁶ Bertsch et al. (1983); Barranco et al. (2004) and refs. therein. It is to be noted that in the case in which the renormalized vibrational modes, i.e. the initial and final wavy lines in Fig. 1.2.5 have angular momentum and parity $\lambda^\pi = 0^+$, and one uses a model in which there is symmetry between the particle and the hole subspaces, the four diagrams sum to zero, because of particle (gauge) conservation.

1.2.5), as well as of the bare NN -interaction, in particular 1S_0 component (bare pairing interaction)¹⁷.

The analytic procedures equivalent to the diagrammatic ones to obtain the HF (Fig. 1.2.2) and RPA (Fig. 1.2.3) solutions associated with the bare NN -interaction v is provided by the relations (1.1.16) and (1.1.15) respectively, replacing the corresponding Hamiltonians by $(T + v)$, where T is the kinetic energy operator. The phonon operator associated with surface vibrations is defined as,

$$\Gamma_\alpha^\dagger = \sum_{ki} X_{ki}^\alpha \Gamma_{ki}^\dagger + Y_{ki}^\alpha \Gamma_{ki}, \quad (1.2.14)$$

the normalization condition being,

$$[\Gamma_\alpha, \Gamma_\alpha^\dagger] = \sum_{ki} (X_{ki}^{\alpha 2} - Y_{ki}^{\alpha 2}) = 1. \quad (1.2.15)$$

The operator $\Gamma_{ki}^\dagger = a_k^\dagger a_i (\epsilon_k > \epsilon_F, \epsilon_i \leq \epsilon_F)$ creates a particle-hole excitation acting on the HF vacuum state $|0\rangle_F$. It is assumed that

$$[\Gamma_{ki}, \Gamma_{k'i'}^\dagger] = \delta(k, k')\delta(i, i'). \quad (1.2.16)$$

Within this context, RPA is a harmonic, quasi-boson approximation.

From being antithetic views of the nuclear structure, a proper analysis of the experimental data testifies to the fact that the collective and the independent particle pictures of the nuclear structure require and support each other¹⁸. To obtain a quantitative description of nucleon motion and nuclear phonons (vibrations), one needs a proper description of the k - and ω -dependent “dielectric” function of the nuclear medium, in a similar way in which a proper description of the reaction processes used as probes of the nuclear structure requires the use of the optical potential (continuum “dielectric” function).

The NFT solutions of (1.2.10) provide all the elements to calculate the structure properties of nuclei, and also the optical potential needed to describe nucleon-nucleus as well as nucleus-nucleus elastic scattering and reaction processes¹⁹. Furthermore, the NFT solutions of (1.2.10) show that both single-particle (fermionic) and collective (bosonic) elementary modes of excitation emerge from the same properties of the NN -interaction. For example, a bunching of levels of the same or opposite parity just below and above the Fermi energy, imply low-lying quadrupole (e.g. $^{50}_{50}\text{Sn}_N$ -isotopes), dipole ($^{11}_3\text{Li}_8$) or octupole ($^{208}_{82}\text{Pb}_{126}$) collective vibrational modes. And, as a bonus, one has the building blocks to construct the nuclear spectrum, and bring quantitative simplicity into the experimental findings. Within this scenario, the NFT solutions of (1.2.10) also indicate the minimum set of experimental probes needed to have a “complete” picture of the nuclear structure associated with a given energy region. This is a consequence of the central role played

¹⁷See e.g. Brink and Broglia (2005) Ch. 10 and references therein.

¹⁸Bohr and Mottelson (1975).

¹⁹However, in the present monograph this subject is not developed in any detail.

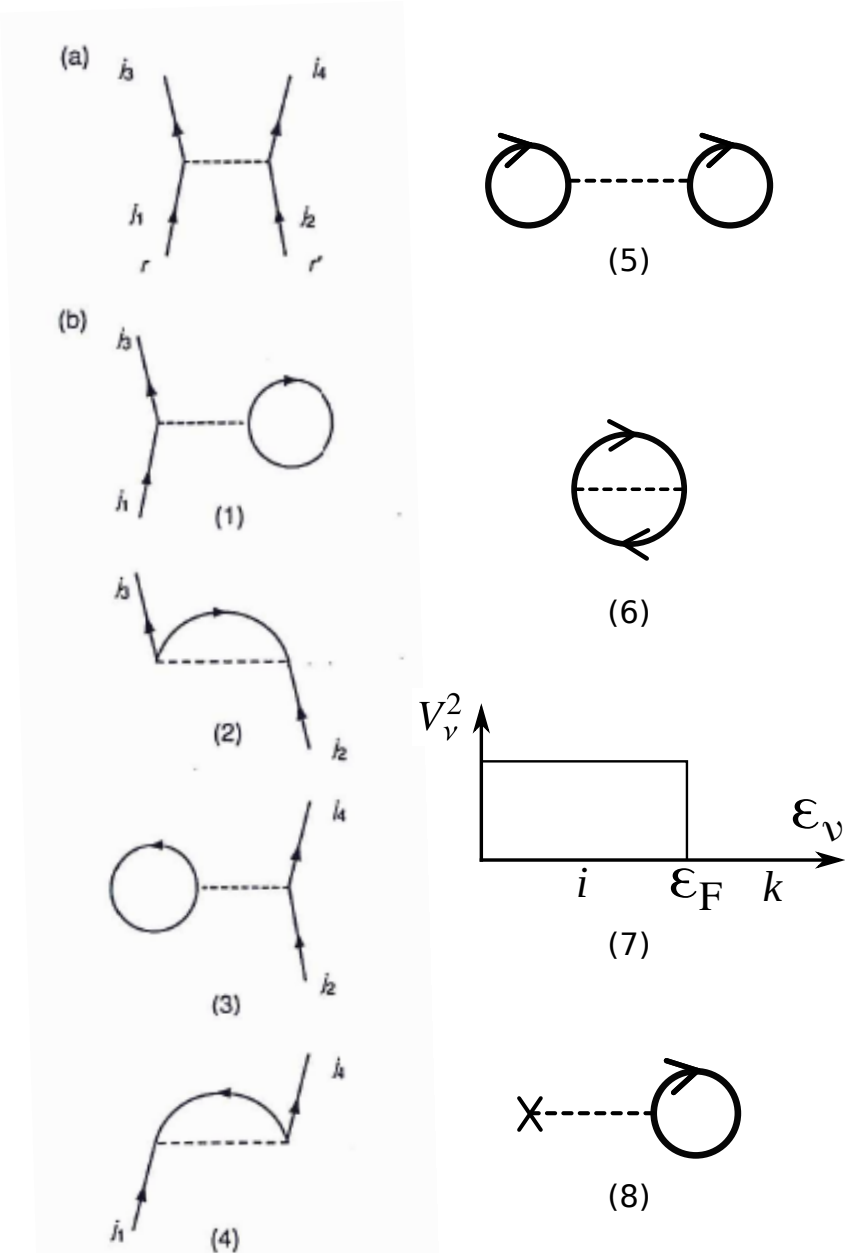


Figure 1.2.2: **(a)** Scattering of two nucleons through the NN -interaction; **(b)** (1) and (3): Contributions to the (direct) Hartree potential; (2) and (4): contributions to the (exchange) Fock potential. In (5) and (6) the ground state correlations associated with the Hartree- and the Fock-terms are displayed. (7) States $|i\rangle$ ($\epsilon_i \leq \epsilon_F$) are occupied with probability $V_i^2 = 1$. States $|k\rangle$ ($\epsilon_k > \epsilon_F$) are empty $V_k^2 = 1 - U_k^2$. (8) Nuclear density, the density operator being represented by a cross followed by a dashed horizontal line. (After Brink and Broglia (2005)).

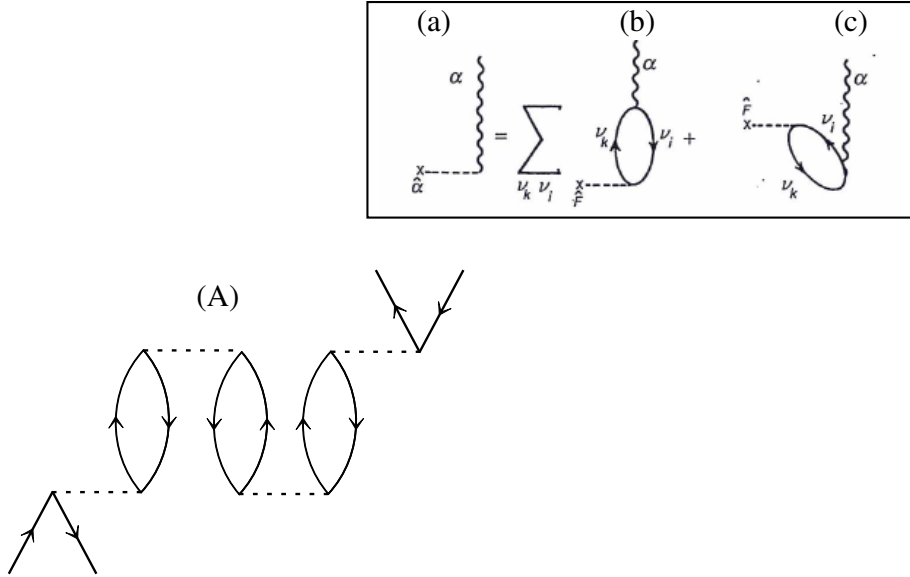


Figure 1.2.3: (A) typical Feynman diagram diagonalizing the NN -interaction $v(|\mathbf{r} - \mathbf{r}'|)$ (horizontal dashed line) in a particle-hole basis provided by the Hartree-Fock solution of v , in the harmonic approximation (RPA). Bubbles going forward in time (inset (b); leading to the amplitudes $X_{ki}^\alpha = \frac{\Lambda_\alpha \langle \tilde{i}|F|k\rangle}{(\epsilon_k - \epsilon_i) - \hbar\omega_\alpha}$) are associated with configuration mixing of particle-hole states, the state $|\tilde{i}\rangle = \tau|i\rangle$ where τ is the time reversal operator. It is of notice that $\epsilon_k > \epsilon_F$ and $\epsilon_i \lesssim \epsilon_F$, and $\epsilon_j = \epsilon_{\bar{j}}$ (Kramers degeneracy). Bubbles going backwards in time (inset (c), leading to the amplitudes $Y_{ki}^\alpha = -\frac{\Lambda_\alpha \langle \tilde{i}|F|k\rangle}{(\epsilon_k - \epsilon_i) + \hbar\omega_\alpha}$) are associated with zero point fluctuations (ZPF) of the ground state (term $(1/2)\hbar\omega$ for each degree of freedom in Eq. (1.1.12)). The self consistent solutions of A, eigenstates of the dispersion relation $\sum_{ki} \frac{2(\epsilon_k - \epsilon_i)(\langle \tilde{i}|F|k\rangle)^2}{(\epsilon_k - \epsilon_i)^2 - (\hbar\omega_\alpha)^2} = 1/\kappa_\alpha$ are represented by a wavy line (inset), that is a collective mode which can be viewed as a correlated particle (arrowed line going upward)- hole (arrowed line going downward) excitation. The quantity $\Lambda_\alpha = \kappa_\alpha \sqrt{\frac{\hbar\omega_\alpha}{2C_\alpha}}$ is the particle-vibration coupling vertex (normalization constant of the RPA amplitudes $\sum_{ki} (X_{ki}^\alpha)^2 - (Y_{ki}^\alpha)^2 = 1$). (Bohm and Pines (1951, 1953), see also Brink and Broglia (2005) Sect. 8.3).

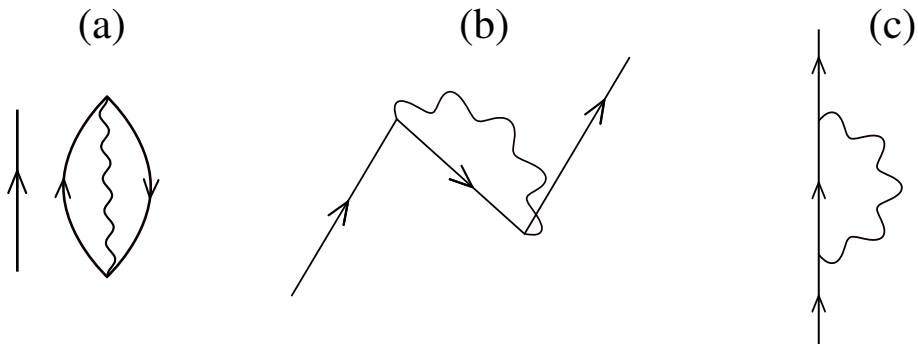


Figure 1.2.4: (a) a nucleon (single arrowed line pointing upward) moving in presence of the zero point fluctuation of the nuclear ground state associated with a collective surface vibration; (b) Pauli principle leads to a dressing process of the nucleon (so called correlation (CO) diagram); (c) time ordering gives rise to the second possible lowest order clothing process (so called polarization (PO) diagram) (time assumed to run upwards). The above are phenomena closely related with the Lamb shift of Quantum Electrodynamics (see e.g. Weinberg (1996) Sect. 14.3).

by the quantal many-body renormalization process which interweave the variety of elementary modes of excitation. Renormalization processes which acts on par on the radial dependence of the wavefunctions (formfactors) and on the single-particle content of the orbitals involved in the reaction process under discussion (see e.g. Sect. 7.2). In other words, structure ad reactions are to be treated on equal footing²⁰.

The development of experimental techniques and associated hardware has allowed for the identification of a rich variety of elementary modes of excitation aside from collective surface vibrations and of independent particle motion: quadrupole and octupole rotational bands, giant resonance of varied multipolarity and isospin, as well as pairing vibrations and rotation, together with giant pairing vibrations of transfer quantum number $\beta \pm 2$. Modes which can be specifically excited in inelastic and Coulomb excitation processes (see App. 2.A), and one- and two-particle transfer reactions (Ch. 5 and 6).

²⁰Within this context, and referring to one-particle transfer reactions for concreteness, the prescription of using the ratio of the absolute experimental cross section of and the theoretical one – calculated in the Distorted Wave Born Approximation (DWBA) making use of Saxon-Woods single-particle wavefunctions as formfactors– to extract the single-particle content of the orbital under study (see e.g. Schiffer et al. (2012)), may not be appropriate.

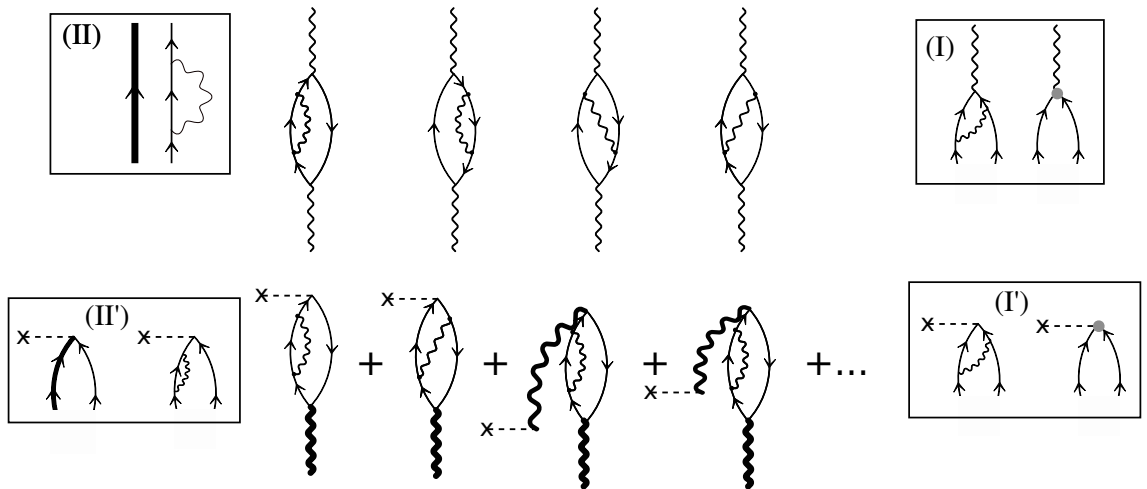


Figure 1.2.5: (Upper part) Examples of renormalization processes dressing a surface collective vibrational state. (Lower part) Intervening with an external electromagnetic field ($E\lambda$: cross followed by dashed horizontal line; bold wavy lines, renormalized vibration of multipolarity λ) the $B(E\lambda)$ transition strength can be measured. In insets (I) and (I'), the hatched circle in the diagram to the right stands for the renormalized PVC strength resulting from the processes described by the corresponding diagrams to the left (vertex corrections). In (II') the bold face arrowed curve represents (left diagram) the motion of a nucleon of effective mass m^* in a potential $(m/m^*)U(r)$, generated by the self-energy process shown to the right (see also (II) right diagram), $U(r)$ being the potential describing the motion of nucleons (drawn as a thin arrowed line) of bare mass m_k (inset (II), right diagrams. (Brink and Broglia (2005) App. B).

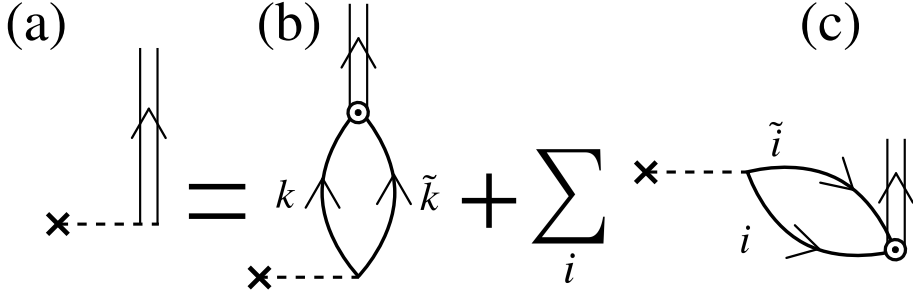


Figure 1.3.1: Graphical representation of the RPA dispersion relation describing the pair addition pairing vibrational mode, represented by a double arrowed line. Making use of the unitary transformation (1.3.6), a cross followed by a dashed horizontal line stands for: (a) the collective operator Γ_α^\dagger , (b) the operator Γ_k^\dagger creating a pair of nucleons moving in time reversal states (k, \tilde{k}) above the Fermi energy ($\epsilon_k > \epsilon_F$); (c) The operator Γ_i^\dagger filling a pair of time reversal holes associated with ground state correlations ($\epsilon_i \leq \epsilon_F$).

1.3 Pairing vibrations

Let us introduce this new type of elementary mode of excitation by making a parallel with quadrupole surface vibrations within the framework of RPA, namely

$$[(H_{sp} + H_i), \Gamma_{k' i'}^\dagger] = \hbar\omega_\alpha \Gamma_{k' i'}^\dagger, \quad (1.3.1)$$

where for simplicity we use, instead of v , an quadrupole-quadrupole separable interaction ($i = QQ$) defined as²¹

$$H_{QQ} = -\kappa Q^\dagger Q \quad (1.3.2)$$

with

$$Q^\dagger = \sum_{ki} \langle k | r^2 Y_{2\mu} | i \rangle a_k^\dagger a_i, \quad (1.3.3)$$

while H_{sp} and Γ_α^\dagger are defined in (1.1.13) and (1.2.14) supplemented by (1.2.15).

In connection with the pairing energy mentioned above (odd-even staggering), it is a consequence of correlation of pairs of like nucleons moving in pairs of time reversed states (v, \tilde{v}). A similar phenomenon to that found in metals at low temperatures and giving rise to superconductivity. The pairing interaction ($i = p$) can be written, within the approximation (1.3.2) used in the case of the quadrupole-quadrupole force, as

$$H_P = -GP^\dagger P, \quad (1.3.4)$$

²¹It is of notice that in this case, and at variance with (1.2.11)–(1.2.13), the fact that the force is attractive is explicitly expressed through the minus sign, assuming $\kappa > 0$. This is done for didactical purposes, to connect with the standard notation for the pairing interaction given in Eq. (1.3.4) below.

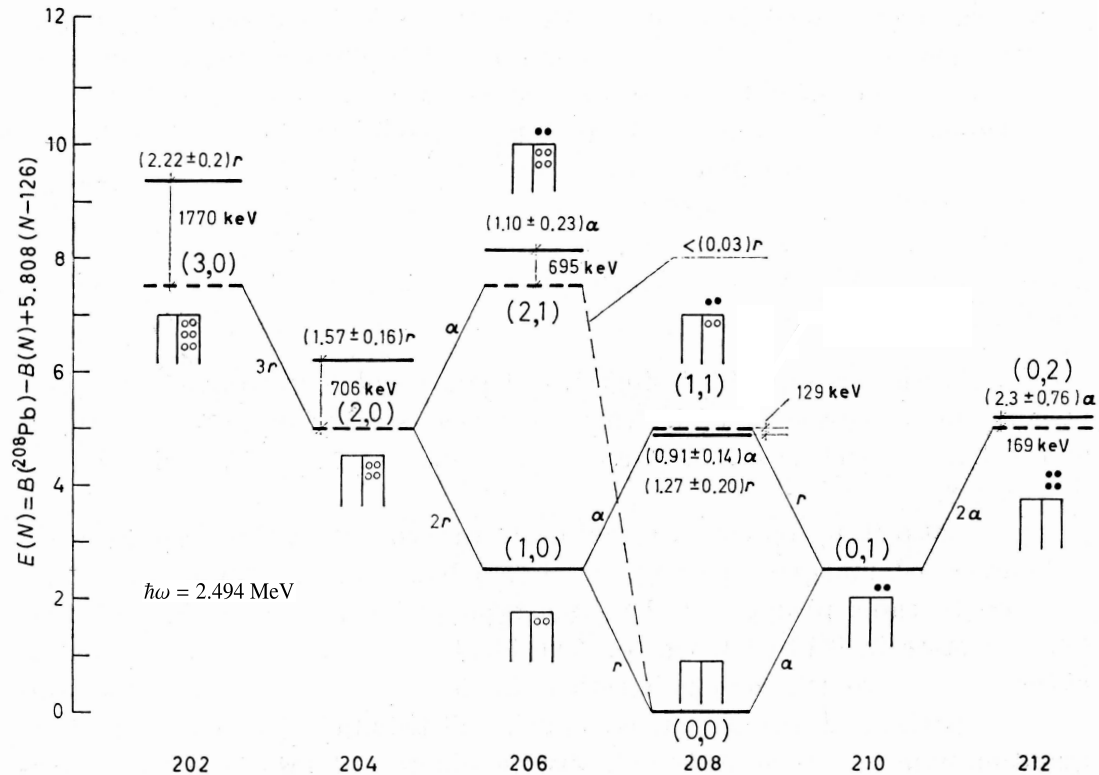


Figure 1.3.2: The many-phonon pairing vibrational spectrum around the “vacuum” ^{208}Pb . The energies predicted by the pairing vibrational model (harmonic approximation) are displayed as dashed horizontal lines. The harmonic quantum numbers (n_r, n_a) are indicated for each level. A schematic representation of the many-particle many-hole structure of the state is also given. The transitions predicted by the model (harmonic approximation) are indicated in units of r and α (see equation (1.3.9) and subsequent text). The corresponding experimental numbers are also given together with their errors, above each level. The dashed line between the states (0,0) and (2,1) indicates that the $^{208}\text{Pb}(p, t)^{206}\text{Pb}$ reaction to the three-phonon state in ^{206}Pb was carried out and an upper limit of $0.03r$ for the corresponding cross-section was determined (see Flynn et al. (1972a) Broglia et al. (1973), also Lanford and McGrory (1973)).

where

$$P^\dagger = \sum_{\nu>0} a_\nu^\dagger a_{\bar{\nu}}^\dagger, \quad (1.3.5)$$

and G is a pairing coupling constant (attractive $G > 0$). Consequently, in this case the concept of independent particle field \hat{Q} (see also (1.2.6) and (1.2.7)) associated with particle-hole (ph) excitations and carrying transfer quantum number $\beta = 0$ has to be generalized to include fields describing independent pair motion of different multipolarity and (normal) parity, in particular 0^+ , in which case $\alpha \equiv (\beta = +2, J^\pi = 0^+)$

$$\Gamma_\alpha^\dagger = \sum_k X_{kk}^\alpha \Gamma_k^\dagger + \sum_i Y_{ii}^\alpha \Gamma_i^\dagger \quad (1.3.6)$$

with

$$\Gamma_k^\dagger = a_k^\dagger a_{\bar{k}}^\dagger (\epsilon_k > \epsilon_F), \quad \Gamma_i^\dagger = a_i^\dagger a_{\bar{i}}^\dagger (\epsilon_i \leq \epsilon_F), \quad (1.3.7)$$

and

$$\sum_k X_{kk}^{\alpha 2} - \sum_i Y_{ii}^{\alpha 2} = 1, \quad (1.3.8)$$

for the pair addition ($(pp), \beta = +2$) mode, and a similar expression for the pair removal ($(hh), \beta = -2$) mode. In Fig. 1.3.1 the NFT graphical representation of the RPA equations for the pair addition mode is given. The state $\Gamma_\alpha^\dagger(\beta = +2)|\tilde{0}\rangle$, where $|\tilde{0}\rangle$ is the correlated ground state of a closed shell nucleus, can be viewed as the nuclear embodiment of a Cooper pair found at the basis of the microscopic theory of superconductivity. While surface vibrations are associated with the normal ($\beta = 0$) nuclear density, pairing vibrations are connected with the so called abnormal ($\beta = \pm 2$) nuclear density (density of Cooper pairs), both static and dynamic.

Similar to the quadrupole and octupole vibrational bands built out of n_α phonons of quantum numbers $\alpha \equiv (\beta = 0, \lambda^\pi = 2^+, 3^-)$ schematically shown in Fig. 1.1.3 and experimentally observed in inelastic and Coulomb excitation and associated γ -decay processes, pairing vibrational bands build of n_α phonons of quantum numbers $\alpha \equiv (\beta = \pm 2, \lambda^\pi = 0^+, 2^+)$ have been identified around closed shells in terms of two-nucleon transfer reactions throughout the mass table. In Fig. 1.3.2, the monopole pairing vibrational band built around the vacuum state $|gs(^{208}\text{Pb})\rangle$ in terms of the pair addition and subtraction modes

$$|a\rangle = |n_a = 1\rangle = |gs(^{210}\text{Pb})\rangle, \quad \text{and} \quad |r\rangle = |n_r = 1\rangle = |gs(^{206}\text{Pb})\rangle, \quad (1.3.9)$$

is displayed. The indices $n_a (= 1, 2, \dots)$ and $n_r (= 1, 2, \dots)$ indicate the number of pair addition and/or of pair removal modes of which the states are made. The label a and r indicate in Fig. 1.3.2, the absolute transition probability, i.e. two-nucleon (Cooper pair) transfer cross section which connects the ground (“vacuum”) state $|gs(^{208}\text{Pb})\rangle$ with $|a\rangle$ and $|r\rangle$ respectively.

1.4 Spontaneously broken symmetry

Because empty space is homogeneous and isotropic, and to the degree of accuracy relevant in many-body problems, also invariant under time-reversal, the nuclear Hamiltonian is translational, rotational and time-reversal invariant. According to quantum mechanics, the corresponding wavefunctions transform in an irreducible way under the corresponding groups of transformation. When the solution of the Hamiltonian does not have some of these symmetries, for example defines a privileged direction in space violating rotational invariance, one is confronted with the phenomenon of spontaneously broken symmetry. Strictly speaking, this can take place only for idealized systems that are infinitely large. But when one sees similar phenomena in atomic nuclei, although not so clear or regular, one recognizes that this system is after all a finite quantum many-body system (FQMBS)²².

1.4.1 Quadrupole deformations in 3D-space

A nuclear embodiment of the spontaneous symmetry breaking phenomenon is provided by a quadrupole deformed mean field. A situation one is confronted with, when the value of the lowest quadrupole frequency ω_2 of the RPA solution (1.1.15) tends to zero ($C_2 \rightarrow 0$, D_2 finite). A phenomenon resulting from the interplay of the interaction v (H_{QQ} in (1.3.2)), and of the nucleons outside closed shell, leading to tidal-like polarization of the spherical core.

Coordinate and linear momentum ((x, p_x) single-particle motion) as well as Euler angles and angular momentum ((φ, I_z) rotational in two-dimensional (2D)-space) are conjugate variables. Similarly, the gauge angle and the number of particles ((ϕ, N) rotation in gauge space), fulfill $[\phi, N] = i$. The operators $e^{-ip_x x}$, $e^{-i\varphi I_z}$ and $e^{-iN\phi}$ induce Galilean transformation and rotations in 2D- and in gauge space respectively, which although in abstract and not real space, is also two-dimensional.

Making again use, for didactical purposes, of H_{QQ} instead of v , and calling $|N\rangle$ the eventual mean field solution of the Hamiltonian $T + H_{QQ}$, one expects

$$\langle N | \hat{Q} | N \rangle = Q_0, \quad (1.4.1)$$

where, for simplicity, we assumed axial symmetry ($\lambda = 2, \mu = 0$). That is, the emergence of a static quadrupole deformation. Rewriting H_{QQ} in terms of $(\hat{Q}^\dagger - Q_0) + Q_0$ and its Hermitian conjugate, one obtains

$$H = H_{sp} + H_{QQ} = H_{MF} + H_{fluct}, \quad (1.4.2)$$

where

$$H_{MF} = H_{sp} - \kappa(\hat{Q}^\dagger + \hat{Q}), \quad (1.4.3)$$

is the mean field, and

$$H_{fluct} = -\kappa(\hat{Q}^\dagger - Q_0)(\hat{Q} - Q_0) \quad (1.4.4)$$

²²Anderson (1972, 1984).

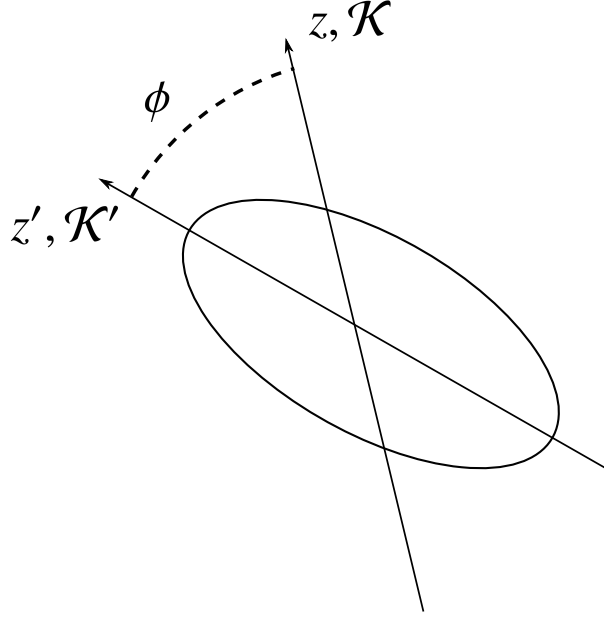


Figure 1.4.1: Schematic representation of deformation in 3D- (gauge-) space, where the laboratory (\mathcal{K}) and the intrinsic (\mathcal{K}' , body fixed) frames of reference making a relative relative angle ((ω , Euler angles); (ϕ , gauge angle)) are indicated (see Eqs. (1.4.6) and (1.4.57)).

the residual interaction inducing fluctuations around Q_0 . Assuming $Q_0 \gg (\hat{Q}^\dagger - Q_0)(\hat{Q} - Q_0)$, we concentrate on H_{MF} . The original realization of it is known as the Nilsson Hamiltonian (Nilsson (1955)). It describes the motion of nucleons in a single-particle potential of radius $R_0(1 + \beta_2 Y_{20}(\hat{r}))$, with β_2 proportional to the intrinsic quadrupole moment²³ Q_0 ($\beta_2 \approx Q_0/(ZR_0^2)$). The reflection invariance and axial symmetry of the Nilsson Hamiltonian implies that parity π and projection Ω of the total angular momentum along the symmetry axis are constants of motion for the one-particle Nilsson states. These states, are two-fold degenerate, since two orbits that differ only in the sign of Ω represent the same motion, apart from the clockwise and anticlockwise sense of revolution around the symmetry axis. One can thus write the Nilsson creation operators in terms of a linear combination of creation operators carrying good total angular momentum j ,

$$\gamma_{a\Omega}^\dagger = \sum_j A_j^a a_{aj\Omega}^\dagger, \quad (1.4.5)$$

where the label a stands for all the quantum numbers aside from Ω , which specify the orbital.

Expressed in the intrinsic, body-fixed, system of coordinates \mathcal{K}' (Fig. 1.4.1) where the 3 (z') axis lies along the symmetry axis and the 1 and 2 (x', y') axis lie

²³Mottelson and Nilsson (1959), where use has been made of $\beta_2 \approx 0.95\delta$ Bohr and Mottelson (1975) p. 47 and Eq. (4-191) (see also Fig. 1.4.2).

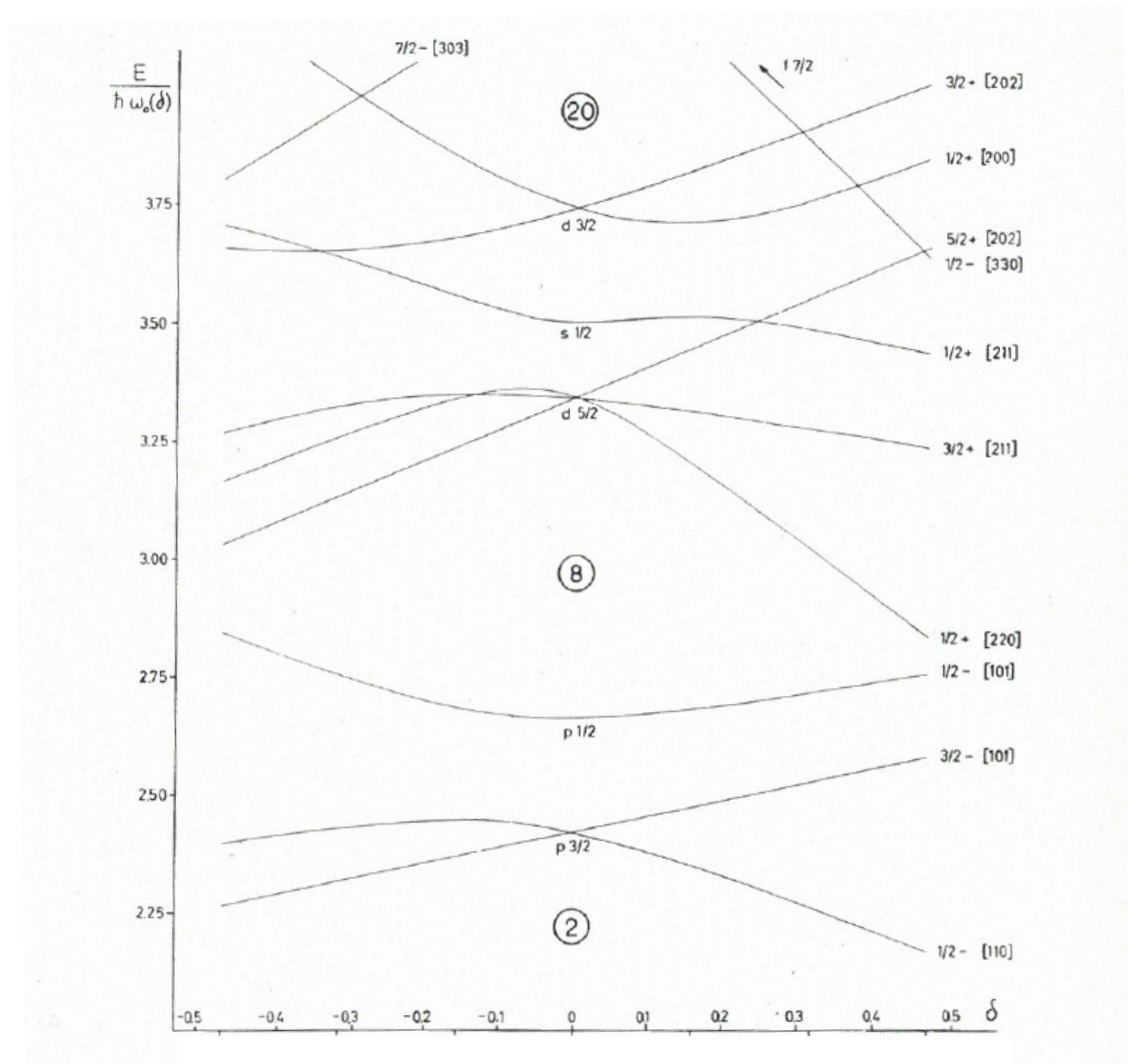
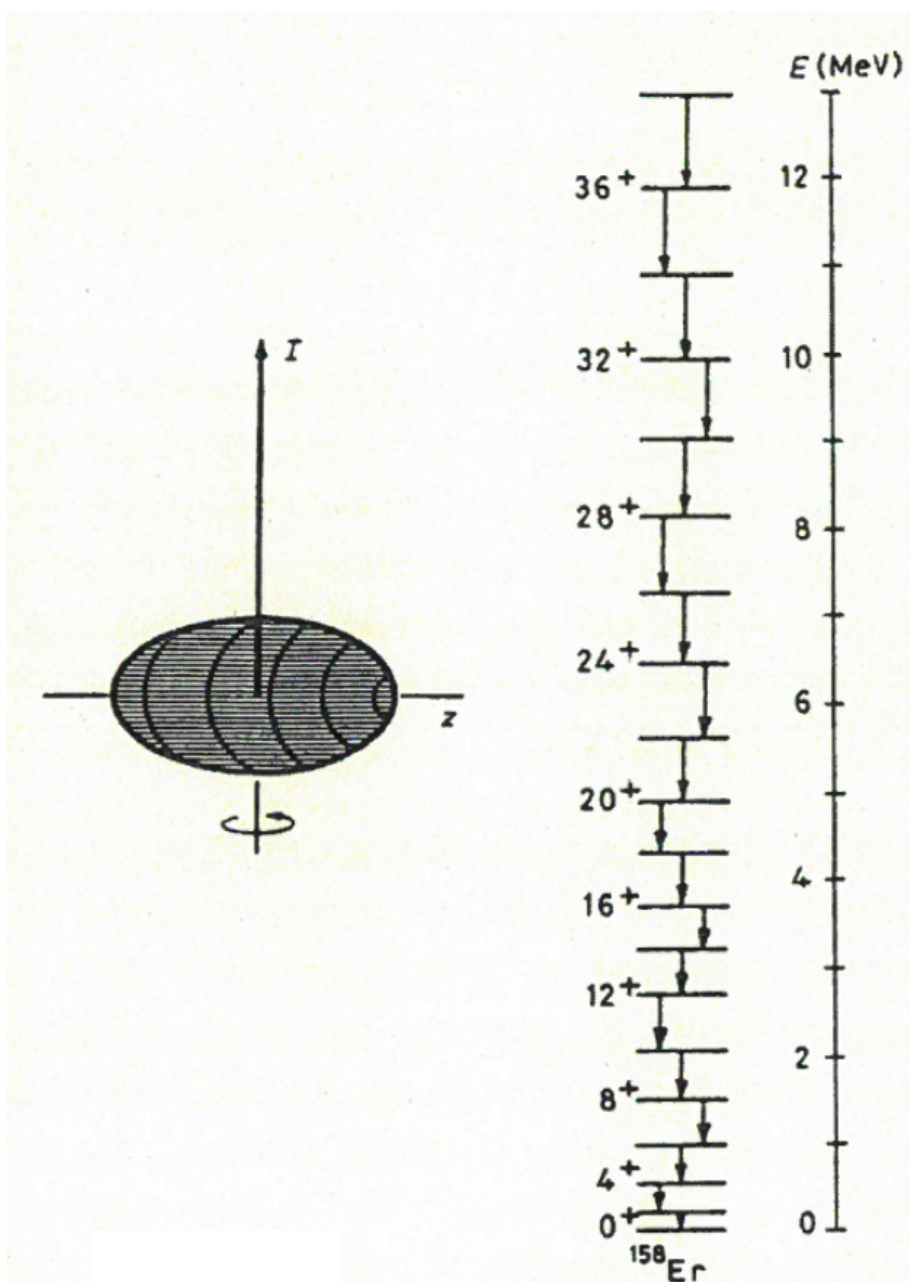


Figure 1.4.2: Single-particle levels in the regions $8 < Z < 20$ and $8 < N < 20$.

Figure 1.4.3: Ground state rotational band of ^{158}Er .

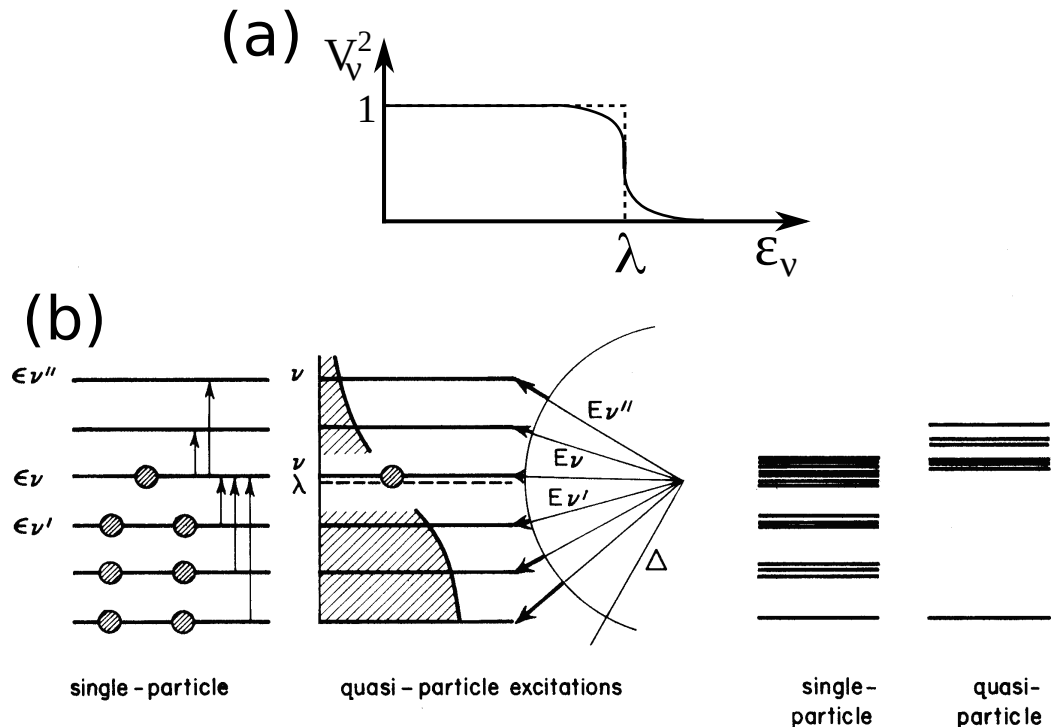


Figure 1.4.4: (a) Independent (dashed line) and BCS occupation numbers; (b) ground state and excited states in the extreme single-particle model and in the pairing-correlated, superfluid model in the case of a system with an odd number of particles. In the first case, the energy of the ground state of the odd system differs from that of the even with one particle fewer by the energy difference $\epsilon_{\nu} - \epsilon_{\nu'}$ while in the second case by the energy $E_{\nu} = \sqrt{(\epsilon_{\nu} - \lambda)^2 + \Delta^2} \approx \Delta$, associated with the fact the odd particle has no partner. Excited states can be obtained in the independent particle case, where it is assumed that levels are two-fold degenerate (Kramers degeneracy) by promoting the odd particle to states above the level ϵ_{ν} , or one particle to states above ν' (arrows). To the left only a selected number of these excitations are shown. In the superfluid case excited states can be obtained by breaking of pairs in any orbit. The associated quasiparticle energy is drawn also here by an arrow of which the thin part indicates the contribution of the pairing gap and the thick part indicates the kinetic energy contribution, i.e. the contribution arising from the single-particle motion. Note the very different density of levels emerging from these two pictures, which are shown at the far right of the figure.

in a plane perpendicular to it, namely

$$\gamma'^{\dagger}_{a\Omega} = \sum_j A_j^a \sum_{\Omega'} \mathcal{D}_{\Omega\Omega'}^2(\omega) a_{a,j\Omega'}^{\dagger}, \quad (1.4.6)$$

one can write the Nilsson state as

$$|N(\omega)\rangle_{\mathcal{K}'} = \prod_{a\Omega>0} \gamma'^{\dagger}_{a\Omega} \gamma'^{\dagger}_{a\Omega} |0\rangle_F, \quad (1.4.7)$$

where ω represent the Euler angles, $|0\rangle_F$ is the particle vacuum, and $|a\tilde{\Omega}\rangle = \gamma'^{\dagger}_{a\tilde{\Omega}} |0\rangle_F$ is the state time-reversed to $|a\Omega\rangle$. For well deformed nuclei, a conventional description of the one-particle motion is based on the similarity of the nuclear potential to that of an anisotropic oscillator potential,

$$V = \frac{1}{2}M \left(\omega_3^2 x_3^2 + \omega_{\perp}^2 (x_1^2 + x_2^2) \right) = \frac{1}{2}M\omega_0 r^2 \left(1 - \frac{4}{3}\delta P_2(\cos\theta) \right), \quad (1.4.8)$$

with $\omega_3\omega_{\perp}^2 = \omega_0^3$. That is a volume which is independent of the deformation $\delta \approx 0.95\beta_2$. The corresponding single-particle states have energy

$$\epsilon(n_3 n_{\perp}) = (n_3 + \frac{1}{2})\hbar\omega_3 + (n_{\perp} + \frac{1}{2})\hbar\omega_{\perp}, \quad (1.4.9)$$

where n_3 and $n_{\perp} = n_1 + n_2$ are the number of quanta along and perpendicular to the symmetry axis. The degenerate states with the same value of n_{\perp} can be specified by the component Λ of the orbital angular momentum along the symmetry axis,

$$\Lambda = \pm n_{\perp}, \pm(n_{\perp} - 2), \dots, \pm 1 \text{ or } 0. \quad (1.4.10)$$

One can then label the Nilsson levels in terms of the asymptotic quantum numbers $\Omega[Nn_3\Lambda]$, where $N = n_3 + n_{\perp}$, is the total oscillator quantum number. The complete expression of the Nilsson potential includes, aside from the central term discussed above, a spin-orbit and a term proportional to the orbital angular momentum quantity squared, so as to make the shape of the oscillator to resemble more that of a Saxon-Woods potential. The resulting levels provide an overall account of the experimental findings, providing detailed evidence in terms of individual states of the interplay between the single-particle and the collective aspects of nuclear structure. An example of relevance for light nuclei (N and $Z < 20$) is given in²⁴ Fig. 1.4.2.

The Nilsson intrinsic state (1.4.7) does not have a definite angular momentum but is rather a superposition of such states,

$$|N(\omega)\rangle_{\mathcal{K}'} = \sum c_I |I\rangle. \quad (1.4.11)$$

Because there is no restoring force associated with different orientations of $|N(\omega)\rangle_{\mathcal{K}'}$, fluctuations in the Euler angle diverge in the right way to restore rotational invariance, leading to a rotational band whose members are

$$|IKM\rangle \sim \int d\omega \mathcal{D}_{MK}^I(\omega) |N(\omega)\rangle_{\mathcal{K}'}, \quad (1.4.12)$$

²⁴Mottelson and Nilsson (1959).

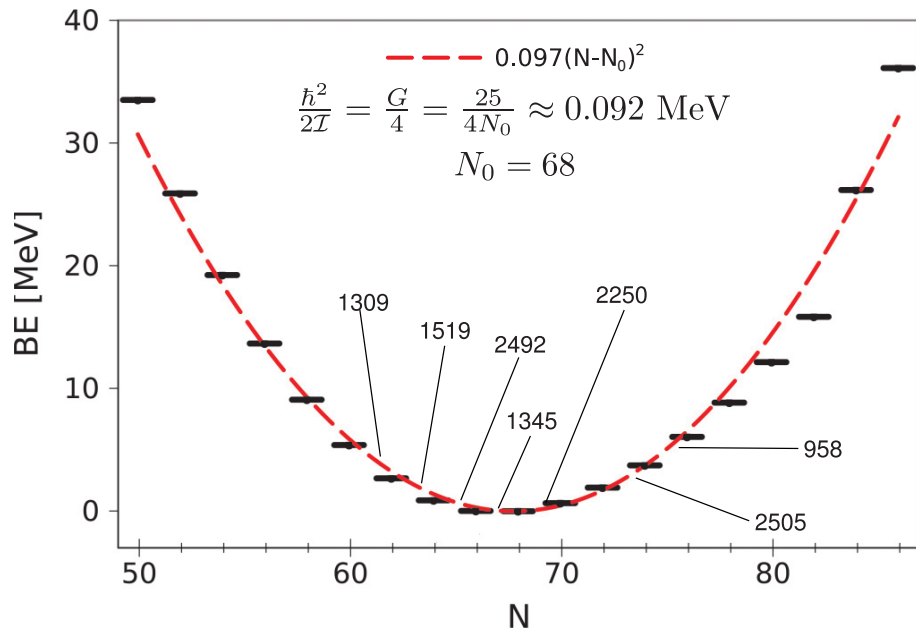


Figure 1.4.5: Pairing rotational band associated with the ground states of the Sn-isotopes. The lines represent the energies calculated according to the expression $BE = B(^{50+N}\text{Sn}_N) - 8.124N + 46.33$ (Brink and Broglia (2005)), subtracting the contribution of the single nucleon addition to the nuclear binding energy obtained by a linear fitting of the binding energies of the whole Sn chain. The estimate of $\hbar^2/2I$ was obtained using the single j -shell model (see, e.g., Brink and Broglia (2005), Appendix H). The numbers indicated with thin lines are the absolute value of the experimental $gs \rightarrow gs$ cross section (in units of μb).

with energy

$$E_I = \frac{\hbar^2}{2I} I(I+1). \quad (1.4.13)$$

The quantum numbers I, M, K are the total angular momentum I , and its third component M and K along the laboratory (z) and intrinsic (z') frame references respectively. Rotational bands have been observed up to rather high angular momenta in terms of individual transitions. In particular, up to $I = 60\hbar$ in the case of ^{152}Dy (Nolan and Twin (1988) and refs. therein). An example of rotational bands is given in Fig. 1.4.3.

1.4.2 Deformation in gauge space

Let us now turn to the pairing Hamiltonian. In the case in which $\hbar\omega(\beta = -2) = \hbar\omega(\beta = 2) = 0$, the system deforms, this time in gauge space. Calling $|BCS\rangle$ the mean field solution of the pairing Hamiltonian, leads to the finite expectation value

$$\alpha_0 = \langle BCS | P^\dagger | BCS \rangle, \quad (1.4.14)$$

of the pair creation operator P^\dagger , quantity which can be viewed as the order parameter of the new deformed phase of the system in gauge space. The total Hamiltonian can be written as

$$H = H_{MF} + H_{fluct}, \quad (1.4.15)$$

where

$$H_{MF} = H_{sp} - \Delta(P^\dagger + P) + \frac{\Delta^2}{G} \quad (1.4.16)$$

and

$$H_{fluct} = -G(P^\dagger - \alpha_0)(P - \alpha_0). \quad (1.4.17)$$

The quantity

$$\Delta = G\alpha_0, \quad (1.4.18)$$

is the so called pairing gap (Fig. 1.4.4), which measures the binding energy of Cooper pairs, the quantity α_0 being the number of Cooper pairs.

The mean field pairing Hamiltonian

$$H_{MF} = \sum_{\nu>0} (\epsilon_\nu - \lambda)(a_\nu^\dagger a_\nu + a_{\tilde{\nu}}^\dagger a_{\tilde{\nu}}) - \Delta \sum_{\nu>0} (\epsilon_\nu - \lambda)(a_\nu^\dagger a_{\tilde{\nu}}^\dagger + a_{\tilde{\nu}} a_\nu) + \frac{\Delta^2}{G} \quad (1.4.19)$$

is a bilinear expression in the creation and annihilation operator, ν labeling the quantum numbers of the single-particle orbitals where nucleons are allowed to correlate (e.g. (nlj, m)), while $\tilde{\nu}$ denotes the time reversal state which in this case is

degenerate with ν and has quantum numbers $(nlj, -m)$, $\nu > 0$ implying that one sums over $m > 0$. It is of notice that

$$\hat{N} = \sum_{\nu>0} (a_\nu^\dagger a_\nu + a_{\bar{\nu}}^\dagger a_{\bar{\nu}}), \quad (1.4.20)$$

is the number operator, and $\lambda\hat{N}$ in Eq. (1.4.19) acts as the Coriolis force in the body-fixed frame of reference in gauge space.

One can diagonalize H_{MF} by a rotation in the (a^\dagger, a) -space. This can be accomplished through the Bogoliubov-Valatin transformation

$$\alpha_\nu^\dagger = U_\nu a_\nu^\dagger - V_\nu a_{\bar{\nu}}, \quad (1.4.21)$$

The BCS solution does not change the energies ϵ_ν (measured in (1.4.19) from the Fermi energy λ) of the single-particle levels or associated wavefunctions $\varphi_\nu(\mathbf{r})$, but the occupation probabilities for levels around the Fermi energy within an energy range 2Δ ($2\Delta/\lambda \approx 2 \text{ MeV}/36 \text{ MeV} \approx 0.06$). The quasiparticle operator α_ν^\dagger creates a particle in the single-particle state ν with probability U_ν^2 , while it creates a hole (annihilates a particle) with probability V_ν^2 . To be able to create a particle, the state ν should be empty, while to annihilate a particle it has to be filled, so U_ν^2 and V_ν^2 are the probabilities that the state ν is empty and is occupied respectively. Within this context, the one quasiparticle states

$$|\nu\rangle = \alpha_\nu^\dagger |BCS\rangle \quad (1.4.22)$$

are orthonormal. In particular

$$\langle \nu | \nu \rangle = 1 = \langle BCS | \alpha_\nu \alpha_\nu^\dagger | BCS \rangle = \langle BCS | \{ \alpha_\nu, \alpha_\nu^\dagger \} | BCS \rangle = U_\nu^2 + V_\nu^2, \quad (1.4.23)$$

where the relations

$$\{a_\nu, a_{\nu'}^\dagger\} = \delta(\nu, \nu') \quad (1.4.24)$$

and

$$\{a_\nu, a_{\nu'}\} = \{a_\nu^\dagger, a_{\nu'}^\dagger\} = 0 \quad (1.4.25)$$

have been used. Note that the $|BCS\rangle$ state is the quasiparticle vacuum

$$\alpha_\nu |BCS\rangle = 0, \quad (1.4.26)$$

in a similar way in which $|0\rangle_F$ is the particle vacuum. Inverting the quasiparticle transformation (1.4.21) and its complex conjugate, i.e. expressing a_ν^\dagger and a_ν (and time reversals (tr)) in terms of α_ν^\dagger and α_ν (and tr) one can rewrite (1.4.19) in terms of quasiparticles.

Minimizing the energy $E_0 = \langle BCS | H | BCS \rangle$ in terms of²⁵ V_ν

$$\frac{\partial E_0}{\partial V_\nu} = 0 \quad (1.4.27)$$

²⁵For details see e.g. Ragnarsson and Nilsson (2005). See also Nathan and Nilsson (1965).

making use of the expression for the average number of particles

$$N_0 = \langle BCS | \hat{N} | BCS \rangle = 2 \sum_{\nu>0} V_\nu^2, \quad (1.4.28)$$

of the number of Cooper pairs²⁶

$$\alpha_0 = \langle BCS | P^\dagger | BCS \rangle = \sum_{\nu>0} U_\nu V_\nu \quad (1.4.29)$$

and of the pairing gap

$$\Delta = G \sum_{\nu>0} U_\nu V_\nu, \quad (1.4.30)$$

one obtains,

$$H_{MF} = H_{11} + U, \quad (1.4.31)$$

where

$$H_{11} = \sum_{\nu} E_\nu \alpha_\nu^\dagger \alpha_\nu, \quad (1.4.32)$$

and

$$U = 2 \sum_{\nu>0} (\epsilon_\nu - \lambda) V_\nu^2 - \frac{\Delta^2}{G}. \quad (1.4.33)$$

The quantity

$$E_\nu = \sqrt{(\epsilon_\nu - \lambda)^2 + \Delta^2} \quad (1.4.34)$$

is the quasiparticle energy, while the occupation (emptiness) probability amplitudes are

$$V_\nu = \frac{1}{\sqrt{2}} \left(1 - \frac{\epsilon_\nu - \lambda}{E_\nu} \right)^{1/2}, \quad (1.4.35)$$

$$U_\nu = \frac{1}{\sqrt{2}} \left(1 + \frac{\epsilon_\nu - \lambda}{E_\nu} \right)^{1/2}. \quad (1.4.36)$$

From the relations (1.4.28), (1.4.30) and (1.4.34) one obtains

$$N_0 = 2 \sum_{\nu>0} V_\nu^2, \quad (1.4.37)$$

²⁶Spontaneously broken invariance invariance in

and

$$\frac{1}{G} = \sum_{\nu>0} \frac{1}{2E_\nu}. \quad (1.4.38)$$

These equations allow one to calculate the parameters λ and Δ from the knowledge of G and ϵ_ν , parameters which completely determine E_ν , V_ν and U_ν and thus the BCS mean field solution (Fig. 1.4.4). The validity of the BCS description of superfluid open shell nuclei have been confirmed throughout the mass table. We provide below recent examples.

The relation (1.4.26) implies, as a consequence of Pauli principle, that

$$\begin{aligned} |BCS\rangle &= \frac{1}{\text{Norm}} \prod_{\nu>0} \alpha_\nu \alpha_{\tilde{\nu}} |0\rangle_F = \prod_{\nu>0} (U_\nu + V_\nu P_\nu^\dagger) |0\rangle_F \\ &= \left(\prod_{\nu>0} U_\nu \right) \sum_{N \text{ even}} \frac{(c_\nu P_\nu^\dagger)^{N/2}}{(N/2)!} |0\rangle_F \\ &= \left(\prod_{\nu>0} U_\nu \right) \sum_{n=0,1,2,\dots} \frac{(c_\nu P_\nu^\dagger)^n}{n!} |0\rangle_F, \end{aligned} \quad (1.4.39)$$

where

$$P_\nu^\dagger = a_\nu^\dagger a_{\tilde{\nu}}^\dagger \quad \left(P^\dagger = \sum_{\nu>0} P_\nu^\dagger \right), \quad c_\nu = V_\nu / U_\nu, \quad (1.4.40)$$

while n denotes the number of pairs of particles ($2n = N$). In the above discussion of BCS we have treated in a rather cavalier fashion the fact that the amplitudes U_ν and V_ν are in fact complex quantities. A possible choice of phasing is²⁷

$$U_\nu = U'_\nu; \quad V_\nu = V'_\nu e^{-2i\phi}, \quad (1.4.41)$$

U'_ν and V'_ν being real quantities, while ϕ is the gauge angle, conjugate variable to the number of particles operator (1.4.20). Then²⁸

$$\hat{\phi} = i\partial/\partial\mathcal{N}, \quad \mathcal{N}, \quad (1.4.42)$$

and

$$[\hat{\phi}, \mathcal{N}] = i, \quad (1.4.43)$$

where $\mathcal{N} \equiv \hat{N}$ (Eq. (1.4.20)), the gauge transformations being induced by the operator

$$\mathcal{G}(\phi) = e^{-i\mathcal{N}\phi}. \quad (1.4.44)$$

²⁷Schrieffer (1973). The same results as those which will be derived are obtained with the alternative choice $U_\nu = U'_\nu e^{i\phi}$, $V_\nu = V'_\nu e^{-i\phi}$ (see e.g. Potel et al. (2013b)).

²⁸See e.g. Brink and Broglia (2005) App. H and refs. therein.

Let us replace the amplitudes (1.4.41) in (1.4.23) in (1.4.39),

$$|BCS\rangle = \left(\prod_{\nu>0} U'_\nu \right) \sum_{N \text{ even}} e^{-iN\phi} |\Phi_N\rangle = \left(\prod_{\nu>0} U'_\nu \right) \sum_{N \text{ even}} e^{-iN\phi} |\Phi_N\rangle, \quad (1.4.45)$$

where

$$|\Phi_N\rangle = \frac{\left(\sum_{\nu>0} c'_\nu P_\nu^\dagger \right)^{N/2}}{(N/2)!} |0\rangle_F, \quad (1.4.46)$$

with $c'_\nu = V'_\nu / U'_\nu$. It is of notice that

$$\sum_{\nu>0} c'_\nu P_\nu^\dagger |0\rangle_F \quad (1.4.47)$$

is the single Cooper pair state. The $|BCS\rangle$ state does not have a definite number of particles, but only in average being a wavepacket in N . In fact, (1.4.45) defines a privileged direction in gauge space, being an eigenstate of $\hat{\phi}$

$$\hat{\phi}|BCS\rangle = i \frac{\partial}{\partial N} \left(\prod_{\nu>0} U'_\nu \right) \sum_{N \text{ even}} e^{-iN\phi} |\Phi_N\rangle = \phi |BCS\rangle. \quad (1.4.48)$$

Expressing it differently (1.4.45) can be viewed as an axially symmetric deformed system in gauge space, whose symmetry axis coincides with the z' component of the body-fixed frame of reference \mathcal{K}' , which makes an angle ϕ with the laboratory z -axis (Fig. 1.4.1).

With the help of Eq. (1.4.39) (first line) one can write

$$|BCS(\phi=0)\rangle_{\mathcal{K}'} = \prod_{\nu>0} (U'_\nu + V'_\nu P_\nu^\dagger) |0\rangle_F, \quad (1.4.49)$$

where use was made of the relations

$$\mathcal{G}(\phi) a_\nu^\dagger \mathcal{G}^{-1}(\phi) = e^{-i\phi} a_\nu^\dagger = a'_\nu^\dagger, \quad (1.4.50)$$

and

$$\mathcal{G}(\phi) P_\nu^\dagger \mathcal{G}^{-1}(\phi) = e^{-2i\phi} P_\nu^\dagger = P'_\nu^\dagger. \quad (1.4.51)$$

It is to be noted that \mathcal{G} induces a counter clockwise rotation²⁹,

$$\mathcal{G}(\chi) \hat{\phi} \mathcal{G}^{-1}(\chi) = \hat{\phi} - \chi. \quad (1.4.52)$$

²⁹

$[\mathcal{N}, \phi] = -i, \quad \mathcal{G}(\chi) = e^{-i\mathcal{N}\chi} \quad \chi : \text{c-number}, \quad [e^{-i\mathcal{N}\chi}, \phi] = e^{-i\mathcal{N}\chi} \phi - \phi e^{-i\mathcal{N}\chi},$
 $[e^{-i\mathcal{N}\chi}, \phi] e^{i\mathcal{N}\chi} = e^{-i\mathcal{N}\chi} \phi e^{i\mathcal{N}\chi} - \phi, \quad e^{-i\mathcal{N}\chi} = 1 - i\mathcal{N}\chi \quad \chi^2 \ll \chi$
 $[1 - i\mathcal{N}\chi, \phi] = -i[\chi, \phi] = -i(\mathcal{N}[\chi, \phi] + [\mathcal{N}, \phi]\chi) = -i(0 - i\chi) = -\chi$
 $[e^{-i\mathcal{N}\chi}, \phi] = -\chi e^{-i\mathcal{N}\chi}$
 $[e^{-i\mathcal{N}\chi}, \phi] e^{i\mathcal{N}\chi} = -\chi e^{-i\mathcal{N}\chi} e^{i\mathcal{N}\chi} = -\chi, \quad -\chi = \mathcal{G}(\chi) \phi \mathcal{G}^{-1}(\chi) - \phi$
 $\mathcal{G}(\chi) \phi \mathcal{G}^{-1}(\chi) = \phi - \chi$

As a consequence, to rotate $|BCS(\phi = 0)\rangle_{\mathcal{K}'}$ back into the laboratory system, use has to be made of the clockwise rotation of angle ϕ induced by $\mathcal{G}^{-1}(\phi)$,

$$\begin{aligned}\mathcal{G}^{-1}(\phi)|BCS(\phi = 0)\rangle_{\mathcal{K}'} &= \prod_{\nu>0} \left(U'_\nu + V'_\nu \mathcal{G}^{-1}(\phi) P_\nu^\dagger \right) |0\rangle_F \\ &= \prod_{\nu>0} \left(U'_\nu + e^{2i\phi} V_\nu P_\nu^\dagger \right) |0\rangle_F = |BCS(\phi)\rangle_{\mathcal{K}}\end{aligned}\quad (1.4.53)$$

where use was made of the invariance of $|0\rangle_F$ with respect to gauge transformations, and of the fact that in (1.4.49), $P'^\dagger = \mathcal{G}(\phi)P_\nu^\dagger \mathcal{G}^{-1}(\phi)$. Thus

$$\mathcal{G}^{-1}(\phi)P_\nu^\dagger \mathcal{G}(\phi) = \mathcal{G}^{-1}(\phi) \left(\mathcal{G}(\phi)P_\nu^\dagger \mathcal{G}^{-1}(\phi) \right) \mathcal{G}(\phi) = P_\nu^\dagger,\quad (1.4.54)$$

leading to

$$|BCS(\phi = 0)\rangle_{\mathcal{K}'} = \prod_{\nu>0} \left(U'_\nu + V'_\nu P_\nu^\dagger \right) |0\rangle_F = \prod_{\nu>0} \left(U_\nu + V_\nu P_\nu^\dagger \right) |0\rangle_F.\quad (1.4.55)$$

Spontaneous broken symmetry in nuclei is, as a rule, associated with the presence of rotational bands, as already found in the case of quadrupole deformed nuclei. *Consequently, one expects in nuclei with $\Delta \neq 0$ rotational bands in which particle number plays the role of angular momentum. That is pairing rotational bands.*

The state with particle number N belonging to such a band can be written as

$$|N_0\rangle = \int d\phi e^{-iN\phi} |BCS(\phi)\rangle_{\mathcal{K}}.\quad (1.4.56)$$

In what follows we discuss the structure of H_{fluct} and single out the term responsible for restoring gauge invariance to the BCS mean field solution giving thus rise to pairing rotational bands for discrete values of the angular momentum in gauge space, namely N , differing in two units from each other. In terms of quasiparticles, H_{fluct} can be expressed as

$$H_{fluct} = H'_p + H''_p + C\quad (1.4.57)$$

where

$$H'_p = -\frac{G}{4} \left(\sum_{\nu>0} (U_\nu^2 - V_\nu^2) (\Gamma_\nu^\dagger + \Gamma_\nu) \right)^2\quad (1.4.58)$$

and

$$H''_p = \frac{G}{4} \left(\sum_{\nu} (\Gamma_\nu^\dagger - \Gamma_\nu) \right)^2,\quad (1.4.59)$$

with

$$\Gamma_\nu^\dagger = \alpha_\nu^\dagger \alpha_\nu^\dagger.\quad (1.4.60)$$

The term C stands for constant terms, as well as for terms proportional to the number of quasiparticles, which consequently vanish when acting on $|BCS\rangle$. The term H'_p gives rise to two-quasiparticle pairing vibrations with energies $\gtrsim 2\Delta$. It can be shown that it is the term H''_p which restores gauge invariance³⁰. In fact,

$$[H_{MF} + H''_p, \hat{N}] = 0. \quad (1.4.61)$$

We now diagonalize $H_{MF} + H''_p$ in the quasiparticle RPA (QRPA),

$$[H_{MF} + H''_p, \Gamma_n^\dagger] = \hbar\omega_n \Gamma_n^\dagger, \quad [\Gamma_n, \Gamma_{n'}^\dagger] = \delta(n, n'), \quad (1.4.62)$$

where

$$\Gamma_n^\dagger = \sum_\nu (a_{n\nu} \Gamma_\nu^\dagger + b_{n\nu} \Gamma_\nu), \quad \Gamma_\nu^\dagger = a_\nu^\dagger a_\nu^\dagger, \quad (1.4.63)$$

is the creation operator of the n th vibrational mode. In the case of the $n = 1$, lowest energy root, it can be written as

$$|1''\rangle = \Gamma_1^{\prime\dagger} |0''\rangle = \frac{\Lambda_1''}{2\Delta} (\hat{N} - N_0) |0''\rangle, \quad (1.4.64)$$

where \hat{N} is the particle number operator written in terms of Γ_ν^\dagger and Γ_ν , and Λ_1'' is the strength of the quasiparticle-mode coupling. The prefactor is the zero point fluctuation (ZPF) of the mode, that is (see Eq. (1.1.11) for the case of surface vibration),

$$\sqrt{\frac{\hbar\omega_1''}{2C_1''}} = \sqrt{\frac{\hbar^2}{2D_1''\hbar\omega_1''}}. \quad (1.4.65)$$

Because the lowest frequency is $\omega_1'' = 0$, the associated ZPF diverge ($\Lambda_1'' \sim (\hbar\omega_1'')^{-1/2}$). It can be seen that this is because $C_1'' \rightarrow 0$, while D_1'' remains finite. In fact,

$$\frac{D_1''}{\hbar^2} = \frac{2\Delta^2}{\Lambda_1''^2 \hbar\omega_1''} = 4 \sum_{\nu>0} \frac{U_\nu^2 V_\nu^2}{2E_\nu}. \quad (1.4.66)$$

A rigid rotation in gauge space can be generated by a series of infinitesimal operations of type $\mathcal{G}(\delta\phi) = e^{i(\hat{N}-N_0)\delta\phi}$, the one phonon state $|1''\rangle = \Gamma_1^{\prime\dagger} |0''\rangle$ is obtained from rotations in gauge space of divergent amplitude. That is, fluctuations of ϕ over the whole $0 - 2\pi$ range. By proper inclusion of these fluctuations one can restore gauge invariance violated by $|BCS\rangle_{\mathcal{K}'}$. The resulting states

$$|N_0\rangle \sim \int_0^{2\pi} d\phi e^{-iN_0\phi} |BCS(\phi)\rangle_{\mathcal{K}'} \left(\sum_{\nu>0} c'_\nu P_\nu^\dagger \right)^{N/2} |0\rangle_F \quad (1.4.67)$$

³⁰For details see Brink and Broglia (2005).

have a definite number of particles and constitute the members of a pairing rotational band. Making use of a simplified model (single j -shell) it can be shown that the energies of those states can be written as,

$$E_N = \lambda(N - N_0) + \frac{G}{4}(N - N_0)^2, \quad (1.4.68)$$

where

$$\frac{G}{4} = \frac{\hbar^2}{2D'_1}. \quad (1.4.69)$$

An example of pairing rotational bands is provided by the ground state of the single open closed shell superfluid isotopes of the $^{50}_A\text{Sn}_N$ -isotopes (Fig. 1.4.5), $N_0 = 68$ having been found to minimize $E_0 = \langle BCS|H|BCS \rangle$ Eq. (1.4.27) used in the solution of the BCS number equation (1.4.37). Theory provides an overall account of the experimental findings. Making use of the BCS pair transfer amplitudes,

$$\langle BCS|P_\nu^\dagger|BCS \rangle = U_\nu V_\nu \quad (1.4.70)$$

in combination with a reaction software and of global optical parameters, one can account for the Cooper absolute value of the pair transfer differential cross section, within experimental errors (see Sect. 3.1 and Chapters 4 and 7, Fig. 7.4.1). The fact that projecting out the different Sn-isotopes from the intrinsic BCS state describing ^{118}Sn one obtains a quantitative description of observations carried out with the help of the specific probe of pairing correlations (Cooper pair transfer), testifies to the fact that pairing rotational bands can be considered elementary modes of nuclear excitation, emergent properties of spontaneous symmetry braking of gauge invariance.

Furthermore, the fact that these results follow the use of QRPA³¹ in the calculation of the ZPF of the collective solutions of the pairing Hamiltonian indicates the importance of conserving approximations to describe quantum many-body problems in general, and the finite size quantum many-body problem (FSQMB), of which the nuclear case represents a paradigmatic example, in particular.

Aside from low-lying collective states, that is rotations and low-energy vibrations, nuclei also display high-lying collective modes known as giant resonances.

1.5 Giant dipole resonance

If one shines a beam of photons on a nucleus it is observed that the system absorbs energy resonantly essentially at a single frequency, of the order of³² $\nu = 5 \times 10^{21}$ Hz, corresponding to an energy of $h\nu \approx 20$ MeV.

³¹Using the Tamm-Dancoff approximation, i.e. setting $Y \equiv 0$ (and thus $\sum X^2 = 1$) in the QRPA approximation does not lead to particle number conservation, in keeping with the fact that the amplitudes Y are closely connected to ZPF.

³²Making use of $h = 4.1357 \times 10^{-15}$ eVs one obtains for $h\nu = 1$ eV the frequency $\nu = 2.42 \times 10^{14}$ Hz and thus $\nu = 4.8 \times 10^{21}$ Hz for $h\nu = 20$ MeV. The wavelength of a photon of energy E is $\lambda = hc/E \approx 2\pi \times 200$ MeV fm/ E , which for $E = 20$ MeV leads to $\lambda \approx 63$ fm.

It is not difficult to understand how γ -rays excite a nuclear dipole vibration. A photon carries with it an oscillating electric field. Although the wavelength of a 20 MeV γ -ray is smaller than that of other forms of electromagnetic radiation such as visible light, it is still large ($\lambda \approx 63$ fm) compared to the dimensions of e.g. ^{40}Ca ($R_0 \approx 4.1$ fm). As a result the photon electric field is nearly uniform across the nucleus at any time. The field exerts a force on the positively charged protons. Consequently, it can set the center of mass into an antenna like, dipole oscillation (Thompson scattering), in which case no photon is absorbed. Another possibility is that it leads to an internal excitation of the system. In this case because the center of mass of the system does not move, the neutrons have to oscillate against the protons, again in an antenna-like motion. The restoring force of the vibration, known as the giant dipole resonance (GDR), is provided by the attractive force between protons and neutrons.

The connotation of giant is in keeping with the fact that it essentially carries the full photo absorption cross section (energy weighted sum rule, see below), and resonance because it displays a Lorentzian-like shape with a full width at half maximum of few MeV ($\lesssim 5$ MeV), considerably smaller than the energy centroid³³ $\hbar\omega_{GDR} \approx 80/A^{1/3}$ MeV. Microscopically, the GDR can be viewed as a correlated particle-hole excitation, that is a state made out of a linear contribution of proton and neutron particle-hole excitations with essentially $\Delta N = 1$, as well as small $\Delta N = 3, 5, \dots$ components (Fig. 1.2.3). Because the difference in energy between major shells is $\hbar\omega_0 \approx 41A^{1/3}$ MeV, one expects that about half of the contribution to the energy of the GDR arises from the neutron-proton interaction. More precisely, from the so called (repulsive) symmetry potential V_1 (see Eq. (1.1.4)), which measures the energy price the system has to pay to separate protons from neutrons. Theoretical estimates lead to

$$(\hbar\omega_{GDR})^2 = (\hbar\omega_0)^2 + \frac{3\hbar^2 V_1}{m\langle r^2 \rangle} = \frac{1}{A^{2/3}} [(41)^2 + (60)^2] \text{ MeV}^2, \quad (1.5.1)$$

resulting in

$$\hbar\omega_{GDR} \approx \frac{73}{A^{1/3}} \approx \frac{87}{R} \text{ MeV}, \quad (1.5.2)$$

where $R = 1.2A^{1/3}$ is the numerical value of the nuclear radius when measured in fm. The above quantity is to be compared with the empirical value $\hbar\omega_{GDR} \approx (80/A^{1/3})$ MeV $\approx (95/R)$ MeV.

³³Within this context we refer to the discussion concerning the renormalization of collective modes carried out in the text after equation (1.2.13), in particular regarding the cancellation between self-energy and vertex corrections (see Fig. 1.2.5 and footnote 16). This is a basic result of NFT –as discussed in later chapters– being connected with sum rule arguments in general, and particle conservation in particular. Argument which has been extended to the case of finite temperature as well as to include relativistic effects Ward (1950); Nambu (1960); Bortignon and Broglia (1981); Bertsch et al. (1983); Bortignon et al. (1998); Litvinova and Wibowo (2018); Wibowo and Litvinova (2019).

It is of notice that the elastic vibrational frequency of a spherical solid made out of particles of mass m can be written as $\omega_{el}^2 \sim \mu/(m\rho R^2) \sim v_t^2/R^2$, where R is the radius, ρ the density and v_t the transverse sound velocity proportional to the Lamé shear modulus of elasticity μ . In other words, giant resonances in general, and the GDR in particular, are embodiments of the elastic response³⁴ of the nucleus to an impulsive external fields, like that provided by a photon. The nuclear rigidity to sudden solicitations is provided by the shell structure, quantitatively measured by the energy separation between major shells.

1.6 Giant pairing vibrations

Due to spatial quantization, in particular to the existence of major shells of pair degeneracy $\Omega (\equiv (2j+1)/2)$, and separated by an energy $\hbar\omega_0 \approx 41/a^{1/3}$ MeV, the Cooper pair model can be extended to encompass pair addition and pair subtraction modes across major shells³⁵. Assuming that both the single-particle energies ϵ_k and ϵ_i appearing in Fig. 1.3.1 are both at an energy $\hbar\omega_0$ away from the Fermi energy, one obtains the dispersion relation

$$-\frac{1}{G} = \frac{\Omega}{W - 2\hbar\omega_0} - \frac{\Omega}{W + 2\hbar\omega_0}, \quad (1.6.1)$$

leading to

$$(2\hbar\omega_0)^2 - W^2 = 4\hbar\omega_0 G, \quad (1.6.2)$$

and implying a high lying pair addition mode of energy

$$W = 2\hbar\omega_0 \left(1 - \frac{G\Omega}{\hbar\omega_0}\right)^{1/2}. \quad (1.6.3)$$

The forwards (backwards) going RPA amplitudes are, in the present case

$$X = \frac{\Lambda_0 \Omega^{1/2}}{2\hbar\omega_0 - W} \quad \text{and} \quad Y = \frac{\Lambda_0 \Omega^{1/2}}{2\hbar\omega_0 + W} \quad (1.6.4)$$

normalized according to the relation

$$1 = X^2 - Y^2 = \Lambda_0^2 \Omega \frac{8\hbar\omega_0 W}{((2\hbar\omega_0)^2 - W^2)^2}, \quad (1.6.5)$$

where Λ_0 stands for the particle-pair vibration coupling vertex. Making use of (1.6.2) one obtains

$$\left(\frac{\Lambda_0}{G}\right)^2 = \Omega \left(1 - \frac{G\Omega}{\hbar\omega_0}\right)^{-1/2} \quad (1.6.6)$$

³⁴Bertsch and Broglia (2005).

³⁵Broglia and Bes (1977).

quantity corresponding, within the framework of the simplified model used, to the two-nucleon transfer cross section. Summing up, the monopole giant pairing vibration has an energy close to $2\hbar\omega_0$, and is expected to be populated in two-particle transfer processes with a cross section of the order of that associated with the low-lying pair addition mode, being this one of the order of Ω . Simple estimates of (1.6.3) and (1.6.6) can be obtained making use of $\Omega \approx \frac{2}{3}A^{2/3}$ and $G \approx 17/A$ MeV lead to

$$W = 0.85 \times 2\hbar\omega_0, \quad \left(\frac{\Lambda_0}{G}\right)^2 \approx 1.2\Omega. \quad (1.6.7)$$

Experimental evidence of GPV in light nuclei have been reported³⁶

1.7 Sum rules

There are important operator identities which restrict the possible matrix elements in a physical system. Let us calculate the double commutator of the Hamiltonian describing the system and a single-particle operator F . That is

$$[\hat{F}, [H, \hat{F}]] = (2\hat{F}H\hat{F} - \hat{F}^2H - H\hat{F}^2) \quad (1.7.1)$$

Let us assume that $\hat{F} = \sum_k F(\mathbf{r}_k)$ and $H = T + v(\mathbf{r}, \mathbf{r}')$, where $v(\mathbf{r}, \mathbf{r}') = -\kappa_1 \hat{F}(\mathbf{r})\hat{F}(\mathbf{r}')$. Thus

$$[\hat{F}, [H, \hat{F}]] = \sum_k \frac{\hbar^2}{m} (\nabla_k F(\mathbf{r}_k))^2 \quad (1.7.2)$$

Let us take the average value on the correlated ground state

$$S(F) = \sum_{\alpha'} |\langle \alpha' | F | \tilde{0} \rangle|^2 (E_{\alpha'} - E_0) = \frac{\hbar^2}{2m} \int d\mathbf{r} |\nabla F|^2 \rho(\mathbf{r}), \quad (1.7.3)$$

where we have used $H|\alpha\rangle = E_\alpha|\alpha\rangle$ and $H|\tilde{0}\rangle = E_0|\tilde{0}\rangle$, and the sum $\sum_{\alpha'}$ is over the complete set of eigenstates of the system. The above result describes the reaction of a system at equilibrium to which one applies an impulsive field, which gives the particles a momentum ∇F . On the average, the particles started at rest so their average energy after the sudden impulse is $\hbar^2|\nabla F|^2/2m$, a result which does not depend on the interaction acting among the nucleons, the energy being absorbed from the (instantaneous) external field before the system is disturbed from equilibrium. The result (1.7.3) is known as the energy weighted sum rule (EWSR).

An important application of (1.7.3) implies a situation where F has a constant gradient. Inserting $\mathbf{F} = z\mathbf{z}$ in (1.7.3), the integral simplifies because $\nabla F = 1$, and

³⁶Cappuzzello et al. (2015); Cavallaro et al. (2019), Bortignon and Broglia (2016). See also Laskin et al. (2016); Id Betan et al. (2002); Dussel et al.; Mouginot et al. (2011); Khan et al. (2004).

the integral leads just to the number of particles,

$$\sum_{\alpha} |\langle \alpha | F | \tilde{0} \rangle|^2 (E_{\alpha} - E_0) = \frac{\hbar^2 N}{2m} \quad (1.7.4)$$

The electric field of a photon is of this form in the dipole approximation, which is valid when the size of the system is small compared to the wavelength of the photon, the single-particle field being

$$F(\mathbf{r}) = e \sum_k \left[\frac{N - Z}{A} - t_z(k) \right] r_k Y_{1\mu}(\hat{r}_k), \quad (1.7.5)$$

with $t_z = -1/2$ for protons and $+1/2$ for neutrons. For the dipole operator referred to the nuclear center of mass one obtains

$$\sum_{\alpha'} |\langle \alpha' | F | \tilde{0} \rangle|^2 (E_{\alpha'} - E_0) = \frac{9}{4\pi} \frac{\hbar^2 e^2}{2m} \frac{NZ}{A}. \quad (1.7.6)$$

The above relation is known as the Thomas-Reiche-Kuhn (TRK) sum rule, and is equal to the maximum energy a system can absorb from the dipole field. The RPA solution respect the EWSR, while the Tamm-Dancoff approximation (TDA), resulting by setting $Y_{ki}^{\alpha} = 0$ and normalizing the X -components ($\sum_{ki} X_{ki}^{\alpha 2} = 1$) fulfill the non-energy weighted sum rule. A fact which testifies to the important role ZPF play in nuclei.

1.8 Ground state correlations

The zero point fluctuations associated with collective nuclear vibrations affect, among other thing, the nuclear mean field properties³⁷. Within the harmonic approximation discussed in Sections 1.1.1 and 1.1.2 in connection with surface vibrational modes, the lowest (ground) state of (1.1.9) has an energy $\frac{1}{2}\hbar\left(\frac{C_{\lambda}}{D_{\lambda}}\right)^{1/2} = \hbar\omega_{\lambda}$ for each degree of freedom (e.g. $(2\lambda + 1)$ in the case of a vibration of multipolarity λ). The associated coordinate-momentum in determining relation assumes its minimum value³⁸

$$\Delta\alpha_{\lambda\mu}^{(n)} \Delta\pi_{\lambda\mu}^{(n)} = \frac{\hbar}{2}, \quad (1.8.1)$$

³⁷Gogny (1978); Esbensen and Bertsch (1983); Reinhard and Drechsel (1979); Khodel et al. (1982); Barranco and Broglia (1987) see also Brown and Jacob (1963); Anderson and Thouless (1962) (it is likely a coincidence in connection with this inaugural issue of Phys. Lett. that short of hundred pages after, one finds the paper of B. D. Josephson, Possible new effects in superconducting tunneling, Phys. Lett. **1**, 251 (1962)).

³⁸The same result is found for Ψ_n describing a state with n -quanta, and the basis that solutions with $n \gg 1$ behaves as “quasiclassical” or “coherent” states of the harmonic oscillator (Glauber (2007)) in keeping with the fact that the contribution of the zero point energy is negligible in such case ($(n + 1/2)\hbar\omega \approx n\hbar\omega$) and that the many quanta wavepacket always attain the lower limit of (1.8.1) (Basdevant and Dalibard (2005) pp. 153,465) (discussions with Pier Francesco Bortignon in March 2018 concerning coherent states are gratefully acknowledged). Schrödinger used this result in a paper (Schrödinger (1926b)) to suggest that waves (material waves) described by his wave func-

in keeping with the fact that

$$\Delta\alpha_{\lambda\mu}^{(n)} = \sqrt{\frac{\hbar\omega_\lambda}{2C_\lambda}}, \quad (1.8.2)$$

and $\Delta\pi_{\lambda\mu} = \sqrt{\hbar D\omega_\lambda/2}$, in keeping with the fact that $|\Psi_0|^2$ is mathematically a Poisson distribution. The fact that $\Delta\alpha_{\lambda\mu}^2(n) = \hbar\omega_\lambda(n)/2C_\lambda(n)$ implies that the mean square radius will be modified from its mean field value R_0 (Eq. (1.8.1)) and thus also the nuclear density distribution. The value of $\hbar\omega_\lambda(n)/2C_\lambda(n)$ can be determined by calculating the collective mode $|n_\lambda(n)=1\rangle = \Gamma_{\lambda\mu}^\dagger(n)|\tilde{0}\rangle$ in RPA. As seen from the caption to Fig. 1.2.3 the zero point fluctuation of the mode enter the definition of the X, Y -amplitudes of the mode. Let us start by calculating the effect of the zero point fluctuations on the nuclear density distribution. The corresponding operator can be written as

$$\hat{\rho}(\mathbf{r}) = a^\dagger(\mathbf{r})a(\mathbf{r}), \quad (1.8.3)$$

where $a^\dagger(\mathbf{r})$ is the creation operator of a nucleon at point \mathbf{r} . It can be expressed in terms of the phase space creation operators $a_\nu^\dagger (\nu \equiv n, l, j, m)$ as

$$a^\dagger(\mathbf{r}) = \sum_\nu \varphi_\nu^*(\mathbf{r})a_\nu^\dagger, \quad (1.8.4)$$

where $\varphi_\nu(\mathbf{r})$ are the single-particle wavefunctions. Thus

$$\hat{\rho}(\mathbf{r}) = \sum_{\nu\nu'} \varphi_\nu^*(\mathbf{r})\varphi_{\nu'}(\mathbf{r})a_\nu^\dagger a_{\nu'}. \quad (1.8.5)$$

The matrix element in the HF ground state is (Fig. 1.2.2)

$$\rho_0(\mathbf{r}) =_F \langle 0 | \hat{\rho}(\mathbf{r}) | 0 \rangle_F = \sum_{i, (\epsilon_i \leq \epsilon_F)} |\varphi_i(\mathbf{r})|^2. \quad (1.8.6)$$

To lowest order of perturbation theory in the particle-vibration coupling vertex, the NFT diagrams associated with the change of ρ_0 due to ZPF are shown in Fig. 1.8.1. Graphs (a) and (b) and (c) and (d) describe the changes in the density operator and in the single-particle potential respectively. This can be seen from the insets (I) and (II). The dashed horizontal line starting with a cross and ending at a hatched circle represents the renormalized density operator. This phenomenon is similar

tion are the only reality, particles being only derivative things. In support of his view he considered a superposition of linear harmonic oscillator wavefunctions and showed that the wave group holds permanently together in the course of time. And he adds that the same will be true for the electron as it moves in high orbits of the hydrogen atom, hoping that wave mechanics would turn out to be a branch of classical physics (Pais (2000)). It was Born who first provided the correct interpretation of Schrödinger's wavefunction (modulus square) in his paper "Quantum mechanical collision phenomena" (Born (1926a)). In it it is stated that the result of solving with wave mechanics the process of elastic scattering of a beam of particles by a static potential is not what the state after the collision is, but how probable is a given effect of the collision.

to that encountered in connection with vertex renormalization in Fig. 1.2.5, that is the renormalization of the particle-vibration coupling (insets (I) and (I')). Concerning potential renormalization, the bold face arrowed line shown in inset (II) of Fig. 1.8.1 represents the motion of a renormalized nucleon due to the self-energy process induced by the coupling to vibrational modes. A phenomenon which can be described at profit through an effective mass, the so called ω -mass m_ω , in which case particle motion is described by the Hamiltonian³⁹ $(\hbar^2/2m_\omega)\nabla^2 + (\frac{m}{m_\omega})U(r)$. The ω -mass can be written as $m_\omega = (1 + \lambda)m$, where m is the nucleon mass and λ is the so called mass enhancement factor $\lambda = N(0)\Lambda$, where $N(0)$ is the density of levels at the Fermi energy, and Λ the PVC vertex strength, typical values being $\lambda = 0.4$.

The fact that in calculating $\delta\rho$, that is, the correction to the nuclear density distribution (renormalization of the density operator), one finds to the same order of perturbation a correction to the potential, is in keeping with the self consistency existing between the two quantities (Eq. (1.2.8)). *Now, what changes is not only the single-particle energy, but also the single-particle content as well as the radial dependence of the wavefunctions of the states measured by $Z_\omega = m/m_\omega$.* It is of notice that the effective mass approximation, although being quite useful, cannot take care of the energy dependence of the renormalization process which leads, in the case of single-particle motion to renormalized energies, spectroscopic amplitudes and wavefunctions. The analytic expressions associated with diagrams (a) and (c) of Fig. 1.8.1 are

$$\delta\rho(r)_{(a)} = \frac{(2\lambda + 1)}{4\pi} \sum_{\nu_1\nu_2n} [Y_n(\nu_1\nu_2; \lambda)]^2 R_{\nu_1}(r)R_{\nu_2}(r), \quad (1.8.7)$$

and

$$\begin{aligned} \delta\rho(r)_{(c)} &= (2\lambda + 1)\Lambda_n(\lambda) \sum_{\nu_1\nu_2\nu_3} \frac{M(\nu_1, \nu_3; \lambda)}{\epsilon_{\nu_1} - \epsilon_{\nu_2}} (2j_1 + 1)^{-1/2} \\ &\times Y_n(\nu_3\nu_2; \lambda) \times R_{\nu_1}(r)R_{\nu_2}(r), \end{aligned} \quad (1.8.8)$$

where M is the matrix element of $\frac{R_0}{\kappa}\frac{\partial U}{\partial r}Y_{\lambda\mu}(\hat{r})$ and $n = 1, 2 \dots$ the first, second, etc vibrational modes as a function of increasing energy, and Λ_n is the strength of the particle-vibration coupling associated with the n -mode of multipolarity λ . The functions $R(r)$ are the radial wavefunctions associated with the states ν_1 and ν_2 . While $\delta\rho_{(a)}$ can be written in terms of the RPA Y -amplitudes which are directly associated with the zero point fluctuations of harmonic motion (Fig. 1.2.3 (c)), $\delta\rho_{(c)}$ contains a scattering vertex not found in RPA – that is going beyond the harmonic approximation– and essential to describe renormalization processes of the different degrees of freedom, namely single-particle (energy, single-particle

³⁹The ratio (m/m_ω) gives a measure of the single-particle energy content (Mahaux et al. (1985), Eq. (3.5.18)), while m_ω is proportional to the (energy-) slope of the (single-particle) self-energy dispersion relation (Sect. 5.A.1; see also Brink and Broglia (2005) and refs. therein).

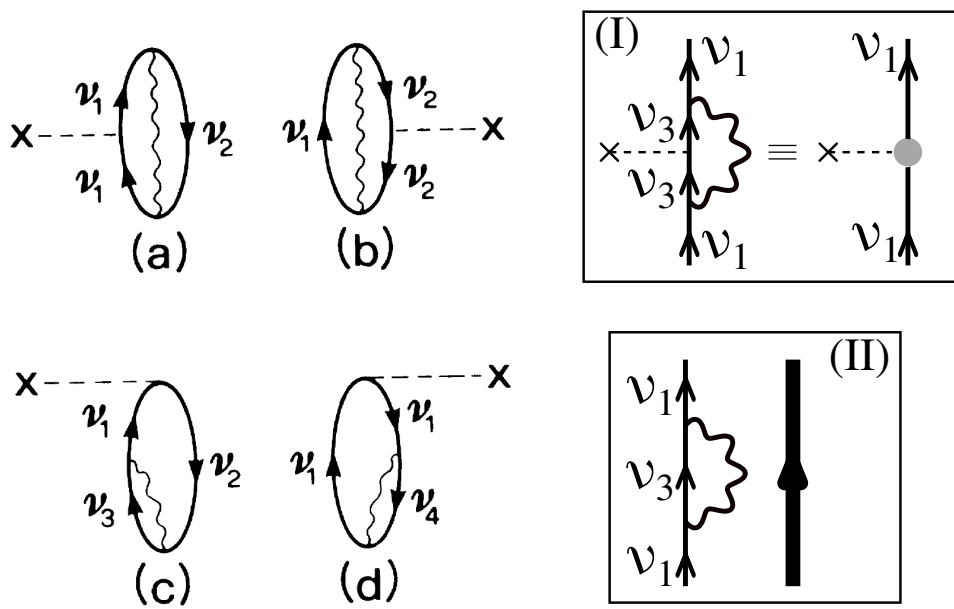


Figure 1.8.1: Lowest-order corrections in the particle-vibration coupling vertex of the nuclear density due to the presence of zero-point fluctuations associated with density vibrations. An arrowed line pointing upwards denotes a particle, while one pointing downward a hole. A wavy line represents a surface phonon. The density operator is described through a dotted horizontal line starting with a cross. Graphs (a) and (b) are typical examples of density contributions to $\delta\rho$ (see inset (I)); the dashed horizontal line starting with a cross and ending at a hatched circle in the diagram to the right, represents the renormalized density operator, resulting from the processes displayed to the left; (c) and (d) are of potential contributions (see inset (II)); the bold face arrowed line represents the renormalized single-particle state due to the coupling to the vibrations leading to the self energy process shown to the left).

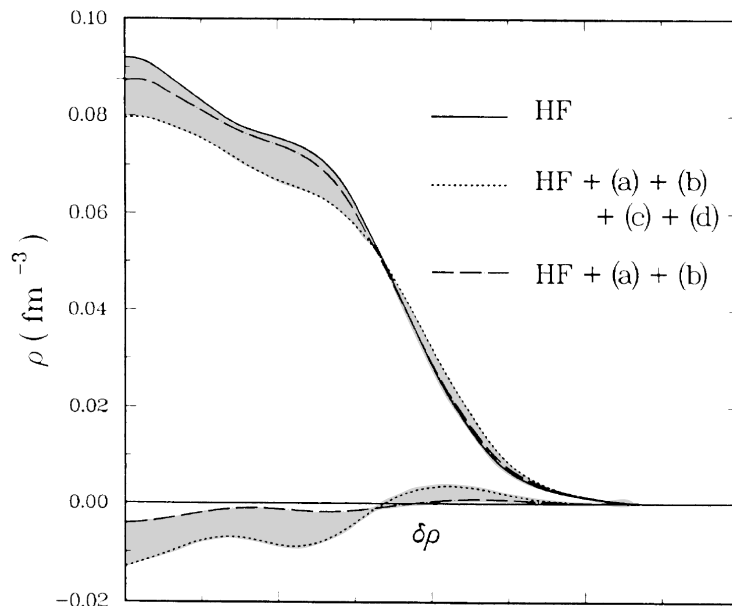


Figure 1.8.2: Modification in the charge density of ^{40}Ca induced by the zero-point fluctuations associated with vibrations of the surface modes. The results labeled HF, HF+(a)+(b), and HF+(a)+(b)+(c)+(d) are the Hartree-Fock density, and that resulting from adding to it the corrections $\delta\rho$ associated with the processes (a)+(b) and (a)+(b)+(c)+(d) displayed in Fig. 1.8.1, respectively. In the lower part of the figure the quantities $\delta\rho$ are displayed.

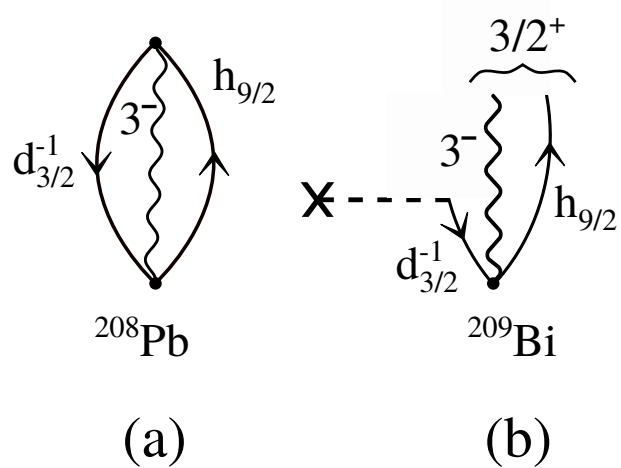


Figure 1.8.3: (a) Example of zero point fluctuation of the ground state of the double-magic nucleus $^{208}_{82}\text{Pb}_{126}$ associated with the low-lying octupole vibration of this system, observed at an energy of 2.615 MeV and displaying a collective electromagnetic decay to the ground state. The proton particle-hole component $(h_{9/2}, d_{3/2}^{-1})_{3^-}$ displayed carries a large amplitude in the octupole vibration wavefunction. (b) Diagram representing the transfer of one proton to ^{208}Pb , which fills the $d_{3/2}^{-1}$ hole state leading to a $3/2^+$ in $^{209}_{83}\text{Bi}_{126}$, member of the septuplet of states $|(3^- \otimes h_{9/2} J^\pi)\rangle$ with $J^\pi = 3/2^+, 5/2^+, \dots, 15/2^+$. The horizontal dashed line starting with a cross stands for the stripping process $(^3\text{He}, d)$.

content and radial dependence of the wavefunction) and collective motion, as well as interactions. In particular the pairing interaction.

In Fig. 1.8.2 results of calculations of $\delta\rho$ carried out for the closed shell nucleus ^{40}Ca are shown. The vibrations were calculated by diagonalizing separable interactions of multipolarity λ in the RPA. All the roots of multipolarity and parity $\lambda^\pi = 2^+, 3^-, 4^+$ and 5^- which exhaust the EWSR were included in the calculations. Both isoscalar and isovector degrees of freedom were considered, as well low-lying and giant resonances.

From the point of view of the single-particle motion the vibrations associated with low-lying modes display very low frequency ($\hbar\omega_\lambda/\epsilon_F \approx 0.1$) and lead to an ensemble of adiabatic deformed shapes. Nucleons can thus reach to distances from the nuclear center which are considerably larger than the radius R of the static spherical potential. Because the frequency of the giant resonances are of similar magnitude to those corresponding to the single-particle motion, the associated surface deformations average out.

Said it differently, the low-lying vibrational modes account for most of the contributions to the changes in the density distribution⁴⁰. Making use of the corresponding $(\delta\rho)_{low-lying}$, the mean square radius of ^{40}Ca was calculated⁴¹, leading to $\langle r^2 \rangle = (3/5)R_0^2 = 10.11 \text{ fm}^2$ ($R_0 = 1.2A^{1/3} \text{ fm} = 4.1 \text{ fm}$), in overall agreement with the experimental findings. Similar calculations to the ones discussed above, but in this case taking into account only the contributions of the low-lying octupole vibration⁴² indicate that nucleons are to be found a reasonable part of the time in higher shells than those assigned to them by the shell model. The average number of “excited” particles being ≈ 2.4 . If these are present, pickup reactions such as (p, d) and (d, t) will show them. From the nature of the correlations, the pickup of such a particle will leave the residual nucleus in an excited state composed of a hole and a vibration (Fig. 1.8.3). Conversely, because of the presence of hole states in the closed shell nucleus, one can transfer a nucleon to states below the Fermi energy in, for example, (d, p) or $(^3\text{He}, d)$ one-neutron or one-proton stripping reactions respectively, leaving the final nucleus with one-nucleon above closed shell coupled to the vibrations.

Systematic studies of such multiplets have been carried out throughout the mass table. In particular around the closed shell nucleus $^{208}_{82}\text{Pb}_{126}$ (Fig. 1.8.3). Within this context it is not only quite natural but also necessary, to deal with structure and reactions on equal footing. This is one of the main goals of the present monograph.

⁴⁰Another example of the recurrent central role played by low-frequency modes in determining the properties and behavior of systems at all levels of organization, from the atomic nucleus to the Casimir effect in QED, to phonons in superconductors as well as to the folding of proteins and brain activity ($\nu < 0.1 \text{ Hz}$) (Mitra et al. (2018)).

⁴¹Barranco and Broglia (1987).

⁴²Brown and Jacob (1963).

1.9 Interactions

A number of subjects are not touched upon in the present monograph. In particular, the role temperature plays in the structure and decay of nuclei and that of bare (e.g. the Argonne NN -potential) and/or effective forces (e.g. Gogny, Skyrme, etc.). In what follows we briefly elaborate on this last point, referring to Bortignon et al. (1998) and refs. therein concerning the first one.

The Coulomb interaction resulting from the exchange of photons between charged particles defines the domain area of quantum electrodynamics (QED). Being the electron and the photon fields in interaction, what we call an electron is only partially to be associated with the electron field alone. It is also partially to be associated with the photon field which dresses the electron field. And conversely what is called the photon field can materialize itself in space in terms of an electron and a positron⁴³.

The Coulomb interaction is the best known of all physical interactions, and QED constitutes the paradigm of theories which can be considered correct. In natural units in which the magnetic moment of the electron emerging from Dirac equation has the value of 1, the results of QED corrections agree –once divergent contributions have been renormalized by properly adjusting the value of the bare electron mass and charge⁴⁴–, within experimental errors, that is down to the eleventh decimal figure, with observation. That is $1.00115965221 \pm 0.00000000003$ (exp.); $1.00115965246 \pm 0.00000000020$ (QED)⁴⁵.

The energy difference between the $2S_{1/2}$ and the $2P_{1/2}$ states of the hydrogen atom which according to Dirac's theory should be degenerate, emerges naturally, according to QED, from the dressing of the hydrogen's electron by the photon associated with the zero point fluctuation of the electromagnetic vacuum. The measured value of the Lamb shift⁴⁶ is 1057.845 (9) MHz, an experimental value⁴⁷ whose accuracy is limited by the ≈ 100 MHz natural line width of the $2P_{1/2}$ state. The best QED value, limited by uncertainties in the radius of the proton, is 1057.865 MHz⁴⁸

The above two numbers (electron magnetic moment and Lamb shift) are results of *ab initio* calculations within the framework of an effective field theory (QED). *Ab initio* to the extent that quantum mechanics in general⁴⁹ and the Dirac equation⁵⁰ in particular can be considered, on grounds of their universal validity, to be

⁴³Schwinger (2001).

⁴⁴Changing indirectly the Coulomb interaction. Not that observed in the laboratory and acting between physical (dressed) electrons, but the “bare” Coulomb interaction acting between the “naked” electron fields, and used in the calculation of the variety of processes through which the photon field dresses the electrons.

⁴⁵Kinoshita (1990).

⁴⁶Lamb Jr (1964).

⁴⁷Lundeen and Pipkin (1981, 1986); Pipkin (1990).

⁴⁸Sapirstein and Yennie (1990); Grotch (1994).

⁴⁹Heisenberg (1925); Born and Jordan (1925); Born et al. (1926); Dirac (1925); Schrödinger (1926b); Born (1926a); Heisenberg (1927); Pauli (1925).

⁵⁰Dirac (1928a,b).

so, including QED with its bare mass and charge parameters used to cure infinities (renormalization)⁵¹.

Nuclear field theory (NFT) was developed following the (graphical) approach adopted by Feynman in his formulation of QED, making use of the correspondence electron→nucleon, photons→collective vibrations, fine structure constant→particle-vibration coupling. In keeping with the fact that in Feynman's QED *nothing is really free*⁵² (*bare*) and of the very large value of the induced (retarded) nuclear pairing interaction –as large or larger than that of the bare NN -interaction in e.g. the case of the 1S_0 (pairing channel)⁵³– arising from the exchange of collective vibrations between nucleons, the role which specific (bare) nuclear forces (four-point vertices v) play in the results of NFT calculations, becomes somewhat blurred.

Starting from the mean field (see Eq. (1.2.8)) at the basis of the non-observable bare single-particle energies, one employs a generic shape (Woods-Saxon), adjusting the depth, radius and diffusivity of the central potential, and the depth of the spin-orbit one in connection with an r -dependent effective k -mass (exchange potential) so that the dressed single-particle states reproduce the experimental findings⁵⁴. Parallel to the bare mass parameter entering renormalized QED. In connection with the coupling between nucleons and surface vibrations, namely the strength Λ_α , one adjusts κ so as to reproduce the properties of the collective modes (see inset Fig. 1.2.3), a procedure which parallels the tuning of the bare charge, and thus the strength of the coupling between electrons and photons (and of the bare Coulomb interaction) in renormalized QED. In other words, renormalized nuclear field theory (NFT)_{ren}

The Mayer and Jensen sequence of levels around the $N = 8$ magic nuclei is $1p_{1/2}, 1d_{5/2}, 2s_{1/2}$ (Fig. 1.1.2), while experimentally ${}^4_4\text{Be}_7$ displays the sequence⁵⁵ $1/2^+, 1/2^-$ (bound), $5/2^+$ (resonance). A consequence of the dressing of the bare $1p_{1/2}, 1d_{5/2}$ and $2s_{1/2}$ states by the quadrupole vibration⁵⁶ of ${}^{10}\text{Be}$ ($\beta_2 \approx 0.9$). This extremely large value of the dynamical deformation parameter implies a Lamb-shift like mechanism which shifts the bare $1p_{1/2}$ and $2s_{1/2}$ orbitals by more than 3 MeV with respect to each other, the resulting dressed levels coinciding with the experimental ones ($\epsilon_{1/2^+} = -0.5$ MeV, $\epsilon_{1/2^-} = -0.18$ MeV, i.e. $\Delta\epsilon_{1/2^+ - 1/2^-} = 0.32$ MeV, see Figs. 7.2.1 and 7.3.1). It is of notice that at the same time, the bare $d_{5/2}$ resonance is moved down, from its bare energy, by ≈ 6 MeV. The resulting centroid

⁵¹Feynman (1949); Schwinger (1948); Tomonaga (1946); see also Dyson (1949); Schwinger (1958); Schweber (1994).

⁵²Feynman (1975).

⁵³For example, concerning the contribution to the pairing gap of ${}^{120}\text{S}$ ($\Delta \approx 1.45$ MeV) arising from the bare 1S_0 (pairing) interaction v_{14} (Argonne NN -potential) and that associated with the exchange of collective vibrational modes between nucleons moving in time reversal states close to the Fermi energy (Idini et al. (2015)). In the case of ${}^{11}\text{Li}$, essentially all of the pairing interaction which binds the two halo neutrons to the core ${}^9\text{Li}$, arise from the exchange between them, of the soft E1-mode (pygmy dipole resonance of ${}^{11}\text{Li}$). (Barranco et al. (2001); Broglia et al. (2019a)).

⁵⁴See e.g. Barranco et al. (2017) and Barranco et al. (2020).

⁵⁵Kwan et al. (2014).

⁵⁶Barranco et al. (2017).

and width of the dressed $\widetilde{5/2}^+$ resonance is ≈ 1.45 MeV ($\Gamma = 0.17$ MeV) to be compared with the experimental values of 1.28 MeV and $\Gamma = 0.15$ MeV. The predicted $E1$ -decay between the parity inverted levels is $B(E1; \widetilde{1/2}^- \rightarrow \widetilde{1/2}^+) = 0.11e^2 \text{ fm}^2$, a value to be compared to the experimental value $B(E1) = 0.102 \pm 0.002e^2 \text{ fm}^2$. The two (three) numbers ($\epsilon_{\widetilde{1/2}^+}$, $\epsilon_{\widetilde{1/2}^-}$ ($\Delta\epsilon$), and $B(E1)$) can, arguably, be used to assess the accuracy of renormalized NFT results on something which one can call equal footing, with the two numbers (electron magnetic moment and Lamb shift) discussed above in connection with the assessment of the level of accuracy of QED results.

It would be computationally useful and conceptually satisfying to have a bare NN -potential eventually derived from QCD, reproducing the NN -phase shifts and which, employed in nuclear structure calculations, lead to bare static (Eq. (1.2.8)) and time-dependent (dynamic, Eq. (1.2.9)) mean fields whose solutions (bare single-particle states and bare vibrational modes), interweaved according to the rules of an (effective) field theory, e.g. NFT (Sect. 2.7.2), accounted for the value of the observable resulting from a “complete” set of probes (see e.g. Figs. 2.11.1 and 7.3.1). Concerning single-particle motion: energies, absolute one-particle transfer differential cross sections and thus insight into both single-particle content and renormalized single-particle wavefunctions (form factors), γ -decay and associated effective charges, etc. Concerning collective vibrations: energies, γ -decay, absolute differential cross sections for inelastic and Coulomb excitations (surface modes) and for two-nucleon transfer processes (pairing vibrations). Until such desideratum becomes reality, the aim at shedding light onto the physics at the basis of new experimental results and that of providing guidance in the quest to achieve a deeper and unified picture of nuclear structure and reactions can be carried out in terms of empirical renormalization, i.e. $(\text{NFT})_{\text{ren}}$.

In keeping with the fact that the domain area of QED is all of chemistry and much of biology (Feynman (2006)), the important *renormalization effects* undergone by *bare forces* when used to describe even the simplest (real) many-body systems –e.g. the hydrogen atom in the case of the Coulomb interaction– is quite universal. Because of the variety of facets and the importance this issue has in connection with the unified nuclear field theory of structure and reactions we discuss in the present monograph, taylored after Feynman’s diagrammatic version of QED, we attempt a shedding light on bare force-renormalization process phenomena through a number of interdisciplinary examples. A crown example is provided by dispersive (retarded) forces like the van der Waals interaction (App. 3.D). Also by the Casimir effect and the hydrophobic force (App. 7.G), let alone in the renormalizations the Coulomb force undergoes in metals (App. 4.A). Dressing changing not only the value, but also the sign of the interaction and resulting in the phenomenon of superconductivity. Hallmarks of which are perfect conductivity and perfect diamagnetism, and the special effects found in terms of the renormalized Coulomb force acting across a Josephson junction (Sect. 4.6). Within this scenario one can mention that at the basis of the mechanism which inverts, in the odd $N = 7$

isotones ${}^3_3\text{Li}$ and ${}^4_4\text{Be}$, the standard Mayer-Jensen sequence of levels $1d_{5/2}$ and $2s_{1/2}$ and comes close to do so also concerning the $1d_{5/2}$ and $1p_{1/2}$ single-particle levels constitutes, arguably, the strongest Lamb shift-like phenomenon displayed by a physical system.

1.10 Hindsight

In order for a nucleon moving in a level close to the Fermi energy to display a mean free path larger than nuclear dimensions and to be reflected at the nuclear surface through an elastic process, all other nucleons must move in a rather ordered, correlated fashion. Within this context to posit that single-particle motion is the most collective of all nuclear motions⁵⁷ seems natural. Associated with mean field and single-particle motion one finds the typical bunching of the corresponding levels closely connected with the major shells lying above and below the Fermi energy. A fact which determines the parity (and angular momentum) of the lowest energies needed to promote a nucleon across the Fermi surface. By correlating these excitations through the same components of the NN -interaction leading to the single-particle bunching within the mean field approximation, one obtains the collective multipole vibrations of particle-hole type. Similar arguments result in the presence of multipole pairing vibrations in the low-energy spectrum, and in their coupling to single-particle motion.

It is then natural to consider single-particle motion and collective states on equal footing, and as basis states of a physical description of the atomic nucleus in which to diagonalize both three point (PVC) and four-point (v) vertices , eventually taking in this second case also $3N$ terms into account. Such an approach also provides direct indication of the minimum set of experiments needed to obtain a “complete” picture (test) of the theoretical description of the atomic nucleus. These, are the specific probes of each of the basis states (elementary modes of excitation). Namely inelastic scattering and Coulomb excitation (particle-hole collective vibrations and rotations), one-particle transfer processes (independent-particle motion) and two-particle transfer reactions (pairing vibrations and rotations). Summing up, because of the interweaving existing between the variety of elementary modes of excitation, experimental probes associated with fields which carry transfer quantum number $\beta = 0, \pm 1$ and ± 2 , and different multipolarities, spins and isospins are needed to characterize the structure of nuclei. This is what we attempt at explaining and formulating in the following chapters, setting special emphasis in transfer processes, in which case the relative motion of the reacting nuclei and the intrinsic motion of the nucleons in target and projectile cannot be separated, and one is forced to treat structure and reactions in an unified way.

⁵⁷Mottelson (1962),

Chapter 2

Structure and reactions

In what follows the connection between the concept of elementary modes of excitation and associated specific probes is discussed in terms of selected experiments. Connection which finds its ultimate test in terms of predicted and measured absolute transition probabilities and differential cross sections.

2.1 Elementary modes of excitation and specific probes

Subject to external probes which couple weakly to the nucleus, that is in such a way that the system can be expressed in terms of the properties of the excitation in the absence of probes¹, the nucleus reacts in terms of single-particle (-hole) motion (one-particle transfer), vibrations (surface, spin, etc.) and rotations (Coulomb excitation and inelastic scattering) and pairing vibrations and rotations (two-nucleon transfer reactions), that is, in terms of elementary modes of excitation.

Collective vibrations in nuclei can be characterized by a variety of quantum numbers. In particular angular momentum (J), parity (π) and transfer quantum number (β). Let us consider the doubly magic nucleus $^{208}_{82}\text{Pb}_{126}$ to illustrate some aspects of β . The ground state of this nucleus $|\text{gs}(^{208}\text{Pb})\rangle$ has angular momentum 0 and positive parity. It can be viewed as the vacuum state of the variety of elementary modes of excitation at the basis of the nuclear field theory (NFT) description of this system. The lowest lying collective vibration ($E_x \approx 2.6$ MeV) is an octupole surface vibration. Microscopically, it can be viewed as a correlated particle-hole (p, h) excitation. Consequently, this state is characterized by the quantum numbers $J^\pi = 3^-, \beta = 0$. A neutron moving around ^{208}Pb in levels above the Fermi energy can have quantum numbers $j^\pi = 9/2^+, 11/2^+, 5/2^+, \dots (2g_{9/2}, 1i_{11/2}, 3d_{5/2}, \dots)$, all of them having $\beta = 1$.

In the case of quantum electrodynamics (Feynman graphical formulation²),

¹See e.g. Pines and Nozières (1966), Bohr and Mottelson (1975) and refs. therein. Within the context of linear response see also Sect. 7.6.3, text after Eq. (7.6.1).

²“The practical usefulness of the Feynman rules and diagrams made them one of the most essential elements of the scientific training of every theoretical physicist” J. Mehra.

theory after which NFT was worked out, these two modes (octupole and single-particle modes) parallel the photon and the electron. The nucleus ^{208}Pb , aside from having a rich variety of $\beta = 0$ collective (p, h) correlated modes (“photons”) like the $J^\pi = 2^+$ (4.1 MeV) and 5^- (3.2 MeV) states, it also displays collective $\beta = \pm 2$ modes. These pairing vibrations can be viewed as correlated two-particle ($\beta = +2$), two-hole ($\beta = -2$) vibrations. For example, pair addition modes ($\beta = +2$) with quantum numbers $J^\pi = 0^+, 2^+, 4^+, \dots$ correspond to the ground state and to the lowest $2^+, 4^+, \dots$ states of ^{210}Pb . In particular, the $|J^\pi = 0_1^+, \beta = 2\rangle \equiv |\text{gs}(\text{gs}(^{210}\text{Pb}))\rangle$ can be viewed as a nuclear embodiment of a Cooper pair: a weakly correlated pair of fermions moving in time reversal states lying close to the Fermi energy. Cooper pairs are the building blocks of the microscopic theory of superconductivity developed by Bardeen, Cooper, Schrieffer (BCS)³.

In Figs. 2.1.1–2.1.3, examples of specific reactions which have identified different elementary modes of excitation of ^{208}Pb mentioned above, are given. In particular, a cartoon representation (color online) of elastic, inelastic, one- and two-particle direct transfer reactions induced by alpha, deuteron and triton projectiles impinging on ^{208}Pb are shown. In all cases a standard setup is used, in which a light projectile is aimed at a fixed target (thin foil made out of ^{208}Pb). The outgoing particles carrying the corresponding physical information, i.e. momentum, angular momentum, energy, etc. transferred to or from the target, are deflected by the electromagnetic fields of a spectrometer and eventually recorded at a given angle by particle detectors (points a,b,... in magnet). Those events provide structural information as shown in the two dimensional strength function displayed below the cartoon laboratory setup.

These strength functions, recorded at a wide range of angles provide the absolute differential cross sections associated with each of the nuclear states populated in the process. They are typically measured in⁴ millibarns per steradian (mb/sr). To translate these quantities into nuclear structure information, a model of structure and of reactions is needed to calculate the absolute cross sections, to be compared with the data. The risks of using relative cross section is that of overlooking limitations in the description of the reaction mechanism or in that of the structure description of the states involved in the reaction under study. Or of both.

In this connection, it is of notice that either one sets equal weight in correctly calculating the static and dynamic properties of the single-particles and of the collective modes respectively, and on their interweaving leading to renormalized, physical modes, than in working out the reaction mechanism, or the confrontation between theoretical predictions and experimental observation may not be fruitful⁵.

³Bardeen et al. (1957a,b). See also Brink and Broglia (2005) and references therein.

⁴A barn is defined as $1\text{b}=10^{-28}\text{m}^2 = 100\text{fm}^2$. In three dimensions, the solid angle Ω is related to the area of the spherical surface A it spans ($\Omega = A/R^2$ sr), in a similar way in which in two dimensions, an angle θ is related to the length L of the circular arc it spans. $\theta = L/R$ rad.

⁵*Structure and Reactions.* Within this context one can ask how one understands which the correct elements are to describe a reaction process, if one does not know in detail the structure of the initial and final states? In a nutshell: how can one understand reaction without knowing structure

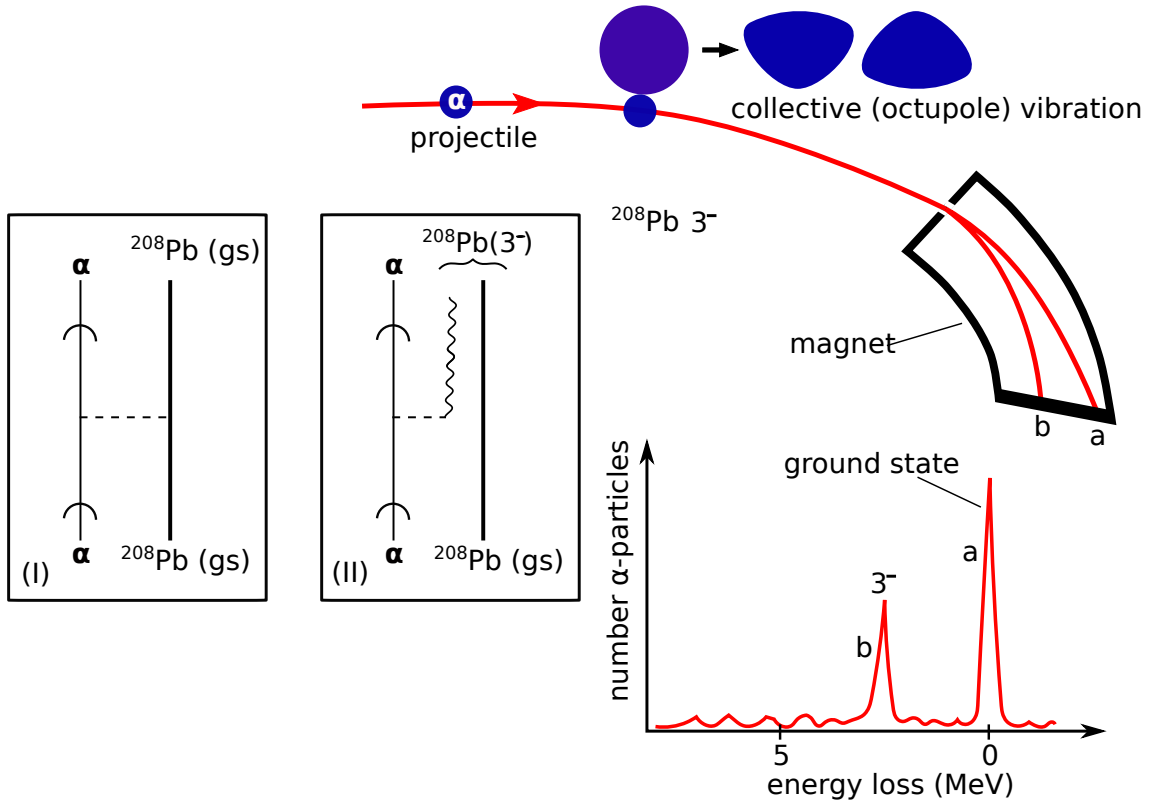


Figure 2.1.1: (color online) Schematic representation of: **elastic** a (population of the ground state), and **inelastic** b (population lowest octupole vibration at 2.62 MeV) processes associated with the reaction $^{208}\text{Pb}(\alpha, \alpha')^{208}\text{Pb}^*$ (for more details see Sect. 2.3 and App. 2.A). In the inset (I) a schematic Nuclear Field Theory (reaction plus structure) (NFT(r+s)) diagram describing the elastic process (potential scattering, dashed horizontal line) is displayed (see e.g. Broglia et al. (2016) and refs. therein). The α -projectile moving in the continuum is represented by an arrowed (curved) line. From the measurement of the elastic differential cross section one can deduce the partial wave phase shifts (Appendix 2.C). In the inset (II) a schematic NFT(r+s) diagram describing the inelastic excitation (see Fig. 2.C.1) of the low-lying octupole vibration (wavy line) of ^{208}Pb by the action of the transient field created by the α -particle on the target (horizontal dashed line) is given. Outgoing α particles are deflected in a spectograph and recorded in a detector. The corresponding excitation function is given in the lowest part of the figure.

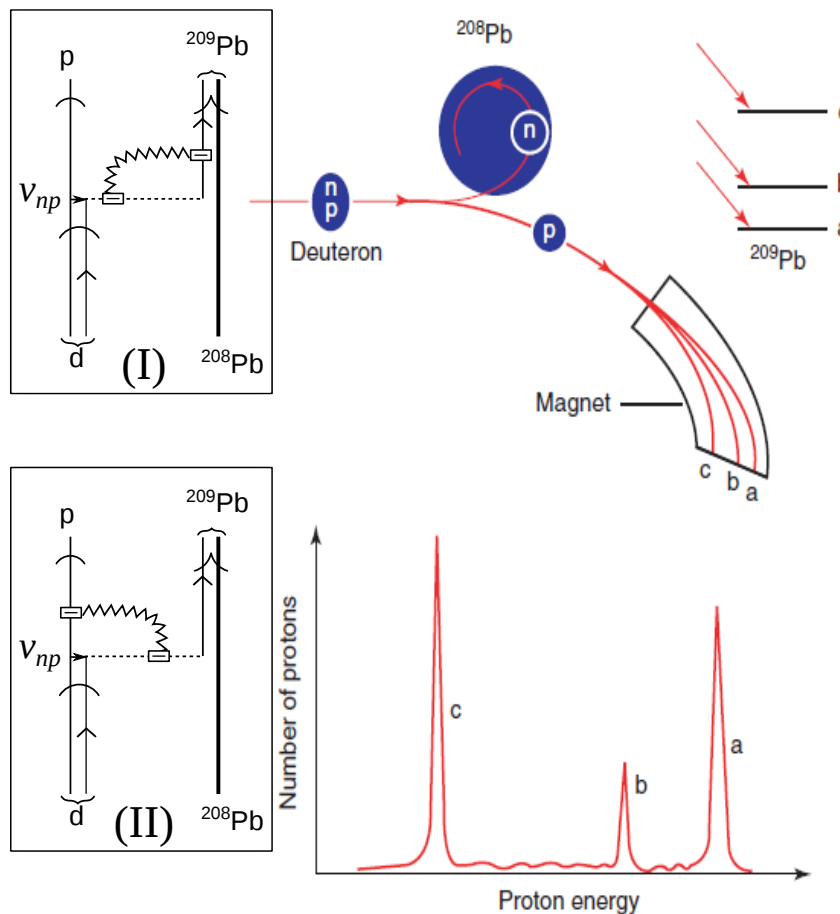


Figure 2.1.2: (Color online) Schematic representation of the one–nucleon transfer reaction $^{208}\text{Pb}(d, p)^{209}\text{Pb}$ populating valence single–particle states of ^{209}Pb . In the inset a schematic NFT($r+s$) diagram describing the process is shown. Curved arrowed lines describe the projectile d (deuteron) and outgoing particle p (proton) moving in the continuum. The short horizontal arrowed line labeled v_{np} represents the proton–neutron interaction inducing the transfer process (dashed horizontal line) while the open dashed rectangle indicates the Particle Recoil Coupling (PRC) vertex. That is, the coupling of the relative motion to the recoil process described in terms of a jagged line (App. 2.C). This information is carried out in the center of mass system by the outgoing particles in the final channel. Within this context the jagged line is involved in a virtual process (insets (I) and (II)). The energy and momentum of the outgoing proton reflects the recoil, the Q –value of the reaction and the excitation energy of the final state as analyzed in the magnet and recorded in the particle detector (a,b,c).

(eyes without object)? Vice versa, how can one understand what the elements needed for a correct

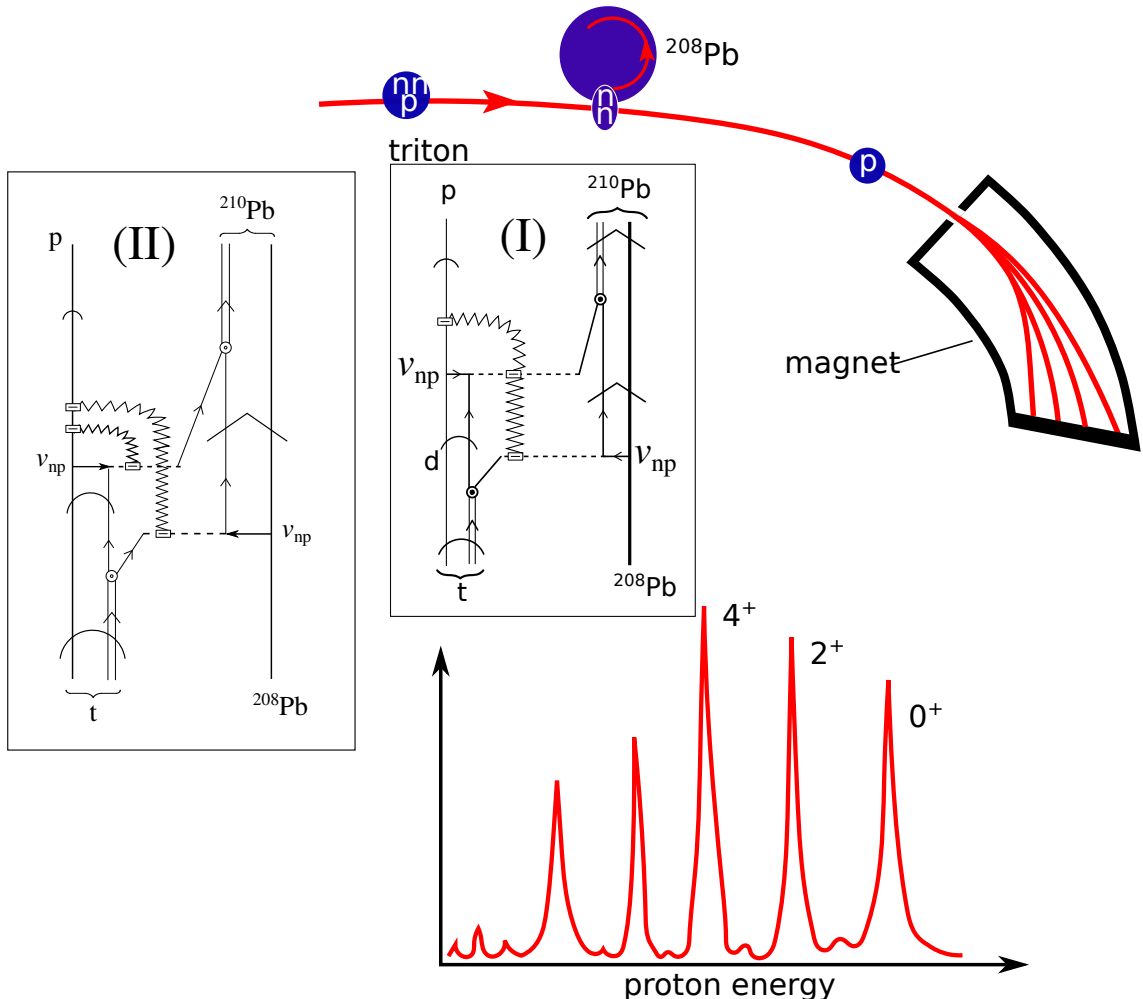


Figure 2.1.3: (Color online) Schematic representation of the two-nucleon transfer reaction $^{208}\text{Pb}(t, p)^{210}\text{Pb}$ process populating the ground state 0^+ , and two particle excited states 2^+ and 4^+ . That is, monopole, quadrupole and hexadecapole pair addition modes (multipole pairing vibrations) of ^{208}Pb (App. 7.F; see also Brink and Broglia (2005) Sect. 5.3.1 p. 108). In the inset (I) a $\text{NFT}(r+s)$ diagram of the (successive) transfer process is displayed. The jagged line brings information to the outgoing nuclei in the exit channel (CM system), of the change in scaling in the asymptotic outgoing waves with respect to the incoming ones, concerning the different mass partitions (recoil) of summed value $2m$ (App. 2.C; concerning the apparent non-linearity that is the direct coupling of two recoil modes, this can be avoided drawing the process as shown in inset (II); see also Sect. 2.B.3), this information is carried out to the detector by the outgoing proton.

Echoing Heisenberg's requirement⁶ that no concept enters the quantal description of a physical system which has no direct relation to experiments, and Landau's findings that a weakly excited state of a quantal many-body system may be regarded as a gas of weakly interacting elementary modes of excitation⁷, Bohr, Mottelson⁸ and coworkers developed a unified description of the nuclear structure. In particular, a Nuclear Field Theory (NFT)⁹ in terms of Feynman diagrams describing the behavior of quasiparticles, vibrations and rotations, and of their couplings both in 3D¹⁰ – as well as in gauge¹¹ – and other “abstract” spaces, which had close connections with direct nuclear reactions¹². Within this context one gives in Figs. 2.1.1–2.1.3 (insets) schematic representations of *unified NFT diagrams of structure and reactions (NFT(s+r))*¹³, which microscopically describe the variety of structure and reaction processes in terms of Feynman diagrams in a basis of elementary modes of excitation. That is, in the present case in which the target is a closed shell system, a particle-hole (inelastic scattering), one-particle (single-particle stripping) and two-particle (Cooper pair transfer) modes.

In inset (I) of Fig. 2.1.1 a diagram describing elastic scattering is shown, while in inset (II) a NFT(r+s) diagram describing the inelastic excitation of the low-lying octupole vibration of ^{208}Pb is displayed. A pointed (curved) arrow on a line indicates propagation of a nucleon inside the projectile or in the target nucleus (in the continuum with asymptotic waves). An up (down) pointing arrowed line indicates a nucleon (nucleon-hole) moving above (in) the Fermi sea. The horizontal dashed line represents the action of the mean field or of the bare interaction (see also Fig. 2.2.1), while the solid dot stands for the particle-vibration coupling vertex in the case of particle-hole collective modes.

In the insets of Fig. 2.1.2 a NFT(r+s) diagrams describing the process $^{208}\text{Pb}(d, p)^{209}\text{Pb}$ are schematically shown. A standard pointed arrowed line indicates the neutron moving with the proton in the deuteron (double, curve arrowed, line), or around the (assumed, for simplicity, inert) ^{208}Pb core (bold face line). The jagged curve represents the recoil mode coupling the intrinsic and the relative mo-

description of the structure of levels is, if one does not know how to observe them (specific probe), how to bring that information to the detector?. In other words, how can one understand structure without knowing reaction (object without eyes)? The answer to both questions is that one cannot.

⁶Heisenberg (1949).

⁷Landau (1941).

⁸Bohr (1964), Bohr and Mottelson (1969), Bohr (1976), Mottelson (1976), Bohr and Mottelson (1975), Bohr et al. (1958) and references therein.

⁹Bès et al. (1974); Broglia et al. (1976); Bohr and Mottelson (1975); Bès and Kurchan (1990); ? and refs. therein.

¹⁰Nilsson (1955); Bohr and Mottelson (1975) and refs. therein. See also Broglia (2019b).

¹¹Bohr et al. (1958); Belyaev (1959); Högaasen-Feldman (1961); Bès and Broglia (1966); Bjerregaard et al. (1966); Broglia and Riedel (1967); Bohr and Mottelson (1975).

¹²Alder et al. (1956), Alder and Winther (1975), Broglia and Winther (2004); concerning the general development of direct nuclear reactions see Austern (1970), Jackson (1970), Satchler (1980), Satchler (1983), Brink (1985), Glendenning (2004); Thompson and Nunes (2009), and refs. therein.

¹³Broglia (1975); Broglia and Winther (2004); Potel et al. (2013a); Broglia et al. (2016).

tion¹⁴, thus accounting for the mass partition and the change in scaling between entrance and exit channel distorted waves. The corresponding momentum mismatch being taken care of by a Galilean transformation (recoil effects)¹⁵. Because one is working in the center of mass (CM) system, the jagged curve can transfer the information of momentum mismatch to either the residual nucleus (inset (I)) or to the outgoing particle, i.e. the proton (inset (II)). Horizontal short arrowed lines stand for the proton–neutron (nucleon–nucleon) bare interaction inducing transfer¹⁶. It is of notice that choosing in an appropriate way the (post or prior) representation to describe the reaction process (energy conservation), one can evidence the single-particle mean field or the proton–neutron interaction as inducing the transfer process¹⁷.

In Fig. 2.1.3 a schematic representation of the $^{208}\text{Pb}(t, p)^{210}\text{Pb}$ process is given. In the insets a schematic NFT(r+s) diagram describing the $^{208}\text{Pb}(t, p)^{210}\text{Pb}$ process is shown. The dineutron moving in the triton and around the ^{208}Pb core, (pair addition mode) is represented by a double arrowed line. Each individual transferred neutron is indicated with a single arrowed line. The curved arrows on the triton and on the proton indicate motion in the continuum with incoming and outgoing asymptotic waves, respectively. The pointed arrow encompassing the pair addition mode and the core ^{208}Pb , indicate intrinsic (structure) motion. In selecting this NFT diagram the assumption was made, following the results of detailed calculations, that the main contribution to the process arises from the successive transfer of the nucleons. Two jagged curves are shown. One connecting the first and the second transfer process at the particle–recoil mode coupling vertex (PRCV, dashed open square), in keeping with the fact that the channel $^{209}\text{Pb}+d$ has no asymptotic waves. The second one emerges from the second PRCV and carries the mismatch information associated with a transfer of mass $2m$ to either the outgoing proton (not shown) or residual nucleus ^{210}Pb (CM description; see App. 2.C, in particular paragraph after Eq. (2.C.40))¹⁸. Within this context, see also inset (II).

It is of notice that the successive transfer of neutrons described in insets (I) and (II) can be related to the successive tunneling of pairs of electrons involved in the Josephson effect¹⁹, in particular in connection with what is known as direct current effect (dc effect; see Sect. 4.7, in particular the discussion following Eq. (4.7.1)).

As discussed in the following Chapters, Cooper pairs are extended objects, the fermionic partners being correlated over distances much larger than nuclear dimensions (correlation length $\xi \approx 15 \text{ fm} \gg R_0 \approx 6 \text{ fm}$ ($A = 120$)). Because the single particle potential acts on these pairs as a rather strong external field,

¹⁴See App. 2.C.

¹⁵See App. 2.C; also Ch. 6, in particular Figs. 6.C.1 and 6.C.2.

¹⁶For more details see Figs. 2.10.2 and 2.10.3, see also App. 6.C.

¹⁷See e.g. Fig. 5.1.1 and App. 6.C.

¹⁸Concerning the apparent non linearity of the recoil process (two jagged lines associated with a single PRCV, we refer to Fig. 2.B.2 and associated discussion).

¹⁹Josephson (1962); Anderson (1964b). See also Brink and Broglia (2005) App. L and refs. therein.

this correlation length feature is not obvious in structure calculations, becoming apparent in reaction calculations.

Elementary modes of excitation, that is single-particle and collective motion, are the way nuclei react to external probes, and thus closely connected with the physical observables. Namely, absolute transition probabilities and absolute differential cross sections. Within this context, bare elementary modes of excitation already contain an important fraction of nuclear many-body correlations, thus making the diagonalization of the nuclear Hamiltonian leading to dressed elementary modes of excitation, a low-dimension problem. For example, in terms of $10^2 \times 10^2$ matrices, each matrix element containing already much physical insight into nuclear structure at large²⁰.

In keeping with the fact that all the nuclear degrees of freedom are exhausted by those of the nucleons, and that the different reactions, that is elastic, Coulomb and inelastic excitations, as well as one- and two-particle transfer reactions project particular, but somewhat overlapping components of the total wavefunction, the nuclear elementary modes of excitation give rise to an overcomplete, non orthogonal, Pauli principle violating basis, both concerning structure as well as reactions. Nuclear Field Theory²¹, provides the conserving sum rules protocol to diagonalize these couplings to any order of perturbation theory, also infinite if so required for specific processes (see Sect. 2.7). The dressed physical elementary modes resulting from the interweaving of the bare modes are orthogonal to each other and fulfill Pauli principle, providing a microscopic solution to the many-body nuclear problem. NFT(s+r) diagrams²² (see e.g. Figs. 2.10.3 (a) and 2.10.5) embody predictions in terms of absolute differential cross sections and transition probabilities. They can be directly compared with the observables whose values are obtained by studying the nuclear system with the variety of ever more precise and varied arsenal of experimental probes (see e.g. Fig. 7.1.3).

At this point a proviso or two are in place. The original elementary modes of nuclear excitation due to their interweaving, melt together into effective fields²³. Each of them display properties which reflect that of all the others, their individuality resulting from the actual relative importance of each one of them. What one calls a physically (clothed) particle is only partially to be associated with that particle field alone. It is also partially to be associated with the vibrational fields (surface, density, spin²⁴, pairing²⁵, etc. vibrational modes), because they are in in-

²⁰Illuminating discussion with B. A. Brown during the 15th International Conference on Nuclear Reactions Mechanisms (Varenna, June 2018) regarding this, and related issues are gratefully acknowledged (RAB).

²¹Bès et al. (1974), Bès et al. (1976b), Bès et al. (1976c), Bès et al. (1976a), Bès and Broglia (1975), Broglia et al. (1976), Bès et al. (1975a), Mottelson (1976), Bès and Broglia (1977), Bortignon et al. (1977), Bortignon et al. (1978), Broglia and Winther (2004), Reinhardt (1975), Reinhardt (1978a), Reinhardt (1978b), Reinhardt (1980). See also Broglia (2019b).

²²Broglia (1975); Broglia and Winther (2004); Broglia et al. (2016).

²³Within this context see Dickhoff and Van Neck (2005) and references therein.

²⁴Bertsch and Broglia (2005) Chs. 6,7,8.

²⁵Brink and Broglia (2005) Ch. 5.

teraction through the particle–vibration coupling vertices²⁶. And conversely, what one calls a nuclear vibration can couple to particle–hole (in the case of a surface vibration), two–particle (in the case of a pair addition) or a two–hole (in the case of a pair removal) configurations.

Thus nucleons (fermions) couple to vibrational modes (bosons) and, eventually, can reabsorb them returning to the original state. The same is true concerning bosons degrees of freedom and their coupling to fermions. The outcome of such processes, namely the dressed physical elementary modes of excitation, is closely connected with the renormalization program of quantum electrodynamics (QED)²⁷ implemented in NFT in terms of Feynman diagrams. Renormalized NFT, i.e (NFT)_{ren} implies that the intermediate, virtual states clothing the elementary modes of excitation, are fully dressed²⁸.

The specific experimental probes of the bare elementary modes of nuclear excitation reveal only one aspect, in most cases likely the most important one of the physical (clothed) elementary modes. Renormalized NFT reflects the physical unity of low–energy nuclear research requiring the melting not only of elementary modes of excitation but also of structure and reaction theory, let alone of the different experimental techniques developed to study the atomic nucleus. In other words the need for a complete set of experimental probes to reveal the multi faceted properties of clothed elementary modes of excitation resulting from the implementation of a consistent program of structure and reactions (within this context see Fig. 2.11.1).

As seen from the contents of the present monograph, the accent is set at relating theoretical predictions with experimental findings, through the unification of structure and reactions. In particular the unification of pairing and two–nucleon transfer processes, where the two subjects are blended together, which is what happens in nature. Once the NFT rules to work out the variety of elements (spectroscopic and, with the help of them, reaction amplitudes) have been laid out and/or the pertinent literature refer to, concrete embodiments are provided and eventual absolute cross sections and transition probabilities calculated and confronted with the experimental data.

As already stated in the previous chapter, an essential test theory has to pass is connected with some operator identities which are known as sum rules²⁹. An overcomplete (non-orthogonal) set of basis states, like that provided by elementary modes of excitation, will violate sum rules. For example, a hole and a pair addition is non orthogonal to a particle and a surface ($p - h$) vibration (Sect. 2.5; also 2.7.4). As we shall see, taking into account the couplings between these modes following the rules of NFT (see Sect. 2.7) eliminates such violations.

A similar situation is found in the case of e.g. two-nucleon transfer, because the

²⁶Bohr and Mottelson (1975).

²⁷Feynman (1975); Schwinger (2001).

²⁸Barranco et al. (2017), see also Broglia et al. (2016), see also Ch. 7.

²⁹See e.g. Bohr and Mottelson (1975), Bertsch and Broglia (2005) Ch. 4, Bortignon et al. (1998), Chs. 3 and 8 and refs. therein.

single-particle states in projectile and target are, as a rule, non-orthogonal. Taking into account such overlaps one can remove the overcounting (see Sects. 4.2, 6.2.9 and Apps. 6.C).

2.2 Sum rules revisited

A quantitative measure of the overcompleteness of the elementary modes of excitation basis is provided by the use of exact and of empirical sum rules that the observables (cross sections) associated with the variety of probes to which the nucleus is subject, have to fulfill. Examples of the first type are given by the Thomas-Reiche-Kuhn (TRK) sum rule^{30,31}, and by a sum rule which relates one- with two-particle transfer processes³². Within the framework of simple, but still physically relevant models, connected with inelastic scattering processes, we refer to Sect. 2.7.2 in general and Eq. (2.7.44) in particular. And concerning one-particle transfer sum rules we refer to Sect. 2.7.3 and Eq. (2.7.82). For examples of the second type (empirical, physical sum rules), we refer to sum rules associated with two-nucleon transfer reactions (TNTR)³³ discussed in Sect. 2.2.1 and³⁴ in Sect. 7.4.1.

Physically, they provide information concerning: 1) the maximum amount of energy which the quantal system can absorb from a beam of photons (γ -rays) shined on it; 2) the total two-nucleon transfer cross section (ring area fraction of the geometrical reaction cross section) exhausted by the final ($A \pm 2$) states populated in the transfer process.

In other words, these sum rules provide a quantitative measure of the single-particle subspace the quantal system under study, in particular the nucleus, uses to correlate particle-hole excitations and thus induce the antenna-like motion of protons against neutrons or, to correlate pairs of nucleons moving in time reversal states around the Fermi energy, leading to a, static or dynamic, sigmoidal distribution of the associated pair ($\nu, \bar{\nu}$) level occupancy around the Fermi energy.

As shown in Sect.. 1.7, the TRK sum rule can, in the nuclear case, be written as

$$S(E1) = \sum_{\alpha} \left| \langle \alpha | F | \tilde{0} \rangle \right|^2 (E_{\alpha} - E_0) = \frac{9}{4\pi} \frac{\hbar^2 e^2}{2m} \frac{NZ}{A}, \quad (2.2.1)$$

where $|\alpha\rangle$ labels a complete set of excited dipole states which can be reached acting with the dipole operator F on the initial correlated vacuum state $|\tilde{0}\rangle$. Each bosonic

³⁰Bohr and Mottelson (1975), Sect. 6-4.

³¹Bertsch and Broglia (2005), Chapter 3, in particular Sect. 3.3.

³²Bayman and Clement (1972); Lanford (1977).

³³Broglia et al. (1972).

³⁴Within this context, the absolute two-nucleon transfer cross section populating the ground state of a superfluid nucleus is proportional to the number of Cooper pairs contributing to the nuclear condensate (modulus squared). This quantity is rather stable along a pairing rotational band, in keeping with the fact that the “intrinsic” $|BCS\rangle$ -state of the deformed system in gauge space, is essentially the same for all members of the band. This fact is at the basis of a newly found physical sum rule (Potel et al. (2017); see also Ch. 7 Sect. 7.4.1).

elementary mode of excitation provides, within the harmonic approximation, a specific contribution to the total zero point fluctuations of the ground state (ZPF, see introduction to Sects. 2.7 and 2.9), that is,

$$\langle \tilde{0}|F^2|\tilde{0}\rangle = \frac{\hbar\omega}{2C_\alpha} = \frac{\hbar^2}{2D_\alpha} \frac{1}{\hbar\omega_\alpha}. \quad (2.2.2)$$

Where C_α and D_α are the restoring force and the inertia parameters of the collective mode of frequency ω_α ($= (C_\alpha/D_\alpha)^{1/2}$). The label α indicates the quantum numbers characterizing the vibrational mode. For example, in the case of surface multipole vibrations $\alpha \equiv (\beta = 0, \lambda\mu)$.

As mentioned in the previous chapter, ZPF perturb the static nucleon Fermi sea, that is the set of occupied levels of the mean field potential (Fig. 2.2.2)

$$U(r) = \int d\mathbf{r}' \rho(r') v(|\mathbf{r} - \mathbf{r}'|), \quad (2.2.3)$$

inducing virtual particle–hole excitations (k, i , i.e. $\epsilon_i \leq \epsilon_F$ and $\epsilon_k > \epsilon_F$, Eqs. (2.2.5) and (2.4.1); see Fig. 2.2.2). In the above equation, $\rho(r)$ is the nuclear density and v is the nuclear two–body interaction.

Because $|\langle \alpha | F | \tilde{0} \rangle|^2$ measures the probability with which the state $|\alpha\rangle$ is populated, the α –sum in (2.2.1) gives a measure of the maximum energy that the nucleus can absorb from the γ –beam. It is customary to measure $|\langle \alpha | F | \tilde{0} \rangle|^2$ in single–particle (sp) units (Weisskopf (W) units)

$$\begin{aligned} B_{sp}(E1; j_1 \rightarrow j_2) &= \frac{3}{4\pi} e_{E1}^2 \langle j_1 \frac{1}{2} 1 0 | j_2 \frac{1}{2} \rangle^2 \times \langle j_2 | r | j_1 \rangle^2, \\ &\approx \frac{0.81}{4\pi} A^{2/3} e_{E1}^2 \text{ fm}^2 = B_W(E1), \end{aligned} \quad (2.2.4)$$

where $(e)_{E1} = (N/A)e$ for protons and $(e)_{E1} = -(Z/A)e$ for neutrons, in keeping with the fact that the motion of a nucleon is associated with a recoil of the rest of the nucleus. This is because the center of mass of the system remains, in an intrinsic excitation³⁵, at rest.

Within this context is that independent–particle motion in general and the existence of a mean field ((MF), Hartree–Fock (HF) solution) in particular can be viewed as the most collective of all nuclear phenomena³⁶, in keeping with the fact that,

$$\begin{aligned} S(E1) &= \sum_n |\langle n | F | \tilde{0} \rangle|^2 (E_n - E_0) \\ &= \sum_{k,i} |\langle k, i | F | \text{gs}(\text{MF}) \rangle|^2 (\epsilon_k - \epsilon_i), \end{aligned} \quad (2.2.5)$$

³⁵See, e.g. Broglia et al. (2016) App. G and references therein.

³⁶Mottelson (1962).

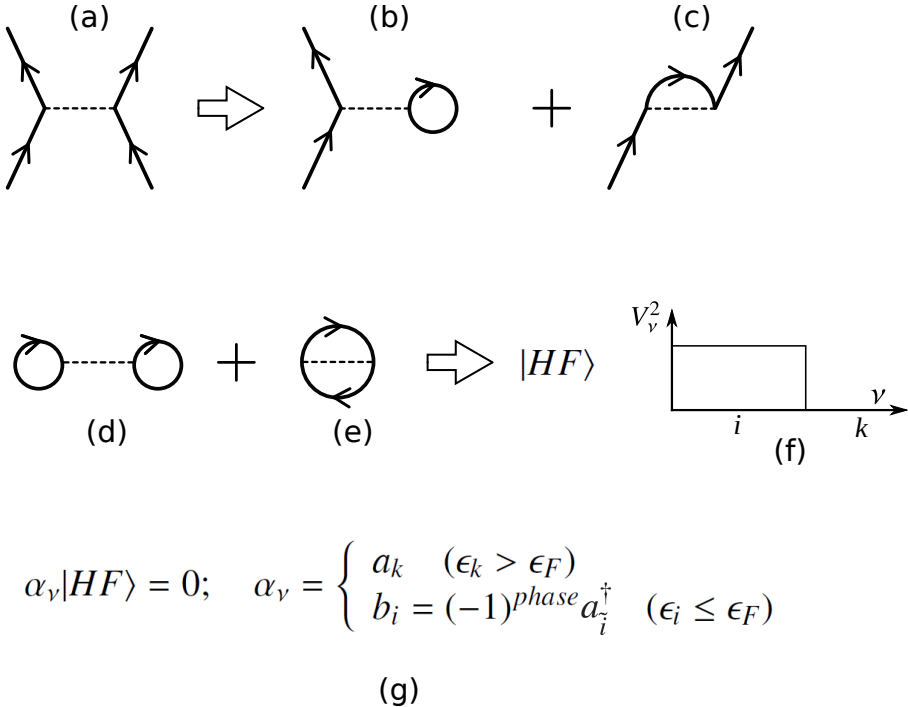


Figure 2.2.1: Schematic representation of the processes characterizing the Hartree–Fock ground state (single-particle vacuum), in terms of Feynman diagrams. (a) nucleon–nucleon interaction through the bare (instantaneous) NN –potential. (b) Hartree mean field contribution. (c) Fock mean field contribution. (d,e) ground state correlations (ZPF) associated with the Hartree and Fock processes. (f) There is, in HF (mean field) theory, a complete decoupling between occupied and empty states, labeled i and k respectively, and thus a sharp discontinuity at the Fermi energy of the occupation probability, from the value of 1 to 0. (g) This decoupling allows for the definition of two annihilation operators: a_k (b_i) particle (hole) annihilation operators, implying the existence of hole (antiparticle) states ($b_i^\dagger |HF\rangle$) with quantum numbers time reversed to that of particle states, (for details see e.g. Brink and Broglia (2005) App. A). In other words, the $|HF\rangle$ ground (vacuum) state is filled to the rim (ϵ_F) with N nucleons. The system with $(N - 1)$ nucleons can, within the language of (Feynman’s) field theory, be described in terms of the degrees of freedom of that of the missing nucleon (hole–, antiparticle state). Such a description is considerably more economic than that corresponding to an antisymmetric wavefunction with $(N - 1)$ spatial and spin coordinates (\mathbf{r}_i, σ_i) . Within the above scenario, a stripping reaction $N(d, p)(N + 1)$ can be viewed as the creation of a particle state ($a_k^\dagger |HF\rangle = |k\rangle$) and that of a pickup reaction $N(p, d)(N - 1)$ as that of a hole state ($b_i^\dagger |HF\rangle \equiv |\tilde{i}\rangle$).

provided $|\tilde{0}\rangle$ contains the ground state correlations mentioned in connection with Eq. (2.2.2), and that $|\text{gs(MF)}\rangle$ those associated with $\Delta x \Delta p \geq \hbar$ (see Fig. 2.2.1). In

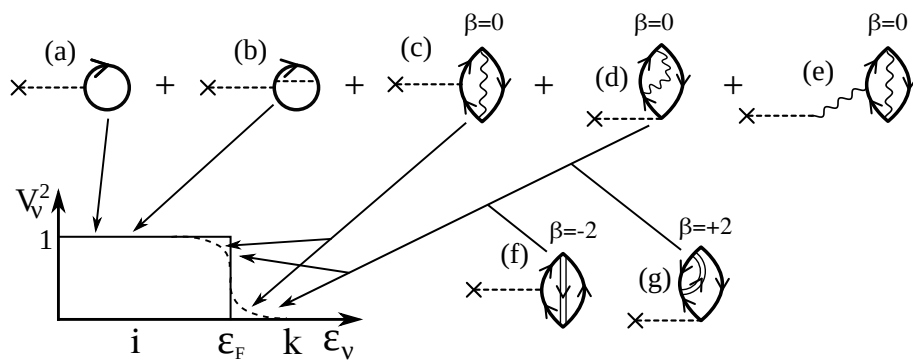


Figure 2.2.2: Schematic representation of the Fermi distribution. The sharp, continuous line drawn step function schematically represents the Hartree–Fock occupation numbers. The associated nuclear density measured with the help of an external field (cross attached to a dashed line) through processes of type (a) (Hartree: H) and (b) (Fock: F) is expected to display a diffusivity of the order of the strong force range. Zero Point Fluctuations (ZPF) associated with collective particle–hole vibrations, i.e. processes with transfer quantum number $\beta = 0$ (Bohr (1964)) and shown in (c), (d) and (e), and with pairing vibrations, i.e. pair removal (graph (f)) and pair addition modes (graph (g)), smooth out the occupation numbers around the Fermi energy (dashed curve) and lead to a nuclear density of larger (dynamical) diffusivity and radius than that associated with HF (see Sect. 1.8). One- and two-particle strengths which in this (mean field) approximation are found in a single A -mass system are, as a result of ZPF ($\beta = 0, \pm 1, \pm 2$) distributed over a number of nuclei ($A, A \pm 1, A \pm 2$) (see also App. 5.H, Fig. 5.H.1).

other words, provided

$$|HF\rangle = |gs(MF)\rangle = \prod_{i \in occup} a_i^\dagger |0\rangle \quad (2.2.6)$$

where $|0\rangle$ is the particle vacuum state ($a_j|0\rangle = 0$), and $\Gamma_\alpha|\tilde{0}\rangle = 0$, Γ_α^\dagger being the creation operator of a dipole Random Phase Approximation (RPA) correlated particle-hole like mode ($\Gamma_\alpha^\dagger = \sum_{ki} X_{ki}^\alpha a_k^\dagger a_i + Y_{ki}^\alpha (a_k^\dagger a_i)^\dagger$)³⁷.

Relation (2.2.5) is a consequence of the fact that $S(E1)$ is proportional to the average value of the double commutator $[[H, F], F]$ in the ground state of the system ($|\tilde{0}\rangle$ or $|HF\rangle$). Because F is a function of only the nucleon coordinates, and assuming $v(|\mathbf{r} - \mathbf{r}'|)$ to be velocity independent, the only contribution to the double commutator arises from the (universal) kinetic energy term of the Hamiltonian. Thus, the value (2.2.1) is model independent. In other words, this value does not depend on the correlations acting among the nucleons, but on the number of them participating in the motion and on their mass (inertia) as testified by the fact that $\sum_\alpha \hbar\omega_\alpha \left(\frac{\hbar\omega_\alpha}{2C_\alpha} \right) = \sum_\alpha \left(\frac{\hbar^2}{2D_\alpha} \right)$. *It is then not surprising that the TRK sum rule was used in the early stages of quantum mechanics, to determine the number of electrons in atoms.*

2.2.1 Empirical two-nucleon transfer sum rules

Let us now consider two-nucleon transfer (pairing) processes. The absolute cross sections associated with the population of final states can be set essentially on equal footing with respect to each other concerning Q -value and recoil effects, with the help of empirically determined global functions³⁸. In this way, the theoretical absolute cross section associated with e.g. the $A(t, p)A + 2$ population (we assume N to be even) of the n th final state of spin J and parity $(-1)^J$ can be written as

$$\sigma^{(n)}(J = L, Q_0) = \left| \sum_{j_1 \geq j_2} B(j_1 j_2; J_n) S(j_1 j_2; L, Q_0) \right|^2, \quad (2.2.7)$$

where

$$S^2(j_1 j_2; L, Q_0) = \sigma(j_1, j_2; L, Q_0), \quad (2.2.8)$$

the quantity $\sigma(j_1, j_2; L, Q_0)$ being the absolute two-nucleon transfer cross section associated with the two particle configuration $(j_1, j_2)_L$. The quantity

$$B(j_1 j_2; J_n) = \left\langle \Phi_{J_n}(\xi_{A+2}) \left| \Phi_{J_i=0}(\xi_A) \frac{[a_{j_1}^\dagger a_{j_2}^\dagger]_J}{[1 + \delta(j_1, j_2)]^{1/2}} \right. \right\rangle, \quad (2.2.9)$$

³⁷Bertsch and Broglia (2005), Ch. 4, and Brink and Broglia (2005) Ch. 8, Sect. 8.3, Bohr and Mottelson (1975) Sect. 6-5 h. As can be seen from Fig 2.C.1, in the RPA approximation no scattering vertices (Fig. 2.3.1) are present. Consequently, the coupling between one- and two- phonon states is, within this (harmonic) approximation, not possible.

³⁸see Broglia et al. (1972)

is the two-nucleon spectroscopic amplitude, $\Phi_{J_i=0}(\xi_A)$ being the wavefunction describing the ground state of the initial nucleus, $\Phi_{J_n}(\xi_{A+2})$ that of the final state, ξ labeling the relative radial and spin intrinsic coordinates. Assuming A to be a closed shell system, and $J = 0$, one can write

$$|0_n^+\rangle = \sum_{j_1 \geq j_2} c^{(n)}(j, j; J = 0) |j, j; J = 0\rangle, \quad (2.2.10)$$

where $n = 1, 2, 3, \dots$ labels the final nucleus states of spin and parity $J^\pi = 0^+$ in increasing energy order. Making use of the completeness relation of the coefficients $c^{(n)}(j, j; J = 0)$ one obtains,

$$\sum_n \sigma^{(n)}(J = L = 0, Q_0) = \sum_j \sigma(j, j; L = 0, Q_0). \quad (2.2.11)$$

The above equation parallels (2.2.5), aside from the fact that the Q -value effect is, in connection with (2.2.5), analytically dealt with, while $\sigma(\{Q\})$ is a functional of Q . The complete separation of the relative and intrinsic motion coordinates taking place in e.g. (2.2.5) is in keeping with the fact that in elastic and inelastic processes the mass partition is equal in both entrance and exit channels. Thus, the intrinsic (structure) and the relative motion (reaction) coordinates can be treated separately. This is not the case for transfer processes, both intrinsic and reaction coordinates being interweaved through the recoil process (particle-recoil mode coupling (dashed open square), jagged curves (recoil mode), see e.g. Fig. 2.1.3 as well as Figs. 2.10.2 and 2.10.3; see also Sect. 2.6).

A parallel with the discussion carried out in connection with (2.2.4) regarding the TRK sum rule, can be drawn defining two-particle units as,

$$\sigma_{2pu}^{max}(A, L, Q_0) = \max [\sigma(j_1, j_2; L, Q_0)], \quad (2.2.12)$$

where $\max[\]$ indicates that the largest two-particle absolute cross section in the single-particle subspace considered (*hot orbital*), is to be considered. In this way one can write the relation (2.2.11) in dimensionless units. Another quite useful, this time exact, two-particle transfer sum rule has been introduced in the literature³⁹, which relates two-nucleon stripping and pick-up reactions cross sections, with single-particle transfer processes⁴⁰.

The above arguments carried out for nuclei around closed shells can, equally well, be applied to the case of open shell nuclei, making use of the corresponding two-nucleon spectroscopic amplitudes⁴¹. In particular, in the case of independent pair motion, i.e. the BCS mean field solution of the pair problem, the summed spectroscopic pair transfer amplitudes, each term weighted with $(j + 1/2)^{1/2}$, is

³⁹Bayman and Clement (1972). In this connection, and within the context of a schematic model, see Eq. (2.7.79) and subsequent discussion.

⁴⁰Lanford (1977)

⁴¹See App. 2 of Broglia et al. (1973), Yoshida (1962).

given by

$$\begin{aligned}\alpha'_0 &= \langle BCS(N+2) | P'^\dagger | BCS(N) \rangle \\ &= \sum_j \frac{2j+1}{2} U'_j(N) V'_j(N+2),\end{aligned}\quad (2.2.13)$$

where⁴²

$$P'^\dagger = \sum_{m>0} a'_{jm}^\dagger a'_{jm}^\dagger = \sum_j \sqrt{\frac{2j+1}{2}} T'^\dagger(j^2(0)), \quad (2.2.14)$$

creates two nucleons in time reversal states,

$$T'^\dagger(j^2(0)) = \frac{[a'_j^\dagger a'_j^\dagger]^0}{\sqrt{2}}, \quad (2.2.15)$$

being the two-nucleon (Cooper pair) transfer operator. The associated expectation value in the $|BCS\rangle$ ground state is the two-nucleon transfer spectroscopic amplitude

$$B(j^2(0), N \rightarrow N+2) = \sqrt{\frac{2j+1}{2}} U'_j(N) V'_j(N+2). \quad (2.2.16)$$

The ZPF associated with pairing vibrations, similar to those associated with particle-hole-like excitations, smooth out the sharp HF Fermi surface (Fig. 2.2.2). The number of pairs in each level participating in this smoothing is $(2j+1)/2$ their occupancy being measured by the simultaneous, and apparently contradictory, property of being a particle (amplitude V'_j) and a hole (amplitude U'_j). In other words α'_0 measures the number of pairs of nucleons (Cooper pairs) participating in the smoothing out of the Fermi surface⁴³ and thus can be viewed as the spectroscopic amplitude associated with the population of pairing rotational bands in two-nucleon transfer processes. It is expected that α'_0 depends weakly on N and is about conserved along a pairing rotational band. Because $d\sigma(gs(N) \rightarrow gs(N+2))/d\Omega \approx |\alpha'_0|^2$, conservation is also expected for these absolute cross section. But in this case, it is a conservation of a physical character, and not a mathematical one (see Sect. 7.4.1). If one finds that at the angle where $L = 0$ two-nucleon transfer differential cross sections have the first maximum, as a rule close to 0° in (t, p) or (p, t) reaction, the two nucleon strength function is dominated by a single peak, that associated with the ground state, and this is so for a number of isotopes differing in mass number by two, it can be concluded that one is in presence of a pairing rotational band (see Figs. 3.1.3 and 3.1.4). This is one of the reasons why (2.2.13) can

⁴²The primed quantities are the particle creation operators and BCS occupation amplitudes referred to the intrinsic system of reference in gauge space (see Fig. 1.4.1; also Sect. 3.4 and 4.8). See also Potel et al. (2013b).

⁴³Schrieffer (1964); Potel et al. (2017) and refs. therein.

be viewed as the order parameter of the nuclear superfluid phase and, in keeping with (2.2.14), two-nucleon transfer reaction regarded as the specific tool to probe pairing in nuclei.

Because in a finite many-body system like the nucleus, quantal fluctuations in general and those of particle number in particular, are much larger than in bulk systems, a dynamic parallel to α_0 (Eq. (2.2.13)) can be defined at profit (see Fig. 3.5.7)⁴⁴.

2.3 Fluctuations and damping

The Hamiltonian describing a system of independent particles and of collective surface vibrations can be written as⁴⁵ (see previous chapter)

$$H = H_M + H_{coll} + H_c, \quad (2.3.1)$$

where

$$H_M = T + U \quad (2.3.2)$$

is the mean field Hamiltonian, sum of the single-particle kinetic energy and of the self-consistent potential $U = f(\rho)$, functional of the density. That is,

$$U = U_H + U_x, \quad (2.3.3)$$

where

$$U_H = \int d\mathbf{r}' \rho(r') v(|\mathbf{r} - \mathbf{r}'|), \quad (2.3.4)$$

is the Hartree potential, and

$$U_x = - \sum_{i(\epsilon_i \leq \epsilon_F)} \varphi_i^*(\mathbf{r}') v(|\mathbf{r} - \mathbf{r}'|) \varphi_i^*(\mathbf{r}), \quad (2.3.5)$$

is the exchange (Fock) potential. It is well established that the nucleus can react collectively to external sollicitations. In particular the nuclear surface⁴⁶ can vibrate in certain normal modes which, in the harmonic approximation can be described as⁴⁷

$$H_{coll} = \frac{\hat{\Pi}_\alpha^2}{2D_\alpha} + \frac{C_\alpha}{2} \hat{\alpha}^2, \quad (2.3.6)$$

where,

$$\hat{\alpha} = \sqrt{\frac{\hbar\omega_\alpha}{2C_\alpha}} (\Gamma_\alpha^\dagger + \Gamma_\alpha), \quad (2.3.7)$$

⁴⁴See also Potel et al. (2017).

⁴⁵Bohr and Mottelson (1975); Brink and Broglia (2005)

⁴⁶We consider in the present section only this type of collective modes

⁴⁷Concerning the dimension of the parameters C_α and D_α see App. 2.A, Eq. (2.A.10) and subsequent discussion. See also Sect. 5.A.1 of App. 5.A, Eq. (5.A.19) and following comments.

is the collective coordinate, $\hat{\Pi}_\alpha$ being the corresponding conjugate momentum, while $\Gamma_\alpha^\dagger(\Gamma_\alpha)$ is the creation (annihilation) operator of the corresponding quanta. Microscopically, these modes can be calculated in the RPA as correlated particle-hole excitations⁴⁸. The particle-vibration coupling Hamiltonian can be written as,

$$H_c = \kappa \hat{\alpha} \hat{F}, \quad (2.3.8)$$

with

$$\hat{F} = \sum_{\nu_1 \nu_2} \langle \nu_1 | F | \nu_2 \rangle a_{\nu_1}^\dagger a_{\nu_2}, \quad (2.3.9)$$

and

$$F = -\frac{1}{\kappa} R_0 \frac{\partial U(r)}{\partial r} Y_{LM}^*(\hat{r}). \quad (2.3.10)$$

It is of notice that κ characterizes the relationship between potential and density, of the mode considered. The self-consistent value is ($\langle F \rangle = \alpha$)⁴⁹,

$$\kappa = \int R_0 \frac{\partial U}{\partial r} R_0 \frac{\partial \rho}{\partial r} r^2 dr. \quad (2.3.11)$$

Both the coupling constant and the potential U are negative, for attractive fields. H_c embodies the coupling of the motion of a single-nucleons with the collective vibrations of the surface, with a matrix element (see Fig. 2.3.1)

$$V_{\nu, \alpha'} = \langle n_\alpha = 1, \nu' | H_c | \nu \rangle = \Lambda_\alpha \langle \nu' | F | \nu \rangle, \quad (2.3.12)$$

where

$$\Lambda_\alpha = \kappa \sqrt{\frac{\hbar \omega_\alpha}{2C_\alpha}} \sim \frac{\kappa \beta_\alpha}{\sqrt{2L_\alpha + 1}}, \quad (2.3.13)$$

is the particle-vibration coupling strength, while β_α is the (dynamic) deformation parameter. For didactical purposes we shall assume in this section that $\beta_L^2 \ll \beta_L$ and thus treat H_c perturbatively. It is of notice that confronted with processes requiring to be summed to infinite order of perturbation theory, this can be done without much difficulty (see e.g. App. 5.B).

Making use of the single-particle energies obtained by solving (2.3.2) and of the particle vibration matrix element (2.3.12) the microscopic, RPA description of the collective states can be obtained by solving the dispersion relation displayed in the inset of Fig. 2.3.1.

Making the ansatz that the physical (clothed) single-particle states results from the coupling to only surface vibrations, the Hamiltonian (2.3.1) can be regarded as being complete to describe the elementary modes of excitation and their couplings. Adding to (2.3.1) the terms describing the spin, spin-isospin, etc. particle-hole modes, as well as those associated with multipole pairing vibrations (see Sect. 3.5

⁴⁸Bohm and Pines (1951); Pines and Bohm (1952); Bohm and Pines (1953); see also Bertsch and Broglia (2005), Ch. 4 and refs. therein.

⁴⁹Bohr and Mottelson (1975) Sect. 6-5 h.

as well as caption to Fig. 2.1.3), i.e. pair addition and pair subtraction modes (with $\lambda^\pi = 0^+, 2^+, 4^+ \dots$, and eventually $1^-, 3^- \dots$, concerning 1^- see App. 7.F), and the corresponding coupling terms, and diagonalizing perturbatively the resulting Hamiltonian, will lead to the physical single-particle states of spherical normal systems (nuclei around close shells). For spherical open-shell nuclei effects arising from the coupling to the condensate⁵⁰ will somewhat affect the actual value of the results, e.g. the energy of the two-quasiparticle phonon states⁵¹.

2.3.1 Fluctuation and damping

To second order in the particle-vibration coupling strength one finds⁵²,

$$\begin{aligned} & \left(-\frac{\hbar^2}{2m} \nabla_r^2 + U_H(r) \right) \varphi_j(r) + \int d^3r' U_x(\vec{r}, \vec{r}') \varphi_j(\vec{r}'), \\ & + (\Delta E_j + iW_j) \varphi_j(\vec{r}) \\ & \approx \left(-\frac{\hbar^2}{2m_k} \nabla_r^2 + U''_H(r) + \Delta E''_j + iW''_j \right) \varphi_j(\vec{r}), \\ & = \varepsilon_j \varphi_j(\vec{r}), \quad \left(U''_H = \frac{m}{m_k} U \text{ and similarly for } \Delta E'' \text{ and } W'' \right), \end{aligned} \quad (2.3.14)$$

where $m_k = \left(1 + \frac{m}{\hbar^2 k} \partial U_x / \partial k \right)^{-1} \approx 0.7m$ is the k -mass⁵³, while

$$\Delta E_j(\omega) = \lim_{\Delta \rightarrow 0} \sum_{\alpha'} \frac{V_{\nu, \alpha'}^2(\omega - E_{\alpha'})}{(\omega - E_{\alpha'})^2 + (\frac{\Delta}{2})^2}, \quad (2.3.15)$$

and

$$W_j(\omega) = \lim_{\Delta \rightarrow 0} \sum_{\alpha'} \frac{V_{\nu, \alpha'}^2}{(\omega - E_{\alpha'})^2 + (\frac{\Delta}{2})^2}, \quad (2.3.16)$$

are the real and imaginary contributions to the self-energy calculated in second order of perturbation theory, where ω is the single-particle energy⁵⁴ (see Fig. 2.3.2; note that in this case $E_{\alpha'} = \epsilon_{\nu_2} + \hbar\omega_\alpha$).

⁵⁰see Bès and Kurchan (1990)

⁵¹see Barranco et al. (2004)

⁵²see e.g. Brink and Broglia (2005), Mahaux et al. (1985) and references therein. See also Bernard and Giai (1981).

⁵³This is in keeping with the fact that the non-local component of the mean field can be parametrized at profit as $0.4E$, where $E = |(\hbar^2 k^2 / 2m) - \epsilon_F|$ (Perey and Buck (1962)) see also Sect. 2.10.1.

⁵⁴Given a Hamiltonian H_c , the contribution to the energy in second order perturbation theory is

$$\Sigma_\nu(\omega) = \sum_{\alpha'} \frac{V_{\nu, \alpha'}^2}{\omega - E_{\alpha'}},$$

where $|\alpha'\rangle \equiv |n_\alpha = 1, \nu'\rangle$ are the intermediate states which can couple to the initial single-particle

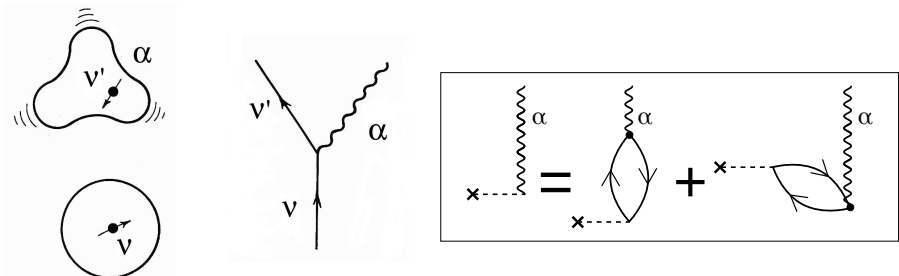


Figure 2.3.1: Schematic representation of the process by which a nucleon excites vibrations of the nuclear surface through the particle–vibration coupling vertex. In the inset, the graphical RPA dispersion relation which determines the properties of the collective mode α , e.g. the low–lying octupole vibration of ^{208}Pb , is displayed.

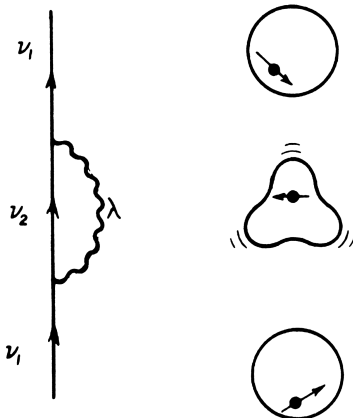


Figure 2.3.2: Self-energy (polarization, PO, see e.g. Fig. 7.2.2 and App. 5.H) graph renormalizing a single-particle. Time ordering leads to the corresponding correlation diagram (CO) (see e.g. Fig. 2.4.2 diagrams (e) and (f), as well as Figs. 5.B.1 and 5.C.2; within this context see also Brink and Broglia (2005) Fig. 9.2 of this reference).

state ν . Note that the expression above is not well defined, in that the energy denominator may vanish. As a rule, textbooks in quantum mechanics deal with such a situation by stating that accidental degeneracies are to be eliminated by diagonalization. Now, this is not a real solution of the problem, because it does not contemplate the case where there are many intermediate states with $E_{\alpha'} \approx \omega$. In other words, where the particle can decay into a more complicated (doorway-) states $|\alpha'\rangle$ (Feshbach (1958)), starting in the single-particle level ν of energy ω , without changing its energy (real process). This is a typical dissipative (diffusion) process, and has to be solved by direct diagonalization (see Fig. 2.3.5 and App. 5.B). Another way around, is to extend the function $\sum_\nu(\omega)$ into the complex plane ($E_{\alpha'} \rightarrow E_{\alpha'} + \frac{i\Delta}{2}$) thus *regularizing the divergence* through a coarse grain approximation, determining the finite contributions and then taking the limit for $\Delta \rightarrow 0$ (Eqs.(2.3.15) and (2.3.16)). The resulting complex potential (*optical potential* from the *complex dielectric function* of optics), parametrizes in simple terms the shift of the centroid of the single-particle state and its finite lifetime.

For many purposes ΔE can be treated in terms of an effective mass

$$m_\omega = m(1 + \lambda), \quad (2.3.17)$$

where

$$\lambda = -\frac{\partial \Delta E}{\partial \omega}, \quad (2.3.18)$$

is the *mass enhancement factor*, while

$$Z_\omega = m/m_\omega,$$

measures the single-particle content (discontinuity) at the Fermi energy.

Consequently, Eq.(2.3.14) can be rewritten as

$$\left(-\frac{\hbar^2}{2m^*} \nabla_r^2 + U'_H + iW'(\omega) \right) \varphi_j(\vec{r}) = \varepsilon_j \varphi_j(\vec{r}), \quad (2.3.19)$$

with

$$m^* = \frac{m_k m_\omega}{m}. \quad (2.3.20)$$

and $U'_H = (m/m^*)U$ and similarly for W' . Because $\lambda \approx 0.4$ (i.e. the dressed single-particle m_ω is heavier than the bare nucleon, as it has to carry a phonon along or, better, move in a cloud of phonons) and $m_k = 0.7m$, $m^*/m \approx 1$ and $Z_\omega \approx 0.7$. Furthermore, due to the fact that $\hbar\omega_a \approx 2 - 2.5 \text{ MeV}$, the range of single-particle energy $E = \varepsilon - \varepsilon_F$ over which the particle-vibration coupling process displayed in Fig.2.3.2 is effective is $\approx \pm 2\hbar\omega_a \approx 4 - 5 \text{ MeV}$ around the Fermi energy (see Figs.2.3.3 and 2.3.4)

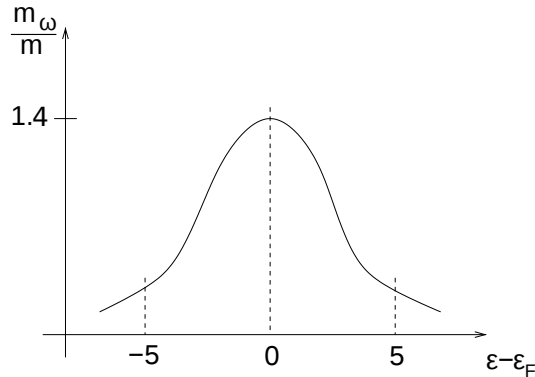


Figure 2.3.3: Schematic representation of the ω -mass as a function of the single-particle energy.

It is of notice that ΔE_j (Eq.(2.3.15)) indicates the shift of the centroid of the "dressed" single-particle state due to the coupling to the doorway states, while $\Gamma = 2W$ measures the energy range over which the single-particle state spreads due to this coupling (see Fig.2.3.5). While a large number of states contribute to

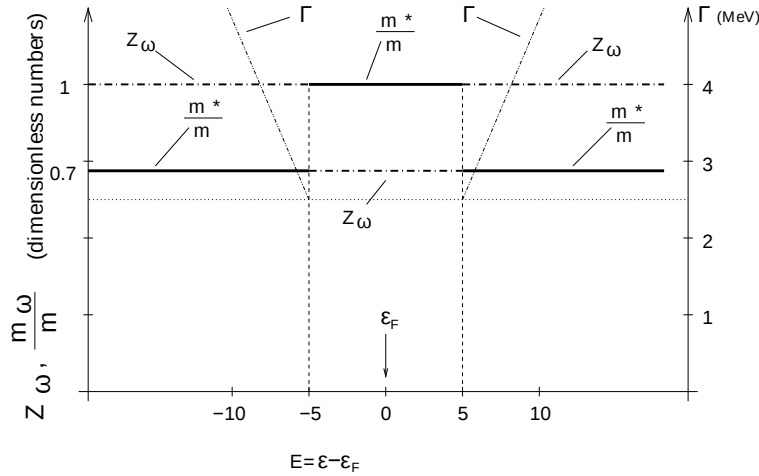


Figure 2.3.4: Schematic representation of the behaviour of m_ω/m , $Z_\omega = (m_\omega/m)^{-1}$ and Γ as a function of $E = \epsilon - \epsilon_F$.

ΔE (“off-the-energy-shell process”, i.e. intermediate, virtual processes in which energy is not conserved), only “on-the-energy-shell processes”, that is processes which conserve energy, contribute to Γ . In fact

$$\lim_{\Delta \rightarrow 0} \frac{\Delta}{(\omega - E_{\alpha'})^2 + \left(\frac{\Delta}{2}\right)^2} = 2\pi\delta(\omega - E_{\alpha'}),$$

and

$$\Gamma(\omega) \approx 2\pi\bar{V}^2 n(\omega), \quad (2.3.21)$$

where \bar{V}^2 is the average value of $V_{\nu,\alpha'}^2$, while

$$n(\omega) = \sum_{\alpha'} \delta(\omega - E_{\alpha'}), \quad (2.3.22)$$

is the density of energy-conserving states α' . Eq.(2.3.21) is known as *Fermi Golden rule*.

Assuming the distribution of single-particle levels is symmetric with respect to the Fermi energy,

$$\Delta E(\omega) = \lim_{\Delta \rightarrow 0} \sum_{\alpha'} \frac{V_{\nu,\alpha'}^2(\omega - E_{\alpha'})}{(\omega - E_{\alpha'})^2 + \left(\frac{\Delta}{2}\right)^2} = 0 \quad (2.3.23)$$

as there are equally many states pushing the state down than up in energy (see Fig.2.3.5).

In the above discussion, the imaginary potential was introduced as an approximation to the breaking of a stationary state into many, more complicated stationary states through the coupling to doorway states (Fig. 2.3.5(b)). This is the correct

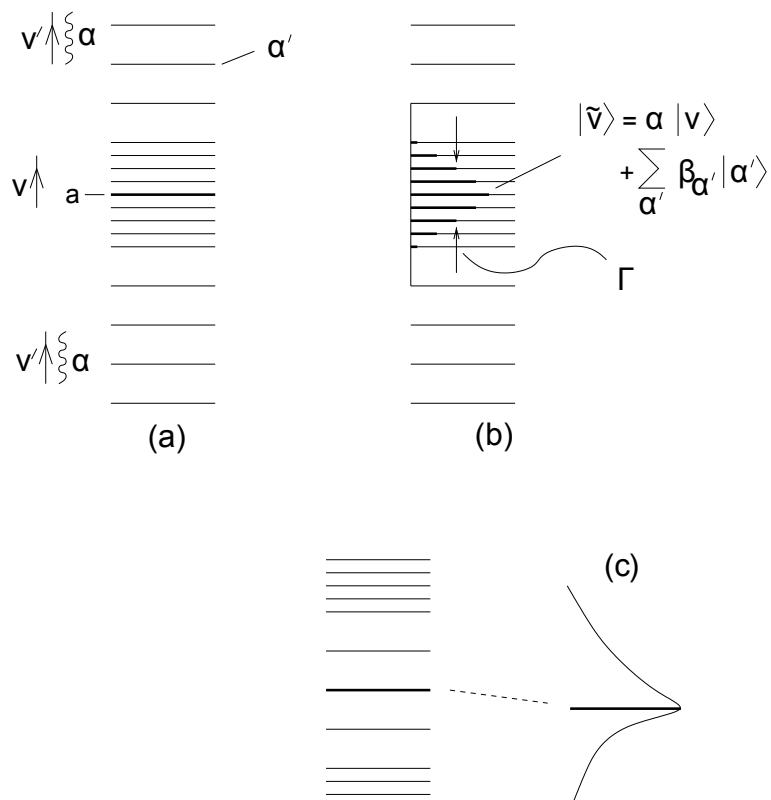


Figure 2.3.5: Schematic representation of the result of the diagonalization of H_c in a basis consisting of the single-particle states $|\nu\rangle$ and the $|\alpha'\rangle = |\nu', \alpha\rangle$ doorway states. In (c) we show a situation where there are more states $|\alpha'\rangle$ above $|\alpha\rangle$ than below.

picture to describe the coupling of a nucleon moving in a single-particle state with more complicated configurations^{55,56}. However, such a description can become quite involved. On the other hand, to account for the change of the centroid energy and of its spreading width in terms of an *optical potential* $\Delta E + iW$ is very economic and convenient. In any case Γ measures the range of energy over which the "pure" single-particle state $|\alpha\rangle$ spreads due to the coupling to the more complicated doorway states $|\alpha'\rangle$. In other words, a stationary state

$$\varphi_\nu(\vec{r}, t) = e^{i\omega t} \varphi_\nu(\vec{r}), \quad (2.3.24)$$

has a probability density

$$\int d^3r |\varphi_\nu(\vec{r}_i t)|^2 = \int d^3r |\varphi_\nu(\vec{r})|^2 = 1, \quad (2.3.25)$$

which does not depend on time. That is, if at $t = 0$, the probability that the particle is in a state ν is 1, it will have this probability also at $t = \infty$, implying an infinite lifetime. If however

$$\begin{aligned} \hbar\omega &= \varepsilon_\nu^{(0)} + \Delta E_\nu(\omega) + i\frac{\Gamma_\nu}{2}(\omega), & = \varepsilon_\nu + i\frac{\Gamma_\nu}{2}(\omega) & , (\varepsilon_\nu = \varepsilon_\nu^{(0)} + \Delta E_\nu) \\ \varphi_\nu(\vec{r}_i t) &= e^{i\frac{\varepsilon_\nu t}{\hbar}} e^{-\frac{\Gamma_\nu t}{2\hbar}}, \\ \int d^3r |\varphi_\nu(\vec{r}_i t)|^2 &= e^{-\frac{\Gamma_\nu t}{\hbar}}, \end{aligned} \quad (2.3.26)$$

implying a lifetime for the single-particle state given by

$$\tau = \Gamma_\nu/\hbar. \quad (2.3.27)$$

One may ask, how is it possible that the coupling to complicate (but still simple) states like $|\alpha'\rangle = |n_\alpha = 1, \nu'\rangle$ made out of a nucleon in the state ν' and a one phonon state of quantum numbers α , can explain the damping of a single-particle state lying 8-10 MeV from the Fermi energy ε_F , where the density of levels is expected to be consistent? This is because the Hamiltonian given in Eq. (2.3.1) contains the basic physics needed to describe the dressed single-particle motion as far as surface modes are concerned (within this context see the discussion carried out following Eq. (2.3.13)). Couplings to more complicated states go through a hierarchy of couplings. In other words, the variety of couplings should first go through the coupling

⁵⁵See however Caldeira and Leggett (1981), Caldeira and Leggett (1983) and refs. therein.

⁵⁶To be noted that if we spread the strength of a stationary quantal state in a number of doorway stationary states over an energy range Γ (of the order of few MeV in the case of the GDR), and set all components in phase at $t = 0$, they will essentially be out of phase at time $t = \tau = \hbar/\Gamma$. In other words, each component will behave independent of each other and the original correlated state, created at $t = 0$ with probability 1 essentially ceases to exist at $t = \tau$. This does not imply that each of the incoherent members of the original coherent state cannot γ -decay at a much later stage ($\Gamma_{\gamma_0}/\Gamma \lesssim 10^{-2}$), see Bortignon et al. (1998). Discussions with B. Herskind on this issue are acknowledged.

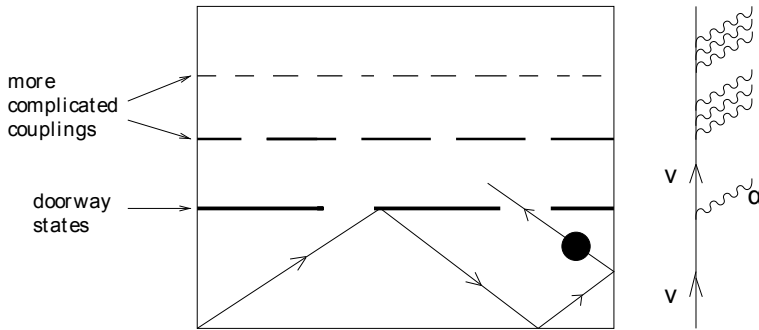


Figure 2.3.6: Schematic representation of the different levels of couplings leading to the damping of a single-particle state. It is essentially the first doorway coupling which controls the probability the ball (black dot) reflecting elastically on the walls of the box has to remain passed the first compartment.

to states of type $|\alpha'\rangle$ which act as proper doorway states (see Fig.2.3.6)⁵⁷. Summing up, in the nuclear case, the *doorway coupling provides the basic mechanism to break the single-particle strength*, while higher-order couplings essentially *fill in valleys* (see Fig.2.3.7).

In the case of the $1s_{1/2}$ orbital of ^{40}Ca ($\epsilon - \epsilon_F = -8$ MeV), simple estimates⁵⁸ lead to $\bar{V}^2 \approx 0.3$ MeV for the coupling to an $L = 2$ phonon, and $n(\epsilon_F) \approx 2$ MeV⁻¹. Consequently

$$\Gamma \approx 4\text{MeV}, \quad (2.3.28)$$

in overall agreement with the experimental findings (see Fig. 2.3.8).

The result given in Eq.(2.3.28) is a particular example of the general (empirical) result (see Fig. 2.3.4)⁵⁹.

$$\Gamma_{sp}(E) = \begin{cases} 0.5|E| & |E| > 5 \text{ MeV}, \\ 0 & E \leq 5 \text{ MeV}, \end{cases} \quad (2.3.29)$$

where

$$E = |\epsilon - \epsilon_F|. \quad (2.3.30)$$

2.3.2 Induced interaction

A nucleon close to the Fermi energy which, by bouncing inelastically off the nuclear surface excites a collective mode moving in the process to another, or remaining in the same state, has no other choices than to continue in such a state, or to reabsorb the vibration at a later instant of time (self-energy, Fig. 2.3.2). In the

⁵⁷Feshbach (1958).

⁵⁸Mahaux et al. (1985)

⁵⁹Bertsch et al. (1983)

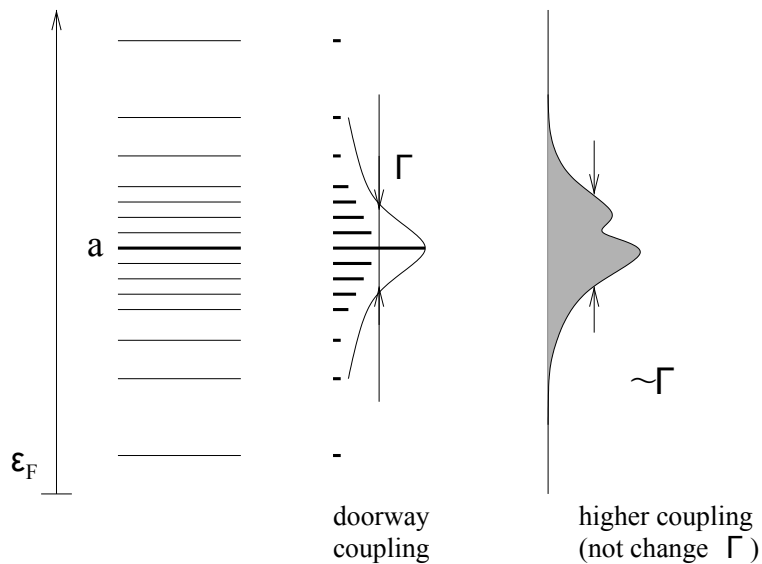


Figure 2.3.7: Schematic representation of the breaking of a single particle state $|a\rangle$ (heavy black horizontal line) through the coupling to doorway states ($|\alpha'\rangle = |n_\alpha = 1, \nu'\rangle$; thin horizontal lines) and eventually to increasingly more complicated (many-particle)–(many-hole) configurations.

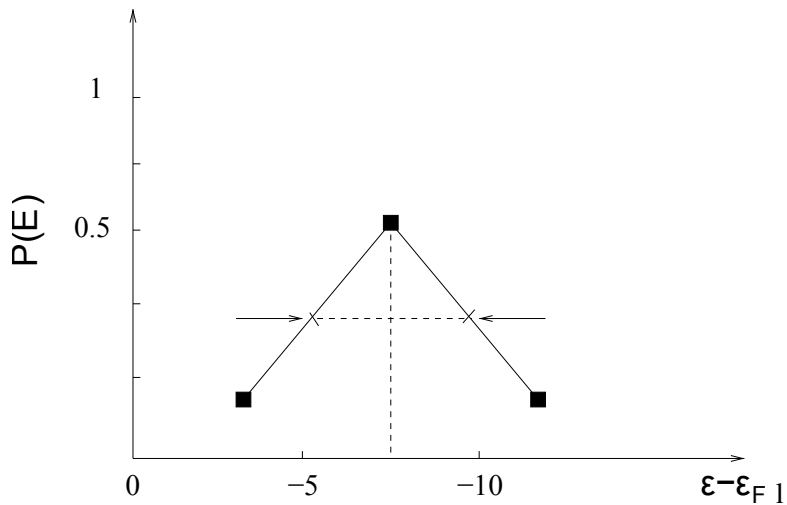


Figure 2.3.8: Schematic representation of the experimental strength function (solid squares) associated with the $2s$ state of ^{40}Ca . Also indicated is the full width at half maximum (FWHM) (after Mahaux et al. (1985) Fig. 2.12).

presence of another nucleon, the excited collective vibration by one nucleon may be absorbed by the second one (Fig.2.3.9), the exchange of a vibration leading to an (induced) interaction.

Simple estimates of this induced interaction leads, in the case of ^{210}Pb , that

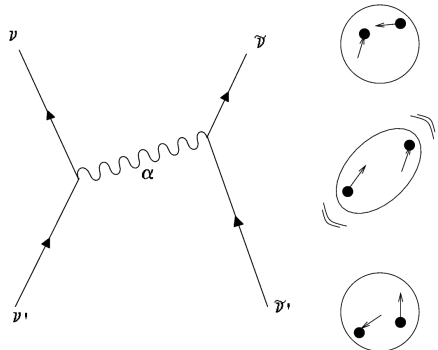


Figure 2.3.9: Schematic representation of the exchange of phonons between nucleons.

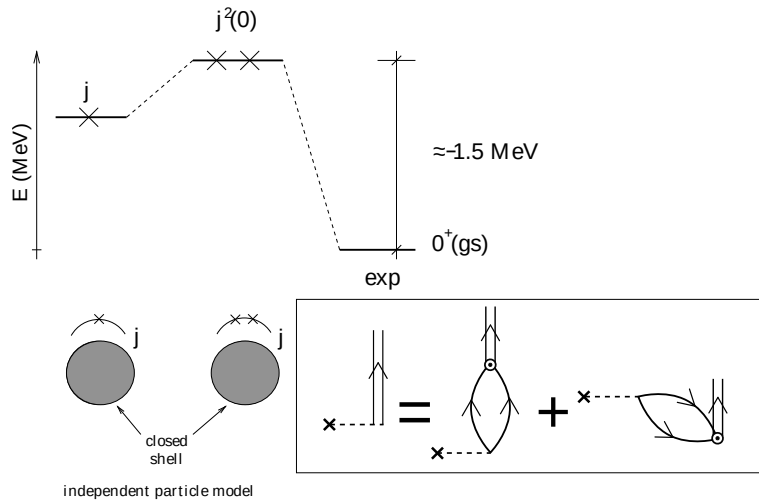


Figure 2.3.10: Schematic representation of the predictions of the independent particle model for one- and two-particles outside closed shell, in comparison with the experimental findings (e.g. for the case of ^{210}Pb , where $j = g_{9/2}$). In the inset, the graphical RPA dispersion relation of the monopole pair addition mode of ^{208}Pb , i.e. $|^{210}\text{Pb(gs)}$) is shown.

is two neutrons above the $N = 126$ closed shell, to correlation energies for pairs of particles moving around it and coupled to angular momentum $J^\pi = 0^+$ of ≈ -1.5 MeV (see Fig. 2.3.10), when α is summed over the different multipolarities ($\lambda^\pi = 2^+, 3^-, 5^-$, label α in Fig. 2.3.9), and about half that value if one takes into account the fact that $Z_\omega \approx 0.7$ for each of the interacting particles. From this result one can conclude that the pairing interaction induced by the process depicted in Fig. 2.3.9, renormalizes in an important way the bare, $NN(^1S_0)$ -short range pairing interaction. This issue is taken up in detail later on, in particular in connection with exotic halo nuclei (see e.g. Fig. 2.10.1 and Sect. 3.6.1). Concerning nuclei lying along the stability valley, see next section.

2.4 Well funneled nuclear structure landscape

Let us now return to the subject of the finite overlap existing between the elementary modes of nuclear excitation⁶⁰. That is, to the fact that one is working in a basis of states which contains already much of the physics one likes to describe, but which has the shortcoming of being overcomplete. An orthogonalization protocol, like a generalized Gram–Schmidt procedure, but leading to an effective field theory, where the different modes melt to some extent together, is called for.

A similar situation is found in the case of transfer processes in general, and of two-nucleon transfer in particular. One can work out the associated transfer amplitude by orthogonalizing, making use of second order perturbation theory, the single-particle wavefunctions of target and projectile. This can be done both within the semiclassical approximation (see App. 6.C, and Sect. 2.6) or the DWBA (Sect. 4.2 and 6.1; see also Sect. 4.7 in connection with weak coupled metallic superconductors and of the Josephson effect).

Because the coupling between elementary modes of excitation is proportional to their overlap, and in keeping with the fact that mean field theory is the natural starting point of nuclear structure and reaction calculations, overcompleteness of the basis is tantamount to the appearance of linear couplings between quasiparticles and collective modes⁶¹, which in the case of reactions corresponds to the recoil modes⁶².

Basis orthogonalization thus implies the diagonalization of the bare NN -interaction (four-point vertices) and of the associated particle-vibration coupling Hamiltonian H_c (three-point vertices). The rules to do so have been casted into a graphical effective field theory, namely the Nuclear Field Theory. In it, the free fields are to be calculated in the HF (HFB) approximation (particle (quasiparticle)) and in the RPA (QRPA) (vibrations). These elementary modes of excitation interact through the particle-vibration coupling vertices, while particles can also interact through

⁶⁰ And of which the particle–vibration coupling discussed above is a consequence.

⁶¹ See Sect. 2.3 and App. 2.A in the case of surface modes and Sect. 2.7.4 in the case of the simultaneous treatment of surface and of pairing modes; see also Fig. 2.7.10.

⁶² See e.g. Figs. 2.1.2, 2.1.3 and 2.10.2–2.10.6. Also Figs. 6.C.1, 6.C.2, 5.1.1 and App. 2.C.

four-point vertices (NN -bare interaction)⁶³.

The NFT rules for evaluating the effect of these couplings between fermions and bosons involve a number of restrictions concerning initial and intermediate states as compared with the usual rules of perturbation theory that are to be used in evaluating the effect of the original (bare) nucleon–nucleon interaction properly renormalized by the exchange of vibrations between nucleons. This is in keeping with the fact that the collective modes contain, from the start, the correlations arising from forwards and backwards going particle–hole ($\beta = 0$) as well as particle–particle ($\beta = +2$) and hole–hole ($\beta = -2$) bubbles, where β is the transfer quantum number⁶⁴. Furthermore these (quasi) bosons are not elementary but composite fields, made out of pairs of fermions, and thus subject to the Pauli principle.

The general validity of NFT rules have been demonstrated by proving the equivalence existing, to each order of perturbation theory, between the many–body finite nuclear system propagator calculated in terms of Feynman diagrams involving only the fermionic degrees of freedom i.e. explicitly respecting Pauli in a complete and not overcomplete basis, also known as Feynman–Goldstone propagator, and the propagator constructed in terms of Feynman diagrams involving fermion and phonon degrees of freedom (NFT Feynman diagrams) in the case of a general two–body interaction and an arbitrary distribution of single–particle levels⁶⁵.

Concerning the actual embodiment of NFT one can recognize the practical difficulties of respecting the corresponding rules. This is in keeping with the fact that at present there is not a single bare, well behaved, low- k NN -force (eventually with $3N$ and higher order corrections) with which it is possible to generate a mean field (Eq. (2.2.3), also Fock potential see Fig. 2.2.1 (c)) to determine the single-particle states and, by introducing a periodic time-dependence with the constrain

$$\delta U(r) = \int d\mathbf{r} \delta\rho(r') v(|\mathbf{r} - \mathbf{r}'|), \quad (2.4.1)$$

calculate the collective modes associated with the variety of particle–hole ($\beta = 0$; density, spin, isospin, etc.) and pairing ($\beta = \pm 2$; monopole and multipole pair addition and pair subtraction) modes. If this was possible, one could then diagonalize, within the framework of NFT and to the desired order of perturbation, also infinite order, the resulting particle–vibration couplings, and thus obtain renormalized quantities which can be directly compared with the data. In other words, a real physical *ab initio* calculation could be done, resulting in a single, common ground state which, corrected with the corresponding ZPF lead eventually to the “exact” ground state concerning the degrees of freedom considered, as well as to properly dressed modes and interactions.

On the other hand, implementation of the NFT rules (renormalization)⁶⁶ have

⁶³In connection with the reaction processes one finds again four–point (e.g. the proton-neutron interaction in the (p, d) reaction) and three-point vertices (e.g. particle-recoil coupling vertices).

⁶⁴Bohr (1964).

⁶⁵Bès and Broglia (1975) and Bès et al. (1976a); see also Baranger (1969) and the lecture notes of McFarlane (1969).

⁶⁶Broglia et al. (2016).

been carried out, making use of the bare Argonne v_{14} potential, and of Skyrme like SLy4⁶⁷ forces (or Saxon–Woods parametrizations and $m_k \approx 0.7m$) to determine the mean field and spin vibrational channels, and of multipole–multipole forces with self–consistent coupling constants for the variety of density vibrational channels.

The resulting predictions are, as a rule, able to provide, together with the specific reaction software, in particular COOPER and SINGLE, an overall account of “complete” sets of experimental data, obtained with the help of Coulomb, inelastic and one– and two–nucleon transfer data, able to map out the nuclear structure and reaction landscape⁶⁸. Similar, but more accurate results are obtained by freely parametrising the bare potential so that the dressed particle reproduce experiment⁶⁹ (Table 2.4.1, last column). Summing up, the nuclear structure description given by the elementary modes of nuclear excitation approach within the framework of NFT, provides a unified description of the variety of observables. At the same time, each cross section or transition probability is connected to essentially all others.

To illustrate this point we bring together in this Section one– and two–particle transfer with the rest of the observables for the open–shell nucleus ^{120}Sn lying along the stability valley. From this example one can see that: 1) it is possible to predict, with few free parameters, most of them strongly constrained by empirical input, the experimental findings within a 10% level of accuracy; 2) the nuclear landscape, as it emerges from NFT based on elementary modes of excitation and of their interweaving through the particle–vibration coupling, is well funneled (Fig. 2.4.1, see also table 2.4.1), its minimum essentially coinciding with the global minimum resulting from the empirical renormalization⁷⁰ choice of basic quantities (m_k , strength bare pairing, properties of few low–lying collective ($p-h$) modes and pairing vibrations) An important proviso concerning the above parlance is that one considers a group of homogeneous nuclei as e.g. open shell spherical superfluid nuclei (like the Sn isotopes), or nuclei around closed shells (like $^{208,209,210}\text{Pb}$, ^{209}Bi , ^{210}Po , etc., or $^{10,11,12}\text{Be}$, $^{9,10,11}\text{Li}$, etc.)⁷¹. In connection with light exotic halo nuclei we refer to Sect. 2.10 of the present Chapter and to Sects. 5.2.2, 7.2 and 7.6.

Let us now comment on Fig. 2.4.1. In it, the root mean square deviations $\sigma(x)$ (see Table 2.4.1) between theoretical predictions and experimental values of the different structural properties which “completely” characterize ^{120}Sn are displayed. The calculations involve the island of open–shell superfluid nuclei $^{118,119,120,121,122}\text{Sn}$. The root mean square deviations are displayed in Fig. 2.4.1 (see also Table 2.4.1) as a function of the pairing coupling constant G (referred to $G_0 = 0.22$ MeV), the k –mass m_k ($(m_k)_0 = 0.7m$), the dynamical quadrupole deformation parameter β_2 ($(\beta_2)_0 = 0.13$) and in general of x (x_0), measured with respect to the minimum value $\sigma_{\min} = \sigma(x_{\min})$, displayed in the interval $0.5 \leq x/x_0 \leq 1.5$ and normalized according to $0 \leq N(\sigma(x) - \sigma_{\min}) \leq 1$. The curves represent

⁶⁷Chabanat et al. (1997)

⁶⁸Idini et al. (2015, 2014); Potel et al. (2013a).

⁶⁹Barranco et al. (2017). This approach parallels renormalization in QED (see Sect. 7.6).

⁷⁰See Sect. 7.5.

⁷¹Within this context we refer to the conclusions of Idini et al. (2015).

(color online): the deviation of the pairing gap associated with the $h_{11/2}$ orbital ($\Delta_{h_{11/2}}(G/G_0)$ (solid black curve); $\Delta_{h_{11/2}}(m_k/(m_k)_0)$ (dotted blue curve); $\Delta_{h_{11/2}}(\beta_2/(\beta_2)_0)$ (dashed green curve)); the deviation of the quasiparticle spectrum ($E_{qp}(G/G_0)$ (dashed brown curve); $E_{qp}(\beta_2/(\beta_2)_0)$ (dash-dotted green curve); the deviation of the $h_{11/2} \otimes 2^+$ multiplet splitting $E_{h_{11/2} \otimes 2^+}(\beta_2/(\beta_2)_0)$ (dash-dotted purple curve); the deviation of the centroid position of the $d_{5/2}$ strength function $S_{d_{5/2}}(\beta_2/(\beta_2)_0)$ (dash-dotted cyan curve); the deviation of the width of the $d_{5/2}$ strength function $S_{d_{5/2}}(\beta_2/(\beta_2)_0)$ (dash-dotted pink curve); the deviation of the quadrupole transition strength $B(E2)(\beta_2/(\beta_2)_0)$ (dashed orange curve). For an overview see⁷² Fig. 2.11.1. The remarkable feature of Fig. 2.4.1 is the fact that, in spite of the fluctuations of the results typical of finite many-body systems, they clearly define a funnel in which all minima fall within a narrow window of x/x_0 values (1 ± 0.2). This is a novel and unexpected result, which can be considered as an emergent property of a description of structure and reactions carried out in a basis of elementary modes of excitations, interacting through the PVC and PRC vertices according to the NFT rules.

The concept of a well funneled energy landscape is easy to understand in the case in which the number of particles $N \rightarrow \infty$ (thermodynamic limit). For example, a swing will have a very simple and well funneled potential energy landscape. A similar concept which still retains the classical viewpoint, but now referred to the free energy of large molecules, has been used in an attempt to describe protein folding⁷³. One has hypothesized that the results of an all atom, explicit solvent classical molecular dynamic simulations can be interpret in terms of a somewhat rugged, but still well funneled free energy landscape.

When we see such a behaviour in the nuclear case, even not so well defined, and somehow imperfect, we recognize that the nucleus is, after all, not macroscopic. Concepts strictly valid for $N \rightarrow \infty$ are strongly renormalized by quantal finite size effects, in particular zero point fluctuations (ZPF, Fig. 2.4.2)⁷⁴.

In other words, it is likely that the “imperfect” nature of the nuclear structure landscape funnel, an example of which is shown in Fig. 2.4.1, embodies more ac-

⁷²For details see Idini et al. (2015).

⁷³Wolynes (2016); Wolynes et al. (2012); see also cover figure of the issue of PNAS in which this reference was published.

⁷⁴This nuclear result in turn, may be used at profit to shed light into the physics which is at the basis of protein folding. These systems are after all quantal systems, and the associated quantal fluctuations are likely to play an important role in fleeting transition states. The fact that average values and shapes of the transit-time distributions agree well with the simplest one-dimensional theory may only reflect the large uncertainties of the tunneling probabilities, small changes in the barrier’s parameters compensating for the lack of quantal phenomena, let alone the fact that being most high-dimensional models, as well as real processes, “sloppy”, their behavior depend on very few parameters (collective variables (CV), see Buchanan (2015), Transtrum et al. (2015), and references therein). It is unlikely that one or few of them are not related to quantal fluctuations. This is particularly true if one considers a NMR chemical shift biased molecular dynamic simulation, in keeping with the fact that NMR, based on the precession of nuclear spins is by its essence, a quantal phenomenon. Within this context one is reminded of α - and exotic-decay (see e.g. Ch. 7 of Brink and Broglia (2005) and references therein).

curately the physics of quantal many-body systems than that of a smooth, more pedagogical construct essentially based on potential energy, even with the entropic contribution (free energy). This is in keeping with the fact that the interaction terms (potential energy) of the Hamiltonian contain the last vestiges of Newton's conception of force or, causation, being thus too much anchored to classical mechanics⁷⁵.

Within this context we refer to Fig. 2.4.2, and to the fact that the ground state (nuclear vacuum) contains all the physics of the system in terms of virtual processes. This is demonstrated by the fact that acting on the system with the variety of probes available in the laboratory one obtains as on-shell final states, which eventually can be observed with the help of the appropriate detectors and setups, the variety of dressed (renormalized) elementary modes of excitation of the nucleus under study. In particular, diagrams (b), (c) of Fig 2.4.2 describe inelastic and two-nucleon transfer processes while diagrams (d)–(f) portray one-nucleon transfer reactions.

In all orders in the particle vibration coupling vertex ((PVC), solid dot), starting from second order (graph (f)), NFT diagrams take care of the Pauli principle acting between the quasiparticles considered explicitly (continuous curves) and those participating in the modes (double wavy lines), as well as between modes. As a consequence, self energy processes based on pure or little collective two quasiparticle excitations are screened out or eliminated.

2.5 Non-orthogonality

Let us now consider a system based on a closed shell nucleus, namely two protons moving around ^{208}Pb . The ground state of $^{210}_{84}\text{Po}_{126}$ can be viewed as the proton pair addition mode of the doubly closed shell nucleus $^{208}_{82}\text{Pb}_{126}$, mode displaying $J^\pi = 0^+$ and $\beta = +2$ (transfer-) quantum numbers. Within this framework $^{209}_{83}\text{Bi}_{126}$ is expected to be a *bona fide* proton single-particle system ($\beta = +1$), in which the $g_{7/2}, d_{5/2}, h_{11/2}, d_{3/2}$ and $s_{1/2}$ valence orbitals are occupied, the odd proton occupying, in the ground state, a substate of the $h_{9/2}$ orbital.

This picture can be specifically probed through one-proton stripping and pick up reactions, e.g. with the help of $^{210}\text{Po}(t, \alpha)^{209}\text{Bi}$ and $^{208}\text{Pb}({}^3\text{He}, d)^{209}\text{Bi}$ transfer processes⁷⁶. The pick-up reaction cross section is, in the case of e.g. the states $1/2^+(s_{1/2})$ and $11/2^-(h_{11/2})$, essentially consistent with a single peak displaying full $(2j+1)$ occupancy. On the other hand, two $3/2^+$ states with essentially equal strength and exhausting the associated $(2j+1=4)$ strength are observed. Furthermore, the four peaks mentioned above are essentially not excited in the stripping process (see Table 2.5.1). In an attempt to further clarify the structure of the two $3/2^+$, use is made of the inelastic process $^{209}\text{Bi}(d, d')$. Both states are excited

⁷⁵Born (1948) pp. 95,103; Pais (1986) p 258.

⁷⁶It is of notice that in the present case, as well as in Sect. 2.7, and at variance with the rest of the monograph, use will be made, for the sake of being didactic, of spectroscopic factors (see end of Sect. 3.1 as well as App. 5.H).

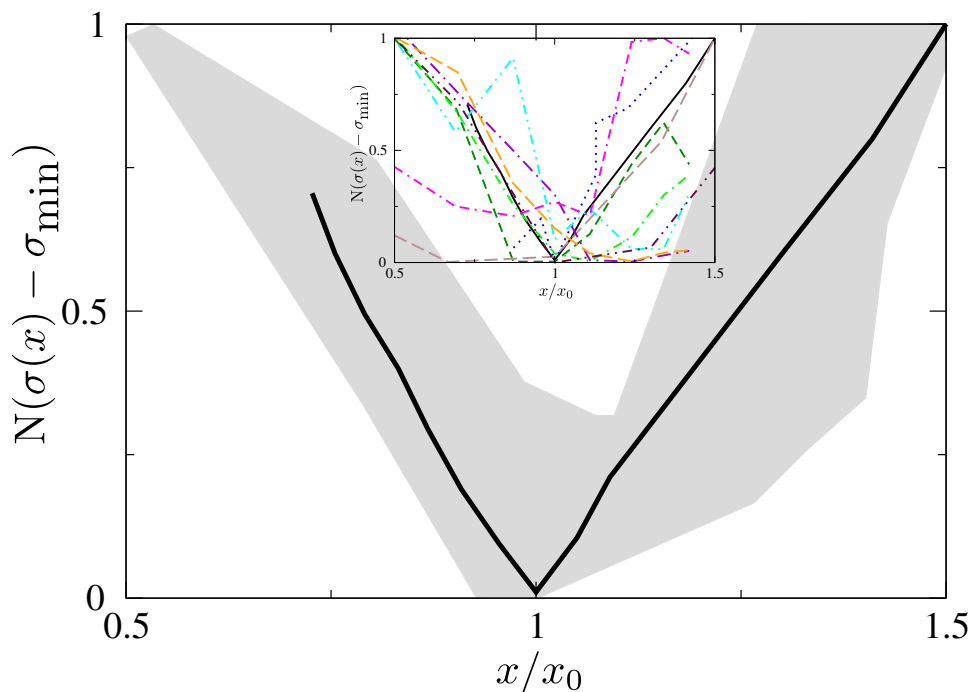


Figure 2.4.1: (Color online) Root mean square deviations $\sigma(x)$ (see Table 2.4.1) between theoretical predictions and experimental values of the different structural properties which “completely” characterize the open-shell nucleus ^{120}Sn (Idini et al. (2015)). After Broglia et al. (2016).

Observables	SLy4	$d_{5/2}$ shifted	Opt. levels
Δ	10 (0.7%)	10 (0.7 %)	50 (3.5 %)
E_{qp}	190 (19%)	160 (16%)	45 (4.5 %)
Mult. splitt.	50 (7%)	70 (10%)	59 (8.4 %)
$d_{5/2}$ strength (centr.)	200 (20%)	40 (4%)	40 (4%)
$d_{5/2}$ strength (width)	160 (20%)	75 (9.3%)	8 (1%)
$B(E2)$	1.4 (14%)	1.34 (13%)	1.43 (14%)
$\sigma_{2n}(p, t)$	40 (2%)	40 (2%)	40 (2%)

Table 2.4.1: Root mean square deviation σ between the experimental data and the theoretical values expressed in keV for the pairing gap, quasiparticle energies, multiplet splitting, centroid and width of the $5/2^+$ low-lying single-particle strength distribution (Fig. 5.2.3). In single-particle units B_{sp} for the γ -decay ($B(E2)$ transition probabilities) and in mb for $\sigma_{2n}(p, t)$ (Fig. 7.4.1). In brackets the ratio $\sigma_{rel} = \sigma/L$ between σ and the experimental range L of the corresponding quantities: 1.4 MeV (Δ), 1 MeV (E_{qp}), 700 keV (mult. splitting), 1 MeV ($d_{5/2}$ centroid), 809 keV (=1730–921) keV ($d_{5/2}$ width), 10 B_{sp} ($B(E2)$), 2250 μb ($\sigma_{2n}(p, t)$)) is given (for details see Idini et al. (2015), also Fig. 2.11.1). Columns 2,3, and 4 contain the results of NFT calculations making use of bare single-particle levels from Hartree–Fock with Sly4, same but for a 600keV shift towards the Fermi energy of the $\epsilon_{d_{5/2}}$ orbital, and optimal values of ϵ_j for all valence levels so that the dressed quasiparticle states provide the best fit to that data, respectively.

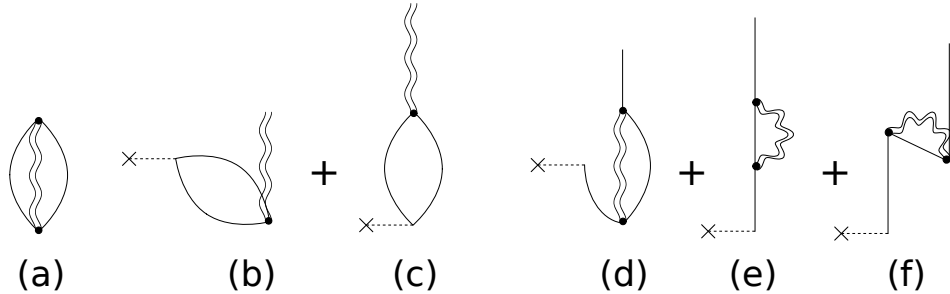


Figure 2.4.2: Schematic representation of the NFT(s+tr) diagrams at the basis of the characterization of a superfluid nucleus like e.g. ^{120}Sn . (a) Nuclear structure (NFT(s)). Zero point fluctuations (ZPF) characterizing the nucleus ground state. Continuous lines describe quasiparticle (qp) states, double wavy curves correlated two quasiparticle ($2qp$) vibrational modes. Because $\alpha_\nu^\dagger = U_\nu a_\nu^\dagger - V_\nu a_\nu$ these modes encompass both particle–hole (ph) like vibrations, e.g. surface quadrupole vibrations, as well as correlated (pp) and (hh) monopole and multipole pairing vibrations. Intervening with an external field (cross followed by dashed line) one can excite (b) and (c) multipole (ph -like; inelastic scattering) and pairing ($2p$ -like) vibrations (two-particle transfer) as well as (d)-(f) single-quasiparticle states.

in inelastic scattering, the associated angular distributions revealing the octupole character of such excitation (Tables 2.5.2 and 2.5.3).

In keeping with the fact that the same experiment reveals a multiplet (septuplet) of states with centroid around 2.6 MeV and with summed $L = 3$ inelastic cross section consistent with that of the lowest collective (2.615 MeV, $B(E3)/B_{sp} \approx 32$) octupole vibration of ^{208}Pb , one can posit that the two $3/2^+$ states are a linear combination of the unperturbed (two particles)–(one hole) ($2p-1h$) states,

$$|\alpha\rangle = |d_{3/2}^{-1} \otimes gs(^{210}\text{Pb}); 3/2^+\rangle, \quad (2.5.1)$$

and

$$|\beta\rangle = |h_{9/2} \otimes 3^-(^{208}\text{Pb}); 3/2^+\rangle. \quad (2.5.2)$$

Because these states lie very close in energy they mix. According to NFT, the most important contribution to this mixing arises from the process given in Fig. 2.5.1. The resulting physical (mixed) states can be written as,

$$|I\rangle = -0.53|\alpha\rangle + 0.76|\beta\rangle, \quad (2.5.3)$$

and

$$|II\rangle = 1.02|\alpha\rangle + 0.80|\beta\rangle, \quad (2.5.4)$$

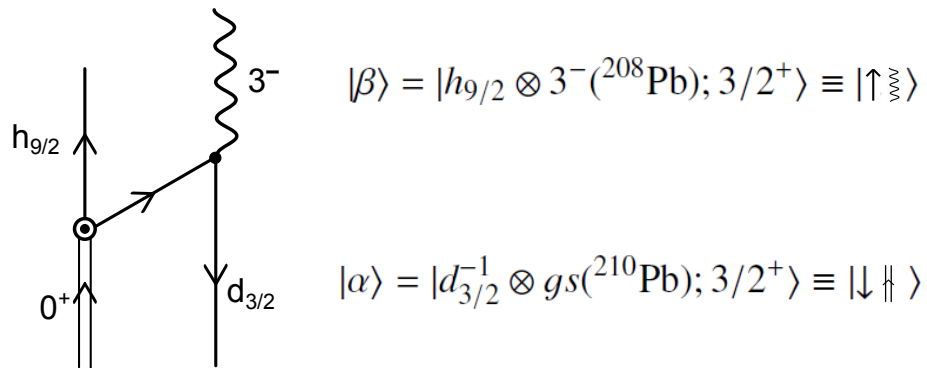


Figure 2.5.1: NFT diagram describing one of the most important processes coupling the $2p - 1h$ states $|\alpha\rangle$ and $|\beta\rangle$ (see Eqs. (2.5.1) and (2.5.2)), product of bare elementary modes of excitation consisting in the ${}^{208}\text{Pb}$, 0^+ pair addition mode and the $d_{3/2}$ proton hole state, and of the lowest octupole vibration of ${}^{208}\text{Pb}$ and of a proton moving in the $h_{9/2}$ orbital.

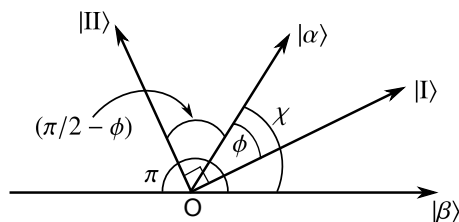


Figure 2.5.2: Schematic representation of the $3/2^+$ states entering the NFT calculation of the process displayed in Fig. 2.5.1. The basis state $|\alpha\rangle$ carries the full (t, α) transfer strength (tr) σ^{tr} , while the basis state $|\beta\rangle$ the full octupole (oct) strength σ^{oct} (see Tables 2.5.1–2.5.3). The overlap between these states is $\cos\chi$. The physical states obtained through the (Feynman) diagrammatic “orthogonalization process” are denoted $|I\rangle$ and $|II\rangle$ (see Eqs. (2.5.3) and (2.5.4)).

	$E_x(\text{MeV})$	$S(t, \alpha)(2j + 1)$	$S(^3\text{He}, d)$
3/2 ⁺	2.49	$1.8 \pm 0.3 (4)$	< 0.01
3/2 ⁺	2.95	$2.2 \pm 0.3 (4)$	< 0.01
1/2 ⁺	2.43	1.8 (2)	< 0.02
11/2 ⁻	3.69	10 (12)	< 0.05

Table 2.5.1: Single-particle strength associated with the transfer reactions $^{210}\text{Po}(t, \alpha)^{209}\text{Bi}$ and $^{208}\text{Pb}(^3\text{He}, d)^{209}\text{Bi}$ (see Bortignon et al. (1977)).

	$E_x(\text{MeV})$	$\frac{\sigma(^{209}\text{Bi}(9/2^-; gs) \rightarrow ^{209}\text{Bi}(3/2^+; E))}{\sigma(^{208}\text{Pb}(gs) \rightarrow (3^-; 2.615 \text{ MeV}))}$
3/2	2.49	0.042 ± 0.003
3/2	2.95	0.011 ± 0.002

Table 2.5.2: The total inelastic cross section σ^{oct} associated with the lowest octupole vibrational state of ^{208}Pb can be written in terms of that associated with a single magnetic substate σ' as $\sigma_{3^-}^{oct} = 7\sigma'$. That associated with the multiplet $(h_{9/2} \otimes 3^-)_{J^+}(J = 3/2 - 15/2)$ as $\sigma_{3^-}^{oct} = 70\sigma'$, in keeping with the fact that the $h_{9/2}$ state has 10 magnetic substates. Thus, the strength associated with the 3/2 channel is $4/70=0.057$ to be compared with the observed summed (percentage) strength $0.053 \pm 0.005 (= (0.042 \pm 0.003) + (0.011 \pm 0.002))$ associated with the 2.45 MeV and the 2.95 MeV 3/2⁺ states; see Bortignon et al. (1977) Table 4.11.

as resulting from the calculation of the diagram displayed in Fig. 2.5.1 to all orders of perturbation, with the help of Brillouin–Wigner perturbation theory (diagonalization of the corresponding effective Hamiltonian⁷⁷, see Sect. 2.7.4).

Let us now calculate the overlap $O = \langle \alpha | \beta \rangle$ between the basis states $|\alpha\rangle$ and $|\beta\rangle$, that is $O = \cos \chi$ (see Fig. 2.5.2). Following this figure one can write,

$$\sqrt{\sigma_I^{tr}} = \cos \phi; \quad \sqrt{\sigma_{II}^{tr}} = \cos \left(\frac{\pi}{2} - \phi \right) = \sin \phi, \quad (2.5.5)$$

where

$$\sigma^{tr} = \sigma_I^{tr} + \sigma_{II}^{tr} = 1, \quad (2.5.6)$$

⁷⁷See p. 316 Bortignon et al. (1977) and references therein.

	$E_n(\text{MeV})$		$\frac{\sigma(h_{9/2} \rightarrow 3/2^+)}{\sigma(0^+ \rightarrow 3^-)} (\%)$		$S(t, \alpha)$		$S(^3\text{He}, d)$	
	Theory	Exp	Theory	Exp	Theory	Exp	Theory	Exp
3/2	2.480	2.494	3.76	4.2 ± 0.3	1.83	1.8 ± 0.3	0.02	< 0.01
3/2	3.125	2.95	1.56	1.1 ± 0.2	2.25	2.2 ± 0.3	10^{-5}	< 0.01

Table 2.5.3: Summary of NFT predictions concerning the structure of the two lowest 3/2⁺ state of ^{209}Bi , in comparison with the experimental data (see Table 4.7 of Bortignon et al. (1977)).

in keeping with the fact that the absolute cross sections of the states $|I\rangle$ and $|II\rangle$ are normalized in terms of the total cross section.

In the same way

$$\sqrt{\sigma_I^{oct}} = \cos(\chi - \phi) = \cos \chi \cos \phi + \sin \chi \sin \phi, \quad (2.5.7)$$

and

$$\sqrt{\sigma_{II}^{oct}} = \cos\left(\pi - \left(\frac{\pi}{2} - \phi + \chi\right)\right) = -\cos\left(\frac{\pi}{2} + (\phi - \chi)\right) = \sin \phi \cos \chi + \sin \chi \cos \phi. \quad (2.5.8)$$

Thus

$$\sqrt{\sigma_I^{oct}} = \cos \chi \sqrt{\sigma_I^{tr}} + \sin \chi \sqrt{\sigma_{II}^{tr}}, \quad (2.5.9)$$

and

$$\sqrt{\sigma_{II}^{oct}} = -\cos \chi \sqrt{\sigma_{II}^{tr}} + \sin \chi \sqrt{\sigma_I^{tr}}. \quad (2.5.10)$$

Multiplying the above relations by $\sqrt{\sigma_I^{tr}}$ and $\sqrt{\sigma_{II}^{tr}}$ respectively one obtains,

$$\sqrt{\sigma_I^{tr} \sigma_I^{oct}} = \cos \chi \sigma_I^{tr} + \sin \chi \sqrt{\sigma_I^{tr} \sigma_{II}^{tr}}, \quad (2.5.11)$$

and

$$\sqrt{\sigma_{II}^{tr} \sigma_{II}^{oct}} = -\cos \chi \sigma_{II}^{tr} + \sin \chi \sqrt{\sigma_I^{tr} \sigma_{II}^{tr}}, \quad (2.5.12)$$

which, upon subtraction leads to the expression of the overlap

$$\cos \chi = \frac{\sqrt{\sigma_I^{tr} \sigma_I^{oct}} - \sqrt{\sigma_{II}^{tr} \sigma_{II}^{oct}}}{\sigma_I^{tr} + \sigma_{II}^{tr}}. \quad (2.5.13)$$

Making use of the values of Tables 2.5.1–2.5.3 (see also Fig. 2.7.11 (e) last column labeled *experiment*)⁷⁸ one obtains

$$O = \cos \chi = \frac{\sqrt{1.8 \times 4.2} - \sqrt{2.2 \times 1.1}}{4} = 0.298 \quad (2.5.14)$$

Regarding the NFT results related to the above questions we refer to Sect. 2.7.4 as well as to App. 2.B (Sect. 2.B.2). In what follows we provide simple, necessarily qualitative estimates making use of the relations⁷⁹.

$$\begin{aligned} \langle I|I\rangle &= (-0.53)^2 + (0.76)^2 - 2 \times 0.53 \times 0.75 O = 1, \\ \langle II|II\rangle &= (1.02)^2 + (0.80)^2 + 2 \times 1.02 \times 0.80 O = 1, \end{aligned}$$

⁷⁸See Table 4.7 of Bortignon et al. (1977).

⁷⁹see Tables 4.5 and 4.6 Bortignon et al. (1977).

and $\langle \text{I}|\text{II} \rangle = -0.53 \times 1.02 + 0.76 \times 0.80 + (-0.53 \times 0.80 + 0.76 \times 1.02) O = 0$ leading to $O = -0.18, -0.42$ and -0.19 respectively and, thus, to the average value of -0.26 . Of course, one can hardly expect to obtain the sign to agree with that of the NFT expression, as it is associated with a free choice of the axis of references (Fig. 2.5.2). Note also the fact that the quantities σ appearing above are well defined, while $\sqrt{\sigma}$ is indetermined by an overall sign.

2.6 Coupling between intrinsic and relative motion

In what follows, we consider the reaction



within the framework of the semiclassical approximation⁸⁰. In the center-of-mass system, the total Hamiltonian may be written

$$H = T_{aA} + H_a + H_A + V_{aA} = T_{bB} + H_b + H_B + V_{bA}, \quad (2.6.2)$$

in keeping with energy conservation. Within this context other, mixed, representations are possible.

One then solves the time-dependent Schrödinger equation

$$i\hbar \frac{\partial \Psi}{\partial t} = H\Psi, \quad (2.6.3)$$

with the initial conditions that the nuclei a and A are in their ground states, and where the relative motion is described by a narrow wavepacket of rather well defined impact parameter and velocity.

We expand Ψ on (stationary) channel wavefunctions

$$\Psi = \sum_{\beta} c_{\beta} (\mathbf{r}_{\beta} - \mathbf{R}_{\beta}) \Psi_{\beta} e^{-iE_{\beta}t/\hbar}, \quad (2.6.4)$$

where

$$\Psi_{\beta}(t) = \Psi_m^b(\xi_b) \Psi_n^B(\xi_B) \exp(i\delta_{\beta}). \quad (2.6.5)$$

The index β labels both the partition of nuclei (b, B) as well as the quantal states of the two nucleons (m, n).

The phase δ_{β} is defined as

$$\delta_{\beta} = \frac{1}{\hbar} \left\{ m_{\beta} \mathbf{v}_{\beta}(t) \cdot (\mathbf{r}_{\beta} - \mathbf{R}_{\beta}(t)) - \int_0^t \left(U_{\beta}(\mathbf{R}_{\beta}(t')) - \frac{1}{2} m_{\beta} \mathbf{v}_{\beta}(t')^2 \right) dt' \right\}, \quad (2.6.6)$$

where an extra phase has been added to eliminate, as far as possible, the diagonal matrix elements in the coupled equations. The phase factor $\exp(i\delta_{\beta})$ acting

⁸⁰Broglia and Winther (2004) and references therein.

on the channel wavefunction is essentially a Galilean transformation (see jagged “phonon” in the NFT reaction diagrams displayed in Figs. 5.1.1 (one-particle transfer) and Figs. 6.C.1 and 6.C.2 (two-particle transfer); see also Figs. 2.1.2, 2.1.3 and 2.10.2–2.10.6).

The function c_β can be expressed as

$$c_\beta = a_\beta(t)\chi_\beta(\mathbf{r}_\beta - \mathbf{R}_\beta(t), t) \quad (2.6.7)$$

product of an amplitude a_β of asymptotic values ($t = \pm\infty, 0$ or 1), and a normalized shape (wavepacket) function, $R_\beta(t)$ being the relative motion elastic trajectory.

Properly combining the above quantities and making use of the time-dependent Schrödinger equation one obtains

$$i\hbar \sum_\beta \dot{a}_\beta(t) \langle \Psi_\xi | \Psi_\beta \rangle_{\mathbf{R}_\xi} e^{iE_\beta t/\hbar} = \sum_\gamma \langle \Psi_\xi | V_\gamma - U_\gamma(r_\gamma) | \Psi_\gamma \rangle_{\mathbf{R}_\xi} a_\gamma(t) e^{iE_\beta t/\hbar}, \quad (2.6.8)$$

where

$$f(\mathbf{R}) = \langle \Psi_\xi | V_\gamma - U_\gamma(r_\gamma) | \Psi_\gamma \rangle_{\mathbf{R}} \quad (2.6.9)$$

are the formfactors, and

$$g(\mathbf{R}) = \langle \Psi_\xi | \Psi_\beta \rangle_{\mathbf{R}} \quad (2.6.10)$$

the *overlaps between the intrinsic channel wavefunctions*.

The coupled equations can be written in a more compact form by introducing the adjoint channel wavefunction

$$\omega_\xi = \sum_\gamma g_{\xi\gamma}^{-1} \Psi_\gamma, \quad (2.6.11)$$

where g^{-1} is the reciprocal of the *overlap matrix*

$$g_{\xi\gamma} = \langle \Psi_\xi | \Psi_\gamma \rangle. \quad (2.6.12)$$

Thus

$$(\omega_\xi, \Psi_\beta) = \delta(\xi, \beta), \quad (2.6.13)$$

and

$$i\hbar \dot{a}_\beta(t) = \sum_\gamma \langle \omega_\beta | V_\gamma - U_\gamma | \Psi_\gamma \rangle_{\mathbf{R}_\beta} e^{(E_\beta - E_\gamma)t/\hbar} a_\gamma(t). \quad (2.6.14)$$

Consequently, the proper tunneling Hamiltonian is obtained by a *basis orthogonalization process*. These coupled equations, being first order in time, can be solved knowing the initial conditions at time $t = -\infty$,

$$a_\gamma(-\infty) = \delta(\gamma, \alpha), \quad (2.6.15)$$

where α labels the entrance channel, that is, the nuclei a and A in their ground state. The cross section for the reaction $\alpha \rightarrow \beta$ is

$$\left(\frac{d\sigma}{d\Omega} \right)_{\alpha \rightarrow \beta} \sim |a_\beta(t = +\infty)|^2. \quad (2.6.16)$$

2.7 Nuclear Field Theory for pedestrians

Nuclear Field Theory (NFT) was tailored after Feynman's graphical version of quantum electrodynamics (QED)⁸¹. It is then natural that in discussing NFT analogies with QED will be recurrent. Arguably, as a consequence of special relativity which put an end to the concept of ether, the field-free and matter-free vacuum was rightly considered as *bona fide* empty space. The advent of quantum mechanics changed this situation, the vacuum becoming populated. In quantum mechanics an oscillator, for example, cannot be at rest. The oscillatory nature of the radiation field requires zero point fluctuations (ZPF) of the electromagnetic fields in the vacuum state of lower energy. The occupation of the negative kinetic energy electron states and the subsequent calculation of the cross section for pair creation by photons, contributed another step in the understanding of the QED vacuum, let alone the Lamb shift⁸².

When the fields are expressed in terms of creation and annihilation operators, the interaction between fermion and boson fields is proportional to the product of two fermion creation or destruction operator a^\dagger or a , and of one boson operator Γ^\dagger or Γ : e.g. $a_\nu^\dagger a_\nu \Gamma_\alpha^\dagger$, (see Fig. 2.7.1). That is, bilinear in the fermion fields and linear in the boson fields.

⁸¹“The diagrams were intended to represent physical processes and the mathematical expressions to describe them... I would see electrons going along, being scattered at on point... emitting a photon and the photon goes over there... I thought that if they really turn out to be useful it would be fun to see them in the pages of Physical Review” R. P. Feynman.

⁸²In high energy collisions and accelerator laboratories some of the original beam energy can be consumed by ripping electron-positron pairs out of the vacuum (Bruce et al. (2007)).

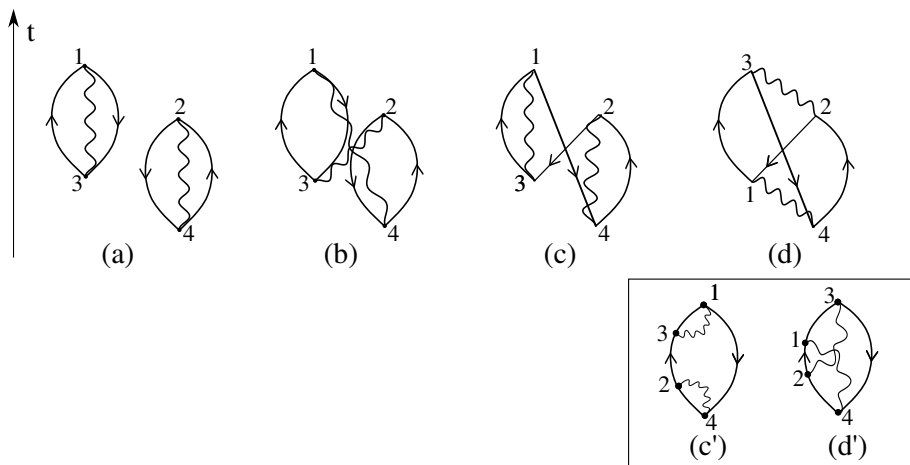


Figure 2.7.1: Oyster diagrams describing the correlation of the nuclear ground state associated with the ZPF of collective particle–hole–like excitations. In (a) we show two of such diagrams. In (b) and (c) we display a symmetrized (boson exchange), and antisymmetrized (fermion exchange) correction to (a), while (d) contains a simultaneous boson and fermion exchange. In all the diagrams shown, only ground state correlation vertices are present. They are connected with the $Y_{k_i}^\alpha$ –components ($\epsilon_k > \epsilon_F$, $\epsilon_i \leq \epsilon_F$) of the RPA wavefunction describing the collective mode (wavy line). While this is so for any time ordering, i.e., the sequence with which the particle-vibration coupling vertex (black dot) appear in the case of the processes shown in (a) and (b), this is not the case in connection with processes shown in (c) and (d) as can be seen from the corresponding diagrams (c') and (d') shown in the inset. Because of Pauli principle between particles (holes) present and those involved in the collective modes, the harmonic approximation has to be corrected. This is diagrammatically reflected by the presence of scattering vertices.

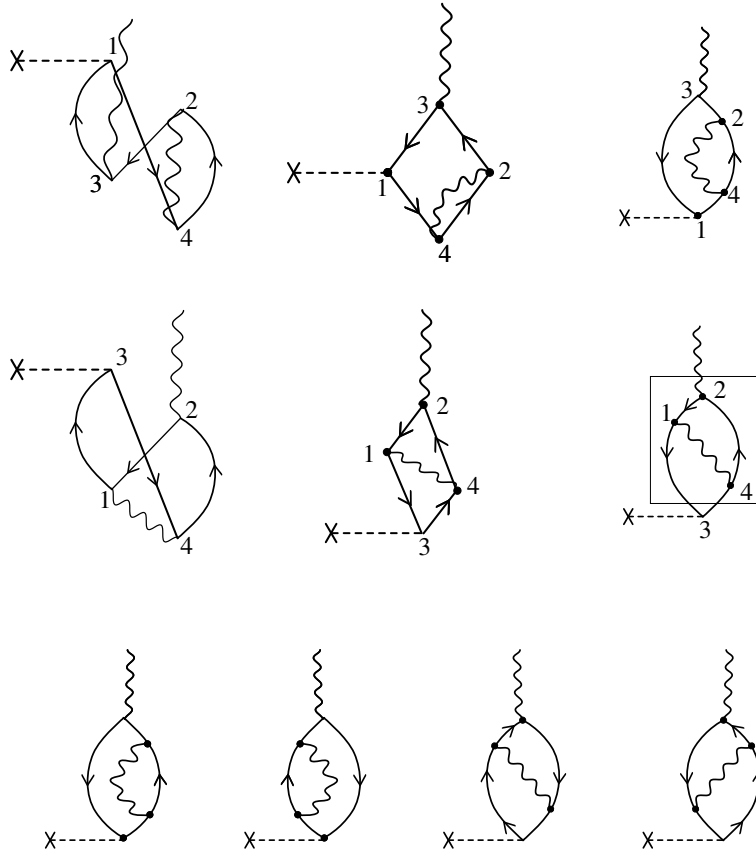


Figure 2.7.2: Some of the possible outcomes resulting from acting with an external single-particle field, i.e. that associated with inelastic processes (represented by a horizontal dashed line starting with a \times) on the ZPF of a nucleus ground state associated with particle-hole correlated vibrations. Within this context one returns to the question of renormalization mentioned in the text (see end of Sect. 2.1 and Sect. 2.4, see also Idini et al. (2015), Broglia et al. (2016), Barranco et al. (2017); see also Sect. 7.5) The diagrams of the first row result by intervening the virtual process shown in Fig. 2.7.1 (c) and eventual time orderings. Similar for those of the second row but in connection with diagram (b) of Fig. 2.7.1. The boxed processes correspond to particle self-energy (first row) and vertex correction (second row). Reversing the sense in which the fermions (arrowed lines) circle the loop from anticlockwise to clockwise, one obtains two new graphs. The complete set of processes obtained in this way are shown in the third and last row, and constitute a sum rule conserving set of diagrams.

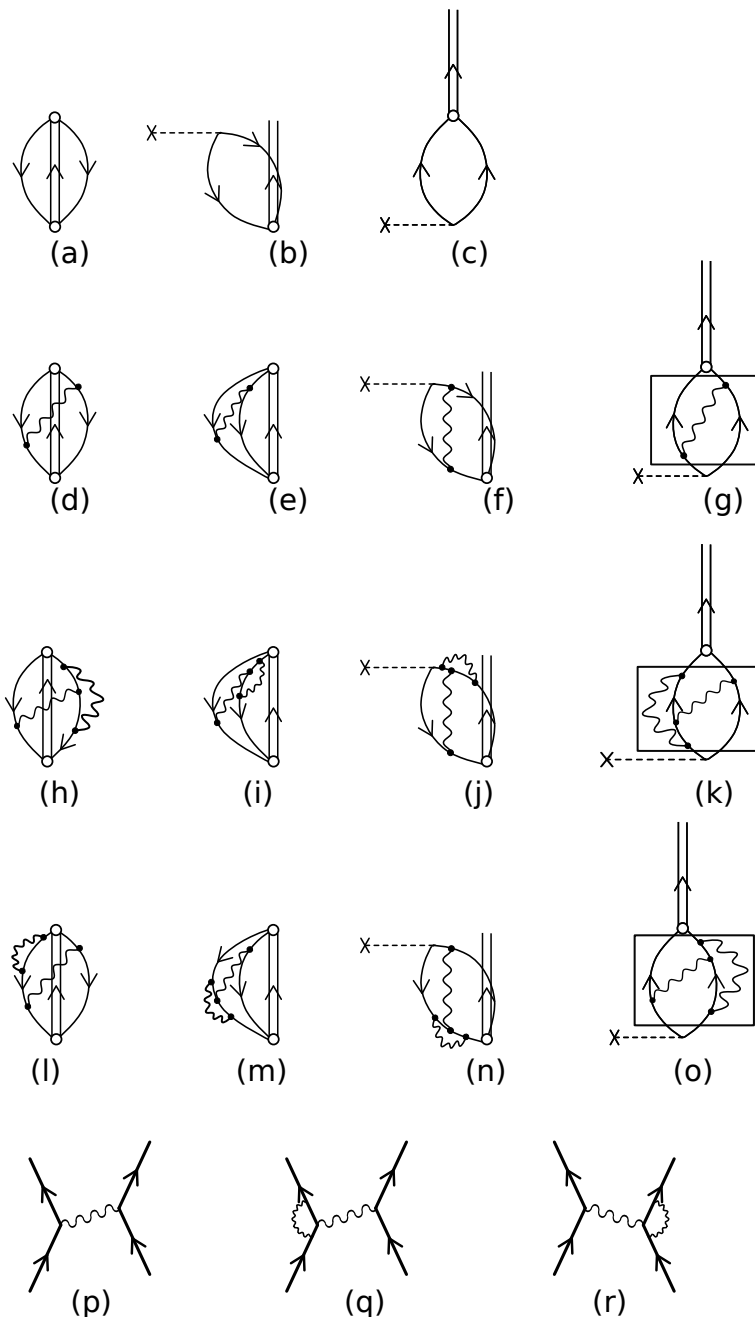


Figure 2.7.3: ZPF associated with the pair addition mode taking into account the interweaving of nucleons with density modes. The processes boxed in (g), (k) and (o), are associated with the induced pairing interaction (medium polarization effects; (p), (q), (r)) resulting from the exchange of density modes between nucleons moving in time reversal states, including also vertex corrections. The two-nucleon stripping and pickup external field is labeled by a dashed horizontal line which starts with a \times . The possibility of using pairing vibrational modes as intermediate bosons contributing to the induced pairing interaction, not only in 1S_0 channels but also in other channels (multipole modes) is discussed in App. 7.F. In particular, in connection with the possible presence of “vortex-like” pair addition modes, in exotic, halo nuclei, with $J^\pi = 1^-$ and $\beta = +2$ quantum numbers.

A detailed graphical NFT treatment of the vacuum has an important consequence concerning the probing of nuclear structure with reactions. By intervening it with an external field one will excite the modes whose properties can be compared with experiment without further ado.

In other words, if one is in doubt of which are the properly dressed elementary, physical modes of excitation, one should find out how to specifically excite the mode in question, by acting with an external field on the ZPF of the vacuum (Hawking-like radiation⁸³; see also Sect. 7.6.2 in particular Fig. 7.6.2). That is, carry out a *gedanken*, NFT-like *experiment* as in Fig. 2.7.2 for $p - h$ -vibrations and in Fig. 2.7.3 regarding pairing vibrations. Because the corresponding processes deal with physical states, they translate with ease into a laboratory setup. In keeping with the fact that the vacuum contains all the information (right physical degrees of freedom) of the quantal system under study. Forcing virtual processes associated with vacuum ZPF to become real, one is guaranteed to get, in each instance, the real, dressed, physical particle.

The fact that one can treat fully quantum mechanically and on equal footing both structure and reaction processes is apparent from these figures and considerations⁸⁴. Thus unification of structure and reactions, and dressing of energies, vertices (interactions) and formfactors (single-particle radial wavefunctions and associated transition densities), results in a single vacuum correlated state (e.g. Figs. 2.7.1 and 2.9.2). Vacuum states which through its fluctuations, reflect both single-particle, normal and abnormal (pairing) density vibrations and their interweaving. It also indicates the set of specific probes which make these virtual states to collapse into on-the-energy shell states, providing the corresponding physical information to the outgoing particles, also photons, which eventually interact with the corresponding detectors (e.g. Figs. 2.7.2, 2.7.3 and 2.10.2). Structure and reaction processes free of non-orthogonality, overcompleteness and Pauli violation contributions.

Summing up, the last line of Fig. 2.7.2 displays, together with the corresponding time orderings, the lowest order self-energy and vertex correction renormalising vibrational states. It thus gives rise to the physical collective vibrations whose properties can be directly compared with the experimental findings (within this context see last paragraph of the next section). In other words, the processes shown in the last line of Fig. 2.7.2 imply that the elementary modes participating in the virtual states have to display, exception made for energy (off-shell modes) the same properties of the physical, dressed (renormalized), on-shell modes whose properties can be directly compared with experiment⁸⁵ (renormalized NFT). This because one can, through an experiment force such virtual states to become real (on-shell) on short call.

Let us now provide an introduction to NFT for pedestrians and see how the

⁸³Barranco et al. (2019).

⁸⁴Full fledge embodiments being found in e.g. Figs. 2.10.1 and 2.10.2 and Figs. 7.3.1 and 7.6.2.

⁸⁵Examples of these processes in the case of giant resonances are found in Bortignon and Broglia (1981); Bertsch et al. (1983). For low-lying states see Barranco et al. (2004).

above considerations become concretely implemented⁸⁶

2.7.1 The concept of elementary modes of excitation⁸⁷

The Hamiltonian of a many–body system of noninteracting particles, bosons or fermions, can be written as

$$H = \sum_i H_i, \quad (2.7.1)$$

where the summation is over all the particles of the system and where each H_i depends only on the variables of the i -th particle. The single–particle Schrödinger equation is

$$H_i \psi_k(\mathbf{r}_i) = \epsilon_k \psi_k(\mathbf{r}_i), \quad (2.7.2)$$

where ϵ_k is the single–particle energy eigenvalue and

$$\psi_k(\mathbf{r}_i) \equiv \langle \mathbf{r}_i | a_k^\dagger | 0 \rangle \quad (2.7.3)$$

is the corresponding wave function. The operator a_k^\dagger creates a particle in the state k when acting in the vacuum state $|0\rangle$. The energy levels of the system are given by the equation

$$E_n = \sum_k n_k \epsilon_k, \quad (2.7.4)$$

the corresponding eigenstates being

$$|n\rangle = \prod_k \frac{(a_k^\dagger)^{n_k}}{\sqrt{n_k!}} |0\rangle, \quad (2.7.5)$$

where $n_k = 0$ or 1 in the case of fermions and $n_k = 0, 1, 2, \dots$ in the case of bosons.

Now we consider a system of interacting particles. The Hamiltonian will in this case be

$$H = \sum_i H_i + \frac{1}{2} \sum_{i,j} H_{ij}, \quad (2.7.6)$$

where i, j label the co–ordinates of the i -th and j -th particle.

In some cases it is possible to recast the two–body Hamiltonian in the form

$$H = \sum_\tau H'_\tau, \quad (2.7.7)$$

⁸⁶For details we refer to Bortignon et al. (1977) and refs. therein.

⁸⁷Bès and Broglia (1977)

with the associated Schrödinger equation

$$H'_\tau \psi_\tau(\zeta) = \epsilon_\tau \psi_\tau(\zeta), \quad (2.7.8)$$

ζ representing a general variable⁸⁸ (e.g. the single-particle co-ordinate, the gap parameter, the shape of the nucleus, etc.). The wave function $\psi_\tau(\zeta)$ is the ζ -co-ordinate representation of the eigenstate $\alpha_\tau^\dagger |\tilde{0}\rangle$. The operator α_τ^\dagger creates an excitation with the quantum number τ when acting in the state $|\tilde{0}\rangle$, the correlated vacuum of all the excitations τ .

The energy of the levels of the system, or at any rate of the most important ones to determine the physical response of it to external probes can be written in the form

$$E_m = \sum_\tau n_\tau \epsilon_\tau. \quad (2.7.9)$$

The corresponding eigenstate can be written in the same way as before, *i.e.*

$$|n\rangle = \prod_\tau \frac{(\alpha_\tau^\dagger)^{n_\tau}}{\sqrt{n_\tau!}} |\tilde{0}\rangle. \quad (2.7.10)$$

Additivity features similar to (2.7.9) hold for other physical quantities, *i.e.*

$$\langle n|O|m\rangle = \sum_\tau A_\tau \sqrt{n_\tau} \delta(n_\tau, m_\tau + 1), \quad (2.7.11)$$

where

$$O = \sum_\tau A_\tau \alpha_\tau^\dagger \quad (2.7.12)$$

is the operator which specifically excites the eigenstates described by $\psi_\tau(\xi)$. Because the excitation energies E_m and observables $|\langle m'|O|m\rangle|^2$ (e.g. absolute two-particle transfer cross-section, electromagnetic-transition probabilities, etc.) are linear combinations of ϵ_τ and A_τ , respectively, the eigenstates with energy ϵ_τ and associated observable A_τ are called the *elementary excitations of the system*.

The elementary modes of excitation of a many-body system represent a generalization of the idea of normal modes of vibration. They provide the building blocks of the excitation spectra, giving insight into the deep nature of the system one is studying, aside from allowing for an economic description of complicated spectra in terms of a gas of, as a rule, weakly interacting bosons and fermions. In the nuclear case they correspond to clothed particles and empirically renormalised vibrations (rotations).

⁸⁸Collective, also in the sense of independent particle motion (see Mottelson (1962)) variable or order parameter.

There lie two ideas behind the concept of elementary modes of excitation⁸⁹. First, that one does not need to be able to calculate the total binding energy of a nucleus to accurately describe the low energy excitation spectrum, in much the same way in which one can calculate the normal modes of a metal rod not knowing how to calculate its total cohesive energy. The second idea is that low-lying states ($\hbar\omega \ll \epsilon_F \ll BE$, i.e. binding energy) are of a particularly simple character, and are amenable to a simple treatment, their interweaving being carried out at profit, in many cases, in perturbation theory⁹⁰. Within this context it is necessary to have a microscopic description of the ground state of the system which ensures that it acts as the vacuum state $|\tilde{0}\rangle$ of the elementary modes of excitation. In other words $a_\nu |\tilde{0}\rangle = 0$, $\Gamma_\alpha |\tilde{0}\rangle = 0$, where $a_\nu^+ |\tilde{0}\rangle = |\nu\rangle$ and $\Gamma_\alpha^+ |\tilde{0}\rangle = |\alpha\rangle$ represent a single-particle and a one-phonon state. This implies, in keeping with the indeterminacy relations⁹¹ $\Delta x \Delta p \geq \hbar/2$, $\Delta I \Delta \Omega \geq 1$, $\Delta N \Delta \phi \geq 1$, etc. that $|\tilde{0}\rangle = |0\rangle_F |0\rangle_B$ displays the quantal zero point fluctuations (ZPF) of the many-body system under study.

Within the framework of nuclear field theory (NFT) used below, in which single-particle (fermionic, F) and vibrational (bosonic, B) elementary modes of excitation are to be calculated within the framework of HFB and QRPA respectively, $|\tilde{0}\rangle$ must display the associated ZPF (cf. App. 2.D). In particular for (harmonic) vibrational modes the indeterminacy relation achieves its lowest possible value $\Delta x \Delta p = \hbar/2$, the associated zero point energy amounting to $\hbar\omega/2$ for each degree of freedom. For example $5\hbar\omega/2$ for quadrupole vibrations, $\hbar\omega$ being the energy of the collective vibrational mode under consideration.

An illustrative example of the above arguments is provided by the low-lying quadrupole vibrational state of ^{120}Sn . Diagonalizing SLy4 in QRPA leads to a value of $B(E2)$ ($890 e^2 \text{ fm}^2$) which is about a factor of 2 smaller than experimentally observed ($2030 e^2 \text{ fm}^2$). Taking into account renormalisation effects in NFT, namely in a conserving approximation (self-energy and vertex corrections, generalised Ward identities, see last line of Fig. 2.7.2 and Fig. 5.C.3), one obtains a value ($2150 e^2 \text{ fm}^2$), which essentially coincides with the experimental findings. One does not know how to accurately calculate the absolute ground state energy E_0 (total binding energy) of e.g. ^{120}Sn , but one can accurately work out the properties of the low-energy mode of this nucleus, also the collective energies $\hbar\omega_L = E_L - E_0$, and thus the associated ZPF and zero point energy E_0 , by renormalizing QRPA

⁸⁹This concept was introduced by Landau (Landau (1941)) to describe the spectrum of HeII. It was subsequently utilized by Bohr and Mottelson (Bohr and Mottelson (1975)) to obtain a unified description of the nuclear spectrum.

⁹⁰More precisely, and in keeping with the fact that boson degrees of freedom have to decay through linear particle-vibration coupling vertices of strength Λ into their fermionic components to interact with another vibrational mode, the interweaving between the variety of many-body components clothing a single-particle state or a collective vibration will be described at profit in terms of an arrowed matrix which, assuming perturbation theory to be valid, can be transformed, neglecting contributions of the order of Λ^3 or higher, into a co-diagonal matrix, namely a matrix whose non-zero elements are $(i, i-1)$ and $(i, i+1)$, aside from the diagonal ones (i, i) .

⁹¹The quantities I , N and Ω , ϕ are the angular momentum and particle number, conjugate variables to the Euler and gauge angles respectively.

solutions through self-energy and vertex corrections contributions⁹². Now, if the collective phonons are not the main object of the study, but are to be used to cloth the single-particle states and give rise to the induced pairing interaction, one can make use of phonons which account for the experimental findings (renormalization^{93,94}).

2.7.2 NFT rules and applications

A field theory can be formulated in which the nuclear elementary modes of excitation play the role of the free fields and in which their mutual interweaving takes place through the particle–vibration coupling vertices⁹⁵. This theory provides a graphical perturbative approach to obtain the exact solution of the many-body nuclear-structure problem in the product basis $\psi_\tau(\zeta)\psi_\eta(\Delta)\dots\psi_\gamma(\Gamma)$

Note that the nuclear bosonic fields are built out by utilizing those degrees of freedom (particles and holes) which already exhaust all the nuclear degrees of freedom. It is thus an essential feature of the product basis to be over-complete and to violate the Pauli principle. On the other hand, this basis is directly related to observables of the system. The different experiments project out only one or two of its components.

In what follows we state and apply the nuclear–field–theory rules, to calculate the interactions between the nuclear free fields and the reaction processes between the resulting physical states making use of a schematic model.

⁹²Barranco et al. (2004), Bortignon and Broglia (1981).

⁹³Idini et al. (2015); Broglia et al. (2016); Barranco et al. (2017).

⁹⁴As already mentioned, with the help of experimental probes which couple weakly to the nucleus, i.e. in such a way that the system can be expressed in terms of the properties of the excitation in the absence of probes (see however Sect. 7.6.3), it has been possible to identify the following elementary excitations in systems around closed shells:

- a) single–particle and –holes,
- b) shape vibrations,
- c) spin and isospin vibrations and charge exchange modes,
- d) pairing vibrations.

Away from closed shells one has to add to the above modes:

- e) rotations in 3D–space (e.g. quadrupole rotations)
- f) rotations in gauge space (pairing rotations).

Different probes have been utilized in the process of the identification of the different modes. In particular two-neutron transfer reactions induced by tritons and protons have played a central role in unraveling the basic features of the pairing modes.

⁹⁵Bès et al. (1974); Broglia et al. (1976); Bohr and Mottelson (1975); Mottelson (1976).

Schematic model

The model considered consists of two single-particle levels, each with pair degeneracy⁹⁶ Ω and with a schematic monopole particle-hole interaction coupling the particles in the two levels.

The total Hamiltonian is equal to

$$H = H_{sp} + H_{TB} \quad (2.7.13)$$

where

$$H_{sp} = \frac{\epsilon}{2} N_0, \quad N_0 = \sum_{\sigma=\pm 1, m} \sigma a_{m,\sigma}^\dagger a_{m,\sigma}, \quad (2.7.14)$$

and

$$H_{TB} = -\frac{V}{2} (A^\dagger A + AA^\dagger), \quad A^\dagger = \sum_m a_{m,1}^\dagger a_{m,-1}. \quad (2.7.15)$$

The index σ ($=\pm 1$) labels the two levels, while m labels the degenerate states within each level. The strength of the monopole coupling is denoted by V and the energy difference between the two levels is ϵ . The matrix element of (2.7.15) is given by

$$\langle m, 1; m', -1 | H_{TB} | m'', 1; m''', -1 \rangle = -V \delta(m, m') \delta(m'', m'''). \quad (2.7.16)$$

Field-theoretical solutions

The bare nuclear fields are the elementary modes of excitation comprising surface vibrations and single particles. The boson fields are defined through the random-phase approximation, in terms of particle-hole excitations. The basis utilized to describe the nuclear systems is a product of the different free fields. The closed-shell system of the schematic model under consideration corresponds to the lowest ($\sigma = -1$) level filled with Ω particles, while the upper ($\sigma = 1$) level remains empty. The basis particle and hole states are obtained by adding or removing a single particle to/from this closed-shell configuration. The corresponding wave functions and energies, which should include the Hartree-Fock corrections (see Fig. 2.2.1 (b), (c)) generated by the residual interaction⁹⁷, are

$$\begin{cases} |m, 1\rangle = a_{m,1}^\dagger |0\rangle, & E(m, 1) = \frac{1}{2}(\epsilon + V), \\ |m, -1\rangle = a_{m,-1}^\dagger |0\rangle, & E(m, -1) = \frac{1}{2}(\epsilon + V). \end{cases} \quad (2.7.17)$$

⁹⁶It is of notice the difference of a factor of 2 in the degeneracy of each level as compared to Sect. 2 of Bortignon et al. (1977) in which case it is 2Ω . This is in keeping with the fact that, as a rule, $\Omega = (2j + 1)/2$. See also Eq. (2.7.89) and related discussion.

⁹⁷The Hartree-Fock energy associated with the Hamiltonian (2.7.13) can be obtained from the linearization relation $[H, a_{\sigma,m}^\dagger] = E(m, \sigma) a_{\sigma,m}^\dagger$ acting on the Hartree-Fock vacuum, which in this case coincides with the single-particle vacuum defined by $a_{m,-1}^\dagger |0\rangle = a_{m,1} |0\rangle = 0$



Figure 2.7.4: Graphical representation of the amplitude of the collective phonon (wavy line) on a given particle–hole excitation $((m, 1), (m, -1))$. This amplitude can be written in terms of the interaction vertex denoted by Λ_i , and the energy denominator $\omega_i - \epsilon'$. The particles (holes) are depicted by upward– (downward–) going arrowed lines.

Thus the unperturbed energy for producing a particle–hole excitation with respect to the ground state is

$$\epsilon' = E(m, 1) + E(m, -1) = \epsilon + V. \quad (2.7.18)$$

The contribution V in (2.7.18) is the Hartree–Fock contribution to the particle–hole excitation.

If we define the creation operator of the normal modes as

$$\beta_\nu^\dagger = \sum_m \lambda_m^\nu a_{m,1}^\dagger a_{m,-1}, \quad (2.7.19)$$

the linearization equation

$$[H, \beta_\nu^\dagger] = \omega_\nu \beta_\nu^\dagger, \quad (2.7.20)$$

yields

$$\begin{cases} \omega_1 = \epsilon' - V\Omega, \\ \omega_\nu = \epsilon' \quad (\nu = 2, 3, \dots, \Omega). \end{cases} \quad (2.7.21)$$

Utilizing (2.7.20) and the normalization condition

$$[\beta_\nu, \beta_{\nu'}^\dagger] = \delta(\nu, \nu'), \quad (2.7.22)$$

we obtain for the amplitudes associated with the lowest mode

$$\lambda_m^1 = \frac{1}{\sqrt{\Omega}}. \quad (2.7.23)$$

One can also write this amplitude as the ratio between a coupling matrix element and an energy denominator, i.e.

$$\lambda_m^1 = \frac{\Lambda_1}{\omega_1 - \epsilon'}. \quad (2.7.24)$$

From (2.7.21), (2.7.23) and (2.7.24) we obtain

$$\Lambda_1 = -V \sqrt{\Omega}, \quad (2.7.25)$$

which is the strength with which a particle hole excitation ($m, 1; m, -1$) couples to the collective phonon (see Fig. 2.7.4). This can also be seen by calculating the matrix element of the interaction Hamiltonian (2.7.15) between the normal modes and the single particle-hole state

$$\Lambda_\nu = \langle n_\nu = 1 | H_{TB} | m, 1; m', -1 \rangle = -V \sqrt{\Omega} \delta(m, m') \delta(\nu, 1). \quad (2.7.26)$$

Note that the particle–vibration coupling strengths associated with the other normal modes lying at an energy ϵ' (see (2.7.21)) are equal to zero. The exact solution of (2.7.13) is reproduced by utilizing as the basic degrees of freedom both the vibrations (see (2.7.21)) and the particles (see (2.7.17)) coupled through the interactions (2.7.16) (four-point vertex) and (2.7.26) (particle–vibration coupling)⁹⁸. A significant part of the original interaction has already been included in generating the collective mode (2.7.21). This implies that the rules for evaluating the effect of the couplings (2.7.16) and (2.7.26) between fermions and bosons involve a number of restrictions as compared with the usual rules of perturbation theory that are to be utilized in evaluating the effect of the original interaction (2.7.15) acting in a fermion space. They read as follows:

- I) In initial and final states, proper diagrams involve collective modes and particle modes, but not any particle configuration that can be replaced by a combination of collective modes. This restriction permits an initial state comprising the configuration ($n_\nu = 1; m$), but excludes ($m', 1; m', -1; m, 1$).
- II) The couplings (2.7.16) and (2.7.26) are allowed to act in all orders to generate the different diagrams of perturbation theory; the restriction I) does not apply to internal lines of these diagrams.
- III) The internal lines of diagrams are, however, restricted by the exclusion of diagrams in which a particle–hole pair is created and subsequently annihilated without having participated in subsequent interactions.
- IV) The energies of the uncoupled particle and phonon fields are to be calculated by utilizing the Hartree–Fock approximation (see eq. (2.7.17)) and the RPA (see eq. (2.7.21)), respectively. The contributions of all allowed diagrams are evaluated by the usual rules of perturbation theory.

⁹⁸Bès et al. (1974); Broglia et al. (1976)

We note that the external fields acting on the system are allowed to create any state which may generate the different diagrams of perturbation theory. The corresponding matrix elements should be weighted with the amplitude of the component through which the final state is excited.

The above rules are also valid for those situations which cannot be treated in perturbation theory and where a full diagonalization is called for. Thus, *e.g.*, when the system displays a spurious state (see Sect. 2.7.3).

In what follows we discuss the energy of the $2p - 1h$ -like excitations, simplest modes which can display spuriously. We distinguish between two types of states, namely

$$|n_i = 1; m, 1\rangle, \quad \begin{cases} \omega_1 = \epsilon' - V\Omega, & \Lambda_1 = -\sqrt{\Omega}V \\ & (i = 1; m = 1, 2, \dots, \Omega), \\ \omega_i = \epsilon', & \Lambda_i = 0 \\ & (i = 2, \dots, \Omega; m = 1, 2, \dots, \Omega), \end{cases} \quad (2.7.27)$$

and⁹⁹

$$|m', 1; m', -1; m, 1\rangle, \quad \epsilon' \quad (m, m' = 1, 2, \dots, \Omega), \quad (2.7.28)$$

where as in (2.7.27) only the energy of the particle-hole excitation is given (see (2.7.18)). One can also displace the zero point of the odd system to the value $\epsilon/2$, in which case the unperturbed energy of the basis states $|n_i; m, 1\rangle$ is ω_i . The physical states are to be written as

$$|qm\rangle = \sum_i \xi_{iqm} |n_i = 1; m, 1\rangle, \quad (2.7.29)$$

as (2.7.28) cannot be basis states according to rule I), but only intermediate states. The quantities ξ_{iqm} are the amplitudes of the physical state in the different components of the product basis of elementary excitations. Rule (I) eliminates most of the double counting of two-particle, one-hole states. The model state contains Ω “proper” states of the form $|n_i; m, 1\rangle$, in which case the odd particle is in the state $(m, 1)$. That is $|n_1; m, 1\rangle$ ($\omega_1 = \epsilon' - V\Omega$) and $|n_i; m, 1\rangle$ ($\omega_i = \epsilon'$, $i = 2, \dots, \Omega$). However, there are only $\Omega - 1$ two-particle, one-hole states in which the odd particle is in the state $(m, 1)$ (Fig. 2.7.6). Therefore, a spurious state remains in the spectrum based on elementary modes of excitation. In other words, allowing the quantum number m to run over all possible Ω -states, the model space contains Ω^2 states (one for each value of m), while the correct number is $\Omega(\Omega - 1)$.

Thus the basis $|n_1 = 1; m, 1\rangle$ contains Ω spurious states. Its origin can be traced back to the violation of the Pauli principle (see also Sect. 2.7.3). To obtain the energy of $|qm\rangle$ we have to allow the states $|n_1 = 1; m, 1\rangle$ to interact through the vertices (2.7.16) and (2.7.26) and generate all the different perturbation theory diagrams (see rule II) except those containing bubbles (see rule III)).

⁹⁹Since the states (2.7.28) are restricted to be intermediate states of the perturbation expansion, the configuration $(m, 1; m, -1; m', 1)$ is allowed.

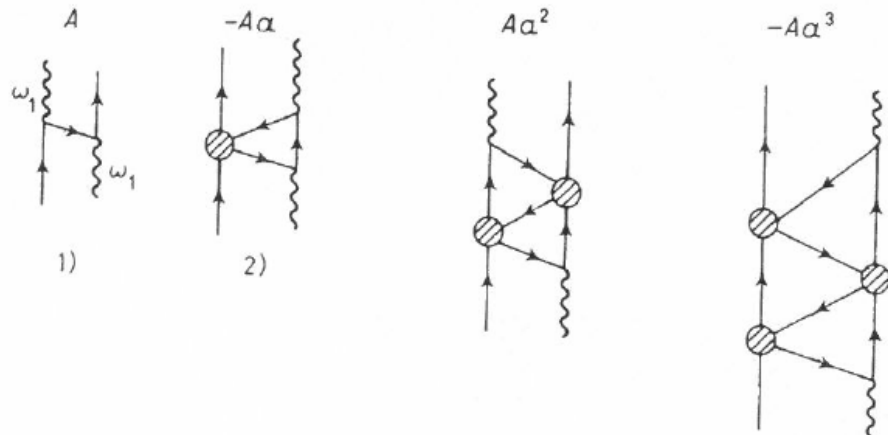


Figure 2.7.5: Contributions to the interaction of a fermion and a collective boson ω_i to order $1/\Omega^4$. The secular equation $E - E^{(0)} = A \sum_n a^n (-1)^n$ is given in terms of the quantities $A = 4\Omega V^2/(3\epsilon' - 2E)$ and $a = 2V/(3\epsilon' - 2E)$. The hatched circle represents the (particle-hole) four-point vertex (2.7.16) (see Fig. 2.7.8, third and fourth diagrams).

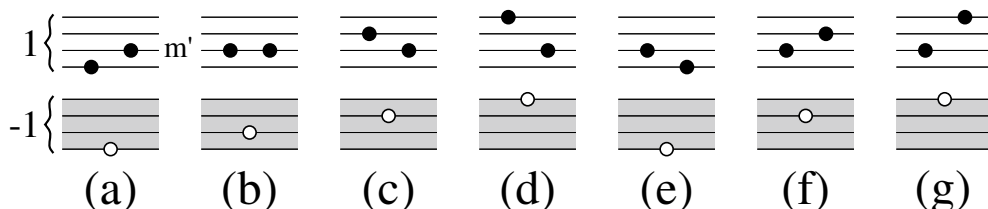


Figure 2.7.6: Schematic two-level model. Count of the states $|m, 1; m-1; m', 1\rangle$ in the case of $j = 3/2$ and $\Omega = 2j+1 = 4$. State (b) is not allowed because of Pauli principle. The states ((a),(e)), ((c),(f)) and ((d),(g)) are pairwise identical, in keeping with the indistinguishability of the particles. Thus, the states (a), (c) and (d) (equivalent (e), (f) (g)) exhaust the degrees of freedom of type (2.7.28). In other words, there are only $\Omega - 1 = 3$ two-particle one-hole states in which the odd particle is in the state $(m', 1)$.

The different graphical contributions calculated in the framework of the Brillouin–Wigner perturbation theory are displayed in Fig. 2.7.6. There is only one (diagonal) matrix element given by a single summation, which can be carried to all orders in the interaction vertices¹⁰⁰, and can be written as

$$\begin{aligned} X_{ii'} &= A \sum_n (-1)^n a^n \delta(i, i') = \\ &= \frac{A}{1+a} \delta(i, i') \delta(n, 1) = -K(E) (\sqrt{\Omega} V)^2 \delta(i, i') \delta(i, 1), \end{aligned} \quad (2.7.30)$$

where a and A are defined in the caption to the figure and

$$K(E) = \left(\frac{3}{2}\epsilon' - E + V \right)^{-1}. \quad (2.7.31)$$

The associated secular equation

$$|(\omega_i - E)\delta(i, i') + X_{ii'}| = 0 \quad (2.7.32)$$

is equivalent to the dispersion relation

$$\frac{1}{K(E)} = \sum_i \frac{(\sqrt{\Omega} V)^2}{\omega_i - E} \delta(i, 1). \quad (2.7.33)$$

Thus the energies of the system are determined by the equation

$$E = \omega_1 + \frac{\Omega V^2}{\frac{3}{2}\epsilon' - E + V}. \quad (2.7.34)$$

It admits the two solutions

$$E_{qm} = \begin{cases} \frac{3}{2}\epsilon', \\ \frac{1}{2}\epsilon' + \omega_1 + V = \frac{3}{2}\epsilon' - \Omega V + V, \end{cases} \quad (2.7.35)$$

and agree with the exact value¹⁰¹.

Because $A = 0$ for $i \neq 1$, there is no summation in (2.7.29) and

$$|qm\rangle = N_{qm}^2 |n_1 = 1; m, 1\rangle, \quad (2.7.36)$$

where

$$1 = N_{qm}^2 \left(1 - \frac{\partial X_{11}}{\partial E} \right) = N_{qm}^2 \left(1 - \frac{\Omega V^2}{\left(\frac{3}{2}\epsilon' - E + V \right)^2} \right). \quad (2.7.37)$$

¹⁰⁰Concerning the proper expansion parameter see Sect. 2.7.4, Eq. (2.7.89).

¹⁰¹The exact solutions can be obtained by noting that the operators A^\dagger, A and $\frac{1}{2}N_0$ are generators of the SU_2 group (see Bortignon et al. (1977)).

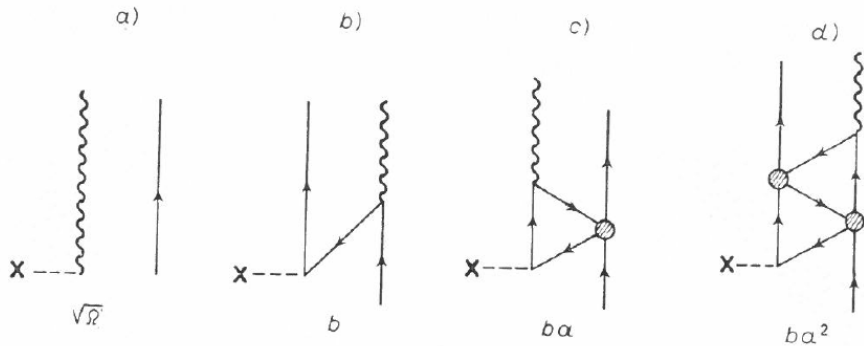


Figure 2.7.7: Graphical representation of the different terms contributing to the matrix element of the inelastic operator $\sqrt{\Omega} A^\dagger$ up to order $1/\Omega^3$. Note that the different contributions b), c), etc. have a one-to-one correspondence with the different contributions to E (see Fig. 2.7.5); $a = -2V/(3\epsilon' - 2E)$, $b = 2\Lambda_1/(3\epsilon' - 2E)$.

For $E_{qm} = \frac{1}{2}\epsilon' + \omega_1 + V$ we obtain

$$N_{qm}^2 = \frac{\Omega}{\Omega - 1}, \quad (2.7.38)$$

while for $E_{qm} = \frac{3}{2}\epsilon'$ the state is non-normalizable as the quantity in parentheses in (2.7.37) is either negative ($\Omega > 1$) or zero ($\Omega = 1$). The state defined by

$$|q, m\rangle = \sqrt{\frac{\Omega}{\Omega - 1}} |n_1 = 1; m, 1\rangle, \quad (2.7.39)$$

and

$$E_{qm} = \frac{1}{2}\epsilon' + \omega_1 + V = \frac{3}{2}\epsilon' - V(\Omega - 1), \quad (2.7.40)$$

exhausts the inelastic sum rule in agreement with the exact results. Note that (2.7.39) is specifically excited in inelastic processes, as can be seen by direct inspection. The external inelastic field can act in two ways, exciting either a particle-hole pair or a phonon, with amplitudes

$$\langle m, 1; m', -1 | A_1^\dagger | 0 \rangle = \delta(m, m'), \quad (2.7.41)$$

and

$$\langle n_i = 1 | A_1^\dagger | 0 \rangle = \sqrt{\Omega} \delta(i, 1), \quad (2.7.42)$$

respectively. The different graphical contributions to the inelastic-scattering process are displayed in Fig. 2.7.7, and can again be summed to all orders in the interaction vertices giving

$$\langle n_1 = 1; m, 1 | A_1^\dagger | m, 1 \rangle = \sqrt{\Omega} + \frac{\Lambda_1}{\frac{3}{2}\epsilon' - E_{qm} + V}. \quad (2.7.43)$$

For $E_{qm} = \frac{3}{2}\epsilon'$ this quantity is equal to zero. Thus, the corresponding states do not carry any inelastic strength, a feature which is closely related to the fact that they cannot be normalized and that they do not display any correlation energy¹⁰². On the other hand, the matrix element associated with (2.7.39) is

$$\langle qm|A^\dagger|m, 1\rangle = \sqrt{\frac{\Omega}{\Omega-1}} \frac{\Omega-1}{\sqrt{\Omega}} = \sqrt{\Omega-1}, \quad (2.7.44)$$

value which agrees with the exact answer. The results (2.7.40) and (2.7.44) can be traced down to Pauli-principle corrections. In fact, the state $|n_i = 1; m, 1\rangle$ has a nonvanishing matrix element, implying a single particle-vibration coupling vertex, with the state $|m, 1; m, -1; m, 1\rangle$. This component, which is spurious, is removed by the different graphs displayed in Figs. 2.7.5 and 2.7.7. The presence of the odd particle $(m, 1)$ blocks the particle-hole excitation $(m, 1; m, -1)$ which was present in the uncoupled system. Thus the system increases its energy by a quantity V . The reduction of the inelastic amplitude from $\sqrt{\Omega}$ to $\sqrt{\Omega-1}$ also indicates that there is one less particle-hole excitation responding to the external probe.

2.7.3 Spurious states

While the model space product of elementary modes of excitation discussed in the last section contains Ω^2 states, only $\Omega(\Omega-1)$ are physically possible, the number of spurious states being Ω , i.e. for each value of m . On the other hand, the agreement between the exact and the nuclear-field-theoretical results shows that the effects of those spurious states are eliminated from all the matrix elements associated with physical observables.

In what follows we show that, in fact, the spurious states are isolated in an explicit way in the nuclear field theory¹⁰³. Their energy coincides with the initial unperturbed energy, while all physical operators have zero off-diagonal matrix elements between any physical state and a spurious state, in particular the unit operator, which measures the overlap of the two types of states. For this purpose we use again a schematic model consisting in a number, Ω , of single-particle levels in which particles interact by means of a “monopole” force,

$$H = H_{sp} + H_{int}, \quad (2.7.45)$$

where

$$H_{sp} = \frac{1}{2} \sum_{m=1}^{\Omega} \epsilon_m (a_{m,1}^\dagger a_{m,1} - a_{m,-1}^\dagger a_{m,-1}), \quad (2.7.46)$$

and

$$H_{int} = -VA^\dagger A, \quad (2.7.47)$$

¹⁰²Note that, even if $N(E_{qm} = \epsilon_m) \rightarrow \infty$, the matrix elements associated with the different transitions tend to zero more rapidly and the final result converges and is equal to zero as expected.

¹⁰³Broglia et al. (1976)

with

$$A^\dagger = \sum_{m=1}^{\Omega} a_{m,1}^\dagger a_{m,1}. \quad (2.7.48)$$

The energy of the i -th phonon is determined by the RPA dispersion relation (see rule IV))

$$\sum_{m=1}^{\Omega} \frac{1}{\epsilon_m - \omega_i} = \frac{1}{V}. \quad (2.7.49)$$

The eigenfunction corresponding to the different modes is

$$|n_i = 1\rangle = \sum_m \frac{\Lambda_i}{\epsilon_m - \omega_i} a_{m,1}^\dagger a_{m,-1}|0\rangle. \quad (2.7.50)$$

The particle-vibration coupling constant is given by

$$\Lambda_i = -\langle n_i = 1 | H_{int} | m, 1; m', -1 \rangle = \left[\sum_m \frac{1}{(\epsilon_m - \omega_i)^2} \right]^{-\frac{1}{2}} \delta(n, n'), \quad (2.7.51)$$

where $|n_i = 1\rangle$ denotes a state containing one phonon, while $|m, 1; m', -1\rangle$ is the eigenstate associated with particle-hole excitation. The other interaction to be included (rule II)) is the four-point vertex which has the value

$$\langle m, 1; m', -1 | H_{int} | m'', 1; m', -1 \rangle = -V \delta(m, m') \delta(m'', m''). \quad (2.7.52)$$

The single-particle energies to be used in calculating the different graphs are $\frac{1}{2}\epsilon_m$, as the Hartree-Fock contribution (see rule IV)) of H_{int} is zero.

Similarly to H_{int} the “inelastic operator” has two different matrix elements, namely

$$\langle n_i = 1 | a_{m',1}^\dagger a_{m',-1} | 0 \rangle = \frac{\Lambda_i}{\epsilon_{m'} - \omega_i} \quad (2.7.53)$$

and

$$\langle m', 1; m'', -1 | a_{m,1}^\dagger a_{m,-1} | 0 \rangle = \delta(m, m') \delta(m', m''). \quad (2.7.54)$$

In what follows we discuss again the system comprising an odd particle, in the orbit $(m, 1)$, in addition to a single phonon excitation of the vacuum. According to rule I) initial and final states may involve both collective modes and particle modes, but not any particle configuration that can be replaced by a combination of collective modes. The exclusion of the states $|m, 1; m', 1; m', -1\rangle$ eliminates most of the double counting of two-particle, one-hole states. The Ω “proper” states of the form $|n_i = 1; m, 1\rangle$ are allowed. However, there are only $\Omega - 1$ (two-particle, one-hole) states in which the odd particle is in the state $(m, 1)$ (see Fig. 2.7.6).

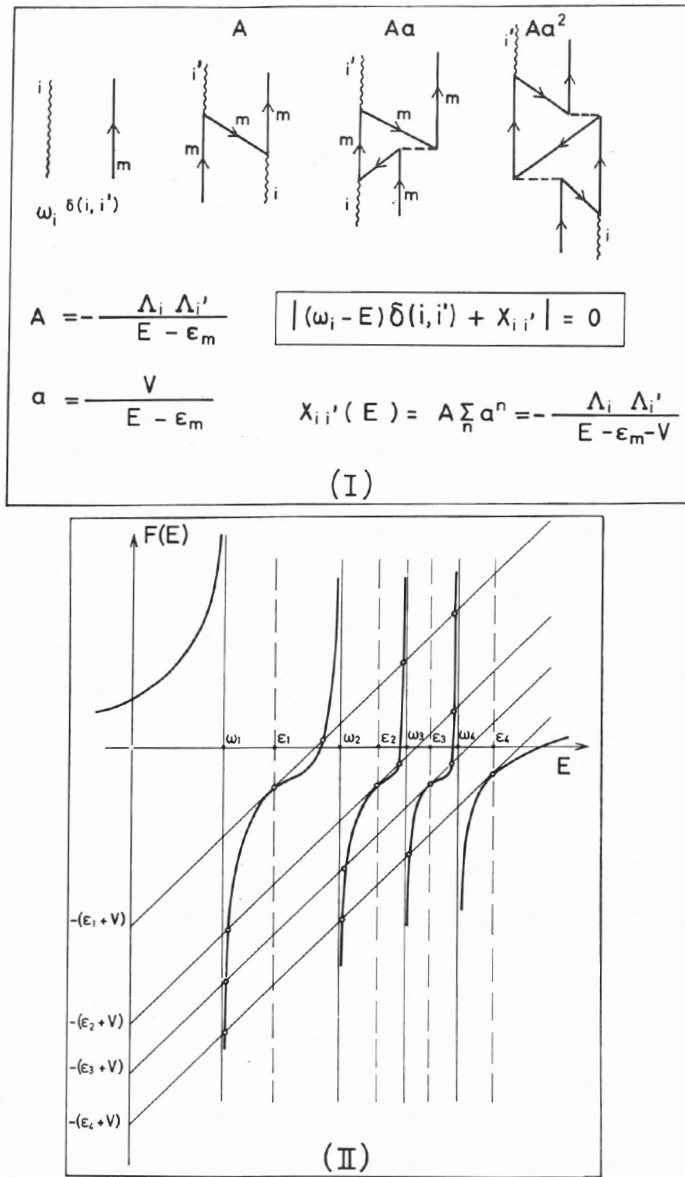


Figure 2.7.8: Lower order contributions to the energy matrix element between the basis states $|n_i = 1; m, 1\rangle$. The dashed line stands for the model bare interaction (see eq. 2.7.52). The quantity $X_{ii'}(E) = A \sum_n a^n = -\Lambda_i \Lambda'_i / (E - \epsilon_m - V)$, where $A = -\Lambda_i \Lambda'_i / (E - \epsilon_m)$ and $a = V / (E - \epsilon_m)$, is the matrix element iterated to all orders in $1/\Omega$. The secular equation of the problem is $|(\omega_i \delta(i, i')) + X_{ii'}| = 0$, and is equivalent to the dispersion relation (2.7.57). II) Graphical solution of the dispersion relation (2.7.57), for the case $\Omega = 4$. The function $F(E) = \sum_i \Lambda_i^2 / (\omega_i - E)$ is displayed as a continuous thick line, while the parallel lines $E - \epsilon_m - V$ have been drawn as thin continuous lines intersecting the ordinates axis at $-(\epsilon_m + V)$. The intersections between the two functions give the eigenvalues of the secular equation. For each value of ϵ_m there are $\Omega + 1$ roots, the root at $E = \epsilon_m$ being double.

Therefore, a spurious state remains in the spectrum of the elementary modes of excitation.

The lower-order corrections to this energy which do not contain bubbles are drawn in Fig. 2.7.8 (I). Iterating these processes to infinite order we obtain the secular equation

$$|(\omega_i - E)\delta(i, i') + X_{ii'}(E)| = 0, \quad (2.7.55)$$

where

$$X_{ii'} = -\frac{\Lambda_i \Lambda_{i'}}{E - \epsilon_m - V}. \quad (2.7.56)$$

The different contributions calculated in the framework of the Brillouin–Wigner perturbation theory are energy dependent, and take into account renormalization effects of the states not explicitly included in the calculations. The dispersion relation fixing the energies E_m of the physical states is (see App. 2.B)

$$E - \epsilon_m - V = \sum_{i=1}^{\Omega} \frac{\Lambda_i^2}{\omega_i - E} = F(E). \quad (2.7.57)$$

There is one equation for each single-particle level because the monopole force cannot change the m-state of the odd particle. The relation (2.7.57) can be solved graphically as shown in Fig. 2.7.8 (II). The energy $E = \epsilon_m$ is always a root of (2.7.57), in fact a double root since

$$\left[\frac{dF(E)}{dE} \right]_{E=\epsilon_m} = \sum_i \frac{\Lambda_i^2}{(\omega_i - \epsilon_m)^2} = 1, \quad (2.7.58)$$

and the line $E - \epsilon_m - V$ is at 45° . The remaining intersections of this line and the function $F(E)$ give rise to $\Omega - 1$ additional roots denoted by (qm) , whose energy E_{qm} agrees with the physical eigenvalues obtained from the exact solution of the model. The eigenvectors associated with the physical states (qm) are

$$|qm\rangle_F = \sum_i \xi_{iqm} |i; m, 1\rangle, \quad (2.7.59)$$

where

$$\xi_{iqm} = -N_{qm} \frac{\Lambda_i}{\omega_i - E_{qm}} = \langle i; m, 1 | qm \rangle_F. \quad (2.7.60)$$

The normalization condition which determines N_{qm} is

$$\begin{aligned} {}_F \langle qm | qm \rangle_F &= 1 = \sum_{i,i'} \left(\delta(i, i') - \frac{\partial X_{ii'}}{\partial E} \right) \xi_{iqm}^* \xi_{i'qm} = \\ &= N_{qm}^2 \left[\sum_i \frac{\Lambda_i^2}{(\omega_i - E_{qm})^2} - \frac{1}{(E_{qm} - \epsilon_m - V)^2} \sum_{i,i'} \frac{\Lambda_i^2 \Lambda_{i'}^2}{(\omega_i - E_{qm})(\omega_{i'} - E_{qm})} \right] = \\ &= N_{qm}^2 \left[\sum_i \frac{\Lambda_i^2}{(\omega_i - E_{qm})^2} - 1 \right], \end{aligned} \quad (2.7.61)$$

where the dispersion relation (2.7.57) has been utilized, and where $X_{ii'}$ is the matrix element appearing in (2.7.55) and defined in (2.7.56). For $E_{qm} = \epsilon_m$ the factor multiplying N_{qm}^2 is zero (see eq. (2.7.58)). Thus, there are only $\Omega - 1$ states which can be normalized when solving the Hamiltonian (2.7.45) in the framework of the nuclear field theory. The full spuriousity of the elementary-mode product basis is concentrated in a single state¹⁰⁴.

The subscript F has been utilized in (2.7.59) to indicate that we are dealing with the nuclear-field solution of the Hamiltonian (2.7.45) (for simplicity it will not be used in the following). Note that these eigenvectors are expressed in terms of only allowed initial or final states (see rule I))

$$|i; m, 1\rangle \equiv a_{m,1}^\dagger |i\rangle, \quad (2.7.62)$$

which are assumed to form an orthonormal basis, in particular in deriving the relation (2.7.61). This is equivalent to the basic assumption of nuclear field theory of the independence of the different modes of excitation, i.e., in the present case,

$$[\Gamma_i, a_{m,1}^\dagger] = 0. \quad (2.7.63)$$

Rules I–IV) discussed in the last section give the proper mathematical framework to this ansatz, which has played a basic role in developing a unified theory of nuclear structure. The above discussion can be illuminated by utilizing a conventional treatment of the residual interaction. Expanding the states $|n_i = 1; m, 1\rangle$ in terms of particle and hole states, we can write, with the help of (2.7.50),

$$a_{m,1}^\dagger |n_i = 1\rangle = a_{m,1}^\dagger \sum_{m' \neq m} \frac{\Lambda_i}{\epsilon' - \omega_i} a_{m',1}^\dagger |0\rangle \quad (2.7.64)$$

The overlap between the states $|n_i = 1; m, 1\rangle$ is thus given by,

$$\begin{aligned} Z(i, i') &= \langle i' | a_{m,1} a_{m,1}^\dagger | i \rangle \\ &= \sum_{m' \neq m} \frac{\Lambda_i \Lambda_{i'}}{(\epsilon_{m'} - \omega_i)(\epsilon_{m'} - \omega_{i'})} = \delta(i, i') - \frac{\Lambda_i \Lambda_{i'}}{(\epsilon_m - \omega_i)(\epsilon_m - \omega_{i'})}, \end{aligned} \quad (2.7.65)$$

where the orthogonality relation,

$$\sum_{m'} \frac{\Lambda_i \Lambda_{i'}}{(\epsilon_{m'} - \omega_i)(\epsilon_{m'} - \omega_{i'})} = \delta(i, i'), \quad (2.7.66)$$

of the RPA solutions in the even system has been utilized. Because of the non-orthogonality of the basis, the eigenvalues of the system are determined by the relation

$$|Z(E)(H - E)| = 0. \quad (2.7.67)$$

¹⁰⁴Note that the mathematical relation $N^2 f(E) = 1, N^2$, being the norm of the state with energy E , implies that such state is spurious if $f(E) = 0$ or $f(E) < 0$ (see eq. (2.7.37) and subsequent discussion).

This is fulfilled for

$$|H - E| = 0, \quad (2.7.68)$$

which yields the $\Omega - 1$ physical roots, as well as for

$$|Z(E)| = 0. \quad (2.7.69)$$

This solution corresponds to the spurious root $E_{qm} = \epsilon_m$ (i.e. $\omega_1 = 0$). In fact¹⁰⁵,

$$\begin{aligned} \lim_{\delta \rightarrow 0} \sum_i \xi_{iqm}(E_{qm} = \epsilon_m + \delta) Z_{ii'} &= \lim_{\delta \rightarrow 0} N_{qm}(E_{qm} = \epsilon_m + \delta) \\ &\times \sum_i \frac{\Lambda_i}{\omega_i - (\epsilon_m + \delta)} \sum_{m' \neq m'} \frac{\Lambda_i \Lambda_{i'}}{(\epsilon_{m'} - \omega_i)(\epsilon_{m'} - \omega_{i'})} = 0, \end{aligned} \quad (2.7.70)$$

since¹⁰⁶

$$\sum_{m' \neq m} \frac{\Lambda_i \Lambda_{i'}}{(\epsilon_{m'} - \omega_i)(\epsilon_{m'} - \omega_{i'})} = \delta(m, m'). \quad (2.7.71)$$

Note that this solution in terms of the overlap Z gives the exact answer in the present case, because of the simplicity of the model. In a general case which includes ground-state correlations this may not be true any longer.

Before dealing with the consequences of the above discussion in connection with reaction matrix elements (one-particle transfer amplitudes), let us return to (2.7.61). The physical amplitudes ξ_{iqm} are connected to $\tilde{\xi}_{iqm}$ by the relation

$$\xi_{iqm} = \frac{\tilde{\xi}_{iqm}}{\sqrt{N_{qm}}}. \quad (2.7.72)$$

Thus,

$$N_{qm} = \sum_{i,i'} \left(\delta(i, i') - \frac{\partial X_{ii'}}{\partial E} \right) \tilde{\xi}_{qm}^* \tilde{\xi}_{qm} = \sum_{i,i'} \tilde{M}_{ii'}^{mm} \tilde{\xi}_{qm}^* \tilde{\xi}_{qm}. \quad (2.7.73)$$

In usual perturbation theory

$$\frac{\partial X_{ii'}}{\partial E} \tilde{\xi}_{qm}^* \tilde{\xi}_{qm} < 0, \quad (2.7.74)$$

¹⁰⁵Within the context of renormalization, one first calculates the expressions for a finite value of δ and then takes the limit.

¹⁰⁶It is of notice that the validity of the relations (2.7.66) and (2.7.71) is related to the fact that the RPA conserves the EWSR.

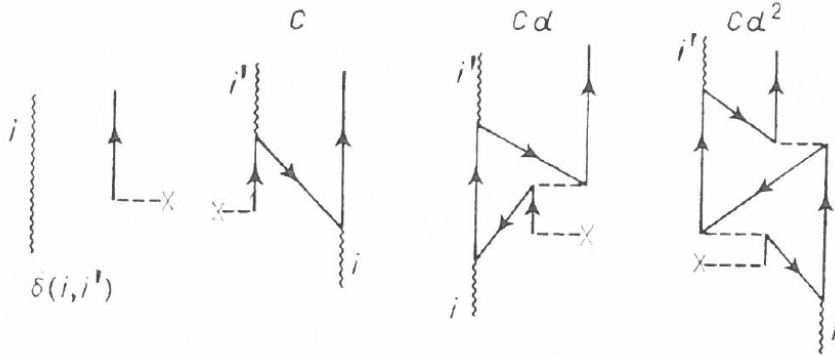


Figure 2.7.9: Lower order contributions to the one-particle transfer reaction induced by $a_{m,1}^\dagger$. The result of iterating the different contributions to all orders in $1/\Omega$ is equal to $T_{qm}(ii') = C \sum_n d^n = -\Lambda_i \Lambda_{i'} / ((\omega_i - \epsilon_m)(E_{qm} - \epsilon_m - V))$, $C = -\Lambda_i \Lambda_{i'} / ((\omega_i - \epsilon_m)(E_{qm} - \epsilon_m))$, $d = |V/(E_{qm} - \epsilon_m)|$.

and N_{qm} is always > 1 . In the present case, however, because the matrix elements of the effective Hamiltonian have to be calculated excluding the contributions containing bubbles, the quantity

$$\sum_{ii'} \frac{\partial X_{ii'}}{\partial E} \xi_{qm}^* \xi_{qm}, \quad (2.7.75)$$

can be either positive, or negative¹⁰⁷. From the above discussion it can be concluded that N_{qm} can vanish for certain states, eliminating the redundant degrees of freedom. Examples are discussed in Sect. 2.7.4 (see also 2.B.2).

We now calculate the one-particle stripping process leading to the odd system. This calculation illustrates the explicit concentration of the whole spuriousity into a single state which has zero correlation energy¹⁰⁸ and zero amplitude for the different physical processes exciting the $\Omega - 1$ physical states.

One has first to calculate the amplitude for the transition to a basis component ($n_i = 1; m, 1$) including only those graphs in which all intermediate states are excluded from appearing as initial or final states. This exclusion reflects the fact that the diagonalization procedure has included all interaction effects that link these allowed states. The final amplitude for the transition to the state (qm) is obtained by summing the amplitudes ($n_i = 1; m, 1$) each weighted by ξ_{iqm} given in Eq. (2.7.60).

The lower-order contributions to the one-particle transfer amplitude between the state $|n_i = 1\rangle$ and the state $|qm\rangle$ are displayed in Fig. 2.7.9. They can be summed

¹⁰⁷Within this context see Bès et al. (1976b) in particular App. B, footnote p. 25.

¹⁰⁸This is because the spurious state has zero phase space to correlate.

up to all orders of $1/\Omega$, the result being equal to

$$\begin{aligned}
 & \langle qm | a_{m,1}^\dagger | n_i = 1 \rangle \\
 &= \sum_{i'} \xi_{i'qm} \left\{ \delta(i, i') - \frac{\Lambda_i \Lambda_{i'}}{(\omega_i - \epsilon_m)(E_{qm} - \epsilon_m)} \left[\frac{1}{1 - V/(E_{qm} - \epsilon_m)} \right] \right\} \\
 &= \sum_{i'} \xi_{i'qm} \{ \delta(i, i') - T_{qm}(i, i') \} = \\
 &= -N_{qm} \left[\frac{\Lambda_i}{\omega_i - E_{qm}} - \frac{\Lambda_i}{(\omega_i - \epsilon_m)(E_{qm} - \epsilon_m - V)} \sum_{i'} \frac{\Lambda_{i'}^2}{\omega_{i'} - E_{qm}} \right] \\
 &= \frac{N_{qm}(E_{qm} - \epsilon_m)\Lambda_i}{(E_{qm} - \omega_i)(\omega_i - \epsilon_m)}. \tag{2.7.76}
 \end{aligned}$$

This quantity is zero for the spurious roots¹⁰⁹ (*i.e.* $E_{qm} = \epsilon_m$) and agrees with the exact result for the $\Omega - 1$ remaining physical roots.

Utilizing the relations

$$\frac{1}{V} = \sum_m \frac{1}{\epsilon_m - \omega_i}, \tag{2.7.77}$$

and

$$\frac{1}{V} = \sum_{m' \neq m} \frac{1}{\epsilon_{m'} - E_{qm}}, \tag{2.7.78}$$

we obtain

$$\sum_{m' \neq m} \frac{1}{(\epsilon_{m'} - E_{qm})(\epsilon_{m'} - \omega_i)} = \frac{1}{(E_{qm} - \omega_i)(\epsilon_m - \omega_i)}. \tag{2.7.79}$$

With the help of this relation we can derive the *one-particle transfer sum rule*. Note that (2.7.77) is the dispersion relation for the free phonon field. The second relation is, however, alien to the field theory results. Nevertheless, one can show that the solutions E_{qm} of (2.7.78) and of the nuclear-field-theory dispersion relation (2.7.57) are identical, except for the root $E_{qm} = \epsilon_m$. One can, therefore, utilize (2.7.78) as a mathematical relation without further justifications in the present context. One obtains

$$\begin{aligned}
 \sum_{qm} \left| \langle qm | a_{m,1}^\dagger | n_i = 1 \rangle \right|^2 &= \sum_{qm} \Lambda_{qm}^2 \Lambda_i^2 \sum_{m' \neq m} \frac{1}{(\epsilon_{m'} - E_{qm})(\epsilon_{m'} - \omega_i)} \\
 &\times \sum_{m' \neq m} \frac{1}{(\epsilon_{m'} - E_{qm})(\epsilon_{m'} - \omega_i)}, \tag{2.7.80}
 \end{aligned}$$

¹⁰⁹In fact, $\lim_{\delta \rightarrow 0} [(E_{qm} - \epsilon_m)N_{qm}]_{E_{qm} + \delta} = \lim_{\delta \rightarrow 0} \left\{ \sqrt{2} \delta^{3/2} / [\sum_i \frac{\Lambda_i}{\omega_i - \epsilon_m}]^{1/2} \right\} = 0$.

where

$$\Lambda_{qm} = -N_{qm}(E_{qm} - \epsilon_m) = \left[\sum_{m' \neq m} \frac{1}{(\epsilon_{m'} - E_{qm})} \right]^{-\frac{1}{2}}. \quad (2.7.81)$$

Thus

$$\sum_{qm} \left| \langle qm | a_{m,1}^\dagger | n_i = 1 \rangle \right|^2 = \Lambda_i^2 \sum_{m' \neq m} \frac{1}{(\epsilon_{m'} - \omega_i)^2} = 1 - \frac{\Lambda_i^2}{(\epsilon_m - \omega_i)^2}, \quad (2.7.82)$$

where use has been made of the orthogonality relation

$$\sum_{m' \neq m} \frac{1}{(\epsilon_{m'} - E_{qm})(\epsilon_{m''} - E_{qm})} = \delta(m', m'') \quad (m', m'' \neq m). \quad (2.7.83)$$

The result (2.7.82) coincides with the exact result. Physically it means that the single-particle orbital $(m, 1)$ is blocked by the amount $\Lambda_i^2/(\epsilon_m - \omega_i)^2$, which is the probability that the phonon $(n_i = 1)$ is in the particle-hole configuration $(m, 1; m, -1)$, *i.e.* with its particle in the orbital $(m, 1)$.

2.7.4 Applications

In what follows we discuss some aspects of the low-lying spectrum of the nucleus ^{209}Bi in terms of fermions, surface ($\beta_n^\dagger(0\lambda)$) and pairing ($\beta_n^\dagger(2\lambda)$) vibrational modes.

The unperturbed states of the closed-shell-plus-one-particle system can be written in terms of the free fields as

$$|n2\lambda, j; IM\rangle = [\beta_n^\dagger(2\lambda)a_j]_{IM}|0\rangle, \quad (2.7.84)$$

and

$$|n0\lambda, j; IM\rangle = [\beta_n^\dagger(0\lambda)a_j^\dagger]_{IM}|0\rangle. \quad (2.7.85)$$

This constitutes the basis set of states $\{\alpha_i\}$. All other states give rise to the complementary Hilbert space $\{a_i\}$.

The elementary modes of excitation interact through the particle-vibration and four-point vertices displayed in Fig. 2.7.10 giving rise to the matrix elements

$$M_1(nj, n'j') \equiv \langle [\beta_n^\dagger(0\lambda)a_{j'}^\dagger]_{IM} | h_{eff}(E) | [\beta_n^\dagger(0\lambda)a_j^\dagger]_{IM} \rangle, \quad (2.7.86)$$

$$M_2(nj, n'j') \equiv \langle [\beta_{n'}^\dagger(2\lambda)a_{j'}]_{IM} | h_{eff}(E) | [\beta_n^\dagger(2\lambda)a_j]_{IM} \rangle, \quad (2.7.87)$$

and

$$M_3(nj, n'j') \equiv \langle [\beta_{n'}^\dagger(2\lambda)a_{j'}]_{IM} | h_{eff}(E) | [\beta_n^\dagger(0\lambda)a_j^\dagger]_{IM} \rangle. \quad (2.7.88)$$

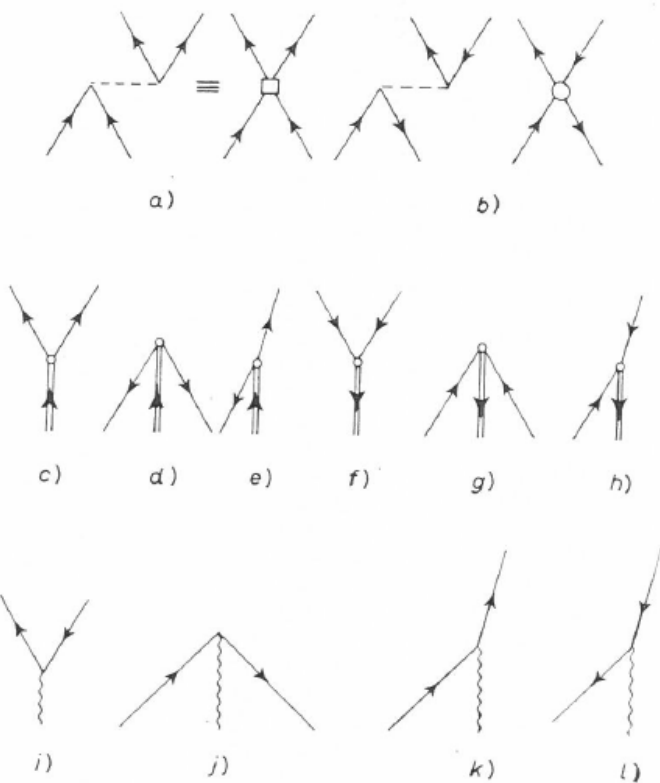


Figure 2.7.10: Interactions coupling the fermion fields with the pairing and surface vibrations. The different fermion and boson free fields are particles, holes, pairing vibrations ($\beta = \pm 2$) and surface vibrations ($\beta = 0$), β being the transfer quantum number. The two possible four-point vertices are given in a) and b). They correspond to the pairing and particle-hole model bare interactions. In graphs c)–h) all possible couplings between the fermion fields (arrowed lines) and the pairing vibrational fields (double lines arrowed) are displayed. Graphs i)–l) are all the possible coupling vertices between the surface vibrations (wavy line) and the fermion fields. Note that there is no direct coupling between the two boson fields, as the field theory we are dealing with is linear in the different field coordinates.

They are to be calculated by utilizing the graphical techniques of perturbation theory and the rules discussed in Sect. 2.7.2. *There are two parameters on which to expand upon in carrying out a perturbative calculation. The first one is the strength of the interaction vertices measured in terms of the average distance between single-particle levels. The second is $1/\Omega$, where $\Omega = \sum_j(j + \frac{1}{2})$ is the effective degeneracy of the valence shells (in connection to this “standard” definition of Ω we refer to footnote⁹⁶). These two parameters are in general connected through involved expressions. In the schematic model discussed in Sect. 2.7.2, however, their relation is explicit and can be expressed as*

$$\epsilon = O(1), \quad \Lambda = O\left(\frac{1}{\sqrt{\Omega}}\right) \quad \text{and} \quad V = O\left(\frac{1}{\Omega}\right). \quad (2.7.89)$$

Another feature which determines the family of diagrams to select to a given order of perturbation is the number of internal lines which can be freely summed up. Each of these summations introduces a multiplicative factor Ω . Based on a wealth of detailed calculations for realistic distributions of levels one can conclude that relations (2.7.89) are valid also in such cases¹¹⁰. In what follows, we give an example of NFT in a realistic situation, namely ^{209}Bi . This nucleus has been investigated by means of high-resolution anelastic process¹¹¹. Through these experiments a septuplet of states around 2.6 MeV of excitation was identified, with spins ranging from $\frac{3}{2}^+$ to $\frac{15}{2}^+$.

In zeroth order these states can be interpreted in terms of a proton moving in the $h_{9/2}$ orbital coupled to the lowest octupole vibration of ^{208}Pb . The $\frac{3}{2}^+$ of this multiplet displays also a large parentage based on the proton pair addition and proton hole moving in the $d_{3/2}$ orbital, as revealed by the (t, α) reaction¹¹² on ^{210}Po . The above results indicate that the (two-particle, one-hole) type of states in ^{209}Bi are amenable to a simple description in term of the basis states

$$|(\beta = 2), \lambda^\pi, j_1^{-1}; IM\rangle \equiv |j_1^{-1} \otimes \lambda^\pi(^{210}\text{Po}); IM\rangle \quad (\lambda^\pi = 0^+, 2^+, 4^+) \quad (2.7.90)$$

and

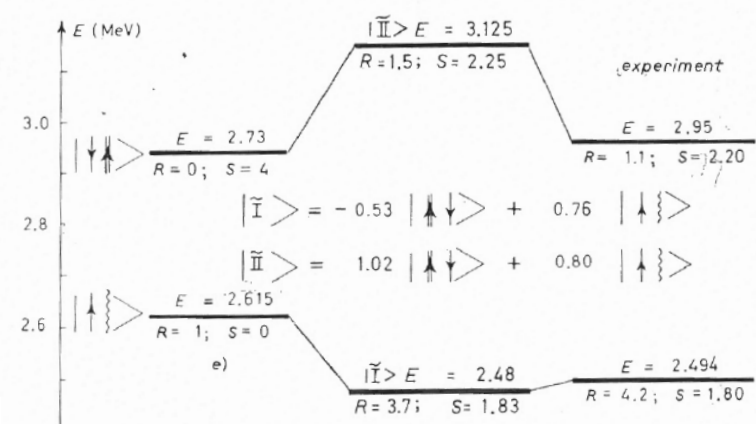
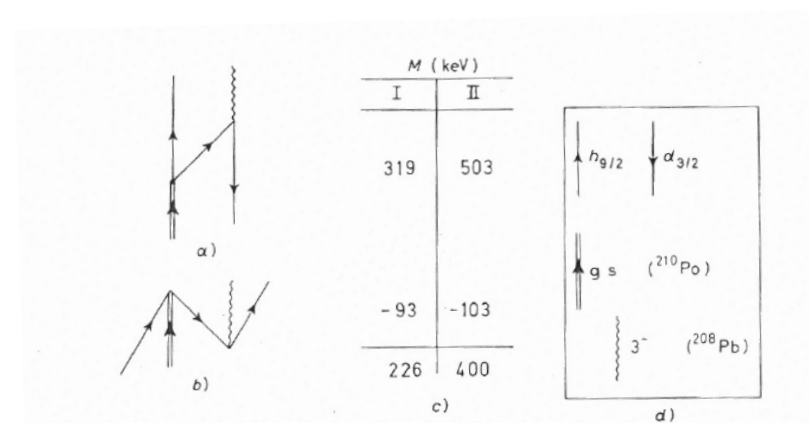
$$|(\beta = 0), \lambda^\pi, j_2; IM\rangle \equiv |j_2 \otimes \lambda^\pi(^{208}\text{Pb}); IM\rangle \quad (\lambda^\pi = 3^-) \quad (2.7.91)$$

Only the lowest states of each spin and parity λ^π are included in the basis states,

¹¹⁰An alternative way to argue concerning the expansion parameter, and in this case in connection with pairing vibrations, is to use the dimensionless quantity $x = 2G\Omega/D$ appropriate of a model made of two j -shells separated by an energy $D = 2\epsilon$ in which pairs of nucleons moving in time-reversal states interact through a pairing coupling constant G . Phase transition takes place at $x \geq 1$, while situations away from phase transitions but still displaying consistent fluctuations typical of nuclei displaying low-lying collective vibrations, correspond to $x \approx 0.5$. Assuming $D(O(\epsilon)) = O(1)$, one obtains $G(O(V)) = O(1/\Omega)$ and naturally $\Lambda = O(1/\sqrt{\Omega})$, in keeping with the fact that the induced interaction can be written as $\Lambda^2/(\epsilon - \omega)$.

¹¹¹Ungrin et al. (1971), Broglia et al. (1970).

¹¹²Barnes et al. (1972).



$$\left\{ \begin{array}{c} -0.53 \\ 1.02 \\ -0.103 \end{array} \right] + \left\{ \begin{array}{c} 0.76 \\ 0.80 \\ 0.135 \end{array} \right]^2 = \frac{2 \times 10^{-2}}{1 \times 10^{-5}}$$

f)

$$4 \times \left\{ \begin{array}{c} -0.53 \\ 1.02 \\ -0.103 \end{array} \right]^2 = \frac{1.12}{4.16}$$

g)

$$4 \times \left\{ \begin{array}{c} -0.53 \\ 1.02 \\ -0.103 \end{array} \right] + \left\{ \begin{array}{c} 0.76 \\ 0.80 \\ -0.211 \\ -0.333 \\ 0.014 \\ 0.015 \end{array} \right]^2 = \frac{1.82}{2.27}$$

h)

$$\frac{1}{10} \left\{ \begin{array}{c} 0.76 \\ 0.80 \\ -0.577 \end{array} \right]^2 = \frac{1.92 \times 10^{-2}}{2.13 \times 10^{-2}} e^2 b^3$$

(3.3 %)
(3.6 %)

i)

$$\begin{aligned}
 & \frac{1}{10} \left\{ -0.53 \left[\begin{array}{c} \text{Diagram 1} \\ \text{Diagram 2} \end{array} \right] + 1.02 \left[\begin{array}{c} \text{Diagram 3} \\ \text{Diagram 4} \end{array} \right] \right\} \\
 & + 0.76 \left[\begin{array}{c} \text{Diagram 5} \\ \text{Diagram 6} \\ \text{Diagram 7} \\ \text{Diagram 8} \\ \text{Diagram 9} \\ \text{Diagram 10} \end{array} \right] + 0.80 \left[\begin{array}{c} \text{Diagram 11} \\ \text{Diagram 12} \\ \text{Diagram 13} \\ \text{Diagram 14} \\ \text{Diagram 15} \\ \text{Diagram 16} \end{array} \right] = \\
 & = \frac{0.0216}{(e^2 b^3)} \quad (3.7\%) \\
 & \quad \quad \quad j) \quad (1.5\%)
 \end{aligned}$$

Figure 2.7.11: In **a**, **b** and **c**) we give the two graphical contributions and the corresponding numerical values to the matrix element $M(E) = \langle d_{3/2}^{-1} \otimes gs(^{210}\text{Po}) | h_{eff}(E) | h_{9/2} \otimes 3^-(^{208}\text{Pb}); 3/2 \rangle$ in lowest order in $1/\Omega$. The resulting wave functions $|\tilde{I}\rangle$ and $|\tilde{II}\rangle$ are displayed in **e**) normalized according to (2.7.72). In **e**) we also give the unperturbed, and the renormalized theoretical energies of the levels. The (t, α) spectroscopic factor corresponding to the reaction $^{210}\text{Po}(t, \alpha)^{209}\text{Bi}$ is denoted by S , while

$$R = \frac{d\sigma(h_{9/2} \rightarrow J)}{d\sigma(gs(^{208}\text{Pb}) \rightarrow 3^-(^{208}\text{Pb}))}.$$

is the ratio of inelastic cross sections. In **d**) we display the free fields, while in **e**) we provide a summary of the results of the calculations in comparison with the data. The zeroth and order $1/\Omega$ contributions to the electromagnetic excitations are collected in **i**) and **j**). The value $0.58e^2b^3$ is the $B(E3; 0 \rightarrow 3)$ value associated with the 2.615 MeV state in ^{208}Pb . In **g**) and **h**) we give the zeroth and order $1/\Omega$ contributions to the spectroscopic factor associated with the $^{210}\text{Po}(t, \alpha)^{209}\text{Bi}$ reaction. Finally in **f**) we display the lowest contribution to the spectroscopic factor associated with the $^{208}\text{Pb}(^3\text{He}, d)$ reaction, which gives a measure of the ground state correlations of ^{208}Pb associated with the existence of an octupole and a pairing vibration (see also Tables 2.5.1–2.5.3).

while all the RPA solutions are included in the intermediate states. The quadrupole surface vibrational modes were allowed only as intermediate states. The single hole and particle states j_1^{-1} and j_2 , respectively, correspond to experimentally known levels around the $Z = 82$ shell closure. In what follows, the two $\frac{3}{2}^+$ states built out of the $|d_{3/2}^{-1} \otimes gs(^{210}\text{Po})\rangle$ and $|h_{9/2} \otimes 3^-(^{208}\text{Pb})\rangle$ configurations are studied in this space. This two-state system provides a rich laboratory to learn about the interplay of surface and pairing modes.

The two basis states

$$|\alpha\rangle \equiv |d_{3/2}^{-1} \otimes gs(^{210}\text{Po}); 3/2^+\rangle \quad (2.7.92)$$

and¹¹³

$$|\beta\rangle \equiv |h_{9/2} \otimes 3^-(^{208}\text{Pb}); 3/2^+\rangle \quad (2.7.93)$$

are 118 keV apart. They mix strongly through the couplings depicted by the graphs a) and b) of Fig. 2.7.11.

Because of the energy dependence of h_{eff} there is a different matrix element for each final state. The diagonalization of the matrices was carried out self-consistently, *i.e.* the energy denominators of the different graphs are to be calculated by utilizing the exact energies¹¹⁴. The corresponding graphical contributions to the single-particle spectroscopic amplitudes, and thus eventually absolute (t, α) differential cross sections, and absolute inelastic scattering cross-sections are also collected in fig. 2.7.11. To be noted is the very different ratio of the (d, d') and (t, α) cross sections. While $R_1 = B(E3; (\frac{3}{2})_1)/B(E3; (\frac{3}{2})_2)$ is approximately equal to 2.5, the ratio $R_2 = \sigma((t, \alpha); (\frac{3}{2})_2)/\sigma((t, \alpha); (\frac{3}{2})_1)$ is close to one. Because the component $|\beta\rangle$ carries the inelastic-scattering strength, while the (t, α) reaction proceeds mainly through the component of type $|\alpha\rangle$, *the difference between R_1 and R_2 can be traced back to the corrections associated with the over-completeness of the unperturbed basis states which give rise to rather different normalizations of the two physical states* (see Sects. 2.5 and 2.7.3, see also App. 2.B, Sect. 2.B.2).

2.8 Elementary modes of excitation and specific probes

The picture of nuclear structure achieved in terms of elementary modes of excitation displays in a transparent manner the correlation aspects of nuclear dynamics. And, as a consequence or better as a result of the physical input at the basis of the picture, it points to the reaction processes specific to bring the structure information to the detector (observer). The wavefunctions resulting from the NFT solution of the finite quantal nuclear many-body problem contains only few components. Each of them make direct reference to a specific probe. In particular

¹¹³Although not likely, the reader is advised not to confuse the label of the state $|\beta\rangle$ with the transfer quantum number β used above.

¹¹⁴for more details, see ref. Bortignon et al. (1977); see also Bortignon et al. (1976).

inelastic scattering and one- and two-particle transfer reactions. That is, each component is related to an observable, and is thus associated with a concrete experiment one knows how to carry out with the help of accelerators, beams (in e.g. inverse kinematics), targets (active or less), detectors and softwares, whose output directly relate to the observer. Said it differently, the elementary modes of excitation picture calls for a unified nuclear field theory description of structure and reactions (see also Sect. 7.6.2). More precisely, to the question concerning how the nuclear structure of the one-proton outside closed shell nucleus $^{209}_{83}\text{Bi}_{126}$ is, a possible answer reads the following: a subtle interplay between the vacuum state, that is the ground state of the double closed shell nucleus $^{208}_{82}\text{Pb}_{126}$, its first excited collective state $|3^-(^{208}\text{Pb}); 2.613 \text{ MeV}\rangle$ and the proton pair addition mode $|gs(^{210}_{84}\text{Po}_{126})\rangle$ as far as boson elementary modes of excitation with $\beta = 0$ and $\beta = +2$ transfer quantum number is concerned, and a one-proton ($\beta = +1$) and one-proton hole ($\beta = -1$) above and in the $Z = 82$, $N = 126$ vacuum state respectively, concerning the fermion degree of freedom. Consistent with this scenario, inelastic scattering and Coulomb excitation ($^{209}\text{Bi}(\alpha, \alpha')$ and $^{209}\text{Bi}(\alpha, \alpha')$ respectively), and one-ptoton stripping and pickup reactions ($^{208}\text{Pb}(^3\text{He}, n)^{209}\text{Bi}$ and $^{210}\text{Po}(t, \alpha)^{209}\text{Bi}$ respectively) together with two-proton stripping processes (e.g. $^{207}\text{Tl}(^3\text{He}, n)^{209}\text{Bi}$, possible only in inverse kinematics), are the specific experimental probes.

The need to include both single-particle and collective modes to describe the elementary excitations (reactions) of nuclei subject to external probes, implies that one employs an overcomplete (non-orthogonal) set of variables.

From the existence of the nuclear shell structure, interactions can be represented in first approximation by an average field. Thus one can describe the coupling between single-particle and collective vibrations by a three-point (-field) vertex (Fig. 2.7.4) rather than a four-point (-field) representing the bare nuclear interaction (Fig. 2.2.1 (a)). It is of notice that according to rule II of NFT, this interaction is also to be considered in working out the different diagrams. Concerning the role of non-orthogonality between elementary modes of excitation we also refer to two-nucleon transfer processes (Fig. 4.1.2, as well as App. 6.C), in which case, simultaneous transfer is partially mediated by the finite overlap of the single-particle wavefunctions in target and projectile, contribution which is to be eliminated from the total transition amplitudes (non-orthogonality (NO) correction). A similar requirement is found at the basis of the derivation of the tunneling Hamiltonian associated with weakly coupled superconductors (Josephson junction, Set. 4.7).

2.9 Competition between the variety of ZPF, in particular those associated with density ($\beta = 0$) and pairing ($\beta = \pm 2$)

Particle-hole like vibrations, as e.g. collective surface quadrupole vibrations, induce dynamical distortions of the mean field which virtually break the magnetic

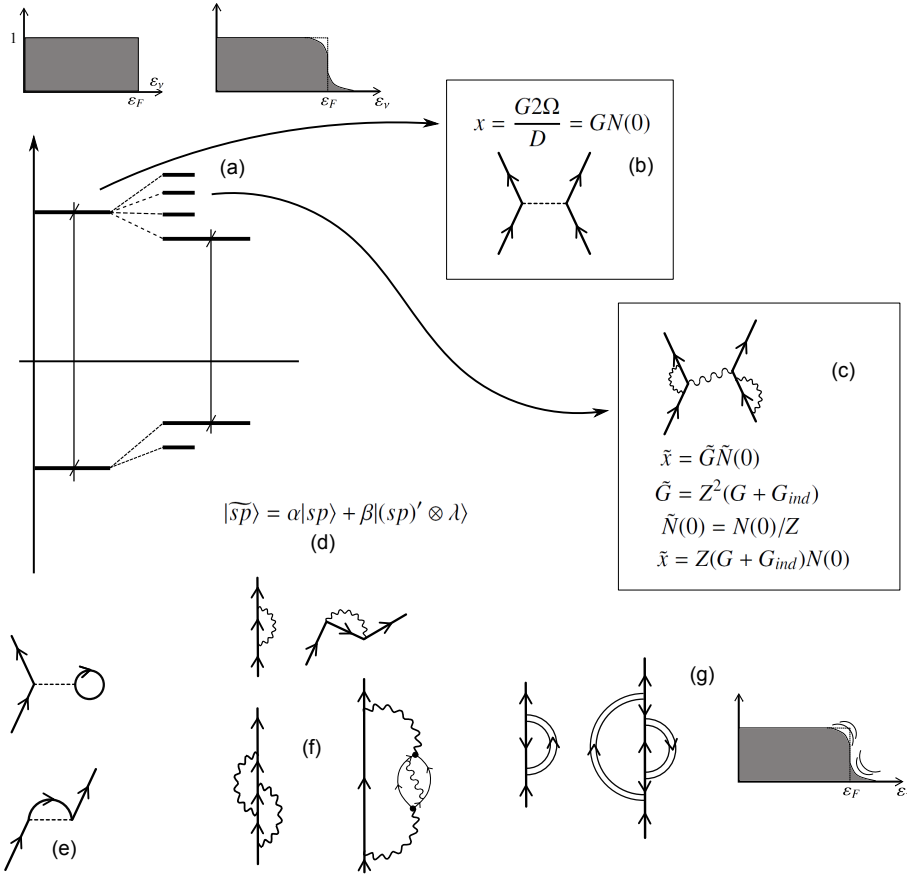


Figure 2.9.1: Schematic representation of some of the consequences the interweaving of the elementary modes of excitation with varied transfer quantum number ($\beta = 0, \pm 1, \pm 2$; **(f)**, **(g)**) have in the (mainly single-particle) nuclear spectrum **(a)**–**(e)**. In particular pair correlations **(b)**, **(c)**, as measured by the (two-level) dimensionless parameter $x = G2\Omega/D = GN(0)$, product of the bare coupling constant G and the density of states (DOS) at the Fermi energy (ratio of the single-particle degeneracy $2\Omega = (2j+1)$, and the single-particle energy separation; see Högaasen-Feldman (1961); Broglia et al. (1968)). Coupling with surface modes **(f)** reduce the effective value of D leading to an increase of $N(0)$ as measured by $1/Z$ but, at the same time decreases, through the breaking of the single-particle strength, the single-particle content **(d)** of each level (as measured by Z ; see e.g. Barranco et al. (2005) and refs. therein). The eventual increase of x , as reflected by \tilde{x} , results from a delicate balance of the two effects eventually overwhelmed by the induced pairing interaction resulting from the exchange of collective ($\beta = 0$) vibrations between pairs of nucleons moving in time reversal states close to the Fermi energy, and by the dynamical smoothing of the Fermi energy through the coupling of single-particle states to $\beta \pm 2$ pairing vibrations **(g)**.

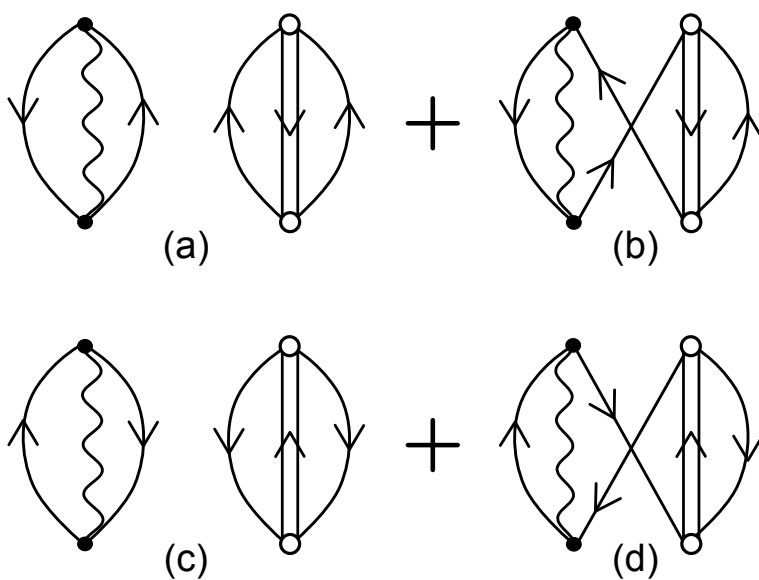


Figure 2.9.2: (a) (c) ZPF associated with $p-h$ and pairing vibrations (pair subtraction and pair addition modes) make use of the same nucleon degrees of freedom to simultaneously, and independently, correlate $p-h$, $p-p$ and $h-h$ excitations, thus violating Pauli principle (harmonic approximation). The NFT processes (b) and (d), which contribute to the correlation energy of the nucleus with opposite sign to that contributed by (a) and (c) (each unavoidable crossing of fermion lines contributes a minus sign), remove Pauli violating contributions to the corresponding order of perturbation in $1/\Omega$ (see Eq. (2.7.89) and related text).

degeneracy of levels into two-fold (Kramer's) degenerate (Nilsson-like) levels and to a reduction of the size of the discontinuity at the Fermi surface typical of non-interacting Fermi systems. Pairing vibrations also smooth out the sharp discontinuity of occupancy taking place around the Fermi energy displayed by closed shell systems through dynamical ($U_j V_j$) weighting factors (see Fig. 4.4.2), which are operative in an energy region¹¹⁵ $\epsilon_F \pm E_{corr}(\beta = \pm 2)$ (see Fig. 2.9.1 (g)). At the same time the dressing of nucleons by particle-hole and pairing vibrations, leads to an effective ω -mass making nucleons heavier, thus approaching the centroid of the valence orbitals lying above and in the Fermi sea towards the Fermi surface. In Fig. 2.9.1 a schematic representation of the subtle effects the interweaving of single-particle motion and collective vibrations has on pairing correlations, is displayed (see also Fig. 5.H.1).

Zero point fluctuations induced by particle-hole like and by pairing modes compete with each other for phase space, through Pauli principle (see Fig. 2.9.2), thus eventually leading to a single ground state containing all of the dressed renormalized ZPF (see Sect. 2.7). The Pauli principle NFT diagrams showed in Figs. 2.9.2 (b) and 2.9.2 (d) are at the basis of the stabilization of the ground state in general and of the competition between (as a rule quadrupole) deformations in 3D-space which breaks single-particle degeneracy (Nilsson potential), and in gauge space which thrives on large degeneracies¹¹⁶. It is also the reason why single open shell nuclei are usually spherical. When tidal-like polarization effects in doubly open shell nuclei become overwhelming, the nucleus makes use of a Jahn-Teller mechanism. This to profit at best and simultaneously, of the quadrupole-quadrupole (alignment) and of the pairing (independent pair motion in Kramers degenerate levels) interactions. In other words, of potential energy (quadrupole deformation, localization) and of pairs of nucleons solidly anchored to each other (localization), over distances $\xi(\gg R_0)$ resulting in strongly overlapping entities and thus little sensitive to the orientation of the quadrupole deformed field (small moment of inertia), effect weakened in turn because of low spatial degeneracy. The fact that the moment of inertia \mathcal{J} of e.g. quadrupole deformed nuclei is found to be appreciably smaller (by about a factor of 2) than the rigid moment of inertia testifies to the role pairing correlations play in nuclei. The fact that \mathcal{J} is considerably larger than the irrotational moment of inertia¹¹⁷ (by a factor of 5), testifies to the subtle effects that spatial quantization, medium polarization effects (within this context see Fig. 4.A.5), let alone the $^1S_0 - NN$ potential, eventually corrected by three-body effects, have in Cooper pair binding.

¹¹⁵ E_{corr} is the correlation energy associated with the pair addition ($\beta = +2$) and pair removal mode ($\beta = -2$).

¹¹⁶This is an example of the competition between pairing and aligned scheme (Bayman (1961); Bès and Sorensen (1969); Mottelson (1962); Bohr and Mottelson (1975)).

¹¹⁷Bohr and Mottelson (1975) p. 75.

2.10 Coupling between structure and reaction channels

In this Section the unification of NFT of structure and reactions is further developed using as example the light exotic two-neutron halo nucleus ^{11}Li . In particular, we dwell upon the variety of renormalization processes and associated form factors needed to calculate one- and two- neutron transfer reactions. The use of the same elements in the eventual calculation of the corresponding polarization contribution to the optical potential¹¹⁸, a subject not treated in the present monograph, is briefly mentioned below.

2.10.1 Bare particles and Hartree-Fock field

Nucleon elastic scattering experiments at energies of tens of MeV can be accurately described in terms of an optical potential in which the real component is parametrized according to the (Woods–Saxon) potential¹¹⁹,

$$U(r) = U f(r), \quad (2.10.1)$$

$f(r)$ being a Fermi (sigmoidal) function, of radius $R_0 = r_0 A^{1/3}$ ($r_0 = 1.2$ fm), diffusivity $a = 0.65$ fm, and strength

$$U = U_0 + 0.4E \quad (2.10.2)$$

where

$$U_0 = V_0 + 30 \frac{N - Z}{A} \text{ MeV}, \quad V_0 = -51 \text{ MeV}, \quad (2.10.3)$$

while E is the energy of the scattered particle $\epsilon_k = \hbar^2 k^2 / 2m$, measured from the Fermi energy, m being the nucleon mass. In the case of $^9\text{Li}_6$, $U_0 \approx -41$ MeV. One can replace the k -dependence in (2.10.2) by the so-called k -mass¹²⁰

$$m_k = m \left(1 + \frac{m}{\hbar^2 k} \frac{dU}{dk} \right)^{-1}, \quad (2.10.4)$$

where the energy independent Woods–Saxon potential has a depth given by $\left(\frac{m}{m_k}\right) U_0 = U'_0$ ¹²¹. For the nucleons of the core, i.e. of ^9Li , $m_k = m(1 + 0.4)^{-1} \approx$

¹¹⁸There exists a vast literature concerning this subject. See e.g. Feshbach (1958, 1962); Jackson (1970); Jeukenne et al. (1976); Sartor and Mahaux (1980); Pollarolo et al. (1983); Satchler (1983); Broglia and Winther (2004); Dickhoff and Van Neck (2005); Montanari et al. (2014); Dickhoff et al. (2017). See also Dickhoff and Charity (2019) and refs. therein.

¹¹⁹cf. e.g. Bohr and Mottelson (1969) and refs. therein.

¹²⁰What in nuclear matter is called the k -mass and is a well defined quantity, in finite systems like the atomic nucleus, in which linear momentum is not a conserved quantity, is introduced to provide a measure of the spatial non-locality of the mean field, and is defined for each state as the expectation value of the quantity inside the parenthesis in Eq. (2.10.4), calculated making use of the corresponding single-particle wavefunction (see e.g. ref. Bernard and Giai (1981), in which case m_k is referred to as the non-locality effective mass)

¹²¹See e.g. Fig. 2.14 Mahaux et al. (1985).

$0.7m$. For the halo neutrons¹²², $m_k/m = (1 + O \times 0.4)^{-1}$, where $O(= (R_0/R)^3)$ is the overlap between the core and the halo nucleons. Making use of the values $R_0 = 2.66$ fm and $R = 4.58$ fm (see Eq. 4.C.4) one obtains $O \approx 0.2$ (see (3.6.8)) and thus, $m_k \approx 0.93 m$.

2.10.2 Physical particles and optical potential

Within the framework of the above scenario, each nucleon moves independently in the average field created by all the other nucleons¹²³ feeling their pushings and pullings only when trying to leave the nucleus, the summed effect being to be forced to scatter elastically off the nuclear surface. Schematically, the full complexity of the many-body nuclear Hamiltonian

$$H = T + v, \quad (2.10.5)$$

has been reduced to

$$H_{HF} = T + U(r) + U_x(\mathbf{r}, \mathbf{r}'). \quad (2.10.6)$$

In other words, and making use of the expression,

$$H = T + v(|\mathbf{r} - \mathbf{r}'|) = H_{HF} + (v(|\mathbf{r} - \mathbf{r}'|) - (U(r) + U_x(|\mathbf{r} - \mathbf{r}'|))) \quad (2.10.7)$$

the full many-body nuclear Hamiltonian has been approximated by the Hartree–Fock Hamiltonian by neglecting the term in parenthesis. That is, by assuming that the sum of the direct and exchange potential gives a sensible approximation to the full two-body interaction v . This approximation (adding an appropriate spin-orbit potential), although providing a number of important insights into the nuclear structure and reactions as the sequence of single-particle levels¹²⁴ (and associated magic numbers), and sensible nucleon–nucleus, elastic phase shifts, disagrees with experiment on a number of points. In particular, leading to a too low level density at the Fermi energy, to an infinite mean free path, also for nucleons moving in states (e.g. deep hole states) far removed from the Fermi energy, let alone the lack of collective electromagnetic transitions and the large value of the elastic cross section.

To move further, one has to go beyond independent particle as well as potential scattering motion. That is, one has to allow the particles (both bound and projectile nucleons) to interact among themselves through four point vertices (see e.g.

¹²²Assuming a velocity independent v , the k -dependence of the mean field stems from the exchange (Fock) potential $U_x(\mathbf{r}, \mathbf{r}') = -\sum_i \varphi_i^*(\mathbf{r}') v(|\mathbf{r} - \mathbf{r}'|) \varphi_i(\mathbf{r})$ (linear in O), while the central potential is written as $U(r) = \sum_i \int d\mathbf{r}' |\varphi_i(\mathbf{r}')|^2 v(|\mathbf{r} - \mathbf{r}'|)$, (independent of O). It is of notice that the coupling between e.g. the quadrupole vibration of the core (⁸He) and a halo neutron is also linear in O , i.e. $\langle H_c \rangle_{2^+(core), n(halo)} = \beta_2 \left\langle \frac{R_0}{\sqrt{5}} \frac{\partial U}{\partial r} \right\rangle O \langle j || Y^2 || 1/2 \rangle$, where $\langle j || Y^2 || 1/2 \rangle \approx 0.7$ ($j = 5/2, 3/2$), and $\left\langle R_0 \frac{\partial U}{\partial r} \right\rangle \approx 1.44 U_0 \approx -60$ MeV, see Brink and Broglia (2005) Eqs. (D20) p. 303 and (D26) p. 304 (see Sect. 2.10.2 and Fig. 2.10.1).

¹²³Pauli principle (Fock potential) takes care of not to count the contribution of a nucleon on itself.

¹²⁴Mayer and Jensen (1955).

(2.7.16) and diagrams a) and b) of Fig. 2.7.10), aside from coupling to the nuclear and to the Fermi surface (diagrams c)–i) of Fig. 2.7.10). Also with spin, spin–isospin, etc. modes (particle vibration coupling, which in the case of surface modes has been introduced in (2.7.26); see also (2.3.13)). In other words, to allow the elementary modes of excitation to interact according to the NFT rules. In the case in which one nucleon moves with asymptotic waves for $r = -\infty$ (e.g. projectile), the interaction in parentheses in (2.10.7) can lead to the coupling to open reaction channels. In particular, one– and two–particle transfer reactions, in which the mass partition changes between entrance and exit channels. Let us exemplify the consequences of the interaction between elementary modes of excitation in the case of $^{11}\text{Li} + p$.

2.10.3 $^{11}\text{Li}_8$ structure in a nutshell

The sequence of single–particle levels for the $^{10}\text{Li}_7$ associated with the mean field potential (2.10.3) implies that the distance between the last occupied neutron state $0p_{1/2}(\epsilon_{1/2^-} = -1.2 \text{ MeV})$ and the first empty one, $1s_{1/2}(\epsilon_{1/2^+} = 1.5 \text{ MeV})$ is 2.7 MeV (see Fig. 2.10.1). In other words, in ^{10}Li the $0s_{1/2}, 0p_{3/2}$ neutron orbitals are fully occupied, while $0p_{1/2}$ carries one neutron, making ^{11}Li a single closed shell system. There is experimental evidence which testifies to the fact that the first unoccupied states of ^{10}Li are a virtual $1/2^+$ ($\epsilon_{1/2^+} = 0.2 \text{ MeV}$) and a resonant $1/2^-$ ($\epsilon_{1/2^-} = 0.5 \text{ MeV}$) state¹²⁵. According to NFT, this is a consequence of the self–energy renormalization of the bare $1/2^+$ state and of the $1/2^-$ state through a mainly PO (polarization) and CO (correlation) process respectively¹²⁶ (Fig. 2.10.1). Thus parity inversion and the melting of the $N = 8$ closed shell in favor of the new magic number $N = 6$. While ^{10}Li is not bound, ^{11}Li displays a two–neutron separation energy $S_{2n} \approx 400 \text{ keV}$. This value is the result of a subtle bootstrap mechanism. Being at threshold and basically not feeling a centrifugal barrier, the $1/2^+$ and $1/2^-$ states, are essentially not available for the short range bare NN –pairing interaction, requiring a Cooper pair binding mechanism mediated by the exchange of long wavelength collective modes. This is the natural scenario of a very low–lying collective dipole mode for two main reasons. First, the presence of an eventual dipole particle–hole transition $1/2^+ \rightarrow 1/2^-$, with energy about 1 MeV. The second one is related to the fact that the neutron halo in ^{11}Li can hardly sustain multiple surface vibrations, e.g. quadrupole vibrations, aside from displaying a very large radius as compared to that of the closed shell core $^9\text{Li}_6$, and thus a small overlap with it. This single–particle controlled phenomenon¹²⁷

¹²⁵Zinser et al. (1995). Note however Cavallaro et al. (2017) and Sanetullaev et al. (2016); see also Barranco et al. (2020) and Moro et al. (2019).

¹²⁶Barranco et al. (2001), CO (involving ground state correlation vertices), PO (particle moving around closed shells and polarizing the core).

¹²⁷Within this context one is essentially forced to make a subtle extension of the statement according to which the single–particle motion is the most collective of all nuclear motions (Mottelson (1962)), emerging from the same properties of the nuclear interaction (both bare and induced) as collective motion does, and in turn at the basis of the detailed properties of each collective mode, acting

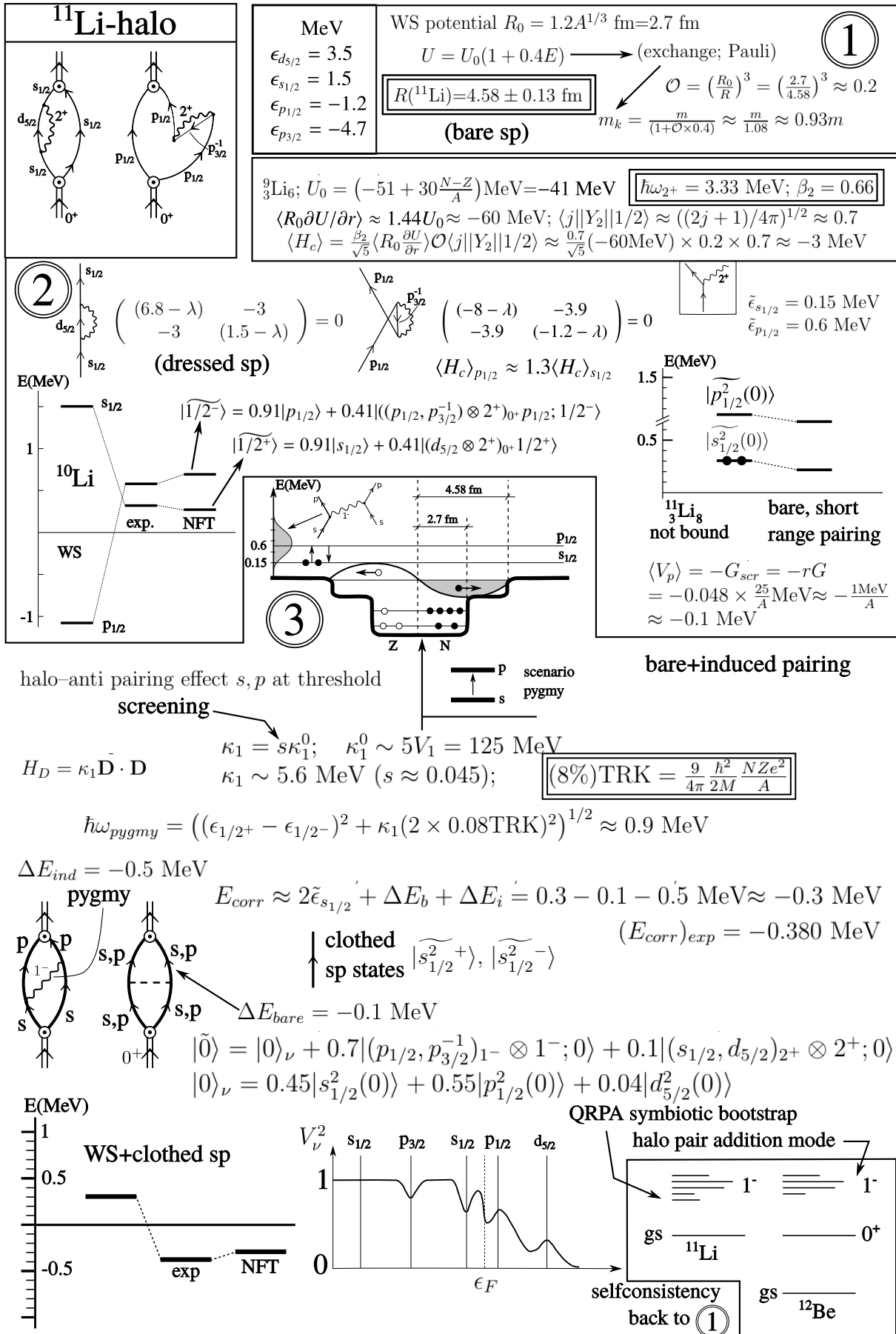


Figure 2.10.1

has a three-fold consequence: i) to screen the bare $NN-^1S_0$ short range pairing interaction making it subcritical, ii) to screen the (repulsive) symmetry interaction, and (consequently), iii) to allow the presence at low energies of a consistent fraction of the TRK-sum rule associated with the GDR at ≈ 36 MeV. In fact, a 1^- resonance carrying $\approx 8\%$ of the TRK sum rule and with centroid at an energy $\lesssim 1$ MeV have been observed¹²⁸. Thus, the connotation of pygmy dipole resonance (PDR)¹²⁹. Exchanged between the heavily dressed neutrons moving in parity inverted states provides, together with the contribution of the strongly screened, bare NN -pairing interaction, the glue needed to bind the neutron halo Cooper pair to the ^9Li core. With some experimental input¹³⁰, NFT allows to, accurately and economically, propagate dressing effects which not only renormalizes mean field, but overwhelms it providing an overall account of the experimental findings. The many-body effects at the basis of these phenomena are carried out in three steps, as schematically displayed in Fig. 2.10.1 and described below¹³¹

(for details see Sect. 3.6)¹³²:

1) Starting with well defined elements: Woods–Saxon (WS) potential, and the parameters characterizing the low-lying quadrupole vibration of the core ^9Li

as scaffolds and filters of the variety of embodiments. In fact, one has to add the characterisation of “physical” to “single-particle motion” (i.e. clothed) to englobe in the above statement also the present situation (parity inversion). In other words, while the bare $s_{1/2}$ and $p_{1/2}$ orbitals could never lead to a low-lying dipole strength, the corresponding clothed, physical states do so in a straightforward manner, the dressing effects being in this case of the same order of magnitude of the mean field effects. Consequently: “physical, clothed single-particle motion, is one of the most collective of nuclear motions”, seems to be the right statement.

¹²⁸Kanungo et al. (2015); Sackett et al. (1993); Zinser et al. (1997)

¹²⁹See Broglia et al. (2019a) and references therein.

¹³⁰See e.g. the corresponding discussion in Barranco et al. (2017).

¹³¹The information contained in this figure, has its origin going back to predictions made in 2001 (Barranco et al. (2001); see Fig. 3.6.3). They found confirmation in a *tour of force*-like experiment carried out at TRIUMF (Vancouver) by Tanihata et al. (2008) (see also Tanihata et al. (2013) and Fig. 7.1.3) providing evidence of phonon mediated pairing in nuclei (Potel et al. (2010)). Figure 2.10.1 displays an analytic synthesis of a nuclear field theory solution –(NFT) presented and discussed at the pedestrian level in Sect. 2.7– of the structure of one- and two- neutron halo nuclei lying at the dripline (^{10}Li (Barranco et al. (2020)) and ^{11}Li Barranco et al. (2001)) and thus, of the unified interpretation of the results of almost two decades of cutting edge experimental research carried and, being carried out at major laboratories around the world (TRIUMF (Vancouver; Tanihata et al. (2008)), ISOLDE (CERN; Jeppesen et al. (2006)), LNS (Catania; Cavallaro et al. (2017)), etc.). Figs. 2.10.1, 2.10.2 and 2.10.3 condense also a number of facets about pygmy resonances in nuclei (see Kanungo et al. (2015); Broglia et al. (2019a) and references therein), and of quantal dipole fluctuations mediated pairing, an intermediate boson also found at the basis of the van der Waals interaction. Within this scenario, see the Section 3.6 *Halo pair addition mode and pygmy*, as well as the parallel carried out in connection with the role the van der Waals interaction plays in molecular systems in general, and proteins in particular (see Appendix 3.A and 3.D). It is also of notice that the results condensed in Figs. 2.10.1 and 2.10.2 are at the basis of a nuclear physics analogue (embodiment) of Hawking Radiation (Barranco et al. (2019)). It is rather simple to reproduce the results shown in Fig. 2.10.1, and thus understand its content and message, making use of the few parameters displayed at the beginning of the figure (see also Sect. 3.6 and Broglia et al. (2019b)).

¹³²It is of notice that in discussing Fig. 2.10.1 use is made of the values calculated in NFT. This is also true in connection with the estimates carried out in Sect. 3.6.1.

(**input**, double boxed quantities), calculate the single-particle levels and collective vibration (separable interaction) and determine the corresponding particle-vibration coupling vertices (strength and form factors). From the ratio of the WS radius (R_0) and of the observed one ($R(^{11}\text{Li})$ **input**) determine the overlap O . Because $O \ll 1$, the contribution of the exchange (Fock) potential to the empirical WS potential is small concerning the halo neutrons¹³³. Consequently the neutron halo k -mass m_k has a value close to the bare mass m ;

2) Making use of the above elements one can cloth the bare single-particle states, in particular the $s_{1/2}$ and $p_{1/2}$ states. Parity inversion ensues, with $1/2^+$ and $1/2^-$ at threshold. As a consequence the $N = 8$ shell closure melts away, $N = 6$ becoming a new magic number, testifying to the fact that large amplitude fluctuations can be, in nuclei, as important or even more important than static mean field effects. As a result ${}^3_3\text{Li}_7$ is not bound. Adding one more neutron and switching on the bare pairing interaction (e.g. a contact force $V(r_{12}) = -4\pi V_0 \delta(\mathbf{r}_1 - \mathbf{r}_2)$ with constant matrix element¹³⁴ $G = 1.2 \text{ fm}^{-3} V_0/A \approx (25/A) \text{ MeV}$), the screening $r = \frac{(M_j)\text{halo}}{(M_j)\text{core}} \approx \frac{2}{2j+1} \left(\frac{R_0}{R} \right)^3 \approx 0.048$ (see Eq. (3.6.3)) resulting from the poor overlap between halo and core neutrons leads to a value of the strength of the pairing interaction $(G)_{scr} = r \times G$ which is subcritical, and thus to an unbound system (see Sect. 3.6 and App. 3.B). In fact, $G_{scr} = 0.048 \times 25/A \text{ MeV} \approx 0.1 \text{ MeV}$ and $\Delta E = 2\tilde{\epsilon}_{s_{1/2}} - G_{scr} \approx 0.3 \text{ MeV} - 0.1 \text{ MeV} \approx 0.2 \text{ MeV}$. Summing up, $G_{scr} < G_c$, G_c being the minimum value of the pairing coupling constant leading to a bound state¹³⁵,

3) Considering the sloshing back and forth of the halo neutrons (with a small contribution from the core neutrons) against the core protons, leads to a dipole mode feeling a strongly screened repulsive symmetry potential. In keeping with the fact that $\kappa_1^0 \sim 1/R^2(^{11}\text{Li})$, the screening factor can be estimated as $((R(^{11}\text{Li})/\xi)^2(R =$

¹³³See Sect. 2.10.1.

¹³⁴Brink and Broglia (2005), pp 40-42. It is of notice that the difference with the number found in this reference $G \approx 28/A \text{ MeV}$ is within the margin of uncertainties.

¹³⁵At the basis of superconductivity one finds the result obtained by Cooper (1956). He worked out the problem of two electrons interacting through an attractive interaction above a quiescent Fermi sea. Thus, all but two of the electrons are assumed to be noninteracting. The background of electrons enter the total problem only through the Pauli principle by blocking states below the Fermi surface from participating in the remaining two-particle problem. If one measures the kinetic energy ϵ_k relative to its value at the Fermi surface only states with $\epsilon_k > 0$ are available to the interacting pair of electrons. Cooper found that a bound state of the pair always exists for arbitrarily weak coupling so long as the potential is attractive near the Fermi surface, a mechanism which implies the instability of the normal phase, and found at the basis of superconductivity. Cooper pair binding is a rather remarkable result for the usual two-body problem. If one has only two particles coupled by an attractive interaction of finite range, they would not form bound states unless the attractive interaction exceeds a certain critical value, Cooper reduces the above 3-dimensional to a 1-dimensional quantal system (Gor'kov (2012)). Now, in ${}^{11}\text{Li}$ the last two neutrons are very weakly bound. Consequently they move away from the neutron closed shell core ${}^9\text{Li}$, lowering in the process their relative momentum and forming a misty cloud or halo. One can thus view this system as the nuclear embodiment of a Cooper pair. The question then arises, why there is a critical value for the pairing interaction. The answer is spatial quantization, which is a three-dimensional feature, and is associated with the fact that the nucleus is a finite system.

4.58 fm , $\xi = 20 \text{ fm}$, $s \approx 0.052$), the value obtained in Sect. 3.6 being $s = 0.043$. In other words, while it takes a quantity proportional to $5V_1 = 125 \text{ MeV}$ to separate protons from neutrons in the core, this price is reduced to $s \times 5V_1 = 5.4 \text{ MeV}$ ($(V_1)_{scr} = sV_1 \approx 1 \text{ MeV}$) for halo neutrons. This is at the basis of the fact that $\approx 8\%$ of the Thomas–Reiche–Kuhn sum rule (**input**) gets down to $\lesssim 1 \text{ MeV}$. Another way to say the same thing is that $(V_1)_{scr} = sV_1$ is at the basis of the fact that the $s_{1/2} - p_{1/2}$ energy difference ($\Delta\tilde{\epsilon} \approx 0.45 \text{ MeV}$) is only increased by a modest value ($\hbar\omega_{pygmy} \approx 1 \text{ MeV} \approx 10^{21} \text{ Hz}$), while the $E1$ single-particle strength remains essentially unchanged. Typical values in the case of nuclei lying along the stability valley being $\approx 10^{-4}B_W(E1)$ for low-energy single-particle transitions, while in the present case one finds a value close to $1B_W(E1)$.

Now, the two halo neutrons dressed by the vibrations of the core (heavy arrowed lines in lowest left corner of Fig. 2.10.1) and interacting through the bare NN -pairing force are not bound. Consequently, the pygmy resonance will fade away almost as soon as it is generated (essentially lasting the neutron transversal time $\approx 10^{-21} \text{ s}$). This, unless it is exchanged between the two neutrons forcing them to jump from the configuration $s_{1/2}^2(0)$ at threshold ($2 \times \tilde{\epsilon}_{s_{1/2}} \approx 0.3 \text{ MeV}$) into $p_{1/2}^2(0)$, also close to threshold ($2 \times \tilde{\epsilon}_{p_{1/2}} \approx 1.2 \text{ MeV}$). In other words, one finds the dipole pygmy resonance acting as an intermediate boson which couples to the halo neutrons with a strength $\Lambda \approx 0.5 \text{ MeV}$ (QRPA calculation). As a result, it contributes to the binding of the neutron halo Cooper pair with $\approx 0.5 \text{ MeV}$ binding. Thus, the corresponding correlation energy $E_{corr} \approx -0.3 \text{ MeV}$ is mainly due to the dipole pygmy exchange process. The resulting symbiotic halo pair addition mode of ^{11}Li can, in principle, be used as a building block of the nuclear spectrum, amenable to be moved around. A possible candidate for such a role is the first excited 0^+ state of ^{12}Be , together with the associated dipole state built on it and eventually other fragments of the associated $E1$ –low energy–strength.

To calculate the pygmy dipole resonance (PDR) of ^{11}Li one needs to know the ground state of this nucleus (halo–pair addition mode) so as to be able to determine microscopically the occupation factors of the $1s_{1/2}, 1p_{3/2}, \epsilon s_{1/2}, \epsilon p_{1/2}, \epsilon d_{5/2}, \dots$, etc. states. This is the basic input needed to work out the corresponding QRPA equations, whose diagonalization provide the energy, transition density and probability of the mode. But to do so one is required to know the PDR. Arrived to this point, the protocol schematically presented in Fig. 2.10.1 implies to go back to 1 and repeat the whole procedure until convergence is achieved.

2.10.4 $^{11}\text{Li}(p, p)^{11}\text{Li}$ and transfer reaction channels

NFT is based on elementary modes of excitation, modes which carry a large fraction of the nuclear correlation. Because its rules have no limitations concerning whether the excitations studied lie or not in the continuum, or whether the single-particle motion displays asymptotic conditions, it allows for a unified description of structure (s) and reactions (r) (NFT(s+r)). An example of the above statement is provided by Fig. 2.10.2. Graph (a) is a NFT–diagram describing one of the pro-

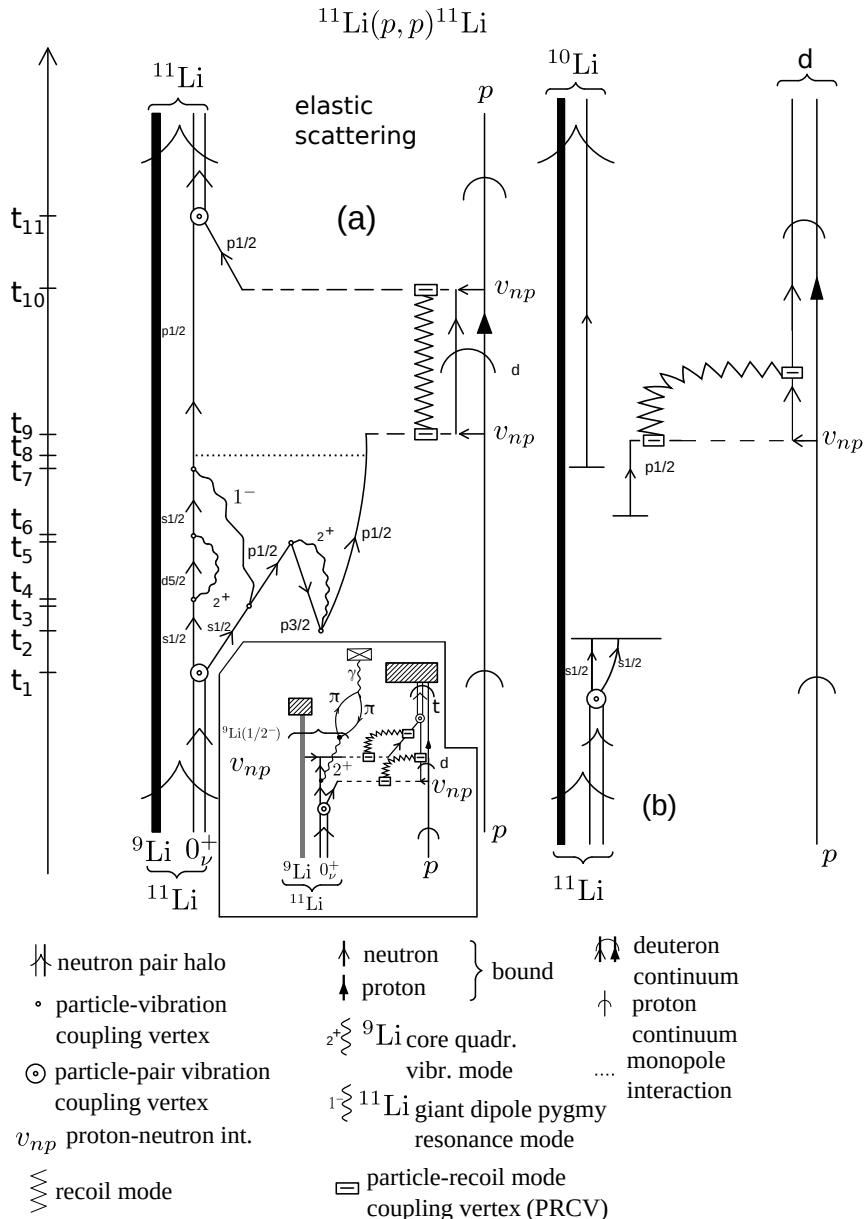


Figure 2.10.2: (a) NFT-diagram describing one of the processes contributing to the elastic reaction $^{11}\text{Li}(p, p)^{11}\text{Li}$ as the system propagates in time (polarization contribution to the global (mean field) optical potential). In the inset, a schematic NFT diagram describing the process $^{11}\text{Li}(p, t)^{9}\text{Li}(1/2^-)$ is displayed. A dashed open rectangle indicates the particle-recoil coupling vertex. A crossed box represents a γ -detector, while hatched rectangles particle detectors. (b) Schematic NFT diagram describing the reaction $^{11}\text{Li}(p, d)^{10}\text{Li}$, i.e. same as in (a) up to time t_8 (reason for which no details are repeated between t_2 and t_8). From there on the deuteron continues to propagate to the detector bringing to it, aside from nuclear structure information, the information resulting from its interaction with the recoil mode. Likely, the neutron in ^{10}Li will break up almost as soon as it is formed. Summing up, in the center of mass reference frame both p and ^{11}Li display asymptotic states in entrance as well as in exit channels in case (a), and only in the entrance channel in case (b), while in the exit channel it is the ^{10}Li ($^9\text{Li} + n$) and the deuteron that do so.

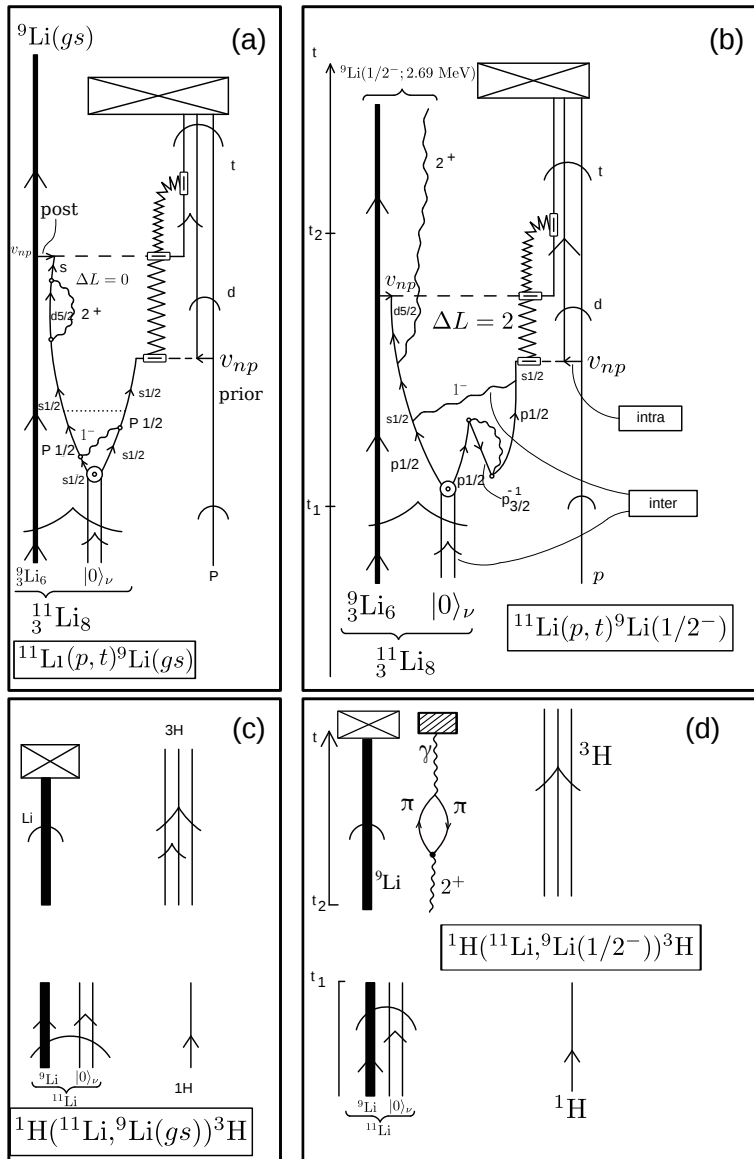


Figure 2.10.3: NFT representation of the reactions (a) $^{11}\text{Li}(p, t)^9\text{Li}(\text{gs})$, (b) $^{11}\text{Li}(p, t)^9\text{Li}(1/2^-)$, (c) $^1\text{H}(^{11}\text{Li}, ^9\text{Li}(\text{gs}))^3\text{H}$ and (d) $^1\text{H}(^{11}\text{Li}, ^9\text{Li}(1/2^-))^3\text{H}$. Time is assumed to run upwards. A single arrowed line represents a fermion (proton (p) or neutron (n)). A double arrowed line two correlated nucleons. In the present case two correlated (halo) neutrons (halo-neutron pair addition mode $|0\rangle_\nu$). A heavy arrowed line represents the core system $^9\text{Li}(\text{gs})$. A standard pointed arrow refers to structure, while "round" arrows refer to reaction. A wavy line represents (particle-hole) collective vibrations, like the low-lying quadrupole mode of ^9Li , or the dipole pygmy resonant state which, together with the bare pairing interaction (horizontal dotted line) binds the neutron halo Cooper pair to the core. A short horizontal arrow labels the proton–neutron interaction v_{np} responsible for the single-particle transfer processes, represented by an horizontal dashed line. A dashed open square indicates the particle-recoil coupling vertex. The jagged line represents the recoil normal mode resulting from the mismatch between the relative centre of mass coordinates associated with the mass partitions $^{11}\text{Li}+p$, $^{10}\text{Li}+d$ (virtual) and $^9\text{Li}+t$. The γ -detector is represented by a hatched box (see Fig. 7.6.2), the particle detector by a crossed rectangle. For further details see caption Fig. 2.10.2.

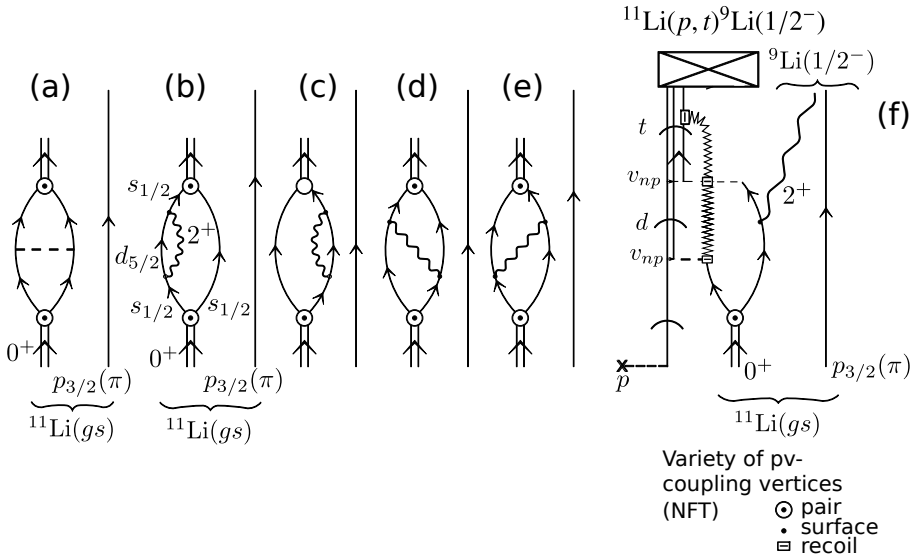


Figure 2.10.4: (a–e) Lowest order, NFT diagrams associated with the processes contributing to the binding of the neutron halo Cooper pair (double arrowed line) of ^{11}Li to the core ^{9}Li through the bare pairing interaction (dashed line) as well as the exchange of the core quadrupole phonon and of the soft dipole mode of ^{11}Li (wavy line). Single arrowed lines describe the nucleon independent-particle motion of neutrons ($s_{1/2}, d_{5/2}$, etc.) as well as of the $p_{3/2}(\pi)$ proton considered as a spectator; (a) Bare pairing interaction, four-point vertex (horizontal dotted line); (b, c) self energy, effective mass polarization (PO) process dressing the $s_{1/2}(v)$ single-particle state (a similar diagram, but corresponding to correlation (CO) processes (see Fig. 5.2.4) dressing the $p_{1/2}$ state is not shown, see Figs. 2.10.2 and 2.10.3); (d, e) vertex correction (induced interaction) renormalizing the vertex with which the pair addition mode couples to the fermion (dotted open circle); (f) NFT diagram describing the reaction $^{11}\text{Li}(p, t)^{9}\text{Li}(1/2^-)$ populating the first excited state of ^{9}Li , the dashed horizontal line starting with a cross standing for the (p, t) probe. The successive transfer of the two halo neutrons ($^{11}\text{Li}(\text{gs}) + p \rightarrow ^{10}\text{Li} + d \rightarrow ^{9}\text{Li}(1/2^+) + t$) is shown, in keeping with the fact that this process, that is successive transfer, provides the largest contribution to the absolute differential cross section. The jagged line represents the recoil mode carrying to the outgoing particle the effect of the momentum mismatch associated with the transfer process (recoil).

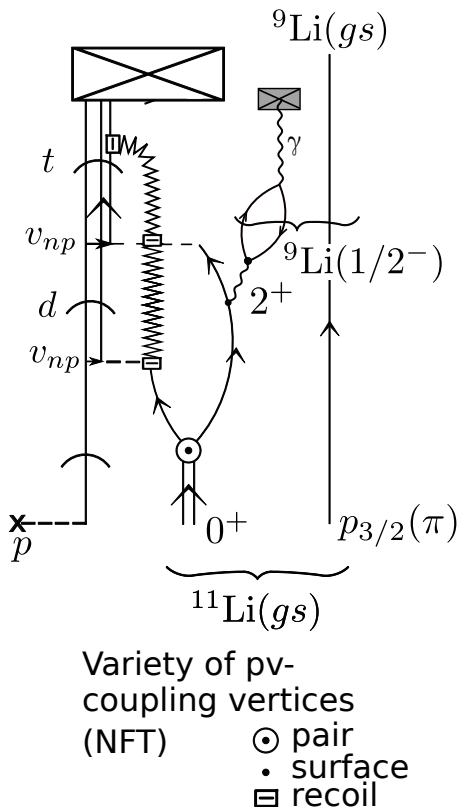


Figure 2.10.5: Gedanken γ -ray coincidence experiment $^1\text{H}(^{11}\text{Li}, ^9\text{Li})^3\text{H}$ and $^9\text{Li}(\text{gs}) + \gamma(E2; 2.69 \text{ MeV})$. In this case, the virtual quadrupole phonon associated with self-energy and vertex correction processes becomes real through the action of the (p, t) external field. Thus, it is not only that recoil modes are “measured” by detectors in connection with outgoing particles which have asymptotic wavefunctions, but also the quadrupole vibration, whose eventual γ -decay (see Fig. 7.6.2 (II)) can be measured by the γ -detector. The apparent bubble process made out of a proton particle-hole component of the quadrupole mode does not contradict NFT rule III (Sect. 2.7). In fact, the initial vertex (solid dot) corresponds to a nuclear PVC, while the second couples the proton excitation to the electromagnetic field, leading to spontaneous γ -decay.

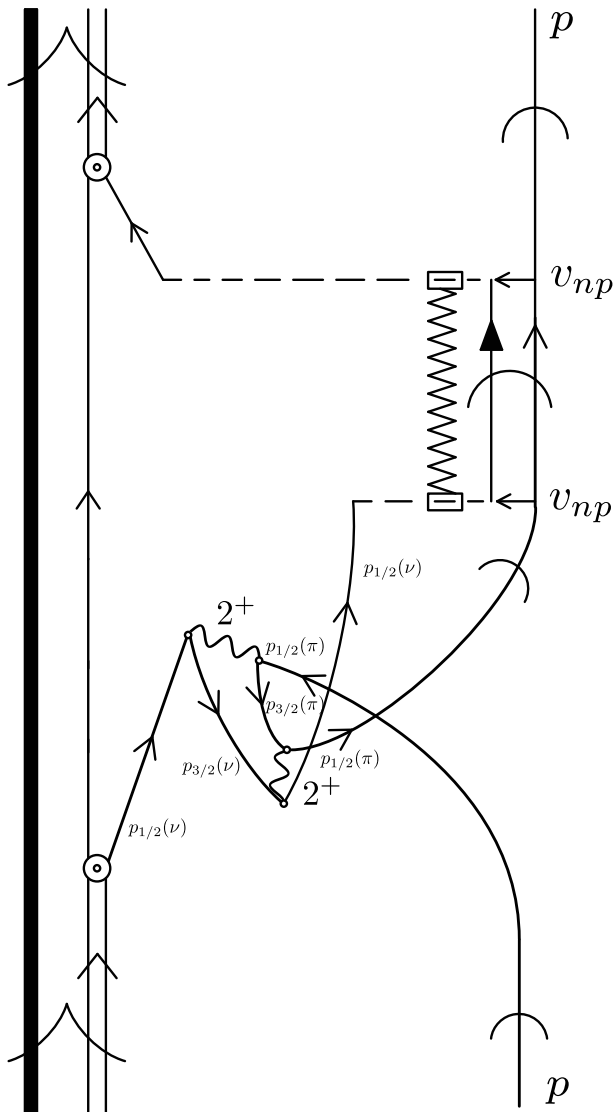


Figure 2.10.6: In keeping with standard direct reaction praxis, neither in Fig. 2.10.2 nor in 2.10.3 antisymmetrization is carried out between the impinging proton and the protons of ^{11}Li . Within the present discussion ($^{11}\text{Li}(p, p)^{11}\text{Li}$), an example of such processes corresponds to the exchange of a proton participating in the quadrupole vibration of the core, with the projectile, as shown in the figure. Such a process will not only be two orders higher in perturbation in the particle–vibration coupling vertex than the original one shown in graph (a) of Fig. 2.10.2. It will be strongly reduced by the square of the overlap between a proton moving in the continuum, and a $p_{1/2}$ proton of the ^9Li core.

cesses contributing to the elastic reaction $^{11}\text{Li}(p, p)^{11}\text{Li}$ as the system propagates in time. This graph describes a polarization contribution to the global (mean field)

optical potential describing proton elastic scattering off ${}^9\text{Li}$.

In what follows we describe the processes taking place in Fig. 2.10.2 (a) in the interval of time $t_1 - t_{11}$, starting from the $t = -\infty$ situation in which a proton impinges on ${}^{11}\text{Li}$. At time t_1 , the halo pair addition mode $|0_v\rangle$ couples to a pure, bare configuration $s_{1/2}^2(0)$. At time t_2 , and due to the zero point fluctuations associated with the quadrupole vibration of the ${}^{11}\text{Li}$ core, the virtual state $((p_{1/2}, p_{3/2}^{-1})_{2^+} \otimes 2^+)_{0^+}$ is created. At time t_4 , one of the continuum $s_{1/2}$ neutrons excites the quadrupole vibration of the core reabsorbing it at time t_6 . As a result of this self energy process, its energy is lowered to threshold, becoming a virtual state. The other $s_{1/2}$ continuum neutron state excites at t_3 the PDR and moves into the $p_{1/2}$ orbital after which, and due to Pauli principle, becomes exchanged with the homologous $p_{1/2}$ of the $(p_{1/2}, p_{3/2}^{-1})_{2^+}$ configuration, exchange process which is completed by time t_5 . As a result the $p_{1/2}$ state undergoes a conspicuous repulsion, becoming a resonant state. At time t_7 the $s_{1/2}$ neutron absorbs the PDR and moves into a $p_{1/2}$ state. At time t_8 it interacts, through the bare 1S_0 -(pairing) interaction, with the other $p_{1/2}$ neutron, completing the process by which the halo pair addition mode binds to the core ${}^{11}\text{Li}$. Before the two $p_{1/2}$ neutrons couple to the $|0_v\rangle$ state one of them is picked up at time t_9 under the action of the proton–neutron interaction v_{np} , by the projectile (proton), to form a virtual deuteron. The recoil effect associated with the new mass partition being taken care of by the particle–recoil coupling vertex. At time t_{10} , again under the effect of v_{np} , the neutron of the virtual deuteron is transferred back to the virtual ${}^{10}\text{Li}$ nucleus to form again ${}^{11}\text{Li}$ and thus the original mass partition, as testified by the fact that the recoil phonon (jaggy line initiated at time t_9) is reabsorbed by a second particle–recoil coupling vertex. The resulting $(p_{1/2}^2(0))$ configuration couples to the $|0_v\rangle$ state leading to the $|{}^{11}\text{Li(gs)}\rangle$ state. The system has thus returned to the entrance channel configuration, namely that of ${}^{11}\text{Li} + p$, which propagates to $t \rightarrow +\infty$, the proton eventually bringing the nuclear structure information to the detector.

The real and imaginary part of the diagram shown in Fig 2.10.2 (a), contribute to the corresponding terms of the polarization components of the optical potential, providing the A -dependence of, and to be added to, the experimentally determined (global) ${}^AX + p$ elastic scattering optical potential¹³⁶. The mass number A represents the region of the mass table¹³⁷ associated with nuclei close to the neutron drip line region $A \approx 11$. It is of notice that Fig. 2.10.2 exemplifies the elements needed to extend and formalize NFT rules of structure so as to be able to deal also

¹³⁶In relation with the program of NFT(r+s) one can mention that Landau felt that a Feynman diagram have an independent basic importance, because the possibility of relating them directly to physical observables. Feynman diagrams allow to describe processes where one set of particles with given energies, momenta, angular momenta, go in and another set (or the same) comes out. At the basis of this approach one finds vertex processes and dispersion relations. Now, vertex processes can simply mean the variety of processes connecting the incoming particles with the outgoing ones. In other words, within the present framework the processes taking place between times $t_2 - t_{11}$ (Fig. 2.10.2) and $t_1 - t_2$ (Fig. 2.10.3) (Landau (1959); ter Haar (1969)). See also Sect. 7.5.

¹³⁷Similar to the island of superfluid nuclei involved in the characterization of ${}^{120}\text{Sn}$ discussed in the next Section (see Idini et al. (2015) and references therein).

with reactions.

As schematically shown in Fig. 2.10.1, to each nuclear structure process displayed in diagram (a) of Fig. 2.10.2, it corresponds a specific equation, amplitude, etc., and thus a number with appropriate units. This is also so regarding the reaction aspects of the diagram, and thus reaction amplitudes and eventual absolute differential cross sections. A fact which is exemplified in detail in Sect. 7.1 and App. 7.B in connection with graphs (a) and (b) of Fig. 2.10.3.

In Fig. 2.10.2 (b) one assumes the same processes to take place as in (a) up to time t_8 (reason for which no details are repeated between t_2 and t_8). From there on the deuteron continues to propagate to the detector, and the effect of the particle-recoil coupling vertex is to be worked out and the corresponding outgoing distorted waves modified accordingly. Likely, the neutron in ^{10}Li will break up before it can be recorded by the particle detector. Summing up, in the center of mass reference frame both p and ^{11}Li display asymptotic states in entrance as well as in exit channels in case (a), and only in the entrance channel in case (b), while in the exit channel only $^{10}\text{Li}(^9\text{Li}+n)$ and the deuteron do so.

Another examples of the NFT diagrams of structure and reactions are given in Fig. 2.10.3. In (a) one contribution associated with the reaction $^{11}\text{Li}(p, t)^9\text{Li}(\text{gs})$ is shown, while in (b) one associated with the population of the first excited $1/2^-$ (2.69 MeV) state of ^9Li . Within this context we refer to Figs. 2.10.4 and 2.10.5 for a compact graphical representation of this last process. The importance of such process is that it provided, likely for the first time, direct evidence of phonon mediated pairing interaction in nuclei as theoretically predicted¹³⁸.

Returning to the process displayed in Fig. 2.10.2 concerning the question of Pauli principle in reaction processes (also essential in the case of structure NFT), in this case not between e.g. the two halo neutrons, but between the incoming proton and the collective modes of the core (^9Li) we refer to¹³⁹ Fig. 2.10.6.

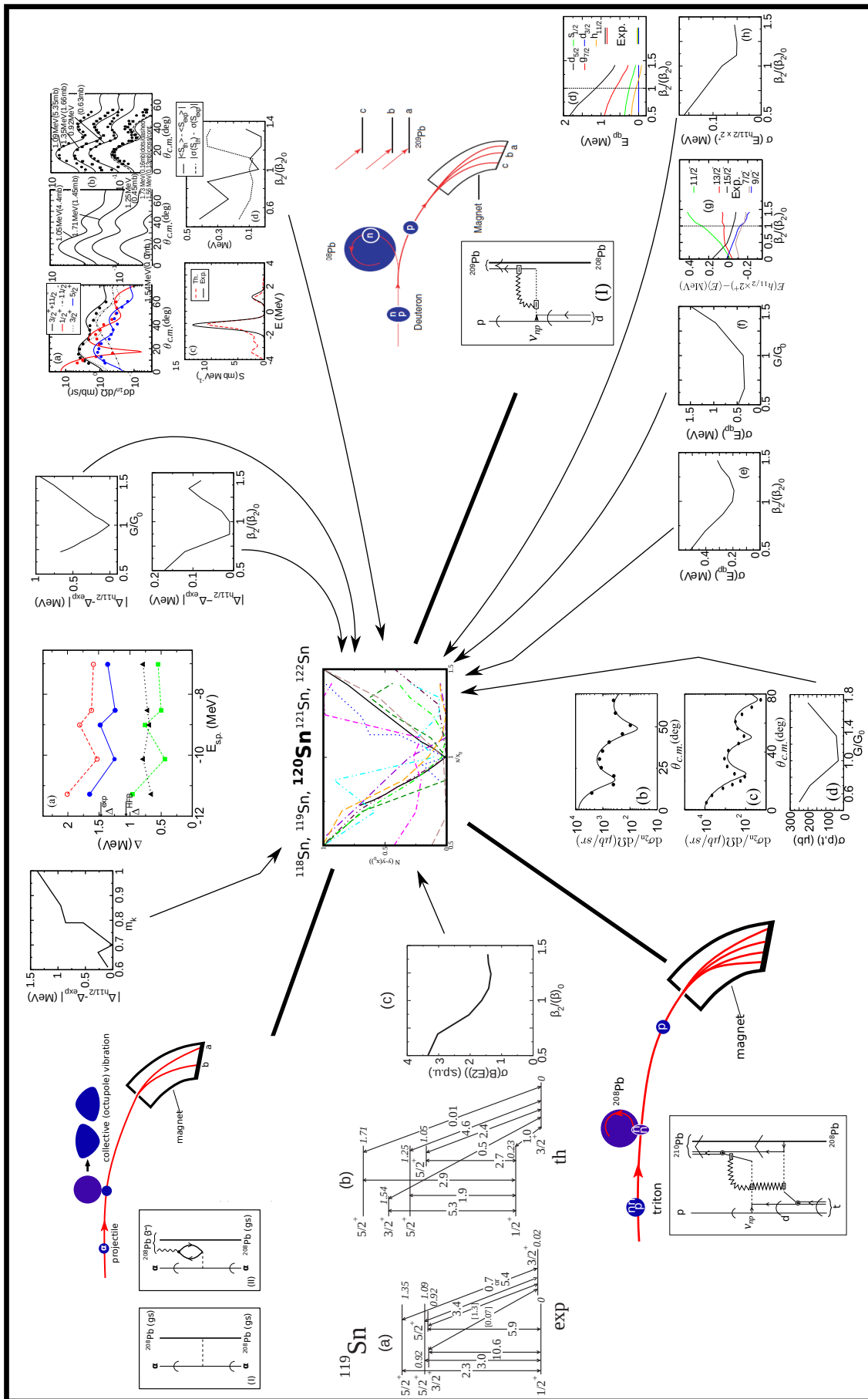
2.11 Characterization of an open-shell nucleus: ^{120}Sn

In this section we aim at giving an overall view of the versatility of $(\text{NFT})_{\text{ren}}(s+r)$ to describe both structure as well as the results of experimental probes which provide an essentially complete characterization of an atomic nucleus. Details of the structure and reaction calculations, techniques and software employed to achieve such characterization will be provided in the following chapters.

In keeping with the fact that ^{120}Sn is a typical example of superfluid nuclei, it has been studied extensively with a variety of probes. Elastic, anelastic (Coulomb

¹³⁸Barranco et al. (2001) Tanihata et al. (2008); Potel et al. (2010); Tanihata et al. (2013); Beceiro-Novo et al. (2015).

¹³⁹It is of notice that making use of global optical potentials to describe the elastic channel, or mean field optical potentials to which one adds polarization contributions like those displayed in Fig. 2.10.2 (a), the effect of Pauli principle between a nucleon projectile and the nucleons of the target can, approximately be taken care of through the energy-dependent Perey–Buck potential (Perey and Buck (1962)), intimately connected with the k -mass.

Figure 2.11.1: Characterization of ^{120}Sn .

excitation and subsequent γ -decay as well as inelastic scattering). Also one- and two-particle transfer reactions. The corresponding absolute differential cross sections and transition probabilities involve as targets and residual systems the island of superfluid nuclei^{118,119,120,121,122}Sn.

A theoretical description of the variety of observables have been carried out solving the Nambu Gorkov equation to propagate the different $(\text{NFT})_{\text{ren}}(s)$ processes dressing the single-particle states and renormalizing the bare pairing interaction, as well as spectroscopic and transition amplitudes¹⁴⁰. With the help of the softwares SINGLE and COOPER, tailored to propagate the $(\text{NFT})_{\text{ren}}(s)$ spectroscopic amplitude content to the detector, one- and two-nucleon transfer reactions have been worked out $((\text{NFT})_{\text{ren}}(r))$. Also the γ -decay transition probabilities. In Fig. 2.11.1 theory is compared to experiment in terms of renormalized energies, absolute differential cross sections and electromagnetic transition probabilities.

In what follows we describe the contents of this figure. In the **upper left** part, (color online), the cartoon representation displayed in Fig. 2.1.1 is here used to schematically illustrate¹⁴¹ anelastic processes, Coulomb excitation and the quadrupole γ -decay of ^{119}Sn (**middle left** (a) experiment, (b) theory, (c) standard deviation between theory and experiment calculated as a function of β_2 normalized with respect to the experimental value $(\beta_2)_0$). The resulting values are displayed in terms of the dashed orange curve of the center boxed landscape (see Fig. 2.4.1 and Table 2.4.1). Also displayed in the upper left part of the figure are NFT diagrams describing elastic and inelastic processes.

In the **bottom left** part of the figure, a schematic representation of an experimental setup to measure two-nucleon transfer processes is given. Also a $(\text{NFT})_{\text{ren}}(s+r)$ diagram describing successive transfer is displayed. In the **bottom middle** part of the figure, the theoretical absolute differential cross sections (continuous curves) associated with the reactions $^{120}\text{Sn}(p,t)^{118}\text{Sn}(\text{gs})$ and $^{122}\text{Sn}(p,t)^{120}\text{Sn}(\text{gs})$ are displayed ((b) and (c)), in comparison with the experimental data (solid dots). The theoretical cross sections were recalculated as a function of the pairing strength G , normalized with respect to the (equivalent) value G_0 of v_{14} (Argonne 1S_0 bare NN -interaction), and the corresponding standard deviation with respect to the experimental value determined (only the values corresponding to $^{120}\text{Sn}(p,t)^{118}\text{Sn}$ are displayed in (d)). It is of notice that the corresponding relative standard deviation σ/L for $G = G_0$ (L being the experimental cross section), is quite small ($70\mu\text{b}/2250\mu\text{b} \approx 0.03$)¹⁴².

¹⁴⁰See Idini et al. (2015) and refs. therein, see also Broglia et al. (2016).

¹⁴¹While in Fig. 2.1.1 one refers to the excitation of an octupole mode, in the present case we deal with a quadrupole vibration.

¹⁴²This result is related with the fact that $\sigma \sim |\alpha_0|^2$, α_0 being the BCS order parameter (number of Cooper pairs participating in the condensate which measure the deformation in gauge space). Because the state $|BCS\rangle$ describing independent pair motion (Cooper pair condensate) is a coherent state displaying off-diagonal-long-range-order (ODLO), it is not surprising that $|\alpha|^2 = \left| \sum_{v>0} U_v V_v \right|^2 = \left| \langle BCS | P^\dagger | BCS \rangle \right|^2 = \left| \langle BCS | P | BCS \rangle \right|^2$ plays the role of a, physical, non-energy weighted sum rule (Potel et al. (2017)). See Sect. 7.4.1.

In the **upper middle** part of the figure and under the label (a), the state dependent pairing gap for the five valence orbitals of ^{120}Sn (blue line) is displayed, in comparison with the experimental findings ($\Delta^{\exp} \approx 1.45$ MeV, arrow left). The gap associated with the lowest quasiparticle state $h_{11/2}$ calculated as a function of m_k (different Skyrme interaction) as well as of G/G_0 and $\beta_2/(\beta_2)_0$ have been used to work out the corresponding standard deviations with respect to the experimental findings and are displayed to the right and the left of (a) (see also dotted blue curve, dashed brown curve and dashed green curve in the central boxed plot, i.e. Fig. 2.4.1). In the **upper right** part of the figure absolute differential cross sections and strength functions associated with the one-particle transfer processes $^{120}\text{Sn}(d, p)^{121}\text{Sn}$, are displayed. In (a), the absolute differential cross sections associated with the low-lying states $h_{11/2}, d_{3/2}, s_{1/2}$ and $d_{5/2}$ are shown (theory: continuous curve; data: solid dots). In (b) (left) the calculated $^{121}\text{Sn}(5/2^+)$ absolute differential cross sections (continuous curves) are shown and compared with the experimental data (right, solid dots; also given here are DWBA fits used in the analysis of the experimental data). In (c) the calculated strength function associated with the $5/2^+$ state (red dashed curve) is compared to the data (black continuous curve), while in (d) the difference between the centroid width of the experimental and calculated $d_{5/2}$ strength function is shown as a function of the ratio $\beta_2/(\beta_2)_0$ in terms of the solid and dashed curves. In the **middle right** part of the figure, a cartoon representation of a setup to measure one-nucleon transfer reactions is displayed. Also shown is a $(\text{NFT})_{\text{ren}}(s+r)$ diagram describing the process. In the **lower right** part of the figure, the lowest quasiparticle energy values are displayed as a function of $\beta_2/(\beta_2)_0$ in comparison with the data. The root mean-square deviation between the experimental and theoretical levels as a function of a function of $\beta_2/(\beta_2)_0$ and of G/G_0 are shown in (e) and (f) respectively. In (g) the experimental energies of the members of the $h_{11/2} \times 2^+$ multiplet shown in (d), are compared with the theoretical values calculated as a function of the ratio $\beta_2/(\beta_2)_0$. Finally in (h) the root mean-square deviation between the experimental and theoretical energies of the members of the $h_{11/2} \times 2^+$ multiplet shown in (g) are given as a function of $\beta_2/(\beta_2)_0$.

Summing up, the nuclear structure landscape is well funneled and theory provides an overall account of the data, when the physical values of β_2, G and m_k are used.

2.12 Summary

In Fig. 2.11.1 the results of a “complete” $(\text{NFT})_{\text{ren}}(r+s)$ description of the open shell superfluid nucleus ^{120}Sn in terms of the $^{120}\text{Sn}(p, t)^{118}\text{Sn}(\text{gs}), ^{122}\text{Sn}(p, t)^{120}\text{Sn}(\text{gs}), ^{120}\text{Sn}(p, d)^{119}\text{Sn}, ^{121}\text{Sn}(p, d)^{120}\text{Sn}, ^{119}\text{Sn}(\alpha, \alpha')^{119}\text{Sn}$ (γ -decay) cross sections, energies and transition probabilities are displayed in comparison with the experimental findings. Arbitrarily forcing the particle-vibration coupling (PVC) strength, the strength of the bare pairing force and the value of the k -mass to depart from their

“physical” values, one can test the robustness of the NFT(r+s) picture of ^{120}Sn given, and of the well funneled character of the associated nuclear structure and reaction landscape.

In a very real sense this, namely the results collected in Fig. 2.11.1 is a nucleus¹⁴³. That is, the summed experimental and theoretical structural information accessed through asymptotic states¹⁴⁴, outcome of simultaneously probing the system with a complete array of experiments (elastic, anelastic and associated γ -decay, as well as one- and two-nucleon transfer reactions), and of calculating the corresponding observables with an equally ample array of theoretical tools, as provided by $(\text{NFT})_{\text{ren}}(r+s)$.

Appendix 2.A Inelastic Scattering

In this Appendix we briefly discuss how to extract values of the effective deformation parameter β_L from inelastic scattering absolute differential cross sections in the most simple and straightforward way, ignoring all the complications associated with the spin carried by the particles, the spin-orbit dependence of the optical model potential, etc. The deformation parameter β_L enter e.g. the particle-vibration coupling Hamiltonian (Eqs. (2.3.8–2.3.13)).

2.A.1 (α, α') -scattering

We start assuming that the interaction V'_β is equal to $V'_\beta = V'_\beta(\xi_\beta, r_\beta)$, which is usually called the stripping approximation. We can then write the differential cross section in the Distorted Wave Born Approximation (DWBA) as (see e.g. App 6.E) as,

$$\frac{d\sigma}{d\Omega} = \frac{k_\beta}{k_\alpha} \frac{\mu_\alpha \mu_\beta}{(2\pi\hbar^2)} |\langle \psi_\beta(\xi_\beta) \chi^{(-)}(k_\beta, \vec{r}_\beta), V'_\beta(\xi_\beta, r_\beta) \psi_\alpha(\xi_\alpha) \chi^{(+)}(k_\alpha, \vec{r}_\alpha) \rangle|^2. \quad (2.A.1)$$

For the case of inelastic scattering $\xi_\alpha = \xi_\beta = \xi$, thus

$$\psi_\beta(\xi_\beta) = \psi_{M_\beta}^{I_\beta}(\xi), \quad (2.A.2a)$$

$$\psi_\alpha(\xi_\alpha) = \psi_{M_\alpha}^{I_\alpha}(\xi), \quad (2.A.2b)$$

$$\vec{r}_\alpha = \vec{r}_\beta, \quad \mu_\alpha = \mu_\beta, \quad (2.A.2c)$$

i.e we are always in the mass partition of the entrance channel.

Equation (2.A.1) can now be rewritten as

$$\frac{d\sigma}{d\Omega} = \frac{k_\beta}{k_\alpha} \frac{m_\alpha^2}{(2\pi\hbar^2)^2} \frac{1}{2I_\alpha + 1} \sum_{M_\alpha M_\beta} |\langle \chi^{(-)}(k_\beta, \vec{r}_\beta), V_{\text{eff}}(\vec{r}) \chi^{(+)}(k_\alpha, \vec{r}_\alpha) \rangle|^2, \quad (2.A.3)$$

¹⁴³For details, see Idini et al. (2015), and Broglia et al. (2016), see also Fig. 2.4.1.

¹⁴⁴Another examples being provided by the result displayed in Fig. 2.10.1 concerning ^{11}Li and Fig. 7.3.1 regarding ^{11}Be (see also Sect. 7.6.2).

where

$$\begin{aligned} V_{eff} &= \int d\xi \psi_{M_{I\beta}}^{I_\beta^*}(\xi) V'_\beta(\xi, \vec{r}) \psi_{M_{I\alpha}}^{I_\alpha}(\xi), \\ &= \int d\xi \psi_{M_{I\beta}}^{I_\beta^*}(\xi) V_\beta(\xi, \vec{r}) \psi_{M_{I\alpha}}^{I_\alpha}(\xi), \end{aligned} \quad (2.A.4)$$

as ψ^{I_β} and ψ^{I_α} are orthogonal (remember $V'_\beta = V_\beta - \bar{U}(r)$). We now expand the interaction in spherical harmonics, i.e.

$$\begin{aligned} V_\beta(\xi, \vec{r}) &= \sum_{LM} V_M^L(\xi, r) Y_M^L(\hat{r}) \\ &= \sum_{LM} V_M^L(\xi, \vec{r}). \end{aligned} \quad (2.A.5)$$

Defining

$$\int d\xi \psi_{M_{I\beta}}^{I_\beta^*}(\xi) [V_M^L(\xi, r) \psi^{I_\alpha}(\xi)]_{M_{I\beta}}^{I_\beta} = F_L(r), \quad (2.A.6)$$

we can write eq.(2.A.4) as

$$V_{eff}(\vec{r}) = \sum_{LM} (LMI_\alpha M_\alpha | I_\beta M_\beta) F_L(r) Y_M^L(\hat{r}). \quad (2.A.7)$$

Inserting (2.A.7) into (2.A.3) we obtain

$$\begin{aligned} \frac{d\sigma}{d\Omega} &= \frac{k_\beta}{k_\alpha} \frac{m_\alpha^2}{(2\pi\hbar^2)^2} \frac{1}{2I_\alpha + 1} \sum_{M_\alpha M_\beta} \left| \sum_{LM} (LMI_\alpha M_\alpha | I_\beta M_\beta) \right. \\ &\quad \times \left. \int d\vec{r} \chi^{(-)*}(k_\beta, \vec{r}_\beta) F_L(r) Y_M^{L*}(\hat{r}) \chi^{(+)}(k_\beta, \vec{r}_\beta) \right|^2 \\ &= \frac{k_\beta}{k_\alpha} \frac{m_\alpha^2}{(2\pi\hbar^2)^2} \frac{2I_\beta + 1}{2I_\alpha + 1} \\ &\quad \times \sum_{LM} \frac{1}{2L + 1} \left| \int d\vec{r} \chi^{(-)*}(k_\beta, \vec{r}_\beta) F_L(r) Y_M^{L*}(\hat{r}) \chi^{(+)}(k_\beta, \vec{r}_\beta) \right|^2, \end{aligned} \quad (2.A.8)$$

where we have used the orthogonality relation between Clebsch-Gordan coefficients

$$\begin{aligned} &\sum_{M_\alpha M_\beta} (LMI_\alpha M_\alpha | I_\beta M_\beta) (L'MI_\alpha M_\alpha | I_\beta M_\beta) \\ &= \sqrt{\frac{(2I_\beta + 1)^2}{(2L + 1)(2L' + 1)}} \sum_{M_\alpha M_\beta} (I_\beta - M_\beta I_\alpha M_\alpha | L - M) \\ &\quad \times (I_\beta - M_\beta I_\alpha M_\alpha | L' - M) = \frac{2I_\beta + 1}{2L + 1} \delta_{LL'}, \end{aligned} \quad (2.A.9)$$

(fixed M).

Let us now discuss the case of inelastic scattering of even spherical nuclei.

The macroscopic Hamiltonian describing the dynamics of the multipole surface vibrations in such nuclei can be written, in the harmonic approximation as

$$H = \sum_{L,M} \left\{ \frac{D_L}{2} |\dot{\alpha}_M^L|^2 + \frac{C_L}{2} |\alpha_M^L|^2 \right\} = \sum_{L,M} \left\{ \frac{|\Pi_M^L|^2}{2D_L} + \frac{C_L}{2} |\alpha_M^L|^2 \right\}, \quad (2.A.10)$$

where the collective coordinate α_M^L is defined through the equation of the radius

$$R(\hat{r}) = R_0 \left[1 + \sum_{L,M} \alpha_M^L Y_M^{L*}(\hat{r}) \right], \quad (2.A.11)$$

and where $R_0 = r_0 A^{1/3}$ fm, and

$$\Pi_M^L = D_L |\dot{\alpha}_M^L|. \quad (2.A.12)$$

It is of notice that α_M^L is a dimensionless variable. Consequently, the dimensions of the inertia and of the restoring force parameters are

$$[D_L] = \text{MeV s}^2 \quad \text{and} \quad [C_L] = \text{MeV}, \quad (2.A.13)$$

while that of the conjugate momentum is

$$[\Pi_M^L] = \text{MeV s}. \quad (2.A.14)$$

The collective mode is generated from the interaction of the multipole field carried by each particle and the field of the rest of the particles. In turn this coupling modifies the single-particle motion. In particular the incoming projectile would feel this coupling. The potential V'_β is equal to

$$\begin{aligned} V'_\beta(\xi, \vec{r}) &= U(r - R(\hat{r})) \\ &= U(r - R_0 - R_0 \sum_{L,M} \alpha_M^L Y_M^{L*}(\hat{r})) \\ &= U(r - R_0) - R_0 \sum_{L,M} \alpha_M^L Y_M^{L*}(\hat{r}) \frac{dU(r - R_0)}{dr} \end{aligned} \quad (2.A.15)$$

$$\begin{aligned} &= V_\beta(\xi, r) - \bar{U}_\beta(r), \\ \bar{U}_\beta(r) &= -U(r - R_0) \\ V_\beta(\xi, \vec{r}) &= R_0 \frac{d\bar{U}_\beta(r)}{dr} \sum_{L,M} \alpha_M^L Y_M^{L*}(\hat{r}). \end{aligned} \quad (2.A.16)$$

Comparing with eq. (2.A.5) we obtain

$$V_M^L(\alpha, r) = R_0 \frac{d\bar{U}_\beta(r)}{dr} \alpha_M^L. \quad (2.A.17)$$

Note that H defined in Eq. (2.A.10) is the Hamiltonian of an L -dimensional harmonic oscillator, and that a_M^L is a classical variable. One can quantize this Hamiltonian in the standard way,

$$a_M^L = \sqrt{\frac{\hbar\omega_L}{2C_L}}(a_M^L - a_{-M}^{+L}), \quad (2.A.18)$$

where $\hbar\omega_L$ is the energy of the vibration, and a_M^{+L} is the creation operator of a phonon. For an even nucleus

$$\begin{aligned} |\Psi_{M_\alpha}^{I_\alpha}\rangle &= |0\rangle \quad (I_\alpha = M_\alpha = 0), \\ |0\rangle &: \text{ ground (vacuum) state.} \end{aligned} \quad (2.A.19)$$

The one-phonon state can be written as,

$$\begin{aligned} |\Psi_{M_\alpha}^{I_\alpha}\rangle &= |I; LM\rangle = a_M^{+L}|0\rangle, \\ (I_\beta &= L; M_{I_\beta} = M). \end{aligned} \quad (2.A.20)$$

We can now calculate the matrix element of the operator (2.A.17), which connects states which differ in one phonon. Starting from the ground state we obtain

$$\begin{aligned} \langle I; LM | V_M^L(\alpha, r) | 0 \rangle &= (-1)^{L-M} R_0 \frac{d\bar{U}_\beta(r)}{dr} \sqrt{\frac{\hbar\omega_L}{2C_L}} \langle 0 | (a_M^L - a_{-M}^{+L}) | 0 \rangle \\ &= R_0 \frac{d\bar{U}_\beta(r)}{dr} \sqrt{\frac{\hbar\omega_L}{2C_L}} = -\frac{R_0}{\sqrt{2L+1}} \frac{d\bar{U}_\beta(r)}{dr} \beta_L, \end{aligned} \quad (2.A.21)$$

where

$$\beta_L = \sqrt{\frac{(2L+1)\hbar\omega_L}{2C_L}}. \quad (2.A.22)$$

Substituting (2.A.21) into eq. (2.A.8) and making use of eqs. (2.A.19) and (2.A.20) we get

$$\begin{aligned} \frac{d\sigma}{d\Omega} &= \frac{k_\beta}{k_\alpha} \frac{\mu_\alpha^2}{(2\pi\hbar^2)^2} (\beta_L R_0)^2 \\ &\times \sum_M \frac{1}{2L+1} \left| \int d\vec{r} \chi^{(-)*}(k_\beta, \vec{r}) \frac{dU(r)}{dr} Y_M^{L*}(\hat{r}) \chi^{(+)}(k_\alpha, \vec{r}_\beta) \right|^2. \end{aligned} \quad (2.A.23)$$

Let us now assume that the nucleus has a permanent quadrupole ($L = 2$) axially-symmetric deformation. For a $K = 0$ band, the nuclear wave function has the form¹⁴⁵

$$\Psi_{IMK=0} = \sqrt{\frac{2I+1}{8\pi^2}} \mathcal{D}_{M0}^I(\omega) \chi_{K=0} \quad (\text{intrinsic}), \quad (2.A.24)$$

¹⁴⁵see e.g. Bohr and Mottelson (1975) and refs. therein.

where we have used $(\omega) = (\theta, \phi, \psi)$ to label the Eulerian angles which serve as orientation parameters.

In the intrinsic frame (which we take to coincide with the space-fixed axis when $\theta = \phi = \psi = 0$) the nuclear surface has the shape

$$R(\hat{r}) = R_0 \left[1 + \sum_L b_L Y_0^L(\hat{r}) \right], \quad (2.A.25)$$

where the b_L introduced here is a_0^L in the intrinsic frame. When the nucleus has orientation ω , this shape is rotated into

$$\hat{R}_\omega R(\hat{r}) = R_0 \left[1 + \sum_L b_L \mathcal{D}_{M0}^L(\omega) Y_0^L(\hat{r}) \right]. \quad (2.A.26)$$

One can then write,

$$W(r - R(\hat{r})) = W(r - R_0) - R_0 \frac{dW(r - R_0)}{dr} \sum_L b_L \mathcal{D}_{M0}^L(\omega) Y_0^L(\hat{r}), \quad (2.A.27)$$

which is the equivalent to Eq. (2.A.15) for the case of deformed nuclei. Then

$$V_M^L(b, r; \omega) = -\frac{d\bar{U}_\beta(r - R_0)}{dr} b_L \mathcal{D}_{M0}^L(\omega). \quad (2.A.28)$$

The effective interaction is now equal to

$$\begin{aligned} \langle \Psi_{IMK=0}, V_M^L(b, r; \omega) \Psi_{000} \rangle &= \\ &- R_0 \frac{d\bar{U}(r - R_0)}{dr} b_L \sqrt{\frac{(2L+1)^2}{8\pi^2}} \int d\omega \mathcal{D}_{M0}^{L*}(\omega) \mathcal{D}_{M0}^L(\omega) = \\ &- R_0 \frac{d\bar{U}(r - R_0)}{dr} b_L = -\frac{R_0}{\sqrt{(2L+1)}} \frac{d\bar{U}(r - R_0)}{dr} \beta_L = F_L(r), \\ &(\beta_L = \sqrt{(2L+1)} b_L), \end{aligned} \quad (2.A.29)$$

in complete analogy to (2.A.21). Thus the same formfactor is used for both types of collective excitation. Within the above simple scheme of structure and reaction, the normalization factor $(\beta_L R_0)^2$ is the only free parameter that can be obtained from the comparison of the experimental and theoretical (DWBA) differential cross section. The quantity β_L is known as the multipole deformation (dynamic or static) parameter, and gives a direct measure of the coupling of the projectile to the vibrational field. The value of β_L can also be obtained from the $B(EL)$ reduced transition probability, in which case one has a measure of the electric moment, instead of the mass moment.

Appendix 2.B Technical details NFT

In this Appendix we briefly discuss two technical aspects related to the overcompleteness of the basis used in NFT.

2.B.1 Graphical solution

The dispersion relation (2.7.57), which is central in the discussion concerning spurious states in the overcomplete basis of elementary modes of excitation used to develop NFT, is solved numerically in Sect. 2.7 (Fig. 2.7.8 (II)). The technical details of the corresponding implementation emerges natural by making a parallel with the dispersion relation associated with the Cooper pair problem, taking into account the energy separation existing in nuclei between single-particle levels due to the fact that it is a finite system (spatial quantization). In this case, the wavefunction of the two-particle system can be written as

$$|0^+\rangle = \frac{1}{\sqrt{2}} \sum_j \alpha_j [a_j^\dagger a_j^\dagger]_0^0 |0\rangle, \quad (2.B.1)$$

where $|0\rangle$ is the vacuum state and a_j^\dagger creates a particle in the orbital j with time-reversal properties $\tau a_{jm}^\dagger \tau^{-1} = (-1)^{j-m} a_{j-m}^\dagger$. The amplitudes α_j are determined by the secular equation

$$(2\epsilon_j - E)\alpha_j = \sum_{j'} (j + 1/2)^{1/2} (j' + 1/2)^{1/2} G(j', j', j, j) \alpha_j. \quad (2.B.2)$$

If one replaces the radial integrals $G(j', j', j, j) = -(V_0/4\pi) \int u_j^2(r) u_{j'}^2(r) r^2 dr$ (assuming the pairing force to be a contact interaction, see Sect. 3.6) by an average value G , the eigenvalues E are determined by the secular equation,

$$\frac{1}{G} = \sum_j \frac{(j + 1/2)}{2\epsilon_j - E} = \sum_j \sum_{m>0} \frac{1}{2\epsilon_j - E} = F(E). \quad (2.B.3)$$

The nature of the solution is illustrated in Fig. 2.B.1. When E goes from a value smaller to a value larger than $2\epsilon_j$, $F(E)$ decreases from $+\infty$ to $-\infty$ going through zero. The eigenvalues E are given by the intersection of $F(E)$ with the line G^{-1} . While all other eigenvalues than the lowest one, are trapped between the unperturbed energies $2\epsilon_j$, the ground state correlation can freely increase as G increases.

Making use of the correspondence

$$\sqrt{j + 1/2} \leftrightarrow \Lambda_1 \quad (2.B.4)$$

and

$$G \leftrightarrow (E - \epsilon_m - V)^{-1}, \quad (2.B.5)$$

one can transform (2.B.3) into (2.7.57). Consequently, the graphical solution shown in Fig. 2.B.1 can be used for this dispersion relation (Fig. 2.7.8).

Let us now return to the Cooper pair problem, and the dispersion relation (2.B.3). If the nucleus was a large box with the states j belonging to the continuum, Eq. (2.B.3) would indicate that there would exist a bound state for an

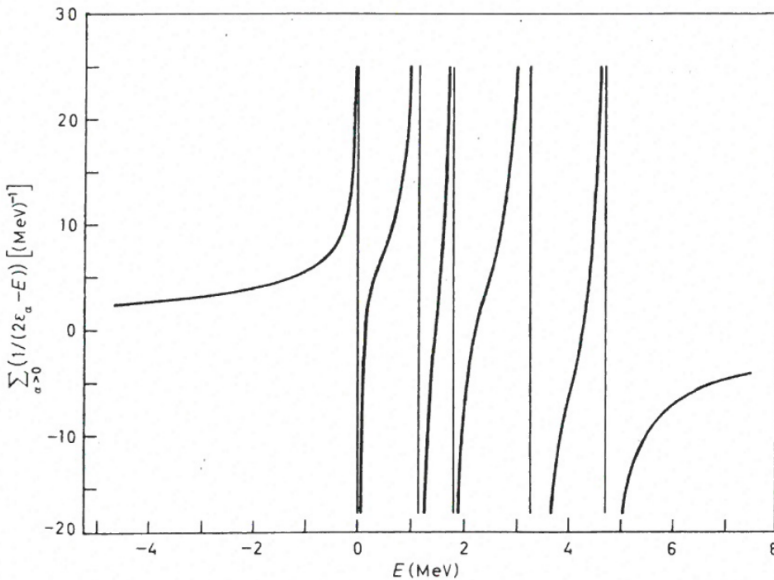


Figure 2.B.1: Dispersion relation for ^{206}Pb . The single-hole states available to the neutron holes (in MeV) are $p_{1/2}(0)$, $f_{5/2}(0.57)$, $p_{3/2}(0.89)$, $i_{13/2}(1.63)$, $f_{7/2}(2.34)$. The label α denotes the quantum numbers (j, m) (after Bayman (1960)).

arbitrary weak coupling provided that the potential was attractive near the Fermi surface. This result was first pointed out by Cooper in connection with the problem of electrons moving in a metal at low temperatures¹⁴⁶.

2.B.2 Overlap

The states $|\alpha\rangle$ and $|\beta\rangle$ mix strongly through the couplings depicted by the graphs (a) and (b) of Fig. 2.7.11. Because of the energy dependence of the effective Hamiltonian (see (2.7.55), (2.7.56)) there is one matrix element for each state. The eigenvectors resulting from the diagonalization procedure were normalized according to (2.7.73). The corresponding amplitudes ξ_{iqm} (2.7.60) are displayed in Fig. 2.7.11 (e).

The normalization matrices $\tilde{M}_{ii'}^{mm}$ associated with the two $3/2^+$ states discussed in Sect. 2.5 and 2.7, are given in Table 2.B.1. Details concerning the off-diagonal matrix elements are collected in Table 2.B.2.

It is of notice that in a conventional two-state model calculation implying a single matrix one would obtain

$$|I\rangle = A|\alpha\rangle + B|\beta\rangle$$

¹⁴⁶Cooper (1956); Bayman (1960).

	$ \alpha\rangle$	$ \beta\rangle$		$ \alpha\rangle$	$ \beta\rangle$		$ \alpha\rangle$	$ \beta\rangle$
$ \alpha\rangle$	-0.010	-0.168	$ \alpha\rangle$	-0.012	-0.434	$ \alpha\rangle$	-0.011	-0.271
$ \beta\rangle$		0.009	$ \beta\rangle$		0.070	$ \beta\rangle$		0.03

Table 2.B.1: Normalization matrices (see Eq. (2.7.73)) associated with the two $3/2^+$ states of ^{209}Bi , $|I\rangle$ and $|II\rangle$ (Fig. 2.7.11 (e)) (Bortignon et al. (1977), table 4.6).

		Fig. 1.7.10		
m	m'	(b)	(c)	(b)+(c)
I	II	0.013	-0.181	-0.168
II	II	0.016	-0.450	-0.434
I	II	0.014	-0.285	-0.271

Table 2.B.2: Contributions to the off diagonal elements of the overlap matrix $M_{ii'}^{mm'}$ associated with the $3/2$ states in the basis $|\alpha\rangle, |\beta\rangle$ (Table 2.B.1). See also figure 4.1 of Bortignon et al. (1977).

and

$$|II\rangle = -B|\alpha\rangle + A|\beta\rangle, \quad (2.B.6)$$

with $A^2 + B^2 = 1$. This model would predict the value $R = (\alpha/\beta)^2$ for the (t, α) ratio $R(t, \alpha) = \sigma_I^{tr}/\sigma_{II}^{tr}$ and $1/R$ for the (α, α') ratio $R(\alpha, \alpha') = \sigma_I^{oct}/\sigma_{II}^{oct}$ (see Sect. 2.7.4). The ratio $R_{th}(t, \alpha) = 1.83/2.25 = 0.81$ (against $R_{exp}(t, \alpha) = 1.8/2.2 = 0.82$) and $R_{th}(\alpha, \alpha') = 3.7/1.5 = 2.5$ (against $R_{exp}(\alpha, \alpha') = 4.2/1.1 = 3.8$) is a direct consequence of the overcompleteness of the basis which is taken care of by the nuclear field theory. While this is a systematic mathematical procedure to deal with the spurious state (in this case due to the overcompleteness of the basis $\{|\alpha\rangle, |\beta\rangle\}$) one can also relate, within the framework of shell model calculations (see Eq. (2.B.1)), the asymmetry between $R(t, \alpha)$ and $R(\alpha, \alpha')$ to the finite overlaps between states $|\alpha\rangle$ and $|\beta\rangle$, as discussed in Sect. 2.5.

2.B.3 NFT(r+s): linear theory

NFT is linear in the variety of particle–vibration coupling vertices (see e.g. Fig. 2.7.10). This is also valid concerning its extension to describe reaction processes, as can be seen from graph (a) of Fig. 2.B.2. For simplicity, this diagram and similar ones are drawn as displayed in Fig. 2.B.2 (b) (see also Fig. 2.1.3). However, in all cases the effects of recoil are properly taken into account following (a), as shown in e.g. Fig. 4.1.2 as well as in Sect. 6.1 within the framework of DWBA, and in App. 6.C (Eq. (6.C.7)) in the semiclassical approximation.

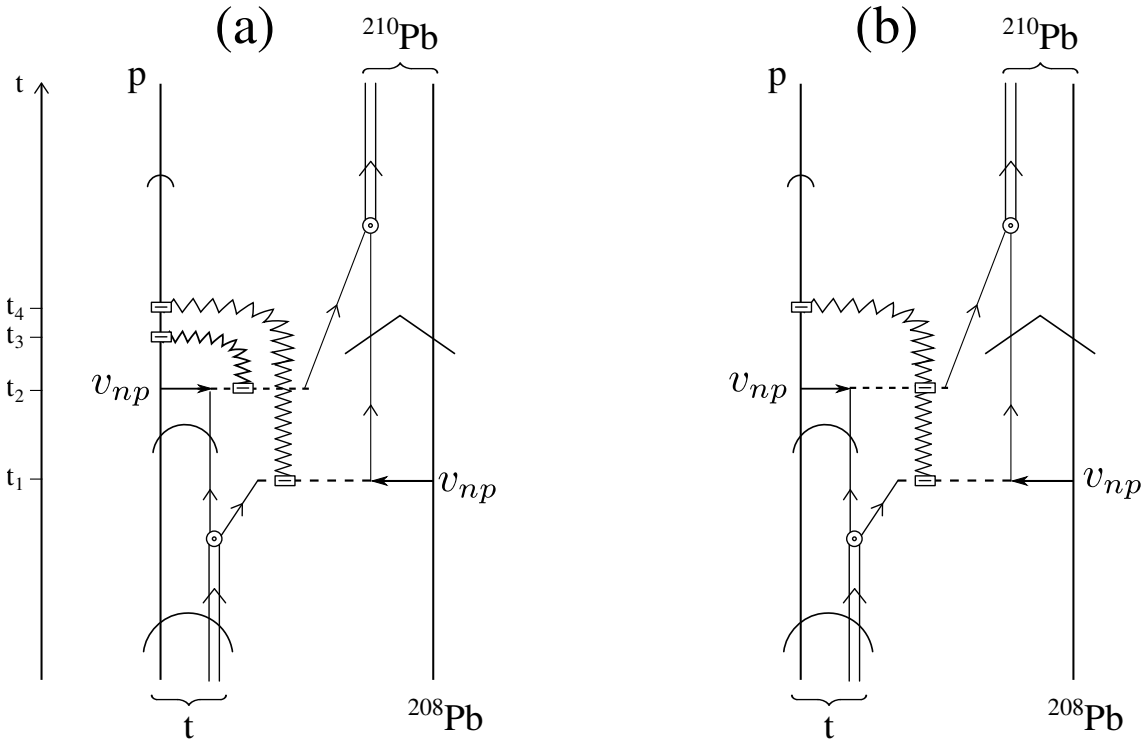


Figure 2.B.2: NFT($r+s$) diagram describing the reaction $^{208}\text{Pb}(t, p)^{210}\text{Pb}(\text{gs})$. That is the population of the lowest energy, monopole pair addition mode of ^{208}Pb . Concerning the different symbols used, we refer to Figs. 2.1.3 and 2.10.2. In particular concerning the recoil mode (jagged line) and the associated particle–recoil mode coupling vertex (dashed open rectangle). Also, of all the possible contributions associated with the different sequence of the processes taking place in this graph at times t_1, t_2, t_3 and t_4 , with the final outcome that the outgoing particle carries information to the detector of a transfer of two neutron masses. With this proviso in mind, and only for simplicity is that one may replace diagram (a) by diagram (b).

Appendix 2.C NFT and reactions

Nuclear Field Theory was systematically developed to describe nuclear structure processes. This fact did not prevent the translation into this graphical language of expressions which embodied the transition amplitude of a variety of reaction processes, in particular second order (in v_{np}) transition amplitudes associated with two nucleon transfer reactions¹⁴⁷.

The new feature to be considered regarding transfer processes and not encountered neither in structure, nor in elastic or anelastic processes, is the graphical representation of recoil effects. That is, a physical phenomenon associated with the change in the coordinate of relative motion reflecting the difference in mass partition between entrance (intermediate, if present) and exit channels. In fact, nuclear structure processes, do not affect the center of mass, with a proviso. In fact, the shell model potential violates the translational of the total nuclear Hamiltonian and, thus, single-particle excitations can be produced by a field proportional to the total center-of-mass coordinate. The translational invariance can be restored by including the effects of the collective field generated by a small displacement α of the nucleus. Such a displacement, in the x -direction, gives rise to a coupling which can be written as,

$$H_c = \kappa\alpha F, \quad (2.C.1)$$

where

$$F = -\frac{1}{\kappa} \frac{\partial}{\partial x}, \quad (2.C.2)$$

and

$$\kappa = \int \frac{\partial}{\partial x} \frac{\partial \rho_0}{\partial x} d\tau = -A \left\langle \frac{\partial^2 U}{\partial x^2} \right\rangle, \quad (2.C.3)$$

corresponding to a normalization of α such that $\langle F \rangle = \alpha$. It is of notice that both κ and U are negative for attractive fields (p. 356 of¹⁴⁸)

The spectrum of normal modes generated by the field coupling (2.C.1), namely by a Galilean transformation of amplitude α , contains an excitation mode with zero energy for which zero point fluctuations diverge in just the right way to restore translational invariance to leading order in α . In fact, while the zero point fluctuations (ZPF)

$$\lim_{\omega_\alpha \rightarrow 0} \left(\frac{\hbar\omega_\alpha}{2C_\alpha} \right)^{1/2} = \lim_{\omega_\alpha \rightarrow 0} \left(\frac{\hbar^2}{2D_\alpha \hbar\omega_\alpha} \right)^{1/2}, \quad (2.C.4)$$

diverge the inertia remains finite and equal to $D_\alpha = AM$, as expected, C_α being the restoring force constant. The additional dipole roots include, in particular, the isoscalar dipole modes associated with $\hat{D} = \sum_{i=1}^A r_i^3 Y_{1\mu}(\hat{r}_i)$, which can be viewed as a non-isotropic compression mode¹⁴⁹.

¹⁴⁷Broglia (1975).

¹⁴⁸Bohr and Mottelson (1975).

¹⁴⁹See e.g. Colò et al. (2000).

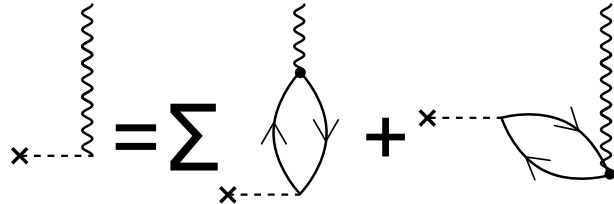


Figure 2.C.1: Self-consistent condition for normal modes

The operators leading to transformations associated with the change in the co-ordinates of relative motion (recoil effects) are Galilean operators ($\sim \exp(\mathbf{k}_{\alpha\beta} \cdot (\mathbf{r}_\beta - \mathbf{r}_\alpha))$). Their action (on e.g. the entrance channel), as that of (2.C.1) (on the shell model ground state), can be graphically represented in terms of NFT diagrams (or eventual extensions of them). In Figs 2.1.2 and 2.1.3 as well as 2.10.2–2.10.6 they are drawn in terms of jagged lines. How do we calculate such couplings? Let us elaborate on this point.

When one states that the small displacement α of the nucleus leads to a coupling (2.C.1) one means a coupling between the single-particle and the collective displacement of the system as a whole. When one talks about the spectrum of normal modes associated with such a coupling, one refers to the harmonic approximation (RPA). Thus, to the solutions of the dispersion relation¹⁵⁰,

$$-\frac{2\kappa}{\hbar} \sum_i \frac{|F_i|^2 \omega_i}{\omega_i^2 - \omega_a^2} = 1, \quad (2.C.5)$$

where the sum is over dipole particle-hole excitations. This dispersion relation can be represented graphically through the diagrams shown in Fig. 2.C.1. In particular, α acting on the vacuum creates the collective mode. This can also be seen by expressing α in second quantization, namely

$$\alpha = \sqrt{\frac{\hbar\omega_\alpha}{2C_\alpha}} (\Gamma_\alpha^\dagger + \Gamma_\alpha), \quad (2.C.6)$$

where $\sqrt{\hbar\omega_\alpha/2C_\alpha} = \sqrt{\frac{\hbar^2}{2D_\alpha} \frac{1}{\hbar\omega_\alpha}}$ is the zero-point amplitude of the collective (displacement) mode. Now, none of the above arguments lose their meaning in the case in which there is a root with $\omega_\alpha = 0$, also in keeping with the fact the inertia remains finite. In Figs. 2.10.2–2.10.6 we do something similar to what is done in Fig. 2.C.1. The dot, which in this figure represents the particle-vibration coupling, is replaced by a small dashed open square, which we label “particle-recoil coupling vertex” (see labels Fig. 2.10.2). It constitutes a graphical mnemonic to count the degrees of freedom that are at play. In this case the coordinates of relative motion. Also the fact that in connection with the appearance of such vertices one has to

¹⁵⁰Bohr and Mottelson (1975); Eq. (6-244), Brink and Broglia (2005), Sect. 8.3.1.

calculate matrix elements of precise form factors which involve the recoil phases. As far as the actual calculation of a particle-mode vertex in which $\omega_a \rightarrow 0$, an empirical way out is that of a coarse-grained-like symmetry restoration. In this case κ is adjusted in such a way, that the lowest solution of Eq. (2.C.5), although being smaller than the rest of them, remains finite¹⁵¹.

2.C.1 Potential scattering

The elastic differential cross section expressed in terms of partial waves is

$$\sigma(\theta) = |f(\theta)|^2 = \frac{1}{k^2} \left| \sum_{l=0}^{\infty} (2l+1) e^{i\delta_l} \sin \delta_l P_l(\cos \theta) \right|^2, \quad (2.C.7)$$

where

$$f(\theta) = \frac{1}{2ik} \sum_{l=0}^{\infty} (2l+1) (e^{2i\delta_l} - 1) P_l(\cos \theta), \quad (2.C.8)$$

is the scattering amplitude. The total cross section

$$\sigma = 2\pi \int_0^{\infty} \sigma(\theta) \sin \theta d\theta = \frac{4\pi}{k^2} \sum_{l=0}^{\infty} (2l+1) \sin^2 \delta_l \quad (2.C.9)$$

expressed in term of f , namely,

$$\sigma = \frac{4\pi}{k} \Im f(0), \quad (2.C.10)$$

being a particular case of the optical theorem. The quantity δ_l is known as the phase shift of the l th partial wave, namely the difference in phase between the asymptotic form of the actual radial wavefunction describing the scattering process and the radial wavefunction $j_l(kr)$ in the absence of potential. The phase shifts which completely determine the scattering lead to a change in the scaling between incoming and outgoing waves which results, as expressed in (2.C.10), in the interference between them, so that particle intensity is smaller behind the scattering region ($\theta \approx 0$) than in front of it. It is of notice that δ_l cannot be measured directly. In fact, with the exception of the $l = 0$ phase shift, obtained from low-energy scattering experiments, the values of δ_l are inferred as empirical quantities from the parametrization of the potential. It is of notice that a degree of ambiguity concerning the uniqueness of the findings may remain.

¹⁵¹Within this context we refer to Bohr and Mottelson (1975), p. 446. With no coupling H_c (Eq. (2.C.1)), the ZPF $\alpha_0^{(0)}$ of the nuclear CM are small ($\sim A^{-1/3}$). Thus, it is possible to tune κ so as to make the ZPF associated with the lowest root large as compared to $\alpha_0^{(0)}$, but still compatible with the ansatz at the basis of RPA (small amplitude harmonic vibrations).

2.C.2 Transfer

We now consider a general reaction



in which the nucleus a impinges on the nucleus A in the entrance channel $\alpha(a, A)$ and where the two nuclei in the exit channel β , namely b and B may differ from those in α , by the transfer of one or more nucleons.

In the center-of-mass system, the total Hamiltonian may be written as

$$\begin{aligned} H &= T_{aA} + H_a + H_A + V_{aA}, \\ &= T_{bB} + H_b + H_B + V_{bB}, \end{aligned} \quad (2.C.12)$$

where T_{aA} is the kinetic energy of the relative motion in channel α

$$T_{aA} = -\frac{\hbar^2}{2m_{aA}} \nabla_{aA}^2, \quad (m_{aA} = \frac{m_a m_A}{m_a + m_A}), \quad (2.C.13)$$

and similarly for T_{bB} . Assuming the nuclei in (2.C.11) to be heavy ions, we shall solve the time-dependent Schrödinger equation

$$i\hbar \frac{\partial \Psi}{\partial t} = H\Psi \quad (2.C.14)$$

with the initial condition that a and A are in their ground states, and that the relative motion is described as a narrow wave-packet of rather well-defined impact parameter and velocity. Because of the quantal nature of the process under consideration, we study the quantal description in the limit of small wavelength of relative motion (semiclassical approximation). One expands Ψ on the channel wavefunctions

$$\Psi_\beta(t) = \Psi_m^b(\xi_b) \Psi_n^B(\xi_B) e^{i\delta_\beta} \quad (2.C.15)$$

where Ψ^b and Ψ^B describe the structure of the two nuclei and satisfy the equations

$$H_b \Psi_m^b(\xi_b) = E_m^b \Psi_m^b(\xi_b) \quad (2.C.16)$$

and

$$H_B \Psi_n^B(\xi_B) = E_n^B \Psi_n^B(\xi_B), \quad (2.C.17)$$

while ξ_b and ξ_B denote the intrinsic coordinates. the phase δ_β is defined by

$$\delta_\beta = \frac{1}{\hbar} \left\{ m_\beta \mathbf{v}_\beta(t) (\mathbf{r}_\beta - \mathbf{R}_\beta(t)) - \int_0^t \left(U_\beta(R_\beta(t')) - \frac{1}{2} m_\beta v_\beta^2(t') \right) dt' \right\}. \quad (2.C.18)$$

The index β labels both the partition of nucleons into b and B , as well as the quantal states of the two nuclei. The quantity U_β is the ion-ion potential in this channel.

It is equal to the expectation value of $V_\beta = V_{bB}$ in the channel β . The distance between the centers of mass of the two systems is denoted by

$$\mathbf{r}_\beta = \mathbf{r}_{bB} = \mathbf{r}_b - \mathbf{r}_B. \quad (2.C.19)$$

The quantity \mathbf{R}_β and its derivative $\mathbf{v}_\beta = \dot{\mathbf{R}}_\beta$ describe the motion of the centers of mass of the wavepackets, and satisfy the corresponding classical equation of motion,

$$m_\beta \dot{\mathbf{v}}_\beta = -\nabla U_\beta(\mathbf{R}_\beta). \quad (2.C.20)$$

The phase factor $e^{i\delta_\beta}$ in the channel wavefunction, is essentially a Galilean transformation where an additional phase (related with the Q -value) has been added to eliminate, as far as possible, the diagonal matrix elements of the coupled equations. Using the notation $E_\beta = E_m^b + E_n^B$ and inserting the ansatz

$$\Psi = \sum_\beta c_\beta((r_\beta - R_\beta), t) \Psi_\beta(t) e^{-iE_\beta t/\hbar} \quad (2.C.21)$$

in eq. (2.C.14) one obtains, assuming narrow wavepackets, product of an amplitude $a_\beta(t)$ and a shape $\chi_\beta(\mathbf{r} - \mathbf{R}_\beta(t), t)$, ($c_\beta = a_\beta \chi_\beta$),

$$\begin{aligned} i\hbar \sum_\beta \dot{a}_\beta(t) \langle \Psi_\xi | \Psi_\beta \rangle_{\mathbf{R}_{\xi\gamma}} e^{-iE_\beta t/\hbar} \\ = \sum_\gamma \langle \Psi_\xi | V_\gamma - U_\gamma(r_\gamma) | \Psi_\gamma \rangle_{\mathbf{R}_{\xi\gamma}} a_\gamma(t) e^{-iE_\gamma t/\hbar}. \end{aligned} \quad (2.C.22)$$

where the sub-index on the matrix elements indicate that the integration over the degree of freedom of the two nuclei, the average center-of-mass coordinate $\mathbf{r}_{\beta\gamma} = (\mathbf{r}_\beta + \mathbf{r}_\gamma)/2$ should be identified with the average classical coordinate, i.e.

$$\mathbf{r}_{\beta\gamma} \rightarrow \mathbf{R}_{\beta\gamma} = \frac{1}{2}(\mathbf{R}_\beta + \mathbf{R}_\gamma), \quad (2.C.23)$$

and the functions $\langle \Psi_\xi | V_\gamma - U_\gamma(r_\gamma) | \Psi_\gamma \rangle_{\mathbf{R}_{\xi\gamma}}$ are the form factors. The coupled equations (2.C.22) can be written in a more compact way by an orthogonalization procedure, which makes use of the *adjoint channel wavefunctions*

$$\omega_\xi = \sum_\gamma g_{\xi\gamma}^{-1} \Psi_\gamma, \quad (2.C.24)$$

where g^{-1} is the inverse of the overlap matrix

$$g_{\xi\gamma} = \langle \Psi_\xi | \Psi_\gamma \rangle, \quad (2.C.25)$$

that is

$$\sum_\xi g_{\gamma\xi} g_{\xi\beta}^{-1} = \sum_\xi g_{\gamma\xi}^{-1} g_{\xi\beta} = \delta(\gamma, \beta). \quad (2.C.26)$$

With this definition,

$$(\omega_\xi, \Psi_\beta) = \delta(\xi, \beta), \quad (2.C.27)$$

which takes care of non-orthogonality. Making use of the above relations one can rewrite (2.C.22) in the form

$$i\hbar \dot{a}_\beta(t) = \sum_\gamma \langle \omega_\beta | V_\gamma - U_\gamma | \Psi_\gamma \rangle_{\mathbf{R}_{\beta\gamma}} e^{i(E_\beta - E_\gamma)t/\hbar} a_\gamma(t). \quad (2.C.28)$$

That is, the proper transfer (tunneling) equations are obtained from (2.C.22) by a basis orthogonalization process¹⁵². By solving these coupled equations with the condition that at $t = -\infty$ the system is in the ground state of a and A (entrance channel α), that is $a_\gamma(-\infty) = \delta_{\gamma,\alpha}$, one can calculate the differential cross section

$$\frac{d\sigma_{\alpha \rightarrow \beta}}{d\Omega} = P_{\alpha \rightarrow \beta} \sqrt{\left(\frac{d\sigma_\alpha}{d\Omega} \right)_{el} \left(\frac{d\sigma_\beta}{d\Omega} \right)_{el}}, \quad (2.C.29)$$

where $P_{\alpha \rightarrow \beta}$ is the absolute value squared of the transition amplitude $|a_\beta(t = +\infty)|^2$. It gives the probability that the system at $t = +\infty$ is in the final channel. The quantities $(d\sigma/d\Omega)_{el}$ are the (semiclassical) elastic cross sections.

We now solve the coupled equations in first order perturbation theory. For this purpose we insert $\delta(\gamma, \alpha)$ at the place of $a_\gamma(t)$ obtaining

$$\begin{aligned} a_\beta(t) &= \frac{1}{i\hbar} \int_{-\infty}^t \langle \omega_\beta | V_\alpha - U_\alpha | \Psi_\alpha \rangle_{\mathbf{R}_{\beta\alpha}(t')} \exp^{i(E_\beta - E_\alpha)t'/\hbar} dt' \\ &= \frac{1}{i\hbar} \int_{-\infty}^t dt' \langle \Psi_\beta | V_\alpha - U_\alpha | \Psi_\alpha \rangle_{\mathbf{R}_{\beta\alpha}(t')} \exp^{i(E_\beta - E_\alpha)t'/\hbar} \end{aligned} \quad (2.C.30)$$

where the expansion,

$$\omega_\beta = \Psi_\beta - \langle \Psi_\alpha | \Psi_\beta \rangle_{\mathbf{R}_{\beta\alpha}(t)}, \quad (2.C.31)$$

has been used, and the ansatz made, that the global optical potentials (U : real part), and standard nucleon–nucleon interactions V fulfill the relation

$$\langle \Psi_\alpha | V_\alpha - U_\alpha | \Psi_\alpha \rangle = 0. \quad (2.C.32)$$

Let us consider for simplicity the one-particle transfer reaction¹⁵³

$$a (= b + 1) + A \rightarrow b + B (= A + 1). \quad (2.C.33)$$

¹⁵²Within this connection we refer to Sect. 4.7 where the tunneling Hamiltonian used in connection with the Josephson effect is discussed.

¹⁵³Concerning the question of non-orthogonality in one-particle transfer processes, the first contribution arises in second order of perturbation theory, within the framework of DWBA (Thompson and Nunes (2009)).

Making use of (2.C.15), that is,

$$\Psi_\alpha = \Psi^a \Psi^A e^{i\delta_\alpha}, \quad (2.C.34)$$

and

$$\Psi_\beta = \Psi^b \Psi^B e^{i\delta_\beta}, \quad (2.C.35)$$

one can write

$$\begin{aligned} \langle \Psi_\beta | V_\alpha - U_\alpha | \Psi_\alpha \rangle_{\mathbf{R}_{ab}} &= \langle \Psi^b \Psi^B | (V_\alpha - U_\alpha) e^{i\sigma_{ab}} | \Psi^a \Psi^A \rangle_{\mathbf{R}_{ab}} e^{i\gamma_{ab}} \\ &= \langle \phi^{B(A)}(S^B(n), r_{1A}), U(r_{1b}) e^{i\sigma_{ab}} \phi^{a(b)}(S^a(n), r_{1b}) \rangle_{\mathbf{R}_{ab}} e^{i\gamma_{ab}}. \end{aligned} \quad (2.C.36)$$

To obtain the above relation, we have separated the difference $\delta_{ab} = \delta_\alpha - \delta_\beta$ between the phases δ_α and δ_β into a part γ_{ab} which only depends on time and is related to the effective Q -value of the reaction process, and a phase σ_{ab} which also depends on the center-of-mass coordinate of the transferred particles. That is

$$\begin{aligned} \gamma_{ab}(t) &= \int_0^t \left\{ U_\alpha(R_\alpha(t)) - \frac{1}{2} m_\alpha v_\alpha^2(t') - U_\beta(R_\beta(t')) + \frac{1}{2} m_\beta v_\beta^2(t') \right\} \\ &\quad + \mathbf{k}_{ab}(t)(\mathbf{R}_\alpha - \mathbf{R}_\beta), \end{aligned} \quad (2.C.37)$$

where \mathbf{k}_{ab} is the average wave vector

$$\mathbf{k}_{ab} = \frac{1}{2\hbar} (m_\alpha \mathbf{v}_\alpha(t) + m_\beta \mathbf{v}_\beta(t)). \quad (2.C.38)$$

Similarly

$$\sigma_{ab} = \mathbf{k}_{ab}(t) \cdot (\mathbf{r}_\beta - \mathbf{r}_\alpha). \quad (2.C.39)$$

The phase σ is characteristic for transfer processes since the dynamical variables \mathbf{r}_α and \mathbf{r}_β are identical for inelastic scattering. It arises from the change in the center-of-mass coordinate taking place when mass is transferred from one system to other. It gives rise to the recoil effect. Within the framework of DWBA it leads to a change of scaling of the DW (see also section elastic transfer). Summing up, the one-particle transfer amplitude reads

$$\begin{aligned} (a_\beta(t = +\infty))^{(1)} &= \int_{-\infty}^{\infty} \langle \phi^{B(A)}(S^B(n), \mathbf{r}_{1A}), U_{1b}(r_{1b}) e^{\sigma_{ab}} \phi^{a(b)}(S^a(n), \mathbf{r}_{1b}) \rangle_{\mathbf{R}_{ab}} \\ &\quad \times \exp \left\{ i \left[(E_\beta - E_\alpha)t' / \hbar + \gamma_{ab} \right] \right\} \end{aligned} \quad (2.C.40)$$

The phases δ_{ab} ($\sigma_{ab} + \gamma_{ab}$) play a similar role in the determination of transfer processes reaction amplitudes as δ_l does in connection with elastic scattering cross sections. In fact, δ_{ab} determines the shift between incoming and outgoing waves and thus the interference process which is at the basis of the absolute value of the transfer differential cross section. In other words, the reaction part of the elastic

and one-nucleon-transfer reaction cross section are embodied in δ_l and $\delta_{\alpha\beta}$ respectively. The nuclear structure part is contained in the reduced mass μ and potential U in the case of elastic scattering, and in the single-particle wavefunctions, potential U_{1b} and Q -value phase in the transfer case. Within the diagrammatic representation of particle-transfer reaction theory, the recoil phase is represented by a jagged line. Similar to δ_l , $\delta_{\alpha\beta}$ and $\sigma_{\alpha\beta}$ cannot be measured directly, but can in principle be inferred from the absolute differential cross section¹⁵⁴. In other words, the jagged line does not display asymptotic behavior, representing in all cases a virtual process.

Let us conclude this section by making some comments concerning two nucleon transfer processes

$$\alpha \equiv a (= b + 2) + A \rightarrow b + B (= A + 2) \equiv \beta, \quad (2.C.41)$$

and associated sum rules. For such reactions, the overlap appearing in Eq. (2.C.31) contributes with an amplitude $\langle \Psi_\beta | \mathbb{1} | \Psi_\gamma \rangle \langle \Psi_\gamma | V_\alpha - U_\alpha | \Psi_\alpha \rangle$, where $\mathbb{1}$ is the unit operator, while $\gamma \equiv f (= b + 1) + F (= A + 1)$, denotes the mass partition of the intermediate channel. The above expression indicates that a consistent description of two-nucleon transfer reactions in a non-orthogonal basis involves three strongly interwoven reaction channels¹⁵⁵, namely α , γ and β and consequently has to be worked out, at least, up to second order of perturbation theory, and thus the need to calculate also $a^{(2)}(t)$. That is, including simultaneous and successive transfer and non-orthogonality corrections.

Regarding the sum-rule subject we consider, for simplicity, the simultaneous transfer amplitude (2.C.30) (see also App. 6.C, Eq. (6.C.4)). That is,

$$a^{(1)}(t = +\infty) = \frac{1}{i\hbar} \int_{-\infty}^{\infty} dt \exp\left[\frac{i}{\hbar}(E^{bB} - E^{aA})t + \gamma_{\beta\alpha}(t)\right] \times \langle \phi^{B(A)}(\mathbf{r}_{1A}, \mathbf{r}_{2A}) | U(r_{1b}) | e^{i\sigma_{\beta\alpha}} \phi^{a(b)}(\mathbf{r}_{1b}, \mathbf{r}_{2b}) \rangle_{\mathbf{R}_{\alpha\beta}(t)}, \quad (2.C.42)$$

where

$$\sigma_{\beta\alpha} = \frac{1}{\hbar} \frac{m_n}{m_A} (m_{aA} \mathbf{v}_{aA}(t) + m_{bB} \mathbf{v}_{bB}(t)) \cdot (\mathbf{r}_\alpha - \mathbf{r}_\beta), \quad (2.C.43)$$

takes care of recoil effects, the phase factor $e^{i\sigma_{\beta\alpha}}$ being a generalized Galilean transformation associated with the mismatch between entrance and exit channels, while the phase

$$\begin{aligned} \gamma_{\beta\alpha}(t) &= \int_0^t dt' \left\{ U_\beta(\mathbf{R}_\beta(t')) - \frac{1}{2} m_\beta v_\beta^2(t') - U_\alpha(\mathbf{R}_\alpha(t')) + \frac{1}{2} m_\alpha v_\alpha^2(t') \right\} \\ &\quad + \frac{1}{2\hbar} (m_\alpha \mathbf{v}_\alpha(t) + m_\beta \mathbf{v}_\beta(t)) \cdot (\mathbf{R}_\beta(t) - \mathbf{R}_\alpha(t)), \end{aligned} \quad (2.C.44)$$

¹⁵⁴For more detail see Broglia and Winther (2004), in particular Section V.4 p. 308 and subsequent.

¹⁵⁵This is also testified by the fact that their formal expression can be shifted around by changing representation, among post-post, prior-prior, and prior-post, see e.g. Eq. (2.6.2) as well as Fig. 6.C.2.

is related to the effective Q -value of the reaction.

The rate of change of the formfactor $\langle \phi^{B(A)}, U(r_{1b})e^{i\sigma_{ab}}\phi^{a(b)} \rangle$ with time is slow, being completely overshadowed by the rapidly varying phase factor $\exp\left[\frac{i}{\hbar}(E^{bB} - E^{aA})t + \gamma_{\beta\alpha}(t)\right]$. Similar relations concerning recoil and Q -value effects can be obtained from the amplitudes associated to successive and to non-orthogonality terms i.e. $a^{(2)}$ and $a^{(NO)}$ (see Ch. 6, Sect. 6.C).

Summing up, to compare two-nucleon transfer cross sections on equal structural footing, one has to eliminate the kinematical oscillating phase which can completely distort the “intrinsic” (reduced matrix element) value of the two-nucleon cross section. And for that, one has to work on each of the three amplitudes to extract at best the phases which couple relative and intrinsic motion.

Let us make a parallel with the sum rule associated with electromagnetic decay (Coulomb excitation, γ -decay). The absolute transition probability for absorption (emission) of a photon from nuclear dipole states is measured in sec^{-1} by

$$T(E1; I_1 \rightarrow I_2) = (1.59 \times 10^{15}) \times (E)^3 \times B(E1; I_1 \rightarrow I_2), \quad (2.C.45)$$

where E is the energy of the transition and $B(E1) = \langle I_2 | \mathcal{M}(E1) | I_1 \rangle / \sqrt{3}$ is¹⁵⁶ the reduced transition probability¹⁵⁷. The TRK-sum rule is written as

$$S(E1) = \langle 0 | [[H, \mathcal{M}(E1)], \mathcal{M}(E1)] | 0 \rangle / 2, \quad (2.C.46)$$

Now, in this particular case the Q -value dependence of the observed absolute transition probabilities can be eliminated analytically (E^3 dependence), as well as the overall factor (1.59×10^{15}), in keeping with the fact that the mass partition ($a+A \rightarrow a+A^*$) as well as the overall factor does not change between entrance and exit channels or, equivalently, the coordinate of relative motion $\mathbf{R}_{aa'}(t)$ is always that describing the relative center of mass position of target and projectile.

Expressed it differently, and returning to the expression of the first order (simultaneous) two-nucleon transfer amplitude $a^{(1)}(t = +\infty)$ one can only devise empirical protocols to try to extract the γ - and σ -phase dependence from it (see Eqs. (2.C.42)–(2.C.44)), and set differential absolute two-nucleon transfer cross sections $d\sigma/d\Omega \sim |a|^2$ on equal footing regarding kinematics, so as to be able to compare the intrinsic, reduced transition probabilities (structure). That is, extract the structure information contained in, e.g.,¹⁵⁸

$$\phi^{B(A)}(\mathbf{r}_{1A}, \mathbf{r}_{2A}) = \langle \mathbf{r}_{1A}, \mathbf{r}_{2A} | \Gamma_1^\dagger(\beta = +2) | \tilde{0} \rangle, \quad (2.C.47)$$

as well as in

$$\phi^{B(A)}(\mathbf{r}_{1A}, \mathbf{r}_{2A}) = \langle \mathbf{r}_{1A}, \mathbf{r}_{2A} | [a_k^\dagger a_k^\dagger]_0 | 0 \rangle. \quad (2.C.48)$$

¹⁵⁶ $\mathcal{M}(E1) = e \sum_k \left(\left(\frac{N-Z}{A} - t_Z \right) r Y_{1\mu} \right)_k$.

¹⁵⁷ Bohr and Mottelson (1969) p. 382.

¹⁵⁸ Where $\Gamma_n^\dagger(\beta = +2) = \sum_k X_k^n [a_k^\dagger a_k^\dagger]_0 - \sum_i Y_i^n [a_i^\dagger a_i^\dagger]_0$, is the RPA pair creation addition mode acting on a closed shell system $|\tilde{0}\rangle$.

Namely, in the RPA pair addition mode representation and in the pure two-particle configuration $|j_k^2(0)\rangle$ describing two nucleons moving in time reversal states around the close shell system $|0\rangle$. If one was able to disentangle the γ and σ dependence of $a^{(1)}$ (as well as that of $a^{(2)}$ and $a^{(NO)}$, see above) from its formfactor dependence, the comparison between the quantities $\sum_{n,k} |c_k^{(n)}|^2$, and¹⁵⁹ $\sum_{n,j} \left| \sum_k X_k^{(n)} \delta(j, k) - \sum_i Y_i^{(n)} \delta(j, i) \right|^2$ could eventually be phrased in terms of exact sum rules. This not being the case, one has to deal with approximate TNTR sum rules. With this proviso in mind, such sum rules are quite useful (see Sect. 7.4.1; also end of Sect. 2.2).

Appendix 2.D NFT vacuum polarization

The role zero point fluctuations play in the nuclear ground state, i.e. in the NFT vacuum can be clarified by relating it to the polarization of the QED vacuum. Let us briefly dwell on the "reality" of such a phenomenon by recalling the fact that to the question of Rabi of whether the polarization of the QED vacuum could be measured¹⁶⁰ in particular the change in charge density felt by the electrons of an atom, e.g. the electron of a hydrogen atom, due to virtual creation and annihilation of electron-positron pairs - Lamb gave a quantitative answer, both experimentally and theoretically¹⁶¹. The corresponding correction (Lamb shift) implies that the $2s_{1/2}$ level lies higher than the $2p_{1/2}$ level by about 1000 megacycles/s as experimentally observed.

In connection with the discussion of Feynman of vacuum polarisation, where a field produces a pair, the subsequent pair annihilation producing a new field, namely a close loop, he implemented in his space-time trajectories Wheeler's idea of electrons going backwards in time (positrons). Such trajectories would be like an N in time, that is electrons which would back up for a while, and go forward again. Being connected with a minus sign, these processes are associated with Pauli principle in the self-energy of electrons (see Fig. 2.4.2 (f)). The divergences affecting such calculations could be renormalised by first computing the self-energy diagram in second order and finding the answer which is finite, but contains a cut-off to avoid a logarithmic divergence. Expressing the result in terms of the experimental mass, one can take the limit (cut-off $\rightarrow \infty$) which now exists (see also Sect. 7.6). Concerning radiative corrections to scattering, in particular that associated with the process in which the potential creates an electron-positron pair which then reannihilates, emitting a quantum which scatters the electron, the renormalisation procedure should be applied to the electric charge, introducing the observed one (Bethe and Pauli)¹⁶².

In the nuclear case, for example Skyrme effective interactions give rise to particle-vibration coupling vertices which, because of the contact character of these

¹⁵⁹ See e.g. Broglia and Riedel (1967).

¹⁶⁰ Pais (1986) pp. 450, 451; Pais (2000) pp. 255-267.

¹⁶¹ Lamb Jr and Rutherford (1947); Kroll and Lamb (1949)

¹⁶² See Mehra (1996) p. 295; see also Bjorken and Drell (1998).

interactions may lead to divergent zero point energies¹⁶³, unless a cut-off is introduced¹⁶⁴. The Gogny force being finite range does not display such problems. Nonetheless, the associated results concerning zero point energies may not be very stable and/or accurate carrying out a complete summation over both collective and non collective contributions. In this case one can eliminate such a problem by going to higher orders in the oyster diagrams (see Figs. 2.4.2 (a), 2.7.1 and 2.9.2, as well as App. 6.A). The fermion exchange between two of these diagrams (Pauli principle) eliminates non-collective contributions, leading to convergent, accurate results.

An economic and reliable method to achieve a similar result, is that of using renormalization. That is, to calculate the lowest order diagrams but introducing, in the intermediate states, the dressed physical (empirical) states.

¹⁶³See Hellemans et al. (2013); Pastore et al. (2015) and refs. therein.

¹⁶⁴Let alone the fact that the velocity dependent component of these forces weaken the PVC vertices leading to poorly collective low-lying vibrations, and to equally poor clothed valence states. The question emerges of which are the provisos to be taken in the use of effective forces to higher orders of the PVC. Within this context cf. Mahaux et al. (1985), also Broglia et al. (2016); Barranco et al. (2017) concerning the implementation of renormalization in both configuration and 3D-spaces within the framework of NFT. In a nutshell, the bare mean field exists but its properties cannot be measured (not any more than the bare electron mass in renormalized quantum electrodynamics), and corresponds to a set of parameters of a Fermi-like function which ensure that the clothed states reproduce all of the experimental findings, for both structure and reactions.

Chapter 3

Pairing with transfer

3.1 Nuclear Structure in a nutshell

The low-energy properties of the finite, quantal, many-body nuclear system, in which nucleons interact through the strong force of strength $v_0 (\approx -100 \text{ MeV})$ and range $a (\approx 0.9 \text{ fm})$ are controlled, in first approximation, by independent particle motion. This is a consequence of the fact that nucleons display a sizable value of the quantal zero point (kinetic) energy of localization ($\hbar^2/Ma \approx 50 \text{ MeV}$) as compared to the absolute value of the strength of the NN -potential¹ $|v_0| = 100 \text{ MeV}$

The corresponding ground state $|HF\rangle = \Pi_i a_i^\dagger |0\rangle$ describes a step function in the probability of the occupied ($\epsilon_i \leq \epsilon_F$) and empty ($\epsilon_k > \epsilon_F$) states, displaying a sharp discontinuity at the Fermi energy and thus $Z_\omega = 1$. Pushing the system it reacts with an inertia AM , sum of the nucleon masses (App. 2.C). Setting it into rotation, assuming the density $\rho(r) = \sum_i |\langle \mathbf{r}|i\rangle|^2 (|i\rangle = a_i^\dagger |0\rangle)$ to be spatially deformed, it responds with the rigid moment of inertia. This is because the single-particle orbitals are solidly anchored to the mean field (Fig. 3.3.3).

Pairing acting on nucleons moving in time reversal states $\nu, \bar{\nu}$ ($\nu \equiv (nlj)$), in configurations of the type $((l)_{L=0}^2, (s)_{S=0}^2)$, and lying close to the Fermi energy $\epsilon_F (\approx 36 \text{ MeV})$, alter this picture in a conspicuous way². Within an energy range of the order of the absolute value of the pair correlation energy³ $|E_{corr}| (\approx 3 \text{ MeV})$

¹The corresponding ratio $q = \left(\frac{\hbar^2}{Ma^2}\right) \frac{1}{|v_0|}$ is known as the quantality parameter and was first used in connection with the study of condensed matter (de Boer (1948, 1957); de Boer and Lundbeck (1948); Nosanow (1976)). It was introduced in nuclear physics in Mottelson (1998) where its value $q = 0.5$ testifies to the validity of independent particle motion. It is f notice that questions like the one posed in connection with localization and long mean free path were already discussed by Lindemann (1910) in connection with the study of the stability or less of crystals. The generalization to aperiodic crystals, like e.g. proteins (Schrödinger (1944)) was carried out in Stillinger and Stillinger (1990). Its possible application to the atomic nucleus is discussed in App. 3.C

²Bohr et al. (1958); for a recent compilation of ongoing research in the field see Broglia and Zelevinsky (2013).

³In BCS, $E_{corr} \approx -\frac{N(0)}{2} \Delta^2$, where $N(0) = \frac{g}{2}$ is the density of states at the Fermi energy and for one spin orientation, $g_i = i/16 \text{ MeV}^{-1}$ ($i = N, Z$) being the result of an empirical estimate which

centered around ϵ_F ($|E_{corr}|/\epsilon_F \ll 1$), the role of independent particles is taken over by independent pairs of nucleons, correlated distances $\xi \approx \hbar v_F/(\pi\Delta)$ (≈ 17 fm; $\Delta = 1.1$ MeV), which flicker in and out of the corresponding $L = 0, S = 0$ configuration (Cooper pairs^{4,5}).

For intrinsic⁶ nuclear excitation energies and rotational frequencies⁷ sensibly smaller than $|E_{corr}/2|$ and $\hbar\omega_{rot} \approx 0.5$ MeV respectively, the system can be described in terms of independent pair motion. This is a consequence of the fact that the kinetic energy of (Cooper) pair confinement ($\hbar^2/(2M\xi^2) \approx 10^{-2}$ MeV), is much smaller than the absolute value of the pair binding energy $|E_{corr}|$, implying that each pair behaves as an entity⁸ of mass $2M$ and spin $S = 0$. Cooper pairs respect Bose–Einstein statistics, the single-particle orbits on which they correlate become dynamically detached from the mean field, leading to a bosonic-like condensate. It is however very different from a standard condensate of real bosons, as will be extensively discussed below. Within this context see e.g. Figs. 3.3.4 and 3.3.5.

In any case, this quasi boson condensate has a number of consequences. In particular, the moment of inertia \mathcal{J} of quadrupole rotational bands of superfluid nuclei with open shells of both protons and neutrons is found to be smaller than the rigid moment of inertia by a factor of 2. The observed values, however, are a factor of 5 larger than the irrotational moment of inertia⁹, testifying to a subtle interplay between pairing and shell effects.

Cooper pairs exist also in situations in which the environmental conditions are above critical. For example, in metals at room temperature, in closed shell nuclei as well as in deformed open shell ones at high values of the angular momentum. However, in such circumstances, they break essentially as soon as they are generated (pairing vibrations). While these pair addition and subtraction fluctuations have little effect in condensed matter systems with the exception than at¹⁰

takes surface effects into account (Bohr and Mottelson (1975); Bortignon et al. (1998)), while Δ is the pairing gap. For a typical superfluid, quadrupole deformed nucleus like ^{170}Yb , $N(0) = 5.3$ MeV⁻¹, $\Delta \approx 1.1$ MeV and $E_{corr} = -3.2$ MeV (Shimizu et al. (1989)).

⁴Cooper (1956).

⁵Brink and Broglia (2005).

⁶As opposed to collective excitations, excitations which do not alter the temperature of the system.

⁷Coriolis force acts oppositely on each member of a Cooper pair. When the difference in rotational energy between superfluid and normal rotation becomes about equal to the correlation energy, the nucleon moving opposite to the collective rotation becomes so much retarded in its revolution period with respect to the partner nucleon, that eventually it cannot correlate any more with it and “align” its motion (and spin) with the rotational motion, becoming again a pair of fermions and not participating any more in the condensate. This happens for a (critical) angular momentum $I_c \approx (120 \times |E_{corr}|)^{1/2} \approx 20\hbar$, corresponding to a rotational frequency $\hbar\omega_c \approx 0.5$ MeV (see Bohr and Mottelson (1975), Brink and Broglia (2005), Broglia and Zelevinsky (2013) and references therein).

⁸The ratio $q_\xi = \frac{\hbar^2}{2M\xi^2} \frac{1}{|E_{corr}|} \approx 0.02$ provides a generalized quantality parameter. It testifies to the stability of nuclear Cooper pairs in superfluid nuclei.

⁹Bohr and Mottelson (1975); Belyaev (1959, 2013).

¹⁰See Schmidt (1968), Schmid (1969) Abrahams and Woo (1968); concerning superfluid ^3He see Wölfe (1978).

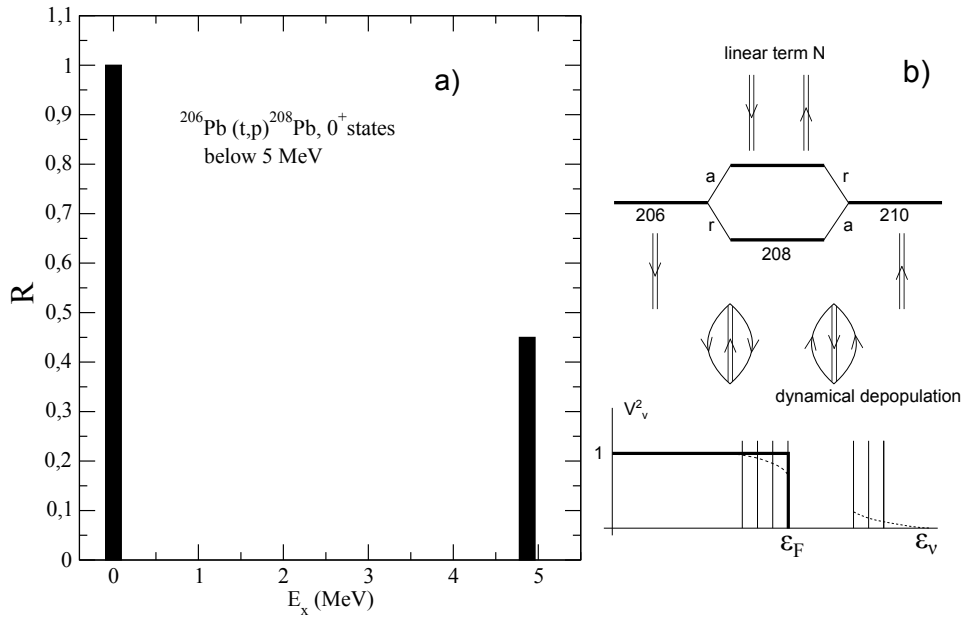


Figure 3.1.1: (a) Ratio of the absolute $L = 0$ differential cross sections $d\sigma(E_x, \theta = 59^\circ)/d\sigma(gs, \theta = 59^\circ)$ ($= (0.05 \text{ mb/sr})/(0.12 \text{ mb/sr})$) below 5 MeV for the reaction $^{206}\text{Pb}(t, p)^{208}\text{Pb}$ at the second maximum ($\theta = 59^\circ$; Bjerregaard et al. (1966)). It is of notice the large experimental errors of the corresponding angular distributions associated with the poor statistics of the cross section at the first maximum $\theta = 5^\circ$. This is the reason why the maximum at 59° was preferred to report the ratio of the cross sections. (b) Schematic representation of the pairing vibrational spectrum around ^{208}Pb . Also shown is a cartoon representation of the softening of the sharp mean field Fermi surface due to the ZPF of the pairing vibrational modes. The label a and r indicate the pair addition and pair removal modes. It is to be noted that a linear term in N has been added to the binding energy to make the binding energy values associated with ^{206}Pb ($N = 124$) and ^{210}Pb ($N = 128$), equal, in an attempt to emphasize a harmonic picture for the two-phonon state. Concerning the anharmonicities of the modes cf. last paragraph Sect. 3.5.

$T \approx T_c$, (critical normal–superconducting temperature) they play an important role in normal (non–superfluid) nuclei. In particular in nuclei around closed shells (Fig. 3.1.1), and specially in the case of light, highly polarizable, exotic halo nuclei¹¹. From this vantage point one can posit that it is not so much, or, at least not only, the superfluid phase which is abnormal in the nuclear case, but the normal state around closed shell systems¹². In particular in connection with the self–energy of nucleons moving around closed shells¹³. It is of notice nonetheless, the role pairing vibrations play in the transition between superfluid and normal nuclear phases (cf. Fig. 3.1.2) as a function of the rotational frequency (angular momentum) as emerged from the experimental studies of high spin states carried out by, among others, Garrett and collaborators¹⁴.

From Fig. 3.1.2 it is seen that while the (dynamic) pairing gap associated with pairing vibrations leads to a $\approx 20\%$ increase of the static pairing gap for low rotational frequencies, it becomes the overwhelming contribution above the critical frequency¹⁵. In any case, the central role played by pairing vibrations within the present circumstances is that to restore particle–number conservation, another example after that provided by the quantality parameter and by its generalization to pair motion, of the fact that potential functionals are, as a rule, best profited by special arrangements of fermions (spontaneous symmetry breaking), while fluctuations favour symmetry¹⁶.

Within this context, there are a number of methods which allows one to go beyond BCS mean–field approximation, or of its generalization known as the Hertree–Fock–Bogolyubov approximation (HFB). Generally referred to as number projection methods¹⁷(NP), they make use of a variety of techniques (Generator Coordinate Method, Pfaffians, etc.) as well as protocols (variation after projection, gradient method, etc.). The advantages of NP methods over the RPA is to lead to smooth functions for both the correlation energy and the pairing gap at the pairing phase transition between normal and superfluid phases. That is, between the pairing vibrational and pairing rotational schemes¹⁸.

In Fig. 3.1.3 we display the excitation function associated with the reaction $^{122}\text{Sn}(p,t)^{120}\text{Sn}(J^\pi)$, populating the low–energy states of the single open shell neutron superfluid nucleus ^{120}Sn . The angle selected to report the value of the absolute

¹¹See Sects. 3.5 and 3.6; Bohr and Mottelson (1975) , Bès and Broglia (1966), Högaasen–Feldman (1961), Schmidt (1972), Schmidt (1968), Barranco et al. (2001), Potel et al. (2013a), Potel et al. (2014).

¹²See Potel et al. (2013a) and refs. therein. Also Potel et al. (2013b) in connection with the closed shell system ^{132}Sn .

¹³See e.g. Bès and Broglia (1971a); Flynn et al. (1971).

¹⁴Garrett (1985); Garrett et al. (1986), see also Shimizu et al. (1989), Barranco et al. (1987) and Ch. 6 of Brink and Broglia (2005).

¹⁵Shimizu et al. (1989), Shimizu and Broglia (1990), Shimizu (2013), Dönau et al. (1999) Shimizu et al. (2000).

¹⁶Anderson and Stein (1984); Anderson (1976).

¹⁷cf. Ring and Schuck (1980), Egido (2013), Robledo and Bertsch (2013); cf. also Frauendorf (2013), Ring (2013), Heenen et al. (2013), and references therein.

¹⁸See Bès and Broglia (1966), Bohr and Mottelson (1975) and references therein.

differential cross sections, that is 5° , corresponds to the first, and largest, peak of the absolute $L = 0$ differential two-nucleon transfer cross section. Essentially all the strength in the $L = 0$ channel is concentrated in the ground state, the strongest 0^+ -excited state carrying a cross section of the order of 3% of that of the ground state. Within this context, the difference with the results displayed in Fig. 3.1.1 is apparent.

In the inset to Fig. 3.1.3 a quantity closely related to the Sn-isotopes binding energy is displayed (bold face levels). Namely $B(^{50+N}\text{Sn}_N)$ -8.124 N MeV+46.33 MeV, obtained by subtracting the contribution of the single nucleon addition to the nuclear binding energy. The linear function in N was obtained by a linear fitting of the binding energies of all the Sn-isotopes. Also displayed is the parabolic fit to these energies, a quantity to be compared with $E_N = (\hbar^2/2I)(N - N_0)^2$, namely the energy associated with the members of the pairing rotational band. The difference with the spectrum of pair addition and subtraction modes displayed in Fig. 3.1.1 b) is again evident.

A simple estimate of the pairing rotational band moment of inertia is provided by the single j -shell model¹⁹, namely $(\hbar^2/2I)=G/4 \approx 25/(4N_0)$ MeV. This estimate turns out to be rather accurate. Certainly better than one can expect. On the other hand, one is reminded of the fact that we are discussing properties which specifically characterize a coherent state²⁰, namely $|BCS\rangle$.

Also reported in the inset of Fig. 3.1.3 are the integrated values of the measured absolute two-neutron transfer cross sections, quantities which are reproduced by the theoretical predictions within experimental errors (Fig. 3.1.6). In principle, one could have expected a sensible constancy of these cross sections (transitions) as the pairing rotational model implies a common intrinsic deformed state in gauge space, namely $|BCS\rangle$ (see Sect. 3.4.2). On the other hand, the number of Cooper pairs α'_0 which defines deformation in gauge space is rather small (≈ 6) and thus subject to conspicuous fluctuations ($\Delta\alpha'_0/\alpha'_0 \approx \sqrt{6}/6 \approx 0.4$). Fluctuations which also affect the two particle transfer absolute cross sections (because $\sigma \sim \alpha'^2_0$, one can expect fluctuations in σ of the order of 100%).

In keeping with the analogy discussed in Figs. 3.3.3 and 3.4.1 between pairing and quadrupole rotational bands, we note that in the electromagnetic decay of these last bands one expects, in the case of heavy nuclei, fluctuations of the order of $(\sqrt{250}/250)^2$, i.e. less than 1%. Within this context, the average value of the absolute experimental cross sections displayed in the inset of Fig. 3.1.3 is 1762 μb , while the average difference between experimental and predicted values is 94 μb (see Fig. 3.1.6)²¹. Thus, the discrepancies between theory and experiment are bound in the interval $0 \leq |1 - \sigma_{th}(i \rightarrow f)/\sigma_{exp}(i \rightarrow f)| \leq 0.09$, the average discrepancy being 5%.

In Fig. 3.1.4 the excited pairing rotational bands based on 0^+ pairing vibra-

¹⁹See e.g. Brink and Broglia (2005) App. H and refs. therein.

²⁰See App. 4.E and Sect. 7.4; see also Potel et al. (2017).

²¹Potel et al. (2013b).

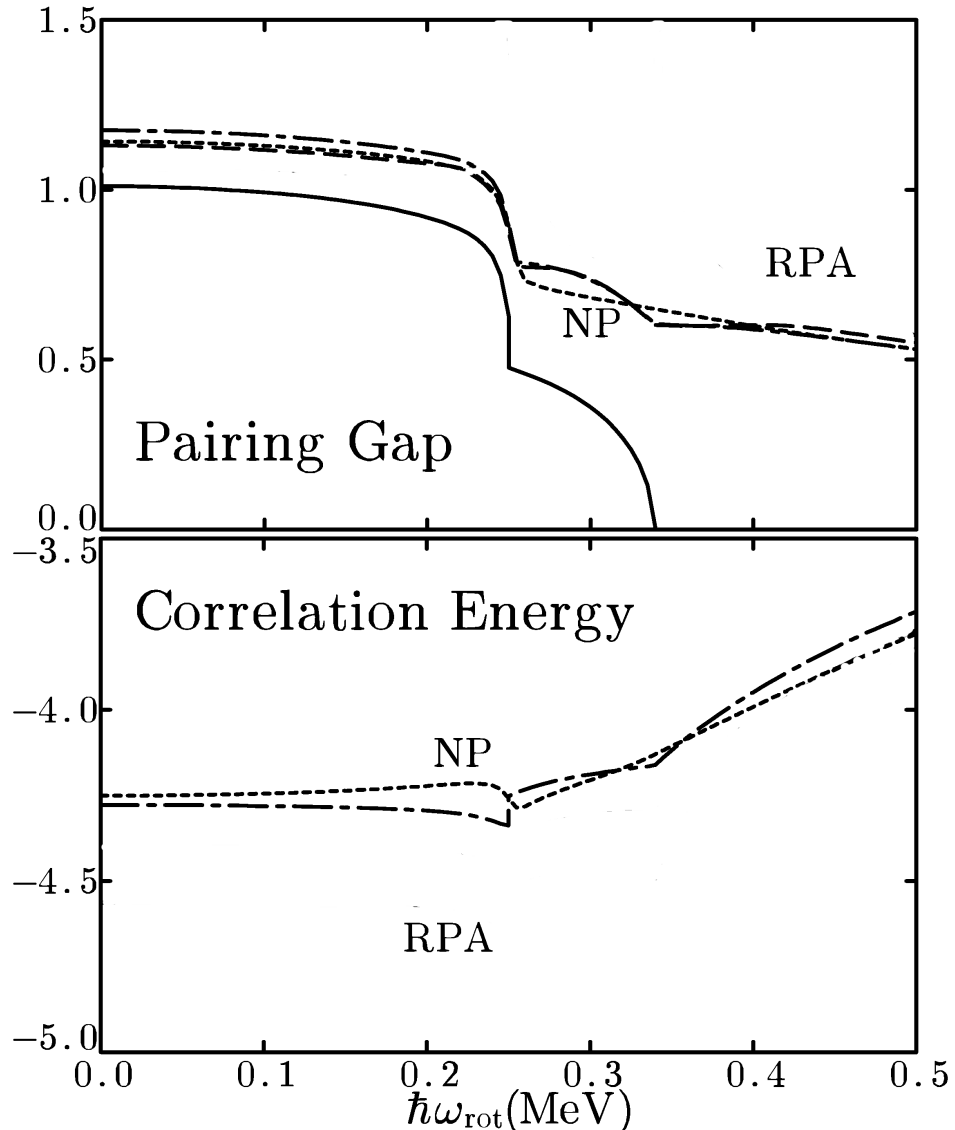


Figure 3.1.2: Pairing gap calculated taking into account the correlation associated with pair vibrations in the RPA approximation ($\Delta = (\Delta_{BCS}^2 + \frac{1}{2}G^2 S_0(RPA))^1/2$) (upper panel) and RPA correlation energy (lower panel) for neutrons in ^{164}Er as a function of the rotational frequency (Brink and Broglia (2005), Sect. 6.6). Both quantities are in MeV (dashed-dotted curves). The value of the static (mean-field) pairing gap Δ , which vanishes at $\hbar\omega_{rot} = 0.34$ MeV, is also displayed in the upper panel (continuous curve). The results of the number-projection (NP) calculations are shown as dotted curves. $S_0(RPA) = \sum_{n \neq AGN} [< n|P|0 > + < n|P^\dagger|0 >]_{RPA}^2$, $P^\dagger = \sum_{\nu>0} a_\nu^\dagger a_\nu^\dagger$ and where $\Delta_{BCS} = G < BCS | P^\dagger | BCS >$ is the standard, static BCS pairing gap, while G is the pairing force strength. The non-energy weighted sum rule $S_0(RPA)$ describes the contribution of pairing fluctuations to the effective (RPA) gap, and is intimately associated with projection in particle number. It is of notice that $\sum_{n \neq AGN}$ means that the divergent contribution from the zero energy mode (Anderson, Goldstone, Nambu mode, see e.g. Broglia et al. (2000) and references therein), associated with the lowest ($\hbar\omega_0$) solution of the $H = H_p + H''_p$ is to be excluded (see Sect 4.8.1, discussion before Eq. (4.8.26) as well as Brink and Broglia (2005) App. J). After Shimizu and Broglia (1990).

tional modes are displayed as a single band, and are associated with the average value of the 0^+ excited states with energy ≤ 3 MeV. The best parabolic fit is shown. Also given are the relative (p, t) absolute integrated cross sections normalized to the corresponding values of the ground state rotational band. The cross talk between bands is in all cases $\leq 8\%$, the single j -shell value estimate being²² 6%.

The above results underscore the fact that, at the basis of an operative coarse grained approximation to the nuclear many-body problem (within this context cf. App. 2.C, in particular the discussion following Eq. (2.C.5)), one finds a judicious choice of the collective coordinates²³. In other words, pairing vibrations are elementary modes of excitation containing the right physics to restore gauge invariance through their interweaving with quasiparticle states. Within the framework of the above picture, one can introduce at profit a collective coordinate α_0 (order parameter; see Sect. 7.4.1) which measures the number of Cooper pairs participating in the pairing condensate, and define a wavefunction for each pair $(U'_v + V'_v a'_v a'_{\bar{v}}^\dagger) |0\rangle$ (independent pair motion, BCS approximation, see Figs. 3.4.1, 3.4.2 and 3.4.3), adjusting the occupation parameters V_v and U_v (probability amplitudes that the two-fold, Kramer's-degenerate pair state (v, \bar{v}) , is either occupied or empty), so as to minimize the energy of the system under the condition that the average number of nucleons is equal to N_0 (the Coriolis-like force felt, in the intrinsic system in gauge space by the Cooper pairs, being equal to $-\lambda N_0$). Thus, $|BCS\rangle = \prod_{v>0} (U'_v + V'_v a'_v a'_{\bar{v}}^\dagger) |0\rangle$ provides a valid description of the independent pair mean field ground state, and of the associated order parameter $\alpha'_0 = \langle BCS | P'^\dagger | BCS \rangle = \sum_{v>0} U'_v V'_v$, $P'^\dagger = \sum_{v>0} a'_v a'_{\bar{v}}^\dagger$ being the pair creation operator²⁴. It is then natural to posit that two-particle transfer reactions are specific to probe pairing correlations in many-body fermionic systems. Examples are provided by the Josephson effect²⁵ between e.g. metallic superconductors, and (t, p) and (p, t) reactions in atomic nuclei²⁶.

Within this context we now take the basic consequence of pairing condensation in nuclei regarding reaction mechanisms. For this purpose let us consider a *gedanken experiment* in which the superfluid target and the projectile can at best come in such weak contact that only single-nucleon transfer leads to a yield falling within the sensitivity range of the measuring setup. Because $(\hbar^2 / 2M\xi^2) / |E_{corr}| \approx 10^{-2}$, Cooper pairs in superfluid nuclei behave as particles of mass $2M$ over distances ξ , even in the case in which the NN -potential vanishes in the zone between the weakly overlapping densities of the two interacting nuclei. One then expects Cooper pair transfer to be observed. Not only. One also expects that the associated

²²Brink and Broglia (2005) App. H.

²³In this connection, we quote allegedly from S. Weinberg: "In solving a problem you may choose to use the degrees of freedom you like. But if you choose the wrong ones you will be sorry".

²⁴cf. Bardeen et al. (1957a), Bardeen et al. (1957b), Schrieffer (1964), Schrieffer (1973) and references therein.

²⁵Josephson (1962).

²⁶cf. e.g. Yoshida (1962), Broglia et al. (1973), Bayman (1971), Glendenning (1965), Bohr (1964), Hansen (2013) and Potel et al. (2013a) and references therein.

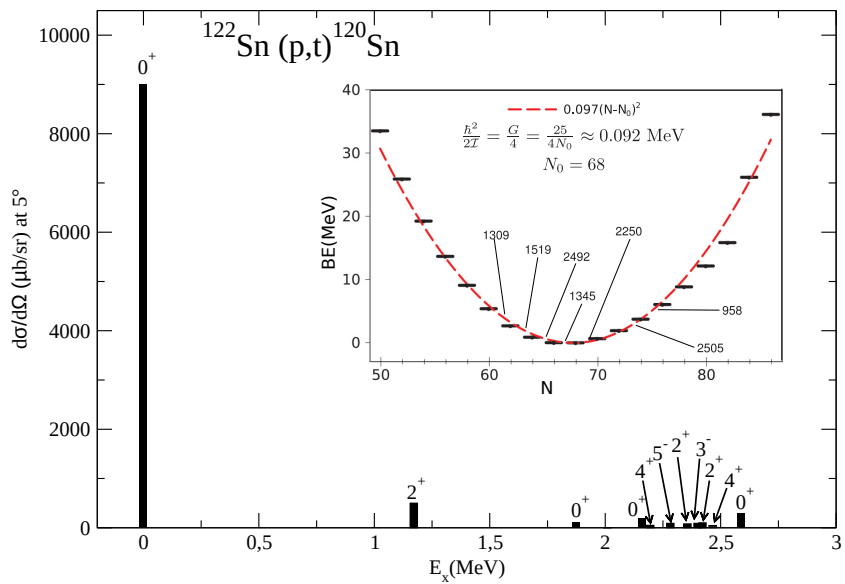


Figure 3.1.3: Excitation function associated with the reaction $^{122}\text{Sn}(p, t)^{120}\text{Sn}(J^\pi)$. The absolute experimental values of $d\sigma(J^\pi)/d\Omega|_{5^\circ}$ are given as a function of the excitation energy E_x (after Guazzoni et al. (2011)). In the inset the full neutron pairing rotational band between magic numbers $N = 50$ and $N = 82$ is also displayed, the absolute $^{A+2}\text{Sn}(p, t)^A\text{Sn}$ experimental cross sections are reported in the abscissa (Guazzoni et al. (1999), Guazzoni et al. (2004), Guazzoni et al. (2006), Guazzoni et al. (2008), Guazzoni et al. (2011), Guazzoni et al. (2012); see also Potel et al. (2011), Potel et al. (2013b)).

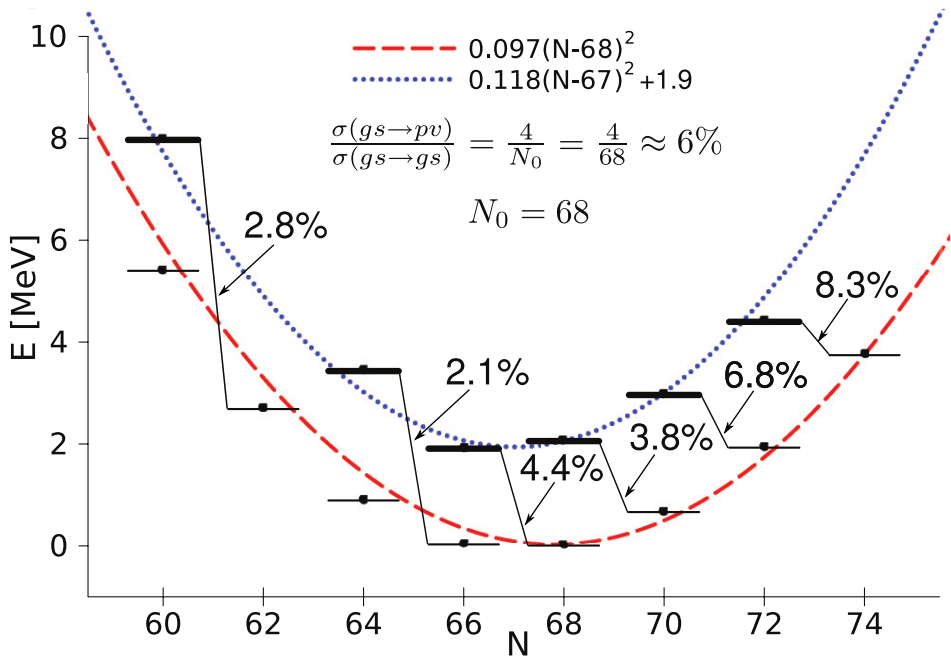


Figure 3.1.4: The weighted average energies ($E_{exc} = \sum_i E_i \sigma_i / \sum_i \sigma_i$) of the excited 0^+ states below 3 MeV in the Sn isotopic chain are shown on top of the pairing rotational band, already displayed in Fig. 3.1.3. Also indicated is the percentage of cross section for two-neutron transfer to excited states, normalized to the cross sections populating the ground states (after Potel et al. (2013b)). The estimate of the ratio of cross sections displayed on top of the figure was obtained making use of the single j -shell model (see Eq. (4.2.3); see also Brink and Broglia (2005) and references therein).

absolute differential cross section contains, for the particular choice of mass number made and within the framework of the theory of quantum measurement, all the information needed to work out a comprehensive description of nuclear superfluidity.

Because $\alpha_0 \sim N(0)$, cross sections associated with the transfer of Cooper pairs between members of a pairing rotational band, are proportional to the density of single-particle levels quantity squared. As a consequence, absolute two-nucleon transfer cross sections are expected to be of the same order of magnitude than one-nucleon transfer ones, and to be dominated by successive transfer (see Sects. 4.2 and 4.4). These expectations have been confirmed experimentally and by detailed numerical calculations, respectively. The above parlance, being at the basis of the Josephson effect, reflects both one of the most solidly established results in the study of BCS pairing, and explains the workings of a paradigmatic probe of spontaneous symmetry breaking phenomena.

Due to the fact that, away from the Fermi energy pair motion becomes independent particle motion (see Sect. 3.4), one-particle transfer reactions like e.g. (d, p) and (p, d) can be used together with (t, p) and (p, t) processes, as valid tools to cross check pair correlation predictions (see Chapter 5). In particular, to shed light on the origin of pairing in nuclei: in a nutshell, the relative importance of the bare NN -interaction and the induced pairing interaction (within this context see Sect. 3.6 and Fig. 2.10.1).

While the calculation of two-nucleon transfer spectroscopic amplitudes and differential cross sections are, *a priori*, more involved to be worked out than those associated with one-nucleon transfer reactions, the former are, as a rule, more “intrinsically” accurate than the latter ones. This is because, in the case of two nucleon transfer reactions, the quantity (order parameter α'_0) which expresses the collectivity of the members of a pairing rotational band, reflects the properties of a coherent state ($|BCS\rangle$). In other words, it results from the sum over many contributions ($\sqrt{j_\nu + 1/2} U'_\nu V'_\nu$, see Sect. 3.4, also Sect. 7.4.1), all of them having the same phase. Consequently, the relative error decreases as the square root of the number contributions ($\approx N(0)\Delta \approx 4 \text{ MeV}^{-1} \times 1.4 \text{ MeV} \approx 6$ in the case of the superfluid nucleus ^{120}Sn).

There is a further reason which confers $\alpha'_0 = \sum_j (j + 1/2) U'_j V'_j$ a privileged position with respect to the single contributions $(j + 1/2) U'_j V'_j$. It is the fact that $\alpha'_0 = e^{2i\phi} \sum_j (j + 1/2) U_j V_j = e^{2i\phi} \alpha_0$ defines a privileged orientation in gauge space, α_0 being the order parameter referred to the laboratory system which makes an angle ϕ in gauge space with respect to the intrinsic system to which α'_0 is referred²⁷. In other words, the quantities α'_0 which measure the deformation of the superfluid nuclear system in gauge space, and the rotational frequency $\lambda = \hbar\dot{\phi}$ in this space, and associated Coriolis force $-\lambda N_0$ felt by the nucleons referred to the body fixed frame, are the result of solving selfconsistently the BCS number $N_0 = \sum_{jm} V_j^2 = \sum_j ((2j + 1)/2)(1 + ((\epsilon_j - \lambda)/\Delta)^2)^{-1}$ and gap equation $\frac{1}{G} \sum_{jm>0} \frac{1}{2E_j} = \frac{1}{\Delta'} \sum_j ((2j +$

²⁷See Sect. 3.4.2, see Potel et al. (2013b).

$1)/2)U_j'V_j = \alpha'_0/\Delta'$ that is $\alpha'_0 = \Delta'/G$, and $\alpha'_0 = \sum_j(j + 1/2)U_j'V_j'$ making use as inputs ϵ_ν and N_0 , that is single-particle energies and the average number of particles.

Similar arguments can be used regarding the excitation of pairing vibrations in terms of Cooper pair transfer from closed shells as compared to one-particle transfer. As seen from Fig. 3.1.5 (b)–(c), the random phase approximation (RPA) amplitudes X_ν^a and Y_ν^a sum coherently over pairs of time reversal states²⁸ to give rise to the spectroscopic amplitudes associated with the direct excitation of the pair addition mode displayed in (d). Because of the (dispersion) relation (b)+(c) \equiv (d), the X_ν - and Y_ν -amplitudes are correlated, among themselves as well as in phase. As seen from (g) and (h), the situation is quite different in the case of one-particle transfer. The soundness of the above parlance reflects itself in the calculation of the elements resulting from the encounter of structure and reaction, namely one- and two-nucleon modified transfer formfactors. While it is usually considered that these quantities carry all the structure information associated with the calculation of the corresponding cross sections, a consistent NFT treatment of structure and reaction will posit that equally much is contained in the distorted waves describing the relative motion of the colliding systems. This is because the state dependent components of the optical potential which determines the scattering waves, emerges from the same elements used in the calculation of the structure properties²⁹. In other words, to describe a two-nucleon transfer reaction like $A+t \rightarrow B(=A+2)+p$, one needs to know what the single-particle states and collective modes of the system $F(=A+1)$ are, equally well than those of nuclei A and B . In principle, also the deuteron wavefunction as one knows the triton wavefunction (see Chapter 4 Sect. 4.2, see also Chapter 6, Section 6.1). Furthermore one needs to take into account the interweaving of different modes and degrees of freedom resulting in dressed particle states (quasiparticles; fermions) and renormalized normal vibrational modes of excitation (bosons). And these are also, essentially, all the elements needed to calculate the processes leading to the depopulation of e.g. the flux in the incoming channel ($A+t$ in the case under discussion). In particular, and assuming to work with spherical nuclei, one-particle transfer is, as a rule, the main depopulation process³⁰. This is a consequence of the long range tail of the associated formfactors as compared to that of other processes, e.g. inelastic processes (see e.g. Fig. 4.6.5).

In keeping with this fact, and because U and W are connected by the Kramers–Krönig generalized dispersion relation³¹, it is possible to calculate the polarization contribution to the nuclear dielectric function (optical potential) associated

²⁸Brink and Broglia (2005) Ch. 5.

²⁹See Sect. 4.6; cf also Broglia et al. (1981), Pollarolo et al. (1983), Broglia and Winther (2004), Fernández-García et al. (2010a), Fernández-García et al. (2010b), Dickhoff and Van Neck (2005), Jenning (2011), Montanari et al. (2014) Barbieri and Jennings (2005); Dickhoff et al. (2017); Rourreau et al. (2017).

³⁰Again, one is referring to doorway states processes (Feshbach (1958)).

³¹See e.g. Mahaux et al. (1985) and references therein.

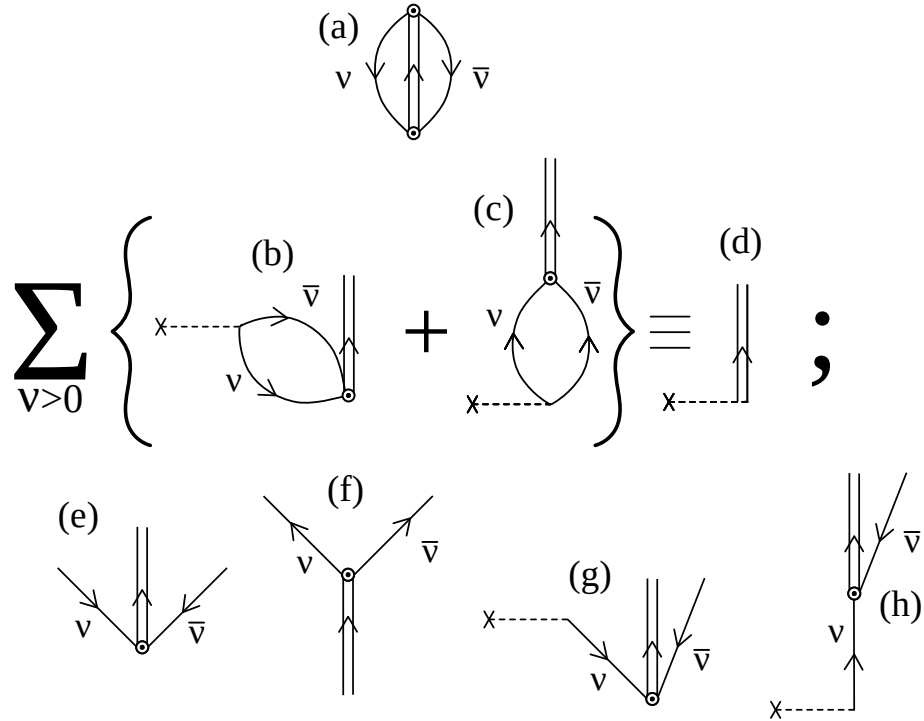


Figure 3.1.5: NFT diagrams associated with one- and two-particle transfer from closed shell. (a) ZPF associated with the virtual excitation of a pair addition mode and two uncorrelated holes. (b) two-particle transfer filling the holes, (c) diagram obtained from the previous one by time ordering. These processes receive contribution from all (v, \bar{v}) pairs (sum over $v > 0$), leading to (d), the direct excitation of the pair addition mode. The relation $(b)+(c)\equiv(d)$ is the NFT graphical representation of the random phase approximation (RPA) dispersion relation used to calculate the properties of the pair addition mode in the harmonic approximation (Section 3.5). The backwards and forwards going RPA amplitudes are displayed in Figs. (e) and (f) respectively. (g) One-particle stripping proceeding through the filling of a hole associated with the ZPF, (h) processes obtained from the previous by time ordering.

with the elastic channels under discussion (i.e. (A, t) , $(F(= A + 1), d)$ and $(B(= A + 2), p)$ in the present case) by first calculating W –which only involves on-shell contributions– making use of the above described elements, and from its knowledge work out U .

We conclude this section by remarking that, in spite of the fact that one is dealing with the connection between structure and direct transfer reactions, no mention has been made of spectroscopic factors in relation with one-particle transfer processes, let alone when discussing two-particle transfer.

Within the above context, we provide below two examples of B -coefficients

associated with coherent states. Namely, one for the case in which A and $B(= A+2)$ are members of a pairing rotational band. A second one, in the case in which they are members of a pairing vibrational band. That is,

$$\begin{aligned} \mathbf{1}), B(nlj, nlj; 000) &= \langle BCS(N+2) | \frac{[a_{nlj}^\dagger a_{nlj}^\dagger]_0^0}{\sqrt{2}} | BCS(N) \rangle \\ &= \sqrt{j+1/2} U_{nlj}(N) V_{nlj}(N+2), \end{aligned} \quad (3.1.1)$$

and

$$\begin{aligned} \mathbf{2}), B(nlj, nlj; 000) &= \langle (N_0 + 2)(gs) | \frac{[a_{nlj}^\dagger a_{nlj}^\dagger]_0^0}{\sqrt{2}} | N_0(gs) \rangle \\ &= \begin{cases} \sqrt{j_k + 1/2} X^a(n_k l_k j_k) & (\epsilon_{j_k} > \epsilon_F) \\ \sqrt{j_k + 1/2} Y^a(n_i l_i j_i) & (\epsilon_{j_k} \leq \epsilon_F). \end{cases} \end{aligned} \quad (3.1.2)$$

Where the X and Y coefficients are the forwardgoing and backwardsgoing RPA amplitudes of the pair addition mode³². For actual numerical values see Sect. 3.4, Table 3.4.1 and Sect. 3.5 Tables 3.5.2–3.5.5. Making use of these spectroscopic amplitudes and treating explicitly the intermediate deuteron channel in terms of successive transfer, correcting both this and the simultaneous transfer channels for non-orthogonality contributions, makes the above picture the quantitative probe of Cooper pair correlations in nuclei³³ (Fig. 3.1.6).

Summing up, one will use throughout the present monograph, exception made when explicitly mentioned, absolute cross sections as the solely link between spectroscopic amplitudes and experimental observations.

3.2 Renormalization and spectroscopic amplitudes

Elementary modes of nuclear excitation, namely single-particle motion, vibrations and rotations, being tailored to economically describe the nuclear response to external probes, contain a large fraction of the many-body correlations. Consequently, their wavefunctions are non-orthogonal to each other, in keeping with the fact that all the degrees of freedom of the nucleus are exhausted by those of the nucleons (see Chapter 2). The corresponding overlaps give a measure of the strength with which the different modes couple to each other. The resulting particle-vibration coupling Hamiltonian can be diagonalized, making use of Nuclear Field Theory³⁴, and of the BRST techniques³⁵ in the case of particle-rotor coupling.

³²Brink and Broglia (2005).

³³Bayman and Chen (1982) and Potel et al. (2013a).

³⁴NFT, cf. Bortignon et al. (1977), Bortignon et al. (1978).

³⁵cf. Bès and Kurchan (1990) and refs. therein.

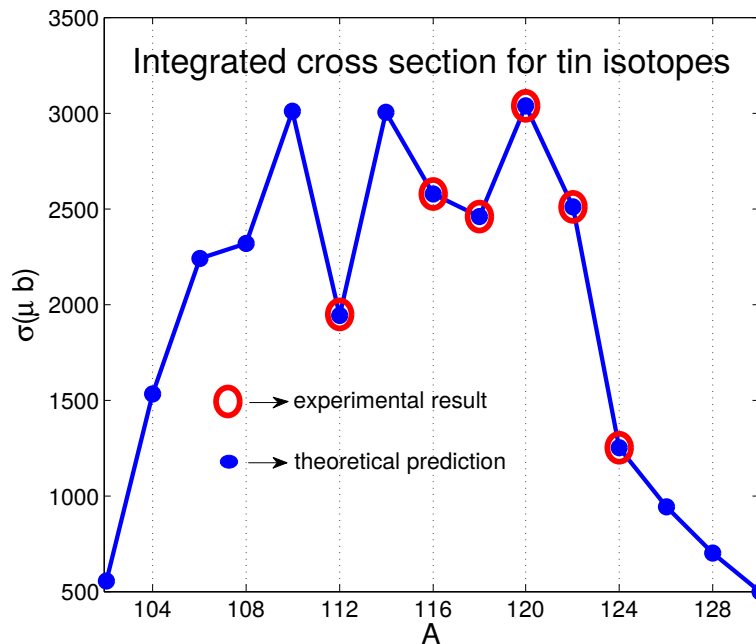


Figure 3.1.6: Absolute value of the two-nucleon transfer cross section $^{A+2}\text{Sn}(p, t)^A\text{Sn}(\text{gs})$ ($A = 112, 116, 118, 120, 122, 124$ cf. Potel et al. (2013a) Potel et al. (2013b)) calculated taking into account successive and simultaneous transfer in second order DWBA, properly corrected for non-orthogonality contributions in comparison with the experimental data (Guazzoni et al. (1999), Guazzoni et al. (2004), Guazzoni et al. (2006), Guazzoni et al. (2008), Guazzoni et al. (2011), Guazzoni et al. (2012)).

As a result of the interweaving of single-particle and collective motion, the nucleons acquire a state dependent self energy³⁶ $\Delta E_j(\omega)$. Consequently, the single-particle potential which was already non-local in space (exchange potential, related to the Pauli principle) becomes also non-local in time (retardation effects; cf. e.g. Fig 3.6.3 (I)). There are a number of techniques to make it local. In particular the Local Density Approximation (LDA) and the effective mass approximation. In this last case one can describe the single-particle motion in terms of a local (complex) potential with a real part given by $U'(r) = (m/m^*)U(r)$, where $m^* = m_k m_\omega / m$ is the effective nucleon mass, m_k being the so-called k -mass (non-locality in space in keeping with the fact that $\Delta x \Delta k_x \geq 1$), and $m_\omega = m(1 + \lambda)$ being the ω -mass (non-locality in time, as implied by the relation $\Delta \omega \Delta t \geq 1$), $\lambda = -\partial \Delta E(\omega) / \partial \hbar \omega$ being the so-called mass enhancement factor. It reflects the ability with which vibrations cloth single-particles. In other words, it measures the probability with which a nucleon moving at $t = -\infty$ in a “pure” orbital j can be found at a later time in a $2p - 1h$ like (doorway state) $|j'L; j\rangle$, L being the multipolarity of a vibrational state. Within this context, the discontinuity taking place at the Fermi energy in the dressed particle picture ($Z_\omega = (m/m_\omega)$) is connected with the single-particle occupancy probability³⁷.

It is of notice that dressed particles automatically imply an induced pairing interaction (see e.g. Figs. 3.6.3 (I) and (II)) resulting from the exchange of the clothing vibrations between pairs of nucleons moving in time reversal states close to the Fermi energy (see e.g. Fig. 4.A.3; also Fig. 7.G.1 (b),(d),(e)). In other words, fluctuations in the normal density $\delta\rho$ and the associated δU (Time-Dependent HF) and particle-vibration coupling vertices lead to abnormal (superfluid) density (deformation in gauge space). Whether this is a dynamic or static effect, depends on whether the parameter (cf. Fig. 3.5.7)³⁸

$$x' = G'N'(0), \quad (3.2.1)$$

product of the effective pairing strength (see footnote 110),

$$G' = Z_\omega^2(v_p^{bare} + v_p^{ind}), \quad (3.2.2)$$

and of the renormalized density of levels $N'(0)$ is considerable smaller (larger) than $\approx 1/2$. The quantity G' is the sum of the bare and induced pairing interaction, renormalized by the degree of single-particle content of the levels where nucleons correlate. The quantity

$$N'(0) = Z_\omega^{-1}N(0) = (1 + \lambda)N(0) \quad (3.2.3)$$

is the similarly renormalized density of levels at the Fermi energy. From the above relations one obtains

$$x' = Z_\omega(v_p^{bare} + v_p^{ind})N(0). \quad (3.2.4)$$

³⁶For levels far away from the Fermi energy it can be parametrized at profit by an extension to the complex-energy-plane.

³⁷See e.g. Brink and Broglia (2005) Ch. 9.

³⁸Brink and Broglia (2005) App. H. Sect. H4 and refs. therein; Barranco et al. (2005).

It is of notice that typical values of $Z_\omega \approx 0.7$, while for nuclei along the stability valley bare and induced pairing contributions are about equal which, according to Eq. (3.2.2) implies $G' \approx G = v_p^{\text{bare}}$, as in the case of a non-renormalized situation. On the other hand the physics is radically changed, particles being a consistent fraction of the time in excited states coupled to collective vibrations, pairing acquiring a state dependence.

All of the above many-body, ω -dependent effects which imply in many cases a coherent sum of amplitudes, together with the corresponding renormalizations of the single-particle radial wavefunctions (formfactors) not discussed within the present framework, are not simple to capture in a spectroscopic factor³⁹ in connection with one-particle transfer, let alone two-nucleon transfer processes⁴⁰.

3.3 Quantality Parameter

The quantality parameter⁴¹ is defined as the ratio of the quantal kinetic energy of localization (confinement) and potential energy, (cf. Fig. 3.3.1 and Table 3.3.1). Fluctuations, quantal or classical, favor symmetry: gases and liquids are homogeneous. Potential energy on the other hand prefers special arrangements: atoms like to be at specific distances and orientations from each other (spontaneous breaking of translational and of rotational symmetry reflecting the homogeneity and isotropy of empty space⁴²).

When q is small, quantal effects are small and the lower state for $T < T_c$ will have a crystalline structure, T_c denoting the critical temperature. For sufficiently large values of $q (> 0.15)$ the system will display particle delocalization and, likely, be amenable, within some approximation, to a mean field description (Figs. 3.3.2

³⁹In keeping with the fact that $m_k \approx 0.6 - 0.7m$ and that $m^* \approx m$, as testified by the satisfactory fitting standard Saxon-Woods potentials provides for the valence orbitals of nucleons of mass m around closed shells, one obtains $m_\omega \approx 1.4 - 1.7m$. Thus $Z_\omega \approx 0.6 - 0.7$. It is still an open question how much of the observed single-particle depopulation can be due to hard core effects, which shifts the associated strength to high momentum levels (see Dickhoff and Van Neck (2005), Jenning (2011), Kramer et al. (2001), Barbieri (2009), Schiffer et al. (2012), Duguet and Hagen (2012), Furnstahl and Schwenk (2010)). An estimate of such an effect of about 20% will not quantitative change the long wavelength estimate of Z_ω given above. Arguably, a much larger depopulation through hard core effects remains an open problem within the overall picture of elementary modes of nuclear excitation and of medium polarization effects. It remains an open question the role of the renormalization of the radial dependence of the single-particle wavefunctions due to many-body effects can play.

⁴⁰See Barranco et al. (2005, 1999).

⁴¹Nosanow (1976), de Boer (1957), de Boer (1948), de Boer and Lundbeck (1948), Mottelson (1998).

⁴²Within this general context the physics embodied in the quantality parameter is closely related to that which is at the basis of the classical Lindemann criterion (Lindemann (1910)) to measure whether a system is ordered (e.g. a crystal) or disordered (e.g. a melted system) (Bilgram (1987), Löwen (1994), Stillinger and Stillinger (1990); Stillinger (1995)). The above statement concerning the competition between potential energy and fluctuations, is also valid for the generalized Lindemann parameter (Stillinger and Stillinger (1990), Zhou et al. (1999)), used to provide similar insight into inhomogeneous finite systems like e.g. proteins (aperiodic crystals Schrödinger (1944), see also Ehrenfest's theorem (Basdevant and Dalibard (2005) pag. 138 see also App. 3.C).

constituents	M/M_n	$a(\text{cm})$	$v_0(\text{eV})$	q	phase($T = 0$)
${}^3\text{He}$	3	2.9(-8)	8.6(-4)	0.19	liquid ^{a)}
${}^4\text{He}$	4	2.9(-8)	8.6(-4)	0.14	liquid ^{a)}
H_2	2	3.3(-8)	32(-4)	0.06	solid ^{b)}
${}^{20}\text{Ne}$	20	3.1(-8)	31(-4)	0.007	solid ^{b)}
nucleons	1	9(-14)	100(+6)	0.4	liquid ^{a),c),d)}

Table 3.3.1: Zero temperature phase for a number of systems of mass M (M_n : nucleon mass), the first four depending on atomic interactions (range Å, strength meV), the last one referring to the atomic nucleus. a) delocalized (condensed), b) localized, c) non-Newtonian solid (cf. e.g. Bertsch (1988), De Gennes (1994)), that is, systems which react elastically to sudden solicitations and plastically under prolonged strain, d) paradigm of quantal, strongly fluctuating, finite many-body systems. Delocalization or less does not seem to depend much on whether one is dealing with fermions or bosons (Mottelson (1998) and refs. therein; cf also Ebran et al. (2014b), Ebran et al. (2014a), Ebran et al. (2013), Ebran et al. (2012)).

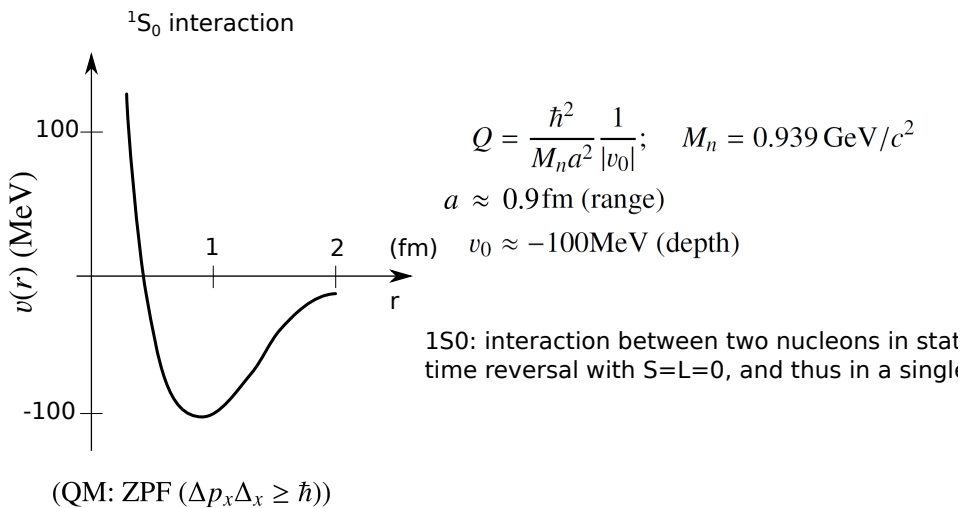


Figure 3.3.1: Schematic representation of the bare NN -interaction acting among nucleons displayed as a function of the relative coordinate $r = |\mathbf{r}_1 - \mathbf{r}_2|$, used to estimate the quantality parameter Q , ratio of the zero point fluctuations (ZPF) of confinement and the potential energy.

and 3.3.3). In fact, the step delocalization → mean field is certainly not automatic, neither guaranteed. In any case, not for all properties neither for all levels of the system. Let us elaborate on these points. Independent particle motion can be viewed as the most collective of all nuclear properties, reflecting the effect of all nucleons on a given one resulting in a macroscopic effect. Namely confinement with long mean free path as compared with nuclear dimensions. Consequently, it should be possible to calculate the mean field in an accurate manner. Arguably, as accurately as one can calculate collective vibrations, e.g. quadrupole vibrations. But this does not mean that one knows how to correctly calculate the energy and associated deformation parameter of each single state of the quadrupole response function. Within this context one may find through mean field approximation a good description for the energy of the valence orbitals of a nucleus but for specific levels (e.g. the $d_{5/2}$ level of $^{119-120}\text{Sn}$, cf. e.g. Fig 5.2.3). It is not said that including particle-vibration coupling corrections, a process which in average makes theory come closer to experiment⁴³, single specific quasiparticle energies will agree better with the data⁴⁴. Cases like this one constitute a sobering experience concerning the intricacies of the many-body problem in general, and the nuclear one (finite many-body system, FMBS) in particular where spatial quantization plays a central role. In other words, one is dealing with a self-confined, strongly interacting, finite many-body system generated from collisions originally associated with a variety of astrophysical events and thus with the coupling and interweaving of different scattering channels and resonances, a little bit as e.g. the Hoyle monopole resonance ($\alpha + \alpha + \alpha \rightarrow ^{12}\text{C}$). Within the anthropomorphic (grand design) scenario such phenomena are found in the evolution of the Universe to eventually allow for the presence of organic matter and, arguably, life on earth⁴⁵ more likely than to make mean field approximation an “exact” description of nuclear structure and reactions.

3.4 Cooper pairs

Let us assume that the motion of nucleons is described by the Hamiltonian,

$$H = \sum_{j_1 j_2} \langle j_1 | T | j_2 \rangle a_{j_1}^\dagger a_{j_2} + \frac{1}{4} \sum_{j_1 j_2 j_3 j_4} \langle j_1 j_2 | v | j_3 j_4 \rangle a_{j_2}^\dagger a_{j_1}^\dagger a_{j_3} a_{j_4},$$

written in second quantization⁴⁶. In what follows it will be schematically shown how mean field is extracted from such a Hamiltonian, both in the case of single-particle motion (HF) and of independent pair motion (BCS).

⁴³See e.g. Bohr and Mottelson (1975), Bortignon et al. (1977), Mahaux et al. (1985), Bès and Broglia (1971a); Flynn et al. (1971), Bortignon et al. (1976), Bès et al. (1988), Barranco et al. (1987), Barranco et al. (2001) and references therein.

⁴⁴cf. also Tarpanov et al. (2014).

⁴⁵cf. e.g. Rees (2000), ? and references therein.

⁴⁶cf. e.g. Brink and Broglia (2005), App. A.

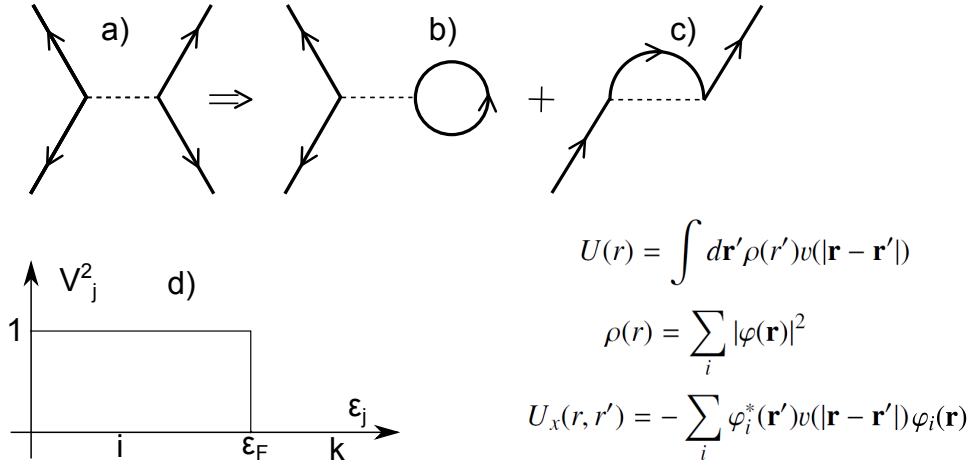


Figure 3.3.2: Schematic representation of (a) nucleon–nucleon scattering through the bare NN –interaction, (b) the associated contribution to the Hartree potential $U(r)$ and, (c) to the Fock (exchange) potential $U_x(r, r')$, $\rho(r)$ being the nucleon density. (d) the Hartree–Fock solution leads to a sharp discontinuity at the Fermi energy ϵ_F . That is, single–particle levels with energy $\epsilon_i \leq \epsilon_F$ are fully occupied. Those with $\epsilon_k \geq \epsilon_F$ empty.

3.4.1 independent-particle motion

In the previous section it was shown that the value of the quantity parameter associated with nuclei ($q \approx 0.4$) leads to particle delocalization and likely makes the system amenable to a mean field description (Fig. 3.3.2; see however the provisos expressed at the end of Sect. 3.3). In such a case, Hartree–Fock approximation is tantamount to a selfconsistent relation between density and potential, weighted by the nucleon–nucleon interaction v , and leading to a complete separation between occupied ($|i\rangle$) and empty ($|k\rangle$) single–particle states,

$$(U_\nu^2 + V_\nu^2) = 1; \quad |\varphi_\nu\rangle = \bar{a}_\nu^\dagger |0\rangle = (U_\nu + V_\nu a_\nu^\dagger) |0\rangle; \quad V_\nu^2 = \begin{cases} 1 & \epsilon_\nu \equiv \epsilon_i \leq \epsilon_F, \\ 0 & \epsilon_\nu \equiv \epsilon_k > \epsilon_F. \end{cases} \quad (3.4.1)$$

The Hartree–Fock ground state can then be written as,

$$|HF\rangle = |\det(\varphi_\nu)\rangle = \Pi_\nu \bar{a}_\nu^\dagger |0\rangle = \Pi_i a_i^\dagger |0\rangle = \Pi_{i>0} a_i^\dagger a_i^\dagger |0\rangle, \quad (3.4.2)$$

where $|\tilde{i}\rangle$ is the time reversed state to $|i\rangle$.

To be solved, the above self–consistent equations have to be given boundary conditions. In particular, make it explicit whether the system has a spherical or, for example, a quadrupole shape. That is, whether $\langle HF | Q_2 | HF \rangle$ is zero or has a finite value, $Q_{2M} = \sum_{j_1 j_2} \langle j_2 | r^2 Y_M^2 | j_1 \rangle [a_{j_1}^\dagger a_{j_2}]_M^2$ being the quadrupole operator which carries particle transfer quantum number $\beta = 0$, in keeping with its particle–hole character. In the case in which $\langle Q_{2M} \rangle = 0$, the system can display a spectrum of low–lying, large amplitude, collective quadrupole vibrations of frequency

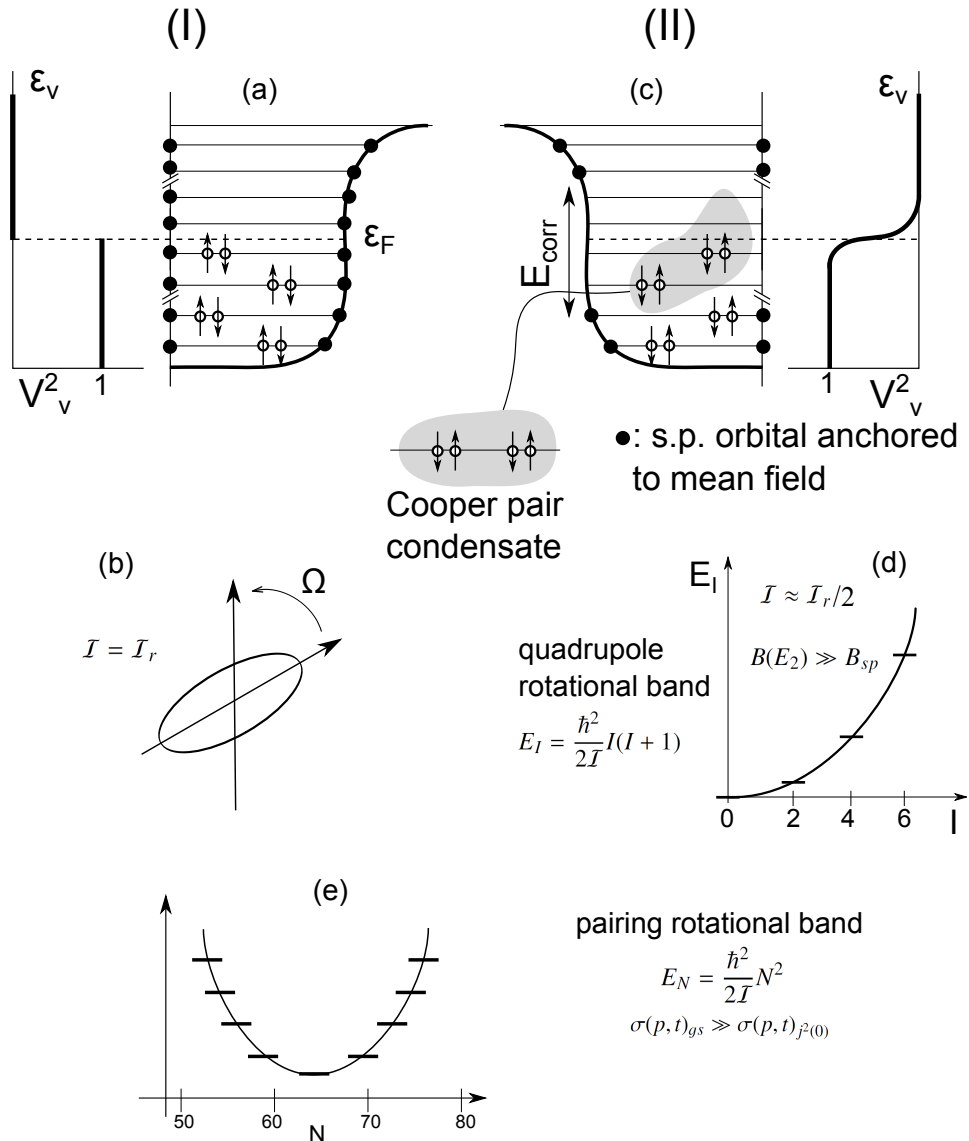


Figure 3.3.3: **(I)** (a) Schematic representation of “normal” (independent-particle) motion of nucleons in two-fold degenerate (Kramers, time-reversal degeneracy) orbits solidly anchored to the mean field (solid dots at the ends of the single-particle levels) and displaying a sharp, step-function-like, discontinuity in the occupancy at the Fermi energy lead to a deformed (Nilsson (1955)) rotating nucleus with a rigid moment of inertia $I = I_r$ (b). **(II)** Schematic representation of independent nucleon Cooper pair motion in which few (of the order of 5-8) pairs lead to (c) a sigmoidal occupation function at the Fermi energy and, having uncoupled themselves from the fermionic mean field (no solid dot at the end of the Kramers invariant single-particle levels) being now (quasi) bosons they contribute in a reduced fashion to (d) the moment of inertia of quadrupole rotational bands leading to $I \approx I_r/2$ (cf. Belyaev (2013), Belyaev (1959), Bohr and Mottelson (1975) and references therein), (e) pairing rotational bands in gauge space, an example of which is provided by the ground states of the superfluid Sn-isotopes (see also Figs. 3.1.3 and 3.1.4).

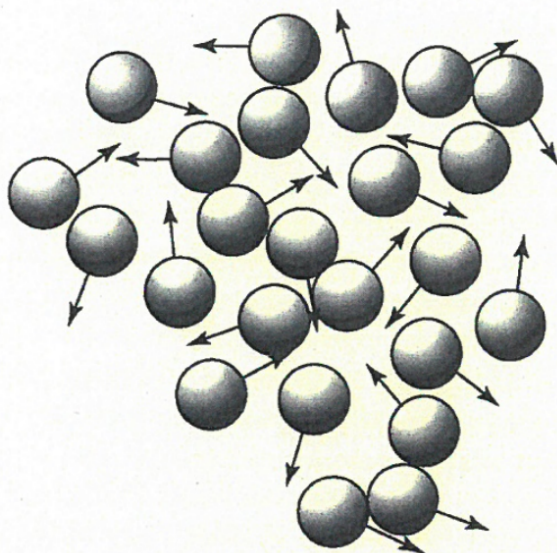


Figure 3.3.4: A system of independent Cooper pairs (Schafroth pairs). This situation corresponds to the incoherent solution of the many Cooper pair problem, the so called Fock state. In cold gases it describes the system beyond the Feschbach resonance leading to BEC (after Rogovin and Scully (1976)).

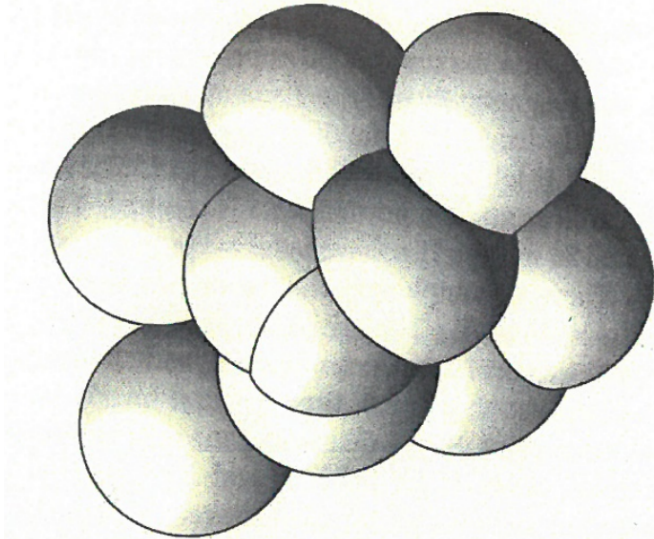


Figure 3.3.5: There are about 10^{12} Cooper pairs per cm^3 in a superconducting metal. A Cooper pair has a spatial extension of about 10^{-4} cm. Thus a given Cooper pair will overlap with 10^6 other Cooper pairs. This picture emerges from the many Cooper pair solution of the superconducting state of metal (coherent state), also valid in atomic nuclei (cf. Schrieffer (1964), Brink and Broglia (2005), and references therein). (After Rogovin and Scully (1976)).

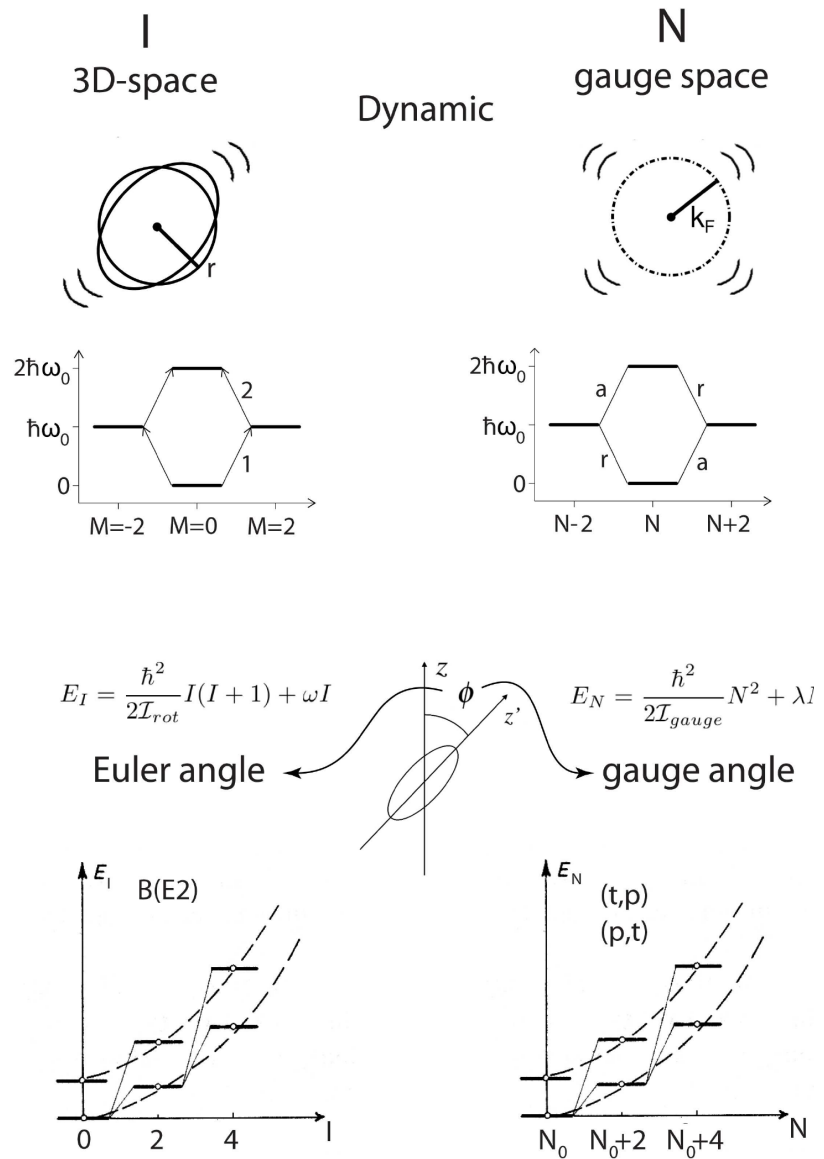


Figure 3.4.1: Parallel between dynamic and static deformations in 3D– and in gauge–space for the nuclear finite many body system. In the first case, the angular momentum \mathbf{I} and the Euler angles are conjugate variables. In the second, particle number N and gauge angle. While the fingerprint of static (quadrupole and gauge) deformations are quadrupole and pairing rotational bands, vibrational bands are the expression of such phenomena in non deformed systems.

$(C/D)^{1/2}$, the associated ZPF = $(\hbar^2/(2D\hbar\omega))^{1/2}$ leading to dynamical violations of rotational invariance. In the above relations, C and D stand for the restoring force constant and the inertia of the vibrational mode, respectively. In the case in which $\langle Q_{2M} \rangle \neq 0$, the $|HF\rangle$ state is known as the Nilsson state, $|\text{Nilsson}\rangle$, defining a privileged orientation in 3D-space and thus an intrinsic, body-fixed system of reference \mathcal{K}' which makes an angle Ω (Euler angles) with the laboratory frame⁴⁷ \mathcal{K} . Because there is no restoring force associated with the different orientations, fluctuations in Ω diverge in just the right way to restore rotational invariance, leading to a rotational band displaying a rigid moment of inertia (cf. Figs. 3.3.3 and 3.4.1), and whose members are the states⁴⁸,

$$|IKM\rangle \sim \int d\Omega \mathcal{D}_{MK}^I(\Omega) |\text{Nilsson}(\Omega)\rangle; E_I = (\hbar^2/2\mathcal{I})I(I+1); \mathcal{I} = \mathcal{I}_{rig}. \quad (3.4.3)$$

One can also view such bands as the limit ($C \rightarrow 0, D (= \mathcal{I})$ finite) of low energy ($\omega \rightarrow 0$), large-amplitude collective vibration. Similar dynamic and static spontaneous symmetry breaking phenomena take place in connection with particle-particle ($\beta = +2$ transfer quantum number) and hole-hole ($\beta = -2$) correlations, namely in gauge space (see Fig. 3.4.1; subject discussed also in Sect. 3.5 (dynamic: pairing vibration) and also below (static: pairing rotation); see also Figs. 3.1.1, 3.1.3 and 3.1.4). For a consistent discussion of these subjects⁴⁹.

3.4.2 independent-pair motion

Let us make use of the constant pairing matrix element approximation $\langle j_1 j_2 | v | j_3 j_4 \rangle = G$, that is,

$$H_P = -G \sum_{\nu, \nu' > 0} a_\nu^\dagger a_{\bar{\nu}}^\dagger a_{\nu'} a_{\bar{\nu'}}. \quad (3.4.4)$$

The abnormal density is related to the finite value of the pair operator. The associated independent pair states are written in the BCS approximation as

$$(U_\nu^2 + V_\nu^2) = 1; \quad |\varphi_{\nu\bar{\nu}}\rangle = (U_\nu + V_\nu a_\nu^\dagger a_{\bar{\nu}}^\dagger) |0\rangle, \quad \left. \frac{V_\nu}{U_\nu} \right\} = \frac{1}{\sqrt{2}} \left(1 \mp \frac{\epsilon_\nu}{E_\nu} \right)^{1/2}, \quad (3.4.5)$$

where $E_\nu = \sqrt{\epsilon_\nu^2 + \Delta^2}$ and $\epsilon_\nu = \varepsilon_\nu - \lambda$, $\lambda = \varepsilon_F$. The BCS ground state,

$$|BCS\rangle = \Pi_{\nu>0} (U_\nu + V_\nu a_\nu^\dagger a_{\bar{\nu}}^\dagger) |0\rangle, \quad (3.4.6)$$

describes independent pair motion, namely a situation correctly described in term of strongly overlapping (quasibosonic) pairs of fermions (Fig. 3.3.5), at variance with of that (erroneous) shown in Fig. 3.3.4. Let us introduce the phasing⁵⁰,

⁴⁷Nilsson (1955).

⁴⁸Bohr and Mottelson (1975).

⁴⁹See Bès and Kurchan (1990).

⁵⁰cf. e.g. Schrieffer (1973).

$$U_\nu = |U_\nu| = U'_\nu; \quad V_\nu = e^{-2i\phi} V'_\nu; \quad (V'_\nu \equiv |V_\nu|) (\nu \equiv j, m), \quad (3.4.7)$$

where ϕ is the gauge angle. One can then write the (BCS) wavefunction as,

$$\begin{aligned} |BCS(\phi)\rangle_{\mathcal{K}} &= \prod_{\nu>0} (U'_\nu + V'_\nu e^{-2i\phi} a_\nu^\dagger a_{\bar{\nu}}^\dagger) |0\rangle = \prod_{\nu>0} (U'_\nu + V'_\nu a_\nu^{\dagger'} a_{\bar{\nu}}^{\dagger'}) |0\rangle \\ &= |BCS(\phi=0)\rangle_{\mathcal{K}'} : \text{lab. system, } \mathcal{K} : \text{intr. system } \mathcal{K}', \end{aligned} \quad (3.4.8)$$

where $a_\nu^{\dagger'} = e^{-i\phi} a_\nu^\dagger$ is the single-particle creation operator referred to the intrinsic system. The BCS order parameter, two-nucleon spectroscopic amplitudes and number and gap equations are^{51,52},

$$\langle BCS | \sum_{\nu>0} a_\nu^\dagger a_{\bar{\nu}}^\dagger | BCS \rangle = \alpha'_0 e^{-2i\phi}; \quad \alpha'_0 = \sum_{\nu>0} U'_\nu V'_\nu; \quad ; \Delta = G\alpha_0, \quad (3.4.9)$$

$$B_\nu = \langle BCS | \frac{[a_\nu^{\dagger'} a_{\bar{\nu}}^{\dagger'}]_0}{\sqrt{2}} | BCS \rangle = (j_\nu + 1/2)^{1/2} U'_\nu V'_\nu, \quad (3.4.10)$$

and

$$N_0 = 2 \sum_{\nu>0} V_\nu^2; \quad \frac{1}{G} = \sum_{\nu>0} \frac{1}{2E_\nu}. \quad (3.4.11)$$

Examples of B_ν -coefficients for the reaction $^{124}\text{Sn}(p, t)^{122}\text{Sn}$ (gs) are given in Table 3.4.1.

The wavefunction and energies of the members of the pairing rotational band, can be written as

$$\begin{aligned} |N_0\rangle &\sim \int_0^{2\pi} d\phi e^{-iN_0\phi} |BCS(\phi)\rangle_{\mathcal{K}} \sim \left(\sum_{\nu>0} c_\nu a_\nu^\dagger a_{\bar{\nu}}^\dagger \right)^{N_0/2} |0\rangle, \quad c_\nu = V_\nu / U_\nu; \\ E_N &= (\hbar^2/2I)N^2; \quad I \approx 2\hbar^2/G, \end{aligned}$$

respectively⁵³.

In the case of a superfluid quadrupole deformed nucleus, the system acquires not only a privileged orientation in gauge space, but also in 3D-space. As summarized above, in a superfluid system, Cooper pairs and not single-particles are

⁵¹See Potel et al. (2017) and references therein.

⁵²It is of notice that the square root of $\alpha_0 = e^{-2i\phi} \alpha'_0$, normalized to a proper volume element V , that is, $\Psi = e^{-i\phi} \sqrt{n_S}$, where $n_S = \alpha_0/V$ is the density of superconducting electrons, constitutes the order parameter at the basis of the Ginzburg–Landau theory of superconductivity (Ginzburg and Landau (1950)), called by Ginzburg the Ψ –theory of superconductivity (Ginzburg (2004)), published seven years before than BCS.

⁵³See e.g. Brink and Broglia (2005) App. H; Mottelson (1998) and refs. therein.

the building blocks of the system (see Figs. 3.4.2 and 3.3.5)⁵⁴. But while the mean square radius of a nucleon at the Fermi energy ($\langle r^2 \rangle^{1/2} \approx (3/5)^{1/2} R_0$ ($R_0 = 1.2A^{1/3}$ fm)) is about 4.6 fm ($A \approx 120$), that of a Cooper pair is determined by the correlation length⁵⁵ ($\xi \approx \hbar v_F / 2\Delta \approx 23$ fm; $v_F/c \approx 0.27$, $\Delta \approx 1.2$ MeV) between the two nucleons forming the pair (see Figs. 3.3.3 and 3.3.5). Consequently, orienting the quadrupole deformed potential in different directions (Euler angles Ω), will have less effect on Cooper pairs than on independent particles. Thus the reduction of the moment of inertia from \mathcal{I}_r to $\approx \mathcal{I}_r/2$, \mathcal{I}_r being the rigid moment of inertia. Within this context one can mention the fact that low-lying nuclear collective vibrations (and rotations) are essentially not observed at intrinsic excitation energies corresponding to temperatures of $\approx 1-2$ MeV. In this case, this is because the surface is strongly fluctuating (thermally) and thus not well defined, making it non operative its anisotropic orientation in space.

Because in FMBS quantal fluctuations are very important⁵⁶, deformation in such systems explicit themselves through rotational bands. In particular, superfluid nuclei display well defined pairing rotational bands, an example of such bands being provided by the ground states of the superfluid Sn-isotopes. In this case, the moment of inertia is directly related to the pairing interaction. Pairing rotational bands are specifically excited in two nucleon transfer reactions (cf, Figs. 3.1.3 and 3.1.4). A summary of the physics which is at the basis of independent single-particle and single-pair motion is given in Figs. 3.4.2 and 3.4.3.

3.5 Two-nucleon spectroscopic amplitudes associated with pairing vibrational modes in closed shell systems: the ^{208}Pb case.

The solution of the pairing Hamiltonian

$$H = H_{sp} + H_p,$$

where

$$H_{sp} = \sum_{\nu} \epsilon_{\nu} a_{\nu}^{\dagger} a_{\nu},$$

and

$$H_p = -GP^{\dagger}P,$$

⁵⁴In connection with Fig. 3.4.2, the estimate $2R = 20/k_F$ was carried out with the help of the Fermi gas model (see e.g. Bohr and Mottelson (1969)). The Fermi momentum is written as $k_F \approx (3\pi^2 A/2V)^{1/3} \approx (\frac{3\pi^2}{2}\rho(0))^{1/3}$. Making use of $\rho(0) \approx 0.17 \text{ fm}^{-3}$ one obtains $k_F \approx 1.36 \text{ fm}^{-1}$. Let us now rewrite the relation between k_F and the volume $V (= (4\pi/3)R^3 = (4\pi/3)r_0^3 A)$. That is $k_F \approx (9\pi/8)^{1/3}/r_0 (= 1.52/r_0)$. To employ $r_0 = 1.2 \text{ fm}$ and still keep 1.36 fm^{-1} , one has to modify the above relation to $k_F \approx 1.63/r_0$. We now write the diameter of a heavy nucleus of mass $A \approx 200$ ($A^{1/3} \approx 5.85$). i.e. $2R = 2r_0 A^{1/3} \approx 20/k_F$. This is the value used in Fig. 3.4.2.

⁵⁵It is of notice that a much employed expression for the correlation length is that introduced by Pippard, $\xi = (\hbar v_F / (\pi\Delta))$ (Schrieffer (1964)).

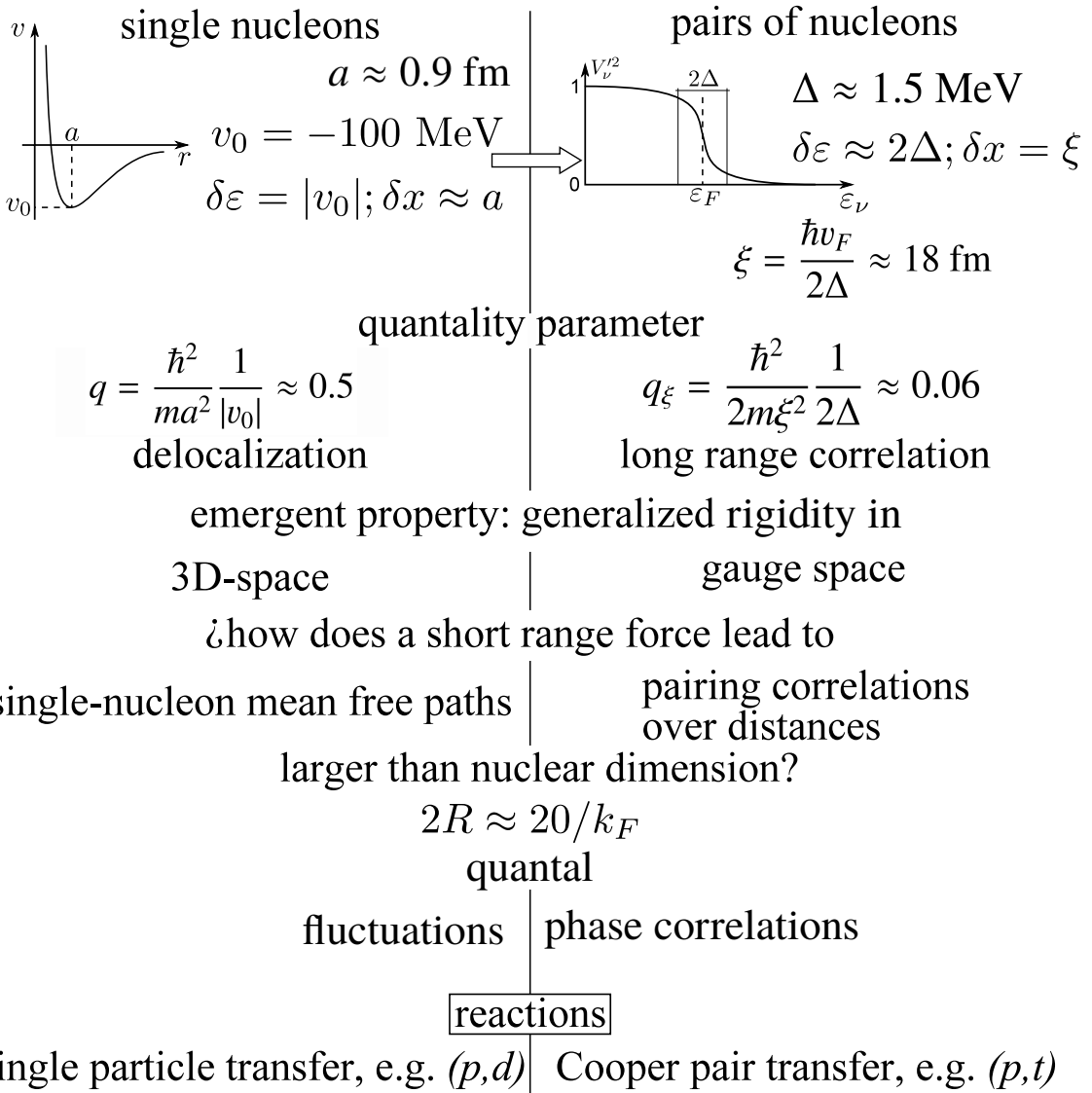
⁵⁶see Bertsch and Broglia (2005) and references therein.

Interplay between classical localization and quantal ZPF

$$\delta x \delta k \geq 1 \quad \varepsilon = \frac{\hbar^2 k^2}{2m} \quad \delta k = \frac{\delta \varepsilon}{\hbar v_F} \quad (v_F/c \approx 0.27)$$

structure

Independent motion of



the *absolute cross section* reflects the full renormalized nucleon transfer amplitude (energy, single-particle content, radial dependence of the wave function (formfactor))

Successive (dominant mechanism) and simultaneous transfer amplitude contributions to the *absolute cross section* carry in a equal efficient manner information concerning pair correlations

Figure 3.4.2: Classical localization and zero point fluctuations, associated with independent-particle (normal density) and independent-pair (abnormal density) motion.

$$H = T + v = \underbrace{T + U + V_p}_{\text{mean field}} + (v - U - V_p)$$

diagonalization

Kramers degeneracy $v\bar{v}$

$$\alpha_v^\dagger = U_v a_v^\dagger - V_{\bar{v}} a_{\bar{v}};$$

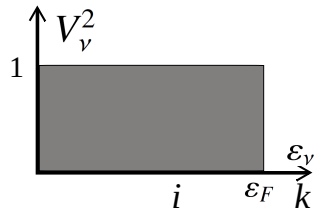
ground state

$$\alpha_\nu |\tilde{0}\rangle = 0$$

$$|\tilde{0}\rangle = \prod_{\nu>0} \alpha_\nu \alpha_{\bar{\nu}} |0\rangle \sim \prod_{\nu>0} \left(U_\nu + V_\nu a_\nu^\dagger a_{\bar{\nu}}^\dagger \right) |0\rangle$$

Ansatz 1: $|\tilde{0}\rangle$ sharp step-funct. occ.

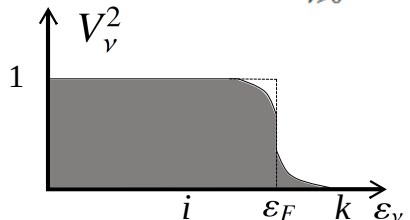
$$|HF\rangle = \prod_{i>0} a_i^\dagger a_i^\dagger |0\rangle = \prod_i a_i^\dagger |0\rangle$$



independent particle motion (**fermions**)

Ansatz 2: $|\tilde{0}\rangle$ sigmoidal distr. occ.

$$|BCS\rangle = \prod_{\nu>0} \left(U_\nu + V_\nu a_\nu^\dagger a_\nu^\dagger \right) |0\rangle$$



independent pair motion (*quasi*) **bosons**)

Figure 3.4.3: Schematic representation of the steps to be taken to extract from a two-body interaction independent particle motion (U , mean field) and independent pair motion ($V_p = -G\alpha_0(P^\dagger + P)$, pair potential, P^\dagger being the pair creation operator), in terms of a generalized quasiparticle transformation, and leading to a sharp step-function occupation distribution and a smooth (sigmoidal) occupation distribution around the Fermi surface respectively.

$nlj^a)$	$^{112}\text{Sn}(p, t)^{110}\text{Sn}(\text{gs})$	$^{124}\text{Sn}(p, t)^{122}\text{Sn}(\text{gs})$	$\text{BCS}^b)$	$V_{low-k}^c)$	$\text{BCS}^d)$	$\text{NuShell}^e)$
$1g_{7/2}$	0.96	-1.1073	0.44	0.63		
$2d_{5/2}$	0.66	-0.7556	0.35	0.60		
$2d_{3/2}$	0.54	-0.4825	0.58	0.72		
$3s_{1/2}$	0.45	-0.3663	0.36	0.52		
$1h_{11/2}$	0.69	-0.6647	1.22	-1.24		

Table 3.4.1: Two–nucleon transfer spectroscopic amplitudes associated with the reactions $^{112}\text{Sn}(p, t)^{110}\text{Sn}(\text{gs})$ and $^{124}\text{Sn}(p, t)^{122}\text{Sn}(\text{gs})$. **a)** quantum numbers of the two–particle configurations $(nlj)_{J=0}^2$ coupled to angular momentum $J = 0$. **b)** and **d)** $\langle \text{BCS} | T_\nu | \text{BCS} \rangle = \sqrt{(2j_\nu + 1)/2} U_\nu(A) V_\nu(A + 2)$ ($A + 2 = 112$ and 124 respectively), where $T_\nu = [a_\nu^\dagger a_\nu]_0^0 / \sqrt{2}$ ($\nu \equiv nlj$) (cf. Potel et al. (2011, 2013a,b)) **c)** two–nucleon transfer spectroscopic amplitudes calculated making use of initial and final state wavefunctions obtained by diagonalizing a v_{low-k} , that is a renormalized, low–momentum interaction derived from the CD–Bonn nucleon–nucleon potential (see Guazzoni et al. (2006) and references therein). **e)** Two–neutron overlap functions obtained making use of the shell–model wavefunctions for the ground state of ^{122}Sn and ^{124}Sn calculated with the code NuShell (Brown and Rae, 2007). The wavefunctions were obtained starting with a G –matrix derived from the CD–Bonn nucleon–nucleon interaction Machleidt et al. (1996). These amplitudes were used in the calculation of $^{124}\text{Sn}(p, t)^{122}\text{Sn}$ absolute cross sections carried out by I.J. Thompson (Thompson, 2013).

with

$$P^\dagger = \sum_{\nu>0} a_\nu^\dagger a_{\bar{\nu}}^\dagger,$$

lead, in the case of closed shell systems and within the harmonic approximation (RPA), to pair addition (*a*) pair removal (*r*) two–particle, two–hole correlated modes, the associated creation and annihilation operator being

$$\Gamma_a^\dagger(n) = \sum_k X_n^a(k) \Gamma_k^\dagger + \sum_i Y_n^a(i) \Gamma_i,$$

and

$$\Gamma_r^\dagger(n) = \sum_i X_n^r(i) \Gamma_i^\dagger + \sum_k Y_n^r(k) \Gamma_k,$$

with

$$\sum X^2 - Y^2 = 1,$$

and

$$\Gamma_k^\dagger = a_k^\dagger a_{\bar{k}}^\dagger, \quad (\epsilon_k > \epsilon_F).$$

Similarly,

$$\Gamma_i^\dagger = a_i^\dagger a_i, \quad (\epsilon_i \leq \epsilon_F).$$

The relations

$$[H, \Gamma_a^\dagger(n)] = \hbar W_n(\beta = +2),$$

and

$$[H, \Gamma_r^\dagger(n)] = \hbar W_n(\beta = -2),$$

where β is the transfer quantum number, while n labels the roots of the corresponding dispersion relations⁵⁷,

$$\frac{1}{G(\pm 2)} = \sum_k \frac{(\Omega_k/2)}{2\epsilon_k \mp W_n(\pm 2)} + \sum_i \frac{(\Omega_i/2)}{2\epsilon_i \pm W_n(\pm 2)},$$

n labeling the corresponding solutions in increasing order of energy. In the above equation, $\Omega_j = j + 1/2$ is the pair degeneracy of the orbital with total angular momentum j .

For the case of the (neutron) pair addition and pair subtraction modes of ^{208}Pb the above equations are graphically solved in Fig 3.5.1 (see also Table 3.5.1). The minimum of the dispersion relation defines the Fermi energy of the system under study. This is in keeping with the fact that in the case in which $W_1(\beta = +2) = W_1(\beta = -2) = 0$, situation corresponding to the transition between normal and superfluid phases, the energy value at which the dispersion relation touches for the first time the energy axis, coincides with the BCS λ variational parameter. It is of notice that, as a rule, the Fermi energy of closed shell nuclei is empirically defined as half the energy difference between the last occupied and the first empty single particle state⁵⁸. Making use of the values (see Fig. 3.5.1 and Table 3.5.1)

$$\begin{cases} E_{corr}(+2) = BE(208) + BE(210) - 2BE(209) = 1.248 \text{ MeV}, \\ E_{corr}(-2) = BE(208) + BE(206) - 2BE(207) = 0.640 \text{ MeV}, \end{cases}$$

one obtains $W_1(-2) + W_1(+2) = (BE(208) - BE(206)) - (BE(210) - BE(208)) = 14.11 - 9.115 = 4.995 \text{ MeV}$. Notice that in the above calculations all energies differences are positive. In particular (see Table 3.5.1)

$$\epsilon_i < \epsilon_F \Rightarrow \epsilon_F - \epsilon_i = -|\epsilon_F| + |\epsilon_i| = |\epsilon_i| - |\epsilon_F| > 0,$$

and

$$\epsilon_k > \epsilon_F \Rightarrow \epsilon_k - \epsilon_F = -|\epsilon_k| + |\epsilon_F| = |\epsilon_F| - |\epsilon_k| > 0.$$

Thus,

$$\begin{cases} 2(\epsilon_F - \epsilon_{p_{1/2}}) = W_1(-2) + E_{corr}(-2) > 0, \\ 2(\epsilon_{g_{9/2}} - \epsilon_F) = W_1(+2) + E_{corr}(+2) > 0. \end{cases}$$

From Fig. 3.5.1 and Table 3.5.1 one can then write,

$$2 \times (-5.825 - (-7.5)) \text{ MeV} = 2.650 \text{ MeV} = W_1(-2) + 0.640 \text{ MeV}$$

⁵⁷cf. Bès and Broglia (1966).

⁵⁸cf. e.g. Mahaux et al. (1985).

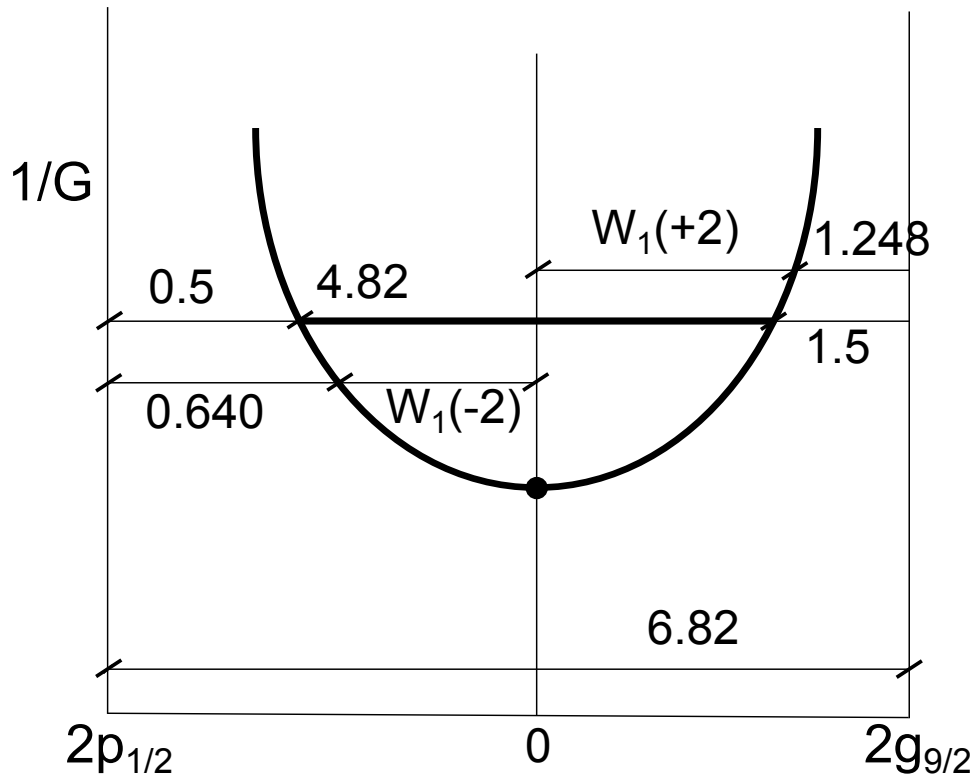


Figure 3.5.1: The right hand side of the RPA pairing vibrational dispersion relation for neutrons in the case of the closed shell system ^{208}Pb (cf. Bès and Broglia (1966)) in the region between the two neighboring shells ($p_{1/2}$ and $g_{9/2}$). All quantities are in MeV. For each G there is a straight horizontal line, which is divided by the the curve in three sections. The first one from the left corresponds to the pairing correlation energy of the nucleus ^{206}Pb (two correlated neutron hole states) while the last segment to the right measures the pairing correlation energy of ^{210}Pb (two correlated neutrons above closed shell) the intermediate segment measures the energy of the two phonon (correlated $(2p - 2h)$) pairing vibrational state of ^{208}Pb .

orbit	ϵ_j	$\epsilon_{p_{1/2}} - \epsilon_k \equiv \epsilon_k - \epsilon_{p_{1/2}} $
$0h_{9/2}$	-10.62	3.47
$1f_{7/2}$	-9.50	2.35
$0i_{13/2}$	-8.79	1.64
$2p_{3/2}$	-8.05	0.90
$1f_{5/2}$	-7.72	0.57
$2p_{1/2}$	-7.15	0
$\epsilon_F = -5.825$ MeV		$\epsilon_k - \epsilon_{g_{9/2}} \equiv \epsilon_{g_{9/2}} - \epsilon_k $
$1g_{9/2}$	-3.74	0.
$0i_{11/2}$	-2.97	0.77
$0j_{15/2}$	-2.33	1.41
$2d_{5/2}$	-2.18	1.56
$3s_{1/2}$	-1.71	2.03
$1g_{7/2}$	-1.27	2.47
$2d_{3/2}$	-1.23	2.51

Table 3.5.1: Valence single-particle levels of ^{208}Pb . In the upper part the occupied levels ($\epsilon_i \leq \epsilon_F$) are shown while in the lower part the empty levels ($\epsilon_k \geq \epsilon_F$). Of notice that $\epsilon_{p_{1/2}} - \epsilon_{g_{9/2}} = 3.41$ MeV, is the single-particle gap associated with $N = 126$ shell closure (from Nuclear Data Center).

and

$$2 \times (-3.74 \text{ MeV} - (-5.825) \text{ MeV}) = 4.17 \text{ MeV} = W_1(+2) + 1.248 \text{ MeV}.$$

Consequently,

$$W_1(-2) = 2.01 \text{ MeV} \quad \text{and} \quad W_1(+2) = 2.92 \text{ MeV},$$

leading to,

$$W_1(+2) + W_1(-2) = 4.93 \text{ MeV}. \quad (3.5.1)$$

3.5.1 Pair removal mode

In Fig. 3.5.2 the graphical representation of the forwards going RPA amplitude of the pair removal mode is shown. Its expression is

$$X_1^r(i) = \frac{\frac{1}{2}\Omega_i^{1/2}\Lambda(-2)}{2(\epsilon_F - \epsilon_i) - W_1(-2)},$$

where

$$\begin{aligned} 2 \times (\epsilon_F - \epsilon_i) - W_1(-2) &= 2 \times (\epsilon_F - \epsilon_i) - 2 \times (\epsilon_F - \epsilon_{p_{1/2}}) + E_{corr}(-2) \\ &= 2 \times (\epsilon_{p_{1/2}} - \epsilon_i) + E_{corr}(-2) = 2 \times (|\epsilon_i| - |\epsilon_{p_{1/2}}|) + E_{corr}(-2). \end{aligned}$$

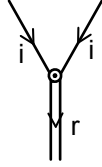


Figure 3.5.2: NFT representation of the forwards going RPA amplitude of the pair removal mode (double downward going arrowed line) describing a two correlated hole state (single downward going arrowed line for each hole with quantum numbers collectively labeled i).

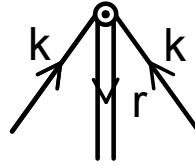


Figure 3.5.3: Same as Fig. 3.5.2 but for the backwards going amplitudes.

Thus,

$$X_1^r(i) = \frac{\frac{1}{2}\Omega_i^{1/2}\Lambda(-2)}{2(|\epsilon_i| - |\epsilon_{p_{1/2}}|) + E_{corr}(-2)}.$$

Making use of the empirical value of $E_{corr}(-2)$ worked out above one obtains,

$$X_1^r(i) = \frac{\frac{1}{2}\Omega_i^{1/2}\Lambda(-2)}{2(|\epsilon_i| - |\epsilon_{p_{1/2}}|) + 0.640 \text{ MeV}}.$$

In Fig. 3.5.3 we display the graphical process associated with the backwards going RPA amplitude,

$$Y_1^r(k) = \frac{\frac{1}{2}\Omega_k^{1/2}\Lambda(-2)}{2(\epsilon_k - \epsilon_F) + W_1(-2)}.$$

Making use of

$$2 \times (\epsilon_F - \epsilon_{p_{1/2}}) - E_{corr}(-2) = W_1(-2),$$

one can write

$$2 \times (\epsilon_F - \epsilon_{p_{1/2}}) + 2 \times (\epsilon_k - \epsilon_F) - E_{corr}(-2) = 2 \times (\epsilon_k - \epsilon_F) + W_1(-2),$$

leading to

$$2 \times (|\epsilon_{p_{1/2}}| - |\epsilon_k|) - E_{corr}(-2) = 2 \times (|\epsilon_{p_{1/2}}| - |\epsilon_{g_{9/2}}|) + 2 \times (|\epsilon_{g_{9/2}}| - |\epsilon_k|) - E_{corr}(-2).$$

Thus,

$$Y_1^r(k) = \frac{\frac{1}{2}\Omega_k^{1/2}\Lambda(-2)}{2(|\epsilon_{g_{9/2}}| - |\epsilon_k|) + 2(|\epsilon_{p_{1/2}}| - |\epsilon_{g_{9/2}}|) - E_{corr}(-2)}.$$

With the help of $2 \times (|\epsilon_{p_{1/2}}| - |\epsilon_{g_{9/2}}|) - E_{corr}(-2) = 6.82 \text{ MeV} - 0.640 \text{ MeV} = 6.18 \text{ MeV}$, one obtains,

$$Y_1^r(k) = \frac{\frac{1}{2}\Omega_k^{1/2}\Lambda(-2)}{2(|\epsilon_{g_{9/2}}| - |\epsilon_k|) + 6.18 \text{ MeV}}.$$

The above expressions of $X_1^r(i)$ and $Y_1^r(k)$ contain the experimental values of the 2-hole correlation energies (0.640 MeV). Because (see Fig. 3.5.1) the associated values of G does not lead to the observed correlation energy of the pair addition mode (1.248 MeV), we prefer to choose a single intermediate value of G and use the resulting $E_{corr}(-2)$ (=0.5 MeV) and $E_{corr}(+2)$ (=1.5 MeV), correlation energies, to calculate the corresponding X, Y amplitudes for both the lowest removal and lowest addition pairing modes. Making use of,

$$\begin{aligned} 2 \times (|\epsilon_{p_{1/2}}| - |\epsilon_{g_{9/2}}|) &= 6.82 \text{ MeV} \quad \text{and} \quad 2 \times (|\epsilon_{p_{1/2}}| - |\epsilon_{g_{9/2}}|) - E_{corr}(-2) \\ &= (6.82 - 0.5) \text{ MeV} = 6.32 \text{ MeV}, \end{aligned}$$

one can write

$$\begin{aligned} X_1^r(i) &= \frac{\frac{1}{2}\Omega_i^{1/2}\Lambda(-2)}{2(|\epsilon_i| - |\epsilon_{p_{1/2}}|) + 0.5 \text{ MeV}}, \\ Y_1^r(k) &= \frac{\frac{1}{2}\Omega_k^{1/2}\Lambda(-2)}{2(|\epsilon_{g_{9/2}}| - |\epsilon_k|) + 6.32 \text{ MeV}}. \end{aligned}$$

Tables 3.5.2 and 3.5.3 contain the amplitudes of the pair removal mode of ^{208}Pb ($\Gamma_r^\dagger(1) = \sum X_1^r(i)\Gamma_i^\dagger + \sum Y_1^r(k)\Gamma_k$), that is of the two neutron correlated hole state describing $|^{206}\text{Pb}(\text{gs})\rangle = \Gamma_r^\dagger(1)|0\rangle$.

It is of notice that the coupling strength $\Lambda(-2)$ with which the pair removal mode couples to the single-particle (-hole) states is calculated by normalizing the amplitudes: 1) (Tamm Dancoff, TD) $\sum_i A^2(i) = 1.5549 \text{ MeV}^{-2}$ and thus $\Lambda(-2) = 0.802 \text{ MeV}$, ($\sum X(i)_{TD}^2 = 1$); 2) RPA, $\Lambda_1^2(-2) \times (\sum_i A^2(i) - \sum_k B^2(k)) = \Lambda_1^2(-2) \times 1.45073 = 1$. Thus $\Lambda_1(-2) = 0.830 \text{ MeV}$. The above results shows that there is a few percentage difference between the two values of Λ (TD and RPA), as well as for the corresponding X amplitudes. Nonetheless, ground state correlations as expressed by the Y amplitudes, gives rise to a 52% increase in the $^{206}\text{Pb}(t, p)^{208}\text{Pb}(\text{gs})$ absolute cross section, from 0.34 mb to 0.52 mb to be compared with experimental data $\sigma = 0.68 \pm 0.24 \text{ mb}$ (see Fig. 4.5.4).

3.5.2 Pair addition mode

In Fig. 3.5.4 the X -amplitude of the pair addition mode is shown (NFT diagram). The associated expression

$$X_1^a(k) = \frac{\frac{1}{2}\Omega_k^{1/2}\Lambda_1(+2)}{2(\epsilon_k - \epsilon_F) - W_1(+2)},$$

units		MeV	MeV ⁻¹	RPA	TD
<i>nlj</i>	Ω_i	$ \epsilon_i - \epsilon_{p_{1/2}} $	$A(i) = \frac{\frac{1}{2}\Omega_i^{1/2}}{2(\epsilon_i - \epsilon_{p_{1/2}}) + 0.5 \text{ MeV}}$	$X_1^r(i)$	$X_1^r(i)$
$2p_{1/2}$	1	0	1	0.83	0.80
$1f_{5/2}$	3	0.57	0.528	0.44	0.42
$2p_{3/2}$	2	0.90	0.307	0.25	0.25
$0i_{13/2}$	7	1.64	0.350	0.29	0.28
$1f_{7/2}$	4	2.35	0.192	0.16	0.15
$0h_{9/2}$	5	3.47	0.150	0.12	0.12

Table 3.5.2: Forwards going RPA amplitudes of the pair removal mode of ^{208}Pb (i.e. $|^{206}\text{Pb}\rangle$ state), cf. Table XVI Broglia et al. (1973).

units		MeV	MeV ⁻¹	RPA
<i>nlj</i>	Ω_k	$ \epsilon_{g_{9/2}} - \epsilon_k $	$B(k) = \frac{\frac{1}{2}\Omega_k^{1/2}}{2(\epsilon_{g_{9/2}} - \epsilon_k) + 6.23 \text{ MeV}}$	$Y_1^r(i)$
$1g_{9/2}$	5	0	0.179	-0.15
$0i_{11/2}$	6	0.77	0.158	-0.13
$0j_{15/2}$	8	1.41	0.156	-0.13
$2d_{5/2}$	3	1.56	0.093	-0.08
$3s_{1/2}$	1	2.03	0.046	-0.04
$1g_{7/2}$	4	2.47	0.090	-0.07
$2d_{3/2}$	2	2.51	0.063	-0.05

Table 3.5.3: Same as Table 3.5.2 but for the backwards amplitude.

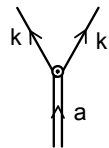


Figure 3.5.4: Same as Fig. 3.5.2 but for the pair addition mode

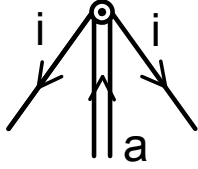


Figure 3.5.5: Same as Fig. 3.5.3 but for the pair addition mode

can be written, making use of

$$\begin{aligned} 2 \times (\epsilon_k - \epsilon_F) - W_1(+2) &= 2 \times (\epsilon_k - \epsilon_F) - 2 \times (\epsilon_{g_{9/2}} - \epsilon_F) + E_{corr}(+2) \\ &= 2 \times (\epsilon_k - \epsilon_{g_{9/2}}) + E_{corr}(+2) = 2 \times (|\epsilon_{g_{9/2}}| - |\epsilon_k|) + E_{corr}(+2), \end{aligned}$$

as

$$X_1^a(k) = \frac{\frac{1}{2}\Omega_k^{1/2}\Lambda_1(+2)}{2(|\epsilon_{g_{9/2}}| - |\epsilon_k|) + E_{corr}(+2)}.$$

Similarly (cf. Fig. 3.5.5),

$$Y_1^a(i) = \frac{\frac{1}{2}\Omega_i^{1/2}\Lambda_1(+2)}{2(\epsilon_F - \epsilon_i) + W_1(+2)},$$

can be written, with the help of the relation

$$\begin{aligned} 2 \times (\epsilon_F - \epsilon_i) + W_1(+2) &= 2 \times (\epsilon_F - \epsilon_i) - 2 \times (\epsilon_{g_{9/2}} - \epsilon_F) - E_{corr}(+2) \\ &= 2 \times (\epsilon_{p_{1/2}} - \epsilon_i) + 2 \times (\epsilon_{g_{9/2}} - \epsilon_{p_{1/2}}) - E_{corr}(+2) \\ &= 2 \times (|\epsilon_i| - |\epsilon_{p_{1/2}}|) + 2 \times (|\epsilon_{p_{1/2}}| - |\epsilon_{g_{9/2}}|) - E_{corr}(+2), \end{aligned}$$

as

$$Y_1^a(i) = \frac{\frac{1}{2}\Omega_i^{1/2}\Lambda_1(+2)}{2(|\epsilon_i| - |\epsilon_{p_{1/2}}|) + 2\Delta\epsilon_{sp} - E_{corr}(+2)}.$$

Making use of $E_{corr}(+2) = 1.5$ MeV (cf. Fig. 3.5.1) and

$$\Delta\epsilon_{sp} = 2 \times (|\epsilon_{p_{1/2}}| - |\epsilon_{g_{9/2}}|) = 6.28 \text{ MeV},$$

one can write $2\Delta\epsilon_{sp} - E_{corr}(+2) = (6.82 - 1.5)$ MeV = 5.32 MeV, leading to

$$\begin{cases} X_1^a(k) = \frac{\frac{1}{2}\Omega_k^{1/2}\Lambda(-2)}{2(|\epsilon_{g_{9/2}}| - |\epsilon_k|) + 1.5 \text{ MeV}}, \\ Y_1^a(i) = -\frac{\frac{1}{2}\Omega_i^{1/2}\Lambda(+2)}{2(|\epsilon_i| - |\epsilon_{p_{1/2}}|) + 5.32 \text{ MeV}}. \end{cases}$$

The corresponding numerical values are displayed in Tables 3.5.4 and 3.5.5, while in Fig. 3.5.6 we display a schematic summary of the graphical solution of the dispersion relations.

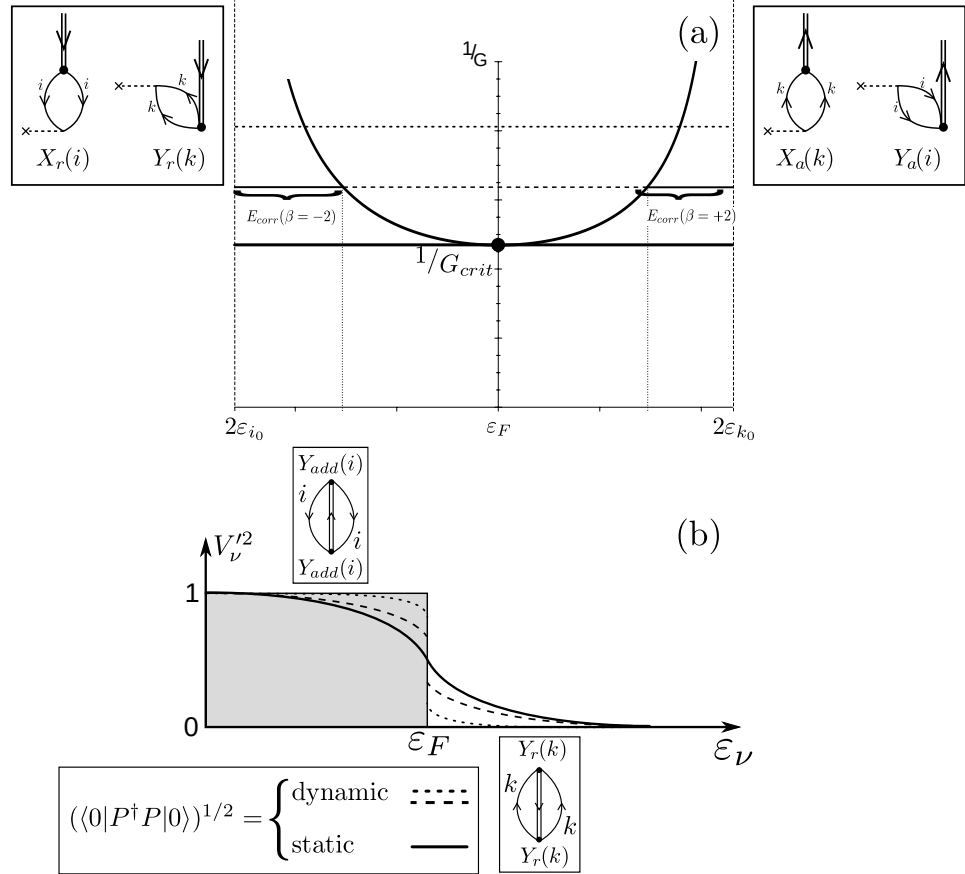


Figure 3.5.6: Schematic representation of the quantal phase transition taking place as a function of the pairing coupling constant in a (model) closed shell nucleus. (a) dispersion relation associated with the RPA diagonalization of the Hamiltonian $H = H_{sp} + H_p$ for the pair addition and pair removal modes. In the insets are shown the two-particle transfer processes exciting these modes, which testify to the fact that the associated zero point fluctuations (ZPF) which diverge at $G = G_{crit}$, blur the distinction between occupied and empty states typical of closed shell nuclei. (b) occupation number associated with the single-particle levels. For $G < G_{crit}$ there is a dynamical depopulation (population) of levels $i(k)$ below (above) the Fermi energy. For $G > G_{crit}$, the deformation of the Fermi surface becomes static, although with a non-vanishing dynamic component (cf. Fig. 3.1.2).

units		MeV	MeV ⁻¹	
<i>nlj</i>	Ω_k	$ \epsilon_{g9/2} - \epsilon_k $	$C(k) = \frac{\frac{1}{2}\Omega_k^{1/2}}{2(\epsilon_{g9/2} - \epsilon_k) + 1.5 \text{ MeV}}$ a)	$X_1^a(k)$
$1g_{9/2}$	5	0	0.745	0.82
$0i_{11/2}$	6	0.77	0.403	0.44
$0j_{15/2}$	8	1.41	0.327	0.36
$2d_{5/2}$	3	1.56	0.187	0.21
$3s_{1/2}$	1	2.03	0.090	0.10
$1g_{7/2}$	4	2.47	0.155	0.17
$2d_{3/2}$	2	2.51	0.108	0.12

Table 3.5.4: Forwards going RPA amplitudes associated with the pair addition mode of ^{208}Pb (cf. Table XVI Broglia et al. (1973)). a) $\sum_k C^2(k) = 0.903$

units		MeV	MeV ⁻¹	
<i>nlj</i>	Ω_i	$ \epsilon_i - \epsilon_{p_{1/2}} $	$D(i) = \frac{\frac{1}{2}\Omega_i^{1/2}}{2(\epsilon_i - \epsilon_{p_{1/2}}) + 5.32 \text{ MeV}}$ a)	$Y_1^a(i)$
$2p_{1/2}$	1	0	-0.094	-0.1
$1f_{5/2}$	3	0.57	-0.134	-0.15
$2p_{3/2}$	2	0.90	-0.099	-0.11
$0i_{13/2}$	7	1.64	-0.154	-0.17
$1f_{7/2}$	4	2.35	-0.100	-0.11
$0h_{9/2}$	5	3.47	-0.091	-0.10

Table 3.5.5: Same as Table 3.5.4 but for the backwards going amplitude. a) $\sum_i D^2(i) = 0.079$ and $\Lambda^2(+2)(\sum_k C^2(k) - D^2(i)) = \Lambda^2(+2)(0.903 - 0.079) \text{ MeV}^{-2} = 0.824 \text{ MeV}^{-2}$; $\Lambda(+2) = (0.824)^{-1/2} \text{ MeV}$, thus $\Lambda(+2) = 1.102 \text{ MeV}$.

Let us conclude this Section by noting that while the harmonic (RPA) description of the pair vibrational mode of ^{208}Pb provides a fair picture of the two neutron transfer spectroscopic amplitudes, in keeping with the collective character of these (coherent) states, conspicuous anharmonicities in the multi-phonon spectrum have been observed and calculated⁵⁹. Within the framework of Fig. 3.4.1, we schematically emphasize in Fig. 3.5.7 the relative importance of dynamic and static pairing distortions, in comparison with the corresponding quantities in the case of quadrupole surface distortions in 3D-space⁶⁰. These results underscore the major role pairing vibrations play in nuclei around closed shells, while those shown in Fig. 3.1.2 their importance in gauge invariance restoration in systems far away from closed shells.

3.6 Halo pair addition and pygmy dipole modes: a new mechanism to break gauge invariance

Pairing is intimately connected with particle number violation and thus spontaneous breaking of gauge invariance, as testified by the order parameter $\langle BCS | P^\dagger | BCS \rangle = \alpha_0$. In the nuclear case and, at variance with condensed matter, dynamical breaking of gauge symmetry is similarly important to that associated with static distortions (e.g. pairing vibrations around closed shell nuclei, cf. Figs. 3.1.1 and 3.5.7). The fact that the average single-particle field acts as an external potential is one of the reasons of the existence of a critical value G_c of the pairing strength G to bind Cooper pairs in nuclei. Spatial quantization in finite systems at large and in nuclei in particular, is intimately connected with the paramount role the surface plays in these systems⁶¹. Another consequence of this role is the fact that in nuclei an important fraction ($\approx 50\%$ in the case of nuclei lying along the stability valley, even more for light halo nuclei) of Cooper pair binding is due to the exchange of collective vibrations between the partners of the pair⁶², the rest being associated with the bare NN -interaction in the 1S_0 channel (cf. Fig. 3.6.1) plus possible $3N$ corrections⁶³. Within this context we note that the results displayed in Fig. 3.1.2 provide one of the clearest quantitative examples of the central and ubiquitous role pairing vibrations play in nuclear pairing correlations.

The study of light exotic nuclei lying along the neutron drip line have revealed a novel aspect of the interplay between shell effects and induced pairing interaction. It has been found that there are situations in which spatial quantization screens,

⁵⁹Cf. for example Flynn et al. (1972a), Lanford and McGrory (1973), Bortignon et al. (1978), Clark et al. (2006).

⁶⁰For details cf. Bès and Broglia (1977), Broglia et al. (1968), Bès et al. (1988), Barranco and Broglia (1987) Shimizu et al. (1989), Shimizu (2013), Vaquero et al. (2013) and references therein.

⁶¹See Bohr and Mottelson (1975); see also Broglia (2002) and references therein.

⁶²Cf. e.g. Barranco et al. (1999), Brink and Broglia (2005), Saperstein and Baldo (2013), Avdeenkov and Kamerdzhiev (2013), Lombardo et al. (2013), and references therein; cf. also Bohr and Mottelson (1975), p. 432, Barranco et al. (2001) and Potel et al. (2010).

⁶³Cf. e.g. Lesinski et al. (2012), Pankratov et al. (2011), Hergert and Roth (2009).

$$P^\dagger = \sum_{\nu>0} a_\nu^\dagger a_{\bar{\nu}}^\dagger$$

$$x' = \frac{2G\Omega'}{D} = GN(0)$$

$x > 1$ $\alpha_0 = \langle P^\dagger \rangle = \frac{\Delta}{G} \approx 7$	$x < 1$ $\alpha_{dyn} = \frac{\langle PP^\dagger \rangle^{1/2} + \langle P^\dagger P \rangle^{1/2}}{2}$ $\approx \frac{1}{2} \left(\frac{E_{corr}(A+2)}{G} + \frac{E_{corr}(A-2)}{G} \right) \approx 10$ $\frac{\alpha_0}{\alpha_{dyn}} \approx 0.7$
--	---

$$\frac{\beta_2}{(\beta_2)_{dyn}} \approx 3 - 6$$

Figure 3.5.7: Relative importance of dynamic and static pairing distortion (α_{dyn} and α_0 respectively) associated with closed shell and open shell nuclei, calculated in terms of a two level model, as compared with similar quantities for the case of quadrupole surface degrees of freedom (β_2 -values). The parameter x' (product of the effective pairing strength $G' = Z_\omega^2(v_p^{bare} + v_p^{ind})$ and of the effective density of levels at the Fermi energy $N'(0) = Z_\omega^{-1}N(0) = Z_\omega^{-1}(2\Omega/D) = 2\Omega'/D = 2\Omega/D'; \Omega' = Z_\omega^{-1}\Omega, D' = Z_\omega D$), measures the relative importance of the single-particle gap $D' = Z_\omega D$ and of the pair correlation $G'\Omega$ (cf. Brink and Broglia (2005) App. H, Sect. H.4).

essentially completely, the bare nucleon–nucleon paring interaction. This happens in the case in which the nuclear valence orbitals are s, p –states at threshold⁶⁴. An example of situations of this type is provided by $N = 7$ (parity inversion; see Chapter 5, Section 5.2.2 and Section 7.2) isotones.

In what follows we discuss the (unbound) nucleus ^{10}Li , in connection with the (bound) two–neutron halo system ^{11}Li . The $N = 7$ isotope ^{10}Li displays a virtual $s_{1/2}$ and a resonant $p_{1/2}$ state⁶⁵. Let us elaborate on this point. The binding provided by a contact pairing interaction $V_\delta(|\mathbf{r} - \mathbf{r}'|)$ (δ –force) to a pair of fermions moving in time–reversal states in a single j –shell⁶⁶ is given by the matrix element,

$$M_j = \langle j^2(0)|V_\delta|j^2(0)\rangle = -\frac{(2j+1)}{2}V_0 I(j) \approx -\frac{(2j+1)}{2}V_0 \frac{3}{R^3}. \quad (3.6.1)$$

Of notice that $G = V_0 I(j)$ ($\approx 25/A$ MeV ≈ 2.3 MeV ($A = 11$)). The ratio of the above matrix element associated with the two halo neutrons of ^{11}Li and with an hypothetical normal nucleus of mass $A = 11$ is

$$r = \frac{(M_j)_{\text{halo}}}{(M_j)_{\text{core}}} = \frac{2}{(2j+1)} \left(\frac{R_0}{R}\right)^3. \quad (3.6.2)$$

The quantities $R_0 = 1.2A^{1/3}\text{fm} = 2.7\text{fm}$ ($A = 11$), and $R = \sqrt{\frac{5}{3}}\langle r^2 \rangle_{^{11}\text{Li}}^{1/2} = \sqrt{\frac{5}{3}}(3.55 \pm 0.1)$ fm $= (4.58 \pm 0.13)$ fm are the radius of a stable nucleus of mass $A = 11$ (systematics), and the measured radius of ^{11}Li , respectively. The quantity j is the effective angular momentum of a single j –shell which can accommodate 8 neutrons ($j \sim k_F R_0 \approx 1.36 \text{ fm}^{-1} \times 2.7 \text{ fm} \approx 3.7$). One thus obtains

$$r = 0.048. \quad (3.6.3)$$

Consequently, the bare NN –nucleon pairing interaction is expected to become strongly screened, the resulting effective G –value

$$G_{\text{scr}} = r \times G = 0.048 \times 25 \text{ MeV}/A \approx 1 \text{ MeV}/A \approx 0.1 \text{ MeV}, \quad (3.6.4)$$

becoming subcritical and thus unable to bind the halo Cooper pair ($2\tilde{\epsilon}_{s_{1/2}} = 0.3$ MeV, see Fig. 2.10.1) to the ^9Li core.

Further insight into this question can be shed making use of the multipole expansion of a general interaction

$$v(|\mathbf{r}_1 - \mathbf{r}_2|) = \sum_\lambda V_\lambda(r_1, r_2) P_\lambda(\cos \theta_{12}). \quad (3.6.5)$$

Because the function P_λ drops from its maximum at $\theta_{12} = 0$ in an angular distance $1/\lambda$, particles 1 and 2 interact through the component λ of the force, only if $r_{12} =$

⁶⁴Pairing anti–halo effect; Bennaceur et al. (2000), Hamamoto and Mottelson (2003), Hamamoto and Mottelson (2004).

⁶⁵See however Cavallaro et al. (2017), as well as Barranco et al. (2020) Moro et al. (2019).

⁶⁶cf. e.g. Eq. (2.12) Brink and Broglia (2005).

$|\mathbf{r}_1 - \mathbf{r}_2| < R/\lambda$, where R is the mean value of the radii \mathbf{r}_1 and \mathbf{r}_2 . Thus, as λ increases, the effective force range decreases. For a force of range much greater than the nuclear size, only the lowest λ (long wavelength) terms are important. At the other extreme, a δ -function force has coefficients $V_\lambda(r_1, r_2) \left(= \frac{(2\lambda+1)}{4\pi r_1^2} \delta(r_1 - r_2)\right)$ that increase with λ . In the case of $^{11}\text{Li}(\text{gs})$ one is thus forced to accept the need for a long range, low λ pairing interaction, as responsible for the binding of the dineutron, halo Cooper pair to the ^9Li core. This is equivalent to saying, an induced pairing interaction arising from the exchange of vibrations with low λ -value.

3.6.1 Cooper pair binding: a novel embodiment of the Axel–Brink hypothesis.

In what follows we discuss a possible novel test of the Axel–Brink hypothesis⁶⁷. Within the s, p subspace, the most natural low multipolarity, long wavelength vibration is the dipole mode. From systematics, the centroid of these vibrations is $\hbar\omega_{GDR} \approx 100 \text{ MeV}/R$, R being the nuclear radius⁶⁸. Thus, in the case of ^{11}Li , one expects the centroid of the Giant Dipole Resonance carrying $\approx 100\%$ of the energy weighted sum rule (EWSR) at $\hbar\omega_{GDR} \approx 100 \text{ MeV}/4.6 \approx 22 \text{ MeV}$. Now, such a high frequency mode can hardly be expected to give rise to anything, but polarization effects. On the other hand, there exists experimental evidence which testifies to the presence of a well defined dipole state with centroid at $\lesssim 1 \text{ MeV}$ and carrying $\approx 8\%$ of the EWSR⁶⁹. The existence of this “pygmy (dipole) resonance” (PDR) which can be viewed as a simple consequence of the existence of a low-lying particle–hole state associated with the transition $s_{1/2} \rightarrow p_{1/2}$ testifies, arguably, to the coexistence⁷⁰ of two states with rather different radii in the ground

⁶⁷The color of an object can be determined in two ways: by illuminating it with white light and see which wavelength it absorbs, or by heating it up and see the same wavelength it emits. In both cases one is talking about dipole radiation. To describe the de-excitation process of hot nuclei requires the knowledge of the photon interactions with excited states. The common assumption, known as the Axel–Brink hypothesis, has been that each excited state of a nucleus carries a giant dipole resonance (GDR) on top of it, and that the properties of such resonances are unaffected by any excitation of the nucleus (Brink (1955 (unpublished), Lynn (1968) pag. 321, Axel (1962); cf. also Bertsch and Broglia (1986) and Bortignon et al. (1998))

⁶⁸See Bohr and Mottelson (1975) Bortignon et al. (1998) and Bertsch and Broglia (2005) and refs. therein.

⁶⁹Zinser et al. (1997), T. Nakamura et al. (2006), Shimoura et al. (1995), Ieki et al. (1993), Sackett et al. (1993), Kanungo et al. (2015), Kobayashi et al. (1989).

⁷⁰Within this context one can mention similar situations concerning the coexistence of spherical and quadrupole deformed states (cf. e.g. Wimmer et al. (2010), Federman and Talmi (1965), Federman and Talmi (1966), Dönau et al. (1967) and refs. therein; cf. also Bohr and Mottelson (1963 (unpublished)), typically of nuclei with $N \approx Z$. The fact that the associated inhomogeneous damping on the GDR has modest consequences concerning dipole strength at low energies as compared with radial (isotropic) deformations in ^{11}Li is understood in terms of the (non–Newtonian) plasticity of the atomic nucleus regarding quadrupole deformations (low-lying collective 2^+ surface vibrations, fission, exotic decay (cf. Barranco et al. (1988), Barranco et al. (1989); Bertsch (1988), Bertsch et al. (1987))), and of the little tolerance to both compressibility and rarification displayed by the same system and connected with saturation properties (see also Broglia et al. (2019a) and Broglia et al.

state. One, closely connected with the ${}^9\text{Li}$ core, (≈ 2.5 fm), the second with the diffuse halo (≈ 4.6 fm), namely displaying a large radial deformation (neutron skin), and thus able to induce a conspicuous inhomogeneous damping to the dipole mode.

The importance of this mechanism is underscored by the fact that in ${}^{11}\text{Li}$, displaying a neutron excess $(N - Z)/A \approx 0.45$ as compared to the value of 0.21 in the case of ${}^{208}\text{Pb}$, it is able to bring down by tens of MeV a consistent fraction ($\approx 8\%$) of the GDR. A consequence of the fact that the nucleus is most sensitive to changes in density (saturation phenomena). In the case of the halo of ${}^{11}\text{Li}$ we are confronted with nuclear structure phenomena in a medium displaying a density of $\approx 4\%$ of saturation density (App. 4.C, see also Eq. (4.3.6)).

Before proceeding, let us estimate the overlap O between the two “ground states”. Making use of a schematic expression for the single-particle radial wave-functions⁷¹

$$\mathcal{R} = \sqrt{3/R_0^3} \Theta(r - R_0), \quad (3.6.6)$$

where

$$\Theta = 1 \quad (r \leq R_0); \quad 0 \quad (r > R_0),$$

leading to,

$$\int_0^\infty dr r^2 \mathcal{R}^2(r) = \frac{3}{R_0^3} \int_0^{R_0} dr r^3 / 3 = 1, \quad (3.6.7)$$

one can work out the overlap O between the two halo neutrons and the core nucleons. That is,

$$\begin{aligned} O &= |\langle \mathcal{R}_{\text{halo}} | \mathcal{R}_{\text{core}} \rangle|^2 = \left(\sqrt{\frac{3}{R_0^3}} \sqrt{\frac{3}{R^3}} \int_0^\infty dr r^2 \Theta(r - R) \Theta(r - R_0) \right)^2 \\ &= \left(\sqrt{\frac{3}{R_0^3}} \sqrt{\frac{3}{R^3}} \int_0^{R_0} dr r^3 / 3 \right)^2 = (R_0/R)^3 = 0.20, \end{aligned} \quad (3.6.8)$$

where use has been made of $\Theta(r - R)\Theta(r - R_0) = \Theta(r - R_0)$, $R_0 = 1.2A^{1/3}$ fm = 2.7 fm ($A = 11$) and $R = (4.58 \pm 0.013)$ fm. Because of the small value of this overlap, one can posit that the $E_x \lesssim 1$ MeV ($\Gamma \approx 0.5$ MeV) soft $E1$ -mode of ${}^{11}\text{Li}$ is a *bona fide* dipole resonance based on an exotic, unusually extended $|0_\nu\rangle$ state of radial dimensions equivalent, according to systematics, to a system of effective A mass number about 5 times that of the actual system ($A \approx (4.6/1.2)^3 \approx 60$). Thus consistent with the connotation of PDR.

It is of notice that the small values of r and of O have essentially the same origin. On the other hand, they have apparently, rather different physical consequences. In fact, the first makes the bare pairing interaction strength G subcritical, while the second one screens the repulsive symmetry potential V_1 ($\approx +25$ MeV)⁷²,

(2019b)).

⁷¹Bohr and Mottelson (1969).

⁷²See e.g. Bortignon et al. (1998) Eq. (3.48) and refs. therein.

that is, the price one has to pay to separate protons from neutrons. This effect allows for a consistent fraction of the dipole Thomas–Reiche–Kuhn sum rule, that is of the $J^\pi = 1^-$ energy weighted sum rule (EWSR), to come low in energy ($p_{1/2} - s_{1/2}$ transition) from the value $E_{GDR} \approx (100/R)$ MeV and, acting as an intermediate boson between the two halo neutrons, glue them to the ${}^9\text{Li}$ core. *Summing up, the halo anti-pairing effect $G_{scr} = r \times G \ll G < G_{crit}$ triggers ($OV_1 \ll V_1$) the virtual presence of a “gas” of dipole (pygmy) bosons which, exchanged between the two halo neutrons (cf. Fig. 3.6.2), overcompensates the reduction of the bare pairing interaction, leading to the binding of the halo Cooper pair to the core (anti-halo anti-pairing effect)). It can thus be stated that the halo of ${}^{11}\text{Li}$ and the pygmy dipole resonance built on top of it constitute a pair of symbiotic states (see also Chapter 7, in particular Fig. 7.1.4).*

Let us further elaborate on these issues. Making use of the relation $\langle r^2 \rangle^{1/2} \approx (3/5)^{1/2} R$ between mean square radius and the radius, one may write

$$\langle r^2 \rangle_{{}^{11}\text{Li}} \approx \frac{3}{5} R_{eff}^2({}^{11}\text{Li}). \quad (3.6.9)$$

with

$$R_{eff}^2({}^{11}\text{Li}) = \left(\frac{9}{11} R_0^2({}^9\text{Li}) + \frac{2}{11} \left(\frac{\xi}{2} \right)^2 \right), \quad (3.6.10)$$

where

$$R_0({}^9\text{Li}) = 2.5\text{fm}, \quad (3.6.11)$$

is the ${}^9\text{Li}$ radius ($R_0 = r_0 A^{1/3}$, $r_0 = 1.2\text{fm}$), while ξ is the correlation length of the Cooper pair neutron halo. An estimate of this quantity is provided by the relation

$$\xi = \frac{\hbar v_F}{\pi E_{corr}} \approx 20\text{ fm}, \quad (3.6.12)$$

in keeping with the fact that in ${}^{11}\text{Li}$, $(v_F/c) \approx 0.16$ and $E_{corr} \approx -0.5$ MeV (see App. 7.E). Consequently,

$$R_{eff}({}^{11}\text{Li}) \approx 4.8\text{ fm} \quad (3.6.13)$$

and $\langle r^2 \rangle_{{}^{11}\text{Li}}^{1/2} \approx 3.7\text{ fm}$, to be compared with the experimental value⁷³ $\langle r^2 \rangle_{{}^{11}\text{Li}}^{1/2} = 3.55 \pm 0.1\text{ fm}$. It is of notice that this experimental value implies the radius $R({}^{11}\text{Li}) = \sqrt{5/3 \langle r^2 \rangle_{{}^{11}\text{Li}}} = 4.58 \pm 0.13\text{ fm}$.

We now proceed to the calculation of the centroid of the dipole pygmy resonance of ${}^{11}\text{Li}$ in RPA making use of the separable interaction

$$H_D = -\kappa_1 \vec{D} \cdot \vec{D} \quad (3.6.14)$$

where $\vec{D} = \vec{r}$ and

$$\kappa_1 = \frac{-5V_1}{AR^2}. \quad (3.6.15)$$

⁷³Kobayashi et al. (1989).

$V_1 = 25$ MeV being the symmetry potential energy. The dispersion relation is⁷⁴

$$W(E) = \sum_{k,i} \frac{2(\epsilon_k - \epsilon_i)|\langle i|F|k\rangle|^2}{(\epsilon_k - \epsilon_i)^2 - E^2} = \frac{1}{\kappa_1}. \quad (3.6.16)$$

Making use of this relation and of the fact that (see Fig. 2.10.1) $\epsilon_{\nu_k} - \epsilon_{\nu_i} = \tilde{\epsilon}_{p_{1/2}} - \tilde{\epsilon}_{s_{1/2}} \approx 0.45$ MeV, and that the EWSR associated with the ^{11}Li pygmy resonance is $\approx 8\%$ of the total Thomas–Reiche–Kuhn sum rule⁷⁵

$$\sum_n |\langle 0|F|n\rangle|^2 (E_n - E_0) = \frac{\hbar^2}{2M} \int d\mathbf{r} |\vec{\nabla} F|^2 \rho(r), \quad (3.6.17)$$

which, for $F = r$ has the value $\hbar^2 A / 2M$ one can write⁷⁶,

$$2 \times 0.08 \times \frac{\hbar^2 A}{2M} = \frac{1}{\kappa_1} [(0.45 \text{ MeV})^2 - (\hbar\omega_{pygmy})^2], \quad (3.6.18)$$

and thus

$$(\hbar\omega_{pygmy})^2 = (0.45 \text{ MeV})^2 - 2 \times 0.08 \times \frac{\hbar^2 A}{2M} \kappa_1, \quad (3.6.19)$$

where⁷⁷

$$\kappa_1 = -\frac{5V_1}{A(\xi/2)^2} \left(\frac{2}{11} \right) = -\frac{125 \text{ MeV}}{A 100 \text{ fm}^2} \left(\frac{2}{11} \right) \approx -0.021 \text{ fm}^{-2} \text{ MeV}, \quad (3.6.20)$$

the ratio in parenthesis reflecting the fact that only 2 out of 11 nucleons, slosh back and forth in an extended configuration with little overlap with the other nucleons. The quantity,

$$\kappa_1^0 = -\frac{5V_1}{AR_{ef}^2(^{11}\text{Li})} \approx 0.49 \text{ MeV fm}^{-2}, \quad (3.6.21)$$

is the “standard” self consistent dipole strength⁷⁸. The screening factor $s = (\kappa_1/\kappa_1^0) = 0.043$ is very close in magnitude to the ratio $r (= 0.048$, Eq. (3.6.3)) and has a similar physical origin. It is of notice that $(V_1)_{scr} = sV_1 \approx 1$ MeV. Making use of (3.6.20) one obtains,

$$-2 \times 0.08 \frac{\hbar^2 A}{2M} \kappa_1 \approx 0.74 \text{ MeV}^2 \approx (0.86 \text{ MeV})^2. \quad (3.6.22)$$

Consequently

⁷⁴See (3.30) p.55 of Bortignon et al. (1998).

⁷⁵The Thomas–Reiche–Kuhn sum rule (Bohr and Mottelson (1975); Bortignon et al. (1998)) TRK = $\frac{9}{4\pi} \frac{\hbar^2 e^2}{2m} \frac{NZ}{A} = 14.8 \frac{NZ}{A} e^2 \text{ fm}^2 \text{ MeV}$ has a value of $32.3 e^2 \text{ MeV fm}^2$ for $^{11}\text{Li}_8$. Assuming a systematic behaviour, the centroid of the giant dipole resonance is expected at $\hbar\omega_D \approx 80/A^{1/3}$ MeV ≈ 36 MeV, leading to the ratio $32.3 e^2 \text{ MeV fm}^2/(36 \text{ MeV}) \approx 0.9e^2 \text{ fm}^2$. The $E1$ –single-particle (Weisskopf) unit can be written as (Bohr and Mottelson (1969) p. 389, Eq. (3C-38)) $B_W(E1) \approx ((1.2)^2/4\pi)(3/4)^2 A^{2/3} (e_{E1})^2 \text{ fm}^2 = 0.32(e_{E1})^2 \text{ fm}^2$, e_{E1} being the effective dipole charge equal to $(N/A)e = 0.73e$ for the eight neutrons of ^{11}Li , and $-(Z/A)e =$ for the protons. Making use of the average value one can write $\bar{B}_W(E1) \approx 0.1e^2 \text{ fm}^2$. Thus $8\% \text{TRK}/\bar{B}_W(E1) \approx 0.072/0.1 \approx 0.7$. In other words, about 1 single-particle unit is associated with the eventual γ -decay of the PDR of ^{11}Li .

⁷⁶cf. Bertsch and Broglia (2005) pag. 53.

⁷⁷see Bortignon et al. (1998).

⁷⁸cf. Bohr and Mottelson (1975).

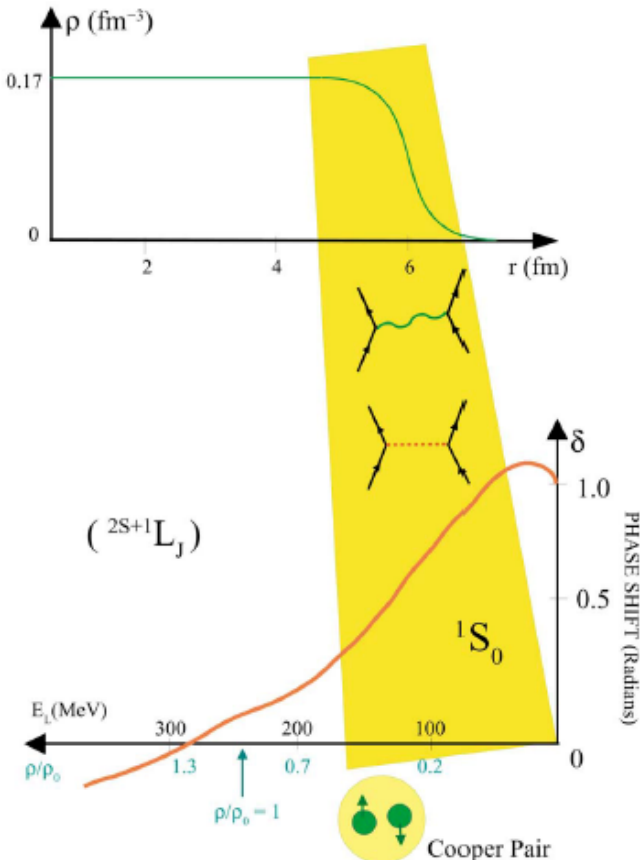


Figure 3.6.1: (top) Nuclear density ρ in units of fm^{-3} , plotted as a function of the distance r (in units of fm) from the centre of a nucleus lying along the stability valley (for comparison with a bound unstable nucleus lying at the neutron drip line see Fig. 4.3.2). Saturation density correspond to $\approx 0.17 \text{ fm}^{-3}$, equivalent to $2.8 \times 10^{14} \text{ g/cm}^3$ (after Bohr and Mottelson (1969)). Because of the short range of the nuclear force, the strong force, the nuclear density changes from 90% of saturation density to 10% within 0.65 fm, i.e. within the nuclear diffusivity. (bottom) Phase shift parameter associated with the elastic scattering of two nucleons moving in states of time reversal, so called 1S_0 phase shift, in keeping with the fact that the system is in a singlet state of spin zero. The solution of the Schrödinger equation describing the elastic scattering of a nucleon from a scattering centre (in this case another nucleon) is, at large distances from the scattering centre a superposition of the incoming wave and of the outgoing, scattering wave. The interaction of the incoming particle with the target particle changes only the amplitude of the outgoing wave. This amplitude can be written in terms of a real phase shift or scattering phase δ . Positive values of δ implies an attractive interaction, negative a repulsive one. For low relative velocities (kinetic energies E_L), i.e. around the nuclear surface where the density is low, the 1S_0 phase shift arizing from the exchange of mesons (e.g. pions, represented by an horizontal dotted line) between nucleons (represented by upward pointing arrowed lines) is attractive. This mechanism provides about half of the glue to nucleons moving in time reversal states to form Cooper pairs. These pairs behaves like quasi-bosons and eventually condense (Fig. 3.3.5) in a single quantal state leading to nuclear superfluidity. Cooper pair formation is further assisted by the exchange of collective surface vibrations (wavy curve in the scattering process) between the members of the pair (after Broglia (2002)).

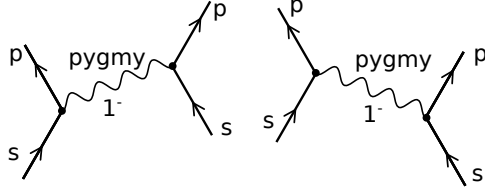


Figure 3.6.2: Diagrammatic representation of the exchange of a collective 1^- pygmy resonance between pairs of nucleons moving in the time-reversal configurations $s_{1/2}^2(0)$ and $p_{1/2}^2(0)$. It is of notice that both these configurations can act as initial states the figure showing only one of the two possibilities. Consequently, the energy denominator to be used in the simple estimate (3.6.25) is the average value $DEN = (DEN_1 + DEN_2)/2 = -\hbar\omega_{pygmy}$ where $DEN_1 = \Delta\epsilon - \hbar\omega_{pygmy}$ and $DEN_2 = -\Delta\epsilon - \hbar\omega_{pygmy}$, while $\Delta\epsilon = \epsilon_{s_{1/2}} - \epsilon_{p_{1/2}}$.

$$\hbar\omega_{pygmy} = \sqrt{(0.45)^2 + (0.86)^2} \text{ MeV} \approx 1 \text{ MeV}, \quad (3.6.23)$$

in overall agreement with the experimental findings⁷⁹. It is of notice that the centroid of the pygmy resonance calculated in RPA with the help of a separable dipole interaction is⁸⁰ $\approx (0.6 \text{ MeV} + 1.6 \text{ MeV})/2 \approx 1.1 \text{ MeV}$.

Let us now estimate the binding energy which the exchange of the pygmy resonance between the two neutrons of the halo Cooper pair of ^{11}Li can provide. The associated particle-vibration coupling⁸¹ is $\Lambda = \left(\partial W(E)/\partial E|_{\hbar\omega_{pygmy}}\right)^{-1/2}$. Note the use in what follows of a dimensionless dipole single-particle field $F' = F/R_{eff}(^{11}\text{Li})$. This is in keeping with the fact that one wants to obtain a quantity with energy dimensions ($[\Lambda] = \text{MeV}$), and that κ_1 has been introduced through the Hamiltonian H_D with the self consistent value normalized in terms of $R_{eff}^2(^{11}\text{Li})$ (Eq. (3.6.21)). One then obtains

$$\begin{aligned} \Lambda &= \left\{ 2\hbar\omega_{pygmy} \frac{2 \times 0.08(\frac{\hbar^2 A}{2M})/R_{eff}^2}{[(\tilde{\epsilon}_{p_{1/2}} - \tilde{\epsilon}_{s_{1/2}})^2 - (\hbar\omega_{pygmy})^2]^2} \right\}^{-1/2}, \\ &= \left\{ 2\text{MeV} \frac{0.16(\hbar^2 A/2M)(1/4.8)^2 \text{ fm}^2}{[(0.45 \text{ MeV})^2 - (1\text{MeV})^2]^2} \right\}^{-1/2}, \\ &= \left(\frac{3 \text{ MeV}^2}{(0.8)^2 \text{ MeV}^4} \right)^{-1/2} \approx 0.5 \text{ MeV}, \end{aligned} \quad (3.6.24)$$

The value of the induced interaction matrix elements is then given by (Fig. 3.6.2),

$$M_{ind} = \frac{2\Lambda^2}{DEN} \approx -\frac{2\Lambda^2}{\hbar\omega_{pygmy}} \approx -0.5 \text{ MeV}, \quad (3.6.25)$$

⁷⁹Zinser et al. (1997), Kanungo et al. (2015).

⁸⁰Barranco et al. (2001); in particular Fig. 2a where the doubled peaked ($\approx 0.6 \text{ MeV}$ and $\approx 1.6 \text{ MeV}$) $dB(E1)/dE$ strength function is displayed.

⁸¹cf. e.g. Brink and Broglia (2005) Eq. (8.42) p.189.

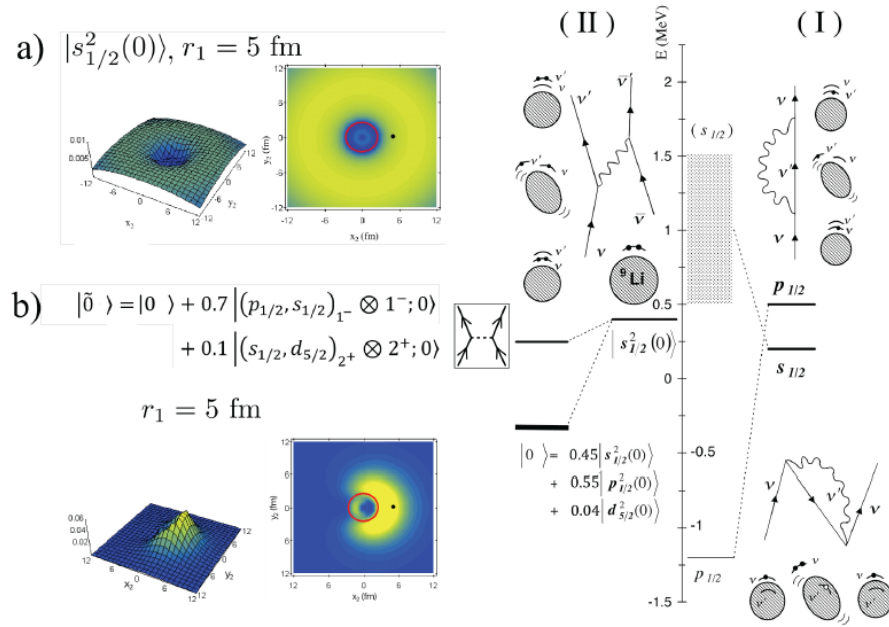


Figure 3.6.3: (Color online) In (I) and (II) the NFT processes renormalizing the single-particle motion (${}^{10}\text{Li}$) and leading to the effective interaction, sum of the bare (horizontal dotted lines) and induced (wavy curves) interactions which bind the two-neutron halo to the core of ${}^9\text{Li}$ thus leading to the $|{}^{11}\text{Li}\rangle$ ground state are displayed. In a) and b) are also displayed the spatial structure of the pure $|s_{1/2}^2(0)\rangle$ configuration and that of the two-neutron halo $|\tilde{0}\rangle$ Cooper pair. The modulus squared wave function $|\Psi_0(\mathbf{r}_1, \mathbf{r}_2)|^2 = |\langle \mathbf{r}_1, \mathbf{r}_1 | 0^+ \rangle|^2$ describing the motion of the two halo neutrons around the ${}^9\text{Li}$ core is shown as a function of the cartesian coordinates of particle 2, for fixed values of the position of particle 1 ($r_1 = 5$ fm) represented by a solid dot, while the core ${}^9\text{Li}$ is shown as a red circle. The numbers appearing on the z -axis of the three-dimensional plots displayed on the left side of the figure are in units of fm^{-2} . After Barranco et al. (2001).

the factor of two arising from the two time ordering contributions. The resulting correlation energy is thus $E_{corr} = 2\tilde{\epsilon}_{s_{1/2}} - G_{scr} + M_{ind} = (0.3 - 0.1 - 0.5) \text{ MeV} \approx -0.3 \text{ MeV}$, in overall agreement with the experimental⁸² findings (-0.380 MeV). It is of notice that in this estimate the (subcritical) effect of the screened bare pairing interaction has also been used (see Eq. (3.6.4))⁸³ Also the theoretical value $\tilde{\epsilon}_{1/2} = 0.15 \text{ MeV}$ (Fig. 2.10.1).

This schematic model⁸⁴ has been implemented with microscopic detail⁸⁵ within the framework of a field theoretical description of the interweaving of collective vibrations and single-particle motion, and is also discussed within the context of single-particle (Chapter 5) and two-particle (Chapter 7) transfer processes. Here we provide a summary of the theoretical findings.

In Fig. 3.6.3 (I), the lowest single-particle neutron virtual and resonant states of ^{10}Li are indicated⁸⁶. The position of the levels $s_{1/2}$ and $p_{1/2}$ determined making use of mean-field theory is shown (left hatched area and thin horizontal line, respectively). The coupling of a single-neutron (upward pointing arrowed line) to a vibration (wavy line) calculated making use of NFT Feynman diagrams (schematically depicted also in terms of either solid dots (neutron) or open circles (neutron hole) moving in a single-particle level around or in the ^9Li core (grey circle)), leads to conspicuous shifts in the energy centroid of the $s_{1/2}$ and $p_{1/2}$ resonances (shown by thick horizontal lines to the right) and eventually to an inversion in their sequence. In Fig. 3.6.3 (II) the processes binding the halo neutron system ^{11}Li are displayed (see also Fig. 2.10.1).

One starts with the dressed mean field picture in which two neutrons (solid dots) coupled to angular momentum zero move in time-reversal states around the core ^9Li (hatched area) in the $s_{1/2}$ virtual state leading to an unbound $s_{1/2}^2(0)$ configuration. The associated spatial structure of the uncorrelated pair is shown in **a**). The exchange of vibrations between the two neutrons displayed in the upper part of the figure leads to a density-dependent interaction which, added to the nucleon-nucleon bare interaction (see boxed inset) which, as can be seen from the figure, is subcritical, correlates the two-neutron system leading to a bound state $|\tilde{0}\rangle$ whose wavefunction is displayed in **b**), together with the spatial structure of the resulting Cooper pair. It is of notice that a large fraction of the induced interaction arises from the exchange of the pygmy resonance (see Fig. 3.6.2) between the two halo neutrons. Within this scenario one can posit that the ^{11}Li dipole pygmy resonance can hardly be viewed but in symbiosis with the ^9Li halo neutron pair addition mode and vice versa. Furthermore, that the two halo neutrons of ^{11}Li , provide the first

⁸²C. Bachelet et al. (2008), Smith et al. (2008).

⁸³That new physics, namely a novel mechanism to (dynamically) violate gauge invariance finds, to express itself, a scenario of a barely bound Cooper pair at the drip line (half life 8.75 ms), seems to confirm a recurrent expectation. That truly new complex phenomena appear at the border between rigid order and randomness (see De Gennes (1994)).

⁸⁴See also Broglia et al. (2019b).

⁸⁵cf. Barranco et al. (2001); see also Potel et al. (2010).

⁸⁶See also Cavallaro et al. (2017), Barranco et al. (2020), Moro et al. (2019).

example of a Van der Waals Cooper pair, the first of its type in nuclei (App. 3.A and Fig. 3.A.1). For further details see Chapter 7 as well as⁸⁷.

Let us conclude this Section by stating that the detailed consequences of the diagonalization of self-energy processes and of the bare and induced interactions tantamount to the diagonalization of the many-body Hamiltonian, provides in the case of ¹⁰Li an example of minimal mean field description (App. 5.A) and, in the case of ¹¹Li, an example of the fact that pairs of dressed single-particle states lead to abnormal density (induced pairing interaction), also in the case of closed shell systems, due to the strong ZPF associated with pairing vibrations (see also discussion around Eq. (3.2.2)). In keeping with the fact that ⁹Li is a normal, bound nucleus, while ¹⁰Li is not bound testifies to the fact that the binding of two neutrons to the ⁹Li core leading to ¹¹Li ground state ($S_{2n} \approx 380$ keV), is a pairing phenomenon.

Appendix 3.A Nuclear van der Waals Cooper pair

The atomic van der Waals (dispersive; retarded) interaction which, like gravitation, acts between all atoms and molecules, also non-polar, can be written for two systems placed at a distance R as (see App. 3.D),

$$\Delta E = -\frac{6 \times e^2 \times a_0^5}{R^6} = -\frac{6 \times e^2}{(R/a_0)^6} \frac{1}{a_0}, \quad (3.A.1)$$

where a_0 is the Bohr radius. A possible nuclear parallel can be established making the following correspondences (see also Fig. 3.A.1),

$$e^2 \rightarrow \Lambda R_0(^{11}\text{Li}) = 0.5 \text{ MeV} \times 2.7 \text{ fm}; \quad a_0 \rightarrow d = 4 \text{ fm}; \quad R \rightarrow R_{eff}(^{11}\text{Li}) = 4.8 \text{ fm}.$$

That is,

$$\begin{aligned} \Delta E &= -\frac{6 \times \Lambda \times R_0}{R^6} = -\frac{6}{(R_{eff}(^{11}\text{Li})/d)^6} \frac{1}{d} = \frac{6 \times 0.5 \text{ MeV} \times 2.7 \text{ fm}}{(4.8/4)^6} \frac{1}{4 \text{ fm}} \\ &\approx -0.7 \text{ MeV} \rightarrow M_{ind}. \end{aligned}$$

Thus,

$$E_{corr} = 2\tilde{\epsilon}_{s_{1/2}} - G_{scr} + \Delta E = 0.3 \text{ MeV} - 0.1 \text{ MeV} - 0.7 \text{ MeV} \approx -0.5,$$

its absolute value to be compared to neutron separation energy,

$$(S_{2n})_{exp} \approx 0.380 \text{ MeV}.$$

⁸⁷Barranco et al. (2001).

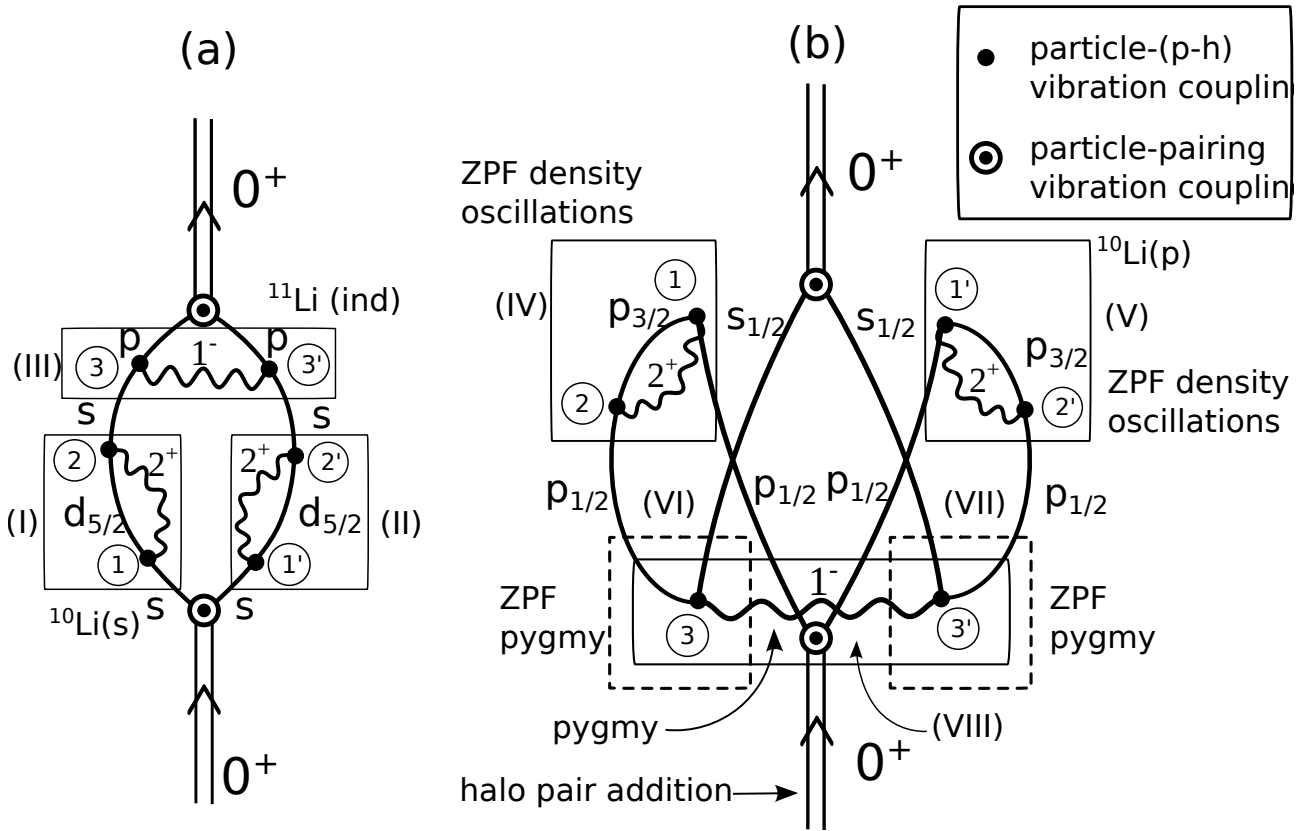


Figure 3.A.1: NFT Feynman diagrams describing the binding of the halo Cooper pair through pygmy. That is, producing the symbiotic mode involving the pair addition mode and the PDR. The single-particle states $s_{1/2}$ and $p_{1/2}$ are labeled in (a) s and p for simplicity. The different particle–vibration coupling vertices (either with the quadrupole (2^+) or with the pygmy (1^-) modes drawn as solid wavy lines) are denoted by a solid dot, and numbered in increasing time sequence so as to show that diagram (b) emerges from (a) through time ordering. The motion of the neutrons are drawn in terms of continuous solid curves. In keeping with the fact that the occupation of the single-particle states is neither 1 nor 0 (see Figs. 2.10.1, 4.C.1 as well as Eqs. (7.1.1)–(7.1.3)), these states are treated as quasiparticle states. Thus no arrow is drawn on them. Diagram (a) emphasizes the self-energy renormalization of the state $s_{1/2}$ lying in the continuum and which through its clothing with the quadrupole mode is brought down becoming a virtual ($\epsilon_{s_{1/2}} = 0.2$ MeV) state (see (I) and (II)), while (III) contributes to the induced pairing interaction through pygmy (see also Fig. 3.6.2). The “eagle” diagram (b) contains ((IV) and (V)) Pauli corrections which push the bound state $p_{1/2}$ into a resonant state in the continuum ($\epsilon_{p_{1/2}} = 0.5$ MeV). In other words, processes (I), (II), (III), (IV) and (V) are at the basis of parity inversion, and of the appearance of the new magic number $N = 6$. Processes (VI) and (VII) are associated with the pygmy ZPF, while (VIII) contributes to the induced pairing interaction through pygmy (van der Waals–like process).

Appendix 3.B Renormalized coupling constants ^{11}Li : résumé

Let us make use of the values,

$$\begin{aligned}\tilde{\epsilon}_{s_{1/2}} &= 0.15 \text{ MeV}, \\ \tilde{\epsilon}_{p_{1/2}} &= 0.60 \text{ MeV}, \\ V_1 &= 25 \text{ MeV},\end{aligned}\quad (3.B.1)$$

and

$$R_0(^{11}\text{Li}) = 1.2(11)^{1/3} \text{ fm} = 2.7 \text{ fm}, \quad (3.B.2)$$

$$\xi = 20 \text{ fm}, \quad (3.B.3)$$

$$R(^{11}\text{Li}) = 4.6 \text{ fm}, \quad (3.B.4)$$

$$G = \frac{25}{A} \text{ MeV} = 2.3 \text{ MeV}, \quad (3.B.5)$$

$$\kappa_1^0 = -\frac{5V_1}{AR_{eff}^2(^{11}\text{Li})} \approx -0.49 \text{ MeV fm}^{-2}, \quad (3.B.6)$$

$$\kappa_1 = -\frac{5V_1}{A(\xi/2)^2} \left(\frac{2}{11} \right) = -0.021 \text{ MeV fm}^{-2}, \quad (3.B.7)$$

One can then calculate the ratio

$$r = \frac{2}{(2j+1)} \left(\frac{R_0}{R} \right)^3 \approx 0.048, \quad (3.B.8)$$

where use was made of $(2j+1) \approx (2k_F R_0 + 1) \approx 8.34$. Thus, the screened bare pairing interaction is,

$$G_{scr} = r \times G = 0.048 \times \frac{25}{A} \text{ MeV} = \frac{1 \text{ MeV}}{A} \approx 0.1 \text{ MeV}. \quad (3.B.9)$$

Similarly

$$\kappa_1 = s \kappa_1^0, \quad (3.B.10)$$

where the screening factor is

$$s = \frac{R_{eff}^2}{(\xi/2)^2} \frac{2}{11} \approx 0.042. \quad (3.B.11)$$

Thus, the screened symmetry potential becomes,

$$(V_1)_{scr} = s V_1 = 0.042 \times 25 \text{ MeV} \approx 1 \text{ MeV}. \quad (3.B.12)$$

The fact that r and s coincide within numerical approximations is in keeping with the fact that both quantities are closely related to the overlap⁸⁸

$$O = \left(\frac{R_0}{R} \right)^3 = \left(\frac{2.7 \text{ fm}}{4.6 \text{ fm}} \right)^3 = 0.2, \quad (3.B.13)$$

quantity which has a double hit effect concerning the mechanism which is at the basis of much of the nuclear structure of exotic nuclei at threshold: **1)** it makes subcritical the screened bare NN -pairing interaction $G_{scr} = r \times G < G_c$ ($G_{scr} = 1 \text{ MeV}/A$); **2)** it screens the symmetry potential drastically, reducing the price one has to pay to separate protons from delocalized neutrons, permitting a consistent chunk ($\approx 8\%$) of the TRK sum rule⁸⁹ to become essentially degenerate with the ground state ($(V_1)_{scr} = 1 \text{ MeV}$). In other words, allowing for, allegedly, the first nuclear example of a van der Waals Cooper pair and a novel mechanism to break dynamically gauge invariance. Namely, dipole-dipole fluctuating fields associated with the exchange of the pygmy dipole resonance between the halo neutrons of ^{11}Li . As a result, a new, (composite) elementary mode of nuclear excitation joins the ranks of the previously known: the halo pair addition mode carrying on top of it, a low-lying collective pygmy resonance. This symbiotic mode can be studied through two-particle transfer reactions, eventually in coincidence with γ -decay. In particular, making use of the reaction $^9\text{Li}(t, p)^{11}\text{Li}(f)$ for

$|f\rangle$: ground state ($L = 0$) and pygmy ($L = 1; E_x \approx 1 \text{ MeV}$).

Similar, but in this case $^{10}\text{Be}(t, p)^{12}\text{Be}(f)$ for

$|f\rangle$: first excited 0^+ state ($E_x = 2.24 \text{ MeV}$),

as well as pygmy ($L = 1$) on top of it, arguably the 1^- state at $E_x = 2.70 \text{ MeV}$ being part of this mode⁹⁰.

Appendix 3.C Lindemann criterion and connection with quantity parameter

The original Lindemann criterion⁹¹ compares the atomic fluctuation amplitude $\langle \Delta r^2 \rangle^{1/2}$ with the lattice constant a of a crystal. If this ratio, which is defined as the disorder parameter Δ_L , reaches a certain value, fluctuations cannot increase without damaging or destroying the crystal lattice. The results of experiments and simulations show that the critical value of Δ_L for simple solids is in the range of 0.10 to 0.15, relatively independent of the type of substance, the nature of the interaction potential, and the crystal structure⁹². Applications of this criterion to an

⁸⁸One can equivalently use $(R_0/R_{eff})^3 \approx (2.7 \text{ fm}/(4.8 \text{ fm}))^3 \approx 0.18$.

⁸⁹Zinser et al. (1997), T. Nakamura et al. (2006), Shimoura et al. (1995), Ieki et al. (1993), Sackett et al. (1993), Kanungo et al. (2015), Kobayashi et al. (1989).

⁹⁰Iwasaki et al. (2000).

⁹¹Lindemann (1910).

⁹²Bilgram (1987); Löwen (1994); Stillinger (1995).

inhomogeneous finite system like a protein in its native state (aperiodic crystal)⁹³, requires evaluation of the generalized Lindemann parameter⁹⁴

$$\Delta_L = \frac{\sqrt{\sum_i \langle \Delta r_i^2 \rangle / N}}{a'}, \quad (3.C.1)$$

where N is the number of atoms and a' the most probable non-bonded near-neighbor distance, \mathbf{r}_i is the position of atom i , $\Delta r_i^2 = (\mathbf{r}_i - \langle \mathbf{r}_i \rangle)^2$, and $\langle \rangle$ denotes configurational averages at the conditions of measurement or simulations (e.g. biological, in which case $T \approx 310$ K, $\text{PH} \approx 7$, etc.⁹⁵). The dynamics as a function of the distance from the geometric center of the protein is characterized by defining an interior (*int*) Lindemann parameter,

$$\Delta_L^{int}(r_{cut}) = \frac{\sqrt{\sum_{i, r_i < r_{cut}} \langle \Delta r_i^2 \rangle / N}}{a'}, \quad (3.C.2)$$

which is obtained by averaging over the atoms that are within a chosen cutoff distance, r_{cut} , from the center of mass of the protein.

Simulations and experimental data for a number of proteins, in particular Barnase, Myoglobin, Crambin and Ribonuclease A indicate 0.14 as the critical value distinguishing between solid-like and liquid-like behaviour, and $r_{cut} \approx 6$ Å. As can be seen from Table 3.C.1, the interior of a protein, under physiological conditions, is solid-like ($\Delta_L < 0.14$), while its surface is liquid-like ($\Delta_L > 0.14$). The beginning of thermal denaturation in the simulations appears to be related to the melting of its interior (i.e. $\Delta_L^{int} > 0.14$), so that the entire protein becomes liquid-like. This is also the situation of the denatured state of a protein under physiological conditions⁹⁶

	$\Delta_L(\Delta_L^{int}(6 \text{ \AA}))(300 \text{ K})$			
	MD simulations		X-ray data	
Proteins	Barnase	Myoglobin	Crambin	Ribonuclease A
all atoms	0.21(0.12)	0.16(0.11)	0.16(0.09)	0.16(0.12)
backbone atoms only	0.16(0.10)	0.12(0.09)	0.12(0.08)	0.13(0.10)
side-chain atoms only	0.25(0.14)	0.18(0.12)	0.19(0.10)	0.19(0.13)

Table 3.C.1: The heavy-atom $\Delta_L(\Delta_L^{int})$ value, for four proteins at 300 K. After Zhou et al. (1999).

⁹³Schrödinger (1944).

⁹⁴Stillinger and Stillinger (1990).

⁹⁵Fluctuations, classical (thermal) or quantal imply a probabilistic description. While one can only predict the odds for a given outcome of an experiment in quantum mechanics, probabilities themselves evolve in a deterministic fashion Born (1948).

⁹⁶see e.g. Rösner et al. (2017).

3.C.1 Lindemann (“disorder”) parameter for a nucleus

An estimate of $\sqrt{\sum_i \langle \Delta r_i^2 \rangle / A}$ in the case of nuclei considered as a sphere of nuclear matter of radius R_0 , is provided by the “spill out” of nucleons due to quantal effects. That is⁹⁷ $\sqrt{ } \approx 0.69 \times a_0$, where a_0 is of the order of the range of nuclear forces (≈ 0.9 fm).

The average internucleon distance can be determined from the relation⁹⁸

$$\left(\frac{V}{A}\right)^{1/3} = \left(\frac{\frac{4\pi}{3}R^3}{A}\right)^{1/3} = \left(\frac{4\pi}{3}\right)^{1/3} \times 1.2 \text{ fm} \approx 2 \text{ fm} \quad (3.C.3)$$

Which gives the radius of the sphere associated with each nucleon in the nucleus. Thus, $a' \approx 4$ fm, and

$$\Delta_L = \frac{0.69a_0}{4 \text{ fm}} \approx 0.16. \quad (3.C.4)$$

While it is difficult to compare among them crystals, aperiodic finite crystals and atomic nuclei, arguably, the above value indicates that a nucleus is liquid-like. More precisely, it is made out of a non-Newtonian fluid, which reacts elastically to sudden solicitations ($\lesssim 10^{-22}$ s), and plastically to long lasting strain ($\gtrsim 10^{-21}$ s). In any case, one expects from $\Delta_L \approx 0.16$ that the nucleon mean free path is long, larger than nuclear dimensions, as also indicated by the quantality parameter (see Sect. 3.3).

Appendix 3.D The van der Waals interaction

Historically one can distinguish two contributions to the van der Waals interaction⁹⁹:

1. **dispersive** retarded contribution¹⁰⁰, emerging from the dynamical dipole-dipole, as well as from higher multipolarities, interaction associated with the quantum mechanical zero point fluctuations (ZPF) of the ground state of the two interacting atoms or molecules associated with the dipole excitations of the systems¹⁰¹
2. **inductive** implying the polarization of one molecule in the permanent dipole or quadrupole field of the other molecule¹⁰²

⁹⁷Bertsch and Broglia (2005), see e.g. Ch. 5.

⁹⁸Brink and Broglia (2005), App. C.

⁹⁹Let us mainly think of non polar (NP) molecules.

¹⁰⁰dispersion: variation of a quantity, e.g. spatial separation of white light (rainbow), as a function of frequency (c.f. e.g. Israelachvili (1985), p.65).

¹⁰¹These forces act between all atoms and molecules, even non-polar, totally neutral ones as hydrogen or helium (noble gas).

¹⁰²Debye (1920, 1921).

It is only the first one which is a *bona fide* van der Waals interaction. In fact with the advent of quantum mechanics it was very early recognized¹⁰³ that for most molecules, interactions of type 2 are small compared with interactions of type 1. That is the interaction corresponding to the mutual polarization of one molecule in the rapidly changing field –due to the instantaneous configuration of electrons and nuclei– of the other molecule¹⁰⁴.

In connection with theories of systems with many degrees of freedom (i.e. fields– and (many–body)–systems) developed in particular by Anderson, Nambu and Goldstone, it has been recognized that the phenomenon of spontaneous symmetry breaking is at the basis of physical emergent properties (see App. 3.E).

Within the present context, an atom violates translational invariance as its center of mass (CM) occupies a definite position in space defining a privileged origin for a reference frame. Setting both ions and electrons in uniform motion through a Galilean transformation restores symmetry, the inertia being the total mass (App. 2.C). Thus, when one pushes the system on one end it starts moving as a rigid body (generalized rigidity), without the need of propagation of information through it.

Such a motion (isoscalar in the case of the atomic nuclei, where N and Z move in phase, equivalent to electrons and ions doing so in the case of condensed or soft matter) display zero restoring force. Thus, the associated ZPF diverge requiring, quantum mechanically, a state orthogonal to it in which the two types of constituents particles (electrons and ions, neutrons and protons), move out of phase. Such a state is, in the nuclear case¹⁰⁵ the GDR and corresponds to a mode in which protons and neutrons slosh back and forth out of phase (isovector mode), a situation which is similar to that of atomic clusters (Mie resonance). In the atomic or molecular case these states (dipole vibration of electrons against the positive ions) are rather directly related to the single-electron atomic shell physics ($1s \rightarrow 2p$ transition in the case of the H atom). Two atoms displaying the above ZPF will interact through van der Waals (dispersive, retarded) interaction.

3.D.1 van der Waals interaction between two hydrogen atoms

For large values of the internuclear distance $r_{AB} = R$, the exchange phenomenon is unimportant (Pauli principle) and one can take as the unperturbed wavefunction for a system of two hydrogen atoms (Fig. 3.D.1) the simple product of two hydrogenlike wavefunctions,

$$\Psi^0 = u_{1sA}(1)u_{1sB}(2). \quad (3.D.1)$$

The perturbation for this wavefunction arises from the potential energy terms

$$H' = \frac{e^2}{r_{12}} + \frac{e^2}{r_{AB}} - \frac{e^2}{r_{A2}} - \frac{e^2}{r_{B1}}, \quad (3.D.2)$$

¹⁰³London (1930).

¹⁰⁴Pauling and Wilson Jr. (1963) p. 384, Born (1969) p. 471.

¹⁰⁵Note however the pygmy halo resonance, soft $E1$ -mode in the neutron halo nuclei like ^{11}Li , which essentially forces a permanent dipole in the $|^{11}\text{Li}(\text{gs})\rangle$.

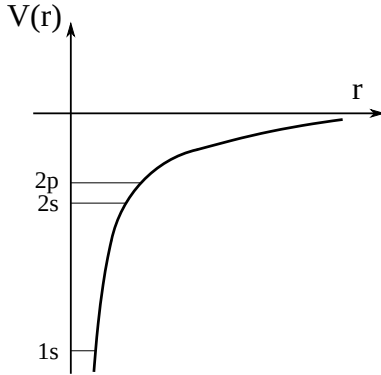


Figure 3.D.1: Schematic representation of the lowest single-particle levels in which the electron can move in a hydrogen atom.

corresponding to the variety of Coulomb interactions involving electrons and protons. Let us assume for simplicity that we are dealing with a one-dimensional problem, in which case one can write (Fig. 3.D.2)

$$\begin{aligned} \mathbf{r}_{12} &= (R + z_1 + z_2) \hat{z}, \\ \mathbf{r}_{AB} &= R \hat{z}, \\ \mathbf{r}_{A2} &= (R + z_2) \hat{z}, \\ \mathbf{r}_{B1} &= (R + z_1) \hat{z}. \end{aligned} \quad (3.D.3)$$

Because all these distances are much larger than the radius of the atom ($a_0 \approx 0.529 \text{ \AA}$, Bohr radius) the expression (3.D.2) can be calculated making use of a Taylor expansion, and diagonalize it with the help of perturbation theory. One obtains

$$r_{12}^2 = (R + z_1 + z_2)^2 = R^2 \left[1 + 2 \frac{(z_1 + z_2)}{R} + \frac{(z_1 + z_2)^2}{R^2} \right], \quad (3.D.4)$$

which leads to

$$\frac{e^2}{r_{12}^2} = \frac{e^2}{R \left[1 + \frac{2(z_1 + z_2)}{R} + \frac{(z_1 + z_2)^2}{R^2} \right]^{1/2}} \approx \frac{e^2}{R} \left[1 - \frac{(z_1 + z_2)}{R} - \frac{(z_1 + z_2)^2}{2R^2} \right]. \quad (3.D.5)$$

Similarly

$$r_{A2}^2 = (R^2 + 2Rz_2 + z_2^2) = R^2 \left(1 + 2 \frac{z_2}{R} + \frac{z_2^2}{R^2} \right), \quad (3.D.6)$$

and

$$r_{B1}^2 = R^2 \left(1 + 2 \frac{z_1}{R} + \frac{z_1^2}{R^2} \right), \quad (3.D.7)$$

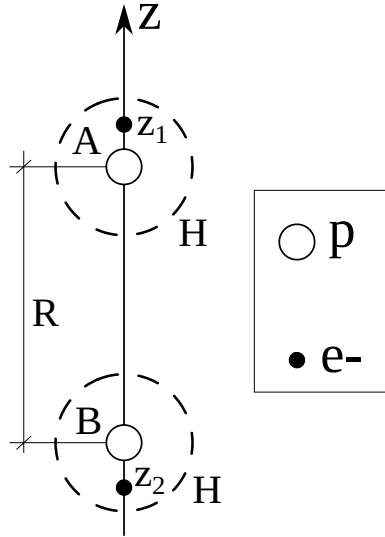


Figure 3.D.2: Planar configuration assumed for two hydrogen atoms at a relative distance R .

leading to

$$-\frac{e^2}{r_{A2}} = -\frac{e^2}{R} \left(1 - \frac{z_2}{R} - \frac{z_2^2}{2R^2} \right), \quad (3.D.8)$$

and

$$-\frac{e^2}{r_{B1}} = -\frac{e^2}{R} \left(1 - \frac{z_1}{R} - \frac{z_1^2}{2R^2} \right). \quad (3.D.9)$$

Finally

$$\frac{e^2}{r_{AB}} = \frac{e^2}{R}. \quad (3.D.10)$$

With the exception of the cross term of (3.D.2) there is complete cancellation between the different contributions to (3.D.2)–(3.D.5). Thus

$$H' = -\frac{\mathbf{D}_1 \cdot \mathbf{D}_2}{R^3}, \quad (3.D.11)$$

where

$$\mathbf{D}_i = e z_i \hat{z} \quad (3.D.12)$$

is the dipole moment operator associated with electron i . Because $R \gg z_i$, one can diagonalize the interaction Hamiltonian (3.D.11) perturbatively. In keeping with the fact that a single-particle quantum state displaying a given parity (and in

the present case angular momentum $(-1)^\ell = \pi$) cannot sustain a permanent dipole moment, in particular

$$\int d\tau u_{1s}(z) z u_{1s}(z) = \int d\tau (u_{1s}(z))^2 z = \int d\tau \rho(z) z = 0, \quad (3.D.13)$$

the lowest perturbative correction to (3.D.1) is of second order. This is in keeping with the fact that we are dealing with interaction through virtual processes. The associated energy correction is given by the relation,

$$\Delta E_z^{(2)} = - \sum_{int} \frac{\langle 0 | H' | int \rangle \langle int | H' | 0 \rangle}{E_{int} - E_0}. \quad (3.D.14)$$

Because we are concerned with the $1s \rightarrow 2p$ transition (Fig. 3.D.3),

$$\Psi^{int} = u_{2pA}(1)u_{2pB}(2), \quad (3.D.15)$$

and thus

$$D_{en} = E_{int} - E_0 = \frac{e^2}{2a_0} = 1 \text{ Ry} = 13.606 \text{ eV}. \quad (3.D.16)$$

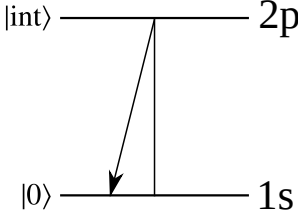


Figure 3.D.3: Schematic representation of the virtual processes associated with (3.D.14).

One can then write

$$\begin{aligned} \Delta E_z^{(2)} &= - \frac{|\langle 0 | H' | 0 \rangle|^2}{D_{en}} = - \frac{e^4}{R^6} \frac{|\langle 0 | z_1^2 z_2^2 | 0 \rangle|^2}{D_{en}}, \\ &= - \frac{e^4}{R^6} \frac{\int d\tau_1 d\tau_2 u_{1s}^2(1) u_{1s}^2(2) z_1^2 z_2^2}{D_{en}}, \\ &= - \frac{e^4}{R^6} \frac{\int d\tau_1 \rho(z_1) z_1^2 \int d\tau_2 \rho(z_2) z_2^2}{D_{en}}, \\ &= - \frac{e^4}{R^6} \frac{\bar{z}_1^2 \bar{z}_2^2}{D_{en}} = - \frac{e^4}{R^6} \frac{a_0^2 a_0^2}{\frac{e^2}{2a_0}} = - \frac{2e^2 a_0^5}{R^6}. \end{aligned} \quad (3.D.17)$$

This result corresponds to the z -degree of freedom of the system (two H atoms at a distance $R \gg a_0$). One has thus to multiply the above result by 3 to take into account the x and y degrees of freedom. Thus

$$\Delta E^{(2)} = - \frac{6e^2 a_0^5}{R^6}. \quad (3.D.18)$$

Let us now calculate the van der Waals interaction between two H-atoms at a distance of the order of ten times the summed radii of the two atoms ($\approx 2a_0 \approx 1\text{\AA}$), that is for $R \approx 10\text{\AA}$,

$$\begin{aligned}\Delta E_{H-H}^{(2)}(10\text{\AA}) &\approx -\frac{6 \times 14.4 \text{ eV \AA}(0.529 \text{ \AA})^5}{(10 \text{ \AA})^6} \\ &\approx -3.6 \times 10^{-6} \text{ eV} = -3.6 \mu\text{eV}\end{aligned}\quad (3.D.19)$$

Making use of the relation

$$1 \text{ eV} = 2.42 \times 10^{14} \text{ Hz}, \quad (1\text{Hz}=\text{s}^{-1}) \quad (3.D.20)$$

one obtains

$$|\Delta E_{H-H}^{(2)}(10 \text{ \AA})| \approx 3.6 \times 10^{-6} \times 2.42 \times 10^{14} \text{ Hz} \approx 9 \times 10^8 \text{ Hz} \approx 10^3 \text{ MHz}, \quad (3.D.21)$$

a quantity which can be compared with the Lamb shift (1058 MHz, Fig. 5.D.1; see also Fig. 7.2.1). It is of notice that $|\Delta E_{H-H}^{(2)}(2.5 \text{ \AA})| \approx 15 \text{ meV/part} \approx 0.35 \text{ kcal/mole}$, ($1\text{meV/part} \approx 0.02306 \text{ kcal/mole}$), a value of the order of $kT/2$. That is, one half of the thermal energy under biological conditions ($T \approx 300 \text{ K}$, $kT \approx 0.6 \text{ kcal/mole}$)¹⁰⁶.

3.D.2 Critical dimension for van der Waals H-H interaction (protein folding domain)

Let us calculate the frequency associated with the $1s \rightarrow 2p$ transition (=1 Ry=13.6 eV),

$$\hbar\omega_e = 13.6 \text{ eV}. \quad (3.D.22)$$

Making use of

$$\hbar c = 2000 \text{ eV \AA}, \quad (3.D.23)$$

one can write

$$\omega_e = \frac{13.6 \text{ eV}}{\hbar c} c \approx 10^{-2} \text{ \AA}^{-1} c. \quad (3.D.24)$$

Now, the exchange of “information” between the ZPF of the two H-atoms must be faster than the electronic revolution period, namely (Fig. 3.D.4)

$$\frac{2R}{c} \lesssim \frac{1}{\omega_e}. \quad (3.D.25)$$

Leading to $R < 50 \text{ fm}$.

¹⁰⁶Huang (2005).

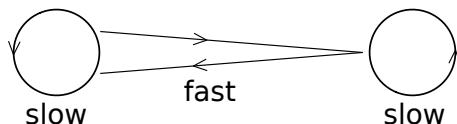


Figure 3.D.4: Schematic representation of the periodic motion associated with the hydrogen atom and the retarded van der Waals interaction.

Otherwise the frequencies of the two periodic motions (ZPF based dipole-dipole interaction and orbiting of electron around proton) would be similar and strong coupling between them would take place. In other words, there would be a strong damping of the retarded, dispersive contribution to the van der Waals interaction.

In keeping with the fact that the linear dimensions of an amino acid are, in average, 0.36 nm, the typical distance between two residues in a protein in its native state is thus $\approx 10 \text{ \AA}$. One would then expect that the maximum number of amino acids of globular protein or of a folding domain, to be of the order of $(50 \text{ \AA}/10 \text{ \AA})^3 \approx 125$, as empirically observed¹⁰⁷.

3.D.3 van der Waals between two amino acids

All of the commonly occurring amino acids in proteins have a central carbon atom (C_α) to which are attached a hydrogen atom, an amino group (NH_2), and a carboxy (COOH) (Fig. 3.D.5). What distinguishes one amino acid from another is the side chain attached to the C_α through its fourth valency. There are 20 different side chains specified by the genetic code. Amino acids are joined end to end during protein synthesis by the formation of peptide bonds. The carboxy group of the first amino acid condenses with the amino group of the next to eliminate water, thus the name residue, and yield a peptide bond.

The van der Waals interaction between two amino acids is,

$$\Delta E^{(2)} = -\frac{6Z^2 e^2 (a_0)^5}{R^6} \quad (3.D.26)$$

where Z is the number of protons of the molecule.

3.D.4 Average interaction between two side chains

Typical dimension of an amino acid is 0.36 nm ($=3.6 \text{ \AA}$). Let us then estimate the average van der Waals interaction of two residues at $R = 8 \text{ \AA}$. For this purpose use

¹⁰⁷Rost (1997).

is made of $30 \leq Z \leq 35$. One can then write,

$$\begin{aligned}\Delta E_{aa}^{(2)} &= -\frac{6 \times Z^2 \times 14.4 \text{ eV } \text{\AA}(0.529 \text{ \AA})^5}{(8 \text{ \AA})^6} \\ &= \begin{cases} -12.3 \frac{\text{meV}}{\text{part}} = -0.28 \frac{\text{kcal}}{\text{mole}}, \\ -16.7 \frac{\text{meV}}{\text{part}} = -0.38 \frac{\text{kcal}}{\text{mole}}, \end{cases} \quad (3.D.27)\end{aligned}$$

Thus

$$\overline{\Delta E_{aa}^{(2)}}(8 \text{ \AA}) \approx -0.33 \frac{\text{kcal}}{\text{mole}}, \quad (3.D.28)$$

a quantity to be compared to $kT = 0.6 \text{ kcal/mole}$.

Summing up, the van der Waals interaction between amino acids is weak, of the order of $kT/2 (\approx 0.3 \text{ kcal/mole})$, with a range $\lesssim 0.5 \text{ nm}$, and non-directional.

Hindsight

The van der Waals interaction is closely related to the restoration of spontaneous symmetry breaking of translational invariance (center of mass of finite systems like atoms and molecules define privileged positions in the otherwise homogeneous and isotropic vacuum), through ZPF of isoscalar and isovector character, some of which diverge although retaining a finite inertia (mass of the system) and associated emergent property, namely rigidity, pushing model; sloshing back and forth of opposite charges with very different spatial distributions (protons and electrons) thus essentially leading to a ground state displaying a low frequency dynamical dipole moment (See App. 2.C, discussion following Eq. (2.C.4)). Of notice that a similar phenomenon is found in atomic nuclei, in the case of light exotic halo neutron dripline systems like e.g. ^{11}Li (App. 3.B).

Appendix 3.E Phase transition and fluctuations¹⁰⁸

Empty space, considering also the quantal vacuum zero point fluctuations, is thought to be homogeneous and isotropic. Translational and rotational symmetry follows. But crystals, for example, of which all rocks are made, are neither homogeneous nor isotropic, displaying emergent properties like rigidity. Not only a crystal occupies and defines a fixed position and a privileged direction in space. Translational symmetry and isotropy is broken everywhere within it, in that the individual atoms all occupy fixed positions and varied groups of them define particular directions. Lattice phonons are the corresponding fluctuations associated and restoring the broken symmetries by the individual atoms, while translation and rotation of the crystal is associated with symmetry restoration of the system as a whole.

¹⁰⁸ See e.g. Anderson and Stein (1984); Anderson (1976, 1964b). For a short overview see Brink and Broglia (2005) Ch. 1, p. 27. A more detailed account of the phenomenon is done in Ch. 6.

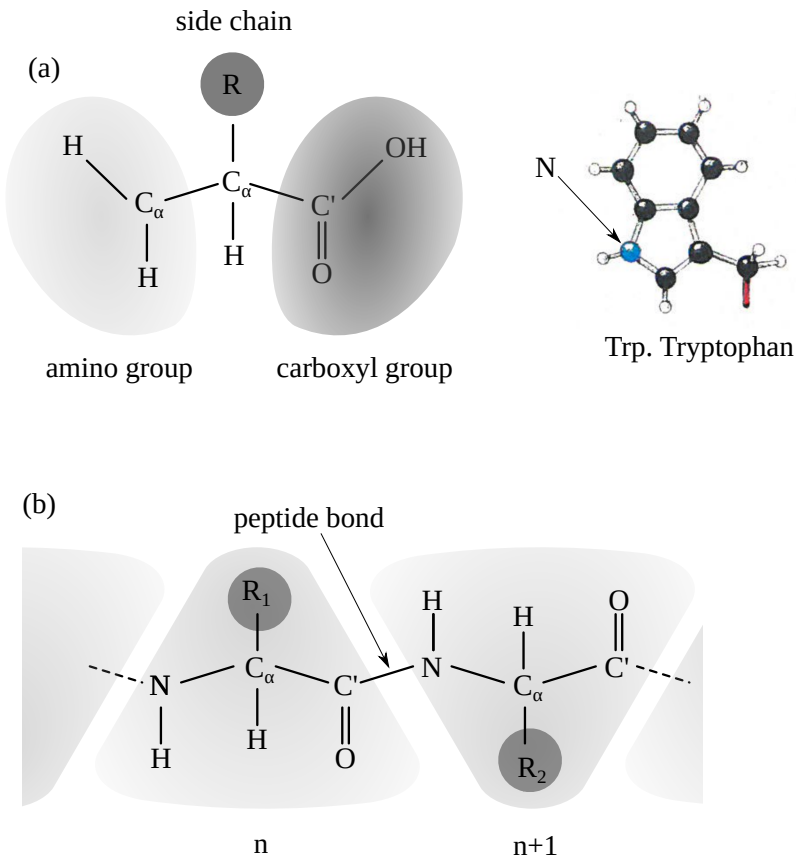


Figure 3.D.5: (Color online) Proteins are built up by amino acids that are linked by peptide bonds into a polypeptide chain. (a) Schematic diagram of an amino acid. A central carbon atom C_α is attached to an amino group, NH_2 , a carboxyl group $C'OOH$, a hydrogen atom H, and a side chain, R. (b) In a polypeptide chain the carboxyl group of amino acid has formed a peptide bond C–N, to the amino group of amino acid $n+1$. One water molecule is eliminated in this process. The repeating units, which are called residues, are divided into main-chain atoms and side chains. The main-chain part, which is identical in all residues, contains a central C_α atom attached to an NH group, a $C'=O$ group, and an H atom. The side-chain R, which is different for different residues is bound to the C_α atom. In the upper right, an example of side chain associated with the amino acid Tryptophan, also denoted Trp or W. Black spheres stand for carbon atoms (C), blue for nitrogen (N). Small, white spheres stand for hydrogen (H) (After Branden and Tooze (1991)).

Similarly, in a ferromagnetic crystal, where magnetization acquires a value different from zero below the Curie temperature breaking rotational invariance. In this case, spin waves are associated with symmetry restoration. In other words, another emergent property of spontaneous symmetry breaking –namely the fact that many–body systems can have ground states which do not have the same symmetry as the Hamiltonian itself– aside from (generalized) rigidity, is the existence of long–wavelength collective motions of the order parameter (amplitude of density waves in a crystal, magnetization in a ferromagnet, etc.), such as phonons and spin waves.

Superconductors break gauge symmetry, intimately related to charge and particle number conservation. A metallic superconductor has a rather perfect internal gauge phase order. Within this context, the BCS mechanism is most relevant to the mass problem because it introduces an energy (mass) gap for fermions, and the Goldstone–zero point motion of the total order parameter α_0 which is large and rapid ($\dot{\phi} = \lambda/\hbar$; pairing rotational bands in nuclei). Another major emergent property in broken symmetry systems is the appearance of singularities and texture of the order parameter like e.g. vortices in superfluid systems –namely, the possibility for a rotational invariant, spherical, quantal system to rotate (note van der Waals 1–Cooper pair in ^{11}Li , see Apps. 3.A and 7.F)– and of domain walls in ferromagnets.

Another feature of **spontaneous symmetry breaking (SSB)** is the possibility of hierarchical¹⁰⁹ SSB or “tumbling”. Namely, SSB can be a cause for another SSB at a lower energy scale, an example being the chain crystal-phonon-superconductivity. Its Goldstone mode is the phonon (few meV) which induces the Cooper pairing of electrons ($T_c \approx 0.5$ meV) to cause superconductivity.

In the nuclear case, and in connection with the state $|^{11}\text{Li}(gs)\rangle$, one could argue that the incipient (dynamical) spontaneous symmetry breaking associated with the almost degeneracy of a soft dipole¹¹⁰ mode, allows for an incipient breaking of gauge invariance at the level of a single Cooper pair ($S_{2n} \approx 380$ keV). The new feature in this case is the symbiotic character of the two incipient (dynamical) SSB phenomena.

3.E.1 Pairing phase transition in small particles

For bulk pure superconductors the large pair coherence length implies a very sharp, extremely narrow critical region as a function of the temperature (or of the magnetic field) so that, for example, the observed specific heat can be accurately described by the standard mean field BCS approach. However, the size of the critical region becomes larger as the dimensions of the system decreases below the coherence length. A limiting case corresponds to particles with dimensions smaller than

¹⁰⁹See Nambu (1991).

¹¹⁰ $E_x \lesssim 1$ MeV, long wavelength $\lambda = 2\pi R/L \approx 2\pi \times 4.58 \text{ fm}/1 \approx 29 \text{ fm}$.

the coherence length which form essentially zero-dimensional systems^{111,112}. An interesting question one may pose is for which size of particles will superconductivity actually cease. It was conjectured¹¹³ that the usual Cooper instability will not exist anymore and therefore superconductivity should disappear if the small superconducting particles are in the quantum-size-effect (QSE) regime when the energy difference δ between two discrete one-electron states is comparable to the energy of the superconducting state (Anderson criterion). This means that small superconductors with fewer than about 10^4 to 10^5 electrons should be affected by this effect. Within this context, important information concerning pairing fluctuations is provided by the study of small Sn-particles at low temperatures¹¹⁴. To describe these fluctuations, use of techniques have been made that take into account large amplitude fluctuations of the order parameter. In particular the static-path approximation¹¹⁵ (SPA) with quadratic corrections¹¹⁶ which mimic the RPA corrections known to be, aside from in a narrow interval around T_c (or H_c ; see Fig. 3.1.2), equivalent to number projection¹¹⁷. The relevant parameter of this sort of calculations is the ratio of δ and kT_c , i.e.

$$\bar{\delta} = \frac{\delta}{kT_c} = \frac{2}{N(0)kT_c}, \quad (3.E.1)$$

where $N(0)$ is the single-particle energy density of one spin orientation states at the Fermi energy. In Fig. 3.E.1 the results of the (SPA)+quadratic correction model for specific heat and spin susceptibility as a function of temperature is shown for $\bar{\delta}$ ranging from $\bar{\delta} = 0.001$ to $\bar{\delta} = 0.5$. The dashed curves show the static path results while the solid lines include the RPA-like corrections. For comparison, the BCS-results labeled by $\bar{\delta} = 0$ corresponding to the bulk system are also displayed.

For small values of $\bar{\delta}$ the system shows a sharp phase transition which can be well described by mean field theory. For $\bar{\delta} \approx 0.5$, corresponding to a small number of particles ($\sim 10^2$), the transition region has broadened so much as to blur the phase transition. RPA corrections are important only for relatively small particles.

¹¹¹See Perenboom et al. (1981); Anderson (1959); Kubo (1962, 1968); Mühlischlegel et al. (1972); Lauritzen et al. (1993).

¹¹²An embodiment of such systems is provided by superfluid nuclei as a function of the rotational frequency (Fig. 3.1.2).

¹¹³Anderson (1959).

¹¹⁴Perenboom et al. (1981).

¹¹⁵Mühlischlegel et al. (1972).

¹¹⁶Lauritzen et al. (1993). It is of notice that in Mühlischlegel et al. (1972), the basic result of the work of the same authors (Denton et al. (1971)) on small normal-metal particles is mentioned to be the restriction to fixed electron number and the assertion is made that in the superconducting case (where they use the grand canonical ensemble) the above restriction to fixed electron number is expected to be even more important.

¹¹⁷Shimizu and Broglia (1990).

3.E.2 Fine Sn particles

The electronic specific heat of small particles of Sn in a matrix with an average diameter ranging from 25 to 220 nm over a temperature range from 0.4 T_c to 1.5 T_c in zero magnetic field (Fig. 3.E.2) have been measured¹¹⁸. In the same figure the results of the model discussed in the previous section is also shown. There is a good quantitative agreement between the results of the model and the experimental findings¹¹⁹.

3.E.3 Time-reversal response function

To explain dirty superconductors a BCS type theory based on pairing in which each one-electron state pairs with its exact time reverse, a generalization of the \mathbf{k} spin up, $-\mathbf{k}$ spin down pairing was developed¹²⁰. It could explain the experimental observation that starting with a pure single crystal of a superconducting material, there is usually a rather sharp initial drop in the superconducting transition temperature as the first small percentage of chemical imperfection is added. If the impurities which are introduced are ordinary ones, the sharp drop stops rather soon and is replaced by a more gradual behavior. On the other hand, if the introduced impurities are magnetic ions rather than ordinary chemical impurities, the initial drop continues, and superconductivity is eventually destroyed.

In fact, when time-reversal transformation cannot be made, that is, when the energy of the state $|\nu\rangle$ is not the same as the energy of $|\bar{\nu}\rangle$, a situation not found in the case of ordinary impurities which do not affect Kramer's degeneracy, pair correlation weakens, and the transition temperature will continue to drop as the degree of magnetic scattering increases. And within this scenario, one comes back again at what degree of (magnetic) scattering will superconductivity cease.

It is of notice that the nucleus is itself a dirty superconductor in the sense that it can be viewed as a very fine particle – spatial quantization forcing it to be close to the QSE regime – with only a very small number of Fermi particles in it, in which Cooper pairs are associated with $|\nu\bar{\nu}\rangle$ correlations. Thus, rapid rotation of the nucleus as a whole which affect differently the different originally Kramers degenerate orbits, can be viewed as introducing an ever increasing amount of magnetic impurities. The associated eventual superfluid–normal phase transition taking place for values of the angular momentum¹²¹ $I_c \approx 20\hbar$. Physically this band crossing between the superfluid S (ground state based) and normal N (pair vibration two-quasiparticle based) bands leads to the phenomenon known as back bending¹²². Within the present scenario the $S - N$ phase transition in nuclei can be studied in

¹¹⁸See Perenboom et al. (1981) and references therein.

¹¹⁹For details we refer to Lauritzen et al. (1993) and Mühlischlegel et al. (1972).

¹²⁰Anderson (1959). Of course such a formalism is standard in the nuclear case See e.g. Bohr and Mottelson (1975); Bohr and Ulfbeck (1988); Broglia (1985).

¹²¹See Bohr and Mottelson (1975) and references therein. See also Brink and Broglia (2005) Ch. 6 Fig. 6.3 and refs. therein.

¹²²Bohr and Mottelson (1975); Stephens and Simon (1972); Johnson et al. (1972).

term of individual quantal states. Although not technically simple, two-nucleon transfer reactions induced by heavy ions can, in principle, be employed in such studies¹²³.

¹²³Broglia and Gallardo (1986); Shimizu et al. (1989), Fig. 39.

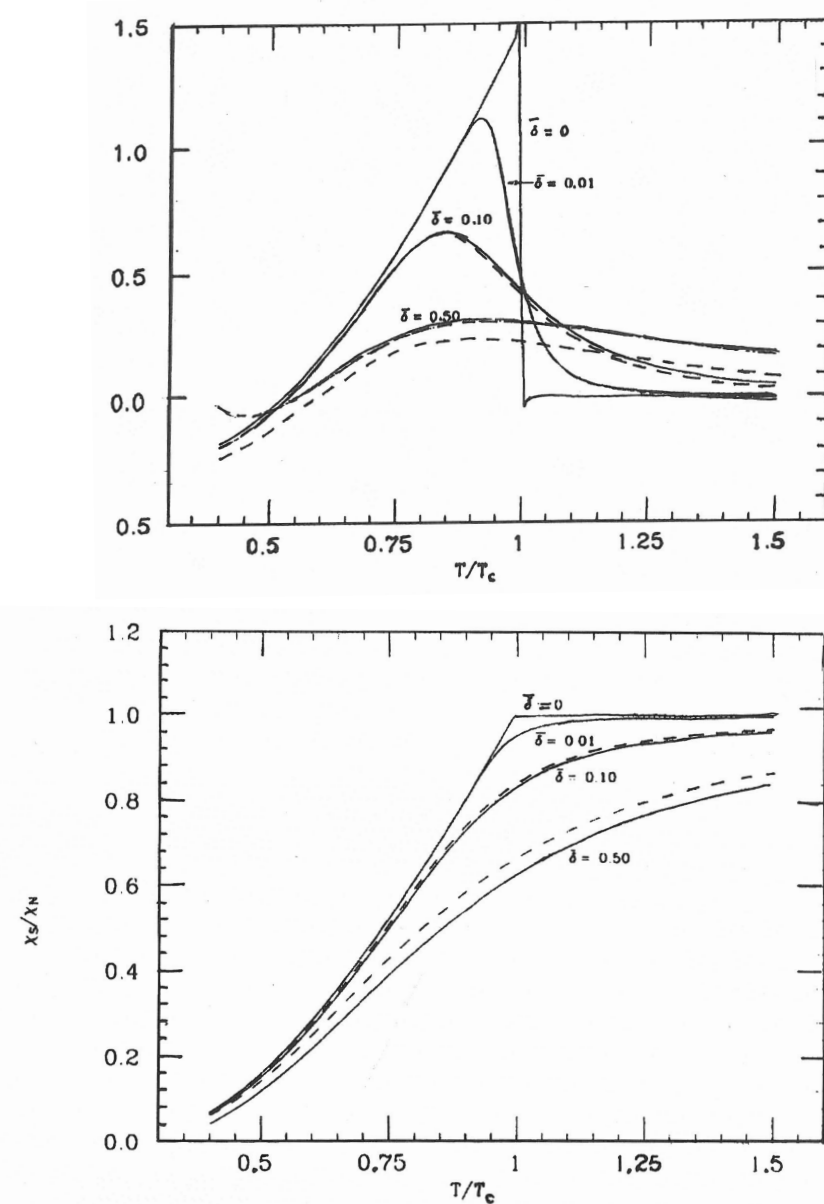


Figure 3.E.1: Specific heat and magnetic susceptibility in the static path approximation (dashed lines) and including quadratic corrections (solid lines). The curves labeled $\bar{\delta} = 0$ show the finite temperature BCS results (after Lauritzen et al. (1993)).

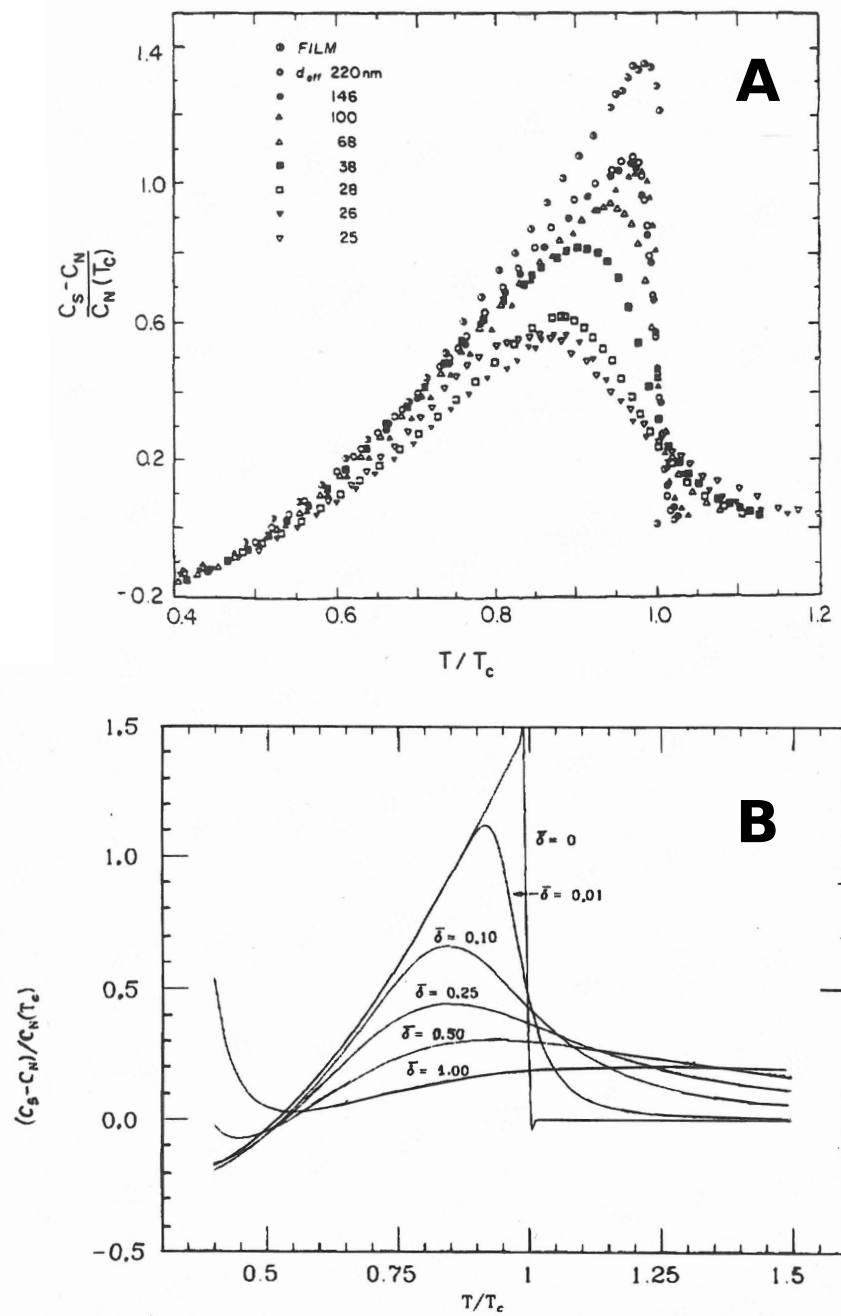


Figure 3.E.2: **A** the measured specific heat is shown for a variety of Sn-particles. The figure is taken from Tsuboi and Suzuki (1977). **B** results of the static path approximation with quadratic (RPA-like) corrections are shown (after Lauritzen et al. (1993)).

Chapter 4

Pair transfer in a nutshell

4.1 Simultaneous versus successive Cooper pair transfer in nuclei

Cooper pair transfer is commonly thought to be tantamount to simultaneous transfer. In this process a nucleon goes over through the NN -interaction v , the second one does it making use of the correlations with its partner (cf. Figs. 4.1.1 and 6.C.1 (I)). Consequently, in the independent particle limit, simultaneous transfer should not be possible (see App. 6.C.1). Nonetheless, it remains operative. This is because, in this limit, the particle transferred through v does it together with a second one which profits from the non-orthogonality of the wavefunctions describing the single-particle motion in target and projectile (Figs. 4.1.2 and 6.C.1 (II)). This is the reason why this (non-orthogonality) transfer amplitude has to be treated on equal footing with the previous one representing, within the overcomplete basis employed, a natural contribution to simultaneous transfer. In other words, $T^{(1)}$ gives the wrong cross section, even at the level of simultaneous transfer, as it violates two-nucleon transfer sum rules¹. In fact $(T^{(1)} - T_{NO}^{(1)})$ is the correct, sum rule conserving two-nucleon transfer amplitude to lowest order (first) in v . The resulting cancellation is quite conspicuous in actual nuclei (see e.g. Figs. 4.5.2 (b) and 4.5.3, see also Fig. 4.5.4). This is in keeping with the fact that Cooper pairs are weakly correlated systems and the reason why the successive transfer process in which v acts twice (implying the mean field U in the post-post representation²), is the dominant mechanism in pair transfer reactions (Sect. 4.4). While this mechanism seems antithetical to the transfer of correlated fermions pairs (bosons), it probes, in the nuclear case, the same pairing correlations as simultaneous transfer does (Sect. 4.5). This is because nuclear Cooper pairs (quasi-bosons) are quite extended objects, the two nucleons being (virtually) correlated over distances much larger than

¹Broglia et al. (1972), Bayman and Clement (1972); cf. also Sect. 2.2

²Poté et al. (2013a), Eq. (A7). Within this context see also Pinkston and Satchler (1982).

typical nuclear dimensions³ (see Fig. 4.1.3). In a two-nucleon transfer process this virtual property becomes real, in the sense that the presence of (normal) density over regions larger than that of the dimensions of each of the interacting nuclei allows for incipient ξ nuclear Cooper pair manifestation.

Within this context, let us refer to the Josephson effect, associated with the Cooper pair tunneling across a thin barrier separating two metallic superconductors. Because the probability of one-electron-tunneling is of the order of 10^{-10} , (conventional) simultaneous tunneling associated with a probability of $(10^{-10})^2$ would hardly be observed (cf. Sect 4.4). Nonetheless, Josephson currents are standard measures in low temperature laboratories⁴.

The same arguments related to the large value of the correlation length is operative in explaining the fact that Coulomb repulsion is rather weak between partners of Cooper pairs which are, in average, at a distance $\xi (\approx 10^4 \text{ \AA})$ much larger than the Wigner–Seitz radius r_s typical of metallic elements ($\approx 1 - 2 \text{ \AA}$). Consequently, it can be overwhelmed by the long range electron–phonon pairing. Similarly, in widely extended light halo nuclei, the short range bare pairing interaction plays little role, becoming subcritical (cf. Sect. 3.6). The fact that such systems are nonetheless bound, although weakly, testifies to the dominant role the exchange of collective vibrations between halo nucleons have in binding the associated halo Cooper pair (e.g. $^{11}\text{Li(gs)}$, and, arguably, also⁵ of $^{12}\text{Be}(0^{++}; 2.251 \text{ MeV})$ to the core $^9\text{Li(gs)}$ and ^{10}Be respectively) (cf. Section 7.1.2).

The above arguments are at the basis of the fact that second order DWBA theory which add both successive and non-orthogonality contributions to the simultaneous transfer amplitudes, provides a quantitative account of the experimental findings (see e.g. Figs. 3.1.6, 4.5.2 (a), 4.5.3 (a) and Chapter 7).

4.2 One- and two-nucleon transfer probabilities

As discussed in Chapter 2, the enhancement factor in a two-nucleon transfer reaction can be defined in terms of two-particle units⁶, similar to what is done in the case of electromagnetic decay (Weisskopf units)⁷. Let us, for simplicity, write such a relation as

$$\left(\frac{d\sigma}{d\Omega} \right)_{2n} = \left| \langle f | P^\dagger | i \rangle \right|^2 \left(\frac{d\sigma}{d\Omega} \right)_{2n}^{(0)}, \quad (4.2.1)$$

where $\left(\frac{d\sigma}{d\Omega} \right)_{2n}^{(0)}$ is the absolute differential cross section associated with a typical pure single-pair configuration $|j^2(0)\rangle$ (or the average value over pairs based on the

³Within this context one can put the following question. Is anybody worried that a photon can, in a two slit experiment, be broken in two? Not likely. Why should then one worry that successive transfer can break a Cooper pair?

⁴cf. e.g. Rogalla and Kes (2012) and references therein.

⁵See e.g. Johansen et al. (2013).

⁶cf. e.g. Broglia et al. (1972, 1973) and references therein.

⁷See e.g. Bohr and Mottelson (1969).

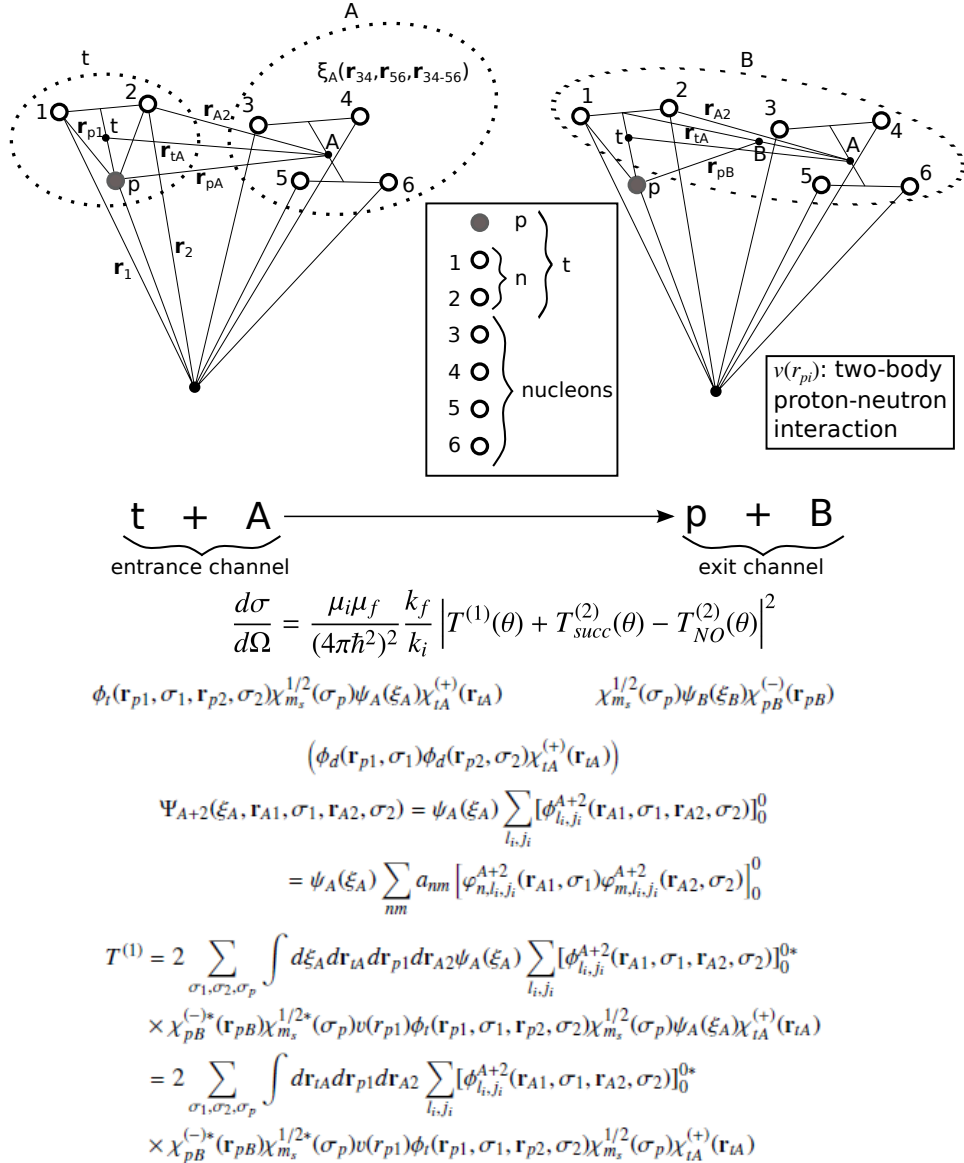
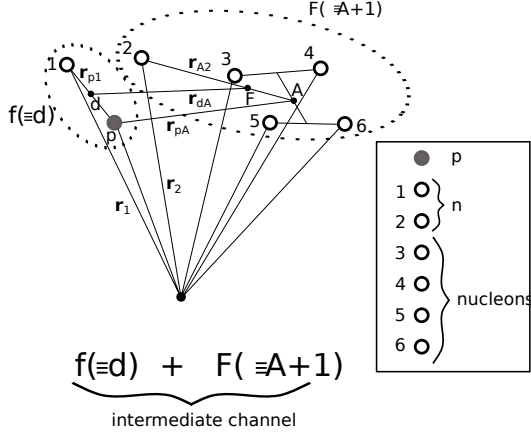


Figure 4.1.1: Contribution of simultaneous transfer, in first order DWBA, to the reaction $A(t, p)B \equiv A + 2$. The nucleus A is schematically assumed to contain four nucleons, the triton being composed of two neutrons and one proton. The set of coordinates used to describe the entrance and exit channels are shown in the upper part (bold face vectors represent the coordinates used to describe the relative motion, while the intrinsic coordinates ξ_A represent \mathbf{r}_{34} , \mathbf{r}_{56} and \mathbf{r}_{34-56}). In the lower part of the figure, the simultaneous two-nucleon transfer amplitude is written (cf. Potel et al. (2013b)). It is of notice that the expression of $T^{(1)}$ violates, in the independent particle basis used, the two-nucleon transfer sum rule by $T_{NO}^{(1)}$, amplitude operative also in lowest order of v (Fig. 4.1.2; see also App. 6.C). It is of notice that of all the relative motion coordinates, only those describing the relative motion of (t, A) and of (p, B) have asymptotic values, being those associated with distorted waves.



$$\begin{aligned}
 & \chi_{m_s}^{1/2}(\sigma_p) \phi_d(\mathbf{r}_{p1}, \sigma_1) \psi_A(\xi_A) \varphi_{l_f, j_f, m_f}^{A+1}(\mathbf{r}_{A2}, \sigma_2) \\
 G(\mathbf{r}_{dF}, \mathbf{r}'_{dF}) &= i \sum_l \sqrt{2l+1} \frac{f_l(k_{dF}, r_<) g_l(k_{dF}, r_>)}{k_{dF} r_{dF} r'_{dF}} \left[Y^l(\hat{r}_{dF}) Y^l(\hat{r}'_{dF}) \right]_0^0 \\
 T_{succ}^{(2)} &= 2 \sum_{l_i, j_i} \sum_{l_f, j_f, m_f} \sum_{\sigma_1 \sigma_2} \int d\xi_A dr_{dF} dr_{p1} dr_{A2} \chi_{pB}^{(-)*}(\xi_B) v(\mathbf{r}_{p1}) \phi_d(\mathbf{r}_{p1}) \varphi_{l_f, j_f, m_f}^{A+1}(\mathbf{r}_{A2}, \sigma_2) \\
 &\quad \times \chi_{m_s}^{1/2}(\sigma_p) \Psi_A(\xi_A) \frac{2\mu_{dF}}{\hbar^2} \int d\xi'_A dr'_{dF} dr'_{p1} dr'_{A2} G(\mathbf{r}_{dF}, \mathbf{r}'_{dF}) \\
 &\quad \times \chi_{tA}^{(+)}(\mathbf{r}_{tA}) \psi_A^*(\xi'_A) v(\mathbf{r}'_{p2}) \phi_d(\mathbf{r}'_{p1}) \varphi_{l_f, j_f, m_f}^{A+1}(\mathbf{r}'_{A2}, \sigma'_2) \\
 &= 2 \sum_{l_i, j_i} \sum_{l_f, j_f, m_f} \sum_{\sigma_1 \sigma_2} \int dr_{dF} dr_{p1} dr_{A2} \chi_{pB}^{(-)*}(\xi_B) v(\mathbf{r}_{p1}) \phi_d(\mathbf{r}_{p1}) \left[\varphi_{l_f, j_f, m_f}^{A+2}(\mathbf{r}_{A1}, \sigma_1, \mathbf{r}_{A2}, \sigma_2) \right]_0^0 \\
 &\quad \times \frac{2\mu_{dF}}{\hbar^2} \int dr'_{dF} dr'_{p1} dr'_{A2} G(\mathbf{r}_{dF}, \mathbf{r}'_{dF}) \chi_{tA}^{(+)}(\mathbf{r}'_{tA}) v(\mathbf{r}'_{p2}) \phi_d(\mathbf{r}'_{p1}, \sigma'_1) \phi_d(\mathbf{r}'_{p2}, \sigma'_2) \varphi_{l_f, j_f, m_f}^{A+1}(\mathbf{r}'_{A2}, \sigma'_2) \\
 T_{NO}^{(1)} &= 2 \sum_{l_i, j_i} \sum_{l_f, j_f, m_f} \sum_{\sigma_1 \sigma_2} \int d\xi_A dr_{dF} dr_{p1} dr_{A2} \chi_{pB}^{(-)*}(\xi_B) \chi_B^*(\xi_B) v(\mathbf{r}_{p1}) \phi_d(\mathbf{r}_{p1}) \varphi_{l_f, j_f, m_f}^{A+1}(\mathbf{r}_{A2}, \sigma_2) \\
 &\quad \times \chi_{m_s}^{1/2}(\sigma_p) \Psi_A(\xi_A) \frac{2\mu_{dF}}{\hbar^2} \int d\xi'_A dr'_{dF} dr'_{p1} dr'_{A2} \\
 &\quad \times \chi_{tA}^{(+)}(\mathbf{r}_{tA}) \psi_A^*(\xi'_A) \phi_d(\mathbf{r}'_{p1}) \varphi_{l_f, j_f, m_f}^{A+1}(\mathbf{r}'_{A2}, \sigma'_2) \\
 &= 2 \sum_{l_i, j_i} \sum_{l_f, j_f, m_f} \sum_{\sigma_1 \sigma_2} \int dr_{dF} dr_{p1} dr_{A2} \chi_{pB}^{(-)*}(\xi_B) v(\mathbf{r}_{p1}) \phi_d(\mathbf{r}_{p1}) \left[\varphi_{l_f, j_f, m_f}^{A+2}(\mathbf{r}_{A1}, \sigma_1, \mathbf{r}_{A2}, \sigma_2) \right]_0^0 \\
 &\quad \times \frac{2\mu_{dF}}{\hbar^2} \int dr'_{dF} dr'_{p1} dr'_{A2} \chi_{tA}^{(+)}(\mathbf{r}'_{tA}) \phi_d(\mathbf{r}'_{p1}, \sigma'_1) \phi_d(\mathbf{r}'_{p2}, \sigma'_2) \varphi_{l_f, j_f, m_f}^{A+1}(\mathbf{r}'_{A2}, \sigma'_2)
 \end{aligned}$$

Figure 4.1.2: Successive and non-orthogonality contributions to the amplitude describing two-nucleon transfer in second order DWBA, entering in the expression of the absolute differential cross section $d\sigma/d\Omega = \frac{\mu_i \mu_f}{(4\pi\hbar^2)^2} \frac{k_f}{k_i} |T^{(1)} + T_{succ}^{(2)} - T_{NO}^{(2)}|^2$.

Concerning $T^{(1)}$ we refer to Fig. 4.1.1. In the upper part of the figure the coordinates used to describe the intermediate channel $d + F(\equiv A + 1)$ are given (bold face vectors represent the coordinates used to describe the relative motion, while the intrinsic coordinates ξ_A represent \mathbf{r}_{34} , \mathbf{r}_{56} and \mathbf{r}_{34-56}). In the lower part of the figure, the expressions corresponding to the (t, p) process are displayed (Potel et al., 2013b). Schematically, the three contributions $T^{(1)}$, $T_{succ}^{(2)}$ and $T_{NO}^{(2)}$ to the transfer amplitude can be written as $\langle pB|v|tA\rangle$, $\sum \langle pB|v|dF\rangle \langle dF|v|tA\rangle$ and $\sum \langle pB|v|dF\rangle \langle dF|\mathbf{1}|tA\rangle$ respectively, where v is the proton-neutron interaction and $\mathbf{1}$ the unit operator. Within this context, while $T_{NO}^{(2)}$ receives contributions from the intermediate (virtual) closed $(d + F)$ channel as $T_{succ}^{(2)}$ does, it is first order in v as $T^{(1)}$ is.

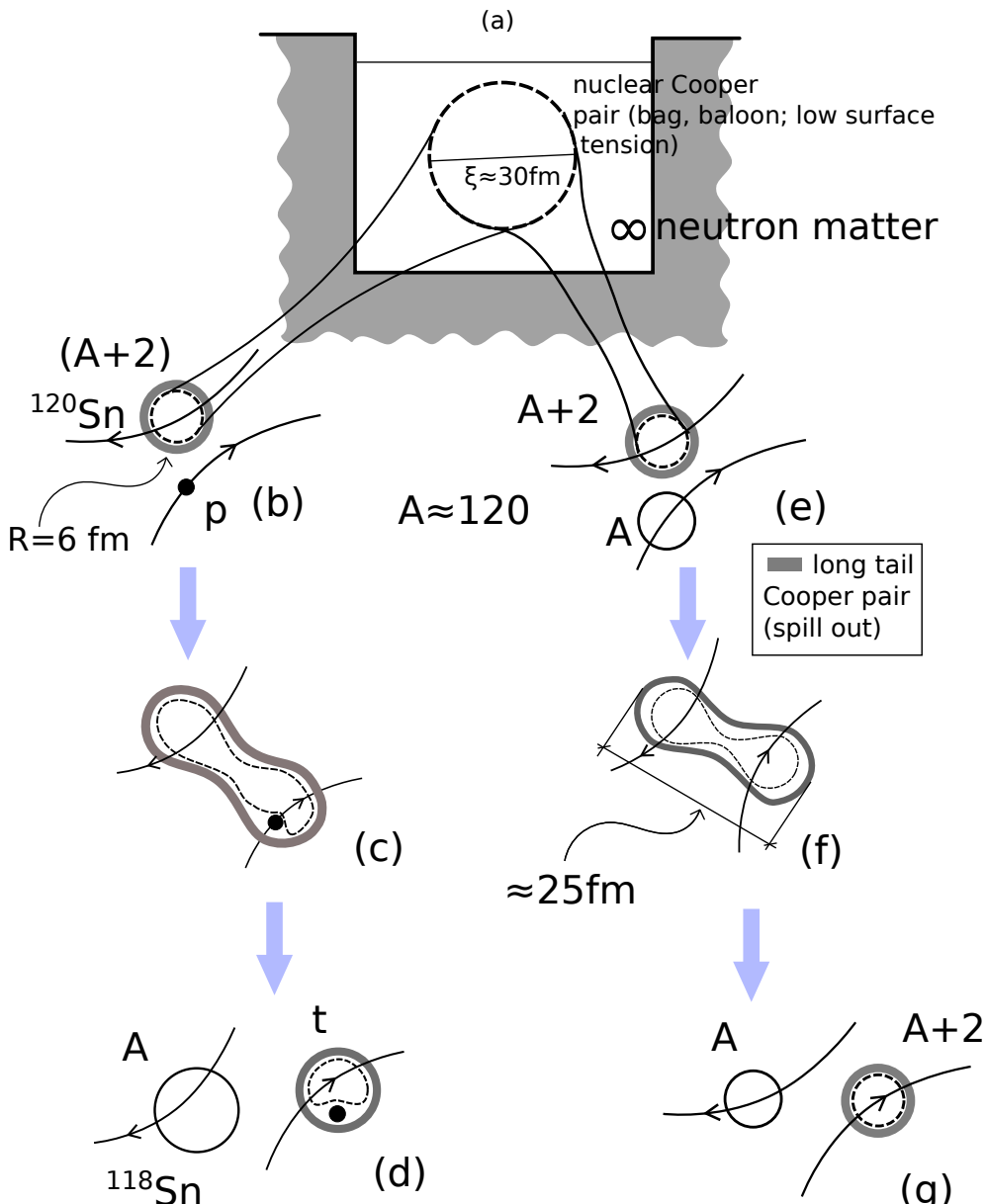


Figure 4.1.3: The correlation length associated with a nuclear Cooper pair is of the order of $\xi \approx \hbar v_F / (\pi \Delta) \approx 14 \text{ fm}$. (a) in neutron matter at typical densities of the order of 0.5–0.8 saturation density, the $NN^{-1}S_0$ short range force, eventually renormalized by medium polarization effects, makes pairs of nucleons moving in time reversal states to correlate over distances larger than nuclear dimensions. How can one get evidence for such an extended object? Hardly when the Cooper bag (balloon) is introduced in (b) the mean field of a superfluid nucleus which, acting as a very strong external field, constrains the Cooper pair to be within the nuclear radius with some spill out (long tail of Cooper pair, grey, shaded area extending outside the nuclear surface defined by $R_0 = 1.2A^{1/3} \text{ fm}$; see also Bertsch and Broglia (2005) p. 88), (d), that is, in the case of two-nucleon transfer process (e.g. (p, t) reaction) in which the absolute cross section can change by orders of magnitude in going from pure two-particle (uncorrelated configurations) to long tail Cooper pair spill outs. This effect is expected to become stronger by allowing , pair transfer between similar superfluid nuclei, in which case one profits of the same type of correlations (superfluidity) as resulting from very similar pair mean fields (e), (f), (g) (see e.g. von Oertzen (2013); von Oertzen and Vitturi (2001), and references therein).

valence orbitals). In the case of a superfluid nucleus like e.g. ^{120}Sn and for $i = \text{gs(A)}$ and $f = \text{gs(A+2)}$ as well as $f = 2qp(\text{A+2})$ one can write

$$\left| \langle f | P^\dagger | i \rangle \right|^2 = \begin{cases} \alpha_0'^2 = (\sum_{\nu>0} U_\nu' V_\nu')^2 = \left(\frac{\Delta}{G} \right)^2 = \left(\frac{12A}{\sqrt{A}25} \right)^2 \approx \frac{A}{4} \approx 30 \ (f = \text{gs}), \\ U_\nu^4 \approx 1 \ (f = 2qp). \end{cases} \quad (4.2.2)$$

Thus, the expected *enhancement* factor⁸ is given by the ratio,

$$R = \frac{\left(\frac{d\sigma}{d\Omega}(\text{gs} \rightarrow \text{gs}) \right)_{2n}}{\left(\frac{d\sigma}{d\Omega}(\text{gs} \rightarrow 2qp) \right)_{2n}} \approx 30. \quad (4.2.3)$$

In other words, in superfluid nuclei one expects the 0^+ pairing vibrational states to carry a (summed) cross section of the order of 3% that of the $\text{gs} \rightarrow \text{gs}$ transition (cf. Fig. 3.1.4). Now, in defining the quantity R used was made of (4.2.1). Because both numerator and denominator are linear in $\left(\frac{d\sigma}{d\Omega} \right)_{2n}^{(0)}$, one could as well posit that one has used (4.2.2) in defining R .

The situation is quite different when one intends to define the *probability* associated with a transfer process. One could be tempted again to use (4.2.1) for the case of $2n$ -transfer and eventually

$$\left(\frac{d\sigma}{d\Omega} \right)_{1n} = S \left(\frac{d\sigma}{d\Omega} \right)_{1n}^{(0)} \quad (4.2.4)$$

in the case of $1n$ -transfer, S being known in the literature as the spectroscopic factor, and used here for illustration purposes only. However, in trying to define an enhancement factor in terms of P_{2n}/P_{1n}^2 , the approximate relations (4.2.1) and (4.2.4) will now condition the physics one is trying to extract from the experimental (empirical) information. In fact, in this case the actual values of $\left(\frac{d\sigma}{d\Omega} \right)_{1n}^{(0)}$ and of $\left(\frac{d\sigma}{d\Omega} \right)_{2n}^{(0)}$ will play an important role, and this could hardly be correct. In fact, the proper definition of the transfer probabilities is to be made in terms of the total reaction cross section.

For this purpose let us remind some useful relations. In particular that of the differential reaction cross section

$$\frac{d\sigma}{d\Omega} = |f(\theta)|^2, \quad (4.2.5)$$

where

$$f(\theta) = \frac{1}{k} \sum_l (2l + 1) e^{i\delta_l} \sin \delta_l P_l(\cos \theta), \quad (4.2.6)$$

⁸See e.g. Brink and Broglia (2005) p. 324

δ_l being the partial wave l phase shift. Let us now use for simplicity the results associated with hard sphere scattering⁹ in the low and high energy limit. Making use of the fact that in the case under discussion the phase shifts δ_l are related to the regular and irregular spherical Bessel functions,

$$\tan \delta_l = \frac{j_l(kR)}{n_l(kR)}, \quad (4.2.7)$$

and that $\sin^2 \delta_l = \tan^2 \delta_l / (1 + \tan^2 \delta_l)$, one can write in the case in which $kR \ll 1$, i.e. in the low-energy, long wavelength, regime

$$\tan \delta_l \approx \frac{-(kR)^{2l+1}}{(2l+1)[(2l-1)!!]^2}, \quad (4.2.8)$$

implying that one can ignore essentially all δ_l with $l \neq 0$. Because $\delta_0 = -kR$ (cf. (4.2.7)) regardless the value of k , one obtains,

$$\frac{d\sigma}{d\Omega} = \frac{\sin^2 \delta_0}{k^2} = R^2, \quad (4.2.9)$$

and thus

$$\sigma_{tot} = \int \frac{d\sigma}{d\Omega} d\Omega = 4\pi R^2 \quad (kR \ll 1), \quad (4.2.10)$$

a cross section which is four times the geometric cross section πR^2 , namely the area of the disc of radius R that blocks the propagation of the incoming (plane) wave, and has the same value as that of a hard sphere. Because $kR \ll 1$ implies long wavelength scattering, it is not surprising that quantal effects are important, so as to overwhelm the classical picture. Let us now consider the high energy limit $kR \gg 1$. The total cross section is in this case, given by

$$\begin{aligned} \sigma_{tot} &= \int |f_l(\theta)|^2 d\Omega = \frac{1}{k^2} \int_0^{2\pi} d\phi \int_{-1}^1 d(\cos \theta) \sum_{l=1}^{kR} \sum_{l'=1}^{kR} (2l+1)(2l'+1) \\ &\times e^{i\delta_l} \sin \delta_l e^{-i\delta_{l'}} \sin \delta_{l'} P_l P_{l'} = \frac{4\pi}{k^2} \sum_{l=1}^{kR} (2l+1) \sin^2 \delta_l. \end{aligned} \quad (4.2.11)$$

Making use of the relation

$$\sin^2 \delta_l = \frac{\tan^2 \delta_l}{1 + \tan^2 \delta_l} = \frac{[j_l(kR)]^2}{[j_l(kR)]^2 + [n_l(kR)]^2} \approx \sin^2 \left(kR - \frac{\pi l}{2} \right), \quad (4.2.12)$$

and the fact that so many l -values contribute to (4.2.11), one can replace $\sin^2 \delta_l$ by its average value $1/2$. Because the number of terms of the sum is roughly kR , the same being true for the average value of $(2l+1)$. Thus one can write

$$\sigma_{tot} = \frac{4\pi}{k^2} (kR)^2 \frac{1}{2} = 2\pi R^2, \quad (kR \gg 1) \quad (4.2.13)$$

⁹cf. e.g. Sakurai (1994)

which, in this short wavelength limit, is not the geometric cross section either. In fact, (4.2.13) can be split into two contributions each of value πR^2 . One due to reflection in which it can be shown that there is no interference amongst contributions from different l -values. A second one (coherent contribution in the forward direction) called shadow because for hard-sphere scattering at high energies, waves with impact parameter less than R must be deflected. Consequently, behind the scatterer there must be zero probability for finding the scattered particle and a shadow must be generated.

In terms of wave mechanics, this shadow is due to the destructive interference between the original wave (which would be there even if the scatterer was absent), and the newly scattered wave. Thus, one needs scattering in order to create a shadow. This contribution is intimately related to the optical theorem¹⁰

$$\sigma_{tot} = \frac{4\pi}{k} \Im[f(\theta = 0, k)] = \frac{4\pi}{k} [f_{shad}(\theta = 0, k)] = \frac{4\pi}{k^2} \sum_l (2l + 1) \sin^2 \delta_l, \quad (4.2.14)$$

to which it provides its physical interpretation. In fact, there are two independent ways of measuring σ_{tot} , namely: i) by integrating the differential cross section $d\sigma/d\Omega = |f(\theta)|^2$ moving around the detector, ii) measuring the attenuation of the incoming beam. Both procedures should give the same result. One then identifies $(4\pi/k)f(\theta = 0, k)$ with the attenuation arising from the interference of the elastic wave with the incoming wave. Of notice that in (4.2.11) the factor $(\pi/k^2)(2l + 1) = \pi\lambda(2l + 1)$ is the area of a ring with radius $b = (l + 1/2)\lambda$ and width λ due to quantal undeterminacy¹¹. Thus

$$\sigma_{tot} = 2\pi(R + \lambda/2)^2 \quad (kR \gg 1). \quad (4.2.15)$$

The quantity

$$\lambda = \frac{\lambda}{2\pi} = \frac{h}{2\pi p} = \frac{\hbar}{p} = \frac{1}{k} = \frac{\hbar}{\sqrt{2mE}}, \quad (4.2.16)$$

is the reduced de Broglie wavelength for a massive particle ($E = p^2/2m$). For a proton of energy $E_p \approx 20$ MeV, typical of beams used in $^{120}\text{Sn}(p, t)^{118}\text{Sn}(\text{gs})$ and $^{120}\text{Sn}(p, d)^{119}\text{Sn}(\text{j})$ reactions (cf. Figs. 5.2.1, 5.2.3, 7.4.1 and 7.4.2)¹² $\lambda \approx 1$ fm, to be compared with the value $R \approx 6$ fm of the radius of ^{120}Sn . Consequently, we are in a situation of type (4.2.15), that is,

$$\sigma_{tot} = 2\pi(6 + 0.5)^2 \text{ fm}^2 \approx 2.7 \text{ b}. \quad (4.2.17)$$

¹⁰Sakurai (1994) pp. 420–421

¹¹The original German word *Unbestimmtheitsprinzip* (“indefiniteness” or “indeterminacy principle”) is sometimes incorrectly translated as “uncertainty principle”. This is very misleading, since it suggests that the electron or the nucleon actually has a definite position and momentum of which one is uncertain. In fact, the quantum formalism simply does not allow the ascription of a definite position and momentum simultaneously (see Leggett (1987)).

¹²Of notice that the reduced wavelength of a photon ($p = E/c$) of the same energy ($E = 20$ MeV) is $\lambda = \lambda/2\pi = \hbar/p = \hbar c/E \approx 10$ fm (cf. Table 2.1 p. 22 Satchler (1980)).

Because typical values of the absolute one-particle cross section associated with the (p, d) reaction mentioned above are few mb (see e.g. Fig. 5.2.3 right panel) one can use, for order of magnitude estimate purposes,

$$P_1 \approx \frac{5.35 \text{ mb}}{2.7 \text{ b}} \approx 10^{-3}, \quad (4.2.18)$$

as the typical probability for such processes. Consequently, one may argue that the probability for a pair of nucleons to simultaneously tunnel in e.g. the (p, t) process mentioned above is $(P_1)^2 \approx 10^{-6}$, as near impossible as no matter. Within this context we note that the integrated $\text{gs} \rightarrow \text{gs}$ absolute cross section $\sigma(^{120}\text{Sn}(p, t)^{118}\text{Sn}(\text{gs})) \approx 2.25 \pm 0.338 \text{ mb}$ (see Figs. 3.1.3, 3.1.6 and 7.4.1). This fact implies that the empirical two-nucleon transfer probability is of the order of $P_2 \approx 10^{-3}$. Consequently, $P_2/(P_1)^2 \approx 10^3$, a ratio which, again, can hardly be explained in terms of a physical enhancement factor.

The above contradictions¹³ are, to a large extent, connected with the fact that one is addressing the subject of pairing correlations in nuclei as probed by two-nucleon transfer reactions, treating separately the associated questions of structure and reactions, while they are but complementary aspects of the same physics. Let us elaborate on this point.

4.3 Phase correlation and enhancement factor

When one turns on, in an open shell atomic nucleus like e.g. $^{120}_{50}\text{Sn}_{70}$, a pairing interaction of strength larger than critical, the system moves into an independent pair regime¹⁴. This fact has essentially no consequence concerning the one-particle transfer mechanism, exception made regarding the size of the mismatch between the relative motion–incoming ($p + ^{120}\text{Sn}(\text{gs})$) and –outgoing ($d + ^{119}\text{Sn}(\text{gs})$) trajectories (Q -value and recoil effect), in keeping with the fact that one has to break a Cooper pair to populate a single quasiparticle state. From a structure point of view the depletion of the occupation probability measured in a (p, d) process is correlated with the corresponding increase in occupation observed in (d, p) (U^2, V^2 factors). Aside from the quantitative values, this is also observed in dressed single-particle states, the single-particle sum rule implying both the (A-1) and (A+1) system (see App. 5.H). Concerning the phase coherence of the pair correlated wavefunction it has no consequence for one-particle transfer process, in keeping

¹³Within this context it is of notice that similar questions were rised by Bardeen (1962, 1961); Pippard (2012); Cohen et al. (1962); McDonald (2001) in connection with the prediction of Josephson (Josephson (1962)) that there should be a contribution to the current through an insulating barrier between two superconductors which would behave like direct tunneling of condensed pairs. This is in keeping with the fact that a single electron had a probability of $\approx 10^{-10}$ of getting through, the “classical” estimate of simultaneous pair tunneling being $\approx 10^{-20}$, an impossible observation.

¹⁴Regime which is conditioned by the “external” mean field. In other words, regime (abnormal density) which express itself provided there is nucleon (normal) density available. It is of notice that pairing in turn may help extend the range over which normal nucleon density is available, as in the case of the neutron halo nucleus ^{11}Li lying (defining) at the neutron drip line.

with the fact that $|e^{i\phi} \sqrt{P_1}|^2 = P_1$. A further evidence, if it was the need, that two-particle transfer is the specific probe of pairing in nuclei.

The situation is very different concerning (Cooper) pair transfer. From a reaction point of view, and in keeping with the non-orthogonality existing between the wavefunctions in target and projectile, the associated contributions to the transfer process have to be eliminated. This is in keeping with the fact that simultaneous two-nucleon transfer can take place also in first order in the proton-neutron interaction v_{np} . When this is a consequence of the pairing correlation between the partners of the Cooper pair it constitutes a *bona fide* contribution. Not when it is a consequence of non-orthogonality. Continuing within the realm of reaction theory, second order processes in v_{np} are to be included and as a rule neglect higher orders in keeping with the small value of P_1 ($\approx 10^{-3}$, cf. also Table 7.B.1). Let us now bring structure into the discussion. The fact that the wave function of the nucleons in the pair are phase-coherent ($(U'_v + V'_v e^{-2i\phi} a_v^\dagger a_v^\dagger) |0\rangle$) implies that one has to add the amplitudes before one takes modulus squared, that is,

$$\begin{aligned} P_2 &= \lim_{\epsilon \rightarrow 0} \left| \frac{1}{\sqrt{2}} (e^{i\phi_1} U \sqrt{P_1} + e^{i\phi_2} V \sqrt{P_1}) \right|^2 \\ &= P_1 \lim_{\epsilon \rightarrow 0} \frac{1 + 2UV \cos \epsilon}{2} \approx P_1 \quad (\epsilon = \phi_2 - \phi_1), \end{aligned} \quad (4.3.1)$$

where the assumption was made that $UV \approx 1/2$. Because the range of v_{np} ($a \approx 1$ fm) is much smaller than the correlation length ($\xi \approx 20-30$ fm), in the successive process (4.3.1), the Cooper pair tunnels between target and projectile equally formed and “unharmed” as in the simultaneous process. Think again that in the nuclear pairing correlated system only Cooper pairs exist (in which the partners nucleons are correlated over distances of the order of 20–30 fm from each other) and not single nucleons (normal system) ≈ 2.4 fm (1.2 fm being the Wigner-Seitz radius of the nucleon cell) from each other (Fig. 4.3.1 (a)). To the extent that the mean field acting as an “external” field allows particle density to be present, the properties of independent Cooper pair motion will explicit themselves. And thus it is a physical condition which is assumed fulfilled each time one makes use of the physical picture provided by Fig. 4.3.1 (b). In other words, inside ^{120}Sn all Cooper pairs will be found within a volume of radius $R_0 \approx 6$ fm, in a similar way in which a Cooper pair will be distributed over two similar volumes during the contact time in e.g. a Sn+Sn heavy ion reaction (Fig. 4.5.1)¹⁵. A phenomenon to which the long-range induced pairing interaction (exchange of phonons) contributes in an

¹⁵The interest of the picture shown in Fig. 4.3.1 (b) can also be exemplified by referring to the fact that the moment of inertia of heavy deformed nuclei is considerably smaller than the rigid moment of inertia, but still larger than the irrotational one ($5\mathcal{J}_{irrot} \lesssim \mathcal{J} \lesssim \mathcal{J}_r/2$). Even confined within the mean field of the nucleus, the small but finite number of pairs of correlated nucleons having the “intrinsic”, infinite-matter-like tendency displayed if Fig. 4.3.1 (b), will, to some extent, average out the different orientations of the rotating system and react to it in terms of an effective deformation smaller than the one related to the $B(E2)$ collective (rotational) values. However, constrained as they are they cannot fully profit of pairing superfluidity.

important way for nuclei along the stability valley, let alone in very extended light halo nuclei like ^{11}Li (Fig. 4.3.2)¹⁶.

Within this context we note that the (approximate) form of the (local) pair wavefunction can be written as¹⁷

$$F(r) \approx \Delta N(0) \frac{\sin k_F r}{k_F} \exp\left(-\frac{\sqrt{2}r}{\xi}\right), \quad (4.3.2)$$

where $N(0)$ is the density of levels at the Fermi energy for one spin orientation. For $r \leq \xi$ the pair wavefunction is approximately proportional to that of two particles at the Fermi energy moving freely in a relative s -wave state. In a typical metallic superconductor ξ is of the order of 10^4 Å, much larger than the inter electron spacing (≈ 2 Å). Note that relative to the Fermi energy, the correlation energy ($E_{corr} = (-1/2)N(0)\Delta^2$) associated with Cooper pairing is very small, $\approx 10^{-7} - 10^{-8}$. Arguably, the most important consequence of this fact, is the exponentially large radius and thus very small value of the relative momentum associated with Cooper pairs. In other words, the typical scenario for a very small value of the localization kinetic energy and thus of the generalized quantality parameter (cf. App. 7.E), implying that the two partners of the Cooper pair, are anchored to each other. This phenomenon is at the basis of the emergence of new elementary modes of excitation (pairing vibrations for single Cooper pairs, pairing rotations for few ones, supercurrents and Josephson currents for macroscopic amounts of them).

The situation of very extended Cooper pairs sound, in principle, very different in the case of condensed matter (e.g. low-temperature superconductors) than in atomic nuclei, in keeping with the fact that nuclear Cooper pairs are, as a rule, subject to an overwhelming external (mean) field ($|E_{corr}| \approx 2\Delta \approx 2.4$ MeV $\ll |U(r \approx R_0)| \approx |V_0/2| \approx 25$ MeV). But even in this case, one can posit that in the transition from independent-particle to independent-pair motion implies that Cooper pair partners recede from each other. Let us clarify this point for the case of a single pair, e.g. $^{210}\text{Pb(gs)}$. It is true that allowing the pair of neutrons to correlate in the valence orbitals leads to a pair wavefunction which is angle correlated ($\Omega_{12} \approx 0$), as compared to e.g. the pure $j^2(0)(j = g_{9/2})$ configuration¹⁸ (App. 4.D). On the other hand, the correlated pair addition mode (Tables 3.5.4 and 3.5.5) will display a sizeable spill out as compared to the pure two particle state, and thus a lower density and larger related average distance between Cooper pair partners. This is also the reason why close to $\approx 40\%$ of the pairing matrix elements is contributed by the induced pairing interaction resulting from the exchange of long wavelength, low-lying, collective modes, the other $\approx 60\%$ resulting from the bare nucleon-nucleon 1S_0 pairing interaction. In carrying out the above arguments the values of

¹⁶In this case $R(^{11}\text{Li}) = \text{micheletti carloni} 4.58 \pm 0.13$ fm, the effective Wigner-Seitz radius being $(r_0)_{eff} \approx 4.58 \text{ fm}/(11)^{1/3} \approx 2.1$ fm.

¹⁷cf. Leggett (2006) p. 185; for the non local nuclear version cf. e.g. Broglia and Winther (1983).

¹⁸Bertsch et al. (1967), Ferreira et al. (1984); Matsuo (2013).

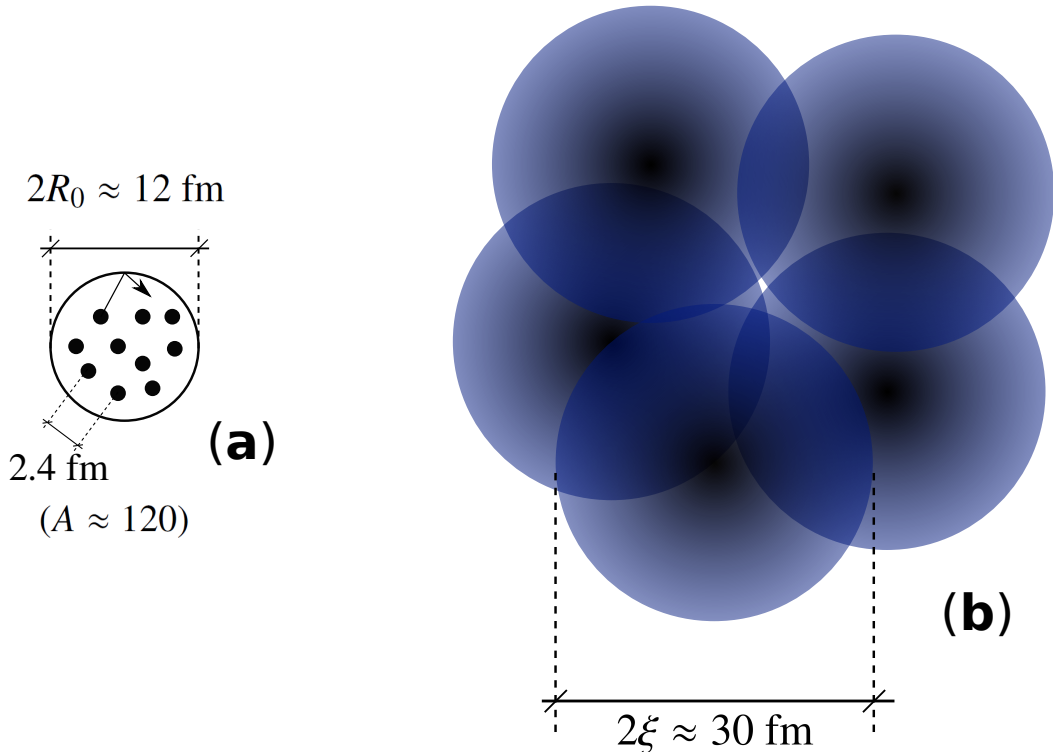


Figure 4.3.1: (a) Schematic representation of independent-particle motion and (b) independent-pair motion. In the first case nucleons (fermions) move independently of each other reflecting elastically from the wall of the mean field created by all the other nucleons, each of which is associated with a Wigner-Seitz cell of volume $(4\pi/3)R_0^3/A = (4\pi/3)r_0^3$, implying a relative distance of $2r_0 (\approx 2.4 \text{ fm})$. Switching on the pairing interaction (bare plus induced) leads to Cooper pair formation in which the correlation length (mean square radius) is ξ . Thus, pair of nucleons moving in time reversal states close to the Fermi energy will tend to recede from each other lowering their relative momentum ($r_0 \rightarrow \xi$) thus boosting the stability of the system, provided that the external mean field allows for it. Or better, if there is nucleon density available to do so, something controlled to a large extent by the single-particle potential. From this point on, and at least for the levels lying close to the Fermi surface, one cannot talk about particles but about Cooper pairs (unless one does not intervene the system with an external field, e.g. (p, d) and provides the energy, angular and linear momentum needed to break a pair). Of course that in the system to the right under the influence of a very strong external field (like e.g. the HF of ^{120}Sn), Cooper pairs will be constrained within its boundaries. But the picture displayed in (b) will be close to be representative in the case of two nuclei of ^{120}Sn at a relative (CM) distance larger than $2R_0 (\approx 12 \text{ fm})$, but still in weak contact. The pair field associated with a Cooper pair will extend from one to the other partner of the heavy ions participating in the reaction through the weakly overlapping interaction region, allowing two nucleons to correlate over a distance ξ and, eventually, in a reaction like e.g. $\text{Sn}+\text{Sn} \rightarrow \text{Sn(gs)}+\text{Sn(gs)}$ allow for the transfer of two nucleons correlated over tens of fm.

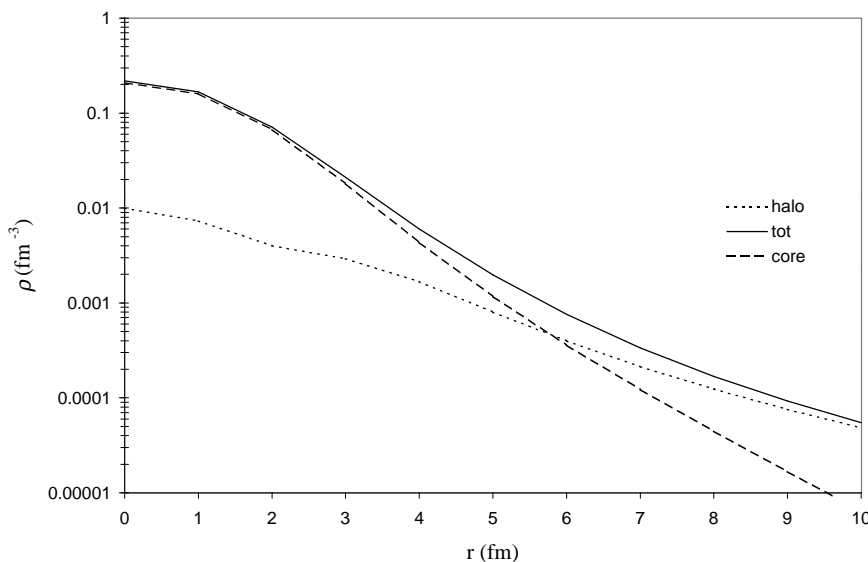


Figure 4.3.2: The nuclear density associated with ^{11}Li , as resulting from the microscopic NFT calculations which are at the basis of the results displayed in Figs. 3.6.3 and 7.1.3 (Barranco et al. (2001)). The contribution arising from the core (^9Li) is displayed with a dashed curve, while that associated with the two halo neutrons (cf. Eqs. (7.1.1)–(7.1.3)) is shown in term of a dotted curve. The sum of these two contributions labeled tot (total) is drawn with a continuous curve.

$(|E_{corr}|/\epsilon_F)^2 \approx \left(\frac{2.4 \text{ MeV}}{36 \text{ MeV}}\right)^2 \approx 10^{-3}$ and $\xi = \frac{\hbar v_F}{\pi \Delta} \approx 14 \text{ fm}$ ($(\frac{v_F}{c}) \approx (k_F)_{\text{fm}^{-1}}/5 \approx 0.27$), typical for superfluid nuclei lying along the stability valley, were used.

The situation described above becomes likely clearer, even if extreme, in the case of ^{11}Li . In this case, the Fermi momentum is $k_F \approx 0.8 \text{ fm}^{-1}$, the radius $R \approx 4.58 \text{ fm}$, much larger than $R_0 = 2.7 \text{ fm}$ expected from systematics. Furthermore essentially all of the correlation energy ($E_{corr} \approx -0.5 \text{ MeV}$, $(E_{corr}/\epsilon_F)^2 \approx (0.5/13)^2 \approx 10^{-3}$, $\xi \approx 20 \text{ fm}$ ($v_F/c \approx 0.2(k_F)_{\text{fm}^{-1}} \approx 0.16$; Eq. (7.E.6) and footnote 55 of Chapter 7)) is associated with the exchange of the dipole pygmy resonance between the halo neutrons¹⁹. It is of notice that in this case, renormalization effects due to the clothing of single-particle states by vibrations, in particular the lowest lying quadrupole vibration of the core ^9Li , are as strong as mean field effects. This is testified by parity inversion and the appearance of a new magic number namely $N = 6$ (see Fig. 3.6.3 (I)). Again in this case $s_{1/2}^2(0)$ and $p_{1/2}^2(0)$ are not correlated in Ω_{12} , while the Cooper state probability density displays a clear angular correlation (see Fig. 3.6.3 (II) (a) and (b)). Nonetheless, the average distance between the partners of the neutron halo Cooper pair, is considerably larger than that associated with the ^9Li core nucleons, as testified by the following numerical estimates (see also Fig. 4.3.2):

$$\text{a)} \quad R(^{11}\text{Li}) = 4.58 \pm 0.13 \text{ fm} \quad (V = (4\pi/3)R^3 = 402.4 \text{ fm}^3) \quad (4.3.3)$$

$$\text{b)} \quad R_0(^{11}\text{Li}) = 2.7 \text{ fm} \quad (V = 82.4 \text{ fm}^3) \quad (4.3.4)$$

$$\text{c)} \quad R_0(^9\text{Li}) = 2.5 \text{ fm} \quad (V = 65.4 \text{ fm}^3), \quad (4.3.5)$$

and associated mean distance between nucleons,

$$\text{a)} \quad \left(\frac{402.4 \text{ fm}^3}{2} \right)^{1/3} \approx 5.9 \text{ fm}, \quad (4.3.6)$$

$$\text{b)} \quad \left(\frac{82.4 \text{ fm}^3}{11} \right)^{1/3} \approx 1.96 \text{ fm}, \quad (4.3.7)$$

$$\text{c)} \quad \left(\frac{65.4 \text{ fm}^3}{9} \right)^{1/3} \approx 1.94 \text{ fm}. \quad (4.3.8)$$

The above quantities are to be compared with the definition²⁰,

$$d = \left(\frac{\frac{4\pi}{3}R^3}{A} \right)^{1/3} = \left(\frac{4\pi}{3} \right)^{1/3} \times r_0 \approx 1.93 \text{ fm}, \quad (4.3.9)$$

consistent with the standard parametrization $R_0 = r_0 A^{1/3}$ of the nuclear radius written in terms of the Wigner–Seitz cell radius r_0 (=1.2 fm) associated with each nucleon, and derived from systematics of stable nuclei lying along the stability valley.

¹⁹See Barranco et al. (2001); see also Broglia et al. (2019a).

²⁰Brink and Broglia (2005) App. C.

4.3.1 Interplay between mean field and correlation length

In Fig. 4.3.1 one displays a schematic representation of two possible *gedanken experiments* situations: **(a)** (*independent particle motion*) system which can be probed in a (p, t) reaction leading insight into non-interacting nucleons confined in a mean field potential, e.g. a Saxon-Woods potential with standard parametrization²¹; **(b)** *independent pair motion*, target of pickup reactions induced in a heavy ion collision between superfluid nuclei. In this case it is assumed that nucleons interact through an effective pairing interaction, sum of a short (v_p^{bare}) and long range (v_p^{ind}) NN -pairing potential and are confined by a mean field, whose parameters are freely adjusted so as to profit at best the pair coupling scheme.

In other words, one moves from a situation in which one assumes: (a) $H = T + v \approx T + U$ (ansatz $\langle v - U \rangle \approx 0$) to another in which (b) $H = T + v \approx T + U' + v_p^{eff}$ (ansatz $\langle v - U' - v_p^{eff} \rangle \approx 0$ and $|U'| \lesssim |U|$, $|v_p^{eff}| \ll |U'|$). Switching from the first to the second situation, pairs of nucleons moving in time reversal states will tend to recede from each other. It can be argued that, to the extent that one is interested in describing nuclei lying along the stability valley like e.g. ^{120}Sn , ansatz (a) is more realistic than (b), in keeping with the fact that $(U' + v_p^{eff})$ represent a much smaller fraction of v than U does. Consequently, the right view seems to be that of (a) plus pairing, in which case Cooper pair partners approach each other, if nothing else, because of angular correlation²² (App. 4.D). Now, this result may be interesting in itself in order to compare (nuclear structure) theory with theory, but not theory with experiment. At least not the experiments associated with the specific probe of Cooper pair correlations, namely two-nucleon transfer reactions, in which case the closest quantity to *be observable is the two-nucleon transfer formfactor* (Sect. 7.6.3). The “correctness” of picture (b) gets strong support from the fact that one- and two-particle transfer absolute cross sections have the same order of magnitude²³.

Within this context we note that the fact that $^9\text{Li}_6$ is well bound ($N = 6$ isotope parity-inverted closed shell), $^{10}\text{Li}_7$ is not while $^{11}\text{Li}_8$ is again bound, indicates that we are confronted with a pairing phenomenon. Allowing the two neutrons moving outside $N = 6$ closed shell to correlate in the configurations $j^2(0)(s_{1/2}^2, p_{1/2}^2, d_{5/2}^2 \dots)$ through a short range bare pairing interaction, e.g. the v_{14} Argonne NN -potential, does not lead to a bound state. The system lowers the relative momentum of the pair by exchanging at the same time the low-lying dipole vibration (soft $E1$ mode, pygmy resonance)²⁴ of the associated diffuse system becoming, eventually, bound, ever so weakly ($S_{2n} = 380$ MeV). The radius of

²¹Bohr and Mottelson (1969)

²²Bertsch et al. (1967); Ferreira et al. (1984); Matsuo (2013) and refs. therein.

²³For example (Fortune et al. (1994)) $^{10}\text{Be}(t, p)^{12}\text{Be}(\text{gs})$ ($\sigma = 1.9 \pm 0.5$ mb, $4.4^\circ \leq \theta_{CM} \leq 54.4^\circ$) as compared to (Schmitt et al. (2013)) $^{10}\text{Be}(d, p)^{11}\text{Be}(1/2^+)$ ($\sigma = 2.4 \pm 0.013$ mb, $5^\circ \leq \theta_{CM} \leq 39^\circ$) in the case of light nuclei around closed shell, and (Bassani et al. (1965)) $^{120}\text{Sn}(p, t)^{118}\text{Sn}(\text{gs})$ ($\sigma = 3.024 \pm 0.907$ mb, $5^\circ \leq \theta_{CM} \leq 40^\circ$) as compared to (Bechara and Dietzsch (1975)) $^{120}\text{Sn}(d, p)^{121}\text{Sn}(7/2^+)$ ($\sigma = 5.2 \pm 0.6$ mb, $2^\circ \leq \theta_{CM} \leq 58^\circ$).

²⁴Broglia et al. (2019a).

the resulting system ($R(^{11}\text{Li})=4.58 \pm 0.13$ fm) corresponds, in the parametrization $R_0 = 1.2A^{1/3}$ fm, to an effective mass number $A \approx 60$. So undoubtedly the system has swelled in moving from $A = 9$ to $A = 11$ in a manner that goes beyond the $1.2A^{1/3}$ (fm) expected dependence. Although the correlation length of the neutron Cooper is restricted to $2 \times R(^{11}\text{Li}) \approx 9.2$ fm, half of the estimated value $\xi \approx 20$ fm, it is almost double as large as $2 \times R_0(^{11}\text{Li}) \approx 5.4$ fm. Consequently, the function ($|\Psi_0(\mathbf{r}_1, \mathbf{r}_2)|^2$) displayed in Fig. 3.6.3 (II) b) should be read with care. Within this context, it is noted that the associated mean field potential can be parametrized in terms of a standard Woods–Saxon potential²⁵ of depth $U' \approx -41$ MeV (Fig. 2.10.1), much weaker than the typical value of $U \approx -50$ MeV.

It will be surprising if the above mentioned bootstrap-like mechanism²⁶ namely that of profiting from low, unstable, nuclear densities to generate transient medium polarization effects to stabilize a Cooper pair halo system, was a unique property of ^{11}Li . In fact, one can expect particular situations of s and p states at threshold eventually leading to a symbiotic halo Cooper pair with such a small value of S_{2n} , which eventually gives rise to a value of $2R \approx \xi$, a situation which can eventually materialize also in connection with nuclear excited states. A problem in the quest of such exotic, but standard Cooper pair picture in condensed matter superconductors, may be related in the nuclear case to the very short lifetime of the resulting system (within this context one is reminded of the fact that $\tau_{1/2}(^{11}\text{Li})=8.75$ ms).

In the above discussion, mention has been made to a bootstrap generation of infinite, condensed-matter-like situation (also in connection with Figs. 4.5.1 and 4.8.1, in which one is referring to finite density overlap across barriers between superfluid nuclei). We remind us that such a methodologic approach is not new to nuclear physics. For this purpose we can use as example the definition of a nuclear temperature and of the associated energy reservoir which can be shared statistically. How does one make a heat reservoir in the nucleus? While it is not a thermal bath in the classical sense, when the system emits a neutron or a γ -ray in the cooling process, it exchanges energy statistically with the freed particle. This is in keeping with the fact that the energy distribution of the emitted nucleon or γ -ray is determined by the density of levels of the daughter states. Concerning the γ -decay of the compound nucleus, it proceeds through $E1$ –transitions, essentially profiting of the Axel–Brink ansatz²⁷ introduced in nuclear physics to deal with this type of cooling processes. Within the bootstrap ansatz of symbiotic Cooper pair binding, we introduce a straightforward generalization of the Axel–Brink hypothesis based on well established experimental results. Namely the fact that the line shape and thus also the percentage of EWSR per energy interval as well as the decay properties of the GDR will reflect the static (splitting) and dynamic (motional narrowing) deformation properties of the state on which the GDR is built upon²⁸

²⁵See Bohr and Mottelson (1969), Eq. (2–182) p. 239.

²⁶See Fig. 2.10.1, see also App. 7.A.

²⁷Namely, the hypothesis that on top of each excited level of the nuclear spectrum is built a GDR equal to that built on the ground state; Axel (1962); Brink (1955 (unpublished)).

²⁸Le Tourneau (no. 11, 1965); Bohr and Mottelson (1975); Bortignon et al. (1998) and refs.

In the case of halo nuclei this generalization is not only quantitative but also qualitative. A sensible fraction of the TRK sum rule is found almost degenerate with the ground state. From the elastic antenna-like response typical of the high energy GDR ($\hbar\omega_{GDR} \approx 80\text{MeV}/A^{1/3}$) one is now confronted with a very low energy ($\lesssim 1\text{ MeV}, \Gamma \approx 0.5\text{ MeV}$)²⁹ plastic dipole response (PDR, pygmy dipole resonance, or low-energy $E1$ mode). Regarding the consequences this phenomenon has for the $L = 1$ induced interaction between nucleons, one moves from dipole-dipole (static moment interactions) to dispersive (retarded) contributions, emerging essentially from quantum mechanical ZPF. In other words, and making use of an analogy with atomic physics, one moves from an interaction between polar molecules, to a “purely” quantal interaction arising from the mutual polarization of one molecule in the rapidly changing field of the other (due to the instantaneous configuration of electrons and nuclei associated with ZPF) and viceversa, only one operative in the case of non-polar molecules. It is this second one which dominates the van der Waals interaction (App. 3.A) and, similarly, it is one which can lead to an almost resonant gluing of Cooper pair halos, a mechanism found also at the basis of superconductivity in metals.

In other words, the energy centroid, the width and the percentage of the TRK sum rule (EWSR) of dipole resonances can be strongly affected by dynamical fluctuations and deformations which, in turn, depend onpairing, and thus on Cooper pairs. Because of angular momentum conservation, such phenomenon is restricted in lowest order to fluctuations and deformations of quadrupole and monopole type. In the case of ^{11}Li –with $R(^{11}\text{Li}) \approx 4.6\text{ fm}$, much larger than $R_0(^{11}\text{Li}) = 1.2A^{1/3}\text{ fm} \approx 2.7\text{ fm}$ – to an isotropic radial deformation, build up by the two less bound neutrons. This highly extended, low-momentum neutron halo, vibrating out of phase against the nucleons of the core (^9Li), gives rise to the soft $E1$ -mode (PDR). Being built on two quasiparticle configurations with radial wavefunctions displaying little overlap with that of the core, it can retain a conspicuous fraction of the TRK-sum rule ($\approx 8\%$)³⁰. It can be viewed as the taylored glue which, exchanged between the halo neutrons, bind the resulting neutron halo Cooper pair to the core.

The challenges faced to learn about the physical basis of pairing in nuclei are comparable to those encountered to extract a collective vibration from a background much larger than the signal, as it was the case in the discovery of the GDR in hot nuclei³¹. In trying to observe pairing effects in nuclei close to the ground state, one has the advantage to start with the system at zero temperature for free. On the other hand one needs to subtract the very large, state dependent effects of the “external” mean field, a challenge not second to that faced by condensed matter practitioners to study low-temperature superconductivity in general, and the Josephson effect in particular. Within this context, ^{11}Li provides a textbook

therein.

²⁹Kanungo et al. (2015).

³⁰Broglia et al. (2019a).

³¹See e.g. Bortignon et al. (1998) Figs. 1.4 and 6.8, and refs. therein.

example of the fact that, given the possibility³², nuclear pair partners recede from each other lowering in the process the momentum of relative motion and thus the confinement kinetic energy³³, allowing to extend the limits of stability of nuclear species through a subtle long range pairing mechanism.

4.4 Correlations between nucleons in Cooper pair tunneling

Let us call x_1 and x_2 the coordinates of the Cooper pair partners. Let us furthermore assume they can only take two values: 0 when they are bound to the target nucleus, 1 when they have tunneled and become part of the outgoing particle (see Fig. 4.4.1).

The correlation between the two nucleons is measured by the value³⁴

$$\langle x_1 x_2 \rangle - \langle x_1 \rangle \langle x_2 \rangle = \int d\gamma P_2 \times 1 \times 1 - \int d\gamma P_1 \times 1 \int d\gamma' P'_1 \times 1 = P_2 - P_1 P'_1, \quad (4.4.1)$$

$d\gamma$ being the differential volume in phase space, normalized with respect to the corresponding standard deviations, that is, with respect to

$$\sigma_{x_1} \sigma_{x_2} = [\langle x_1^2 \rangle - \langle x_1 \rangle^2] [\langle x_2^2 \rangle - \langle x_2 \rangle^2]^{1/2}. \quad (4.4.2)$$

Making use of the fact that

$$\langle x_1^2 \rangle = \int d\gamma P_1 \times 1^2 = P_1, \quad (4.4.3)$$

and

$$\langle x_1 \rangle = \int d\gamma P_1 \times 1 = P_1, \quad (4.4.4)$$

one can calculate the function which measures the correlations between nucleons 1 and 2, namely,

$$Corr = \frac{\langle x_1 x_2 \rangle - \langle x_1 \rangle \langle x_2 \rangle}{\sqrt{[\langle x_1^2 \rangle - \langle x_1 \rangle^2] [\langle x_2^2 \rangle - \langle x_2 \rangle^2]}} = \frac{P_2 - P_1 P'_1}{\sqrt{(P_1 - P_1^2)(P'_1 - P'_1^2)}}. \quad (4.4.5)$$

³²Namely, the presence of normal density. A feature which in the present case goes hand in hand with the presence of abnormal density (single Cooper pair).

³³That is, from $\hbar^2/(ma^2) \approx 50$ MeV ($a = 0.9$ fm) to $\hbar^2/(m(2R(^{11}\text{Li}))^2) \approx 0.5$ MeV ($R(^{11}\text{Li})=4.6$ fm; within this context it is of notice that the overlap between radial wavefunctions of the halo neutrons and of the core is $O = (R_0/R)^3 \approx 0.2$ see Fig. 2.10.1; see also Broglia et al. (2019b)). While the system loses in this way a consistent fraction of the bare, short range pairing interaction through screening, it opens up for long-range pairing contributions which, ever so weak, can still bind the halo Cooper pair to the core. In the case of superconducting metals, the correlation length is $\xi \approx 10^4$ Å, a distance to be compared to the Wigner-Seitz radius of ≈ 2 Å. This variation leads to a decrease of the Coulomb repulsion of 4 orders of magnitude. From $U_c = e^2/r = 14.4$ eV Å/(2 Å)=7.2 eV to $U_c = 14.4$ eV Å/(10⁴ Å)=1.4 meV.

³⁴Basdevant and Dalibard (2005).

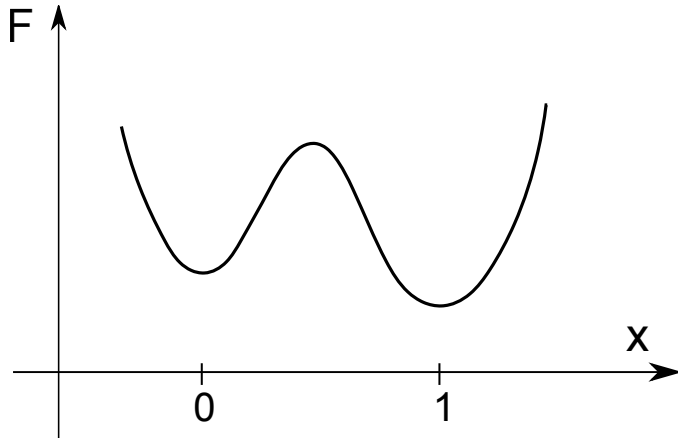


Figure 4.4.1: A schematic representation of nucleon tunneling between target and projectile. The free energy $F = U - TS$ which for the zero temperature situation under consideration (e.g. $^{120}\text{Sn}(p, d)^{119}\text{Sn}$, $^{120}\text{Sn}(p, d)^{118}\text{Sn}$) coincides with the potential energy as a function of the nucleon coordinate x . For $x = 0$ the nucleon is assumed to be bound to the target system. For $x = 1$ the nucleon has undergone tunneling becoming bound to the outgoing particle. In other words x_1 jumps from the value 0 to the value 1 in the tunneling process ($x, 0 \rightarrow 1$), the same for the coordinate of the second nucleon.

Because both nucleons are identical and thus interchangeable, $P_1 = P'_1$. Thus

$$\text{Corr} = \frac{P_2 - P_1^2}{P_1 - P_1^2}. \quad (4.4.6)$$

Making use of the empirical values

$$P_1 \approx P_2 \approx 10^{-3} \quad (4.4.7)$$

leads to,

$$\text{Corr} = \frac{10^{-3} - 10^{-6}}{10^{-3} - 10^{-6}} \approx 1. \quad (4.4.8)$$

In other words, within the independent pair motion regime, nucleon partners are solidly anchored to each other: if one nucleon goes over, the other does it also. This is so in spite of the very liable and fragile structure of the nuclear Cooper pairs ($2\Delta/\epsilon_F \ll 1$). A clear example of this scenario is provided by ^{11}Li . In fact, if one picks-up a neutron from ^{11}Li ($^{11}\text{Li}(p, d)^{10}\text{Li}$), the other one breaks up essentially instantaneously, ^{10}Li being unbound. In spite of this fact, the probability associated

$$\text{Order parameter} \quad \left(\langle \tilde{0}|PP^\dagger|\tilde{0} \rangle \right)^{1/2} = \begin{cases} \alpha_0 = \sum_{\nu>0} U'_\nu V'_\nu \\ \alpha_{dyn} = \sum_{\nu>0} U_\nu^{eff} V_\nu^{eff} \end{cases}$$

pairing vibrations

$$(U_\nu^{eff})^2 = 2Y_a^2(j_\nu)/\Omega_\nu; \quad (V_\nu^{eff})^2 = 1 - (U_\nu^{eff})^2$$

$$\begin{aligned} X_n(j_\nu) \\ Y_n(j_\nu) \end{aligned} \Bigg\} = \frac{\left(\sqrt{\Omega_j}/2\right)\Gamma_n}{2|E_j| \mp W_n}$$

pairing rotations

$$\begin{aligned} U'_\nu \\ V'_\nu \end{aligned} \Bigg\} = \frac{1}{\sqrt{2}} \left(1 \pm \frac{\epsilon_\nu}{\sqrt{\epsilon_\nu^2 + \Delta^2}} \right)^{1/2}$$

Figure 4.4.2: Order parameter associated with static and dynamic pair correlations (see Potel et al. (2013b)).

with the reaction³⁵ ${}^{35}\text{H}({}^{11}\text{Li}, {}^9\text{Li(gs)}){}^3\text{H}$ is given by

$$P_2 = \frac{(5.7 \pm 0.9) \text{ mb}}{2\pi((4.58 \pm 0.13) \text{ fm})^2} \approx (4.3 \pm 1)10^{-3}. \quad (4.4.9)$$

This value is much larger than the value of 4.85×10^{-6} associated with the breakup process mentioned above³⁶, let alone than $P_1^2 = (1.02 \times 10^{-3})^2 \approx 10^{-6}$ reported in entry $l = 0$ of Table 4.4.1.

In keeping with the fact that both of the two-nucleon transfer reaction cross sections ($\gtrsim 80\%$) is associated with successive transfer one could, in principle, be surprised of this result. The explanation for the fact that $P_2 \approx P_1$ is contained in the relation (4.3.1) applicable both for static and dynamic pair modes, in keeping with the fact that in nuclei, dynamic spontaneous breaking of gauge invariance is of similar importance as the static one³⁷.

Summing up, a direct consequence of the above parlance is the fact that the Cooper pair rigidity emerges from phase coherence (in gauge space), and leads

³⁵See Fig. 7.1.3, App. 7.B and Table 7.B.1 concerning the experimental value of $\sigma({}^{11}\text{Li} \rightarrow {}^9\text{Li (gs)})$ and Eq. (3.6.9) and following paragraph concerning the experimental (and estimated) value of $R({}^{11}\text{Li})$.

³⁶See entry $l = 0$ of column **3** of Table 7.B.1. It is of notice that the value given in Eq. (4.4.9) essentially coincides with that shown in $l = 0$, column **1** of the same table.

³⁷cf. Fig. 3.5.7, cf. also Sect. 4.9 and Fig. 4 of Potel et al. (2013b); cf. Fig. 4.4.2.

	p_l
0	1.02×10^{-3}
1	2.40×10^{-3}
2	1.26×10^{-2}
3	1.84×10^{-2}
4	6.13×10^{-3}
5	1.39×10^{-3}
6	2.89×10^{-4}
7	5.04×10^{-5}
8	6.51×10^{-6}
9	5.87×10^{-7}

Table 4.4.1: Probabilities p_l (see Sect. 4.2 and App. 7.B) associated with the reaction ${}^1\text{H}({}^{11}\text{Li}, {}^{10}\text{Li(gs)}){}^2\text{H}$ calculated with the same bombarding conditions as those associated with ${}^1\text{H}({}^{11}\text{Li}, {}^9\text{Li(gs)}){}^3\text{H}$ (see Table 7.B.1). It was assumed that the amplitude with which the single particle orbital $s_{1/2}$ enters in the $|{}^{10}\text{Li}(1/2^+)\rangle$ ground state (gs) is $\sqrt{0.5}$ (see Eqs. (7.1.1)–(7.1.3)).

to the generalized rigidity of pairing rotational (static) and vibrational (dynamic) bands which can be instantaneously set into rotation (vibration) with just the push imparted in gauge space by the transferred pair.

4.5 Pair transfer

The semiclassical two-nucleon transfer amplitudes fulfill, in the **independent particle limit**, the relations³⁸,

$$a_{sim}^{(1)} = a_{NO}^{(1)}, \quad (4.5.1)$$

and

$$a_{succ}^{(2)} = a_{one-part}^{(1)} \times a_{one-part}^{(1)}, \quad (4.5.2)$$

with

$$a + A \rightarrow f + F \rightarrow b + B, \quad (4.5.3)$$

corresponding to the product of two single nucleon transfer processes. On the other hand, in the **strong correlation limit** one can write, making use of the post-prior representation

$$\tilde{a}_{succ}^{(2)} = a_{succ}^{(2)} - a_{NO}^{(1)}. \quad (4.5.4)$$

Thus

$$\lim_{E_{corr} \rightarrow \infty} \tilde{a}_{succ}^{(2)} = 0, \quad (4.5.5)$$

³⁸see App. 6.C, also Potel et al. (2013a).

and all transfer is, in this case, due to simultaneous transfer (App. 6.C). Actual nuclei are close to the independent particle limit ($E_{corr} \approx (1\text{--}2 \text{ MeV}) \ll \epsilon_F (\approx 36 \text{ MeV})$). Then successive transfer is the major contribution to pair transfer processes. But successive transfer seems to break the pair *right? Wrong. Why?* let us see below.

4.5.1 Cooper pair dimensions

At the basis of the relations used to estimate the dimensions of a Cooper pair (correlation length; mean square radius) one finds

$$\delta x \delta p \geq \hbar \quad \delta \epsilon \approx |E_{corr}|, \quad (4.5.6)$$

where

$$\epsilon = \frac{p^2}{2m}; \quad \delta \epsilon = \frac{2p \delta p}{m} \approx v_F \delta p, \quad (4.5.7)$$

and thus

$$\delta \epsilon \approx |E_{corr}| \approx v_F \delta p, \quad (4.5.8)$$

leading to

$$\xi \approx \delta x \approx \frac{\hbar}{\delta p} \approx \frac{\hbar v_F}{|E_{corr}|} \quad (\text{correlation length}). \quad (4.5.9)$$

In what follows we use, for normal systems,

$$\xi = \frac{\hbar v_F}{\pi |E_{corr}|}, \quad (4.5.10)$$

and, in the case of open shell superfluid nuclei³⁹

$$\xi = \frac{\hbar v_F}{\pi \Delta}. \quad (4.5.11)$$

For Sn-isotopes, a typical value of the pairing gap is $\Delta \approx 1.2 \text{ MeV}$. Making use of $k_F = 1.36 \text{ fm}^{-1}$ associated with nuclei lying along the stability valley, and thus ($v_F/c \approx 0.2(k_F)_{\text{fm}^{-1}} \approx 0.27$),

$$\xi \approx 14 \text{ fm}. \quad (4.5.12)$$

Consequently, successive and simultaneous transfer feel equally well the pairing correlations giving rise to long range order⁴⁰. This virtual property can become⁴¹ real in e.g. a pair transfer between two superfluid tin isotopes (see Figs. 4.1.3 and 4.5.1).

³⁹See Schrieffer (1964) p. 18 and 34, Leggett (2006) p. 184, Annett (2013) p. 62.

⁴⁰See e.g. Potel et al. (2017) and references therein.

⁴¹See von Oertzen (2013); von Oertzen and Vitturi (2001).

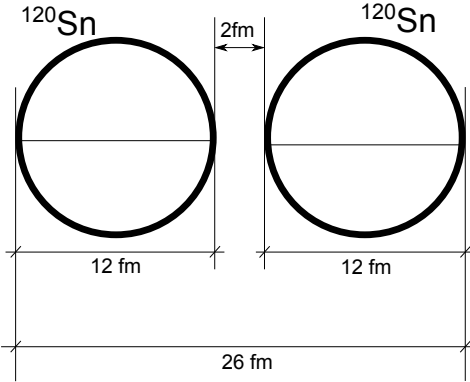


Figure 4.5.1: Schematic representation of two Sn-isotopes (radius $R_0 \approx 6$ fm) at the distance of closest approach in a heavy ion collision.

Objection

What about $v_{pairing}(= G)$ becoming zero, e.g. between the two nuclei?

Answer

$$\frac{d\sigma(a(= b + 2) + A \rightarrow b + B(= A + 2))}{d\Omega} \sim |\alpha_0|^2, \quad (4.5.13)$$

$$\alpha_0 = \langle BCS(A + 2)|P^\dagger|BCS(A)\rangle = \sum_{\nu>0} U_\nu(A) V_\nu(A + 2). \quad (4.5.14)$$

Objection

Relation (4.5.14) is only valid for simultaneous transfer, *right? Wrong.*

Answer

The order parameter can also be written as,

$$\begin{aligned} \alpha_0 &= \sum_{\nu, \nu' > 0} \langle BCS | a_\nu^\dagger | int(\nu') \rangle \langle int(\nu') | a_{\bar{\nu}}^\dagger | BCS \rangle \\ &\approx \sum_{\nu, \nu' > 0} \langle BCS(A + 2) | a_\nu^\dagger a_{\nu'}^\dagger | BCS(A + 1) \rangle \langle BCS(A + 1) | \alpha_{\nu'} a_{\bar{\nu}}^\dagger | BCS(A) \rangle \\ &= \sum_{\nu, \nu' > 0} \langle BCS(A + 2) | V_\nu(A + 2) \alpha_{\bar{\nu}} a_{\nu'}^\dagger | BCS(A + 1) \rangle \\ &\times \langle BCS(A + 1) | \alpha_{\nu'} U_\nu(A) a_{\bar{\nu}}^\dagger | BCS(A) \rangle = \sum_{\nu > 0} V_\nu(A + 2) U_\nu(A), \quad (4.5.15) \end{aligned}$$

where the (inverse) quasiparticle transformation relation $a_\nu^\dagger = U_\nu a_\nu^\dagger + V_\nu a_{\bar{\nu}}^\dagger$ was

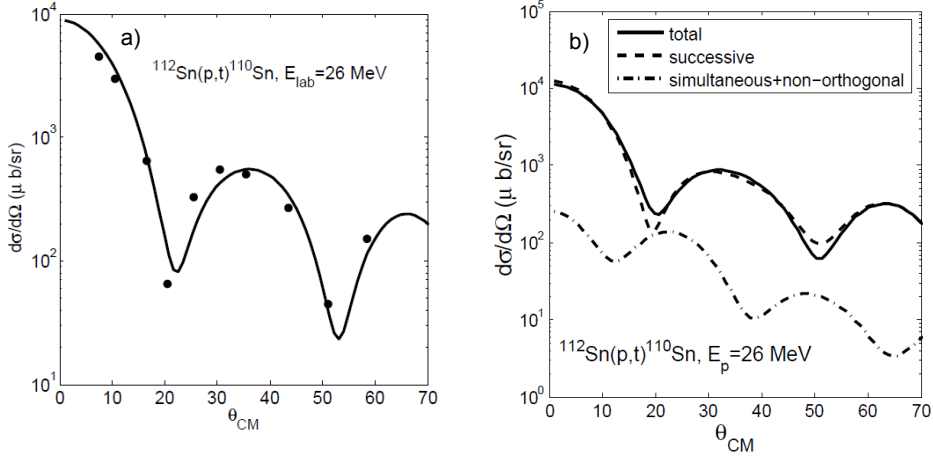


Figure 4.5.2: a) Absolute differential cross section associated with the reaction $^{112}\text{Sn}(p,t)^{110}\text{Sn}(\text{gs})$ calculated with the software COOPER (App. 7.C) in comparison with the experimental data (Guazzoni et al. (2006)). b) Details of the different contributions to the total absolute (p,t) differential cross section (for details see Potel et al. (2013a), Potel et al. (2013b)).

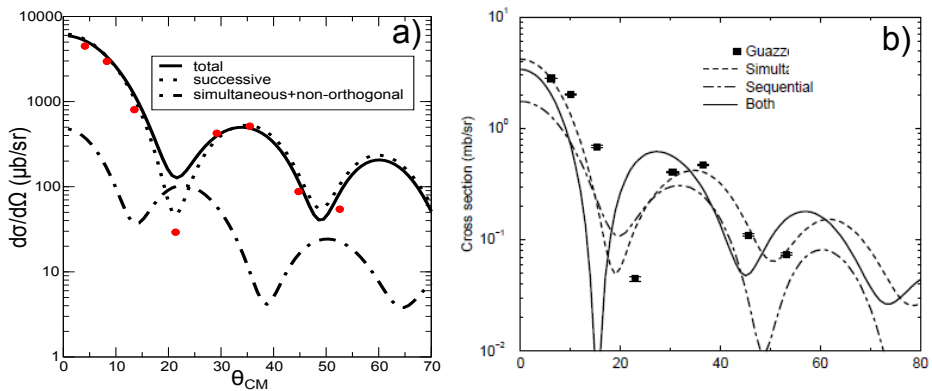


Figure 4.5.3: Absolute differential cross section associated with the reaction $^{124}\text{Sn}(p,t)^{122}\text{Sn}(\text{gs})$ calculated making use of: a) second order DWBA taking into account non-orthogonality corrections and the two-nucleon spectroscopic amplitudes resulting from BCS (see Table 3.4.1, third column; for details see Potel et al. (2013a), Potel et al. (2013b)) in comparison with experimental data (Guazzoni et al. (2011)). b) As above, but making use of FRESCO (reaction) and of shell model two-nucleon overlaps (structure); cf. Table 3.4.1 fourth column (for details cf. Thompson (2013)).

used⁴². Examples of two-nucleon spectroscopic amplitudes involving superfluid targets, namely those associated with the reactions $^{112}\text{Sn}(p, t)^{110}\text{Sn}(\text{gs})$ and $^{124}\text{Sn}(p, t)^{122}\text{Sn}(\text{gs})$ are given in Tables 3.4.1 and 7.4.1. Making use of some of these amplitudes (first column of Table 3.4.1) and of global optical parameters (Table 7.4.2), the two-nucleon transfer absolute differential cross section of the reaction $^{112}\text{Sn}(p, t)^{110}\text{Sn}(\text{gs})$ at center of mass bombarding energy of $E_p = 26$ MeV, was calculated making use of the software COOPER based on second order DWBA and taking into account successive and simultaneous transfer properly corrected for non-orthogonality (cf. Chapter 6 and App. 7.C). It is compared with experimental data in Fig. 4.5.2 (a). The corresponding absolute integrated cross sections are $1310 \mu\text{b}$ and $1309 \pm 200 \mu\text{b}$ respectively. The largest contribution to the cross section arises from successive transfer, the cancellation between simultaneous and non-orthogonality amplitudes being important (Fig. 4.5.2 (b)). The above is a typical example of results of a systematic study of two-nucleon transfer reactions in terms of absolute cross sections⁴³ (Figs. 3.1.6 and 7.4.1).

Making use of two-nucleon spectroscopic amplitudes worked out within the framework of an extended shell model calculation (Table 3.4.1, second column) one obtains very similar results to those displayed in Fig. 4.5.2 (a). In Fig. 4.5.3 (a) we report results similar to those displayed in Fig. 4.5.2, but for the case of the reaction $^{124}\text{Sn}(p, t)^{122}\text{Sn}(\text{gs})$ calculated within second order DWBA making use of the BCS spectroscopic amplitudes (Table 3.4.1 third column). We display in Fig. 4.5.3 (b) the absolute differential cross section calculated with NuShell spectroscopic amplitudes and the coupled channel software FRESCO⁴⁴.

Let us now provide an example of two-nucleon transfer around a closed shell nucleus displaying well defined collective pairing vibrational modes. We refer, in particular, to the pair removal mode of ^{206}Pb , that is, to the reaction, $^{206}\text{Pb}(t, p)^{208}\text{Pb}(\text{gs})$. Making use of the spectroscopic amplitudes displayed in Tables 3.5.2 and 3.5.3 and of global optical parameters, the associated absolute differential cross sections was calculated again with the software COOPER. It is displayed in Fig. 4.5.4 in comparison with experimental findings. In the same figure, the total differential cross section is compared with that associated with the TD (Tamm-Dancoff) description of $^{206}\text{Pb}(\text{gs})$, that is, setting the pairing ground state correlations to zero ($\sum_i X_r^2(i) = 1$, $Y_r(k) \equiv 0$, see Table 3.5.2). In this case, theory underpredicts observation by about a factor of 2. Also given in Fig. 4.5.4 is the predicted cross section associated with the pure configuration $|p_{1/2}^{-2}(0)\rangle$.

It is of notice, that within the effective reaction mechanism described in App. 6.B pairing correlations increase the value of $\Omega_0 (\approx 0.97)$. As a consequence the $l = n = 0$ two-neutron system gives a much larger contribution to the two-nucleon transfer process than those associated with $n = 1$ and 2, that is those proportional to Ω_1 and Ω_2 whose values are 0.25 and 0.06 respectively (cf. Eq. (6.B.13)). All these

⁴²See e.g. Brink and Broglia (2005) App. G.

⁴³Potel et al. (2013a), Potel et al. (2013b).

⁴⁴Thompson (2013).

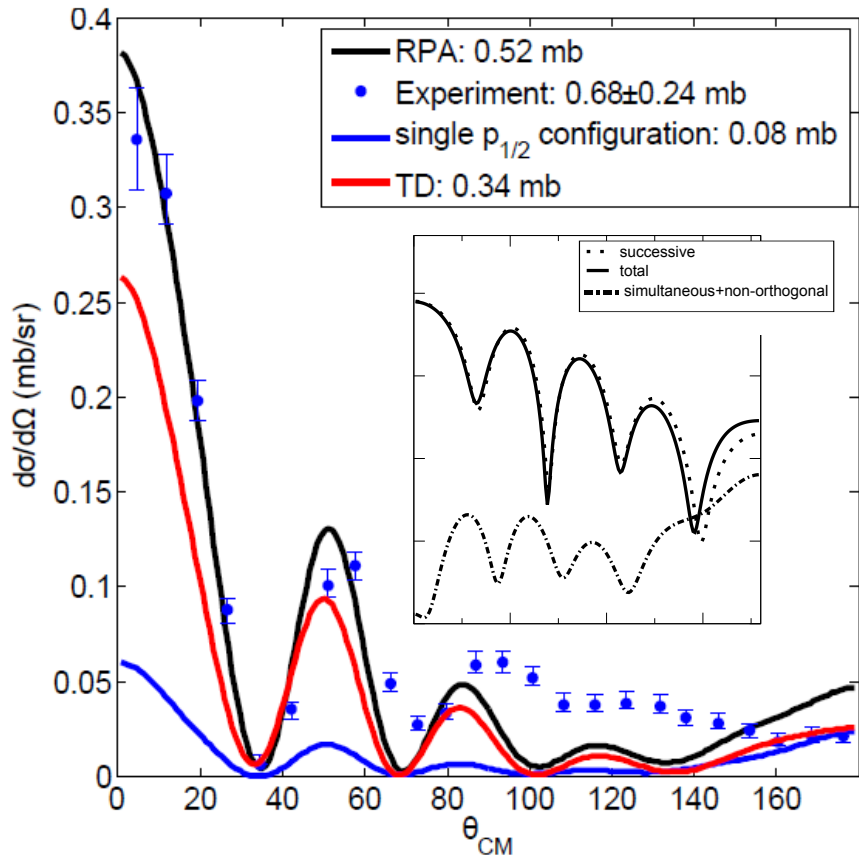


Figure 4.5.4: Absolute two-nucleon transfer differential cross section associated with the $^{206}\text{Pb}(t, p)^{208}\text{Pb}(\text{gs})$ transfer reaction, that is, the annihilation of the pair removal mode of ^{208}Pb in comparison with the data (Bjerregaard et al. (1966)). The theoretical cross sections were calculated making use of the spectroscopic amplitudes given in Tables 3.5.2 and 3.5.3 and of global optical parameters as reported in the reference above. Both RPA and TD amplitudes were used as well as a pure configuration $p_{1/2}^2(0)$.

features boost the effective absolute two-nucleon transfer cross section. While the results displayed in Fig. 4.5.4 were calculated making use of the full formalism of second order DWBA (Figs. 4.1.1 and 4.1.2) the simplified expressions given in Eqs. (6.B.1–6.B.3) and (6.B.13–6.B.16) were useful to gain physical insight into the effective two-nucleon transfer formfactors $u_{LSJ}^{J_i J_f} f(R)$. In fact, these functions, multiplied by the factors D_0 , provide a simple parametrization to account for the absolute two-nucleon transfer differential cross sections. *On the other hand, they were a source of misunderstanding concerning the reaction mechanism of two-nucleon transfer; let alone of the spatial structure of Cooper pairs*⁴⁵.

Let us elaborate on this point, making use of an analogy. Collective surface vibrations of closed shell nuclei can be viewed as correlated particle-hole excitations. The phase coherence existing between the different RPA amplitudes of the corresponding wavefunction leads to a decrease of the average distance (angular correlation) between the particle and the hole, as compared with pure ph -configurations, similar to what happens in pair addition (subtraction) modes (concerning this parallel see also Fig. 4.B.3). In this case are the pp (hh) which approach each other. It has been argued that this is the reason why both pairing and surface vibrations of closed shell nuclei display enhanced (t, p) cross sections as compared to pure configurations⁴⁶. The two neutrons lie rather close to each other in the triton.

Now, in the case of collective surface vibrations of closed shell nuclei, like e.g. the octupole vibration of ^{208}Pb ($E_x = 2.65$ MeV), the specific probe is not two-nucleon transfer, but Coulomb excitation or inelastic scattering, the wavelength of the γ -ray associated with the corresponding electromagnetic decay being $\lambda \approx 460$ fm. This is about two orders of magnitude larger than nuclear dimensions. Within this scenario, whether the particle lies closer to the hole or less in the correlated as compared to the pure $p - h$ state can hardly be of any relevance to explain the enhancement of the absolute transition probability ($B(E3) = 32$ Bsp). Not only this, it sets a question mark on the validity of the argument as applied to Cooper pair transfer and pairing correlations. This question is taken up in Sect. 4.9 and Apps. 4.B–4.D.

4.6 Comments on the optical potential

The following is to be read with the proviso mentioned in the starting of Sect. 2.10. Within this context see also footnote 118 in Ch. 2.

As a rule, the depopulation of the entrance, elastic channel $\alpha(a, A)$ (see Fig. 4.6.1) is mainly due to one-particle transfer channels $\phi(f(= a - 1), F(= A + 1))$.

Other channels, like e.g. inelastic ones $\beta(a^*, A)$, $\gamma(a, A^*)$ being operative in particular situations, for example, when deformed nuclei are involved in the reaction process. Let us assume that this is not the case. Thus, quite likely, the one-particle transfer channel ϕ is expected to be the main depopulating channel of the entrance

⁴⁵For more (historic) details see Broglia (2019a) (Overview).

⁴⁶Bertsch et al. (1967)

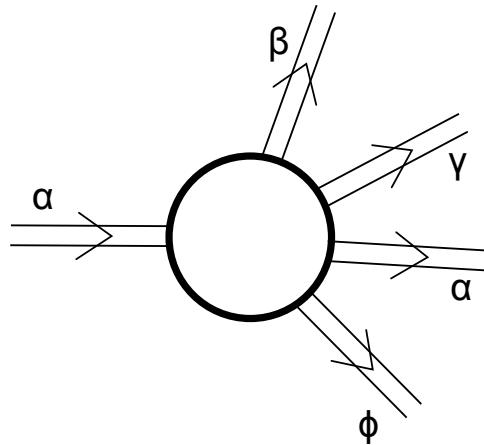


Figure 4.6.1: Schematic representation of entrance (α) and exit channels ($\beta, \gamma, \alpha, \phi$) of a nuclear reaction and of the interaction region.

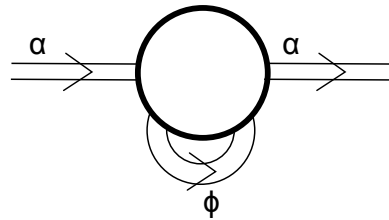


Figure 4.6.2: Schematic representation of the change in role of the one-nucleon transfer channel ϕ from being an open channel, (Fig. 4.6.1) to one which acts as a virtual channel contributing to the optical potential.

channel α (cf. Fig. 4.6.2). This is in keeping with the fact that the tail of the corresponding form factors, reaches further away than that of any other channel (cf. Fig. 4.6.5). In this case, the calculation of the optical potential⁴⁷, is quite reminiscent to the calculation of two-particle transfer (2nd order process), and can be carried out with essentially the same tools. In fact,

$$\begin{aligned} T_{succ}^{(2)} &\sim \langle fin|v|int\rangle\langle int|v|in\rangle \\ T_{NO}^{(2)} &\sim \langle fin|v|int\rangle\langle int|\mathbf{1}|in\rangle, \end{aligned} \quad (4.6.1)$$

where $|in\rangle = |a, A\rangle$, $|int\rangle = |f, F\rangle$ and $|fin\rangle = |b, B\rangle$ are the initial, intermediate, and final channels in a two-nucleon transfer reactions, which become

$$\begin{aligned} \langle in|v|int\rangle\langle int|v|in\rangle \\ \langle in|v|int\rangle\langle int|\mathbf{1}|in\rangle, \end{aligned} \quad (4.6.2)$$

as contributions to the optical potential (Fig. 4.6.2).

Let us elaborate on the above arguments within the context, for concreteness, of ^{11}Li and of the reaction $^{11}\text{Li}(p, t)^9\text{Li}$. In keeping with the fact that structure and reactions are just but two aspects of the same physics and that in the study of light halo nuclei, bound and continuum states are to be treated on, essentially, equal footing in the calculation of the wavefunctions (structure) as well as of the asymptotic distorted waves entering the calculation of the absolute two-particle transfer differential cross sections (reaction; see Figs. 4.6.3 (a) and (b)), the determination of the optical potentials is essentially within reach (reaction, see Figs. 4.6.3 (c) and 4.6.4). Because the real and imaginary parts of complex functions are related by simple dispersion relations⁴⁸ it is sufficient to calculate only one of the two (real or imaginary) components of the self-energy function to obtain the full scattering, complex self energy contribution to the nuclear dielectric function (optical potentials). Now, absorption is controlled by on-the-energy-shell contributions. It is

⁴⁷It is of notice that the optical potential can be viewed as the complex “dielectric” function of direct nuclear reactions. In other words, the function describing the properties of the medium in which incoming and outgoing distorted waves propagate, properties which are, as a rule determined through the analysis of elastic scattering processes, under the assumption that the coupling between the relative motion(reaction) and intrinsic (structure) coordinates, occur only through a Galilean transformation (recoil effect) which smoothly matches the incoming with te outgoing waves (trajectories). Now, within the present context, namely that of the microscopic calculation of $\Delta E + iW$ (Fig. 4.6.4), non-locality and ω -dependence can be microscopically treated on equal footing through the calculation of structure properties. In particular, within the framework of NFT, taking into account the variety of polarization and correlation (self energy) contributions to the optical potential, arising from couplings between single-particle and collective motion, elementary modes of nuclear excitation. Such an approach to structure and reaction provides the elements and rules for a microscopic calculations of the texture of the corresponding vacuum states, and thus of the bound and continuum properties of the nuclear quantal system by itself and in interaction. It is of notice that such a scenario includes also limiting situations like sub-barrier fusion processes (cf. e.g. Sargsyan et al. (2013) and refs. therein) and also exotic decay (cf. e.g. Barranco et al. (1988, 1990); Montanari et al. (2014), cf. also Brink and Broglia (2005)).

⁴⁸See, e.g., Mahaux et al. (1985) and references therein; Dickhoff and Van Neck (2005).

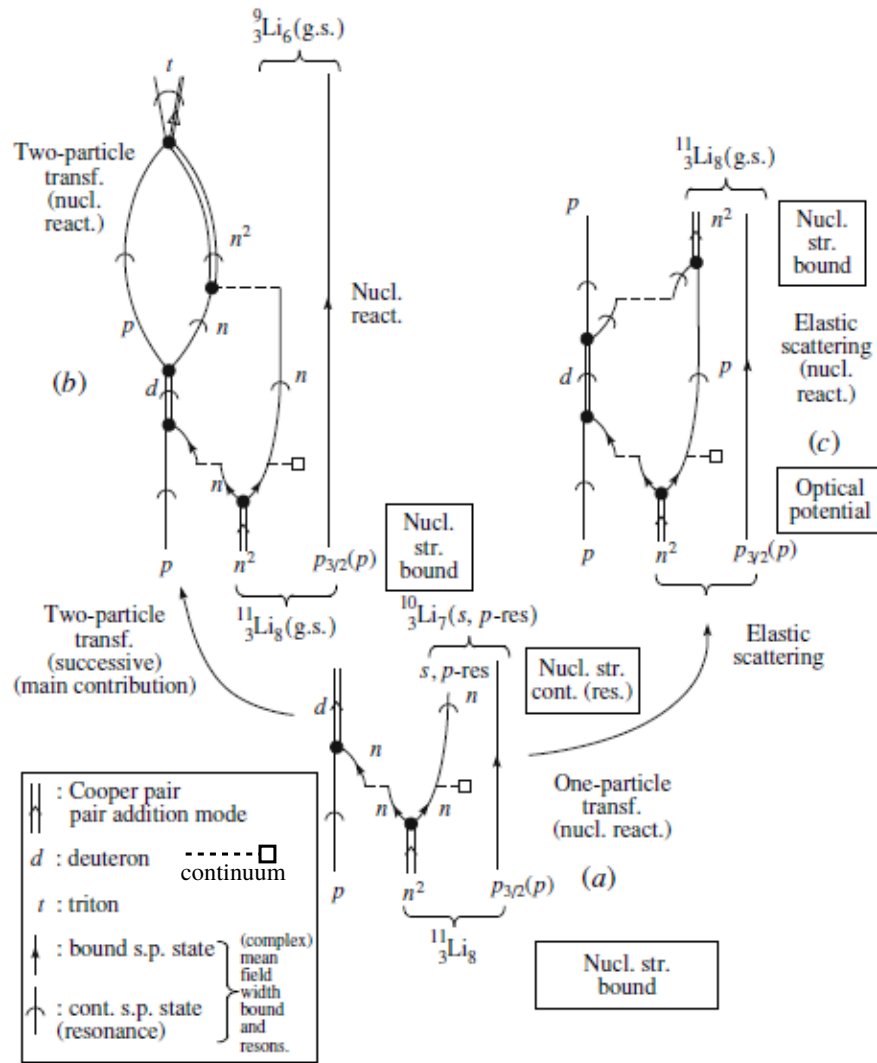


Figure 4.6.3: Simplified NFT diagrams summarizing the physics which is at the basis of the structure of ^{11}Li (Barranco et al. (2001)) and of the analysis of the $^{11}\text{Li}(p, t)^9\text{Li}(\text{g.s.})$ reaction (Potel et al. (2010)). In the figure emphasis is set on intermediate (like, e.g., $^{10}\text{Li} + d$, see (a) and (b)) and elastic (see (c), see also Fig. 4.6.4) channels. It is of notice that for simplicity the recoil mode has not been drawn (within this connection see Figs. 2.10.2 and 2.10.3).

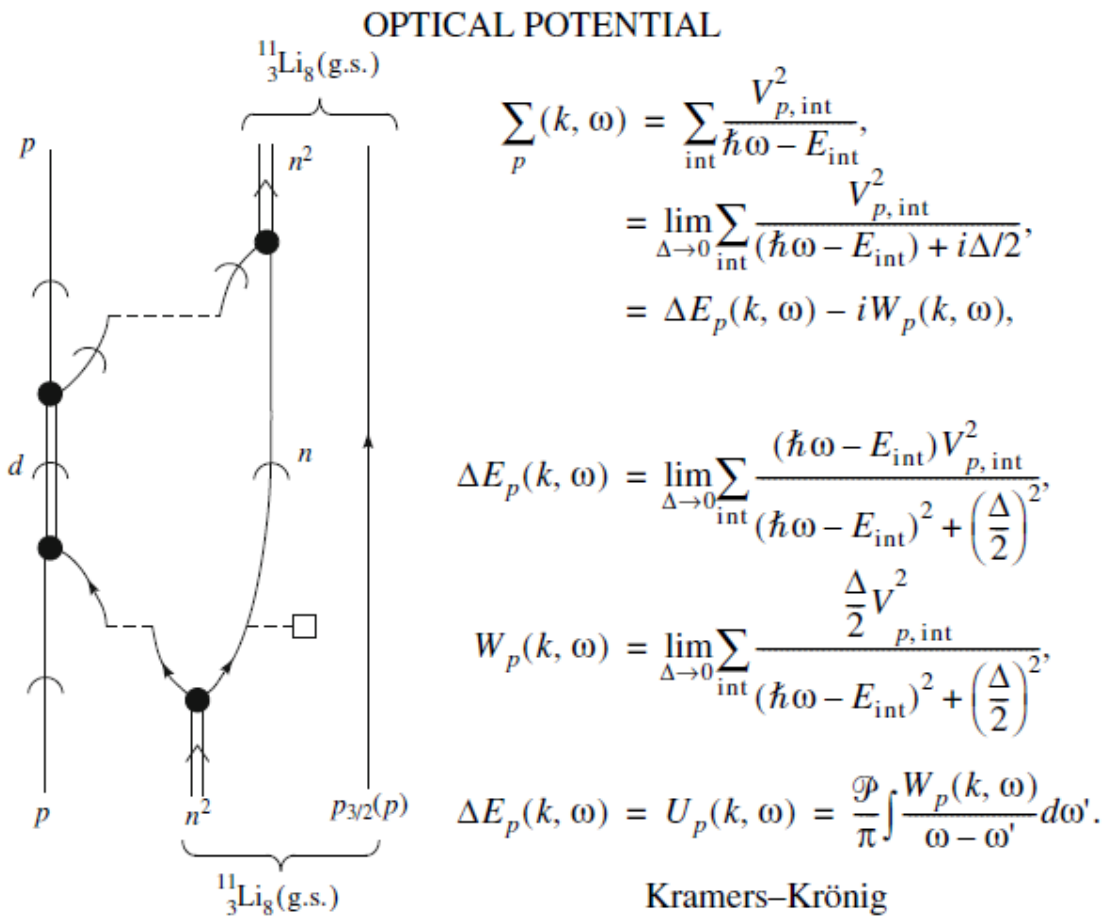


Figure 4.6.4: Schematic NFT diagrams and summary of the expression (see, e.g., Mahaux et al. (1985) and references therein) entering the calculation of one of the contributions (that associated with one-particle transfer and, arguably, the dominant one) to the $^{11}\text{Li} + p$ elastic channel optical potential (for details see Fig. 2.10.2). The self-energy function is denoted Σ_p , while the real and imaginary parts are denoted $\Delta E_p (= U_p)$ and W_p , respectively, the subindex p indicating the incoming proton. These quantities are, in principle, functions of frequency and momentum.

then likely that the simplest way to proceed is that of calculating the absorptive potential and then obtain the real part by dispersion⁴⁹. Of notice that in heavy-ion reactions, one is dealing with leptodermous systems. Thus, the real part of the optical potential can, in principle, be obtained by convolution of the nuclear densities and of the surface tension⁵⁰. Within the present context, one can mention the ambiguities encountered in trying to properly define a parentage coefficient relating the system of $(A + 1)$ nucleons to the system of A nucleons, and thus a spectroscopic amplitude. In other words, a prefactor which arguably allows to express the absolute one-particle transfer differential cross section in terms of the elastic cross section. Making use of NFT diagrams like the one schematically shown in Fig. 4.6.4, it is possible to calculate, one at a time, the variety of contributions leading to one- and two-particle transfer processes as well as of the associated optical potential with the proper renormalized single-particle contents and radial wavefunctions (formfactors). Summing up the different contributions, taking also proper care of those arising from three- and four-point vertex, tadpole processes, etc., a consistent description of the different channels can be worked out, in which the predicted quantities to be directly compared with observables are absolute differential cross sections, or, more generally, absolute values of strength functions for different scattering angles.

4.7 Weak link between superconductors

Two-nucleon transfer reactions involving superfluid nuclei display some similarities with Cooper pair tunneling between weakly coupled superconductors, in particular when discussing heavy ion reactions, but not only⁵¹. Within this context it is useful to remind the basic elements of the pair tunneling which is at the basis of the Josephson effect. In this section we essentially reproduce the description of the tunneling of Cooper pairs between two weakly coupled superconductors to be found in⁵², likely the best physical presentation of the Josephson effect⁵³.

One starts with the many-body Hamiltonian of⁵⁴

$$H = H_1 + H_2 + \sum_{kq} T_{kq} (a_{k\uparrow}^\dagger a_{q\uparrow} + a_{-q\downarrow}^\dagger a_{-k\downarrow}) + hc \quad (4.7.1)$$

where H_1 and H_2 are the separate Hamiltonians of the two superconductors on each side of the barrier, T_{kq} being the (exponentially) small tunneling matrix element from state k on one side to q on the other.

One can arrive to (4.7.1) by first finding sets of single-particle wavefunctions for each side separately, in the absence of the potential of the other system. *Then*

⁴⁹Mahaux et al. (1985). See also App. 5.H.

⁵⁰Cf. e.g. Broglia and Winther (2004) and references therein.

⁵¹von Oertzen and Vitturi (2001); von Oertzen (2013); Broglia and Winther (2004).

⁵²Anderson (1964b)

⁵³Josephson (1962).

⁵⁴Cohen et al. (1962)

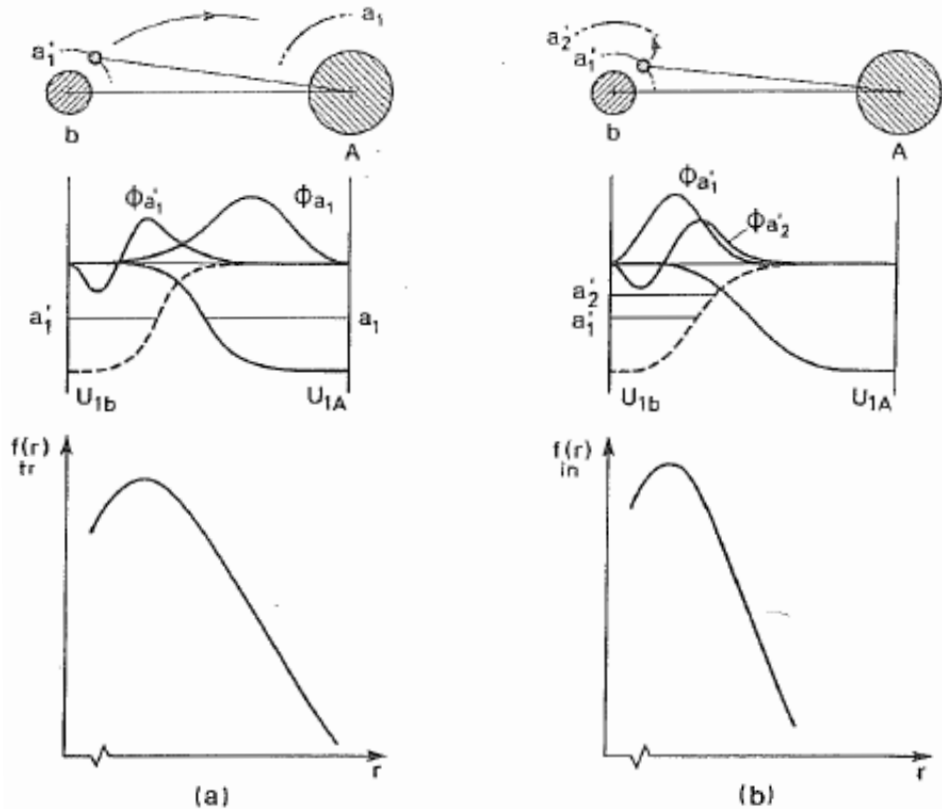


Figure 4.6.5: Schematic representation of the radial dependence of the one-particle transfer and inelastic form factors in a heavy ion collision. In (a) a nucleon moving in the orbital with quantum numbers a'_1 in the projectile a is transferred under the action of the shell model potential U_{1A} to the target nucleus A into an orbital a_1 . The dependence of the form factor on the distance between the two nuclei is determined by the overlap of the product of the single-particle wavefunctions $\phi_{a'_1}$ and ϕ_{a_1} with the potential U_{1A} . A schematic representation of this dependence is given at the bottom of (a). In (b) a nucleon in the projectile a is excited under the influence of the target field U_{1A} from the single-particle orbital with quantum numbers a'_1 to the orbital with quantum numbers a'_2 . The dependence of the form factor on the distance between the cores is here determined by the overlap of the product of the functions $\phi_{a'_1}$ and $\phi_{a'_2}$ with the potential U_{1A} . A representation of this dependence is shown at the bottom of (b) (after Broglia and Winther (2004)).

one eliminates the non-orthogonality effects by perturbation theory (cf. the similarity with the arguments used in Sect. 4.2 as well as App. 6.C; for further details see Sect. 6.1). It is of notice that a nuclear embodiment of such strategy but for the case superfluid–normal⁵⁵ tunneling is worked out in Ch. 6 and implemented in COOPER⁵⁶. It is of notice that at the basis of the Josephson effect one finds $P_2 \approx P_1$ which, in the nuclear case implies $\sigma_{2p} \approx \sigma_{1p}$. A remarkable finding whether both or a single of the interacting systems is a superfluid nucleus.

Let us now calculate the second order expression of (4.7.1) in the case in which the gaps of the two weakly linked superconductors are different. Making use of relations presented in Sect. 3.4.2 one can write, for $T = 0$,

$$\Delta E_2 = -2 \sum_{kq} |T_{kq}|^2 \frac{|V_k U_q + V_q U_k|^2}{E_k + E_q}. \quad (4.7.2)$$

With the help of

$$2U_k V_k^* = \frac{\Delta_k}{E_k}, \quad 2U_q V_q^* = \frac{\Delta_q}{E_q}, \quad (4.7.3)$$

and

$$|U_k|^2 - |V_k|^2 = \frac{\epsilon_k}{E_k}, \quad |U_q|^2 - |V_q|^2 = \frac{\epsilon_q}{E_q}, \quad (4.7.4)$$

where

$$E = \sqrt{\epsilon^2 + \Delta^2} \quad (4.7.5)$$

and

$$\Delta_k = \Delta_1 e^{i\phi_1}, \quad \Delta_q = \Delta_2 e^{i\phi_2}, \quad (4.7.6)$$

one can write for the numerator of Eq. (4.7.2),

$$\begin{aligned} NUM &= (V_k U_q + V_q U_k)(V_k^* U_q^* + V_q^* U_k^*) \\ &= \{V_k^2 U_q^2 + V_q^2 U_k^2\} + [(U_k^* V_k)(U_q V_q^*) + (U_q^* V_q)(U_k V_k^*)]. \end{aligned} \quad (4.7.7)$$

⁵⁵It is of notice that because pairing vibrations in nuclei are quite collective, leading to effective U and V occupation factor (cf. Fig. 4.4.2) (see also Potel et al. (2013b)), the nuclear and the condensed matter expressions for Cooper tunneling processes are very similar. Of course no supercurrent is expected between nuclei. However, the systems ¹²⁰Sn(gs), ¹¹⁹Sn(j), ¹¹⁸Sn(gs) form an ensemble of weakly coupled Fermi superfluids, with different (average) number of particles ($N, N - 1, N - 2$), to which essentially all the BCS techniques, including those of the present Appendix can be applied (cf. Fig. 4.8.1). It is of notice the parallel of this scenario with that associated with nuclei excited at rather high intrinsic excitation energies for which one defines a temperature. This is possible, because the excited (thermalized) nucleus is in equilibrium with the particles, namely neutrons and gamma-rays it emits, particles which act as a thermal bath, let alone the very high density of levels, of the compound nucleus (cf. Bertsch and Broglia (2005) p 171, Bortignon et al. (1998) p. 7).

⁵⁶Cf. App. 7.C; cf. also Broglia and Winther (2004).

It is of notice that, for simplicity, throughout this Appendix

$$V^2 \equiv |V|^2. \quad (4.7.8)$$

With the help of (4.7.3) the expression in the squared bracket in (4.7.7) can be written as

$$[] = \frac{1}{4E_k E_q} (\Delta_k^* \Delta_q + (\Delta_k^* \Delta_q)^*) = \frac{1}{4E_k E_q} 2\Re(\Delta_k^* \Delta_q). \quad (4.7.9)$$

Making use of the relations

$$\begin{aligned} (U_k^2 - V_k^2)(U_q^2 - V_q^2) &= U_k^2 U_q^2 - U_k^2 V_q^2 - V_k^2 U_q^2 + V_k^2 V_q^2 \\ &= -(U_k^2 V_q^2 + V_k^2 U_q^2) + (U_k^2 U_q^2 + V_k^2 V_q^2), \end{aligned} \quad (4.7.10)$$

and

$$\begin{aligned} 1 &= (U_k^2 + V_k^2)(U_q^2 + V_q^2) = U_k^2 U_q^2 + U_k^2 V_q^2 + V_k^2 U_q^2 + V_k^2 V_q^2 \\ &= (U_k^2 V_q^2 + V_k^2 U_q^2) + (U_k^2 U_q^2 + V_k^2 V_q^2), \end{aligned} \quad (4.7.11)$$

one obtains,

$$1 - (U_k^2 - V_k^2)(U_q^2 - V_q^2) = 2(U_k^2 V_q^2 + V_k^2 U_q^2), \quad (4.7.12)$$

that is, twice the expression written in curly brackets in (4.7.7). Consequently

$$\{ \} = \frac{1}{2} (1 - (U_k^2 - V_k^2)(U_q^2 - V_q^2)) = \frac{1}{2} \left(1 - \frac{\epsilon_k \epsilon_q}{E_k E_q} \right). \quad (4.7.13)$$

Thus, the sum of (4.7.9) and (4.7.13) leads to,

$$NUM = \frac{1}{2} \left(1 - \frac{\epsilon_k \epsilon_q}{E_k E_q} + \frac{\Re(\Delta_q^* \Delta_k)}{E_k E_q} \right) \quad (4.7.14)$$

and

$$\Delta E_2 = - \sum_{kq} \frac{|T_{kq}|^2}{E_k + E_q} \left(1 - \frac{\epsilon_k \epsilon_q}{E_k E_q} + \frac{\Re(\Delta_q^* \Delta_k)}{E_k E_q} \right). \quad (4.7.15)$$

With the help of (4.7.6) one can write

$$\Delta_k \Delta_q^* = \Delta_1 \Delta_2 e^{i(\phi_1 - \phi_2)} = \Delta_1 \Delta_2 (\cos(\phi_1 - \phi_2) + i \sin(\phi_1 - \phi_2)). \quad (4.7.16)$$

Thus

$$\Re(\Delta_k \Delta_q^*) = \Delta_1 \Delta_2 \cos(\phi_1 - \phi_2), \quad (4.7.17)$$

where \Re stands for real part. Making use of

$$\sum_k \rightarrow N_1 \int d\epsilon_1, \quad \sum_q \rightarrow N_2 \int d\epsilon_2 \quad (4.7.18)$$

where N_1 and N_2 are the density of levels of one spin at the Fermi energy one finally obtains⁵⁷

$$\begin{aligned} \Delta E_2 &\approx -N_1 N_2 \Delta_1 \Delta_2 \langle |T_{kq}|^2 \rangle \cos(\phi_1 - \phi_2) \int_{-\infty}^{\infty} \int_{-\infty}^{\infty} \frac{d\epsilon_1 d\epsilon_2}{E_1 E_2 (E_1 + E_2)} \\ &\approx -2\pi N_1 N_2 \langle |T_{kq}|^2 \rangle \cos(\phi_1 - \phi_2) \left(\pi \frac{\Delta_1 \Delta_2}{\Delta_1 + \Delta_2} \right). \end{aligned} \quad (4.7.19)$$

Replacing the phase difference in (4.7.19) by the gauge-invariant phase difference $\gamma = (\phi_1 - \phi_2) - \frac{2e}{\hbar} \int_1^2 \mathbf{A} \cdot d\ell$, where \mathbf{A} is the magnetic vector potential ($\nabla \times \mathbf{A} = \mathbf{B}$), and the line integral is carried across the barrier of thickness d ($\int_1^2 d\ell = d$), one can calculate the supercurrent⁵⁸ whose maximum value for two identical superconductors is⁵⁹

$$J_0 = \left(\frac{\pi \Delta}{2e} \right) \times \frac{1}{R_b} = \frac{\pi}{4} \frac{V_{equiv}}{R_b}, \quad (4.7.20)$$

where

$$\frac{1}{R_b} = \frac{4\pi e^2}{\hbar} N^2 \langle |T|^2 \rangle, \quad (4.7.21)$$

R_n being the tunneling resistance per unit area of the junction when both metals are in the normal state, and $V_{equiv} = 2\Delta/e$ is the minimum voltage at which a normal current, upon the breaking of Cooper pairs, starts to flow. For Pb and Sn, the gaps are 1.4 meV and 0.7 meV, leading to eV_{equiv} (V_{equiv}) ≈ 2.8 meV (2.8 mV) and 1.4 meV (1.4 mV) respectively. Assuming R_n to be of the order of 1Ω per unit area, implies maximum values of the Josephson supercurrent $J = J_0 \sin \gamma$ ($\gamma = \phi_1 - \phi_2 - \frac{2e}{\hbar c} \int_1^2 \mathbf{A} \cdot d\ell$, where \mathbf{A} is the vector potential), of the order of $J_0 \approx 2$ mA as experimentally observed.

It is suggestive that the expression (4.7.19) is formally similar to that of the ion-ion potential acting between two heavy ions in weak contact, namely at a distance a diffusivity away from the grazing distance r_g . In this case the role of the reduced

⁵⁷It is of notice that ΔE_2 is bilinear in the density of levels (see Potel et al. (2017)).

⁵⁸ $I = \frac{1}{d} (\delta(\Delta E_2)/\delta \mathbf{A}) = (2e/\hbar) N_a N_A \langle |T|^2 \rangle 2\pi (\Delta_a \Delta_A / (\Delta_a + \Delta_A)) \sin \left((\phi_1 - \phi_2) - \frac{2e}{\hbar} \int_1^2 \mathbf{A} \cdot d\ell \right)$, where one has divided by the thickness of the barrier d , so as to obtain a supercurrent per unit area ($\langle |T|^2 \rangle$ assumed to be an energy squared per unit area).

⁵⁹Tinkham (1996) Ch. 6, Eq. (6-4) and subsequent discussion; see also Anderson (1964a) Eq. (11) and following discussion.

gap is played by a quantity closely related to the reduced radius of curvature⁶⁰

$$U_{aA}^N(r_g + a) \sim \gamma \frac{R_a R_A}{R_a + R_A} a, \quad (4.7.22)$$

In the above expression $\gamma \approx 0.9$ MeV/fm² is the surface tension, $a = 0.63$ fm the diffusivity of the potential, $R_i (= (1.233A^{1/3} - 0.98A^{-1/3})$ fm) being the radii of nuclei $i = a, A$. For two identical nuclei $R_a = R_A = R$ and $V_0 = 8\pi\gamma Ra$. In the case in which the interacting nuclei are two ¹²⁰Sn systems $U_{aA}^N(r_g + a) = U_{aA}^N(13.43$ fm) ≈ -9 MeV.

Nuclei being leptodermous systems can be described at profit, concerning a number of properties, with the help of the liquid drop. Because at the grazing distance the two leptodermous objects overlap, although weakly, two “unit” areas disappear. To reconstruct them one has to separate the two nuclei until these areas are reconstructed again. The energy needed to do so has to compensate the value (4.7.22) which, in the present case is ≈ 6 MeV. Microscopically, the interaction (4.7.22) arises from a kind of, weak, covalent mechanism. The single-particle orbitals of the two individual nuclei a and A , are shared when in contact, leading to a common mean field.

Similarly, the weak limit (4.7.19) between the two superconductors 1 and 2, is associated with the situations in which each partner of a Cooper pair is in a different superconductor, a kind of covalent phenomenon, each Cooper pair being simultaneously shared by the two superconductors.

4.8 Rotation in gauge space

The occurrence of rotation as a feature of the nuclear spectrum, e.g. of pairing rotational bands, originates in the phenomenon of spontaneous symmetry breaking of rotational invariance in the two dimensional gauge space. In other words, violation of particle number conservation, which introduces a deformation that makes it possible to specify an orientation of the system in gauge space.

The condensate in the nuclear superfluid system involve a deformation of the field that creates the fermion pairs. The process of addition or removal of a Cooper pair constitutes a rotational mode in gauge space in which particle number plays the role of angular momentum. Pairing rotational bands represents the collective mode associated with spontaneous symmetry of particle number conservation (Goldstone mode).

Let us elaborate on the above points within the framework of a simple model which contains the basic physical features one is interested in discussing.

⁶⁰Broglia and Winther (2004) p.114 Eq. (40), $U_{aA}^N(r) = -V_0/(1 + \exp(\frac{r-R_0}{a}))$, $V_0 = 16\pi\gamma R_{aA}a$, $R_0 = R_a + R_A + 0.29$ fm, which for two ¹²⁰Sn nuclei ($R = 5.883$ fm) leads to $R_0 \approx 12.1$ fm and $V_0 = 83.8$ MeV. For energies somewhat above the Coulomb barrier, the grazing distance (Eq. (25) p. 128) of the above reference is $r_g = r_B - \delta \approx 12.8$ fm ($r_B \approx 13.3$ fm, $\delta \approx 0.5$ fm). Thus $(1 + \exp(\frac{r_g+a-R}{a})) \approx 10.1$.

We consider N nucleons moving in a single j -shell⁶¹ of energy ϵ_j and total angular momentum $(ls)j$. The number of pairs moving in time reversal state which can be accommodated in the shell is $\Omega = (2j + 1)/2$. Consequently, the value of the BCS occupation parameters is $V = (N/2\Omega)^{1/2}$ and $U = (1 - N/2\Omega)^{1/2}$. Setting $\epsilon_j = 0$. The solution of the BCS number and gap equations associated with a pairing force with constant matrix elements G are

$$\lambda = -\frac{G}{2}(\Omega - N), \quad (4.8.1)$$

and

$$\Delta = \frac{G}{2} \sqrt{N(2\Omega - N)}, \quad (4.8.2)$$

respectively.

The BCS ground state energy of the superfluid system is

$$U = 2 \sum_{\nu>0} (\epsilon_\nu - \lambda) V_\nu^2 - \frac{\Delta^2}{G}. \quad (4.8.3)$$

Using (4.8.1) and (4.8.2), one can write

$$U \approx \frac{\hbar^2}{2\mathcal{J}} N^2, \quad (4.8.4)$$

where

$$\mathcal{J} = \frac{2\hbar^2}{G}, \quad (4.8.5)$$

is the moment of inertia of the associated pairing rotational band. The fact that the single-particle energies are measured with respect to λ implies that the nucleons feel the Coriolis force ($\hbar\dot{\phi} = \lambda$) associated with rotation in gauge space (Eq. (4.8.10) below). In other words, the BCS solution is carried out in the intrinsic system of reference \mathcal{K}' (see below). In fact, the ground state energy in the laboratory system \mathcal{K} is (see Fig. 3.1.3)

$$E_0 = U + \lambda N = \lambda N + \frac{\hbar^2}{2\mathcal{J}} N^2, \quad (4.8.6)$$

a quantity which approaches zero linearly in N , as expected for a Goldstone mode.

4.8.1 Phase coherence

The phase of a wavefunction and the number of nucleons (electrons in condensed matter) are conjugate variables. In other words, the gauge angle and the particle number operators $\hat{\phi}$ and \hat{N} satisfy the commutation relation,

$$[\hat{\phi}, \hat{N}] = i. \quad (4.8.7)$$

⁶¹For details see e.g. App. H of Brink and Broglia (2005) and refs. therein.

In the particle number representation

$$\hat{N} = -i\partial/\partial\phi, \quad \hat{\phi} = \phi, \quad (4.8.8)$$

while

$$\hat{N} = N, \quad \hat{\phi} = i\partial/\partial N, \quad (4.8.9)$$

in the gauge angle representation. The time derivative of the gauge angle is given by the equation of motion⁶²,

$$\dot{\phi} = \frac{i}{\hbar} [H, \phi] = \frac{1}{\hbar} \frac{\partial H}{\partial N} = \frac{1}{\hbar} \lambda, \quad (4.8.10)$$

where λ is the chemical potential (Fermi energy).

Gauge invariance, i.e. invariance under phase changes, implies number of particle conservation in a similar way that rotational invariance implies angular momentum conservation.

Example: let us introduce the trivially invariant many-body wavefunction⁶³,

$$\Psi = a_1^\dagger a_2^\dagger \cdots a_N^\dagger \Psi_{vac}, \quad (4.8.11)$$

and rotate it an angle ϕ making use of the operator

$$\mathcal{G}(\phi) |\Psi_N\rangle = e^{-iN\phi} |\Psi\rangle = |\Psi'\rangle, \quad (4.8.12)$$

where

$$|\Psi'\rangle = a_1'^\dagger a_2'^\dagger \cdots a_N'^\dagger |0\rangle, \quad (4.8.13)$$

and

$$\mathcal{G}^{-1}(\phi) a_\nu^\dagger \mathcal{G}(\phi) = e^{-i\phi} a_\nu^\dagger = a_\nu'^\dagger, \quad (4.8.14)$$

thus

$$|\Psi_N\rangle = e^{iN\phi} |\Psi'_N\rangle, \quad (4.8.15)$$

and

$$\hat{N} |\Psi_N\rangle = -i \frac{\partial}{\partial \phi} |\Psi_N\rangle = N |\Psi_N\rangle. \quad (4.8.16)$$

A phase change for a gauge invariant function is just a trivial operation. Like to rotate a rotational invariant function. Quantum mechanically nothing happens rotating a spherical, symmetry conserving, system (in 3D-, gauge, etc.) space.

⁶²See e.g. Brink and Broglia (2005) App. I.

⁶³Anderson (1964b).

The situation is very different in the case of the wavefunction

$$\begin{aligned}
 |\text{BCS}(\phi)\rangle_{\mathcal{K}} &= \prod_{\nu>0} (U_\nu + V_\nu a_\nu^\dagger a_{\bar{\nu}}^\dagger) |0\rangle, \\
 &= \prod_{\nu>0} (U'_\nu + e^{-2i\phi} V'_\nu a_\nu^\dagger a_{\bar{\nu}}^\dagger) |0\rangle, \\
 &= \prod_{\nu>0} (U'_\nu + V'_\nu a_\nu'^\dagger a_{\bar{\nu}}'^\dagger) |0\rangle, \\
 &= |\text{BCS}(\phi = 0)\rangle_{\mathcal{K}'}, \tag{4.8.17}
 \end{aligned}$$

where

$$U_\nu = |U_\nu| = U'_\nu; \quad V_\nu = e^{-2i\phi} V'_\nu (V'_\nu = |V_\nu|). \tag{4.8.18}$$

In fact,

$$|\text{BCS}(\phi)\rangle_{\mathcal{K}} = \left(\prod_{\nu>0} U'_\nu \right) \sum_{N \text{ even}} \frac{e^{-iN\phi}}{(N/2)!} \left(\sum_{\nu>0} c'_\nu P_\nu^\dagger \right)^{N/2} |0\rangle, \tag{4.8.19}$$

with

$$c'_\nu = \frac{V'_\nu}{U'_\nu}; \quad P_\nu^\dagger = a_\nu^\dagger a_{\bar{\nu}}^\dagger, \tag{4.8.20}$$

is a coherent state in particle number which can be written as,

$$|\text{BCS}(\phi)\rangle_{\mathcal{K}} = \sum_N f_N(\phi) |\Psi_N\rangle \tag{4.8.21}$$

Let us now apply the gauge angle operator to it,

$$\hat{\phi} |\text{BCS}(\phi)\rangle_{\mathcal{K}} = \hat{\phi} \sum_N f_N(\phi) |\Psi_N\rangle, \tag{4.8.22}$$

that is,

$$i \frac{\partial}{\partial N} f_N(\phi) = \phi f_N(\phi). \tag{4.8.23}$$

Thus,

$$f_N(\phi) \sim e^{-iN\phi}, \tag{4.8.24}$$

and

$$|\text{BCS}(\phi)\rangle_{\mathcal{K}} \sim \sum_N e^{-iN\phi} |\Psi_N\rangle, \tag{4.8.25}$$

the state $|\text{BCS}(\phi = 0)\rangle_{\mathcal{K}'}$ being aligned in gauge space in which it defines a privileged orientation (z').

An isolated nucleus will not remain long in this product type state. Due to the term⁶⁴ $(G/4) \left(\sum_{\nu>0} (U_\nu^2 + V_\nu^2) (\Gamma_\nu^\dagger - \Gamma_\nu) \right)^2$ in the residual quasiparticle Hamiltonian it will fluctuate (QM, ZPF, Goldstone mode), and decay into a state

$$|N\rangle \sim \int d\phi e^{iN\phi} |BCS(\phi)\rangle_{\mathcal{K}} \sim \sum_{N'} \int_0^{2\pi} d\phi e^{-i(N'-N)\phi} |\Psi_{N'}\rangle \sim |\Psi_N\rangle \quad (4.8.26)$$

in keeping with the fact that

$$\int_0^{2\pi} d\phi e^{-i(N'-N)\phi} = \begin{cases} 2\pi\delta(N, N') & (N = N'), \\ \frac{i}{N'-N} e^{-i(N'-N)\phi} \Big|_0^{2\pi} = 0 & (N \neq N'). \end{cases} \quad (4.8.27)$$

The state $|N\rangle$ is a member of the pairing rotational band centered around neutron number N_0 . In the example discussed in connection with Figs. 3.1.2 and 3.1.3, $|N\rangle$ is one of the ground states of the Sn-isotopes around $N_0 = 68$. Making use of the fact that $E_R = (\hbar^2/2I)(N-N_0)^2$ and that $\delta N \delta\phi \approx 1$, the coherent state (4.8.21) will decay into one of the states $|N\rangle$, likely the one corresponding to $N = \sum_{\nu>0} 2V_\nu^2$, in a time \hbar/E_R . The member of Cooper pairs participating in the nuclear condensate in the case of ¹²⁰Sn is $\alpha'_0 \approx 5 - 6$, the number of neutrons being $2\alpha'_0 \approx 10$. Because $\delta N \sim \sqrt{N} \sim 3$ ($\delta\phi \sim 0.3$ rad, that is⁶⁵ $\delta\phi \sim 0.3/0.017 \approx 17^\circ$), one obtains $E_R \approx 0.092 \text{ MeV} \times (3)^2 \approx 1 \text{ MeV}$ ($\hbar^2/2I \approx G/4 \approx 25 \text{ MeV}/(4N_0) \approx 0.092 \text{ MeV}$, see Fig. 3.1.3). Consequently $\hbar/E_R \approx 10^{-21} \text{ s}$. Further insight into the same question can be obtained making use of (4.8.10). That is $1/\dot{\phi} \approx \hbar/\epsilon_F \approx \hbar/(36 \text{ MeV}) \approx 3 \times 10^{-23} \text{ s}$. In other words, superfluid nuclei prepared in isolation, in a state displaying a coherent superposition of N -values, will decay into a member of the corresponding pairing rotational band of which (4.8.19) (see also 4.8.21) is the intrinsic state, becoming stabilized on the particular state $|N\rangle$ after about 30 revolutions. The common assumption that N is fixed and ϕ not, is correct.

This is also the case for metallic superconductors. In fact, the state (4.8.17) even if prepared in isolation will dissipate because there is a term in the energy of the superconductor depending on N , namely the electrostatic energy $e^2(N -$

⁶⁴Within BCS theory of pairing, there are two parameters which determines spontaneous symmetry breaking in gauge space. The probability amplitude with which a pair state $(\nu\bar{\nu})$ is occupied, and that with which it is empty. Namely, V_ν and U_ν respectively. As a consequence, there only two fields F which contribute, through terms of type FF^\dagger , to the residual interaction H_{res} acting among quasiparticles, which is neglected in the mean field solution of the pairing Hamiltonian. One which is antisymmetric with respect to the Fermi surface namely $(U_\nu^2 - V_\nu^2)$ and which leads to pairing vibrations of the gauge deformed state $|BCS\rangle$. The other one, $(U_\nu^2 + V_\nu^2)$ is symmetric with respect to ϵ_F and leads to fluctuations which diverge in the long wavelength limit ($W''_1 \rightarrow 0$) in precisely the right way to set $|BCS\rangle$ into rotation with a finite inertia, and restore symmetry. This term can be written as $H_p'' = (G/4) \left(\sum_{\nu>0} (U_\nu^2 + V_\nu^2) (\Gamma_\nu^\dagger - \Gamma_\nu) \right)^2 = (G/4) \left(\sum_{\nu>0} (\Gamma_\nu^\dagger - \Gamma_\nu) \right)^2$, where $\Gamma_\nu^\dagger(\Gamma_\nu)$ is the two quasiparticle creation (annihilation) operator in the harmonic (quasiboson) approximation $[\Gamma_\nu, \Gamma_{\nu'}^\dagger] = \delta(\nu, \nu')$ see Brink and Broglia (2005), eq. 4.24 and Sect. I.4. For more details see App. J of this reference.

⁶⁵ $\delta\phi \approx 0.3/(\pi/180) \approx 0.3/0.017 \approx 17^\circ$.

$N_0)^2/2C$, where C is the electrostatic capacity⁶⁶. Because the number of overlapping Cooper pairs contributing to superconductivity is $\alpha'_0 \approx 10^6$ and thus the associated number of electrons $2\alpha'_0 \approx 2 \times 10^6$, $\delta N \sim \sqrt{N} \sim 10^3$, one can write $E_{el} = \frac{e^2}{2C}(\delta N)^2 \approx \frac{14.4 \text{ eV} \times 10^{-8} \text{ cm}}{2 \times 1 \text{ cm}} (10)^3 \approx 10^{-7} \text{ eV}$, and $\hbar/E_{el} \approx 10^{-14} \text{ s}$. Similarly as done in connection with atomic nuclei, we estimate $(\dot{\phi})^{-1} = \hbar/(4 \text{ eV}) \sim 10^{-16} \text{ s}$, implying in this case about 10^2 revolutions to loose the original N -wavepacket coherence. In this case $\delta\phi \sim 10^{-3}$ radians, that is $\delta\phi \sim 10^{-3}/0.017 \sim 1^\circ$. The opposite situation is that of the case in which one considers different parts of the same superconductor. In this case one can define relative variables $n = N_1 - N_2$ and $\phi = \phi_1 - \phi_2$ and again $n = -i\partial/\partial\phi$ and $\phi = i\partial/\partial n$. Thus, locally there is a superposition of different n states: ϕ is fixed so n is uncertain. It is obvious that there must be a dividing line between these two behaviors, perfect phase coherence and negligible coherence, namely the Josephson effect.

Clearly, again, the total phase of the assembly is not physical. However, the relative phases can be given a meaning when one observes, as one does in e.g. metallic superconductors, that electrons can pass back and forth through the barrier, leading to the possibility of coherence between states in which the total number of electrons is not fixed *locally*. Under such conditions there is, for instance, a coherence between the state with $N/2$ electrons in one half of the block and $N/2$ in the other, and that with $(N/2) + 2$ on one side and $(N/2) - 2$ on the other.

In the nuclear case, one can view the systems $|BCS(A+2)\rangle$ and $|BCS(A)\rangle$ as parts of a fermion superfluid (superconductor) which, in presence of a proton ($p + (A+2)$) are in weak contact to each other, the $d + |BCS(A+1)\rangle$ system (without scattering, running waves, but as a closed, virtual, channel) acting as the dioxide layer of a Josephson junction (Fig. 4.8.1).

Under favorable conditions, in particular of Q -value for the different channels involved and, similarly to the so called backwards rise effect, one may, arguably, observe signals of the coherence between systems $(A+2)$ and A in the elastic scattering process ${}^{A+2}X + p \rightarrow {}^A X + t \rightarrow {}^{A+2}X$, t denoting a member of a pairing rotational band (cf. Fig. 4.8.1, see also Fig 3.1.3).

Whether an effect which may parallel that shown in (c) (backwards rise) can be seen or not depends on a number of factors, but very likely it is expected to be a weak effect. This was also true in the case of the Josephson effect in its varied versions (AC, DC, etc.). In fact, its observation required to take into account the effect of the earth magnetic field, let alone quantal and thermal fluctuations.

A direct observation of weak coupling coherent phenomena between states $|BCS(A+2)\rangle$ and $|BCS(A)\rangle$ in $A+a \rightarrow A+a$ process could arguably, be achieved in e.g. the virtual transfer of two protons in the case in which the system A is superfluid in Z , and of the observation of associated γ -rays of frequency $\nu = Q_{2p}/\hbar$, where Q_{2p} is the Q -value of the two proton transfer process. It is of notice that a similar effect will be observed in the case of two-neutron transfer between superfluid systems in N , in keeping with the neutron effective charge.

⁶⁶The capacity of a sphere is $C = R$. Below we use $R = 1\text{cm}$ (see Anderson (1964b)).

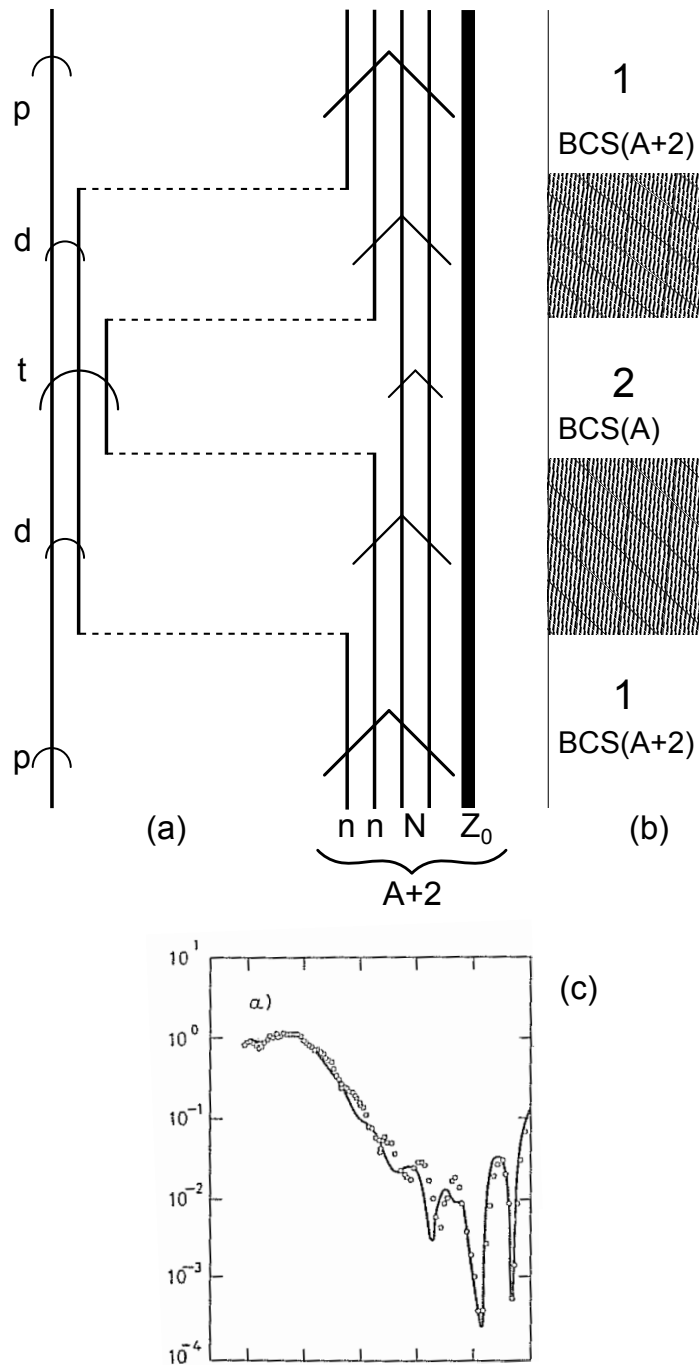


Figure 4.8.1: Gedanken experiment concerning the possibility of observing weak coupling coherence phenomena between states $|BCS(A + 2)\rangle$ and $|BCS(A)\rangle$ in an elastic reaction involving superfluid nuclei (a), e.g. $p + {}^{120}\text{Sn} \rightarrow p + {}^{120}\text{Sn}$, the system ${}^{119}\text{Sn} + d$ acting as a dynamical barrier (hatched areas arguably play role of that of dioxide layers in Josephson junctions) between the two even N superfluid systems arising from the successive transfer of two nucleons (b) and eventually allowing for a time dependent gauge phase difference between the $(A + 2)$ and A superfluid systems, thus leading, in the case in which Q -value effects are appropriate, to an oscillating enhancement of the elastic cross section at large angles as observed, for quite different reasons, in the case of the elastic angular distribution of the reaction ${}^{16}\text{O} + {}^{28}\text{Si}$ (cf. Pollarolo and Broglia (1984)).

4.9 Hindsight

The formulation of superconductivity (BCS theory) described by Gor'kov⁶⁷ allows, among other things for a simple visualization of spatial dependences. In this formulation $F(\mathbf{x}, \mathbf{x}')$ is the amplitude for two Fermions (electrons) at \mathbf{x}, \mathbf{x}' , to belong to the Cooper pair (within the framework of nuclear physics cf. e.g. Fig. 3.6.3 $\Psi_0(\mathbf{r}_1, \mathbf{r}_2)$; see also App. 4.B). The phase of F is closely related to the angular orientation of the spin variable in Anderson's quasispin formulation of BCS theory⁶⁸. The gap function $\Delta(x)$ is given by $V(\mathbf{x})F(\mathbf{x}, \mathbf{x})$ where $V(\mathbf{x})$ is the local two-body interaction at the point \mathbf{x} . In the insulating barrier between the two superconductors of a Josephson junction, $V(\mathbf{x})$ is zero and thus $\Delta(x)$ is also zero.

The crucial point is that vanishing⁶⁹ $\Delta(x)$ does not imply vanishing F , provided, of course, that one has within the insulating barrier, a non-zero particle (electron) density, resulting from the overlap of densities from right (R) and left (L) superconductors. Now, these barriers are such that they allow for one-electron-tunneling with a probability of the order of 10^{-10} and, consequently, the above requirement is fulfilled. Nonetheless, conventional (normal) simultaneous pair transfer, with a probability of $(10^{-10})^2$ will not be observed⁷⁰. But because one electron at a time can tunnel profiting of the small, but finite electron density within the layer, $F(\mathbf{x}, \mathbf{x}')$ can have large amplitude for Cooper pairs with partners electrons one on each side of the barrier (i.e. $\mathbf{x} \in L$ and $\mathbf{x}' \in R$), separated by distances $|\mathbf{x} - \mathbf{x}'|$ up to the coherence length. Hence, for barriers thick to only allow for essentially the tunneling of one electron at a time, but thin compared with the coherence length, two electrons on opposite sides of the barrier can still be correlated and the pair current be consistent. An evaluation of its value shows that, at zero temperature, the pair current is equal to $\pi/4$ times the single particle current at an equivalent voltage⁷¹ $2\Delta/e$.

The translation of the above parlance to the language of nuclear physics has to come to terms with the basic fact that nuclei are self-bound, finite many-body systems in which the surface, as well as space quantization, play a very important role both as a static element of confinement, as well as a dynamic source for renor-

⁶⁷Gor'kov (1958, 1959).

⁶⁸Anderson (1958); within the framework of nuclear physics cf. e.g. Bohr and Ulfbeck (1988), Potel et al. (2013b) and references therein.

⁶⁹This point was likely misunderstood by Bardeen who writes "...In my view, virtual pair excitations do not extend across the layer...", see McDonald (2001), see also Bardeen (1961) and Bardeen (1962).

⁷⁰Pippard (2012) see also McDonald (2001).

⁷¹In the case of Pb at low temperatures (≈ 7.19 K (0.62 meV)) this voltage is ≈ 1 meV/ $e = 1$ mV leading to ≈ 2 mA current for a barrier resistance of $R \sim 1\Omega$ (Ambegaokar and Baratoff (1963); McDonald (2001); Tinkham (1996)).

malization effects^{72,73}. Under the influence of the average potential which can be viewed as very strong external field ($|V_0| \approx 50$ MeV), Cooper pairs ($|E_{corr}| \approx 1.5$ MeV; see e.g. Fig. 3.5.1) will become constrained within its boundaries with some amount of spill out. In the case of the single open shell superfluid nucleus ^{120}Sn , the boundary can be characterized by the radius $R_0 \approx 6$ fm ($\ll \xi \approx 14$ fm), the spill out being connected with the diffusivity $a \approx 0.65$ fm.

Let us now consider a two nucleon transfer reaction in the collision Sn+Sn assuming a distance of closest approach of ≈ 14 fm, in which the two nuclear surfaces are separated by ≈ 2 fm (Fig 4.5.1). In keeping with the fact that this distance is about $3 \times a$, the heavy ion system will display a few percent (of saturation) density overlap in the interacting region. Ever so small this overlap of the nuclear surfaces, and so narrow the hole between the two leptodermic systems resulting from it, Cooper pairs can now extend over the two volumes, in a similar way as electron Cooper pairs could be partially found in the R and L superconductors in a Josephson junction. If this is the case, Cooper pair partners can be at distance as large as 26 fm, of the same order of magnitude as twice the correlation length. In other words, in the reaction $\text{Sn}+\text{Sn} \rightarrow \text{Sn(gs)}+\text{Sn(gs)}$ one expects (mainly successive) Cooper pair transfer of two neutrons which are away from each other by tens of fm.

As previously stated, an example of the fact that Cooper pairs will “expand” if the external mean field is weakened, is provided by ^{11}Li in which case, profiting of the weak binding (≈ 380 keV), the extension of the constrained Cooper pair (≈ 4.58 fm ± 0.13 fm) is similar to that expected in a nucleus of mass number $A \approx 60$, assuming a standard radial behavior, i.e. $r_0 A^{1/3}$ fm. In keeping with this scenario, it could be expected that moving from one neutron pair addition 0^+ mode of the $N = 6$ isotones⁷⁴ to another one ($|^{11}\text{Li(gs)}\rangle$, $|^{12}\text{Be(gs)}\rangle$ and $|^{12}\text{Be}(0^{++}; 2.24 \text{ MeV})\rangle$) one would see the system expanding, contracting and expanding again, respectively, in keeping with the fact that the external (mean) field is weak, strong, weak respectively, as testified by S_{2n} (380 keV, 3672 keV, 1432 keV). Within this context, the dipole strength (pygmy resonance) found on top of them is expected to vary in energy from very low ($\lesssim 1$ MeV) to high (2.71 MeV) to low (0.460 MeV), that is from a symbiotic, to an independent, and, likely, to a (quasi) symbiotic role again. Within this context, in Fig. 4.9.1 an overall view of the pairing vibrational modes associated with $N = 6$ parity inverted closed shell isotones, together

⁷²Within this context it is of notice that the liquid drop model is a very successful nuclear model, able to accurately describe not only large amplitude motion (fission, exotic decay, low-lying collective density and surface vibrations, cf. e.g. Bohr and Wheeler (1939), Barranco et al. (1990), Bertsch (1988), see also Brink and Broglia (2005) and references therein), but also the masses of nuclides (see e.g. Møller et al. (1995)), provided the superfluid inertia and shell corrections respectively, are properly considered. Thus, it is an open question whether in the quest of developing more predictive theoretical tools of the global nuclear properties one should develop ever more “accurate” zero range (Skyrme-like) forces, or deal also with the long wavelength, renormalization effects and induced interaction.

⁷³Broglia (2002).

⁷⁴See e.g. Gori et al. (2004).

with low-energy $E1$ -strength modes is given. The possible candidates to the role of neutron halo pair addition modes and symbiotic state are explicitly indicated (boxed levels).

Appendix 4.A Medium polarization effects and pairing

In many-body systems, medium polarization effects play an important role in renormalizing single-particle motion and the four-point vertices, namely Coulomb interaction in condensed matter and the bare NN -potential in nuclei. In what follows, special attention is paid to this mechanism in connection with the pairing interaction.

4.A.1 Nuclei

In many-body systems, medium polarization effects play an important role in renormalising single-particle motion and four-point vertices, namely the Coulomb interaction in condensed matter, and the bare NN -potential in nuclei. In what follows special attention is paid to medium polarization effect in connection with the pairing interaction.

Polarization contributions to the bare nucleon–nucleon pairing interaction through elementary modes of excitation

Elementary modes of excitation constitute a basis of states in which correlations, as found in observables, play an important role. As a consequence, it allows for an economic solution of the nuclear many–body problem of structure and reaction. A first step in this quest is to eliminate the non–orthogonality associated with single–particle motion in different nuclei (target and projectile (*reaction*)). Also between single–particle degrees of freedom and collective modes (vibrations and rotations (*structure*)) typical of an overcomplete , Pauli principle violating, basis. This can be done by diagonalizing, making use of the rules of nuclear field theory (NFT), the particle–vibration coupling (PVC), and the v_{np} (v : four point vertex, bare NN) interaction. In this way one obtains quantities (energies, transition probabilities, absolute value of reaction cross sections) which can be directly compared with the experimental findings. Such a protocol can be carried out, in most cases, within the framework of perturbation theory. For example, second order perturbation theory, in both reaction and structure, as exemplified in Fig. 2.10.3 displaying a NFT (r+s) graphical representation of contributions to the $^{11}\text{Li}(p,t)^9\text{Li}(\text{gs})$ and $^{11}\text{Li}(p,t)^9\text{Li}(1/2^-; 2.69 \text{ MeV})$ processes (see also Fig. 7.1.3). As a result, single-particle states move in a gas of vibrational quanta and become clothed by coupling to them. Similar couplings renormalize the bare NN -interaction in the different channels. In particular in the 1S_0 (pairing) channel.

Also as a result of their interweaving, the variety of elementary modes of excitation may break in a number of states, eventually acquiring a lifetime and, within

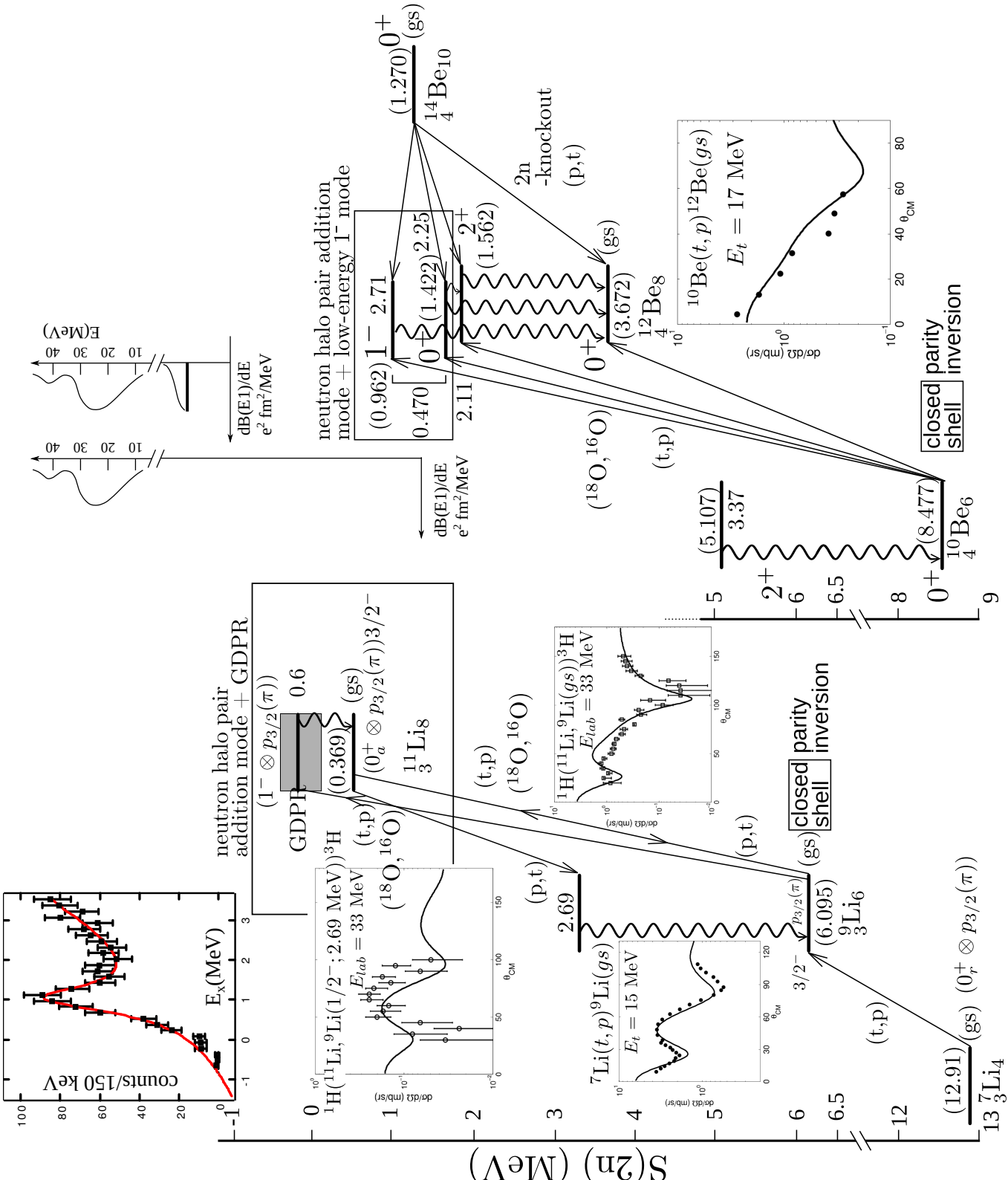


Figure 4.9.1: Monopole pairing vibrational modes associated with $N = 6$ parity inverted closed shell isotones, together with low-energy E1-strength modes. The levels are displayed as a function of the two-neutron separation energies $S(2n)$. These quantities are shown in parenthesis on each level, the excitation energies with respect to the ground state are quoted in MeV. Absolute differential cross sections from selected (t, p) and (p, t) reactions calculated as described in the text (cf. Potel et al. (2010, 2014)), in comparison with the experimental data (Young and Stokes (1971); Fortune et al. (1994)).

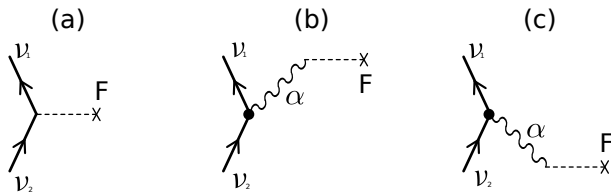


Figure 4.A.1: (a) F -moment of single-particle and (b,c) renormalization effects induced by the collective vibration α .

a coarse grain approximation, a damping width (imaginary component of the self energy). Moving into the continuum, as for example in the case of direct reactions, one such component is the imaginary part of the optical potential operating in the particular channel selected. It can be calculated microscopically using similar techniques and elements as e.g. those used in the calculation of the damping width of giant resonances. With the help of dispersion relations, the real part of the optical potential can be obtained from the knowledge of the energy dependence of the absorptive potential. In this way, the consistency circle structure-reaction based on elementary modes and codified by NFT could be closed. The rich variety of emergent properties found along the way eventually acquiring a conspicuous level of physical validation. In the case of halo exotic nuclei, in particular in the case of ^{11}Li (bootstrap, Van der Waals Cooper binding, halo pair addition mode (symbiosis of pairing vibration and pygmy) being few of the associated emergent properties) one is rather close to this goal. At that time it would be possible, arguably if there is one, to posit that the *ultima ratio* of structure and reactions, in any case that associated with pairing and Cooper pair transfer in nuclei, have been unveiled⁷⁵

Effective moments

At the basis of the coupling between elementary modes of excitation, for example of single-particle motion and of collective vibrations, one finds the fact that, in describing the nuclear structure it is necessary to make reference to both of them simultaneously and in an unified way.

Within the harmonic approximation the above statement is economically embodied in e.g. the relation existing between the collective ($\hat{\alpha}$) and the single-particle (\hat{F}) representation of the operator creating a particle-hole excitation. That

⁷⁵In the above paragraph we allowed ourselves to paraphrase Jacques Monod writing in connection with biology and life: *L'ultima ratio de toutes les structures et performances télémorphiques des êtres vivants est donc enfermée dans les séquences des radicaux des fibres polypeptidiques "embryons" de ces démons de Maxwell biologiques que sont les protéines globulaires. En un sens, très réel, c'est à ce niveau d'organisation chimique qui gît, s'il y en a un, le secret de la vie. Et saurait-on non seulement décrire les séquences, mais énoncer la loi d'assemblage à laquelle obéissent, on pourrait dire que le secret est percé, l'ultima ratio découverte (Monod (1970)).*

is⁷⁶,

$$\begin{aligned}
\hat{F} &= \left\{ \langle k|F|\tilde{i}\rangle \Gamma_{ki}^\dagger + \langle \tilde{i}|F|k\rangle \Gamma_{ki} \right\} \\
&= \sum_{k,i,\alpha'} X_{ki}^{\alpha'} \Gamma_{\alpha'}^\dagger - Y_{ki}^{\alpha'} \Gamma_{\alpha'} \\
&= \sum_{\alpha'} \Lambda_{\alpha'} \sum_{ki} \frac{|\langle \tilde{i}|F|k\rangle|^2}{(\epsilon_k - \epsilon_i)^2 - (\hbar\omega_{\alpha'})^2} (\Gamma_{\alpha'}^\dagger + \Gamma_{\alpha'}) \\
&= \sum_{\alpha'} \frac{\Lambda_{\alpha'}}{\kappa} (\Gamma_{\alpha'}^\dagger + \Gamma_{\alpha'}) = \sum_{\alpha'} \sqrt{\frac{\hbar\omega_{\alpha'}}{2C'_\alpha}} (\Gamma_{\alpha'}^\dagger + \Gamma_{\alpha'}) = \hat{\alpha}. \tag{4.A.1}
\end{aligned}$$

This is a consequence of the self consistent relation

$$\delta U(r) = \int d\mathbf{r}' \delta\rho(r)v(|\mathbf{r}-\mathbf{r}'|), \tag{4.A.2}$$

existing between density (collective) and potential (single-particle) distortion, typical of normal modes of many-body systems.

Relation (4.A.1) implies that at the basis of these normal modes one finds the attractive $\kappa < 0$ separable interaction

$$H = \frac{\kappa}{2} \hat{F} \hat{F}, \tag{4.A.3}$$

but where now (Fig. 4.A.1 (a))

$$\hat{F} = \sum_{\nu_1, \nu_2} \langle \nu_1 | F | \nu_2 \rangle a_{\nu_1}^\dagger a_{\nu_2}, \tag{4.A.4}$$

is a general single-particle operator, while \hat{F} in Eq. (4.A.1) is its harmonic representation acting in the particle (k)–hole (i) space, Γ_{ki}^\dagger and Γ_{ki} being (quasi) bosons, i.e. respecting the commutation relation

$$[\Gamma_{ki}, \Gamma_{k'i'}^\dagger] = \delta(k, k')\delta(i, i'). \tag{4.A.5}$$

In other words, the representation (4.A.1), which is at the basis of the RPA (as well as QRPA), does not allow for scattering vertices, processes which become operative by rewriting (4.A.3) in terms of the particle–vibration coupling Hamiltonian

$$H_c = \kappa \hat{\alpha} \hat{F} \tag{4.A.6}$$

It is of notice that κ is negative for an attractive field. Let us now calculate the effective single-particle moments (cf. Fig. 4.A.1 (b)),

$$\begin{aligned}
\langle \nu_2 | \hat{F} | \nu_1 \rangle_{(b)} &= \frac{\langle \nu_2 | \hat{F} | \nu_2, n_\alpha = 1 \rangle \langle \nu_2, n_\alpha = 1 | H_c | \nu_1 \rangle}{(\epsilon_{\nu_1} - \epsilon_{\nu_2}) - \hbar\omega_\alpha}, \\
&= \frac{\langle 0 | \hat{\alpha} | n_\alpha = 1 \rangle \kappa \alpha \langle \nu_2 | F | \nu_1 \rangle}{(\epsilon_{\nu_1} - \epsilon_{\nu_2}) - \hbar\omega_\alpha}, \\
&= \kappa \alpha^2 \frac{\langle \nu_2 | F | \nu_1 \rangle}{(\epsilon_{\nu_1} - \epsilon_{\nu_2}) - \hbar\omega_\alpha}, \tag{4.A.7}
\end{aligned}$$

⁷⁶cf. Bohr and Mottelson (1975), cf. also Brink and Broglia (2005) App. C.

and (Fig. 4.A.1 (c))⁷⁷

$$\begin{aligned}\langle v_2 | \hat{F} | v_1 \rangle_{(c)} &= \frac{\langle v_2 | H_c | v_1, n_\alpha = 1 \rangle \langle v_1, n_\alpha = 1 | F | v_1 \rangle}{\epsilon_{v_2} - (\epsilon_{v_1} + \hbar\omega_\alpha)}, \\ &= \kappa\alpha^2 \left(-\frac{\langle v_2 | F | v_1 \rangle}{(\epsilon_{v_1} - \epsilon_{v_2}) + \hbar\omega_\alpha} \right),\end{aligned}\quad (4.A.8)$$

leading to

$$\begin{aligned}\langle v_2 | \hat{F} | v_1 \rangle_{(b)} + \langle v_2 | \hat{F} | v_1 \rangle_{(c)} &= \kappa\alpha^2 \frac{2\hbar\omega_\alpha \langle v_2 | F | v_1 \rangle}{(\epsilon_{v_1} - \epsilon_{v_2})^2 - (\hbar\omega_\alpha)^2}, \\ &= \frac{\kappa}{C_\alpha} \frac{(\hbar\omega_\alpha)^2 \langle v_2 | F | v_1 \rangle}{(\epsilon_{v_1} - \epsilon_{v_2})^2 - (\hbar\omega_\alpha)^2}.\end{aligned}\quad (4.A.9)$$

This is in keeping with the fact that the ZPF of the α -vibrational mode is,

$$\alpha = \sqrt{\frac{\hbar\omega_\alpha}{2C_\alpha}}, \quad (4.A.10)$$

the particle-vibration coupling strength being

$$\Lambda_\alpha = \kappa\alpha. \quad (4.A.11)$$

Together with $\langle v_2 | \hat{F} | v_1 \rangle_{(a)} = \langle v_2 | F | v_1 \rangle$ (see Fig. 4.A.1 (a)) one obtains

$$\langle v_2 | \hat{F} | v_1 \rangle = (1 + \chi(\omega)) \langle v_2 | F | v_1 \rangle, \quad (4.A.12)$$

where

$$\chi_\alpha(\omega) = \frac{\kappa}{C_\alpha} \frac{\omega_\alpha^2}{\omega^2 - \omega_\alpha^2} \quad (4.A.13)$$

is the polarizability coefficient while

$$\omega = |\epsilon_{v_1} - \epsilon_{v_2}|/\hbar. \quad (4.A.14)$$

In the static limit, e.g. in the case in which α is a giant resonance and $\omega_\alpha \gg \omega$ one obtains

$$\chi_\alpha(0) = -\frac{\kappa}{C_\alpha}. \quad (4.A.15)$$

The sign of $\chi_\alpha(0)$ is opposite to that of κ , since the static polarization effect produced by an attractive coupling ($\kappa < 0$) is in phase with the single-particle moment,

⁷⁷In calculating the energy denominators one takes the difference between the energy of the initial and of the intermediate states. However, when an external field like \hat{F} acts on the system, before the PVC or four-point vertices operate, being equivalent to an observation, the energy denominator is to be calculated as the energy difference between the final and the intermediate states.

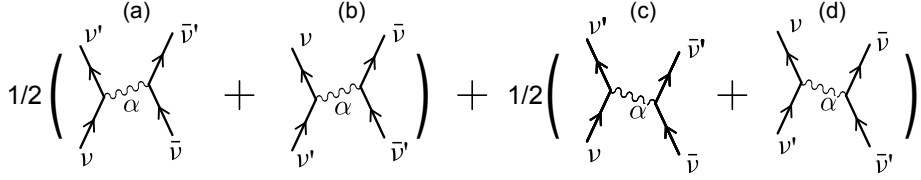


Figure 4.A.2: Diagrams associated with nuclear pairing induced interaction.

while a repulsive coupling ($\kappa > 0$) implies opposite phases for the polarization effect and the one-particle moment⁷⁸.

Let us now calculate the two-body pairing induced interaction (Fig. 4.A.2) arising from the exchange of collective vibrations⁷⁹ (summing over the two time orderings and symmetrizing between initial and final states)⁸⁰

$$\begin{aligned}
 v_{\nu\nu'}^{ind}(a) + v_{\nu\nu'}^{ind}(b) &= \kappa^2 \alpha^2 |\langle \nu' | F | \nu \rangle|^2 \left(\frac{1}{\epsilon_\nu - \epsilon_{\nu'} - \hbar\omega_\alpha} + \frac{1}{\epsilon_{\nu'} - \epsilon_\nu - \hbar\omega_\alpha} \right), \\
 &= \kappa^2 \alpha^2 |\langle \nu' | F | \nu \rangle|^2 \left(\frac{1}{(\epsilon_\nu - \epsilon_{\nu'}) - \hbar\omega_\alpha} - \frac{1}{(\epsilon_\nu - \epsilon_{\nu'}) + \hbar\omega_\alpha} \right), \\
 &= \Lambda_\alpha^2 |\langle \nu' | F | \nu \rangle|^2 \left(\frac{2\hbar\omega_\alpha}{(\epsilon_\nu - \epsilon_{\nu'})^2 - (\hbar\omega_\alpha)^2} \right), \\
 &= v_{\nu\nu'}^{ind}(c) + v_{\nu\nu'}^{ind}(d).
 \end{aligned} \tag{4.A.16}$$

Thus

$$\begin{aligned}
 v_{\nu\nu'}^{ind} &= \frac{1}{2} (v_{\nu\nu'}^{ind}(a) + v_{\nu\nu'}^{ind}(b)) + \frac{1}{2} (v_{\nu\nu'}^{ind}(c) + v_{\nu\nu'}^{ind}(d)) \\
 &= \Lambda_\alpha^2 |\langle \nu' | F | \nu \rangle|^2 \left(\frac{2\hbar\omega_\alpha}{(\hbar\omega)^2 - (\hbar\omega_\alpha)^2} \right).
 \end{aligned} \tag{4.A.17}$$

The diagonal matrix element,

$$v_{\nu\nu}^{ind} \equiv -\frac{2\Lambda_\alpha^2 |\langle \nu | F | \nu \rangle|^2}{\hbar\omega_\alpha},$$

testifies to the fact, for values of $\omega_\alpha \gtrsim \omega$, with

$$\omega = |\epsilon_\nu - \epsilon_{\nu'}|/\hbar, \tag{4.A.18}$$

namely the frequencies of the single-particle excitation energy, the induced pairing interaction is attractive. Summing to (4.A.17) the matrix element of the bare

⁷⁸Bohr and Mottelson (1975); Mottelson (1962). Think in the first case about the effect the GQR ($\tau = 0$) plays in $(e(E2))_{eff}$, in the second that played by the GDR ($\tau = 1$) in $(e(E1))_{eff}$.

⁷⁹In the present discussion we do not consider spin modes. For details see e.g. Idini et al. (2015). See also Bortignon et al. (1983).

⁸⁰Cf. Brink and Broglia (2005) p. 217.

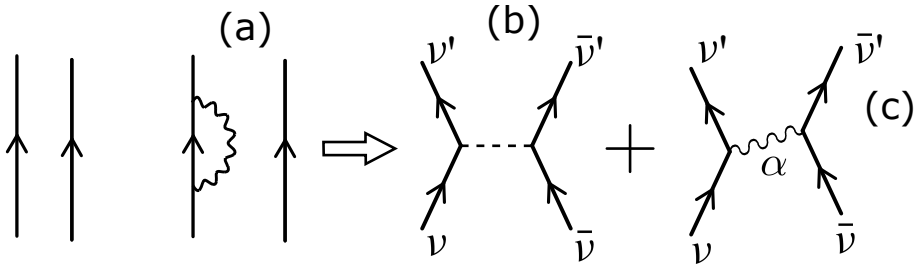


Figure 4.A.3: Starting with two bare nucleons moving around a closed shell system N_0 in Hartree-Fock orbitals (arrowed lines far left), a graphical (NFT) representation of (a) self energy processes and of (b) bare and (c) induced pairing interactions are displayed.

interaction (4.A.3), (Fig. 4.A.3 (b))⁸¹

$$v_{vv'}^{bare} = \kappa |\langle v' | F | v \rangle|^2, \quad (4.A.19)$$

one obtains for the total pairing matrix element⁸²

$$\begin{aligned} v_{vv'} &= \kappa |\langle v' | F | v \rangle|^2 + \frac{\kappa^2}{C_\alpha} |\langle v' | F | v \rangle|^2 \frac{(\hbar\omega_\alpha)^2}{\omega^2 - \omega_\alpha^2} \\ &= v_{vv'}^{bare} \left(1 + v_{vv'}^{bare} \Pi_{vv'}(\omega, \omega_\alpha) \right) = v_{vv'}^{bare} + \left(v_{vv'}^{bare} \right)^2 \Pi_{vv'}(\omega, \omega_\alpha). \end{aligned} \quad (4.A.20)$$

where

$$\Pi_{v,v'} = \begin{cases} \left(C_\alpha |\langle v' | F | v \rangle|^2 \right)^{-1} \frac{\omega_\alpha^2}{\omega^2 - \omega_\alpha^2}, \\ \left(D_\alpha |\langle v' | F | v \rangle|^2 \right)^{-1} \frac{1}{\omega^2 - \omega_\alpha^2}, \end{cases} \quad (4.A.21)$$

both expressions being equivalent in keeping with the fact that $\omega_\alpha = (C_\alpha/D_\alpha)^{1/2}$. In the second expression of $\Pi_{vv'}$ the inertia of the phonon appears in the denominator, similar to the factor (Z/AM) in (4.A.66) below. The unit of both C_α and \hbar^2/D_α is MeV.

It is of notice that $v_{vv'}$ can display a resonant behaviour leading to attraction regardless whether $v_{vv'}^{bare}$ is attractive or repulsive ($\lim_{\omega \rightarrow \omega_\alpha} \Pi_{vv'} \rightarrow -\infty$), a situation found in the case of dielectric polarization effects in metals. In this case,

⁸¹Within the framework of (4.A.3) and of its role in (4.A.20) one finds, in the case of superconductivity in metals to be discussed below, that the bare unscreened Coulomb interaction can be written as

$$U_c(r) = \frac{1}{2} \sum_{i,j} \frac{q_i q_j}{|\mathbf{r}_i - \mathbf{r}_j|},$$

i, j running over all particles (nuclei and electrons) and $q_i = -e$ for electrons and Ze for nuclei.

⁸²It is of notice that $\Pi_{vv'}$ is closely related with Lindhard's function (Lindhard (no. 8, 1954)). See Eq. (4.A.66) below.

the resulting effective electron-electron interaction (phonon exchange) is attractive (see Eq. (4.A.69)), and is at the basis of Cooper pair correlation and BCS superconductivity.

Let us discuss the case of ^{11}Li , in which case Cooper pair binding results mainly from the exchange of the low-lying dipole mode between the two halo nuclei. Making use of the bare screened interaction⁸³ $G_{scr} \approx 0.05G \approx 0.1$ MeV ($G \approx 28/A$ MeV) ($v_{vv'}^{bare} = -G_{scr} = -0.1$ MeV), and of the induced pairing interaction $v_{vv'}^{ind} (= M_{ind} \approx -0.6$ MeV), one can write for the last term in (4.A.20), $(0.1 \text{ MeV})^2 \Pi_{vv'}(\omega_\alpha, \omega) = -0.6$ MeV leading to $\Pi_{vv} = -60 \text{ MeV}^{-1}$. This large effect is not a resonant phenomenon, although the energies $\hbar\omega (= \tilde{\epsilon}_{p_{1/2}} - \tilde{\epsilon}_{s_{1/2}} \approx 0.5$ MeV) and $\hbar\omega_\alpha (\gtrsim 0.7 \text{ MeV})$ are rather similar.

At the basis of the quite small value of the energy centroid of the ^{11}Li soft $E1$ -mode (pygmy dipole resonance⁸⁴), one finds the screening potential ($V_1 = 125$ MeV) which arises from the poor overlap between the core (^9Li) and the halo neutron wavefunctions, as in the case of G_{scr} can be assumed, for order of magnitude estimates, to be equal to it (i.e. ≈ 0.05). Thus $(V_1)_{scr} \approx 6$ MeV. Making use of the parametrization⁸⁵ $\hbar\omega_\alpha = \hbar\omega_0 (1 + \kappa/C^{(0)})^{1/2}$, where $\kappa \approx V_1 A^{-5/3}$ MeV fm $^{-2}$, $C^{(0)} = 41 A^{-5/3}$ MeV fm $^{-2}$ and $\hbar\omega_0 = 41 \text{ MeV}/A^{1/3}$ in the case of nuclei lying along the stability valley, one obtains $\hbar\omega_\alpha = 41 \text{ MeV}(1 + V_1/41)^{1/2} \approx 80 \text{ MeV} A^{-1/3}$. In the case of ^{11}Li $\hbar\omega_0 \approx \tilde{\epsilon}_{p_{1/2}} - \tilde{\epsilon}_{s_{1/2}} \approx 0.5$ MeV, and V_1 is to be replaced by $(V_1)_{scr}$. Thus $\hbar\omega_\alpha \approx 0.5 \times (1.2)^{1/2} \text{ MeV} \approx 0.6 \text{ MeV}$.

Let us now carry a simple estimate of the contribution of the induced pairing interaction to the (empirical) nuclear pairing gap. For this purpose we introduce the quantity

$$\lambda = N(0)v_{vv'}^{ind} \quad (4.A.22)$$

where $N(0)$ is the density of levels of a single spin orientation at the Fermi energy. The above quantity is known as the nuclear mass enhancement factor. This is because of the role it plays in the nucleon ω -mass (see App. 5.A and App. 5.H)

$$m_\omega = (1 + \lambda)m. \quad (4.A.23)$$

Systematic studies of this quantity, and of the related discontinuity occurring by the single-particle occupation number at the Fermi energy, namely $Z_\omega = (m/m_\omega)$ testifies to the fact that $\lambda \approx 0.4$.

The BCS expressions of the pairing gap in terms of λ are

$$\Delta = \begin{cases} 2\hbar\omega_D e^{-1/\lambda}, & (\text{weak coupling } \lambda \ll 1) \\ \hbar\omega_D \lambda, & (\text{strong coupling } \lambda \geq 1) \end{cases} \quad (4.A.24)$$

⁸³See Broglia et al. (2019b).

⁸⁴Broglia et al. (2019a)

⁸⁵Bohr and Mottelson (1975) Eq. (6-315a).

where ω_D is the limiting frequency of the low-lying collective modes of nuclear excitation, typically of quadrupole and octupole vibrations. While for weak coupling one can use $\hbar\omega_D \approx 10$ MeV, for the strong coupling situation it seems more proper $\hbar\omega_D \approx 2$ MeV.

Making use of $\lambda = 0.4$, intermediate between weak and strong coupling situation one obtains

$$\Delta \approx 1.6 \text{ MeV} \quad (4.A.25)$$

and

$$\Delta \approx 0.8 \text{ MeV}, \quad (4.A.26)$$

to be compared with the empirical value

$$\Delta \approx 1.4 \text{ MeV} \quad (4.A.27)$$

of superfluid medium heavy mass nuclei like ^{120}Sn .

While the relations (4.A.24) can hardly be relied to provide a quantitative number, they testify to the fact that induced pairing is expected to play an important role in nuclei. These expectations have been confirmed by detailed confrontation of theory and experiment⁸⁶.

Hindsight

Static polarization effects can be important in clothing single-particle states. For example, effective charges and induced interactions associated with moments induced by giant resonances⁸⁷. However, retarded ω -dependent self-energy effects and induced interactions are essential in describing structure and reactions of many-body systems. Examples are provided by the bootstrap binding of the halo neutrons (pair addition mode) to ^9Li , leading to the fragile $|^{11}\text{Li}(gs)\rangle$, displaying a $S_{2n} \approx 0.380$ MeV as compared to typical values of $S_{2n} \approx 18$ MeV as far as structure goes, and by the $^1\text{H}(^{11}\text{Li}, ^9\text{Li}(1/2^-; 2.69 \text{ MeV}))^3\text{H}$ population of the lowest member of the $(2^+ \times p_{3/2}(\pi))_{J^-}$ multiplet of ^9Li with a cross section $\sigma(3/2^- \rightarrow 1/2^-; 2.69 \text{ MeV}) \approx 1 \text{ mb}$, as far as reaction goes. If there was need for support coming from other fields of research, one can mention just two: van der Waals force and superconductivity.

It was recognized early in the study of dipole-dipole interaction in atomic systems that, of the variety of contributions to the van der Waals interaction, the retarded, fully quantal contribution, arising from (dipole) zero point fluctuations (ZPF) of the two interacting atoms or molecules, and the only active in the case of non-polar molecules⁸⁸, play the most important role, static-induced interactions

⁸⁶See e.g. Idini et al. (2015).

⁸⁷See e.g. Bohr and Mottelson (1975), Eqs. (6-217) and (6-228).

⁸⁸Within this context van der Waals and gravitation are two forces which are universally operative, acting among all bodies. In connection with quantal fluctuations and van der Waals forces, see London (1937).

being less important (App. 3.D). A consequence of this result is the fact that the limiting size of globular proteins ($\approx 50 \text{ \AA}$) is controlled by the strong damping undergone by the retarded contribution to the amino acid interaction, when the frequency associated with the back and forth propagation of the force matches the molecules electronic frequencies⁸⁹.

Concerning superconductivity, the overscreening effect which binds weakly Cooper pairs stems from a delicate ω -dependent interaction, interaction which in the case of low temperature superconductors leads, eventually, to one of the first macroscopic manifestations of quantum mechanics, as e.g. “permanent” magnetic fields associated with persistent supercurrents.

The statement “*Life at the edge of chaos*” coined in connection with the study of emergent properties in biological molecules (e.g. protein evolution, folding and stability) reflects the idea, as expressed by de Gennes⁹⁰, that truly important new properties and results can emerge in systems lying at the border between rigid order and randomness, as testified by the marginal stability and conspicuous fluctuations characterizing, for example, nuclear Cooper pairs at the dripline and in metals, and that of proteins of e.g. viral particles like the HIV-1- and HCV-proteases⁹¹.

Let us conclude by quoting again de Gennes but doing so with the hindsight of twenty years of nuclear research which have elapsed since “*Les objets fragiles*” was first published. The chapter entitled “*Savoir s’arrêter, savoir changer*” starting at p. 180 opens with the statement “En ce moment, la physique nucléaire (la science des noyaux atomiques) est une science qui, à mon avis, se trouve en fin de parcours... C’est une physique qui demande des moyens coûteux, et qui s’est constituée par ailleurs en un puissant lobby. Mais elle me semble naturellement exténuée... je suis tenté de dire: “Arretons”... mais ce serait aussi absurde que de vouloir arrêter un train à grande vitesse. Le mieux serait d’aguiller ce train sur une autre voie, plus nouvelle et plus utile à la collectivité.”

In a way, and even without knowing de Gennes remark, part of the nuclear physics community have followed them, capitalizing on the novel embodiment that concepts like elementary modes of excitation, spontaneous symmetry breaking and phase transitions have had in this paradigm of finite quantum many-body (FQMB) system the nucleus represents, where fluctuations can dominate over potential energy effects. The use of these concepts tainted by FQMB system effects

⁸⁹It is of notice that similar arguments (cf. Sect. 3.6) are at the basis of the estimate (3.6.13) concerning the size of the halo nucleus ^{11}Li , a quantity which is influenced to a large extent by the maximum distance (correlation length) over which partners of a Cooper pair are virtually (of course only if particle, normal, density allows for it) but solidly anchored to each other (localized), and have to be seen as an (extended) bosonic entity and not as two fermions. The fact that Cooper pair transfer proceeds mainly in terms of successive transfer controlled by the single-particle mean field, reinforces the above physical picture of nuclear pairing. Even under the effect of extremely large, as compared to the pair correlation energy, external single-particle fields, namely that of target and projectile, the Cooper pair field extends over the two nuclei, permeating the whole summed nuclear volume also through tiny density overlaps.

⁹⁰De Gennes (1994).

⁹¹See e.g. Broglia (2013).

as applied to proteins, in particular to the understanding of protein folding may, arguably, shed light on the possibility of designing leads to drugs which are less prone to create resistance⁹², let alone all the parallels that one has been able to establish and the associated progress resulting from them concerning cluster and quantum dots physics, a particular example being the discovery of super shells⁹³.

4.A.2 Metals

Plasmons and phonons (jellium model)

The expression of the electron plasmon (ep) frequency of the antenna-like oscillations of the free, conduction electrons of mass m_e and charge $-e$, against the positive charged background (jellium model) is

$$\omega_{ep}^2 = \frac{4\pi n_e e^2}{m_e} = \frac{3e^2}{m_e r_s^3}, \quad (4.A.28)$$

where

$$n_e = \frac{3}{4\pi} \frac{1}{r_s^3}, \quad (4.A.29)$$

are the number of electrons per unit volume, r_s being the radius of a sphere whose volume is equal to the volume per conduction electron,

$$r_s = \left(\frac{3}{4\pi n_e} \right)^{1/3}, \quad (4.A.30)$$

that is, the radius of the Wigner–Seitz cell.

For⁹⁴ metallic Li

$$n_e = 4.70 \frac{10^{22}}{\text{cm}^3} = \frac{4.7 \times 10^{-2}}{\text{\AA}^3}, \quad (4.A.31)$$

while

$$r_s = \left(\frac{3\text{\AA}^3}{4\pi \times 4.7 \times 10^{-2}} \right)^{1/3} = 1.72\text{\AA}, \quad (4.A.32)$$

implying a value $(r_s/a_0) = 3.25$ in units of Bohr radius ($a_0 = 0.529\text{\AA}$). Making use of

$$\alpha = 7.2973 \times 10^{-3} = \frac{e^2}{\hbar c} \quad (4.A.33)$$

and

$$e^2 = 14.4 \text{ eV \AA}, \quad (4.A.34)$$

⁹²See e.g. Broglia (2013, 2005); Rösner et al. (2017) and refs. therein.

⁹³Pedersen et al. (1991); de Heer et al. (1987); Brack (1993); Pacheco et al. (1991); Lipparini (2003); Martin et al. (1994); Bjornhølm et al. (1994).

⁹⁴cf. page 5, table 1.1 of Ashcroft and Mermin (1987).

one obtains

$$\hbar c = \frac{14.4 \text{ eV } \text{\AA}}{7.2973 \times 10^{-3}} = 1973.3 \text{ eV } \text{\AA}. \quad (4.A.35)$$

Making use of the above values and of

$$m_e c^2 = 0.511 \text{ MeV}, \quad (4.A.36)$$

one can write

$$\hbar^2 \omega_{ep}^2 = \frac{(\hbar c)^2}{m_e c^2} \frac{3e^2}{r_s^3} = \frac{(1973.3 \text{ eV } \text{\AA})}{0.511 \times 10^6 \text{ eV}} \frac{3 \times 14.4 \text{ eV } \text{\AA}}{(1.72 \text{ \AA})^3} = 64.7 \text{ eV}^2 \quad (4.A.37)$$

leading to⁹⁵

$$\hbar \omega_{ep} = 8.04 \text{ eV} \approx 1.94 \times 10^9 \text{ MHz} \quad (4.A.38)$$

For the case of metal clusters of Li, the Mie resonance frequency is⁹⁶

$$\hbar \omega_M = \frac{\hbar \omega_{ep}}{\sqrt{3}} = 4.6 \text{ eV}. \quad (4.A.39)$$

4.A.3 Elementary theory of phonon dispersion relation

Again, within the framework of the jellium model, one can estimate the long wavelength ionic plasma (ip) frequency introducing, in (4.A.28) the substitution $e \rightarrow Ze$, $m_e \rightarrow AM$ ($A = N + Z$, mass number, M nucleon mass), $n_e \rightarrow n_i = n_e/Z$,

$$\omega_{ip}^2 = \frac{4\pi n_i (Ze)^2}{AM} = \frac{Z m_e}{AM} \omega_{ep}^2, \quad (4.A.40)$$

$AM(Ze)$ being the mass (charge) of the ions⁹⁷. For metallic Li, one obtains

$$\begin{aligned} \hbar \omega_{ip} &= \left(\frac{Z m_e}{AM} \right)^{1/2} \hbar \omega_{ep} = \left(\frac{3 \times 0.5}{9 \times 10^3} \right)^{1/2} \times 1.94 \times 10^{15} \text{ sec}^{-1} \\ &\approx 2.5 \times 10^{13} \text{ sec}^{-1} \approx 10^{13} \text{ sec}^{-1} \approx 1.04 \times 10^2 \text{ meV}. \end{aligned} \quad (4.A.41)$$

Now, both the relations (4.A.28) and (4.A.40), although being quite useful, are wrong from a many-body point of view: ω_{ep} because electrons appear as bare electrons not dressed by the phonons, neither by the plasmons; ω_{ip} because the static negative background does not allow for an exchange of electron plasmons between ions, exchange eventually leading to a screened, short-range ionic Coulomb repulsive field. Namely ions interact, in the approximation used above, in terms of the “bare” ion-ion Coulomb interaction. Being it infinite range it does not allow for a dispersion relation linear in k at long wavelengths (sound waves) but forces a finite “mass” also to the lattice phonons. Allowing for electron screening of the “bare”

⁹⁵Kittel (1996) Table 2, p. 278.

⁹⁶See Bertsch and Broglia (2005), Sect. 5.1, also Table 5.1.

⁹⁷Ketterson and Song (1999), p. 230.

ion-ion Coulomb interaction, as embodied in the electron gas dielectric function $1/\epsilon(0, q) = q^2/(k_s^2 + q^2)$, one obtains the dressed phonon frequency

$$\omega_q^2 = \frac{\omega_{ip}^2}{\epsilon(0, q)} = \frac{Zm_e}{AM} \frac{\omega_{ep}^2}{q^2 + k_s^2} q^2 = \frac{\omega_{ip}^2}{q^2 + k_s^2} q^2. \quad (4.A.42)$$

The quantity

$$k_S = \left(\frac{6\pi n_e e^2}{\epsilon_F} \right)^{1/2} = \left(\frac{4k_F}{\pi a_0} \right)^{1/2} = 0.82 k_F \left(\frac{r_S}{a_0} \right)^{1/2} \quad (4.A.43)$$

is the Thomas-Fermi screening wave vector, a quantity which is of the order of the Fermi momentum, the associated screening length being then of the order of the Wigner-Seitz radius. In writing the above relations use has been made of

$$k_F = \left(\frac{9\pi}{4} \right)^{1/3} \frac{1}{r_s} = \frac{1.92}{r_s}, \quad (4.A.44)$$

and

$$\epsilon_F = \frac{e^2 a_0}{2} k_F^2. \quad (4.A.45)$$

In the case of metallic Li ($k_F = 1.12 \text{ \AA}$, $r_S = 1.72 \text{ \AA}$),

$$k_S = 1.6 \text{ \AA}^{-1}. \quad (4.A.46)$$

Let us return to (4.A.43), and take the long wavelength limit of ω_q . One finds

$$\lim_{q \rightarrow 0} \omega_q = c_S q \quad (4.A.47)$$

the sound velocity (squared) being

$$c_s^2 = \frac{Zm_e}{AM} \frac{4\pi n_e e^2}{m_e} \frac{\epsilon_F}{6\pi n_e e^2} = \frac{2Z}{3AM} \epsilon_F = \frac{Zm_e}{3AM} v_F^2, \quad (4.A.48)$$

where use has been made of

$$n_e = \frac{3}{4\pi} \frac{1}{r_s^3} = 4.7 \times 10^{-2} \text{ \AA}^{-3} \quad (r_s = 1.72 \text{ \AA}, \text{Li}), \quad (4.A.49)$$

and

$$\epsilon_F = \frac{50.1}{(r_s/a_0)} \approx 15.42 \text{ eV} \quad (r_s/a_0 = 3.25, \text{Li}), \quad (4.A.50)$$

With the help of

$$k_F = \frac{1.92}{r_s}, \quad (4.A.51)$$

and of the velocity of light,

$$c = 3 \times 10^{10} \text{ cm/sec}, \quad (4.A.52)$$

one obtains,

$$\begin{aligned} v_F &= \left(\frac{\hbar}{m_e} \right) k_F = \left(\frac{\hbar c}{m_e c^2} \right) \times 3 \times 10^{10} \frac{\text{cm}}{\text{sec}} \frac{1.92}{r_s} \\ &= \left(\frac{1973.3 \text{ \AA eV}}{0.511 \times 10^6 \text{ eV}} \right) \times 3 \times 10^{10} \frac{\text{cm}}{\text{sec}} \frac{1.92}{1.72 \text{ \AA}} \approx 1.29 \times 10^8 \frac{\text{cm}}{\text{sec}} \end{aligned} \quad (4.A.53)$$

Consequently,

$$c_s^2 = \frac{1}{3} \frac{3m_e}{9M} v_F^2 \approx 6 \times 10^{-5} v_F^2, \quad (4.A.54)$$

and

$$c_s \approx 7.8 \times 10^{-3} v_F \approx 1.0 \times 10^6 \frac{\text{cm}}{\text{sec}}. \quad (4.A.55)$$

That is, about a hundredth of the Fermi velocity⁹⁸.

Let us now discuss the effective electron-electron interaction. Within the jellium model used above one can write it as

$$V(\mathbf{q}, \omega) = \frac{U_c(q)}{\epsilon(\mathbf{q}, \omega)}, \quad (4.A.56)$$

where the dielectric function

$$\epsilon(\mathbf{q}, \omega) = \frac{\omega^2(q^2 + k_s^2) - \omega_{ip}^2 q^2}{\omega^2 q^2} \quad (4.A.57)$$

contains the effects due to both the ions and the background electrons, while

$$U_c(q) = \frac{4\pi e^2}{q^2} \quad (4.A.58)$$

is the Fourier transform of the bare Coulomb interaction

$$U_c(r) = \frac{e^2}{r}. \quad (4.A.59)$$

For $\omega \gg \omega_{ip}$ one obtains the so called screened Coulomb field,

$$V(\mathbf{q}, 0) = \frac{U_c(q)}{\epsilon(0, q)} = \frac{4\pi e^2 n_e}{q^2 + k_s^2} = U_c^{scr}(q), \quad (4.A.60)$$

its \mathbf{r} space Fourier transform being

$$U_c^{scr}(r) = \frac{e^2}{r} e^{-k_s r}. \quad (4.A.61)$$

⁹⁸Ashcroft and Mermin (1987), p. 51, Ketterson and Song (1999) p. 234.

A quantity that for large values of r falls off exponentially. Thus, in the high frequency limit, the electron–electron interaction, although strongly renormalized by the exchange of plasmons, as testified by the fact that (e.g. for Li),

$$U_c^{scr}(r = 5 \text{ \AA}) \approx U_c(r = 5 \text{ \AA}) e^{-1.6 \times 5} \approx 1 \text{ meV}, \quad (4.A.62)$$

as compared to $U_c(r = 5 \text{ \AA}) \approx 2.9 \text{ eV}$, is still repulsive.

Let us now consider frequencies $\omega \ll \omega_{ip}$ but for values of q of the order of a^{-1} , where a is the lattice constant ($a \approx 3 - 5 \text{ \AA}$, $a^{-1} \approx 0.25 \text{ \AA}^{-1}$) to be compared to $k_s \approx 1.6 \text{ \AA}^{-1}$ and $k_F \approx 1.12 \text{ \AA}^{-1}$ (metallic Li). In the case in which $\omega_{ip}^2/\omega^2 > (q^2 + k_s^2)/q^2$, V is attractive. This behavior explicitly involves the ions through ω_{ip} (electron–phonon coupling).

The dispersion relation of the associated frequency collective modes follows from

$$\epsilon(\mathbf{q}, \omega) = 0. \quad (4.A.63)$$

In other words, making use of Eq. (4.A.57) one obtains the relation (4.A.42). One can now rewrite the reciprocal of the dielectric functions in terms of ω_q , that is,

$$\begin{aligned} \frac{1}{\epsilon(\mathbf{q}, \omega)} &= \frac{\omega^2 q^2}{\omega^2(q^2 + k_s^2) - \omega_{ip}^2 q^2} = \frac{\omega^2 q^2}{\omega^2(q^2 + k_s^2)} \left(\frac{1}{1 - \frac{\omega_{ip}^2 q^2}{\omega^2(q^2 + k_s^2)}} \right) \\ &= \frac{q^2}{q^2 + k_s^2} \left[1 + \frac{\omega_q^2}{\omega^2 - \omega_q^2} \right]. \end{aligned} \quad (4.A.64)$$

For $\omega \gg \omega_q$ one recovers the Thomas–Fermi dielectric function (4.A.42). For ω near, but smaller than ω_q the interaction eventually becomes attractive⁹⁹. The effective electron–electron interaction can be then written as

$$\begin{aligned} V(q, \omega) &= \frac{4\pi e^2 n_e}{q^2 + k_s^2} + \frac{4\pi e^2 n_e}{q^2 + k_s^2} \frac{\omega_q^2}{\omega^2 - \omega_q^2} \\ &= U_c^{scr}(q) + U_c^{scr}(q) \frac{\omega_q^2}{\omega^2 - \omega_q^2} \\ &= U^{scr}(q) (1 + U^{scr}(q) \Pi(q, \omega)), \end{aligned} \quad (4.A.65)$$

where

$$\Pi(q, \omega) = \left(\frac{Z}{AM} \right) \frac{q^2}{\omega^2 - \omega_q^2}. \quad (4.A.66)$$

In working out the last expression Eqs. (4.A.42) and (4.A.28) have been used. In other words $\omega_q^2 = (Zm_e/AM)(\omega_{ep}^2/(q^2 + k_s^2)q^2) = (Z/AM)(4\pi n_e e^2/(q^2 + k_s^2))q^2$.

⁹⁹Schrieffer (1964), Fig. 6–11, p. 152.

This quantity is intimately connected with Lindhard's function¹⁰⁰. See also the close relation with the expression (4.A.20) of the nuclear renormalized pairing interaction. The first term of $V(q, \omega)$ contains the screened Coulomb field arising from the exchange of plasmons between electrons (cf. Fig. 4.A.4). The second term with the exchange of collective low frequency phonons calculated making use of the same screened interaction as emerges from (4.A.65).

Concerning the parallels discussed above between pairing in nuclei and in metals, it is also important to point out to the important differences. At least concerning the possibility of developing a unified theoretical working tool.

In metals the bare interaction emerges from the exchange of photons, a process which can be described at profit in terms of an instantaneous Coulomb interaction. While major progress have been made concerning the bare nucleon interaction at large, and the NN -pairing interaction in particular, taking also into account three-body processes and carrying out ab initio calculations, we are not yet in possess of the equivalent of the Coulomb interaction. Let alone of a so called low- k version of such interaction, which could allow to work on equal footing Hartree-Fock-Bogoliubov solutions, and QRPA microscopic calculations of low-lying collective modes in the variety of channels (density, spin, charge-exchange, etc.).

Concerning these phonons, they are built of the same nucleon degrees of freedom which already exhaust the nuclear phase space. Double counting and Pauli principle violations have to be taken care of in using the collective modes as intermediate bosons. In metals, phonons are associated with lattice vibrations, that is degrees of freedom different from the electronic ones.

On the other hand, the fact that in nuclei one can describe in terms of individual quantal states and of single Cooper pairs, if not identical, rather similar phenomena as those leading to some of the most remarkable and technically transferable quantum phenomena (persistent currents, high magnetic fields, the Josephson effect), makes the nuclear pairing paradigm a unique laboratory of low-temperature many-body physics.

Let us now introduce the dimensionless quantity

$$\lambda = \langle F|V|I \rangle = N(0)U_c^{scr} (1 + U_c^{scr}\Pi). \quad (4.A.67)$$

In the weak coupling limit ($\lambda^2 \ll \lambda$)

$$\Delta = 2\omega_D e^{-1/\lambda}, \quad (4.A.68)$$

where ω_D is the Debye energy. Now, provided that we are in a situation in which ω is consistently different from ω_q ,

$$\frac{1}{\lambda} = \frac{1}{N(0)U_c^{scr}(1 + U_c^{scr}\Pi)} \approx \frac{1}{N(0)U_c^{scr}} (1 - U_c^{scr}\Pi), \quad (4.A.69)$$

¹⁰⁰Lindhard (no. 8, 1954).

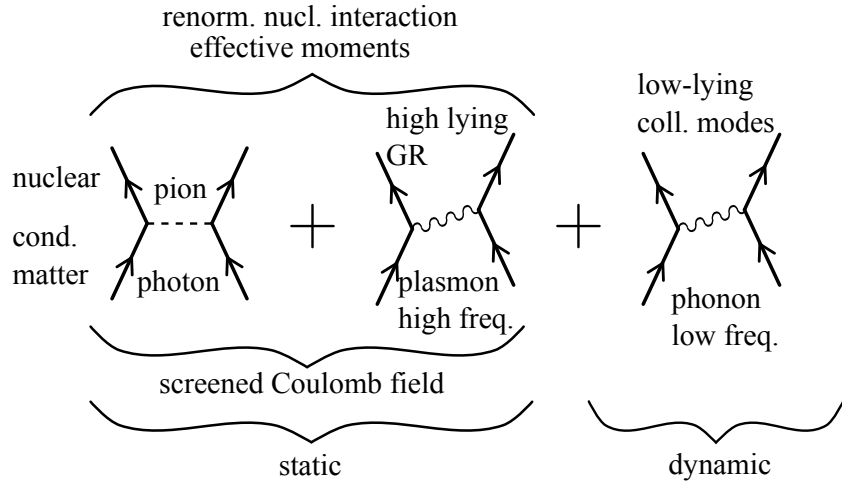


Figure 4.A.4: Schematic representation of the variety of contributions to the effective interaction in nuclei and in metals.

Thus

$$\frac{1}{\lambda} = \frac{1}{N(0)U_c^{scr}} - \frac{\Pi}{N(0)}, \quad (4.A.70)$$

and

$$\Delta = \left(2\omega_D e^{\frac{\Pi}{N(0)}} \right) e^{-\frac{1}{N(0)U_c^{scr}}}. \quad (4.A.71)$$

Consequently, the renormalization effects of the pairing gap associated with phonon exchange are independent of the approximation used to calculate U_c^{scr} (Thomas–Fermi in the above discussion), provided one has used the same “bare” (screened) Coulomb interaction to calculate ω_q^2 . Otherwise, the error introduced through a resonant renormalization process entering the expression of e.g. the pairing gap may be quite large.

4.A.4 Pairing condensation (correlation) energy beyond level density

The condensation energy, namely the energy difference $W_N - W_S$ between the normal N – and superfluid S –state is defined as (Eq. (2-35) of ref¹⁰¹)

$$W_{con} = W_N - W_S = \frac{1}{2} N(0) \Delta_0^2, \quad (4.A.72)$$

where $N(0)$ is the density of single-electron states of one-spin orientation evaluated at the Fermi surface (p. 31 of ref.¹⁰²), and Δ_0 is the pairing gap at $T = 0$.

¹⁰¹Schrieffer (1964).

¹⁰²Schrieffer (1964).

System	Δ_0		N_0		W_{con}		E_{cohe}	BE/A	$\frac{W_{con}}{E_c}$	$\frac{W_{con}}{BE}$
	meV	MeV	$\frac{\text{mev}^{-1}}{\text{atom}}$	MeV^{-1}	$\frac{\text{mev}}{\text{atom}}$	MeV	$\frac{\text{mev}}{\text{atom}}$	$\frac{\text{MeV}}{A}$	10^{-7}	10^{-3}
Pb	^{120}Sn	1.4	1.5	276	4	3×10^{-4}	4.3	2030	8.5	

Table 4.A.1: Summary of the quantities entering the calculation of the condensation energy superconducting lead (Pb), and of the single open shell superfluid nucleus ^{120}Sn .

The correlation energy E_{corr} introduced in equation (6-618) of ¹⁰³

$$E_{corr} = -\frac{1}{2d}\Delta^2 \quad (4.A.73)$$

to represent $W_S - W_N$ in the nuclear case, was calculated making use of a (single particle) spectrum of two-fold degenerate (Kramer degeneracy) equally spaced (spacing d) single-particle levels. Consequently, $2/d$ corresponds to the total level density, and $1/d = N(0)$. In keeping with the fact that a nucleus in the ground state (or in any single quantal state), is at zero temperature, (4.A.72) coincides with (4.A.73), taking into account the difference in sign in the definitions.

Nuclei

The empirical value of the level density parameter for both states ($\nu, \bar{\nu}$) (Kramers degeneracy, both spin orientations) is $a = A/8 \text{ MeV}^{-1}$, $A = N + Z$ being the mass number. Thus, for neutrons one can write $a_N = N/8$ and $N_N(0) = N/16 \text{ MeV}^{-1}$. For $^{120}_{50}\text{Sn}$, $N_N(0) \approx 4 \text{ MeV}^{-1}$. Because $\Delta = 1.46 \text{ MeV}$, (Table 4.A.1)

$$W_{con} = \frac{1}{2} \times 4 \text{ MeV}^{-1} \times (1.46)^2 \text{ MeV}^2 \approx 4.3 \text{ MeV}. \quad (4.A.74)$$

The binding energy per nucleon is $BE/A = 8.504 \text{ MeV}$. Thus $BE = 120 \times 8.504 \text{ MeV} = 1.02 \times 10^3 \text{ MeV}$, and

$$\frac{W_{con}}{BE} \approx 4.2 \times 10^{-3}. \quad (4.A.75)$$

Superconducting lead

Making use of the value¹⁰⁴

$$N(0) = \frac{0.276 \text{ eV}^{-1}}{\text{atom}}, \quad (4.A.76)$$

and of $\Delta_0 = 1.4 \text{ meV}$, one obtains

$$W_{con} = 0.27 \times 10^{-6} \text{ eV/atom}. \quad (4.A.77)$$

¹⁰³Bohr and Mottelson (1975).

¹⁰⁴Beck and Claus (1970).

In keeping with the fact that the cohesive energy of lead, namely the energy required to break all the bonds associated with one of its atoms is

$$E_{cohe} = 2.03 \frac{\text{eV}}{\text{atom}}, \quad (4.A.78)$$

one obtains

$$\frac{W_{con}}{E_{cohe}} \approx 1.3 \times 10^{-7}. \quad (4.A.79)$$

The different quantities are summarized in Table 4.A.1.

4.A.5 Hindsight

The function $\Pi(q, \omega)$ essentially at resonance ($\omega \lesssim \omega_q$) and its nuclear analogue $\Pi(\omega, \omega_\alpha)$ again close to resonance ($\omega \lesssim \omega_\alpha$), are the sources of new physics eventually leading to observable emergent properties, provided one finds the proper embodiments. In the case of metals at low temperature there are permanent magnetic fields in a superconducting ring, the Josephson effect, etc. In the case of halo neutron drip line nuclei one finds (see App. 4.C in particular paragraph before Eq. (4.C.6)) symbiotic pair addition modes, and essentially an equality of the absolute one- and two-particle transfer cross sections, phenomenon at the basis of the Josephson effect.

In Fig. 4.A.5 we present a schematic parallel between the physical mechanisms at the basis of the origin of pairing in metals and in nuclei, and of some of the consequences associated with spontaneous breaking of gauge symmetry in these systems, in particular Cooper pair tunneling.

Appendix 4.B Cooper pair: radial dependence

The fact that one is still trying to understand (BCS-like) pairing (abnormal density) in nuclei is, to a non negligible extent, due to the fact that, as a rule, pairing in these systems is constrained to manifest itself subject to a very strong “external” (mean, normal density) field¹⁰⁵. Also, to some extent, due to the fact that the analysis of two-nucleon transfer data was made, as a rule, in terms of relative cross sections and not absolute cross sections as done now¹⁰⁶. Within this context, Cooper pair transfer was viewed as simultaneous transfer, successive implying a breakup or, at least an anti-pairing disturbance of the pair. There exist a number of evidences which testify to the fact that the picture in which nucleon Cooper pairs are viewed as independent correlated entities over distances of the order of tens of fm (Fig. 4.3.1), contains a number of correct elements (see e.g. Fig. 4.B.1). In

¹⁰⁵c.f. e.g. Matsuo (2013).

¹⁰⁶See Potel et al. (2013a) and references therein.

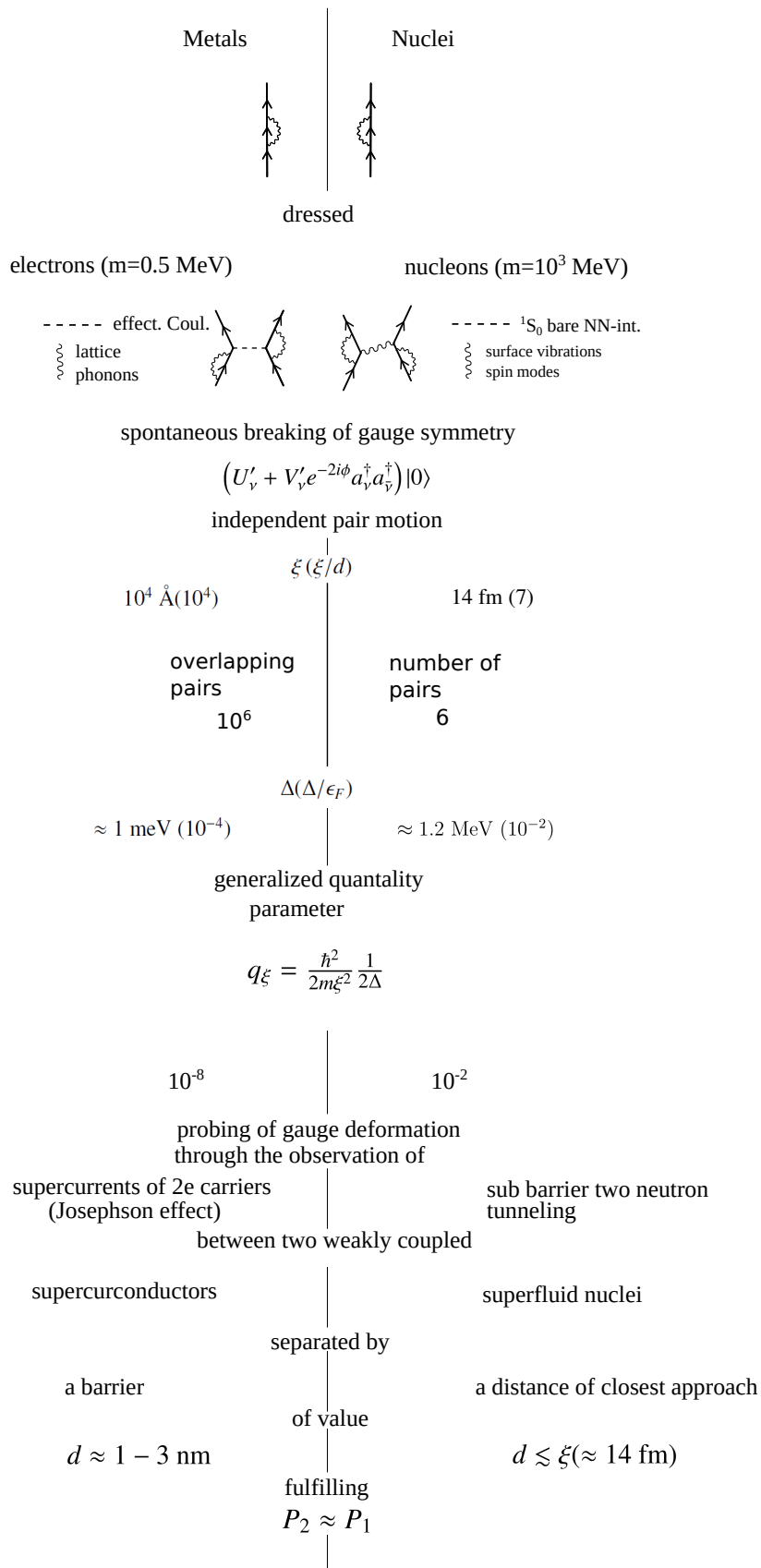


Figure 4.A.5

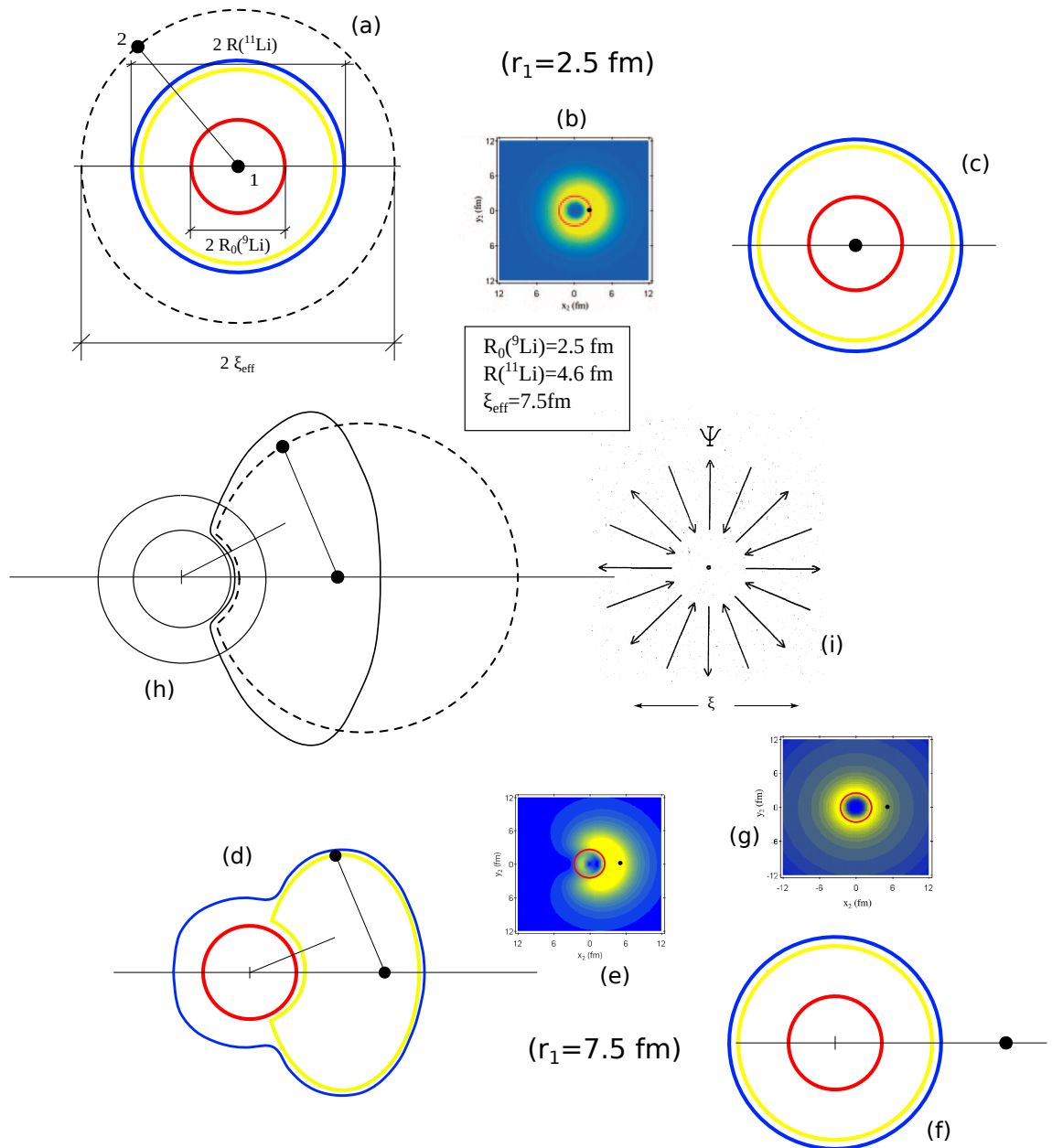


Figure 4.B.1

this Appendix an attempt at summarizing these evidences, already mentioned or partially discussed above, is made¹⁰⁷.

The problem that Cooper solved was that of a pair of electrons which interact above a quiescent Fermi sea with an interaction of the kind that might be expected due to phonon exchange and a screened Coulomb field¹⁰⁸. What he showed approximating this retarded interaction by an instantaneous non-local one, active on a thin energy shell near (above) the Fermi surface¹⁰⁹, was that the resulting spectrum has an eigenvalue $E = 2\epsilon_F - 2\Delta$, regardless how weak the interaction is, and consequently the binding energy 2Δ of the pair, so long as the interaction is attractive. This result is a consequence of the Fermi statistic and of the existence of a Fermi sea background –the two electrons interact with each other but not with those in the sea, except via the Pauli principle– since it is known that binding does not ordinarily occur in the two-body problem in three dimensions, until the strength of the attraction exceeds a finite threshold value.

The wavefunction of the two electrons can be written as

$$\Psi(\mathbf{r}_1\sigma_1; \mathbf{r}_2\sigma_2) = \phi_q(\mathbf{r})e^{i\mathbf{q}\cdot\mathbf{R}}\chi(\sigma_1, \sigma_2) \quad (4.B.1)$$

where $\mathbf{R} = (\mathbf{r}_1 + \mathbf{r}_2)/2$, $\mathbf{r} = \mathbf{r}_1 - \mathbf{r}_2$, and σ_1 and σ_2 denote the spins¹¹⁰.

Let us consider the state with zero center of mass ($q = 0$) and with zero relative momentum, so that the two electrons carry equal and opposite momenta, aside of being in the singlet spin state state, with

$$\chi = \frac{1}{\sqrt{2}} \left[\begin{pmatrix} 1 \\ 0 \end{pmatrix} \begin{pmatrix} 0 \\ 1 \end{pmatrix} - \begin{pmatrix} 0 \\ 1 \end{pmatrix} \begin{pmatrix} 1 \\ 0 \end{pmatrix} \right] \quad (4.B.2)$$

We have thus a pair of electrons moving in time reversal states and can write¹¹¹,

$$\phi_0(\mathbf{r}) = \sum_{k>k_F} g(\mathbf{k})e^{i\mathbf{k}\cdot\mathbf{r}} = \sum_{k>k_F} g(\mathbf{k})e^{i\mathbf{k}\cdot\mathbf{r}_1} e^{-i\mathbf{k}\cdot\mathbf{r}_2}. \quad (4.B.3)$$

In the above wavefunction Pauli principle ($k > k_F$) and translational invariance (dependence on the relative coordinate \mathbf{r}) are apparent. The pair wavefunction is likely a superposition of one-electron levels with energies of the order of 2Δ close to ϵ_F ,

¹⁰⁷Of course such manifestation will be latent, expressing themselves indirectly. In other words, abnormal density can only be present when normal density, at ever so low values already is present. The pairing field does not have within this context an existence by itself uncoupled from the normal density. On the other hand this, in most cases latent (virtual), and in only few cases factual existence, has important consequences on nuclear properties. Within this context one can mention that the neutron halo normal density in ^{11}Li is not there before the associated abnormal density is operative. In fact in this case abnormal density requires the normal one to develop in this neutron dripline nucleus, and viceversa.

¹⁰⁸Cooper (1956).

¹⁰⁹States below the Fermi surface are frozen because of Pauli principle.

¹¹⁰In the limit $q \rightarrow 0$ the relative coordinate problem is spherically symmetric so that $\phi_0(\mathbf{r})$ is an eigenfunction of the angular momentum operator (Schrieffer (1964)).

¹¹¹In other words, one expands the $l = 0$ wavefunction ϕ_0 in terms of s -states of relative momentum k and total momentum zero.

since tunneling experiments indicate that for higher energies the one-electron density is little altered from the form it has in normal metals. The spread in momenta of the single-electron levels entering (4.B.3) is thus fixed by the condition

$$2\Delta \approx \delta E \approx \delta \left(\frac{p^2}{2m} \right)_{\epsilon_F} \approx v_F \delta p. \quad (4.B.4)$$

Consequently

$$\frac{\delta p}{p_F} = \frac{2\Delta}{mv_F^2} = \frac{\Delta}{\epsilon_F} \ll 1. \quad (4.B.5)$$

Thus, $\phi_0(\mathbf{r})$ consists mainly of waves of wavenumber k_F . Now, because the wavefunction of a Cooper pair represents a bound s -state, the motion it describes is a periodic back and forth movement of the two electrons in directions which are uniformly distributed, covering a relative distance ($\delta x \delta p = \hbar$)

$$\xi = \delta x = \frac{\hbar}{\delta p} = \frac{\hbar v_F}{2\Delta} \quad (4.B.6)$$

as schematically¹¹² shown in Fig. 4.B.1 (i). It is analogous to the motion of the two nucleon in a deuteron or the main ($L = 0$) component of the two neutrons in the triton. The hydrogen atom in s -state is also an example; in that case it is the electron that does most of the back and forth moving, whereas the proton only recoils slightly.

In keeping with the above arguments and with (4.B.6), $\phi_0(\mathbf{r})$ will look like $e^{i\mathbf{k}_F \cdot \mathbf{r}}$ for $r \ll \xi$, while for $r \gg \xi$ the waves $e^{i\mathbf{k} \cdot \mathbf{r}}$ weighted by $g(k)$ will destroy themselves by interference (Fig. 4.B.2). From the above physical arguments, $\phi_0(\mathbf{r})$ will look like $e^{i\mathbf{k}_F \cdot \mathbf{r}}$ for $r \ll \xi$ while for $r \gtrsim \xi$ one can approximate the weighing function as,

$$g(k) \sim \delta(\mathbf{k}, \mathbf{k}_F + i\hat{\mathbf{k}}_F/\xi), \quad (4.B.7)$$

where $\hat{\mathbf{k}}_F$ is a unit vector. One then obtains,

$$\phi_0(\mathbf{r}) \sim e^{-r/\xi} e^{ik_F r}. \quad (4.B.8)$$

Because we are dealing with a singlet state, and the total wavefunction has to be antisymmetric,

$$\phi_0(\mathbf{r}) \sim e^{-r/\xi} \cos k_F r, \quad (4.B.9)$$

A more proper solution of the Cooper pair problem leads to¹¹³

$$\phi_0(\mathbf{r}) \sim K_0(r/\pi\xi) \cos k_F r, \quad (4.B.10)$$

¹¹²Weisskopf (1981).

¹¹³Kadin (2007).

where K_0 is the zeroth-order modified Bessel function. For $x \gg 0$, $K_0(x) \sim (\pi/2x)^{1/2} \exp(-x)$, where $x = r/\pi\xi$.

A wavefunction which extends over distances much larger than the binding potential is a well-known phenomenon when the binding energy is small. For example, as in the case of the deuteron mentioned above.

Be as it may, the large size of the Cooper pair wavefunction also explains why the electrostatic repulsion between electron pairs does not appreciably influence the binding. The repulsion acts only over distances of the order of the correlation length.

Going back to Fig. 4.B.1, it is illustrative to compare the two (NFT calculated) situations displayed in (b) and (e), concerning the relative distribution of the halo neutrons of ^{11}Li . Pairing correlations being, in particular in this case, mainly a surface phenomenon bring, for $r_1 = 7.5$ fm, the two nucleons close to each other as compared to the uncorrelated situation (diagram (g)). The fact that this result, which is not under discussion, is more subtle than just expressed, emerges by looking at (h), where the situation displayed in (b) and (e) (see also (a) and (d)), are schematically drawn in a single plot. The pairing, Cooper pair phenomenon (dashed curve) implies that the two neutrons recede from each other. However, the average potential $U(r) = \int d\mathbf{r}' v(|\mathbf{r} - \mathbf{r}'|)$ acting as a strong external field which determines where normal ($\rho(r)$), and thus abnormal density can find themselves, distorts the halo Cooper pair, leading to the situation represented with the continuous (irregular) curve. Thus, to a situation in which the two halo neutrons have come closer to each other as compared to the uncorrelated situation. And to do so, the finite quantal system under discussion uses the mechanism discussed in App. 4.D (spatial quantization, i.e. independent particle motion, opposed to independent pair motion).

Now, the situation depicted in Fig. 4.B.1 (e) is not observable with the specific probe, namely a two-particle pick up reaction ($^1\text{H}(^{11}\text{Li}, ^9\text{Li})^3\text{H}$). In fact, during the period of time the proton is around the grazing distance, and one of the halo neutrons joins it to form a virtual deuteron, the other neutron can be at the antipode, essentially one diameter apart. The situation will essentially evolve into the density distribution represented with the dashed curve in (h), the two members of the halo Cooper pair being at a distance of the order of the correlation length and carrying a much lower relative momentum than that typical of the situation (e) (continuous irregular curve). It is the natural that successive transfer dominates the absolute differential cross section.

Caption Fig 4.B.1

Synthesis of the spatial structure of ^{11}Li neutron halo Cooper pair calculated in NFT (Barranco et al. (2001)). To make more direct the comparison between the simple estimates and the results of the above reference, it is assumed that $\xi = 7.5$

fm (dashed circle) instead¹¹⁴ of ≈ 12 fm. Diagrams (a) and (d) are the schematic representations of the modulus square $|\Psi_0(\mathbf{r}_1, \mathbf{r}_2)|^2 = |\langle \mathbf{r}_1, \mathbf{r}_2 | 0 \rangle|^2$ describing the motion of the two halo neutrons of ^{11}Li , moving around the ^9Li core as a function of the cartesian coordinates of neutron 2, for fixed (small and large as compared to $R(^{11}\text{Li})=4.6$ fm) values of the position r_1 of neutron 1 (for more details see Caption to Fig. 3.6.3). Diagrams (b), (e) and (g) are the results of NFT (see also Fig. 3.6.3 (II) a) and b)). **(a)** The circles drawn with continuous lines correspond to the relative distance r at the radius of the ^9Li core and of ^{11}Li . The Cooper pair “intrinsic coordinate” r_{12} is also shown. Particle 1 of the Cooper pair is assumed to occupy the center of the nucleus ($r_1 = 0$). **(b)** Result of NFT for a situation similar to the above. **(c)** Schematic representation of an uncorrelated pair in a potential weakly binding the pure configuration $p_{1/2}^2(0)(r_1 = 0)$. **(d)** Same as (a) but for $r_1 = 7.5$ fm. **(e)** Result of the NFT calculation for a similar setup ($r_1 = 5$ fm). **(f)** Schematic representation of a pure configuration $p_{1/2}^2(0)(r_1 = 7.5$ fm), **(g)** The result of the microscopic calculation for a weakly bound $p_{1/2}^2(0)$ configuration ($r_1 = 5$ fm). **(h)** The variety of situations found in (a) and (d) in comparison to each other in a single cartoon. **(i)** Schematic picture of the dynamics of the partners fermions in the quantum state of the Cooper pair. It is a linear combination of motions away and towards one another. The fermions stay within a distance of the order ξ , root mean square radius of the Cooper pair (After Weisskopf (1981), see also Kadin (2007) and van Witsen (2014)).

Within the nuclear scenario, to interact at profit through long wavelength medium polarization pairing, pairs of nucleons have to have low momentum. To do so they have to reduce the effect of the strong external (mean) field by moving away from it, possible mechanisms being among others: halo (Fig. 4.B.1), transfer processes (see e.g. Fig. 4.5.1), exotic decay¹¹⁵ (see Fig. 4.B.3) and, if nothing else, some amount of spill out.

4.B.1 Number of overlapping pairs

The coherence length for low temperature superconductors is of the order of 10^4 Å. In the case of e.g. bulk Pb, for which¹¹⁶ $\Delta = 1.4$ meV and $v_F = 1.83 \times 10^8$ cm/s one obtains $\xi \approx 0.3 \times 10^{-4}$ cm.

¹¹⁴In connection with this figure we have estimated the Fermi momentum associated with the two halo neutrons of ^{11}Li as $k_F = (3\pi^2 \times 2 / ((4\pi/3)(4.6)^3 - (2.5)^3))^{1/3} \approx 0.56$, the denominator being the volume associated with the halo. Thus $(v_F/c) \approx 0.2(k_F)_{\text{fm}^{-1}} \approx 0.1$ and $\xi = \hbar v_F / (\pi \times 0.5 \text{ MeV}) \approx 12$ fm (see also Eq. (4.C.5) as well as the end of caption to Fig. 4.B.3; see also App. 7.E).

¹¹⁵In Fig. 4.B.3, a parallel is made between correlation lengths associated with (pairing) particle-particle or hole-hole modes and particle-hole vibrations. These last modes also display a consistent spatial correlation (see e.g. Broglia et al. (1971c)).

¹¹⁶The experimental value of the critical temperature for Pb is $T_c = 7.193$ K ($k_B T_c = 0.62$ meV). Then $\Delta_0(0)/k_B T_c = 2.26$, to be compared with the BCS prediction of 1.76.

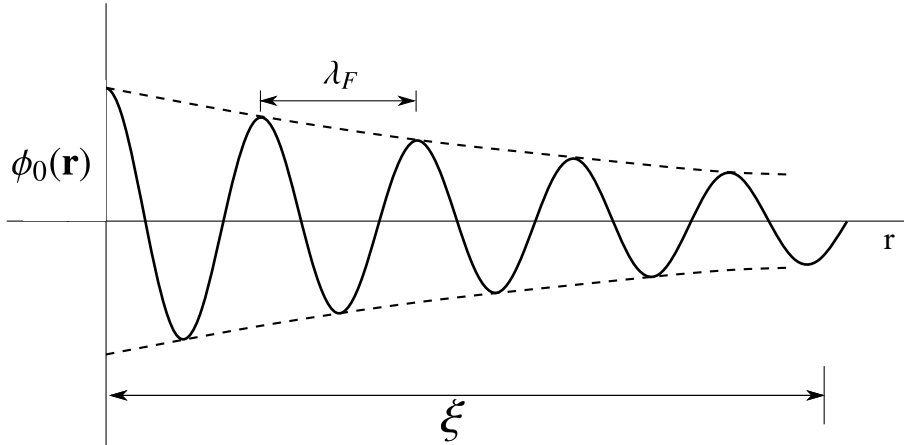


Figure 4.B.2: Schematic representation of the Cooper pair wavefunction. Indicated are the coherence length ξ and the Fermi wavelength $\lambda_F = h/p_F = 2\pi/k_F$. In the nuclear case, and for nuclei along the stability valley $\lambda_F \approx 4.6$ fm and $\xi \approx \hbar v_F/\pi\Delta \approx 14$ fm ($k_F \approx 1.36$ fm $^{-1}$, $v_F/c \approx 0.27$, $\Delta \approx 1.2$ MeV). Thus $\xi/\lambda_F \approx 3$ (after Weisskopf (1981)).

Since electrons in metals typically occupy a volume of the order of $(2\text{\AA})^3$ (Wigner–Seitz cell radius), there would be of the order of¹¹⁷ $\xi^3/(2\text{\AA})^3 \approx 3 \times 10^9$ other electrons within a “coherence volume”. Eliminating the electrons deep within the Fermi sea as they behave essentially as if the metal was in the normal phase¹¹⁸, one gets¹¹⁹ $\approx 10^6$. In other words, about a million of other Cooper pairs have their center of mass falling inside the coherence volume of a pair. Thus, the isolated pair picture (Fig. 3.3.4) is not correct, but yes that displayed in Fig. 3.3.5.

In the nuclear case, the number of Cooper pairs participating in the condensate

$$\alpha_0 = \langle BCS | P'^{\dagger} | BCS \rangle = \sum_j \frac{2j+1}{2} U'_j V'_j. \quad (4.B.11)$$

A simple estimate of this number can be made with the help of the single j –shell model, in which case $V_j = (N/2\Omega)^{1/2}$ and $U_j = (1 - N/2\Omega)^{1/2}$, where $\Omega = (2j + 1)/2$. For a half-filled shell ($N = \Omega$) one obtains¹²⁰ $\alpha'_0 = \Omega/2$. With the help of the approximate expression $\Omega \approx (2/3)A^{2/3}$ one obtains, for ^{120}Sn ($N = 70$), $\alpha \approx 6$.

¹¹⁷Ketterson and Song (1999) p. 198.

¹¹⁸The BCS ground state at $T = 0$ consists in two classes of electrons: those deep inside the Fermi sea, which behave essentially in the same way as those in the normal state, and those near the Fermi surface, which form the overlapping Cooper pairs. These latter electrons cannot scatter because they are in a coherent state. The former electrons inside the sea cannot scatter either because being far from the Fermi surface, they are blocked by Pauli principle. At $T = 0$, all electrons of both classes contribute to the lossless supercurrent Waldrum (1996).

¹¹⁹Schrieffer (1964) p. 43. That is $3 \times 10^9 \times (2\Delta/\epsilon_F) \approx 10^6$ ($2\Delta/\epsilon_F \approx 2.8$ meV/9.47 eV $\approx 3 \times 10^{-4}$).

¹²⁰Making use of the harmonic oscillator, one can write $\Omega = \frac{1}{2}(N + 1)(N + 2) \sim A^{2/3}$, where the proportionality constant has a value between 1/2 and 2/3.

In keeping with the fact that $\xi > R_0$, in the nuclear case one has a complete overlap between all Cooper pairs participating in the condensate. This, together with the fact that the nuclear Cooper pairs press against the nuclear surface in an attempt to expand and are forced to bounce elastically off from it, receive strong circumstantial evidence from the following experimental results: **1)** while the moment of inertia of rotational bands is $\mathcal{J}_r/2$ it is $5\mathcal{J}_{irrot}$. In other words, while pairing in nuclei is important, its role is only partially exhausted, and certainly strongly distorted by the mean field; **2)** One- and two-nucleon transfer reactions in pairing correlated nuclei have the same order of magnitude. For example $\sigma(^{120}\text{Sn}(p,d)^{119}\text{Sn}(5/2^+; 1.09 \text{ MeV})) = 5.35 \text{ mb}$ ($2^\circ < \theta_{cm} < 55^\circ$), while $\sigma(^{120}\text{Sn}(p,t)^{118}\text{Sn}(gs)) = 2.25 \text{ mb}$ ($7.6^\circ < \theta_{cm} < 59.7^\circ$). In this last reaction Cooper pair partners can be as far as 12–13 fm away; **3)** The decay constant of the exotic decay $^{223}_{88}\text{Ra}_{135} \rightarrow ^{14}_6\text{C}_8 + ^{209}_{82}\text{Pb}_{127}$ has been measured to be $\lambda_{exp} = 4.3 \times 10^{-16} \text{ sec}^{-1}$. For theoretical purposes it can be written as $\lambda = P f T$, product of the formation probability P of ^{14}C in ^{223}Ra (saddle configuration, see bottom Fig. 4.B.3), the knocking rate f and the tunneling probability T . These two last quantities hardly depend on pairing. On the other hand P changes from $\approx 2 \times 10^{-76}$ to 2.3×10^{-10} , and consequently the associated lifetimes from 10^{75} y to the observed value of 10^8 y allowing Cooper pairs to be correlated over distances which can be as large as 20 fm.

Within the above context, and as discussed in App. 4.C, exotic halo nuclei open new possibilities to understand the physics at the basis of pairing in nuclei. In fact, one may be able to hide away in a bare 1S_0 NN -potential the $\approx 50\%$ contribution associated with the induced pairing interaction to the pairing gap in ^{120}Sn . Hardly, essentially all of the binding energy ($S_{2n} \approx 380 \text{ keV}$) of the neutron halo Cooper pair of ^{11}Li to the core ^9Li . At the basis of the large magnitude of renormalization effects of elementary modes of excitation and of medium polarization contributions to the pairing interaction observed in light exotic halo nuclei like e.g. ^{11}Li , one finds a fundamental parameter of NFT, namely the effective degeneracy $\Omega (\approx 2/3A^{2/3})$ of the single-particle phase space, $1/\Omega$ being the small expansion parameter. In the case of ^{11}Li , Ω is rather small (≈ 3) as compared with heavy nuclei like e.g. ^{210}Pb ($\Omega \approx 24$). Furthermore, in the case of ^{11}Li , the surface (S) to volume (V) ratio ($= aS/V$, a being the nuclear diffusivity) is much larger¹²¹ (≈ 0.72) than in the case of heavy nuclei lying along the stability valley (≈ 0.27 in the case of ^{210}Pb).

4.B.2 Coherence length and quantity parameter for (*ph*) vibrations

As seen from Fig. 2.2.2, both $\beta = 0$ and $\beta = \pm 2$ modes lead to a sigmoidal shape of the single-particle occupation probabilities within an energy region $\delta\epsilon = |E_{corr}|$ around the Fermi energy. Consequently, the arguments used in Sect. 4.5.1 and

¹²¹In carrying out this estimate use was made of $a_{eff} = (R(^{11}\text{Li})/R_0(^{11}\text{Li}))a$ (within this context see Fig. 4.3.2).

leading to

$$\xi = \frac{\hbar v_F}{\pi |E_{corr}|}, \quad (4.B.12)$$

for pairing modes and resulting in

$$\xi = \frac{\hbar v_F}{\pi \Delta} \quad (4.B.13)$$

for the case of superfluid nuclei, can be used equally well in connection with $\beta = 0$ modes. In other words, in a similar way in which pair addition and subtraction modes (Cooper pairs) can be viewed as correlated pp and hh modes over distances of the order ξ , $\beta = 0$ collective vibrations can be pictured as ph modes correlated again over distances inversely proportional to the correlation energy of e.g. the RPA collective roots. Summing up, ξ describe, both in the case of $\beta = \pm 2$ and $\beta = 0$ modes, a similar physical property of the vibration: the length over which pairs of fermions ((ph), (pp), (hh)) are correlated in normal and in superfluid nuclei (see Fig. 4.B.3).

Caption Fig 4.B.3

Vibrations can be classified by the transfer quantum number β . Collective modes with $\beta = 0$ correspond to correlated particle-hole (ph) excitations. For example low-lying quadrupole or octupole (surface) vibrations. Modes with $\beta = \pm 2$ correspond to correlated (pp) or (hh) modes, that is, pair addition and pair subtraction modes. Thinking of these modes propagating in uniform nuclear matter, the associated correlation length can be calculated making use of Eq. (4.B.12), the correlation energy being, as a rule estimated from the shift of the lowest root of the RPA solution for both, ph and pairing modes, from the lowest unperturbed configuration (pole). The (generalized) quantality parameter, ratio of the quantal kinetic energy of localization and the correlation energy, gives a measure of the tendency to independent particle ($q_\xi \approx 1$) or independent pp , hh , ph ($q_\xi \ll 1$) motion. This is in keeping with the fact that potential energy is best profited by special arrangements between nucleons and thus lower symmetry than the original Hamiltonian, while fluctuations favor symmetry. A concrete example which testifies to the fact that (ph) excitations (large amplitude surface distortion) and independent pair motion (superfluidity) are correlated over dimensions larger than typical nuclear dimensions, is provided by e.g. fission and exotic decay, in particular $^{223}\text{Ra} \rightarrow ^{14}\text{C} + ^{209}\text{Pb}$. In the related estimates use has been made of¹²² $\Delta = 12/\sqrt{A}$ MeV; $C = 18.1$ MeV, $D/\hbar^2 = 29.1$ MeV $^{-1}$ and¹²³ $\hbar\omega = \hbar(C/D)^{1/2} \approx 0.8$ MeV; $E = 1.4$ MeV, while¹²⁴ $E_{corr} = -(E - \hbar\omega)$. In keeping with the uncertainties affecting the above simple estimates (factor 2 or π in the denominator of ξ , $\langle r^2 \rangle_{Cooper}^{1/2}$, $\sqrt{\frac{5}{3}} \langle r^2 \rangle_{Cooper}^{1/2}$, etc.), it

¹²²Bohr and Mottelson (1969).

¹²³Brink and Broglia (2005) Sect. 7.1.

¹²⁴Bohr and Mottelson (1975) Fig. 6-38.

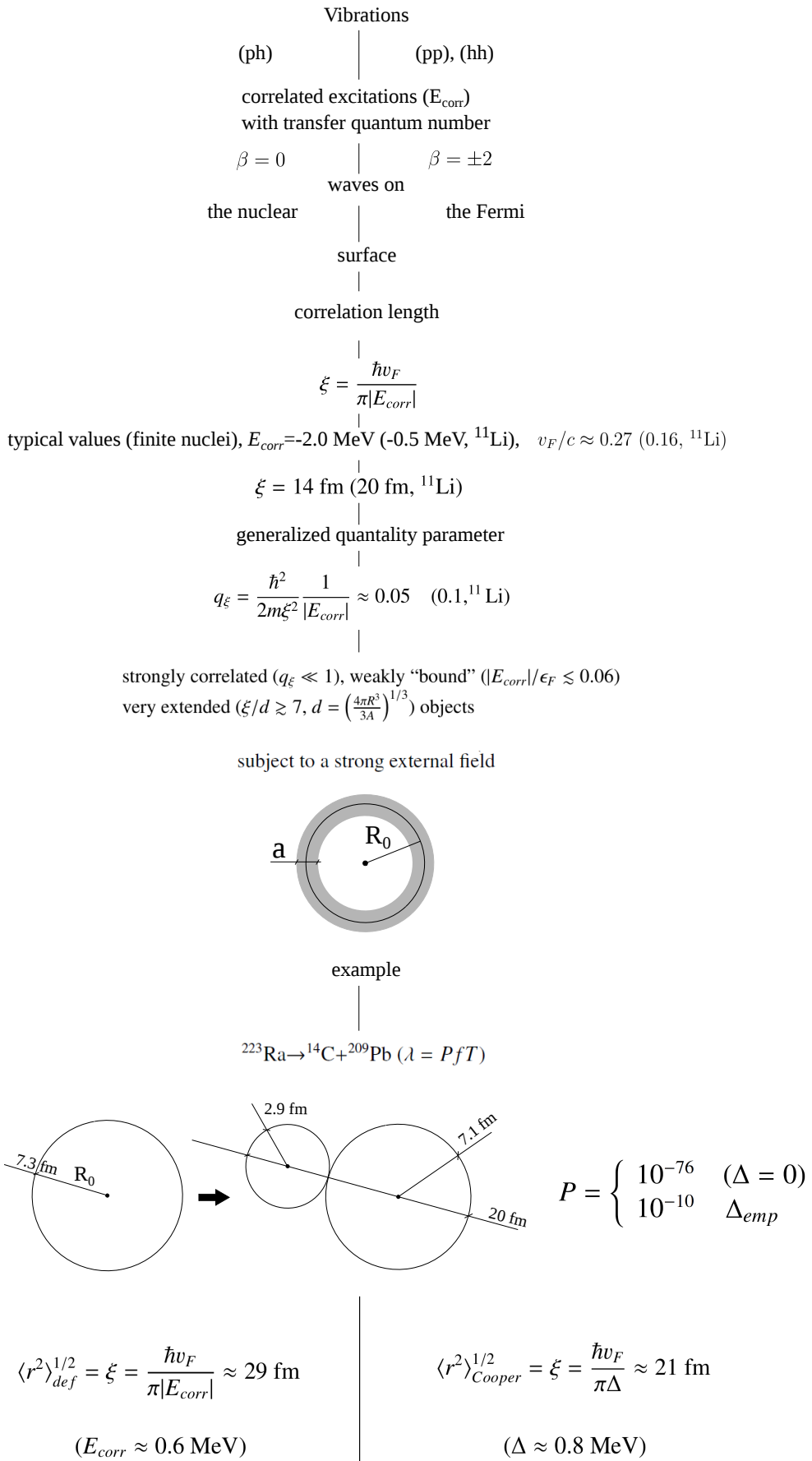


Figure 4.B.3

seems fair to conclude that $15 \text{ fm} \lesssim \xi \lesssim 25 \text{ fm}$. Thus, one is likely faced with an intermediate situation in which $2 \lesssim \xi/R \lesssim 3$.

f		$\sigma(gs \rightarrow f)/\sigma(gs \rightarrow gs)$	Table A
J^π	E_x		
$0^+(gs)$	0	100	pair removal (hh)
3^-	2.62	21	(ph) collective mode
5^-	3.20	45	(ph) collective mode
0^+	4.87	45	pair addition

Table 4.B.1: Relative two-nucleon transfer cross sections $\sigma(^{206}\text{Pb}(t, p)^{208}\text{Pb}(f)/\sigma(^{206}\text{Pb}(t, p)^{208}\text{Pb}(gs))$ integrated in the range $5^\circ - 175^\circ$ of cm angles. (After Broglia et al. (1973), Table A. VIII b)

J^π	$\sigma(gs \rightarrow f)$ (mb)	$\sigma(gs \rightarrow f)/\sigma(gs \rightarrow gs)$
$0^+(gs)$	2250 ± 338	100
2^+	613 ± 92	27

Table 4.B.2: Absolute cross section associated with the reaction $^{120}\text{Sn}(p, t)^{118}\text{Sn}$ to the ground state and first excited state integrated in the range $7.6^\circ < \theta_{cm} < 69.7^\circ$. After Guazzoni et al. (2008).

Some typical orders of magnitude: $E_{corr} \approx -1.2$ MeV and $\Delta \approx 1.2$ MeV for medium heavy nuclei lying along the stability valley. Thus

$$\xi = \frac{\hbar v_F}{\pi |E_{corr}|} \approx \frac{\hbar c(v_F/c)}{3.8 \text{ MeV}} \approx \frac{200 \text{ MeV fm} \times 0.27}{3.8} \approx 14 \text{ fm.} \quad (4.B.14)$$

In the case of ^{11}Li , $E_{corr} \approx -500$ keV and $v_F/c \approx 0.16$. Thus

$$\xi \approx \frac{200 \text{ MeV fm} \times 0.16}{1.6} \approx 20 \text{ fm.} \quad (4.B.15)$$

Generalized quantity parameter

$$q_\xi = \frac{\hbar^2}{2m\xi^2} \frac{1}{|E_{corr}|} = \begin{cases} \frac{20 \text{ MeV fm}}{14^2 \times 2 \times 1.2 \text{ MeV}} \approx 0.04 \\ \frac{20 \text{ MeV fm}}{20^2 \times 0.5 \text{ MeV}} \approx 0.10 \quad ^{11}\text{Li} \end{cases} \quad (4.B.16)$$

The parallel which can be traced between Cooper pairs and correlated particle-hole excitations is further testified by the fact that two-nucleon transfer reaction do excite quite strongly also these modes (see Tables 4.B.1 and 4.B.2).

This parallel between $\beta = 0$ and $\beta = \pm 2$ modes emerged already in the analysis¹²⁵ of the $^{206}\text{Pb}(t, p)^{208}\text{Pb}$ which provided the experimental confirmation of the theoretical predictions concerning pairing vibrations. In particular concerning the population of the pair addition mode ($|gs(^{208}\text{Pb})\rangle$; see Fig. 3.1.1 (b) transition denoted a (indicating addition mode) predicted at an excitation energy¹²⁶ of 4.9 MeV

¹²⁵Broglia and Riedel (1967).

¹²⁶See Fig. 5 Bès and Broglia (1966).

(Fig. 3.5.1) in ^{208}Pb , and observed¹²⁷ at 4.87 MeV. Now, because the lowest excited state populated with a sizable cross section ($21\pm3\%$) of that associated with the ground state transition (and thus populating the pair removal mode ($|gs(^{206}\text{Pb})\rangle$), see Fig. 3.1.1(b) transition denoted r) was observed at $E_x = 2.619$ MeV, much effort and time was dedicated to experimentally disentangled and eventually $J^\pi = 0^+$, essentially degenerated with the octupole vibration at $E_x = 2.62 \pm 0.01$ MeV. This was in keeping with the idea that around close shell nuclei, only pairing vibration were strongly populated, this not being the case for $\beta = 0$ collective surface state.

The analysis of the data dispelled such believe, as testified already by the title of the paper reporting the results. In fact, collective $\beta = 0$ and $\beta = \pm 2$ are similarly strongly populated in two-nucleon transfer reactions, the main difference being the fact that while the Y -component (ground state correlations, see Tables 3.5.2 and 3.5.3) contribute constructively coherent to the cross section, the similar components of the $\beta = 0$ modes give rise to destructive coherence. Again an example of the competition for phase space between pairing and (dynamical) surface deformation (see e.g. Fig. 2.9.2). These results originally found in Pb, were extended to other mass regions and $\beta = 0$ modes¹²⁸. Within this scenario one can look forward to the test of the $^9\text{Li}(t, p)^{11}\text{Li}$ predictions, concerning the population of both the ground state and the DPR ($E_x \lesssim 1$ MeV). Also to compare to which extent the 0^{++} ^{12}Be excited state and 1^- excitation on top of it, can be viewed as related elementary modes of excitation (see Fig. 4.9.1).

4.B.3 tunneling probabilities

The state $|BCS(\phi)\rangle_{\mathcal{K}} = \prod_{\nu>0} (U'_\nu + V'_\nu e^{-2i\phi} a_\nu^\dagger a_{\bar{\nu}}^\dagger) |0\rangle$ (see Eq. (4.8.17)) displays off-diagonal-long-range-order (ODLRO) because each pair is in a state $(U'_\nu + V'_\nu e^{-2i\phi} a_\nu^\dagger a_{\bar{\nu}}^\dagger) |0\rangle$ with the same phase as all the others. In fact, the above wavefunction leads to a two-particle density matrix with the property $\lim_{\mathbf{r}_1, \mathbf{r}_2, \mathbf{r}_3, \mathbf{r}_4 \rightarrow \infty} \phi(\mathbf{r}_1, \mathbf{r}_2; \mathbf{r}_3, \mathbf{r}_4) \neq 0$ under the assumption that $r_{12}, r_{34} < \xi$, $(\mathbf{r}_1, \mathbf{r}_2)$ and $(\mathbf{r}_3, \mathbf{r}_4)$ being the coordinates of a Cooper pair, r_{ij} the relative modulus of it and ξ the coherence length¹²⁹.

Bringing the above argument into reaction implies, as shown in Eq. (4.3.1), that $P_2 = P_1$. In keeping with the parallel made with superconductors (see Fig. 4.A.5) one can mention that Josephson showed that at very low temperatures, the pair current is equal to the single-particle current at an equivalent voltage¹³⁰ $\frac{\pi}{4} \frac{2\Delta}{e}$. Experiments observed values of maximum Josephson current of ≈ 1 mA, consistent with junctions resistances of 1Ω per unit area (see Sect. 4.7). The importance of this result concerning the mechanism at the basis of Cooper pair transfer is connected with the fact that the probability of one-electron-tunneling across a typical

¹²⁷Bjerregaard et al. (1966).

¹²⁸Broglia et al. (1971c).

¹²⁹See e.g. Ambegaokar (1969) and refs. therein, see also Potel et al. (2017).

¹³⁰In the case of Pb $\Delta = 1.4$ meV (see footnote¹¹⁶) this voltage is $(\pi \times 1.4/2) \times 10^{-3} \times \text{eV/e} \approx 2 \text{mV}$ (see e.g. McDonald (2001)).

dioxide layer giving rise to a weak $S - S$ coupling¹³¹ is of the order of 10^{-10} . Consequently, simultaneous pair transfer between two superconductors (S), with a probability $(10^{-10})^2$ would not be observed¹³². Thus, the Josephson current of carriers of charge $2e$ results from the tunneling of a Cooper pair partner at a time, equally pairing correlated when they are in the same superconductor (S) within the correlation length ξ , than when each of them is on a different of the two weakly coupled S .

One could argue that in the reaction $^{120}\text{Sn}(p, t)^{118}\text{Sn}(\text{gs})$ one can hardly consider the triton as a pairing condensate. While this is correct one can hardly claim either that six–eight Cooper pairs (^{120}Sn) make a *bona fide* one. In any case, when one experimentally observes such unexpected phenomenon $\sigma_{2n} \approx \sigma_{1n}$, one is likely somewhat authorized at using similar concepts¹³³.

4.B.4 Nuclear correlation (condensation) energy

The BCS mean field can be written as¹³⁴

$$H_{MF} = U + H_{11} \quad (4.B.17)$$

where

$$U = 2 \sum_{\nu>0} (\epsilon_\nu - \epsilon_F) V_\nu^2 - G \alpha_0^2 \quad (4.B.18)$$

while

$$H_{11} = \sum_{\nu>0} E_\nu (\alpha_\nu^\dagger \alpha_\nu + \alpha_{\bar{\nu}}^\dagger \alpha_{\bar{\nu}}), \quad (4.B.19)$$

E_ν being the quasiparticle energy, and α_ν^\dagger the quasiparticle creation operator. The pair-correlation energy is the difference between the energy with and without pairing. The energy including pair correlations is

$$E_p = 2 \sum_{\nu>0} |V_\nu|^2 \epsilon_\nu - G |\alpha_0|^2 \quad (4.B.20)$$

while the energy without correlation is

$$E_0 = \sum_{\nu>0} |V_\nu^0|^2 \epsilon_\nu. \quad (4.B.21)$$

The occupation probabilities $|V_\nu^0|$ are unity below the Fermi energy level and zero above. In both Eqs. (4.B.20) and (4.B.21) the Fermi energy has to be chosen to give the correct number of particles. The pairing correlation energy is

$$E_{corr} = E_S - G |\alpha_0|^2, \quad (4.B.22)$$

¹³¹Pippard (2012).

¹³²See e.g. McDonald (2001).

¹³³Anderson (1972).

¹³⁴Brink and Broglia (2005), Appendix G.

where

$$E_S = \sum_{\nu>0} 2(|V_\nu|^2 - |V_\nu^0|^2) \epsilon_\nu. \quad (4.B.23)$$

The pairing energy $-G|\alpha_0|^2$ is partially canceled by the first term describing the fact that, in the BCS ground state, particles moving in levels close to the Fermi energy are partially excited across the Fermi surface, in keeping with the fact that V_ν^2 changes smoothly from 1 to 0 around ϵ_F , being 1/2 at the Fermi energy.

In other words, the energy gain resulting from the potential energy term, where G is the pairing coupling constant while $|\alpha_0|$ measures the number of Cooper pairs is partially compensated by a quantal, zero point fluctuation like term. It can, in principle, be related to the Cooper pair kinetic energy of confinement $T_\xi = \frac{\hbar^2}{2m\xi^2}$ already discussed in connection with the generalized quantality parameter, through the relation $2|\alpha_0|T_\xi$ (for one type of nucleons), in keeping with the fact that (4.B.23) is expressed in terms of single particle energies. Let us make a simple estimate which can help at providing a qualitative example of the above argument, and consider for the purpose the nucleus ^{223}Ra and $G \approx (22/A) \text{ MeV}$, $|\alpha_0| \approx 5$ and $\xi \approx 20 \text{ fm}$: $T_\xi \approx 0.1 \text{ MeV}$, $2 \times (2 \times |\alpha_0| \times T_\xi) = 2 \text{ MeV}$, $2 \times (-G|\alpha_0|^2) = -5 \text{ MeV}$ ¹³⁵ (factors of 2, both protons and neutrons). The resulting pairing correlation energy thus being $E_{corr} = -3 \text{ MeV}$. This number can be compared with a “realistic” estimate provided by the relation¹³⁶

$$E_{corr} = -\frac{g\Delta^2}{4}, \quad (4.B.24)$$

where $g_n = N/16 \text{ MeV}^{-1}$ and $g_p = Z/16 \text{ MeV}^{-1}$. Taking into account both types of particles $g = g_n + g_p = A/16 \text{ MeV}^{-1}$ and making use of $\Delta = 12/\sqrt{A} \text{ MeV}$, one obtains $E_{corr} = -\frac{143}{64} \text{ MeV} = -2.23 \text{ MeV}$. With the help of E_{corr} and T_ξ , one can estimate the generalized quantality parameter, $q_\xi = T_\xi/|E_{corr}| = 0.1/2 \approx 0.05$, as well as make a consistency check on the value of ξ used, namely $\hbar v_F/(2|E_{corr}|) \approx 13.5 \text{ fm}$.

4.B.5 Summary

The nuclear Cooper pair not only is forced to exist in a very strong external field, the HF mean field, of very reduced dimensions as compared to the correlation length. Because of spatial quantization, it is also forced to exist on selected orbitals of varied angular momentum and parity¹³⁷ (App. 4.D).

¹³⁵This quantity, but divided by 2, i.e. -2.5 MeV can be compared with the effective pairing matrix element $v = \left(\frac{\Delta_n^2 + \Delta_p^2}{4} \approx -2.9\right) \text{ MeV}$, operative at level crossing in the calculation of the inertia of the exotic decay $^{223}\text{Ra} \rightarrow ^{14}\text{Ca} + ^{209}\text{Pb}$, cf. Brink and Broglia (2005) p.159 and refs. therein.

¹³⁶Brink and Broglia (2005).

¹³⁷Some of them allowing for pure $j^2(0)$ configurations, with large (little) probability of $L = 0$ relative motion, which behaves as hot (cold) orbitals, their contribution to pairing correlations and to

Correlations, in particular pairing correlations within such constraints will have opposite and apparently contradictory effects. As an example, let us consider two neutrons moving around ${}^9\text{Li}$ in the $s_{1/2}^2(0)$ or in the $p_{1/2}^2(0)$ (pure) configurations. In such a situation, fixing one of the neutrons of the pair at a radius r_1 , the other one will display equal probability to be close or in the opposite side of the nucleus ($\theta_{12} = 0^\circ$ or $\theta_{12} = 180^\circ$), the average distance between neutrons being of the order of $d = \left(\frac{\frac{4\pi}{3}R^3}{A}\right)^{1/3} \approx 2 \text{ fm}$ (3.3 fm using $R({}^{11}\text{Li})=4.6 \text{ fm}$ instead of $R = 1.2A^{1/3} \text{ fm}$).

By exchanging the PDR between the two outer neutrons, the halo Cooper pair is stabilized, becoming weakly bound ($S_{2n} = 380 \text{ keV}$). Assuming that the odd proton $p_{3/2}(\pi)$ plays only a spectator role, the ground state of ${}^{11}\text{Li}$ can be written as $|{}^{11}\text{Li}(gs)\rangle = |\tilde{0}\rangle \otimes |p_{3/2}(\pi)\rangle$, the neutron halo Cooper pair state being

$$|\tilde{0}\rangle = |\tilde{0}\rangle + 0.71|(p_{1/2}, s_{1/2})_{1^-} \otimes 1^-; 0\rangle + 0.1|(s_{1/2}, d_{5/2})_{2^+} \otimes 2^+; 0\rangle. \quad (4.B.25)$$

where

$$|\tilde{0}\rangle = 0.45|s_{1/2}^2(0)\rangle + 0.55|p_{1/2}^2(0)\rangle + 0.04|d_{5/2}^2(0)\rangle \quad (4.B.26)$$

Studying this state microscopically one observes two contrasting effects taking place:

1) The two neutrons will switch from a regime of single-particle motion to that of independent pair motion and adopt the configuration proper to a Cooper pair (radial motion against each other) and expand radially consistent with the fact that its mean square radius is $\approx 20 \text{ fm}$ ($\xi = \langle r^2 \rangle_{\text{Cooper}}^{1/2} \approx \frac{\hbar v_F}{\pi E_{\text{corr}}} \approx \hbar c(v_F/c)/\pi E_{\text{corr}} \approx \frac{200 \text{ MeV fm} \times 0.16}{\pi \times 0.5 \text{ MeV}} = 20 \text{ fm}$, $\epsilon_F({}^{11}\text{Li}) \approx 13 \text{ MeV} \rightarrow v_F/c \approx 0.16$). This can be appreciated by the fact that the radius of ${}^{11}\text{Li}$ is much larger than that expected from systematic ($R({}^{11}\text{Li}) = 4.6 \text{ fm}$, corresponding to an effective mass number $A_{\text{eff}} \approx 60$).

2) Interference between positive ($(-1)^l = +1$) and negative ($(-1)^l = -1$) single-particle based $|(l, j)_0^2\rangle$ configurations, constructive at $\theta = 0^\circ$ and destructive at $\theta = 180^\circ$, $\theta = r_1 \hat{r}_2$ been the relative angle between the coordinates \mathbf{r}_1 and \mathbf{r}_2 of the Cooper pair partners. In other words the two nucleons will tend to be close to each other, in particular on the nuclear surface. As can be seen from (4.B.26), this effect is extreme in the case of the ground state of ${}^{11}\text{Li}$. Now, such an effect has not much to do with pairing, BCS pairing at it and thus superconductivity¹³⁸, but

two-nucleon transfer reactions being very inhomogeneous, at variance of the situation found in solid state (see e.g. Broglia (2005)). This is also the reason why the second-order-like phase transition normal-superfluid taking place in nuclei as e.g. a function of the number of pairs of nucleons moving outside closed shells, affected by strong pairing fluctuations, are conspicuously blurred as compared to the $N \rightarrow \infty$ case.

¹³⁸Within this context it is of notice that in condensed matter literature Cooper pairs are viewed as fragile, extended di-electron entities, overlapping with a conspicuous number of other pairs, and displaying a delicate “rigid” quantal correlation between partners (generalized quantity parameter) and among Cooper pairs (off diagonal long range order). In fact, Weisskopf’s representation of the radial (opposite) motion of electrons provides a useful picture of Cooper pair internal dynamics, In other words, approaching to or recessing from each other does not favour a particular anisotropic configuration , the two electrons being at the mean square radius of the Cooper pair, i.e. the coherence length ξ .

with the properties of the nuclear mean field, result of spatial quantization which not only distorts the Cooper pair through isotropic confinement, but through admixtures of odd and even parity states controlled also by the very strong spin orbit term. Within this context see Sect. 7.6.3.

Summing up, the difficulties of understanding pairing in nuclei as compared with condensed matter is (at least threefold): **a**) the bare interaction is attractive, a fact which lead to the idea that pairing force is short range and delayed the discovery of the other half of pairing, namely the retarded, medium polarization interaction, for a long time¹³⁹; **b**) particle number is small, thus pairing vibrations are important, and renormalize in a conspicuous way the variety of nuclear phenomena, in particular single-particle motion. The fact that such effects are still not being really considered is testified by the fact that a serious treatment of multipole pairing vibrations is still missing; **c**) spatial quantization leading to phenomena which by themselves can be very interesting¹⁴⁰, but which are not directly related to pairing correlations and nonetheless has conditioned nuclear structure research, let alone reaction mechanism studies and the physics emerging from their interweaving.

Appendix 4.C Absolute Cooper pair tunneling cross section: quantitative novel physics at the edge between stability and chaos

In the study of many-body systems, in particular of finite quantum many-body systems (FQMBS) like the atomic nucleus, much can be learned from symmetries (group theory) as well as from the general phenomena of spontaneous symmetry breaking. However, it is the texture of the associated emergent properties, concrete embodiment of symmetry breaking (potential energy) and of its restoration (fluctuations, collective modes), which provides insight into the eventual new physics. In fact, when one understands the many-body under study in terms of the detailed motion of single-particles (nucleons) and collective motion, taking properly into account their couplings and associated zero point fluctuations, is that one can hope to have reached a solid, quantitative, understanding of the problem and of its solutions. Even more, that these solutions are likely transferable, at profit, to the study of other FQMBS like e.g. metal clusters, fullerenes¹⁴¹, quantum dots¹⁴², and eventually soft matter, in particular proteins¹⁴³, let alone the fact that one can make predictions. Predictions which, in connection with the study of halo nu-

¹³⁹A long held picture: pairing plus long range force, i.e. pairing short range, many (high) relative angular momenta contributing (Kisslinger and Sorensen (1963); Soloviev (1965); Mottelson (1962, 1998).

¹⁴⁰Bertsch et al. (1967); Ferreira et al. (1984); Lotti et al. (1989); Matsuo (2006, 2013)

¹⁴¹Cf. e.g. Gunnarsson (2004), Broglia et al. (2004) and refs. therein.

¹⁴²Lipparini (2003).

¹⁴³Broglia (2013).

clei, in particular of pairing¹⁴⁴ in such exotic, highly extended systems lying at the nucleon drip line, involve true novel physics¹⁴⁵. Within this context one can quote from Leon Cooper's contribution to the volume¹⁴⁶ BCS: 50 years: "It has become fashionable... to assert... that once gauge symmetry is broken the properties of superconductors follow... with no need to inquire into the mechanism by which the symmetry is broken¹⁴⁷. This is not... true, since broken gauge symmetry might lead to molecule-like and a Bose-Einstein rather than BCS condensation... in 1957... the major problem was to show... how... an order parameter or condensation in momentum space could come about... to show how... gauge-invariant symmetry of the Lagrangian could be spontaneously broken due to interactions which were themselves gauge invariant".

Nuclear physics has brought this quest a step further. This time in connection with the "extension" of the study of BCS condensation to its origin, a single Cooper pair in the rarified atmosphere resulting from the strong radial (isotropic) deformation observed in light halo, exotic nuclei in general, and in ^{11}Li in particular. During the last few years, the probing of this system in terms of absolute two-nucleon transfer (pick-up) reactions, has made this field a quantitative one, errors below the %10 limit being the rule. This achievement which has its basis on the remarkable experiments of Tanihata et al. (2008), is also the result of the combined effort made in treating the structure and reaction aspects of the subject, two sides of the same physics, on equal footing.

4.C.1 Saturation density, spill out and halo

In the incipit to the Chapter on bulk properties of nuclei of Bohr and Mottelson¹⁴⁸ one reads: "The almost constant density of nuclear matter is associated with the finite range of nuclear forces; the range of the forces is r_0 (where r_0 enters the nuclear radius in the expression $R = r_0 A^{1/3}$) thus small compared to nuclear size. This "saturation" of nuclear matter is also reflected in the fact that the total binding energy of the nucleus is roughly proportional to A . In a minor way, these features

¹⁴⁴Cf. e.g. Broglia and Zelevinsky (2013).

¹⁴⁵Cf. e.g. Barranco et al. (2001); Tanihata et al. (2008); Potel et al. (2010) and references therein.

¹⁴⁶Cooper (2011).

¹⁴⁷Quoting (Weinberg (2011)): "... In consequence of this spontaneous symmetry breaking, products of any even number of electron fields have non-vanishing expectation values in a superconductor, though a single electron field does not. All of the dramatic exact properties of superconductors – zero electric resistance, the expelling of the magnetic fields from superconductors known as the Meissner effect, the quantization of magnetic flux through a thick superconducting ring, and the Josephson formula for the frequency of the ac current at a junction between two superconductors with different voltages – follow from the assumption that electromagnetic gauge invariance is broken in this way, with no need to inquire into the mechanism by which the symmetry is broken." The above quotation is similar to saying that once the idea of a double DNA helix was thought, all about inheritance was solved and known, and that one could forget the X-ray plates of Rosalind Franklin, Maurice Wilkins and collaborators, let alone how DNA and proteins interact with each other (cf. e.g. Stent (1980) and references therein).

¹⁴⁸Bohr and Mottelson (1969) p. 139.

are modified by surface effects and long-range Coulomb forces acting between the protons".

Electron scattering experiments (see the figure 2-1, p. 159 of the above reference) yield

$$\rho(0) = 0.17 \text{ fm}^{-3}. \quad (4.C.1)$$

Thus, one can posit that

$$\frac{4\pi}{3} R_0^3 \rho(0) = A, \quad (4.C.2)$$

leading to

$$r_0 = \left(\frac{3}{4\pi} \frac{1}{\rho(0)} \right)^{1/3} \approx 1.12 \text{ fm}. \quad (4.C.3)$$

Because the above relations imply a step function distribution, we have to add to (4.C.3) the nucleon spill out¹⁴⁹ ($a_0/R_0 \ln 2 \approx (0.5/5.5) \ln 2 \approx 0.06 (A = 120)$) associated with the fact that a more realistic distribution is provided by a Fermi function of diffusivity $a_0 \approx 0.5 \text{ fm}$. Thus $r_0 = (1.12 + 0.06) \text{ fm} \approx 1.2 \text{ fm}$. In the case of the nucleus ^{11}Li , observations indicate a mean square (gyration radius¹⁵⁰) radius $\langle r^2 \rangle^{1/2} = 3.55 \pm 0.1 \text{ fm}$ ¹⁵¹. Thus

$$R(^{11}\text{Li}) = \sqrt{\frac{5}{3}} \langle r^2 \rangle^{1/2} \approx 4.58 \pm 0.13 \text{ fm}. \quad (4.C.4)$$

Making use of the relation $R (= R_0) \approx 1.2A^{1/3} \text{ fm}$, the quantity (4.C.4) leads to $(4.58/1.2)^3 \approx 56$, an effective mass number larger five times the actual value $A = 11$. To be noted that the actual mass number predicts a "systematic" value of the nuclear radius $R_0(^{11}\text{Li}) \approx 2.7 \text{ fm}$.

The above results testify to a very large "*isotropic radial deformation*", or halo region (skin), in keeping with the fact¹⁵² that $R(^{11}\text{Li}) - R_0(^9\text{Li}) = R_0(^9\text{Li}) \left(\frac{R(^{11}\text{Li})}{R_0(^9\text{Li})} - 1 \right) = 0.83R_0(^9\text{Li})$. In other words, ^{11}Li can be viewed as made out of a normal ^9Li core and of a skin made out of two neutrons extending over a shell radius of the order of that of the core. But even more important, it is the fashion in which the above mentioned "deformation" affects nuclear matter. Matter which is little compliant to undergo either compressions or, for that sake, "depressions", without resulting in nuclear instability. In one case, through a mini supernova. In the second, by

¹⁴⁹Bertsch and Broglia (2005).

¹⁵⁰The radius of gyration R_g is a measure of an object of arbitrary shape, R_g^2 being the second moment in 3D space. In the case of a sphere of radius R , $R_g^2 = 3R^2/5$.

¹⁵¹Kobayashi et al. (1989).

¹⁵²Let us parametrize the radius of ^{11}Li as (see Bohr and Mottelson (1975)), $R = R_0(1 + \alpha_{00}Y_{00}) = R_0(1 + \beta_0 \frac{1}{\sqrt{4\pi}})$. Thus $\beta_0 = \sqrt{4\pi}(\frac{R}{R_0} - 1) \approx 2.5$ which testifies to the extreme "exoticity" of the phenomenon.

obliterating the effect of the short range strong force acting in the 1S_0 channel (screening effect of the bare pairing interaction).

In fact, in the case of the halo Cooper pair of ${}^{11}\text{Li}$, that is of the last two weakly bound neutrons, one is dealing with a rarefied nuclear atmosphere of density

$$\rho \approx \frac{2}{\frac{4\pi}{3}(R^3({}^{11}\text{Li}) - R_0^3({}^9\text{Li}))} \approx 0.6 \times 10^{-2} \text{ fm}^{-3} \quad (4.\text{C}.5)$$

where the value $R_0({}^9\text{Li}) \approx 2.5$ fm was used. That is, we are dealing with pairing in a nuclear system at a density which is only 4% of saturation density.

The quest for the long range pairing mechanism which is at the basis of the binding of the halo Cooper pair of ${}^{11}\text{Li}$ to the ${}^9\text{Li}$ core ($S_{2n} \approx 0.380$ keV, to be compared to typical systematic values of $S_{2n} \approx 16$ MeV), has lead to the discovery of what can be considered a novel nuclear mode of elementary excitation. The symbiotic halo pair addition mode, which has to carry its own source of binding (glue) like the hermit crab who carries a gastropod shell to protect his body. A novel embodiment of the Axel–Brink scenario in which not only the line shape, but the main structure of the resonance depends on the state on which it is built, and to which it is deeply interweaved as to guarantee its stability¹⁵³ and thus its own existence. It also provides a novel realization of the Bardeen-Fröhlich-Pines¹⁵⁴ microscopic mechanism to break gauge invariance: through the exchange of quite large ZPF which ensures the same symmetries of the original Hamiltonian to a system displaying essentially a permanent dipole moment, as a consequence of the almost degeneracy of the dipole pygmy resonance (centroid $\lesssim 1$ MeV) with the ground state. To our knowledge, this is the first example of a van der Waals Cooper pair, atomic or nuclear (App. 3.A).

The NFT diagram shown in Fig. 3.A.1 describing this binding seems quite involved and high order. Thus unlikely to be at the basis of a new elementary mode of nuclear excitation, if nothing else because of the apparent lack of “elementarity”. This is not the case and, in fact, the physics at the basis of the process depicted by the oyster-like and eagle-like networks displayed in (a) and (b) is quite simple and recurrent throughout nuclear structure and reactions, let alone many-body theories and QED. In fact, it encompasses (see Fig. 3.A.1): (I,II) the changes in energy of single-particle levels as a function of dynamical quadrupole dynamical deformations leading to a Jahn-Teller like effect (III) the interaction between particles through the exchange of (bosons) vibrations, (IV,V) Pauli principle, (VI,VII) the softening of collective modes due to ground state correlations ((ZPF)-components, QRPA),(VIII) the interaction between two non-polar systems through virtual, ZPF associated dipoles. Referring to general many-degree of freedom systems, (I,II) and (III) are at the basis of the fact that, in QED, the coupling between one and two photons is zero (Furry’s theorem). It is also at the basis, through cancellation, of the small width displayed by giant resonances as compared with single-particle

¹⁵³Axel (1962); Brink (1955 (unpublished)).

¹⁵⁴Bardeen and Pines (1955); Fröhlich (1952).

widths of similar excitation energies, as well as of inhomogeneous damping in rotational motion at finite temperatures¹⁵⁵, in NMR of molecules and in GDR of atomic nuclei. Concerning (VIII), one can mention resonant interactions between fluctuating systems like e.g. two coupled harmonic oscillators¹⁵⁶. It is like to find a new particle. Either one is at the right energy (on-shell) or one would not see it.

In the case of halo Cooper pair binding by PDR in ¹¹Li, the system although not being on resonance it is not far from it, in keeping with the fact $\epsilon_{p_{1/2}} - \epsilon_{s_{1/2}} \approx 0.3$ MeV and $\hbar\omega_{PDR} \lesssim 1$ MeV, and that independent particle motion emerges from the same properties of the force from which collective modes emerge. In other words the ¹⁰Li inverted parity system is poised to acquire a permanent dipole moment or, almost equivalent, to display a large amplitude, dipole mode at very low energy as well as a collective $B(E1)$ to the halo ground state, of the order of a single-particle unit $B_W(E1)$. The PDR (see Fig. 4.C.1, see also Fig. 2.10.1) with centroid about $\lesssim 1$ MeV, 8% of the EWSR and screened from the GDR through the poor overlap between core and halo single-particle wavefunctions so as to be able to retain essentially all of its B_W , $E1$ -strength which can rightly be considered a new mode of excitation. In other words we are faced, already at the level of single-particle spectrum, with the possibility of a plastic large amplitude dipole mode, as it materializes in ¹¹Li. In this case, and making use of the relation

$$\frac{dn}{d\beta_L} = \frac{1}{4} \sqrt{\frac{2L+1}{3\pi}} A \quad (4.C.6)$$

defining the number of crossings n in terms of deformation¹⁵⁷, one obtains for $L = 0$ and $\beta_0 = 2.5$, $n \approx 2$. That is, one is in presence of a large amplitude plastic mode.

It is of notice that all of these processes takes place inside the halo neutron pair addition vibrational mode of the closed shell system ⁹₃Li₆(gs), and thus in terms of virtual states. On the other hand intervening the processes depicted in Fig. 3.A.1 with external fields, e.g. those associated with one-and two-particle transfer processes, can shed light on much of the physics which is at the basis of the exotic properties of ¹⁰Li and ¹¹Li (see e.g. Figs. 3.6.3 (I), 2.10.4 and 2.10.5. See also Fig. 7.1.3).

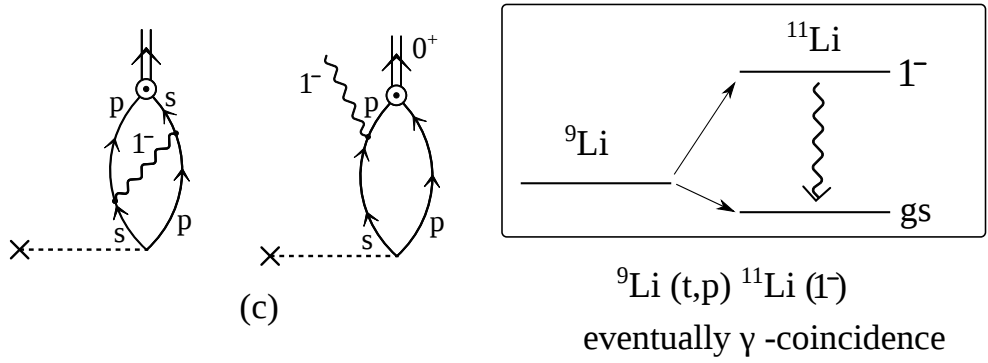
But let us now proceed one step at a time. A simple and economic picture of parity inversion in ¹⁰Li, and thus in ¹¹Li and, as a result of the mechanism at the basis of the existence of the dipole pygmy resonance in ¹¹Li was proposed in¹⁵⁸. To explain parity inversion use is made of the fact that, for large prolate quadrupole deformations ($\beta_2 \approx 0.6 - 0.7$), the $m = 1/2$ member of the $1d_{5/2}$ and $1p_{1/2}$ orbitals, i.e. [220 1/2] and [101 1/2] in the Nilsson labeling of levels ([$Nn_3\Lambda\Omega$]), cross. This is in keeping with the fact that quadrupole distortion changes the energy of single-particle states; those having orbits lying in a plane containing the poles become, in

¹⁵⁵ Broglia et al. (1987).

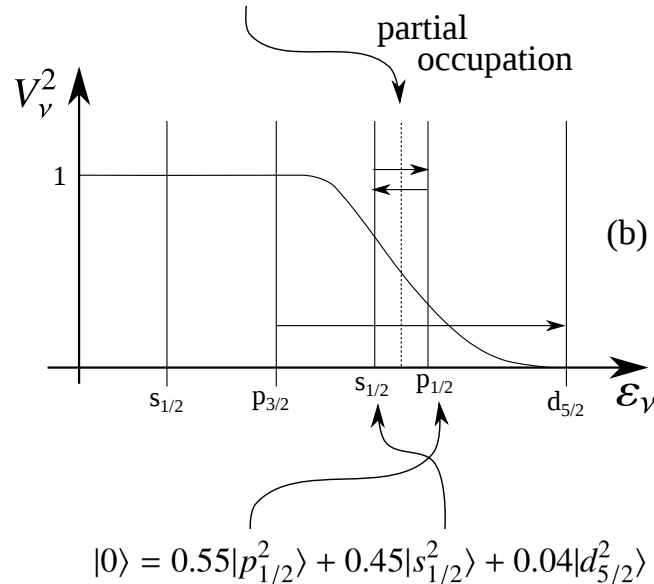
¹⁵⁶ See e.g. Born (1969), App. XL p. 471.

¹⁵⁷ Brink and Broglia (2005), Eq. (7.35) and refs. therein.

¹⁵⁸ Hamamoto and Shimoura (2007).



$$|0\rangle_v = |0\rangle + 0.7|(p_{1/2}, s_{1/2})_{1^-} \otimes 1^-; 0\rangle + 0.1|(s_{1/2}, d_{5/2})_{2^+} \otimes 2^+; 0\rangle$$



$$|1^-, \text{pygmy}\rangle = \alpha \Gamma_{\text{pygmy}}^\dagger |\text{halo}\rangle + \beta \Gamma_{\text{GDR}}^\dagger |\text{core}\rangle$$

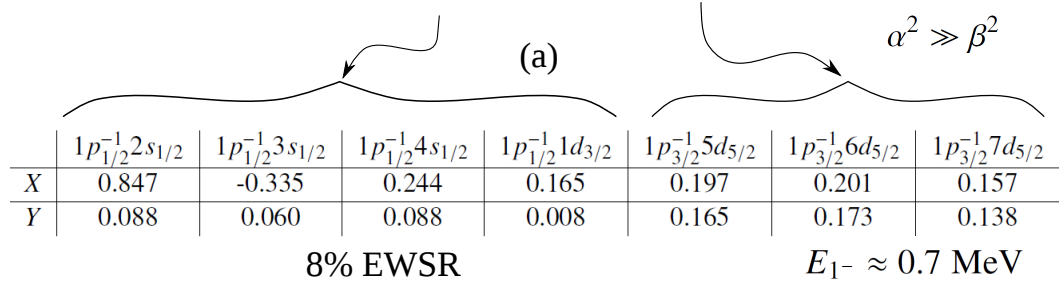


Figure 4.C.1: Schematic representation of (a) the QRPA calculation of the PDR of ^{11}Li and associated results: namely X and Y amplitudes divided, for didactical purposes, into low-lying (pygmy) and high lying (PDR) $p - h$ excitations. It is of notice that throughout the odd $p_{3/2}$ proton state is not shown being treated as a spectator, although the corresponding couplings are properly taken into account in the actual microscopic calculations (Barranco et al. (2001)). (b) Schematic representation of the connection between occupation numbers and NFT wavefunction describing the two halo neutrons. (c) Gedanken eksperiment ($^9\text{Li}(t, p)^{11}\text{Li}(\text{PDR})$) to probe the PDR wavefunction.

the case of prolate deformations, lower in energy, while those lying preferentially in a plane perpendicular to the symmetry axis, increase their energy. Now, for such value of deformation parity inversion is observed between the resonant $1/2^-$ (≈ 0.5 MeV) and the virtual $1/2^+$ (≈ 0.2 MeV) states of ^{10}Li ($p_{1/2}$ and $2_{1/2}$ states). Thus, the energy difference of 0.3 MeV is not very different from the value of 0.6-0.7 MeV of the PDR centroid. In any case, adjusting β_2 to the appropriate value this centroid energy is within reach.

Furthermore, the fact that the observed $\approx 8\%$ of the EWSR below ≈ 5 MeV for the PDR corresponds to about $1B_W(E1)$ for a single particle transition, provides another confirmation of the attractiveness of the model.

On the other hand, because the radius is affected by deformation, one can posit that the above model predicts $R = R_0(1 + \frac{\beta_2}{\sqrt{5}} \sqrt{\frac{5}{4\pi}}) = 2.7 \text{ fm} \times 1.2 \text{ fm} \approx 3.2 \text{ fm}$ ($\beta_2 \approx 0.7$), in disagreement with the experimental finding.

Now, static models (including also the group theoretical models like that provided by SU_3) imply that single-particle states are either occupied or empty. Experimentally, this does not seem the case in the reaction $^9\text{Li}(d, p)^{10}\text{Li}$, although one can argue that the situation is different in the case of the single-particle states in ^{11}Li .

Finally the fact that the dipole resonance observed in a (d, d') experiment¹⁵⁹ at $E_x \leq 1$ MeV and width 0.5 MeV displays a single peak testifies against the presence of a static quadrupole deformation¹⁶⁰.

Let us now go back to the calculation of the giant dipole pygmy resonance based on the ground state of ^{11}Li . To do so, one needs to know the occupation factors of the $s_{1/2}$ and $p_{1/2}$ states (Fig. 4.C.1). This has been done microscopically making use of the diagonalization of the NFT diagrams taking into account self-energy and induced interaction (vertex renormalization processes) leading to¹⁶¹

$$|\tilde{0}\rangle = |\tilde{0}\rangle + 0.71|(p_{1/2}, s_{1/2})_{1^-} \otimes 1^-; 0\rangle + 0.1|(s_{1/2}, d_{5/2})_{2^+} \otimes 2^+; 0\rangle, \quad (4.C.7)$$

and

$$|\tilde{0}\rangle = 0.45|s_{1/2}^2\rangle + 0.55|p_{1/2}^2\rangle + 0.04|d_{5/2}^2\rangle. \quad (4.C.8)$$

In Eq. (4.C.7), the state $|1^-\rangle$ and $|2^+\rangle$ stand for the pygmy dipole resonance, and for the low-lying collective quadrupole vibration of ^9Li , respectively. To calculate the microscopic structure of the state $|1^-\rangle$ (both wavefunction and transition density and consequently the particle-vibration coupling vertex) one needs to calculate $|\tilde{0}\rangle$. But to do so one needs to know the same $|1^-\rangle$ state, the vibrational mode which exchanged between the two neutrons of the halo provides most of its glue to the ^9Li core. From here, the symbiotic character of the $|\tilde{0}^+\rangle$ and $|1^-\rangle$ states.

¹⁵⁹Kanungo et al. (2015).

¹⁶⁰See e.g. Bohr and Mottelson (1975).

¹⁶¹Barranco et al. (2001).

Appendix 4.D Pairing spatial correlation: simple estimate

Let us assume two equal nucleons above closed shell as the nuclear embodiment of Cooper's model. The two-particle wave function in configuration space can be written as,

$$\Psi(\mathbf{r}_1\sigma_1, \mathbf{r}_2\sigma_2) = \Psi_0(\mathbf{r}_1, \mathbf{r}_2)\chi_{S=0}(\sigma_1, \sigma_2) + [\Psi_1(\mathbf{r}_1, \mathbf{r}_2)\chi_{S=1}(\sigma_1\sigma_2)]_0, \quad (4.D.1)$$

where $\chi_{S=0}$ and $\chi_{S=1}$ are the singlet and triplet spin wavefunctions, respectively.

In what follows we shall consider a pairing interaction acting on pairs of particles moving in time reversal states. Consequently we shall concentrate in the spin singlet radial component of (4.D.1). In the Tamm–Dancoff approximation (in keeping with Cooper ansatz) one can write

$$\Psi_0(\mathbf{r}_1, \mathbf{r}_2) = \sum_{nn'lj} X_{nn'lj} R_{nl}(r_1) R_{n'l}(r_2) \sqrt{\frac{2j+1}{2(2l+1)}} [Y_l(\hat{r}_1) Y_l(\hat{r}_2)]_0. \quad (4.D.2)$$

This wave function can be rewritten as

$$\begin{aligned} \Psi_0(\mathbf{r}_1, \mathbf{r}_2) &= \Psi_0(|\mathbf{r}_1|, |\mathbf{r}_2|, \theta) \\ &= \sum_{n'n'lj} X_{n'n'lj} R_{nl}(r_1) R_{n'l}(r_2) \sqrt{\frac{2j+1}{2}} \frac{1}{4\pi} P_l(\cos \theta), \end{aligned} \quad (4.D.3)$$

where $\theta = \widehat{r_1 r_2}$. A convenient way to display two-particle correlation is by plotting $|\Psi_0(|\mathbf{r}_1|, |\mathbf{r}_2|, \theta)|^2$ in the $x - z$ plane.

In the case of pure configurations $a \equiv nlj$,

$$\Psi_0(|\mathbf{r}_1|, |\mathbf{r}_2|, \theta) = R_{nl}(r_1) R_{nl}(r_2) \sqrt{\frac{2j+1}{2}} \frac{1}{4\pi} P_l(\cos \theta). \quad (4.D.4)$$

In keeping with the fact that the specific probe of pairing correlation is two-nucleon transfer, a phenomenon which takes place mainly, although not only, on the nuclear surface, we shall set $r_1 = r_2 = R_0$, and use the empirical relation

$$R_{nl}(R_0) = \left(\frac{1.4}{R_0^3} \right)^{1/2}, \quad (4.D.5)$$

Thus

$$\Psi_0(R_0, R_0, \theta) = \left(\frac{1.4}{R_0^3} \right) \sqrt{\frac{2j+1}{2}} \frac{1}{4\pi} P_l(\cos \theta). \quad (4.D.6)$$

and

$$|\Psi_0(R_0, R_0, \theta)|^2 \sim |P_l(\cos \theta)|^2. \quad (4.D.7)$$

It is seen that the two particles have the same probability to be on top of each other ($\theta = 0^\circ$; $P_l(1) = 1$), or on opposite sides of the nucleus ($\theta = 180^\circ$; $P_l(-1) = (-1)^l$). Taking into account the actual radial dependence of $R_{nl}^2(r_1)$ for $r_1 = R_0$, the width of the two probability peaks is found to be ≈ 2 fm i.e. $d \approx \left(\frac{4\pi}{3}R^3/A\right)^{1/3}$.

Let us now consider the general expression (4.D.3), and assume, aside from $n = n'$, that the two nucleons are allowed to correlate in a phase space composed of N single-particle levels, and that all amplitudes are equal,

$$X \approx \frac{1}{\sqrt{N}}. \quad (4.D.8)$$

Thus

$$\Psi_0(R_0, R_0, \theta) = \left(\frac{1.4}{R_0^3}\right) \frac{1}{\sqrt{N}} \frac{1}{4\pi} \sqrt{\frac{2j+1}{2}} \sum_l P_l(\cos \theta), \quad (4.D.9)$$

where again (4.D.5) have been used. One can then write

$$|\Psi_0(R_0, R_0, \theta)|^2 \sim \left| \sum_l P_l(\cos \theta) \right|^2. \quad (4.D.10)$$

Assuming the closed shell nucleus to be ^{208}Pb and the N single-particle levels the neutron valence orbitals $2g_{9/2}, 1i_{11/2}, 1j_{15/2}, 3d_{5/2}, 4s_{1/2}, 2g_{7/2}$ and $3d_{3/2}$, one obtains

$$\frac{|\Psi_0(R_0, R_0, \theta = 0^\circ)|^2}{|\Psi_0(R_0, R_0, \theta = 180^\circ)|^2} \approx \left(\frac{7}{5}\right)^2 \approx 2, \quad (4.D.11)$$

in keeping with the fact that there is only a single state of opposite parity (intruder $j_{15/2}$).

Making use of an extended basis, containing a similar amount of positive and negative natural parity states, that is taking into account a large number of major shells ($\pi = (-1)^N, N$ principal quantum number), one can reduce in a consistent fashion the value of¹⁶² $|\Psi_0(R_0, R_0, \theta = 180^\circ)|^2$. This of course materializes already within the basis of valence states in e.g. ^{11}Li , in keeping with the fact that in this case $s_{1/2}$ and $p_{1/2}$ play a similar role.

Summing up, the above results have something to do with the Cooper pair problem, but much more with the peculiarities of spatial quantization associated with the nuclear self-bound many-body system. That is, the nuclear Cooper pair phenomenon is to be expressed under the influence of a very strong external field which imposes not only confinement, but also spatial quantization with strong spin orbit effects resulting, among other things, in intruder states and thus parity mixing.

¹⁶²Ferreira et al. (1984).

Appendix 4.E Coherent state

The BCS ground state can be written as¹⁶³,

$$\begin{aligned} |BCS(\phi)\rangle_{\mathcal{K}} &= \prod_{\nu>0} \left(U_{\nu} + V_{\nu} a_{\nu}^{\dagger} a_{\bar{\nu}}^{\dagger} \right) |0\rangle = \prod_{\nu>0} U_{\nu} \left(1 + \frac{V_{\nu}}{U_{\nu}} a_{\nu}^{\dagger} a_{\bar{\nu}}^{\dagger} \right) |0\rangle \\ &= \left(\prod_{\nu>0} U_{\nu} \right) \left(\prod_{\nu>0} \left(1 + c_{\nu} P^{\dagger} \right) \right) |0\rangle, \end{aligned} \quad (4.E.1)$$

where

$$c_{\nu} = \frac{V_{\nu}}{U_{\nu}} \quad \text{and} \quad P^{\dagger} = a_{\nu}^{\dagger} a_{\bar{\nu}}^{\dagger}. \quad (4.E.2)$$

In what follows, we worked out a couple of simple examples:

a) $\nu=1,2$ (two pairs),

$$\begin{aligned} \prod_{\nu>0} \left(1 + c_{\nu} P^{\dagger} \right) &= \left(1 + c_1 P_1^{\dagger} \right) \left(1 + c_2 P_2^{\dagger} \right) = 1 + c_1 P_1^{\dagger} + c_2 P_2^{\dagger} \\ &+ c_1 c_2 P_1^{\dagger} P_2^{\dagger} = 1 + \sum_{\nu>0} c_{\nu} P_{\nu}^{\dagger} + \frac{1}{2!} \left(\sum_{\nu>0} c_{\nu} P_{\nu}^{\dagger} \right)^2, \end{aligned} \quad (4.E.3)$$

where use has been made of

$$\left(c_1 P_1^{\dagger} + c_2 P_2^{\dagger} \right)^2 = 2 c_1 c_2 P_1^{\dagger} P_2^{\dagger}, \quad (4.E.4)$$

in keeping with the fact that

$$\left(P_1^{\dagger} \right)^2 = \left(P_2^{\dagger} \right)^2 = 0, \quad [P_i^{\dagger}, P_j^{\dagger}] = 0. \quad (4.E.5)$$

b) $\nu=1,2,3$ (three pairs):

$$\begin{aligned} \prod_{\nu>0} \left(1 + c_{\nu} P^{\dagger} \right) &= \left(1 + c_3 P_3^{\dagger} \right) \left(1 + c_2 P_2^{\dagger} \right) \left(1 + c_1 P_1^{\dagger} \right) \\ &= \left(1 + c_3 P_3^{\dagger} \right) \left(1 + c_1 P_1^{\dagger} + c_2 P_2^{\dagger} + c_1 c_2 P_1^{\dagger} P_2^{\dagger} \right) \\ &= 1 + \left(c_1 P_1^{\dagger} + c_2 P_2^{\dagger} + c_3 P_3^{\dagger} \right) + \left(c_1 c_2 P_1^{\dagger} P_2^{\dagger} + c_1 c_3 P_1^{\dagger} P_3^{\dagger} + c_2 c_3 P_2^{\dagger} P_3^{\dagger} \right) \\ &+ c_1 c_2 c_3 P_1^{\dagger} P_2^{\dagger} P_3^{\dagger} = 1 + \sum_{\nu>0} c_{\nu} P_{\nu}^{\dagger} + \frac{1}{2!} \left(\sum_{\nu>0} c_{\nu} P_{\nu}^{\dagger} \right)^2 + \frac{1}{3!} \left(\sum_{\nu>0} c_{\nu} P_{\nu}^{\dagger} \right)^3 \end{aligned} \quad (4.E.6)$$

where use has been made of the relations (4.E.5) and of,

$$\begin{aligned} [(a+b+c)(a+b+c)] &= ab + ac + ba + bc + ca + cb = 2ab + 2ac + 2bc, \\ a^2 &= b^2 = c^2 = 0, \end{aligned}$$

¹⁶³See e.g. Potel et al. (2013b), and references therein.

together with

$$(a + b + c)[(a + b + c)(a + b + c)] = 2abc + 2bac + 2cab = 6abc. \quad (4.E.7)$$

Thus,

$$\left(\sum_{\nu>0} c_\nu P_\nu^\dagger \right)^3 = 6c_1 c_2 c_3 P_1^\dagger P_2^\dagger P_3^\dagger = 3! c_1 c_2 c_3 P_1^\dagger P_2^\dagger P_3^\dagger \quad (4.E.8)$$

Making use of

$$e^x = 1 + x + \frac{x^2}{2!} + \frac{x^3}{3!} + \dots, \quad (4.E.9)$$

one can write

$$\begin{aligned} |BCS(\phi)\rangle_{\mathcal{K}} &= \left(\prod_{\nu>0} U_\nu \right) \left\{ 1 + \frac{1}{1!} \left(\sum_{\nu>0} c_\nu P_\nu^\dagger \right) + \frac{1}{2!} \left(\sum_{\nu>0} c_\nu P_\nu^\dagger \right)^2 + \frac{1}{3!} \left(\sum_{\nu>0} c_\nu P_\nu^\dagger \right)^3 + \dots \right\} |0\rangle \\ &= \left(\prod_{\nu>0} U'_\nu \right) \left\{ 1 + \frac{e^{-2i\phi}}{1!} \left(\sum_{\nu>0} c'_\nu P_\nu^\dagger \right) + \frac{e^{-4i\phi}}{2!} \left(\sum_{\nu>0} c'_\nu P_\nu^\dagger \right)^2 + \frac{e^{-6i\phi}}{3!} \left(\sum_{\nu>0} c'_\nu P_\nu^\dagger \right)^3 + \dots \right\} |0\rangle \end{aligned} \quad (4.E.10)$$

where

$$c_\nu = e^{-2i\phi} c'_\nu, \quad c'_\nu = V'_\nu / U'_\nu. \quad (4.E.11)$$

Thus,

$$|BCS(\phi)\rangle_{\mathcal{K}} = \left(\prod_{\nu>0} U_\nu \right) \exp \left(\sum_{\nu>0} c_\nu P_\nu^\dagger \right) |0\rangle = \left(\prod_{\nu>0} U'_\nu \right) \sum_{N \text{ even}} \frac{e^{-iN\phi}}{(N/2)!} \left(\sum_{\nu>0} c'_\nu P_\nu^\dagger \right)^{N/2} |0\rangle \quad (4.E.12)$$

(see Eq. (4.8.27)) and

$$\begin{aligned} |N_0\rangle &= \int d\phi e^{iN_0\phi} |BCS(\phi)\rangle_{\mathcal{K}} \\ &= \left(\prod_{\nu>0} U'_\nu \right) \sum_{N \text{ even}} \int d\phi e^{iN_0\phi} \frac{e^{-iN\phi}}{(N/2)!} \left(\sum_{\nu>0} c'_\nu P_\nu^\dagger \right)^{N/2} |0\rangle \sim \left(\sum_{\nu>0} c'_\nu P_\nu^\dagger \right)^{N_0/2} |0\rangle \end{aligned} \quad (4.E.13)$$

is the member with N_0 particles of the pairing rotational band, while

$$\left(\sum_{\nu>0} c'_\nu P_\nu^\dagger \right) |0\rangle \quad (4.E.14)$$

is the Cooper pair state. Because $U'_\nu \rightarrow 0$ for $\epsilon \ll \epsilon_F$, (4.E.14) is to be interpreted to be valid for values of ϵ_ν close to ϵ_F . Making use of the single j -shell model

$$V' = \sqrt{\frac{N}{2\Omega}}, \quad U' = \sqrt{1 - \frac{N}{2\Omega}}, \quad (4.E.15)$$

and

$$\frac{V'}{U'} = \sqrt{\frac{N}{2\Omega - N}} \approx U'V' \left(1 + O\left(\frac{N}{2\Omega}\right)\right) \quad (4.E.16)$$

for a number of particles considerably smaller than the full degeneracy of the single-particle subspace in which nucleons can correlate, that is for $N \ll 2\Omega$. Consequently, one can write

$$|\tilde{0}\rangle \approx \frac{1}{\sqrt{N}} \sum_{\nu>0} (\alpha'_0)_\nu P_\nu^\dagger |0\rangle, \quad (4.E.17)$$

where

$$(\alpha'_0)_\nu = \langle BCS | P_\nu^\dagger | BCS \rangle = U'_\nu V'_\nu, \quad (4.E.18)$$

and

$$N = \sum_{\nu>0} (\alpha'_0)_\nu^2. \quad (4.E.19)$$

Chapter 5

One-particle transfer

In what follows we present a derivation of the one-particle transfer differential cross section within the framework of the distorted wave Born approximation (DWBA)¹.

The structure input in the calculations are, as a rule, single-particle states dressed, within the formalism of nuclear field theory², through the coupling with the variety of collective, (quasi-) bosonic vibrations, leading to modified formfactors³. With the help of these modified formfactors⁴, and of global optical potentials, one can calculate the absolute differential cross sections, quantities which can be directly compared with the experimental findings.

In this way one avoids to introduce, let alone use spectroscopic factors, quantities which are rather elusive to calculate consistently⁵. This is in keeping with the fact that as a nucleon moves through the nucleus it feels the presence of the other nucleons whose configurations change as time proceeds. It takes time for this information to be feed back on the nucleon. This renders the average potential nonlocal in time⁶. A time-dependent operator can always be transformed into an energy-dependent operator, implying an ω -dependence of the properties which are usually adscribed to particles like (effective) mass, charge, etc. Furthermore, due to Pauli principle, the average potential is also non local in space. Consequently,

¹See Tobocman (1961), Austern (1963), Jackson (1970) Satchler (1980); Broglia and Winther (2004), Satchler (1983), Austern (1970), Glendenning (2004), Thompson and Nunes (2009), and refs. therein.

²Bès et al. (1974); Bès and Broglia (1975); Bohr and Mottelson (1975); Bès et al. (1976a,b,c); Mottelson (1976); Broglia et al. (1976); Bès and Broglia (1977); Bortignon et al. (1977); Bès and Kurchan (1990).

³It is of notice that single-particle modified formfactors (see e.g. Fig. 5.2.4) have their counterpart in the renormalised transition densities (App. 2.A) and in the modified two-nucleon transfer formfactors (Chapter 6, Eqs. (6.2.48; simultaneous), (6.2.134–6.2.136; successive) and (6.2.154–6.2.156; non-orthogonality) associated with inelastic and with pair transfer reactions (see Broglia et al. (1973); Potel et al. (2013a) and refs. therein), respectively.

⁴See also Vaagen et al. (1979); Bang et al. (1980); Hamamoto (1970) and refs. therein. See also Barranco et al. (2017) and Sect. 5.2.2.

⁵Duguet and Hagen (2012); Jenning (2011); Dickhoff and Barbieri (2004); Dickhoff and Van Neck (2005), and refs. therein. See also Feshbach (1992); Tamura (1974); Tamura et al. (1980).

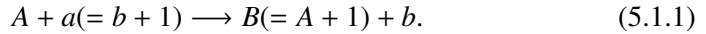
⁶See Mahaux et al. (1985) and references therein, see also App. 5.H.

one is forced to deal with nucleons which carry around a cloud of (quasi) bosons, aside from exchanging its position with that of the other nucleons, and thus with renormalized energies, single-particle amplitude content and wavefunctions (form-factors) which eventually result in a dynamical shell model. It is of notice that the above mentioned phenomena are not only found in nuclear physics, but are universal within the framework of many-body systems as well as of field theories like quantum electrodynamics (QED). In fact, a basic result of such theories is that nothing is really free⁷. A textbook example of this fact is provided by the Lamb shift, resulting from the dressing of the hydrogen's atom electron, as a result of the exchange of this electron with those participating in the spontaneous, virtual excitation (zero point fluctuations (ZPF)) of the QED vacuum (see Apps 5.C, 5.D and 5.E; see also Fig. 7.2.1). Within this context, in Section 5.2.1 we provide examples of one-particle transfer processes between nuclei lying along the stability valley, populating strongly renormalized quasiparticle states.

In Section 7.2 we again take up the subject, but in this case for the exotic, halo nucleus ^{11}Be , in connection with the $N = 6$ magic number related with the phenomenon of parity inversion. Furthermore, in Sect. 5.2.2 we discuss the close relation existing, in particular in halo exotic nuclei, between $\beta = 0, \pm 1, \pm 2$ modes.

5.1 General derivation

We now proceed to derive the transition amplitude for the reaction (Fig. 5.1.1).



For a simplified version –no recoil plus plane wave limit (see also Sect. 5.1.2)– we refer to App 5.F, while for an alternative derivation within the framework of one-particle knock-out reactions we refer to App 5.G.

Let us assume that the nucleon bound initially to the core b is in a single-particle state with orbital and total angular momentum l_i and j_i respectively, and that the nucleon in the final state (bound to core A) is in the l_f, j_f state. The total spin and magnetic quantum numbers of nuclei A, a, B, b are $\{J_A, M_A\}, \{J_a, M_a\}, \{J_B, M_B\}, \{J_b, M_b\}$ respectively. Denoting ξ_A and ξ_b the intrinsic coordinates of the wavefunctions describing the structure of nuclei A and b , and \mathbf{r}_{An} and \mathbf{r}_{bn} the relative coordinates of the transferred nucleon with respect to the CM of nuclei A and b respectively, one can write the “intrinsic” wavefunctions of the colliding nuclei A, a as

$$\begin{aligned} &\phi_{M_A}^{J_A}(\xi_A), \\ &\Psi(\xi_b, \mathbf{r}_{b1}) = \sum_{m_i} \langle J_b \ j_i \ M_b \ m_i | J_a \ M_a \rangle \phi_{M_b}^{J_b}(\xi_b) \psi_{m_i}^{j_i}(\mathbf{r}_{bn}, \sigma), \end{aligned} \quad (5.1.2)$$

⁷Feynman (1975).

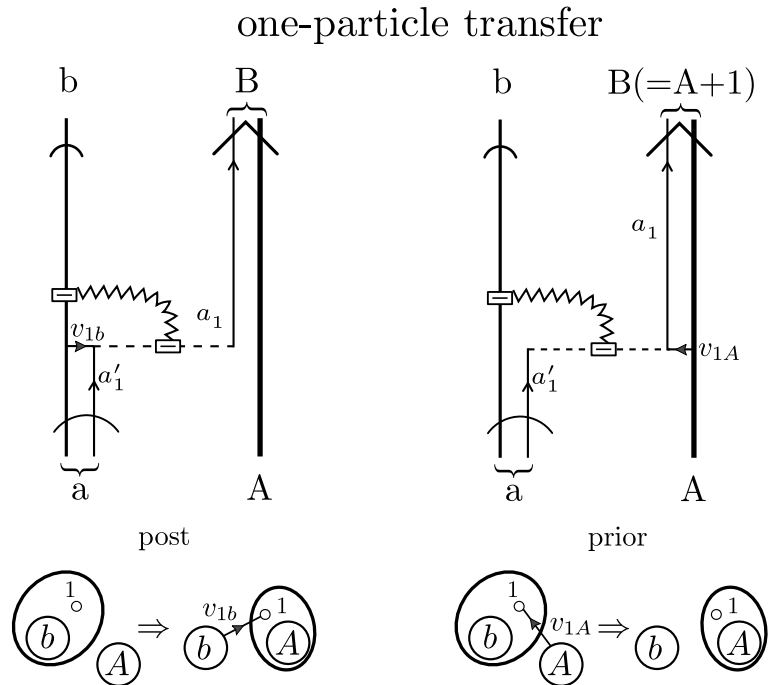


Figure 5.1.1: NFT graphical representation of the one-particle transfer reaction $a (= b + 1) + A \rightarrow b + B (= A + 1)$ (see Figs. 6.C.1 and 6.C.2 and the last paragraph before Sect. 6.C.1 of App. 6.C). The time arrow is assumed to point upwards. The quantum numbers characterizing the states in which the transferred nucleon moves in projectile and target are denoted a'_1 and a_1 respectively. The interaction inducing the nucleon to be transferred can act either in the entrance channel $((a, A); v_{1A}$, prior representation) or in the exit channel $((b, B); v_{1b}$, post representation), in keeping with energy conservation. In the transfer process, the nucleon changes orbital at the same time that a change in the mass partition takes place. The corresponding relative motion mismatch is known as the recoil process, and is represented by a jagged curve (this is the recoil elementary mode, mode which couples to the particle degrees of freedom through a Galilean transformation operator). The recoil mode provides information on the evolution of r_{1A} (r_{1b}). In other words, on the coupling between structure and reaction (relative motion) degrees of freedom.

while the “intrinsic” wavefunctions describing the structure of nuclei B and b are

$$\begin{aligned} \phi_{M_b}^{J_b}(\xi_b), \\ \Psi(\xi_A, \mathbf{r}_{A1}) = \sum_{m_f} \langle J_A \ j_f \ M_A \ m_f | J_B \ M_B \rangle \phi_{M_A}^{J_A}(\xi_A) \psi_{m_f}^{j_f}(\mathbf{r}_{An}, \sigma). \end{aligned} \quad (5.1.3)$$

For an unpolarized incident beam (sum over M_A, M_a and divide by $(2J_A + 1), (2J_a + 1)$), and assuming that one does not detect the final polarization (sum over M_B, M_b), the differential cross section in the DWBA can be written as

$$\begin{aligned} \frac{d\sigma}{d\Omega} = \frac{k_f}{k_i} \frac{\mu_i \mu_f}{4\pi^2 \hbar^4} \frac{1}{(2J_A + 1)(2J_a + 1)} \\ \times \sum_{\substack{M_A, M_a \\ M_B, M_b}} \left| \sum_{m_i, m_f} \langle J_b \ j_i \ M_b \ m_i | J_a \ M_a \rangle \langle J_A \ j_f \ M_A \ m_f | J_B \ M_B \rangle T_{m_i, m_f} \right|^2, \end{aligned} \quad (5.1.4)$$

where k_i and k_f are the relative motion linear momentum in both initial and final channels (flux), while μ_i and μ_f are the corresponding relative masses. The two quantities within $\langle \rangle$ brackets are Clebsch–Gordan coefficients taking care of angular momentum conservation⁸.

The transition amplitude T_{m_i, m_f} is

$$T_{m_i, m_f} = \sum_{\sigma} \int d\mathbf{r}_f d\mathbf{r}_{bn} \chi^{(-)*}(\mathbf{r}_f) \psi_{m_f}^{j_f*}(\mathbf{r}_{An}, \sigma) V(r_{bn}) \psi_{m_i}^{j_i}(\mathbf{r}_{bn}, \sigma) \chi^{(+)}(\mathbf{r}_i), \quad (5.1.5)$$

where

$$\psi_{m_i}^{j_i}(\mathbf{r}_{An}, \sigma) = u_{j_i}(r_{bn}) \left[Y^{l_i}(\hat{r}_i) \chi(\sigma) \right]_{j_i m_i}, \quad (5.1.6)$$

is the single-particle wavefunction describing the motion of the nucleon to be transferred, when in the initial state, u , Y and χ being the radial, angular (spherical harmonics) and spin components. Similarly for $\psi_{m_f}^{j_f}$. The distorted waves describing the relative motion of the incoming projectile and of the target nucleus and of the outgoing system and the residual nucleus are,

$$\chi^{(+)}(\mathbf{k}_i, \mathbf{r}_i) = \frac{4\pi}{k_i r_i} \sum_l i^l e^{i\sigma_i^l} g_l(\hat{r}_i) \left[Y^l(\hat{r}_i) Y^l(\hat{k}_i) \right]_0^0, \quad (5.1.7)$$

and

$$\chi^{(-)*}(\mathbf{k}_f, \mathbf{r}_f) = \frac{4\pi}{k_f r_f} \sum_l i^{-l} e^{i\sigma_f^l} f_l(\hat{r}_f) \left[Y^l(\hat{r}_f) Y^l(\hat{k}_f) \right]_0^0, \quad (5.1.8)$$

respectively. In the above relations f and g are, respectively, the solutions of the radial Schrödinger equation describing the relative motion associated with the corresponding optical potential (“elastic” scattering) in entrance and exit channel. Let

⁸Brink and Satchler (1968) and Edmonds (1960), also Bohr and Mottelson (1969).

us now discuss the angular components involved in the reaction process, starting with the relation

$$\begin{aligned} \left[Y^l(\hat{r}_f) Y^l(\hat{k}_f) \right]_0^0 \left[Y^{l'}(\hat{r}_i) Y^{l'}(\hat{k}_i) \right]_0^0 &= \sum_K ((ll)_0(l'l')_0 | (ll')_K (ll')_K)_0 \\ &\times \left\{ \left[Y^l(\hat{r}_f) Y^{l'}(\hat{r}_i) \right]^K \left[Y^l(\hat{k}_f) Y^{l'}(\hat{k}_i) \right]^K \right\}_0^0. \end{aligned} \quad (5.1.9)$$

The 9*j*-symbol can be explicitly evaluated to give,

$$((ll)_0(l'l')_0 | (ll')_K (ll')_K)_0 = \sqrt{\frac{2K+1}{(2l+1)(2l'+1)}}, \quad (5.1.10)$$

while the coupled expression can be written as

$$\begin{aligned} \left\{ \left[Y^l(\hat{r}_f) Y^{l'}(\hat{r}_i) \right]^K \left[Y^l(\hat{k}_f) Y^{l'}(\hat{k}_i) \right]^K \right\}_0^0 &= \sum_M \langle K \ K \ M \ -M | 0 \ 0 \rangle \left[Y^l(\hat{r}_f) Y^{l'}(\hat{r}_i) \right]_M^K \\ &\times \left[Y^l(\hat{k}_f) Y^{l'}(\hat{k}_i) \right]_{-M}^K = \sum_M \frac{(-1)^{K+M}}{\sqrt{2K+1}} \left[Y^l(\hat{r}_f) Y^{l'}(\hat{r}_i) \right]_M^K \left[Y^l(\hat{k}_f) Y^{l'}(\hat{k}_i) \right]_{-M}^K. \end{aligned} \quad (5.1.11)$$

Thus,

$$\begin{aligned} \left[Y^l(\hat{r}_f) Y^l(\hat{k}_f) \right]_0^0 \left[Y^{l'}(\hat{r}_i) Y^{l'}(\hat{k}_i) \right]_0^0 &= \sum_{K,M} \frac{(-1)^{K+M}}{\sqrt{(2l+1)(2l'+1)}} \left[Y^l(\hat{r}_f) Y^{l'}(\hat{r}_i) \right]_M^K \left[Y^l(\hat{k}_f) Y^{l'}(\hat{k}_i) \right]_{-M}^K. \end{aligned} \quad (5.1.12)$$

For the angular integral to be different from zero, the integrand must be coupled to zero angular momentum (scalar). Noting that the only variables over which one integrates in the above expression are \hat{r}_i, \hat{r}_f , we have to couple the remaining functions of the angular variables, namely the wavefunctions $\psi_{m_f}^{j_f*}(\mathbf{r}_{An}, \sigma) = (-1)^{j_f-m_f} \psi_{-m_f}^{j_f}(\mathbf{r}_{An}, -\sigma)$ and $\psi_{m_i}^{j_i}(\mathbf{r}_{bn}, \sigma)$ to angular momentum K , as well as to fulfill $M = m_f - m_i$. Let us then consider

$$\begin{aligned} (-1)^{j_f-m_f} \psi_{-m_f}^{j_f}(\mathbf{r}_{An}, -\sigma) \psi_{m_i}^{j_i}(\mathbf{r}_{bn}, \sigma) &= (-1)^{j_f-m_f} u_{j_f}(r_{An}) u_{j_i}(r_{bn}) \\ &\times \sum_P \langle j_f \ j_i \ -m_f \ m_i | P \ m_i - m_f \rangle \left\{ \left[Y^{l_f}(\hat{r}_{An}) \chi^{1/2}(-\sigma) \right]^{j_f} \left[Y^{l_i}(\hat{r}_{bn}) \chi^{1/2}(\sigma) \right]^{j_i} \right\}_{m_i-m_f}^P. \end{aligned} \quad (5.1.13)$$

Recoupling the spherical harmonics to angular momentum K and the spinors to $S = 0$, only one term survives the angular integral in (5.1.5), namely

$$\begin{aligned} & (-1)^{j_f - m_f} u_{j_f}(r_{An}) u_{j_i}(r_{bn}) ((l_f \frac{1}{2})_{j_f} (l_i \frac{1}{2})_{j_i} | (l_f l_i)_K (\frac{1}{2} \frac{1}{2})_0)_K \\ & \times \langle j_f \ j_i \ -m_f \ m_i | K \ m_i - m_f \rangle [Y^{l_f}(\hat{r}_{An}) Y^{l_i}(\hat{r}_{bn})]_{m_i - m_f}^K [\chi(-\sigma) \chi(\sigma)]_0^0. \quad (5.1.14) \end{aligned}$$

Making use of the fact that the sum over spins yields a factor $-\sqrt{2}$, and in keeping with the fact that $M = m_f - m_i$, one obtains,

$$\begin{aligned} T_{m_i, m_f} = & (-1)^{j_f - m_f} \frac{-16 \sqrt{2} \pi^2}{k_f k_i} \sum_{l'} i'^{-l} e^{\sigma'_f + \sigma'_i} \sum_K ((l_f \frac{1}{2})_{j_f} (l_i \frac{1}{2})_{j_i} | (l_f l_i)_K (\frac{1}{2} \frac{1}{2})_0)_K \\ & \times \langle j_f \ j_i \ -m_f \ m_i | K \ m_i - m_f \rangle [Y^l(\hat{k}_f) Y^{l'}(\hat{k}_i)]_{m_i - m_f}^K \int d\mathbf{r}_f d\mathbf{r}_{bn} \frac{f_l(r_f) g_{l'}(r_i)}{r_f r_i} \\ & \times u_{j_f}(r_{An}) u_{j_i}(r_{bn}) V(r_{bn}) (-1)^{K+m_f-m_i} [Y^l(\hat{r}_f) Y^{l'}(\hat{r}_i)]_{m_f - m_i}^K [Y^{l_f}(\hat{r}_{An}) Y^{l_i}(\hat{r}_{bn})]_{m_i - m_f}^K. \quad (5.1.15) \end{aligned}$$

Again, the only term of the expression

$$\begin{aligned} & (-1)^{K+m_f-m_i} [Y^l(\hat{r}_f) Y^{l'}(\hat{r}_i)]_{m_f - m_i}^K [Y^{l_f}(\hat{r}_{An}) Y^{l_i}(\hat{r}_{bn})]_{m_i - m_f}^K = \\ & (-1)^{K+m_f-m_i} \sum_P \langle K \ K \ m_f - m_i \ m_i - m_f | P \ 0 \rangle \left\{ [Y^l(\hat{r}_f) Y^{l'}(\hat{r}_i)]^K [Y^{l_f}(\hat{r}_{An}) Y^{l_i}(\hat{r}_{bn})]^K \right\}_0^P \end{aligned}$$

which survives after angular integration is the one with $P = 0$, that is,

$$\begin{aligned} & \frac{1}{\sqrt{(2K+1)}} \left\{ [Y^l(\hat{r}_f) Y^{l'}(\hat{r}_i)]^K [Y^{l_f}(\hat{r}_{An}) Y^{l_i}(\hat{r}_{bn})]^K \right\}_0^0 \\ & = \frac{1}{\sqrt{(2K+1)}} \sum_{M_K} \langle K \ K \ M_K \ -M_K | 0 \ 0 \rangle [Y^l(\hat{r}_f) Y^{l'}(\hat{r}_i)]_{M_K}^K \\ & \times [Y^{l_f}(\hat{r}_{An}) Y^{l_i}(\hat{r}_{bn})]_{-M_K}^K = \frac{1}{\sqrt{(2K+1)}} \sum_{M_K} \frac{(-1)^{K+M_K}}{\sqrt{(2K+1)}} [Y^l(\hat{r}_f) Y^{l'}(\hat{r}_i)]_{M_K}^K \\ & \times [Y^{l_f}(\hat{r}_{An}) Y^{l_i}(\hat{r}_{bn})]_{-M_K}^K \\ & = \frac{1}{2K+1} \sum_{M_K} (-1)^{K+M_K} [Y^l(\hat{r}_f) Y^{l'}(\hat{r}_i)]_{M_K}^K [Y^{l_f}(\hat{r}_{An}) Y^{l_i}(\hat{r}_{bn})]_{-M_K}^K, \end{aligned}$$

an expression which is spherically symmetric. One can evaluate it for a particular configuration, for example setting $\hat{r}_f = \hat{z}$ and the center of mass A, b, n in the $x - z$ plane (see Fig. 5.1.2). Once the orientation in space of this “standard” configuration is specified (through, for example, a rotation $0 \leq \alpha \leq 2\pi$ around \hat{z} , a rotation $0 \leq \beta \leq \pi$ around the new x axis and a rotation $0 \leq \gamma \leq 2\pi$ around

\hat{r}_{bB}), the only remaining angular coordinate is θ , while the integral over the other three angles yields $8\pi^2$. Setting $\hat{r}_f = \hat{z}$ one obtains

$$\left[Y^l(\hat{r}_f) Y^{l'}(\hat{r}_i) \right]_{M_K}^K = \langle l' l' 0 M_K | K M_K \rangle \sqrt{\frac{2l+1}{4\pi}} Y_{M_K}^{l'}(\hat{r}_i). \quad (5.1.16)$$

Because of $M = m_i - m_f$, and $m = m_f$, $T_{m_i, m_f} \equiv T_{m, M}$ where

$$\begin{aligned} T_{m, M} &= (-1)^{j_f - m} \frac{-64\sqrt{2}\pi^{7/2}}{k_f k_i} \sum_{ll'} i'^{-l} e^{\sigma_f^l + \sigma_i^{l'}} \sqrt{2l+1} \sum_K \frac{(-1)^K}{2K+1} ((l_f \frac{1}{2})_{j_f} (l_i \frac{1}{2})_{j_i} | (l_f l_i)_K (\frac{1}{2} \frac{1}{2})_0)_K \\ &\times \langle j_f j_i - m M + m | K M \rangle \left[Y^l(\hat{k}_f) Y^{l'}(\hat{k}_i) \right]_M^K \int d\mathbf{r}_f d\mathbf{r}_{bn} \frac{f_l(r_f) g_{l'}(r_i)}{r_f r_i} \\ &\times u_{j_f}(r_{An}) u_{j_i}(r_{bn}) V(r_{bn}) \sum_{M_K} (-1)^{M_K} \langle l' l' 0 M_K | K M_K \rangle \left[Y^{l_f}(\hat{r}_{An}) Y^{l_i}(\hat{r}_{bn}) \right]_{-M_K}^K Y_{M_K}^{l'}(\hat{r}_i). \end{aligned} \quad (5.1.17)$$

We now turn our attention to the sum

$$\sum_{\substack{M_A, M_a \\ M_B, M_b}} \left| \sum_{m, M} \langle J_b j_i M_b m | J_a M_a \rangle \langle J_A j_f M_A M | J_B M_B \rangle T_{m, M} \right|^2, \quad (5.1.18)$$

appearing in the expression for the differential cross section (5.1.4). For any given value m', M' of m, M , the sum will be

$$\begin{aligned} &\sum_{M_a, M_b} \left| \langle J_b j_i M_b m' | J_a M_a \rangle \right|^2 \sum_{M_A, M_B} \left| \langle J_A j_f M_A M' | J_B M_B \rangle \right|^2 \left| T_{m', M'} \right|^2 \\ &= \frac{(2J_a + 1)(2J_B + 1)}{(2j_i + 1)(2j_f + 1)} \sum_{M_a, M_b} \left| \langle J_b J_a M_b - M_a | j_i m' \rangle \right|^2 \\ &\times \sum_{M_A, M_B} \left| \langle J_A J_B M_A - M_B | j_f M' \rangle \right|^2 \left| T_{m', M'} \right|^2, \end{aligned} \quad (5.1.19)$$

by virtue of the symmetry property of Clebsch–Gordan coefficients

$$\langle J_b j_i M_b m | J_a M_a \rangle = (-1)^{J_b - M_b} \sqrt{\frac{(2J_a + 1)}{(2j_i + 1)}} \langle J_b J_a M_b - M_a | j_i m \rangle. \quad (5.1.20)$$

The sum over the Clebsch–Gordan coefficients in (5.1.19) is equal to 1, so (5.1.18) becomes

$$\frac{(2J_a + 1)(2J_B + 1)}{(2j_i + 1)(2j_f + 1)} \sum_{m, M} \left| T_{m, M} \right|^2, \quad (5.1.21)$$

and the differential cross section can be written as,

$$\frac{d\sigma}{d\Omega} = \frac{k_f}{k_i} \frac{\mu_i \mu_f}{4\pi^2 \hbar^4} \frac{(2J_B + 1)}{(2j_i + 1)(2j_f + 1)(2J_A + 1)} \sum_{m, M} \left| T_{m, M} \right|^2. \quad (5.1.22)$$

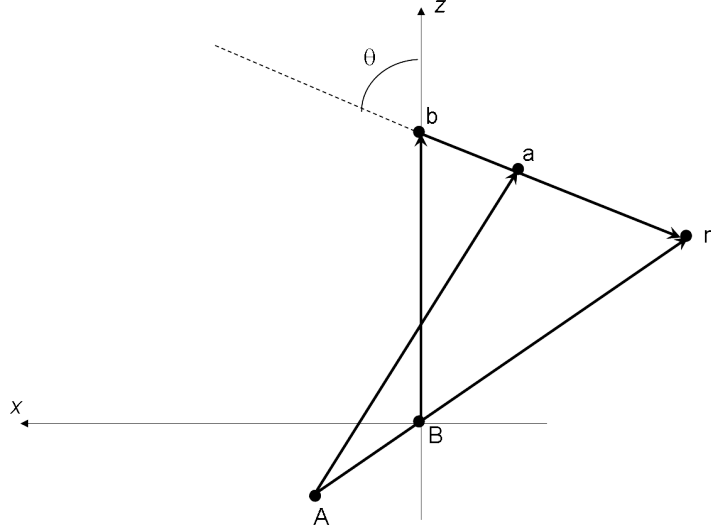


Figure 5.1.2: Coordinate system in the “standard” configuration. Note that $\mathbf{r}_f \equiv \mathbf{r}_{Bb}$, and $\mathbf{r}_i \equiv \mathbf{r}_{Aa}$.

where

$$T_{m,M} = \sum_{Kll'} (-1)^{-m} \langle j_f j_i - m | M + m | K M \rangle \left[Y^l(\hat{k}_f) Y^{l'}(\hat{k}_i) \right]_M^K t_{ll'}^K. \quad (5.1.23)$$

Orienting \hat{k}_i along the incident z -direction leads to,

$$\left[Y^l(\hat{k}_f) Y^{l'}(\hat{k}_i) \right]_M^K = \langle l l' M 0 | K M \rangle \sqrt{\frac{2l'+1}{4\pi}} Y_M^l(\hat{k}_f), \quad (5.1.24)$$

and

$$T_{m,M} = \sum_{Kll'} (-1)^{-m} \langle l l' M 0 | K M \rangle \langle j_f j_i - m | M + m | K M \rangle Y_M^l(\hat{k}_f) t_{ll'}^K, \quad (5.1.25)$$

with

$$\begin{aligned} t_{ll'}^K &= (-1)^{K+j_f} \frac{-32\sqrt{2}\pi^3}{k_f k_i} i^{l'-l} e^{\sigma_f^l + \sigma_i^{l'}} \frac{\sqrt{(2l+1)(2l'+1)}}{2K+1} ((l_f \frac{1}{2})_{j_f} (l_i \frac{1}{2})_{j_i} | (l_f l_i)_K (\frac{1}{2} \frac{1}{2})_0)_K \\ &\times \int dr_f dr_{bn} d\theta r_{bn}^2 \sin \theta r_f \frac{f_l(r_f) g_{l'}(r_i)}{r_i} u_{j_f}(r_{An}) u_{j_i}(r_{bn}) V(r_{bn}) \\ &\times \sum_{M_K} (-1)^{M_K} \langle l l' 0 | M_K | K M_K \rangle \left[Y^{l_f}(\hat{r}_{An}) Y^{l_i}(\hat{r}_{bn}) \right]_{-M_K}^K Y_{M_K}^{l'}(\hat{r}_i). \end{aligned} \quad (5.1.26)$$

5.1.1 Coordinates

To perform the integral in (5.1.26), one needs the expression of $r_i, r_{An}, \hat{r}_{An}, \hat{r}_{bn}, \hat{r}_i$ in term of the integration variables r_f, r_{bn}, θ . Because one is interested in evaluating these quantities in the particular configuration depicted in Fig. 5.1.2, one has

$$\mathbf{r}_f = r_f \hat{z}, \quad (5.1.27)$$

$$\mathbf{r}_{bn} = -r_{bn}(\sin \theta \hat{x} + \cos \theta \hat{z}), \quad (5.1.28)$$

$$\mathbf{r}_{Bn} = \mathbf{r}_f + \mathbf{r}_{bn} = -r_{bn} \sin \theta \hat{x} + (r_f - r_{bn} \cos \theta) \hat{z}. \quad (5.1.29)$$

One can then write

$$\mathbf{r}_{An} = \frac{A+1}{A} \mathbf{r}_{Bn} = -\frac{A+1}{A} r_{bn} \sin \theta \hat{x} + \frac{A+1}{A} (r_f - r_{bn} \cos \theta) \hat{z}, \quad (5.1.30)$$

$$\mathbf{r}_{an} = \frac{b}{b+1} \mathbf{r}_{bn} = -\frac{b}{b+1} r_{bn} (\sin \theta \hat{x} + \cos \theta \hat{z}), \quad (5.1.31)$$

and

$$\mathbf{r}_i = \mathbf{r}_{An} - \mathbf{r}_{an} = -\frac{2A+1}{(A+1)A} r_{bn} \sin \theta \hat{x} + \left(\frac{A+1}{A} r_f - \frac{2A+1}{(A+1)A} r_{bn} \cos \theta \right) \hat{z}, \quad (5.1.32)$$

where A, b are the number of nucleons of nuclei A and b respectively.

5.1.2 Zero-range approximation

In the zero range approximation,

$$\int dr_{bn} r_{bn}^2 u_{j_i}(r_{bn}) V(r_{bn}) = D_0; \quad u_{j_i}(r_{bn}) V(r_{bn}) = \delta(r_{bn})/r_{bn}^2. \quad (5.1.33)$$

It can be shown (see Fig. 5.1.2) that for $r_{bn} = 0$

$$\mathbf{r}_{An} = \frac{m_A + 1}{m_A} \mathbf{r}_f, \quad \mathbf{r}_i = \frac{m_A + 1}{m_A} \mathbf{r}_f. \quad (5.1.34)$$

One then obtains

$$t_{ll'}^K = \frac{-16\sqrt{2}\pi^2}{k_f k_i} (-1)^K \frac{D_0}{\alpha} i'^{-l} e^{\sigma_f^l + \sigma_i'^l} \frac{\sqrt{(2l+1)(2l'+1)(2l_i+1)(2l_f+1)}}{2K+1} ((l_f \frac{1}{2})_{j_f} (l_i \frac{1}{2})_{j_i} | (l_f l_i)_K (\frac{1}{2} \frac{1}{2})_0)_K \\ \times \langle l' l' 0 0 | K 0 \rangle \langle l_f l_i 0 0 | K 0 \rangle \int dr_f f_l(r_f) g_{l'}(\alpha r_f) u_{j_f}(\alpha r_f), \quad (5.1.35)$$

with

$$\alpha = \frac{A+1}{A}. \quad (5.1.36)$$

5.2 Examples and Applications

In the calculation of absolute reaction cross section two elements melt together: reaction and structure. In the case of weakly coupled probes like, as a rule, direct one-particle transfer processes are, the first element can be further divided into two essentially separated components: elastic scattering (optical potentials), and transfer amplitudes connecting entrance and exit channels. In other words, the habitat of DWBA.

5.2.1 $^{120}\text{Sn}(p, d)^{119}\text{Sn}$ and $^{120}\text{Sn}(d, p)^{121}\text{Sn}$ reactions.

The calculation of the structure properties of the Sn-isotopes probed through (d, p) and (p, d) reactions, were carried out making use of an effective Skyrme interaction⁹, SLy4, to determine the mean field (HFB) and the collective modes (QRPA), and a $v_{14}(^1S_0)(\equiv v_p^{bare})$ Argonne pairing interaction¹⁰ Hartree-Fock-Bogoliubov (HFB) results provide the bare quasiparticle spectrum, while QRPA a realization of density ($J^\pi = 2^+, 3^-, 4^+, 5^-$) and spin ($2^\pm, 3^\pm, 4^\pm, 5^\pm$) modes.

Taking into account renormalization processes (self-energy, vertex corrections) in terms of the PVC mechanism, the dressed particles and the induced pairing interaction v_p^{ind} were calculated. Adding it to v_p^{bare} , the total pairing interaction v_p^{eff} was determined. It is found that v_p^{bare} and v_p^{ind} contribute about equally to the state dependent pairing gap.

Making use of the above input, the lowest order NFT renormalizing diagrams (self-energy and vertex correction) were propagated to infinite order making use of Nambu-Gorkov equation¹¹ In Fig. 5.2.1 (a), the absolute differential cross section associated with the population of the low-lying state $|^{119}\text{Sn}(7/2^+; 788\text{keV})\rangle$ in the one-particle pick-up process $^{120}\text{Sn}(p, d)^{119}\text{Sn}$ and worked out with the help of the software ONE¹², of global optical parameters¹³ and of NFT spectroscopic amplitudes (Table 5.2.1), is compared with the experimental data.

Similar calculations (ONE, NFT spectroscopic amplitudes (Table 5.2.2) and global optical parameters), have been carried for the reaction $^{120}\text{Sn}(d, p)^{121}\text{Sn} (j^\pi; E_x)$ in connection with the population of the $|3/2^+; \text{gs}\rangle$ and $|11/2^-; E_x \approx 0 \text{ MeV}\rangle$ states. In the stripping experiment¹⁴ the ground state and the $11/2^-$ state were not resolved in energy. This is the reason why theory and experiment are only compared to the data for the summed $l = 2 + 5$ differential cross section (cf. Fig. 5.2.2 (a)), the separate theoretical predictions been displayed in Figs. 5.2.2 (b) and (c).

Let us now turn to the most fragmented low-lying quasiparticle state around ^{120}Sn , namely that associated with the $d_{5/2}$ orbital¹⁵ As shown in Fig. 5.2.3 five

⁹Chabanat et al. (1997).

¹⁰Wiringa et al. (1984).

¹¹For details see Idini et al. (2015).

¹²Potel (2012a).

¹³Dickey et al. (1982).

¹⁴Bechara and Dietzsch (1975).

¹⁵cf. Idini (2013), Idini et al. (2015).

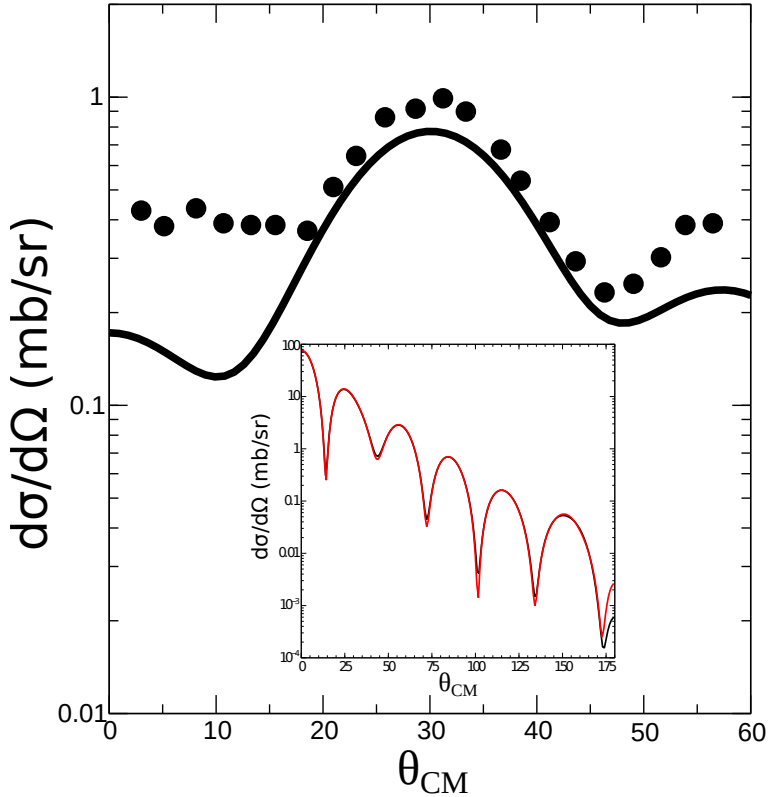


Figure 5.2.1: The absolute differential cross section $^{120}\text{Sn}(p,d)^{119}\text{Sn}(j^\pi)$ associated with the state $j^\pi = 7/2^+$. The theoretical prediction (continuous curve) is displayed in comparison with the experimental data (solid dots, Dickey et al. (1982)). The corresponding integrated cross sections are 5.0 and 5.2 ± 0.6 mb respectively. In the inset, and for the sake of accuracy control, the absolute differential cross sections associated with the reaction $^{124}\text{Sn}(p,d)^{123}\text{Sn}(\text{gs})$ calculated making use of the softwares ONE (red) and FRESCO (black (Thompson (1988))) are displayed.

	$^{120}\text{Sn}(p,d)^{119}\text{Sn}$		
	Exp.	Th.	
$j^\pi(lj)$	$Ex(\text{MeV})$	E'_x	\tilde{V}
$7/2^+(g7/2)$	0.788	0.37	0.81

Table 5.2.1: Experimental (E_x) and theoretical (E'_x) quasiparticle excitation energies and theoretical effective occupation probability $\tilde{V}^2 (= 0.66)$ associated with valence orbital $g_{7/2}$ (Idini et al. (2015)).

low-lying $5/2^+$ states have been populated in the reaction $^{120}\text{Sn}(p, d)^{119}\text{Sn}$ with a summed cross section¹⁶ $\sum_{i=1}^5 \sigma(2^\circ - 25^\circ) \approx 8 \text{ mb} \pm 2 \text{ mb}$ while four are theoretically predicted with $\sum_{i=1}^4 \sigma(2^\circ - 25^\circ) = 6.2 \text{ mb}$. Within the present context, namely that of probing the single-particle content of an elementary excitation (coupling to doorway states¹⁷), the study of the $5/2^+$ quasiparticle strength is a rather trying situation, providing a measure of the limitations encountered in such studies.

Analysis of the type presented above allows one to posit that structure and reactions are but just two aspects of the same physics. If one adds to this picture the fact that the optical potential –that is, the energy and momentum dependent nuclear dielectric function describing the medium where direct nuclear chemistry takes place– can be calculated microscopically¹⁸ in terms of the same elements entering structure calculations (i.e. spectroscopic amplitudes, renormalized single-particle wavefunctions and transition densities and thus effective formfactors), the structure-reaction circle closes itself. Allowing halo nuclei to be part of the daily nuclear structure paradigm, the equivalence between structure and reactions becomes even stronger, in keeping with the central role the continuum plays in the structure of these nuclei.

It seems then fair to state that the importance of the coupled channels approach to reactions¹⁹ is not so much, or at least not only, that it is able to handle situations like for example one-particle transfer to members of a quadrupole rotational band, alas at the expenses of including effects to all orders which can be treated in lowest one²⁰, but that it reminds us how intimately connected probed and probe are in nuclei.

On the other hand, for most of the situations dealt with in the present monograph, it is transparent the power, also to reflect the physics, of the approach based in perturbative DWBA (e.g. 1st order for one-nucleon transfer and 2nd for Cooper pair tunneling), coupled with NFT elementary modes of nuclear excitation. To which extent a FRESCO like software built on a NFT basis will ever be attempted is an open question. Note in any case the important attempts made at incorporating so called core excitations within the FRESCO framework²¹.

We conclude this section by recalling the fact that the dressing of single particles with pairing vibrations plays also a central role in the structure properties of nuclei²².

¹⁶Dickey et al. (1982).

¹⁷Feshbach (1958), Rawitscher (1987), Bortignon and Broglia (1981), Bertsch et al. (1983).

¹⁸Mahaux et al. (1985), Fernández-García et al. (2010a), Fernández-García et al. (2010b), Broglia et al. (1981), Pollarolo et al. (1983), Broglia and Winther (2004), Dickhoff and Van Neck (2005), Jennings (2011), Montanari et al. (2014), Rotureau et al. (2017).

¹⁹Thompson (1988), Thompson (2013), Tamura et al. (1970), Asciutto and Glendenning (1969), Asciutto and Glendenning (1970), Asciutto et al. (1971), Asciutto and Sørensen (1972); cf. also Fernández-García et al. (2010a), Fernández-García et al. (2010b).

²⁰Within this context see e.g. the couple channel Born approximation treatment of $^{208}\text{Pb}(t, p)^{210}\text{Pb}(3^-)$ carried out in Flynn et al. (1972b).

²¹Fernández-García et al. (2010a), Fernández-García et al. (2010b).

²²Barranco et al. (1987), Bès et al. (1988), Baroni et al. (2004).

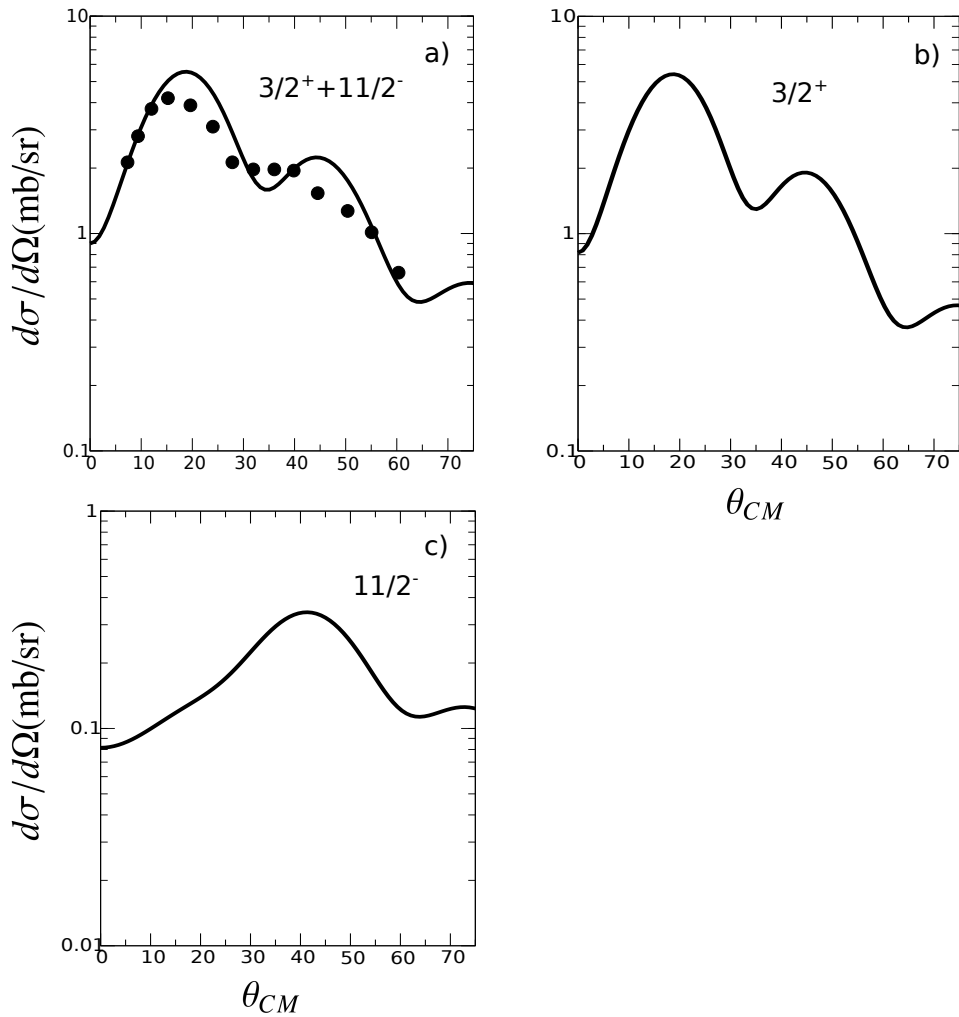


Figure 5.2.2: The theoretical absolute differential cross section (continuous curve) associated with the reaction $^{120}\text{Sn}(d, p)^{121}\text{Sn}$ and populating the low-lying states $3/2^+$ and $11/2^-$ are shown in b) and c), while the summed differential cross section is displayed in a) in comparison with the data (Bechara and Dietzsch (1975)).

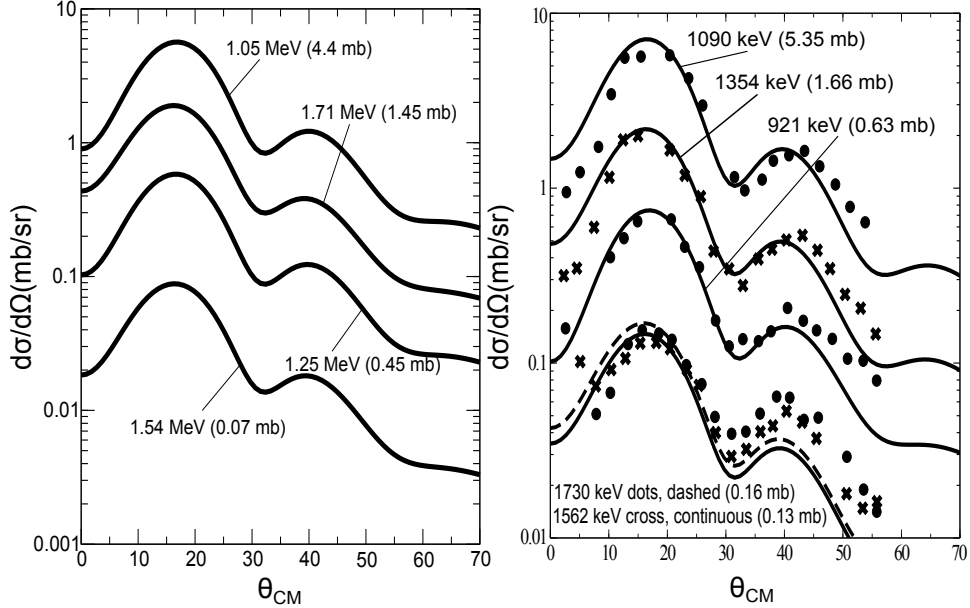


Figure 5.2.3: $^{120}\text{Sn}(p, d)^{119}\text{Sn}(5/2^+)$ absolute experimental cross sections (solid dots, Dickey et al. (1982)), together with the DWBA fit carried out in the analysis of the data (right panel) in comparison with the finite range, full recoil DWBA calculations carried out with the same global optical potentials making use of NFT structure inputs as explained in the text (after Idini et al. (2015)) and of the software ONE (Potel (2012a)); see also App. 7.C.

		$^{120}\text{Sn}(p, d)^{119}\text{Sn}(j)$	$^{120}\text{Sn}(d, p)^{121}\text{Sn}(j)$
j	\tilde{E}_j (MeV)	\bar{V}_j^2	\bar{U}_j^2
$h_{11/2}$	1.54	(1.34) 0.25 (0.28)	(1.25) 0.55 (0.49)
$d_{3/2}$	1.27	(1.27) 0.35 (0.41)	(1.25) 0.41 (0.44)

Table 5.2.2: The properties $(\tilde{E}_j, \tilde{V}_j^2, \tilde{U}_j^2)$ of the main peaks of the $h_{11/2}$ and $d_{3/2}$ strength functions of ^{120}Sn calculated taking into account the interweaving of fermionic and bosonic elementary modes of excitation within NFT and of their consequences in both the normal and abnormal densities (cf. Idini et al. (2012); Idini (2013) see also Idini et al. (2015) where the spin degree of freedom, solely repulsive component of the pairing channel (1S_0) in finite nuclei, has also been included). In parenthesis in the third and fourth columns, experimental (energies) and empirical (single-particle strength) data are given (Bechara and Dietzsch (1975), Dickey et al. (1982)).

5.2.2 Dressing of single-particle states: parity inversion in ^{11}Li

The $N = 6$ isotope of ^9Li displays quite ordinary structural properties and can, at first glance, be thought of a two-neutron hole system in the $N = 8$ closed shell. That this is not the case emerges clearly from the fact that ^{10}Li is not bound. In addition, the observation that the two lowest unoccupied states are the virtual ($1/2^+$) and the resonant ($1/2^-$) states²³, testify to the fact that, in the present case, $N = 6$ is a far better magic neutron number than $N = 8$. In addition, the observation that the unbound $s_{1/2}$ state lies lower than the unbound $p_{1/2}$ state, a phenomenon known in the literature as parity inversion (see Figs. 2.10.1 and 3.6.3), is in plain contradiction with static mean field theory. Dressing the (standard) mean field²⁴ single-particle states with vibrations of the ^9Li core in terms of polarization (effective mass-like) and correlation (vacuum zero point fluctuations (ZPF)) diagrams, similar to those associated with the (lowest order) Lamb shift Feynman diagrams, (cf. App 5.D), shifts the $s_{1/2}$ and $p_{1/2}$ mean field levels around. In particular the $p_{1/2}$ from a bound state ($\approx -1.2\text{ MeV}$) to a resonant state lying at $\approx 0.5\text{ MeV}$ (Pauli principle, vacuum ZPF process), the $s_{1/2}$ being lowered and becoming a virtual state ($\approx 0.2\text{ MeV}$) (cf. Fig. 3.6.3)²⁵. While ^{10}Li is not bound, adding a second dressed neutron and allowing them to exchange density vibrations of the core, as well as the pygmy dipole resonance²⁶ resulting from the sloshing back and forth of the outer neutrons against those of the core (^9Li), binds the Cooper pair to it. The system $^{11}_3\text{Li}_8$ displays a two-neutron separation energy $S_{2n} \approx 400\text{ keV}$.

The two-dimensional landscapes (surfaces) displayed in Figs. 3.6.3 (II) a) and b) attempt at describing the becoming of the neutron halo Cooper pair of ^{11}Li , from an uncorrelated $s_{1/2}^2(0)$ configuration to a correlated, (weakly) bound two-neutron state. It is of notice that the bare interaction (boxed inset in (II)), lowers the $s_{1/2}^2(0)$, as well as the $p_{1/2}^2(0)$ pure configurations, by only 100 keV, and thus it is not able, by itself, to bind the pair, nor to give rise to any significant mixing between these two configurations.

How can one check that correlation (CO) and polarization (PO) like processes as the ones shown in Figs. 3.6.3 (I) and 5.2.4 (cf. also Fig. 5.B.1) are the basic processes dressing the odd neutron of ^{10}Li , and thus the mechanism at the basis of parity inversion? The answer is, forcing these virtual processes to become real. In other words, act on the system with an external field so that certain off-the-energy shell states become on-the-energy shell. In fact, a reaction like $^1\text{H}(^{11}\text{Li}, ^{10}\text{Li})^2\text{H}$ can populate single-particle states in ^{10}Li (see Fig. 5.2.5), in particular the two lowest states of ^{10}Li , namely the virtual and the resonant $|s_{1/2}\rangle$ and $|p_{1/2}\rangle$ states respectively. The same can be of course done through the²⁷ reactions $^2\text{H}(^9\text{Li}, ^{10}\text{Li})^1\text{H}$

²³See however Cavallaro et al. (2017).

²⁴Saxon–Woods potential, cf. Bohr and Mottelson (1969) Eqs. (2–181)–(2–182).

²⁵Barranco et al. (2001); and refs. therein, Tanihata et al. (2013), Sanetullaev et al. (2016); see however Cavallaro et al. (2017).

²⁶Broglia et al. (2019a).

²⁷Orrigo and Lenske (2009) and Jeppesen et al. (2004); Cavallaro et al. (2017).

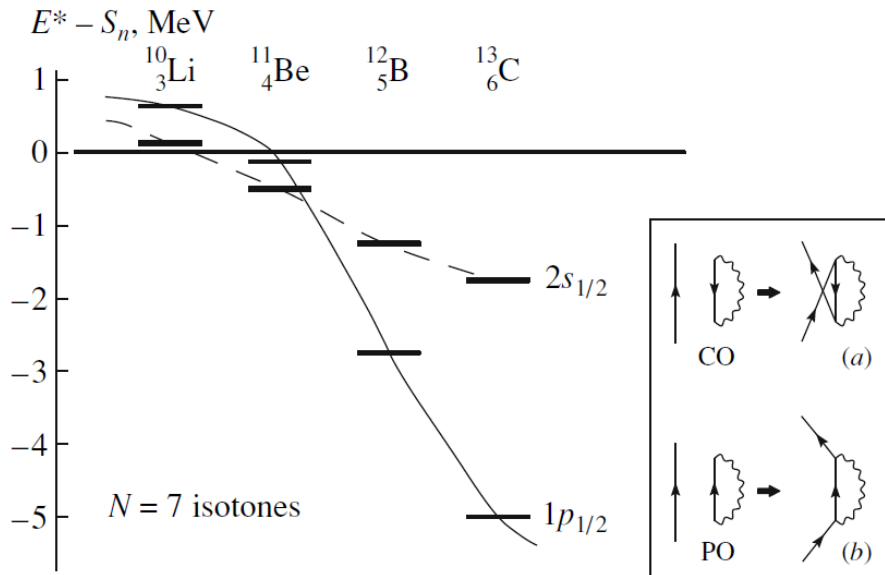


Figure 5.2.4: Single-particle states for $N = 7$ isotones around ^{11}Be associated with parity inversion. The thin horizontal lines represent the $1p_{1/2}$ single-particle state, while the thick ones the $2s_{1/2}$ orbital. In the case of ^{10}Li one reports the centroid of the virtual and of the resonant states. E^* stands for excitation energy and S_n is the neutron separation energy. In the case of ^{10}Li e.g. $S_n = 0$, while $E_{s_{1/2}}^* = 0.2$ MeV and $E_{p_{1/2}}^* = 0.5$ MeV (see however Cavallaro et al. (2017)). In the inset the correlation (CO) and polarization (PO) (virtual) contribution to the single-particle self-energy are shown. An arrowed line pointing upwards represents a particle moving in a level with energy $\epsilon_k > \epsilon_F$, a downwards pointing line represents a hole state $\epsilon_i < \epsilon_F$, while a wavy line stands for a ph-like vibrational state. Their contribution to the real (single-particle “legs” propagating to $\pm\infty$ times) processes dressing the $1p_{1/2}$ and $2s_{1/2}$ neutron states of ^{10}Li are (a) and (b), respectively. The phonon corresponds essentially only to the 2^+ vibration of the corresponding core (^9Li and ^{10}Be , respectively) and pushes, in the process (a), the orbital upwards (Pauli principle, Lamb–shift–like process) making the dressed $p_{1/2}$ orbital considerably less bound than what it was originally in the Woods–Saxon potential. In the case of the $2s_{1/2}$ orbital, it is mainly the process (b) which dresses the state making it almost bound (virtual state) as compared with the Woods–Saxon state. Within this context, it is of notice that in the binding of the two halo neutrons of ^{11}Li to the ^9Li core, it is essentially the pygmy resonance of ^{11}Li which provides the largest contribution, the coupling to the 2^+ vibration of the core ^9Li giving a small shift in energy (nonetheless, it is this weak component of the self energy which is responsible for the excitation, in the $^{11}\text{Li}(p,t)^9\text{Li}$ reaction, of the $1/2$, 2.69 MeV state). It is of notice that graphs (a) and (b) give rise to an effective mass known as the ω –mass. Associated with it are the $Z(\omega) = (m_\omega/m)^{-1}$ occupation factors (discontinuity at the Fermi energy). After Potel et al. (2014).

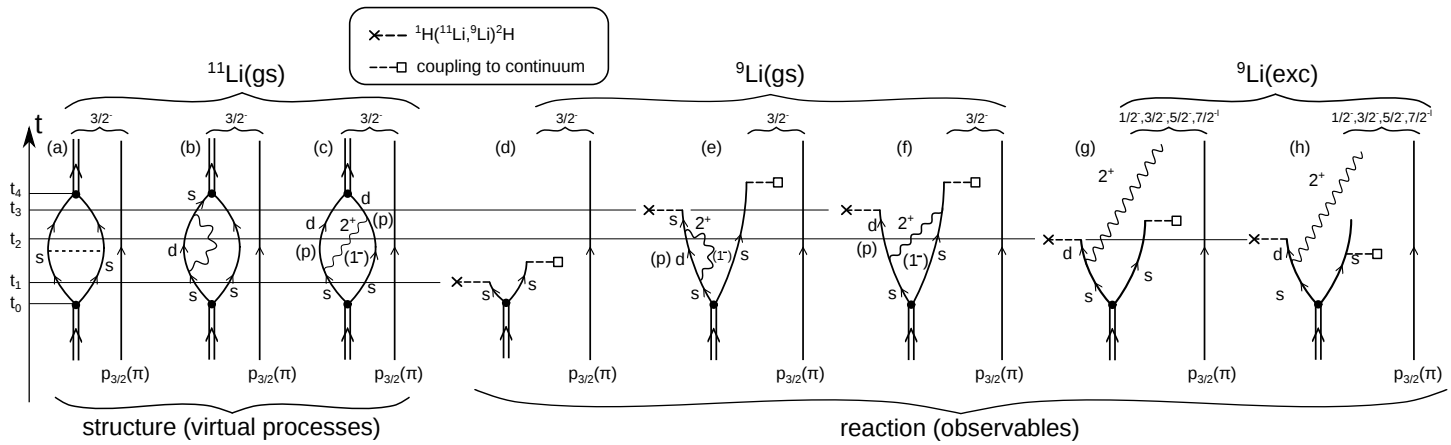


Figure 5.2.5: Nuclear Field Theory diagrams describing the basic, lowest order processes, by which the di-neutron halo binds to the ${}^9\text{Li}_6$ core to give rise to ${}^{11}\text{Li}$ ground state (**structure**), and those associated with a one-neutron pick-up process, e.g. ${}^1\text{H}({}^{11}\text{Li}, {}^{10}\text{Li})^2\text{H}$ (**reaction**). In this case, and for simplicity the mode associated with recoil (jagged line) is not shown (within this context see Fig. 2.10.2 (b)). The vibrational states of the core ${}^9\text{Li}$ are here represented by the quadrupole mode 2^+ , although in the calculations particle-hole modes with $\lambda^\pi = 3^-, 4^+$ and 5^- were also considered. The state (1^-) associated with the $s \rightarrow (p)$ single-particle states shown in (c) corresponds to the dipole pygmy resonance of ${}^{11}\text{Li}$ (see α -component in Eq. (7.1.1)). The contribution of this mode to the binding of the Cooper pair is overwhelming.

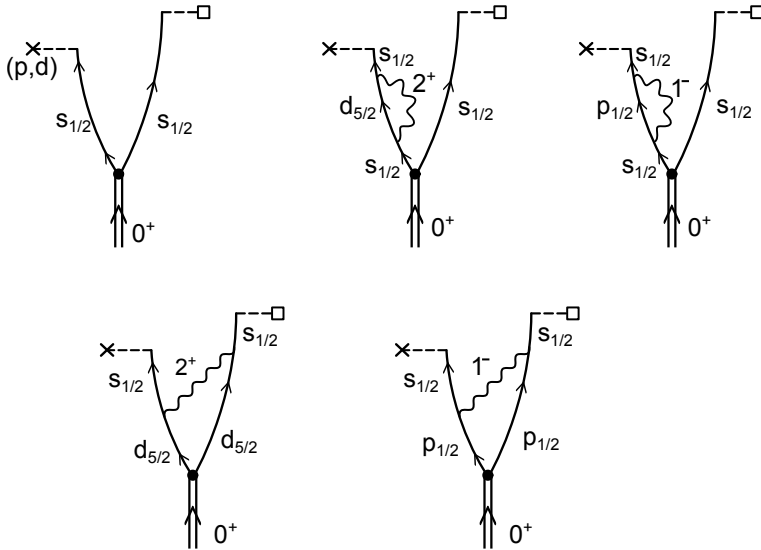


Figure 5.2.6: Lowest order, schematic NFT contributions, to the population of the $s_{1/2}$ lowest resonant $^{10}\text{Li}(1/2^+)$ through the pick-up reaction $^1\text{H}(^{11}\text{Li}, ^{10}\text{Li}(1/2^+))^2\text{H}$. Concerning the notation see Caption to Fig. 5.2.5. Concerning the recoil mode (jagged line) we refer to Fig. 2.10.2 (b).

and $^9\text{Li}(d, p)^{10}\text{Li}$. Being these states embedded in the continuum the system will eventually decay into both the ground and excited states of ^9Li .

Now, indirect information on this questions can also be obtained with the help of two-particle transfer processes, namely that associated with inverse kinematics (p, t) reaction²⁸ $^1\text{H}(^{11}\text{Li}, ^9\text{Li}(2.69\text{MeV}; 1/2^-))^3\text{H}$ populating the first excited state of ^9Li , thought to be the lowest member of the multiplet $2^+ \otimes p_{3/2}(\pi)$ (cf. Figs. 7.1.1–7.1.3 and 2.10.3). A price to pay for not using the specific probe for single-particle modes (one-particle transfer), is that of adding to the self-energy contributions in question those corresponding to vertex corrections (for details cf. App 5.E, Figs 5.E.1 and 5.E.2).

Within the present context, it is difficult if not impossible to talk about single-particle motion without also referring to collective vibrational states (cf. e.g. Fig. 3.6.3 (II)), or to talk about pair addition and pair subtraction modes, without at the same time talking about correlated particle-hole (e.g. density) vibrations and dressed quasiparticle motion, again concerning both structure and reactions.

Let us now return to the discussion of the one-particle transfer process $^1\text{H}(^{11}\text{Li}, ^{10}\text{Li})^2\text{H}$, that is the pickup of a neutron from the pair addition halo state $|^{11}\text{Li(gs)}\rangle$ (cf. Fig. 5.2.5). In keeping with the fact that ^{10}Li is not bound, such a reaction populates only transiently the virtual and resonant states of ^{10}Li and eventually, after the second neutron of the pair, spoliated of its dynamical glue, leaves the system by decaying into the continuum, a state in ^9Li is populated (see Figs.

²⁸Tanihata et al. (2008).

5.2.5 (d)–(f) and (g) and (h)). In drawing the different NFT diagrams time t is assumed to run upwards. External fields and the bare NN –interaction are assumed to act instantaneously, while the couplings to the phonon modes (wavy lines) lead to retarded (ω –dependent) effects. The halo Cooper pair (pair addition mode of the $N = 6$ closed shell system) carries angular momentum 0^+ and is represented by a double arrowed line, the odd proton (π) which occupies a $p_{3/2}$ state, is represented by a single arrowed line and is here treated as a spectator. The di-neutron system binds to the core through (a) the bare interaction (horizontal dashed line) acting between the two neutrons, each represented by a single arrowed line, and through the renormalizing processes associated with the coupling of the neutrons with vibrations; (b) effective mass processes associated with the quadrupole vibration of ${}^9\text{Li}$ (wavy line) renormalizing the energy of the $s_{1/2}$ continuum state (only one known) and leading to an almost bound (virtual) state (≈ 0.2 MeV) as well as of the p –state²⁹ and giving rise to a resonant state (≈ 0.5 MeV); (c) Vertex correction (induced pairing interaction) associated with the quadrupole vibration of ${}^9\text{Li}$ and with the pygmy dipole resonance of ${}^{11}\text{Li}$.

While the quadrupole vibration is essential for parity inversion (single-particle renormalization effect) it plays little role regarding vertex corrections (induced pairing interaction), the pygmy resonance of ${}^{11}\text{Li}$ playing the central role in binding the Cooper pair, as testified by components $\beta (= 0.1)$ and $\alpha (= 0.7)$ of $|{}^{11}\text{Li}(gs)\rangle$ (see Eq. (4.C.7)). Of course, the pygmy resonance does not contribute to parity inversion in ${}^{10}\text{Li}$, being an excitation of ${}^{11}\text{Li}$. Picking up a neutron from the halo pair addition mode of ${}^9\text{Li}$ (that is $|{}^{11}\text{Li}(gs)\rangle$), it obliterates this symbiotic pygmy resonant state. This is a peculiar example of the fact that not all virtual states can be forced to become real even with the proper external field. In particular not a mode resulting from a bootstrap mechanism. On the other hand, the absolute cross section associated with the reaction ${}^1\text{H}({}^{11}\text{Li}, {}^{10}\text{Li}(1/2^+)) {}^2\text{H}$ will depend on the variety of renormalization processes displayed³⁰ in Fig. 5.2.6.

Let us now return to Fig. 5.2.5 and discuss processes associated with the population of $|{}^{11}\text{Li}(gs)\rangle$. In (d) it is shown that intervening the process (a) at any time after t_0 and before t_4 with an external single-neutron pick-up field (cross followed by an horizontal dashed line), and processes (b) and (c) at $t_0 < t < t_1$, leads to the ground state of ${}^9\text{Li}$. This is in keeping with the fact that the second neutron will leave the system almost immediately, ${}^{10}\text{Li}$ not being stable; (e) same as above but in connection with process (b) and now after the nucleon has reabsorbed the quadrupole phonon and before t_4 , i.e. acting at $t_3 < t < t_4$ leads again to the population of the ${}^9\text{Li}$ ground state; (f) same as (e) but in this case the external field acts on the process (c). Let us now consider the one-nucleon pickup processes populating the $(2^+ \otimes p_{3/2}(\pi))_{J^\pi}, (J^\pi = 1/2^-, 3/2^-, 5/2^- \text{ and } 7/2^-)$ multiplet of ${}^9\text{Li}$, in particular the lowest $|1/2^-; 2.69 \text{ MeV}\rangle$ state. In this case the external field has

²⁹For this Lamb–shift–like process see Fig. 2.10.2, process taking place in the interval t_2 – t_5 .

³⁰It is of notice that the (simplified) notation used in the present Section in referring to the population of the virtual $1/2^+$ state of ${}^{10}\text{Li}$ is not correct. Because of the presence of the odd $p_{3/2}(\pi)$ proton, two states are associated with the $1/2^+$, namely $(\tilde{s}_{1/2}(\nu), p_{3/2}(\pi))_{1^+, 2^+}$ (See Ch. 7).

to act at a time \mathbf{t}_2 ($\mathbf{t}_1 < \mathbf{t}_2 < \mathbf{t}_3$) on either (b) or (c), in which case it leads to identical final states (see (g) and (h)). While the single contribution associated with mass renormalization process ((b)→(g)) and vertex corrections ((c)→(h)) cannot be distinguished experimentally, one can estimate the relative contribution to the corresponding absolute cross section making use of, microscopic wavefunctions³¹.

Before concluding the present section, and in connection with Figs. 5.2.5 (g,h) and 2.10.3 (b), it may be useful to remind us what, within the framework of quantum mechanics, one can learn from a reaction experiment. It is not “what is the state after the collision” but “how probable is a given effect of the collision”. Within this context let us quote: “The motion of particles follows probability laws, but the probability itself propagates according to the laws of causality”³².

Appendix 5.A Minimal requirements for a consistent mean field theory

In what follows the question of why, rigorously speaking, one cannot talk about single-particle motion, let alone spectroscopic factors, not even within the framework of mean field theory, is briefly touched upon (see also App. 5.H).

As can be seen from Fig. 5.A.1 the minimum requirements of selfconsistency to be imposed upon single-particle motion requires both non-locality in space (HF) and in time (TDHF)

$$i\hbar \frac{\partial \varphi_\nu}{\partial t} = -\frac{\hbar^2}{2m} \nabla^2 \varphi_\nu(x, t) + \int dx' dt' U(x - x', t - t') \varphi_\nu(x', t'), \quad (5.A.1)$$

and consequently also of collective vibrations and, consequently, from their interweaving to dressed single-particles (quasiparticles), let alone renormalized collective modes (cf. Fig. 5.C.3). Assuming for simplicity infinite nuclear matter (confined by a constant potential of depth V_0), and thus plane wave solutions, the

³¹Barranco et al. (2001).

³²Born (1926a). If there is a lesson to be learned from the above discussion is the fact that, in dealing with a specific feature of a quantal many-body system, e.g. single-particle motion in nuclei (structure) and one-particle transfer process (reaction), one can hardly avoid to talk about other elementary modes of excitation and reaction channels, respectively. Within the scenario of the chosen example, this is because a nucleon which, in first approximation is in a mean field stationary state, can actually be viewed as a fermion moving through a gas of ephemeral $2p - 2h$ composite virtual excitations, that is $(p - h) +$ density and/or $2h(2p) +$ pair addition (subtraction) modes, arising from vacuum (ground state) ZPF and giving rise to the nuclear vacuum (ω -dependent dielectric function). Because of Pauli principle (Pauli, 1947) the nucleon in question is forced to exchange role with the virtual, off-the-energy-shell nucleons, thus leading to CO processes (Fig. 5.B.1 (b)) and eventually, through time ordering, to PO ones (Fig. 5.B.1 (a)). Such processes, eventually carried out to higher orders of perturbation in the nucleon-vibration coupling, diagonalize the nuclear Hamiltonian. In this way, one takes care of the overcompleteness (non-orthogonality) and of Pauli violations of the basis made out of elementary modes of nuclear excitation. The results of the diagonalization are dressed (observable) modes, single-particle states in the present case, whose properties, e.g. absolute single-particle transfer cross sections, can be compared with the data without further ado.

above time-dependent Schrödinger equation leads to the quasiparticle dispersion relation

$$\hbar\omega = \frac{\hbar^2 k^2}{2m^*} + \frac{m}{m^*} V_0, \quad (5.A.2)$$

where the effective mass

$$m^* = \frac{m_k m_\omega}{m}, \quad (5.A.3)$$

in the product of the k -mass

$$m_k = m \left(1 + \frac{m}{\hbar^2 k} \frac{\partial U}{\partial k} \right)^{-1}, \quad (5.A.4)$$

closely connected with the Pauli principle ($\frac{\partial U}{\partial k} \approx \frac{\partial U_x}{\partial k}$), while the ω -mass

$$m_\omega = m \left(1 - \frac{\partial U}{\partial \hbar\omega} \right), \quad (5.A.5)$$

results from the dressing of the nucleon through the coupling with the (quasi) bosons. Because typically $m_k \approx 0.7m$ and $m_\omega \approx 1.4m$, $m^* \approx m$. One could then be tempted to conclude that the results embodied in the dispersion relation (5.A.2) reflects the fact that the distribution of levels around the Fermi energy can be described in terms of the solutions of a Schrödinger equation in which nucleons of mass equal to the bare nucleon mass m move in a Saxon–Woods potential of depth V_0 .

Now, it can be shown that the occupancy of levels around ε_F is related to Z_ω , a quantity which measures the discontinuity at the Fermi energy (Fig. 5.A.1 (h)) and which is equal to $m/m_\omega = 1/(1 + \lambda) \approx 0.7$, λ being the mass enhancement factor ($\lambda = N(0)g_{p-v}$), product of the density of levels at the Fermi energy and the particle–vibration coupling parameter³³. This is in keeping with the fact that the time the nucleon is coupled to the vibrations it cannot behave as a single-particle and can thus not contribute to e.g. the single-particle pickup cross section. The particle-vibration coupling not only renormalizes energies and single-particle content but also the radial dependence of the wavefunction (formfactors).

It is of notice that the self-consistence requirements for the iterative solution of Eq. (5.A.1) (see Fig. 5.A.1 (d) and (d')) reminds very much those associated with the solution of the Kohn–Sham equations in finite systems,

$$H^{KS} \varphi_\gamma(\mathbf{r}) = \lambda_\gamma \varphi_\gamma(\mathbf{r}), \quad (5.A.6)$$

where

$$H^{KS} = -\frac{\hbar^2}{2m_e} \nabla^2 + U_H(\mathbf{r}) + V_{ext}(\mathbf{r}) + U_{xc}(\mathbf{r}), \quad (5.A.7)$$

H^{KS} being known as the Kohn–Sham Hamiltonian, $V_{ext}(\mathbf{r})$ being the field created by the ions and acting on the electrons. Both the Hartree and the exchange–correlation potentials $U_H(\mathbf{r})$ and $U_{xc}(\mathbf{r})$ depend on the (local) density, hence on the

³³Barranco et al. (2005); Brink and Broglia (2005) and refs. therein.

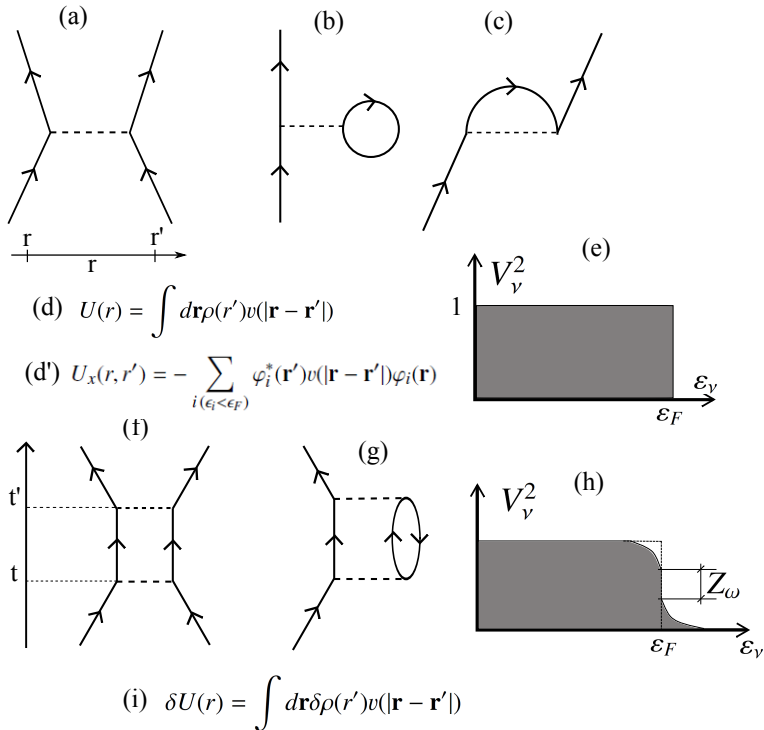


Figure 5.A.1: (a) Scattering of two nucleons through the bare NN interaction $v|\mathbf{r} - \mathbf{r}'|$, (b) contribution to the direct (U , Hartree) and (c) to the exchange (U_x , Fock) potential, resulting in (d) the (static) self-consistent relation between potential and density (non-local (d')), which (e) uncouples occupied ($\epsilon_v \leq \epsilon_F$) from empty states ($\epsilon_v > \epsilon_F$), (f) multiple scattering of two nucleons lead, through processes like the one depicted in (g), eventually propagated to all orders, to: (h) softening of the discontinuity of the occupancy of levels at ϵ_F , as well as to: (i) generalization of the static selfconsistency into a dynamic relation encompassing also collective vibrations (Time-Dependent HF solutions of the nuclear Hamiltonian, conserving energy weighted sum rules (EWSR)).

whole set of wavefunctions $\varphi_\gamma(\mathbf{r})$. Thus, the set of KS –equations must be solved selfconsistently³⁴.

5.A.1 Density of levels

Making use of Eq. (5.A.2) ($E = \hbar\omega$), one can calculate dE/dk for a single nucleon and one spin orientation³⁵. The inverse of this expression is

$$\frac{dk}{dE} = \frac{m^*}{\hbar^2 k}, \quad (5.A.8)$$

which testifies to the fact that the energy spacing between levels, i.e. the density of levels (see below), changes as m^* does.

One can then calculate the average value over the Fermi distribution, obtaining

$$\left\langle \frac{dk}{dE} \right\rangle = \frac{m^*}{\hbar^2(2/3)k_F}. \quad (5.A.9)$$

Let us now take into account all nucleons, both spin orientations and eliminate the unit (inverse) length, i.e.

$$\frac{2A}{k_F} \left\langle \frac{dk}{dE} \right\rangle = 3A \frac{m^*}{\hbar^2 k_F^2} = 3A \frac{m^*}{2m\epsilon_F}. \quad (5.A.10)$$

Assuming $m^* = m_\omega m_k/m \approx m$, where m is the bare mass one obtains

$$\frac{3}{2} \frac{A}{\epsilon_F}, \quad (5.A.11)$$

a value which coincides with the Fermi gas model estimate for the one-particle level density g_0 ³⁶. Taking properly into account the geometry of the system, one obtains

$$a = \frac{\pi^2}{6} \frac{3}{2} \frac{A}{\epsilon_F} \quad (5.A.12)$$

for the prefactor in the exponential of the Fermi expression of the total density of single particle levels. Making use of $\epsilon_F = 36$ MeV leads to,

$$a \approx \frac{A}{14} \text{MeV}^{-1}. \quad (5.A.13)$$

In keeping with the fact that one can interpret dE/dk as the rate of change in energy when the momentum changes or, equivalently, when the number of nodes per unit length changes, and this can be used to label the single-particle states, (5.A.13)

³⁴See e.g. Broglia et al. (2004) and refs. therein.

³⁵Mahaux et al. (1985), p. 17.

³⁶See e.g. Bohr and Mottelson (1969) Eq. (2-48).

can be confronted at profit with the average degeneracy per unit energy of valence orbitals (see Table 5.A.1).

Within this context it is of notice that an estimate of the quantity a based on the harmonic oscillator, leads to $a \approx \frac{\pi^2}{6} \frac{(N_{max}+3/2)^2}{\hbar\omega_0}$ i.e. an expression inversely proportional to the (constant) energy separation of levels³⁷. In an attempt to bridge the gap between the nuclear matter expressions discussed above and finite nuclei, i.e. potential wells of finite range, we consider

$$H = \frac{p^2}{2D} + \frac{C}{2}x^2, \quad (5.A.14)$$

($p = D\dot{x}$) which leads to a constant level spacing,

$$\hbar\omega_0 = \hbar \sqrt{\frac{C}{D}}, \quad (5.A.15)$$

and implies that the density of states is proportional to the square root of the particle inertia (mass). However, this result follows from the assumption that the potential remains unchanged if the bare mass (in which case D is, for example, set equal to the HF k -mass, m_k) is replaced by an effective mass m^* (e.g. $m_k m_\omega / m$, Eq. (5.A.3)). In this case the ground state wavefunction

$$\varphi_0 \sim \exp\left(-\frac{x^2}{2b^2}\right), \quad (5.A.16)$$

with,

$$b = \sqrt{\frac{\hbar}{m^*\omega_0}}, \quad (5.A.17)$$

for a dressed nucleon of effective mass $m^* > D$ will shrink in space compared with the one of mass D and consequently the mean square radius of the system

$$\langle r^2 \rangle = \frac{\hbar}{m^*\omega_0} \left(N + \frac{3}{2} \right) = b^2 \left(N + \frac{3}{2} \right) \quad (5.A.18)$$

will decrease. This is not correct, and one has to impose the condition $b^2=\text{constant}$. A condition which implies that the energy difference between levels is inversely proportional to the effective mass of the nucleon, that is,

$$\hbar\omega_0 = \frac{\hbar^2}{m^*b^2}. \quad (5.A.19)$$

Let us conclude this Appendix with a remark concerning the dimensions of the parameters D and C entering Eq. (5.A.14). Because the variable x has dimensions of length ([x]=fm), the dimensions of the inertia and restoring force parameters are

³⁷See Bohr and Mottelson (1969) p. 188, Eq (2-125a).

	MeV ⁻¹	
	empirical	<i>a</i>
²⁰⁸ Pb ₁₂₆ 82	17(10 ^a + 7 ^b)	15(9 ^a + 6 ^b)
¹²⁰ Sn ₁₂₆ 50	4 ^a)	5 ^a)

a) neutrons
b) protons

Table 5.A.1: Comparison of the factor (5.A.13) ($a = n/14\text{MeV}^{-1}$) corresponding to ²⁰⁸Pb for both $n = N$ and $n = Z$ and for ¹²⁰Sn for $n = N$, in comparison with the empirical value associated with the valence orbitals of these nuclei. That is ($h_{9/2}, f_{7/2}, i_{13/2}, p_{3/2}, f_{5/2}, p_{1/2}, g_{9/2}, i_{11/2}, d_{5/2}, j_{15/2}, s_{1/2}, g_{7/2}, d_{3/2}$) and ($g_{7/2}, d_{5/2}, h_{11/2}, d_{3/2}, s_{1/2}, h_{9/2}, f_{7/2}, i_{13/2}$) for neutrons and protons in ²⁰⁸Pb, leading to $\sum_j^N (2j+1)/\Delta E_N = 102/10 \text{ MeV} = 10 \text{ MeV}^{-1}$ and $\sum_j^Z (2j+1)/\Delta E_Z = 64/(9 \text{ MeV}) \approx 7 \text{ MeV}^{-1}$, where ΔE_N is the experimental energy interval over which the valence orbitals are distributed (see e.g. Bohr and Mottelson (1969) p. 325, Fig. 3-3). In the case of neutrons of ¹²⁰Sn, use is made of the dressed valence orbitals $d_{5/2}, g_{7/2}, s_{1/2}, d_{3/2}, h_{11/2}$ resulting from the renormalization of HF-Sly4 levels through the coupling of collective modes making use of nuclear field theory plus Nambu–Gorkov techniques ((NFT)+(NG); for details see Idini et al. (2015) and Table I of Potel et al. (2017)). The result, taking into account the breaking of the single-particle strength, in particular that of the $d_{5/2}$ orbital is $\sum_j^N (2j+1)/\Delta E_N = 32/8 \text{ MeV} \approx 4 \text{ MeV}^{-1}$.

$$[C] = \text{MeV fm}^{-2} \quad \text{and} \quad [D] = \text{MeV fm}^{-2}\text{s}^2.$$

Consequently the associated zero point fluctuations

$$\sqrt{\frac{\hbar\omega_0}{2C}} = \sqrt{\frac{\hbar^2}{2D} \frac{1}{\hbar\omega_0}} \quad (5.\text{A}.20)$$

have dimensions of fm. It is of notice that in the case of the harmonic oscillator Hamiltonian (2.A.10), the associated ZPF is a *c*-number, in keeping with the fact that the dynamic (2.A.18) and static (2.A.26) deformation parameters in the different notations (α_M^L, β_L, b_L) are dimensionless (collective) variables (CV).

Appendix 5.B Model for single-particle strength function: Dyson equation

In the previous Appendix we schematically introduced arguments regarding the “impossibility” of defining a “bona fide” single-particle spectroscopic factor. It was done with the help of Feynman (NFT) diagrams. In what follows we essentially repeat the arguments, but this time in terms of Dyson’s (Schwinger) language.

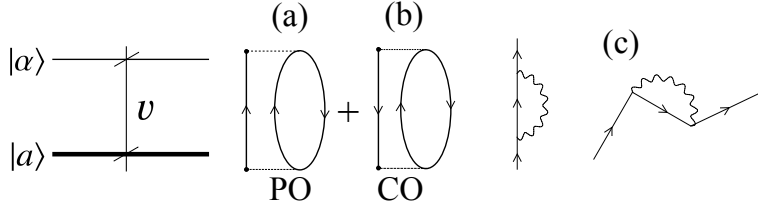


Figure 5.B.1: Two state schematic model describing the breaking of the strength of the pure single-particle state $|a\rangle$, through the coupling to collective vibrations (wavy line) associated with polarization (PO) and correlation (CO) processes.

For simplicity, we consider a two-level model where the pure single-particle state $|a\rangle$ couples to a more complicated (doorway) state $|\alpha\rangle$, made out of a fermion (particle or hole), coupled to a particle-hole excitation which, if iterated to all orders can give rise to a collective state (Fig. 5.B.1). The Hamiltonian describing the system is³⁸

$$H = H_0 + v, \quad (5.B.1)$$

where

$$H_0|a\rangle = E_a|a\rangle, \quad (5.B.2)$$

and

$$H_0|\alpha\rangle = E_\alpha|\alpha\rangle. \quad (5.B.3)$$

Let us call $\langle a|v|\alpha\rangle = v_{a\alpha}$ and assume $\langle a|v|a\rangle = \langle a|v|\alpha\rangle = 0$.

From the secular equation

$$\begin{pmatrix} E_\alpha - E_i & v_{a\alpha} \\ v_{a\alpha} & E_a - E_i \end{pmatrix} \begin{pmatrix} C_\alpha(i) \\ C_a(i) \end{pmatrix} = 0, \quad (5.B.4)$$

and associated normalization condition

$$C_a^2(i) + C_\alpha^2(i) = 0, \quad (5.B.5)$$

one obtains

$$C_a^2(i) = \left(1 + \frac{v_{a\alpha}^2}{(E_\alpha - E_i)^2} \right)^{-1}, \quad (5.B.6)$$

and

$$\Delta E_a(E) = E_a - E = \frac{v_{a\alpha}^2}{E_a - E}. \quad (5.B.7)$$

The energy of the correlated state

$$|\tilde{a}\rangle = C_a(i)|a\rangle + C_\alpha(i)|\alpha\rangle, \quad (5.B.8)$$

is obtained by the (iterative) solution of the Dyson equation (5.B.7), which propagate the diagrams shown in Figs 5.B.1 (a) and (b) to infinite order leading to collective vibrations (see Fig. 5.B.1 (c)).

³⁸Bohr and Mottelson (1969).

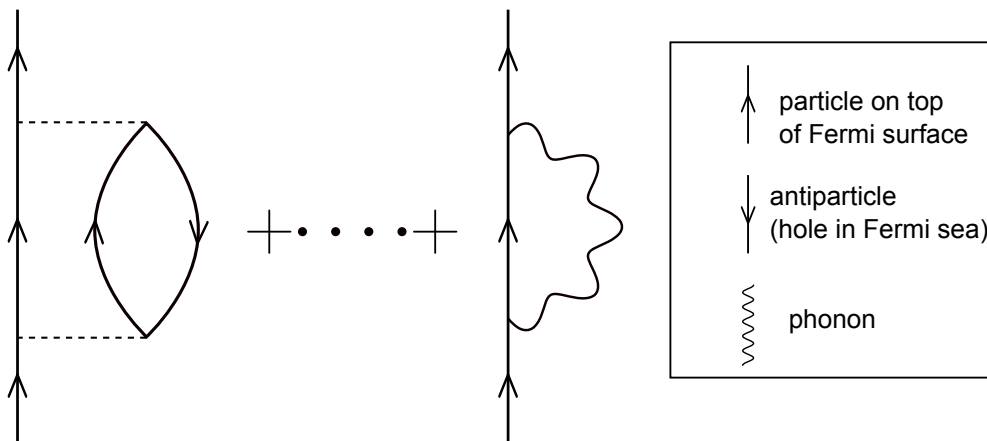


Figure 5.C.1: Feynman diagrams renormalizing the properties of a fermion.

With the help of the definition given in eq (5.A.5), and making use of the fact that in the present case, the quantity U appearing in this equation coincides, within the present context with $\Delta E_a(E)$, one obtains that the discontinuity of the single-particle levels at the Fermi energy is given by

$$Z_\omega = C_a^2(i) = \left(\frac{m_\omega}{m} \right)^{-1}. \quad (5.B.9)$$

Making use of the solution of the Dyson equation (5.B.7), and of the relations (5.B.5) and (5.B.6), one can calculate the renormalized state $|\tilde{a}\rangle$ (Eq. 5.B.8) to be employed in working out the associated, modified, single-particle transfer form factor needed in the calculation of the absolute value of one-particle transfer cross sections (cf. e.g. Sect. 5.2.1, where the above concepts and techniques are applied to the study of one-neutron transfer reactions in open shell, superfluid (^{120}Sn)).

Appendix 5.C Antiparticles: proof of concept of the quantal vacuum and of medium polarization effects

Let us consider a massive quantal particle, e.g., an electron, which moves at a velocity close of that of light. Because of Heisenberg relations, there exists a finite possibility to observe the particle moving at a velocity larger than its average velocity, and thus faster than light, a possibility ruled out by special relativity. The only way to avoid this, is by introducing antiparticles, that is a hole in the “vacuum” filled to the rim (Fermi energy) with particles, thus providing the physics to the negative energy solutions of Dirac equation.

In other words, when an electron approaches the maximum speed with which information propagates in a medium, like e.g. in the case of an electron in the QED

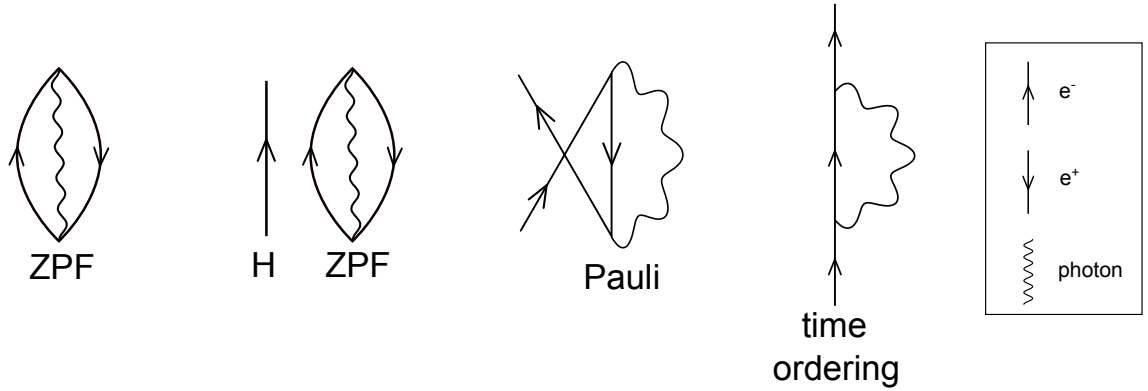


Figure 5.C.2: QED vacuum fluctuation (ZPF). In presence of e.g. an hydrogen atom (H), its electron is forced by Pauli principle to exchange with that of the ZPF, leading to a CO (correlation) like process. Time ordering leads to PO (polarization) processes.

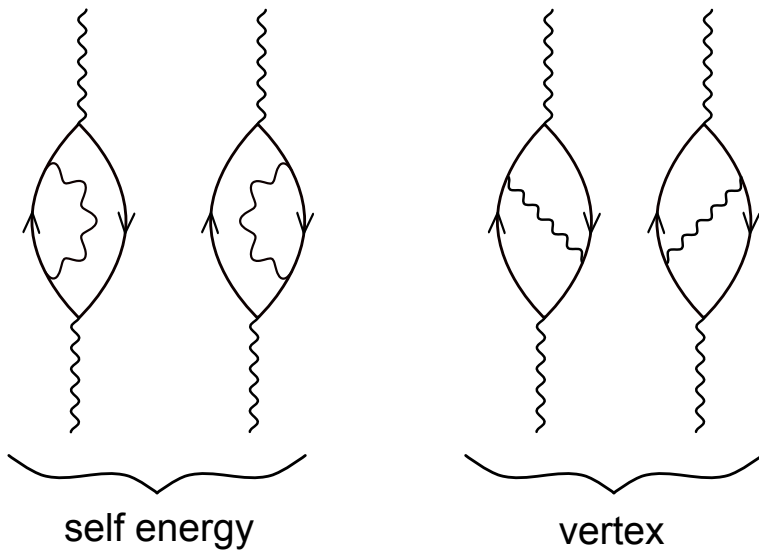


Figure 5.C.3: Lowest order diagrams which dress collective nuclear vibrations and GR.

vacuum, processes like the one depicted in Fig. 5.C.1 become operative. In other words, one can take care of the position indeterminacy of a quantal particle (electron) accepting the possibility to observe it through specific measurements which unavoidably create different particles, each of them identical to the original one, but with different positions, to keep track of conserved quantum numbers, these particles are to be accompanied by an equal number of antiparticles (positrons).

Similar results can be obtained by considering vacuum fluctuations (ZPF), and forcing them to become real through e.g. the Pauli principle (Pauli, 1947), as observed in the Lamb shift (Fig. 5.C.2, cf. also Fig. 5.D.1).

In the nuclear case the medium can, due to spatial quantization typical of Finite Quantal Many-Body Systems (FQMBS), propagate information with varied frequency. Typically, few MeV (low-lying collective vibrations of which one has to add dipole pygmy resonances ($\hbar\omega_{GDPR} \leq 1$ MeV) as for example that involved in the glue of the halo neutrons of $^{11}\text{Li(gs)}$), and tens of MeV (giant resonances), leading to a rich number of CO and PO processes. This is in keeping with the fact that the intermediate boson (photon QED, vibrations of nuclear medium) propagates in a medium which is not isotropic, thus undergoing fragmentation of the associated strength (inhomogeneous damping, Fig. 5.C.3). To make even richer the nuclear scenario, collisional damping plays also a role in the strength function of giant resonances (GR). Nonetheless, the associated widths (lifetimes) are controlled by the coupling to doorway states ($(2p - 2h)$ intermediate states built out of uncorrelated $p - h$ excitations and of a collective vibration), even at nuclear temperatures of 1–2 MeV, let alone when the GR is based on the ground state³⁹. The strong cancellation found between self-energy and vertex correction diagrams, testify to the collectivity of nuclear vibrations (generalized Ward identities), and reminds of Furry's theorem (no coupling between one- and two-photon states or, more generally, diagrams containing loops with an odd number of quanta in it, are zero⁴⁰).

Summing up, nothing is really free in the quantal world (App. 5.E). Selected measurements carried out with specific probes, can make virtual processes become real, and shed light on the variety of the mechanisms leading to renormalized elementary modes of nuclear excitation (dressed fermions and bosons).

Appendix 5.D The Lamb Shift

In Fig. 5.D.1 we display a schematic summary of the electron–photon processes, associated with Pauli principle corrections, leading to the splitting of the lowest s, p states of the hydrogen atom known as the Lamb shift⁴¹.

In the upper part of the figure the predicted position of the electronic single-particle levels of the hydrogen atom as resulting from the solution of the Schrödinger

³⁹Fig. 5.C.3; cf. Bortignon et al. (1998) and refs. therein, cf. also Broglia et al. (1987).

⁴⁰See e.g. Mehra (1996) p 264.

⁴¹Lamb Jr and Rutherford (1947); Kroll and Lamb (1949).

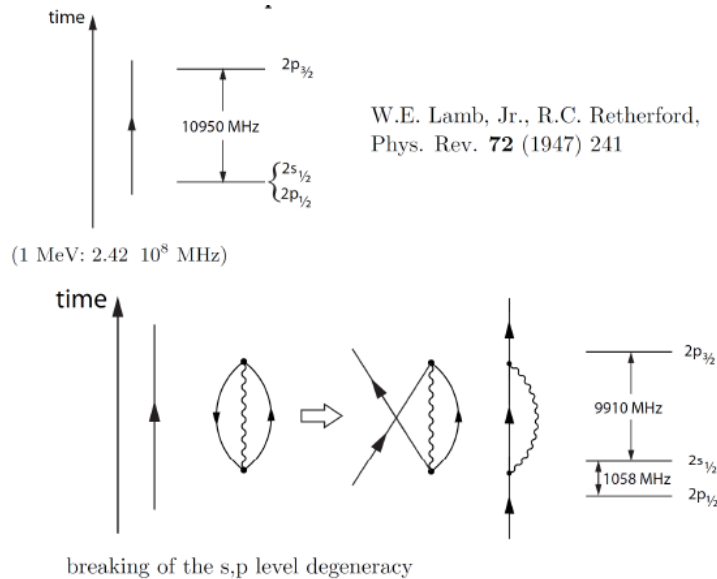


Figure 5.D.1: Schematic representation of the processes associated with the Lamb shift.

equation (Coulomb field). In the lowest part of the figure one displays the electron of an hydrogen atom (upwards going arrowed line) in presence of vacuum ZPF (electron–positron pair plus photon, oyster-like diagram). Because the associated electron virtually occupies states already occupied by the hydrogen’s electron, thus violating Pauli principle, one has to antisymmetrize the corresponding two-electron state. Such process gives rise to the exchange of the corresponding fermionic lines and thus to CO-like diagrams as well as, through time ordering, to PO-like diagrams. The results provide a quantitative account of the experimental findings (see also Fig. 7.2.1).

Appendix 5.E Self-energy and vertex corrections

In Fig. 5.E.1 an example of the fact that in field theories (e.g. QED or NFT), nothing is really free and that e.g., the bare mass of a fermion (electron or nucleon), is the parameter one adjusts (m_k) so that the result of a measurement gives the observed mass (single particle energy). In Fig. 5.E.2, lowest order diagrams associated with the renormalization of the fermion–boson interaction (vertex corrections) are given. The sum of contributions (a) and (b) can, in principle, be represented by a renormalized vertex (cf. diagram (c)). It is of notice, however, that there is, as a rule, conspicuous interference (e.g. cancellation) in the nuclear case between vertex and self-energy contributions (see diagrams (a) and (d)+(e) of Fig. 5.E.2,

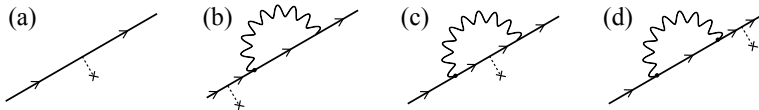


Figure 5.E.1: Self energy (effective-mass-like) processes. The result of the probing with an external field (dotted line started with a cross, observer) of the properties (mass, single-particle energy, etc) of a fermion (e.g. an electron or a nucleon, arrowed line) dressed through the coupling of (quasi) bosons (photons or collective vibrations, wavy line), corresponds to the modulus squared of the sum of the amplitudes associated with each of the four diagrams (a)–(d) (cf. (Feynman, 1975)). A concrete embodiment of the above parlance is provided by the process $^1\text{H}(^{11}\text{Li}, ^{10}\text{Li})^2\text{H}$ (cf. Figs. 5.2.5 and 5.2.6).

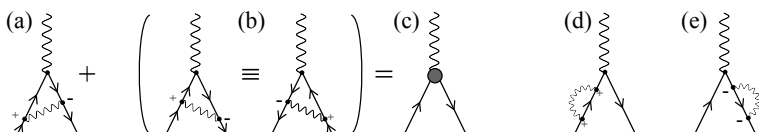


Figure 5.E.2: (a), (b) Vertex corrections. These are triple-interaction diagrams (phonon, particle and hole lines) in which none of the incoming lines can be detached from either of the other two by cutting one line. In connection with condensed matter Migdal's theorem (Migdal (1958)) states that for phonons, (Bardeen and Pines (1955), Fröhlich (1952)) vertex corrections can be neglected (cf. also Anderson (1964a)). Vertex corrections are, as a rule, important in the nuclear case where they lead to conspicuous cancellations of the self-energy contributions (d) and (e) (cf. e.g. Bortignon et al. (1983), cf. also Anderson (1964a)). The solid grey circle in (c) represents the effective, renormalized vertex.

a phenomenon closely related with conservation laws⁴². In particular, cancellation in the case in which the bosonic modes are of isoscalar character⁴³. Consequently, one has to sum explicitly the different amplitudes with the corresponding phases and eventually take the modulus squared of the result to eventually obtain the quantities to be compared with the data, a fact that precludes the use of an effective, ω -independent (renormalized) vertex.

Within the framework of QED the above mentioned cancellations are exact implying that the interaction between one- and two-photon states vanishes (Furry theorem). The physics at the basis of the cancellation found in the nuclear case can be exemplified by looking at a spherical nucleus displaying a low-lying collective quadrupole vibration. The associated zero point fluctuations (ZPF) lead to time dependent shapes with varied instantaneous values of the quadrupole moment, and of its orientation (dynamical spontaneous breaking of rotational invariance). In other words, a component of the ground state wavefunction ($|(\vec{j}_p \otimes \vec{j}_h^{-1})_{2^+} \otimes 2^+; 0^+\rangle$), which can be viewed as a gas of quadrupole (quasi) bosons promoting a nucleon across the Fermi energy (particle-hole excitation) will lead to fermionic states which behave as having a positive (particle) and a negative (hole) effective quadrupole moment, in keeping with the fact that the closed shell system is spherical, thus carrying zero quadrupole moment.

Appendix 5.F Single-nucleon transfer for pedestrians

In what follows we discuss some aspects of the relations existing between nuclear structure and one-particle transfer cross sections. To do so, we repeat some of the steps carried out above, but this time in a simpler and straightforward way, ignoring the complications associated with the spin carried out by the particles, the spin-orbit dependence of the optical model potential, the recoil effect, etc.

We consider the case of $A(d, p)A + 1$ reaction, namely that of neutron stripping. The intrinsic wave functions ψ_α and ψ_β , where $\alpha = (A, d)$ and $\beta = ((A + 1), p)$,

$$\psi_\alpha = \psi_{M_A}^{I_A}(\xi_A)\phi_d(\vec{r}_{np}), \quad (5.F.1a)$$

$$\begin{aligned} \psi_\beta &= \psi_{M_{A+1}}^{I_{A+1}}(\xi_{A+1}) \\ &= \sum_{l, I'_A} (I'_A; l \mid I_{A+1}) [\psi_{M_A}^{I'_A}(\xi_A)\phi_l(\vec{r}_n)]_{M_{A+1}-M_A}^{I_{A+1}}, \end{aligned} \quad (5.F.1b)$$

where $(I'_A; l \mid I_{A+1})$ is a generalized fractional parentage coefficient. It is of notice that this fractional parentage expansion is not well defined. In fact, as a rule, $(I'_A; l \mid I_{A+1})\phi_l(\vec{r}_n)_{M_{A+1}-M_A}$ is an involved, dressed quasiparticle state containing only a fraction of the “pure” single particle strength. For simplicity we assume the expansion to be operative. To further simplify the derivation we assume we are

⁴²Schrieffer (1964)); see also Fig. 5.C.3 and refs. Bortignon and Broglia (1981); Bertsch et al. (1983) and Bortignon et al. (1998) pp. 82–86.

⁴³Bortignon et al. (1983).

dealing with spinless particles. This is the reason why no “intrinsic” proton wavefunction appears in Eq. (5.F.1b). The variable \vec{r}_{np} is the relative coordinate of the proton and the neutron (see Fig. 5.F.1).

The transition matrix element can now be written as

$$\begin{aligned} T_{d,p} &= \langle \psi_{M_{A+1}}^{I_{A+1}}(\xi_{A+1}) \chi_p^{(-)}(k_p, \vec{r}_p), V'_\beta \psi_{M_A}^{I_A}(\xi_A) \chi_d^{(+)}(k_d, \vec{r}_d) \rangle \\ &= \sum_{\substack{l, I'_A \\ M'_A}} (I'_A; l | I_{A+1})(I'_A M'_A l M_{A+1} - M' A | I_{A+1} M_{A+1}) \\ &\quad \times \int d\vec{r}_n d\vec{r}_p \chi_p^{*(-)}(k_p, \vec{r}_p) \phi_{M_{A+1}-M'_A}^{*l}(\vec{r}_n) (\psi_{M_A}^{I_A}(\xi_A), V'_\beta \psi_{M'_A}^{I'_A}(\xi_A)) \\ &\quad \times \phi_d(\vec{r}_{np}) \chi_d^{(+)}(k_d, \vec{r}_d) \delta_{I'_A, I_A} \delta_{M'_A, M_A}. \end{aligned} \quad (5.F.2)$$

In the stripping approximation

$$\begin{aligned} V'_\beta &= V_\beta(\xi, \vec{r}_\beta) - \bar{U}_\beta(r_\beta) \\ &= V_\beta(\xi_A, \vec{r}_{pA}) + V_\beta(\vec{r}_{pn}) - \bar{U}_\beta(r_{pA}). \end{aligned} \quad (5.F.3)$$

Then

$$\begin{aligned} (\psi_{M_A}^{I_A}(\xi_A), V'_\beta \psi_{M_A}^{I_A}(\xi_A)) &= (\psi_{M_A}^{I_A}(\xi_A), V_\beta(\xi_A, \vec{r}_{pA}) \psi_{M_A}^{I_A}(\xi_A)) \\ &\quad + (\psi_{M_A}^{I_A}(\xi_A), V_\beta(\vec{r}_{pn}) \psi_{M_A}^{I_A}(\xi_A)) - \bar{U}_\beta(r_{pA}). \end{aligned} \quad (5.F.4)$$

We assume

$$U_\beta(r_{pA}) = (\psi_{M_A}^{I_A}(\xi_A), V_\beta(\xi_A, \vec{r}_{pA}) \psi_{M_A}^{I_A}(\xi_A)). \quad (5.F.5)$$

Then

$$(\psi_{M_A}^{I_A}(\xi_A), V'_\beta \psi_{M_A}^{I_A}(\xi_A)) = V_{np}(\vec{r}_{pn}). \quad (5.F.6)$$

Inserting eq. (5.F.6) into eq. (5.F.2) we obtain

$$\begin{aligned} T_{d,p} &= \sum_l (I_A; l | I_{A+1})(I_A M_A l M_{A+1} - M_A | I_{A+1} M_{A+1}) \\ &\quad \times \int d\vec{r}_n d\vec{r}_p \chi_p^{*(-)}(k_p, \vec{r}_p) \phi_{M_{A+1}-M_A}^{*l}(\vec{r}_n) V(\vec{r}_{pn}) \phi_d(\vec{r}_{np}) \chi_d^{(+)}(k_d, \vec{r}_d) \end{aligned} \quad (5.F.7)$$

The differential cross section is then equal to

$$\frac{d\sigma}{d\Omega} = \frac{2}{3} \frac{\mu_p \mu_d}{(2\pi\hbar^2)^2} \frac{(2I_{A+1} + 1)}{(2I_A + 1)} \frac{k_p}{k_d} \sum_{l, m_l} \frac{(I_A; l | I_{A+1})^2}{2l + 1} |B_{m_l}^l|^2, \quad (5.F.8)$$

where

$$B_{m_l}^l(\theta) = \int d\vec{r}_n d\vec{r}_p \chi_p^{*(-)}(k_p, \vec{r}_p) Y_m^{*l}(\hat{r}_n) u_{nl}(r_n) V(\vec{r}_{pn}) \phi_d(\vec{r}_{np}) \chi_d^{(+)}(k_d, \vec{r}_d) \quad (5.F.9)$$

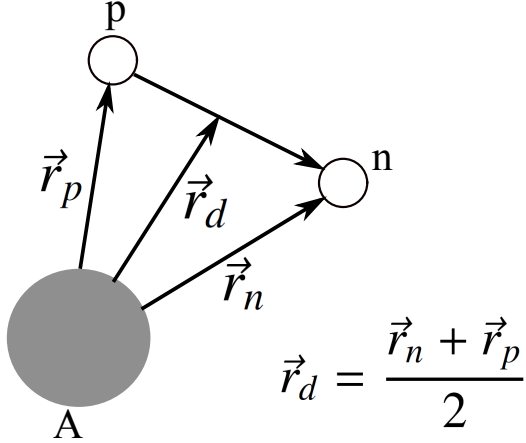


Figure 5.F.1: Coordinates used in the description of the $A(d, p)(A + 1)$ stripping process.

and

$$\phi_m^l(\vec{r}_n) = u_{nl}(r_n)Y_m^l(\hat{r}_n), \quad (5.F.10)$$

is the single-particle wave function of a neutron bound to the core A. For simplicity, the radial wave function $u_{nl}(r_n)$ can be assumed to be a solution of a Saxon-Woods potential of parameters $V_0 \approx 50$ MeV, $a = 0.65$ fm and $r_0 = 1.25$ fm.

The relation (5.F.8) gives the cross section for the stripping from the projectile of a neutron that would correspond to the n^{th} valence neutron in the nucleus $(A + 1)$. If we now want the cross section for stripping any of the valence neutrons of the final nucleus from the projectile, we must multiply eq. (5.F.8) by n . A more careful treatment of the antisymmetry with respect to the neutrons shows this to be the correct answer.

Finally we get

$$\frac{d\sigma}{d\Omega} = \frac{(2I_{A+1} + 1)}{(2I_A + 1)} \sum_l S_l \sigma_l(\theta), \quad (5.F.11)$$

where

$$S_l = n(I_A; l|I_{A+1})^2, \quad (5.F.12)$$

and

$$\sigma_l(\theta) = \frac{2}{3} \frac{\mu_p \mu_d}{(2\pi\hbar^2)^2} \frac{k_p}{k_d} \frac{1}{2l + 1} \sum_m |B_m^l|^2 \quad (5.F.13)$$

The distorted wave softwares evaluate numerically the quantity $B_m^l(\theta)$, using for the wave functions $\chi^{(-)}$ and $\chi^{(+)}$ the solution of the optical potentials that fit the elastic scattering, i.e.

$$(-\nabla^2 + \bar{U} - k^2)\chi = 0, \quad (5.F.14)$$

Note that if the target nucleus is even-even, $I_A = 0$, $l = I_{A+1}$. That is, only one l value contributes in Eq. (5.F.8), and the angular distribution is uniquely

given by $\sum_m |B_m^l|^2$. The l -dependence of the angular distributions helps to identify $l = I_{A+1}$. The factor S_l needed to normalize the calculated function to the data yields (assuming a good fit to the angular distribution), is known in the literature as the spectroscopic factor. It was assumed in the early stages of studies of nuclear structure with one-particle transfer reactions not only that it could be defined, but also that it contained all the nuclear structure information (aside from that associated with the angular distribution) which could be extracted from single-particle transfer. In other words, that it was the bridge directly connecting theory with experiment. *Because nucleons are never bare, but are dressed by the coupling to collective modes, coupling which renormalizes not only the single-particle content but also the single-particle wavefunctions (formfactors), the spectroscopic factor approximation is at best a helpful tool to get order of magnitude information from one-particle transfer data.*

There is a fundamental problem which makes the handling of integrals like that of (5.F.9) difficult to handle, if not numerically at least conceptually. This difficulty is connected with the so called recoil effect⁴⁴, namely the fact that the center of mass of the two interacting particles in entrance ($\mathbf{r}_\alpha : \alpha = a + A$) and exit ($\mathbf{r}_\beta : \beta = b + B$) channels is different. This is at variance with what one is accustomed to deal with in nuclear structure calculations, in which the Hartree potential depends on a single coordinate, as well as in the case of elastic and inelastic reactions, situations in which $\mathbf{r}_\alpha = \mathbf{r}_\beta$. When $\mathbf{r}_\alpha \neq \mathbf{r}_\beta$ we enter a rather more complex many-body problem, in particular if continuum states are to be considered, than nuclear structure practitioners were accustomed to.

Of notice that similar difficulties have been faced in connection with the non-local Fock (exchange) potential. As a rule, the corresponding (HF) mean field equations are rendered local making use of the k -mass approximation or within the framework of Local Density Functional Theory (DFT), in particular with the help of the Kohn-Sham equations⁴⁵. Although much of the work in this field is connected with the correlation potential (interweaving of single-particle and collective motion), an important fraction is connected with the exchange potential.

In any case, and returning to the subject of the present appendix, it is always useful to be able to introduce approximations which can help the physics which is at the basis of the phenomenon under discussion (single-particle motion) emerge in a natural way, if not to compare in detail with the experimental data. Within this context, to reduce the integral (5.F.9) one can assume that the proton-neutron interaction V_{np} has zero-range, i.e.

$$V_{np}(\vec{r}_{np})\phi_d(\vec{r}_{np}) = D_0\delta(\vec{r}_{np}) \quad (5.F.15)$$

⁴⁴While this effect could be treated in a cavalier fashion in the case of light ion reactions ($m_a/m_A \ll 1$), this was not possible in the case of heavy ion reactions, as the change in momenta involved was always sizeable (cf. Broglia and Winther (2004) and refs. therein).

⁴⁵Mahaux et al. (1985), Broglia et al. (2004) and refs. therein; see also App. 5.A.

so that B_m^l becomes equal to

$$B_{m_l}^l(\theta) = D_0 \int d\vec{r} \chi_p^{*(-)}(k_p, \vec{r}) Y_{m_l}^{*l}(\hat{r}) u_l(r) \chi_d^{(+)}(k_d, \vec{r}), \quad (5.F.16)$$

which is a three dimensional integral, but in fact essentially a one-dimensional integral, as the integration over the angles can be worked out analytically.

5.F.1 Plane-wave limit

If in Eq. (5.F.14) one sets $\bar{U} = 0$, the distorted waves become plane waves i.e.

$$\chi_d^{(+)}(k_d, \vec{r}) = e^{i\vec{k}_d \cdot \vec{r}}, \quad (5.F.17a)$$

$$\chi_d^{*(-)}(k_p, \vec{r}) = e^{-i\vec{k}_p \cdot \vec{r}}. \quad (5.F.17b)$$

Equation (5.F.16) can now be written as

$$B_m^l = D_0 \int d\vec{r} e^{i(\vec{k}_d - \vec{k}_p) \cdot \vec{r}} Y_m^{*l}(\hat{r}) u_l(r). \quad (5.F.18)$$

The linear momentum transferred to the nucleus is $\vec{k}_d - \vec{k}_p = \vec{q}$. Let us expand $e^{i\vec{q} \cdot \vec{r}}$ in spherical harmonics, i.e.

$$\begin{aligned} e^{i\vec{q} \cdot \vec{r}} &= \sum_l l! j_l(qr) (2l+1) P_l(\hat{q} \cdot \hat{r}) \\ &= 4\pi \sum_l l! j_l(qr) \sum_m Y_m^{*l}(\hat{q}) Y_m^l(\hat{r}), \end{aligned} \quad (5.F.19)$$

so

$$\int d\hat{r} e^{i\vec{q} \cdot \vec{r}} Y_m^l(\hat{r}) = 4\pi l! j_l(qr) Y_m^{*l}(\hat{q}). \quad (5.F.20)$$

Then

$$\begin{aligned} \sum_m |B_m^l|^2 &= \sum_m |Y_m^l(\hat{q})|^2 D_0^2 16\pi^2 \times \\ &\quad \left| \int r^2 dr j_l(qr) u_l(r) \right|^2 \\ &= \frac{2l+1}{4\pi} D_0^2 16\pi^2 \left| \int r^2 dr j_l(qr) u_l(r) \right|^2. \end{aligned} \quad (5.F.21)$$

Thus, the angular distribution is given by the integral $\left| \int r^2 dr j_l(qr) u_l(r) \right|^2$. If one assumes that the process takes place mostly on the surface, the angular distribution will be given by $|j_l(qR_0)|^2$, where R_0 is the nuclear radius.

We then have

$$\begin{aligned} q^2 &= k_d^2 + k_p^2 - 2k_d k_p \cos(\theta) \\ &= (k_d^2 + k_p^2 - 2k_d k_p) + 2k_d k_p (1 - \cos(\theta)) \\ &= (k_d - k_p)^2 + 4k_d k_p (\sin(\theta/2))^2 \\ &\approx 4k_d k_p (\sin(\theta/2))^2, \end{aligned} \quad (5.F.22)$$

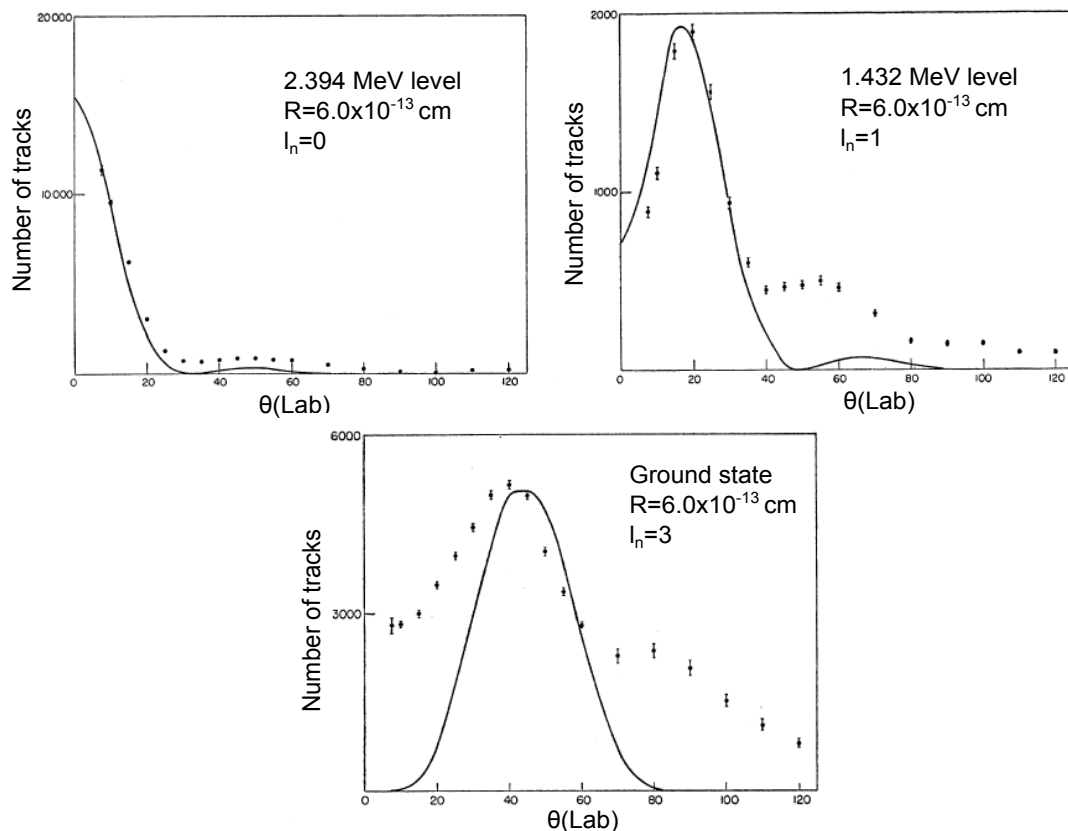


Figure 5.F.2: Plane wave approximation analysis of three $^{44}\text{Ca}(\text{d},\text{p})^{45}\text{Ca}$ differential cross sections leading to the ground state ($l_n = 3$) and to the 1.9 MeV state ($l_n = 1$) and 2.4 MeV ($l_n = 0$) excited states, i.e. $f_{9/2}$, $p_{1/2}$ and $s_{1/2}$ states (Cobb and Guthe, 1957).

since $k_d \approx k_p$ for stripping reactions at typical energies. Thus the angular distribution has a diffraction-like structure given by

$$|j_l(qR_0)|^2 = j_l^2(2R_0 \sqrt{k_d k_p} \sin(\theta/2)). \quad (5.F.23)$$

The function $j_l(x)$ has its first maximum at $x = l$, i.e. where

$$\sin(\theta/2) = \frac{l}{2R_0 k}, \quad (k_p \approx k_d = k), \quad (5.F.24)$$

Examples of the above relation are provided in Fig. 5.F.2.

Appendix 5.G One-particle knockout within DWBA

5.G.1 Spinless particles

We are going to consider the reaction $A + a \rightarrow a + b + c$, in which the cluster b is knocked out from the nucleus $A (= c + b)$. Cluster b is thus initially bound, while the final states of a, b and the initial state of a are all in the continuum, and can be described with distorted waves defined as scattering solutions of an optical potential. A schematic depiction of the situation is shown in Fig. 5.G.1. While the derivation presented below is quite general, special emphasis is set to one-particle knock-out processes.

Transition amplitude

A first derivation will be given in which, for simplicity, all the “particles” (nuclei) involved in the reaction process are spinless and inert. Use is made of central, complex optical potentials ($U(r_{aA}), U(r_{cb}), U(r_{ac})$) potentials without a spin-orbit term. In addition, the interaction $v(r_{ab})$ between a and b is taken to be a function of the distance r_{ab} . Within this scenario, the transition amplitude which is at the basis of the evaluation of the multi-differential cross section is the 6-dimensional integral

$$T_{mb} = \int d\mathbf{r}_{aA} d\mathbf{r}_{bc} \chi^{(-)*}(\mathbf{r}_{ac}) \chi^{(-)*}(\mathbf{r}_{bc}) v(r_{ab}) \chi^{(+)}(\mathbf{r}_{aA}) u_{l_b}(r_{bc}) Y_{mb}^{l_b}(\hat{\mathbf{r}}_{bc}). \quad (5.G.1)$$

Coordinates

The vectors $\mathbf{r}_{ab}, \mathbf{r}_{ac}$ can easily be written in function of the integration variables $\mathbf{r}_{aA}, \mathbf{r}_{bc}$ (see Fig. 5.G.1), namely

$$\begin{aligned} \mathbf{r}_{ac} &= \mathbf{r}_{aA} + \frac{b}{A} \mathbf{r}_{bc}, \\ \mathbf{r}_{ab} &= \mathbf{r}_{aA} - \frac{c}{A} \mathbf{r}_{bc}, \end{aligned} \quad (5.G.2)$$

where b, c, A stand for the number of nucleons of the species b, c and A respectively.

Distorted waves in the continuum

A standard way to reduce the dimensionality of the integral (5.G.1) consists in expanding the continuum wave functions $\chi^{(+)}(\mathbf{r}_{aA}), \chi^{(-)*}(\mathbf{r}_{ac}), \chi^{(-)*}(\mathbf{r}_{bc})$ in a basis of eigenstates of the angular momentum operator (partial waves). Then one can exploit the transformation properties of these eigenstates under rotations to conveniently carry out the angular integrations. Making use of time-reversed phasing, that is

$$Y_m^l(\theta, \phi) = i^l \sqrt{\frac{2l+1}{4\pi} \frac{(l-m)!}{(l+m)!}} P_l^m(\cos \theta) e^{im\phi}, \quad (5.G.3)$$

the general form of these expansions is

$$\chi^{(+)}(\mathbf{k}, \mathbf{r}) = \sum_l \frac{4\pi}{kr} i^l \sqrt{2l+1} e^{i\sigma_l} F_l(r) [Y^l(\hat{\mathbf{r}}) Y^l(\hat{\mathbf{k}})]_0^0, \quad (5.G.4)$$

and

$$\chi^{(-)*}(\mathbf{k}, \mathbf{r}) = \sum_l \frac{4\pi}{kr} i^{-l} \sqrt{2l+1} e^{i\sigma_l} F_l(r) [Y^l(\hat{\mathbf{r}}) Y^l(\hat{\mathbf{k}})]_0^0, \quad (5.G.5)$$

σ_l being the Coulomb phase shift. The radial functions $F_l(r)$ are regular (finite at $r = 0$) solutions of the one-dimensional Schrödinger equation with an effective potential $U(r) + \frac{\hbar^2 l(l+1)}{2\mu r^2}$ and suitable asymptotic behaviour at $r \rightarrow \infty$ as boundary conditions. Thus, the distorted waves appearing in (5.G.1) are,

$$\chi^{(+)}(\mathbf{k}_a, \mathbf{r}_{aA}) = \sum_{l_a} \frac{4\pi}{k_a r_{aA}} i^{l_a} \sqrt{2l_a+1} e^{i\sigma^{l_a}} F_{l_a}(r_{aA}) [Y^{l_a}(\hat{\mathbf{r}}_{aA}) Y^{l_a}(\hat{\mathbf{k}}_a)]_0^0, \quad (5.G.6)$$

describing the relative motion of A and a in the entrance channel as determined by the complex optical potential $U(r_{Aa})$,

$$\chi^{(-)*}(\mathbf{k}'_a, \mathbf{r}_{ac}) = \sum_{l'_a} \frac{4\pi}{k'_a r_{ac}} i^{-l'_a} \sqrt{2l'_a+1} e^{i\sigma^{l'_a}} F_{l'_a}(r_{ac}) [Y^{l'_a}(\hat{\mathbf{r}}_{ac}) Y^{l'_a}(\hat{\mathbf{k}}'_a)]_0^0, \quad (5.G.7)$$

which describes the relative motion of c and a , in the final channel controlled by the complex optical potential $U(r_{ac})$, and finally

$$\chi^{(-)*}(\mathbf{k}'_b, \mathbf{r}_{bc}) = \sum_{l'_b} \frac{4\pi}{k'_b r_{bc}} i^{-l'_b} \sqrt{2l'_b+1} e^{i\sigma^{l'_b}} F_{l'_b}(r_{bc}) [Y^{l'_b}(\hat{\mathbf{r}}_{bc}) Y^{l'_b}(\hat{\mathbf{k}}'_b)]_0^0, \quad (5.G.8)$$

final channel wavefunction describing the relative motion of b and c , as defined by the complex optical potential $U(r_{bc})$.

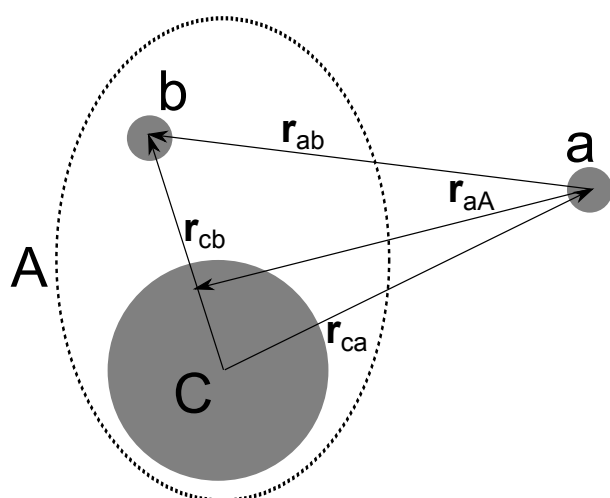


Figure 5.G.1: System of coordinates used to describe the reaction $A+a \rightarrow a+b+c$. The nucleus A is viewed as an inert cluster b bounded to an inert core c .

Recoupling of angular momenta

One now proceeds to the evaluation of the 6-dimensional integral

$$\begin{aligned} & \frac{64\pi^3}{k_a k'_a k'_b} \int d\mathbf{r}_{aA} d\mathbf{r}_{bc} u_{l_b}(r_{cb}) v(r_{ab}) \sum_{l_a, l'_a, l'_b} \sqrt{(2l_a + 1)(2l'_a + 1)(2l'_b + 1)} \\ & \times e^{i(\sigma^{l_a} + \sigma^{l'_a} + \sigma^{l'_b})} \frac{F_{l_a}(r_{aA}) F_{l'_a}(r_{ac}) F_{l'_b}(r_{bc})}{r_{ac} r_{aA} r_{bc}} \\ & \times \left[Y^{l_a}(\hat{\mathbf{r}}_{aA}) Y^{l_a}(\hat{\mathbf{k}}_a) \right]_0^0 \left[Y^{l'_a}(\hat{\mathbf{r}}_{ac}) Y^{l'_a}(\hat{\mathbf{k}}'_a) \right]_0^0 \left[Y^{l'_b}(\hat{\mathbf{r}}_{bc}) Y^{l'_b}(\hat{\mathbf{k}}'_b) \right]_0^0 Y^{l_b}_{m_b}(\hat{\mathbf{r}}_{bc}), \end{aligned} \quad (5.G.9)$$

an expression which explicitly depends on the asymptotic kinetic energies and scattering angles ($\hat{\mathbf{k}}_a, \hat{\mathbf{k}}'_a, \hat{\mathbf{k}}'_b$) of a, b as determined by k_a, k'_a, k'_b and $\hat{\mathbf{k}}_a, \hat{\mathbf{k}}'_a, \hat{\mathbf{k}}'_b$ respectively. In what follows we will take advantage of the partial wave expansion to reduce the dimensionality of the integral from 6 to 3. A possible strategy to follow is that of recoupling together all the terms that depend on the integration variables to a global angular momentum and retain only the term coupled to 0 as the only one surviving the integration. Let us start to separately couple the terms corresponding to particles a and b . For particle a we write

$$\begin{aligned} & \left[Y^{l_a}(\hat{\mathbf{r}}_{aA}) Y^{l_a}(\hat{\mathbf{k}}_a) \right]_0^0 \left[Y^{l'_a}(\hat{\mathbf{r}}_{ac}) Y^{l'_a}(\hat{\mathbf{k}}'_a) \right]_0^0 = \sum_K ((l_a l_a)_0 (l'_a l'_a)_0 | (l_a l'_a)_K (l_a l'_a)_K)_0 \\ & \times \left\{ \left[Y^{l_a}(\hat{\mathbf{r}}_{aA}) Y^{l'_a}(\hat{\mathbf{r}}_{ac}) \right]_M^K \left[Y^{l_a}(\hat{\mathbf{k}}_a) Y^{l'_a}(\hat{\mathbf{k}}'_a) \right]_{-M}^K \right\}_0^0. \end{aligned} \quad (5.G.10)$$

We can now evaluate the $9j$ -symbol,

$$((l_a l_a)_0 (l'_a l'_a)_0 | (l_a l'_a)_K (l_a l'_a)_K)_0 = \sqrt{\frac{2K+1}{(2l'_a+1)(2l_a+1)}}, \quad (5.G.11)$$

and expand the coupling,

$$\begin{aligned} & \left\{ \left[Y^{l_a}(\hat{\mathbf{r}}_{aA}) Y^{l'_a}(\hat{\mathbf{r}}_{ac}) \right]_M^K \left[Y^{l_a}(\hat{\mathbf{k}}_a) Y^{l'_a}(\hat{\mathbf{k}}'_a) \right]_{-M}^K \right\}_0^0 = \sum_M \langle K \ K \ M \ -M | 0 \ 0 \rangle \\ & \times \left[Y^{l_a}(\hat{\mathbf{r}}_{aA}) Y^{l'_a}(\hat{\mathbf{r}}_{ac}) \right]_M^K \left[Y^{l_a}(\hat{\mathbf{k}}_a) Y^{l'_a}(\hat{\mathbf{k}}'_a) \right]_{-M}^K = \sum_M \frac{(-1)^{K+M}}{\sqrt{2K+1}} \\ & \times \left[Y^{l_a}(\hat{\mathbf{r}}_{aA}) Y^{l'_a}(\hat{\mathbf{r}}_{ac}) \right]_M^K \left[Y^{l_a}(\hat{\mathbf{k}}_a) Y^{l'_a}(\hat{\mathbf{k}}'_a) \right]_{-M}^K. \end{aligned} \quad (5.G.12)$$

Thus,

$$\begin{aligned} & \left[Y^{l_a}(\hat{\mathbf{r}}_{aA}) Y^{l_a}(\hat{\mathbf{k}}_a) \right]_0^0 \left[Y^{l'_a}(\hat{\mathbf{r}}_{ac}) Y^{l'_a}(\hat{\mathbf{k}}'_a) \right]_0^0 = \sqrt{\frac{1}{(2l'_a+1)(2l_a+1)}} \\ & \times \sum_{KM} (-1)^{K+M} \left[Y^{l_a}(\hat{\mathbf{r}}_{aA}) Y^{l'_a}(\hat{\mathbf{r}}_{ac}) \right]_M^K \left[Y^{l_a}(\hat{\mathbf{k}}_a) Y^{l'_a}(\hat{\mathbf{k}}'_a) \right]_{-M}^K. \end{aligned} \quad (5.G.13)$$

One can further simplify the above expression by choosing the direction of the initial momentum to be parallel to the z axis, so that $Y_m^{l_a}(\hat{\mathbf{k}}_a) = Y_m^{l_a}(\hat{\mathbf{z}}) = \sqrt{\frac{2l_a+1}{4\pi}}\delta_{m,0}$. Then,

$$\begin{aligned} \left[Y^{l_a}(\hat{\mathbf{r}}_{aA}) Y^{l_a}(\hat{\mathbf{k}}_a) \right]_0^0 \left[Y^{l'_a}(\hat{\mathbf{r}}_{ac}) Y^{l'_a}(\hat{\mathbf{k}}'_a) \right]_0^0 &= \sqrt{\frac{1}{4\pi(2l'_a + 1)}} \sum_{KM} (-1)^{K+M} \\ &\times \langle l_a 0 l'_a - M | K - M \rangle \left[Y^{l_a}(\hat{\mathbf{r}}_{aA}) Y^{l'_a}(\hat{\mathbf{r}}_{ac}) \right]_M^K Y_{-M}^{l'_a}(\hat{\mathbf{k}}'_a). \end{aligned} \quad (5.G.14)$$

For particle b we have

$$Y_{m_b}^{l_b}(\hat{\mathbf{r}}_{bc}) \left[Y^{l'_b}(\hat{\mathbf{r}}_{bc}) Y^{l'_b}(\hat{\mathbf{k}}'_b) \right]_0^0 = Y_{m_b}^{l_b}(\hat{\mathbf{r}}_{cb}) \sum_m \frac{(-1)^{l'_b+m}}{\sqrt{2l'_b + 1}} Y_m^{l'_b}(\hat{\mathbf{r}}_{bc}) Y_{-m}^{l'_b}(\hat{\mathbf{k}}'_b), \quad (5.G.15)$$

and can write

$$Y_{m_b}^{l_b}(\hat{\mathbf{r}}_{bc}) Y_m^{l'_b}(\hat{\mathbf{r}}_{bc}) = \sum_{K'} \langle l_b m_b l'_b m | K' m_b + m \rangle \left[Y^{l_b}(\hat{\mathbf{r}}_{bc}) Y^{l'_b}(\hat{\mathbf{r}}_{bc}) \right]_{m_b+m}^{K'}. \quad (5.G.16)$$

In order to couple to 0 angular momentum with (5.G.14) we must only keep the term with $K' = K$, $m = -M - m_b$ so

$$\begin{aligned} Y_{m_b}^{l_b}(\hat{\mathbf{r}}_{bc}) \left[Y^{l'_b}(\hat{\mathbf{r}}_{bc}) Y^{l'_b}(\hat{\mathbf{k}}'_b) \right]_0^0 &= \frac{(-1)^{l'_b-M-m_b}}{\sqrt{2l'_b + 1}} \langle l_b m_b l'_b - M - m_b | K - M \rangle \\ &\times \left[Y^{l_b}(\hat{\mathbf{r}}_{bc}) Y^{l'_b}(\hat{\mathbf{r}}_{bc}) \right]_{-M}^{K'} Y_{-M-m_b}^{l'_b}(\hat{\mathbf{k}}'_b), \end{aligned} \quad (5.G.17)$$

and (5.G.9) becomes

$$\begin{aligned} \frac{32\pi^2}{k_a k'_a k'_b} \sum_{KM} (-1)^{K+l'_b-m_b} \langle l_a 0 l'_a - M | K - M \rangle \langle l_b m_b l'_b - M - m_b | K - M \rangle \\ \times \sum_{l_a, l'_a, l'_b} \sqrt{(2l_a + 1)} e^{i(\sigma^{l_a} + \sigma^{l'_a} + \sigma^{l'_b})} Y_{-M-m_b}^{l'_b}(\hat{\mathbf{k}}'_b) Y_{-M}^{l'_a}(\hat{\mathbf{k}}'_a) \int d\mathbf{r}_{aA} d\mathbf{r}_{bc} u_{l_b}(r_{bc}) v(r_{ab}) \\ \times \frac{F_{l_a}(r_{aA}) F_{l'_a}(r_{ac}) F_{l'_b}(r_{bc})}{r_{ac} r_{aA} r_{bc}} \left[Y^{l_a}(\hat{\mathbf{r}}_{aA}) Y^{l'_a}(\hat{\mathbf{r}}_{ac}) \right]_M^K \left[Y^{l_b}(\hat{\mathbf{r}}_{bc}) Y^{l'_b}(\hat{\mathbf{r}}_{bc}) \right]_{-M}^K. \end{aligned} \quad (5.G.18)$$

Note that

$$\begin{aligned} \left[Y^{l_a}(\hat{\mathbf{r}}_{aA}) Y^{l'_a}(\hat{\mathbf{r}}_{ac}) \right]_M^K \left[Y^{l_b}(\hat{\mathbf{r}}_{bc}) Y^{l'_b}(\hat{\mathbf{r}}_{bc}) \right]_{-M}^K &= \sum_P \langle K M K - M | P 0 \rangle \\ &\times \left\{ \left[Y^{l_a}(\hat{\mathbf{r}}_{aA}) Y^{l'_a}(\hat{\mathbf{r}}_{ac}) \right]_0^K \left[Y^{l_b}(\hat{\mathbf{r}}_{bc}) Y^{l'_b}(\hat{\mathbf{r}}_{bc}) \right]_0^K \right\}_0^P, \end{aligned} \quad (5.G.19)$$

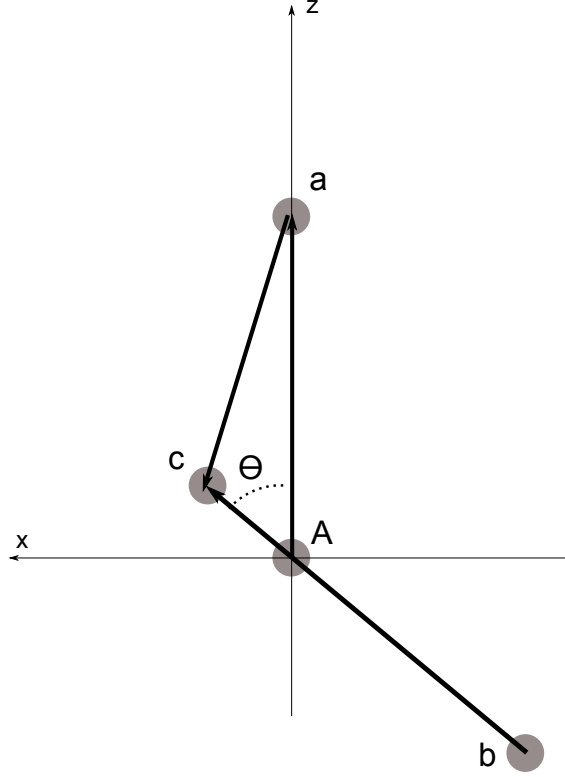


Figure 5.G.2: Coordinates in the “standard” configuration.

and that to survive the integration the rotational tensors must be coupled to $P = 0$. Keeping only this term in the sum over P , we get

$$\begin{aligned} & \left[Y^{l_a}(\hat{\mathbf{r}}_{aA}) Y'^a(\hat{\mathbf{r}}_{ac}) \right]_M^K \left[Y^{l_b}(\hat{\mathbf{r}}_{bc}) Y'^b(\hat{\mathbf{r}}_{bc}) \right]_{-M}^K = \\ & \frac{(-1)^{K+M}}{\sqrt{2K+1}} \left\{ \left[Y^{l_a}(\hat{\mathbf{r}}_{aA}) Y'^a(\hat{\mathbf{r}}_{ac}) \right]_M^K \left[Y^{l_b}(\hat{\mathbf{r}}_{bc}) Y'^b(\hat{\mathbf{r}}_{bc}) \right]_{-M}^K \right\}_0^0. \end{aligned} \quad (5.G.20)$$

The coordinate-dependent part of the latter expression is a rotationally invariant scalar, so it can be evaluated in any conventional “standard” configuration such as the one depicted in Fig. 5.G.2. It must then be multiplied by a factor resulting of the integration of the remaining angular variables, which accounts for the rigid rotations needed to connect any arbitrary configuration to one of this type. This factor turns out to be $8\pi^2$ (a 4π factor for all possible orientations of, say, \mathbf{r}_{aA} and a

2π factor for a complete rotation around its direction). According to Fig. 5.G.2,

$$\begin{aligned}\mathbf{r}_{bc} &= r_{bc} (\sin \theta \hat{x} + \cos \theta \hat{z}), \\ \mathbf{r}_{aA} &= -r_{aA} \hat{z}, \\ \mathbf{r}_{ac} &= \frac{b}{A} r_{bc} \sin \theta \hat{x} + \left(\frac{b}{A} r_{bc} \cos \theta - r_{aA} \right) \hat{z}.\end{aligned}\quad (5.G.21)$$

As \mathbf{r}_{aA} lies parallel to the z axis, $Y_{M_K}^{l_a}(\hat{\mathbf{r}}_{aA}) = \sqrt{\frac{2l_a+1}{4\pi}} \delta_{M_K,0}$ and

$$\begin{aligned}\left[Y^{l_a}(\hat{\mathbf{r}}_{aA}) \ Y^{l'_a}(\hat{\mathbf{r}}_{ac}) \right]_{M_K}^K &= \sum_m \langle l_a \ m \ l'_a \ M_K - m | K \ M_K \rangle Y_m^{l_a}(\hat{\mathbf{r}}_{aA}) Y_{M_K-m}^{l'_a}(\hat{\mathbf{r}}_{ac}) = \\ &\sqrt{\frac{2l_a+1}{4\pi}} \langle l_a \ 0 \ l'_a \ M_K | K \ M_K \rangle Y_{M_K}^{l'_a}(\hat{\mathbf{r}}_{ac}).\end{aligned}\quad (5.G.22)$$

Then

$$\begin{aligned}\left\{ \left[Y^{l_a}(\hat{\mathbf{r}}_{aA}) Y^{l'_a}(\hat{\mathbf{r}}_{ac}) \right]^K \left[Y^{l_b}(\hat{\mathbf{r}}_{bc}) Y^{l'_b}(\hat{\mathbf{r}}_{bc}) \right]^K \right\}_0^0 &= \\ \sum_{M_K} \langle K \ M_K \ K - M_K | 0 \ 0 \rangle \left[Y^{l_a}(\hat{\mathbf{r}}_{aA}) Y^{l'_a}(\hat{\mathbf{r}}_{ac}) \right]_{M_K}^K \left[Y^{l_b}(\hat{\mathbf{r}}_{bc}) Y^{l'_b}(\hat{\mathbf{r}}_{bc}) \right]_{-M_K}^K &= \\ \sqrt{\frac{2l_a+1}{4\pi}} \sum_{M_K} \frac{(-1)^{K+M_K}}{\sqrt{2K+1}} \langle l_a \ 0 \ l'_a \ M_K | K \ M_K \rangle \\ &\times \left[Y^{l_b}(\hat{\mathbf{r}}_{bc}) Y^{l'_b}(\hat{\mathbf{r}}_{bc}) \right]_{-M_K}^K Y_{M_K}^{l'_a}(\hat{\mathbf{r}}_{ac}).\end{aligned}\quad (5.G.23)$$

Remembering the $8\pi^2$ factor, the term arising from (5.G.20) to be considered in the integral is

$$\begin{aligned}4\pi^{3/2} \frac{\sqrt{2l_a+1}}{2K+1} (-1)^K \sum_{M_K} (-1)^{M_K} \langle l_a \ 0 \ l'_a \ M_K | K \ M_K \rangle \\ \times \left[Y^{l_b}(\cos \theta, 0) Y^{l'_b}(\cos \theta, 0) \right]_{-M_K}^K Y_{M_K}^{l'_a}(\cos \theta_{ac}, 0),\end{aligned}\quad (5.G.24)$$

with

$$\cos \theta_{ac} = \frac{\frac{b}{A} r_{bc} \cos \theta - r_{aA}}{\sqrt{\left(\frac{b}{A} r_{bc} \sin \theta \right)^2 + \left(\frac{b}{A} r_{bc} \cos \theta - r_{aA} \right)^2}}, \quad (5.G.25)$$

(see (5.G.21)). The final expression of the transition amplitude is

$$\begin{aligned}T_{m_b}(\mathbf{k}'_a, \mathbf{k}'_b) &= \frac{128\pi^{7/2}}{k_a k'_a k'_b} \sum_{KM} \frac{(-1)^{l'_b+m_b}}{2K+1} \langle l_a \ 0 \ l'_a - M | K - M \rangle \langle l_b \ m_b \ l'_b - M - m_b | K - M \rangle \\ &\times \sum_{l_a, l'_a, l'_b} (2l_a + 1) e^{i(\sigma^{l_a} + \sigma^{l'_a} + \sigma^{l'_b})} Y_{-M-m_b}^{l'_b}(\hat{\mathbf{k}}'_b) Y_{-M}^{l'_a}(\hat{\mathbf{k}}'_a) \mathcal{I}(l_a, l'_a, l'_b, K),\end{aligned}\quad (5.G.26)$$

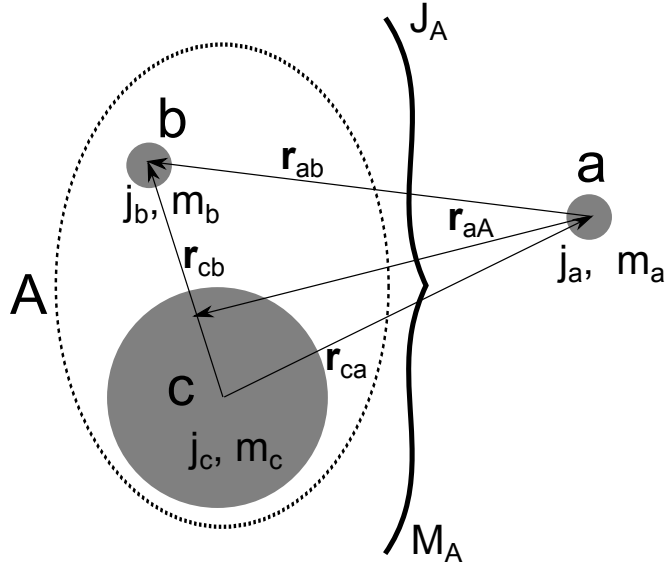


Figure 5.G.3: In the present case all three clusters a, b, c have definite spins and projections. The nucleus A is coupled to total spin J_A, M_A .

where

$$\begin{aligned} \mathcal{I}(l_a, l'_a, l'_b, K) = & \int dr_{aA} dr_{bc} d\theta r_{aA} r_{bc} \frac{\sin \theta}{r_{ac}} u_{l_b}(r_{bc}) v(r_{ab}) F_{l_a}(r_{aA}) F_{l'_a}(r_{ac}) F_{l'_b}(r_{bc}) \\ & \times \sum_{M_K} (-1)^{M_K} \langle l_a \ 0 \ l'_a \ M_K | K \ M_K \rangle [Y^{l_b}(\cos \theta, 0) Y^{l'_b}(\cos \theta, 0)]_{-M_K}^K Y^{l'_a}_{M_K}(\cos \theta_{ac}, 0) \end{aligned} \quad (5.G.27)$$

is a 3-dimensional integral that can be numerically evaluated with the help of, e.g., Gaussian integration.

5.G.2 Particles with spin

We now treat the case in which the clusters have a definite spin (see Fig. 5.G.3), and the complex optical potentials $U(r_{aA}), U(r_{cb}), U(r_{ac})$ contain now a spin-orbit term proportional to the product $\mathbf{l} \cdot \mathbf{s} = 1/2(j(j+1) - l(l+1) - 3/4)$ for particles with spin $1/2$. In addition, the interaction $V(r_{ab}, \sigma_a, \sigma_b)$ between a and b is taken to be a separable function of the distance r_{ab} and of the spin orientations, $V(r_{ab}, \sigma_a, \sigma_b) = v(r_{ab})v_\sigma(\sigma_a, \sigma_b)$. Note that this ansatz rules out spin-orbit as well

as tensor terms in the NN -interaction. For the time being we will assume that the spin-dependent interaction is rotationally invariant (scalar with respect to rotations), such as, e.g., $v_\sigma(\sigma_a, \sigma_b) \propto \sigma_a \cdot \sigma_b$. Again, this assumption excludes tensor terms in the interaction. The transition amplitude is then,

$$\begin{aligned} T_{m_a, m_b}^{m'_a, m'_b} = & \sum_{\sigma_a, \sigma_b} \int d\mathbf{r}_{aA} d\mathbf{r}_{bc} \chi_{m'_a}^{(-)*}(\mathbf{r}_{ac}, \sigma_a) \chi_{m'_b}^{(-)*}(\mathbf{r}_{bc}, \sigma_b) \\ & \times v(r_{ab}) v_\sigma(\sigma_a, \sigma_b) \chi_{m_a}^{(+)}(\mathbf{r}_{aA}, \sigma_a) \psi_{m_b}^{l_b, j_b}(\mathbf{r}_{bc}, \sigma_b). \end{aligned} \quad (5.G.28)$$

Distorted waves

The distorted waves in (5.G.28) $\chi_m(\mathbf{r}, \sigma) = \chi(\mathbf{r}) \phi_m^{1/2}(\sigma)$ have a spin dependence contained in the spinor $\phi_m^{1/2}(\sigma)$, where σ is the spin degree of freedom and m the projection of the spin along the quantization axis. The superscript $1/2$ reminds us that we are considering spin $1/2$ particles, which have important consequences when dealing with the spin-orbit term of the optical potentials. As for the spin-dependent term $v_\sigma(\sigma_a, \sigma_b)$, the actual value of the spin of particles involved in the reaction process do not make much difference, *as long as this term is rotationally invariant*. Following (5.G.4),

$$\chi^{(+)}(\mathbf{k}, \mathbf{r}) \phi_m(\sigma) = \sum_{l,j} \frac{4\pi}{kr} i^l \sqrt{2l+1} e^{i\sigma l} F_{l,j}(r) \left[Y^l(\hat{\mathbf{r}}) Y^l(\hat{\mathbf{k}}) \right]_0^0 \phi_m^{1/2}(\sigma). \quad (5.G.29)$$

Note that now one also sums over the total angular momentum j , as the radial functions $F_{l,j}(r)$ depend both on j as well as on l , in keeping with the fact that they are solutions of an optical potential containing a spin-orbit term proportional to $1/2(j(j+1) - l(l+1) - 3/4)$. One must then couple the radial and spin functions to total angular momentum j , noting that

$$\begin{aligned} \left[Y^l(\hat{\mathbf{r}}) Y^l(\hat{\mathbf{k}}) \right]_0^0 \phi_m^{1/2}(\sigma) = & \sum_{m_l} \langle l \ m_l \ | \ l - m_l | 0 \ 0 \rangle Y_{m_l}^l(\hat{\mathbf{r}}) Y_{-m_l}^l(\hat{\mathbf{k}}) \phi_m^{1/2}(\sigma) = \\ & \sum_{m_l} \frac{(-1)^{l-m_l}}{\sqrt{2l+1}} Y_{m_l}^l(\hat{\mathbf{r}}) Y_{-m_l}^l(\hat{\mathbf{k}}) \phi_m^{1/2}(\sigma), \end{aligned} \quad (5.G.30)$$

and

$$Y_{m_l}^l(\hat{\mathbf{r}}) \phi_m^{1/2}(\sigma) = \sum_j \langle l \ m_l \ | \ 1/2 \ m | j \ m_l + m \rangle \left[Y^l(\hat{\mathbf{r}}) \phi^{1/2}(\sigma) \right]_{m_l+m}^j, \quad (5.G.31)$$

we can write

$$\begin{aligned} \left[Y^l(\hat{\mathbf{r}}) Y^l(\hat{\mathbf{k}}) \right]_0^0 \phi_m^{1/2}(\sigma) = & \sum_{m_l, j} \frac{(-1)^{l+m_l}}{\sqrt{2l+1}} \langle l \ m_l \ | \ 1/2 \ m | j \ m_l + m \rangle \\ & \times \left[Y^l(\hat{\mathbf{r}}) \phi^{1/2}(\sigma) \right]_{m_l+m}^j Y_{-m_l}^l(\hat{\mathbf{k}}), \end{aligned} \quad (5.G.32)$$

and the distorted waves in (5.G.28) are

$$\begin{aligned} \chi_{m_a}^{(+)}(\mathbf{r}_{aA}, \mathbf{k}_a, \sigma_a) &= \sum_{l_a, m_{l_a}, j_a} \frac{4\pi}{k_a r_{aA}} i^{l_a} (-1)^{l_a + m_{l_a}} e^{i\sigma^{l_a}} F_{l_a, j_a}(r_{aA}) \\ &\times \langle l_a \ m_{l_a} \ 1/2 \ m_a | j_a \ m_{l_a} + m_a \rangle [Y^{l_a}(\hat{\mathbf{r}}_{aA}) \phi^{1/2}(\sigma_a)]_{m_{l_a} + m_a}^{j_a} Y_{-m_{l_a}}^{l_a}(\hat{\mathbf{k}}_a), \end{aligned} \quad (5.G.33)$$

$$\begin{aligned} \chi_{m'_b}^{(-)*}(\mathbf{r}_{bc}, \mathbf{k}'_b, \sigma_b) &= \sum_{l'_b, m_{l'_b}, j'_b} \frac{4\pi}{k'_b r_{bc}} i^{-l'_b} (-1)^{l'_b + m_{l'_b}} e^{i\sigma^{l'_b}} F_{l'_b, j'_b}(r_{bc}) \\ &\times \langle l'_b \ m_{l'_b} \ 1/2 \ m'_b | j'_b \ m_{l'_b} + m'_b \rangle [Y^{l'_b}(\hat{\mathbf{r}}_{bc}) \phi^{1/2}(\sigma_b)]_{m_{l'_b} + m'_b}^{j'_b*} Y_{-m_{l'_b}}^{l'_b*}(\hat{\mathbf{k}}'_b), \end{aligned} \quad (5.G.34)$$

$$\begin{aligned} \chi_{m'_a}^{(-)*}(\mathbf{r}_{ac}, \mathbf{k}'_a, \sigma_a) &= \sum_{l'_a, m_{l'_a}, j'_a} \frac{4\pi}{k'_a r_{ac}} i^{-l'_a} (-1)^{l'_a + m_{l'_a}} e^{i\sigma^{l'_a}} F_{l'_a, j'_a}(r_{ac}) \\ &\times \langle l'_a \ m_{l'_a} \ 1/2 \ m'_a | j'_a \ m_{l'_a} + m'_a \rangle [Y^{l'_a}(\hat{\mathbf{r}}_{ac}) \phi^{1/2}(\sigma_a)]_{m_{l'_a} + m'_a}^{j'_a*} Y_{-m_{l'_a}}^{l'_a*}(\hat{\mathbf{k}}'_a). \end{aligned} \quad (5.G.35)$$

The initial bound particle b wavefunction is

$$\psi_{m_b}^{l_b, j_b}(\mathbf{r}_{bc}, \sigma_b) = u_{l_b, j_b}(r_{bc}) [Y^{l_b}(\hat{\mathbf{r}}_{bc}) \phi^{1/2}(\sigma_b)]_{m_b}^{j_b}, \quad (5.G.36)$$

Substituting in (5.G.28), one obtains,

$$\begin{aligned} T_{m_a, m_b}^{m'_a, m'_b}(\mathbf{k}'_a, \mathbf{k}'_b) &= \frac{64\pi^3}{k_a k'_a k'_b} \sum_{\sigma_a, \sigma_b} \sum_{l_a, m_{l_a}, j_a} \sum_{l'_a, m_{l'_a}, j'_a} \sum_{l'_b, m_{l'_b}, j'_b} e^{i(\sigma^{l_a} + \sigma^{l'_a} + \sigma^{l'_b})} i^{l_a - l'_a - l'_b} (-1)^{l_a - m_{l_a} + l'_a - j'_a + l'_b - j'_b} \\ &\times \langle l'_a \ m_{l'_a} \ 1/2 \ m'_a | j'_a \ m_{l'_a} + m'_a \rangle \langle l_a \ m_{l_a} \ 1/2 \ m_a | j_a \ m_{l_a} + m_a \rangle \langle l'_b \ m_{l'_b} \ 1/2 \ m'_b | j'_b \ m_{l'_b} + m'_b \rangle \\ &\times Y_{-m_{l_a}}^{l_a}(\hat{\mathbf{k}}_a) Y_{-m_{l'_a}}^{l'_a}(\hat{\mathbf{k}}'_a) Y_{-m_{l'_b}}^{l'_b}(\hat{\mathbf{k}}'_b) \int d\mathbf{r}_{aA} d\mathbf{r}_{bc} [Y^{l'_a}(\hat{\mathbf{r}}_{ac}) \phi^{1/2}(\sigma_a)]_{-m_{l'_a} - m'_a}^{j'_a} [Y^{l'_b}(\hat{\mathbf{r}}_{bc}) \phi^{1/2}(\sigma_b)]_{-m_{l'_b} - m'_b}^{j'_b} \\ &\times \frac{F_{l_a, j_a}(r_{aA}) F_{l'_a, j'_a}(r_{ac}) F_{l'_b, j'_b}(r_{bc})}{r_{ac} r_{aA} r_{bc}} u_{l_b, j_b}(r_{bc}) v(r_{ab}) v_\sigma(\sigma_a, \sigma_b) \\ &\times [Y^{l_a}(\hat{\mathbf{r}}_{aA}) \phi^{1/2}(\sigma_a)]_{m_{l_a} + m_a}^{j_a} [Y^{l_b}(\hat{\mathbf{r}}_{bc}) \phi^{1/2}(\sigma_b)]_{m_b}^{j_b}, \end{aligned} \quad (5.G.37)$$

where use was made of the relation

$$[Y^l(\hat{\mathbf{r}}) \phi^{1/2}(\sigma)]_m^{j*} = (-1)^{j-m} [Y^l(\hat{\mathbf{r}}) \phi^{1/2}(\sigma)]_{-m}^j. \quad (5.G.38)$$

Recoupling of angular momenta

Let us now separate spatial and spin coordinates, noting that the spin functions must be coupled to $S = 0$, a consequence of the fact that the interaction $v_\sigma(\sigma_a, \sigma_b)$ is rotationally invariant. Starting with particle a ,

$$\begin{aligned} & \left[Y^{l'_a}(\hat{\mathbf{r}}_{ac}) \phi^{1/2^*}(\sigma_a) \right]_{-m_{l'_a}-m'_a}^{j'_a} \left[Y^{l_a}(\hat{\mathbf{r}}_{aA}) \phi^{1/2}(\sigma_a) \right]_{m_{l_a}+m_a}^{j_a} = \\ & \quad \sum_K ((l'_a \frac{1}{2})_{j'_a} (l_a \frac{1}{2})_{j_a} | (l_a l'_a)_K (\frac{1}{2} \frac{1}{2})_0)_K \\ & \quad \times \left[Y^{l'_a}(\hat{\mathbf{r}}_{ac}) Y^{l_a}(\hat{\mathbf{r}}_{aA}) \right]_{-m_{l'_a}-m'_a+m_{l_a}+m_a}^K \left[\phi^{1/2^*}(\sigma_a) \phi^{1/2}(\sigma_a) \right]_0^0. \end{aligned} \quad (5.G.39)$$

For particle b ,

$$\begin{aligned} & \left[Y^{l'_b}(\hat{\mathbf{r}}_{bc}) \phi^{1/2^*}(\sigma_b) \right]_{-m_{l'_b}-m'_b}^{j'_b} \left[Y^{l_b}(\hat{\mathbf{r}}_{bc}) \phi^{1/2}(\sigma_b) \right]_{m_b}^{j_b} = \\ & \quad \sum_{K'} ((l'_b \frac{1}{2})_{j'_b} (l_b \frac{1}{2})_{j_b} | (l_b l'_b)_{K'} (\frac{1}{2} \frac{1}{2})_0)_{K'} \\ & \quad \times \left[Y^{l'_b}(\hat{\mathbf{r}}_{bc}) Y^{l_b}(\hat{\mathbf{r}}_{bc}) \right]_{-m_{l'_b}-m'_b+m_b}^{K'} \left[\phi^{1/2^*}(\sigma_b) \phi^{1/2}(\sigma_b) \right]_0^0. \end{aligned} \quad (5.G.40)$$

The spin summation yields a constant factor,

$$\sum_{\sigma_a, \sigma_b} \left[\phi^{1/2^*}(\sigma_a) \phi^{1/2}(\sigma_a) \right]_0^0 \left[\phi^{1/2^*}(\sigma_b) \phi^{1/2}(\sigma_b) \right]_0^0 v_\sigma(\sigma_a, \sigma_b) \equiv T_\sigma, \quad (5.G.41)$$

and what we have yet to do is very similar to what we have done in the case of spinless particles. First of all note that the constrain of coupling all angular momenta to 0, imposes $K' = K$ and $m_{l_a} + m_a - m_{l'_a} - m'_a = m_{l'_b} + m'_b - m_b$ (see (5.G.39) and (5.G.40)). If we set $M = m_{l_a} + m_a - m_{l'_a} - m'_a$ and take, as before, $\hat{\mathbf{k}}_a \equiv \hat{z}$

$$\begin{aligned} T_{m_a, m_b}^{m'_a, m'_b}(\mathbf{k}'_a, \mathbf{k}'_b) &= \frac{32\pi^{5/2}}{k_a k'_a k'_b} T_\sigma \sum_{l_a, j_a} \sum_{l'_a, j'_a} \sum_{l'_b, j'_b} \sum_{K, M} e^{i(\sigma^{l_a} + \sigma^{l'_a} + \sigma^{l'_b})} i^{l_a - l'_a - l'_b} (-1)^{l_a + l'_a + l'_b - j'_a - j'_b} \\ & \quad \times \sqrt{2l_a + 1} ((l'_a \frac{1}{2})_{j'_a} (l_a \frac{1}{2})_{j_a} | (l_a l'_a)_K (\frac{1}{2} \frac{1}{2})_0)_K ((l'_b \frac{1}{2})_{j'_b} (l_b \frac{1}{2})_{j_b} | (l_b l'_b)_K (\frac{1}{2} \frac{1}{2})_0)_K \\ & \quad \times \langle l'_a m_a - m'_a - M \rangle \langle l'_a m'_a | j'_a m_a - M \rangle \langle l_a 0 \rangle \langle l_a 1/2 m_a | j_a m_a \rangle \langle l'_b m_b - m'_b + M \rangle \langle l'_b m'_b | j'_b M + m_b \rangle \\ & \quad \times Y_{m'_b - m_b - M}^{l'_b}(\hat{\mathbf{k}}'_b) Y_{m'_a - m_a + M}^{l'_a}(\hat{\mathbf{k}}'_a) \int d\mathbf{r}_{aA} d\mathbf{r}_{bc} \frac{F_{l_a, j_a}(r_{aA}) F_{l'_a, j'_a}(r_{ac}) F_{l'_b, j'_b}(r_{bc})}{r_{ac} r_{aA} r_{bc}} \\ & \quad \times u_{l_b, j_b}(r_{bc}) v(r_{ab}) \left[Y^{l_a}(\hat{\mathbf{r}}_{aA}) Y^{l'_a}(\hat{\mathbf{r}}_{ac}) \right]_M^K \left[Y^{l_b}(\hat{\mathbf{r}}_{bc}) Y^{l'_b}(\hat{\mathbf{r}}_{bc}) \right]_{-M}^K. \end{aligned} \quad (5.G.42)$$

The integral of the above expression is similar to the one in (5.G.18), so we obtain

$$\begin{aligned}
 T_{m_a, m_b}^{m'_a, m'_b}(\mathbf{k}'_a, \mathbf{k}'_b) = & \frac{128\pi^4}{k_a k'_a k'_b} T_\sigma \sum_{l_a, j_a} \sum_{l'_a, j'_a} \sum_{l'_b, j'_b} \sum_{K, M} e^{i(\sigma^{l_a} + \sigma^{l'_a} + \sigma^{l'_b})} i^{l_a - l'_a - l'_b} (-1)^{l_a + l'_a + l'_b - j'_a - j'_b} \\
 & \times \frac{2l_a + 1}{2K + 1} ((l'_a \frac{1}{2})_{j'_a} (l_a \frac{1}{2})_{j_a} | (l_a l'_a)_K (\frac{1}{2} \frac{1}{2})_0)_K ((l'_b \frac{1}{2})_{j'_b} (l_b \frac{1}{2})_{j_b} | (l_b l'_b)_K (\frac{1}{2} \frac{1}{2})_0)_K \\
 & \times \langle l'_a m_a - m'_a - M 1/2 m'_a | j'_a m_a - M \rangle \langle l'_b m_b - m'_b + M 1/2 m'_b | j'_b M + m_b \rangle \\
 & \times \langle l_a 0 1/2 m_a | j_a m_a \rangle Y_{m'_b - m_b - M}^{l'_b}(\hat{\mathbf{k}}'_b) Y_{m_a - m'_a + M}^{l'_a}(\hat{\mathbf{k}}'_a) \mathcal{I}(l_a, l'_a, l'_b, j_a, j'_a, j'_b, K),
 \end{aligned} \tag{5.G.43}$$

with

$$\begin{aligned}
 \mathcal{I}(l_a, l'_a, l'_b, j_a, j'_a, j'_b, K) = & \int dr_{aA} dr_{bc} d\theta r_{aA} r_{bc} \frac{\sin \theta}{r_{ac}} u_{l_b}(r_{bc}) v(r_{ab}) \\
 & \times F_{l_a, j_a}(r_{aA}) F_{l'_a, j'_a}(r_{ac}) F_{l'_b, j'_b}(r_{bc}) \\
 & \times \sum_{M_K} \langle l_a 0 l'_a M_K | K M_K \rangle \left[Y^{l_b}(\cos \theta, 0) Y^{l'_b}(\cos \theta, 0) \right]_{-M_K}^K Y_{M_K}^{l'_a}(\cos \theta_{ac}, 0). \tag{5.G.44}
 \end{aligned}$$

Again, this is a 3-dimensional integral that can be evaluated with the method of Gaussian quadratures. The transition amplitude $T_{m_a, m_b}^{m'_a, m'_b}(\mathbf{k}'_a, \mathbf{k}'_b)$ depends explicitly on the initial (m_a, m'_a) and final (m'_a, m'_b) polarizations of a, b . If the particle b is initially coupled to core c to total angular momentum J_A, M_A , the amplitude to be considered is rather

$$T_{m_a}^{m'_a, m'_b}(\mathbf{k}'_a, \mathbf{k}'_b) = \sum_{m_b} \langle j_b m_b j_c M_A - m_b | J_A M_A \rangle T_{m_a, m_b}^{m'_a, m'_b}(\mathbf{k}'_a, \mathbf{k}'_b), \tag{5.G.45}$$

and the multi-differential cross section for detecting particle c (or a) is

$$\frac{d\sigma}{d\mathbf{k}'_a d\mathbf{k}'_b} \Big|_{m_a}^{m'_a, m'_b} = \frac{k'_a}{k_a} \frac{\mu_{aA} \mu_{ac}}{4\pi^2 \hbar^4} \left| \sum_{m_b} \langle j_b m_b j_c M_A - m_b | J_A M_A \rangle T_{m_a, m_b}^{m'_a, m'_b}(\mathbf{k}'_a, \mathbf{k}'_b) \right|^2. \tag{5.G.46}$$

All spin-polarization observables (analysing powers, etc.,) can be derived from this expression. But let us now work out the expression of the cross section for an unpolarized beam (sum over initial spin orientations divided by the number of such orientations) and when we do not detect the final polarizations (sum over final spin orientations),

$$\begin{aligned}
 \frac{d\sigma}{d\mathbf{k}'_a d\mathbf{k}'_b} = & \frac{k'_a}{k_a} \frac{\mu_{aA} \mu_{ac}}{4\pi^2 \hbar^4} \frac{1}{(2J_A + 1)(2j_a + 1)} \\
 & \times \sum_{\substack{m_a, m'_a \\ M_A, m'_b}} \left| \sum_{m_b} \langle j_b m_b j_c M_A - m_b | J_A M_A \rangle T_{m_a, m_b}^{m'_a, m'_b}(\mathbf{k}'_a, \mathbf{k}'_b) \right|^2. \tag{5.G.47}
 \end{aligned}$$

The sum above can be simplified a bit. Let us consider a single particular value of m_b in the sum over m_b ,

$$\begin{aligned} \sum_{m_a, m'_a, m'_b} & \left| T_{m_a, m_b}^{m'_a, m'_b}(\mathbf{k}'_a, \mathbf{k}'_b) \right|^2 \sum_{M_A} \left| \langle j_b \ m_b \ j_c \ M_A - m_b | J_A \ M_A \rangle \right|^2 = \\ & \frac{2J_A + 1}{2j_b + 1} \sum_{m_a, m_a, m'_b} \left| T_{m_a, m_b}^{m'_a, m'_b}(\mathbf{k}'_a, \mathbf{k}'_b) \right|^2 \\ & \times \sum_{M_A} \left| \langle J_A - M_A \ j_c \ M_A - m_b | j_b \ m_b \rangle \right|^2, \end{aligned} \quad (5.G.48)$$

where we have used

$$\langle j_b \ m_b \ j_c \ M_A - m_b | J_A \ M_A \rangle = (-1)^{j_c - M_A + m_b} \sqrt{\frac{2J_A + 1}{2j_b + 1}} \langle J_A - M_A \ j_c \ M_A - m_b | j_b \ m_b \rangle. \quad (5.G.49)$$

As

$$\sum_{M_A} \left| \langle J_A - M_A \ j_c \ M_A - m_b | j_b \ m_b \rangle \right|^2 = 1, \quad (5.G.50)$$

we finally have

$$\frac{d\sigma}{d\mathbf{k}'_a d\mathbf{k}'_b} = \frac{k'_a}{k_a} \frac{\mu_{aA} \mu_{ac}}{4\pi^2 \hbar^4} \frac{1}{(2j_b + 1)(2j_a + 1)} \sum_{m_a, m'_a, m'_b} \left| \sum_{m_b} T_{m_a, m_b}^{m'_a, m'_b}(\mathbf{k}'_a, \mathbf{k}'_b) \right|^2. \quad (5.G.51)$$

Zero range approximation.

The zero range approximation consists in taking $v(r_{ab}) = D_0 \delta(r_{ab})$. Then, (see (5.G.21))

$$\begin{aligned} \mathbf{r}_{aA} &= \frac{c}{A} \mathbf{r}_{bc}, \\ \mathbf{r}_{ac} &= \mathbf{r}_{bc}. \end{aligned} \quad (5.G.52)$$

The angular dependence of the integral can be readily evaluated. From (6.D.20), noting that $\hat{\mathbf{r}}_{aA} = \hat{\mathbf{r}}_{ac} = \hat{\mathbf{r}}_{bc} \equiv \hat{\mathbf{r}}$,

$$\begin{aligned} & \left[Y^{l_a}(\hat{\mathbf{r}}) Y^{l'_a}(\hat{\mathbf{r}}) \right]_M^K \left[Y^{l_b}(\hat{\mathbf{r}}) Y^{l'_b}(\hat{\mathbf{r}}) \right]_{-M}^K = \\ & \frac{(-1)^{K-M}}{\sqrt{2K+1}} \left\{ \left[Y^{l_a}(\hat{\mathbf{r}}) Y^{l'_a}(\hat{\mathbf{r}}) \right]_M^K \left[Y^{l_b}(\hat{\mathbf{r}}) Y^{l'_b}(\hat{\mathbf{r}}) \right]_0^K \right\}_0^0. \end{aligned} \quad (5.G.53)$$

We can as before evaluate this expression in the configuration shown in Fig. 5.G.2 ($\hat{\mathbf{r}} = \hat{z}$), but now the multiplicative factor is 4π . The corresponding contribution to the integral is

$$\frac{(-1)^K}{4\pi(2K+1)} \langle l_a \ 0 \ l'_a \ 0 | K \ 0 \rangle \sqrt{(2l_a + 1)(2l'_a + 1)(2l_b + 1)(2l'_b + 1)}, \quad (5.G.54)$$

and

$$\begin{aligned}
T_{m_a, m_b}^{m'_a, m'_b}(\mathbf{k}'_a, \mathbf{k}'_b) = & \frac{16\pi^2}{k_a k'_a k'_b A} D_0 T_\sigma \sum_{l_a, j_a} \sum_{l'_a, j'_a} \sum_{l'_b, j'_b} \sum_{K, M} e^{i(\sigma^{l_a} + \sigma^{l'_a} + \sigma^{l'_b})} i^{l_a - l'_a - l'_b} (-1)^{l_a + l'_a + l'_b - j'_a - j'_b} \\
& \times \sqrt{(2l_a + 1)(2l'_a + 1)(2l_b + 1)(2l'_b + 1)} \langle l_a 0 l'_a 0 | K 0 \rangle \\
& \times \frac{2l_a + 1}{2K + 1} ((l'_a \frac{1}{2})_{j'_a} (l_a \frac{1}{2})_{j_a} | (l_a l'_a)_K (\frac{1}{2} \frac{1}{2})_0)_K ((l'_b \frac{1}{2})_{j'_b} (l_b \frac{1}{2})_{j_b} | (l_b l'_b)_K (\frac{1}{2} \frac{1}{2})_0)_K \\
& \times \langle l'_a m_a - m'_a - M 1/2 m'_a | j'_a m_a - M \rangle \langle l'_b m_b - m'_b + M 1/2 m'_b | j'_b M + m_b \rangle \\
& \times \langle l 0 1/2 m_a | j m_a \rangle Y_{M+m_b+m'_b}^{l'_b}(\hat{\mathbf{k}}'_b) Y_{m_a+m'_a-M}^{l'_a}(\hat{\mathbf{k}}'_a) \mathcal{I}_{ZR}(l_a, l'_a, l'_b, j_a, j'_a, j'_b), \quad (5.G.55)
\end{aligned}$$

where now the 1-dimensional integral to solve is

$$\mathcal{I}_{ZR}(l_a, l'_a, l'_b, j_a, j'_a, j'_b) = \int dr u_{l_b}(r) F_{l_a, j_a}(\frac{c}{A} r) F_{l'_a, j'_a}(r) F_{l'_b, j'_b}(r)/r. \quad (5.G.56)$$

5.G.3 One-particle transfer

It may be interesting to state the expression for the one particle transfer reaction within the same context and using the same elements, in order to better compare these two type of experiments. In particle transfer, the final state of b is a bound state of the $B (= a + b)$ nucleus (cf. Fig. 7.G.4), and we can carry on in a similar way as done previously just by substituting the distorted wave (continuum) wave function (5.G.34) with

$$\psi_{m'_b}^{l'_b, j'_b*}(\mathbf{r}_{ab}, \sigma_b) = u_{l'_b, j'_b}^*(r_{ab}) \left[Y^{l'_b}(\hat{\mathbf{r}}_{ab}) \phi^{1/2}(\sigma_b) \right]_{m'_b}^{j'_b*}, \quad (5.G.57)$$

so the transition amplitude is now

$$\begin{aligned}
T_{m_a, m_b}^{m'_a, m'_b}(\mathbf{k}'_a) = & \frac{8\pi^{3/2}}{k_a k'_a} \sum_{\sigma_a, \sigma_b} \sum_{l_a, j_a} \sum_{l'_a, m_{l'_a}, j'_a} e^{i(\sigma^{l_a} + \sigma^{l'_a})} i^{l_a - l'_a} (-1)^{l_a + l'_a - j'_a - j'_b} \\
& \times \sqrt{2l_a + 1} \langle l'_a m_{l'_a} 1/2 m'_a | j'_a m_{l'_a} + m'_a \rangle \langle l_a 0 1/2 m_a | j_a m_a \rangle \\
& \times Y_{-m_{l'_a}}^{l'_a}(\hat{\mathbf{k}}'_a) \int d\mathbf{r}_{aA} d\mathbf{r}_{bc} \left[Y^{l'_a}(\hat{\mathbf{r}}_{bc}) \phi^{1/2}(\sigma_a) \right]_{-m_{l'_a} - m'_a}^{j'_a} \left[Y^{l'_b}(\hat{\mathbf{r}}_{ab}) \phi^{1/2}(\sigma_b) \right]_{-m'_b}^{j'_b} \\
& \times \frac{F_{l_a, j_a}(r_{aA}) F_{l'_a, j'_a}(r_{bc})}{r_{bc} r_{aA}} u_{l'_b, j'_b}^*(r_{ab}) u_{l_b, j_b}(r_{bc}) v(r_{ab}) v_\sigma(\sigma_a, \sigma_b) \\
& \times \left[Y^{l_a}(\hat{\mathbf{r}}_{aA}) \phi^{1/2}(\sigma_a) \right]_{m_a}^{j_a} \left[Y^{l_b}(\hat{\mathbf{r}}_{bc}) \phi^{1/2}(\sigma_b) \right]_{m_b}^{j_b}. \quad (5.G.58)
\end{aligned}$$

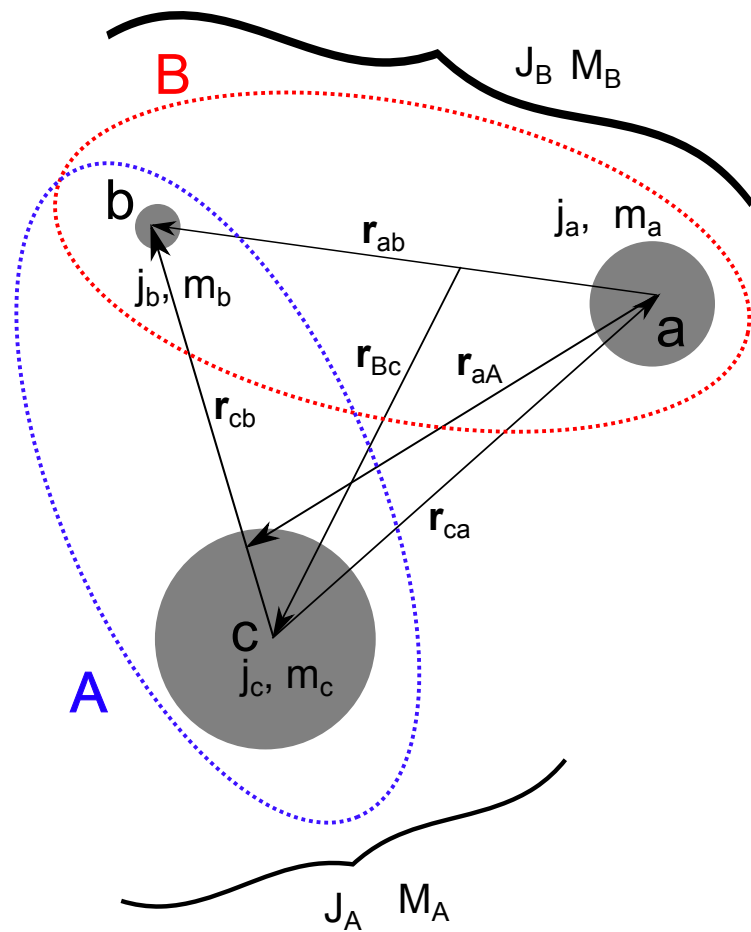


Figure 5.G.4: One particle transfer reaction $A(= c + b) + a \rightarrow B(= a + b) + c$.

Using (5.G.39), (5.G.40), (6.F.4), and setting $M = m_a - m'_a - m_{l'_a}$

$$\begin{aligned} T_{m_a, m_b}^{m'_a, m'_b}(\mathbf{k}'_a) &= \frac{8\pi^{3/2}}{k_a k'_a} T_\sigma \sum_{l_a, j_a} \sum_{l'_a, j'_a} \sum_{K, M} e^{i(\sigma^{l_a} + \sigma^{l'_a}) l_a - l'_a} (-1)^{l_a + l'_a - j'_a - j'_b} \\ &\times ((l'_a \frac{1}{2})_{j'_a} (l_a \frac{1}{2})_{j_a} | (l_a l'_a)_K (\frac{1}{2} \frac{1}{2})_0)_K ((l'_b \frac{1}{2})_{j'_b} (l_b \frac{1}{2})_{j_b} | (l_b l'_b)_K (\frac{1}{2} \frac{1}{2})_0)_K \\ &\times \sqrt{2l_a + 1} \langle l'_a m_a - m'_a - M 1/2 m'_a | j'_a m_a - M \rangle \langle l_a 0 1/2 m_a | j_a m_a \rangle \\ &\times Y_{m_a - m'_a - M}^{l'_a}(\hat{\mathbf{k}}'_a) \int d\mathbf{r}_{aA} d\mathbf{r}_{bc} \frac{F_{l_a, j_a}(r_{aA}) F_{l'_a, j'_a}(r_{bc})}{r_{bc} r_{aA}} u_{l'_b, j'_b}^*(r_{ab}) u_{l_b, j_b}(r_{bc}) v(r_{ab}) \\ &\times [Y^{l_a}(\hat{\mathbf{r}}_{aA}) Y^{l'_a}(\hat{\mathbf{r}}_{bc})]_M^K [Y^{l_b}(\hat{\mathbf{r}}_{bc}) Y^{l'_b}(\hat{\mathbf{r}}_{ab})]_{-M}^K. \quad (5.G.59) \end{aligned}$$

Aside from (5.G.21), we also need

$$\mathbf{r}_{Bc} = \frac{a+B}{B} \mathbf{r}_{aA} + \frac{b}{A} \mathbf{r}_{bc}. \quad (5.G.60)$$

From (5.G.20–5.G.25), one gets

$$\begin{aligned} T_{m_a, m_b}^{m'_a, m'_b}(\mathbf{k}'_a) &= \frac{32\pi^3}{k_a k'_a} T_\sigma \sum_{l_a, j_a} \sum_{l'_a, j'_a} \sum_{K, M} e^{i(\sigma^{l_a} + \sigma^{l'_a}) l_a - l'_a} (-1)^{l_a + l'_a - j'_a - j'_b} \\ &\times ((l'_a \frac{1}{2})_{j'_a} (l_a \frac{1}{2})_{j_a} | (l_a l'_a)_K (\frac{1}{2} \frac{1}{2})_0)_K ((l'_b \frac{1}{2})_{j'_b} (l_b \frac{1}{2})_{j_b} | (l_b l'_b)_K (\frac{1}{2} \frac{1}{2})_0)_K \\ &\times \frac{2l_a + 1}{2K + 1} \langle l'_a m_a - m'_a - M 1/2 m'_a | j'_a m_a - M \rangle \\ &\times \langle l_a 0 1/2 m_a | j_a m_a \rangle Y_{m_a - m'_a - M}^{l'_a}(\hat{\mathbf{k}}'_a) I(l_a, l'_a, j_a, j'_a, j'_b, K), \quad (5.G.61) \end{aligned}$$

with

$$\begin{aligned} I(l_a, l'_a, j_a, j'_a, K) &= \int dr_{aA} dr_{bc} d\theta r_{aA} r_{bc}^2 \frac{\sin \theta}{r_{bc}} \\ &\times F_{l_a, j_a}(r_{aA}) F_{l'_a, j'_a}(r_{ac}) u_{l'_b, j'_b}^*(r_{ab}) u_{l_b, j_b}(r_{bc}) v(r_{ab}) \\ &\times \sum_{M_K} \langle l_a 0 l'_a M_K | K M_K \rangle [Y^{l_b}(\cos \theta, 0) Y^{l'_b}(\cos \theta_{ab}, 0)]_{-M_K}^K Y_{M_K}^{l'_a}(\cos \theta_{Bc}, 0), \quad (5.G.62) \end{aligned}$$

where (see (5.G.21), (5.G.60) and Fig. 5.G.2)

$$\cos \theta_{ab} = \frac{-r_{aA} - \frac{c}{A} r_{bc} \cos \theta}{\sqrt{\left(\frac{c}{A} r_{bc} \sin \theta\right)^2 + \left(r_{aA} + \frac{c}{A} r_{bc} \cos \theta\right)^2}}, \quad (5.G.63)$$

$$\cos \theta_{Bc} = \frac{\frac{a+B}{B} r_{aA} + \frac{b}{A} r_{bc} \cos \theta}{\sqrt{\left(\frac{b}{A} r_{bc} \sin \theta\right)^2 + \left(\frac{a+B}{B} r_{aA} + \frac{b}{A} r_{bc} \cos \theta\right)^2}}, \quad (5.G.64)$$

and

$$r_{Bc} = \sqrt{\left(\frac{b}{A}r_{bc}\sin\theta\right)^2 + \left(\frac{a+B}{B}r_{aA} + \frac{b}{A}r_{bc}\cos\theta\right)^2}. \quad (5.G.65)$$

By the way, (5.G.61) can also be used when particle b populates a resonant state in the continuum of nucleus B .

Appendix 5.H Dynamical shell model in a nutshell

In the extreme shell model the nucleons move independently, feeling the presences of the other nucleons when bouncing elastically off the nuclear surface of the average potential. The properly normalized probability for removing a nucleon from such orbitals is equal to 1 for ω equal to the (unperturbed) energy of the orbital in question and zero otherwise (see Fig. 5.H.1).

In the dynamical shell model⁴⁶, the nucleons can bounce inelastically off the nuclear surface setting the nucleus in a vibrational state and changing their state of motion. In this case the strength of the levels becomes, in general, distributed over a range of energies both below and above the Fermi energy. That is, the state k is found both in the system $(A - 1)$ produced in a pick-up process and in the system $(A + 1)$ populated through a stripping reaction as indicated in Fig 5.H.1 (b).

It is still an open question whether this distribution is concentrated in discrete states or displays a continuous behavior. Both situations can in principle be found depending of whether the original single-particle state is close or far away from the Fermi energy. The sum of the strength functions associated with all the states excited in the pick-up process of a nucleon with quantum numbers k gives the occupation number associated with the orbital, i.e. $\int_{-\infty}^{\epsilon_F} S_h(k; \omega) d\omega = n_k$, where S_h is the (hole) strength function. The full single-particle strength is found adding to this quantity the spectroscopic factors associated with the excitation of states in the $(A + 1)$ system where a particle with quantum numbers k is deposited in the target.

It is noted that the fact that in the dynamical shell model the single-particle strength is distributed not only over an energy range in the $(A - 1)$ system but also in the $(A + 1)$ system is intimately connected with the ground state correlations associated with the vibrational modes which produce particle-hole excitations in the ground state (also pair addition and subtraction modes). In this way single-particle states which originally were filled become partially empty, and vice versa.

The transfer process shown in (b) for both stripping and pick-up reactions are closely associated with the polarization and correlation contributions to the mass operator $\mathcal{M}(k; \omega) = \mathcal{V}(k; \omega) + i\mathcal{W}(k; \omega)$ (Fig. 5.B.1). The associated total strength

⁴⁶Mahaux et al. (1985) and references therein.

distribution

$$\begin{aligned} S(k; \omega) &= S_h(k; \omega) + S_p(k; \omega), \\ &= \frac{1}{2\pi} \frac{\mathcal{W}(k; \omega) + \Delta}{(E_k + \mathcal{V}(k; \omega) - E)^2 + \frac{1}{4}(\mathcal{W}(k; \omega) + \Delta)^2}, \end{aligned} \quad (5.H.1)$$

can display a variety of shapes, as $\mathcal{V}(k; \omega)$ and $\mathcal{W}(k; \omega)$ are energy dependent.

The intermediate states of the polarization and correlation diagrams which in the present discussion are the doorway states to the renormalization of the single-particle motion must be mixed with more complicated configurations. The mechanism for these couplings and their consequences are quite involved and, to some extent, open problems. Thus, the extension in the complex plane of the associated expressions in terms of an imaginary parameter Δ is made to take these effects into account in some average way. In any case, most of the results are not dependent on the detailed value this quantity has.

The picture shown in Fig. 5.H.1 (b) although accurate and controlled by only few parameters is much too rich as compared to the originally extreme shell model picture.

A major simplification can be achieved recognizing that the essential difference between the situation depicted in Figs 5.H.1 (a) and (b) is the value of the mean free path. In the first case it is infinite while in the second it is finite. That is, due to the coupling to the surface modes (and eventually pair modes) single-particle motion acquires a lifetime. In other terms, the coupling to doorway states leads to a breaking of the single-particle strength (see e.g. Fig. 5.2.3). The associated energy range (width Γ), over which this phenomenon takes place, provides insight into the time it takes for the different components to come out of phase ($\approx \hbar/\Gamma$).

Making the ansatz that the single-particle motion decays exponentially a Breit-Wigner shape can be fitted to the different strength concentration resulting from the detailed calculation (Fig. 5.H.1 (b)) The centroid of the corresponding peaks can be viewed as the energy of the dressed single-particle state. On the other hand, caution should be exercised in interpreting the area under the fitted curve as a spectroscopic factor, if only because this quantity can become larger than one (Fig. 5.H.1 (c)). It is only for the levels not too far away from the Fermi energy that such interpretation can be reasonably accurate.

Another quantity which can be used to characterize the dressed single-particle states is the rate of change of the energy shift as a function of the energy, i.e. the effective mass. Again, for the orbitals close to the Fermi energy this quantity is inversely proportional to the area under the Breit-Wigner shapes. The energy range over which the effective mass deviates from one determine the region where the dynamical couplings change the density of single-particle levels.

The trend of the effective masses shown in Fig. 5.H.1 (d) can be quantitatively understood as follows. For single-particle states close to the Fermi energy the intermediate states have all energies larger than the unperturbed single-particle energy, and the resulting shape is δ -like with a tail extending away from the Fermi energy.

For single-particle orbitals 5–7 MeV away from ϵ_F there are a number of intermediate states which have the same energy of the initial state leading to vanishing energy denominators and thus to a marked structure in the strength function. Finally, for single-particle states far away from ϵ_F , the density of intermediate states is so large that the matrix elements of these couplings average out to a constant with a value much larger than typical distances between successive intermediate states. These are the conditions which lead to a Breit–Wigner shape.

It is then to be expected that the single-particle levels in the intermediate region will be associated with strength functions which deviate much from a smooth function and for which comparatively large errors can be made through a Breit–Wigner fitting. This is also seen from Fig. 5.H.1 (d) where the effective mass becomes smaller than one, indicating that the area of the fitted shapes are larger than that of the original strength function $S(k; \omega)$. This result emphasizes the difficulties found in trying to translate effective masses into spectroscopic factors in a general situation.

Starting from the extreme picture shown in Fig. 5.H.1 (a) where the relation $\omega = \hbar^2 k^2 / 2m$ holds, one arrives at the picture (c) where the relation $d\omega = \hbar^2 k \delta k / m^*$ again accounts for the main properties of the single-particle motion and where the effect of the couplings are contained in m^* (see Eq. (5.A.3)). The numerical implementation of the single-particle self-energies scenario have been carried out for different regions of the mass table. In particular, for the valence levels of ^{208}Pb . In this case the mass operator associated with each orbital was calculated as a function of the energy. The numerical derivative of the real part of the mass operator was then calculated and the ω -dependent effective mass obtained as a function of the energy.

The question then arises of how to define an average quantity which depends only on the energy of the orbital and is state independent. Rather different prescriptions have been used to deal with the question. In any case the main result obtained was that the ω -dependent effective mass shows a well defined peak at the Fermi surface, its maximum value being considerably larger than one (≈ 1.4). The associated full width at half maximum is of the order of 10 MeV (i.e. ± 5 MeV around ϵ_F). This quantity is much smaller than the Fermi energy (~ 36 MeV) and is essentially determined by the energy of the low-lying collective modes and of the single-particle gap around closed shell system, e.g. ^{208}Pb .

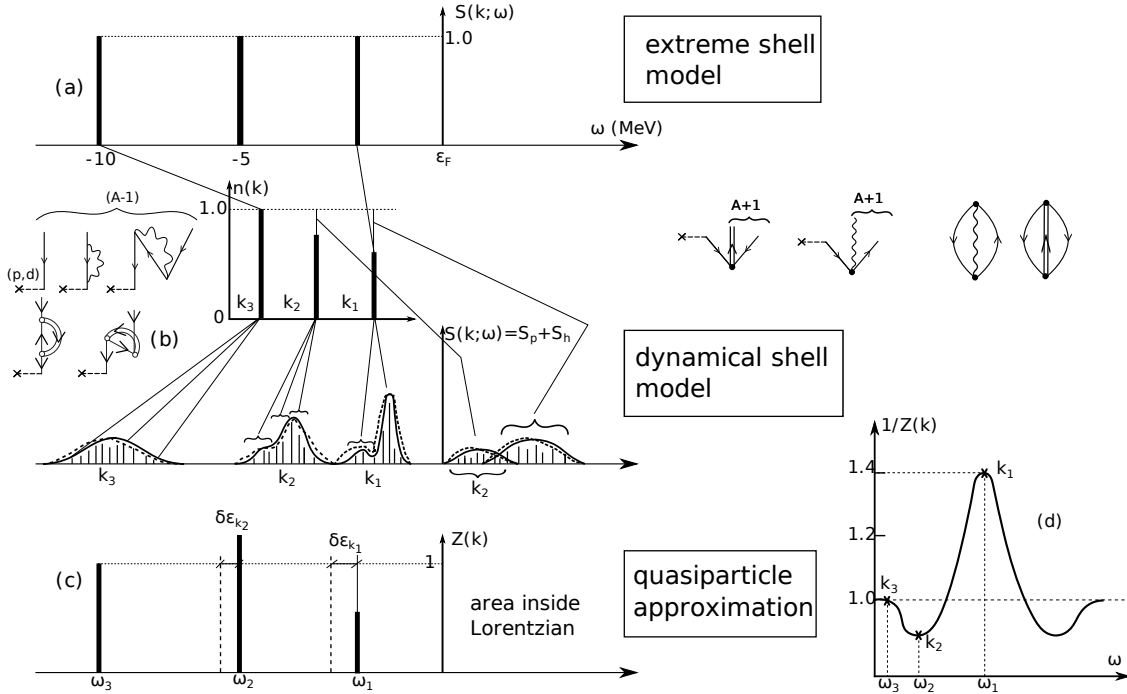


Figure 5.H.1: Schematic representation of the main quantities characterizing the single-particle motion in the nuclear shell model taking into account the residual interaction among the particles at different levels of approximation. In (a) the bare NN -interaction is treated in the Hartree-Fock approximation and the particles feel the presence of the other particles through their own confinement in the average field. The strength function shows sharp peaks, each of them carrying the full strength of the states. In fact, the occupation number associated with each state k contains only one contribution. In (b) the particles still couple only with the average field. However in this case they can set the surface into vibrations by changing its state of motion. The strength associated with each orbital is distributed over a finite energy range. The corresponding occupation numbers arise from the sum of many contributions. Fitting a Breit-Wigner shape to each peak one can regain the simplicity of the extreme shell model by defining new levels with energy equal to that of the centroid and strength equal to that of the area covered by the Lorentzian shape (cf. (c)). In (d) the energy variation of the shift of the centroids is contained into an effective ω -mass according to the relation $\frac{m_\omega}{m} = \left(1 - \frac{\partial \Delta E}{\partial \hbar \omega}\right)$ (see Eq. (5.A.5)). The resulting curve resembles the shape obtained by calculating the inverse of the area below the different Lorentzians (quasiparticle approximation).

Chapter 6

Two-particle transfer

Cooper pairs are the building blocks of pairing correlations in many-body fermionic systems. In particular in atomic nuclei. As a consequence, nuclear superfluidity can be specifically probed through Cooper pair tunneling. In the simultaneous transfer of two nucleons, one nucleon goes over from target to projectile, or viceversa, under the influence of the nuclear interaction responsible of the existence of a mean field potential, while the other follows suit by profiting of: 1) pairing correlations (simultaneous transfer); 2) the fact that the single-particle wavefunctions describing the motion of Cooper pair partners in both target and projectile are solutions of different single-particle potentials (non-orthogonality term). In the limit of independent particle motion, in which all of the nucleon-nucleon interaction is used up in generating a mean field, both contributions to the transfer process (simultaneous and non-orthogonality) cancel out exactly (App. 6.C)

In keeping with the fact that nuclear Cooper pairs are weakly bound ($E_{corr} \ll \epsilon_F$), this cancellation is, in actual nuclei, quite strong. Consequently, successive transfer, a process in which the nuclear interaction acts twice is, as a rule, the main mechanism at the basis of Cooper pair transfer. Because of the same reason (weak binding), the correlation length of Cooper pairs is larger than nuclear dimensions ($\xi = \hbar v_F / (\pi E_{corr}) > R$), a fact which allows the two members of a Cooper pair to move between target and projectile, essentially as a whole, also in the case of successive transfer. In other words, because of its (intrinsic, virtual extension) Cooper pair transfer display equivalent pairing correlations both in simultaneous than in successive transfer.¹

¹In order for a nucleon to display independent particle motion, all other nucleons must act coherently so as to leave the way free making feel their pullings and pushings only when the nucleon in question tries to leave the self-bound system, thus acting as a reflecting surface which inverts the momentum of the particle. It is then natural to consider the nuclear mean field the most striking and fundamental collective feature in all nuclear phenomena (Mottelson (1962)). A close second is provided by the BCS mean field, resulting from the condensation of a number of strongly overlapping Cooper pairs ($\approx \langle BCS | \sum_{\nu>0} a_\nu^\dagger a_\nu^\dagger | BCS \rangle = \alpha_0 \neq 0$) and leading to independent pair motion. It is a rather unfortunate perversity of popular terminology that regards these collective fields (HF and HFB) as well as successive transfer, as in some sense an antithesis to the nuclear collective modes and to simultaneous transfer respectively. Within this context it is of notice that the differential cross

The present Chapter is structured in the following way. In Section 6.1 we present a summary of two-nucleon transfer reaction theory. It provides, together with Section 4.1 the elements needed to calculate the absolute two-nucleon transfer differential cross sections in second order DWBA, and thus to compare theory with experiment. For the practitioner in search of details and clarification we present in section 6.2 a derivation of the equations presented in section 6.1. These equations are implemented and made operative in the software COOPER used in the applications (cf. App. 7.C).

A number of Appendices are provided. Appendix 6.A briefly reminds the quantal basis for the dressing of elementary modes of excitation and of pairing interaction. In App. 6.B the derivation of first order DWBA simultaneous transfer is worked out within a formalism tailored to focus the attention on the nuclear structure correlations aspects of the process leading to effective two-nucleon transfer form factors. In App. 6.C the variety of contributions to two-nucleon transfer amplitudes (successive, simultaneous and non-orthogonality) are discussed in detail within the framework of the semi-classical approximation which provides a rather intuitive vision of the different processes. Appendices 6.D–6.G contain relations used in Sect. 6.2 as well as in the derivation of two-nucleon transfer spectroscopic amplitudes. Finally Appendix 6.H provides a glimpse of original material due to Ben Bayman² which was instrumental to render quantitative the studies of two-nucleon transfer, studies which can now be carried out in terms of absolute cross sections and not relative ones as done previously.

6.1 Summary of second order DWBA

Let us illustrate the theory of second order DWBA two-nucleon transfer reactions with the $A + t \rightarrow B(\equiv A + 2) + p$ reaction, in which $A + 2$ and A are even nuclei in their 0^+ ground state. The extension of the expressions to the transfer of pairs coupled to arbitrary angular momentum is discussed in subsection 6.2.10.

The wavefunction of the nucleus $A + 2$ can be written as

$$\Psi_{A+2}(\xi_A, \mathbf{r}_{A1}, \sigma_1, \mathbf{r}_{A2}, \sigma_2) = \psi_A(\xi_A) \sum_{l_i, j_i} [\phi_{l_i, j_i}^{A+2}(\mathbf{r}_{A1}, \sigma_1, \mathbf{r}_{A2}, \sigma_2)]_0^0, \quad (6.1.1)$$

where

$$[\phi_{l_i, j_i}^{A+2}(\mathbf{r}_{A1}, \sigma_1, \mathbf{r}_{A2}, \sigma_2)]_0^0 = \sum_{nm} a_{nm} [\varphi_{n, l_i, j_i}^{A+2}(\mathbf{r}_{A1}, \sigma_1) \varphi_{m, l_i, j_i}^{A+2}(\mathbf{r}_{A2}, \sigma_2)]_0^0, \quad (6.1.2)$$

while the wavefunctions $\varphi_{n, l_i, j_i}^{A+2}(\mathbf{r})$ are single-particle wavefunctions. The radial dependence of the wavefunction of the two neutrons in the triton is written as

section associated with the two-nucleon transfer processes between the ground state of superfluid nuclei is proportional to α_0^2 and not to Δ^2 . In fact, Cooper pairs partners remain correlated even over regions in which $G = 0$, of course provided normal density is different from 0.

²Bayman and Kallio (1967), Bayman (1970), Bayman (1971), Bayman and Chen (1982).

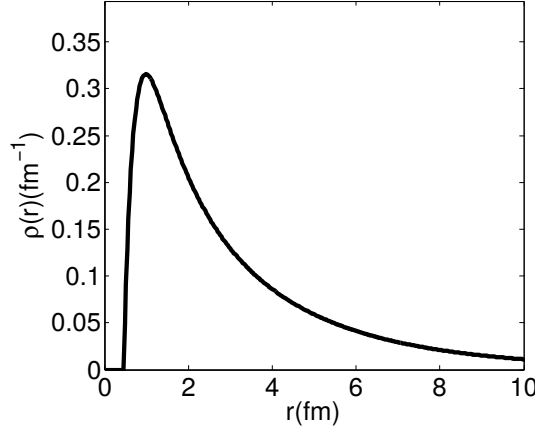


Figure 6.1.1: Radial function $\rho(r)$ (hard core 0.45 fm) entering the tritium wavefunction (cf. Tang and Herndon (1965)).

$\phi_t(\mathbf{r}_{p1}, \mathbf{r}_{p2}) = \rho(r_{p1})\rho(r_{p2})\rho(r_{12})$, where r_{p1}, r_{p2}, r_{12} are the distances between neutron 1 and the proton, neutron 2 and the proton and between neutrons 1 and 2 respectively, while $\rho(r)$ is the hard core ($r_{core} = 0.45$ fm) potential wavefunction depicted in Fig 6.1.1.

The two-nucleon transfer differential cross section is written as

$$\frac{d\sigma}{d\Omega} = \frac{\mu_i \mu_f}{(4\pi\hbar^2)^2} \frac{k_f}{k_i} \left| T^{(1)}(\theta) + T_{succ}^{(2)}(\theta) - T_{NO}^{(2)}(\theta) \right|^2, \quad (6.1.3)$$

where³,

$$T^{(1)}(\theta) = 2 \sum_{l_i, j_i} \sum_{\sigma_1 \sigma_2} \int d\mathbf{r}_{tA} d\mathbf{r}_{p1} d\mathbf{r}_{A2} [\phi_{l_i, j_i}^{A+2}(\mathbf{r}_{A1}, \sigma_1, \mathbf{r}_{A2}, \sigma_2)]_0^{0*} \chi_{pB}^{(-)*}(\mathbf{r}_{pB}) \\ \times v(\mathbf{r}_{p1}) \phi_t(\mathbf{r}_{p1}, \sigma_1, \mathbf{r}_{p2}, \sigma_2) \chi_{tA}^{(+)}(\mathbf{r}_{tA}), \quad (6.1.4a)$$

$$T_{succ}^{(2)}(\theta) = 2 \sum_{l_i, j_i} \sum_{l_f, j_f, m_f} \sum_{\sigma'_1 \sigma'_2} \int d\mathbf{r}_{dF} d\mathbf{r}_{p1} d\mathbf{r}_{A2} [\phi_{l_i, j_i}^{A+2}(\mathbf{r}_{A1}, \sigma_1, \mathbf{r}_{A2}, \sigma_2)]_0^{0*} \chi_{pB}^{(-)*}(\mathbf{r}_{pB}) v(\mathbf{r}_{p1}) \\ \times \phi_d(\mathbf{r}_{p1}, \sigma_1) \varphi_{l_f, j_f, m_f}^{A+1}(\mathbf{r}_{A2}, \sigma_2) \int d\mathbf{r}'_{dF} d\mathbf{r}'_{p1} d\mathbf{r}'_{A2} G(\mathbf{r}_{dF}, \mathbf{r}'_{dF}) \\ \times \phi_d(\mathbf{r}'_{p1}, \sigma'_1)^* \varphi_{l_f, j_f, m_f}^{A+1*}(\mathbf{r}'_{A2}, \sigma'_2) \frac{2\mu_{dF}}{\hbar^2} v(\mathbf{r}'_{p2}) \phi_d(\mathbf{r}'_{p1}, \sigma'_1) \phi_d(\mathbf{r}'_{p2}, \sigma'_2) \chi_{tA}^{(+)}(\mathbf{r}'_{tA}), \quad (6.1.4b)$$

³See Bayman and Chen (1982) and App. 6.H.

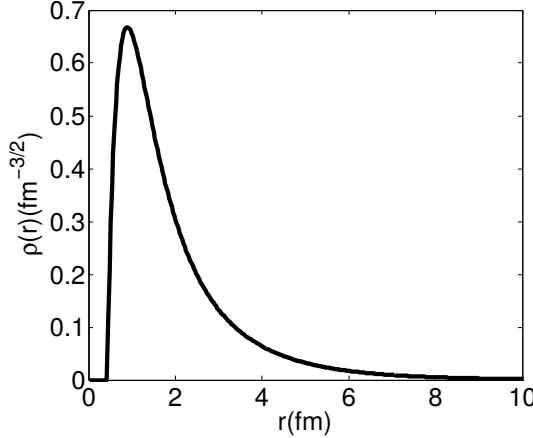


Figure 6.1.2: Radial wavefunction $\rho_d(r)$ (hard core 0.45 fm) entering the deuteron wavefunction (cf. Tang and Herndon (1965)).

$$\begin{aligned}
 T_{NO}^{(2)}(\theta) = & 2 \sum_{l_i, j_i} \sum_{l_f, j_f, m_f} \sum_{\sigma_1 \sigma_2} \int d\mathbf{r}_{dF} d\mathbf{r}_{p1} d\mathbf{r}_{A2} [\phi_{l_i, j_i}^{A+2}(\mathbf{r}_{A1}, \sigma_1, \mathbf{r}_{A2}, \sigma_2)]_0^{0*} \chi_{pB}^{(-)*}(\mathbf{r}_{pB}) v(\mathbf{r}_{p1}) \\
 & \times \phi_d(\mathbf{r}_{p1}, \sigma_1) \varphi_{l_f, j_f, m_f}^{A+1}(\mathbf{r}_{A2}, \sigma_2) \int d\mathbf{r}'_{p1} d\mathbf{r}'_{A2} d\mathbf{r}'_{dF} \\
 & \times \phi_d(\mathbf{r}'_{p1}, \sigma'_1)^* \varphi_{l_f, j_f, m_f}^{A+1*}(\mathbf{r}'_{A2}, \sigma'_2) \phi_d(\mathbf{r}'_{p1}, \sigma'_1) \phi_d(\mathbf{r}'_{p2}, \sigma'_2) \chi_{tA}^{(+)}(\mathbf{r}'_{tA}). \quad (6.1.4c)
 \end{aligned}$$

The quantities $\mu_i, \mu_f(k_i, k_f)$ are the reduced masses (relative linear momenta) in both entrance (initial, i) and exit (final, f) channels, respectively. In the above expressions, $\varphi_{l_f, j_f, m_f}^{A+1}(\mathbf{r}_{A1})$ are the wavefunctions describing the intermediate states of the nucleus $F (\equiv (A + 1))$, generated as solutions of a Woods-Saxon potential, $\phi_d(\mathbf{r}_{p2})$ being the deuteron bound wavefunction (see Fig. 6.1.2). Note that some or all of the single-particle states described by the wavefunctions $\varphi_{l_f, j_f, m_f}^{A+1}(\mathbf{r}_{A1})$ may lie in the continuum (case in which the nucleus F is loosely bound or unbound). Although there are a number of ways to exactly treat such states, discretization processes may be sufficiently accurate. They can be implemented by, for example, embedding the Woods-Saxon potential in a spherical box of sufficiently large radius. In actual calculations involving e.g. the halo nucleus ^{11}Li , and where $|F\rangle = |^{10}\text{Li}\rangle$, one achieved convergence making use of approximately 20 continuum states and a box of 30 fm of radius. Concerning the components of the triton wavefunction describing the relative motion of the dineutron, it was generated with the $p - n$ interaction⁴

$$v(r) = -v_0 \exp(-k(r - r_c)) \quad r > r_c \quad (6.1.5)$$

$$v(r) = \infty \quad r < r_c, \quad (6.1.6)$$

⁴Tang and Herndon (1965).

where $k = 2.5 \text{ fm}^{-1}$ and $r_c = 0.45 \text{ fm}$, the depth v_0 being adjusted to reproduce the experimental separation energies. The positive-energy wavefunctions $\chi_{tA}^{(+)}(\mathbf{r}_{tA})$ and $\chi_{pB}^{(-)}(\mathbf{r}_{pB})$ are the ingoing distorted wave in the initial channel and the outgoing distorted wave in the final channel respectively. They are continuum solutions of the Schrödinger equation associated with the corresponding optical potentials.

The transition potential responsible for the transfer of the pair is, in the *post* representation (cf. Fig. 6.C.1),

$$V_\beta = v_{pB} - U_\beta, \quad (6.1.7)$$

where v_{pB} is the interaction between the proton and nucleus B , and U_β is the optical potential in the final channel. We make the assumption that v_{pB} can be decomposed into a term containing the interaction between A and p and the potential describing the interaction between the proton and each of the transferred nucleons, namely

$$v_{pB} = v_{pA} + v_{p1} + v_{p2}, \quad (6.1.8)$$

where v_{p1} and v_{p2} is the hard-core potential (6.1.5). The transition potential is

$$V_\beta = v_{pA} + v_{p1} + v_{p2} - U_\beta. \quad (6.1.9)$$

Assuming that $\langle \beta | v_{pA} | \alpha \rangle \approx \langle \beta | U_\beta | \alpha \rangle$ (i.e., assuming that the matrix element of the core–core interaction between the initial and final states is very similar to the matrix element of the real part of the optical potential), one obtains the final expression of the transfer potential in the *post* representation, namely,

$$V_\beta \simeq v_{p1} + v_{p2} = v(\mathbf{r}_{p1}) + v(\mathbf{r}_{p2}). \quad (6.1.10)$$

We make the further approximation of using the same interaction potential in all the (i.e. initial, intermediate and final) channels.

The extension to a heavy-ion reaction $A + a (\equiv b + 2) \longrightarrow B (\equiv A + 2) + b$ imply no essential modifications in the formalism. The deuteron and triton wavefunctions appearing in Eqs. (6.1.4a), (6.1.4b) and (6.1.4c) are to be substituted with the corresponding wavefunctions $\Psi_{b+2}(\xi_b, \mathbf{r}_{b1}, \sigma_1, \mathbf{r}_{b2}, \sigma_2)$, constructed in a similar way as those appearing in (6.1.1 and 6.1.2). The interaction potential used in Eqs. (6.1.4a), (6.1.4b) and (6.1.4c) will now be the Saxon–Woods used to define the initial (final) state in the post (prior) representation, instead of the proton–neutron interaction (6.1.5).

The Green's function $G(\mathbf{r}_{dF}, \mathbf{r}'_{dF})$ appearing in (6.1.4b) propagates the intermediate channel d, F . It can be expanded in partial waves as,

$$G(\mathbf{r}_{dF}, \mathbf{r}'_{dF}) = i \sum_l \sqrt{2l+1} \frac{f_l(k_{dF}, r_<) g_l(k_{dF}, r_>)}{k_{dF} r_{dF} r'_{dF}} \left[Y^l(\hat{r}_{dF}) Y^l(\hat{r}'_{dF}) \right]_0^0. \quad (6.1.11)$$

The $f_l(k_{dF}, r)$ and $g_l(k_{dF}, r)$ are the regular and the irregular solutions of a Schrödinger equation for a suitable optical potential and an energy equal to the kinetic energy

of the intermediate state. In most cases of interest, the result is hardly altered if we use the same energy of relative motion for all the intermediate states. This representative energy is calculated when both intermediate nuclei are in their corresponding ground states. It is of notice that the validity of this approximation can break down in some particular cases. If, for example, some relevant intermediate state become off shell, its contribution is significantly quenched. An interesting situation can arise when this happens to all possible intermediate states, so they can only be virtually populated.

6.2 Detailed derivation of second order DWBA

6.2.1 Simultaneous transfer: distorted waves

For a (t, p) reaction, the triton is represented by an incoming distorted wave. We make the assumption that the two neutrons are in an $S = L = 0$ state, and that the relative motion of the proton with respect to the dineutron is also $l = 0$. Consequently, the total spin of the triton is entirely due to the spin of the proton. We will explicitly treat it, as we will consider a spin-orbit term in the optical potential acting between the triton and the target⁵.

Following (6.E.1), we can write the triton distorted wave as

$$\psi_{m_t}^{(+)}(\mathbf{R}, \mathbf{k}_i, \sigma_p) = \sum_{l_t} \exp(i\sigma_{l_t}^t) g_{l_t j_t} Y_0^{l_t}(\hat{\mathbf{R}}) \frac{\sqrt{4\pi(2l_t + 1)}}{k_i R} \chi_{m_t}(\sigma_p), \quad (6.2.1)$$

where use was made of $Y_0^{l_t}(\hat{\mathbf{k}}_i) = i^{l_t} \sqrt{\frac{2l_t + 1}{4\pi}} \delta_{m_t, 0}$, in keeping with the fact that \mathbf{k}_i is oriented along the z -axis. Note the phase difference with eq. (7) of Bayman (1971), due to the use of time-reversal rather than Condon–Shortley phase convention. Making use of the relation

$$Y_0^{l_t}(\hat{\mathbf{R}}) \chi_{m_t}(\sigma_p) = \sum_{j_t} \langle l_t 0 1/2 m_t | j_t m_t \rangle [Y^{l_t}(\hat{\mathbf{R}}) \chi(\sigma_p)]_{m_t}^{j_t}, \quad (6.2.2)$$

we have

$$\begin{aligned} \psi_{m_t}^{(+)}(\mathbf{R}, \mathbf{k}_i, \sigma_p) &= \sum_{l_t, j_t} \exp(i\sigma_{l_t}^t) \frac{\sqrt{4\pi(2l_t + 1)}}{k_i R} g_{l_t j_t}(R) \\ &\quad \times \langle l_t 0 1/2 m_t | j_t m_t \rangle [Y^{l_t}(\hat{\mathbf{R}}) \chi(\sigma_p)]_{m_t}^{j_t}. \end{aligned} \quad (6.2.3)$$

We now turn our attention to the outgoing proton distorted wave, which, following (6.E.3) can be written as

$$\psi_{m_p}^{(-)}(\zeta, \mathbf{k}_f, \sigma_p) = \sum_{l_p j_p} \frac{4\pi}{k_f \zeta} i^{l_p} \exp(-i\sigma_{l_p}^p) f_{l_p j_p}^*(\zeta) \sum_m Y_m^{l_p}(\hat{\zeta}) Y_m^{l_p *}(k_f) \chi_{m_p}(\sigma_p). \quad (6.2.4)$$

⁵In what follows we will use the notation of Bayman (1971), see also App. 6.H.

Making use of the relation

$$\begin{aligned} \sum_m Y_m^{l_p}(\hat{\zeta}) Y_m^{l_p*}(\hat{\mathbf{k}}_f) \chi_{m_p}(\sigma_p) &= \sum_{m, j_p} Y_m^{l_p*}(\hat{\mathbf{k}}_f) \langle l_p m 1/2 m_p | j_p m + m_p \rangle \\ &\times [Y^{l_p}(\hat{\zeta}) \chi_{m_p}(\sigma_p)]_{m+m_p}^{j_p} \\ &= \sum_{m, j_p} Y_{m-m_p}^{l_p*}(\hat{\mathbf{k}}_f) \langle l_p m - m_p 1/2 m_p | j_p m \rangle [Y^{l_p}(\hat{\zeta}) \chi_{m_p}(\sigma_p)]_m^{j_p}, \end{aligned} \quad (6.2.5)$$

one obtains

$$\begin{aligned} \psi_{m_p}^{(-)}(\zeta, \mathbf{k}_f, \sigma_p) &= \frac{4\pi}{k_f \zeta} \sum_{l_p j_p m} i^{l_p} \exp\left(-i\sigma_{l_p}^p\right) f_{l_p j_p}^*(\zeta) Y_{m-m_p}^{l_p*}(\hat{\mathbf{k}}_f) \\ &\times \langle l_p m - m_p 1/2 m_p | j_p m \rangle [Y^{l_p}(\hat{\zeta}) \chi(\sigma_p)]_m^{j_p}. \end{aligned} \quad (6.2.6)$$

6.2.2 matrix element for the transition amplitude

We now turn our attention to the evaluation of

$$\begin{aligned} \langle \Psi_f^{(-)}(\mathbf{k}_f) | V(r_{1p}) | \Psi_i^{(+)}(k_i, \hat{\mathbf{z}}) \rangle &= \frac{(4\pi)^{3/2}}{k_i k_f} \sum_{l_p l_t j_p j_t m} ((\lambda \frac{1}{2})_k (\lambda \frac{1}{2})_k | (\lambda \lambda)_0 (\frac{1}{2} \frac{1}{2})_0)_0 \sqrt{2l_t + 1} \\ &\times \langle l_p m - m_p 1/2 m_p | j_p m \rangle \langle l_t 0 1/2 m_t | j_t m_t \rangle i^{-l_p} \exp[i(\sigma_{l_p}^p + \sigma_{l_t}^t)] \\ &\times 2 Y_{m-m_p}^{l_p}(\hat{\mathbf{k}}_f) \sum_{\sigma_1 \sigma_2 \sigma_p} \int \frac{d\zeta d\mathbf{r} d\boldsymbol{\eta}}{\zeta R} u_{\lambda k}(r_1) u_{\lambda k}(r_2) [Y^\lambda(\hat{\mathbf{r}}_1) Y^\lambda(\hat{\mathbf{r}}_2)]_0^{0*} \\ &\times f_{l_p j_p}(\zeta) g_{l_t j_t}(R) [\chi(\sigma_1) \chi(\sigma_2)]_0^{0*} [Y^{l_p}(\hat{\zeta}) \chi(\sigma_p)]_m^{j_p*} V(r_{1p}) \\ &\times \theta_0^0(\mathbf{r}, \mathbf{s}) [\chi(\sigma_1) \chi(\sigma_2)]_0^0 [Y^{l_t}(\hat{\mathbf{R}}) \chi(\sigma_p)]_{m_t}^{j_t}, \end{aligned} \quad (6.2.7)$$

where

$$\begin{aligned} \mathbf{r} &= \mathbf{r}_2 - \mathbf{r}_1, \\ \mathbf{s} &= \frac{1}{2}(\mathbf{r}_1 + \mathbf{r}_2) - \mathbf{r}_p, \\ \boldsymbol{\eta} &= \frac{1}{2}(\mathbf{r}_1 + \mathbf{r}_2), \\ \zeta &= \mathbf{r}_p - \frac{\mathbf{r}_1 + \mathbf{r}_2}{A + 2}. \end{aligned} \quad (6.2.8)$$

The sum over σ_1, σ_2 in (6.2.7) is found to be equal to 1. We will now simplify the term $[Y^{l_p}(\hat{\zeta}) \chi(\sigma_p)]_m^{j_p*} [Y^{l_t}(\hat{\mathbf{R}}) \chi(\sigma_p)]_{m_t}^{j_t}$, noting that, (6.D.13)

$$[Y^{l_p}(\hat{\zeta}) \chi(\sigma_p)]_m^{j_p*} = (-1)^{1/2 - \sigma_p + j_p - m} [Y^{l_p}(\hat{\zeta}) \chi(-\sigma_p)]_{-m}^{j_p}. \quad (6.2.9)$$

and that

$$\begin{aligned} & \left[Y^{l_p}(\hat{\zeta}) \chi(-\sigma_p) \right]_{-m}^{j_p} \left[Y^{l_t}(\hat{\mathbf{R}}) \chi(\sigma_p) \right]_{m_t}^{j_t} = \sum_{JM} \langle j_p - m | j_t | m_t | J M \rangle \\ & \times \left\{ \left[Y^{l_p}(\hat{\zeta}) \chi(-\sigma_p) \right]_{-m}^{j_p} \left[Y^{l_t}(\hat{\mathbf{R}}) \chi(\sigma_p) \right]_{m_t}^{j_t} \right\}_M^J \end{aligned} \quad (6.2.10)$$

The only term which does not vanish after the integration is performed is the one in which the angular and spin functions are coupled to $L = 0, S = 0, J = 0$. Thus,

$$\begin{aligned} & \langle j_p - m | j_t | m_t | 0 0 \rangle \left\{ \left[Y^{l_p}(\hat{\zeta}) \chi(-\sigma_p) \right]_{-m}^{j_p} \left[Y^{l_t}(\hat{\mathbf{R}}) \chi(\sigma_p) \right]_{m_t}^{j_t} \right\}_0^0 \delta_{l_p l_t} \delta_{j_p j_t} \delta_{mm_t} \\ & = \frac{(-1)^{j_p + m_t}}{\sqrt{2j_p + 1}} \left\{ \left[Y^{l_p}(\hat{\zeta}) \chi(-\sigma_p) \right]_{-m}^{j_p} \left[Y^{l_t}(\hat{\mathbf{R}}) \chi(\sigma_p) \right]_{m_t}^{j_t} \right\}_0^0 \delta_{l_p l_t} \delta_{j_p j_t} \delta_{mm_t}. \end{aligned} \quad (6.2.11)$$

Coupling separately the spin and angular functions, one obtains

$$\begin{aligned} & \left\{ \left[Y^l(\hat{\zeta}) \chi(-\sigma_p) \right]^j \left[Y^l(\hat{\mathbf{R}}) \chi(\sigma_p) \right]^j \right\}_0^0 \\ & = ((l\frac{1}{2})_j (l\frac{1}{2})_j | (ll)_0 (\frac{1}{2}\frac{1}{2})_0)_0 \left[\chi(-\sigma_p) \chi(\sigma_p) \right]_0^0 \left[Y^l(\hat{\zeta}) Y^l(\hat{\mathbf{R}}) \right]_0^0. \end{aligned} \quad (6.2.12)$$

We substitute (6.2.9), (6.2.30), (6.2.31) in (6.2.7) to obtain

$$\begin{aligned} & \langle \Psi_f^{(-)}(\mathbf{k}_f) | V(r_{1p}) | \Psi_i^{(+)}(k_i, \hat{\mathbf{z}}) \rangle = - \frac{(4\pi)^{3/2}}{k_i k_f} \sum_{lj} ((\lambda\frac{1}{2})_k (\lambda\frac{1}{2})_l | (\lambda\lambda)_0 (\frac{1}{2}\frac{1}{2})_0)_0 \sqrt{\frac{2l+1}{2j+1}} \\ & \times \langle l | m_t - m_p | 1/2 | m_p | j | m_t \rangle \langle l | 0 | 1/2 | m_t | j | m_t \rangle i^{-l} \exp[i(\sigma_l^p + \sigma_l^t)] \\ & \times 2Y_{m_t - m_p}^l(\hat{\mathbf{k}}_f) \int \frac{d\zeta d\mathbf{r} d\mathbf{n}}{\zeta R} u_{\lambda k}(r_1) u_{\lambda k}(r_2) \left[Y^\lambda(\hat{\mathbf{r}}_1) Y^\lambda(\hat{\mathbf{r}}_2) \right]_0^{0*} \\ & \times f_{lj}(\zeta) g_{lj}(R) \left[Y^l(\hat{\zeta}) Y^l(\hat{\mathbf{R}}) \right]_0^0 V(r_{1p}) \theta_0^0(\mathbf{r}, \mathbf{s}) \\ & \times ((l\frac{1}{2})_j (l\frac{1}{2})_j | (ll)_0 (\frac{1}{2}\frac{1}{2})_0)_0 \sum_{\sigma_p} (-1)^{1/2 - \sigma_p} \left[\chi(-\sigma_p) \chi(\sigma_p) \right]_0^0. \end{aligned} \quad (6.2.13)$$

The last sum over σ_p leads to

$$\begin{aligned} & \sum_{\sigma_p} (-1)^{1/2 - \sigma_p} \left[\chi(-\sigma_p) \chi(\sigma_p) \right]_0^0 = \sum_{\sigma_p m} (-1)^{1/2 - \sigma_p} \langle 1/2 | m | 1/2 | -m | 0 0 \rangle \\ & \times \chi_m(-\sigma_p) \chi_{-m}(\sigma_p) \\ & = \frac{1}{\sqrt{2}} \sum_{\sigma_p m} (-1)^{1/2 - \sigma_p} (-1)^{1/2 - m} \delta_{m, -\sigma_p} \delta_{-m, \sigma_p} = -\sqrt{2}. \end{aligned} \quad (6.2.14)$$

The $9j$ -symbols can be evaluated to find

$$\begin{aligned} ((\lambda \frac{1}{2})_k (\lambda \frac{1}{2})_k | (\lambda \lambda)_0 (\frac{1}{2} \frac{1}{2})_0)_0 &= \sqrt{\frac{2k+1}{2(2\lambda+1)}} \\ ((l \frac{1}{2})_j (l \frac{1}{2})_j | (ll)_0 (\frac{1}{2} \frac{1}{2})_0)_0 &= \sqrt{\frac{2j+1}{2(2l+1)}}, \end{aligned} \quad (6.2.15)$$

and consequently,

$$\begin{aligned} \langle \Psi_f^{(-)}(\mathbf{k}_f) | V(r_{1p}) | \Psi_i^{(+)}(k_i, \hat{\mathbf{z}}) \rangle &= \frac{(4\pi)^{3/2}}{k_i k_f} \sum_{lj} \sqrt{\frac{2k+1}{2\lambda+1}} \\ &\times \langle l m_t - m_p 1/2 m_p | j m_t \rangle \langle l 0 1/2 m_t | j m_t \rangle i^{-l} \exp[i(\sigma_l^p + \sigma_l^t)] \\ &\times \sqrt{2} Y_{m_t - m_p}^l(\hat{\mathbf{k}}_f) \int \frac{d\zeta d\mathbf{r} d\boldsymbol{\eta}}{\zeta R} u_{\lambda k}(r_1) u_{\lambda k}(r_2) [Y^\lambda(\hat{\mathbf{r}}_1) Y^\lambda(\hat{\mathbf{r}}_2)]_0^{0*} \\ &\times f_{lj}(\zeta) g_{lj}(R) [Y^l(\hat{\zeta}) Y^l(\hat{\mathbf{R}})]_0^0 V(r_{1p}) \theta_0^0(\mathbf{r}, \mathbf{s}). \end{aligned} \quad (6.2.16)$$

The values of the Clebsh–Gordan coefficients are, for $j = l - 1/2$,

$$\begin{aligned} \langle l m_t - m_p 1/2 m_p | l - 1/2 m_t \rangle \langle l 0 1/2 m_t | l - 1/2 m_t \rangle \\ = \begin{cases} \frac{l}{2l+1} & \text{if } m_t = m_p \\ -\frac{\sqrt{l(l+1)}}{2l+1} & \text{if } m_t = -m_p \end{cases} \end{aligned} \quad (6.2.17)$$

and, for $j = l + 1/2$:

$$\begin{aligned} \langle l m_t - m_p 1/2 m_p | l + 1/2 m_t \rangle \langle l 0 1/2 m_t | l + 1/2 m_t \rangle \\ = \begin{cases} \frac{l+1}{2l+1} & \text{if } m_t = m_p \\ \frac{\sqrt{l(l+1)}}{2l+1} & \text{if } m_t = -m_p \end{cases} \end{aligned} \quad (6.2.18)$$

One thus can write,

$$\begin{aligned} \langle \Psi_f^{(-)}(\mathbf{k}_f) | V(r_{1p}) | \Psi_i^{(+)}(k_i, \hat{\mathbf{z}}) \rangle &= \frac{(4\pi)^{3/2}}{k_i k_f} \sum_l \frac{1}{(2l+1)} \sqrt{\frac{(2k+1)}{(2\lambda+1)}} \exp[i(\sigma_l^p + \sigma_l^t)] i^{-l} \\ &\times \sqrt{2} Y_{m_t - m_p}^l(\hat{\mathbf{k}}_f) \int \frac{d\zeta d\mathbf{r} d\boldsymbol{\eta}}{\zeta R} u_{\lambda k}(r_1) u_{\lambda k}(r_2) [Y^\lambda(\hat{\mathbf{r}}_1) Y^\lambda(\hat{\mathbf{r}}_2)]_0^{0*} \\ &\times V(r_{1p}) \theta_0^0(\mathbf{r}, \mathbf{s}) [Y^l(\hat{\zeta}) Y^l(\hat{\mathbf{R}})]_0^0 \\ &\times \left[(f_{l+1/2}(\zeta) g_{l+1/2}(R)(l+1) + f_{l-1/2}(\zeta) g_{l-1/2}(R)l) \delta_{m_p, m_t} \right. \\ &\left. + (f_{l+1/2}(\zeta) g_{l+1/2}(R) \sqrt{l(l+1)} - f_{l-1/2}(\zeta) g_{l-1/2}(R) \sqrt{l(l+1)}) \delta_{m_p, -m_t} \right]. \end{aligned} \quad (6.2.19)$$

We can further simplify this expression using

$$\begin{aligned}
[Y^\lambda(\hat{\mathbf{r}}_1)Y^\lambda(\hat{\mathbf{r}}_2)]_0^{0*} &= [Y^\lambda(\hat{\mathbf{r}}_1)Y^\lambda(\hat{\mathbf{r}}_2)]_0^0 = \sum_m \langle \lambda m \lambda - m | 0 0 \rangle Y_m^\lambda(\hat{\mathbf{r}}_1)Y_{-m}^\lambda(\hat{\mathbf{r}}_2) \\
&= \sum_m (-1)^{\lambda-m} \langle \lambda m \lambda - m | 0 0 \rangle Y_m^\lambda(\hat{\mathbf{r}}_1)Y_m^{l*}(\hat{\mathbf{r}}_2) \\
&= \frac{1}{\sqrt{2\lambda+1}} \sum_m Y_m^\lambda(\hat{\mathbf{r}}_1)Y_m^{l*}(\hat{\mathbf{r}}_2) \\
&= \frac{\sqrt{(2\lambda+1)}}{4\pi} P_\lambda(\cos \theta_{12}).
\end{aligned} \tag{6.2.20}$$

Note that when using Condon–Shortley phases this last expression is to be multiplied by $(-1)^\lambda$, and that

$$\begin{aligned}
[Y^l(\hat{\boldsymbol{\zeta}})Y^l(\hat{\mathbf{R}})]_0^0 &= \sum_m \langle l m l - m | 0 0 \rangle Y_m^l(\hat{\boldsymbol{\zeta}})Y_{-m}^l(\hat{\mathbf{R}}) \\
&= \frac{1}{\sqrt{(2l+1)}} \sum_m (-1)^{l+m} Y_m^l(\hat{\boldsymbol{\zeta}})Y_{-m}^l(\hat{\mathbf{R}}).
\end{aligned} \tag{6.2.21}$$

Because the integral of the above expression is independent of m , one can eliminate the m -sum and multiply by $2l+1$ the $m=0$ term, leading to

$$\begin{aligned}
[Y^l(\hat{\boldsymbol{\zeta}})Y^l(\hat{\mathbf{R}})]_0^0 &\Rightarrow (-1)^l \sqrt{(2l+1)} Y_0^l(\hat{\boldsymbol{\zeta}})_0 Y^l(\hat{\mathbf{R}}) \\
&= \sqrt{(2l+1)} Y_0^l(\hat{\boldsymbol{\zeta}}) Y_0^{l*}(\hat{\mathbf{R}}).
\end{aligned} \tag{6.2.22}$$

We now change the integration variables from $(\boldsymbol{\zeta}, \mathbf{r}, \boldsymbol{\eta})$ to $(\mathbf{R}, \alpha, \beta, \gamma, r_{12}, r_{1p}, r_{2p})$, the quantity

$$\left| \frac{\partial(\mathbf{r}, \boldsymbol{\eta}, \boldsymbol{\zeta})}{\partial(\mathbf{R}, \alpha, \beta, \gamma, r_{12}, r_{1p}, r_{2p})} \right| = r_{12} r_{1p} r_{2p} \sin \beta, \tag{6.2.23}$$

being the Jacobian of the transformation. Finally,

$$\begin{aligned}
\langle \Psi_f^{(-)}(\mathbf{k}_f) | V(r_{1p}) | \Psi_i^{(+)}(k_i, \hat{\mathbf{z}}) \rangle &= \frac{\sqrt{8\pi}}{k_i k_f} \sum_l \sqrt{\frac{2k+1}{2l+1}} \exp[i(\sigma_l^p + \sigma_l^t)] i^{-l} \\
&\times Y_{m_l-m_p}^l(\hat{\mathbf{k}}_f) \int d\mathbf{R} Y_0^{l*}(\hat{\mathbf{R}}) \int \frac{d\alpha d\beta d\gamma dr_{12} dr_{1p} dr_{2p} \sin \beta}{\zeta R} Y_0^l(\hat{\boldsymbol{\zeta}}) \\
&\times u_{\lambda k}(r_1) u_{\lambda k}(r_2) V(r_{1p}) \theta_0^0(\mathbf{r}, \mathbf{s}) P_\lambda(\cos \theta_{12}) r_{12} r_{1p} r_{2p} \\
&\times \left[(f_{ll+1/2}(\zeta) g_{ll+1/2}(R)(l+1) + f_{ll-1/2}(\zeta) g_{ll-1/2}(R)l) \delta_{m_p, m_l} \right. \\
&\left. + (f_{ll+1/2}(\zeta) g_{ll+1/2}(R) \sqrt{l(l+1)} - f_{ll-1/2}(\zeta) g_{ll-1/2}(R) \sqrt{l(l+1)}) \delta_{m_p, -m_l} \right].
\end{aligned} \tag{6.2.24}$$

It is noted that the second integral is a function of solely \mathbf{R} transforming under rotations as $Y_0^l(\hat{\mathbf{R}})$, in keeping with the fact that the full dependence on the orientation

of \mathbf{R} is contained in the spherical harmonic $Y_0^l(\hat{\zeta})$. The second integral can thus be cast into the form

$$\begin{aligned} A(R)Y_0^l(\hat{\mathbf{R}}) = & \int d\alpha d\beta d\gamma dr_{12} dr_{1p} dr_{2p} \sin\beta \\ & \times F(\alpha, \beta, \gamma, r_{12}, r_{1p}, r_{2p}, R_x, R_y, R_z). \end{aligned} \quad (6.2.25)$$

To evaluate $A(R)$, we set \mathbf{R} along the z -axis

$$\begin{aligned} A(R) = & 2\pi i^{-l} \sqrt{\frac{4\pi}{2l+1}} \int d\beta d\gamma dr_{12} dr_{1p} dr_{2p} \sin\beta \\ & \times F(\alpha, \beta, \gamma, r_{12}, r_{1p}, r_{2p}, 0, 0, R), \end{aligned} \quad (6.2.26)$$

where a factor 2π results from the integration over α , the integrand not depending on α . Substituting (6.2.25) and (6.2.26) in (6.2.24) and, after integration over the angular variables of \mathbf{R} , we obtain

$$\begin{aligned} \langle \Psi_f^{(-)}(\mathbf{k}_f) | V(r_{1p}) | \Psi_i^{(+)}(k_i, \hat{\mathbf{z}}) \rangle = & 2 \frac{(2\pi)^{3/2}}{k_i k_f} \sum_l \sqrt{\frac{2k+1}{2l+1}} \exp[i(\sigma_l^p + \sigma_l^t)] i^{-l} \\ & \times Y_{m_t-m_p}^l(\hat{\mathbf{k}}_f) \int dR d\beta d\gamma dr_{12} dr_{1p} dr_{2p} R \sin\beta r_{12} r_{1p} r_{2p} \\ & \times u_{\lambda k}(r_1) u_{\lambda k}(r_2) V(r_{1p}) \theta_0^0(\mathbf{r}, \mathbf{s}) P_\lambda(\cos\theta_{12}) P_l(\cos\theta_\zeta) \\ & \times \left[(f_{ll+1/2}(\zeta) g_{ll+1/2}(R)(l+1) + f_{ll-1/2}(\zeta) g_{ll-1/2}(R)l) \delta_{m_p, m_t} \right. \\ & \left. + (f_{ll+1/2}(\zeta) g_{ll+1/2}(R) \sqrt{l(l+1)} - f_{ll-1/2}(\zeta) g_{ll-1/2}(R) \sqrt{l(l+1)}) \delta_{m_p, -m_t} \right] / \zeta, \end{aligned} \quad (6.2.27)$$

where use was made of the relation

$$Y_0^l(\hat{\zeta}) = i^l \sqrt{\frac{2l+1}{4\pi}} P_l(\cos\theta_\zeta). \quad (6.2.28)$$

The final expression of the differential cross section involves a sum over the spin orientations:

$$\frac{d\sigma}{d\Omega}(\hat{\mathbf{k}}_f) = \frac{k_f}{k_i} \frac{\mu_i \mu_f}{(2\pi\hbar^2)^2} \frac{1}{2} \sum_{m_t m_p} |\langle \Psi_f^{(-)}(\mathbf{k}_f) | V(r_{1p}) | \Psi_i^{(+)}(k_i, \hat{\mathbf{z}}) \rangle|^2. \quad (6.2.29)$$

When $m_p = 1/2, m_t = 1/2$ or $m_p = -1/2, m_t = -1/2$, the terms proportional to δ_{m_p, m_t} including the factor

$$|Y_{m_t-m_p}^l(\hat{\mathbf{k}}_f) \delta_{m_p, m_t}| = |Y_0^l(\hat{\mathbf{k}}_f)| = \left| i^l \sqrt{\frac{2l+1}{4\pi}} P_l^0(\cos\theta) \right|, \quad (6.2.30)$$

in the case in which $m_p = -1/2, m_t = 1/2$

$$|Y_{m_t-m_p}^l(\hat{\mathbf{k}}_f) \delta_{m_p, -m_t}| = |Y_1^l(\hat{\mathbf{k}}_f)| = \left| i^l \sqrt{\frac{2l+1}{4\pi}} \frac{1}{l(l+1)} P_l^1(\cos\theta) \right|, \quad (6.2.31)$$

and

$$|Y_{m_t-m_p}^l(\hat{\mathbf{k}}_f)\delta_{m_p,-m_t}| = |Y_{-1}^l(\hat{\mathbf{k}}_f)| = |Y_1^l(\hat{\mathbf{k}}_f)| = \left| i^l \sqrt{\frac{2l+1}{4\pi}} \frac{1}{l(l+1)} P_l^1(\cos \theta) \right|, \quad (6.2.32)$$

when $m_p = 1/2, m_t = -1/2$. Taking the squared modulus of (6.2.27), the sum over m_t and m_p yields a factor 2 multiplying each one of the 2 different terms of the sum ($m_t = m_p$ and $m_t = -m_p$). This is equivalent to multiply each amplitude by $\sqrt{2}$, so the final constant that multiply the amplitudes is

$$\frac{8\pi^{3/2}}{k_i k_f}. \quad (6.2.33)$$

Now, for the triton wavefunction we use

$$\theta_0^0(\mathbf{r}, \mathbf{s}) = \rho(r_{1p})\rho(r_{2p})\rho(r_{12}), \quad (6.2.34)$$

$\rho(r)$ being a Tang–Herndon (1965) wave function also used by Bayman (1971). We obtain

$$\frac{d\sigma}{d\Omega}(\hat{\mathbf{k}}_f) = \frac{1}{2E_i^{3/2}E_f^{1/2}} \sqrt{\frac{\mu_f}{\mu_i}} \left(|I_{\lambda k}^{(0)}(\theta)|^2 + |I_{\lambda k}^{(1)}(\theta)|^2 \right), \quad (6.2.35)$$

where

$$\begin{aligned} I_{\lambda k}^{(0)}(\theta) &= \sum_l P_l^0(\cos \theta) \sqrt{2k+1} \exp[i(\sigma_l^p + \sigma_l^t)] \\ &\times \int dR d\beta d\gamma dr_{12} dr_{1p} dr_{2p} R \sin \beta \rho(r_{1p})\rho(r_{2p})\rho(r_{12}) \\ &\times u_{\lambda k}(r_1)u_{\lambda k}(r_2)V(r_{1p})P_\lambda(\cos \theta_{12})P_l(\cos \theta_\zeta)r_{12}r_{1p}r_{2p} \\ &\times (f_{ll+1/2}(\zeta)g_{ll+1/2}(R)(l+1) + f_{ll-1/2}(\zeta)g_{ll-1/2}(R)) / \zeta, \end{aligned} \quad (6.2.36)$$

and

$$\begin{aligned} I_{\lambda k}^{(1)}(\theta) &= \sum_l P_l^1(\cos \theta) \sqrt{2k+1} \exp[i(\sigma_l^p + \sigma_l^t)] \\ &\times \int dR d\beta d\gamma dr_{12} dr_{1p} dr_{2p} R \sin \beta \rho(r_{1p})\rho(r_{2p})\rho(r_{12}) \\ &\times u_{\lambda k}(r_1)u_{\lambda k}(r_2)V(r_{1p})P_\lambda(\cos \theta_{12})P_l(\cos \theta_\zeta)r_{12}r_{1p}r_{2p} \\ &\times (f_{ll+1/2}(\zeta)g_{ll+1/2}(R) - f_{ll-1/2}(\zeta)g_{ll-1/2}(R)) / \zeta. \end{aligned} \quad (6.2.37)$$

Note that the absence of the $(-1)^l$ factor with respect to what is found in the work of Bayman⁶, is due to the use of time-reversed phases instead of Condon–Shortley phasing. This is compensated in the total result by a similar difference in the expression of the spectroscopic amplitudes. This ensures that, in either case, the contribution of all the single particle transitions tend to have the same phase for superfluid nuclei, adding coherently to enhance the transfer cross section.

⁶Bayman (1971).

Heavy-ion Reactions

In dealing with a heavy ion reaction, $\theta_0^0(\mathbf{r}, \mathbf{s})$ are be the spatial part of the wave-function

$$\begin{aligned}\Psi(\mathbf{r}_{b1}, \mathbf{r}_{b2}, \sigma_1, \sigma_2) &= [\psi^{j_i}(\mathbf{r}_{b1}, \sigma_1)\psi^{j_i}(\mathbf{r}_{b2}, \sigma_2)]_0^0 \\ &= \theta_0^0(\mathbf{r}, \mathbf{s})[\chi(\sigma_1)\chi(\sigma_2)]_0^0,\end{aligned}\quad (6.2.38)$$

where $\mathbf{r}_{b1}, \mathbf{r}_{b2}$ are the positions of the two neutrons with respect to the b core. It can be shown to be

$$\theta_0^0(\mathbf{r}, \mathbf{s}) = \frac{u_{l_i j_i}(r_{b1})u_{l_i j_i}(r_{b2})}{4\pi} \sqrt{\frac{2j_i + 1}{2}} P_{l_i}(\cos \theta_i), \quad (6.2.39)$$

where θ_i is the angle between \mathbf{r}_{b1} and \mathbf{r}_{b2} . Neglecting the spin-orbit term in the optical potential, as is usually done for heavy ion reactions, one obtains

$$\frac{d\sigma}{d\Omega}(\hat{\mathbf{k}}_f) = \frac{\mu_f \mu_i}{16\pi^2 \hbar^4 k_i^3 k_f} |T^{(1)}(\theta)|^2, \quad (6.2.40)$$

where

$$\begin{aligned}T^{(1)}(\theta) &= \sum_l (2l + 1) P_l(\cos \theta) \sqrt{(2j_i + 1)(2j_f + 1)} \exp[i(\sigma_l^p + \sigma_l^t)] \\ &\times \int dR d\beta d\gamma dr_{12} dr_{b1} dr_{b2} R \sin \beta u_{l_i j_i}(r_{b1})u_{l_i j_i}(r_{b2}) \\ &\times u_{l_f j_f}(r_{A1})u_{l_f j_f}(r_{A2})V(r_{b1})P_\lambda(\cos \theta_{12})P_l(\cos \theta_\zeta) \\ &\times r_{12}r_{b1}r_{b2}P_{l_i}(\cos \theta_i)\frac{f_l(\zeta)g_l(R)}{\zeta},\end{aligned}\quad (6.2.41)$$

obtained by using Eq. (6.2.39) in Eq. (6.2.7) instead of (6.2.34), $\mathbf{r}_{A1}, \mathbf{r}_{A2}$ being the coordinates of the two transferred neutrons with respect to the A core.

For control, in what follows we work out the same transition amplitude but starting from the distorted waves for a reaction taking place between spinless nuclei, namely

$$\psi^{(+)}(\mathbf{r}_{Aa}, \mathbf{k}_{Aa}) = \sum_l \exp(i\sigma_l^i) g_l Y_0^l(\hat{\mathbf{r}}_{aA}) \frac{\sqrt{4\pi(2l+1)}}{k_{aA} r_{aA}}, \quad (6.2.42)$$

and

$$\psi^{(-)}(\mathbf{r}_{bB}, \mathbf{k}_{bB}) = \frac{4\pi}{k_{bB} r_{bB}} \sum_{\tilde{l}} i^{\tilde{l}} \exp(-i\sigma_{\tilde{l}}^f) f_{\tilde{l}}^*(r_{bB}) \sum_m Y_m^{\tilde{l}*}(\hat{\mathbf{k}}_{bB}) Y_m^{\tilde{l}}(\hat{\mathbf{r}}_{bB}). \quad (6.2.43)$$

One can then write,

$$\begin{aligned}
T_{2N}^{1step} = & \langle \Psi_f^{(-)}(\mathbf{k}_{bB}) | V(r_{1p}) | \Psi_i^{(+)}(k_{aA}, \hat{\mathbf{z}}) \rangle = \frac{(4\pi)^{3/2}}{k_{aA} k_{bB}} \sum_{\tilde{l}\tilde{m}} ((l_f \frac{1}{2})_{j_f} (l_f \frac{1}{2})_{j_f} | (l_f l_f)_0 (\frac{1}{2} \frac{1}{2})_0)_0 \\
& \times ((l_i \frac{1}{2})_{j_i} (l_i \frac{1}{2})_{j_i} | (l_i l_i)_0 (\frac{1}{2} \frac{1}{2})_0)_0 \sqrt{2l+1} i^{-l_p} \exp[i(\sigma_{\tilde{l}}^f + \sigma_l^i)] \\
& \times 2Y_m^{\tilde{l}}(\hat{\mathbf{k}}_{bB}) \sum_{\sigma_1 \sigma_2} \int \frac{d\mathbf{r}_{bB} d\mathbf{r} d\boldsymbol{\eta}}{r_{bB} r_{aA}} u_{l_f j_f}(r_{A1}) u_{l_f j_f}(r_{A2}) u_{l_i j_i}(r_{b1}) u_{l_i j_i}(r_{b2}) \\
& \times [Y^{l_f}(\hat{\mathbf{r}}_{A1}) Y^{l_f}(\hat{\mathbf{r}}_{A2})]_0^{0*} [Y^{l_i}(\hat{\mathbf{r}}_{b1}) Y^{l_i}(\hat{\mathbf{r}}_{b2})]_0^0 \\
& \times f_{\tilde{l}}(r_{bB}) g_l(r_{aA}) [\chi(\sigma_1) \chi(\sigma_2)]_0^{0*} Y_m^{\tilde{l}*}(\hat{\mathbf{r}}_{bB}) V(r_{1p}) \\
& \times [\chi(\sigma_1) \chi(\sigma_2)]_0^0 Y_0^l(\hat{\mathbf{r}}_{aA}),
\end{aligned} \tag{6.2.44}$$

which, after a number of simplifications becomes

$$\begin{aligned}
\langle \Psi_f^{(-)}(\mathbf{k}_{bB}) | V(r_{1p}) | \Psi_i^{(+)}(k_{aA}, \hat{\mathbf{z}}) \rangle = & \frac{(4\pi)^{3/2}}{k_{aA} k_{bB}} \sum_{\tilde{l}\tilde{m}} \sqrt{\frac{(2j_f+1)(2j_i+1)}{(2l_f+1)(2l_i+1)}} \\
& \times \sqrt{2l+1} i^{-\tilde{l}} \exp[i(\sigma_{\tilde{l}}^f + \sigma_l^i)] \\
& \times Y_m^{\tilde{l}}(\hat{\mathbf{k}}_{bB}) \int \frac{d\mathbf{r}_{bB} d\mathbf{r} d\boldsymbol{\eta}}{r_{bB} r_{aA}} u_{l_f j_f}(r_{A1}) u_{l_f j_f}(r_{A2}) u_{l_i j_i}(r_{b1}) u_{l_i j_i}(r_{b2}) \\
& \times [Y^{l_f}(\hat{\mathbf{r}}_{A1}) Y^{l_f}(\hat{\mathbf{r}}_{A2})]_0^{0*} [Y^{l_i}(\hat{\mathbf{r}}_{b1}) Y^{l_i}(\hat{\mathbf{r}}_{b2})]_0^0 \\
& \times f_{\tilde{l}}(r_{bB}) g_l(r_{aA}) Y_m^{\tilde{l}*}(\hat{\mathbf{r}}_{bB}) V(r_{1p}) Y_0^l(\hat{\mathbf{r}}_{aA}),
\end{aligned} \tag{6.2.45}$$

where $l = \tilde{l}$ and $m = 0$. Making use of Legendre polynomials leads to,

$$\begin{aligned}
\langle \Psi_f^{(-)}(\mathbf{k}_{bB}) | V(r_{1p}) | \Psi_i^{(+)}(k_{aA}, \hat{\mathbf{z}}) \rangle = & \frac{(4\pi)^{-1/2}}{k_{aA} k_{bB}} \sum_l \sqrt{(2j_f+1)(2j_i+1)} \\
& \times \sqrt{2l+1} i^{-l} \exp[i(\sigma_l^f + \sigma_l^i)] Y_0^l(\hat{\mathbf{k}}_{bB}) \\
& \times \int \frac{d\mathbf{r}_{bB} d\mathbf{r} d\boldsymbol{\eta}}{r_{bB} r_{aA}} u_{l_f j_f}(r_{A1}) u_{l_f j_f}(r_{A2}) u_{l_i j_i}(r_{b1}) u_{l_i j_i}(r_{b2}) \\
& \times P_{l_f}(\cos \theta_A) P_{l_i}(\cos \theta_b) \\
& \times f_l(r_{bB}) g_l(r_{aA}) Y_0^{l*}(\hat{\mathbf{r}}_{bB}) V(r_{1p}) Y_0^l(\hat{\mathbf{r}}_{aA}).
\end{aligned} \tag{6.2.46}$$

Changing the integration variables and proceeding as in last section, (implying the

multiplicative factor $2\pi \sqrt{\frac{4\pi}{2l+1}}$, the above expression becomes

$$\begin{aligned} \langle \Psi_f^{(-)}(\mathbf{k}_{bB}) | V(r_{1p}) | \Psi_i^{(+)}(k_{aA}, \hat{\mathbf{z}}) \rangle &= \frac{2\pi}{k_{aA} k_{bB}} \sum_l \sqrt{(2j_f + 1)(2j_i + 1)} \\ &\times i^{-l} \exp[i(\sigma_l^f + \sigma_l^i)] Y_0^l(\hat{\mathbf{k}}_{bB}) \\ &\times \int dr_{aA} d\beta d\gamma dr_{12} dr_{b1} dr_{b2} r_{aA} \sin \beta r_{12} r_{b1} r_{b2} \\ &\times P_{l_f}(\cos \theta_A) P_{l_i}(\cos \theta_b) u_{l_f j_f}(r_{A1}) u_{l_f j_f}(r_{A2}) u_{l_i j_i}(r_{b1}) u_{l_i j_i}(r_{b2}) \\ &\times f_l(r_{bB}) g_l(r_{aA}) Y_0^{l*}(\hat{\mathbf{r}}_{bB}) V(r_{1p}) / r_{bB}, \end{aligned} \quad (6.2.47)$$

which eventually can be recasted, through the use of Legendre polynomials, in the expression,

$$\begin{aligned} T_{2N}^{1step} = \langle \Psi_f^{(-)}(\mathbf{k}_{bB}) | V(r_{1p}) | \Psi_i^{(+)}(k_{aA}, \hat{\mathbf{z}}) \rangle &= \frac{1}{2k_{aA} k_{bB}} \sum_l \sqrt{(2j_f + 1)(2j_i + 1)} \\ &\times i^{-l} \exp[i(\sigma_l^f + \sigma_l^i)] P_l(\cos \theta) (2l + 1) \\ &\times \int dr_{aA} d\beta d\gamma dr_{12} dr_{b1} dr_{b2} r_{aA} \sin \beta r_{12} r_{b1} r_{b2} \\ &\times P_{l_f}(\cos \theta_A) P_{l_i}(\cos \theta_b) u_{l_f j_f}(r_{A1}) u_{l_f j_f}(r_{A2}) V(r_{1p}) \\ &\times u_{l_i j_i}(r_{b1}) u_{l_i j_i}(r_{b2}) f_l(r_{bB}) g_l(r_{aA}) P_l(\cos \theta_{if}) / r_{bB}, \end{aligned} \quad (6.2.48)$$

expression which gives the same results as (6.2.41)

6.2.3 Coordinates for the calculation of simultaneous transfer

In what follows we explicit the coordinates used in the calculation of the above equations. Making use of the notation of Bayman (1971), we find the expression of the variables appearing in the integral as functions of the integration variables $r_{1p}, r_{2p}, r_{12}, R, \beta, \gamma$ (remember that $\mathbf{R} = R \hat{\mathbf{z}}$, see last section). \mathbf{R} being the center of mass coordinate. Thus, one can write

$$\mathbf{R} = \frac{1}{3} (\mathbf{r}_1 + \mathbf{r}_2 + \mathbf{r}_p) = \frac{1}{3} (\mathbf{R} + \mathbf{d}_1 + \mathbf{R} + \mathbf{d}_2 + \mathbf{R} + \mathbf{d}_p), \quad (6.2.49)$$

so

$$\mathbf{d}_1 + \mathbf{d}_2 + \mathbf{d}_p = 0. \quad (6.2.50)$$

Together with

$$\mathbf{d}_1 + \mathbf{r}_{12} = \mathbf{d}_2 \quad \mathbf{d}_2 + \mathbf{r}_{2p} = \mathbf{d}_p, \quad (6.2.51)$$

we find

$$\mathbf{d}_1 = \frac{1}{3} (2\mathbf{r}_{12} + \mathbf{r}_{2p}), \quad (6.2.52)$$

and

$$d_1^2 = \frac{1}{9} (4r_{12}^2 + r_{2p}^2 + 4\mathbf{r}_{12}\mathbf{r}_{2p}). \quad (6.2.53)$$

Making use of

$$\begin{aligned} \mathbf{r}_{12} + \mathbf{r}_{2p} &= \mathbf{r}_{1p} \\ r_{1p}^2 &= r_{12}^2 + r_{2p}^2 + 2\mathbf{r}_{12}\mathbf{r}_{2p} \\ 2\mathbf{r}_{12}\mathbf{r}_{2p} &= r_{1p}^2 - r_{12}^2 - r_{2p}^2. \end{aligned} \quad (6.2.54)$$

one obtains

$$d_1 = \frac{1}{3} \sqrt{2r_{12}^2 + 2r_{1p}^2 - r_{2p}^2}. \quad (6.2.55)$$

Similarly,

$$d_2 = \frac{1}{3} \sqrt{2r_{12}^2 + 2r_{2p}^2 - r_{1p}^2} \quad d_p = \frac{1}{3} \sqrt{2r_{2p}^2 + 2r_{1p}^2 - r_{12}^2}. \quad (6.2.56)$$

We now express the angle α between \mathbf{d}_1 and \mathbf{r}_{12} . We have

$$-\mathbf{d}_1 \mathbf{r}_{12} = r_{12} d_1 \cos(\alpha), \quad (6.2.57)$$

and

$$\begin{aligned} \mathbf{d}_1 + \mathbf{r}_{12} &= \mathbf{d}_2 \\ d_1^2 + r_{12}^2 + 2\mathbf{d}_1\mathbf{r}_{12} &= d_2^2. \end{aligned} \quad (6.2.58)$$

Consequently,

$$\cos(\alpha) = \frac{d_1^2 + r_{12}^2 - d_2^2}{2r_{12}d_1}. \quad (6.2.59)$$

The complete determination of $\mathbf{r}_1, \mathbf{r}_2, \mathbf{r}_{12}$ can be made by writing their expression in a simple configuration, in which the triangle lies in the xz -plane with \mathbf{d}_1 pointing along the positive z -direction, and $\mathbf{R} = 0$. Then, a first rotation $\mathcal{R}_z(\gamma)$ of an angle γ around the z -axis, a second rotation $\mathcal{R}_y(\beta)$ of an angle β around the y -axis, and a translation along \mathbf{R} will bring the vectors to the most general configuration. In other words,

$$\begin{aligned} \mathbf{r}_1 &= \mathbf{R} + \mathcal{R}_y(\beta)\mathcal{R}_z(\gamma)\mathbf{r}'_1, \\ \mathbf{r}_{12} &= \mathcal{R}_y(\beta)\mathcal{R}_z(\gamma)\mathbf{r}'_{12}, \\ \mathbf{r}_2 &= \mathbf{r}_1 + \mathbf{r}_{12}, \end{aligned} \quad (6.2.60)$$

with

$$\mathbf{r}'_1 = \begin{bmatrix} 0 \\ 0 \\ d_1 \end{bmatrix}, \quad (6.2.61)$$

$$\mathbf{r}'_{12} = r_{12} \begin{bmatrix} \sin(\alpha) \\ 0 \\ -\cos(\alpha) \end{bmatrix}, \quad (6.2.62)$$

and the rotation matrixes are

$$\mathcal{R}_y(\beta) = \begin{bmatrix} \cos(\beta) & 0 & \sin(\beta) \\ 0 & 1 & 0 \\ -\sin(\beta) & 0 & \cos(\beta) \end{bmatrix}, \quad (6.2.63)$$

and

$$\mathcal{R}_z(\gamma) = \begin{bmatrix} \cos(\gamma) & -\sin(\gamma) & 0 \\ \sin(\gamma) & \cos(\gamma) & 0 \\ 0 & 0 & 1 \end{bmatrix}. \quad (6.2.64)$$

then

$$\mathbf{r}_1 = \begin{bmatrix} d_1 \sin(\beta) \\ 0 \\ R + d_1 \cos(\beta) \end{bmatrix}, \quad (6.2.65)$$

$$\mathbf{r}_{12} = \begin{bmatrix} r_{12} \cos(\beta) \cos(\gamma) \sin(\alpha) - r_{12} \sin(\beta) \cos(\alpha) \\ r_{12} \sin(\gamma) \sin(\alpha) \\ -r_{12} \sin(\beta) \cos(\gamma) \sin(\alpha) - r_{12} \cos(\alpha) \cos(\beta) \end{bmatrix}, \quad (6.2.66)$$

$$\mathbf{r}_2 = \begin{bmatrix} d_1 \sin(\beta) + r_{12} \cos(\beta) \cos(\gamma) \sin(\alpha) - r_{12} \sin(\beta) \cos(\alpha) \\ r_{12} \sin(\gamma) \sin(\alpha) \\ R + d_1 \cos(\beta) - r_{12} \sin(\beta) \cos(\gamma) \sin(\alpha) - r_{12} \cos(\alpha) \cos(\beta) \end{bmatrix}. \quad (6.2.67)$$

We also need $\cos(\theta_{12})$, ζ and $\cos(\theta_\zeta)$, θ_{12} being the angle between \mathbf{r}_1 and \mathbf{r}_2 , $\zeta = \mathbf{r}_p - \frac{\mathbf{r}_1 + \mathbf{r}_2}{A+2}$ the position of the proton with respect to the final nucleus, and θ_ζ the angle between ζ and the z -axis:

$$\cos(\theta_{12}) = \frac{\mathbf{r}_1 \cdot \mathbf{r}_2}{r_1 r_2}, \quad (6.2.68)$$

and

$$\zeta = 3\mathbf{R} - \frac{A+3}{A+2}(\mathbf{r}_1 + \mathbf{r}_2), \quad (6.2.69)$$

where we have used (6.2.49).

For heavy ions, we find instead

$$\mathbf{R} = \frac{1}{m_a} (\mathbf{r}_{A1} + \mathbf{r}_{A2} + m_b \mathbf{r}_{Ab}), \quad (6.2.70)$$

$$\mathbf{d}_1 = \frac{1}{m_a} (m_b \mathbf{r}_{b2} - (m_b + 1) \mathbf{r}_{12}), \quad (6.2.71)$$

$$d_1 = \frac{1}{m_a} \sqrt{(m_b + 1)r_{12}^2 + m_b(m_b + 1)r_{b1}^2 - m_b r_{b2}^2}, \quad (6.2.72)$$

$$d_2 = \frac{1}{m_a} \sqrt{(m_b + 1)r_{12}^2 + m_b(m_b + 1)r_{b2}^2 - m_b r_{b1}^2}, \quad (6.2.73)$$

and

$$\zeta = \frac{m_a}{m_b} \mathbf{R} - \frac{m_B + m_b}{m_b m_B} (\mathbf{r}_{A1} + \mathbf{r}_{A2}). \quad (6.2.74)$$

The rest of the formulae are identical to the (t, p) ones. We list them for convenience,

$$\mathbf{r}_{A1} = \begin{bmatrix} d_1 \sin(\beta) \\ 0 \\ R + d_1 \cos(\beta) \end{bmatrix}, \quad (6.2.75)$$

$$\mathbf{r}_{A2} = \begin{bmatrix} d_1 \sin(\beta) + r_{12} \cos(\beta) \cos(\gamma) \sin(\alpha) - r_{12} \sin(\beta) \cos(\alpha) \\ r_{12} \sin(\gamma) \sin(\alpha) \\ R + d_1 \cos(\beta) - r_{12} \sin(\beta) \cos(\gamma) \sin(\alpha) - r_{12} \cos(\alpha) \cos(\beta) \end{bmatrix}. \quad (6.2.76)$$

We we also find

$$\mathbf{r}_{b1} = \frac{1}{m_b} (\mathbf{r}_{A2} + (m_b + 1) \mathbf{r}_{A1} - m_a \mathbf{R}), \quad (6.2.77)$$

and

$$\mathbf{r}_{b2} = \frac{1}{m_b} (\mathbf{r}_{A1} + (m_b + 1) \mathbf{r}_{A2} - m_a \mathbf{R}). \quad (6.2.78)$$

One can readily obtain

$$\cos \theta_{12} = \frac{r_{A1}^2 + r_{A2}^2 - r_{12}^2}{2r_{A1}r_{A2}}, \quad (6.2.79)$$

and

$$\cos \theta_i = \frac{r_{b1}^2 + r_{b2}^2 - r_{12}^2}{2r_{b1}r_{b2}}. \quad (6.2.80)$$

6.2.4 Matrix element for the transition amplitude (alternative derivation)

In what follows we work out an alternative derivation of T_{2N}^{1step} , more closely related to heavy ion reactions⁷, that is

$$\begin{aligned} T^{(1)}(\theta) = & 2 \frac{(4\pi)^{3/2}}{k_{Aa} k_{Bb}} \sum_{l_p j_p m_l l_t j_p} i^{-l_p} \exp[i(\sigma_{l_p}^p + \sigma_{l_t}^t)] \sqrt{2l_t + 1} \\ & \times \langle l_p \ m - m_p \ 1/2 \ m_p | j_p \ m \rangle \langle l_t \ 0 \ 1/2 \ m_t | j_t \ m_t \rangle Y_{m-m_p}^{l_p}(\hat{\mathbf{k}}_{Bb}) \\ & \times \sum_{\sigma_1 \sigma_2 \sigma_p} \int d\mathbf{r}_{Cc} d\mathbf{r}_{b1} d\mathbf{r}_{A2} [\psi^{j_f}(\mathbf{r}_{A1}, \sigma_1) \psi^{j_f}(\mathbf{r}_{A2}, \sigma_2)]_0^{0*} \\ & \times v(r_{b1}) [\psi^{j_i}(\mathbf{r}_{b1}, \sigma_1) \psi^{j_i}(\mathbf{r}_{b2}, \sigma_2)]_0^0 \frac{g_{l_t j_t}(r_{Aa}) f_{l_p j_p}(r_{Bb})}{r_{Aa} r_{Bb}} \\ & \times [Y^{l_t}(\hat{\mathbf{r}}_{Aa}) \chi(\sigma_p)]_{m_t}^{j_t} [Y^{l_p}(\hat{\mathbf{r}}_{Bb}) \chi(\sigma_p)]_m^{j_p*}. \end{aligned} \quad (6.2.81)$$

⁷Bayman and Chen (1982).

As shown above one can write,

$$\begin{aligned} \sum_{\sigma_p} \langle l_p m - m_p 1/2 m_p | j_p m \rangle \langle l_t 0 1/2 m_t | j_t m_t \rangle & \left[Y^{l_t}(\hat{\mathbf{r}}_{Aa}) \chi(\sigma_p) \right]_{m_t}^{j_t} \left[Y^{l_p}(\hat{\mathbf{r}}_{Bb}) \chi(\sigma_p) \right]_m^{j_p*} \\ &= -\frac{\delta_{l_p, l_t} \delta_{j_p, j_t} \delta_{m, m_t}}{\sqrt{2l+1}} \left[Y^l(\hat{\mathbf{r}}_{Aa}) Y^l(\hat{\mathbf{r}}_{Bb}) \right]_0^0 \begin{cases} \frac{l}{2l+1} & \text{if } m_t = m_p \\ -\frac{\sqrt{l(l+1)}}{2l+1} & \text{if } m_t = -m_p \end{cases} \end{aligned} \quad (6.2.82)$$

when $j = l - 1/2$ and

$$\begin{aligned} \sum_{\sigma_p} \langle l_p m - m_p 1/2 m_p | j_p m \rangle \langle l_t 0 1/2 m_t | j_t m_t \rangle & \left[Y^{l_t}(\hat{\mathbf{r}}_{Aa}) \chi(\sigma_p) \right]_{m_t}^{j_t} \left[Y^{l_p}(\hat{\mathbf{r}}_{Bb}) \chi(\sigma_p) \right]_m^{j_p*} \\ &= -\frac{\delta_{l_p, l_t} \delta_{j_p, j_t} \delta_{m, m_t}}{\sqrt{2l+1}} \left[Y^l(\hat{\mathbf{r}}_{Aa}) Y^l(\hat{\mathbf{r}}_{Bb}) \right]_0^0 \begin{cases} \frac{l+1}{2l+1} & \text{if } m_t = m_p \\ \frac{\sqrt{l(l+1)}}{2l+1} & \text{if } m_t = -m_p \end{cases} \end{aligned} \quad (6.2.83)$$

if $j = l + 1/2$. One then gets

$$\begin{aligned} T^{(1)}(\mu = 0; \theta) = & 2 \frac{(4\pi)^{3/2}}{k_{Aa} k_{Bb}} \sum_l i^{-l} \frac{\exp[i(\sigma_l^p + \sigma_l^t)]}{2l+1} Y_{m_t - m_p}^l(\hat{\mathbf{k}}_{Bb}) \\ & \times \sum_{\sigma_1 \sigma_2} \int \frac{d\mathbf{r}_{Cc} d\mathbf{r}_{b1} d\mathbf{r}_{A2}}{r_{Aa} r_{Bb}} \left[\psi^{j_f}(\mathbf{r}_{A1}, \sigma_1) \psi^{j_f}(\mathbf{r}_{A2}, \sigma_2) \right]_0^{0*} \\ & \times v(r_{b1}) \left[\psi^{j_i}(\mathbf{r}_{b1}, \sigma_1) \psi^{j_i}(\mathbf{r}_{b2}, \sigma_2) \right]_0^0 \left[Y^l(\hat{\mathbf{r}}_{Aa}) Y^l(\hat{\mathbf{r}}_{Bb}) \right]_0^0 \\ & \times \left[(f_{ll+1/2}(r_{Bb}) g_{ll+1/2}(r_{Aa})(l+1) + f_{ll-1/2}(r_{Bb}) g_{ll-1/2}(r_{Aa})l) \delta_{m_p, m_t} \right. \\ & \left. + (f_{ll+1/2}(r_{Bb}) g_{ll+1/2}(r_{Aa}) \sqrt{l(l+1)} - f_{ll-1/2}(r_{Bb}) g_{ll-1/2}(r_{Aa}) \sqrt{l(l+1)}) \delta_{m_p, -m_t} \right]. \end{aligned} \quad (6.2.84)$$

Making use of the relations,

$$\begin{aligned} & \left[\psi^{j_f}(\mathbf{r}_{A1}, \sigma_1) \psi^{j_f}(\mathbf{r}_{A2}, \sigma_2) \right]_0^{0*} \\ &= ((l_f \frac{1}{2})_{j_f} (l_f \frac{1}{2})_{j_f} | (l_f l_f)_0 (\frac{1}{2} \frac{1}{2})_0)_0 u_{l_f}(r_{A1}) u_{l_f}(r_{A2}) \\ & \times \left[Y^{l_f}(\hat{\mathbf{r}}_{A1}) Y^{l_f}(\hat{\mathbf{r}}_{A2}) \right]_0^{0*} [\chi(\sigma_1) \chi(\sigma_2)]_0^{0*} \\ &= \sqrt{\frac{2j_f + 1}{2(2l_f + 1)}} u_{l_f}(r_{A1}) u_{l_f}(r_{A2}) \\ & \times \left[Y^{l_f}(\hat{\mathbf{r}}_{A1}) Y^{l_f}(\hat{\mathbf{r}}_{A2}) \right]_0^{0*} [\chi(\sigma_1) \chi(\sigma_2)]_0^{0*} \\ &= \sqrt{\frac{2j_f + 1}{2}} \frac{u_{l_f}(r_{A1}) u_{l_f}(r_{A2})}{4\pi} P_{l_f}(\cos \omega_A) [\chi(\sigma_1) \chi(\sigma_2)]_0^{0*}, \end{aligned} \quad (6.2.85)$$

and

$$\begin{aligned}
& \left[\psi^{j_i}(\mathbf{r}_{b1}, \sigma_1) \psi^{j_i}(\mathbf{r}_{b2}, \sigma_2) \right]_0^0 \\
&= ((l_i \frac{1}{2})_{j_i} (l_i \frac{1}{2})_{j_i} | (l_i l_i)_0 (\frac{1}{2} \frac{1}{2})_0)_0 u_{l_i}(r_{b1}) u_{l_i}(r_{b2}) \\
&\quad \times \left[Y^{l_i}(\hat{\mathbf{r}}_{b1}) Y^{l_i}(\hat{\mathbf{r}}_{b2}) \right]_0^0 [\chi(\sigma_1) \chi(\sigma_2)]_0^0 \\
&= \sqrt{\frac{2j_i + 1}{2(2l_i + 1)}} u_{l_i}(r_{b1}) u_{l_i}(r_{b2}) \\
&\quad \times \left[Y^{l_i}(\hat{\mathbf{r}}_{b1}) Y^{l_i}(\hat{\mathbf{r}}_{b2}) \right]_0^0 [\chi(\sigma_1) \chi(\sigma_2)]_0^0 \\
&= \sqrt{\frac{2j_i + 1}{2}} \frac{u_{l_i}(r_{b1}) u_{l_i}(r_{b2})}{4\pi} P_{l_i}(\cos \omega_b) [\chi(\sigma_1) \chi(\sigma_2)]_0^0,
\end{aligned} \tag{6.2.86}$$

where ω_A is the angle between \mathbf{r}_{A1} and \mathbf{r}_{A2} , and ω_b is the angle between \mathbf{r}_{b1} and \mathbf{r}_{b2} . Consequently

$$\begin{aligned}
T^{(1)}(\theta) &= (4\pi)^{-3/2} \frac{\sqrt{(2j_i + 1)(2j_f + 1)}}{k_{Aa} k_{Bb}} \sum_l i^{-l} \frac{\exp[i(\sigma_l^p + \sigma_l^t)]}{\sqrt{2l + 1}} Y_{m_t - m_p}^l(\hat{\mathbf{k}}_{Bb}) \\
&\quad \times \int \frac{d\mathbf{r}_{Cc} d\mathbf{r}_{b1} d\mathbf{r}_{A2}}{r_{Aa} r_{Bb}} P_{l_f}(\cos \omega_A) P_{l_i}(\cos \omega_b) P_l(\cos \omega_{if}) \\
&\quad \times v(r_{b1}) u_{l_i}(r_{b1}) u_{l_i}(r_{b2}) u_{l_f}(r_{A1}) u_{l_f}(r_{A2}) \\
&\quad \times \left[(f_{ll+1/2}(r_{Bb}) g_{ll+1/2}(r_{Aa})(l+1) + f_{ll-1/2}(r_{Bb}) g_{ll-1/2}(r_{Aa})l) \delta_{m_p, m_t} \right. \\
&\quad \left. + (f_{ll+1/2}(r_{Bb}) g_{ll+1/2}(r_{Aa}) \sqrt{l(l+1)} - f_{ll-1/2}(r_{Bb}) g_{ll-1/2}(r_{Aa}) \sqrt{l(l+1)}) \delta_{m_p, -m_t} \right],
\end{aligned} \tag{6.2.87}$$

where ω_{if} is the angle between \mathbf{r}_{Aa} and \mathbf{r}_{Bb} . For heavy ions, we can consider that the optical potential does not have a spin-orbit term, and the distorted waves are independent of j . We thus have

$$\begin{aligned}
T^{(1)}(\theta) &= (4\pi)^{-3/2} \frac{\sqrt{(2j_i + 1)(2j_f + 1)}}{k_{Aa} k_{Bb}} \sum_l i^{-l} \exp[i(\sigma_l^p + \sigma_l^t)] Y_0^l(\hat{\mathbf{k}}_{Bb}) \sqrt{2l + 1} \\
&\quad \times \int \frac{d\mathbf{r}_{Cc} d\mathbf{r}_{b1} d\mathbf{r}_{A2}}{r_{Aa} r_{Bb}} P_{l_f}(\cos \omega_A) P_{l_i}(\cos \omega_b) P_l(\cos \omega_{if}) \\
&\quad \times v(r_{b1}) u_{l_i}(r_{b1}) u_{l_i}(r_{b2}) u_{l_f}(r_{A1}) u_{l_f}(r_{A2}) f_l(r_{Bb}) g_l(r_{Aa}).
\end{aligned} \tag{6.2.88}$$

Changing variables one obtains,

$$\begin{aligned}
 T^{(1)}(\theta) = & (4\pi)^{-1} \frac{\sqrt{(2j_i + 1)(2j_f + 1)}}{k_{Aa} k_{Bb}} \sum_l \exp[i(\sigma_l^p + \sigma_l^t)] P_l(\cos \theta) (2l + 1) \\
 & \times \int dr_{1A} dr_{2A} dr_{Aa} d(\cos \beta) d(\cos \omega_A) d\gamma r_{1A}^2 r_{2A}^2 r_{Aa}^2 \\
 & \times P_{l_f}(\cos \omega_A) P_{l_i}(\cos \omega_b) P_l(\cos \omega_{if}) v(r_{b1}) \\
 & \times u_{l_i}(r_{b1}) u_{l_i}(r_{b2}) u_{l_f}(r_{A1}) u_{l_f}(r_{A2}) f_l(r_{Bb}) g_l(r_{Aa}).
 \end{aligned} \tag{6.2.89}$$

6.2.5 Coordinates used to derive Eq. (6.2.89)

We determine the relation between the integration variables in (6.2.87) and the coordinates needed to evaluate the quantities in the integrand. Noting that

$$\mathbf{r}_{Aa} = \frac{\mathbf{r}_{A1} + \mathbf{r}_{A2} + m_b \mathbf{r}_{Ab}}{m_b + 2}, \tag{6.2.90}$$

one has

$$\mathbf{r}_{b1} = \mathbf{r}_{bA} + \mathbf{r}_{A1} = \frac{(m_b + 1)\mathbf{r}_{A1} + \mathbf{r}_{A2} - (m_b + 2)\mathbf{r}_{Aa}}{m_b}, \tag{6.2.91}$$

$$\mathbf{r}_{b2} = \mathbf{r}_{bA} + \mathbf{r}_{A2} = \frac{(m_b + 1)\mathbf{r}_{A2} + \mathbf{r}_{A1} - (m_b + 2)\mathbf{r}_{Aa}}{m_b}, \tag{6.2.92}$$

and

$$\begin{aligned}
 \mathbf{r}_{Cc} = \mathbf{r}_{CA} + \mathbf{r}_{A1} + \mathbf{r}_{1c} &= -\frac{1}{m_A + 1} \mathbf{r}_{A2} + \mathbf{r}_{A1} - \frac{m_b}{m_b + 1} \mathbf{r}_{b1} \\
 &= \frac{m_b + 2}{m_b + 1} \mathbf{r}_{Aa} - \frac{m_b + 2 + m_A}{(m_b + 1)(m_A + 1)} \mathbf{r}_{A2}
 \end{aligned} \tag{6.2.93}$$

Since,

$$\mathbf{r}_{AB} = \frac{\mathbf{r}_{A1} + \mathbf{r}_{A2}}{m_A + 2}, \tag{6.2.94}$$

one obtains

$$\mathbf{r}_{Bb} = \mathbf{r}_{BA} + \mathbf{r}_{Ab} = \frac{m_b + 2}{m_b} \mathbf{r}_{Aa} - \frac{m_A + m_b + 2}{(m_A + 2)m_b} (\mathbf{r}_{A1} + \mathbf{r}_{A2}). \tag{6.2.95}$$

Using the same rotations as those used in Section 6.2.3 one gets,

$$\mathbf{r}_{A1} = r_{A1} \begin{bmatrix} \sin \alpha \\ 0 \\ \cos \alpha \end{bmatrix}, \tag{6.2.96}$$

and

$$\mathbf{r}_{A2} = r_{A2} \begin{bmatrix} -\cos \alpha \cos \gamma \sin \omega_A + \sin \alpha \cos \omega_A \\ -\sin \gamma \sin \omega_A \\ \sin \alpha \cos \gamma \sin \omega_A + \cos \alpha \cos \omega_A \end{bmatrix}, \tag{6.2.97}$$

with

$$\cos \alpha = \frac{r_{A1}^2 - d_1^2 + r_{Aa}^2}{2r_{A1}r_{Aa}}, \quad (6.2.98)$$

and

$$d_1 = \sqrt{r_{A1}^2 - r_{Aa}^2 \sin^2 \beta} - r_{Aa} \cos \beta. \quad (6.2.99)$$

Note that though β, r_{1A}, r_{Aa} are independent integration variables, they have to fulfill the condition

$$r_{Aa} \sin \beta \leq r_{A1}, \quad \text{for } 0 \leq \beta \leq \pi. \quad (6.2.100)$$

The expression of the remaining quantities appearing in the integral are now straightforward,

$$\begin{aligned} r_{b1} &= m_b^{-1} |(m_b + 1)\mathbf{r}_{A1} + \mathbf{r}_{A2} - (m_b + 2)\mathbf{r}_{Aa}| \\ &= m_b^{-1} \left((m_b + 2)^2 r_{Aa}^2 + (m_b + 1)^2 r_{A1}^2 + r_{A2}^2 \right. \\ &\quad \left. - 2(m_b + 2)(m_b + 1)\mathbf{r}_{Aa} \mathbf{r}_{A1} - 2(m_b + 2)\mathbf{r}_{Aa} \mathbf{r}_{A2} + 2(m_b + 1)\mathbf{r}_{A1} \mathbf{r}_{A2} \right)^{1/2}, \end{aligned} \quad (6.2.101)$$

$$\begin{aligned} r_{b2} &= m_b^{-1} |(m_b + 1)\mathbf{r}_{A2} + \mathbf{r}_{A1} - (m_b + 2)\mathbf{r}_{Aa}| \\ &= m_b^{-1} \left((m_b + 2)^2 r_{Aa}^2 + (m_b + 1)^2 r_{A2}^2 + r_{A1}^2 \right. \\ &\quad \left. - 2(m_b + 2)(m_b + 1)\mathbf{r}_{Aa} \mathbf{r}_{A2} - 2(m_b + 2)\mathbf{r}_{Aa} \mathbf{r}_{A1} + 2(m_b + 1)\mathbf{r}_{A2} \mathbf{r}_{A1} \right)^{1/2}, \end{aligned} \quad (6.2.102)$$

$$\begin{aligned} r_{Bb} &= \left| \frac{m_b + 2}{m_b} \mathbf{r}_{Aa} - \frac{m_A + m_b + 2}{(m_A + 2)m_b} (\mathbf{r}_{A1} + \mathbf{r}_{A2}) \right| \\ &= \left[\left(\frac{m_b + 2}{m_b} \right)^2 r_{Aa}^2 + \left(\frac{m_A + m_b + 2}{(m_A + 2)m_b} \right)^2 (r_{A1}^2 + r_{A2}^2 + 2\mathbf{r}_{A1} \mathbf{r}_{A2}) \right. \\ &\quad \left. - 2 \frac{(m_b + 2)(m_A + m_b + 2)}{(m_A + 2)m_b^2} \mathbf{r}_{Aa} (\mathbf{r}_{A1} + \mathbf{r}_{A2}) \right]^{1/2}, \end{aligned} \quad (6.2.103)$$

$$\begin{aligned} r_{Cc} &= \left| \frac{m_b + 2}{m_b + 1} \mathbf{r}_{Aa} - \frac{m_b + 2 + m_A}{(m_b + 1)(m_A + 1)} \mathbf{r}_{A2} \right| \\ &= \left[\left(\frac{m_a}{(m_a - 1)} \right)^2 r_{Aa}^2 + \left(\frac{m_A + m_a}{(m_A + 1)(m_a - 1)} \right)^2 r_{A2}^2 \right. \\ &\quad \left. - 2 \frac{m_A m_a + m_a^2}{(m_A + 1)(m_a - 1)^2} \mathbf{r}_{Aa} \mathbf{r}_{A2} \right]^{1/2}, \end{aligned} \quad (6.2.104)$$

$$\cos \omega_b = \frac{\mathbf{r}_{b1} \mathbf{r}_{b2}}{r_{b1} r_{b2}}, \quad (6.2.105)$$

$$\cos \omega_{if} = \frac{\mathbf{r}_{Ad} \mathbf{r}_{Bb}}{r_{Aa} r_{Bb}}, \quad (6.2.106)$$

with

$$\mathbf{r}_{Aa}\mathbf{r}_{A1} = r_{Aa}r_{A1} \cos \alpha, \quad (6.2.107)$$

$$\mathbf{r}_{Aa}\mathbf{r}_{A2} = r_{Aa}r_{A2}(\sin \alpha \cos \gamma \sin \omega_A + \cos \alpha \cos \omega_A), \quad (6.2.108)$$

$$\mathbf{r}_{A1}\mathbf{r}_{A2} = r_{A1}r_{A2} \cos \omega_A. \quad (6.2.109)$$

6.2.6 Successive transfer

The successive two-neutron transfer amplitudes can be written as (Bayman and Chen (1982)):

$$\begin{aligned} T_{succ}^{(2)}(\theta) = & \frac{4\mu_{Cc}}{\hbar^2} \sum_{\substack{\sigma_1 \sigma_2 \\ \sigma'_1 \sigma'_2 \\ KM}} \int d^3 r_{Cc} d^3 r_{b1} d^3 r_{A2} d^3 r'_{Cc} d^3 r'_{b1} d^3 r'_{A2} \chi^{(-)*}(\mathbf{k}_{Bb}, \mathbf{r}_{Bb}) \\ & \times \left[\psi^{j_f}(\mathbf{r}_{A1}, \sigma_1) \psi^{j_f}(\mathbf{r}_{A2}, \sigma_2) \right]_0^{0*} v(r_{b1}) \left[\psi^{j_f}(\mathbf{r}_{A2}, \sigma_2) \psi^{j_i}(\mathbf{r}_{b1}, \sigma_1) \right]_M^K \\ & \times G(\mathbf{r}_{Cc}, \mathbf{r}'_{Cc}) \left[\psi^{j_f}(\mathbf{r}'_{A2}, \sigma'_2) \psi^{j_i}(\mathbf{r}'_{b1}, \sigma'_1) \right]_M^{K*} v(r'_{c2}) \\ & \times \left[\psi^{j_i}(\mathbf{r}'_{b1}, \sigma'_1) \psi^{j_i}(\mathbf{r}'_{b2}, \sigma'_2) \right]_0^0 \chi^{(+)}(\mathbf{r}'_{Aa}). \end{aligned} \quad (6.2.110)$$

It is of notice that the time-reversal phase convention is used throughout. Expanding the Green function and the distorted waves in a basis of angular momentum eigenstate one can write,

$$\chi^{(-)*}(\mathbf{k}_{Bb}, \mathbf{r}_{Bb}) = \sum_{\tilde{l}} \frac{4\pi}{k_{Bb} r_{Bb}} i^{-\tilde{l}} e^{i\sigma_f^{\tilde{l}}} F_{\tilde{l}} \sum_m Y_m^{\tilde{l}}(\hat{r}_{Bb}) Y_m^{\tilde{l}*}(\hat{k}_{Bb}), \quad (6.2.111)$$

the sum over m being

$$\sum_m (-1)^{\tilde{l}-m} Y_m^{\tilde{l}}(\hat{r}_{Bb}) Y_{-m}^{\tilde{l}}(\hat{k}_{Bb}) = \sqrt{2\tilde{l}+1} \left[Y^{\tilde{l}}(\hat{r}_{Bb}) Y^{\tilde{l}}(\hat{k}_{Bb}) \right]_0^0, \quad (6.2.112)$$

where we have used (6.D.2) and (6.D.18), so

$$\chi^{(-)*}(\mathbf{k}_{Bb}, \mathbf{r}_{Bb}) = \sum_{\tilde{l}} \sqrt{2\tilde{l}+1} \frac{4\pi}{k_{Bb} r_{Bb}} i^{-\tilde{l}} e^{i\sigma_f^{\tilde{l}}} F_{\tilde{l}}(r_{Bb}) \left[Y^{\tilde{l}}(\hat{r}_{Bb}) Y^{\tilde{l}}(\hat{k}_{Bb}) \right]_0^0. \quad (6.2.113)$$

Similarly,

$$\chi^{(+)}(\mathbf{r}'_{Aa}) = \sum_l i^l \sqrt{2l+1} \frac{4\pi}{k_{Aa} r'_{Aa}} e^{i\sigma_i^l} F_l(r'_{Aa}) \left[Y^l(\hat{r}'_{Aa}) Y^l(\hat{k}_{Aa}) \right]_0^0 \quad (6.2.114)$$

where we have taken into account the choice $\hat{k}_{Aa} \equiv \hat{z}$. The Green function can be written as

$$G(\mathbf{r}_{Cc}, \mathbf{r}'_{Cc}) = i \sum_{l_c} \sqrt{2l_c + 1} \frac{f_{l_c}(k_{Cc}, r_<) P_{l_c}(k_{Cc}, r_>)}{k_{Cc} r_{Cc} r'_{Cc}} \left[Y^{l_c}(\hat{r}_{Cc}) Y^{l_c}(\hat{r}'_{Cc}) \right]_0^0. \quad (6.2.115)$$

Finally

$$\begin{aligned} T_{succ}^{(2)}(\theta) = & \frac{4\mu_{Cc}(4\pi)^2 i}{\hbar^2 k_{Aa} k_{Bb} k_{Cc}} \sum_{l, l_c, \tilde{l}} e^{i(\sigma_i^l + \sigma_f^{\tilde{l}}) t^{l-\tilde{l}}} \sqrt{(2l+1)(2l_c+1)(2\tilde{l}+1)} \\ & \times \sum_{\sigma_1 \sigma_2} \int d^3 r_{Cc} d^3 r_{b1} d^3 r_{A2} d^3 r'_{Cc} d^3 r'_{b1} d^3 r'_{A2} v(r_{b1}) v(r'_{c2}) \left[Y^{\tilde{l}}(\hat{r}_{Bb}) Y^{\tilde{l}}(\hat{k}_{Bb}) \right]_0^0 \\ & \times \left[Y^l(\hat{r}'_{Aa}) Y^l(\hat{k}'_{Aa}) \right]_0^0 \left[Y^{l_c}(\hat{r}_{Cc}) Y^{l_c}(\hat{r}'_{Cc}) \right]_0^0 \frac{F_{\tilde{l}}(r_{Bb})}{r_{Bb}} \frac{F_l(r'_{Aa})}{r'_{Aa}} \\ & \times \frac{f_{l_c}(k_{Cc}, r_<) P_{l_c}(k_{Cc}, r_>)}{r_{Cc} r'_{Cc}} \left[\psi^{j_f}(\mathbf{r}_{A1}, \sigma_1) \psi^{j_f}(\mathbf{r}_{A2}, \sigma_2) \right]_0^{0*} \\ & \times \left[\psi^{j_i}(\mathbf{r}'_{b1}, \sigma'_1) \psi^{j_i}(\mathbf{r}'_{b2}, \sigma'_2) \right]_0^0 \sum_{KM} \left[\psi^{j_f}(\mathbf{r}_{A2}, \sigma_2) \psi^{j_i}(\mathbf{r}_{b1}, \sigma_1) \right]_M^K \\ & \times \left[\psi^{j_f}(\mathbf{r}'_{A2}, \sigma'_2) \psi^{j_i}(\mathbf{r}'_{b1}, \sigma'_1) \right]_M^{K*}. \end{aligned} \quad (6.2.116)$$

Let us now perform the integration over \mathbf{r}_{A2} ,

$$\begin{aligned} & \sum_{\sigma_1 \sigma_2} \int d\mathbf{r}_{A2} \left[\psi^{j_f}(\mathbf{r}_{A1}, \sigma_1) \psi^{j_f}(\mathbf{r}_{A2}, \sigma_2) \right]_0^{0*} \left[\psi^{j_f}(\mathbf{r}_{A2}, \sigma_2) \psi^{j_i}(\mathbf{r}_{b1}, \sigma_1) \right]_M^K \\ &= \sum_{\sigma_1 \sigma_2} (-1)^{1/2-\sigma_1+1/2-\sigma_2} \int d\mathbf{r}_{A2} \left[\psi^{j_f}(\mathbf{r}_{A1}, -\sigma_1) \psi^{j_f}(\mathbf{r}_{A2}, -\sigma_2) \right]_0^0 \left[\psi^{j_f}(\mathbf{r}_{A2}, \sigma_2) \psi^{j_i}(\mathbf{r}_{b1}, \sigma_1) \right]_M^K \\ &= - \sum_{\sigma_1 \sigma_2} (-1)^{1/2-\sigma_1+1/2-\sigma_2} \int d\mathbf{r}_{A2} \left[\psi^{j_f}(\mathbf{r}_{A2}, -\sigma_2) \psi^{j_f}(\mathbf{r}_{A1}, -\sigma_1) \right]_0^0 \left[\psi^{j_f}(\mathbf{r}_{A2}, \sigma_2) \psi^{j_i}(\mathbf{r}_{b1}, \sigma_1) \right]_M^K \\ &= -((j_f j_f)_0 (j_f j_i)_K |(j_f j_f)_0 (j_f j_i)_K)_K \sum_{\sigma_1 \sigma_2} (-1)^{1/2-\sigma_1+1/2-\sigma_2} \\ & \quad \times \int d\mathbf{r}_{A2} \left[\psi^{j_f}(\mathbf{r}_{A2}, -\sigma_2) \psi^{j_f}(\mathbf{r}_{A2}, \sigma_2) \right]_0^0 \left[\psi^{j_f}(\mathbf{r}_{A1}, -\sigma_1) \psi^{j_i}(\mathbf{r}_{b1}, \sigma_1) \right]_M^K \\ &= \frac{1}{2j_f + 1} \sqrt{2j_f + 1} ((l_f \frac{1}{2})_{j_f} (l_i \frac{1}{2})_{j_i} |(l_f l_i)_K (\frac{1}{2} \frac{1}{2})_0)_K \\ & \quad \times u_{l_f}(r_{A1}) u_{l_i}(r_{b1}) \left[Y^{l_f}(\hat{r}_{A1}) Y^{l_i}(\hat{r}_{b1}) \right]_M^K \sum_{\sigma_1} (-1)^{1/2-\sigma_1} \left[\chi^{1/2}(-\sigma_1) \chi^{1/2}(\sigma_1) \right]_0^0 \\ &= - \sqrt{\frac{2}{2j_f + 1}} ((l_f \frac{1}{2})_{j_f} (l_i \frac{1}{2})_{j_i} |(l_f l_i)_K (\frac{1}{2} \frac{1}{2})_0)_K \left[Y^{l_f}(\hat{r}_{A1}) Y^{l_i}(\hat{r}_{b1}) \right]_M^K u_{l_f}(r_{A1}) u_{l_i}(r_{b1}), \end{aligned} \quad (6.2.117)$$

where we have evaluated the 9*j*-symbol

$$((j_f j_f)_0 (j_f j_i)_K | (j_f j_f)_0 (j_f j_i)_K)_K = \frac{1}{2j_f + 1}, \quad (6.2.118)$$

as well as (6.D.19). We proceed in a similar way to evaluate the integral over \mathbf{r}'_{b1} ,

$$\begin{aligned} & \sum_{\sigma'_1, \sigma'_2} \int d\mathbf{r}'_{b1} [\psi^{j_i}(\mathbf{r}'_{b1}, \sigma'_1) \psi^{j_i}(\mathbf{r}'_{b2}, \sigma'_2)]_0^0 [\psi^{j_f}(\mathbf{r}'_{A2}, \sigma'_2) \psi^{j_i}(\mathbf{r}'_{b1}, \sigma'_1)]_M^{K*} \\ &= -(-1)^{K-M} \sum_{\sigma'_1, \sigma'_2} \int d\mathbf{r}'_{b1} [\psi^{j_f}(\mathbf{r}'_{A2}, -\sigma'_2) \psi^{j_i}(\mathbf{r}'_{b1}, -\sigma'_1)]_{-M}^K \\ & \times [\psi^{j_i}(\mathbf{r}'_{b2}, \sigma'_2) \psi^{j_i}(\mathbf{r}'_{b1}, \sigma'_1)]_0^0 (-1)^{1/2-\sigma'_1+1/2-\sigma'_2} \\ &= -(-1)^{K-M} ((j_f j_i)_K (j_i j_i)_0 | (j_f j_i)_K (j_i j_i)_0)_K (-\sqrt{2j_i + 1}) \\ & \times ((l_f \frac{1}{2})_{j_f} (l_i \frac{1}{2})_{j_i} | (l_f l_i)_K (\frac{1}{2} \frac{1}{2})_0)_K (-\sqrt{2}) u_{l_f}(r'_{A2}) u_{l_i}(r'_{b2}) [Y^{l_f}(\hat{r}'_{A2}) Y^{l_i}(\hat{r}'_{b2})]_{-M}^K \\ &= -\sqrt{\frac{2}{2j_i + 1}} ((l_f \frac{1}{2})_{j_f} (l_i \frac{1}{2})_{j_i} | (l_f l_i)_K (\frac{1}{2} \frac{1}{2})_0)_K [Y^{l_f}(\hat{r}'_{A2}) Y^{l_i}(\hat{r}'_{b2})]_M^{K*} u_{l_f}(r'_{A2}) u_{l_i}(r'_{b2}). \end{aligned} \quad (6.2.119)$$

Setting the different elements together one obtains

$$\begin{aligned} T_{succ}^{(2)}(\theta) &= \frac{4\mu_{Cc}(4\pi)^2 i}{\hbar^2 k_{Aa} k_{Bb} k_{Cc}} \frac{2}{\sqrt{(2j_i + 1)(2j_f + 1)}} \sum_{K,M} ((l_f \frac{1}{2})_{j_f} (l_i \frac{1}{2})_{j_i} | (l_f l_i)_K (\frac{1}{2} \frac{1}{2})_0)_K^2 \\ & \times \sum_{l_c, l, \tilde{l}} e^{i(\sigma'_i + \sigma'_f)} \sqrt{(2l_c + 1)(2l + 1)(2\tilde{l} + 1)} i^{l-\tilde{l}} \\ & \times \int d^3 r_{Cc} d^3 r_{b1} d^3 r'_{Cc} d^3 r'_{A2} v(r_{b1}) v(r'_{c2}) u_{l_f}(r_{A1}) u_{l_i}(r_{b1}) u_{l_f}(r'_{A2}) u_{l_i}(r'_{b2}) \\ & \times [Y^{l_f}(\hat{r}'_{A2}) Y^{l_i}(\hat{r}'_{b2})]_M^{K*} [Y^{l_f}(\hat{r}_{A1}) Y^{l_i}(\hat{r}_{b1})]_M^K \frac{F_l(r'_{Aa}) F_{\tilde{l}}(r'_{Bb}) f_{l_c}(k_{Cc}, r_{<}) P_{l_c}(k_{Cc}, r_{>})}{r'_{Aa} r_{Bb} r_{Cc} r'_{Cc}} \\ & \times [Y^{\tilde{l}}(\hat{r}_{Bb}) Y^{\tilde{l}}(\hat{k}_{Bb})]_0^0 [Y^l(\hat{r}'_{Aa}) Y^l(\hat{k}_{Aa})]_0^0 [Y^{l_c}(\hat{r}_{Cc}) Y^{l_c}(\hat{r}'_{Cc})]_0^0. \end{aligned} \quad (6.2.120)$$

We now proceed to write this expression in a more compact way. For this purpose one writes

$$\begin{aligned} & [Y^{\tilde{l}}(\hat{r}_{Bb}) Y^{\tilde{l}}(\hat{k}_{Bb})]_0^0 [Y^l(\hat{r}'_{Aa}) Y^l(\hat{k}_{Aa})]_0^0 = \\ & ((l l)_0 (\tilde{l} \tilde{l})_0 | (l \tilde{l})_0 (l \tilde{l})_0)_0 [Y^{\tilde{l}}(\hat{r}_{Bb}) Y^l(\hat{r}'_{Aa})]_0^0 [Y^{\tilde{l}}(\hat{k}_{Bb}) Y^l(\hat{k}_{Aa})]_0^0 \\ & = \frac{\delta_{\tilde{l}l}}{2l + 1} [Y^l(\hat{r}_{Bb}) Y^l(\hat{r}'_{Aa})]_0^0 [Y^l(\hat{k}_{Bb}) Y^l(\hat{k}_{Aa})]_0^0. \end{aligned} \quad (6.2.121)$$

Taking into account the relations

$$\left[Y^l(\hat{k}_{Bb}) Y^l(\hat{k}_{Aa}) \right]_0^0 = \frac{(-1)^l}{\sqrt{4\pi}} Y_0^l(\hat{k}_{Bb}) l^l, \quad (6.2.122)$$

and

$$\begin{aligned} & \left[Y^l(\hat{r}_{Bb}) Y^l(\hat{r}'_{Aa}) \right]_0^0 \left[Y^{l_c}(\hat{r}_{Cc}) Y^{l_c}(\hat{r}'_{Cc}) \right]_0^0 = \\ & \quad ((ll)_0(l_c l_c)_0 | (ll_c)_K (ll_c)_K)_0 \left\{ \left[Y^l(\hat{r}_{Bb}) Y^{l_c}(\hat{r}_{Cc}) \right]^K \left[Y^l(\hat{r}'_{Aa}) Y^{l_c}(\hat{r}'_{Cc}) \right]^K \right\}_0^0 \\ & \quad = \sqrt{\frac{2K+1}{(2l+1)(2l_c+1)}} \\ & \quad \times \sum_{M'} \frac{(-1)^{K+M'}}{\sqrt{2K+1}} \left[Y^l(\hat{r}_{Bb}) Y^{l_c}(\hat{r}_{Cc}) \right]_{-M'}^K \left[Y^l(\hat{r}'_{Aa}) Y^{l_c}(\hat{r}'_{Cc}) \right]_{M'}^K \\ & \quad = \sqrt{\frac{1}{(2l+1)(2l_c+1)}} \\ & \quad \times \sum_{M'} \left[Y^l(\hat{r}_{Bb}) Y^{l_c}(\hat{r}_{Cc}) \right]_{M'}^{K*} \left[Y^l(\hat{r}'_{Aa}) Y^{l_c}(\hat{r}'_{Cc}) \right]_{M'}^K. \end{aligned} \quad (6.2.123)$$

It is of notice that the integrals

$$\int d\hat{r}_{Cc} d\hat{r}_{b1} \left[Y^l(\hat{r}_{Bb}) Y^{l_c}(\hat{r}_{Cc}) \right]_M^{K*} \left[Y^{l_f}(\hat{r}_{A1}) Y^{l_i}(\hat{r}_{b1}) \right]_M^K, \quad (6.2.124)$$

and

$$\int d\hat{r}'_{Cc} d\hat{r}'_{A2} \left[Y^l(\hat{r}'_{Aa}) Y^{l_c}(\hat{r}'_{Cc}) \right]_M^K \left[Y^{l_f}(\hat{r}'_{A2}) Y^{l_i}(\hat{r}'_{b2}) \right]_M^{K*}, \quad (6.2.125)$$

over the angular variables do not depend on M . Let us see why this is so with the help of (6.2.124),

$$\begin{aligned} & \left[Y^l(\hat{r}_{Bb}) Y^{l_c}(\hat{r}_{Cc}) \right]_M^{K*} \left[Y^{l_f}(\hat{r}_{A1}) Y^{l_i}(\hat{r}_{b1}) \right]_M^K = (-1)^{K-M} \left[Y^l(\hat{r}_{Bb}) Y^{l_c}(\hat{r}_{Cc}) \right]_{-M}^K \\ & \quad \times \left[Y^{l_f}(\hat{r}_{A1}) Y^{l_i}(\hat{r}_{b1}) \right]_M^K = (-1)^{K-M} \sum_J \langle K \ K \ M \ - M | J \ 0 \rangle \\ & \quad \times \left\{ \left[Y^l(\hat{r}_{Bb}) Y^{l_c}(\hat{r}_{Cc}) \right]^K \left[Y^{l_f}(\hat{r}_{A1}) Y^{l_i}(\hat{r}_{b1}) \right]^K \right\}_0^J. \end{aligned} \quad (6.2.126)$$

After integration, only the term

$$\begin{aligned} & (-1)^{K-M} \langle K \ K \ M \ - M | 0 \ 0 \rangle \left\{ \left[Y^l(\hat{r}_{Bb}) Y^{l_c}(\hat{r}_{Cc}) \right]^K \left[Y^{l_f}(\hat{r}_{A1}) Y^{l_i}(\hat{r}_{b1}) \right]^K \right\}_0^0 = . \\ & \quad \frac{1}{\sqrt{2K+1}} \left\{ \left[Y^l(\hat{r}_{Bb}) Y^{l_c}(\hat{r}_{Cc}) \right]^K \left[Y^{l_f}(\hat{r}_{A1}) Y^{l_i}(\hat{r}_{b1}) \right]^K \right\}_0^0 \end{aligned} \quad (6.2.127)$$

corresponding to $J = 0$ survives, which is indeed independent of M . We can thus omit the sum over M in (6.2.120) and multiply by $(2K + 1)$, obtaining

$$\begin{aligned} T_{succ}^{(2)}(\theta) &= \frac{64\mu_{Cc}(\pi)^{3/2}i}{\hbar^2 k_{Aa} k_{Bb} k_{Cc}} \frac{i^{-l}}{\sqrt{(2j_i + 1)(2j_f + 1)}} \\ &\times \sum_K (2K + 1)((l_f \frac{1}{2})_{j_f} (l_i \frac{1}{2})_{j_i} | (l_f l_i)_K (\frac{1}{2} \frac{1}{2})_0)_K^2 \\ &\times \sum_{l_c, l} \frac{e^{i(\sigma_i^l + \sigma_f^l)}}{\sqrt{(2l + 1)}} Y_0^l(\hat{k}_{Bb}) S_{K, l, l_c}, \end{aligned} \quad (6.2.128)$$

where

$$\begin{aligned} S_{K, l, l_c} &= \int d^3 r_{Cc} d^3 r_{b1} v(r_{b1}) u_{l_f}(r_{A1}) u_{l_i}(r_{b1}) \frac{s_{K, l, l_c}(r_{Cc})}{r_{Cc}} \frac{F_l(r_{Bb})}{r_{Bb}} \\ &\times [Y^{l_f}(\hat{r}_{A1}) Y^{l_i}(\hat{r}_{b1})]_M^K [Y^{l_c}(\hat{r}_{Cc}) Y^l(\hat{r}_{Bb})]_M^{K*}, \end{aligned} \quad (6.2.129)$$

and

$$\begin{aligned} s_{K, l, l_c}(r_{Cc}) &= \int_{r_{Cc, fixed}} d^3 r'_{Cc} d^3 r'_{A2} v(r'_{c2}) u_{l_f}(r'_{A2}) u_{l_i}(r'_{b2}) \frac{F_l(r'_{Aa})}{r'_{Aa}} \frac{f_l(k_{Cc}, r_{<}) P_{l_c}(k_{Cc}, r_{>})}{r'_{Cc}} \\ &\times [Y^{l_f}(\hat{r}'_{A2}) Y^{l_i}(\hat{r}'_{b2})]_M^{K*} [Y^{l_c}(\hat{r}'_{Cc}) Y^l(\hat{r}'_{Aa})]_M^K. \end{aligned} \quad (6.2.130)$$

It can be shown that the integrand in (6.2.129) is independent of M . Consequently, one can sum over M and divide by $(2K + 1)$, to get

$$\begin{aligned} \frac{1}{2K + 1} v(r_{b1}) u_{l_f}(r_{A1}) u_{l_i}(r_{b1}) \frac{s_{K, l, l_c}(r_{Cc})}{r_{Cc}} \frac{F_l(r_{Bb})}{r_{Bb}} \\ \times \sum_M [Y^{l_f}(\hat{r}_{A1}) Y^{l_i}(\hat{r}_{b1})]_M^K [Y^{l_c}(\hat{r}_{Cc}) Y^l(\hat{r}_{Bb})]_M^{K*}. \end{aligned} \quad (6.2.131)$$

This integrand is rotationally invariant (it is proportional to a T_M^L spherical tensor with $L = 0, M = 0$), so one can evaluate it in the “standard” configuration in which \mathbf{r}_{Cc} is directed along the z -axis and multiply by $8\pi^2$ (see Bayman and Chen (1982)), obtaining the final expression for S_{K, l, l_c} :

$$\begin{aligned} S_{K, l, l_c} &= \frac{4\pi^{3/2} \sqrt{2l_c + 1}}{2K + 1} i^{-l_c} \\ &\times \int r_{Cc}^2 dr_{Cc} r_{b1}^2 dr_{b1} \sin \theta d\theta v(r_{b1}) u_{l_f}(r_{A1}) u_{l_i}(r_{b1}) \\ &\times \frac{s_{K, l, l_c}(r_{Cc})}{r_{Cc}} \frac{F_l(r_{Bb})}{r_{Bb}} \\ &\times \sum_M \langle l_c 0 l M | K M \rangle [Y^{l_f}(\hat{r}_{A1}) Y^{l_i}(\theta + \pi, 0)]_M^K Y_M^{l*}(\hat{r}_{Bb}). \end{aligned} \quad (6.2.132)$$

Similarly, one has

$$\begin{aligned}
 s_{K,l,l_c}(r_{Cc}) &= \frac{4\pi^{3/2} \sqrt{2l_c + 1}}{2K + 1} i^{l_c} \\
 &\times \int r'_{Cc}^2 dr'_{Cc} r'^2_{A2} dr'_{A2} \sin \theta' d\theta' v(r'_{c2}) u_{l_f}(r'_{A2}) u_{l_i}(r'_{b2}) \\
 &\times \frac{F_l(r'_{Aa})}{r'_{Aa}} \frac{f_{l_c}(k_{Cc}, r_<) P_{l_c}(k_{Cc}, r_>)}{r'_{Cc}} \\
 &\times \sum_M \langle l_c 0 l M | K M \rangle [Y^{l_f}(\hat{r}'_{A2}) Y^{l_i}(\hat{r}'_{b2})]_M^{K*} Y_M^l(\hat{r}'_{Aa}).
 \end{aligned} \tag{6.2.133}$$

Introducing the further approximations $\mathbf{r}_{A1} \approx \mathbf{r}_{C1}$ and $\mathbf{r}_{b2} \approx \mathbf{r}_{c2}$, one obtains the final expression

$$\begin{aligned}
 T_{succ}^{(2)}(\theta) &= \frac{1024\mu_{Cc}\pi^{9/2}i}{\hbar^2 k_{Aa} k_{Bb} k_{Cc}} \frac{1}{\sqrt{(2j_i+1)(2j_f+1)}} \\
 &\times \sum_K \frac{1}{2K+1} ((l_f \frac{1}{2})_{j_f} (l_i \frac{1}{2})_{j_i} | (l_f l_i)_K (\frac{1}{2} \frac{1}{2})_0)_K^2 \\
 &\times \sum_{l_c, l} e^{i(\sigma_i^l + \sigma_f^l)} \frac{(2l_c + 1)}{\sqrt{2l + 1}} Y_0^l(\hat{k}_{Bb}) S_{K,l,l_c},
 \end{aligned} \tag{6.2.134}$$

with

$$\begin{aligned}
 S_{K,l,l_c} &= \int r_{Cc}^2 dr_{Cc} r_{b1}^2 dr_{b1} \sin \theta d\theta v(r_{b1}) u_{l_f}(r_{C1}) u_{l_i}(r_{b1}) \\
 &\times \frac{s_{K,l,l_c}(r_{Cc})}{r_{Cc}} \frac{F_l(r_{Bb})}{r_{Bb}} \\
 &\times \sum_M \langle l_c 0 l M | K M \rangle [Y^{l_f}(\hat{r}_{C1}) Y^{l_i}(\theta + \pi, 0)]_M^K Y_M^{l*}(\hat{r}_{Bb}),
 \end{aligned} \tag{6.2.135}$$

and

$$\begin{aligned}
 s_{K,l,l_c}(r_{Cc}) &= \int r'_{Cc}^2 dr'_{Cc} r'^2_{A2} dr'_{A2} \sin \theta' d\theta' v(r'_{c2}) u_{l_f}(r'_{A2}) u_{l_i}(r'_{c2}) \\
 &\times \frac{F_l(r'_{Aa})}{r'_{Aa}} \frac{f_{l_c}(k_{Cc}, r_<) P_{l_c}(k_{Cc}, r_>)}{r'_{Cc}} \\
 &\times \sum_M \langle l_c 0 l M | K M \rangle [Y^{l_f}(\hat{r}'_{A2}) Y^{l_i}(\hat{r}'_{c2})]_M^{K*} Y_M^l(\hat{r}'_{Aa}).
 \end{aligned} \tag{6.2.136}$$

6.2.7 Coordinates for the successive transfer

In the standard configuration in which the integrals (6.2.135) and (6.2.136) are to be evaluated, we have

$$\mathbf{r}_{Cc} = r_{Cc} \hat{\mathbf{z}}, \quad \mathbf{r}_{b1} = r_{b1}(-\cos \theta \hat{\mathbf{z}} - \sin \theta \hat{\mathbf{x}}). \tag{6.2.137}$$

Now,

$$\begin{aligned}\mathbf{r}_{C1} &= \mathbf{r}_{Cc} + \mathbf{r}_{c1} = \mathbf{r}_{Cc} + \frac{m_b}{m_b + 1} \mathbf{r}_{b1} \\ &= \left(r_{Cc} - \frac{m_b}{m_b + 1} r_{b1} \cos \theta \right) \hat{\mathbf{z}} - \frac{m_b}{m_b + 1} r_{b1} \sin \theta \hat{\mathbf{x}},\end{aligned}\quad (6.2.138)$$

and

$$\mathbf{r}_{Bb} = \mathbf{r}_{BC} + \mathbf{r}_{Cb} = -\frac{1}{m_B} \mathbf{r}_{C1} + \mathbf{r}_{Cb}. \quad (6.2.139)$$

Substituting the relation

$$\mathbf{r}_{Cb} = \mathbf{r}_{Cc} + \mathbf{r}_{cb} = \mathbf{r}_{Cc} - \frac{1}{m_b + 1} \mathbf{r}_{b1}, \quad (6.2.140)$$

in (6.2.139) one gets

$$\mathbf{r}_{Bb} = \left(\frac{m_B - 1}{m_B} r_{Cc} + \frac{m_b + m_B}{m_B(m_b + 1)} r_{b1} \cos \theta \right) \hat{\mathbf{z}} + \frac{m_b + m_B}{m_B(m_b + 1)} r_{b1} \sin \theta \hat{\mathbf{x}}. \quad (6.2.141)$$

The primed variables are arranged in a similar fashion,

$$\mathbf{r}'_{Cc} = r'_{Cc} \hat{\mathbf{z}}, \quad \mathbf{r}'_{A2} = r'_{A2} (-\cos \theta' \hat{\mathbf{z}} - \sin \theta' \hat{\mathbf{x}}). \quad (6.2.142)$$

Thus,

$$\mathbf{r}'_{c2} = \left(-r'_{Cc} - \frac{m_A}{m_A + 1} r'_{A2} \cos \theta' \right) \hat{\mathbf{z}} - \frac{m_A}{m_A + 1} r'_{A2} \sin \theta' \hat{\mathbf{x}}, \quad (6.2.143)$$

and

$$\mathbf{r}'_{Aa} = \left(\frac{m_a - 1}{m_a} r'_{Cc} - \frac{m_A + m_a}{m_a(m_A + 1)} r'_{A2} \cos \theta' \right) \hat{\mathbf{z}} - \frac{m_A + m_a}{m_a(m_A + 1)} r'_{A2} \sin \theta' \hat{\mathbf{x}}. \quad (6.2.144)$$

6.2.8 Simplifying the vector coupling

We will now turn our attention to the vector-coupled quantities in (6.2.135) and (6.2.136),

$$\sum_M \langle l_c 0 l M | K M \rangle \left[Y^{l_f}(\hat{r}_{C1}) Y^{l_i}(\theta + \pi, 0) \right]_M^K Y_M^{l*}(\hat{r}_{Bb}), \quad (6.2.145)$$

and

$$\sum_M \langle l_c 0 l M | K M \rangle \left[Y^{l_f}(\hat{r}'_{A2}) Y^{l_i}(\hat{r}'_{c2}) \right]_M^{K*} Y_M^l(\hat{r}'_{Aa}). \quad (6.2.146)$$

We can express them both as

$$\sum_M f(M), \quad (6.2.147)$$

where e.g. in the case of (6.2.145), one has

$$f(M) = \langle l_c 0 l M | K M \rangle \left[Y^{l_f}(\hat{r}_{C1}) Y^{l_i}(\theta + \pi, 0) \right]_M^K Y_M^{l^*}(\hat{r}_{Bb}). \quad (6.2.148)$$

Note that all the vectors that come into play in the above expressions are in the (x, z) -plane. Consequently, the azimuthal angle ϕ is always equal to zero. Under these circumstances and for time-reversed phases, $(Y_M^{L^*}(\theta, 0) = (-1)^L Y_M^L(\theta, 0))$ one has

$$f(-M) = (-1)^{l_c + l_f + l_i + l} f(M). \quad (6.2.149)$$

Consequently,

$$\begin{aligned} \sum_M \langle l_c 0 l M | K M \rangle f(M) &= \langle l_c 0 l 0 | K 0 \rangle f(0) \\ &+ \sum_{M>0} \langle l_c 0 l M | K M \rangle f(M) \left(1 + (-1)^{l_c + l + l_i + l_f} \right). \end{aligned} \quad (6.2.150)$$

Consequently, in the case in which $l_c + l + l_i + l_f$ is odd, we have only to evaluate the $M = 0$ contribution. This consideration is useful to restrict the number of numerical operations needed to calculate the transition amplitude.

6.2.9 non-orthogonality term

We write the non-orthogonality contribution to the transition amplitude (see Bayman and Chen (1982)):

$$\begin{aligned} T_{NO}^{(2)}(\theta) = & 2 \sum_{\substack{\sigma_1 \sigma_2 \\ \sigma'_1 \sigma'_2 \\ KM}} \int d^3 r_{Cc} d^3 r_{b1} d^3 r_{A2} d^3 r'_{b1} d^3 r'_{A2} \chi^{(-)*}(\mathbf{k}_{Bb}, \mathbf{r}_{Bb}) \\ & \times \left[\psi^{j_f}(\mathbf{r}_{A1}, \sigma_1) \psi^{j_f}(\mathbf{r}_{A2}, \sigma_2) \right]_0^{0*} v(r_{b1}) \left[\psi^{j_f}(\mathbf{r}_{A2}, \sigma_2) \psi^{j_i}(\mathbf{r}_{b1}, \sigma_1) \right]_M^K \\ & \times \left[\psi^{j_f}(\mathbf{r}'_{A2}, \sigma'_2) \psi^{j_i}(\mathbf{r}'_{b1}, \sigma'_1) \right]_M^{K*} \left[\psi^{j_i}(\mathbf{r}'_{b1}, \sigma'_1) \psi^{j_i}(\mathbf{r}'_{b2}, \sigma'_2) \right]_0^0 \chi^{(+)}(\mathbf{r}'_{Aa}). \end{aligned} \quad (6.2.151)$$

This expression is equivalent to (6.2.110) if we make the replacement

$$\frac{2\mu_{Cc}}{\hbar^2} G(\mathbf{r}_{Cc}, \mathbf{r}'_{Cc}) v(r'_{A2}) \rightarrow \delta(\mathbf{r}_{Cc} - \mathbf{r}'_{Cc}). \quad (6.2.152)$$

Looking at the partial-wave expansions of $G(\mathbf{r}_{Cc}, \mathbf{r}'_{Cc})$ and $\delta(\mathbf{r}_{Cc} - \mathbf{r}'_{Cc})$ (see App. 6.D), we find that we can use the above expressions for the successive transfer with the replacement

$$i \frac{2\mu_{Cc}}{\hbar^2} \frac{f_{l_c}(k_{Cc}, r_<) P_{l_c}(k_{Cc}, r_>)}{k_{Cc}} \rightarrow \delta(r_{Cc} - r'_{Cc}). \quad (6.2.153)$$

We thus have

$$\begin{aligned} T_{2NT}^{NO} = & \frac{512\pi^{9/2}}{k_{Aa}k_{Bb}} \frac{1}{\sqrt{(2j_i+1)(2j_f+1)}} \\ & \times \sum_K ((l_f \frac{1}{2})_{j_f} (l_i \frac{1}{2})_{j_i} | (l_f l_i)_K (\frac{1}{2} \frac{1}{2})_0)_K^2 \\ & \times \sum_{l_c, l} e^{i(\sigma_i^l + \sigma_f^l)} \frac{(2l_c + 1)}{\sqrt{2l + 1}} Y_0^l(\hat{k}_{Bb}) S_{K, l, l_c}, \end{aligned} \quad (6.2.154)$$

with

$$\begin{aligned} S_{K, l, l_c} = & \int r_{Cc}^2 dr_{Cc} r_{b1}^2 dr_{b1} \sin \theta d\theta v(r_{b1}) u_{l_f}(r_{C1}) u_{l_i}(r_{b1}) \\ & \times \frac{s_{K, l, l_c}(r_{Cc})}{r_{Cc}} \frac{F_l(r_{Bb})}{r_{Bb}} \\ & \times \sum_M \langle l_c 0 l M | K M \rangle [Y^{l_f}(\hat{r}_{C1}) Y^{l_i}(\theta + \pi, 0)]_M^K Y_M^{l*}(\hat{r}_{Bb}), \end{aligned} \quad (6.2.155)$$

and

$$\begin{aligned} s_{K, l, l_c}(r_{Cc}) = & r_{Cc} \int dr'_{A2} r'^2_{A2} \sin \theta' d\theta' u_{l_f}(r'_{A2}) u_{l_i}(r'_{c2}) \frac{F_l(r'_{Aa})}{r'_{Aa}} \\ & \times \sum_M \langle l_c 0 l M | K M \rangle [Y^{l_f}(\hat{r}'_{A2}) Y^{l_i}(\hat{r}'_{c2})]_M^{K*} Y_M^l(\hat{r}'_{Aa}). \end{aligned} \quad (6.2.156)$$

6.2.10 Arbitrary orbital momentum transfer

We will now examine the case in which the two transferred nucleons carry an angular momentum Λ different from 0. Let us assume that two nucleons coupled to angular momentum Λ in the initial nucleus A are transferred into a final state of zero angular momentum in nucleus B . The transition amplitude is given by the integral

$$\begin{aligned} 2 \sum_{\sigma_1 \sigma_2} \int d\mathbf{r}_{cC} d\mathbf{r}_{A2} d\mathbf{r}_{b1} \chi^{(-)*}(\mathbf{r}_{bB}) [\psi^{j_f}(\mathbf{r}_{A1}, \sigma_1) \psi^{j_f}(\mathbf{r}_{A2}, \sigma_2)]_0^{0*} \\ \times v(r_{b1}) \Psi^{(+)}(\mathbf{r}_{aA}, \mathbf{r}_{b1}, \mathbf{r}_{b2}, \sigma_1, \sigma_2). \end{aligned} \quad (6.2.157)$$

If we neglect core excitations, the above expression is exact as long as $\Psi^{(+)}(\mathbf{r}_{aA}, \mathbf{r}_{b1}, \mathbf{r}_{b2}, \sigma_1, \sigma_2)$ is the exact wavefunction. We can instead obtain an approximation for the transfer amplitude using

$$\begin{aligned} \Psi^{(+)}(\mathbf{r}_{aA}, \mathbf{r}_{b1}, \mathbf{r}_{b2}, \sigma_1, \sigma_2) \approx & \chi^{(+)}(\mathbf{r}_{aA}) [\psi^{j_{i1}}(\mathbf{r}_{b1}, \sigma_1) \psi^{j_{i2}}(\mathbf{r}_{b2}, \sigma_2)]_\mu^\Lambda \\ & + \sum_{K, M} \mathcal{U}_{K, M}(\mathbf{r}_{cC}) [\psi^{j_f}(\mathbf{r}_{A2}, \sigma_2) \psi^{j_{i1}}(\mathbf{r}_{b1}, \sigma_1)]_M^K \end{aligned} \quad (6.2.158)$$

as an approximation for the incoming state. The first term of (6.2.158) gives rise to the simultaneous amplitude, while from second one leads to both the successive and the non-orthogonality contributions. To extract the amplitude $\mathcal{U}_{K,M}(\mathbf{r}_{cC})$, we define $f_{KM}(\mathbf{r}_{cC})$ as the scalar product

$$f_{KM}(\mathbf{r}_{cC}) = \left\langle \left[\psi^{j_f}(\mathbf{r}_{A2}, \sigma_2) \psi^{j_{i1}}(\mathbf{r}_{b1}, \sigma_1) \right]_M^K \middle| \Psi^{(+)}(\mathbf{r}_{aA}, \mathbf{r}_{b1}, \mathbf{r}_{b2}, \sigma_1, \sigma_2) \right\rangle \quad (6.2.159)$$

for fixed \mathbf{r}_{cC} , which can be seen to obey the equation

$$\begin{aligned} & \left(\frac{\hbar^2}{2\mu_{cC}} k_{cC}^2 + \frac{\hbar^2}{2\mu_{cC}} \nabla_{r_{cC}}^2 - U(r_{cC}) \right) f_{KM}(\mathbf{r}_{cC}) \\ &= \left\langle \left[\psi^{j_f}(\mathbf{r}_{A2}, \sigma_2) \psi^{j_{i1}}(\mathbf{r}_{b1}, \sigma_1) \right]_M^K \middle| v(r_{c2}) \middle| \Psi^{(+)}(\mathbf{r}_{aA}, \mathbf{r}_{b1}, \mathbf{r}_{b2}, \sigma_1, \sigma_2) \right\rangle. \end{aligned} \quad (6.2.160)$$

The solution can be written in terms of the Green function $G(\mathbf{r}_{cC}, \mathbf{r}'_{cC})$ defined by

$$\left(\frac{\hbar^2}{2\mu_{cC}} k_{cC}^2 + \frac{\hbar^2}{2\mu_{cC}} \nabla_{r_{cC}}^2 - U(r_{cC}) \right) G(\mathbf{r}_{cC}, \mathbf{r}'_{cC}) = \frac{\hbar^2}{2\mu_{cC}} \delta(\mathbf{r}_{cC} - \mathbf{r}'_{cC}). \quad (6.2.161)$$

Thus,

$$\begin{aligned} f_{KM}(\mathbf{r}_{cC}) &= \frac{2\mu_{cC}}{\hbar^2} \int d\mathbf{r}'_{cC} G(\mathbf{r}_{cC}, \mathbf{r}'_{cC}) \left\langle \left[\psi^{j_f}(\mathbf{r}'_{A2}, \sigma'_2) \psi^{j_{i1}}(\mathbf{r}'_{b1}, \sigma'_1) \right]_M^K \middle| v(r_{c2}) \middle| \Psi^{(+)}(\mathbf{r}'_{aA}, \mathbf{r}'_{b1}, \mathbf{r}'_{b2}, \sigma'_1, \sigma'_2) \right\rangle \\ &\approx \frac{2\mu_{cC}}{\hbar^2} \sum_{\sigma'_1 \sigma'_2} \int d\mathbf{r}'_{cC} d\mathbf{r}'_{A2} d\mathbf{r}'_{b1} G(\mathbf{r}_{cC}, \mathbf{r}'_{cC}) \left[\psi^{j_f}(\mathbf{r}'_{A2}, \sigma'_2) \psi^{j_{i1}}(\mathbf{r}'_{b1}, \sigma'_1) \right]_M^{K*} \\ &\quad \times v(r'_{c2}) \chi^{(+)}(\mathbf{r}'_{aA}) \left[\psi^{j_{i1}}(\mathbf{r}'_{b1}, \sigma'_1) \psi^{j_{i2}}(\mathbf{r}'_{b2}, \sigma'_2) \right]_\mu^\Lambda = \mathcal{U}_{K,M}(\mathbf{r}_{cC}) \\ &\quad + \left\langle \left[\psi^{j_f}(\mathbf{r}'_{A2}, \sigma_2) \psi^{j_{i1}}(\mathbf{r}'_{b1}, \sigma_1) \right]_M^K \middle| \chi^{(+)}(\mathbf{r}'_{aA}) \left[\psi^{j_{i1}}(\mathbf{r}'_{b1}, \sigma'_1) \psi^{j_{i2}}(\mathbf{r}'_{b2}, \sigma'_2) \right]_\mu^\Lambda \right\rangle. \end{aligned} \quad (6.2.162)$$

Therefore

$$\begin{aligned} \mathcal{U}_{K,M}(\mathbf{r}_{cC}) &= \frac{2\mu_{cC}}{\hbar^2} \sum_{\sigma'_1 \sigma'_2} \int d\mathbf{r}'_{cC} d\mathbf{r}'_{A2} d\mathbf{r}'_{b1} G(\mathbf{r}_{cC}, \mathbf{r}'_{cC}) \left[\psi^{j_f}(\mathbf{r}'_{A2}, \sigma'_2) \psi^{j_{i1}}(\mathbf{r}'_{b1}, \sigma'_1) \right]_M^{K*} \\ &\quad \times v(r'_{c2}) \chi^{(+)}(\mathbf{r}'_{aA}) \left[\psi^{j_{i1}}(\mathbf{r}'_{b1}, \sigma'_1) \psi^{j_{i2}}(\mathbf{r}'_{b2}, \sigma'_2) \right]_\mu^\Lambda \\ &\quad - \left\langle \left[\psi^{j_f}(\mathbf{r}'_{A2}, \sigma_2) \psi^{j_{i1}}(\mathbf{r}'_{b1}, \sigma_1) \right]_M^K \middle| \chi^{(+)}(\mathbf{r}'_{aA}) \left[\psi^{j_{i1}}(\mathbf{r}'_{b1}, \sigma'_1) \psi^{j_{i2}}(\mathbf{r}'_{b2}, \sigma'_2) \right]_\mu^\Lambda \right\rangle. \end{aligned} \quad (6.2.163)$$

When we substitute $\mathcal{U}_{K,M}(\mathbf{r}_{cC})$ into (6.2.158) and (6.2.157), the first term gives rise to the successive amplitude for the two-particle transfer, while the second term is responsible for the non-orthogonal contribution.

6.2.11 Successive transfer contribution

We need to evaluate the integral

$$\begin{aligned} T_{succ}^{(2)}(\theta; \mu) = & \frac{4\mu_{cC}}{\hbar^2} \sum_{\sigma_1 \sigma_2} \sum_{KM} \int d\mathbf{r}_{cC} d\mathbf{r}_{A2} d\mathbf{r}_{b1} d\mathbf{r}'_{cC} d\mathbf{r}'_{A2} d\mathbf{r}'_{b1} [\psi^{j_f}(\mathbf{r}_{A1}, \sigma_1) \psi^{j_f}(\mathbf{r}_{A2}, \sigma_2)]_0^{0*} \\ & \times \chi^{(-)*}(\mathbf{r}_{bB}) G(\mathbf{r}_{cC}, \mathbf{r}'_{cC}) [\psi^{j_f}(\mathbf{r}'_{A2}, \sigma'_2) \psi^{j_{i1}}(\mathbf{r}'_{b1}, \sigma'_1)]_M^{K*} \chi^{(+)}(\mathbf{r}'_{aA}) v(r'_{c2}) v(r_{b1}) \\ & \times [\psi^{j_{i1}}(\mathbf{r}'_{b1}, \sigma'_1) \psi^{j_{i2}}(\mathbf{r}'_{b2}, \sigma'_2)]_\mu^K [\psi^{j_f}(\mathbf{r}_{A2}, \sigma_2) \psi^{j_{i1}}(\mathbf{r}_{b1}, \sigma_1)]_M^K, \end{aligned} \quad (6.2.164)$$

where we must substitute the Green function and the distorted waves by their partial wave expansions (see App. 6.E). The integral over \mathbf{r}'_{b1} is:

$$\begin{aligned} & \sum_{\sigma'_1} \int d\mathbf{r}'_{b1} [\psi^{j_f}(\mathbf{r}'_{A2}, \sigma'_2) \psi^{j_{i1}}(\mathbf{r}'_{b1}, \sigma'_1)]_M^{K*} [\psi^{j_{i1}}(\mathbf{r}'_{b1}, \sigma'_1) \psi^{j_{i2}}(\mathbf{r}'_{b2}, \sigma'_2)]_\mu^K \\ &= \sum_{\sigma'_1} \int d\mathbf{r}'_{b1} (-1)^{-M+j_f+j_{i1}-\sigma_1-\sigma_2} [\psi^{j_{i1}}(\mathbf{r}'_{b1}, -\sigma'_1) \psi^{j_f}(\mathbf{r}'_{A2}, -\sigma'_2)]_{-M}^K [\psi^{j_{i1}}(\mathbf{r}'_{b1}, \sigma'_1) \psi^{j_{i2}}(\mathbf{r}'_{b2}, \sigma'_2)]_\mu^K \\ &= \sum_{\sigma'_1} \int d\mathbf{r}'_{b1} (-1)^{-M+j_f+j_{i1}-\sigma_1-\sigma_2} \sum_P \langle K \Lambda - M \mu | P \mu - M \rangle ((j_{i1} j_f)_K (j_{i1} j_{i2})_\Lambda | (j_{i1} j_{i1})_0 (j_f j_{i2})_P)_P \\ & \quad \times [\psi^{j_{i1}}(\mathbf{r}'_{b1}, -\sigma'_1) \psi^{j_{i1}}(\mathbf{r}'_{b1}, \sigma'_1)]_0^0 [\psi^{j_f}(\mathbf{r}'_{A2}, -\sigma'_2) \psi^{j_{i2}}(\mathbf{r}'_{b2}, \sigma'_2)]_{\mu-M}^P \\ &= (-1)^{-M+j_f+j_{i1}} \sqrt{2j_{i1}+1} u_{l_f}(r_{A2}) u_{l_{i2}}(r'_{b2}) \sum_P \langle K \Lambda - M \mu | P \mu - M \rangle \\ & \quad \times ((j_{i1} j_f)_K (j_{i1} j_{i2})_\Lambda | (j_{i1} j_{i1})_0 (j_f j_{i2})_P)_P ((l_f \frac{1}{2})_{j_f} (l_{i2} \frac{1}{2})_{j_{i2}} | (l_f l_{i2})_P (\frac{1}{2} \frac{1}{2})_0)_P \\ & \quad \times [Y^{l_f}(\hat{\mathbf{r}}'_{A2}) Y^{l_{i2}}(\hat{\mathbf{r}}'_{b2})]_{\mu-M}^P u_{l_f}(r_{A2}) u_{l_{i2}}(r_{b2}). \end{aligned} \quad (6.2.165)$$

Integrating over \mathbf{r}_{A2} (see (6.2.117)) leads to,

$$\begin{aligned} & \sum_{\sigma_2} \int d\mathbf{r}_{A2} [\psi^{j_f}(\mathbf{r}_{A1}, \sigma_1) \psi^{j_f}(\mathbf{r}_{A2}, \sigma_2)]_0^{0*} [\psi^{j_f}(\mathbf{r}_{A2}, \sigma_2) \psi^{j_{i1}}(\mathbf{r}_{b1}, \sigma_1)]_M^K \\ &= - \sqrt{\frac{2}{2j_f+1}} ((l_f \frac{1}{2})_{j_f} (l_{i1} \frac{1}{2})_{j_{i1}} | (l_f l_{i1})_K (\frac{1}{2} \frac{1}{2})_0)_K [Y^{l_f}(\hat{\mathbf{r}}_{A1}) Y^{l_{i1}}(\hat{\mathbf{r}}_{b1})]_M^K u_{l_f}(r_{A1}) u_{l_{i1}}(r_{b1}). \end{aligned} \quad (6.2.166)$$

Let us examine the term

$$\sum_M (-1)^M \langle K \Lambda - M \mu | P \mu - M \rangle [Y^{l_f}(\hat{\mathbf{r}}_{A1}) Y^{l_{i1}}(\hat{\mathbf{r}}_{b1})]_M^K [Y^{l_f}(\hat{\mathbf{r}}'_{A2}) Y^{l_{i2}}(\hat{\mathbf{r}}'_{b2})]_{\mu-M}^P. \quad (6.2.167)$$

Making use of the relation

$$\langle l_1 l_2 m_1 m_2 | L M_L \rangle = (-1)^{l_2-m_2} \sqrt{\frac{2L+1}{2l_1+1}} \langle L l_2 - M_L m_2 | l_1 - m_1 \rangle, \quad (6.2.168)$$

the expression (6.2.168) is equivalent to,

$$(-1)^K \sqrt{\frac{2P+1}{2\Lambda+1}} \left\{ \left[Y^{l_f}(\hat{\mathbf{r}}'_{A2}) Y^{l_{i2}}(\hat{\mathbf{r}}'_{b2}) \right]^P \left[Y^{l_f}(\hat{\mathbf{r}}_{A1}) Y^{l_{i1}}(\hat{\mathbf{r}}_{b1}) \right]^K \right\}_\mu^\Lambda. \quad (6.2.169)$$

We now recouple the term

$$\left[Y^{l_a}(\hat{\mathbf{r}}'_{aA}) Y^{l_a}(\hat{\mathbf{k}}_{aA}) \right]_0^0 \left[Y^{l_b}(\hat{\mathbf{r}}_{bB}) Y^{l_b}(\hat{\mathbf{k}}_{bB}) \right]_0^0, \quad (6.2.170)$$

arising from the partial wave expansion of the incoming and outgoing distorted waves to have,

$$((l_a l_a)_0 (l_b l_b)_0 | (l_a l_b)_\Lambda (l_a l_b)_\Lambda)_0 \left\{ \left[Y^{l_a}(\hat{\mathbf{r}}'_{aA}) Y^{l_b}(\hat{\mathbf{r}}_{bB}) \right]^\Lambda \left[Y^{l_a}(\hat{\mathbf{k}}_{aA}) Y^{l_b}(\hat{\mathbf{k}}_{bB}) \right]_0^\Lambda \right\}_0^0. \quad (6.2.171)$$

The only term which does not vanish upon integration is

$$\frac{(-1)^{\Lambda-\mu}}{\sqrt{(2l_a+1)(2l_b+1)}} \left[Y^{l_a}(\hat{\mathbf{r}}'_{aA}) Y^{l_b}(\hat{\mathbf{r}}_{bB}) \right]_{-\mu}^\Lambda \left[Y^{l_a}(\hat{\mathbf{k}}_{aA}) Y^{l_b}(\hat{\mathbf{k}}_{bB}) \right]_\mu^\Lambda. \quad (6.2.172)$$

Again, the only term surviving

$$\left\{ \left[Y^{l_f}(\hat{\mathbf{r}}'_{A2}) Y^{l_{i2}}(\hat{\mathbf{r}}'_{b2}) \right]^P \left[Y^{l_f}(\hat{\mathbf{r}}_{A1}) Y^{l_{i1}}(\hat{\mathbf{r}}_{b1}) \right]^K \right\}_\mu^\Lambda \left[Y^{l_a}(\hat{\mathbf{r}}'_{aA}) Y^{l_b}(\hat{\mathbf{r}}_{bB}) \right]_{-\mu}^\Lambda \quad (6.2.173)$$

is

$$\begin{aligned} & \frac{(-1)^{\Lambda+\mu}}{\sqrt{2\Lambda+1}} \left[\left\{ \left[Y^{l_f}(\hat{\mathbf{r}}'_{A2}) Y^{l_{i2}}(\hat{\mathbf{r}}'_{b2}) \right]^P \right. \right. \\ & \left. \left. \left[Y^{l_f}(\hat{\mathbf{r}}_{A1}) Y^{l_{i1}}(\hat{\mathbf{r}}_{b1}) \right]^K \right\}^\Lambda \left[Y^{l_a}(\hat{\mathbf{r}}'_{aA}) Y^{l_b}(\hat{\mathbf{r}}_{bB}) \right]_0^\Lambda \right]. \end{aligned} \quad (6.2.174)$$

We now couple this last term with the term $\left[Y^{l_c}(\hat{\mathbf{r}}'_{cC})Y^{l_c}(\hat{\mathbf{r}}_{cC}) \right]_0^0$, arising from the partial wave expansion of the Green function. That is,

$$\begin{aligned}
& \left\{ \left[Y^{l_f}(\hat{\mathbf{r}}'_{A2})Y^{l_{i2}}(\hat{\mathbf{r}}'_{b2}) \right]^P \left[Y^{l_f}(\hat{\mathbf{r}}_{A1})Y^{l_{i1}}(\hat{\mathbf{r}}_{b1}) \right]^K \right\}^\Lambda \left[Y^{l_a}(\hat{\mathbf{r}}'_{aA})Y^{l_b}(\hat{\mathbf{r}}_{bB}) \right]^\Lambda \Big|_0^0 \left[Y^{l_c}(\hat{\mathbf{r}}'_{cC})Y^{l_c}(\hat{\mathbf{r}}_{cC}) \right]_0^0 \\
& = ((l_a l_b)_\Lambda (l_c l_c)_0 | (l_a l_c)_P (l_b l_c)_K)_\Lambda \left\{ \left[Y^{l_f}(\hat{\mathbf{r}}'_{A2})Y^{l_{i2}}(\hat{\mathbf{r}}'_{b2}) \right]^P \left[Y^{l_f}(\hat{\mathbf{r}}_{A1})Y^{l_{i1}}(\hat{\mathbf{r}}_{b1}) \right]^K \right\}^\Lambda \\
& \left\{ \left[Y^{l_a}(\hat{\mathbf{r}}'_{aA})Y^{l_c}(\hat{\mathbf{r}}'_{cC}) \right]^P \left[Y^{l_b}(\hat{\mathbf{r}}_{bB})Y^{l_c}(\hat{\mathbf{r}}_{cC}) \right]^K \right\}^\Lambda \Big|_0^0 = ((l_a l_b)_\Lambda (l_c l_c)_0 | (l_a l_c)_P (l_b l_c)_K)_\Lambda \\
& \times ((PK)_\Lambda (PK)_\Lambda | (PP)_0 (KK)_0)_0 \left\{ \left[Y^{l_f}(\hat{\mathbf{r}}'_{A2})Y^{l_{i2}}(\hat{\mathbf{r}}'_{b2}) \right]^P \left[Y^{l_a}(\hat{\mathbf{r}}'_{aA})Y^{l_c}(\hat{\mathbf{r}}'_{cC}) \right]^P \right\}_0^0 \\
& \times \left\{ \left[Y^{l_f}(\hat{\mathbf{r}}_{A1})Y^{l_{i1}}(\hat{\mathbf{r}}_{b1}) \right]^K \left[Y^{l_b}(\hat{\mathbf{r}}_{bB})Y^{l_c}(\hat{\mathbf{r}}_{cC}) \right]^K \right\}_0^0 = ((l_a l_b)_\Lambda (l_c l_c)_0 | (l_a l_c)_P (l_b l_c)_K)_\Lambda \\
& \times \sqrt{\frac{2\Lambda + 1}{(2K + 1)(2P + 1)}} \left\{ \left[Y^{l_f}(\hat{\mathbf{r}}'_{A2})Y^{l_{i2}}(\hat{\mathbf{r}}'_{b2}) \right]^P \left[Y^{l_a}(\hat{\mathbf{r}}'_{aA})Y^{l_c}(\hat{\mathbf{r}}'_{cC}) \right]^P \right\}_0^0 \\
& \times \left\{ \left[Y^{l_f}(\hat{\mathbf{r}}_{A1})Y^{l_{i1}}(\hat{\mathbf{r}}_{b1}) \right]^K \left[Y^{l_b}(\hat{\mathbf{r}}_{bB})Y^{l_c}(\hat{\mathbf{r}}_{cC}) \right]^K \right\}_0^0. \tag{6.2.175}
\end{aligned}$$

Collecting all the contributions (including the constants and phases arising from the partial wave expansion of the distorted waves and the Green function), we get

$$\begin{aligned}
T_{succ}^{(2)}(\theta; \mu) & = (-1)^{j_f + j_{i1}} \frac{2048\pi^5 \mu_{Cc}}{\hbar^2 k_{Aa} k_{Bb} k_{Cc}} \sqrt{\frac{(2j_{i1} + 1)}{(2\Lambda + 1)(2j_f + 1)}} \sum_{K,P} ((l_f \frac{1}{2})_{j_f} (l_i \frac{1}{2})_{j_{i1}} | (l_f l_i)_P (\frac{1}{2} \frac{1}{2})_0)_P \\
& \times ((l_f \frac{1}{2})_{j_f} (l_i \frac{1}{2})_{j_{i1}} | (l_f l_i)_K (\frac{1}{2} \frac{1}{2})_0)_K ((j_{i1} j_f)_K (j_{i1} j_{i2})_0 | (j_{i1} j_{i1})_0 (j_f j_{i2})_P)_P \\
& \times \frac{(-1)^K}{(2K + 1) \sqrt{2P + 1}} \sum_{l_c, l_a, l_b} ((l_a l_b)_\Lambda (l_c l_c)_0 | (l_a l_c)_P (l_b l_c)_K)_\Lambda e^{i(\sigma_i^{l_a} + \sigma_f^{l_b})} i^{l_a - l_b} \\
& \times (2l_c + 1)^{3/2} \left[Y^{l_a}(\hat{\mathbf{k}}_{aA})Y^{l_b}(\hat{\mathbf{k}}_{bB}) \right]_\mu^K S_{K,P,l_a,l_b,l_c}, \tag{6.2.176}
\end{aligned}$$

with (note that we have reduced the dimensionality of the integrals in the same fashion as for the $L=0$ -angular momentum transfer calculation, see (6.2.132))

$$\begin{aligned}
S_{K,P,l_a,l_b,l_c} & = \int r_{Cc}^2 dr_{Cc} r_{b1}^2 dr_{b1} \sin \theta d\theta v(r_{b1}) u_{l_f}(r_{C1}) u_{l_i}(r_{b1}) \\
& \times \frac{s_{P,l_a,l_c}(r_{Cc})}{r_{Cc}} \frac{F_{l_b}(r_{Bb})}{r_{Bb}} \\
& \times \sum_M \langle l_c 0 l_b M | K M \rangle \left[Y^{l_f}(\hat{r}_{C1})Y^{l_{i1}}(\theta + \pi, 0) \right]_M^K Y^{l_b}_{-M}(\hat{r}_{Bb}), \tag{6.2.177}
\end{aligned}$$

and

$$\begin{aligned} s_{P,l_a,l_c}(r_{Cc}) &= \int r'_{Cc} dr'_{Cc} r'_{A2}^2 dr'_{A2} \sin \theta' d\theta' v(r'_{c2}) u_{l_f}(r'_{A2}) u_{l_i}(r'_{c2}) \\ &\times \frac{F_{l_a}(r'_{Aa})}{r'_{Aa}} \frac{f_{l_c}(k_{Cc}, r_<) P_{l_c}(k_{Cc}, r_>)}{r'_{Cc}} \\ &\times \sum_M \langle l_c 0 l_a M | P M \rangle \left[Y^{l_f}(\hat{r}'_{A2}) Y^{l_i}(r'_{c2}) \right]_M^P Y_{-M}^{l_a}(\hat{r}'_{Aa}). \end{aligned} \quad (6.2.178)$$

We have evaluated the transition matrix element for a particular projection μ of the initial angular momentum of the two transferred nucleons. If they are coupled to a core of angular momentum J_f to total angular momentum J_i, M_i , the fraction of the initial wavefunction with projection μ is $\langle \Lambda \mu J_f M_i - \mu | J_i M_i \rangle$, and the cross section will be

$$\frac{d\sigma}{d\Omega}(\hat{\mathbf{k}}_{bB}) = \frac{k_{bB}}{k_{aA}} \frac{\mu_{aA}\mu_{bB}}{(2\pi\hbar^2)^2} \left| \sum_\mu \langle \Lambda \mu J_f M_i - \mu | J_i M_i \rangle T_{succ}^{(2)}(\theta; \mu) \right|^2. \quad (6.2.179)$$

For a non polarized incident beam,

$$\frac{d\sigma}{d\Omega}(\hat{\mathbf{k}}_{bB}) = \frac{k_{bB}}{k_{aA}} \frac{\mu_{aA}\mu_{bB}}{(2\pi\hbar^2)^2} \frac{1}{2J_i + 1} \sum_{M_i} \left| \sum_\mu \langle \Lambda \mu J_f M_i - \mu | J_i M_i \rangle T_{succ}^{(2)}(\theta; \mu) \right|^2. \quad (6.2.180)$$

This would be the differential cross section for a transition to a definite final state M_f . If we do not measure M_f we have to sum for all M_f ,

$$\frac{d\sigma}{d\Omega}(\hat{\mathbf{k}}_{bB}) = \frac{k_{bB}}{k_{aA}} \frac{\mu_{aA}\mu_{bB}}{(2\pi\hbar^2)^2} \frac{1}{2J_i + 1} \sum_\mu |T_{succ}^{(2)}(\theta; \mu)|^2 \sum_{M_i, M_f} |\langle \Lambda \mu J_f M_f | J_i M_i \rangle|^2. \quad (6.2.181)$$

The sum over M_i, M_f of the Clebsh–Gordan coefficients gives $(2J_i + 1)/(2\Lambda + 1)$ (see Eq. (6.D.26)). One then gets,

$$\frac{d\sigma}{d\Omega}(\hat{\mathbf{k}}_{bB}) = \frac{k_{bB}}{k_{aA}} \frac{\mu_{aA}\mu_{bB}}{(2\pi\hbar^2)^2} \frac{1}{(2\Lambda + 1)} \sum_\mu |T_{succ}^{(2)}(\theta; \mu)|^2, \quad (6.2.182)$$

where one can write

$$\begin{aligned} T_{succ}^{(2)}(\theta; \mu) &= \sum_{l_a, l_b} C_{l_a, l_b} \left[Y^{l_a}(\hat{\mathbf{k}}_{aA}) Y^{l_b}(\hat{\mathbf{k}}_{bB}) \right]_\mu^\Lambda \\ &= \sum_{l_a, l_b} C_{l_a, l_b} i^{l_a} \sqrt{\frac{2l_a + 1}{4\pi}} \langle l_a l_b 0 \mu | \Lambda \mu \rangle Y_\mu^{l_b}(\hat{\mathbf{k}}_{bB}). \end{aligned} \quad (6.2.183)$$

Note that (6.2.182) takes into account only the spins of the heavy nucleus. In a (t, p) or (p, t) reaction, we have to sum over the spins of the proton and of the triton

and divide by 2. If a spin-orbit term is present in the optical potential, the sum yields the combination of terms shown in Section (6.2.2),

$$\frac{d\sigma}{d\Omega}(\hat{\mathbf{k}}_{bB}) = \frac{k_{bB}}{k_{aA}} \frac{\mu_{aA}\mu_{bB}}{(2\pi\hbar^2)^2} \frac{1}{2(2\Lambda+1)} \sum_{\mu} |A_{\mu}|^2 + |B_{\mu}|^2. \quad (6.2.184)$$

Appendix 6.A ZPF and Pauli principle at the basis of medium polarization effects: self-energy, vertex corrections and induced interaction

In keeping with a central objective of the formulation of quantum mechanics, namely that the basic concepts on which it is based relate directly to experiment⁸, elementary modes of nuclear excitation (single-particle, collective vibrations and rotations), are solidly anchored on observation (inelastic and Coulomb excitation, one- and two-particle transfer reactions). Of all quantal phenomena, zero point fluctuations (ZPF), closely connected with virtual states, are likely to be most representative of the essential difference existing between quantum and classical mechanics. In fact, ZPF are intimately connected with the complementary principle⁹, and thus with indeterminacy¹⁰ and non-commutative¹¹ relations, and with the probabilistic interpretation¹² of the (modulus squared) of the wavefunctions, solution of Schrödinger's or Dirac's equations¹³. Pauli principle¹⁴ brings about essential modifications of the virtual fluctuations of the many-body system, modifications which are instrumental in the dressing and interweaving of the elementary modes of excitation¹⁵.

In Fig. 6.A.1, NFT diagrams are given which correspond to the lowest order medium polarization effects renormalizing the properties of a particle-hole collective mode (wavy line), correlated particle-hole excitation which in the shell model basis corresponds to a linear combination of particle-hole excitations ((up-going)-(down-going) arrowed lines) calculated within the random phase approximation

⁸Heisenberg (1925). The abstract of this reference reads: "In this paper it will be attempted to secure foundations for a quantum theoretical mechanics which is exclusively based on relations between quantities which in principle are observables". Within the present context, namely that of probing the nuclear structure (e.g. pairing correlations) with direct nuclear reactions, in particular Cooper pair transfer, one can hardly think of a better *incipit* for the introduction of elementary modes of excitation, modes which carry within them most of the correlations one aims at mapping out in microscopic detail, thus requiring for their theoretical treatment an effective field theory, like e.g. NFT to properly deal with the intrinsic overcompleteness of the basis (non-orthogonality) as well as of Pauli violating processes.

⁹Bohr (1928).

¹⁰Heisenberg (1927).

¹¹Born and Jordan (1925), Born et al. (1926).

¹²Born (1926a).

¹³Schrödinger (1926a), Dirac (1930).

¹⁴Pauli (1925).

¹⁵Within the present context, see also Schrieffer (1964).

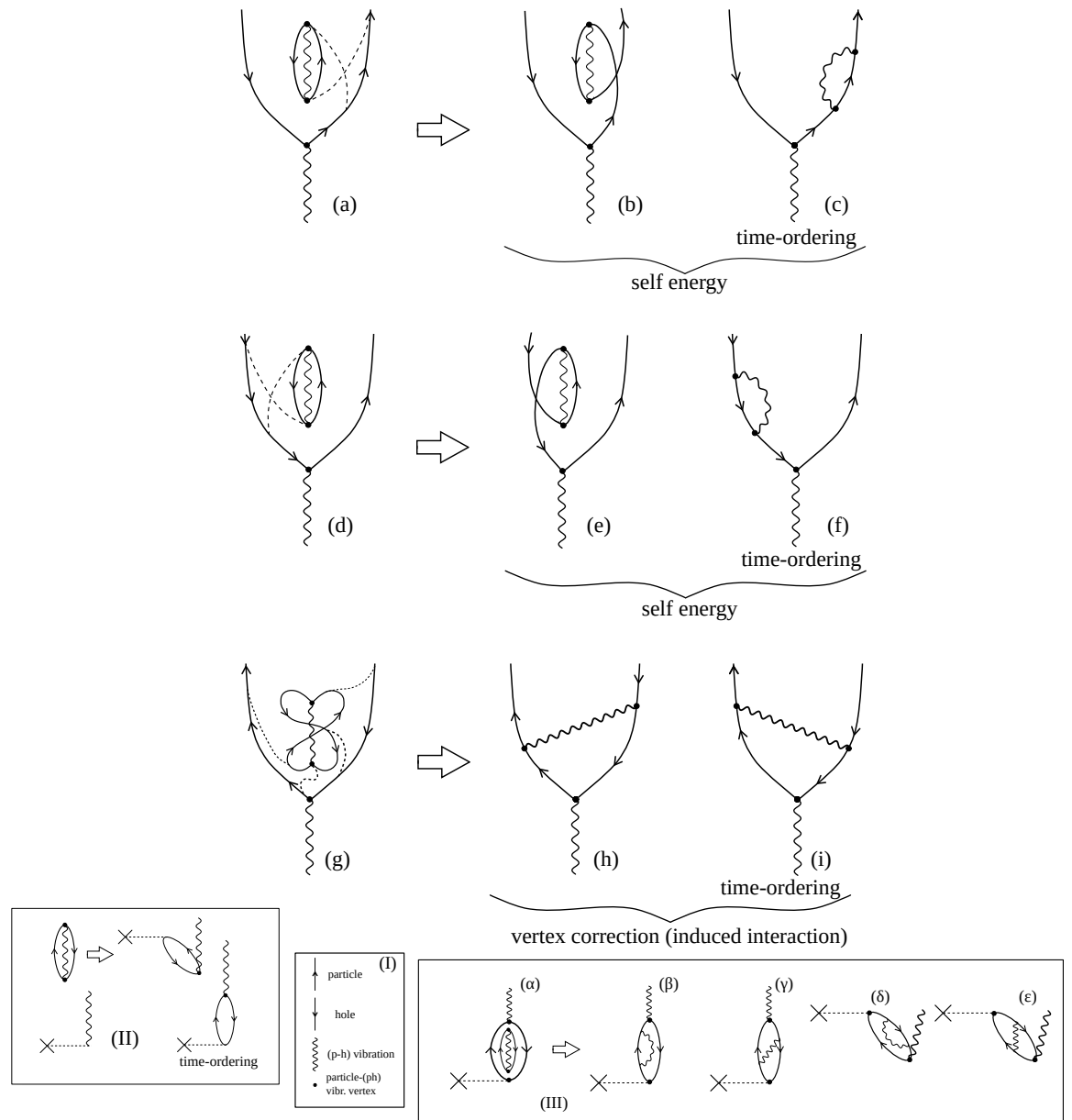


Figure 6.A.1: Nuclear field theory (NFT) diagrams describing renormalization processes associated with ZPF. For details see caption to Fig. 6.A.2.

(RPA,QRPA), and leading to the particle-vibration coupling vertex (formfactor and strength, i.e. transition density (solid dot), see inset (I), bottom). The action of an external field on the zero point fluctuations (ZPF) of the vacuum (inset (II)), forces a virtual process to become real, leading to a collective vibration by annihilating a (virtual, spontaneous) particle-hole excitation (backwards RPA Y -amplitude) or,

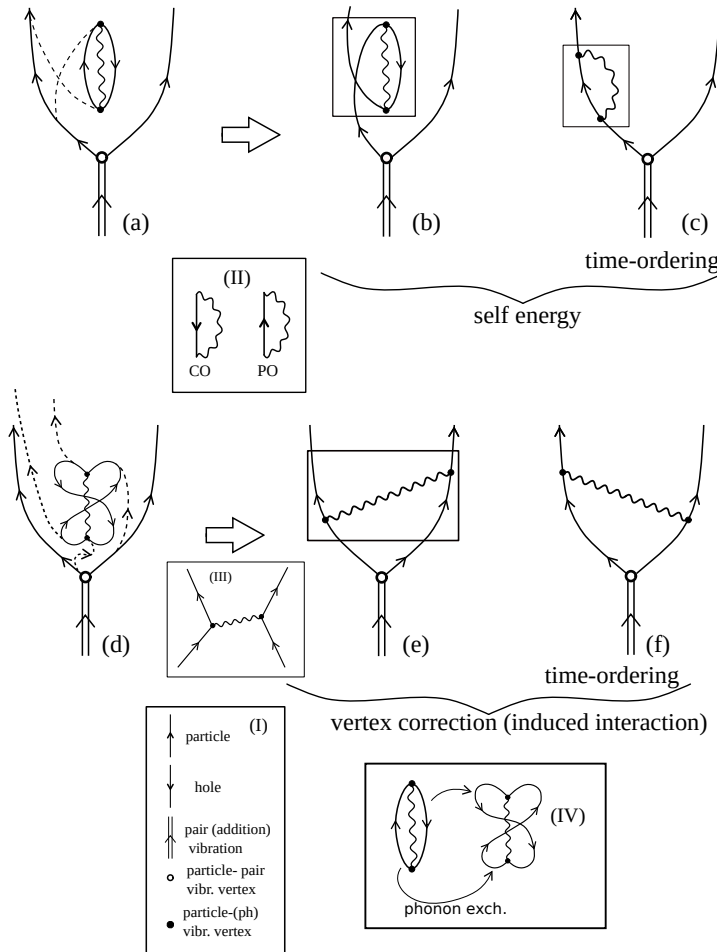


Figure 6.A.2: Pauli effects associated (p-h) ZPF dressing a pairing vibrational (pair addition) mode (see inset I) in terms of self-energy (graphs (a)–(c); correlation (CO) and polarization (PO) diagrams, inset II) and vertex correction (graphs (d)–(f); induced particle-particle (pairing) interaction processes (inset (III)), associated with phonon exchange (inset (IV)).

in the time ordered process, by creating a particle-hole excitation which eventually, through the particle-vibration coupling vertex, correlate into the collective (coherent) state (forwardgoing X -amplitudes). Now, oyster-like diagrams associated with the vacuum ZPF can occur at any time (see inset (III) of Fig. 6.A.1). Because the texture of the vacuum is permeated by symmetry rules (while one can violate energy conservation in a virtual state one cannot violate e.g. angular momentum conservation or the Pauli principle). The process shown in the inset III (α) leads, through Pauli principle correcting diagrams (exchange of fermionic arrowed lines) to self-energy (inset III (β), (δ)) and vertex corrections (induced $p - h$ inter-

action; inset III (γ), (ε), see also graphs (c), (f), (h) and (i) of Fig. 6.A.1) processes (phonon exchange, cf. inset (IV) of Fig. 6.A.2). Similar processes are found in the interplay between ZPF and pair addition modes as shown in Fig. 6.A.2. Note the parallel between diagrams 6.A.1 (g)–(i) and 6.A.2 (d)–(f).

The collective vibrational modes can be viewed as coherent states¹⁶ exhausting a consistent fraction of the EWSR (e.g. a Giant Resonance or a low-lying $E1$ -strength concentration, like in ^{11}Li in which case the mode has an energy $E_x \lesssim 1$ MeV and carries $\approx 8\%$ of the TRK sum rule) for which the associated uncertainty relations in momentum and coordinate fulfills the absolute minimum consistent with the indeterminacy relations ($\Delta\alpha_{\lambda\mu}\Delta\pi_{\lambda\mu} = \hbar/2$), $\alpha_{\lambda\mu} = (\hbar\omega_{\lambda}/2C_{\lambda}^{1/2})(\Gamma_{\lambda\mu}^{\dagger} + \Gamma_{\lambda\mu})$ being the (harmonic) collective coordinate, $\pi_{\lambda\mu}$ being the conjugate momentum. As a consequence, there is a strong cancellation between the contribution of the associated self-energy and vertex correction diagrams¹⁷. This implies small anharmonicities and long lifetimes. That is, $\Gamma/E \ll 1$, where Γ is the width and E the centroid of the mode $|\lambda\mu\rangle = \Gamma_{\lambda\mu}^{\dagger}|0\rangle$, $(\hbar\omega_{\lambda}/2C_{\lambda})^{1/2}$ being the ZPF amplitude.

Appendix 6.B Coherence and effective formfactors

In what follows we shall work out a simplified derivation of the simultaneous two-nucleon transfer amplitude, within the framework of first order DWBA specially suited to discuss correlation aspects of pair transfer in general, and of the associated effective formfactors in particular¹⁸.

We will concentrate on (t, p) reaction, namely reactions of the type $A(\alpha, \beta)B$ where $\alpha = \beta + 2$ and $B = A + 2$.

The intrinsic wave functions are in this case

$$\begin{aligned} \psi_{\alpha} &= \psi_{M_i}^{J_i}(\xi_A) \sum_{ss'_f} \left[\chi^s(\sigma_{\alpha}) \chi^{s'_f}(\sigma_{\beta}) \right]_{M_{s_i}}^{s_i} \phi_t^{L=0} \left(\sum_{i < j} |\vec{r}_i - \vec{r}_j| \right) \\ &= \psi_{M_i}^{J_i}(\xi_A) \sum_{M_s M'_{s_f}} (s M'_s s'_f M'_{s_f} | s_i M_{s_i}) \chi_{M'_s}^s(\sigma_{\alpha}) \chi_{M'_{s_f}}^{s'_f}(\sigma_{\beta}) \quad (6.B.1) \\ &\quad \times \phi_t^{L=0} \left(\sum_{i < j} |\vec{r}_i - \vec{r}_j| \right) \end{aligned}$$

while

¹⁶See e.g. Glauber (1969, 2007).

¹⁷Bortignon and Broglia (1981).

¹⁸Glendenning (1965); Bayman and Kallio (1967).

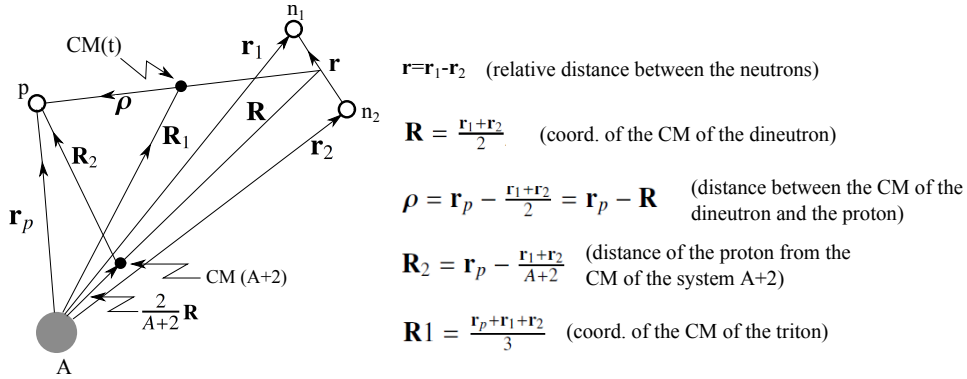


Figure 6.B.1: Coordinate system used in the calculation of the two–nucleon transfer amplitude.

$$\begin{aligned}
 \psi_\beta &= \psi_{M_f}^{J_f}(\xi_{A+2}) \chi_{M_{s_f}}^{s_f}(\sigma_\beta) \\
 &= \sum_{\substack{n_1 l_1 j_1 \\ n_2 l_2 j_2}} B(n_1 l_1 j_1, n_2 l_2 j_2; J J'_i J_f) \left[\phi^J(j_1 j_2) \phi^{J'_i}(\xi_A) \right]_{M_f}^{J_f} \\
 &\quad \times \chi_{M_{s_f}}^{s_f}(\sigma_\beta)
 \end{aligned} \tag{6.B.2}$$

Making use of the above equation one can define the spectroscopic amplitude B as

$$\begin{aligned}
 B(n_1 l_1 j_1, n_2 l_2 j_2; J J'_i J_f) \\
 = \left\langle \psi^{J_f}(\xi_{A+2}) \left| \left[\phi^J(j_1 j_2) \phi^{J_i}(\xi_A) \right]^{J_f} \right. \right\rangle,
 \end{aligned} \tag{6.B.3}$$

where

$$\phi^J(j_1 j_2) = \frac{\left[\phi_{j_1}(\vec{r}_1) \phi_{j_2}(\vec{r}_2) \right]^J - \left[\phi_{j_1}(\vec{r}_2) \phi_{j_2}(\vec{r}_1) \right]^J}{\sqrt{1 + \delta(j_1, j_2)}}, \tag{6.B.4}$$

is an antisymmetrized, normalized wave function of the two transferred particles. The function $\chi_{M_s}^s(\sigma_\beta)$ appearing both in eq. (6.B.1) and (6.B.2) is the spin wave function of the proton while

$$\chi^s(\sigma_\alpha) = [\chi^{s_1}(\sigma_{n_1}) \chi^{s_2}(\sigma_{n_2})]^s, \tag{6.B.5}$$

is the spin function of the two–neutron system.

A convenient description of the intrinsic degrees of freedom of the triton is obtained by using a wavefunction symmetric in the coordinates of all particles, i.e.

$$\begin{aligned}\phi_t^{L=0} \left(\sum_{i < j} |\vec{r}_i - \vec{r}_j| \right) &= N_t e^{[(r_1 - r_2)^2 + (r_1 - r_p)^2 + (r_2 - r_p)^2]} \\ &= \phi_{000}(\vec{r}) \phi_{000}(\vec{\rho}),\end{aligned}\quad (6.B.6)$$

where

$$\phi_{000}(\vec{r}) = R_{nl}(v^{1/2}r) Y_{lm}(\hat{r}). \quad (6.B.7)$$

The coordinate $\vec{\rho}$ is the radius vector which measures the distance between the center of mass of the dineutron and the proton, while the vector \vec{r} is the dineutron relative coordinate (cf. Fig. 6.B.1).

To obtain the DWBA cross section we have to calculate the integral

$$T(\theta) = \int d\xi_A d\vec{r}_1 d\vec{r}_2 d\vec{r}_p \chi_p^{(-)}(\vec{R}_2) \psi_\beta^*(\xi_{A+2}, \sigma_\beta) V_\beta \psi_\alpha(\xi_A, \sigma_\alpha, \sigma_\beta) \psi_t^{(+)}(\vec{R}_1) \quad (6.B.8)$$

where the final state effective interaction $V_\beta(\rho)$ is assumed to depend only on the distance ρ between the center of mass of the di-neutron and of the proton. Instead of integrating over $\xi_A, \vec{r}_1, \vec{r}_2$ and \vec{r}_p we would integrate over $\xi_A, \vec{r}', \vec{r}'$ and \vec{r}_p . The Jacobian of the transformation is equal to 1, i.e. $\partial(\vec{r}_1, \vec{r}_2)/\partial(\vec{r}', \vec{r}') = 1$.

To carry out the integral (6.B.8) we transform the wave function (6.B.4) into center of mass and relative coordinates. If we assume that both $\phi_{j_1}(\vec{r}_1)$ and $\phi_{j_2}(\vec{r}_2)$ are harmonic oscillator wave functions (used as a basis to expand the Saxon-Woods single-particle wavefunctions), this transformation can be carried with the aid of the Moshinsky brackets. If $|n_1 l_1, n_2 l_2; \lambda \mu\rangle$ is a complete system of wave functions in the harmonic oscillator basis, depending on \vec{r}_1 and \vec{r}_2 and $|nl, NL; \lambda \mu\rangle$ is the corresponding one depending on \vec{r} and \vec{R} , we can write

$$\begin{aligned}|n_1 l_1, n_2 l_2; \lambda \mu\rangle &= \sum_{nlNL} |nl, NL; \lambda \mu\rangle \langle nl, NL; \lambda \mu| |n_1 l_1, n_2 l_2; \lambda \mu\rangle \\ &= \sum_{nlNL} |nl, NL; \lambda \mu\rangle \langle nl, NL; \lambda \mu| n_1 l_1, n_2 l_2; \lambda \rangle\end{aligned}\quad (6.B.9)$$

The labels n, l are the principal and angular momentum quantum numbers of the relative motion, while N, L are the corresponding ones corresponding to the center of mass motion of the two-neutron system. Because of energy and parity conservation we have

$$\begin{aligned}2n_1 + l_1 + 2n_2 + l_2 &= 2n + l + 2N + L \\ (-1)^{l_1 + l_2} &= (-1)^{l + L}.\end{aligned}\quad (6.B.10)$$

The coefficients $\langle nl, NL, L | n_1 l_1, n_2 l_2, L \rangle$ are tabulated and were first discussed by Moshinsky¹⁹.

¹⁹Moshinsky (1959).

With the help of eq. (6.B.9) we can write the wave function $\psi_{M_f}^{J_f}(\xi_{A+2})$ as

$$\begin{aligned}
 \psi_{M_f}^{J_f}(\xi_{A+2}) &= \sum_{\substack{n_1 l_1 j_1 \\ n_2 l_2 j_2 \\ J J_i}} B(n_1 l_1 j_1, n_2 l_2 j_2; J J'_i J_f) [\phi^J(j_1 j_2) \phi^{J'_i}(\xi_A)]_{M_f}^{J_f} \\
 &= \sum_{\substack{n_1 l_1 j_1 \\ n_2 l_2 j_2 \\ J J_i}} B(n_1 l_1 j_1, n_2 l_2 j_2; J J'_i J_f) \\
 &\quad \times \sum_{M_J M'_{J_i}} \langle J M_J J'_i M_{J_i} | J_f M_{J_f} \rangle \psi_{M'_{J_i}}^{J'_i}(\xi_A) \\
 &\quad \times \sum_{L S'} \langle S' L J | j_1 j_2 J \rangle \sum_{M_L M'_S} \langle L M_L S' M'_S | J M_J \rangle \chi_{M'_S}^{S'}(\sigma_\alpha) \\
 &\quad \times \sum_{n l N \Lambda} \langle n l, N \Lambda, L | n_1 l_1, n_2 l_2, L \rangle \\
 &\quad \times \sum_{m_l M_\Lambda} \langle l m_l \Lambda M_\Lambda | L M_L \rangle \phi_{nlm_l}(\vec{r}) \phi_{N \Lambda M_\Lambda}(\vec{R})
 \end{aligned} \tag{6.B.11}$$

Integration over \vec{r} gives

$$\langle \phi_{nlm_l}(\vec{r}) | \phi_{000}(\vec{r}) \rangle = \delta(l, 0) \delta(m_l, 0) \Omega_n \tag{6.B.12}$$

where

$$\Omega_n = \int R_{nl}(\nu_1^{1/2} r) R_{00}(\nu_2^{1/2} r) r^2 dr \tag{6.B.13}$$

Note that there is no selection rule in the principal quantum number n , as the potential in which the two neutrons move in the triton has a frequency ν_2 which is different from the one that the two neutrons are subjected to, when moving in the system A (non-orthogonality effect).

Integration over ξ_A and multiplication of the spin functions gives

$$\begin{aligned}
 (\psi_{M_{J_i}}^{J_i}, V'_\beta(\rho) \psi_{M'_{J_i}}^{J'_i}) &= \delta(J_i, J'_i) \delta(M_{J_i}, M_{J'_i}) V(\rho), \\
 (\chi_{M_S}^S(\sigma_\alpha), \chi_{M'_{S'}}^{S'}(\sigma_\alpha)) &= \delta(S, S') \delta(M_S, M_{S'}), \\
 (\chi_{M_{S_f}}^{S_f}(\sigma_\beta), \chi_{M'_{S'_f}}^{S'_f}(\sigma_\beta)) &= \delta(S_f, S'_f) \delta(M_{S_f}, M_{S'_f}).
 \end{aligned} \tag{6.B.14}$$

The integral (6.B.8) can then be written as

$$\begin{aligned}
T(\theta) = & \sum_{n_1 l_1 j_1} \sum_{JM_J} \sum_{nN} \sum_S B(n_1 l_1 j_1, n_2 l_2 j_2; JJ_i J_f) \\
& \times \langle JM_J J_i M_{J_i} | J_f M_{J_f} \rangle \langle S L J | j_1 j_2 J \rangle \\
& \times \langle LM_L S M_S | JM_J \rangle \langle n0, NL, L | n_1 l_1, n_2 l_2, L \rangle \\
& \times \langle S M_S S_f M_{S_f} | S_i M_{S_i} \rangle \Omega_n \\
& \times \int d\vec{R} d\vec{r}_p \chi_t^{(+)*}(\vec{R}_1) \phi_{NLM_L}^*(\vec{R}) V(\rho) \phi_{000}(\vec{\rho}) \chi_t^{(+)}(\vec{R}_1),
\end{aligned} \tag{6.B.15}$$

where we have approximated V'_β by an effective interaction depending on $\rho = |\vec{\rho}|$.

We now define the effective two-nucleon transfer form factor as

$$\begin{aligned}
u_{LSJ}^{J_i J_f}(R) = & \sum_{n_1 l_1 j_1} \sum_{nN} B(n_1 l_1 j_1, n_2 l_2 j_2; JJ_i J_f) \langle S L J | j_1 j_2 J \rangle \\
& \langle n0, NL, L | n_1 l_1, n_2 l_2; L \rangle \Omega_n R_{NL}(R).
\end{aligned} \tag{6.B.16}$$

We can now rewrite eq. (6.B.15) as

$$\begin{aligned}
T(\theta) = & \sum_J \sum_L \sum_S (JM_J J_i M_{J_i} | J_f M_{J_f} \rangle) (S M_S S_f M_{S_f} | S_i M_{S_i} \rangle) (LM_L S M_S | JM_J \rangle) \\
& \times \int d\vec{R} d\vec{r}_p \chi_p^{*(-)}(\vec{R}_2) u_{LSJ}^{J_i J_f}(R) Y_{LM_L}^* V(\rho) \phi_{000}(\vec{\rho}) \chi_t^{(+)}(\vec{R}_1).
\end{aligned} \tag{6.B.17}$$

Because the di-neutron has $S = 0$, we have that

$$(LM_L 00 | JM_J) = \delta(J, L) \delta(M_L, M_J), \tag{6.B.18}$$

and the summations over S and L disappear from eq. (6.B.17). Let us now make also here, as done in App. 5.F, Eq. (5.F.15) for one-particle transfer reactions, the zero range approximation, that is,

$$V(\rho) \phi_{000}(\vec{\rho}) = D_0 \delta(\vec{\rho}), \tag{6.B.19}$$

where D_0 is an empirical parameter ($D_0^2 = (31.6 \pm 9.3) \times 10^4 \text{ MeV}^2 \text{fm}^2$) determined to reproduce, in average, the observed absolute cross sections²⁰. This means that the proton interacts with the center of mass of the di-neutron, only when they are at the same point in space. Within this approximation (cf. Fig. 6.B.1)

$$\begin{aligned}
\vec{R} = & \vec{R}_1 = \vec{r}, \\
\vec{R}_2 = & \frac{A}{A+2} \vec{R},
\end{aligned} \tag{6.B.20}$$

²⁰Broglia et al. (1973).

Then Eq. (6.B.15) can be written as

$$T = D_0 \sum_L (LM_L J_i M_{J_i} | J_f M_{J_f}) \\ \times \int d\vec{R} \chi_p^{*(-)} \left(\frac{A}{A+2} \vec{R} \right) u_L^{J_i J_f}(R) Y_{LM_L}^*(\hat{R}) \chi_t^{(+)}(\vec{R}) \quad (6.B.21)$$

From Eq. (6.B.21) it is seen that the change in parity implied by the reaction is given by $\Delta\pi = (-1)^L$. Consequently, the selection rules for (t, p) and (p, t) reactions in zero-range approximation are,

$$\begin{aligned} \Delta S &= 0 \\ \Delta J &= \Delta L = L \\ \Delta\pi &= (-1)^L \end{aligned} \quad (6.B.22)$$

i.e. only normal parity states are excited.

The integral appearing in Eq. (6.B.21) has the same structure as the DWBA integral appearing in Eq. (5.F.16) which was derived for the case of one-nucleon transfer reactions.

The difference between the two processes manifests itself through the different structure of the two form factors. While $u_l(r)$ is a single-particle bound state wave function (cf. Eq. (5.F.1a)), $u_L^{J_i J_f}$ is a coherent summation over the center of mass states of motion of the two transferred neutrons (see Eq. (6.B.16)). In other words, an effective quantity (function). It is of notice that this difference essentially vanishes, when one considers dressed particles resulting from the coupling to collective motion, and leading, among other things, to ω -dependent effective masses (see e.g. 7.2.3). Examples of two-nucleon transfer form factors are given in Figs 6.B.2, 6.B.3 and 6.B.4.

Appendix 6.C Relative importance of successive and simultaneous transfer and non-orthogonality corrections

In what follows we discuss the relative importance of successive and simultaneous two-neutron transfer and of non-orthogonality corrections associated with the reaction

$$\alpha \equiv a (= b + 2) + A \rightarrow b + B (= A + 2) \equiv \beta, \quad (6.C.1)$$

in the limits of independent particles and of strongly correlated Cooper pairs, making use for simplicity of the semiclassical approximation²¹, in which case the two-particle transfer differential cross section can be written as

²¹For details cf. Broglia and Winther (2004).

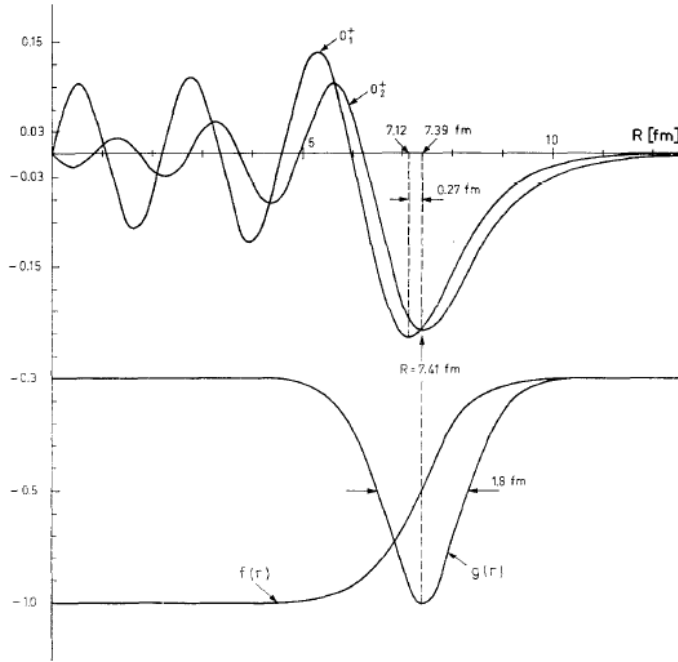


Figure 6.B.2: The upper part of the figure shows the modified formfactor for the $^{206}\text{Pb}(t,\text{p})^{208}\text{Pb}$ transition to the ground state (0_1^+) and the pairing vibrational state (0_2^+) at 4.87 MeV. Both curves are matched with appropriate Hankel functions. In the lower part the form factors of the real ($f(r)$) and the imaginary ($g(r)$) part of the optical potential used to calculate the differential cross sections (cf. Fig. 4.5.4), are given in the same scale for the radius. After Broglia and Riedel (1967).

$$\frac{d\sigma_{\alpha \rightarrow \beta}}{d\Omega} = P_{\alpha \rightarrow \beta}(t = +\infty) \sqrt{\left(\frac{d\sigma_\alpha}{d\Omega} \right)_{el}} \sqrt{\left(\frac{d\sigma_\beta}{d\Omega} \right)_{el}}, \quad (6.C.2)$$

where P is the absolute value squared of a quantum mechanical transition amplitude. It gives the probability that the system at $t = +\infty$ is found in the final channel. The quantities $(d\sigma/d\Omega)_{el}$ are the classical elastic cross sections in the center of mass system, calculated in terms of the deflection function, namely the functional relating the impact parameter and the scattering angle.

The transfer amplitude can be written as

$$a(t = +\infty) = a^{(1)}(\infty) - a^{(NO)}(\infty) + \tilde{a}^{(2)}(\infty), \quad (6.C.3)$$

where $\tilde{a}^{(2)}(\infty)$ at $t = +\infty$ labels the successive transfer amplitude expressed in the post-prior representation (see below). The simultaneous transfer amplitude is given by (see Fig. 6.C.1 (I))

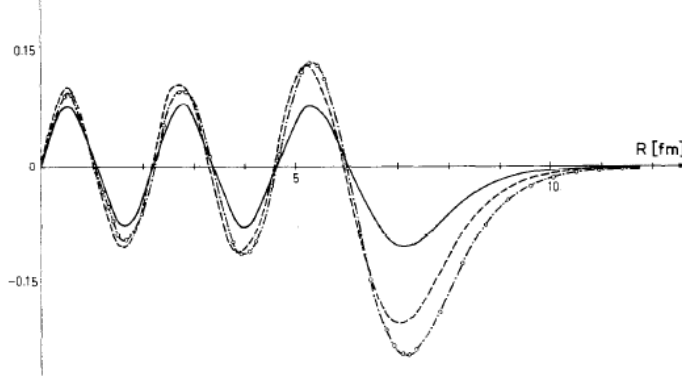


Figure 6.B.3: Modified formfactor for the transition to the ground state ($^{206}\text{Pb}(t,p)^{208}\text{Pb}(\text{gs})$; see Fig. 4.5.4) calculated in different spectroscopic models (pure shell-model configuration ——, shell model plus pairing residual interaction ——, including ground state correlations -o-o-). After Broglia and Riedel (1967).

$$\begin{aligned}
 a^{(1)}(\infty) &= \frac{1}{i\hbar} \int_{-\infty}^{\infty} dt (\psi^b \psi^B, (V_{bB} - V_{bB}) \psi^a \psi^A) \times \exp\left[\frac{i}{\hbar}(E^{bB} - E^{aA})t\right] \\
 &\approx \frac{2}{i\hbar} \int_{-\infty}^{\infty} dt \left(\phi^{B(A)}(S_{(2n)}^B; \vec{r}_{1A}, \vec{r}_{2A}), U(r_{1b}) e^{i(\sigma_1 + \sigma_2)} \phi^{a(b)}(S_{(2n)}^a; \vec{r}_{1b}, \vec{r}_{2b}) \right) \\
 &\quad \times \exp\left[\frac{i}{\hbar}(E^{bB} - E^{aA})t + \gamma(t)\right]
 \end{aligned} \tag{6.C.4}$$

where

$$\sigma_1 + \sigma_2 = \frac{1}{\hbar} \frac{m_n}{m_A} (m_{aA} \vec{v}_{aA}(t) + m_{bB} \vec{v}_{bB}(t)) \cdot (\vec{r}_{1a} - \vec{r}_{2a}), \tag{6.C.5}$$

in keeping with the fact that $\exp(i(\sigma_1 + \sigma_2))$ takes care of recoil effects (Galilean transformation associated with the mismatch between entrance and exit channels). The phase $\gamma(t)$ is related with the effective Q -value of the reaction. In the above expression, ϕ indicates an antisymmetrized, correlated two-particle (Cooper pair) wavefunction, $S(2n)$ being the two-neutron separation energy (see Fig. 6.C.3), $U(r_{1b})$ being the single particle potential generated by nucleus b ($U(r) = \int d^3 r' \rho^b(r') v(|r - r'|)$). The contribution arising from non-orthogonality effects can be written as (see Fig. 6.C.1 (II))

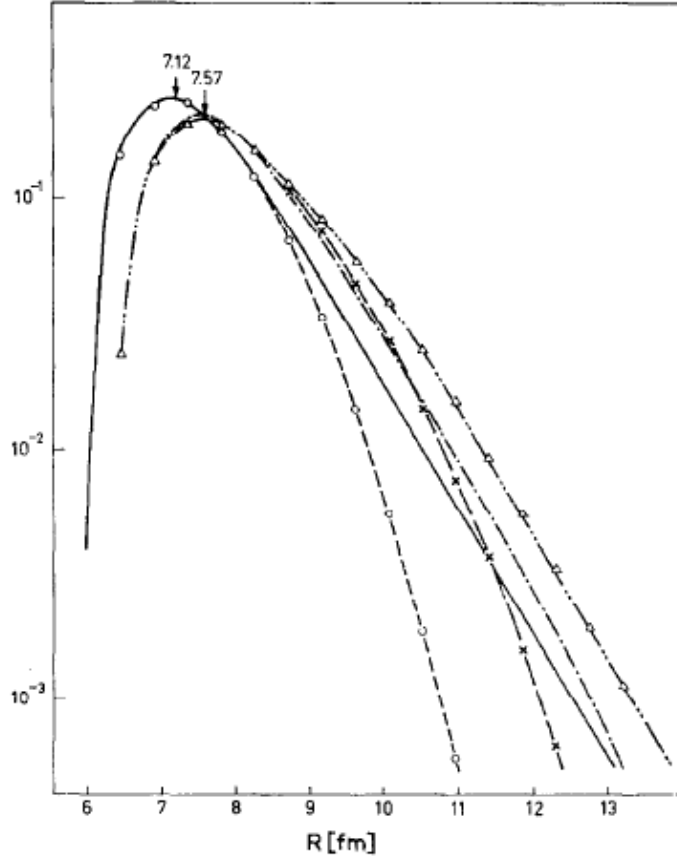


Figure 6.B.4: Asymptotic behavior of the modified formfactor for the $^{206}(\text{t},\text{p})^{208}\text{Pb}(\text{gs})$ ground state transition for oscillator plus Hankel wave functions (continuous solid curve), oscillator wave functions alone (dash point dashed curve), and Saxon-Woods wave functions with a variety of asymptotic matchings (cf. Broglia and Riedel (1967)).

$$\begin{aligned}
 a^{(NO)}(\infty) &= \frac{1}{i\hbar} \int_{-\infty}^{\infty} dt (\psi^b \psi^B, (V_{bB} - V_{bB}) \psi^f \psi^F) (\psi^f \psi^F, \psi^a \psi^A) \exp\left[\frac{i}{\hbar}(E^{bB} - E^{aA})t\right] \\
 &\approx \frac{2}{i\hbar} \int_{-\infty}^{\infty} \phi^{B(F)}(S_{(n)}^B, \vec{r}_{1A}), U(r_{1b}) e^{i\sigma_1} (\phi^{f(b)}(S^f(n), \vec{r}_{1b}) \\
 &\quad \times \phi^{F(A)}(S^F(n), \vec{r}_{2A}) e^{i\sigma_2} \phi^{a(f)}(S^a(n), \vec{r}_{2b})) \exp\left[\frac{i}{\hbar}(E^{bB} - E^{aA})t + \gamma(t)\right],
 \end{aligned} \tag{6.C.6}$$

the reaction channel $f = (b+1) + F (= A+1)$ having been introduced, the quantity $S(n)$ being the one-neutron separation energy (see Fig. 6.C.3). The summation

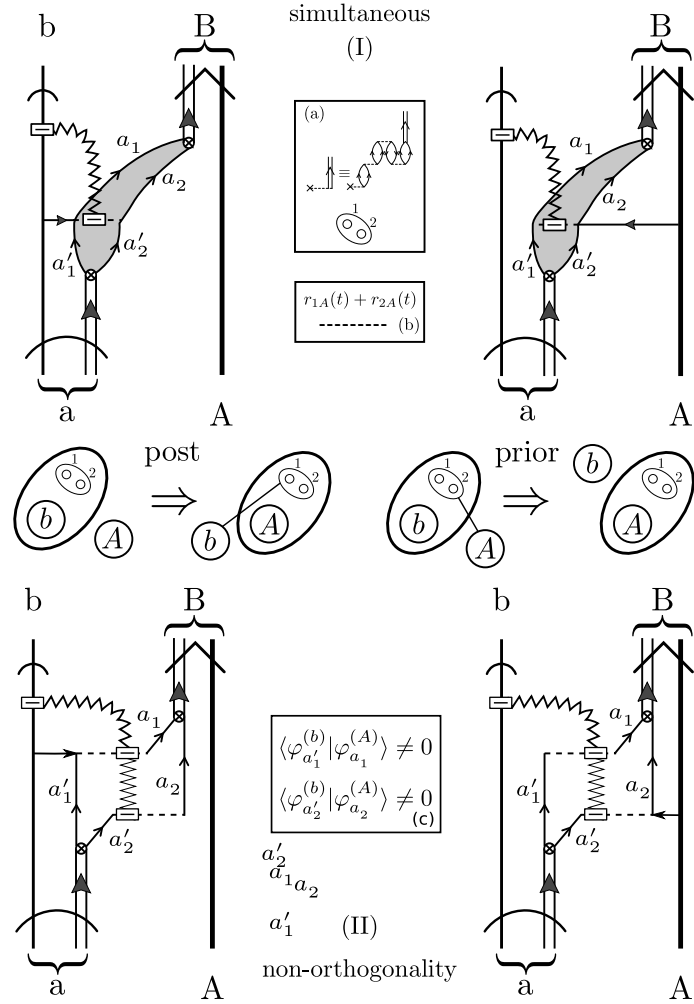


Figure 6.C.1: Graphical representation of simultaneous (I) and non-orthogonality (II) transfer processes. For details see text and cf. caption to Fig. 6.C.2. In this figure, as well as in Fig. 6.C.2, and at variance with, e.g. Fig. 2.10.2, the particle-pair vibration coupling vertex is represented by a crossed circle. Concerning the jagged line representing recoil see Sect. 2.B.3.

over $f(\equiv a'_1, a'_2)$ and $F(\equiv a_1, a_2)$ involves a restricted number of states, namely the valence shells in nuclei B and a . It is of notice that the NFT(r+s) diagrams appearing in Fig. 6.C.1 (II) are the only ones we have encountered in which to a particle-recoil coupling vertex (dashed open rectangle) and thus the starting or/and ending of a recoil mode (jagged line) does not correspond the action of the nuclear interaction or mean field (horizontal short arrow) inducing a transfer process.

The successive transfer amplitude $\tilde{a}_\infty^{(2)}$ written making use of the post-prior

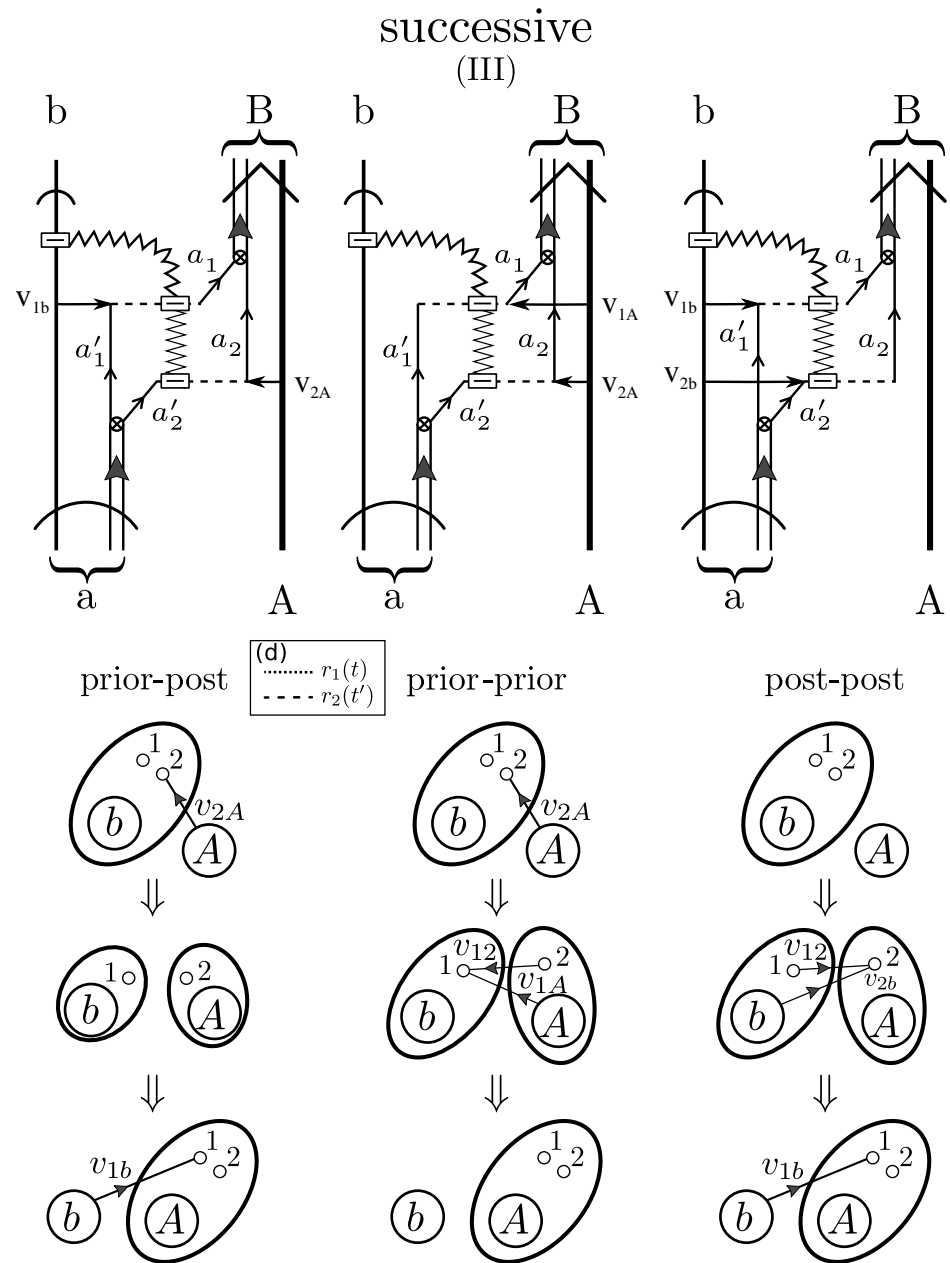


Figure 6.C.2: Graphical representation of the successive transfer of two nucleons. For details see text.

representation is equal to (see Fig. 6.C.2 (III))

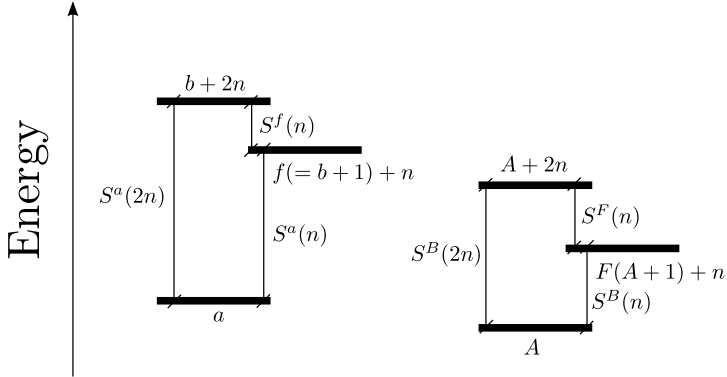


Figure 6.C.3: One- and two-neutron separation energies $S(n)$ and $S(2n)$ associated with the channels $\alpha \equiv a (= b + 2) + A \rightarrow \gamma \equiv f (= b + 1) + F (= A + 1) \rightarrow \beta \equiv b + B (= A + 2)$.

$$\begin{aligned} \tilde{a}^{(2)}(\infty) = & \frac{1}{i\hbar} \int_{-\infty}^{\infty} dt (\psi^b \psi^B, (V_{bB} - V_{bB}) e^{i\sigma_1} \psi^f \psi^F) \\ & \times \exp\left[\frac{i}{\hbar}(E^{bB} - E^{fF})t + \gamma_1(t)\right] \\ & \times \frac{1}{i\hbar} \int_{-\infty}^t dt' (\psi^f \psi^F, (V_{fF} - V_{fF}) e^{i\sigma_2} \psi^a \psi^A) \\ & \times \exp\left[\frac{i}{\hbar}(E^{fF} - E^{aA})t' + \gamma_2(t')\right]. \end{aligned} \quad (6.C.7)$$

To gain insight into the relative importance of the three terms contributing to Eq. (6.C.3) we discuss two situations, namely, the independent-particle model and the strong-correlation limits.

Before doing so, let us describe in some detail the graphical description of the transfer amplitudes (6.C.4) (6.C.6) and (6.C.7) displayed in Figs. 6.C.1 and 6.C.2. It is of notice that the time arrow is assumed to point upwards: (I) Simultaneous transfer, in which one particle is transferred by the nucleon-nucleon interaction (note that $U(r) = \int d^3r' \rho(r') v(|\vec{r} - \vec{r}'|)$) acting either in the entrance $\alpha \equiv a + A$ channel (prior) or in the final $\beta \equiv b + B$ channel (post), while the other particle follows suit making use of the particle-particle correlation (grey area) which binds the Cooper pair (see upper inset labelled (a)), represented by a solid arrow on a double line, to the projectile (curved arrowed lines) or to the target (opened arrowed lines). The above argument provides the explanation why when e.g. v_{1b} acts on one nucleon, the other nucleon also reacts instantaneously. In fact a Cooper pair displays generalized rigidity (emergent property in gauge space). A crossed open circle represents the particle-pair vibration coupling. The associated strength, together with an energy denominator, determines the amplitude $X_{a'_1 a'_2}$ with which the

pair mode (Cooper pair) is in the (time reversed) two particle configuration $a'_1 a'_2$. In the transfer process, the relative motion orbit changes, the readjustement of the corresponding trajectory mismatch being operated by a Galilean transformation induced by the operator $(\exp\{\vec{k} \cdot (\vec{r}_{1A}(t) + \vec{r}_{2A}(t))\})$. This phenomenon, known as recoil process, is represented by a jagged line which provides simultaneous information on the two transferred nucleons (single time appearing as argument of both single-particle coordinates r_1 and r_2 ; see inset labeled (b)). In other words, information on the coupling of structure and reaction modes. (II) Non-orthogonality contribution. While one of the nucleons of the Cooper pairs is transferred under the action of v , the other goes, uncorrelatedly over, profiting of the non-orthogonality of the associated single-particle wavefunctions (see inset (c)). In other words of the non-vanishing values of the overlaps, as shown in the inset. (III) Successive transfer. In this case, there are two time dependences associated with the acting of the nucleon-nucleon interaction twice (see inset (d)).

From a physical point of view the recoil-related coupling (jagged line) is similar to the one involved in the restoration of translational invariance violated by the shell-model potential U . This is done by including the effects of the collective field generated by a small displacement of the nucleus, giving rise to a coupling Hamiltonian proportional to the gradient of U . The spectrum of normal modes generated by such coupling contains a zero frequency mode, orthogonal to the additional normal modes which represent 1^- states, displaying a divergent ZPF but a finite inertia equal to AM , result which testifies to translational invariance restoration²².

6.C.1 Independent particle limit

In the independent particle limit, the two transferred particles do not interact among themselves but for antisymmetrization. Thus, the separation energies fulfill the relations (see Fig. 6.C.3)

$$S^B(2n) = 2S^B(n) = 2S^F(n), \quad (6.C.8)$$

and

$$S^a(2n) = 2S^a(n) = 2S^f(n). \quad (6.C.9)$$

In this case

$$\phi^{B(A)}(S^B(2n), \vec{r}_{1A}, \vec{r}_{2A}) = \sum_{a_1 a_2} \phi_{a_1}^{B(F)}(S^B(n), \vec{r}_{1A}) \phi_{a_2}^{F(A)}(S^F(n), \vec{r}_{2A}), \quad (6.C.10)$$

and

$$\phi^{a(b)}(S^a(2n), \vec{r}_{1b}, \vec{r}_{2b}) = \sum_{a'_1 a'_2} \phi_{a'_1}^{a(f)}(S^a(n), \vec{r}_{2b}) \phi_{a'_2}^{f(b)}(S^f(n), \vec{r}_{1b}), \quad (6.C.11)$$

where $(a_1, a_2) \equiv F$ and $(a'_1, a'_2) \equiv f$ span, as mentioned above, shells in nuclei B and a respectively.

²²Bohr and Mottelson (1975) p. 445.

Inserting Eqs. (6.C.8–6.C.11) in Eq. (6.C.4) one can show that

$$a^{(1)}(\infty) = a^{(NO)}(\infty). \quad (6.C.12)$$

It can be further demonstrated that within the present approximation, $\text{Im } \tilde{a}^{(2)} = 0$, and that

$$\begin{aligned} \tilde{a}^{(2)}(\infty) &= \frac{1}{i\hbar} \int_{-\infty}^{\infty} dt (\psi^b \psi^B, (V_{bB} - \langle V_{bB} \rangle) e^{i\sigma_1} \psi^f \psi^F) \\ &\quad \times \exp\left[\frac{i}{\hbar}(E^{bB} - E^{fF})t + \gamma_1(t)\right] \\ &\times \frac{1}{i\hbar} \int_{-\infty}^{\infty} dt' (\psi^f \psi^F, (V_{fF} - \langle V_{fF} \rangle) e^{i\sigma_2} \psi^a \psi^A) \\ &\quad \times \exp\left[\frac{i}{\hbar}(E^{fF} - E^{aA})t' + \gamma_2(t')\right]. \end{aligned} \quad (6.C.13)$$

The total absolute differential cross section (6.C.2), where $P = |a(\infty)|^2 = |\tilde{a}^{(2)}|^2$, is then equal to the product of two one-particle transfer cross sections (see Fig. 5.1.1), associated with the (virtual) reaction channels

$$\alpha \equiv a + A \rightarrow f + F \equiv \gamma, \quad (6.C.14)$$

and

$$\gamma \equiv f + F \rightarrow b + B \equiv \beta. \quad (6.C.15)$$

In fact, Eq.(6.C.13) involves no time ordering and consequently the two processes above are completely independent of each other. This result was expected because being $v_{12} = 0$, the transfer of one nucleon cannot influence, aside from selecting the initial state for the second step, the behaviour of the other nucleon.

6.C.2 Strong correlation (cluster) limit

The second limit to be considered is the one in which the correlation between the two nucleons is so strong that (see Fig. 6.C.3)

$$S^a(2n) \approx S^a(n) \gg S^f(n), \quad (6.C.16)$$

and

$$S^B(2n) \approx S^B(n) \gg S^F(n). \quad (6.C.17)$$

That is, the magnitude of the one-nucleon separation energy is strongly modified by the pair breaking.

There is a different, although equivalent way to express (6.C.3) which is more convenient to discuss the strong coupling limit. In fact, making use of the post-prior representation one can write

$$\begin{aligned} a^{(2)}(t) &= \tilde{a}^{(2)}(t) - a^{(NO)}(t) = \frac{1}{i\hbar} \int_{-\infty}^{\infty} dt (\psi^b \psi^B, (V_{bB} - \langle V_{bB} \rangle) e^{i\sigma_1} \psi^f \psi^F) \\ &\quad \times \exp\left[\frac{i}{\hbar}(E^{bB} - E^{fF})t + \gamma_1(t)\right] \\ &\quad \times \frac{1}{i\hbar} \int_{-\infty}^t dt' (\psi^f \psi^F, (V_{fF} - \langle V_{fF} \rangle) e^{i\sigma_2} \psi^a \psi^A) \\ &\quad \times \exp\left[\frac{i}{\hbar}(E^{fF} - E^{aA})t' + \gamma_2(t')\right]. \end{aligned} \quad (6.C.18)$$

The relations (6.C.16), (6.C.17) imply

$$E^{fF} - E^{aA} = S^a(n) - S^F(n) \gg \frac{\hbar}{\tau}, \quad (6.C.19)$$

where τ is the collision time. Consequently the real part of $a^{(2)}(\infty)$ vanishes exponentially with the Q -value of the intermediate transition, while the imaginary part vanishes inversely proportional to this energy. One can thus write,

$$\operatorname{Re} a^{(2)}(\infty) \approx 0, \quad (6.C.20)$$

and

$$\begin{aligned} a^{(2)}(\infty) &\approx \frac{1}{i\hbar} \frac{\tau}{<E^{fF}> - E^{bB}} \sum_{fF} (\psi^b \psi^B, (V_{bB} - <V_{bB}>) \psi^f \psi^F)_{t=0} \\ &\times (\psi^f \psi^F, (V_{aA} - <V_{aA}>) \psi^a \psi^A)_{t=0}, \end{aligned} \quad (6.C.21)$$

where one has utilized the fact that $E^{bB} \approx E^{aA}$. For $v_{12} \rightarrow \infty$, ($<E^{fF}> - E^{bB}$) $\rightarrow \infty$) and, consequently,

$$\lim_{v_{12} \rightarrow \infty} a^{(2)}(\infty) = 0. \quad (6.C.22)$$

Thus the total two-nucleon transfer amplitude is equal, in the strong coupling limit, to the amplitude $a^{(1)}(\infty)$.

Summing up, only when successive transfer and non-orthogonal corrections are included in the description of the two-nucleon transfer process, does one obtain a consistent description of the process, which correctly converges to the weak and strong correlation limiting values.

Appendix 6.D Spherical harmonics and angular momenta

With Condon–Shortley phases

$$Y_m^l(\hat{z}) = \delta_{m,0} \sqrt{\frac{2l+1}{4\pi}}, \quad Y_m^{l*}(\hat{r}) = (-1)^m Y_{-m}^l(\hat{r}). \quad (6.D.1)$$

Time-reversed phases consist in multiplying Condon–Shortley phases with a factor i^l , so

$$Y_m^l(\hat{z}) = \delta_{m,0} i^l \sqrt{\frac{2l+1}{4\pi}}, \quad Y_m^{l*}(\hat{r}) = (-1)^{l-m} Y_{-m}^l(\hat{r}). \quad (6.D.2)$$

With this phase convention, the relation with the associated Legendre polynomials includes an extra i^l factor with respect to the Condon–Shortley phase,

$$Y_m^l(\theta, \phi) = i^l \sqrt{\frac{2l+1}{4\pi} \frac{(l-m)!}{(l+m)!}} P_l^m(\cos \theta) e^{im\phi}. \quad (6.D.3)$$

6.D.1 Addition theorem

The addition theorem for the spherical harmonics states that

$$P_l(\cos \theta_{12}) = \frac{4\pi}{2l+1} \sum_m Y_m^l(\mathbf{r}_1) Y_m^{l*}(\mathbf{r}_2), \quad (6.D.4)$$

where θ_{12} is the angle between the vectors \mathbf{r}_1 and \mathbf{r}_2 . This result is independent of the phase convention. With *time-reversed phases*,

$$P_l(\cos \theta_{12}) = \frac{4\pi}{\sqrt{2l+1}} [Y^l(\hat{\mathbf{r}}_1) Y^l(\hat{\mathbf{r}}_2)]_0^0. \quad (6.D.5)$$

With *Condon–Shortley phases*,

$$P_l(\cos \theta_{12}) = (-1)^l \frac{4\pi}{\sqrt{2l+1}} [Y^l(\hat{\mathbf{r}}_1) Y^l(\hat{\mathbf{r}}_2)]_0^0. \quad (6.D.6)$$

6.D.2 Expansion of the delta function

The Dirac delta function can be expanded in multipoles, yielding

$$\begin{aligned} \delta(\mathbf{r}_2 - \mathbf{r}_1) &= \sum_l \delta(r_1 - r_2) \frac{2l+1}{4\pi r_1^2} P_l(\cos \theta_{12}) \\ &= \sum_l \delta(r_1 - r_2) \frac{1}{r_1^2} \sum_m Y_m^l(\mathbf{r}_1) Y_m^{l*}(\mathbf{r}_2). \end{aligned} \quad (6.D.7)$$

This result is independent of the phase convention. With *time-reversed phases*,

$$\delta(\mathbf{r}_2 - \mathbf{r}_1) = \sum_l \delta(r_1 - r_2) \frac{\sqrt{2l+1}}{r_1^2} [Y^l(\hat{\mathbf{r}}_1) Y^l(\hat{\mathbf{r}}_2)]_0^0. \quad (6.D.8)$$

6.D.3 Coupling and complex conjugation

If $\Psi_{M_1}^{I_1*} = (-1)^{I_1-M_1} \Psi_{-M_1}^{I_1}$ and $\Phi_{M_2}^{I_2*} = (-1)^{I_2-M_2} \Phi_{-M_2}^{I_2}$, as it happens to be the case for spherical harmonics with time-reversed phases, then

$$\begin{aligned} [\Psi^{I_1} \Phi^{I_2}]_M^{I*} &= \sum_{\substack{M_1 M_2 \\ (M_1+M_2=M)}} \langle I_1 I_2 M_1 M_2 | IM \rangle \Psi_{M_1}^{I_1*} \Phi_{M_2}^{I_2*} \\ &= \sum_{\substack{M_1 M_2 \\ (M_1+M_2=M)}} (-1)^{I-M_1-M_2} \langle I_1 I_2 -M_1 -M_2 | I-M \rangle \Psi_{-M_1}^{I_1} \Phi_{-M_2}^{I_2} \\ &= (-1)^{I-M} \sum_{\substack{M_1 M_2 \\ (M_1+M_2=M)}} \langle I_1 I_2 -M_1 -M_2 | I-M \rangle \Psi_{-M_1}^{I_1} \Phi_{-M_2}^{I_2} \\ &= (-1)^{I-M} [\Psi^{I_1} \Phi^{I_2}]_{-M}^I, \end{aligned} \quad (6.D.9)$$

where we have used (6.D.23).

Let us care now about the spinor functions $\chi_m^{1/2}(\sigma)$, which have the form

$$\chi^{1/2}(\sigma = 1/2) = \begin{bmatrix} 1 \\ 0 \end{bmatrix} \quad \chi^{1/2}(\sigma = -1/2) = \begin{bmatrix} 0 \\ 1 \end{bmatrix}, \quad (6.D.10)$$

or

$$\chi_m^{1/2}(\sigma) = \delta_{m,\sigma}. \quad (6.D.11)$$

Thus, $\chi_m^{1/2*}(\sigma) = \chi_m^{1/2}(\sigma) = \delta_{m,\sigma}$, but we can also write

$$\chi_m^{1/2*}(\sigma) = (-1)^{1/2-m+1/2-\sigma} \chi_{-m}^{1/2}(-\sigma). \quad (6.D.12)$$

This trick enable us to write

$$\left[Y^l(\hat{r}) \chi^{1/2}(\sigma) \right]_M^{J*} = (-1)^{1/2-\sigma+J-M} \left[Y^l(\hat{r}) \chi^{1/2}(-\sigma) \right]_{-M}^J, \quad (6.D.13)$$

which can be derived in a similar way as (6.D.9).

6.D.4 Angular momenta coupling

Relation between Clebsh–Gordan and $3j$ coefficients:

$$\langle j_1 \ j_2 \ m_1 \ m_2 | JM \rangle = (-1)^{j_1-j_2+M} \sqrt{2J+1} \begin{Bmatrix} j_1 & j_2 & J \\ m_1 & m_2 & -M \end{Bmatrix}. \quad (6.D.14)$$

Relation between Wigner and $9j$ coefficients:

$$\begin{aligned} ((j_1 j_2)_{j_{12}} (j_3 j_4)_{j_{34}} | (j_1 j_3)_{j_{13}} (j_2 j_4)_{j_{24}}))_j = \\ \sqrt{(2j_{12}+1)(2j_{13}+1)(2j_{24}+1)(2j_{34}+1)} \begin{Bmatrix} j_1 & j_2 & j_{12} \\ j_3 & j_4 & j_{34} \\ j_{13} & j_{24} & j \end{Bmatrix}. \end{aligned} \quad (6.D.15)$$

6.D.5 Integrals

Let us now prove

$$\int d\Omega \left[Y^l(\hat{r}) Y^l(\hat{r}) \right]_M^I = \delta_{M,0} \delta_{I,0} \sqrt{2l+1}. \quad (6.D.16)$$

$$\begin{aligned}
\int d\Omega \left[Y^l(\hat{r}) Y^l(\hat{r}) \right]_M^I &= \sum_{\substack{m_1, m_2 \\ (m_1 + m_2 = M)}} \langle l \ l \ m_1 \ m_2 | IM \rangle \int d\Omega Y_{m_1}^l(\hat{r}) Y_{m_2}^l(\hat{r}) \\
&= \sum_{\substack{m_1, m_2 \\ (m_1 + m_2 = M)}} (-1)^{l+m_1} \langle l \ l - m_1 \ m_2 | IM \rangle \int d\Omega Y_{m_1}^{l*}(\hat{r}) Y_{m_2}^l(\hat{r}) \\
&= \delta_{M,0} \sum_m (-1)^{l+m} \langle l \ l - m \ m | I0 \rangle \\
&= \delta_{M,0} \sqrt{2l+1} \sum_m \langle l \ l - m \ m | I0 \rangle \langle l \ l - m \ m | 00 \rangle \\
&= \delta_{M,0} \delta_{I,0} \sqrt{2l+1},
\end{aligned} \tag{6.D.17}$$

where we have used

$$\langle l \ l - m \ m | 0 \ 0 \rangle = \frac{(-1)^{l+m}}{\sqrt{2l+1}} \tag{6.D.18}$$

Let us now prove

$$\begin{aligned}
\sum_{\sigma} \int d\Omega (-1)^{1/2-\sigma} \left[\Psi^j(\hat{r}, -\sigma) \Psi^j(\hat{r}, \sigma) \right]_M^I &= -\delta_{M,0} \delta_{I,0} \sqrt{2j+1}. \tag{6.D.19} \\
\sum_{\sigma} \int d\Omega (-1)^{1/2-\sigma} \left[\Psi^j(\hat{r}, -\sigma) \Psi^j(\hat{r}, \sigma) \right]_M^I &= \sum_{\substack{m_1, m_2 \\ (m_1 + m_2 = M)}} \langle j \ j \ m_1 \ m_2 | IM \rangle \sum_{\sigma} \int d\Omega \Psi_{m_1}^j(\hat{r}, -\sigma) \Psi_{m_2}^j(\hat{r}, \sigma) \\
&= \sum_{\substack{m_1, m_2 \\ (m_1 + m_2 = M)}} \langle j \ j \ m_1 \ m_2 | IM \rangle \sum_{\sigma} (-1)^{j+m_1} \int d\Omega \Psi_{-m_1}^{j*}(\hat{r}, \sigma) \Psi_{m_2}^j(\hat{r}, \sigma) \\
&= \sum_{\substack{m_1, m_2 \\ (m_1 + m_2 = M)}} \langle j \ j \ m_1 \ m_2 | IM \rangle (-1)^{j+m_1} \delta_{-m_1, m_2} \\
&= \delta_{M,0} \sum_m (-1)^{j+m} \langle j \ j \ m - m | I0 \rangle \\
&= -\delta_{M,0} \sqrt{2j+1} \sum_m (-1)^{j+m} \langle j \ j \ m - m | I0 \rangle \langle j \ j \ m - m | 00 \rangle \\
&= -\delta_{M,0} \delta_{I,0} \sqrt{2j+1}.
\end{aligned} \tag{6.D.20}$$

6.D.6 Symmetry properties

Note also another useful property

$$\left[\Psi^{I_1} \Psi^{I_2} \right]_M^I = (-1)^{I_1 + I_2 - I} \left[\Psi^{I_2} \Psi^{I_1} \right]_M^I, \tag{6.D.21}$$

by virtue of the symmetry property of the Clebsh-Gordan coefficients

$$\langle I_1 \ I_2 \ m_1 \ m_2 | IM \rangle = (-1)^{I_1+I_2-I} \langle I_2 \ I_1 \ m_2 \ m_1 | IM \rangle. \quad (6.D.22)$$

Here's another symmetry property of the Clebsh-Gordan coefficients

$$\langle I_1 \ I_2 \ m_1 \ m_2 | IM \rangle = (-1)^{I_1+I_2-I} \langle I_1 \ I_2 \ -m_2 \ -m_1 | I - M \rangle. \quad (6.D.23)$$

Another one, which can be derived from the simpler properties of $3j$ -symbols

$$\langle I_1 \ I_2 \ m_1 \ m_2 | IM \rangle = (-1)^{I_1-m_1} \sqrt{\frac{2I+1}{2I_2+1}} \langle I_1 \ I \ m_1 \ -M | I_2 m_2 \rangle. \quad (6.D.24)$$

Let us use this last property to calculate sums of the type

$$\sum_{m_1, m_3} |\langle I_1 \ I_2 \ m_1 \ m_2 | I_3 m_3 \rangle|^2. \quad (6.D.25)$$

Using (6.D.24), we have

$$\begin{aligned} \sum_{m_1, m_3} |\langle I_1 \ I_2 \ m_1 \ m_2 | I_3 m_3 \rangle|^2 &= \\ \frac{2I_3+1}{2I_2+1} \sum_{m_1, m_3} |\langle I_1 \ I_3 \ m_1 \ -m_3 | I_2 m_2 \rangle|^2 &= \frac{2I_3+1}{2I_2+1}, \end{aligned} \quad (6.D.26)$$

since

$$\sum_{m_1, m_3} |\langle I_1 \ I_3 \ m_1 \ -m_3 | I_2 m_2 \rangle|^2 = \sum_{m_1, m_3} |\langle I_1 \ I_3 \ m_1 \ m_3 | I_2 m_2 \rangle|^2 = 1. \quad (6.D.27)$$

Appendix 6.E distorted waves

Let us have a closer look at the partial wave expansion of the distorted waves

$$\chi^{(+)}(\mathbf{k}, \mathbf{r}) = \sum_l \frac{4\pi}{kr} i^l e^{i\sigma l} F_l \sum_m Y_m^l(\hat{r}) Y_m^{l*}(\hat{k}). \quad (6.E.1)$$

Of notice the very important fact that *this definition is independent of the phase convention*, since the l -dependent phase is multiplied by its complex conjugate.

$$\chi^{(-)}(\mathbf{k}, \mathbf{r}) = \chi^{(+)*}(-\mathbf{k}, \mathbf{r}) = \sum_l \frac{4\pi}{kr} i^{-l} e^{-i\sigma l} F_l^* \sum_m Y_m^{l*}(\hat{r}) Y_m^l(-\hat{k}). \quad (6.E.2)$$

As $Y_m^l(-\hat{k}) = (-1)^l Y_m^l(\hat{k})$, we have

$$\chi^{(-)}(\mathbf{k}, \mathbf{r}) = \sum_l \frac{4\pi}{kr} i^l e^{-i\sigma l} F_l^* \sum_m Y_m^{l*}(\hat{r}) Y_m^l(\hat{k}), \quad (6.E.3)$$

which is also independent of the phase convention. With time-reversed phase convention

$$\chi^{(+)}(\mathbf{k}, \mathbf{r}) = \sum_l \frac{4\pi}{kr} i^l \sqrt{2l+1} e^{i\sigma^l} F_l [Y^l(\hat{r}) Y^l(\hat{k})]_0^0, \quad (6.E.4)$$

while with Condon–Shortley phase convention we get an extra $(-1)^l$ factor:

$$\chi^{(+)}(\mathbf{k}, \mathbf{r}) = \sum_l \frac{4\pi}{kr} i^{-l} \sqrt{2l+1} e^{i\sigma^l} F_l [Y^l(\hat{r}) Y^l(\hat{k})]_0^0. \quad (6.E.5)$$

The partial-wave expansion of the Green function $G(\mathbf{r}, \mathbf{r}')$ is

$$G(\mathbf{r}, \mathbf{r}') = i \sum_l \frac{f_l(k, r_<) P_l(k, r_>)}{krr'} \sum_m Y_m^l(\hat{r}) Y_m^{l*}(\hat{r}'), \quad (6.E.6)$$

where $f_l(k, r_<)$ and $P_l(k, r_>)$ are the regular and the irregular solutions of the homogeneous problem respectively. With *time-reversed* phase convention

$$G(\mathbf{r}, \mathbf{r}') = i \sum_l \sqrt{2l+1} \frac{f_l(k, r_<) P_l(k, r_>)}{krr'} [Y^l(\hat{r}) Y^l(\hat{r}')]_0^0. \quad (6.E.7)$$

Appendix 6.F hole states and time reversal

Let us consider the state $|(jm)^{-1}\rangle$ obtained by removing a ψ_{jm} single-particle state from a $J = 0$ closed shell $|0\rangle$. The antisymmetrized product state

$$\sum_m \mathcal{A}\{\psi_{jm}|(jm)^{-1}\rangle\} \propto |0\rangle \quad (6.F.1)$$

is clearly proportional to $|0\rangle$. This gives us the transformation rules of $|(jm)^{-1}\rangle$ under rotations, which must be such that, when multiplied by a j, m spherical tensor and summed over m , yields a $j = 0$ tensor. It can be seen that these properties imply that $|(jm)^{-1}\rangle$ transforms like $(-1)^{j-m} T_{j-m}$, T_{j-m} being a spherical tensor. It also follows that the hole state $|(j\bar{m})^{-1}\rangle$ transforms like a j, m spherical tensor if $\psi_{j\bar{m}}$ is defined as the \mathcal{R} -conjugate to ψ_{jm} by the relation

$$\psi_{j\bar{m}} \equiv (-1)^{j+m} \psi_{j-m}. \quad (6.F.2)$$

In other words, with the latter definition a *hole state* transforms under rotations with the right phase. We will now show that \mathcal{R} -conjugation is equivalent to a rotation of spin and spatial coordinates through an angle $-\pi$ about the y -axis:

$$e^{i\pi J_y} \psi_{jm} = (-1)^{j+m} \psi_{j-m} \equiv \psi_{j\bar{m}}. \quad (6.F.3)$$

Let us begin by calculating $e^{i\pi L_y} Y_l^m$. The rotation matrix about the y -axis is

$$R_y(\theta) = \begin{pmatrix} \cos(\theta) & 0 & \sin(\theta) \\ 0 & 1 & 0 \\ -\sin(\theta) & 0 & \cos(\theta) \end{pmatrix}, \quad (6.F.4)$$

so for $R_y(-\pi)$ we get

$$R_y(-\pi) = \begin{pmatrix} -1 & 0 & 0 \\ 0 & 1 & 0 \\ 0 & 0 & -1 \end{pmatrix}. \quad (6.F.5)$$

When applied to the generic direction $(\sin(\theta)\cos(\phi), \sin(\theta)\sin(\phi), \cos(\theta))$, we obtain $(-\sin(\theta)\cos(\phi), \sin(\theta)\sin(\phi), -\cos(\theta))$, which corresponds to making the substitutions

$$\theta \rightarrow \pi - \theta, \quad \phi \rightarrow \pi - \phi. \quad (6.F.6)$$

When we substitute these angular transformations in the spherical harmonic $Y_l^m(\theta, \phi)$, we obtain the rotated $Y_l^m(\theta, \phi)$:

$$e^{i\pi L_y} Y_l^m = (-1)^{l+m} Y_l^{-m}. \quad (6.F.7)$$

Let us now turn our attention to the spin coordinates rotation $e^{i\pi s_y} \chi_m$. The rotation matrix in spin space is

$$\begin{pmatrix} \cos(\theta/2) & -\sin(\theta/2) \\ \sin(\theta/2) & \cos(\theta/2) \end{pmatrix}, \quad (6.F.8)$$

which, for $\theta = -\pi$ is

$$\begin{pmatrix} 0 & 1 \\ -1 & 0 \end{pmatrix}. \quad (6.F.9)$$

Applying it to the spinors, we find the rule

$$e^{i\pi s_y} \chi_m = (-1)^{1/2+m} \chi_{-m}, \quad (6.F.10)$$

so

$$\begin{aligned} e^{i\pi J_y} \psi_{jm} &= \sum_{m_l m_s} \langle l \ m_l \ 1/2 \ m_s | j \ m \rangle \ e^{i\pi L_y} Y_l^{m_l} \ e^{i\pi s_y} \chi_{m_s} \\ &= \sum_{m_l m_s} (-1)^{1/2+m_s+l+m_l} \langle l \ m_l \ 1/2 \ m_s | j \ m \rangle \ Y_l^{-m_l} \ \chi_{-m_s} \\ &= \sum_{m_l m_s} (-1)^{1+m-j+2l} \langle l \ -m_l \ 1/2 \ -m_s | j \ -m \rangle \ Y_l^{-m_l} \ \chi_{-m_s} \\ &= (-1)^{m+j} \psi_{j-m} \equiv \psi_{j\bar{m}}, \end{aligned} \quad (6.F.11)$$

where we have used $(-1)^{1+m-j+2l} = -(-1)^{m-j} = (-1)^{m+j}$, as j, m are always half-integers and l is always an integer.

We now turn our attention to the time reversal operation, which amounts to the transformations

$$\mathbf{r} \rightarrow \mathbf{r}, \quad \mathbf{p} \rightarrow -\mathbf{p}. \quad (6.F.12)$$

This is enough to define the operator of time reversal of a spinless particle (see Messiah). In the position representation, in which \mathbf{r} is real and \mathbf{p} pure imaginary, this (unitary antilinear) operator is the complex conjugation operator.

As angular momentum $\mathbf{l} = \mathbf{r} \times \mathbf{p}$ changes sign under time reversal, so does spin:

$$\mathbf{s} \rightarrow -\mathbf{s}, \quad (6.F.13)$$

which, along with (6.F.12), completes the set of rules that define the time reversal operation on a particle with spin. In the representation of eigenstates of s^2 and s_z , complex conjugation alone changes only the sign of s_y , so an additional rotation of $-\pi$ around the y -axis is necessary to change the sign of s_x, s_z and implement the transformation (6.F.13). If we call K the time-reversal operator, we have

$$K\psi_{jm} = e^{i\pi s_y} \psi_{jm}^*. \quad (6.F.14)$$

This is completely general and independent of the phase convention. It only depends on the fact that we have used the \mathbf{r} representation for the spatial wave function and the representation of the eigenstates of s^2 and s_z for the spin part. *If we use time-reversal phases for the spherical harmonics (see (6.D.2)),*

$$Y_m^{l*} = (-1)^{l+m} Y_{-m}^l = e^{i\pi L_y} Y_m^l. \quad (6.F.15)$$

So we can write

$$K\psi_{jm} = e^{i\pi J_y} \psi_{jm} = \psi_{j\bar{m}}. \quad (6.F.16)$$

Note again that this last expression is valid only if we use time-reversal phases for the spherical harmonics. Only in this case time-reversal coincides with \mathcal{R} -conjugation and hole states.

In BCS theory, the quasiparticles are defined in terms of linear combinations of particles and holes. With time-reversal phases, holes are equivalent to time-reversed states, and we get the definitions

$$\begin{aligned} a_\nu^\dagger &= u_\nu a_\nu^\dagger - v_\nu a_{\bar{\nu}} & a_\nu &= u_\nu \alpha_\nu^\dagger + v_\nu \alpha_{\bar{\nu}} \\ a_{\bar{\nu}}^\dagger &= u_\nu a_{\bar{\nu}}^\dagger + v_\nu a_\nu & a_{\bar{\nu}} &= u_\nu \alpha_{\bar{\nu}}^\dagger - v_\nu \alpha_\nu \\ \alpha_\nu &= u_\nu a_\nu - v_\nu a_{\bar{\nu}}^\dagger & a_\nu &= u_\nu \alpha_\nu + v_\nu \alpha_{\bar{\nu}}^\dagger \\ \alpha_{\bar{\nu}} &= u_\nu a_{\bar{\nu}} + v_\nu a_\nu^\dagger & a_{\bar{\nu}} &= u_\nu \alpha_{\bar{\nu}} - v_\nu \alpha_\nu^\dagger \end{aligned} \quad (6.F.17)$$

Appendix 6.G Spectroscopic amplitudes in the BCS approximation

The creation operator of a pair of fermions coupled to J, M can be expressed in second quantization as

$$P^\dagger(j_1, j_2, JM) = N \sum_m \langle j_1 m | j_2 M - m | J M \rangle a_{j_1 m}^\dagger a_{j_2 M-m}^\dagger, \quad (6.G.1)$$

where N is a normalization constant. To determine it, we write the wave function resulting from the action of (6.G.1) on the vacuum

$$\begin{aligned} \Psi &= P^\dagger(j_1, j_2, JM)|0\rangle = \frac{N}{\sqrt{2}} \sum_m \langle j_1 m | j_2 M - m | J M \rangle \\ &\quad \times (\phi_{j_1 m}(\mathbf{r}_1) \phi_{j_2 M-m}(\mathbf{r}_2) - \phi_{j_2 M-m}(\mathbf{r}_1) \phi_{j_1 m}(\mathbf{r}_2)). \end{aligned} \quad (6.G.2)$$

The norm is

$$\begin{aligned} |\Psi|^2 &= \frac{N^2}{2} \sum_{mm'} \langle j_1 m j_2 M - m | J M \rangle \langle j_1 m' j_2 M - m' | J M \rangle \\ &\quad \times (\phi_{j_1 m}(\mathbf{r}_1) \phi_{j_2 M-m}(\mathbf{r}_2) - \phi_{j_2 M-m}(\mathbf{r}_1) \phi_{j_1 m}(\mathbf{r}_2)) \\ &\quad \times (\phi_{j_1 m'}(\mathbf{r}_1) \phi_{j_2 M-m'}(\mathbf{r}_2) - \phi_{j_2 M-m'}(\mathbf{r}_1) \phi_{j_1 m'}(\mathbf{r}_2)). \end{aligned} \quad (6.G.3)$$

Integrating we get

$$\begin{aligned} 1 &= \frac{N^2}{2} \sum_{mm'} \langle j_1 m j_2 M - m | J M \rangle \langle j_1 m' j_2 M - m' | J M \rangle \\ &\quad \times (2\delta_{m,m'} - 2\delta_{j_1,j_2}\delta_{m,M-m'}) \\ &= N^2 \left(\sum_m \langle j_1 m j_2 M - m | J M \rangle^2 \right. \\ &\quad \left. - \delta_{j_1,j_2} \sum_m \langle j_1 m j_2 M - m | J M \rangle \langle j_1 M - m j_2 m | J M \rangle \right) \\ &= N^2 (1 - \delta_{j_1,j_2}(-1)^{2j-J}), \end{aligned} \quad (6.G.4)$$

where we have used the closure condition for Clebsh–Gordan coefficients and (6.D.22), and δ_{j_1,j_2} must be interpreted as a δ function regarding all the quantum numbers but the magnetic one. We see that two fermions with identical quantum numbers (but the magnetic one) *cannot couple to J odd*. If J is even, the normalization constant is

$$N = \frac{1}{\sqrt{1 + \delta_{j_1,j_2}}}. \quad (6.G.5)$$

To sum up,

$$P^\dagger(j_1, j_2, JM) = \frac{1}{\sqrt{1 + \delta_{j_1,j_2}}} \sum_m \langle j_1 m j_2 M - m | J M \rangle a_{j_1 m}^\dagger a_{j_2 M-m}^\dagger. \quad (6.G.6)$$

The spectroscopic amplitude for finding in a $A + 2, J_f, M_f$ nucleus a couple of nucleons with quantum numbers j_1, j_2 coupled to J on top of a A, J_i nucleus is

$$B(J, j_1, j_2) = \sum_{M, M_i} \langle J_i M_i JM | J_f M_f \rangle \langle \Psi_{J_f M_f} | P^\dagger(j_1, j_2, JM) | \Psi_{J_i M_i} \rangle. \quad (6.G.7)$$

This is completely general. It depends on the structure model only through the way the $A + 2$ and A nuclei are treated. We now want to turn our attention to the expression of $B(J, j_1, j_2)$ in the BCS approximation when both the $A + 2$ and the A are 0^+ , zero-quasiparticle ground states. In order to do this, we write (6.G.6) in

terms of quasiparticle operators using (6.F.17)²³:

$$\begin{aligned}
 P^\dagger(j_1, j_2, JM) = & \frac{1}{\sqrt{1 + \delta_{j_1, j_2}}} \sum_{m_1, m_2} \langle j_1 \ m_1 \ j_2 \ m_2 | J \ M \rangle \left(U_{j_1} U_{j_2} \alpha_{j_1 m_1}^\dagger \alpha_{j_2 m_2}^\dagger \right. \\
 & + (-1)^{j_1 + j_2 - M} V_{j_1} V_{j_2} \alpha_{j_1 - m_1} \alpha_{j_2 - m_2} \\
 & + (-1)^{j_2 - m_2} U_{j_1} V_{j_2} \alpha_{j_1 m_1}^\dagger \alpha_{j_2 - m_2} \\
 & - (-1)^{j_1 - m_1} V_{j_1} U_{j_2} \alpha_{j_2 m_2}^\dagger \alpha_{j_1 - m_1} \\
 & \left. + (-1)^{j_1 - m_1} V_{j_1} U_{j_2} \delta_{j_1 j_2} \delta_{-m_1 m_2} \right). \tag{6.G.8}
 \end{aligned}$$

If both nuclei are in zero-quasiparticle states, the only term that survives is the last one in the above expression, and (6.G.7) becomes (see also Sect. 3.4.2 and equation 3.1.1).

$$\begin{aligned}
 B_j = B(j^2(0)) = & \frac{1}{\sqrt{2}} \sum_m \langle j \ m \ j - m | 0 \ 0 \rangle (-1)^{j-m} V_j U_j \\
 = & \frac{1}{\sqrt{2}} \sum_m \frac{(-1)^{j-m}}{\sqrt{(2j+1)}} (-1)^{j-m} V_j U_j \\
 = & \frac{1}{\sqrt{2}} \sum_m \frac{1}{\sqrt{(2j+1)}} V_j U_j. \tag{6.G.9}
 \end{aligned}$$

After carrying out the summation one finds,

$$B_j = B(j^2(0)) = \sqrt{j + 1/2} \ V_j U_j. \tag{6.G.10}$$

Note that in this final expression V_j refers to the A nucleus, while U_j is related to the $A + 2$ nucleus. In practice, it does not make a big difference to calculate both for the same nucleus.

Appendix 6.H Derivation of two-nucleon transfer transition amplitudes including recoil, non-orthogonality and successive transfer.

In the present Appendix we reproduce with the permission of the author the first (manuscript) page (Fig. 6.H.1) of what, arguably, was the first complete derivation²⁴ of the different contributions needed to calculate absolute two-nucleon transfer cross sections in a systematic way²⁵.

²³In what follows, we use the phase convention $\alpha_{j\bar{m}}=(-1)^{j-m}\alpha_{j-m}$ instead of $\alpha_{j\bar{m}}=(-1)^{j+m}\alpha_{j-m}$, consistent with (6.F.2). Had we stick to the definition (6.F.2), the amplitude $B(0, j, j)$ calculated below would have a minus sign, which would not have any physical consequence.

²⁴Bayman (1970) (unpublished).

²⁵Bayman (1971) and Bayman and Chen (1982)). Within this context we refer to Broglia et al. (1973) and Potel et al. (2013a) in particular Fig. 10 of this reference.

$$A + a \xrightarrow{(b+n_1+n_2)} C + c \xrightarrow{(A+n_2)} b + B$$

We need

$$2 \sum_{\sigma_1 \sigma_2} \int d^3 r_{C_1} d^3 r_{B_1} d^3 r_{A_2} \left[\Psi^{f_1 \rightarrow}(\vec{r}_{A_1}, \sigma_1) \Psi^{f_2 \rightarrow}(\vec{r}_{A_2}, \sigma_2) \right]_\mu^* X_f^{(-)}(\vec{F}_{Bb}) U(r_{B_1}) \Psi^{(+)}(\vec{x})$$

$$H = H_C + H_c - \frac{\hbar^2}{2\mu_{C_0}} \nabla_{C_0}^2 + U(r_{C_0}) + V(r_{C_2}), \quad (E - H) \Psi^{(+)} = 0 = [E - H]$$

$$\text{Let } f_{KH}(\vec{r}_{C_c}) = \langle [\psi^{j_2}(\vec{r}_{A2}, \vec{r}_2) \psi^{j_1}(\vec{r}_{B1}, \vec{r}_1)]^K_M | \Psi^{(+)}(\vec{r}_{A2}, \vec{r}_2, \vec{r}_{B1}, \vec{r}_1; \vec{r}_{C_c}) \rangle_{\text{fixed}}$$

$$f_{KM}(\vec{r}_c) = \frac{2\mu_c}{\hbar^2} \int d\vec{r}'_c G(\vec{r}_c, \vec{r}'_c) \left\langle [\Psi^{j_2}(\vec{r}'_2, \vec{r}'_2) \Psi^{j_1}(\vec{r}'_1, \vec{r}'_1)]_M^K | V(r'_c) | \Psi \right\rangle$$

$$\approx \frac{2M_c}{\hbar^2} \sum_{\sigma_1 \sigma_2} \int d^3 \vec{r}_c' d^3 \vec{r}_{A_2}' d^3 \vec{r}_{B_1}' G(\vec{r}_c', \vec{r}_{C_2}') \left[\psi_{(\vec{r}_{A_2}', \sigma_2')}^{j_{F_2}} \psi_{(\vec{r}_{B_1}', \sigma_1')}^{j_1} \right]_M^K V(r_{C_2}') \chi_i^{(+)}(\vec{r}_{A_2}')$$

$$= \langle [\Psi^{j_{F_2}}(\vec{r}_{A_2}, \sigma_2') \Psi^{j_i}(\vec{r}_{B_1}, \sigma_1)]_H^K | x_i^{(+)}(\vec{r}_{A_2}) [\Psi^{j_i}(\vec{r}_{B_1}, \sigma_1') \Psi^{j_i'}(\vec{r}_{B_2}, \sigma_2')]_O^0 \rangle + u_K.$$

$$f_2 = \frac{1}{3} \quad f_{\text{fixed}} = j_1$$

$$\text{Thus } U_{k_1, M}(\vec{r}_{cc}) = \frac{2\mu_{cc}}{\pi^2} \sum_{\sigma_1 \sigma_2'} \int d^3 \vec{r}_{c_1} d^3 \vec{r}_{A_2} d^3 \vec{r}_{b_1} G(\vec{r}_{c_1}, \vec{r}_{c_1}') [\psi^{j_{f_2}}(\vec{r}_{A_2}, \sigma_2') \psi^{j_1}(\vec{r}_{b_1}, \sigma_1')] M^{K^*} V$$

4

Figure 6.H.1: First manuscript page of Ben Bayman's derivation of the two-nucleon transfer reaction amplitude, in second order DWBA approximation.

Chapter 7

Probing Cooper pairs with pair transfer

A superconductor has rather perfect internal phase order... The importance of the Josephson effect... is that... it can pin down the order parameter.

P. W. Anderson

Pairing density, both static ($n_{st} = e^{-2i\phi}\alpha'_0/N$) and dynamic ($\alpha_{dyn}/V; V = (4\pi/3)R^3$) can exist only to the extent that normal density exists. At the basis of normal density one finds independent nucleon (fermion) motion in a mean field created by all nucleons. At the basis of pair density one finds the conversion of this motion into long range correlated motion of extended, strongly overlapping, weakly bound pairs (quasibosons) of nucleons moving in time reversal states close to the Fermi energy. Because the mean square radius of Cooper pairs is considerably larger than nuclear dimensions, the average potential acts on them as a strong external field and affects their structure and dynamics. A fact whose implications have become physically clear in the study of the structure of the two-neutron halo nucleus ^{11}Li and, quantitatively accurate, by probing the system through the transfer of two-nucleons. Said it differently, Cooper pairs are at the basis of both static and dynamic spontaneous breaking of gauge invariance, namely of (pairs) of particle number. To study the specific consequence of a broken symmetry one needs a probe which itself breaks the symmetry. In the present case a probe which changes in two particle number, like a heavy or light ion reaction inducing Cooper pair transfer.

Within the above scenario we apply, in what follows, we apply the formalism worked out in the previous chapters with the help of software developed to calculate absolute one- and two-particle transfer differential cross sections, to analyze reactions induced by both light and heavy ions (see App. 7.C COOPER, ONE).

A number of examples are considered covering nuclei throughout the mass table. Namely, one-particle transfer reactions on ^{10}Be , and two-particle transfer on ^{10}Be , ^7Li , ^{11}Li , ^{48}Ca , and ^{206}Pb (systems around closed shells), and on open shell superfluid medium heavy nuclei (Sn-isotopes).

7.1 The $^1\text{H}(^{11}\text{Li}, ^9\text{Li})^3\text{H}$ reaction: evidence for phonon mediated pairing

We start by discussing the analysis of the two-neutron pickup¹ reaction $^1\text{H}(^{11}\text{Li}, ^9\text{Li})^3\text{H}$. Particular attention is paid to the excitation of the $1/2^-$ first excited state of ^9Li lying² at 2.69 MeV (see Figs. 2.10.4 and 7.1.1). The results provide evidence for a new mechanism of pairing correlations in nuclei: pygmy resonance (low-energy $E1$ -strength) mediated pairing interaction³, which strongly renormalizes the bare, $NN^{-1}S_0$ interaction. This is but a particular embodiment of phonon mediated pairing interaction found throughout in nuclei⁴. The main difference between light halo exotic nuclei and medium heavy superfluid nuclei lying along the valley of stability is the role fluctuations play in dressing particles (quasiparticles) and in renormalizing their properties (mass, charge, etc.) and their interactions. In fact, in the case of e.g. Sn isotopes, mean field effects are dominant, while in the case of halo exotic nuclei renormalization effects can be as large as mean field ones. Concerning the pairing interaction, bare and induced contributions are about equal in the case of i.e. Sn-isotopes, while the second one is the overwhelming contribution in the case of ^{11}Li . The collective modes acting as glue of the Cooper pairs are mainly of quadrupole type in Sn and of dipole (pygmy resonance)⁵ type in the case of Li. In what follows we summarize aspects of structure and reaction which, interweaved shed insight on this single Cooper pair halo nucleus, and allows to compare theory with experiment in terms of absolute differential cross sections.

7.1.1 Structure

Within the scenario presented in Chapter 3 (Sect. 3.6) and Chapter 5 (Sect. 5.2.2) the wavefunction describing the structure of the halo neutrons in the ground state of ^{11}Li (the $p_{3/2}$ proton being assumed to act only as a spectator) can be written as

$$|0\rangle_v = |0\rangle + \alpha|(p_{1/2}, s_{1/2})_{1^-} \otimes 1^-; 0\rangle + \beta|(s_{1/2}, d_{5/2})_{2^+} \otimes 2^+; 0\rangle, \quad (7.1.1)$$

with

$$\alpha = 0.7, \quad \text{and} \quad \beta = 0.1, \quad (7.1.2)$$

¹Tanihata et al. (2008).

²To assess the direct character of the $1/2^-$ excitation process, the importance of inelastic and knockout (cf. Ch.5) channels were considered and found to be small (see App. 7.B).

³Barranco et al. (2001); Potel et al. (2010).

⁴See e.g. Barranco et al. (1999); Gori et al. (2004) cf. also Brink and Broglia (2005).

⁵Within this context see Broglia et al. (2019a).

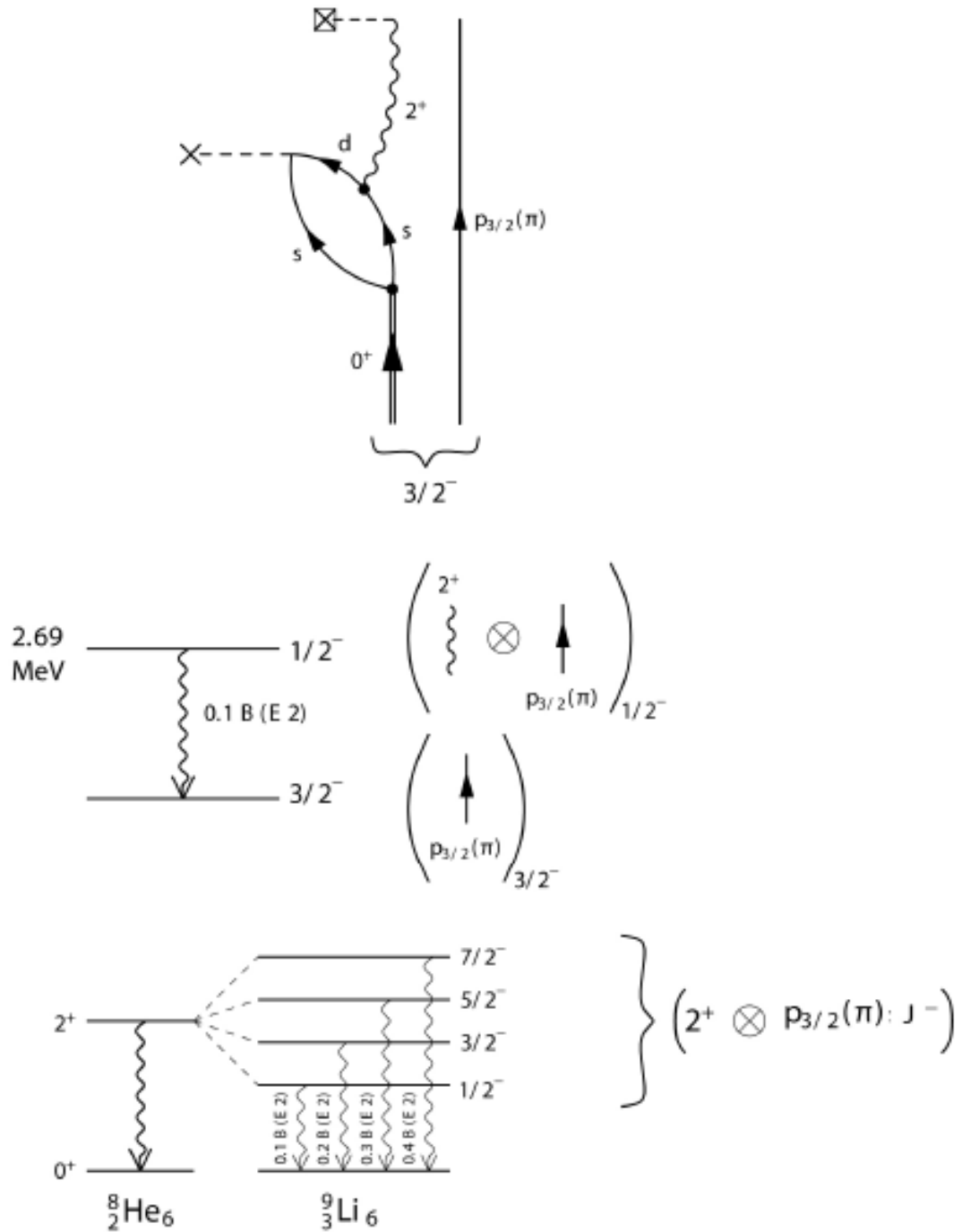


Figure 7.1.1: *Gedanken* (two-particle transfer) coincidence experiments aimed at better individuating the couplings involved in the neutron halo Cooper pair correlations in ^{11}Li and of the $1/2^-$ first excited state of ^9Li populated in the $^1\text{H}(^{11}\text{Li}, ^9\text{Li})^3\text{H}$ reaction (Tanihata et al. (2008); Barranco et al. (2001); Potel et al. (2010)). From Potel et al. (2014). It is of notice the lack of detail regarding the reaction aspect of the process, to emphasize some structural features.

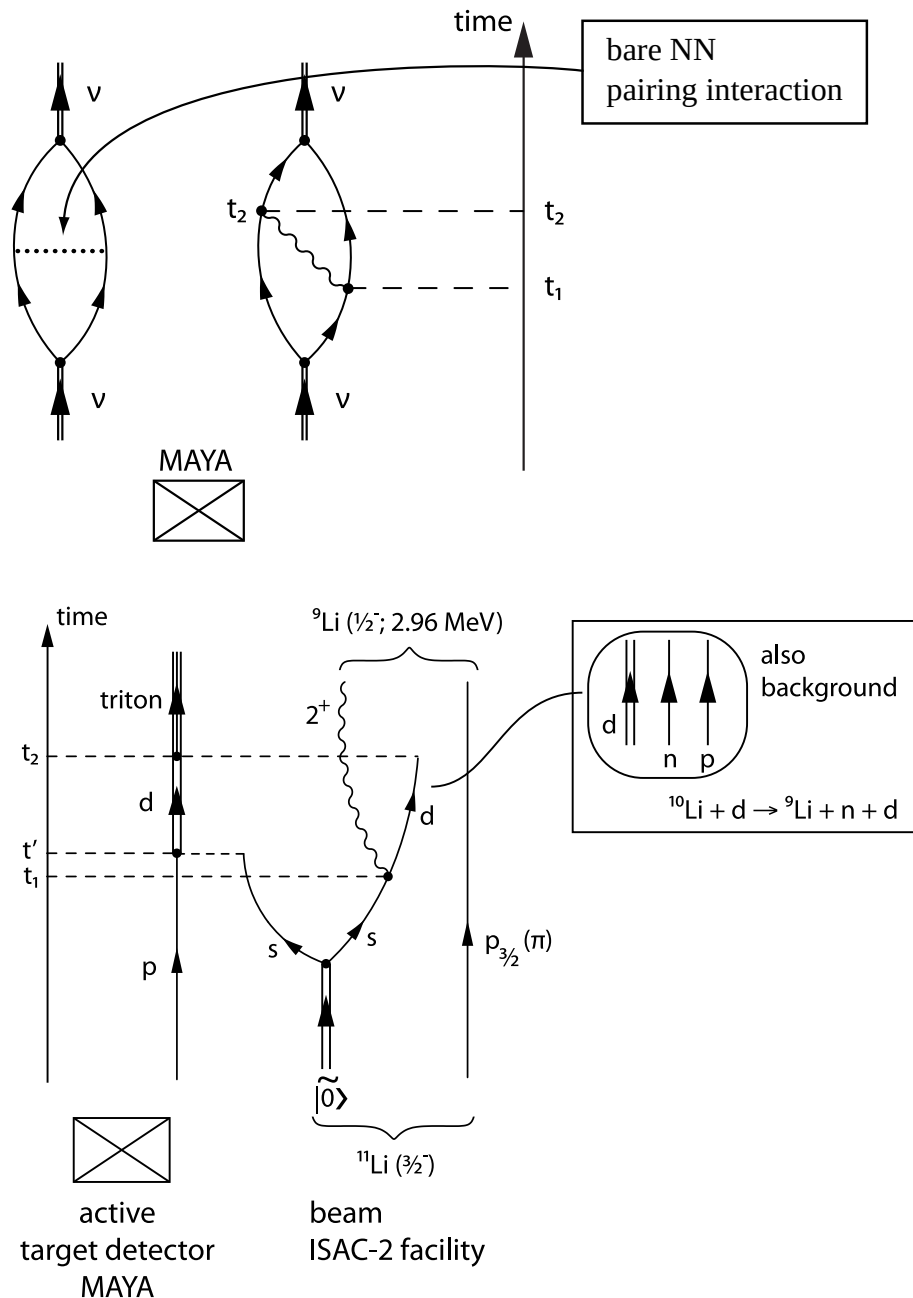


Figure 7.1.2: Schematic representation of the bare nucleon-nucleon and phonon induced pairing correlations (upper part) NFT diagrams, and of the population of the first, excited state of ${}^9\text{Li}(1/2^-; 2.69 \text{ MeV})$, in the TRIUMF experiment reported in ref. Tanihata et al. (2008).

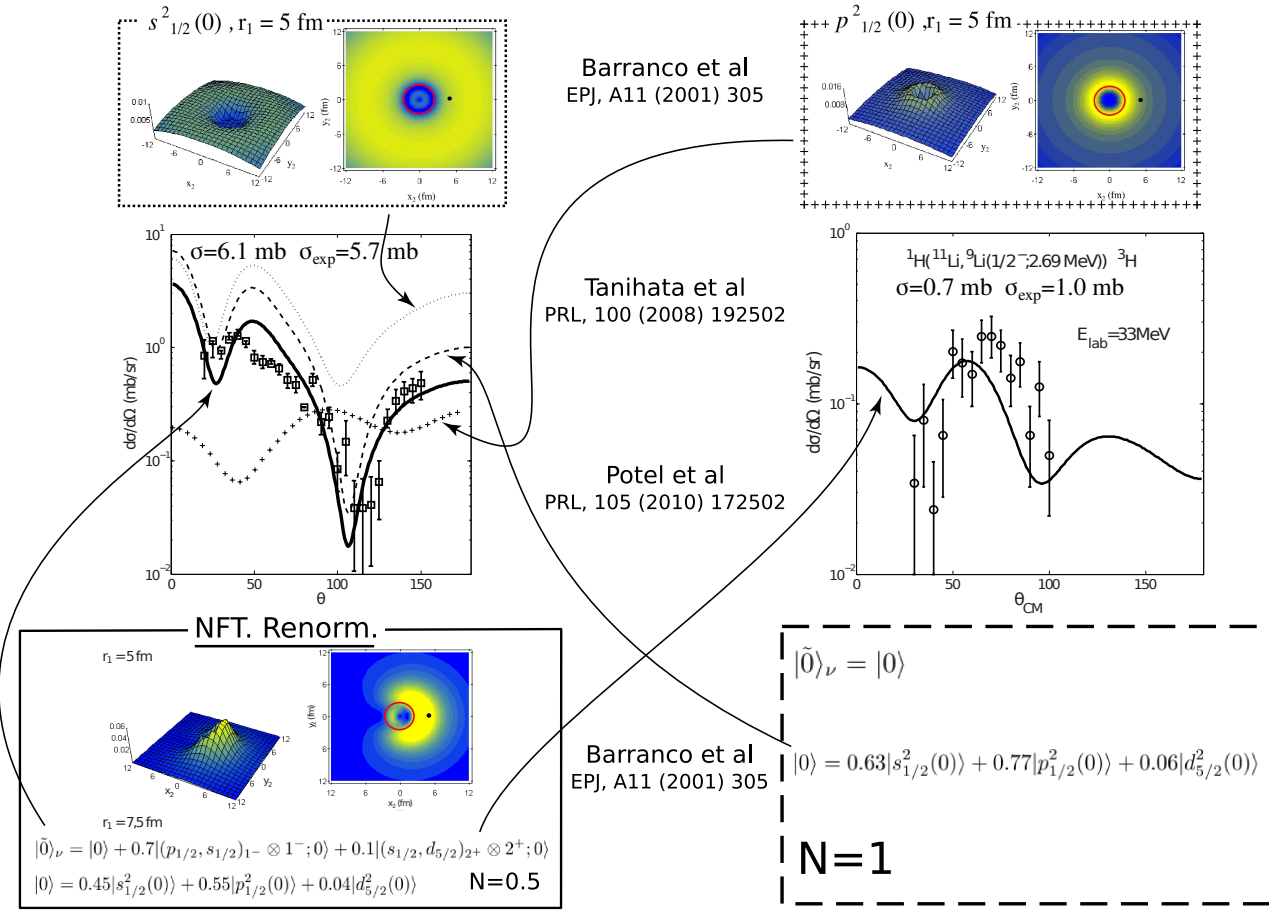


Figure 7.1.3: Absolute, two-nucleon transfer differential cross section associated with the ground state and the first excited state of ${}^9\text{Li}$, excited in the reaction ${}^1\text{H}({}^{11}\text{Li}, {}^9\text{Li}){}^3\text{H}$ (Tanihata et al., 2008) in comparison with the predicted differential cross sections (Potel et al., 2010) worked out making use of spectroscopic amplitudes and Cooper pair wavefunctions calculated with NFT, and of the optical potential collected in Table 7.1.1.

and

$$|0\rangle = 0.45|s_{1/2}^2(0)\rangle + 0.55|p_{1/2}^2(0)\rangle + 0.04|d_{5/2}^2(0)\rangle, \quad (7.1.3)$$

$|1^-\rangle$ and $|2^+\rangle$ being the (RPA) states describing the dipole pygmy resonance of ^{11}Li and the quadrupole vibration of the core. The corresponding NFT diagrams are shown in diagrams (a), (d) and (e) of Fig. 2.10.4 (see also Fig. 3.6.3). The wavy curve represents both the quadrupole and dipole collective vibrational states being exchanged between the two halo neutrons, the horizontal dashed line the bare nuclear pairing interaction.

$^{11}\text{Li}(p, t)^9\text{Li}$												
	V	W	V_{so}	W_d	r_1	a_1	r_2	a_2	r_3	a_3	r_4	a_4
$p, {}^{11}\text{Li}^d)$	63.62	0.33	5.69	8.9	1.12	0.68	1.12	0.52	0.89	0.59	1.31	0.52
$d, {}^{10}\text{Li}^b)$	90.76	1.6	3.56	10.58	1.15	0.75	1.35	0.64	0.97	1.01	1.4	0.66
$t, {}^9\text{Li}^c)$	152.47	12.59	1.9	12.08	1.04	0.72	1.23	0.72	0.53	0.24	1.03	0.83

Table 7.1.1: Optical potentials (cf. Tanihata et al. (2008)) used in the calculation of the absolute differential cross sections displayed in Fig. 7.1.3.

We are then in presence of a paradigmatic nuclear embodiment of Cooper's model which is at the basis of BCS theory: a single weakly bound neutron pair on top of the Fermi surface of the ${}^9\text{Li}$ core. But the analogy goes beyond these aspects, and covers also the very nature of the interaction acting between Cooper pair partners. Due to the the high polarizability of the system under study and of the small overlap of halo and core single particle wavefunctions, most of the Cooper pair correlation energy stems from the exchange of collective vibrations, the role of the strongly screened bare interaction being, in this case, minor (see Sect. 3.6). In other words, we are in the presence of a new realization of the Cooper model in which a totally novel Bardeen-Pines-Frölich-like phonon induced interaction is generated by a self induced collective vibration of the nuclear medium.

In connection with (7.1.1), it is revealing that the two states populated in the inverse kinematics, two-neutron pick up reaction ${}^1\text{H}({}^{11}\text{Li}, {}^9\text{Li}){}^3\text{H}$ are⁶, the $|3/2^-, \text{gs}({}^9\text{Li})\rangle$ and the first excited $|1/2^-, 2.69 \text{ MeV}({}^9\text{Li})\rangle$ level of ${}^9\text{Li}$ (see Figs. 2.10.4 (f) and 7.1.1, 7.1.2 and 7.1.3). The associated absolute differential cross sections calculated making use of the spectroscopic amplitudes displayed in (7.1.1)-(7.1.3) and the optical potentials displayed in Table 7.1.1, provide a quantitative account of the experimental data within the NFT scenario (Fig. 7.1.3).

7.1.2 Reaction

Because second order calculations of inelastic, break up and final state interaction channels, which in principle can provide alternative routes for the population of the first excited state of ${}^9\text{Li}$ (see Fig. 7.B.1 and Table 7.B.1) to the direct one predicted

⁶Tanihata et al. (2008).

by the wavefunction (7.1.1) (β component), lead to absolute cross sections which are smaller by few orders of magnitude than that shown in Fig. 7.1.3, one can posit that quadrupole core polarization effects in $|gs(^{11}\text{Li})\rangle$ is essential to account for the observation of the $|1/2^-, 2.69 \text{ MeV}\rangle$ state, thus providing evidence for phonon mediated pairing in nuclei.

The reason why in the case of ^{11}Li evidence for phonon mediated pairing is, arguably, inescapable, is connected with the fact that reaching the limits of stability associated with drip line nuclei, the system also reaches to situations in which medium polarization effects become overwhelming. In fact, one is, in such cases confronted with elementary modes of nuclear excitation in which dynamic fluctuation effects are as important as static, mean field effects. Within this context we refer to parity inversion (see Figs. 3.6.3 and 7.2.1). Nuclear field theory allows one to sum to infinite order weakly convergent processes or particular important ones⁷ without at the same time to do so with others which are not so, and is thus specially suited to study halo systems⁸. From these studies it emerges a possible new elementary mode of excitation, namely pair addition halo vibration, of which $|gs(^{11}\text{Li})\rangle$ state is a concrete embodiment. It is associated with a novel mechanism for stabilizing Cooper pairs, which arises from a (dynamical) breakup of gauge invariance (see App. 7.A). Their most distinctive feature, namely that of carrying on top of it a (dipole) pygmy resonance at a relative excitation energy of about 1 MeV, a necessary although not sufficient condition for this new mode to exist, can be instrumental for its characterization. While the neutron pair addition mode is, in the case of ^9Li , the ground state of the $A + 2$ system ($|^{11}\text{Li}(gs)\rangle$), in other nuclei it may be an excited state which could be observed in a combined $L = 0$, and $L = 1$, two-particle transfer reaction to excited states, or in terms of $E1$ -decay of the soft mode (pygmy resonance) built on top of it. Within this context, it is an open question whether one could expect to find a realization of such a halo pair addition mode in, for example, the first excited 0^+ state of ^{12}Be (see Fig. 7.1.4).

Single-particle $s_{1/2}$ and $p_{1/2}$ states at threshold in neutron drip-line nuclei have been found to lead, within the framework of a bare, short range, pairing interaction scheme to halo anti-pairing effects⁹. The fact that the two-neutron separation energy of the halo neutrons (halo Cooper pair) of $^{11}\text{Li}(gs)$ is $\approx 400 \text{ keV}$, testifies to the fact that the anti-halo pairing effect is, in this case, overwhelmed by (dynamical) medium polarization effects.

Before concluding this section we provide in Fig. 7.1.5 examples of pairing vibrational states around ^9Li , ^{10}Be , $^{48}_{20}\text{Ca}_{28}$ and $^{208}_{82}\text{Pb}_{126}$, $N = 6$, $N = 28$ and $N = 126$ neutron closed shell systems. The fact that among the (p, t) and (t, p) absolute differential cross sections one also finds the $^{208}\text{Pb}(^{16}\text{O}, ^{18}\text{O})^{206}\text{Pb}(gs)$ absolute differential cross section is in keeping with the fact that the formalism to treat both light and heavy ions two-nucleon transfer reactions and their connection

⁷Bortignon et al. (1978).

⁸Barranco et al. (2001) and Gori et al. (2004).

⁹Bennaceur et al. (2000), cf. also Hamamoto and Mottelson (2003), Hamamoto and Mottelson (2004).

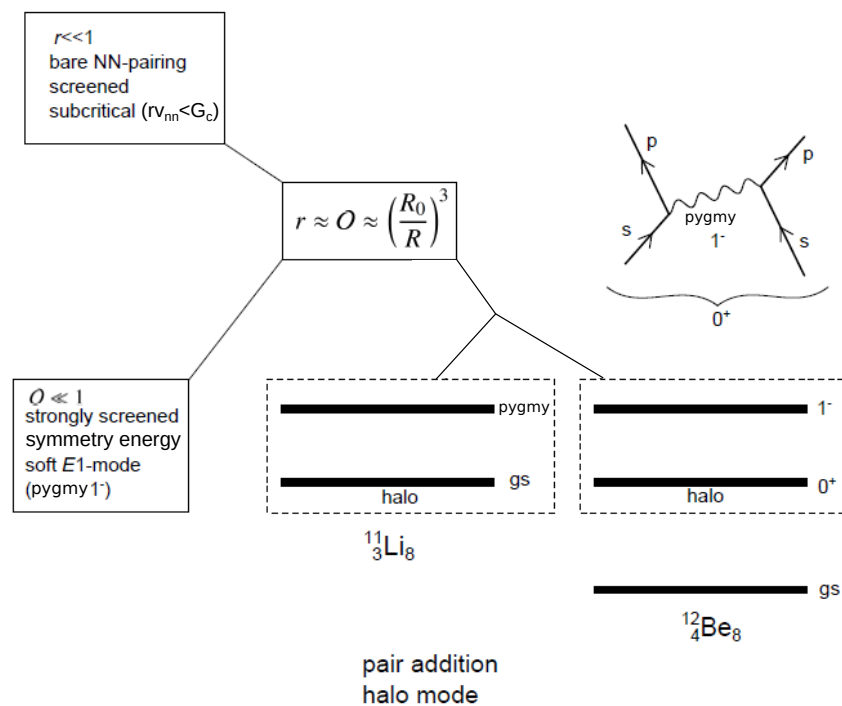


Figure 7.1.4: Schematic representation of a possible realization of halo pair addition mode in terms of the first excited 0^+ state (2.24 MeV) of ^{12}Be (for details see Sect. 3.6).

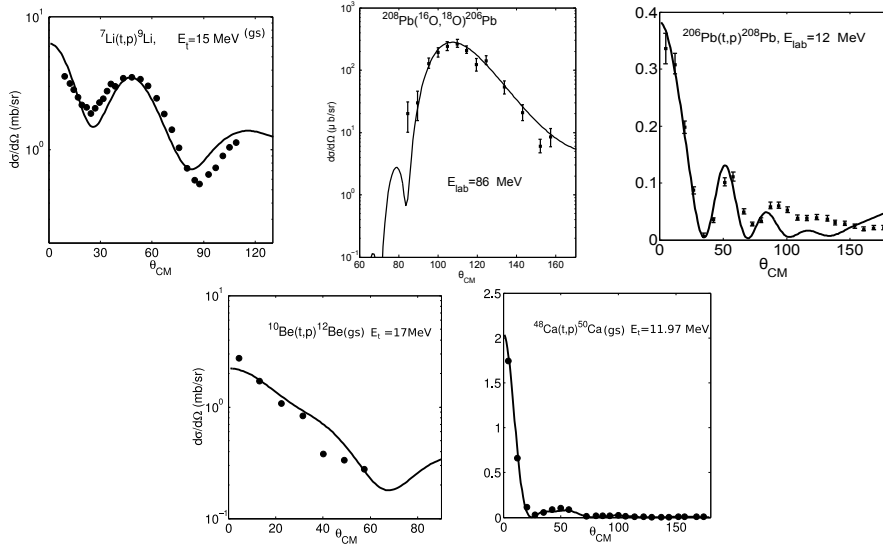


Figure 7.1.5: Absolute two-particle transfer differential cross sections for a number of reactions around closed shell associated with monopole pair addition and removal modes, and populating the ground state of the final system. Making use of spectroscopic amplitudes calculated as described in Sect. 3.5 in the particular case of $N = 6$ (Li,Be), $N = 48$ (Ca) and $N = 126$ (Pb), of global optical parameters and of the software COOPER, the absolute differential cross sections were calculated and are displayed in comparison with the experimental data (after Potel et al. (2013a)).

is well known¹⁰ and rather homogeneous¹¹. Thus, it has been implemented in the software COOPER as a standard option (cf. App. 7.C). As observed, theory provides a quantitative account of experimental findings.

7.2 NFT of ^{11}Be : one-particle transfer in halo nuclei

The nucleus $^{11}_4\text{Be}_7$ constitutes an example of one-neutron halo system, namely a halo neutron outside the $N = 6$ closed shell resulting from the phenomenon of parity inversion¹²

¹⁰Broglia and Winther (2004), Bayman and Chen (1982) and Thompson (1988) and references therein.

¹¹Potel et al. (2013b).

¹²This nucleus has been extensively studied both experimentally (see Iwasaki et al. (2000); Fortier et al. (1999); Winfield et al. (2001); Auton (1970); Zwiglinski et al. (1979); Schmitt et al. (2013); Nörterhäuser et al. (2009); Kwan et al. (2014) and references therein) and theoretically (see Talmi and Unna (1960); Otsuka et al. (1993); Sagawa et al. (1993); Vinh Mau (1995); Gori et al. (2004); Nunes et al. (1996); Fossez et al. (2016); Hamamoto and Shimoura (2007); Kanada-En'yo and Horieuchi (2002); Calci et al. (2016); Krieger et al. (2012); Timofeyuk and Johnson (1999); Keeley et al. (2004); Deltuva (2009, 2013); Lay et al. (2014); de Diego et al. (2014) and references therein).

7.2.1 Outlook¹³

In the core of ^{11}Be , namely $^{10}_4\text{Be}_6$, six neutrons occupy the $1s_{1/2}$ and $1p_{3/2}$ levels (Fig. 7.2.1). The dominant ZPF is of quadrupole type, the main neutron component being the $((p_{1/2}, p_{3/2}^{-1}) \otimes 2^+)_{0+}$ one. Because $\epsilon_{p1/2} - \epsilon_{p3/2} \approx 3.38$ MeV and $\hbar\omega_{2^+} = 3.368$ MeV, the largest amplitude of the quadrupole mode is associated with particle-hole excitation $(p_{1/2}, p_{3/2}^{-1})_{2^+}$. The repulsion due to Pauli principle correction (Fig. 7.2.1 inset (A)) is ≈ 2.8 MeV. The clothing of the $2s_{1/2}$ bare level by the quadrupole mode (Fig. 7.2.1 inset (B)) makes it heavier, lowering its energy by almost 1 MeV (710 keV). The result of the two processes is parity inversion and the appearance of the $N = 6$ new magic number together with the melting away of the $N = 8$ standard one. In a similar way in which the Lamb shift (Fig. 7.2.1, inset C) provides a measure of the fluctuations of the QED vacuum¹⁴, parity inversion measures ZPF of the nuclear vacuum (ground) state.

7.2.2 Calculations

In the calculations one has simultaneously dealt with the $p_{3/2}, p_{1/2}, s_{1/2}$ and $d_{5/2}$ valence single-particle states, treating their interweaving with the low-lying quadrupole collective vibration of the ^{10}Be core and the mixing between bound and continuum states. The bare energies of the single-particle orbitals were determined by freely varying the depth, diffusivity, radius and spin-orbit strength of a Woods-Saxon potential so that, making use of an effective radial dependent effective mass ($m_k(r=0) = 0.7m$, $m_k(r=\infty) = 9/10m$), the fully dressed, renormalized energies best reproduce the experimental findings¹⁵.

The variety of self energy diagrams, renormalizing selfconsistently the motion of the odd neutron of ^{11}Be in both configuration- (Fig. 7.2.2) and conformational 3D-space (Fig. 7.2.3), through the coupling to quadrupole vibrations, have been worked out¹⁶. The resulting states can be written as

$$|\widetilde{1/2^+}\rangle = \sqrt{0.80}|s_{1/2}\rangle + \sqrt{0.20}|(d_{5/2} \otimes 2^+)_{1/2^+}\rangle \quad (7.2.1)$$

$$|\widetilde{1/2^-}\rangle = \sqrt{0.84}|(p_{1/2}\rangle + \sqrt{0.16}|(p_{1/2}, p_{3/2}^{-1})_{2^+} \otimes 2^+)_0, p_{1/2}\rangle \quad (7.2.2)$$

$$|\widetilde{5/2^+}\rangle = \sqrt{0.49}|d_{5/2}\rangle + \sqrt{0.23}|(s_{1/2} \otimes 2^+)_{5/2^+}\rangle + \sqrt{0.28}|(d_{5/2} \otimes 2^+)_{5/2^+}\rangle. \quad (7.2.3)$$

The bare energies ϵ_j and the $((NFT)_{ren})$ values $\tilde{\epsilon}_j$ associated with the renormalised single-particle states are shown in Fig. 7.2.1. These last quantities reproduce

¹³Barranco et al. (2017).

¹⁴Pais (1986) p. 451.

¹⁵Namely, renormalization connected with the bare mass, as found in QED.

¹⁶The results worked out taking also into account the coupling to the octupole vibration and the pair removal mode of the core ^{10}Be is shown in Fig. 7.3.1. There are rather similar to the ones discussed in this Section (Barranco et al. (2017), supplemental material).

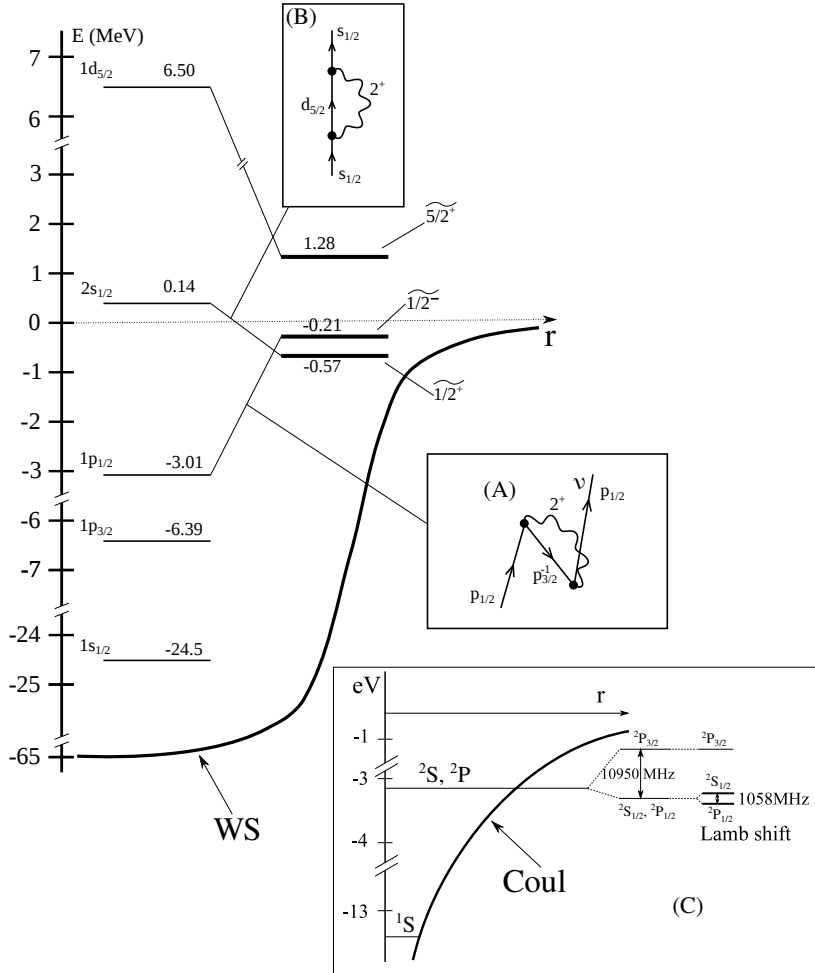


Figure 7.2.1: Bare ϵ_j (upper left thin horizontal lines) and dressed $\tilde{\epsilon}_j$ (bold face) single-particle levels of ^{11}Be . Due to the dressing of neutron motion with quadrupole vibrations of the core ^{10}Be (insets (A), (B) and (D)) inversion in sequence between the $2s_{1/2}$ and $1p_{1/2}$ levels (parity inversion) is observed. The numbers are energies in MeV. The Woods-Saxon (WS) bare mean field is indicated. In inset (C), the lowest energy levels of hydrogen are indicated, the Coulomb potential (Coul) is also schematically shown. The effects of the spin-orbit coupling and Lamb shift associated with the splitting of the $^2S_{1/2}$ and $^2P_{1/2}$ levels are displayed.

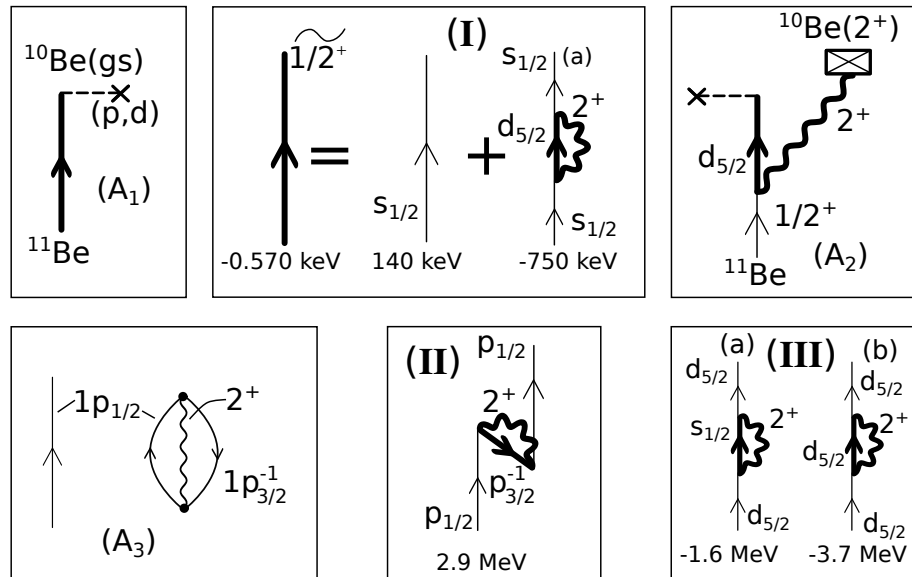


Figure 7.2.2: $(NFT)_{ren}$ diagrams describing the renormalization processes responsible for the different components of the clothed states (Eqs. (7.2.1)-(7.2.3)) associated with (I)-(III)) and the pickup processes populating the ground (A_1) and the first excited 2^+ state (A_2) of ^{10}Be . (A_3) Valence nucleon in presence of a virtual zero point fluctuation of the core ^{10}Be . Bold (thin) arrowed lines pointing upwards (downwards), describe dressed (bare) particle (hole) states. The wavy line represents the quadrupole vibration. A cross followed by a horizontal dashed line stands for an external one-neutron pickup (p,d) field. A crossed box indicates a detector, revealing the γ -ray associated with the eventual decay of the quadrupole vibration of ^{10}Be (Fig 7.6.2 (II)). After Barranco et al. (2017).

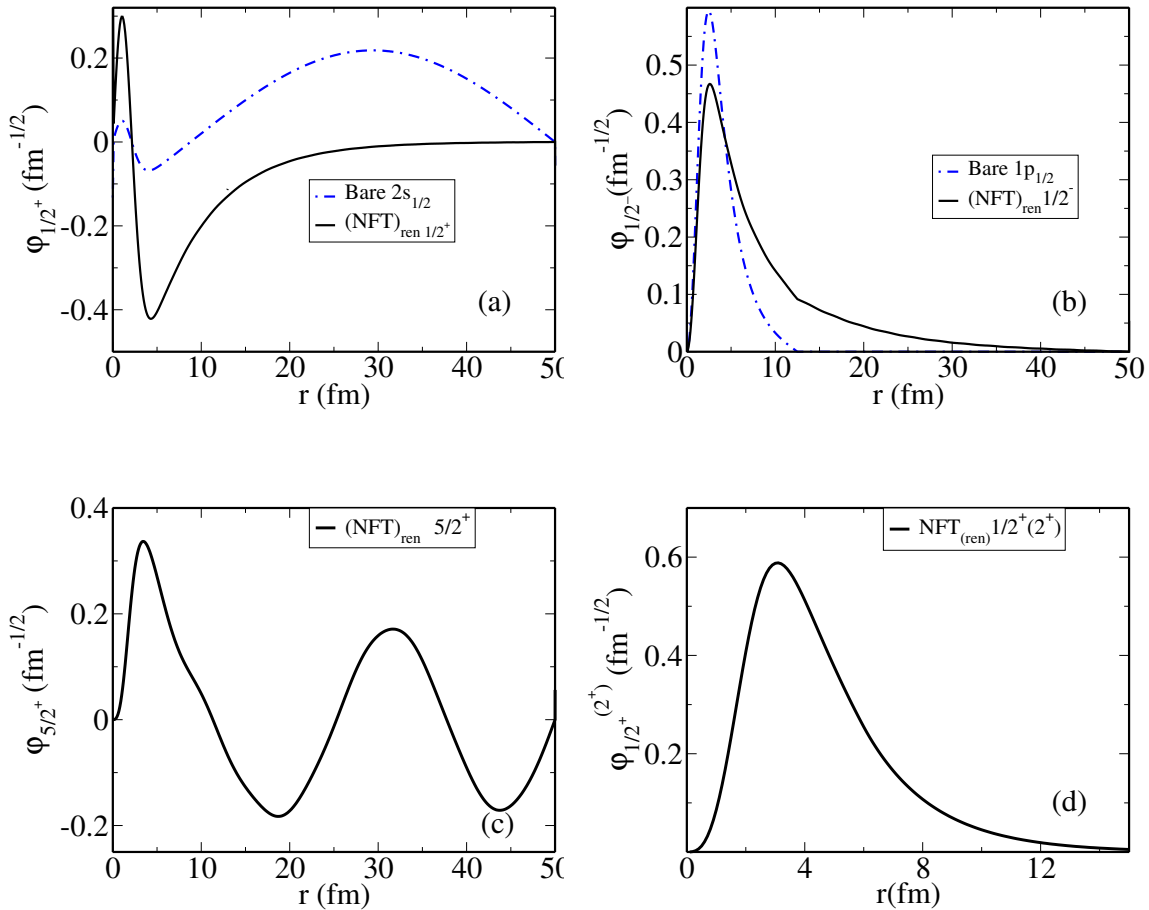


Figure 7.2.3: Form factors of the $1/2^+$ (a), $1/2^-$ (b), $5/2^+$ (c) states; (d) the form factor associated with the reaction $^{11}\text{Be}(\text{p},\text{d})^{10}\text{Be}(2^+)$ calculated within the framework of $(\text{NFT})_{\text{ren}}$ ($a_{1/2^+} = \sqrt{0.80}$, $a_{1/2^-} = \sqrt{0.84}$, $a_{5/2^+} = \sqrt{0.49}$, $a_{(d_{5/2} \otimes 2^+)_1}_{1/2^+} = \sqrt{0.20}$, see Eqs. (7.2.1–7.2.3)). Also shown in (a) and (b) are the wave functions calculated with the bare potential. After Barranco et al. (2017).

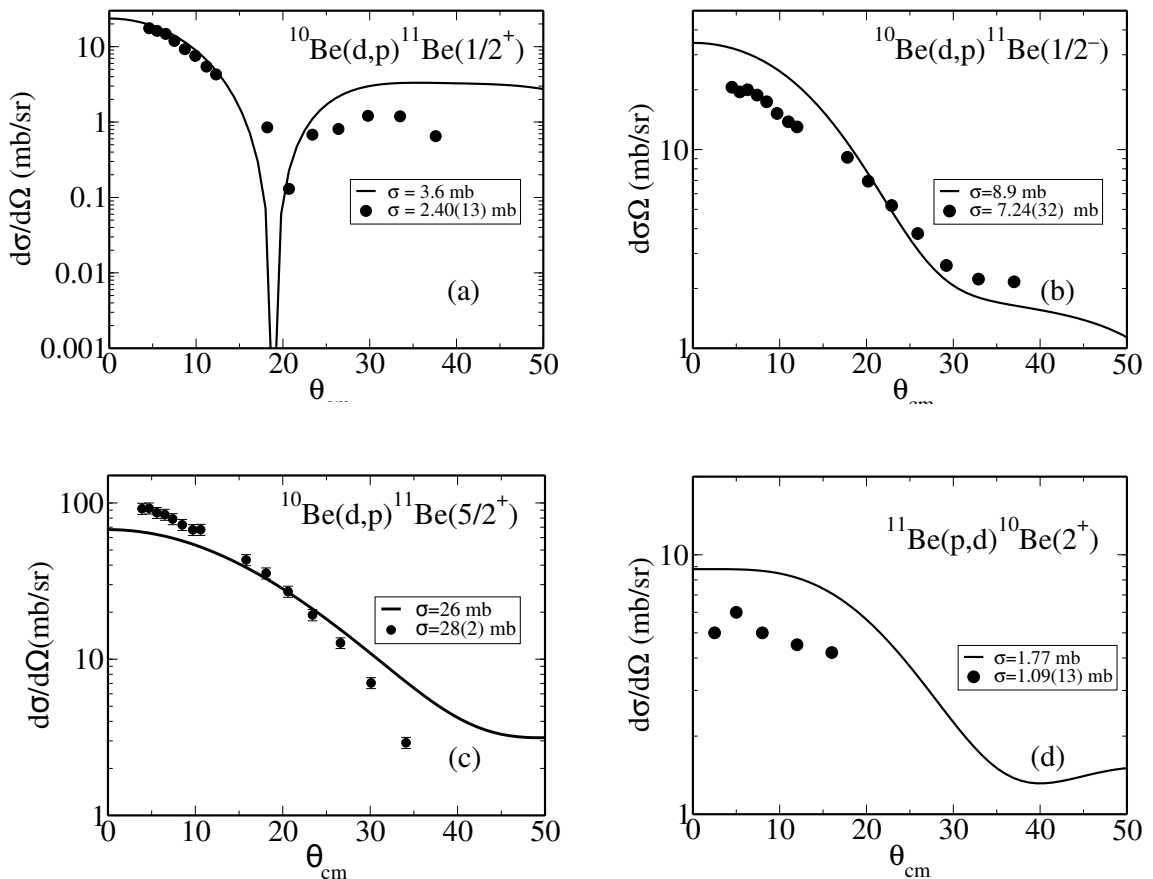


Figure 7.2.4: (a-c) (continuous curve) Absolute differential and summed (inset) cross sections associated with the reactions $^2\text{H}(^{10}\text{Be}, ^{11}\text{Be})^1\text{H}$ at $E=107 \text{ MeV}$, populating the $1/2^+$, $1/2^-$, and $5/2^+$ states. The experimental data Schmitt et al. (2013) are displayed in terms of solid dots. (d) Same as before, but for the reaction $^1\text{H}(^{11}\text{Be}, ^{10}\text{Be})^2\text{H}$ at $E=388.3 \text{ MeV}$, populating the 2^+ state (Winfield et al. (2001)). After Barranco et al. (2017).

quite accurately the experimental findings (Fig. 7.3.1, upper center). The corresponding wavefunctions $\phi_j(r)$ and $\tilde{\phi}_j(r)$ are shown in Fig. 7.2.3. The form factors $\tilde{\phi}_j(r)$ were used, together with global optical potentials¹⁷, to calculate the one-nucleon stripping and pickup absolute differential cross sections of the reactions $^{10}\text{Be}(d, p)^{11}\text{Be}(1/2^+, 1/2^-, \text{ and } 5/2^+)$ and $^{11}\text{Be}(p, d)^{10}\text{Be}(2^+)$. The results provide an overall account of the experimental findings (Fig. 7.2.4).

Within this context we remark that the pickup process shown in inset (A₁) of Fig. 7.2.2 and populating ^{10}Be ground state implies the action of the external (p, d) field on the left hand side of the graphical representation of Dyson equation shown in Fig. 7.2.2(I), and involves, at the same time, the use of the corresponding radial wavefunction as form factor (Fig. 7.2.3(a)). In the case of the population of the first 2^+ excited state of ^{10}Be (inset A₂), the (p, d) field acts on the $(d_{5/2} \otimes 2^+)_{1/2^+}$ virtual state of the second graph of the right hand side of this equation (Fig. 7.2.2(I)(a)), involving this time the radial wave function $\tilde{\phi}_{1/2^+}(r)^{(2^+)}$, namely the odd neutron moving around the quadrupole excited ^{10}Be core, as form factor (Fig. 7.2.3(d)).

Summing up, insets (A₁) and (A₂) and diagrams (I) of Fig. 7.2.2 testify to the subtle effects resulting from the unification of $(\text{NFT})_{\text{ren}}$ of structure and reactions, and operative in the cross sections shown in Fig. 7.2.4, as a result of the simultaneous and self consistent treatment of configuration and 3D-space. Within this context the bold face drawn state $|(d_{5/2} \otimes 2^+)_{1/2^+}\rangle$ shown in Fig. 7.2.2(I)(a) and the radial wave function $(\text{NFT})_{\text{ren}}$ displayed with a continuous curve in Fig. 7.2.3(d), can be viewed as *on par* renormalized structure and reaction intermediate (virtual) elements of the quantal process $^{11}\text{Be}(p, d)^{10}\text{Be}(2^+)$.

7.3 Summary

In Figure 7.3.1 a “complete” $(\text{NFT})_{\text{ren}}(s+r)$ description of the single-neutron outside closed shell halo nucleus ^{11}Be in terms of the reactions $^2\text{H}(^{10}\text{Be}, ^{11}\text{Be})^1\text{H}$ populating the $1/2^+, 1/2^-$ and $5/2^+$ states and of the $^1\text{H}(^{11}\text{Be}, ^{10}\text{Be})^2\text{H}$ process populating the 2^+ mode. Also shown, in comparison with the data, are the $E1$ -transition between the parity inverted states $1/2^+, 1/2^-$ and the isotopic shift of the charge radius of ^{10}Be . Repeating the last paragraph of Sect. 2.12 one can again state that, *in a very real sense, this is a nucleus*.

7.4 Pairing rotational band with two–nucleon transfer: Sn-isotopes

In keeping with the fact that Cooper pair tunneling is proportional to $|\alpha_0|^2$, this quantity plays also the role of a ($L = 0$) two-nucleon transfer sum rule, sum rule which is essentially exhausted by the superfluid nuclear $|BCS\rangle$ ground state (see Fig. 3.1.3).

¹⁷Han et al. (2006); Koning and Delaroche (2003).

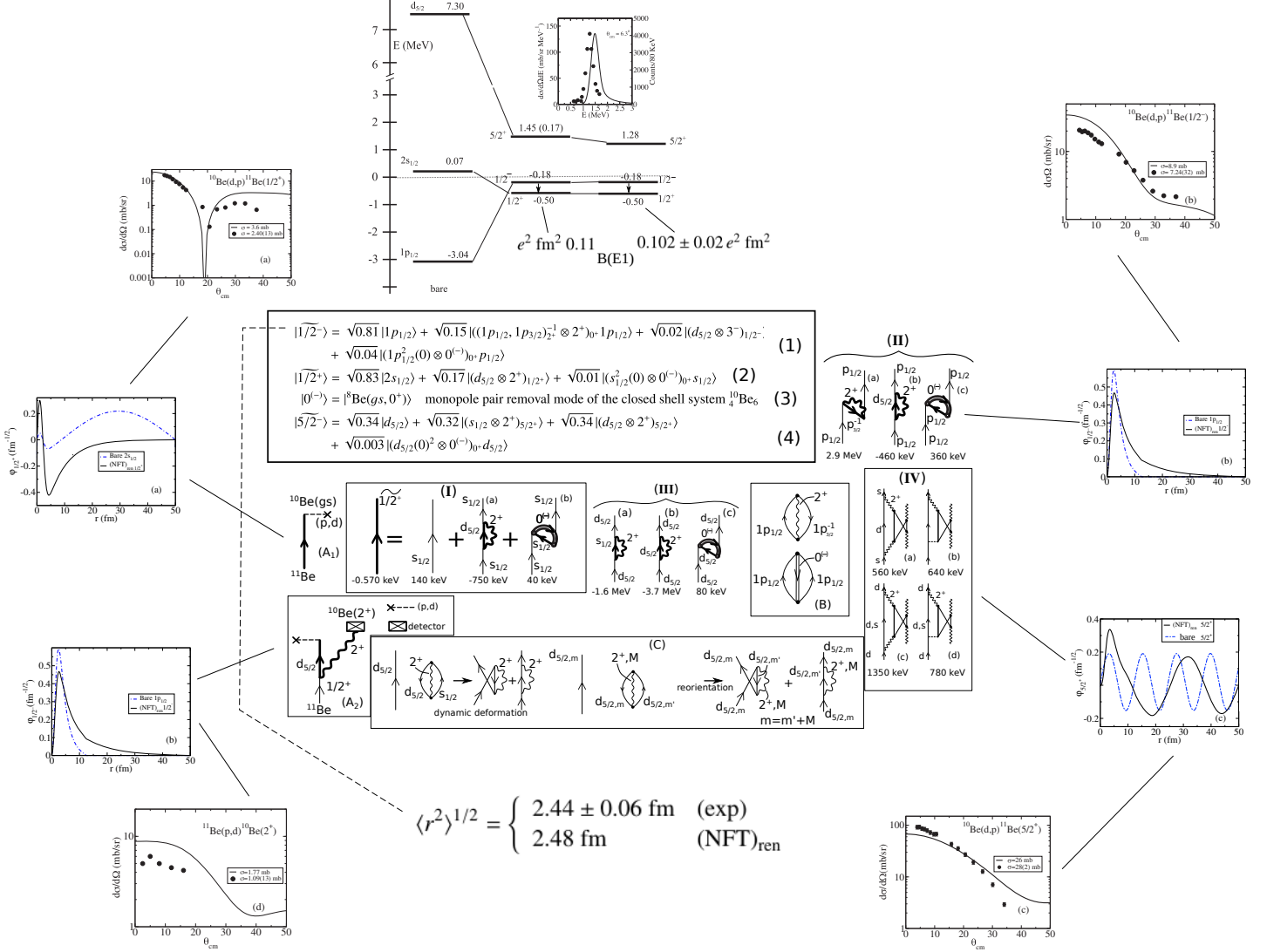


Figure 7.3.1: The clothing of the bare nucleons (single arrowed lines) with quadrupole and octupole particle-hole and monopole pair removal vibrations of the ^{10}Be core following the rules of renormalized nuclear field theory, give rise to values of the (renormalized) energies $\tilde{\epsilon}_j$ in agreement with observation and renormalized single-particle wavefunctions $\tilde{\phi}_j$ which used as formfactors in connection with global optical potentials provide an overall account of the absolute one-nucleon stripping and pickup differential cross sections. The same is true concerning the $B(E1)$ transition between the parity inverted $1/2^+$, $1/2^-$ states and the isotopic shift of the charge radius.

In Table 7.4.1 we collect the two-nucleon spectroscopic amplitudes associated with the reactions $^{A+2}\text{Sn}(p,t)^A\text{Sn}$, for A in the interval 112–126. Making use of these results and of global optical parameters (see Table 7.4.2), the absolute differential cross section $^{A+2}\text{Sn}(p,t)^A\text{Sn}(\text{gs})$ were calculated. They are shown in Fig. 7.4.1 in comparison with the data.

	^{112}Sn	^{114}Sn	^{116}Sn	^{118}Sn	^{120}Sn	^{122}Sn	^{124}Sn
$1d_{5/2}$	0.664	0.594	0.393	0.471	0.439	0.394	0.352
$0g_{7/2}$	0.958	0.852	0.542	0.255	0.591	0.504	0.439
$2s_{1/2}$	0.446	0.477	0.442	0.487	0.451	0.413	0.364
$1d_{3/2}$	0.542	0.590	0.695	0.706	0.696	0.651	0.582
$0h_{11/2}$	0.686	0.720	1.062	0.969	1.095	1.175	1.222

Table 7.4.1: Two-nucleon transfer spectroscopic amplitudes $\langle BCS(A)|P_\nu|BCS(A+2)\rangle = \sqrt{(2j_\nu + 1)/2} U_\nu(A) V_\nu(A+2)$, associated with the reactions connecting the ground states (members of a pairing rotational band) of two superfluid Sn-nuclei $^{A+2}\text{Sn}(p,t)^A\text{Sn}(\text{gs})$ (Potel et al. (2013a,b)).

	$^A\text{Sn}(p,t)^{A-2}\text{Sn}$											
	V	W	V_{so}	W_d	r_1	a_1	r_2	a_2	r_3	a_3	r_4	a_4
$p, {}^A\text{Sn}^a)$	50	5	3	6	1.35	0.65	1.2	0.5	1.25	0.7	1.3	0.6
$d, {}^{A-1}\text{Sn}^b)$	78.53	12	3.62	10.5	1.1	0.6	1.3	0.5	0.97	0.9	1.3	0.61
$t, {}^{A-2}\text{Sn}^a)$	176	20	8	8	1.14	0.6	1.3	0.5	1.1	0.8	1.3	0.6

Table 7.4.2: Optical potentials (see caption Fig. 7.4.1) used in the calculations of the absolute differential cross sections displayed in this figure.

7.4.1 Structure-reaction: stability of the order parameter α_0

As discussed before, the order parameter associated with distortion in gauge space can be written as

$$\alpha'_0 = \sum_{j_a} \sqrt{\frac{2j_a + 1}{2}} B(j_a^2(0), N \rightarrow N+2), \quad (7.4.1)$$

where

$$B(j_a^2(0), N \rightarrow N+2) = \sqrt{\frac{2j_a + 1}{2}} U'_{j_a}(N) V'_{j_a}(N+2) \quad (7.4.2)$$

is the two-nucleon spectroscopic amplitude associated with the ($j^2(0)$) pair transfer between members of a pairing rotational band. Thus

$$\alpha'_0 \approx \sum_{j_a} \frac{2j_a + 1}{2} U'_{j_a} V'_{j_a} = e^{2i\phi} \sum_{j_a} \frac{2j_a + 1}{2} U_{j_a} V_{j_a} = e^{2i\phi} \alpha_0, \quad (7.4.3)$$

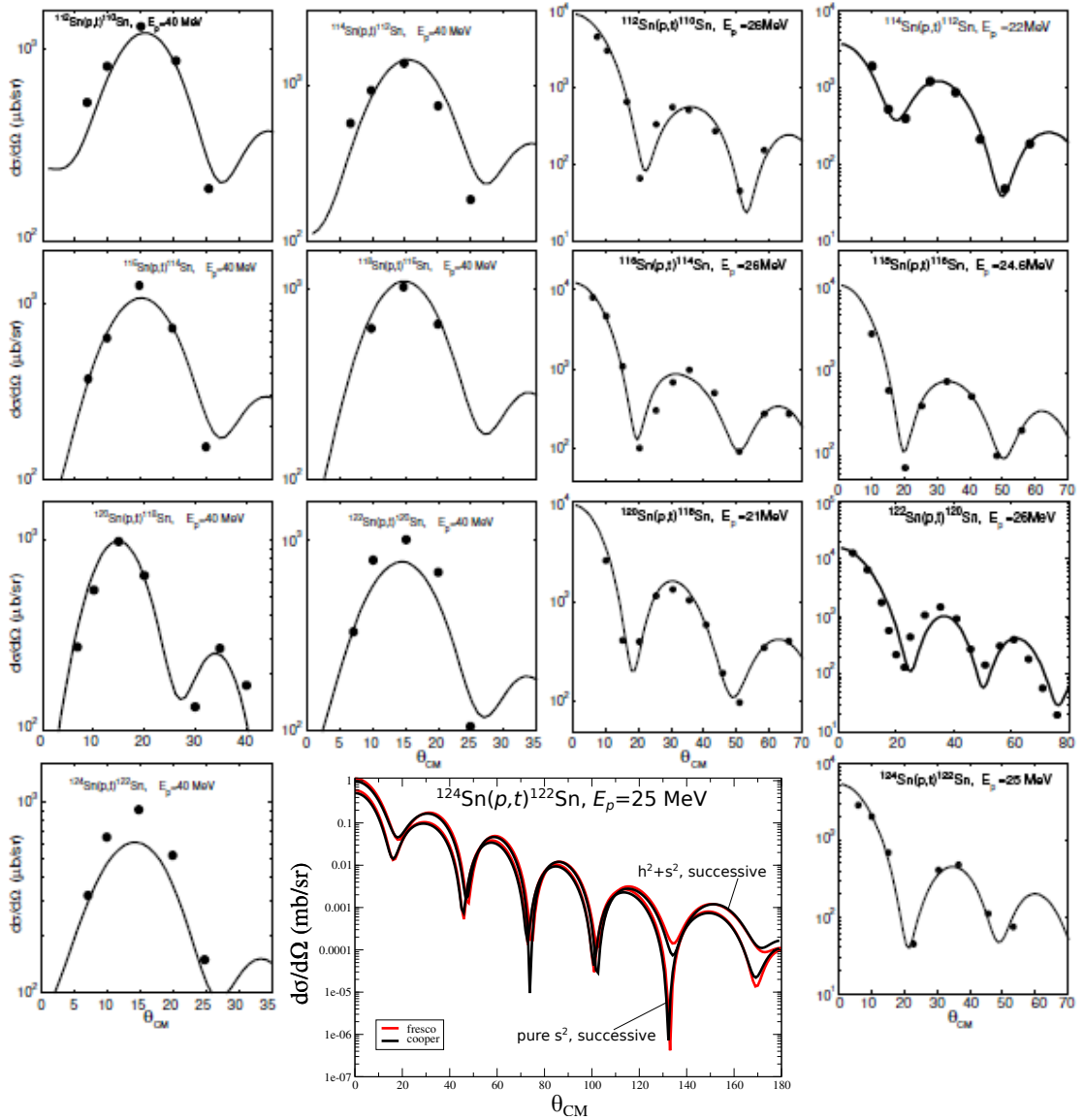


Figure 7.4.1: Predicted (continuous curve, Potel et al. (2013a,b)) absolute differential $A+2\text{Sn}(p,t)^A\text{Sn}(\text{gs})$ cross sections for bombarding energies $E_p=40$ MeV (in the two left columns) and $21 \text{ MeV} \leq E_p \leq 26$ MeV (in the two right columns) in comparison with the experimental data (solid dots, Bassani et al. (1965), Guazzoni et al. (1999), Guazzoni et al. (2004), Guazzoni et al. (2006), Guazzoni et al. (2008), Guazzoni et al. (2011), Guazzoni et al. (2012)). In the center of the lowest row, the absolute differential cross section (successive transfer displayed in the angular interval $0^\circ \leq \theta_{CM} \leq 180^\circ$) associated with the process $^{124}\text{Sn}(p,t)^{122}\text{Sn}(f)$ ($f = h_{11/2}^2(0), s_{1/2}^2(0)$) and calculated with both the software COOPER and FRESCO (Thompson (1988)) are displayed.

defines a privileged orientation in gauge space. Within the unified description of structure and reactions of the present monograph, the quantities (7.4.3) are the weighting factors of the successive, simultaneous and non-orthogonality formfactors involved in the calculation of the corresponding transfer amplitudes. Consequently, in discussing the properties of the order parameter α_0 , in particular in this section, one has in mind the two-nucleon transfer formfactors (Eq. (7.6.1)). The B -coefficients weight the corresponding radial functions, as well as the contributions of energy denominators (Green functions) associated with the different contributions and intermediate channels (see Sect. 7.6.3 as well as Figs. 4.1.1, 4.1.2 and Sect. 4.2).

7.4.2 A two-nucleon transfer physical sum rule

In what follows we analyze the stability of a'_0 making use of three schemes to calculate the B -amplitude¹⁸ associated with the reaction $^{120}\text{Sn}(p, t)^{118}\text{Sn}(\text{gs})$. The first one corresponds to BCS approximation making use of a pairing interaction of constant matrix elements. Starting from the HF solution of a Skyrme interaction, namely Sly4, the gap and number equations are solved in the pairing approximation with $G = 0.26$ MeV leading to the empirical value of the three-point expression of the pairing gap $\Delta^{\exp} \approx 1.4$ MeV. The B -coefficients for the valence orbitals are reported in the fourth column of Table 7.4.3.

In the second calculational scheme, and making use of the same Skyrme interaction and of the v_{14} Argonne, 1S_0 NN -potential and neglecting the influence of the bare pairing force in the mean field, the HFB equation was solved. As a result, this step corresponds to an extended BCS calculation over the HF basis, allowing for the interference between states of equal quantum numbers $a (\equiv l, j)$, but different number of nodes (k, k'). One includes (N_a) states (for each a) up to ≈ 1 GeV, to properly take into account the repulsive core of v_{14} and be able to accurately calculate Δ^{HFB} ($= 1.08$ MeV). The resulting B -coefficients are displayed in the third column of Table 7.4.3.

Going beyond mean field and including the particle-vibration coupling leading to retardation phenomena, both in the quasiparticle self-energy and in the induced pairing interaction, within the framework of renormalized NFT ((NFT)_{ren}) and Nambu-Gorkov (NG) equation leads, in the canonical basis, to the renormalized spectroscopic amplitudes shown in the second column of Table 7.4.3.

Making use of these B -coefficients, together with the global optical parameters reported in Table 7.4.2, the corresponding absolute differential cross sections associated with the reaction $^{120}\text{Sn}(p, t)^{118}\text{Sn}(\text{gs})$ at 21 MeV of bombarding energy were calculated. They are displayed in Fig. 7.4.2 in comparison with the experimental findings. In keeping with the unified structure-reaction physical interpretation of α_0 mentioned following Eq. (7.4.3), and the results shown in Figs 7.4.2 and 7.4.3, namely the fact that the absolute cross section ratio $|\sigma_i - \sigma_{\exp}|/\sigma_{\exp}$ is equal to

¹⁸Potel et al. (2017).

$a \equiv \{l_j\}$	NFT(NG)	HFB v_{14}	BCS(G)
$d_{5/2}$	0.22	0.29	0.41
$g_{7/2}$	0.46	0.47	0.57
$s_{1/2}$	0.37	0.34	0.41
$d_{3/2}$	0.59	0.60	0.66
$h_{11/2}$	0.95	1.0	1.03

Table 7.4.3: Two-nucleon spectroscopic amplitudes associated with the reaction $^{120}\text{Sn}(p, t)^{118}\text{Sn}(\text{gs})$. Note the small difference between the values of the fourth column with those reported in the column labeled ^{120}Sn of Table 7.4.1. They are due to a small difference in the value of the pairing coupling constant used here (Potel et al. (2017)) and that employed in Potel et al. (2017) and Potel et al. (2013b).

0.09, 0.13 and 0.07 ($i = \text{BCS}, \text{HFB}, \text{NFT(NG)}$), one can posit that the relative errors of the associated two-nucleon transfer amplitudes $\alpha_0(\sim \sqrt{\sigma})$ are 4.5%, 6.5% and 3.5%. In other words, spontaneous breaking of gauge symmetry, a feature which is embodied in the three descriptions used (BCS, HFB, NFT(NG)) albeit, at very different levels of many-body refinement, seems to give rise to a new emergent property: a physical sum rule resulting from the intertwining of structure and reaction aspects of pairing in nuclei.

Because the matrix elements of v_{14} for configurations based on the valence orbitals are essentially state independent and $Z^2 \approx 0.5$, setting $v_{ind} = 0$ one expects for the renormalised (NFT(NG)) cross section a value $\approx 1000\mu\text{b}$ ($0.5 \times \sigma_{HFB}$), precluding the above accuracy. Consequently, at the basis of the conservation of two-nucleon transfer amplitudes in going from BCS mean field to NFT(NG) many-body, medium renormalization representations, one also finds the central role played by the induced pairing interaction.

7.5 Virtual states forced to become real through transfer reactions

One of the main subjects which has been discussed in the present monograph concerns the melting of *structure and reactions* and of *bare and virtual states* into a higher unity –likely as it is in nature– which can be described in terms of Feynman diagrams where particles come in and go out, and eventually interact with the detectors whose clicks can be translated in terms of absolute cross sections and lifetimes, conveying to observation the properties of renormalized, dressed, physical elementary modes of excitation.

The initial and final asymptotic states of the $(\text{NFT})_{\text{ren}}(\mathbf{r}+\mathbf{s})$ Feynman diagrams are anchored to the laboratory (incoming beams and target–outgoing particles, including γ -rays and detectors). The intermediate states break open the incoming systems –e.g. a beam of the halo nucleus ^{11}Li , of half life of 8.75 ms, which im-

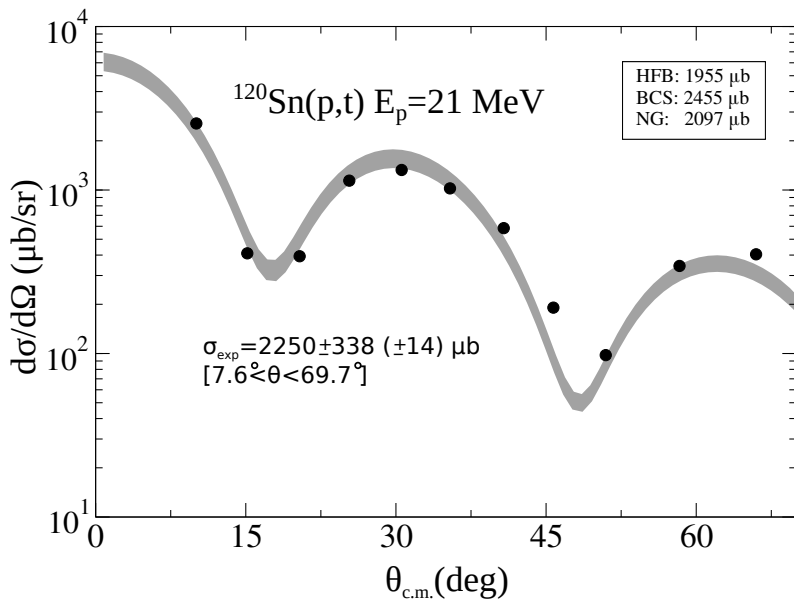


Figure 7.4.2: Absolute differential cross sections associated with the reaction $^{120}\text{Sn}(p,t)^{118}\text{Sn}(\text{gs})$ calculated making use of the BCS, HFB and renormalised NFT(NG) spectroscopic amplitudes and global optical parameters, in comparison with the experimental findings (solid dots) Guazzoni et al. (2008).

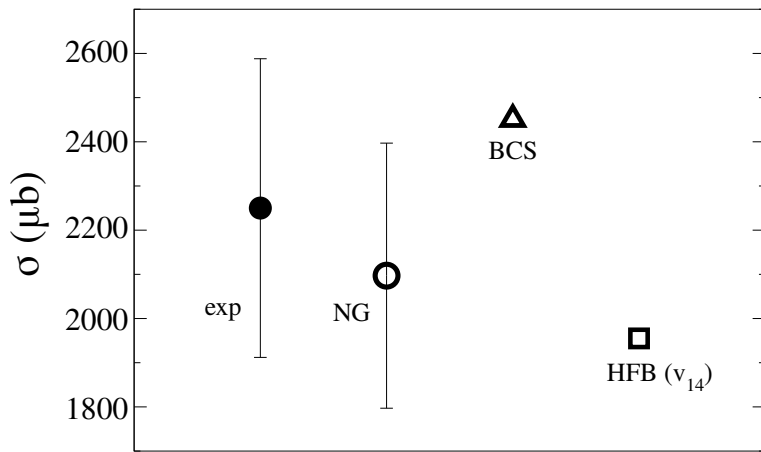


Figure 7.4.3: Integrated absolute cross sections associated with the reaction $^{120}\text{Sn}(p,t)^{118}\text{Sn}(\text{gs})$. The error ascribed to the NFT(NG) theoretical result stems from the variation the spin contribution of the different Skyrme interactions induce in the B -coefficients.

pinges on a hydrogen target (proton) in an inverse kinematic experiment– to allow the elementary modes of excitation which are probed by the experiment to become active, interact (melt) with other modes, and eventually pass the information concerning the properties of the resulting physical modes to the outgoing particles including γ -rays.

Among these diagrams, one finds those associated with reaction processes in which a virtual state is acted upon and forced to become real, eventually reaching the detectors. A sort of Hawking radiation to the extent that one concentrates on the (virtual) \rightarrow (real phenomenon), with the proviso of viewing the action of the external field as the event horizon of the black hole. An example of such diagrams which describes a possible event associated with the reaction ${}^1\text{H}({}^{11}\text{Li}, {}^9\text{Li}(1/2^-)) {}^3\text{H}$ is displayed in Fig. 2.10.3 (b): a virtual quadrupole vibration which, in the process of renormalizing the $s_{1/2}$ state, or of being exchanged between the partners of the neutron halo Cooper pair has been caught in the act by the pair transfer field produced by the ISAAC-2 facility at TRIUMF, forced to become a real final state and to bring this information to the active detector MAYA (see also fig 7.1.2).

7.5.1 Empirical renormalization¹⁹

Most if not all theories able to provide a complete description of structure and reactions of atomic nuclei can hardly avoid the separation between explicit and virtual configuration (phase) spaces²⁰. Once this is recognized, a physical choice concerning the first type of degrees of freedom is: elementary modes of excitation. That is, the response to the variety of external probes of the nuclear system, a choice deeply anchored to the aim that only concepts related to observable quantities enter the theory.

But here empiricism ends²¹. Because the *bare* elementary modes of excitation which potentially contains all of the physics that experiment can eventually provide, are not observables. To become so, they have to loose their elementarity and become mixed, dressed, renormalized, and melt together into effective fields. In fact, what we call a physical nucleon moving inside the nucleus is only partially

¹⁹The practical usefulness of the Feynman rules and diagrams made them one of the most essential elements of the scientific training of every theoretical physicist (Mehra (1996) p. 290).

²⁰While configuration space traditionally refers to structure and phase space to reactions (see e.g. Feshbach (1962)) these connotations tend to melt into a unity in the case of unstable, exotic nuclei like ${}^{11}\text{Li}$ ($\tau_{1/2} \approx 8$ ms), let alone ${}^{10}\text{Li}$, transiently observed in terms of virtual and resonant states in a one-neutron transfer processes (Cavallaro et al. (2017); Barranco et al. (2020) and refs. therein). As a consequence, both structure and reactions are to be worked out in the continuum, discretization being a connotation of methodological, rather than of physical approach. Think only on the central role the tail of the neutron halo Cooper pair, bound by only 380 keV to the core (${}^9\text{Li}$), play in stabilizing ${}^{11}\text{Li}$, and in connection with two-nucleon transfer process (formfactors). Within this scenario, inverse kinematics in e.g. the case of ${}^2\text{H}({}^9\text{Li}, {}^{10}\text{Li}) {}^1\text{H}$ provides, in the laboratory set up, a large but finite box for both the probe (deuteron) and the probed (${}^{10}\text{Li}$).

²¹To the extent of attributing the ancient Greek meaning of “find” and “discover” to the word heuristic (*ευρισκω*) and of “serving to discover” of the Oxford dictionary, one can connotate the above empirical protocol, as heuristic.

to be associated with that nucleon field alone. It is also partially to be associated with the vibrational field, because the two are in interaction . On the other hand, elementary modes participating in virtual states which intervened upon with an appropriate external field can become on-shell²², have to be dressed, fully renormalized modes, poised to be forced to become observable on short call²³.

As shown in Fig. 7.6.2 (see also Fig. 7.6.1), the reaction $^{11}\text{Be}(p, d)^{10}\text{Be}(2^+)$ provides an embodiment of such processes. In fact, this reaction gives information concerning the most important process clothing of the $1/2^+$ parity inverted ground state of $^{11}\text{Be}_7$ through the coupling to the low-lying quadrupole vibration of the core $^{10}_4\text{Be}_6$ (see **I(a)**). A schematic representation of the pickup of the neutron moving around a $N = 6$ closed shell and populating the low-lying quadrupole vibrational state of this core, in coincidence with the corresponding γ -decay is shown in **I(b)**. More detailed structure and reaction NFT diagrams, are shown in **I(d)** and **I(e)**, (the jagged line represents a graphic mnemonic of the recoil effect), together with a cartoon representation in **(f)**. The predicted (continuous curve) and experimental (solid dots) absolute differential cross sections are displayed in **I(c)**. In **I(a)-(e)**, protons and neutrons are labeled π and ν respectively, d stands for deuteron while γ -detectors are represented by a crossed rectangle. Curved arrows indicate motion in the continuum (reaction). Normal arrowed lines, motion inside target or projectile (structure).

At the basis of the spontaneous γ -decay displayed in **I(b)** and **I(e)** we find the processes shown in the lower part of Fig. 7.6.2, as it is explained in what follows. **(II)** Interaction of protons in a nucleus with nuclear vibrations (solid dot, PVC vertex $\beta_L R_0 \partial U / \partial r Y_{LM}^*(\hat{r})$, β_L , dynamical distortion parameter; $U(r)$ central potential) and photons (normal vertex, electromagnetic interaction²⁴ $e \int d^4x J_\mu(x) A^\mu(x)$, A^μ being the vector potential, and J_μ the current density ($\mu = 1, \dots, 4$)). While the variety of diagrams shown have general validity, we have assumed we are dealing with the low-lying correlated particle-hole quadrupole vibration ($L = 2$) of $^{10}_4\text{Be}_6$ lying at 3.368 MeV, $B(E2; 0^+ \rightarrow 2^+) = 0.0052 e^2 b^2$ being associated with $\beta_2 \approx 0.9$. An arrowed line pointing upward (downward) describes a proton (proton hole) moving in the $p_{1/2}$ ($1p_{3/2}$) orbital. Zero point fluctuations of the nuclear ground state associated with : **(a)** the nuclear vibration, **(b)** the electromagnetic field associated with the corresponding spontaneous γ -decay. **(c)** Pauli principle correction to the simultaneous presence of the above two ZPF processes. **(d)** Intervening the virtual excitation of the nuclear vibrations (graph (c)) with an external (inelastic) field (cross followed by a dashed line), in coincidence with the γ -decay (γ -detector, crossed box), the virtual process (c) becomes real. **(e)**, **(f)** Time ordering of the above process correspond to the RPA contributions through backwardsgoing and forwardsgoing amplitudes and subsequent γ -decay.

²²The intervened mode has an on-shell energy consistent with the Q -value of the reaction, and thus may not correspond to that of an actual final state in absence of that probe.

²³As a rule, the collective modes participating in these virtual state are calculated making use of empirical input. Thus, empirical renormalization.

²⁴Holstein (1989).

The above is an example of empirical renormalization (use of dressed elementary modes of excitation, reaction channels) of (renormalized) NFT of structure and reactions²⁵ ((NFT)_{ren(s+r)}).

7.5.2 On-shell energy

It was stated that intermediate states are built out, aside from their energy, of a fully dressed, renormalized physically observable elementary modes of excitation. Concerning the eventual value of the on-shell-energy, it will naturally depend on the reaction process taking place. For example, in the reaction $^{11}\text{Be}(p, d)^{10}\text{Be}(2^+; 3.368 \text{ MeV})$ (Fig. 7.6.2 (b) and (e)) populating the quadrupole vibration of ^{10}Be which, in the virtual $(\widetilde{5/2}^+ \otimes 2^+)_{1/2^+}$ state dress the $|\widetilde{1/2}^+\rangle$ ground state of ^{11}Be (Fig. 7.6.2 (a)), the on-shell-energy coincides with that of that observed in the inelastic process $^{10}\text{Be}(\text{gs} \rightarrow 2^+)$. On the other hand, the $5/2^+$ pickup neutron, while displaying the structural properties of the $5/2^+$ resonance ($\tilde{\epsilon}_{5/2^+} = 1.45 \text{ MeV}$), it has a binding energy equal to $\tilde{\epsilon}_{5/2^+} - \hbar\omega_{2^+} = -3.868 \text{ MeV}$, unrelated to the experimental energy of $+1.28 \text{ MeV}$ (continuum, unbound), recorded in the reaction $^{10}\text{Be}(d, p)^{11}\text{Be}(5/2^+)$. This is a natural outcome of (NFT)_{ren} which, through the PVC and the Pauli mechanism, provides the proper clothing of the $d_{5/2}$ orbital so as to allow it to be able “to exist” inside the $|\widetilde{s}_{1/2}\rangle$ state as a virtual, intermediate configuration. The asymptotic r -behavior results from the coherent superposition of many continuum states.

We now consider the process in which an inelastic field acting on $|^{11}\text{Be}(\text{gs})\rangle$ populates the $5/2^+$ resonance. An important contribution to this excitation results from the action of the external field on the quadrupole vibration of the virtual state $(\widetilde{d}_{5/2} \otimes 2^+)_{1/2^+}$ which renormalizes the $1/2^+$ state (Fig. 7.6.1 (a)) leading to diagram (b) of the same figure. In this case, the external field has to provide an energy equal to $|\tilde{\epsilon}_{1/2} - \tilde{\epsilon}_{5/2^+}| = 1.95 \text{ MeV}$, again unrelated to the on-shell energy of $|^{10}\text{Be}(2^+; 3.868 \text{ MeV})\rangle$ observed in the inelastic process $^{10}\text{Be}(\text{gs} \rightarrow 2^+)$, but needed to dress the bare single-particle valence orbital.

7.6 Perturbation and beyond

In Q.E.D. at the one-loop diagrams level, the renormalized electron mass m_e , that is the observed ($\approx 0.5 \text{ MeV}$) mass, is related to the bare mass m_0 , not observable, by $m_e = m_0 \left(1 + \frac{3\alpha}{\pi} \log \left(\frac{\Lambda_{cut}}{m_0} \right)^2 \right)$, Λ_{cut} being the cutoff of the divergent integrals²⁶. This quantity appears inside the log, and in front of it one has the fine structure constant α which is small ($\approx 1/137$). Therefore, even pushing the cutoff to the Planck scale, $\Lambda_{cut} \sim 10^{19} \text{ GeV}$, with $m_0 \sim \text{MeV}$ one has $\delta m_e/m_e \approx \frac{3\alpha}{\pi} \log \left(\frac{\Lambda_{cut}}{m_0} \right)^2 \approx 0.1$. So δm_e is really a small correction. To reproduce the physical electron mass m_e , one must take a value of m_0 of the same order of magnitude.

²⁵Broglia et al. (2016).

²⁶See Bjorken and Drell (1998) pp 162–166.

Within this context one can compare the value of the four parameters (plus the effective mass functional) which determine the mean field (Saxon–Woods) potential used to calculate the bare single-particle energies of ^{11}Be –imposing the condition that the dressed levels best reproduce the experimental findings– with the value of the corresponding parameters of the standard, global Woods–Saxon potential (and of effective mass equal to the observed mass m). The results displayed in Table 7.6.1 testify to the fact that renormalization in nuclear physics, in particular in the case of halo exotic, parity inverted nuclei, is less “perturbative” than in the case of Q.E.D. This fact becomes even clearer if one compares the overall centroid of the valence orbitals as well as the density of levels associated with the two potentials. Within this context it is of notice that the Lamb (–like) shift taking place between the $s_{1/2}$ and $p_{1/2}$ valence levels of ^{11}Be has a value of approximately 10% ($(\Delta\epsilon_{1/2^+,1/2^-})_{\text{bare}} - (\Delta\epsilon_{1/2^+,1/2^-})_{\text{ren}} \approx 3.11 + 0.32\text{MeV}$) of that of the Fermi energy ($\approx 36\text{ MeV}$). This result can be compared with the ratio of the hydrogen $^2S_{1/2} - ^2P_{1/2}$ Lamb shift ($1058\text{ MHz} \approx 4.3 \times 10^{-9}\text{ eV}$) and the Rydberg constant ($R_H = 13.6\text{ eV}$), i.e. $\approx 10^{-10}$, a result which underscores the strong coupled situation one is confronted with in trying to describe the structure of light halo exotic nuclei (Fig. 7.2.1).

7.6.1 One-particle transfer and optical potential

The fact that in spite of this non-perturbative situation, $(\text{NFT})_{\text{ren}}(\mathbf{r}+\mathbf{s})$ can provide an overall account of an essentially complete set of experimental data which characterizes ^{11}Be , within a 10% error, testifies to the power and flexibility Feynman version of Q.E.D. has. It can be used as paradigm to construct a field theory for both structure and reactions of a strongly interacting finite many-body system like the atomic nucleus. As already mentioned, examples of $(\text{NFT})_{\text{ren}}(\mathbf{r}+\mathbf{s})$ diagrams, aside from that discussed in detail in connection with Fig. 7.6.2, are displayed in Figs. 2.10.3 and 2.10.2. The first describes the process $^1\text{H}(^{11}\text{Li}, ^9\text{Li})^3\text{H}$ providing a quantitative account of the data and first evidence of phonon induced pairing in nuclei. The second shows in (a), one of the most important channels contributing to the optical potential needed to describe the elastic scattering process $^1\text{H}(^{11}\text{Li}, ^{11}\text{Li})^1\text{H}$.

The calculation of the optical potential constitutes a major challenge lying ahead.

7.6.2 $(\text{NFT})_{\text{ren}(\mathbf{s}+\mathbf{r})}$ diagrams, S-matrix

Landau felt that Feynman diagrams, although usually derived from conventional field theory have an independent basic importance²⁷ This work is closely connected with both Heisenberg statement that one should introduce only observable quantities²⁸ into a quantum theory, and with the special role the scattering matrix plays in

²⁷Landau (1959).

²⁸Heisenberg (1925); see english translation W. Heisenberg, Quantum-theoretical re-interpretation of kinematical and mechanical relations, in Van der Waerden (1967) p 261.

	$V_0(\text{MeV})$	$V_l(\text{MeV})$	$R_0(\text{fm})$	$a(\text{fm})$
Standard ^{a)}	-50	17	2.7 ^{c)}	0.65
bare ^{b)}	-68.9	14.47	2.15 ^{d)}	0.77

Table 7.6.1: Parametrization of the standard (Bohr and Mottelson (1969)) and of the bare mean field potential associated with ^{11}Be (Barranco et al. (2017)). Changes of the order of 20-30% are observed. Within this context, in the case of Q.E.D. $\delta m_e/m_e = 0.1$.

^{a)} $m^* = m$

^{b)} $m^*(r=0) = 0.7m$, $m^*(r=\infty) = 10/11m$

^{c)} $R_0 = r_0 A^{1/3}$, $r_0 = 1.2 \text{ fm}$

^{d)} $r_0 \approx 1.03 \text{ fm}$

such a program. As the wavefunctions themselves cannot be observed and because the Hamiltonian formalism is intimately connected with wavefunctions, it may not be the most appropriate to describe quantal systems. The quantities to be studied are the scattering amplitudes where particles go in and another set, including eventually γ -rays, come out and directly determine the cross sections of the different physical processes. Within this context we refer to diagram (e) of Fig. 7.6.2 (I) where the $(\text{NFT})_{\text{ren}}$ ($r+s$) diagram describing the becoming of a virtual process²⁹ real³⁰, is displayed.

7.6.3 The structure of “observable” Cooper pairs

In his Waynflete lectures on Cause and Chance, Max Born³¹, to whom we owe the statistical interpretation of quantum mechanics³², states “... quantum mechanics does not describe an objective state in an independent external world, but the aspect of this world gained by considering it from a certain subjective standpoint, or with certain experimental means and arrangements”. It is within this context that we tried in previous sections to get insight concerning the structure of nuclear Cooper pairs. Specifically, in terms of two-nucleon transfer reactions. Being even more *subjective* (concrete), we were interested in shedding light on the structure of one of the 5-6 Cooper pairs participating in the condensate (intrinsic state in gauge space) of the Sn-isotopes (ground state rotational band³³) through pair transfer processes. That is $^{A+2}\text{Sn}(p,t)^A\text{Sn}(\text{gs})$ processes in general, and $^{120}\text{Sn}(p,t)^{118}\text{Sn}$ in particular. From a strict observational perspective, concerning Cooper pairs, one can only

²⁹Dressing of the $s_{1/2}$ ground state of ^{11}Be , diagram (a), see also Table 7.6.1 for the parameters of the bare potential.

³⁰Through the action of an external field namely $^{11}\text{Be}(p,d)^{10}\text{Be}(2^+)$.

³¹Born (1948).

³²Born (1964); Pais (1986).

³³Potel et al. (2013b, 2017)

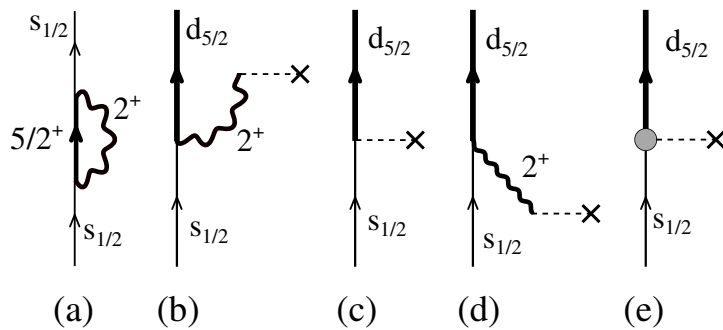


Figure 7.6.1: Inelastic population of the $|^{11}\text{Be}(\widetilde{5/2}^+; 1.45 \text{ MeV})\rangle$ calculated resonance. **(a)** Main process dressing the neutron moving in the $s_{1/2}$ orbital and leading to the ^{11}Be ground state. The virtual state is made out of the fully renormalized (real, empirical) quadrupole vibration of the core ^{10}Be and of the low-lying $5/2^+$ resonance of ^{11}Be , and is indicated by using bold face symbols. **(b)** Intervening process (a) with an external inelastic hadron field (e.g. (p, p')) of quadrupole character (dashed horizontal line starting at a cross), one can excite the $5/2^+$ resonance. This can also happen if the external field acts on the $1/2^+$ state as in **(c)**, or if this field first excites the quadrupole vibration of ^{10}Be which eventually couples to the $1/2^+$ state as in **(d)**. **(e)** If the vibration was a high-lying quadrupole giant resonance the summed contribution of processes (b)–(d) could be replaced at profit by a single graph, namely the equivalent of (c) but with an effective charge (hatched circle). For low-lying modes like the 3.368 MeV quadrupole vibration of ^{10}Be , retardation, ω -dependent effects have to be explicitly taken into account.

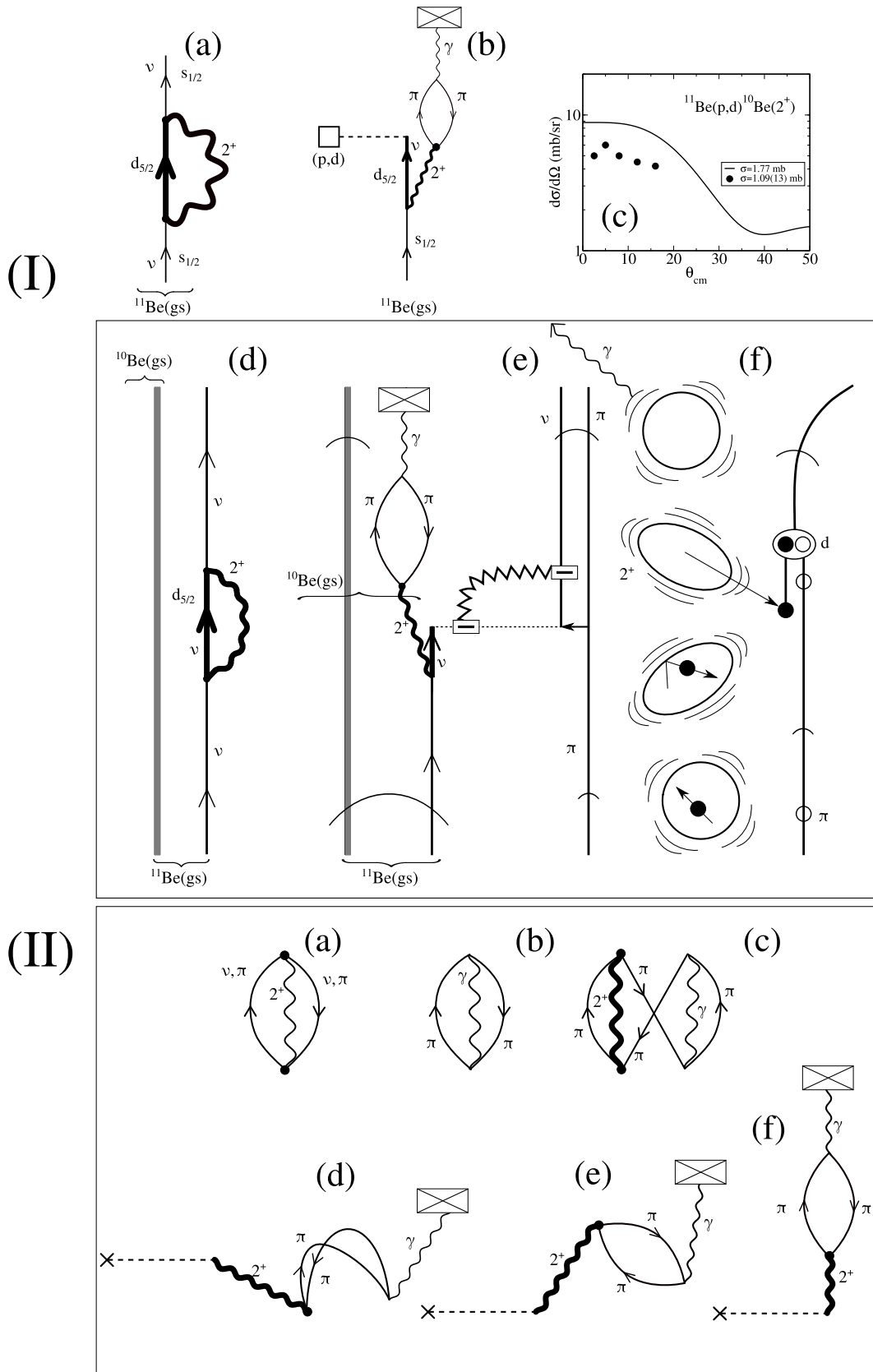


Figure 7.6.2: The reaction $^{11}\text{Be}(p, d)^{10}\text{Be}(2^+)$. A virtual process, namely the self-energy contribution of the renormalization of the $s_{1/2}$ ground state of ^{11}Be through the coupling to the low-lying collective quadrupole vibration of the ^{10}Be becomes real through the action of a one-particle pickup external field.

refer to the information two-nucleon transfer absolute differential cross sections carry on these entities. On the other hand, leaving the discussion regarding the microscopic calculation of the optical potential, the carriers mediating information between structure and differential cross sections, e.g. between target and outgoing particle in a standard laboratory setup, are the distorted waves. These functions can be studied independently of the transfer processes under consideration, in elastic scattering experiments. Consequently, the non-local, correlated formfactors (see Figs. 4.1.1 and 4.1.2),

$$F(\mathbf{r}_1, \mathbf{r}_2, \mathbf{r}_{Ap}) = F_{succ}(\mathbf{r}_1, \mathbf{r}_2, \mathbf{r}_{Ap}) + F_{sim}(\mathbf{r}_1, \mathbf{r}_2, \mathbf{r}_{Ap}) + F_{NO}(\mathbf{r}_1, \mathbf{r}_2, \mathbf{r}_{Ap}), \quad (7.6.1)$$

sum of the corresponding functions associated with successive and simultaneous transfer and with the non-orthogonality correction, and calculated with different sets of two-nucleon spectroscopic amplitudes can be compared at profit to each other. This is in keeping with the fact that they can be related, in an homogeneous fashion, with the absolute cross sections or, better, with the square root of these quantities.

It is also of notice, that the dimension, structure, non-locality and ω -dependence of the function (7.6.1) is expected to be rather different from that of the structure wavefunction of the Cooper pair, observed e.g. in electron scattering, a question closely connected with linear response (see discussion following Eq. (7.4.3)). While this concept has been, and continues to be quite useful in the study of many-body systems, it is a subtle one. In direct two-nucleon transfer reactions induced by both light and heavy (grazing) ion collisions, the contact between the two interacting nuclei is weak. Nonetheless, even a very low density overlap between target and projectile may induce important modifications in Cooper pairs. In particular, allow pairing correlated partner nucleons to profit from the enlarged volume as compared to that available in the target nucleus to expand, recede from each other and, in the process, lower the relative kinetic energy of confinement. As a consequence, one-nucleon can be transferred at a time as a single Cooper pair, successive being the dominant transfer mechanism. This is the reason why Cooper pair transfer displays absolute cross sections of the same order of magnitude of one-nucleon transfer processes.

It can be stated that this picture is again an example of the fruitfulness of linear response to shed light on subtle questions regarding many-body systems. In the case under discussion, it allows the partners of the nuclear Cooper pair to correlate over dimensions larger than nuclear dimensions and in so doing make their intrinsic structure “observable”, almost free of the strong pressures of the mean field³⁴ which acts as a strong external field. The above discussion is schematically illustrated in Fig. 7.6.3. With it one comes back to the original question (Sect. 2.1). Which are the proper variables to be used in an attempt to describe the nuclear system? Elementary modes of excitation is a valid choice. But because these modes

³⁴Within this context, think of the need of being able to distinguish between right and left weakly coupled (dioxide-layer separated) superconductors, to be able to measure gauge phase difference through the Josephson effect. See also Magierski et al. (2017).

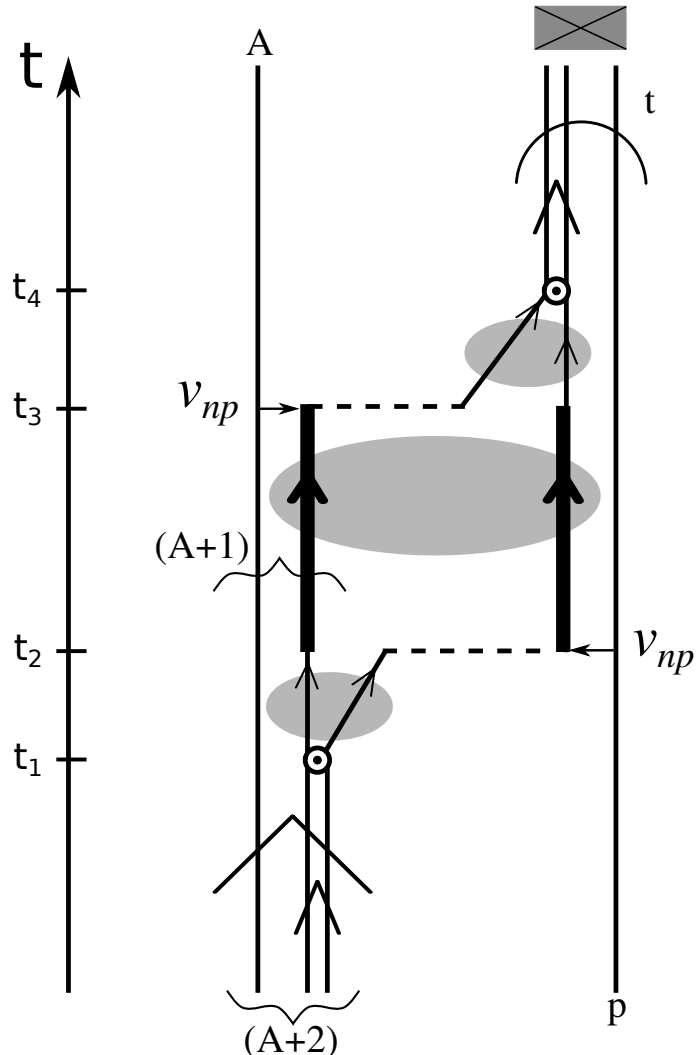


Figure 7.6.3: Diagram describing structure and reaction aspects of the main process through which a Cooper pair (di-neutron) tunnels from target to projectile in the reaction $(A + 2) + p \rightarrow A + t$. In order that the two-step process $(A + 2) + p \rightarrow (A + 1) + d \rightarrow A + t$ takes place, target and projectile have to be in contact at least in the time interval running between t_2 and t_3 . During this time, the two systems create, with local regions of ever so low nucleonic presence, a common density over which the non-local pairing field can be established, and the Cooper pair can be correlated. Even with regions in which the pairing interaction may be zero. Small ellipses (with linear dimensions of the order of the nuclear radius R_0) indicate situations in which the two neutron correlation is distorted by the external mean field of a single of the systems involved of the reaction, i.e. $A + 2$ in the entrance channel, t in the exit one (see e.g. Fig. 3.6.3). The large ellipse (with linear dimensions of the order of the correlation length ξ) indicate the region in which the two partners of the Cooper pair correlate over distances of the order of the correlation length ξ . It is this information that the outgoing particle of a Cooper pair transfer process brings to the detector. In other words, this is the observable Cooper pair in terms of its specific probe, and the reason why the neutrons are described, in the interval $\Delta t = t_3 - t_1$, in terms of bold face arrowed lines.

are in interaction, the above choice is not sufficient (unique). An operative definition requires that also the specific probe, reaction or decay process is specified. In fact, if one were to study Cooper pairs through electron scattering (two-nucleon correlations), one would obtain a picture of the system as that marked by the small ellipses in Fig. 7.6.3 (see Fig. 3.6.3). Thus, rather different from the one which emerges from the specific two-nucleon transfer process (large ellipse, correlation length ξ).

7.6.4 Closing the circle³⁵

In one of the first references of this monograph³⁶ entitled “Quantum mechanics of collision phenomena”, Born considers the elastic scattering of a beam consisting of N electrons which cross a unit area per unit time, scattered by a static potential. The stationary wavefunction describing the scattering process behaves asymptotically as,

$$e^{ikz} + f(\theta, \phi) \frac{e^{kr}}{r}, \quad \left(k = \frac{mv}{\hbar} \right). \quad (7.6.2)$$

The number of particles scattered into the solid angle $d\Omega = \sin \theta d\theta$ is given by $N|f(\theta, \phi)|^2 d\Omega$. To connect with Born notation one has to replace $f(\theta, \phi)$ by Φ_{mn} , where n denotes the initial-state plane wave in the z -direction and m the asymptotic final-state in which the waves move in the direction fixed by the angles (θ, ϕ) . Then Born writes that Φ_{mn} determines the probability for the scattering of the electron from the z - to the (θ, ϕ) -direction, adding a footnote in proof, as already mentioned, stating that a more precise consideration shows that the probability is proportional to the square of Φ_{mn} . In a second paper with the same title of the first³⁷ he states explicitly that the probability is to be connected with the modulus squared³⁸. Within this context, the matrix element between the entrance and exit channel distorted waves of $F(\mathbf{r}_1, \mathbf{r}_2, \mathbf{r}_{Ap})$ is proportional to $f(\theta, \phi)$ and thus Φ_{mn} . The function F is not directly measurable, but the closer one can come of a theoretical construct connecting the Cooper pair ($s+r$) to experiment. For superfluid nuclei lying along the stability valley, this construct does not change much with the theory one uses to calculate the spectroscopic two-nucleon transfer amplitudes, provided they display off diagonal long range order (ODLRO)³⁹, a property closely related with deformation in gauge space. This is the reason why the associated absolute cross sections

³⁵In this section we follow closely Pais (1986)

³⁶Born (1926a).

³⁷Born (1926b)

³⁸The motion of particles follows probability laws but the probability itself propagates according to the law of causality. And concerning the distinction between classical and quantal probabilities he states: “The classical theory introduces the microscopic coordinates which determine the individual processes only to eliminate them because of ignorance by averaging over their values; whereas the new theory get the same results without introducing them at all... We free the forces of their classical duty of determining directly the motion of particles and allow them instead to determine the probability of states”.

³⁹Yang (1962). See also App. A, Potel et al. (2017) and refs. therein.

are rather stable, and α_0 provides a natural order parameter to measure deformation in gauge space.

On the other hand, in the case of halo, weakly bound exotic nuclei like ^{11}Li , the sensitivity of the absolute cross sections to the models used to calculate $F(\mathbf{r}_1, \mathbf{r}_2, \mathbf{r}_{Ap})$ is expected to be more relevant, and directly related to the conspicuous changes which renormalization produces in the radial shape of the single-particle wavefunctions of the halo neutrons forming the Cooper pair. This is in keeping with the fact that the nucleus is a finite many-body system, where surface effects play a central role⁴⁰, and light halo weakly bound exotic nuclei like ^{11}Be and ^{11}Li constitute paradigms⁴¹ of these leptodermic controlled entities. While the surface (S) to volume (V) ratio ($aS/V = 3a/R$, a being the diffusivity) is estimated to be 0.32 in the case of Sn, this value becomes 0.73 for Li.

Within this context, self-consistency in $(\text{NFT})_{\text{ren}}$ implies both the renormalization of single-particle energies and occupancies ($\tilde{\epsilon}_j, Z_j(\omega)$), as well as of radial wavefunctions ($\tilde{\phi}(r)^{(i)}$). For each $\tilde{\epsilon}_j$ there can be more than one radial function, depending on whether the nucleon is moving around the ground state ($i = \text{gs}$) or an excited state ($i = \text{coll}$) of the core. In keeping with the fact that $\tilde{\phi}(r)^{(i)}$ are the formfactors associated with transfer processes, self-consistency in $(\text{NFT})_{\text{ren}}$ is intimately related to unification of (s+r). In nuclei one has thus the unique possibility to study renormalization effects in terms of individual quantum states, and pairing correlations resulting from bare plus induced 1S_0 interactions in systems with few (5-6) Cooper pairs (superfluid nuclei) down to the single Cooper pair (^{11}Li).

7.7 Summary

Nucleons moving in time reversal states lying close to the Fermi energy and interacting through the exchange of mesons (1S_0 NN-interaction) and of collective vibrations (induced pairing interaction), lead to $L = 0, S = 0$ nuclear Cooper pairs. Making use of the two-particle wavefunction describing them, it is found that the partner nucleons come closer to each other, as compared to the uncorrelated pair situation.

Cooper pairs were introduced in physics to describe low temperature superconductivity in metals, and constitute the building blocks of BCS. The BCS ground state wavefunction describes the condensation of these weakly bound (through the exchange of virtual photons and lattice phonons), widely extended (dimensions much larger than typical distances between uncorrelated electrons), strongly overlapping quasi bosons (pair of electrons moving in time reversal states (v, \tilde{v}) with momentum and spin ($\mathbf{k} \uparrow, -\mathbf{k} \downarrow$)).

In presence of an external field, for example that associated with the tunneling interaction of a Josephson junction –involving energies smaller than the transition temperature and thus acting on the Cooper pairs center of mass– all pairs move

⁴⁰Within this context see Broglia (2002) and refs. therein.

⁴¹One could be tempted to say, caricatures.

in an identical (coherent) fashion, leading to a supercurrent across the junction of carriers with charge $q = 2e$. Its (maximum) intensity being equal to the (normal) single-electron current associated with a junction bias equal to the Cooper pair binding energy divided by the electron charge, a relation closely connected with the critical value of the supercurrent.

When the momentum imparted to the center of mass of the condensed Cooper pairs acquires a value of the order of the inverse of the mean square radius of the Cooper pairs (correlation length), the back-and-forth ($\ell = 0$) radial motion of electron partners (intrinsic (v, \tilde{v}) motion) cannot follow suit, getting out of step and resulting in the breaking (unbinding) of the pairs (critical current). As a consequence, supercurrent ceases and only normal current ($q = e$) flows.

The traditional view of nuclear Cooper pairs described above, seems to be partially at odds with that found at the basis of the BCS description of low temperature superconductivity. In particular concerning what can be considered the only (specific) coupling field able to detect Cooper pair (gauge) phase correlation, namely tunneling across a Josephson junction. In each of the two weakly coupled superconductors, pairs of electrons recede from each other as compared to the normal situation. In this way, they lower their relative kinetic energy of confinement, profiting best of the weak, attractive, (retarded) interaction. Being the electron pair phase correlated, with a correlation length much larger than the barrier thickness, although they tunnel one at a time, they do so as a single particle (of mass $2m_e$ and charge $2e$), and the probability of going through the junction is comparable to that of a single electron. It is like interference in optics, with phase coherent waves mixing.

In the transient, time dependent, Josephson-like junction established between two superfluid nuclei in a heavy ion collision about and below the Coulomb barrier, one finds that for bombarding energies leading to distances of closest approach smaller or of the order of the correlation length, quantity much larger than nuclear dimensions, the probability P_2 of pair transfer –process dominated by successive transfer where nuclear Cooper pair partners are about a correlation length apart from each other– is about equal to that of one-nucleon transfer (P_1). For larger distances, for which the intrinsic back and forth relative motion of the partner nucleons characterizing the intrinsic structure of the nuclear Cooper pair gets uncorrelated, and the system undergoes a phase transition from the superfluid (S) to the normal (N) state, this ($P_2 \approx P_1$) is not anymore so. Already for distances of closest approach about 1 fm–1.5 fm larger than the nuclear correlation length, the probability of one-nucleon transfer is an order of magnitude larger than that associated with two-nucleon tunneling. The nuclear S→N phase transition as a function of the distance of closest approach, where the Cooper pair is probed (stressed) beyond the correlation length, parallels that associated with the one undergoing by a low temperature superconductor where Cooper pairs are forced to move with a center of mass moment of the order of the inverse of the correlations length.

The gained homogeneity between the pictures of Cooper pairs in nuclei and in superconductors is a consequence of fulfilling a basic requirement of quantum

mechanics. Namely, that to specify the experimental setup in discussing a physical phenomena. In the present case, that of the structure of nuclear Cooper pairs emerging from probing it through pair tunneling in heavy ion collisions between superfluid nuclei, and comparing theory with experiment in terms of absolute cross sections.

Appendix 7.A Bootstrap particle–phonon mechanism to spontaneously break gauge invariance

In this Appendix we discuss a gedanken experiment, aimed at clarifying the bootstrap pairing mechanism resulting in the binding of the neutron halo of ^{11}Li .

7.A.1 Gedanken eksperiment

Let us assume that one shines a low energy neutron beam on a ^9Li target. If these neutrons felt only the associated single-particle mean field, they will go by essentially as fast as they came in. However, part of the time pairs of these neutrons will bound themselves in presence of phonon (bosonic) excitations of quadrupole and of (pygmy) dipole character, produced also by the field the two neutron create themselves. The first of these collective modes is associated with vibrations of the (even) ^8He core, the second resulting from the sloshing back and forth of the strongly non-local field of two (passing by) neutrons of the beam, together with the neutrons, and against the protons, of the core. Such possibility implies that, for a short time, of the order of the traversal time, the two (unbound) neutrons will move in a gas of virtual bosonic excitations, also made out of dipole pygmy resonances. Consequently, they can profit to be almost at threshold by moving in the $\tilde{s}_{1/2}$ and $\tilde{p}_{1/2}$ states, to get correlated by exchanging these bosonic collective vibrations. The first phenomenon is associated, as discussed above, with phononic backflow (Pauli principle upflow) leading to ^{10}Li -like quasi-bound (s -wave) and resonant (p -wave) dressed single-particle states displaying parity inversion. The second phenomenon, mediated by phonon exchange between halo neutrons, contributes in a major way to the glue which binds the neutron halo Cooper pair to the ^9Li core. Within the above scenario, one can posit that the ^{11}Li dipole pygmy resonance can hardly be viewed but in symbiosis with the ^9Li halo neutron pair addition mode. The above described bootstrap phonon-exchange mechanism can be considered as a novel microscopic embodiment of the Bardeen–Pines–Frölich-like processes to spontaneously break gauge invariance⁴².

To conclude, let us comment on Fig. 7.A.1. As said above, (a) the dressing of single-particle levels by collective vibrations and (b) the renormalization of the bare NN -interaction, in particular of the pairing interaction, through the exchange

⁴²Bootstrapping or booting. The term is often attributed to Rudolf Erich Raspe's story The surprising Adventures of Baron Münchhausen, where the main character pulls himself out of a swamp by his hair. Early 19th century USA: "pull oneself over a fence by one's bootstraps"

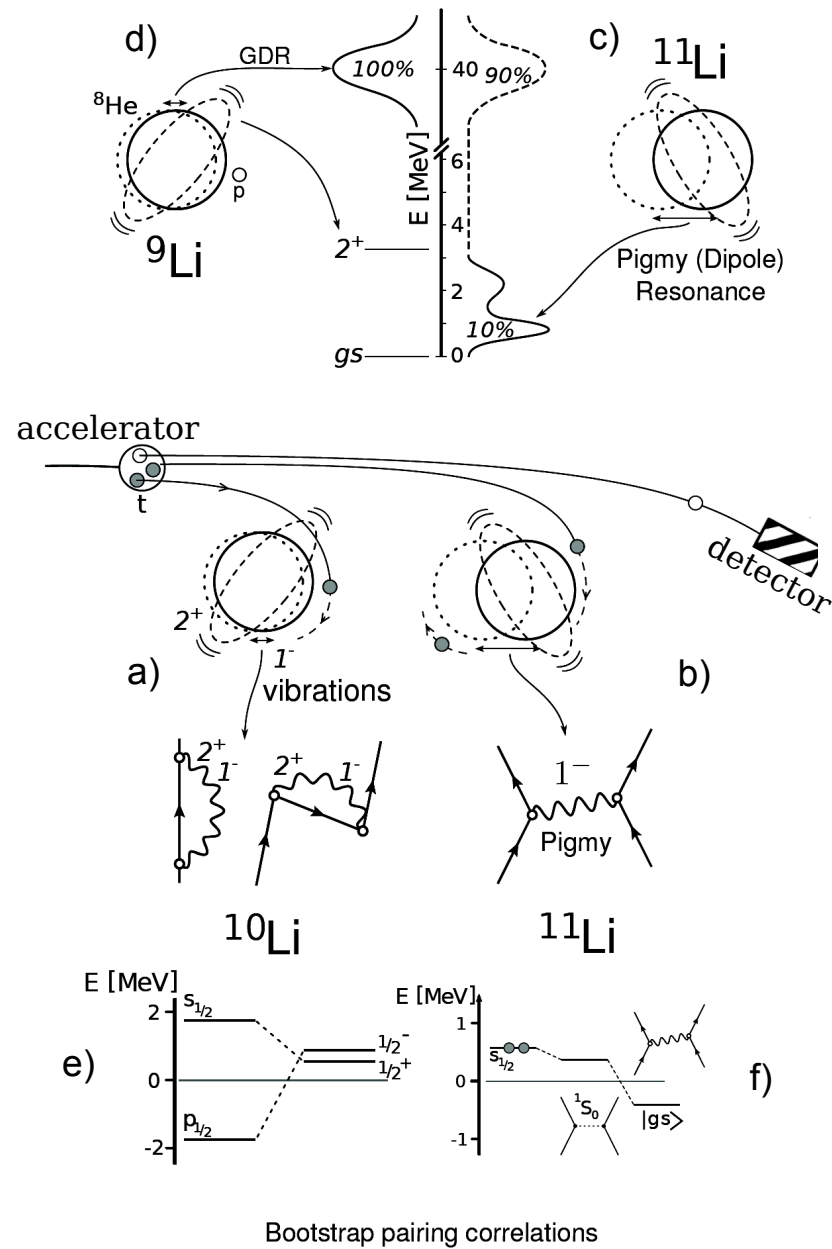


Figure 7.A.1: Schematic representation of the collective quadrupole and dipole response of lithium isotopes, and of a (*t, p*) reaction (in the text one reasons in terms of a flux of low energy neutrons) in which two neutrons are transferred to ⁹Li.

of collective modes between nucleons moving in time reversal states lying close

to the Fermi energy, play a central role in nuclear structure. In particular, in the case of the single Cooper pair system ^{11}Li , most of the glue is provided by the exchange of the dipole pygmy resonance. The pygmy resonance is a chunk of the GDR and arises from radial inhomogeneous damping. This phenomenon, which arises from extreme neutron excess, is responsible for the isoscalar character⁴³ of an antenna-like mode between protons and neutrons⁴⁴.

Appendix 7.B Alternative processes to populate $|^9\text{Li}(1/2^-)\rangle$

The $1/2^-$ (2.69 MeV) first excited state of ^9Li can in principle, not only be populated through a two-particle transfer process, but also through a break up process in which one (see Fig. 7.B.1(a)), or both neutrons (Fig. 7.B.1(b)) are forced into the continuum for then eventually one of them fall into the $1p_{3/2}$ orbital of ^9Li and excite the quadrupole vibration of the core⁴⁵, in keeping with the fact that the main RPA amplitude of this state is precisely $X(1p_{3/2}^{-1}, 1p_{1/2})(\approx 1)$ ⁴⁶. The remaining channel populating the first excited state of ^9Li is associated with an inelastic process (Fig. 7.B.1(c)): two-particle transfer to the ground state of ^9Li and final state interaction (FSI) between the outgoing triton and ^9Li in its ground state, resulting in the inelastic excitation of the $1/2^-$ state.

Making use of the NFT spectroscopic amplitudes, and of a software developed to take into account microscopically the different processes mentioned above, that is 9 different reaction channels and continuum states up to 50 MeV of excitation energy, the corresponding transfer amplitudes and associated probabilities p_l were calculated. In Table 7.B.1 are displayed the probabilities $p_l = |S_l^{(c)}|^2$ associated with each of the processes mentioned above, where the amplitude $S_l^{(c)}$ is related to the total cross section associated with each of the channels c by the expression⁴⁷

$$\sigma_c = \frac{\pi}{k^2} \sum_l (2l+1) |S_l^{(c)}|^2, \quad (7.B.1)$$

k being the wave number of the relative motion between the reacting nuclei.

In keeping with the small values of p_l , in what follows we take into account the interference between the contributions associated with the different reaction paths making use of second order perturbation theory, instead of a coupled channel treatment⁴⁸. In particular, in the case of the $1/2^-$ (2.69 MeV) first excited state of

⁴³Kanungo et al. (2015).

⁴⁴Similar situations are well known in the case of isoscalar and isovector giant quadrupole resonances (see e.g. Bès et al. (1975b) and references therein).

⁴⁵Potel et al. (2010).

⁴⁶Barranco et al. (2001).

⁴⁷Satchler (1980); Landau and Lifshitz (1965).

⁴⁸See e.g. Ascuitto and Glendenning (1969) Tamura et al. (1970) Khoa and von Oertzen (2004) Keeley et al. (2007) Thompson (1988).

$l \backslash c$	1	2	3	4	5
0	4.35×10^{-3}	1.79×10^{-4}	4.81×10^{-6}	2.90×10^{-11}	3.79×10^{-8}
1	3.50×10^{-3}	9.31×10^{-4}	1.47×10^{-5}	1.87×10^{-9}	1.09×10^{-6}
2	7.50×10^{-4}	8.00×10^{-5}	2.45×10^{-5}	1.25×10^{-8}	1.21×10^{-6}
3	6.12×10^{-4}	9.81×10^{-5}	1.51×10^{-6}	6.50×10^{-10}	2.20×10^{-7}
4	1.10×10^{-4}	1.18×10^{-5}	2.21×10^{-7}	4.80×10^{-11}	1.46×10^{-8}
5	3.65×10^{-5}	2.16×10^{-7}	7.42×10^{-9}	6.69×10^{-13}	9.63×10^{-10}
6	1.35×10^{-5}	6.05×10^{-8}	2.88×10^{-10}	8.04×10^{-15}	1.08×10^{-11}
7	4.93×10^{-6}	7.78×10^{-8}	6.01×10^{-11}	4.05×10^{-16}	5.26×10^{-13}
8	2.43×10^{-6}	2.62×10^{-8}	7.4×10^{-12}	1.26×10^{-17}	9.70×10^{-11}

Table 7.B.1: Probabilities p_l associated with the processes described in the text for each partial wave l . The different channels are labeled by a channel number c equal to: **1**, multistep transfer to the ${}^9\text{Li}$ ground state (Fig. 7.B.1(d)); **2**, multistep transfer (Fig. 7.B.1(e)) to the first excited ${}^9\text{Li}$ state, **3**, breakup (Fig. 7.B.1(f)), **4**, breakup (Fig. 7.B.1(g)), and **5** inelastic processes (Fig. 7.B.1(h)) involved in the population of the $1/2^-$ (2.69 MeV) first excited state of ${}^9\text{Li}$. It is of notice that the probabilities displayed in columns **1** and **2** result from the (coherent) sum of three amplitudes namely those associated with successive, simultaneous and non-orthogonality transfer channels (see also Figs. 7.B.2 and 7.B.3) after Potel et al. (2010).

${}^9\text{Li}$,

$$\frac{d\sigma}{d\Omega}(\theta) = \frac{\mu^2}{16\pi^3\hbar^4} \left| \sum_l (2l+1)P_l(\theta) \sum_{c=2}^5 T_l^{(c)} \right|^2, \quad (7.B.2)$$

where μ is the reduced mass and $T_l^{(c)}$ are the transition matrix elements associated with the different channels and for each partial wave of DWBA⁴⁹.

Making use of all the elements discussed above, multistep transfer⁵⁰, breakup and inelastic channels were calculated, and the results displayed in Figs. 7.B.2 and 7.B.3 and in Table 7.B.1. Theory provides an overall account of the experimental findings. In particular, in connection with the $1/2^-$ state, this result essentially emerges from cancellations and coherence effects taking place between the three terms contributing to the multistep two-particle transfer cross section (Fig. 7.B.3), tuned by the nuclear structure amplitudes associated with the process shown in Fig. 7.B.1 (e) as well as Eqs. (7.1.1)–(7.1.3). In fact, and as shown in Figs. 7.B.2 and 7.B.3, the contributions of break up processes and inelastic (Figs. 7.B.1(f),(g) and (h) respectively) to the population of the $1/2^-$ (2.69 MeV) first excited state of

⁴⁹Satchler (1980).

⁵⁰Bayman and Chen (1982), Igarashi et al. (1991), Bayman and Feng (1973) as well as Broglia and Winther (2004).

^9Li are negligible as compared with the process depicted in Fig. 7.B.1(e). In the case of the breakup channel (Figs. 7.B.1(f) and 7.B.1(g)) this is a consequence of the low bombarding energy of the ^{11}Li beam (inverse kinematics), combined with the small overlap between continuum (resonant) neutron $p_{1/2}$ wavefunctions and bound state wavefunctions. In the case of the inelastic process (Fig. 7.B.1(h)), it is again a consequence of the relative low bombarding energy. In fact, the adiabaticity parameters ξ_C, ξ_N ⁵¹ associated with Coulomb excitation and inelastic excitation in the $t+^9\text{Li}$ channel are larger than 1, implying an adiabatic cutoff. In other words, the quadrupole mode is essentially only polarized during the reaction but not excited. The situation is quite different in the case of the intervening of the virtual processes displayed in Fig. 7.B.1 (b) and (c) leading to the population of the $1/2^-$ state displayed in Fig. 7.B.1 (e). Being those off-the-energy shell processes, energy is not conserved, and adiabaticity gets profoundly modified.

Appendix 7.C Software

In this Appendix we provide a brief description of the numerical methods implemented in the code **COOPER**⁵² written to evaluate the differential cross sections. The two-nucleon transfer differential cross section is given by Eq. (6.1.3), so the principal task consists in calculating the transfer amplitudes $T^{(1)}(\theta)$, $T_{succ}^{(2)}(\theta)$ and $T_{NO}^{(2)}(\theta)$ described in Eqs. 6.1.4a-6.1.4c, by numerically evaluating the corresponding integrals. The dimensionality of the integrals can be reduced by expanding in partial waves (eigenfunctions of the angular momentum operator) the distorted waves and wavefunctions present in the corresponding integrands. The resulting expressions are Eqs. (6.2.36) and (6.2.37) for $T^{(1)}(\theta)$, Eqs. (6.2.128), (6.2.129) and (6.2.130) for $T_{succ}^{(2)}(\theta)$, and Eqs. (6.2.154), (6.2.155) and (6.2.156) for $T_{NO}^{(2)}(\theta)$. The integrals are computed numerically with the method of Gaussian quadratures.

The one-dimensional (radial) functions (6.1.2) appearing in the integrands are defined in a spatial grid up to a given maximum radius r_{max} . The bound state wavefunctions are obtained by numerical integration of the radial Schrödinger equation for a Woods-Saxon potential with a spin-orbit term. Along with the optical potentials governing the relative nucleus-nucleus motion in the initial, intermediate, and final channels, they conform the basic structure input needed to define the calculation. They are generated by solving a one-body Schrödinger equation for a Woods-Saxon with standard geometry, where the radius and diffusivity parameters are given as an input. The depth of the potential is adjusted to reproduce the binding energy of the state under consideration, according to the prescription defined below. The resulting potential corresponding to the final (initial) nucleon bound state stands also for the interaction potential featured in the integrand in the prior (post) representation.

⁵¹See eqs. (IV.12) and (IV.14) of ref. Broglia and Winther (2004).

⁵²Potel (2012b).

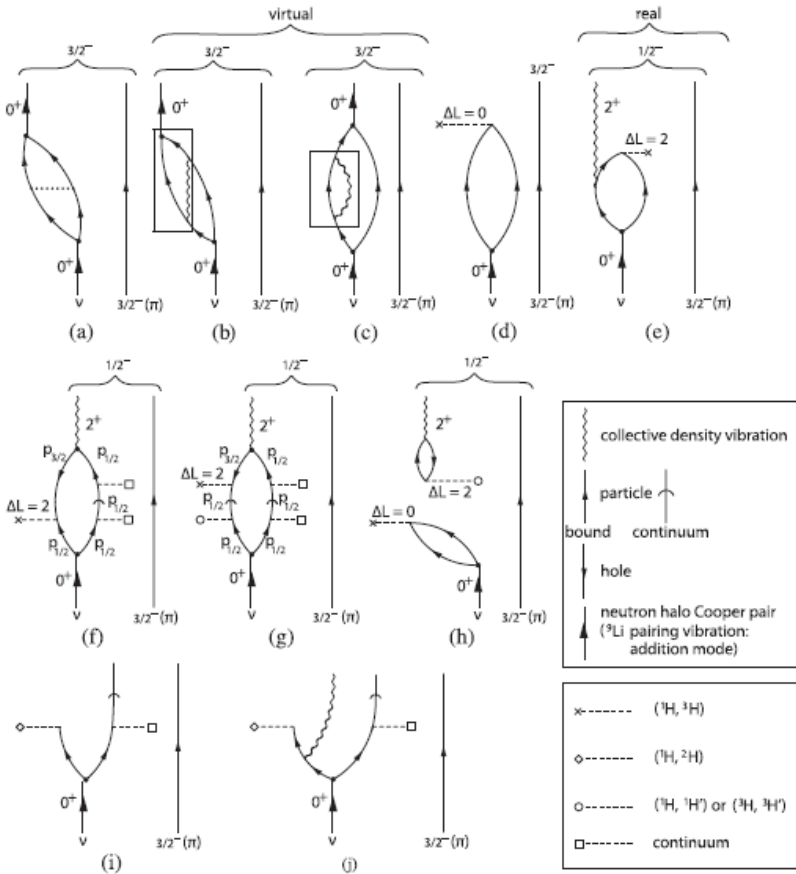


Figure 7.B.1: Representative Nuclear Field Theory–Feynman diagrams associated with correlation process ((a),(b),(c)) and with one- and two-particle pick-up reactions ((i),(j) and (d),(e) respectively) of the halo neutrons of ^{11}Li (Cooper pair, indicated in terms of a double arrowed line). Also shown are the possible diagrams associated with other channels (breakup and inelastic) populating the $1/2^-$ (2.69 MeV) state: f) two-particle pickup reaction involving one of the halo neutrons (the other one going into the continuum, i.e. breaking up from the ^9Li core) together with a neutron from the $p_{3/2}$ orbital of the ^9Li core leading eventually to the excitation of the $1/2^-$ final state (2^+ density mode (wavy line) coupled to the $p_{3/2}(\pi)$), g) the proton field acting once breaks the Cooper pair forcing one of the halo neutrons to populate a $p_{1/2}$ continuum state (the other one follows suit), while acting for the second time picks up one of the neutrons moving in the continuum and another one from those moving in the $p_{3/2}$ orbital of ^9Li eventually leaving the core in the quadrupole mode of excitation. In (h) the two-step transfer to the ^9Li ground state plus the inelastic final channel process exciting the $(2^+ \otimes p_{3/2}(\pi))_{1/2^-}$ state is shown. After Potel et al. (2010).

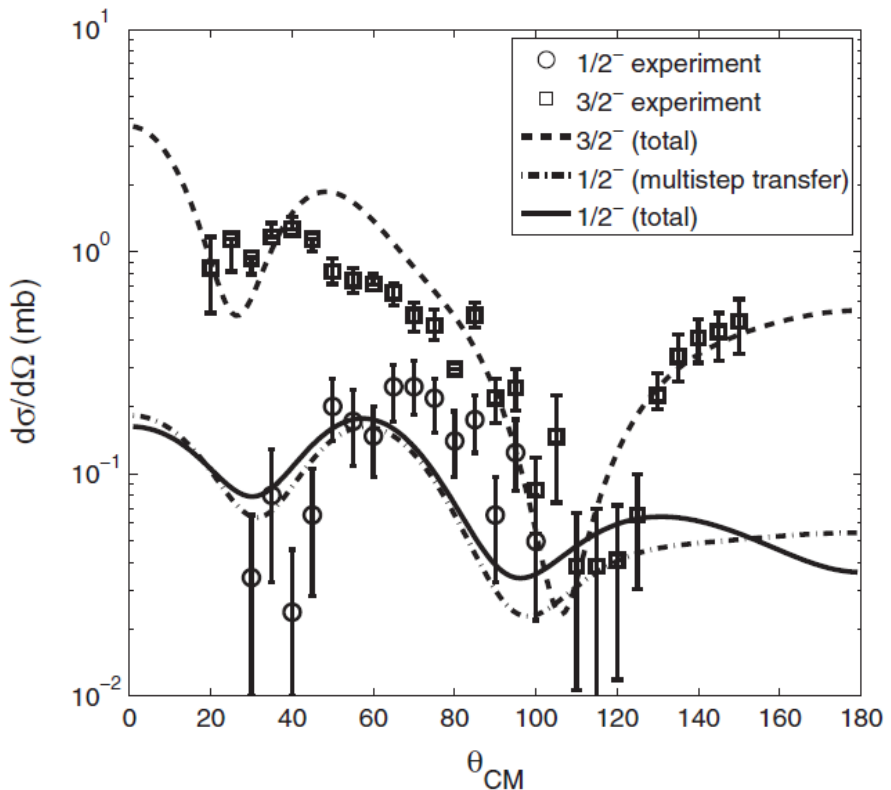


Figure 7.B.2: Experimental (Tanihata et al. (2008)) and theoretical differential cross sections (including multistep transfer as well as breakup and inelastic channels, Potel et al. (2010)) of the ${}^1\text{H}({}^{11}\text{Li}, {}^9\text{Li}){}^3\text{H}$ reaction populating the ground state ($3/2^-$) and the first excited state ($1/2^-$; 2.69 MeV) of ${}^9\text{Li}$. Also shown (dash-dotted curve) is the differential cross section associated with this last state but taking into account only multistep transfer. The optical potentials used are from (Tanihata et al., 2008; An and Cai, 2006), see Table 7.1.1. The absolute cross sections associated with the ground state ($3/2^-$) is predicted to be 6.1 mb (exp: 5.7 ± 0.9 mb) while that corresponding to the first excited state ($1/2^-$; 2.69 MeV) being 0.7 mb (exp: 1.0 ± 0.36 mb).

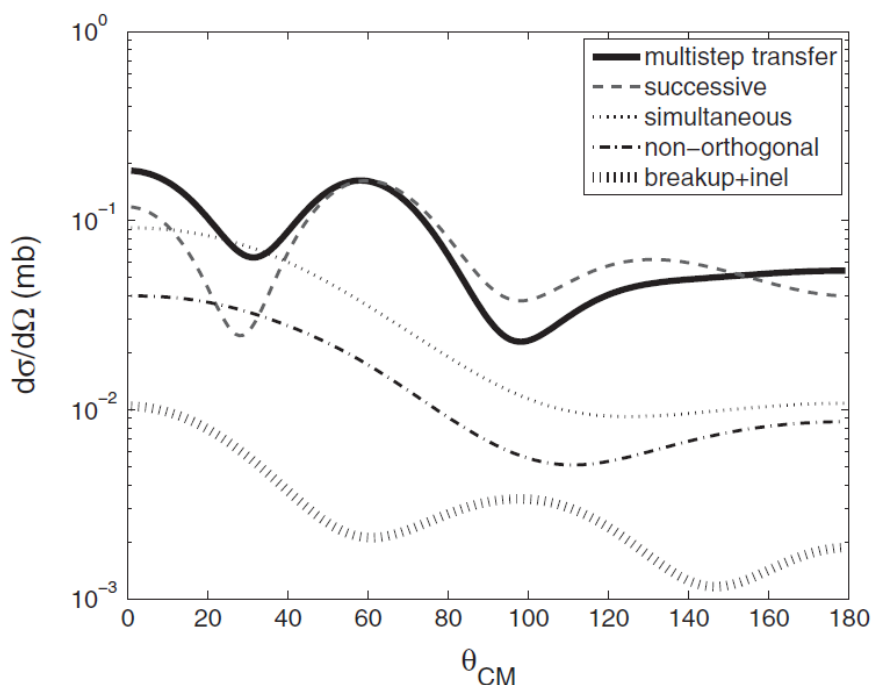


Figure 7.B.3: Successive, simultaneous and non-orthogonality contributions (prior representation) to the ${}^1H({}^{11}Li, {}^9Li){}^3H$ differential cross section associated with the population of the $1/2^-$ state of 9Li , displayed in Fig. 7.B.2. Also shown is the (coherent) sum of the breakup ($c = 3$ and 4) and inelastic ($c = 5$) channel contributions.

	^{120}Sn (I)	^{120}Sn (II)	B
$d_{5/2}$	-9.49	-7.79	0.41
$g_{7/2}$	-8.89	-7.79	0.57
$s_{1/2}$	-7.79	-7.79	0.41
$d_{3/2}$	-7.29	-7.79	0.66
$h_{11/2}$	-5.89	-7.79	1.03

Table 7.C.1: Energies (in MeV) of the single-particle orbitals involved in the description of the ground state of ^{120}Sn . The second column displays the energies of the single-particle orbitals according to the prescription used throughout this monograph (calculation (I)). The $s_{1/2}$ single-particle state, associated with the $1/2^+$ ground state of ^{119}Sn , has a binding energy of half the two-neutron separation energy of ^{120}Sn , $S_{2n}(^{120}\text{Sn})=15.59$ MeV. Calculation (II) (third column) corresponds to binding all the single-particle wavefunctions with half the two-neutron separation energy of ^{120}Sn . The last column displays the spectroscopic amplitudes B obtained from a BCS calculation of the ground state of ^{120}Sn (see Tab. 7.4.3).

The binding energies of the single-particle wavefunctions determine the asymptotic behavior of the transfer formfactors, an essential ingredient for a quantitative account of the two-nucleon transfer cross section (see App. 6.B). According to the prescription followed in the calculations discussed in the present monograph, the orbital corresponding to the spin-parity of the $A + 1$ system will be bound by half the experimental two-neutron separation energy S_{2n} of the $A + 2$ nucleus. The energies of the remaining single-particle states relative to the $A + 1$ ground state are determined from a structure calculation. Let us illustrate this procedure with the $^{120}\text{Sn}(p,t)^{118}\text{Sn}$ reaction with a 21 MeV proton beam. In order to assess the impact of the binding energies of the single-particle orbitals in the absolute value of the transfer cross section, we also show a calculation in which all the single-particle wavefunctions are bound with half the two-neutron separation energy of ^{120}Sn . The binding energies used for the two calculations are collected in Table 7.C.1, and the corresponding results are shown in Fig. 7.C.1. When calculating the successive transfer amplitude, the energy of the Green's function of the intermediate channel $d + (A + 1)$ (Eq. 6.1.11) is taken at the experimental energy of each of the populated states of the $(A + 1)$ system. Off-shell effects due to the virtual population of the different $(A + 1)$ intermediate states are thus fully taken into account. For the study of ^{11}Li , a different approach have been followed: the two-neutron wavefunction have been read from a two-dimensional numerical grid, generated from the NFT structure calculation. The distorted waves are obtained by integrating the radial Schrödinger equation with positive energy from $r = 0$ to r_{max} , and matching the solution with the corresponding Coulomb wave function at a given $r = r_{match}$, big enough to lie outside of the range of the nuclear interaction. The Woods-Saxon optical potentials used to obtain the distorted waves consist on a

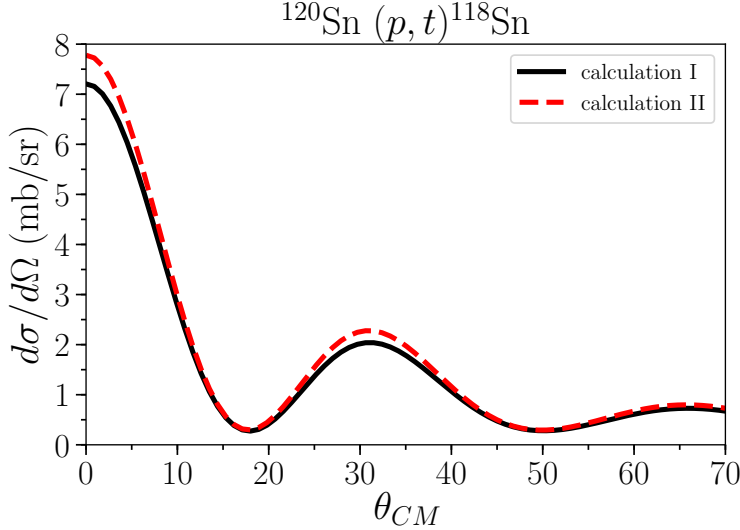


Figure 7.C.1: Numerical computation of the two-neutron transfer cross section corresponding to the reaction $^{120}\text{Sn}(p,t)^{118}\text{Sn}$. The two calculations shown in the figure correspond to the two different prescriptions for defining the binding energies of the single-particle orbitals described in the caption of Tab. 7.C.1.

real Coulomb term, a real and imaginary volume terms, an imaginary surface term, and a real and imaginary spin orbit terms. The parameters needed to specify all those terms are given as an input.

Appendix 7.D Statistics.

Let us consider two identical particles moving in a one-dimensional harmonic oscillator. Let us assume that one is in the ground state and the other is in the first excited state. According to the superposition principle

$$\Phi(x_1, x_2) = \lambda\phi_1(x_1)\phi_0(x_2) + \mu\phi_0(x_1)\phi_1(x_2). \quad (7.D.1)$$

Let us calculate the correlation of these particles, that is, the quantity

$$\text{Corr} = \frac{\langle x_1 x_2 \rangle - \langle x_1 \rangle \langle x_2 \rangle}{\sqrt{(\langle x_1^2 \rangle - \langle x_1 \rangle^2)(\langle x_2^2 \rangle - \langle x_2 \rangle^2)}} \quad (7.D.2)$$

Let us start with

$$\begin{aligned} \langle x_1 x_2 \rangle &= \int dx_1 dx_2 (\lambda^* \phi_1^*(x_1) \phi_0^*(x_2) + \mu^* \phi_0^*(x_1) \phi_1^*(x_2)) \\ &\times (x_1 x_2) (\lambda \phi_1(x_1) \phi_0(x_2) + \mu \phi_0(x_1) \phi_1(x_2)) \\ &= |\lambda|^2 \langle \phi_1 | x_1 | \phi_1 \rangle \langle \phi_0 | x_2 | \phi_0 \rangle + \lambda^* \mu \langle \phi_1 | x_1 | \phi_0 \rangle \langle \phi_0 | x_2 | \phi_1 \rangle \\ &+ \lambda \mu^* \langle \phi_0 | x_1 | \phi_1 \rangle \langle \phi_1 | x_2 | \phi_0 \rangle + |\mu|^2 \langle \phi_0 | x_1 | \phi_0 \rangle \langle \phi_1 | x_2 | \phi_1 \rangle. \end{aligned} \quad (7.D.3)$$

In keeping with the fact that

$$\langle \phi_1 | x | \phi_1 \rangle = \langle \phi_0 | x | \phi_0 \rangle = 0, \quad (7.D.4)$$

and

$$\langle \phi_0 | x | \phi_1 \rangle = \langle \phi_1 | x | \phi_0 \rangle = \sqrt{\frac{\hbar\omega}{2C}}, \quad (7.D.5)$$

one obtains

$$\langle x_1 x_2 \rangle = \left(\frac{\hbar\omega}{2C} \right)^2 \Re(\lambda^* \mu). \quad (7.D.6)$$

And

$$\sqrt{--} = \left(\frac{\hbar\omega}{2C} \right), \quad (7.D.7)$$

for the denominator of Eq. (7.D.2). From the above results the correlation function between particle 1 and 2 is

$$Corr = \frac{2C}{\hbar\omega} \langle x_1 x_2 \rangle = 2\Re(\lambda^* \mu) = \begin{cases} 1 & (\lambda = +\mu = \frac{1}{\sqrt{2}}) \\ -1 & (\lambda = -\mu = \frac{-1}{\sqrt{2}}) \end{cases} \quad (7.D.8)$$

It is of notice that, in quantum mechanics, average values imply the mean outcome of a large number of experiments. In this case, of the (simultaneous) measure of the position of the two particles⁵³.

Appendix 7.E Correlation length and quantality parameter.

The correlation length can be defined as⁵⁴

$$\xi = \frac{\hbar v_F}{\pi\Delta} \approx \frac{\hbar^2}{m} \frac{k_F}{\pi\Delta} \quad (7.E.1)$$

where the Fermi momentum in the case of stable nuclei lying along the stability valley is

$$k_F \approx 1.36 \text{ fm}^{-1}. \quad (7.E.2)$$

Thus,

$$\xi = 40 \text{ MeV fm}^2 \times \frac{1.36}{\pi\Delta} \text{ fm}^{-1} \approx \frac{17}{\Delta} \text{ fm}, \quad (7.E.3)$$

⁵³Basdevant and Dalibard (2005).

⁵⁴See e.g. Annett (2013) p. 62.

and,

$$\xi \approx 14 \text{ fm}, \quad (\Delta \approx 1.2 \text{ MeV}). \quad (7.E.4)$$

Thus, the associated (generalized) quantality parameter is, in the present case,

$$q_\xi = \frac{\hbar^2}{2m\xi^2} \frac{1}{2\Delta} \approx 0.04. \quad (7.E.5)$$

That is, the two partner nucleons are, in the Cooper pair, rigidly correlated with each other.

We now consider $^{11}_3\text{Li}_8$, and calculate k_F (neutrons) with the help of the Thomas-Fermi model⁵⁵

$$k_F = \left(3\pi^2 \frac{8}{\frac{4\pi}{3}(4.58)^3} \right)^{1/3} \text{ fm}^{-1} \approx \frac{(18\pi)^{1/3}}{4.58} \text{ fm}^{-1} \approx 0.8 \text{ fm}^{-1}. \quad (7.E.6)$$

The correlation length can, in the present case, be calculated in terms of the correlation energy ($E_{corr} \approx -0.5 \text{ MeV}$),

$$\xi \approx \frac{\hbar v_F}{\pi |E_{corr}|} \approx \frac{20 \text{ MeV fm} \times 0.16}{\pi \times 0.5 \text{ MeV}} \approx 20 \text{ fm}, \quad (7.E.7)$$

the resulting generalized quantality parameter being

$$q_\xi = \frac{\hbar^2}{2m\xi^2} \frac{1}{|E_{corr}|} \approx 0.1. \quad (7.E.8)$$

It is of notice that this result is but an alternative embodiment of the relation (4.4.8). Now, one could argue that both (4.4.8) and (7.E.8) (as well as (7.E.5) for stable nuclei), are just a manifestation of (7.D.8). That there is more to it is forcefully expressed by the fact that, selecting the pure two-particle configuration $|s_{1/2}^2(0)\rangle$ ($|p_{1/2}^2(0)\rangle$) to describe the halo neutron Cooper pair of ^{11}Li leads to absolute two-particle transfer cross sections which are about one order of magnitude larger (smaller) than the observed cross section (see Fig. 7.1.3). The fact that the NFT result (7.1.1)–(7.1.3) reproduces observations within experimental errors, underscores the central role played by structure on Cooper pair tunneling, through the emergent property of generalized pairing rigidity. Summing up, both the bare NN - and the long range induced pairing interaction changes the statistics of the elementary modes from fermionic to (quasi) bosonic ones⁵⁶ and, at the same time, the value of the quantality parameter from $q \approx 1$ to $q_\xi \ll 1$. That is, from a regime of delocalized single nucleons to one of strongly overlapping, independent pair motion each being governed by the same phased wavefunction $(U'_\nu + V'_\nu e^{-2i\phi} P_\nu^\dagger)|0\rangle$,

⁵⁵ Quantity which can be related to (v_F/c) according to $(v_F/c) = \hbar k_F/(mc) = (\hbar c/(mc^2))k_F \approx 0.2(k_F)\text{fm}^{-1}$. In the case in which $k_F \approx 0.8 \text{ fm}^{-1}$ (see Eq. (7.E.6)), $v_F/c \approx 0.16$.

⁵⁶ Within this context see Sect. 4.8.1.

where $P_{\nu}^{\dagger} = a_{\nu}^{\dagger}a_{\bar{\nu}}^{\dagger}$ create two nucleons in time reversal states⁵⁷. In each pair, the partners are phase correlated to each other (see Eq. (4.3.1)) behaving as a single entity. The operator P_{ν}^{\dagger} , being a product of two fermions, do not fulfill Bose statistics ($(P_{\nu}^{\dagger})^2 = 0$). This property implies the presence of a pairing gap not only for breaking a pair, but also for making a pair move differently from the others⁵⁸. As a result one has long-range-order in the superfluid nuclear system, known as off-diagonal-long-range-order (ODLRO)⁵⁹. This effect leads to generalized gauge rigidity, the detailed renormalizing and dressing mechanisms ultimately deciding on the soundness and applicability of the description under discussion. The fact that in working out the reaction mechanism one uses, for practical reasons, a single-particle basis (second order DWBA corrected by non-orthogonality), reconstructing the pair correlations in term of sums over virtual states, is at the basis of the two-neutron transfer physical sum rule discussed in Sect. 7.4.2.

Appendix 7.F Multipole pairing vibrations.

Although much work has been carried out concerning multipole pairing vibrations⁶⁰, i.e. modes with transfer quantum numbers $\beta = \pm 2$ and multipolarity and parity λ^{π} different from 0^+ , this remains a chapter essentially missing from the subject of pairing in nuclei. Arguably, with the partial exception of quadrupole pairing studied in the multiphonon pairing vibrational spectrum⁶¹ around the closed shell ^{208}Pb , and in connection with strongly excited 0^+ pairing vibrational states in the actinide region⁶², as well as of the quadrupole and hexadecapole pairing vibrations in the multiplet spectrum⁶³ of ^{209}Bi .

In what follows, we shall elaborate on the new insight on pairing vibrational modes, the studies of two-neutron pickup reactions on ^{11}Li have opened. As already explained, because of the small overlap existing between halo neutrons and core nucleons both the 1S_0 , NN- and the symmetry-potential become strongly screened, resulting in a subcritical value of pairing strength and in a weak repul-

⁵⁷Since P_{ν}^{\dagger} commutes for different ν 's, $|BCS\rangle$ represents uncorrelated occupancy of the various pair states.

⁵⁸The BCS state can be written as $|BCS\rangle \sim \Pi_{\nu} \alpha_{\nu} |0\rangle$, where $\alpha_{\nu} = U_{\nu} a_{\nu} - V_{\nu} a_{\bar{\nu}}^{\dagger}$, is the annihilation quasiparticle operator (Bogoliubov (1958); Valatin (1958); see App. G of Brink and Broglia (2005)). Thus, to make e.g. the pair associated with the state ν' to behave differently from the rest of the pairs one has to avoid including in the product above the state ν' , i.e. $\Pi_{\nu \neq \nu'} \alpha_{\nu} |0\rangle$. The resulting state resembles a one-quasiparticle state.

⁵⁹Yang (1962).

⁶⁰See Brink and Broglia (2005) Sect. 5.3 and refs. therein. See also Broglia et al. (1974), Ragnarsson and Broglia (1976), Broglia et al. (1971a), Broglia et al. (1971b), Bès and Broglia (1971b), Bès and Broglia (1971a), Flynn et al. (1971), Bès et al. (1972), Broglia (1981), Bohr and Mottelson (1980), Flynn et al. (1972a), Bortignon et al. (1976); see also Kubo et al. (1970) and references therein.

⁶¹See Flynn et al. (1972a).

⁶²Casten et al. (1972), Bès et al. (1972), Ragnarsson and Broglia (1976). It is of notice that β -vibrations and monopole pairing vibrations become mixed in quadrupole deformed nuclei.

⁶³Bortignon et al. (1976).

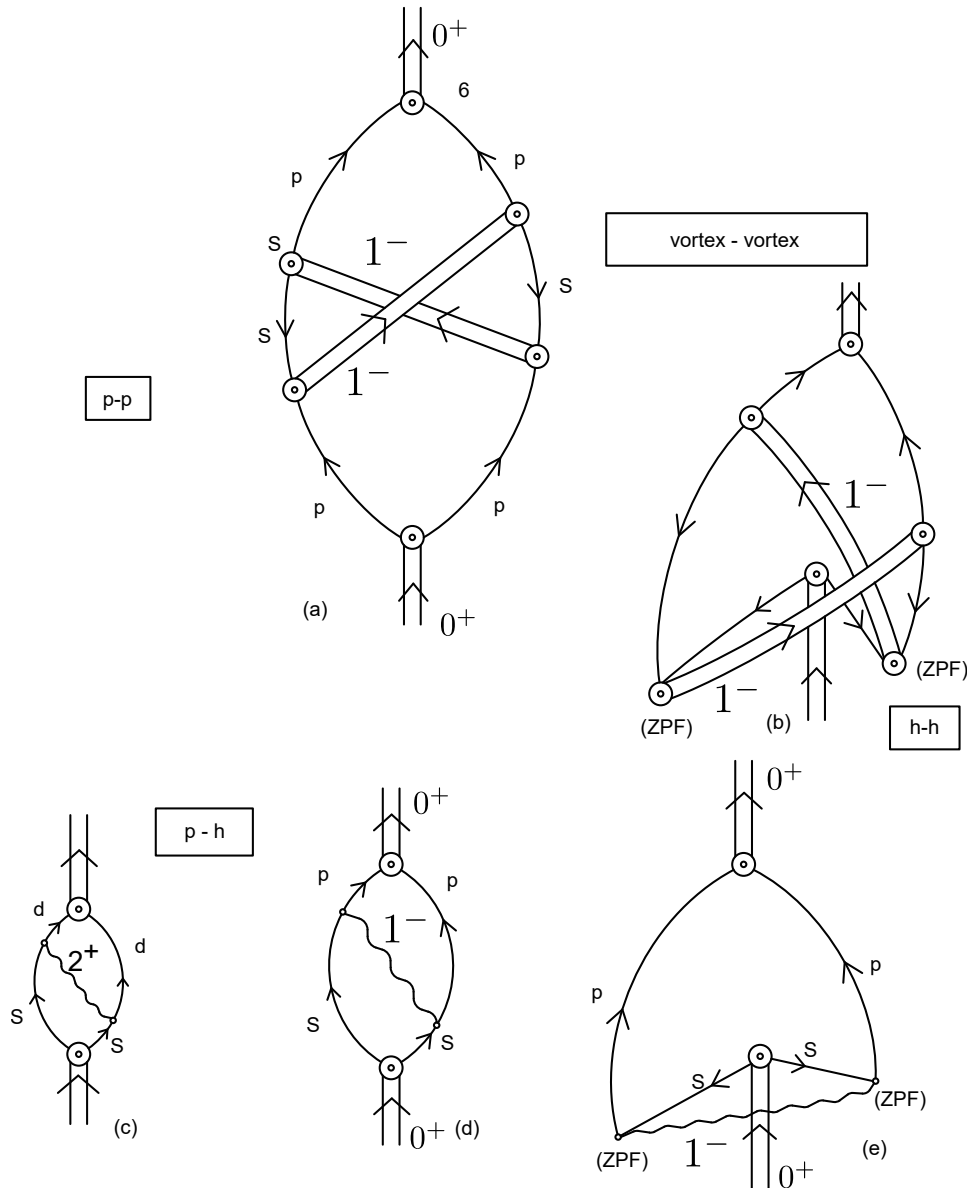


Figure 7.F.1: NFT-Feynman diagrams describing the interweaving between the neutron halo pair addition monopole and dipole modes (double arrowed lines labeled 0^+ and 1^- respectively). Above, the exchange of dipole modes binding the 0^+ pair addition mode through forwards going particle-particle p - p (h - h) components. Below, the assumption is made that the GDR of ^{11}Li can be viewed as a p - h (two quasiparticle), QRPA mode.

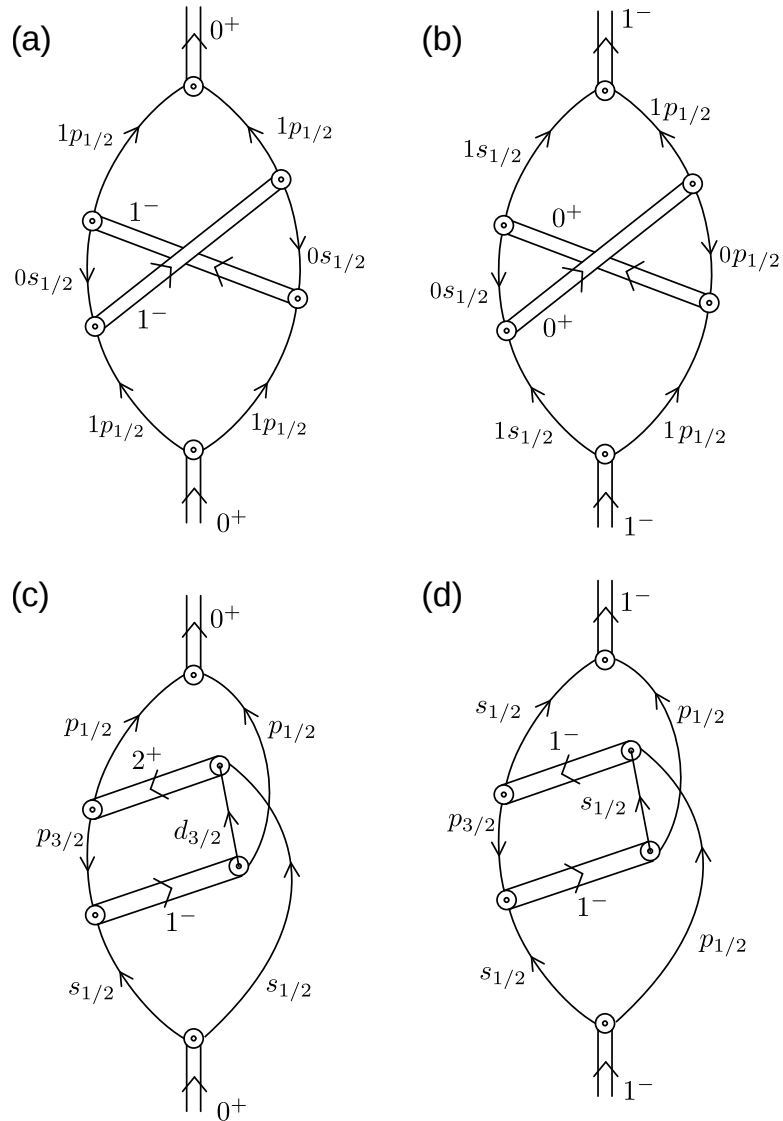


Figure 7.F.2: NFT-Feynman diagrams describing, (a,c) some of the particle-particle (pp), hh and ph processes binding the Cooper pair neutron halo and stabilizing ^{11}Li , as well as (b,d) giving rise to the GDPR.

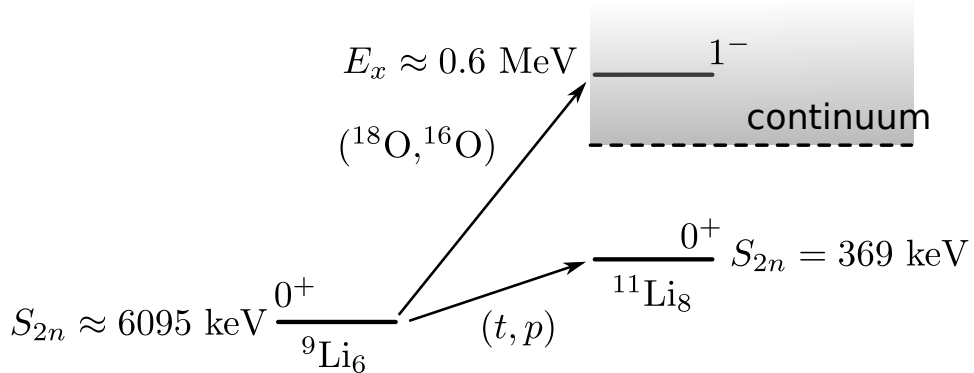


Figure 7.F.3: Schematic representation of levels of ^{11}Li populated (gs), or which eventually could be populated (1^-) in two–nucleon transfer reactions. Indicated in keV are the two–neutron separation energies S_{2n} . In labeling the different states, one has not considered the quantum numbers of the $p_{3/2}$ odd proton.

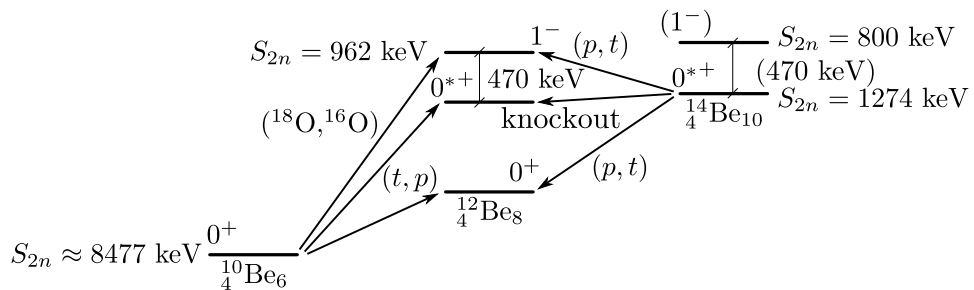


Figure 7.F.4: Levels of ^{12}Be expected to be populated in two-nucleon transfer and knockout processes. S_{2n} are the two-neutron separation energies.

sion to separate protons from neutrons in the dipole channel. As a result, neither the $J^\pi = 0^+$ correlated neutron state (Cooper pair), nor the $J^\pi = 1^-$ one (vortex-like)⁶⁴ are bound (although both qualify to do so) to the core ${}^9\text{Li}$.

Having essentially exhausted the bare NN-interaction channels, the two neutrons can correlate their motion by exchanging vibrations of the medium in which they propagate, namely the halo and the core. Concerning the first one, these modes could hardly be the $\lambda = 2^+, 3^-$ or 5^- surface vibrations found in nuclei lying along the stability valley. This is because the diffusivity of the halo is so large that it blurs the very definition of surface. Those associated with the core (2^+ see Fig. 7.F.1 (c), and eventually also $3^-, 5^-$ etc.) provide some glue, but insufficient to bind any of the two dineutron states in question.

As already mentioned, the next alternative is that of bootstrapping. Namely, that in which the two partners of the (monopole) Cooper pair exchange pairs of vortices (dipole Cooper pair), as well as one dipole Cooper pair and a quadrupole pair removal mode, while those of the vortex exchange pairs of Coopers pairs (monopole pairing vibrations), but also two dipole pairs, as shown in Figs. 7.F.1 and 7.F.2. In other words, by liaising with each other, the two dineutrons contenders at the role of ${}^{11}\text{Li}$ ground state settle the issue. As a result the Cooper pair becomes weakly bound ($S_{2n} = 380$ keV), the vortex state remaining barely unbound, by about 0.5–1 MeV. There is no physical reason why things could not have gone the other way, at least none that we know. Within this context we refer to ${}^3\text{He}$ superfluidity, where condensation involve $S = 1$ pairs. It is of notice that we are not considering spin degrees of freedom in the present case, at least not dynamic ones.

For practical purposes, one can describe the 1^- as a two quasiparticle state and calculate it within the framework of QRPA adjusting the strength of the dipole-dipole separable interaction to reproduce the experimental findings (Fig. 4.C.1). In this basis it is referred to as a Pygmy Dipole Resonance (PDR). Exchanged between the two partners of the Cooper pair (Fig. 7.F.1(d)) leads to essentially the right value of dineutron binding to the ${}^9\text{Li}$ core. Within this context one can view the ${}^{11}\text{Li}$ neutron halo as a van der Waals Cooper pair (Fig. 7.F.1(e)). The transformation between this picture and that discussed in connection with (a) and (b) as well as with Fig. 7.F.2 can be obtained expressing the PDR, QRPA wavefunction, in terms of particle creation and destruction operators (Bogoliubov-Valatin transformation) as seen from Fig. 7.F.1(a) and (b). A vortex-vortex stabilised Cooper pair emerges.

Which of the two pictures is more adequate to describe the dipole mediated condensation is an open question, as each of them reflects important physical properties which characterise the PDR. In any case, both indicate the symbiotic character of the halo Cooper pair addition mode and of the pygmy resonance built on top of, and almost degenerate with it. Insight into this question can be obtained by shedding light on the question of whether the velocity field of each of the symbi-

⁶⁴One of the effects of a vortex is that it allows rotation about an axis of symmetry.

otic states is more similar to that associated with irrotational or vortex-like flow⁶⁵. Two-nucleon transfer reactions, specific probe of (multipole) pairing vibrational modes, contain many of the answers to the above question (Figs. 7.F.3). In fact, ground state correlations will play a very different role in the absolute value of the ${}^9\text{Li}(\text{t},\text{p}){}^{11}\text{Li}$ (1^-) cross section, depending on which picture is correct. In the case in which it can be viewed as a vortex (pair addition dipole mode) it will lead to an increase of the two-particle transfer reaction (positive coherence). It will produce the opposite effect if the correct interpretation of the PDR is that of a ($p - h$)-like excitation⁶⁶. Insight in the above question may also be obtained by studying the properties of a quantal vortex in a Wigner cell with parameters which approximately reproduce the halo of ${}^{11}\text{Li}$. Within this context, and for the solely purpose of providing an analogy, we refer to what is done in the study of vortices in the environment of neutron stars⁶⁷.

A possible test of the soundness of the physics discussed above, concerns the question of whether the first excited, 0^+ halo state ($E_x = 2.24$ MeV) of ${}^{12}\text{Be}$ can be viewed as the $|\text{gs}({}^{11}\text{Li})\rangle$ in a new environment. In other words, to consider the halo neutron pair addition mode a novel mode of elementary excitation: neutron halo pair addition mode of which the $|1^-({}^{12}\text{Be}) ; 2.71 \text{ MeV}\rangle$ is a fraction of its symbiotic PDR partner. One can gain insight concerning this question, by eventually measuring the E1-branching ratio $|1^-(2.71 \text{ MeV})\rangle \rightarrow |0^{+*}(2.24 \text{ MeV})\rangle$, and possibly finding other low-energy E1-transitions populating the 0^* state, as well as through two-nucleon stripping process, and two-nucleon pickup and knockout reactions (Fig. 7.F.4). A resumé of the picture discussed above is given in Fig. 4.9.1.

Appendix 7.G Vacuum fluctuations and interactions: the Casimir effect

In Fig. 7.G.1 (I) (a) an example is given of zero-point fluctuations (ZPF) of the nuclear vacuum (ground state) in which, a surface quantised vibration and an uncor-

⁶⁵See Repko et al. (2013). Within this context, and making use of an analogy, one can mention that a consistent description of the GQR and of the GIQR is obtained assuming that the average eccentricity of neutron orbits is equal to the average eccentricity of the proton orbits (Bès et al. (1975b)), the scenario of neutron skin. The isoscalar quadrupole-quadrupole interaction is attractive. Furthermore, the valence orbitals of nuclei have, as a rule and aside from intruder states, homogeneous parity. These facts preclude the GQR to play the role of the GDPR. In fact, there will always be a low-lying quadrupole vibration closely connected with the aligned coupling scheme and thus with nuclear plasticity. Within this context one can nonetheless posit that the GQR, related to neutron skin, is closely associated with the aligned coupling scheme. Making a parallel, one can posit that the GDPR is closely connected with vortical motion. Arguably, support for this picture is provided by the low-lying E1 strength of ${}^{11}\text{Li}$. It results from the presence of $s_{1/2}$ and $p_{1/2}$ orbitals almost degenerate and at threshold, leading to a low-lying Cooper pair coupled to angular momentum 1^- . (dipole pair addition mode). The scenario of vortical motion.

⁶⁶Broglia et al. (1971c).

⁶⁷Avogadro et al. (2007, 2008).

related particle–hole mode get virtually excited for a short period of time. Adding a nucleon (odd system, Fig. 7.G.1 (I) (b)) leads, through the particle–vibration coupling mechanism to processes which contain the effect of the antisymmetry between the single-particle explicitly considered and the particles out of which the vibrations are built (Fig. 7.G.1 (I)(c)). Time ordering gives rise to the graph shown in Fig. 7.G.1 (I)(d). Processes I(c) and I(d), known as correlation (CO) and polarisation (PO) contributions to the mass operator, clothe the particles and lead to physical nucleons whose properties can be compared with the experimental findings with the help of specific experimental probes. For example one–particle transfer reactions. Summing up, the processes shown in Fig. 7.G.1 (I) are examples of quantum field theory phenomena. They testify to the fact that the clothing of nucleons is at the basis of the quantal description of the atomic nucleus.

Nuclear superfluidity at large, and its incipience in the case of single Cooper pair like e.g. in ^{11}Li in particular, are among the most quantal of all the phenomena displayed by the nuclear many-body system. Even if the bare 1S_0 , NN –interaction was not operative, or was rendered subcritical by screening effects as in the case of ^{11}Li , Cooper binding will still be healthy, as a result of the exchange of vibrations between pairs of physical (clothed) nucleons (Fig. 7.G.1 (II) (a), (c)) moving in time reversal states close to the Fermi energy (Fig. 7.G.1 (II)(b),(d)-(g)), a direct consequence of the ZPF of the nuclear vacuum (ground) state. *Arrived at this point, the reader may find it useful to read again Sect. 1.10, in particular the last paragraph.*

7.G.1 Measuring QED quantum fluctuations

The many–body character of the attractive interaction between nucleons arising from the nuclear (vacuum) ZPF discussed above, and important to describe phenomena occurring close to the surface of the Fermi sea, have a classical analogue. Fittingly, a classical phenomenon which emerges from maritime experience.

At sea, on a windless day in which the water surface can resemble a mirror, free floating ships singly or in groups do not do much, just stay put. The situation is quite different in a strong swell, still on a windless situation. In this case, single, isolated ships end up lying parallel to the wave crests (see Fig. 7.G.2(a)) and start rolling heavily. In the days of the clipper ships it was believed that under those circumstances, two vessels at close distance, attracted each other. This in keeping with the fact that the rigs of the rolling ships became often entangled leading to disaster. It was not until quite recently⁶⁸ that a quantitative understanding of the phenomenon (based on knowledge of similar quantal effects) was achieved, providing evidence that the old tale was true. Only waves with wavelength smaller than the separation of the ships can exist between them. In the region of sea extending away from the ships to the horizon, waves of any wavelength can exist (see Fig. 7.G.2(b)). This fact results into an imbalance between the forces exerted by the

⁶⁸Boersma (1996).

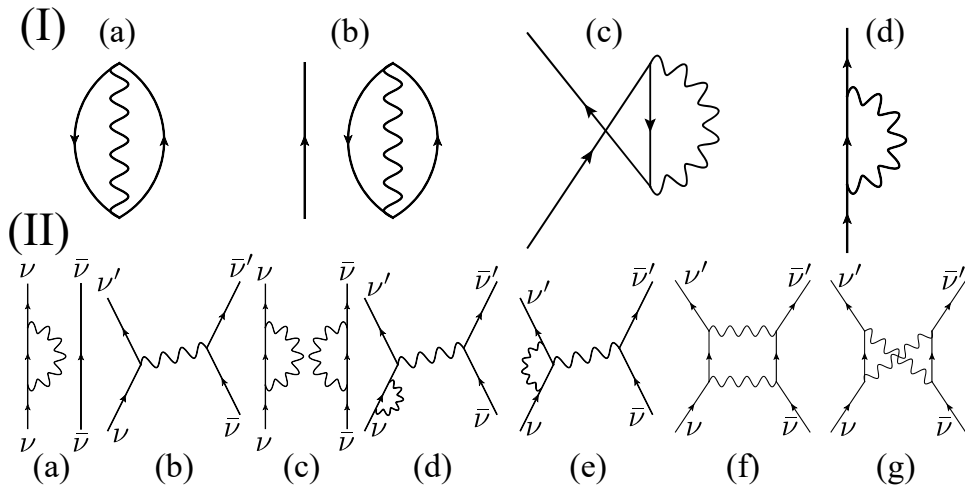


Figure 7.G.1: **(I)** **(a)** ZPF associated with (particle-hole) surface vibrations; **(b)** odd system; **(c)** the antisymmetrization between the particles considered explicitly and those involved in the vibration; **(d)** time ordering of (c). Diagrams (c) and(d) lead to the clothing of single-particle motion in lowest order in the particle-vibration coupling vertex. **(II)** A dressed nucleon moving in a state ν in the presence of: **(a)** a bare nucleon moving in the time reversed state $\bar{\nu}$, **(c)** another dressed nucleon. Exchange of vibration in (a) leads to **(b)**, the NFT lowest-order contribution in the particle-vibration coupling vertex, of the induced pairing interaction. Exchange of vibrations in (c) leads to **(d)** self-energy, **(e)** vertex correction of the induced pairing interaction; **(f)** ladder diagram contributing to the induced pairing interaction. The symmetrisation between the bosons displayed in (c) is shown in (g).

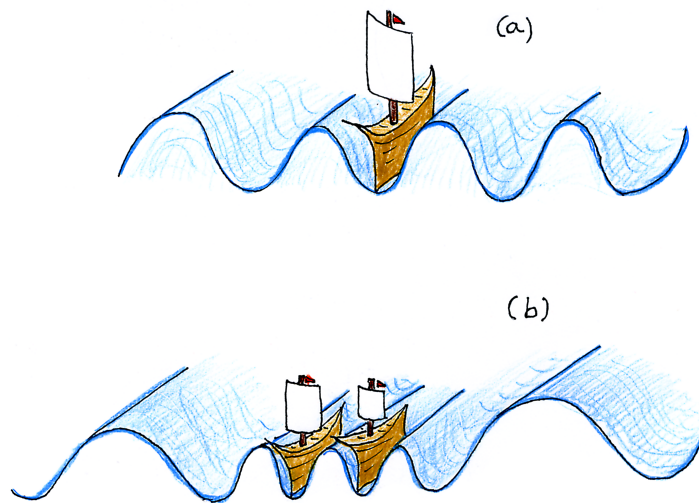


Figure 7.G.2: (Color online) Schematic representation of the behaviour of an isolated ship at sea in a situation of no wind but of strong swell (a), and of two ships close by in similar conditions (b).

internal (between ships) waves, in favour of that exerted by the external waves, leading to a net attraction. Quantum mechanical, such an effect is known as the Casimir effect⁶⁹.

Two conducting, neutral plates at very small distances, of the order of the micron ($1\mu = 10^{-6}$ cm), attract each other, due to the imbalance in electromagnetic field pressure exerted by the bombarding of the surface by electrons and positrons, arising from the ZPF of the electromagnetic field⁷⁰ (see Fig. 7.G.3). It is of notice that the Casimir effect, namely the attraction between two metallic, uncharged, plates (which have been drawn in Fig. 7.G.3 as plane surface but which could, in principle have any shape) is not so different from that experienced by leptodermic systems, that is, systems which display a surface tension. Setting two of such systems in contact “destroys” part of their surface. But this is tantamount to saying that one has to spend some amount of work to separate the systems from each other, namely that associated with “recreating” the surface area associated with the overlap. In other words the two leptodermic systems attract each other with a potential energy proportional to the surface tension of the system (Fig. 7.G.4; see also Eq. (4.7.22) and related discussion). Now, this quantity is a measure of the force that

⁶⁹Casimir (1948).

⁷⁰As stated in the last sentences of the caption to Fig. 7.G.3, long wavelengths play the central role in the Casimir effect. A recurring property of the modes renormalizing the bare interaction or the associated collective variables (elementary modes of excitation) found in condensed matter (phonons of much lower frequency (ω_{ip}) than plasmons (ω_{ep}), nuclei (collective quadrupole and soft- E_1 (pygmy) modes ($\hbar\omega_2$, $\hbar\omega_{PDR}$) $\ll \hbar\omega_{GR}$), proteins (in this connection see Micheletti et al. (2004, 2001, 2002); Hamacher (2010)).

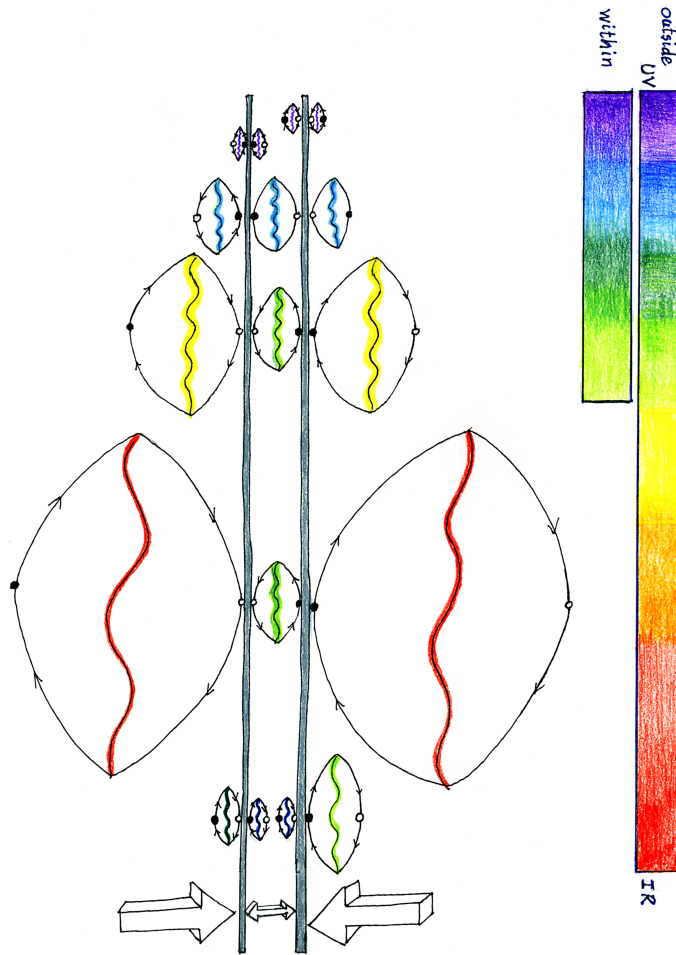


Figure 7.G.3: (Color online) Casimir effect. Two metallic isolated, conducting plates (grey vertical sections) in vacuum attract each other when they are placed at very small distances (of the order of micron). This is known as the Casimir effect. The origin of such a force are, in this work, traced back to quantal zero point fluctuations (ZPF) of the electromagnetic vacuum. In the figure a cartoon of such processes is given. Virtual electrons (e^- , solid dots) and positrons (e^+ , open dots) pop up of the vacuum together with a photon, travel for short distances on timescales of the order of $\hbar/1\text{MeV} \approx 10^{-23}$ s (1 MeV being approximately equal to the summed mass of e^- and e^+). In their way, some of them hit the plates. The different wavelengths of the visible photons (and thus the associate momenta of the fermions), are displayed with the standard color coding of the rainbow. Of course, the spectrum extends beyond such limit (from UV to IR). Because the range of colors (wavelengths) allowed between the plates is smaller than the full spectrum (see colored spectra to the far right of the figure) allowed for the photons associated with the electromagnetic ZPF in the right and left unlimited halves, more fermions or bosons will be knocking the plates from outside than from the in between region, thus leading to an imbalance of the “quantal” pressure and consequently to an effective attractive force. *Within this scenario, there are in fact the long wavelengths of the electromagnetic spectrum which are responsible for the attraction between the metallic plates in the Casimir effect. In other words, quantal pressure by infrared.*

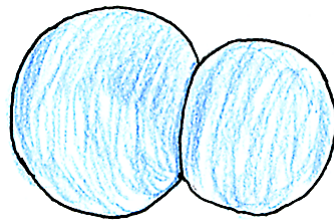


Figure 7.G.4: Two overlapping water droplets attract each other with a potential energy proportional to the surface tension and, making a spherical approximation, as far as the overlapping region is concerned, proportional also to reduced radius or better, to the inverse sum of the curvature. This is also true for two atomic nuclei.

must be applied to surface molecules so that they experience the same force as a molecule in the interior of the liquid.

Summing up, in a similar way in which one can state that there are neither bare fermions (e.g. electrons or nucleons) nor bare bosons (e.g. photons or surface vibrations), one can posit that essentially all bare forces are, with varied degrees of complexity and strength, renormalized by many-body effects. This message comes also from the least suspected of all fundamental forces, the Coulomb interaction, responsible for all of chemistry and most of biophysics (Sect. 4.A.3).

7.G.2 The hydrophobic force

Water has three noteworthy properties: liquid water is heavier than ice, it has an exceptionally large specific heat⁷¹ –the amount of heat needed to raise the temperature of 1 kg of mass 1 degree Kelvin– aside from being an excellent solvent due to its dipole moment.

All these properties follow from the structure of the water molecule H₂O. This, in turn, is connected with the directional, anisotropic structure of the valence, electronic distribution of O. Oxygen is an open shell atom⁷², having in its ground state only four electrons in the last occupied 2p-orbital which can host six ($|gs\rangle = |1s^2\rangle|2s^2\rangle|2p^4\rangle$). It can thus use at profit the electrons of the two H-atoms to dynamically become a closed shell system (²⁰Ne–noble gas–like electronic configuration, Fig. 7.G.5 (c)), a requirement simple to fulfill in the present case. This is in keeping with the fact that the hydrogen atom H is prone to share its electron.

Hybridization between the four orbitals $|2s\rangle$, $|2p_x\rangle$, $|2p_y\rangle$ and $|2p_z\rangle$ leads to a tetrahedral correlation in which the four orbitals $|i\rangle$ point towards the corners of a tetrahedron with the oxygen atom at the center (Fig. 7.G.5 (a), 7.G.6). Because the electronic distribution has its charge center closer to the oxygen atom than to the

⁷¹Water absorbs 4.184 Joules of heat for the temperature of one gram of water to increase 1 degree celsius (°C). For comparison sake, it takes 0.385 Joules of heat to raise 1 gram of Copper 1°C.

⁷²See e.g. Greiner (1998).

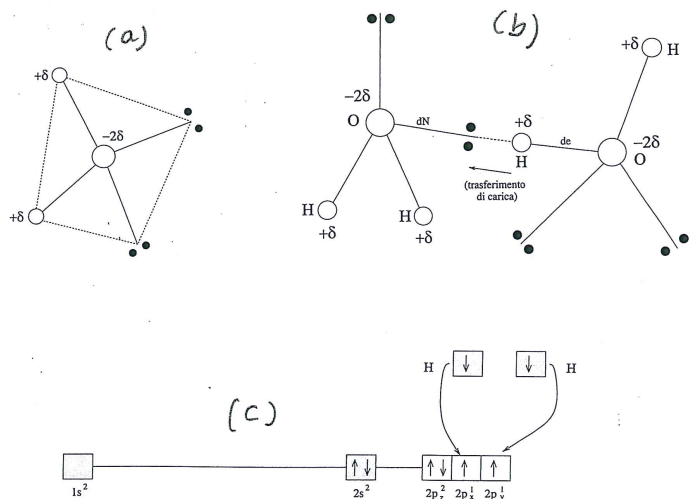


Figure 7.G.5: (a) To understand the behavior of water molecules one has to realize that in the covalent bonds, where the oxygen and the hydrogen atoms share a couple of electrons, the corresponding electronic cloud is somewhat more concentrated on the oxygen than on the hydrogen. The oxygen acquires a partial charge -2δ while each hydrogen gets a positive one $+\delta$. (b) Such charges give rise to an attractive electric force between close lying molecules, in which the hydrogen atoms of a molecule points to the oxygen atom of the other molecule. One can view this attractive force as a type of chemical bond. It is known as hydrogen bond. It is of notice that also in this type of bond there is a component which implies the sharing of electrons. Furthermore, the hydrogen atom in an hydrogen bond does not just stick indiscriminantly to the the oxygen of another molecule. Being positively charged it goes where the electrons are. So the hydrogen bond is a bond between a hydrogen atom and a lone pair (two bold face dots). This means that a water molecule can form four hydrogen bonds: the molecule's two hydrogens form two bonds with neighboring oxygens, while the molecule's two lone pairs interact with neighboring hydrogens. (c) Schematic electronic structure of H_2O .

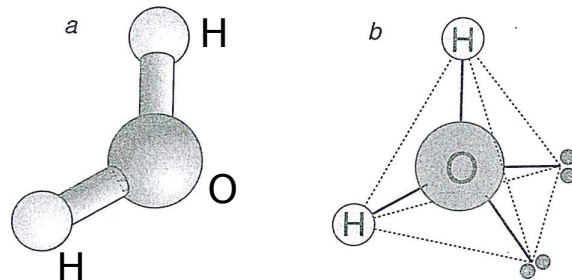


Figure 7.G.6: The water molecule is bent, with the two bonds between oxygen and hydrogen splayed at an angle of 104.5° (a). To understand the structure of liquid water, we must also take into account the two “lone pairs” of electrons on the oxygen atom. The hydrogen atoms and the lone pairs sit more or less at the corners of a tetrahedron (b). (after Ball (2003)).

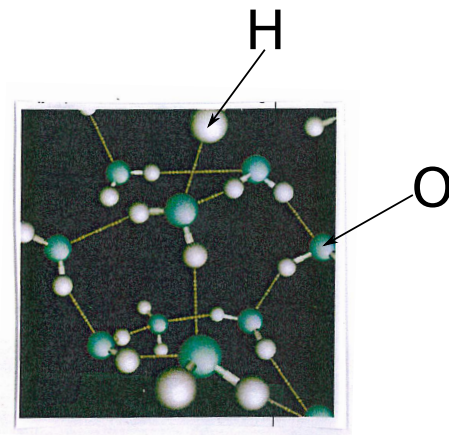


Figure 7.G.7: (Color online) Stick and ball representation (blue O, light grey H) of a network of hydrogen bonds in bulk water (after Chandler (2002)).

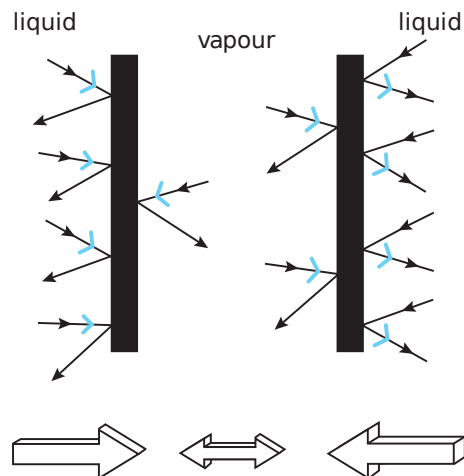


Figure 7.G.8: Schematic representation of water molecules (arrowed lines also blue arrowed) impinging from the outside (liquid) and from the inter space (vapor) of two large parallel hydrophobic plates (after Lum et al. (1999)).

two protons of the H-atoms, H_2O has a sizable dipole moment⁷³ ($\approx 0.68ea_0 \approx 0.6$ D, e being the electron charge, a_0 the Bohr radius and D the Debye unit). Water molecules can form four hydrogen bonds⁷⁴ (hb), a special bond between molecules which is produced in situations when they share an hydrogen nucleus between them. The molecule's two hydrogen atoms form two bonds with neighboring oxygens, while the molecule's two lone pairs interact with neighboring hydrogens⁷⁵ (Figs. 7.G.5 (b)).

Water and oil do not mix. The term hydrophobic (water-fearing) is commonly used to describe substances that, like oil, do not mix (dissolves) with (in) water.

⁷³The dipole moment of a polar molecule is defined as $u = ql$, where l is the distance between the two charges $+q$ and $-q$. Thus, for two electronic charges $q = \pm e$ separated by $l = 0.1$ nm, the dipole moment is $u = 1.602 \times 10^{-19} \text{ C} \times 10^{-10} \text{ m} = 4.8 \text{ D}$, where the Debye=1D=3.336×10⁻³⁰ Cm is the unit of dipole moment. Small polar molecules have moments of the order of 1D (see e.g. Israelachvili (1985)).

⁷⁴Let us consider an H atom in a covalent bond with oxygen. When a second oxygen atom approaches the H atom, its nucleus, the proton, sees a potential with two minima, and tunnels through the corresponding barrier from one minimum to the other. In other words, the effective potential in which the proton moves becomes broader as compared to the single oxygen potential. Thus, the quantum mechanical confinement kinetic energy decreases by roughly a factor of two. This implies that the order of magnitude energy of an hydrogen bond between two oxygen atoms corresponds to the difference in the corresponding ZPF energies, i.e. ≈ 200 meV ($\approx 0.38 \text{ eV} - 0.19 \text{ eV} \approx 0.2 \text{ eV} \approx 4.6 \text{ kcal/mol}$ ($\approx 8 \text{ kT}$), where kT ($\approx 0.6 \text{ kcal/mol} \approx 27 \text{ meV}$) is the thermal energy at room temperature ($\approx 310 \text{ K}$)). For comparison a covalent bond corresponds to $\approx 96 \text{ kcal/mol} \approx 4 \text{ eV}$, while the van der Waals interaction energy between two H at a distance of 2.4 \AA , that is of the order of the hydrogen bond length of 1.83 \AA , is $\approx 20 \text{ meV}$ (see Povh and Rosina (2002))

⁷⁵A possible pedestrian explanation of this is to impersonate a water molecule. Quoting from Ball (2003): "Your hands are hydrogen atoms, your ankles are the lone pairs of electrons of oxygen. Stand legs apart... Twist 90° at the waist, stretch your arms and you're H_2O . The way that water molecules join up has just one rule: hands can grab ankles, but nothing else. That grasp is an hydrogen bond".

Although it may look as if water repels oil, these two types of molecules actually attract each other, e.g. through the van der Waals interaction, but not nearly as strongly as water attracts itself. Mixing enough oil (hydrophobic, non polar (NP) molecules) with water leads to a reduction in favorable bonding. Strong mutual attraction between water molecules induce segregation of NP molecules from water and results in an effective NP–NP (hydrophobic) attraction, as observed e.g. in surface force measurements⁷⁶. For example, the loss of hydrogen bonds near the two extended hydrophobic surfaces depicted in Fig. 7.G.8 causes water to move away from those surfaces⁷⁷, producing thin vapour layers. Fluctuations in the interfaces form in this way can destabilize and expel the remaining liquid contained between these surfaces. The resulting pressure imbalance will cause the surfaces to attract. If the liquid is close to coexistence with the vapor phase, as is the case for water at ambient conditions, this phenomenon occurs for widely separated surfaces. The similarity with a (generalized) Casimir effect is apparent. Within this context, and in keeping with the fact that the hydrophobic force plays a central role in the folding and, as a consequence, in the biological activity of proteins, one can point that water at physiological conditions ($T = 300\text{K}$, $\text{pH}=7$, etc.) can be viewed as the vacuum of the macromolecules responsible for metabolism, and thus one of the two origins of life on earth⁷⁸.

While the many–body basis of hydrophobicity cannot be denied (Fig. 7.G.7) the parallel with the zero–body Casimir effect (Fig. 7.G.3) can hardly be avoided. Neither with the nuclear phenomena displayed in Fig. 7.G.1 nor with those discussed in Sects. 4.A.2 and 4.A.3 in connection with superconductivity in metals.

Within this scenario, one can also observe a (generalized) Nambu-tumbling effect. Namely the chain *hydrogen bond* → *weak and strong hydrophobicity* → *polypeptide chain evolution* → *proteins (second order phase transition, spontaneous symmetry breaking in information space⁷⁹)* → *protein folding (first order phase transition in conformation space)* → *metabolism*. And, at the basis of the

⁷⁶See e.g. Chandler (2002, 2005) and Lum et al. (1999) and references therein.

⁷⁷Hydrophobic molecules do not hydrogen bond to water, creating excluded regions where the density of water molecules vanishes. When these units are small enough, water can reorganize near them without loosing hydrogen bonds, building an ice–like cage around the NP molecule. The entropic cost of this structural change leads to low solubility for small apolar molecules in water. Said it differently, such a force, known as the weak hydrophobic force (WHF) leads only to metastable states of groups of nonpolar molecules (Chandler (2002)). On the other hand, close to a large hydrophobic object, the persistence of an hydrogen bond network –four bond per water molecule– cannot persist, being geometrically impossible. In this case, water molecules near the hydrophobic cluster (surface) have typically three or fewer hydrogen bonds. This force, known as the strong hydrophobic force (SHF, Chandler (2002)) can be viewed as a *bona fide* hydrophobic interaction, stabilizing large aggregates of nonpolar molecules.

⁷⁸To the question “what is life?”(Schrödinger (1944)) one is forced to answer that life is not one but two things (Dyson (1999)). Which ones? Replication and metabolism. The molecules of DNA and RNA are responsible for the first function (Watson and Crick (1953); Watson (1980)), proteins (i.e. polymers made out of the 20 commonly occurring acids in nature), for the second (Sanger (1952)). Because software (replication) is necessary a parasite of hardware (proteins), the becoming of a protein carries, to a large extent, the secret of life (Monod (1970)).

⁷⁹Broglio (2013).

first link of the chain, one finds the difference in the ZPF energy which an hydrogen nucleus feels when in presence of one (O) or two (O_2) oxygen nuclei, quantity closely connected with quantum fluctuation of confinement (Povh and Rosina (2002)).

Bibliography

- E. Abrahams and J. W. F. Woo. Phenomenological theory of the rounding of the resistive transition of superconductors. *Phys. Lett. A*, 27:117, 1968.
- K. Alder and A. Winther. *Electromagnetic Excitations*. North Holland, Amsterdam, 1975.
- K. Alder, A. Bohr, T. Huus, B. Mottelson, and A. Winther. Study of Nuclear Structure by Electromagnetic Excitation with Accelerated Ions. *Rev. Mod. Phys.*, 28:432, 1956.
- V. Ambegaokar. The Green's function method. In R. D. Parks, editor, *Superconductivity, Vol I*, page 259. Marcel Dekker, New York, 1969.
- V. Ambegaokar and A. Baratoff. Tunneling between superconductors. *Phys. Rev. Lett.*, 10:486, 1963.
- H. An and C. Cai. Global deuteron optical model potential for the energy range up to 183 MeV. *Phys. Rev. C*, 73:054605, 2006.
- P. W. Anderson. New method in the theory of superconductivity. *Phys. Rev.*, 110: 985, 1958.
- P. W. Anderson. Theory of dirty superconductors. *Journal of Physics and Chemistry of Solids*, 11:26, 1959.
- P. W. Anderson. Superconductivity. *Science*, 144:373, 1964a.
- P. W. Anderson. Special effects in superconductivity. In E. R. Caianello, editor, *The Many-Body Problem, Vol.2*, page 113. Academic Press, New York, 1964b.
- P. W. Anderson. More is different. *Science*, 177:393, 1972.
- P. W. Anderson. Uses of solid state analogies in elementary particle theory. In R. Arnowitt and P. Nath, editors, *Gauge theories and modern field theories, Proceeding of a conference held at Northeastern University, Boston*, page 311, Cambridge, Mass., 1976. MIT Press.
- P. W. Anderson. *Basic Notions of Condensed Matter*. Addison-Wesley, Reading, Mass, 1984.

- P. W. Anderson and D. L. Stein. Broken symmetry, emergent properties, dissipative structures, life: are they related? In *P. W. Anderson, Basic notions of condensed matter*, page 263. Benjamin, Menlo Park, CA, 1984.
- P. W. Anderson and D. J. Thouless. Diffuseness of the nuclear surface. *Physics Letters*, 1:155, 1962.
- J. F. Annett. *Superconductivity, superfluids and condensates*. Oxford University Press, Oxford, 2013.
- R. J. Asciutto and N. K. Glendenning. Inelastic processes in particle transfer reactions. *Physical Review*, 181:1396, 1969.
- R. J. Asciutto and N. K. Glendenning. Assessment of two-step processes in (p, t) reactions. *Phys. Rev. C*, 2:1260, 1970.
- R. J. Asciutto and B. Sørensen. Coupling effects in ^{208}Pb . *Nuclear Physics A*, 186: 641, 1972.
- R. J. Asciutto, N. K. Glendenning, and B. Sørensen. Confirmation of strong second order processes in (p, t) reactions on deformed nuclei. *Physics Letters B*, 34:17, 1971.
- N. W. Ashcroft and N. D. Mermin. *Solid state physics*. Holt, Reinhardt and Winston, Hong Kong, 1987.
- N. Austern. Direct reactions. In F. Janouch, editor, *Select Topics in Nuclear Theory*, p. 17, Vienna, 1963. IAEA.
- N. Austern. *Direct nuclear reaction theories*. Interscience monographs and texts in physics and astronomy. Wiley–Interscience, 1970.
- D. Auton. Direct reactions on ^{10}Be . *Nuclear Physics A*, 157:305, 1970.
- A. Avdeenkov and S. Kamerdzhiev. Phonon Coupling and the Single-Particle Characteristics of Sn Isotopes. In R. A. Broglia and V. Zelevinsky, editors, *50 Years of Nuclear BCS*, page 274. World Scientific, Singapore, 2013.
- P. Avogadro, F. Barranco, R. A. Broglia, and E. Vigezzi. Quantum calculation of vortices in the inner crust of neutron stars. *Phys. Rev. C*, 75:012805, 2007.
- P. Avogadro, F. Barranco, R. Broglia, and E. Vigezzi. Vortex–nucleus interaction in the inner crust of neutron stars. *Nuclear Physics A*, 811(3):378, 2008.
- P. Axel. Electric Dipole Ground-State Transition Width Strength Function and 7-MeV Photon Interactions. *Phys. Rev.*, 126:671, 1962.
- P. Ball. *$\text{H}_2\text{O} A$ biography of water*. Phoenix, London, 2003.

- J. Bang, S. Ershov, F. Gareev, and G. Kazacha. Discrete expansions of continuum wave functions. *Nuclear Physics A*, 339:89, 1980.
- M. Baranger. Recent progress in the understanding of finite nuclei from the two-nucleon interaction. In M. Jean and R. A. Ricci, editors, *Proceedings of the International school of physics “E. Fermi” Course XL Nuclear Structure and Nuclear Reactions*, page 511. Academic Press, New York, 1969.
- C. Barbieri. Role of Long-Range Correlations in the quenching of spectroscopic factors. *Phys. Rev. Lett.*, 103:202502, 2009.
- C. Barbieri and B. K. Jennings. Nucleon-nucleus optical potential in the particle-hole approach. *Phys. Rev. C*, 72:014613, 2005.
- J. Bardeen. Tunnelling from a many-particle point of view. *Phys. Rev. Lett.*, 6:57, 1961.
- J. Bardeen. Tunneling into superconductors. *Physical Review Letters*, 9:147, 1962.
- J. Bardeen and D. Pines. Electron-phonon interaction in metals. *Phys. Rev.*, 99: 1140, 1955.
- J. Bardeen, L. N. Cooper, and J. R. Schrieffer. Microscopic theory of superconductivity. *Physical Review*, 106:162, 1957a.
- J. Bardeen, L. N. Cooper, and J. R. Schrieffer. Theory of superconductivity. *Physical Review*, 108:1175, 1957b.
- P. Barnes, E. Romberg, C. Ellegard, R. Casten, O. Hansen, and J. Mulligan. Proton-hole states in ^{209}Bi From the $^{210}\text{Po} (t, \alpha)$ reaction. *Nucl. Phys. A*, 195: 146, 1972.
- S. Baroni, M. Armati, F. Barranco, R. A. Broglia, G. Colò, G. Gori, and E. Vigezzi. Correlation energy contribution to nuclear masses. *Journal of Physics G: Nuclear and Particle Physics*, 30:1353, 2004.
- F. Barranco and R. A. Broglia. Effect of surface fluctuations on the nuclear density. *Phys. Rev. Lett.*, 59:2724, 1987.
- F. Barranco, M. Gallardo, and R. A. Broglia. Nuclear field theory of spin dealignment in strongly rotating nuclei and the vacuum polarization induced by pairing vibrations. *Phys. Lett. B*, 198:19, 1987.
- F. Barranco, R. A. Broglia, and G. F. Bertsch. Exotic radioactivity as a superfluid tunneling phenomenon. *Phys. Rev. Lett.*, 60:507, 1988.
- F. Barranco, E. Vigezzi, and R. A. Broglia. Calculation of the absolute lifetimes of the variety of decay modes of ^{234}U . *Phys. Rev. C*, 39:210, 1989.

- F. Barranco, G. F. Bertsch, R. A. Broglia, and E. Vigezzi. Large-amplitude motion in superfluid fermi droplets. *Nuclear Physics A*, 512:253, 1990.
- F. Barranco, R. A. Broglia, G. Gori, E. Vigezzi, P. F. Bortignon, and J. Terasaki. Surface vibrations and the pairing interaction in nuclei. *Phys. Rev. Lett.*, 83: 2147, 1999.
- F. Barranco, P. F. Bortignon, R. A. Broglia, G. Colò, and E. Vigezzi. The halo of the exotic nucleus ^{11}Li : a single Cooper pair. *Europ. Phys. J. A*, 11:385, 2001.
- F. Barranco, R. A. Broglia, G. Colò, G. Gori, E. Vigezzi, and P. F. Bortignon. Many-body effects in nuclear structure. *European Physical Journal A*, 21:57, 2004.
- F. Barranco, P. F. Bortignon, R. A. Broglia, G. Colò, P. Schuck, E. Vigezzi, and X. Viñas. Pairing matrix elements and pairing gaps with bare, effective, and induced interactions. *Phys. Rev. C*, 72:054314, 2005.
- F. Barranco, G. Potel, R. A. Broglia, and E. Vigezzi. Structure and reactions of ^{11}Be : many-body basis for single-neutron halo. *Phys. Rev. Lett.*, 119:082501, 2017.
- F. Barranco, G. Potel, E. Vigezzi, and R. A. Broglia. Radioactive beams and inverse kinematics: Probing the quantal texture of the nuclear vacuum. *The European Physical Journal A*, 55:104, 2019.
- F. Barranco, G. Potel, E. Vigezzi, and R. A. Broglia. $^9\text{Li}(d, p)$ reaction as a specific probe of ^{10}Li , the paradigm of parity-inverted nuclei around the $N = 6$ closed shell. *Phys. Rev. C*, 101:031305, 2020.
- J. L. Basdevant and J. Dalibard. *Quantum Mechanics*. Springer, Berlin, 2005.
- G. Bassani, N. M. Hintz, C. D. Kavaloski, J. R. Maxwell, and G. M. Reynolds. (p, t) Ground-State $L = 0$ Transitions in the Even Isotopes of Sn and Cd at 40 MeV, $N = 62$ to 74. *Phys. Rev.*, 139:B830, 1965.
- B. Bayman. A derivation of the pairing-correlation method. *Nuclear Physics*, 15: 33, 1960.
- B. F. Bayman. Seniority, Quasi-particle and Collective vibrations. *Lecture notes, Palmer Physical Laboratory, Princeton, unpublished*, 1961. (Unpublished).
- B. F. Bayman. Finite-range calculation of the two-neutron transfer reaction. *Phys. Rev. Lett.*, 25:1768, 1970.
- B. F. Bayman. Finite-range calculation of the two-neutron transfer reaction. *Nuclear Physics A*, 168:1, 1971.

- B. F. Bayman and J. Chen. One-step and two-step contributions to two-nucleon transfer reactions. *Phys. Rev. C*, 26:1509, 1982.
- B. F. Bayman and C. F. Clement. Sum rules for two-nucleon transfer reactions. *Phys. Rev. Lett.*, 29:1020, 1972.
- B. F. Bayman and B. H. Feng. Monte Carlo calculations of two-neutron transfer cross sections. *Nuclear Physics A*, 205:513, 1973.
- B. F. Bayman and A. Kallio. Relative-angular-momentum-zero part of two-nucleon wave functions. *Phys. Rev.*, 156:1121, 1967.
- S. Beceiro-Novo, T. Ahn, D. Bazin, and W. Mittig. Active targets for the study of nuclei far from stability. *Progress in Particle and Nuclear Physics*, 84:124, 2015.
- M. J. Bechara and O. Dietzsch. States in ^{121}Sn from the $^{120}\text{Sn}(d, p)^{121}\text{Sn}$ reaction at 17 MeV. *Phys. Rev. C*, 12:90, 1975.
- P. A. Beck and H. Claus. Density of states information from low temperature specific heat measurements. *Journal of Research of the National Bureau of Standards A, Physics and Chemistry*, 74 A:449, 1970.
- S. T. Belyaev. Effect of pairing correlations on nuclear properties. *Kgl. Danske Videnskab. Selskab, Mat.-fys. Medd.*, 31:no. 11, 1959.
- S. T. Belyaev. Pair correlations in nuclei: Copenhagen 1958. In R. A. Broglia and V. Zelevinski, editors, *50 Years of Nuclear BCS*, page 3. World Scientific, Singapore, 2013.
- K. Bennaceur, J. Dobaczewski, and M. Ploszajczak. Pairing anti-halo effect. *Physics Letters B*, 496:154, 2000.
- V. Bernard and N. V. Giai. Single-particle and collective nuclear states and the Green's function method. In R. A. Broglia, R. A. Ricci, and C. H. Dasso, editors, *Proc. of the Int. School of Physics "Enrico Fermi", Course LXXVII*, p. 437. North Holland, Amsterdam, 1981.
- G. Bertsch. Collective motion in Fermi droplets. In R. A. Broglia and J. R. Schrieffer, editors, *International School of Physics "Enrico Fermi" Course CIV, Frontiers and Borderlines in Many-Body Particle Physics*, page 41. North Holland, Amsterdam, 1988.
- G. Bertsch, F. Barranco, and R. A. Broglia. How nuclei change shape. In T. Kuo and I. Speth, editors, *Windsurfing the Fermi sea*, page 33. Elsevier, 1987.
- G. F. Bertsch and R. A. Broglia. Giant resonances in hot nuclei. *Physics Today*, 39 (8):44, 1986.

- G. F. Bertsch and R. A. Broglia. *Oscillations in Finite Quantum Systems*. Cambridge University Press, Cambridge, 2005.
- G. F. Bertsch, R. A. Broglia, and C. Riedel. Qualitative description of nuclear collectivity. *Nucl. Phys. A*, 91:123, 1967.
- G. F. Bertsch, P. F. Bortignon, and R. A. Broglia. Damping of nuclear excitations. *Rev. Mod. Phys.*, 55:287, 1983.
- D. R. Bès and R. A. Broglia. Pairing vibrations. *Nucl. Phys.*, 80:289, 1966.
- D. R. Bès and R. A. Broglia. Effect of the multipole pairing and particle-hole fields in the particle-vibration coupling of ^{209}Pb . I. *Physical Review C*, 3:2349, 1971a.
- D. R. Bès and R. A. Broglia. Effective operators in the analysis of single-nucleon transfer reactions on closed shell nuclei. *Physical Review C*, 3:2389, 1971b.
- D. R. Bès and R. A. Broglia. Equivalence between Feynman–Goldstone and particle–phonon diagrams for finite many body systems. In G. Alaga, V. Paar, and L. Sips, editors, *Problems of Vibrational Nuclei, in Procs. of the topical Conference on Problems of Vibrational Nuclei*, page 1. North Holland, Amsterdam, 1975.
- D. R. Bès and R. A. Broglia. Nuclear superfluidity and field theory of elementary excitations. In A. Bohr and R. A. Broglia, editors, *International School of Physics “Enrico Fermi” Course LXIX, Elementary Modes of Excitation in Nuclei*, page 55. North Holland, Amsterdam, 1977.
- D. R. Bès and J. Kurchan. *The treatment of Collective Coordinates in Many–Body Systems*. World Scientific, Singapore, 1990.
- D. R. Bès and R. A. Sorensen. The pairing–plus–quadrupole model. *Advances in Nuclear Physics*, 2:129, 1969.
- D. R. Bès, R. A. Broglia, and B. Nilsson. Importance of the quadrupole pairing field in the $J^\pi = 0^+$ vibrations of shape deformed nuclei. *Physics Letters B*, 40:338, 1972.
- D. R. Bès, G. G. Dussel, R. A. Broglia, R. Liotta, and B. R. Mottelson. Nuclear field theory as a method of treating the problem of overcompleteness in descriptions involving elementary modes of both quasi–particles and collective type. *Phys. Lett. B*, 52:253, 1974.
- D. R. Bès, R. A. Broglia, G. G. Dussel, and R. Liotta. Simultaneous treatment of surface and pairing nuclear fields. *Phys. Lett. B*, 56:109, 1975a.
- D. R. Bès, R. A. Broglia, and B. Nilsson. Microscopic description of isoscalar and isovector giant quadrupole resonances. *Phys. Rep.*, 16, 1975b.

- D. R. Bès, R. A. Broglia, G. G. Dussel, R. J. Liotta, and R. P. J. Perazzo. On the many-body foundation of the Nuclear Field Theory. *Nucl. Phys. A*, 260:77, 1976a.
- D. R. Bès, R. A. Broglia, G. G. Dussel, R. J. Liotta, and H. M. Sofía. The nuclear field treatment of some exactly soluble models. *Nucl. Phys. A*, 260:1, 1976b.
- D. R. Bès, R. A. Broglia, G. G. Dussel, R. J. Liotta, and H. M. Sofía. Application of the nuclear field theory to monopole interactions which include all the vertices of a general force. *Nucl. Phys. A*, 260:27, 1976c.
- D. R. Bès, R. A. Broglia, J. Dudek, W. Nazarewicz, and Z. Szymański. Fluctuation effects in the pairing field of rapidly rotating nuclei. *Annals of Physics*, 182:237, 1988.
- J. H. Bilgram. Dynamics at the solid-liquid transition: Experiments at the freezing point. *Physics Reports*, 153:1, 1987.
- J. H. Bjerregaard, O. Hansen, O. Nathan, and S. Hinds. States of ^{208}Pb from double triton stripping. *Nucl. Phys.*, 89:337, 1966.
- J. B. Bjorken and S. D. Drell. *Relativistic quantum mechanics*. Mc Graw-Hill, New York, 1998.
- S. Bjornholm, J. Borggreen, K. Hansen, and J. Pedersen. Electronic shells and supershells in metal clusters. In R. A. Broglia and J. R. Schrieffer, editors, *International School of Physics “Enrico Fermi” Course CXXI, Perspectives in many-particle physics*, page 279. North Holland, Amsterdam, 1994.
- S. Boersma. A maritime analogy of the Casimir effect. *Am. J. Phys.*, 64:539, 1996.
- N. Bogoljubov. On a new method in the theory of superconductivity. *Il Nuovo Cimento*, 7:794, 1958.
- D. Bohm and D. Pines. A Collective Description of Electron Interactions. I. Magnetic Interactions. *Phys. Rev.*, 82:625, 1951.
- D. Bohm and D. Pines. A Collective Description of Electron Interactions: III. Coulomb Interactions in a Degenerate Electron Gas. *Phys. Rev.*, 92:609, 1953.
- A. Bohr. Elementary modes of excitation and their coupling. In *Comptes Rendus du Congrès International de Physique Nucléaire*, volume 1, page 487. Centre National de la Recherche Scientifique, 1964.
- A. Bohr. *Rotational Motion in Nuclei, in Les Prix Nobel en 1975*. Imprimerie Royale Norstedts Tryckeri, Stockholm, 1976. p. 59.

- A. Bohr and B. R. Mottelson. Submission letter to H. Lipkin Febr. 13th, 1963 for non publication in his jocular but quite influential journal of non-publishable results in nuclear physics concerning the remarkable (coexistence) properties of low-lying 0^+ excited states in ^{16}O , ^{40}Ca , ^{42}Ca , ^{70}Ge , and ^{24}Mg (5.465 MeV) $l = 0$ strength. February 1963 (unpublished).
- A. Bohr and B. R. Mottelson. *Nuclear Structure, Vol.I.* Benjamin, New York, 1969.
- A. Bohr and B. R. Mottelson. *Nuclear Structure, Vol.II.* Benjamin, New York, 1975.
- A. Bohr and B. R. Mottelson. Features of nuclear deformations produced by the alignment of individual particles or pairs. *Physica Scripta*, 22:468, 1980.
- A. Bohr and O. Ulfbeck. Quantal structure of superconductivity gauge angle. In *First Topsøe summer School on Superconductivity and Workshop on Superconductors*, Roskilde, Denmark Riso/M/2756, 1988.
- A. Bohr, B. R. Mottelson, and D. Pines. Possible analogy between the excitation spectra of nuclei and those of the superconducting metallic state. *Physical Review*, 110:936, 1958.
- N. Bohr. The quantum postulate and the recent development of atomic theory. *Nature*, 121:580, 1928.
- N. Bohr and J. A. Wheeler. The mechanism of nuclear fission. *Phys. Rev.*, 56:426, 1939.
- M. Born. Zur Quantenmechanik der Stoßvorgänge. *Zeitschr. f. Phys.*, 37:863, 1926a.
- M. Born. Zur Quantenmechanik der Stoßvorgänge. *Zeitschr. f. Phys.*, 38:803, 1926b.
- M. Born. *Natural philosophy of cause and chance*. Oxford University Press, Oxford, 1948.
- M. Born. *Nobel Lecture, (1954), The statistical interpretation of quantum mechanics, Nobel Lectures, Physics 1942-1962*, p. 256. Elsevier, 1964.
- M. Born. *Atomic Physics*. Blackie, London, 1969.
- M. Born and P. Jordan. Zur quantenmechanik. *Zeitschr. Phys.*, 34:858, 1925.
- M. Born, P. Jordan, and W. Heisenberg. Zur Quantenmechanik II. *Zeitschr. Phys.*, 35:557, 1926.
- P. F. Bortignon and R. A. Broglia. Role of the nuclear surface in an unified description of the damping of single-particle states and giant resonances. *Nucl. Phys. A*, 371:405, 1981.

- P. F. Bortignon and R. A. Broglia. Elastic response of the atomic nucleus in gauge space: Giant pairing vibrations. *The European Physical Journal A*, 52(9):280, 2016.
- P. F. Bortignon, R. A. Broglia, D. R. Bès, R. Liotta, and V. Paar. On the role of the pairing modes in the ($h_{9/2} \otimes 3^-$) multiplet of ^{209}Bi . *Phys. Lett. B*, 64:24, 1976.
- P. F. Bortignon, R. A. Broglia, D. R. Bès, and R. Liotta. Nuclear field theory. *Physics Reports*, 30:305, 1977.
- P. F. Bortignon, R. A. Broglia, and D. R. Bès. On the convergence of nuclear field theory perturbation expansion for strongly anharmonic systems. *Phys. Lett. B*, 76:153, 1978.
- P. F. Bortignon, R. A. Broglia, and C. H. Dasso. Quenching of the mass operator associated with collective states in many-body systems. *Nuclear Physics A*, 398: 221, 1983.
- P. F. Bortignon, A. Bracco, and R. A. Broglia. *Giant Resonances*. Harwood Academic Publishers, Amsterdam, 1998.
- M. Brack. The physics of simple metal clusters: self-consistent jellium model and semiclassical approaches. *Rev. Mod. Phys.*, 65:677, 1993.
- C. Branden and J. Tooze. *Introduction to protein structure*. Garland Publishing Inc., New York, 1991.
- D. M. Brink. *PhD Thesis*. Oxford University, 1955 (unpublished).
- D. M. Brink. *Semi-classical methods in nucleus-nucleus scattering*. Cambridge University Press, Cambridge, 1985.
- D. M. Brink and R. A. Broglia. *Nuclear Superfluidity*. Cambridge University Press, Cambridge, 2005.
- D. M. Brink and G. R. Satchler. *Angular Momentum*. Clarendon Press, 1968.
- R. A. Broglia. Heavy ion reaction, Notes of lectures delivered during the academic years 1974–1976 at SUNY, Stony Brook at Brookhaven National Laboratory, and at Niels Bohr Institute, unpublished. <http://www.mi.infn.it/vigezzi/HIR/HeavyIonReactions.pdf>, 1975.
- R. A. Broglia. Microscopic structure of the intrinsic state of a deformed nucleus. In F. Iachello, editor, *Interacting Bose–Fermi systems in nuclei*, page 95. Plenum Press, New York, 1981.
- R. A. Broglia. Pairing Phase transition in nuclei. In M. Lozano and G. Madurga, editors, *Theory of nuclear structure and reactions*, page 133. World Scientific, Singapore, 1985.

- R. A. Broglia. The surfaces of compact systems: from nuclei to stars. *Surface Science*, 500:759, 2002.
- R. A. Broglia. From phase transitions in finite systems to protein folding and non-conventional drug design. *La Rivista del Nuovo Cimento*, 28(1):1, 2005.
- R. A. Broglia. More is different: 50 Years of Nuclear BCS. In R. A. Broglia and V. Zelevinsky, editors, *50 Years of Nuclear BCS*, page 642. World Scientific, Singapore, 2013.
- R. A. Broglia, editor. *The Finite Quantum Many-Body Problem, Selected papers of Aage Bohr*. World Scientific, Singapore, 2019a.
- R. A. Broglia, editor. *Aage Bohr and the Quantum Finite Many-Body Problem: Selected Papers*. World Scientific, Singapore, 2019b.
- R. A. Broglia and D. R. Bes. High-lying pairing resonances. *Physics Letters B*, 69:129, 1977.
- R. A. Broglia and M. Gallardo. Random phase approximation treatment of the pairing phase transition in strongly rotating nuclei. *Nuclear Physics A*, 447:489, 1986.
- R. A. Broglia and C. Riedel. Pairing vibration and particle-hole states excited in the reaction $^{206}\text{Pb}(\text{t}, \text{p})^{208}\text{Pb}$. *Nucl. Phys.*, 92:145, 1967.
- R. A. Broglia and A. Winther. On the pairing field in nuclei. *Physics Letters B*, 124:11, 1983.
- R. A. Broglia and A. Winther. *Heavy Ion Reactions*. Westview Press, Boulder, CO., 2004.
- R. A. Broglia and V. Zelevinsky. Preface. In R. A. Broglia and V. Zelevinsky, editors, *50 Years of Nuclear BCS*. World Scientific, Singapore, 2013.
- R. A. Broglia, C. Riedel, and B. Sørensen. Two-nucleon transfer and pairing phase transition. *Nuclear Physics A*, 107:1, 1968.
- R. A. Broglia, J. S. Lilley, R. Perazzo, and W. R. Phillips. Coulomb excitation of ^{209}Bi and the weak-coupling model. *Phys. Rev. C*, 1:1508, 1970.
- R. A. Broglia, V. Paar, and D. R. Bes. Diagrammatic perturbation treatment of the effective interaction between two-photon states in closed shell nuclei: The $J^\pi = 0^+$ states in ^{208}Pb . *Physics Letters B*, 37:159, 1971a.
- R. A. Broglia, V. Paar, and D. R. Bes. Effective interaction between $J^\pi = 2^+$ two-phonon states in ^{208}Pb . Evidence of the isovector quadrupole mode. *Physics Letters B*, 37:257, 1971b.

- R. A. Broglia, C. Riedel, and T. Udagawa. Coherence properties of two-neutron transfer reactions and their relation to inelastic scattering. *Nuclear Physics A*, 169:225, 1971c.
- R. A. Broglia, C. Riedel, and T. Udagawa. Sum rules and two-particle units in the analysis of two-neutron transfer reactions. *Nuclear Physics A*, 184:23, 1972.
- R. A. Broglia, O. Hansen, and C. Riedel. Two-neutron transfer reactions and the pairing model. *Advances in Nuclear Physics*, 6:287, 1973. URL www.mi.infn.it/?vigezzi/BHR/BrogliaHansenRiedel.pdf.
- R. A. Broglia, D. R. Bès, and B. S. Nilsson. Strength of the multipole pairing coupling constant. *Physics Letters B*, 50:213, 1974.
- R. A. Broglia, B. R. Mottelson, D. R. Bès, R. Liotta, and H. M. Sofía. Treatment of the spurious state in Nuclear Field Theory. *Physics Letters B*, 64:29, 1976.
- R. A. Broglia, G. Pollarolo, and A. Winther. On the absorptive potential in heavy ion scattering. *Nuclear Physics A*, 361:307, 1981.
- R. A. Broglia, T. Døssing, B. Lauritzen, and B. R. Mottelson. Nuclear rotational damping: Finite-system analogue to motional narrowing in nuclear magnetic resonances. *Phys. Rev. Lett.*, 58:326, 1987.
- R. A. Broglia, J. Terasaki, and N. Giovanardi. The Anderson–Goldstone–Nambu mode in finite and in infinite systems. *Physics Reports*, 335:1, 2000.
- R. A. Broglia, G. Coló, G. Onida, and H. E. Roman. *Solid State Physics of Finite Systems: metal clusters, fullerenes, atomic wires*. Springer Verlag, 2004.
- R. A. Broglia, P. F. Bortignon, F. Barranco, E. Vigezzi, A. Idini, and G. Potel. Unified description of structure and reactions: implementing the Nuclear Field Theory program. *Phys. Scr.*, 91:063012, 2016.
- R. A. Broglia, F. Barranco, A. Idini, G. Potel, and E. Vigezzi. Pygmy resonances: what's in a name? *Phys. Scr.*, 94:114002, 2019a.
- R. A. Broglia, F. Barranco, G. Potel, and E. Vigezzi. One- and two-neutron at the drip line. From ^{11}Be to ^{11}Li and back: ^{10}Li and parity inversion. *Proceedings of the 15th International Conference on Nuclear Reaction Mechanisms*, Editors F. Cerutti, A. Ferrari, T. Kawano, F. Salvat-Pujol, and P. Talou., page 1, 2019b. doi: <http://dx.doi.org/10.23727/CERN-Proceeding-2019-001>.
- B. A. Brown and W. D. M. Rae. In *NuShell @ MSU*. MSU–NSCL report, 2007.
- G. Brown and G. Jacob. Zero-point vibrations and the nuclear surface. *Nuclear Physics*, 42:177 – 182, 1963.

- R. Bruce, J. M. Jowett, S. Gilardoni, A. Drees, W. Fischer, S. Tepikian, and S. R. Klein. Observations of beam losses due to bound-free pair production in a heavy-ion collider. *Phys. Rev. Lett.*, 99:144801, 2007.
- M. Buchanan. Wheat from the chaff. *Nature Physics*, 11:296, 2015.
- C. Bachelet et al. New Binding Energy for the Two-Neutron Halo of ^{11}Li . *Phys. Rev. Lett.*, 100:182501, 2008.
- A. Calci, P. Navrátil, R. Roth, J. Dohet-Eraly, S. Quaglioni, and G. Hupin. Can ab initio theory explain the phenomenon of parity inversion in ^{11}Be ? *Phys. Rev. Lett.*, 117:242501, 2016.
- A. O. Caldeira and A. J. Leggett. Influence of dissipation on quantum tunneling in macroscopic systems. *Phys. Rev. Lett.*, 46:211, 1981.
- A. O. Caldeira and A. J. Leggett. Quantum tunneling in a dissipative system. *Ann. of Phys.*, 149:374, 1983.
- F. Cappuzzello, D. Carbone, M. Cavallaro, M. Bondí, C. Agodi, F. Azaiez, A. Bonaccorso, A. Cunsolo, L. Fortunato, A. Foti, S. Franchoo, E. Khan, R. Linares, J. Lubian, J. A. Scarpaci, and A. Vitturi. Signatures of the Giant Pairing Vibration in the ^{14}C and ^{15}C atomic nuclei. *Nature Communications*, 6:6743, 2015.
- H. B. G. Casimir. Hydrophobicity at Small and Large Length Scales. *Proc. K. Ned. Akad. Wet.*, 60:793, 1948.
- R. F. Casten, E. R. Flynn, J. D. Garrett, O. Hansen, T. J. Mulligan, D. R. Bès, R. A. Broglia, and B. Nilsson. Search for (t, p) transitions to excited 0^+ states in the actinide region. *Physics Letters B*, 40:333, 1972.
- M. Cavallaro, M. De Napoli, F. Cappuzzello, S. E. A. Orrigo, C. Agodi, M. Bondí, D. Carbone, A. Cunsolo, B. Davids, T. Davinson, A. Foti, N. Galinski, R. Kanungo, H. Lenske, C. Ruiz, and A. Sanetullaev. Investigation of the ^{10}Li shell inversion by neutron continuum transfer reaction. *Phys. Rev. Lett.*, 118:012701, 2017.
- M. Cavallaro, F. Cappuzzello, D. Carbone, and C. Agodi. Giant Pairing Vibrations in light nuclei. *The European Physical Journal A*, 55(12):244, 2019.
- E. Chabanat, P. Bonche, P. Haensel, J. Meyer, and R. Schaeffer. A Skyrme parametrization from subnuclear to neutron star densities. *Nuclear Physics A*, 627:710, 1997.
- D. Chandler. Hydrophobicity: Two faces of water. *Nature*, 417:491, 2002.
- D. Chandler. Interfaces and the driving force of hydrophobic assembly. *Nature*, 437:640, 2005.

- R. M. Clark, A. O. Macchiavelli, L. Fortunato, and R. Krücken. Critical-point description of the transition from vibrational to rotational regimes in the pairing phase. *Phys. Rev. Lett.*, 96:032501, 2006.
- W. R. Cobb and D. B. Guthe. Angular distribution of protons from the $^{44}\text{Ca}(d, p)^{45}\text{Ca}$ reaction. *Phys. Rev.*, 107:181, 1957.
- M. H. Cohen, L. M. Falicov, and J. C. Phillips. Superconductive tunneling. *Phys. Rev. Lett.*, 8:316, 1962.
- G. Colò, N. V. Giai, P. F. Bortignon, and M. R. Quaglia. On dipole compression modes in nuclei. *Physics Letters B*, 485:362, 2000.
- L. N. Cooper. Bound Electron Pairs in a Degenerate Fermi Gas. *Phys. Rev.*, 104: 1189, 1956.
- L. N. Cooper. Rememberance of Superconductivity Past, p.3. In L. Cooper and D. Feldman, editors, *BCS: 50 years*. World Scientific, Singapore, 2011.
- J. de Boer. Quantum theory of condensed permanent gases in the law of corresponding states. *Physica*, 14:139, 1948.
- J. de Boer. Quantum Effects and Exchange Effects on the Thermodynamic Properties of Liquid Helium. volume 2 of *Progress in Low Temperature Physics*, page 1. 1957.
- J. de Boer and R. J. Lundbeck. Quantum theory of condensed permanent gases III. The equation of state of liquids. *Physica*, 14:520, 1948.
- R. de Diego, J. M. Arias, J. A. Lay, and A. M. Moro. Continuum-discretized coupled-channels calculations with core excitation. *Phys. Rev. C*, 89:064609, 2014.
- P. G. De Gennes. *Les objets fragiles*. Plon, 1994.
- W. A. de Heer, W. Knight, M. Chou, and M. L. Cohen. Electronic shell structure and metal clusters. volume 40 of *Solid State Physics*, page 93. 1987.
- P. Debye. Van der Waals cohesion forces. *Phys. Z.*, 21:178, 1920.
- P. Debye. Molecular forces and their electrical interpretation. *Phys. Z.*, 22:302, 1921.
- A. Deltuva. Deuteron stripping and pickup involving the halo nuclei ^{11}Be and ^{15}C . *Phys. Rev. C*, 79:054603, 2009.
- A. Deltuva. Faddeev-type calculation of three-body nuclear reactions including core excitation. *Phys. Rev. C*, 88:011601, 2013.

- R. Denton, B. Mühlischlegel, and D. J. Scalapino. Electronic heat capacity and susceptibility of small metal particles. *Phys. Rev. Lett.*, 26:707, 1971.
- S. A. Dickey, J. Kraushaar, R. Ristinen, and M. Rumore. The $^{120}\text{Sn}(p,d)^{119}\text{Sn}$ reaction at 26.3 MeV. *Nuclear Physics A*, 377:137, 1982.
- W. H. Dickhoff and C. Barbieri. Self-consistent Green's function method for nuclei and nuclear matter. *Progress in Particle and Nuclear Physics*, 52:377, 2004.
- W. H. Dickhoff and R. J. Charity. Recent developments for the optical model of nuclei. *Progress in Particle and Nuclear Physics*, 105:252, 2019.
- W. H. Dickhoff and D. Van Neck. *Many-Body Theory Exposed: Propagator description of quantum mechanics in many-body systems*. World Scientific, Singapore, 2005.
- W. H. Dickhoff, R. J. Charity, and M. H. Mahzoon. Novel applications of the dispersive optical model. *Journal of Physics G: Nuclear and Particle Physics*, 44:033001, 2017.
- P. A. M. Dirac. The fundamental equations of quantum mechanics. *Proc. Roy. Soc. A*, 109(752):642, 1925.
- P. A. M. Dirac. The quantum theory of the electron. *Proceedings of the Royal Society of London. Series A, Containing Papers of a Mathematical and Physical Character*, 117(778):610, 1928a.
- P. A. M. Dirac. The quantum theory of the electron. Part II. *Proceedings of the Royal Society of London. Series A, Containing Papers of a Mathematical and Physical Character*, 118(779):351, 1928b.
- P. A. M. Dirac. *The principles of quantum mechanics*. Oxford University Press, London, 1930.
- F. Dönau, K. Hehl, C. Riedel, R. A. Broglia, and P. Federman. Two-nucleon transfer reaction on oxygen and the nuclear coexistence model. *Nucl. Phys. A*, 101:495, 1967.
- F. Dönau, D. Almehed, and R. G. Nazmitdinov. Integral representation of the random-phase approximation correlation energy. *Phys. Rev. Lett.*, 83:280, 1999.
- T. Duguet and G. Hagen. *Ab initio* approach to effective single-particle energies in doubly closed shell nuclei. *Phys. Rev. C*, 85:034330, 2012.
- G. G. Dussel, R. I. Betan, R. J. Liotta, and T. Vertse. Collective excitations in the continuum. *Phys. Rev. C*, 80:064311.
- F. Dyson. *Origins of life*. Cambridge University Press, Cambridge, 1999.

- F. J. Dyson. The radiation theories of Tomonaga, Schwinger, and Feynman. *Physical Review*, 75:486, 1949.
- J.-P. Ebran, E. Khan, T. Nikšić, and D. Vretenar. How atomic nuclei cluster. *Nature*, 487:341, 2012.
- J.-P. Ebran, E. Khan, T. Nikšić, and D. Vretenar. Localization and clustering in the nuclear fermi liquid. *Phys. Rev. C*, 87:044307, 2013.
- J.-P. Ebran, E. Khan, T. Nikšić, and D. Vretenar. Cluster-liquid transition in finite, saturated fermionic systems. *Phys. Rev. C*, 89:031303, 2014a.
- J.-P. Ebran, E. Khan, T. Nikšić, and D. Vretenar. Density Functional Theory studies of cluster states in nuclei. *Phys. Rev. C*, 90:054329, 2014b.
- A. R. Edmonds. *Angular momentum in quantum mechanics*. Princeton University Press, Princeton, 1960.
- J. L. Egido. Projection Methods, Variational Diagonalization of the Pairing Hamiltonian and Restoration of Rotational and Gauge Invariance. In R. A. Broglia and V. Zelevinski, editors, *50 Years of Nuclear BCS*, page 553. World Scientific, Singapore, 2013.
- W. Elsasser. Sur le principe de Pauli dans les noyaux. *J. Phys. Radium*, 4:549, 1933.
- H. Esbensen and G. F. Bertsch. Nuclear surface fluctuations: Charge density. *Phys. Rev. C*, 28:355, 1983.
- P. Federman and I. Talmi. Coexistence of shell model and deformed states in oxygen isotopes. *Physics Letters*, 19:490, 1965.
- P. Federman and I. Talmi. Nuclear energy levels of Calcium isotopes. *Physics Letters*, 22:469, 1966.
- J. P. Fernández-García, M. A. G. Alvarez, A. M. Moro, and M. Rodríguez-Gallardo. Simultaneous analysis of elastic scattering and transfer/breakup channels for the ${}^6\text{He} + {}^{208}\text{Pb}$ reaction at energies near the Coulomb barrier. *Phys.Lett.*, B693:310, 2010a.
- J. P. Fernández-García, M. Rodríguez-Gallardo, M. A. G. Alvarez, and A. M. Moro. Long range effects on the optical model of ${}^6\text{He}$ around the Coulomb barrier. *Nuclear Physics A*, 840:19, 2010b.
- L. Ferreira, R. Liotta, C. H. Dasso, R. A. Broglia, and A. Winther. Spatial correlations of pairing collective states. *Nuclear Physics A*, 426:276, 1984.
- H. Feshbach. Unified Theory of Nuclear Reactions. *Annals of Physics*, 5:357, 1958.

- H. Feshbach. A Unified Theory of Nuclear Reactions,II. *Annals of Physics*, 19: 287, 1962.
- H. Feshbach. *Theoretical nuclear physics: Nuclear Reactions*. Wiley & Sons, New York, 1992.
- R. P. Feynman. Space-time approach to quantum electrodynamics. *Phys. Rev.*, 76: 769, Sep 1949.
- R. P. Feynman. *Theory of fundamental processes*. Benjamin, Reading, Mass., 1975.
- R. P. Feynman. *QED: The strange theory of light and matter*. Princeton University Press, 2006.
- E. R. Flynn, G. Igo, P. D. Barnes, D. Kovar, D. R. Bès, and R. A. Broglia. Effect of multipole pairing particle-hole fields in the particle-vibration coupling of ^{209}Pb (II). The $^{207}\text{Pb}(t, p)^{209}\text{Pb}$ reaction at 20 MeV. *Phys. Rev. C*, 3:2371, 1971.
- E. R. Flynn, G. J. Igo, and R. A. Broglia. Three-phonon monopole and quadrupole pairing vibrational states in ^{206}Pb . *Phys. Lett. B*, 41:397, 1972a.
- E. R. Flynn, G. J. Igo, R. A. Broglia, S. Landowne, V. Paar, and B. Nilsson. An experimental and theoretical investigation of the structure of ^{210}Pb . *Nuclear Physics A*, 195:97, 1972b.
- S. Fortier, S. Pita, J. Winfield, W. Catford, N. Orr, J. V. de Wiele, Y. Blumenfeld, R. Chapman, S. Chappell, N. Clarke, N. Curtis, M. Freer, S. Gals, K. Jones, H. Langevin-Joliot, H. Laurent, I. Lhenry, J. Maison, P. Roussel-Chomaz, M. Shawcross, M. Smith, K. Spohr, T. Suomijarvi, and A. de Vismes. Core excitation in $^{11}\text{Be}_{gs}$ via the $p(^{11}\text{Be}, ^{10}\text{Be})d$ reaction. *Physics Letters B*, 461: 22, 1999.
- H. T. Fortune, G.-B. Liu, and D. E. Alburger. $(sd)^2$ states in ^{12}Be . *Phys. Rev. C*, 50:1355, 1994.
- K. Fossez, W. Nazarewicz, Y. Jaganathan, N. Michel, and M. Płoszajczak. Nuclear rotation in the continuum. *Phys. Rev. C*, 93:011305, 2016.
- S. Frauendorf. Pairing at high spin. In R. A. Broglia and V. Zelevinski, editors, *50 Years of Nuclear BCS*, page 536. World Scientific, Singapore, 2013.
- H. Fröhlich. Interaction of electrons with lattice vibrations. *Proc. Royal Soc.*, 215:291, 1952.
- R. J. Furnstahl and A. Schwenk. How should one formulate, extract and interpret 'non-observables' for nuclei? *Journal of Physics G*, 37:064005, 2010.

- J. D. Garrett. The “single-particle” spectrum of states: correlated or uncorrelated? In R. A. Broglia, G. B. Hagemann, and B. Herskind, editors, *Nuclear Structure 1985*, page 111, Amsterdam, 1985. North Holland.
- J. D. Garrett, G. B. Hagemann, and B. Herskind. Recent nuclear structure studies in rapidly rotating nuclei. *Annual Review of Nuclear and Particle Science*, 36: 419, 1986.
- I. Giaver. Electron tunneling and superconductivity. In P. Norstedt and Söner, editors, *Le Prix Nobel en 1973*, page 84. 1973.
- V. L. Ginzburg. Nobel lecture: On superconductivity and superfluidity (what i have and have not managed to do) as well as on the “physical minimum” at the beginning of the xxi century. *Rev. Mod. Phys.*, 76:981, 2004.
- V. L. Ginzburg and L. D. Landau. On the theory of superconductivity. *JETP*, 20: 1064, 1950.
- R. J. Glauber. Coherence and Quantum Optics. In R. J. Glauber, editor, *International School of Physics “Enrico Fermi” Course XLII on Quantum Optics*, page 15. New York, Academic Press, 1969.
- R. J. Glauber. *Quantum theory of optical coherence*. Wiley, Weinheim, 2007.
- N. K. Glendenning. Nuclear Spectroscopy with Two–Nucleon Transfer Reactions. *Phys. Rev.*, 137:B102, 1965.
- N. K. Glendenning. *Direct nuclear reactions*. World Scientific, Singapore, 2004.
- D. Gogny. Lecture notes in physics, vol. 108. In H. Arenhövd and D. Drechsel, editors, *Nuclear Physics with Electromagnetic Interactions*, p.88, page 55. Springer Verlag, Heidelberg, 1978.
- G. Gori, F. Barranco, E. Vigezzi, and R. A. Broglia. Parity inversion and breakdown of shell closure in Be isotopes. *Phys. Rev. C*, 69:041302, 2004.
- L. P. Gor’kov. About the energy spectrum of superconductors. *Soviet Phys. JETP*, 7:505, 1958.
- L. P. Gor’kov. Microscopic derivation of the Ginzburg–Landau equations in the theory of superconductivity. *Soviet Phys. JETP*, 9:1364, 1959.
- L. P. Gor’kov. Theory of superconductivity: from phenomenology to microscopic theory. In H. Rogallia and P. H. Kes, editors, *100 years of Superconductivity*, page 72. CRC Press, Florida, 2012.
- W. Greiner. *Quantum Mechanics*. Springer, Berlin, 1998.
- H. Grotch. Status of the theory of the hydrogen Lamb shift. *Foundations of physics*, 24(2):249, 1994.

- P. Guazzoni, M. Jaskola, L. Zetta, A. Covello, A. Gargano, Y. Eisermann, G. Graw, R. Hertenberger, A. Metz, F. Nuoffer, and G. Staudt. Level structure of ^{120}Sn : High resolution (p, t) reaction and shell model description. *Phys. Rev. C*, 60: 054603, 1999.
- P. Guazzoni, L. Zetta, A. Covello, A. Gargano, G. Graw, R. Hertenberger, H.-F. Wirth, and M. Jaskola. High-resolution study of the ^{116}Sn (p, t) reaction and shell model structure of ^{114}Sn . *Phys. Rev. C*, 69:024619, 2004.
- P. Guazzoni, L. Zetta, A. Covello, A. Gargano, B. F. Bayman, G. Graw, R. Hertenberger, H.-F. Wirth, and M. Jaskola. Spectroscopy of ^{110}Sn via the high-resolution $^{112}\text{Sn}(p, t)$ ^{110}Sn reaction. *Phys. Rev. C*, 74:054605, 2006.
- P. Guazzoni, L. Zetta, A. Covello, A. Gargano, B. F. Bayman, T. Faestermann, G. Graw, R. Hertenberger, H.-F. Wirth, and M. Jaskola. ^{118}Sn levels studied by the $^{120}\text{Sn}(p, t)$ reaction: High-resolution measurements, shell model, and distorted-wave Born approximation calculations. *Phys. Rev. C*, 78:064608, 2008.
- P. Guazzoni, L. Zetta, A. Covello, A. Gargano, B. F. Bayman, T. Faestermann, G. Graw, R. Hertenberger, H.-F. Wirth, and M. Jaskola. High-resolution measurement of the $^{118,124}\text{Sn}(p,t)$ $^{116,122}\text{Sn}$ reactions: Shell-model and microscopic distorted-wave Born approximation calculations. *Phys. Rev. C*, 83:044614, 2011.
- P. Guazzoni, L. Zetta, A. Covello, A. Gargano, B. F. Bayman, G. Graw, R. Hertenberger, H. F. Wirth, T. Faestermann, and M. Jaskola. High resolution spectroscopy of ^{112}Sn through the $^{114}\text{Sn}(p, t)$ ^{112}Sn reaction. *Phys. Rev. C*, 85:054609, 2012.
- O. Gunnarsson. *Alkali-doped Fullerides: Narrow-band Solids with Unusual Properties*. World Scientific, Singapore, 2004.
- K. Hamacher. Temperature dependence of fluctuations in HIV-1-protease. *European Biophysics Journal*, 39(7):1051, 2010.
- I. Hamamoto. Single-particle components of particle-vibrational states in the nuclei ^{209}Pb , ^{209}Bi , ^{207}Pb and ^{207}Tl . *Nuclear Physics A*, 141:1, 1970.
- I. Hamamoto and B. R. Mottelson. Pair correlation in neutron drip line nuclei. *Phys. Rev. C*, 68:034312, 2003.
- I. Hamamoto and B. R. Mottelson. Weakly bound $s_{1/2}$ neutrons in the many-body pair correlation of neutron drip line nuclei. *Phys. Rev. C*, 69:064302, 2004.
- I. Hamamoto and S. Shimoura. Properties of ^{12}Be and ^{11}Be in terms of single-particle motion in deformed potential. *Journal of Physics G: Nuclear and Particle Physics*, 34:2715, 2007.

- Y. Han, Y. Shi, and Q. Shen. Deuteron global optical model potential for energies up to 200 MeV. *Phys. Rev. C*, 74:044615, 2006.
- O. Hansen. Experimental establishment of the nuclear pairing phases. In R. A. Broglia and V. Zelevinsky, editors, *50 Years of Nuclear BCS*, page 449. World Scientific, Singapore, 2013.
- O. Haxel, J. H. D. Jensen, and H. E. Suess. On the “Magic Numbers” in nuclear structure. *Phys. Rev.*, 75:1766, 1949.
- P. H. Heenen, V. Hellemans, and R. V. F. Janssens. Pairing correlations at superdeformation. In R. A. Broglia and V. Zelevinski, editors, *50 Years of Nuclear BCS*, page 579. World Scientific, Singapore, 2013.
- W. Heisenberg. Über quantentheoretische umdeutung kinematischer und mechanischer beziehungen. *Z. Phys.*, 33:879, 1925.
- W. Heisenberg. Über der anschaulichen inhalt der quantentheoretischen kinematik und mechanik. *Z. Phys.*, 43:172, 1927.
- W. Heisenberg. *The physical principles of quantum theory*. Dover, New York, 1949.
- V. Hellemans, A. Pastore, T. Duguet, K. Bennaceur, D. Davesne, J. Meyer, M. Bender, and P.-H. Heenen. Spurious finite-size instabilities in nuclear energy density functionals. *Phys. Rev. C*, 88:064323, 2013.
- H. Hergert and R. Roth. Pairing in the framework of the unitary correlation operator method (UCOM): Hartree-Fock-Bogoliubov calculations. *Phys. Rev. C*, 80: 024312, 2009.
- J. Högaasen-Feldman. A study of some approximations of the pairing force. *Nuclear Physics*, 28:258, 1961.
- B. R. Holstein. *Weak interaction in nuclei*. Princeton University Press, New Jersey, 1989.
- K. Huang. *Statistical Physics and Protein Folding*. World Scientific, Singapore, 2005.
- R. Id Betan, R. J. Liotta, N. Sandulescu, and T. Vertse. Two-particle resonant states in a many-body mean field. *Phys. Rev. Lett.*, 89:042501, Jul 2002.
- A. Idini. Renormalization effects in nuclei. *Ph.D. thesis, University of Milan* <http://air.unimi.it/2434/216315>, 2013.
- A. Idini, F. Barranco, and E. Vigezzi. Quasiparticle renormalization and pairing correlations in spherical superfluid nuclei. *Phys. Rev. C*, 85:014331, 2012.

- A. Idini, G. Potel, F. Barranco, E. Vigezzi, and R. A. Broglia. Dual origin of pairing in nuclei. *Physics of Atomic Nuclei*, 79:807, 2014.
- A. Idini, G. Potel, F. Barranco, E. Vigezzi, and R. A. Broglia. Interweaving of elementary modes of excitation in superfluid nuclei through particle-vibration coupling: Quantitative account of the variety of nuclear structure observables. *Phys. Rev. C*, 92:031304, 2015.
- K. Ieki, D. Sackett, A. Galonsky, C. A. Bertulani, J. J. Kruse, W. G. Lynch, D. J. Morrissey, N. A. Orr, H. Schulz, B. M. Sherrill, A. Sustich, J. A. Winger, F. Deák, A. Horváth, A. Kiss, Z. Seres, J. J. Kolata, R. E. Warner, and D. L. Humphrey. Coulomb dissociation of ^{11}Li . *Phys. Rev. Lett.*, 70:730, 1993.
- M. Igarashi, K. Kubo, and K. Yagi. Two-nucleon transfer mechanisms. *Phys. Rep.*, 199:1, 1991.
- J. N. Israelachvili. *Intermolecular and surface forces*. Academic Press, New York, 1985.
- H. Iwasaki, T. Motobayashi, H. Akiyoshi, Y. Ando, N. Fukuda, H. Fujiwara, Z. Flp, K. Hahn, Y. Higurashi, M. Hirai, I. Hisanaga, N. Iwasa, T. Kijima, T. Mine-mura, T. Nakamura, M. Notani, S. Ozawa, H. Sakurai, S. Shimoura, S. Takeuchi, T. Teranishi, Y. Yanagisawa, and M. Ishihara. Quadrupole deformation of ^{12}Be studied by proton inelastic scattering. *Physics Letters B*, 481:7, 2000.
- D. F. Jackson. *Nuclear reactions*. Methuen, London, 1970.
- B. Jenning. Non observability of spectroscopic factors. *arXiv: 1102.3721ve [nucl-th]*, 2011.
- H. Jeppesen, F. Ames, U. C. Bergmann, M. J. G. Borge, J. Cederkäll, S. Emhofer, L. M. Fraile, H. O. U. Fynbo, S. Henry, H. T. Johansson, B. Jonson, M. Meister, T. Nilsson, G. Nyman, M. Pantea, K. Riisager, A. Richter, K. Rudolph, G. Schrieder, T. Siebert, O. Tengblad, E. Tengborn, M. Turrión, R. von Hahn, F. Wenander, and B. Wolf. Experimental investigation of the $^9\text{Li}+\text{d}$ reaction at REX-ISOLDE. *Nuclear Physics A*, 738:511, 2004.
- H. Jeppesen, A. Moro, U. Bergmann, M. Borge, J. Cederkäll, L. Fraile, H. Fynbo, J. Gómez-Camacho, H. Johansson, B. Jonson, M. Meister, T. Nilsson, G. Nyman, M. Pantea, K. Riisager, A. Richter, G. Schrieder, T. Sieber, O. Tengblad, E. Tengborn, M. Turrión, and F. Wenander. Study of ^{10}Li via the $^9\text{Li}(^2\text{H}, p)$ reaction at REX-ISOLDE. *Physics Letters B*, 642:449, 2006.
- J. Jeukenne, A. Lejeune, and C. Mahaux. Many-body theory of nuclear matter. *Physics Reports*, 25(2):83, 1976.
- J. G. Johansen, V. Bildstein, M. J. G. Borge, M. Cubero, J. Diriken, J. Elseviers, L. M. Fraile, H. O. U. Fynbo, L. P. Gaffney, R. Gernhäuser, B. Jonson, G. T.

- Koldste, J. Konki, T. Kröll, R. Krücken, D. Mücher, T. Nilsson, K. Nowak, J. Pakarinen, V. Pesudo, R. Raabe, K. Riisager, M. Seidlitz, O. Tengblad, H. Törnqvist, D. Voulot, N. Warr, F. Wenander, K. Wimmer, and H. De Witte. Experimental study of bound states in ^{12}Be through low-energy $^{11}\text{Be}(d, p)$ -transfer reactions. *Phys. Rev. C*, 88:044619, 2013.
- A. Johnson, H. Ryde, and S. A. Hjorth. Nuclear moment of inertia at high rotational frequencies. *Nuclear Physics A*, 179:753, 1972.
- B. D. Josephson. Possible new effects in superconductive tunnelling. *Phys. Lett.*, 1, 1962.
- A. M. Kadin. Spatial Structure of the Cooper Pair. *Journal of Superconductivity and Novel Magnetism*, 20:285, 2007.
- Y. Kanada-En'yo and H. Horiuchi. Structure of excited states of ^{11}Be studied with antisymmetrized molecular dynamics. *Phys. Rev. C*, 66:024305, 2002.
- R. Kanungo, A. Sanetullaev, J. Tanaka, S. Ishimoto, G. Hagen, T. Myo, T. Suzuki, C. Andreoiu, P. Bender, A. A. Chen, B. Davids, J. Fallis, J. P. Fortin, N. Galinski, A. T. Gallant, P. E. Garrett, G. Hackman, B. Hadinia, G. Jansen, M. Keefe, R. Krücken, J. Lighthall, E. McNeice, D. Miller, T. Otsuka, J. Purcell, J. S. Randhawa, T. Roger, A. Rojas, H. Savajols, A. Shotter, I. Tanihata, I. J. Thompson, C. Unsworth, P. Voss, and Z. Wang. Evidence of soft dipole resonance in ^{11}Li with isoscalar character. *Phys. Rev. Lett.*, 114:192502, 2015.
- N. Keeley, N. Alamanos, and V. Lapoux. Comprehensive analysis method for (d, p) stripping reactions. *Phys. Rev. C*, 69:064604, 2004.
- N. Keeley, R. Raabe, N. Alamanos, and J.-L. Sida. Fusion and direct reactions of halo nuclei at energies around the Coulomb barrier. *Prog. Nucl. Part. Phys.*, 59: 579, 2007.
- J. B. Ketterson and S. N. Song. *Superconductivity*. Cambridge University Press, Cambridge, 1999.
- E. Khan, N. Sandulescu, N. V. Giai, and M. Grasso. Two-neutron transfer in nuclei close to the drip line. *Physical Review C*, 69:014314, 2004.
- D. T. Khoa and W. von Oertzen. Di-neutron elastic transfer in the $^4\text{He}(^6\text{He}, ^6\text{He})^4\text{He}$ reaction. *Physics Letters B*, 595:193, 2004.
- V. A. Khodel, A. P. Platonov, and E. E. Saperstein. On the $^{40}\text{Ca}-^{48}\text{Ca}$ isotope shift. *Journal of Physics G: Nuclear Physics*, 8:967, jul 1982.
- T. Kinoshita, editor. *Quantum electrodynamics*. World Scientific, Singapore, 1990.
- L. S. Kisslinger and R. A. Sorensen. Spherical nuclei with simple residual forces. *Review of Modern Physics*, 35:853, 1963.

- C. Kittel. *Introduction to solid state physics*. Wiley, NJ, 1996.
- T. Kobayashi, S. Shimoura, I. Tanihata, K. Katori, K. Matsuta, T. Minamisono, K. Sugimoto, W. Mller, D. L. Olson, T. J. M. Symons, and H. Wieman. Electromagnetic dissociation and soft giant dipole resonance of the neutron-dripline nucleus ^{11}Li . *Physics Letters B*, 232:51, 1989.
- A. J. Koning and J. P. Delaroche. Local and global nucleon optical models from 1 keV to 200 MeV. *Nucl. Phys. A*, 713:231, 2003.
- G. J. Kramer, H. P. Blok, and L. Lapikás. A consistence analisys of $(e, e' p)$ and $(d, ^3\text{He})$ experiments. *Nucl. Phys. A*, 679:267, 2001.
- A. Krieger, K. Blaum, M. L. Bissell, N. Frömmgen, C. Geppert, M. Hammen, K. Kreim, M. Kowalska, J. Krämer, T. Neff, R. Neugart, G. Neyens, W. Nörterhäuser, C. Novotny, R. Sánchez, and D. T. Yordanov. Nuclear charge radius of ^{12}Be . *Phys. Rev. Lett.*, 108:142501, 2012.
- N. M. Kroll and W. E. Lamb. On the self-energy of a bound electron. *Phys. Rev.*, 75:388, 1949.
- K. Kubo, R. A. Broglia, and T. Riedel, C. Udagawa. Determination of the Y_4 deformation parameter from (p, t) reactions. *Phys. Lett. B*, 32:29, 1970.
- R. Kubo. Electronic Properties of Metallic Fine Particles. I. *Journal of the Physical Society of Japan*, 17:975, 1962.
- R. Kubo. Electrons in small metallic particles. *Comments Solid State Phys.*, 1:61, 1968.
- E. Kwan, C. Wu, N. Summers, G. Hackman, T. Drake, C. Andreoiu, R. Ashley, G. Ball, P. Bender, A. Boston, H. Boston, A. Chester, A. Close, D. Cline, D. Cross, R. Dunlop, A. Finlay, A. Garnsworthy, A. Hayes, A. Laffoley, T. Nano, P. Navrtil, C. Pearson, J. Pore, S. Quaglioni, C. Svensson, K. Starosta, I. Thompson, P. Voss, S. Williams, and Z. Wang. Precision measurement of the electromagnetic dipole strengths in ^{11}Be . *Physics Letters B*, 732:210, 2014.
- W. E. Lamb Jr. Fine structure of the hydrogen atom. In *Nobel Lecture Physics 1942-1962*, page 286. Elsevier, Amsterdan, 1964.
- W. E. Lamb Jr and R. C. Retherford. Fine structure of the hydrogen atom by a microwave method. *Phys. Rev.*, 72:241, 1947.
- L. Landau. The theory of superfluidity in ^2He . *Journ. Phys. USSR*, 5:71, 1941.
- L. Landau. On analytic properties of vertex parts in quantum field theory. *Nuclear Physics*, 13:181, 1959.

- L. Landau and L. Lifshitz. *Quantum Mechanics, 3rd ed.* Pergamon Press, London, 1965.
- W. A. Lanford. Systematics of two-neutron-transfer cross sections near closed shells: A sum-rule analysis of (p, t) strengths on the lead isotopes. *Phys. Rev. C*, 16:988, 1977.
- W. A. Lanford and J. B. McGrory. Two-neutron pickup strengths on the even lead isotopes: the transition from single-particle to “collective”. *Physics Letters B*, 45:238, 1973.
- M. Laskin, R. F. Casten, A. O. Macchiavelli, R. M. Clark, and D. Bucurescu. Population of the giant pairing vibration. *Phys. Rev. C*, 93:034321, 2016.
- B. Lauritzen, A. Anselmino, P. F. Bortignon, and R. A. Broglia. Pairing phase transition in small particles. *Annals of Physics*, 223:216, 1993.
- J. A. Lay, A. M. Moro, J. M. Arias, and Y. Kanada-En’yo. Semi-microscopic folding model for the description of two-body halo nuclei. *Phys. Rev. C*, 89: 014333, 2014.
- J. Le Tourneau. Effect of the Dipole-Quadrupole interaction on the width and structure of the Giant Dipole Line in spherical nuclei. *Mat. Fys. Medd. Dan. Vid. Selsk.*, 34, no. 11, 1965.
- A. J. Leggett. *The problems of Physics*. Oxford University Press, Oxford, 1987.
- A. J. Leggett. *Quantum Liquids*. Oxford University Press, Oxford, 2006.
- T. Lesinski, K. Hebeler, T. Duguet, and A. Schwenk. Chiral three-nucleon forces and pairing in nuclei. *Journal of Physics G: Nuclear and Particle Physics*, 39: 015108, 2012.
- F. A. Lindemann. The calculation of molecular vibration frequencies. *Physik. Z.*, 11:609, 1910.
- J. Lindhard. On the properties of a gas of charged particles. *Kgl. Danske Videnskab. Selskab, Mat. Fys. Medd.*, 28, no. 8, 1954.
- E. Lippmann. *Modern Many-Particle Physics: Atomic gases, Quantum Dots and Quantum Fluids*,. World Scientific, Singapore, 2003.
- E. Litvinova and H. Wibowo. Finite-temperature relativistic nuclear field theory: An application to the dipole response. *Phys. Rev. Lett.*, 121:082501, Aug 2018.
- U. Lombardo, H. J. Schulze, and W. Zuo. Induced Pairing Interaction in Neutron Star Matter. In R. A. Broglia and V. Zelevinsky, editors, *50 Years of Nuclear BCS*, page 338. World Scientific, Singapore, 2013.

- F. London. Zur Theorie der Systematik der Molekularkräfte. *Z. f. Physik*, 63:245, 1930.
- F. London. The general theory of molecular forces, Trans. *Faraday Soc.*, 33:8, 1937.
- P. Lotti, F. Cazzola, P. F. Bortignon, R. A. Broglia, and A. Vitturi. Spatial correlation of pairing modes in nuclei at finite temperature. *Phys. Rev. C*, 40:1791, 1989.
- H. Löwen. Melting, freezing and colloidal suspensions. *Phys. Rep.*, 237:249, 1994.
- K. Lum, D. Chandler, and J. D. Weeks. Hydrophobicity at Small and Large Length Scales. *The Journal of Physical Chemistry B*, 103:4570, 1999.
- S. R. Lundeen and F. M. Pipkin. Measurement of the Lamb Shift in Hydrogen, $n = 2$. *Phys. Rev. Lett.*, 46:232, 1981.
- S. R. Lundeen and F. M. Pipkin. Separated oscillatory field measurement of the Lamb shift in H, $n= 2$. *Metrologia*, 22:9, 1986.
- J. E. Lynn. *Theory of neutron resonance reactions*. Oxford University Press, Oxford, 1968.
- R. Machleidt, F. Sammarruca, and Y. Song. Nonlocal nature of the nuclear force and its impact on nuclear structure. *Phys. Rev. C*, 53:R1483, 1996.
- P. Magierski, K. Sekizawa, and G. Włazłowski. Novel role of superfluidity in low-energy nuclear reactions. *Phys. Rev. Lett.*, 119:042501, 2017.
- C. Mahaux, P. F. Bortignon, R. A. Broglia, and C. H. Dasso. Dynamics of the shell model. *Physics Reports*, 120:1–274, 1985.
- T. P. Martin, U. Näher, and H. Schaber. Metal clusters as giant atomic nuclei. In R. A. Broglia and J. R. Schrieffer, editors, *International School of Physics “Enrico Fermi” Course CXXI, Perspectives in many-particle physics*, page 139. North Holland, Amsterdam, 1994.
- M. Matsuo. Spatial structure of neutron Cooper pair in low density uniform matter. *Phys. Rev. C*, 73:044309, 2006.
- M. Matsuo. Spatial Structure of Cooper Pairs in Nuclei. In R. A. Broglia and V. Zelevinsky, editors, *50 Years of Nuclear BCS*, page 66. World Scientific, Singapore, 2013.
- M. G. Mayer. On closed shells in nuclei. *Phys. Rev.*, 74:235, 1948.
- M. G. Mayer. On closed shells in nuclei. II. *Phys. Rev.*, 75:1969, 1949.

- M. G. Mayer and J. Jensen. *Elementary Theory of Nuclear Structure*. Wiley, New York, NY, 1955.
- M. G. Mayer and E. Teller. On the origin of elements. *Phys. Rev.*, 76:1226, 1949.
- D. G. McDonald. The nobel laureate versus the graduate student. *Physics Today*, page 46, July 2001.
- M. H. McFarlane. The reaction matrix in nuclear shell theory. In M. Jean and R. A. Ricci, editors, *Proceedings of the International school of physics “E. Fermi” Course XL Nuclear Structure and Nuclear Reactions*, page 457. Academic Press, New York, 1969.
- J. Mehra. *The beat of a different drum*. Clarendon Press, Oxford, 1996.
- L. Meitner and O. R. Frisch. Products of the fission of the uranium nucleus. *Nature*, 143:239, 1939.
- C. Micheletti, J. R. Banavar, and A. Maritan. Conformations of proteins in equilibrium. *Physical Review Letters*, 87:088102, 2001.
- C. Micheletti, F. Cecconi, A. Flammini, and A. Maritan. Crucial stages of protein folding through a solvable model: Predicting target sites for enzyme-inhibiting drugs. *Protein science*, 11:1878, 2002.
- C. Micheletti, P. Carloni, and A. Maritan. Accurate and efficient description of protein vibrational dynamics: comparing molecular dynamics and gaussian models. *Proteins: Structure, Function, and Bioinformatics*, 55:635, 2004.
- A. Migdal. Interaction between electrons and lattice vibrations in a normal metal. *Soviet Physics JETP*, 7:996, 1958.
- A. Mitra, A. Kraft, P. Wright, B. Acland, A. Z. Snyder, Z. Rosenthal, L. Czerniewski, A. Bauer, L. Snyder, J. Culver, et al. Spontaneous infra-slow brain activity has unique spatiotemporal dynamics and laminar structure. *Neuron*, 98: 297, 2018.
- P. Møller, J. R. Nix, W. D. Myers, and W. J. Swiatecki. Nuclear Ground-State Masses and Deformations. *Atomic Data and Nuclear Data Tables*, 59:185, 1995.
- J. Monod. *Le hasard et la nécessité*. Editions du seuil, Paris, 1970.
- D. Montanari, L. Corradi, S. Szilner, G. Pollaro, E. Fioretto, G. Montagnoli, F. Scarlassara, A. M. Stefanini, S. Courtin, A. Goasduff, F. Haas, D. Jelavić Malenica, C. Michelagnoli, T. Mijatović, N. Soić, C. A. Ur, and M. Varga Pajtler. Neutron Pair Transfer in $^{60}\text{Ni} + ^{116}\text{Sn}$ Far below the Coulomb Barrier. *Phys. Rev. Lett.*, 113:052501, 2014.

- A. Moro, J. Casal, and M. Gómez-Ramos. Investigating the ^{10}Li continuum through $^9\text{Li}(d, p)^{10}\text{Li}$ reactions. *Physics Letters B*, 793:13 – 18, 2019.
- M. Moshinsky. Transformation brackets for harmonic oscillator functions. *Nucl. Phys.*, 13:104, 1959.
- B. Mottelson. Elementary features of nuclear structure. In H. Nifenecker, J. P. Blaizot, G. F. Bertsch, W. Weise, and F. David, editors, *Trends in Nuclear Physics, 100 years later, Les Houches, Session LXVI*, page 25. Elsevier, Amsterdam, 1998.
- B. R. Mottelson. Selected topics in the theory of collective phenomena in nuclei. In G. Racah, editor, *International School of Physics “Enrico Fermi” Course XV, Nuclear Spectroscopy*, page 44. Academic Press, New York, 1962.
- B. R. Mottelson. *Elementary Modes of Excitation in Nuclei, Le Prix Nobel en 1975*, page 80. Imprimerie Royale Norstedts Tryckeri, Stockholm, 1976.
- B. R. Mottelson and S. G. Nilsson. The intrinsic states of odd-A nuclei having ellipsoidal equilibrium shape. *Kgl. Danske Videnskab, Selskab. Mat.-fys. Skrifter*, 1, no 8, 1959.
- B. Mouginot, E. Khan, R. Neveling, F. Azaiez, E. Z. Buthelezi, S. V. Förtsch, S. Franchoo, H. Fujita, J. Mabiala, J. P. Mira, P. Papka, A. Ramus, J. A. Scarpaci, F. D. Smit, I. Stefan, J. A. Swartz, and I. Usman. Search for the giant pairing vibration through (p,t) reactions around 50 and 60 MeV. *Phys. Rev. C*, 83: 037302, 2011.
- B. Mühlischlegel, D. J. Scalapino, and R. Denton. Thermodynamic properties of small superconducting particles. *Phys. Rev. B*, 6:1767, 1972.
- Y. Nambu. Quasi-particles and gauge invariance in the theory of superconductivity. *Physical Review*, 117:648, 1960.
- Y. Nambu. Dynamical symmetry breaking. In T. Eguchi and K. Nishigama, editors, *Broken Symmetry, Selected papers of Y. Nambu (1995)*, page 436. World Scientific, Singapore, 1991.
- O. Nathan and S. G. Nilsson. Collective nuclear motion and the unified model. In K. Siegbahn, editor, *Alpha- Beta- and Gamma-Ray Spectroscopy, Vol 1*, page 601. North Holland Publishing Company, Amsterdam, 1965.
- S. G. Nilsson. Binding states of individual nucleons in strongly deformed nuclei. *Mat. Fys. Medd. Dan. Vid. Selsk.*, 29, 1955.
- P. J. Nolan and P. J. Twin. Superdeformed shapes at high angular momentum. *Annual Review of Nuclear and Particle Science*, 38:533, 1988.

- W. Nörtershäuser, D. Tiedemann, M. Žáková, Z. Andjelkovic, K. Blaum, M. L. Bissell, R. Cazan, G. W. F. Drake, C. Geppert, M. Kowalska, J. Krämer, A. Krieger, R. Neugart, R. Sánchez, F. Schmidt-Kaler, Z.-C. Yan, D. T. Yordanov, and C. Zimmermann. Nuclear charge radii of $^{7,9,10}\text{Be}$ and the one-neutron halo nucleus ^{11}Be . *Phys. Rev. Lett.*, 102:062503, 2009.
- L. Nosanow. On the possible superfluidity of ^6He —Its phase diagram and those of ^6He - ^4He and ^6He - ^3He mixtures. *Journal of Low Temperature Physics*, 23:605, 1976.
- F. Nunes, I. Thompson, and R. Johnson. Core excitation in one neutron halo systems. *Nuclear Physics A*, 596:171, 1996.
- S. E. A. Orrigo and H. Lenske. Pairing resonances and the continuum spectroscopy of ^{10}Li . *Phys. Lett. B*, 677:214, 2009.
- T. Otsuka, N. Fukunishi, and H. Sagawa. Structure of exotic neutron-rich nuclei. *Phys. Rev. Lett.*, 70:1385, 1993.
- J. M. Pacheco, R. A. Broglia, and B. R. Mottelson. The intrinsic line width of the plasmon resonances in metal microclusters at very low temperatures: quantal surface fluctuations. *Zeitschrift für Physik D Atoms, Molecules and Clusters*, 21:289, 1991.
- A. Pais. *Inward bound*. Oxford University Press, Oxford, 1986.
- A. Pais. *The genius of science*. Oxford University Press, Oxford, 2000.
- S. S. Pankratov, M. V. Zverev, M. Baldo, U. Lombardo, and E. E. Saperstein. Semimicroscopic model of pairing in nuclei. *Phys. Rev. C*, 84:014321, 2011.
- A. Pastore, D. Tarpanov, D. Davesne, and J. Navarro. Spurious finite-size instabilities in nuclear energy density functionals: Spin channel. *Phys. Rev. C*, 92: 024305, 2015.
- W. Pauli. Zur quantenmechanik ii. *Zeitschr. Phys.*, 31:625, 1925.
- W. Pauli. Über gasentartung und paramagnetismus. *Zeitschrift für Physik*, 41(2): 81, Jun 1927.
- W. Pauli. *Exclusion principle and quantum mechanics, Nobel Lecture 1945*. Editions du Griffon, Neuchâtel, Switzerland, 1947.
- L. Pauling and E. B. Wilson Jr. *Quantum Mechanics*. Dover, New York, 1963.
- J. Pedersen, S. Bjornhølm, J. Borggreen, K. Hansen, T. P. Martin, and H. D. Rasmussen. Observation of quantum supershells in clusters of sodium atoms. *Nature*, 353:733, 1991.

- J. A. A. J. Perenboom, P. Wyder, and F. Meier. Electronic properties of small metallic particles. *Physics Reports*, 78:173, 1981.
- F. Perey and B. Buck. A non-local potential model for the scattering of neutrons by nuclei . *Nuclear Physics*, 32:353, 1962.
- D. Pines and D. Bohm. A Collective Description of Electron Interactions: II. Collective vs Individual Particle Aspects of the Interactions. *Phys. Rev.*, 85:338, 1952.
- D. Pines and P. Nozières. *The theory of quantum liquids*. Benjamin, New York, 1966.
- W. Pinkston and G. Satchler. Properties of simultaneous and sequential two-nucleon transfer. *Nuclear Physics A*, 383:61, 1982.
- F. M. Pipkin. Lamb shift measurements. In T. Kinoshita, editor, *Quantum electrodynamics*, page 697. World Scientific, Singapore, 1990.
- A. B. Pippard. The historical context of Josephson discovery. In H. Rogalla and P. H. Kes, editors, *100 years of superconductivity*, page 30. CRC Press, Taylor and Francis, FL, 2012.
- G. Pollarolo and R. A. Broglia. Microscopic Description of the Backward Rise of the Elastic Angular Distribution $^{16}\text{O}+^{28}\text{Si}$. *Nuovo Cimento*, 81:278, 1984.
- G. Pollarolo, R. A. Broglia, and A. Winther. Calculation of the imaginary part of the heavy ion potential. *Nuclear Physics A*, 406:369, 1983.
- G. Potel. ONE: single-particle transfer DWBA code for both light and heavy ions. 2012a. (unpublished).
- G. Potel. COOPER: two-particle transfer in second-order DWBA code for both light and heavy ions. 2012b. (unpublished).
- G. Potel, F. Barranco, E. Vigezzi, and R. A. Broglia. Evidence for phonon mediated pairing interaction in the halo of the nucleus ^{11}Li . *Phys. Rev. Lett.*, 105:172502, 2010.
- G. Potel, F. Barranco, F. Marini, A. Idini, E. Vigezzi, and R. A. Broglia. Calculation of the Transition from Pairing Vibrational to Pairing Rotational Regimes between Magic Nuclei ^{100}Sn and ^{132}Sn via Two-Nucleon Transfer Reactions. *Physical Review Letters*, 107:092501, 2011.
- G. Potel, A. Idini, F. Barranco, E. Vigezzi, and R. A. Broglia. Cooper pair transfer in nuclei. *Rep. Prog. Phys.*, 76:106301, 2013a.
- G. Potel, A. Idini, F. Barranco, E. Vigezzi, and R. A. Broglia. Quantitative study of coherent pairing modes with two-neutron transfer: Sn isotopes. *Phys. Rev. C*, 87:054321, 2013b.

- G. Potel, A. Idini, F. Barranco, E. Vigezzi, and R. A. Broglia. Nuclear Field Theory predictions for ^{11}Li and ^{12}Be : shedding light on the origin of pairing in nuclei. *Phys. At. Nucl.*, 77:941, 2014.
- G. Potel, A. Idini, F. Barranco, E. Vigezzi, and R. A. Broglia. From bare to renormalized order parameter in gauge space: structure and reactions. *Phys. Rev C*, 96:034606, 2017.
- B. Povh and M. Rosina. *Scattering and structures*. Springer, Berlin, 2002.
- I. Ragnarsson and R. A. Broglia. Pairing isomers. *Nuclear Physics A*, 263:315, 1976.
- I. Ragnarsson and S. G. Nilsson. *Shapes and shells in nuclear structure*. Cambridge University Press, Cambridge, 2005.
- G. H. Rawitscher. The microscopic Feshbach optical potential for a schematic coupled channel example. *Nuclear Physics A*, 475:519, 1987.
- M. Rees. *Just six numbers*. Basic Books, New York, 2000.
- P. G. Reinhard and D. Drechsel. Ground state correlations and the nuclear charge distribution. *Zeitschrift für Physik A Atoms and Nuclei*, 290(1):85–91, Mar 1979.
- H. Reinhardt. Foundation of nuclear field-theory. *Nucl. Phys. A*, 241:317, 1975.
- H. Reinhardt. Functional approach to Nuclear Field-theory - schematic model with pairing and particle-hole forces. *Nucl. Phys. A*, 298:60, 1978a.
- H. Reinhardt. Nuclear Field-Theory. *Nucl. Phys. A*, 251:77, 1978b.
- H. Reinhardt. Application of the nuclear-field theory to superfluid nuclei-quasiparticle-phonon multiplet. *Nucl. Phys. A*, 251:176, 1980.
- A. Repko, P. G. Reinhard, V. O. Nesterenko, and J. Kvasil. Toroidal nature of the low-energy E1 mode. *Phys. Rev. C*, 87:04305, 2013.
- P. Ring. Berry phase and backbending. In R. A. Broglia and V. Zelevinski, editors, *50 Years of Nuclear BCS*, page 522. World Scientific, Singapore, 2013.
- P. Ring and P. Schuck. *The Nuclear Many-Body Problem*. Springer, Berlin, 1980.
- R. M. Robledo and G. F. Bertsch. Pairing in Finite Systems: Beyond the HFB Theory. In R. A. Broglia and V. Zelevinski, editors, *50 Years of Nuclear BCS*, page 89. World Scientific, Singapore, 2013.
- H. Rogalla and P. H. Kes, editors. *100 years of superconductivity*. CRC Press, Taylor and Francis, FL, 2012.

- D. Rogovin and M. Scully. Superconductivity and macroscopic quantum phenomena. *Physics Reports*, 25:175, 1976.
- H. J. Rose and G. A. C. Jones. A new kind of natural radioactivity. *Nature*, 307:245, 1984.
- H. I. Rösner, M. Caldarini, A. Prestel, M. A. Vanoni, R. A. Broglia, A. Aliverti, G. Tiana, , and B. B. Kragelund. Cold denaturation of the HIV-1 protease monomer. *Biochemistry*, 156:1029, 2017.
- B. Rost. Protein structures sustained evolutionary drift. *Folding and Design*, 2:19, 1997.
- J. Rotureau, P. Danielewicz, G. Hagen, F. M. Nunes, and T. Papenbrock. Optical potential from first principles. *Phys. Rev. C*, 95:024315, 2017.
- D. Sackett, K. Ieki, A. Galonsky, C. A. Bertulani, H. Esbensen, J. J. Kruse, W. G. Lynch, D. J. Morrissey, N. A. Orr, B. M. Sherrill, H. Schulz, A. Sustich, J. A. Winger, F. Deák, A. Horváth, A. Kiss, Z. Seres, J. J. Kolata, R. E. Warner, and D. L. Humphrey. Electromagnetic excitation of ^{11}Li . *Phys. Rev. C*, 48:118, 1993.
- H. Sagawa, B. A. Brown, and H. Esbensen. Parity inversion in the N=7 isotones and the pairing blocking effect. *Phys. Lett. B*, 309:1, 1993.
- J. J. Sakurai. *Modern Quantum Mechanics*. Addison-Wesley, Cambridge, MA, 1994.
- A. Sanetullaev, R. Kanungo, J. Tanaka, M. Alcorta, C. Andreoiu, P. Bender, A. Chen, G. Christian, B. Davids, J. Fallis, J. Fortin, N. Galinski, A. Gallant, P. Garrett, G. Hackman, B. Hadinia, S. Ishimoto, M. Keefe, R. Krücken, J. Lighthall, E. McNeice, D. Miller, J. Purcell, J. Randhawa, T. Roger, A. Rojas, H. Savajols, A. Shotter, I. Tanihata, I. Thompson, C. Unsworth, P. Voss, and Z. Wang. Investigation of the role of ^{10}Li resonances in the halo structure of ^{11}Li through the $^{11}\text{Li}(p, d)^{10}\text{Li}$ transfer reaction. *Physics Letters B*, 755:481, 2016.
- F. Sanger. The arrangement of aminoacids in proteins. *Adv. Protein Chem.*, VII:1, 1952.
- E. E. Saperstein and M. Baldo. Microscopic Origin of Pairing. In R. A. Broglia and V. Zelevinsky, editors, *50 Years of Nuclear BCS*, page 263. World Scientific, Singapore, 2013.
- J. R. Sapirstein and D. R. Yennie. Theory of Hydrogenic Bound States. In T. Kinoshita, editor, *Quantum electrodynamics*. World Scientific, Singapore, 1990.
- V. V. Sargsyan, G. Scamps, G. G. Adamian, N. V. Antonenko, and D. Lacroix. Neutron-pair transfer in the sub-barrier capture process. *Phys. Rev. C*, 88:064601, 2013.

- R. Sartor and C. Mahaux. Single-particle states in nuclear matter and in finite nuclei. *Physical Review C*, 21(6):2613, 1980.
- G. Satchler. *Introduction to Nuclear Reactions*. Mc Millan, New York, 1980.
- G. Satchler. *Direct Nuclear Reactions*. Clarendon Press, Oxford, 1983.
- J. P. Schiffer, C. R. Hoffman, B. P. Kay, J. A. Clark, C. M. Deibel, S. J. Freeman, A. M. Howard, A. J. Mitchell, P. D. Parker, D. K. Sharp, and J. S. Thomas. Test of sum rules in nucleon transfer reactions. *Phys. Rev. Lett.*, 108:022501, 2012.
- A. Schmid. Diamagnetic susceptibility at the transition to the superconducting state. *Phys. Rev.*, 180:527, 1969.
- H. Schmidt. The onset of superconductivity in the time dependent Ginzburg–Landau theory. *Zeits. Phys.*, 216:336, 1968.
- H. Schmidt. Pairing vibrations in nuclei and solids. In Morinaga H., editor, *Proceedings of the International School of Physics “Enrico Fermi” Course LIII, Developments and Borderlines on Nuclear Physics*, page 144, NY, 1972. Academic Press.
- K. T. Schmitt, K. L. Jones, S. Ahn, D. W. Bardayan, A. Bey, J. C. Blackmon, S. M. Brown, K. Y. Chae, K. A. Chipps, J. A. Cizewski, K. I. Hahn, J. J. Kolata, R. L. Kozub, J. F. Liang, C. Matei, M. Matos, D. Matyas, B. Moazen, C. D. Nesaraja, F. M. Nunes, P. D. O’Malley, S. D. Pain, W. A. Peters, S. T. Pittman, A. Roberts, D. Shapira, J. F. Shriner, M. S. Smith, I. Spassova, D. W. Stracener, N. J. Upadhyay, A. N. Villano, and G. L. Wilson. Reactions of a ^{10}Be beam on proton and deuteron targets. *Phys. Rev. C*, 88:064612, 2013.
- J. R. Schrieffer. *Superconductivity*. Benjamin, New York, 1964.
- J. R. Schrieffer. Macroscopic quantum phenomena from pairing in superconductors. *Physics Today*, 26 (7):23, 1973.
- E. Schrödinger. Quantisierung als eigenwertproblem. *Annalen der Phys.*, 384:273, 1926a.
- E. Schrödinger. Der stetige Übergang von der Mikro-zur Makromechanik. *Naturw.*, 14:644, 1926b.
- E. Schrödinger. *What is life? The physical aspect of the living cell*. Cambridge University Press, 1944.
- S. Schweber. *QED*. Princeton University Press, Princeton, New Jersey, 1994.
- J. Schwinger. On quantum-electrodynamics and the magnetic moment of the electron. *Physical Review*, 73:416, 1948.

- J. Schwinger. *Quantum electrodynamics: selected papers*. Dover Publications, 1958.
- J. Schwinger. *Quantum Mechanics*. Springer, Heidelberg, 2001.
- Y. R. Shimizu. Pairing fluctuations and gauge symmetry restoration in rotating superfluid nuclei. In R. A. Broglia and V. Zelevinsky, editors, *50 Years of Nuclear BCS*, page 567. World Scientific, Singapore, 2013.
- Y. R. Shimizu and R. A. Broglia. A comparison of the RPA and number projection approach for calculations of pairing fluctuations in fast rotating nuclei. *Nucl. Phys. A*, 515:38, 1990.
- Y. R. Shimizu, J. D. Garrett, R. A. Broglia, M. Gallardo, and E. Vigezzi. Pairing fluctuations in rapidly rotating nuclei. *Reviews of Modern Physics*, 61:131, 1989.
- Y. R. Shimizu, P. Donati, and R. A. Broglia. Response function technique for calculating the random-phase approximation correlation energy. *Phys. Rev. Lett.*, 85:2260, 2000.
- S. Shimoura, T. Nakamura, M. Ishihara, N. Inabe, T. Kobayashi, T. Kubo, R. Siemssen, I. Tanihata, and Y. Watanabe. Coulomb dissociation reaction and correlations of two halo neutrons in ^{11}Li . *Physics Letters B*, 348:29, 1995.
- M. Smith, M. Brodeur, T. Brunner, S. Ettenauer, A. Lapierre, R. Ringle, V. L. Ryjkov, F. Ames, P. Bricault, G. W. F. Drake, P. Delheij, D. Lunney, F. Sarazin, and J. Dilling. First penning-trap mass measurement of the exotic halo nucleus ^{11}Li . *Phys. Rev. Lett.*, 101:202501, 2008.
- V. G. Soloviev. Quasi-particle and collective structure of the states of even, strongly-deformed nuclei. *Nuclear Physics*, 69(1):1, 1965.
- G. S. Stent. In G. S. Stent, editor, *The double helix*. Norton and Co., New York, 1980.
- F. S. Stephens and R. S. Simon. Coriolis effects in the yrast states. *Nuclear Physics A*, 183:257, 1972.
- F. H. Stillinger. A topographic view of supercooled liquids and glass formation. *Science*, 237:1935, 1995.
- F. H. Stillinger and D. K. Stillinger. Computational study of transition dynamics in 55-atom clusters. *J. Chem. Phys.*, 93:6013, 1990.
- T. Nakamura et al. Observation of Strong Low-Lying E1 Strength in the Two-Neutron Halo Nucleus ^{11}Li . *Phys. Rev. Lett.*, 96:252502, 2006.
- I. Talmi and I. Unna. Order of Levels in the Shell Model and Spin of Be^{11} . *Phys. Rev. Lett.*, 4:469, 1960.

- T. Tamura. Compact reformulation of distorted-wave and coupled-channel born approximations for transfer reactions between nuclei. *Physics Reports*, 14:59, 1974.
- T. Tamura, D. R. Bès, R. A. Broglia, and S. Landowne. Coupled-channel Born-approximation calculation of two-nucleon transfer reactions in deformed nuclei. *Physical Review Letters*, 25:1507, 1970.
- T. Tamura, T. Udagawa, and C. Mermaz. Direct reaction analyses of heavy-ion induced reactions leading to discrete states. *Physics Reports*, 65:345, 1980.
- Y. C. Tang and R. C. Herndon. Form factors of ^3H and ^4He with repulsive–core potentials. *Phys. Lett.*, 18:42, 1965.
- I. Tanihata, M. Alcorta, D. Bandyopadhyay, R. Bieri, L. Buchmann, B. Davids, N. Galinski, D. Howell, W. Mills, S. Mythili, R. Openshaw, E. Padilla-Rodal, G. Ruprecht, G. Sheffer, A. C. Shotter, M. Trinczek, P. Walden, H. Savajols, T. Roger, M. Caamano, W. Mittig, P. Roussel-Chomaz, R. Kanungo, A. Gallant, M. Notani, G. Savard, and I. J. Thompson. Measurement of the two-halo neutron transfer reaction $^1\text{H}(^{11}\text{Li}, ^9\text{Li})^3\text{H}$ at 3A MeV. *Phys. Rev. Lett.*, 100:192502, 2008.
- I. Tanihata, H. Savajols, and R. Kanungo. Recent experimental progress in nuclear halo structure studies. *Progress in Particle and Nuclear Physics*, 68:215, 2013.
- D. Tarpanov, J. Dobaczewski, J. Toivanen, and B. G. Carlsson. Spectroscopic properties of nuclear skyrme energy density functionals. *Phys. Rev. Lett.*, 113: 252501, 2014.
- D. ter Haar. *Men of Physics: L. D. Landau II*. Bergamon Press, Oxford, 1969.
- I. J. Thompson. Coupled reaction channels calculations in nuclear physics. *Computer Physics Reports*, 7(4):167, 1988.
- I. J. Thompson. Reaction mechanism of pair transfer. In R. A. Broglia and V. Zelevinsky, editors, *50 Years of Nuclear BCS*, page 455. World Scientific, Singapore, 2013.
- I. J. Thompson and F. M. Nunes. *Nuclear Reactions for Astrophysics*. Cambridge University Press, Cambridge, 2009.
- N. K. Timofeyuk and R. C. Johnson. Deuteron stripping and pick-up on halo nuclei. *Phys. Rev. C*, 59:1545, 1999.
- M. Tinkham. *Introduction to Superconductivity*. Mc Graw-Hill, New York, 1996.
- W. Tobocman. *Theory of direct reactions*. Oxford University Press, Oxford, 1961.
- S. Tomonaga. On a relativistically invariant formulation of the quantum theory of wave fields. *Progress of Theoretical Physics*, 1:27, 1946.

- M. K. Transtrum, B. B. Machta, K. S. Brown, B. C. Daniels, C. R. Myers, and J. P. Sethna. Perspective: Sloppiness and emergent theories in physics, biology, and beyond. *The Journal of Chemical Physics*, 143:010901, 2015.
- T. Tsuboi and T. Suzuki. Specific Heat of Superconducting Fine Particles of Tin. I. Fluctuations in Zero Magnetic Field. *Journal of the Physical Society of Japan*, 42:437, 1977.
- J. Ungrin, R. M. Diamond, P. O. Tjøm, and B. Elbek. Inelastic deuteron scattering in the lead region. *Mat. Fys. Medd. Dan. Vid. Selk.*, 38, 1971.
- J. Vaagen, B. Nilsson, J. Bang, and R. Ibarra. One- and two-nucleon overlaps generated by a Sturmian method. *Nuclear Physics A*, 319:143, 1979.
- J. Valatin. Comments on the theory of superconductivity. *Il Nuovo Cimento*, 7: 843, 1958.
- V. L. Van der Waerden. *Sources of quantum mechanics*. Dover, New York, 1967.
- M. van Witsen. Superconductivity in real space. *University of Twente*, 2014. (unpublished).
- N. L. Vaquero, J. L. Egido, and T. R. Rodríguez. Large-amplitude pairing fluctuations in atomic nuclei. *Phys. Rev. C*, 88:064311, 2013.
- N. Vinh Mau. Particle-vibration coupling in one neutron halo nuclei. *Nuclear Physics A*, 592:33, 1995.
- W. von Oertzen. Enhanced two-nucleon transfer due to pairing correlations. In R. A. Broglia and V. Zelevinsky, editors, *50 Years of Nuclear BCS*, page 405. World Scientific, Singapore, 2013.
- W. von Oertzen and A. Vitturi. Pairing correlations of nucleons and multi-nucleon transfer between heavy nuclei. *Reports on Progress in Physics*, 64:1247, 2001.
- J. R. Waldram. *Superconductivity of metals and cuprates*. Institute of Physics, Bristol, 1996.
- J. C. Ward. An identity in quantum electrodynamics. *Phys. Rev.*, 78:182, 1950.
- J. D. Watson. *The double helix*. Norton & C.O., New York, 1980.
- J. D. Watson and F. H. C. Crick. A structure of the deoxyribose nucleic acid. *Nature*, 171:737, 1953.
- L. Weinberg. From BCS to the LHC. In L. Cooper and D. Feldman, editors, *BCS: 50 years*. World Scientific, Singapore, 2011.
- S. Weinberg. *The Quantum Theory of Fields*, volume 1. Cambridge University Press, Cambridge, 1996.

- V. F. Weisskopf. The formation of superconducting pairs and the nature of superconducting currents. *Contemporary Physics*, 22:375, 1981.
- C. F. Weizsäcker. Zur theorie der kernmassen. *Z. Phys.*, 96:431, 1935.
- H. Wibowo and E. Litvinova. Nuclear dipole response in the finite-temperature relativistic time-blocking approximation. *Phys. Rev. C*, 100:024307, Aug 2019.
- K. Wimmer, T. Kröll, R. Krücken, V. Bildstein, R. Gernhäuser, B. Bastin, N. Bree, J. Diriken, P. Van Duppen, M. Huyse, N. Patronis, P. Vermaelen, D. Voulot, J. Van de Walle, F. Wenander, L. M. Fraile, R. Chapman, B. Hadinia, R. Orlandi, J. F. Smith, R. Lutter, P. G. Thirolf, M. Labiche, A. Blazhev, M. Kalkühler, P. Reiter, M. Seidlitz, N. Warr, A. O. Macchiavelli, H. B. Jeppesen, E. Fiori, G. Georgiev, G. Schrieder, S. Das Gupta, G. Lo Bianco, S. Nardelli, J. Butterworth, J. Johansen, and K. Riisager. Discovery of the Shape Coexisting 0^+ State in ^{32}Mg by a Two Neutron Transfer Reaction. *Phys. Rev. Lett.*, 105:252501, 2010.
- J. Winfield, S. Fortier, W. Catford, S. Pita, N. Orr, J. V. de Wiele, Y. Blumenfeld, R. Chapman, S. Chappell, N. Clarke, N. Curtis, M. Freer, S. Gals, H. Langevin-Joliot, H. Laurent, I. Lhenry, J. Maison, P. Roussel-Chomaz, M. Shawcross, K. Spohr, T. Suomijrvi, and A. de Vismes. Single-neutron transfer from $^{11}\text{Be}_{gs}$ via the (p, d) reaction with a radioactive beam. *Nuclear Physics A*, 683:48, 2001.
- R. B. Wiringa, R. A. Smith, and T. L. Ainsworth. Nucleon-nucleon potentials with and without $\Delta(1232)$ degrees of freedom. *Phys. Rev. C*, 29:1207, 1984.
- P. Wölfe. Sound propagation an kinetic coefficients in superfluid ^3He . *Progr. Low Temp. Phys.*, 7:191, 1978.
- P. G. Wolynes. Moments of excitement. *Science*, 352:150, 2016.
- P. G. Wolynes, W. A. Eaton, and F. A. R. Chemical physics of protein folding. *PNAS*, 109:17770, 2012.
- C. N. Yang. Concept of Off-Diagonal Long-Range Order and the Quantum Phases of Liquid He and of Superconductors. *Rev. Mod. Phys.*, 34:694, 1962.
- S. Yoshida. Note on the two-nucleon stripping reaction. *Nuclear Physics*, 33:685, 1962.
- P. G. Young and R. H. Stokes. New States in ^9Li from the Reaction $^7\text{Li}(t, p)^9\text{Li}$. *Phys. Rev. C*, 4:1597, 1971.
- Y. Zhou, D. Vitkup, and M. Karplus. Native proteins are surface–molten solids: applications of the Lindemann Criterion for the solid versus liquid state. *J. Mol. Biol.*, 285:1371, 1999.

- M. Zinser, F. Humbert, T. Nilsson, W. Schwab, T. Blaich, M. J. G. Borge, L. V. Chulkov, H. Eickhoff, T. W. Elze, H. Emling, B. Franzke, H. Freiesleben, H. B. Geissel, K. Grimm, D. Guillemaud-Mueller, P. G. Hansen, R. Holzmann, H. Irnich, B. Jonson, J. G. Keller, O. Klepper, H. Klingler, J. V. Kratz, R. Kulessa, D. Lambrecht, Y. Leifels, and A. Magel. Study of the unstable nucleus ^{10}Li in stripping reactions of the radioactive projectiles ^{11}Be and ^{11}Li . *Phys. Rev. Lett.*, 75:1719, 1995.
- M. Zinser, F. Humbert, T. Nilsson, W. Schwab, H. Simon, T. Aumann, M. J. G. Borge, L. V. Chulkov, J. Cub, T. W. Elze, H. Emling, H. Geissel, D. Guillemaud-Mueller, P. G. Hansen, R. Holzmann, H. Irnich, B. Jonson, J. V. Kratz, R. Kulessa, Y. Leifels, H. Lenske, A. Magel, A. C. Mueller, G. Mnzenberg, F. Nickel, G. Nyman, A. Richter, K. Riisager, C. Scheidenberger, G. Schrieder, K. Stelzer, J. Stroth, A. Surowiec, O. Tengblad, E. Wajda, and E. Zude. Invariant-mass spectroscopy of ^{10}Li and ^{11}Li . *Nuclear Physics A*, 619:151, 1997.
- B. Zwieglinski, W. Benenson, R. Robertson, and W. Coker. Study of the $^{10}\text{Be}(d, p)^{11}\text{Be}$ reaction at 25 MeV. *Nuclear Physics A*, 315:124, 1979.